

Frontiers
in
Artificial
Intelligence
and
Applications

FUZZY SYSTEMS AND DATA MINING VI

Proceedings of FSDM 2020

Edited by
Antonio J. Tallón-Ballesteros

FUZZY SYSTEMS AND DATA MINING VI

The interdisciplinary field of fuzzy logic encompass applications in the electrical, industrial, chemical and engineering realms as well as in areas of management and environmental issues, while data mining covers new approaches to big data, massive data, and scalable, parallel and distributed algorithms.

This book presents papers from the 6th International Conference on Fuzzy Systems and Data Mining (FSDM 2020). The conference was originally due to be held from 13-16 November 2020 in Xiamen, China, but was changed to an online conference held on the same dates due to ongoing restrictions connected with the COVID-19 pandemic. The annual FSDM conference provides a platform for knowledge exchange between international experts, researchers academics and delegates from industry. This year, the committee received 316 submissions, of which 76 papers were selected for inclusion in the conference; an acceptance rate of 24%. The conference covers four main areas: fuzzy theory; algorithms and systems, which includes topics like stability; foundations and control; and fuzzy applications, which are widely used and cover various types of processing as well as hardware and architecture for big data and time series.

Providing a current overview of research and developments in fuzzy logic and data mining, the book will be of interest to all those working in the field of data science.



ISBN 978-1-64368-134-4 (print)

ISBN 978-1-64368-135-1 (online)

ISSN 0922-6389 (print)

ISSN 1879-8314 (online)

FUZZY SYSTEMS AND DATA MINING VI

Frontiers in Artificial Intelligence and Applications

The book series Frontiers in Artificial Intelligence and Applications (FAIA) covers all aspects of theoretical and applied Artificial Intelligence research in the form of monographs, selected doctoral dissertations, handbooks and proceedings volumes. The FAIA series contains several sub-series, including ‘Information Modelling and Knowledge Bases’ and ‘Knowledge-Based Intelligent Engineering Systems’. It also includes the biennial European Conference on Artificial Intelligence (ECAI) proceedings volumes, and other EurAI (European Association for Artificial Intelligence, formerly ECCAI) sponsored publications. The series has become a highly visible platform for the publication and dissemination of original research in this field. Volumes are selected for inclusion by an international editorial board of well-known scholars in the field of AI. All contributions to the volumes in the series have been peer reviewed.

The FAIA series is indexed in ACM Digital Library; DBLP; EI Compendex; Google Scholar; Scopus; Web of Science: Conference Proceedings Citation Index – Science (CPCI-S) and Book Citation Index – Science (BKCI-S); Zentralblatt MATH.

Series Editors:

Joost Breuker, Nicola Guarino, Pascal Hitzler, Joost N. Kok, Jiming Liu,
Ramon López de Mántaras, Riichiro Mizoguchi, Mark Musen, Sankar K. Pal,
Ning Zhong

Volume 331

Recently published in this series

- Vol. 330. B. Brodaric and F. Neuhaus (Eds.), Formal Ontology in Information Systems – Proceedings of the 11th International Conference (FOIS 2020)
- Vol. 329. A.J. Tallón-Ballesteros (Eds.), Modern Management based on Big Data I – Proceedings of MMBD 2020
- Vol. 328. A. Utka, J. Vaičenonienė, J. Kovalevskaitė and D. Kalinauskaitė (Eds.), Human Language Technologies – The Baltic Perspective – Proceedings of the Ninth International Conference Baltic HLT 2020
- Vol. 327. H. Fujita, A. Selamat and S. Omatsu (Eds.), Knowledge Innovation Through Intelligent Software Methodologies, Tools and Techniques – Proceedings of the 19th International Conference on New Trends in Intelligent Software Methodologies, Tools and Techniques (SoMeT_20)
- Vol. 326. H. Prakken, S. Bistarelli, F. Santini and C. Taticchi (Eds.), Computational Models of Argument – Proceedings of COMMA 2020
- Vol. 325. G. De Giacomo, A. Catala, B. Dilkina, M. Milano, S. Barro, A. Bugarín and J. Lang (Eds.), ECAI 2020 – 24th European Conference on Artificial Intelligence – 29 August–8 September 2020, Santiago de Compostela, Spain

ISSN 0922-6389 (print)
ISSN 1879-8314 (online)

Fuzzy Systems and Data Mining VI

Proceedings of FSDM 2020

Edited by

Antonio J. Tallón-Ballesteros

University of Huelva, Spain

IOS
Press

Amsterdam • Berlin • Washington, DC

© 2020 The authors and IOS Press.

This book is published online with Open Access and distributed under the terms of the Creative Commons Attribution Non-Commercial License 4.0 (CC BY-NC 4.0).

ISBN 978-1-64368-134-4 (print)

ISBN 978-1-64368-135-1 (online)

Library of Congress Control Number: 2020948959

doi: 10.3233/FAIA331

Publisher

IOS Press BV

Nieuwe Hemweg 6B

1013 BG Amsterdam

Netherlands

fax: +31 20 687 0019

e-mail: order@iospress.nl

For book sales in the USA and Canada:

IOS Press, Inc.

6751 Tepper Drive

Clifton, VA 20124

USA

Tel.: +1 703 830 6300

Fax: +1 703 830 2300

sales@iospress.com

LEGAL NOTICE

The publisher is not responsible for the use which might be made of the following information.

PRINTED IN THE NETHERLANDS

Preface

This year's edition of the International Conference on Fuzzy Systems and Data Mining (FSDM), the first of the 2020s, has been disrupted due to the COVID-19 pandemic. FSDM has had a short but also very intense history to reach this 6th edition of the series, and has become one of the top conferences the proceedings of which are published in the prestigious book series, *Frontiers in Artificial Intelligence and Applications* (FAIA), by IOS Press. The last two proceedings of the European-Japanese Conference on Information Modelling and Knowledge Bases (EJC-IMKB) can be found in [1] and [2] respectively; the 2019 proceedings of Legal Knowledge Based Systems (JURIX) can be accessed from [3]; and papers for JURIX 2020 are currently under assessment. The – International Conference on Software Methodologies, Tools and Techniques (SOMET) – SOMET 2020 is a newly published book in FAIA [4], and SOMET 2019 can be found in [5]. These are the three conferences with the highest number of edited volumes published as part of the FAIA series.

FSDM 2015 [6] was held in Shanghai, China; FSDM 2016 [7] took place in Macau, China; FSDM 2017 [8] visited Hualien, Taiwan; FSDM 2018 [9] travelled to Bangkok, Thailand; and finally FSDM 2019 [10] was held in Kitakyushu City, Japan.

Nowadays, data science, big data and deep learning are the typical keywords which abound in any high-level conference in the field of machine learning. FSDM is focused on data mining and fuzzy systems, and the aforementioned topics are dealt with in many of the papers included here.

This volume includes the papers accepted and presented at the 6th International Conference on Fuzzy Systems and Data Mining (FSDM 2020), which was initially scheduled to be held from 13–16 November 2020 in Xiamen, China, but which was ultimately changed to an online conference due to ongoing restrictions connected with the COVID-19 pandemic. All sessions were available via live streaming with a high interaction from all participants.

All papers were carefully reviewed by program committee members with regard to the quality, novelty, breadth and depth of the research themes falling within the scope of FSDM. FSDM 2020 was a reference and outstanding conference which attracted three remarkable keynote speakers: Prof. Dr. Rongrong Ji from Xiamen University (China), Prof. Dr. Juan Manuel Corchado, Director of the European IoT Digital Innovation Hub and Director of the BISITE Research Group from the University of Salamanca (Spain) and Prof. Dr. Milan Tuba, Vice Rector for International Relations, Singidunum University, Serbia. This meant that the conference enjoyed three keynotes from very different locations.

The current FAIA volume contains selected contributions from FSDM 2020. If you have contributed to the FSDM conference before or in this edition, we would like to see you on board again. Otherwise, if you have not yet submitted a paper to FSDM, we would like to invite you to prepare a good contribution and for our visit to either Europe or South Korea, one of which will be the location for FSDM 2021.

I am very glad to inform you that FSDM received 316 submissions this year. After an intense discussion stage, the committee, which included many experts, decided to accept 76 papers, which represents an acceptance rate of 24%. The profile of the

authors is very remarkable and the number of full professors who contributed is very high. As a follow-up to the conference, some special issues in well-regarded journals such as the *International Journal of Information Technology and Web Engineering (IJITWE)*, *CMES-Computer Modeling in Engineering & Sciences*, *International Journal of Fuzzy Systems and Mathematics* are scheduled to be published; this is an important leap in the number of journal issues, which is increasing yearly. Special issues with *Intelligent Data Analysis* and *Journal of Nonlinear and Convex Analysis* have been published in previous years.

I would like to take this opportunity to thank all the keynote and invited speakers, as well as the authors who made the effort to prepare a contribution to the conference. Furthermore, I also wish to express our gratitude to everyone, especially the program committee members and reviewers, who devoted time to assessing the papers. It is an honor to continue with the publication of these proceedings in the outstanding series FAIA by IOS Press. My particular thanks and regards also go to J. Breuker, N. Guarino, J.N. Kok, R. López de Mántaras, J. Liu, R. Mizoguchi, M. Musen, S.K. Pal and N. Zhong, the FAIA series editors, for supporting this conference.

1st October 2020
Huelva city, Spain

Antonio J. Tallón-Ballesteros
University of Huelva (Spain)

References

- [1] B. Thalheim, M. Tropmann-Frick, H. Jaakkola & Y. Kiyoki (Eds.). (2020). *Proceedings of the 30th International Conference on Information Modelling and Knowledge Bases (EJC 2020)*.
- [2] A. Dahanayak, J. Huiskonen, & Y. Kiyoki (Eds.). (2020). *Information Modelling and Knowledge Bases XXXI* (Vol. 321). IOS Press.
- [3] M. Araszkiewicz, & V. Rodríguez-Doncel (Eds.). (2019). *Legal Knowledge and Information Systems: JURIX 2019: The Thirty-second Annual Conference* (Vol. 322). IOS Press.
- [4] H. Fujita, A. Selamat, & S. Omatu (Eds.). (2020). *Knowledge Innovation Through Intelligent Software Methodologies, Tools and Techniques*. IOS Press. ISBN 978-1-64368-114-6 DOI:10.3233/FAIA200574.
- [5] H. Fujita, & A. Selamat (Eds.). (2019). *Advancing Technology Industrialization Through Intelligent Software Methodologies, Tools and Techniques: Proceedings of the 18th International Conference on New Trends in Intelligent Software Methodologies, Tools and Techniques (SoMet_19)* (Vol. 318). IOS Press.
- [6] G. Chen, F. Liu, & M. Shojafar (Eds.). (2016). *Fuzzy system and data mining: proceedings of FSDM 2015* (Vol. 281). IOS Press.
- [7] S. L. Sun, A. J. Tallón-Ballesteros, & D. S. Pamučar (Eds.). (2016). *Fuzzy Systems and Data MiningII: Proceedings of FSDM 2016* (Vol. 293). IOS Press.
- [8] A. J. Tallón-Ballesteros, & K. Li (Eds.). (2017). *Fuzzy Systems and Data Mining III: Proceedings of FSDM 2018* (Vol. 299). IOS Press.
- [9] A. J. Tallón-Ballesteros, & K. Li (Eds.). (2018). *Fuzzy Systems and Data Mining IV: Proceedings of FSDM 2018* (Vol. 309). IOS Press.
- [10] A. J. Tallón-Ballesteros (Ed.). (2019). *Fuzzy Systems and Data Mining V: Proceedings of FSDM 2019* (Vol. 320). IOS Press.

Contents

Preface <i>Antonio J. Tallón-Ballesteros</i>	v
Using the Generative Adversarial Network to Generate Recommendations <i>A.V. Prosvetov</i>	1
Study on Generalized Directional Differentiability Problems of Fuzzy Mappings <i>Yu-e Bao, Tingting Li and Linfen Zhang</i>	7
Structure Optimization of Magnetic Levitation Motor Rotor <i>Shuyan Yao, Bo Wu, Qiang Liu and Kang Xu</i>	16
Assessment of Socio-Economic Efficiency of the Scientific and Educational Complex: Approach and System of Indicators <i>Alexey Slavikovsky, Olga Vladimirova and Manon Khusainov</i>	25
Classification of Unbalanced Data Based on RSM and Binomial Distribution <i>Rong Li and Wei-Bai Zhou</i>	33
Facial Expression Analysis Based on Fusion Multi-Layer Convolutional Layer Feature Neural Network <i>Hao Meng, Fei Yuan and Tianhao Yan</i>	43
Investigation of a Method for EEG Signal De-Noising Based on the DIVA Model <i>Shaobai Zhang, Lihong Jiao and Ningning Zhou</i>	52
Origin and Evolution of Conceptual Differences Between Two Measurement Theories <i>Huisheng Shi, Xiaoming Ye, Cheng Xing and Shijun Ding</i>	66
Customer Churn Prediction Based on HMM in Telecommunication Industry <i>Huisheng Zhu and Bin Yu</i>	78
The Diagnosis of Alzheimer's Disease: An Ensemble Approach <i>Jingyan Qiu, Linjian Li, Yida Liu, Yingjun Ou and Yubei Lin</i>	93
An Improved Decision Tree Algorithm for Electricity Theft Prediction and Analysis <i>Xiaofeng Chen, Lipeng Zhang, Zhongping Xu, Feng Zhu and Xiaoming Qi</i>	101
Curves Classification by Using a Local Likelihood Function and Its Practical Usefulness for Real Data <i>Mustapha Rachdi, Ali Laksaci, Ali Hamié, Jacques Demongeot and Idir Ouassou</i>	113
Application of Grey Prediction in a GA-BP Power Theft Algorithm <i>Xiaofeng Chen, Zhongping Xu, Lipeng Zhang, Feng Zhu, Xiaoming Qi and Fangzhen Chen</i>	125

Output Feedback Control Synthesis and Stabilization for Positive Polynomial Fuzzy Systems Under L_1 Performance <i>Aiwen Meng, Hak-Keung Lam, Fucai Liu and Ziguang Wang</i>	135
Distance Metrics of D Numbers <i>Ligu Fei and Yuqiang Feng</i>	146
Comparison of Two Estimators of the Regression Coefficient Vector Under Pitman's Closeness Criterion <i>Jibo Wu</i>	152
Spatial-Spectral Density Peaks Based Discriminant Projection for Classification of Membranous Nephropathy Hyperspectral Pathological Image <i>Meng Lv, Wei Li and Ran Tao</i>	160
Intelligent Identification of Potential Customers for Electricity Substitution <i>Xiaofeng Chen, Yadi Zhao, Zhifeng Wei and Bingqiang Gao</i>	168
A Statistical Analysis of the Social Status of Chinese Women: Data Mining Method Based on MapReduce <i>Xiangdong Liu, Mingzhu Yang and Chengshuai Luo</i>	180
News-Based Research on Forecast of International Natural Gas Price Trend <i>Tianxiang Li, Xiaosong Han, Aoqing Wang, Hui Li, Guosheng Liu and Ying Pei</i>	194
A Virtual Reality Check: Covid-19 & the Challenges Facing Virtual Reality as an off-the-shelf Mainstream EdTech Solution <i>Markus Rach and Russell Scott</i>	201
Machine Learning and Statistical Analysis Techniques on Terrorism <i>Rajesh P, Babitha D, Mansoor Alam, Mansour Tahernezhadi and Monika A</i>	210
Analysis of the Legal Basis to Mitigate Cyberbullying in Social Networks in Ecuador <i>Segundo Moisés Toapanta Toapanta, Ingrid Lilibeth Tacuri López and Luis Enrique Majla Gallegos</i>	223
Neighborhood Based Multi-Granularity Attribute Reduction: An Acceleration Approach <i>Jingjing Song, Huili Dou, Xiansheng Rao, Xiaojing Luo and Xuan Yan</i>	234
Research on Application of Artificial Intelligence in VR Games <i>Wang Xi</i>	247
Fuzzy Expert Pricing Systems and Optimization Techniques in Marketing Science <i>Adeolu Dairo and Krisztián Szűcs</i>	255
ClothNet: A Neural Network Based Recommender System <i>Hao Xing, Zhike Han and Yichen Shen</i>	261
Realistic Face Image Generation System Based on GANs <i>Zhike Han, Bin Yang, Yiren Du, Xingyu Du, Hao Xing and Qinnan Cheng</i>	273

The Coupling Co-Location Pattern: A New Spatial Pattern for Spatial Data Sets <i>Shiran Zhou, Lizhen Wang and Pingping Wu</i>	290
LAR: A User Behavior Prediction Model in Server Log Based on LSTM-Attention Network and RSC Algorithm <i>Yingying Shang</i>	304
The Improved Algorithm of Sample Adaptive Offset Based on Visual Saliency <i>Nana Shan, Wei Zhou and Zhemin Duan</i>	315
The Overview of Genetic Algorithm with Tree Chromosome Structure to Identify Functions <i>Mitsukuni Matayoshi</i>	324
A Pipeline Abnormal Signal Detection Method Based on 1D-Faster R-CNN <i>Zhen Zhang and Weiguo Lin</i>	340
Research on Characteristics of Chinese Herbal Medicine Compounds Based on Bisecting k-Means Algorithm <i>Yushu Wu, Fenfen Xie, Lu Wang, Shoude Zhang, Lei Zhang and Xiaoying Wang</i>	351
Keyword Extraction from TV Program Viewers' Tweet Based on Neural Embedding Model <i>Taiga Kirihsara, Kazuyuki Matsumoto, Minoru Yoshida and Kenji Kita</i>	360
Water Quality Data Outlier Detection Method Based on Spatial Series Features <i>Jianzhuo Yan, Ya Gao and Yongchuan Yu</i>	370
Security and Privacy in Information Management in a Distributed Environment for Public Organizations <i>Segundo Moisés Toapanta Toapanta, Yaritza Julieth Terán Terranova, Bertha Alice Naranjo Sánchez and Luis Enrique Mafla Gallegos</i>	378
Exploring the Potential of GPT-2 for Generating Fake Reviews of Research Papers <i>Alberto Bartoli and Eric Medvet</i>	390
Development of IoT Based Fresh Food Delivery Tracking System Using GPS <i>Man-Ching Yuen, Yip-Hin Choi, Tsun-Hin Ng, Chun-Tung Poon and Kin-Chung Fung</i>	397
Consistency-Check Edge Refinement for Deep Stereo Matching <i>Fangrui Wu and Menglong Yang</i>	405
The Design of ERP Intelligent Sales Management System <i>Jianghui Liu, Qiuyi Chen and Yuexing Qiu</i>	413
Federated Learning in Big Data Application and Sharing <i>Jing Yang, Quan Zhang, Kunpeng Liu, Peng Jin and Guoyi Zhao</i>	423
Exploration on the Construction of Sharing Platform of Power Big Data Application <i>Jing Yang, Quan Zhang, Lihua Gong, Longzhu Zhu and Kunpeng Liu</i>	436

Estimating Observation Error Statistics Using a Robust Filter Method for Data Assimilation <i>Yue Wang and Yulong Bai</i>	449
Community Detection, Pattern Recognition, and Hypergraph-Based Learning: Approaches Using Metric Geometry and Persistent Homology <i>Dong Quan Ngoc Nguyen, Lin Xing and Lizhen Lin</i>	457
A Classification for Electronic Nose Based on Broad Learning System <i>Yu Wang, Xiaoyan Peng, Hao Cui and Pengfei Jia</i>	474
3D Single Person Pose Estimation Method Based on Deep Learning <i>Xinrui Yuan, Hairong Wang and Jun Wang</i>	481
A Review of Inference Methods Based on Knowledge Graph <i> Dexiang Zhang, Hairong Wang and Yudan Ding</i>	492
Recommendation Based on Java Code Analysis and Search <i>Shanqing Fu, Bing Li, Yi Cai, Zhuang Liu and Junxia Guo</i>	514
Research Progress and Advantage Analysis of Big Data Application in Chinese Academic Journals <i>Qin Wu and Hui Wu</i>	522
The Mechanism Analysis of the Accelerator for Support Vector Regression Based on Data Partition <i>Yunsheng Song, Fangyi Li, Jianyu Liu and Juao Zhang</i>	528
Focused Crawler Strategy Based on Improved Energy Landscape Paving Algorithm <i>Jingfa Liu, Wei Zhang, Zhihe Yang and Ziang Liu</i>	536
Mapping Property of Bilateration and Its Application to Human-Following Robot <i>Heungju Ahn, Van Chien Dang, Hyeon Cheol Seo and Sang C. Lee</i>	546
Construction of Cloud ERP Security Evaluation Index System Based on Text Mining <i>Ying Gao, Qin Su, Yue Fang and Pinyan Lai</i>	553
Personalized Mobile Information Recommendation Based on Fine-Grained User Behaviors <i>Yilei Wang and Xueqin Chen</i>	562
Research on the Construction of Cloud ERP Ecosystem Security Evaluation Index System <i>Zhujun Wang, Qin Su and Yue Fang</i>	580
Interval Observer Design for Metzlerian Takagi-Sugeno Systems <i>Dušan Krokavec and Anna Filasová</i>	589
A Cognitive Robotic System for a Human-Following Robot <i>Chien Van Dang, Heungju Ahn, Hyeon C. Seo and Sang C. Lee</i>	601
ASCII Art Classification Model by Transfer Learning and Data Augmentation <i>Akira Fujisawa, Kazuyuki Matsumoto, Kazuki Ohta, Minoru Yoshida and Kenji Kita</i>	608

The Efficiency of Employment Relationship: Through Data Envelopment Analysis <i>Kunyi Wang, Ping Liu and Yujiang Liu</i>	619
An Intelligent Marshalling Model for Enterprise Station Freight Railway <i>Junxia Guo, Gang Lu, Zili Xie, Jiawei Wen and Nanshan Xu</i>	627
Fault Diagnosis of Coal Mining Machinery Based on State Parameters <i>Dong Song</i>	636
Hierarchies and Uncertainty Measures on Pythagorean Fuzzy Approximation Spaces <i>Xiaojing Luo, Jingjing Song, Huili Dou, Xibei Yang and Taihua Xu</i>	643
Data-Driven Modeling of Mechanical Properties of Cast Iron Using Fuzzy Logic <i>He Tan, Vladimir Tarasov, Vasileios Fourlakidis and Attila Dioszegi</i>	656
Reward-Free Reinforcement Learning Algorithm Using Prediction Network <i>Zhen Yu, Yimin Feng and Lijun Liu</i>	663
Differential Privacy Trajectory Data Protection Algorithm Based on Polar Coordinate Transformation <i>Zhenzhen Zhang, Jianping Cai, Lan Sun, Yongyi Guo, Yubing Qiu and Yingjie Wu</i>	671
Visualization of the Artist Relations Using Twitter User Profiles <i>Minoru Yoshida, Shogo Kohno, Kazuyuki Matsumoto and Kenji Kita</i>	682
A New Approach for the Detection of Concrete Cracks Based on Adaptive Morphological Filtering <i>Huan Hou and Weiguo Lin</i>	690
Hardware Detection Method of Transmission Line Patrol Inspection Image Based on Improved YOLOV4 Model <i>Ning Wang, Hanghang Zhao, Wulue Zheng and Chaoshuo Wang</i>	700
The Relation of Career Adaptability to Values Realization Degree and Organizational Citizenship Behavior <i>Qingsong Zhu, Ruiting Tan and Ping Wang</i>	707
Research on the Internal Relationship Characteristics and Their Influences of Knowledge Sharing Multilevel Network in Q&A Community <i>Xiaohui Chen and Ping Hu</i>	716
Characterizing Eating Disorder Issues on Sina Weibo <i>Jingyun Tang, Guang Yu, Zheng Wang and Xiaoxu Yao</i>	722
Optimization of Transit Scheduling Combined with Short-Turn Service Based on Real-Time Passenger Flow <i>Ailing Huang, Yijing Miao and Jiarui Li</i>	732
Monitoring the Development Quality of College Students Based on Knowledge Graph <i>Aiyan Wu and Yongmei Zhang</i>	753

Hierarchy Spatial-Temporal Transformer for Action Recognition in Short Videos <i>Guoyong Cai and Yumeng Cai</i>	760
A Brief Review of Relation Extraction Based on Pre-Trained Language Models <i>Tiange Xu and Fu Zhang</i>	775
Subject Index	791
Author Index	795

Using the Generative Adversarial Network to Generate Recommendations

Prosvetov A.V.^{a,b,c,1}

^a*CleverDATA, Russia*

^b*Space Research Institute, Russian Academy of Science, Russia*

^c*LANIT, Russia*

Abstract. Widely used recommendation systems do not meet all industry requirements, so the search for more advanced methods for creating recommendations continues. The proposed new methods based on Generative Adversarial Networks (GAN) have a theoretical comparison with other recommendation algorithms; however, real-world comparisons are needed to introduce new methods in the industry. In our work, we compare recommendations from the Generative Adversarial Network with recommendation from the Deep Semantic Similarity Model (DSSM) on real-world case of airflight tickets. We found a way to train the GAN so that users receive appropriate recommendations, and during A/B testing, we noted that the GAN-based recommendation system can successfully compete with other neural networks in generating recommendations. One of the advantages of the proposed approach is that the GAN training process avoids a negative sampling, which causes a number of distortions in the final ratings of recommendations. Due to the ability of the GAN to generate new objects from the distribution of the training set, we assume that the Conditional GAN is able to solve the cold start problem.

Keywords. GAN, Recommendations System. Neural network

1. Introduction

Recommendations can be generated using several approaches. While some of the most popular methods are based on matrix decomposition (user-based and item-based collaborative filtering, Alternating Least Squares, SVD and etc), the alternative methods are based on neural networks (restricted Boltzmann machine, deep autoencoders and etc.). Approaches based on neural networks available to use additional information about the composition of items and the user's purchase sequence in embeddings [1], however, widely used matrix decomposition approaches show significant results either. Despite the successes achieved, several unresolved issues still exist, for example, Cold Start problem.

A recommendation system based on matrix decomposition can give each user a rating for each item, but the estimates obtained are in the form of floating point number, while in cases with high uncertainty level the distribution of rating is required. After training the recommendation system, the production implementation requires regular retraining, model monitoring and tuning, so reinforcement learning is very suitable.

¹ Prosvetov A.V.; E-mail: prosvetov@gmail.com.

The discriminative algorithms try to learn $P(Y|X)$ directly or try to learn mappings from space of inputs X to the labels {0,1}. The generative algorithms try to learn $P(X|Y)$. If Y indicates whether an item is interesting to user, then $P(X|Y=1)$ represents the distribution of item features, that are relevant to user. The probability $P(X|Y=0)$ in this case represents the distribution of product features for user, that are non-relevant. In the current work we suggest to solve the cold start problem using Generative Adversarial Network (GAN), that generative approach was proposed by I. Goodfellow et al. [2] in 2014. The GAN architecture combined from two neural networks: the first attempts to create new sample from the same distribution as the training set, while the second neural network trains to classify the real and the generated samples. When the training process is completed, a generative model is obtained. The resulting generative model is capable of generating new samples indistinguishable from objects from the training set. The GAN approach was proposed for unsupervised learning initially, however the reinforced learning is close to GAN architecture [3]. That fact gives additional potential for the implementation of a GAN recommendation system in production.

GAN architecture is commonly used to generate images. Currently GAN can achieve photorealistic results for photo [4], but also GAN was successfully used for prediction of gravitational lensing in a certain direction in the distribution of dark matter [5]. GANs were also proposed for the generation of simulated showers of particles in calorimeters of experiments in high-energy physics. [6,7]. Thus, the potential of GAN generalizations can be used by recommendation systems to offer more relevant products and to augment the data, which is in great demand for solving the cold start problem.

Previous attempts to use the GAN in the recommendation system showed a high potential of the approach with respect to typical datasets [8], however, measured offline metrics cannot guarantee the high quality of recommendations in real cases. In our work, we test the GAN architecture in flight recommendations. Our preliminary results has already published in short form [9], the current paper is present the detailed description of experiment, data preparation and network architecture.

2. GAN details

Assume that GAN consist of generator and discrimination subnetworks. The subnetwork architecture can be multi-layer perceptrons. Assume a prior on input noise variables $p_z(z)$ to learn the generator's distribution p_g over data x . The generator takes place a mapping to data space as $G(z; \theta_g)$, where G is multilayer perceptron with parameters θ_g . Assume that the discriminator is a multilayer perceptron $D(x, \theta_d)$ that outputs a single scalar. We are able to create train set where $D(x)$ models the probability that object x came from the real data set rather than form the set of generated objects. The next step will be training D to maximize the probability of assigning the correct label to both training examples and samples from G . Simultaneously one can train G to minimize $\log(1 - D(G(z)))$. Thus, D and G play the minimax game with value function $V(G, D)$:

$$\min_G \max_D V(D, G) = E_{x \sim p_{data}(x)} [\log(D(x))] + E_{z \sim p_z(z)} [\log(1 - D(G(z)))] \quad (1)$$

During the train one can take k steps of optimizing D and one step of optimizing G

in the loop to avoid overfitting. In this case results in \mathbf{D} being maintained near its optimal solution, so long as \mathbf{G} changes slowly enough. In more general case the discriminator and the generator can have convolutional layers [10] and recurrent cells [11]. If the discriminator and the generator are used conditioned information \mathbf{y} , than the architecture will be upgraded to a conditional model [12]. To get a recommendation system, we used the information about the historical choice of the user. The conditioning was carried out by feeding an additional input layer with historical information to the discriminator and the generator. Two-player minimax game objective function would be the following:

$$\min_G \max_D V(D, G) = E_{x \sim p_{data}(x)} [\log(D(x \vee y))] + E_{z \sim p_z(x)} [\log(1 - D(G(z \vee y)))] \quad (2)$$

The architecture of conditional adversarial network that was tested in our study is illustrated on Figure 1.

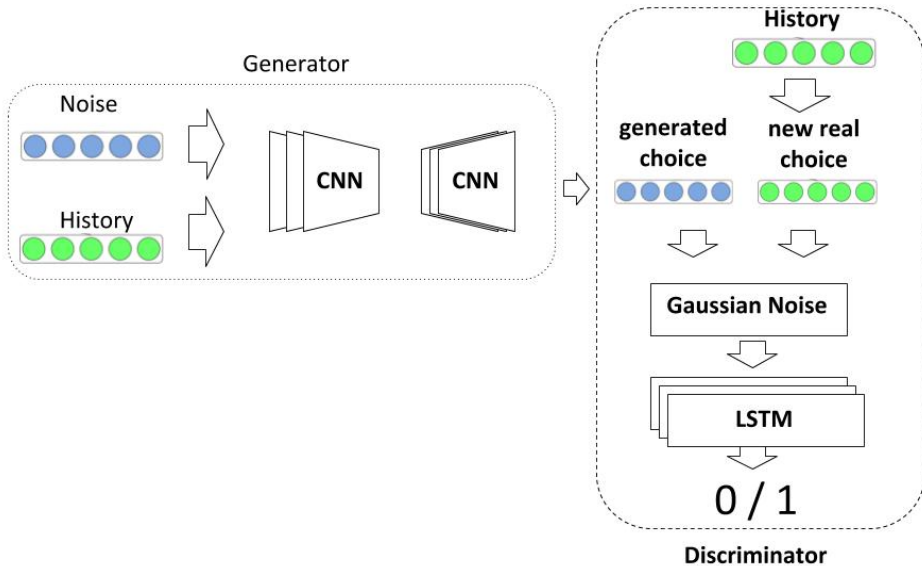


Figure 1. The architecture of recommendation system based on conditional GAN

3. Data preparation

In our experiment, we used a dataset with information about historical air flights provided by our partner. For each user, we used the sequence of airports visited in chronological order. We extracted the home airport from the sequence and coded the airports so that we could work with the sequence as with text. The last airport was extracted from the sequence, the generator was trained to predict the next flight airport, and the discriminator was trained to distinguish between the predicted airport and the real next airport for each user.

4. Recommendation system

Our recommendation system contains generator, discriminator and intermediate layer.

- 1) The aim of generator is to produce new user selection from previous selections and random noise. The generator network uses the following inputs:

- a) the historical choice of the user
- b) random noise.

The embeddings for previous selections input are trainable; however one can use a pre-trained embeddings. The output of generator is a dense layer with the activation function of sigmoidal form. The number of user selection options is equal to the size of the output layer.

- 2) The goal of discriminator is to make a determination whether the input tensor is a real or imitative object. The discriminator uses the following inputs:

- a) historical customer selections
- b) next selection.

The embeddings for historical selections are trainable; however one can use a pre-trained embeddings. The output of discriminator is a dense layer with one neuron with a sigmoidal activation function.

- 3) The intermediate layer is an additional level with Gaussian noise. Gaussian noise is required in order to help generator in producing realistic one-hot-encoded vector of user selection without the rounding operation. The rounding operation prevents the backpropagation, however without rounding the discriminator can easily distinct real objects from generated. The noise layer is intervened between the discriminator and generator. The shape of noise layer is equal to the number of user options to select. The Gaussian distribution density is the following:

$$p(x; \mu, \Sigma) = \frac{1}{(2\pi)^{n/2} |\Sigma|^{1/2}} \exp\left(\frac{-1}{2} (x - \mu)^T \Sigma^{-1} (x - \mu)\right) \quad (3)$$

where μ is a mean vector ($\mu \in R^n$), Σ is a covariance matrix ($\Sigma \in R^{n \times n}$). The noise level is ignored on stage of inference, it is required during the model training. As one can see from the mentioned above architecture description, for the training process the following data is required:

- the historical selections of the client;
- next selection of the client.

Thus, in the proposed architecture, we do not need to perform negative sampling to obtain positive and negative classes for binary classification. The generated objects will serve a purpose of negative objects for the discriminator training. A negative sampling causes a number of distortions in the final ratings of recommendations, since the model has tendency to use the frequency of item occurring in the training set as additional information. Due to the avoidance of negative sampling, the proposed approach is less prone to rating distortion.

5. Results

In order to compare the proposed approach with the current State-of-the-Art method, we trained the GAN model of the architecture described above on the flight dataset.

The data set contains flight information in 840 cities of 5.7 million anonymous customers.

A generator from a trained GAN was used to prepare recommendation ratings, and email offers with personalized recommendations were sent to customers in addition to newsletters.

The generator has encoder-decoder architecture: six sequent convolution layers of encoder using “relu” activation function with intermediate batch normalization, three convolution layers of decoder using “relu” activation function with intermediate batch normalization and upsampling layer.

The discriminator network was a recurrent type: we used three sequential LSTM layers and three fully connected dense layers, adding batch normalization and dropout after each layer.

In the role of competitor was Deep Semantic Similarity Model (DSSM) [13]:

- six convolution sequential layers with activation function “relu”, and max pooling layers in between,
- two fully connected dense layers with activation function “relu”, dropout and batch normalization,
- final fully connected dense layer with “sigmoid” activation function

The results of comparison between GAN and DSSM recommendation system is presented in table 1. A total of 162,978 clients were used to test the recommendations in the A / B test with the control group. In first group we used recommendations from DSSM, in the second group we used recommendations from GAN, in the baseline group we used the random direction. The conversion rate was the main metric for comparison, confidence interval was estimated using 95% significance level.

Table 1. The results of A/B testings of recommendations from DSSM and GAN.

	DSSM	GAN	Baseline (random)
Number of receivers	69688	59602	33688
Number of purchases	1627	1393	744
The rate of conversion	$2.33 \pm 0.11\%$	$2.34 \pm 0.12\%$	2.21 %

The GAN rate of conversion is higher than the DSSM, but the difference is not statistically significant. Thus, GAN can successfully compete with DSSM recommendation system in domain of airflight tickets.

As can be seen from the table 1, the conversion rate of DSSM and GAN recommendations is higher than the baseline, thus from both networks users received relevant offers. The tuning of DSSM network was based on the domain information, while GAN training wasn't used additional domain information.

The proposed approach may encounter problems in cases where the client has a high number of choice options. We used simple architecture for GAN in the current case, however the improvement of recommendations based on GAN can be obtained using more complex loss functions, and more sophisticated network architecture, for example Transformer and additional domain information. The potential of StyleGAN for recommendation preparing require additional exploration and experiments.

6. Conclusion

The object of this paper is to consider possible application of GAN in the field of recommendation systems. The main novelty of the approach is to adapt the GAN to solve the practical problem of constructing recommendations, which is a step towards

the main field of application of the GAN, such as image generation. Additional Gaussian Noise layer allow us to avoid the rounding operation, which prevents the back propagation. The advantage of a GAN-based recommendation system is that training does not require negative sampling. In addition, the GAN allows the researcher to obtain a rating distribution for each product for each item, which is very useful for understanding the confidence interval for rating recommendations. The recommender system based on the GAN was successively trained and showed results that are statistically close to the results of recommendations based on the DSSM neural network. Further study of GAN application is required on the field of recommender systems using the StyleGAN architecture, additional loss functions, and additional domain information.

References

- [1] A Prosvetov, The comparison of autoencoder architectures in improving of prediction models, Journal of Physics: Conference Series, Volume 1117, conference 1 (2018)
- [2] Goodfellow, Ian; Pouget-Abadie, Jean; Mirza, Mehdi; Xu, Bing; Warde-Farley, David; Ozair, Sherjil; Courville, Aaron; Bengio, Yoshua; Generative Adversarial Networks; Proceedings of the International Conference on Neural Information Processing Systems (NIPS 2014). pp. 2672–2680
- [3] Ho, Jonathon; Ermon, Stefano; Generative Adversarial Imitation Learning; Advances in Neural Information Processing Systems; 2016; p. 4565–4573
- [4] Horev, Rani; Style-based GANs – Generating and Tuning Realistic Artificial Faces; 2019; Lymn.AI.
- [5] Mustafa, Mustafa; Bard, Deborah; Bhimji, Wahid; Lukic, Zarija; Al-Rfou, Rami; Kratochvil, Jan M.; CosmoGAN: creating high-fidelity weak lensing convergence maps using Generative Adversarial Networks; 2019; Computational Astrophysics and Cosmology Simulations, Data Analysis and Algorithms 6; 1
- [6] Erdmann, Martin; Glombitza, Jonas; Quast, Thorben; Precise Simulation of Electromagnetic Calorimeter Showers Using a Wasserstein Generative Adversarial Network; 2019; Computing and Software for Big Science 3; 4
- [7] Musella, Pasquale; Pandolfi, Francesco; Fast and Accurate Simulation of Particle Detectors Using Generative Adversarial Networks; Computing and Software for Big Science. 2018;2; 8.
- [8] Homanga Bharadhwaj, Homin Park, and Brian Y. Lim; RecGAN: Recurrent Generative Adversarial Networks for Recommendation Systems; In Twelfth ACM Conference on Recommender Systems; 2018
- [9] Prosvetov, A.V.; GAN for Recommendation System; J. Phys.: Conf. Ser. 1405 012005; 2019
- [10] Zhang, Wei; Shift-invariant pattern recognition neural network and its optical architecture; Proceedings of Annual Conference of the Japan Society of Applied Physics; 1988
- [11] S Hochreiter, J Schmidhuber; Long short-term memory; Neural computation 9.8; 1997; p. 1735-1780
- [12] Mehdi Mirza, Simon Osindero; Conditional Generative Adversarial Nets; arXiv:1411.1784; 2014
- [13] Po-Sen Huang, Xiaodong He, Jianfeng Gao, Li Deng, Alex Acero, Larry Heck; Learning Deep Structured Semantic Models for Web Search using Clickthrough Data; Proceedings of the 22nd ACM international conference on Conference on information & knowledge management; 2013

Study on Generalized Directional Differentiability Problems of Fuzzy Mappings

Yu-e Bao¹, Tingting Li, Linfen Zhang

College of Mathematics, Inner Mongolia University for Nationalities, China

Abstract. This paper discusses the gH-directional differentiability of fuzzy mappings, and proposes the concept of gH-directional differentiability of fuzzy mappings. Based on the concept of gH-directional differentiability of interval-valued mappings and its related properties, two properties of gH-directional differentiability fuzzy mappings are proposed. At the same time, the relation between gH-differentiability and gH-directional differentiability for a fuzzy mapping is discussed, and it is proved that both gH-derivative and gH-partial derivative are directional derivatives of fuzzy mappings in the direction of the coordinate axis.

Keywords. Fuzzy mappings, gH-differentiability, gH-derivative, gH-partial derivative, gH-directional differentiability

1. Introduction

The differentiability concept of fuzzy mappings is closely related to the difference operation (subtraction operation) for fuzzy numbers. Regarding the difference operation of fuzzy numbers, its definition is relatively complicated, and there are multiple definitions. Nonetheless, there are two kinds of difference operations for fuzzy numbers, which are used to discuss the differentiability of fuzzy mappings at present, one is the concept of H-difference introduced by Hukuhara [1]; the other is the concept of generalized H-difference supported by Stefanini[2], i.e., gH-difference concept. The differentiability concept based on H-difference is called differentiability or H-differentiability problem; the concept of differentiability established by using gH-difference is called generalized differentiability or gH-differentiability problem. The generalized differentiability discussed in this paper refers to the problem of gH-differentiability.

In order to overcome some deficiencies of the concept of H-differentiability, in 2013, Barnabás Bede and Luciano Stefanini [3] first discussed the differentiability of fuzzy mappings by using the gH-difference and gave the concept of gH-differentiability. Meanwhile, they put forward a new and feasible method for studying the differentiability of fuzzy mappings and its application. Since then, many scholars have studied the gH-differentiability and application of fuzzy mappings, and obtained a series of valuable results [3-11].

¹ Corresponding Author: Yu-e Bao, College of Mathematics, Inner Mongolia University for Nationalities. E-mail:byebed@163.com.

In the study of the differentiability (H-differentiability) of fuzzy mappings, the concepts of the directional derivative (H-directional derivative) and subgradient of fuzzy mappings are proposed by Guixiang Wang and Congxin Wu in reference[12] , and the concepts are applied in convex fuzzy programming. However, the generalized differentiability (gH-differentiability) problem of fuzzy mappings in the above research work only considers the differentiability problem in the direction of the coordinate axis, and does not consider the differentiability in any particular directions, i.e., the gH-directional differentiability problem. Therefore, it is necessary to discuss the gH-directional differentiability problem of fuzzy mappings, so that the gH-differentiability of fuzzy mappings and its application can be fully discussed and developed, and some conclusions that are convenient for practical application are obtained.

In reference [13] and [14], we discussed respectively the differentiability (H-differentiability) and application in fuzzy programming for fuzzy mappings and the gH-directional differentiability of interval-valued mappings and so on, in the meantime, some important conclusions are obtained. On this basis, in the first section of this article, the concepts of gH-differentiability, gH-derivative, gH-partial derivative of fuzzy mappings and the concept and related properties of gH-differentiability of interval-valued mappings are given in references [3, 10, 14]. In Section 2, the problem of gH-directional differentiability of fuzzy mappings is discussed. Using the concept of gH-directional differentiability and related properties of interval-valued mappings [14], the relevant properties of gH-directional differentiability fuzzy mappings are given; And gH-directional derivative are used to characterize gH-derivative [3], gH-partial derivative [10] and gH-gradient [10].

2. Preliminaries

We denote by R the family of all sets of real numbers, and \mathcal{F} be a set of all fuzzy numbers in R (or fuzzy numbers space). So, for any $u \in \mathcal{F}$, we have that its α - level set be bounded closed intervals and we denote its α - levels by $[u]^\alpha = [\underline{u}_\alpha, \bar{u}_\alpha]$ for all $\alpha \in [0,1]$.

For fuzzy numbers $u, v \in \mathcal{F}$ and $r \in R$, respectively, the addition and the scalar multiplication are defined as follows

$$[u+v]^\alpha = \left[(\underline{u}+v)_\alpha, (\bar{u}+v)_\alpha \right] = [\underline{u}_\alpha + \underline{v}_\alpha, \bar{u}_\alpha + \bar{v}_\alpha], \alpha \in [0,1].$$

$$[ru]^\alpha = \left[(ru)_\alpha, (r\bar{u})_\alpha \right] = [\min\{r\underline{u}_\alpha, r\bar{u}_\alpha\}, \max\{r\underline{u}_\alpha, r\bar{u}_\alpha\}], \alpha \in [0,1].$$

Definition 2.1[3]. For fuzzy numbers $u, v \in \mathcal{F}$, the generalized Hukuhara difference (gH - difference, for short) of u and v is the fuzzy number $w \in \mathcal{F}$, if it exists, such that $u = v + w$ or $v = u + (-1)w$. And we denote as $u \ominus_{gH} v = w$.

If $u \ominus_{gH} v$ exists, then for $\alpha \in [0,1]$, in terms of α - levels, we have

$$[u \ominus_{gH} v]^\alpha = [u]^\alpha \ominus_{gH} [v]^\alpha = [\min\{\underline{u}_\alpha - \underline{v}_\alpha, \bar{u}_\alpha - \bar{v}_\alpha\}, \max\{\underline{u}_\alpha - \underline{v}_\alpha, \bar{u}_\alpha - \bar{v}_\alpha\}].$$

Where, $[u]^\alpha \ominus_{gH} [v]^\alpha$ is the gH - difference of two interval operands [13].

Proposition 2.1[8]. For fuzzy numbers $u, v \in \mathcal{F}$, if the gH - difference $u \ominus_{gH} v$

exists, then for $r \in R$, the $ru \ominus_{gH} rv$ exists, and

$$r[u \ominus_{gH} v] = (ru) \ominus_{gH} (rv).$$

For fuzzy numbers $u, v \in \mathcal{F}$, the Hausdorff distance of u and v is defined by

$$D_H(u, v) = \sup_{\alpha \in [0,1]} d_H([u]^\alpha, [v]^\alpha) = \sup_{\alpha \in [0,1]} \max \{|\underline{u}_\alpha - \underline{v}_\alpha|, |\bar{u}_\alpha - \bar{v}_\alpha|\}.$$

Where, $d_H([u]^\alpha, [v]^\alpha) = \max \{|\underline{u}_\alpha - \underline{v}_\alpha|, |\bar{u}_\alpha - \bar{v}_\alpha|\}$ is the Hausdorff distance of two interval operands $[u]^\alpha$ and $[v]^\alpha$.

Let R^n denote the n-dimensional Euclidean space, and M be a nonempty subset of R^n . We say $F: M \rightarrow \mathcal{F}$ be a fuzzy mapping (or fuzzy-valued function). For $\alpha \in [0,1]$, we can easily obtain a family of interval-valued mappings $F_\alpha: M \rightarrow [R]$, and we denote as $F_\alpha(x) = [F(x)]^\alpha = [\underline{F}_\alpha(x), \bar{F}_\alpha(x)]$, $x \in M$.

Where, (1) $[R]$ indicates the interval number space formed by all bounded closed intervals in R (see the reference[13]).

(2) $\underline{F}_\alpha(x)$ and $\bar{F}_\alpha(x)$ are two real-valued functions defined on M , called endpoint functions.

Definition 2.2[3]. Let $F: (a,b) \rightarrow \mathcal{F}$ be a fuzzy mapping, $x_0 \in (a,b)$ and $x_0 + h \in (a,b)$. Then the gH -derivative of F at x_0 is defined as

$$\lim_{h \rightarrow 0} \frac{F(x_0 + h) \ominus_{gH} F(x_0)}{h} = u.$$

If exists $u \in \mathcal{F}$, we say that F is gH -differentiable, and u is called the gH -derivative of F at x_0 , which is denoted as $F^{gH}(x_0) = u$.

Definition 2.3[10]. Let $F: M \rightarrow \mathcal{F}$ be a fuzzy mapping, and $x^0 = (x_1^0, x_2^0, \dots, x_n^0) \in M$. If fuzzy mapping $H_i(x_i) = F(x_1^0, \dots, x_{i-1}^0, x_i^0, x_{i+1}^0, \dots, x_n^0)$ is gH -differentiable at x_i , then we say that the gH -partial derivative of F at x^0 with respect to x_i , and $H_i^{gH}(x^0)$ is called the gH -partial derivative of F at x^0 , which is denoted as $\partial F / \partial x_i \Big|_{x=x_0} = H_i^{gH}(x^0)$.

We consider that F is gH -differentiable at x^0 if all the partial derivatives exist on some neighborhood of x^0 .

Definition 2.4[10]. Let $F: M \rightarrow \mathcal{F}$ be a fuzzy mapping. If F is gH -differentiable at x_0 , then the gH -gradient of F at x_0 , denoted by $(\partial F / \partial x_1 \Big|_{x=x_0}, \dots, \partial F / \partial x_n \Big|_{x=x_0})$ is a fuzzy vector, defined by

$$\nabla F(x_0) = \left(\left(\partial F / \partial x_1 \Big|_{x=x_0}, \dots, \partial F / \partial x_n \Big|_{x=x_0} \right) \right).$$

Definition 2.5[14]. Let $f: M \rightarrow ([R], d_H)$ be a interval-valued function, and $x \in M$. If for $y \in R^n$, there exists $\delta > 0$ such that $x + hy \in M$ ($x - hy \in M$) for any

$h \in (0, \delta)$, and there exists $A_+ \in [R]$ ($A_- \in [R]$) such that

$$\lim_{h \rightarrow 0^+} \frac{1}{h} (f(x + hy_e) \ominus_{gH} f(x)) = A_+ \left(\lim_{h \rightarrow 0^+} \frac{1}{h} (f(x) \ominus_{gH} f(x - hy_e)) = A_- \right).$$

Then $f(x)$ is (resp. left) gH -differentiable in the direction y at x , and A_+ (A_-) is called the (resp. left) gH -derivative of $f(x)$ in the direction y at x , which is denoted as $f_+^{gH}(x, y) = A_+$ ($f_-^{gH}(x, y) = A_-$).

If $f_+^{gH}(x, y) = f_-^{gH}(x, y)$, we say that $f(x)$ is gH -differentiable in the direction y at x , and denoted as $f^{gH}(x, y) = f_+^{gH}(x, y) = f_-^{gH}(x, y)$, where $f^{gH}(x, y)$ is called the gH -derivative of $f(x)$ in the direction y at x .

Theorem 2.1[13]. Let $F: M \rightarrow [R]$ be an interval-valued mapping, and denoted as $F(x) = [\underline{F}(x), \bar{F}(x)]$. If $\underline{F}(x)$ and $\bar{F}(x)$ are gH -differentiable in the direction y at x_0 , then $F(x)$ is gH -differentiable in the direction y at x_0 , and

$$F^{gH}(x_0, y) = [\min\{\underline{F}(x_0, y), \bar{F}(x_0, y)\}, \max\{\underline{F}(x_0, y), \bar{F}(x_0, y)\}].$$

3. gH-Directional differentiability of fuzzy mapping

Definition 3.1. Let $F: M \rightarrow \mathcal{F}$ be a fuzzy mapping, and $x \in M$. If for $y \in R^n$, there exists $\delta > 0$ such that $x + hy_e \in M$ ($x - hy_e \in M$) for $h \in (0, \delta)$. And gH -difference

$$F(x + hy_e) \ominus_{gH} F(x) (F(x) \ominus_{gH} F(x - hy_e))$$

exists, and there exists $u^+ \in \mathcal{F}$ ($u^- \in \mathcal{F}$) such that

$$\lim_{h \rightarrow 0^+} \frac{F(x + hy_e) \ominus_{gH} F(x)}{h} = u^+ \left(\lim_{h \rightarrow 0^+} \frac{F(x) \ominus_{gH} F(x - hy_e)}{h} = u^- \right).$$

Then the right (resp. left) gH -derivative of F in the direction y at x exists, which is denoted as $u^+(u^-)$, and $F_+^{gH}(x, y) = u^+$ ($F_-^{gH}(x, y) = u^-$).

If $F_+^{gH}(x, y) = F_-^{gH}(x, y)$, we say that F is gH -derivable in the direction y at x , and denoted as

$$F^{gH}(x, y) = F_+^{gH}(x, y) = F_-^{gH}(x, y),$$

Where $F^{gH}(x, y)$ is called the gH -derivative of F in the direction y at x .

Theorem 3.1. Let $F: M \rightarrow \mathcal{F}$ be a fuzzy mapping. If F is gH -derivable in the direction $y \in R^n$ at $x \in M$, then for any $\alpha \in [0, 1]$, $F_\alpha: M \rightarrow [R]$ is an interval-valued mapping, which is gH -derivable in the direction y at x , and

$$F_\alpha^{gH}(x, y) = [F^{gH}(x, y)]^\alpha.$$

Proof. Let $F: M \rightarrow \mathcal{F}$ be a fuzzy mapping, which is gH -derivable in the direction

y at $x \in M$, then there exists $\delta > 0$ such that

$$x + hy_e \in M(x - hy_e \in M) \text{ for any } h \in (0, \delta),$$

and gH -difference

$$F(x + hy_e) \ominus_{gH} F(x) \text{ and } (F(x) \ominus_{gH} F(x - hy_e))$$

exist, and there exists $F^{gH}(x, y) \in \mathcal{F}$ such that

$$\lim_{h \rightarrow 0^+} \frac{F(x + hy_e) \ominus_{gH} F(x)}{h} = \lim_{h \rightarrow 0^+} \frac{F(x) \ominus_{gH} F(x - hy_e)}{h} = F^{gH}(x, y).$$

That is, there exists $\delta' > 0$ such that

$$D_H\left(\frac{F(x + hy_e) \ominus_{gH} F(x)}{h}, F^{gH}(x, y)\right) = D_H\left(\frac{F(x) \ominus_{gH} F(x - hy_e)}{h}, F^{gH}(x, y)\right) < \varepsilon$$

for any $0 < h < \delta'$. From the Definition of D_H and Proposition 2.1, we have

$$d_H\left(\frac{1}{h}\left[F(x + hy_e)\right]^\alpha \ominus_{gH} \left[F(x)\right]^\alpha, \left[F^{gH}(x, y)\right]^\alpha\right) = d_H\left(\frac{1}{h}\left[F(x)\right]^\alpha \ominus_{gH} \left[F(x - hy_e)\right]^\alpha, \left[F^{gH}(x, y)\right]^\alpha\right) < \varepsilon$$

for any $\alpha \in [0, 1]$. So,

$$\lim_{h \rightarrow 0^+} \frac{\left[F(x + hy_e)\right]^\alpha \ominus_{gH} \left[F(x)\right]^\alpha}{h} = \lim_{h \rightarrow 0^+} \frac{\left[F(x)\right]^\alpha \ominus_{gH} \left[F(x - hy_e)\right]^\alpha}{h} = \left[F^{gH}(x, y)\right]^\alpha.$$

Hence, from the Definition 2.5, $F_\alpha(x) = [F(x)]^\alpha$ is a interval-valued mapping, which is gH -differentiable in the direction y at x , and

$$F_\alpha^{gH}(x, y) = \left[F^{gH}(x, y)\right]^\alpha \text{ for any } \alpha \in [0, 1].$$

Theorem 3.2. Let $F : M \rightarrow \mathcal{F}$ be a fuzzy mapping, which is gH -differentiable in the direction y at x . If $F_\alpha(x) = [\underline{F}_\alpha(x), \bar{F}_\alpha(x)]$ for any $\alpha \in [0, 1]$ is an interval-valued mapping, whose two endpoint functions $\underline{F}_\alpha(x)$ and $\bar{F}_\alpha(x)$ are differentiable in the direction y at x , then

$$\left[F^{gH}(x, y)\right]^\alpha = \left[\min\{\underline{F}_\alpha(x, y), \bar{F}_\alpha(x, y)\}, \max\{\underline{F}_\alpha(x, y), \bar{F}_\alpha(x, y)\}\right].$$

Where $\underline{F}_\alpha(x, y)$ and $\bar{F}_\alpha(x, y)$ is the directional derivative of real-valued functions $\underline{F}_\alpha(x)$ and $\bar{F}_\alpha(x)$ in the direction y at x respectively.

Proof. Let $F : M \rightarrow \mathcal{F}$ is gH -differentiable in the direction y at x , then from Theorem 3.1, $F_\alpha(x) = [\underline{F}_\alpha(x), \bar{F}_\alpha(x)]$ is an interval-valued mapping, which is gH -differentiable in the direction y at x , and

$$\left[F^{gH}(x, y)\right]^\alpha = F_\alpha^{gH}(x, y). \quad (1)$$

Moreover, for $\alpha \in [0, 1]$, $\underline{F}_\alpha(x)$ and $\bar{F}_\alpha(x)$ are gH -differentiable in the direction y at x , then by Theorem 2.1, we have

$$F_\alpha^{gH}(x, y) = \left[\min\{\underline{F}_\alpha(x, y), \bar{F}_\alpha(x, y)\}, \max\{\underline{F}_\alpha(x, y), \bar{F}_\alpha(x, y)\}\right]. \quad (2)$$

Therefore, for $\alpha \in [0,1]$, from (1) and (2), we easily obtain

$$[F^{gH}(x,y)]^\alpha = [\min\{F_\alpha(x,y), \bar{F}_\alpha(x,y)\}, \max\{F_\alpha(x,y), \bar{F}_\alpha(x,y)\}]$$

Theorem 3.3. Let $F : (a,b) \rightarrow \mathcal{F}$ be a fuzzy mapping, then F is gH -differentiable in the direction $y=1$ at x if and only if F is gH -differentiable at x , and

$$F^{gH}(x) = F^{gH}(x,1).$$

Proof. Necessity. If $F(x)$ is gH -differentiable in the direction $y=1$ at x , then there exists $\delta > 0$ such that $x-h, x+h \in (a,b)$ and for any $h \in (0, \delta)$, gH -difference

$$F(x+h) \ominus_{gH} F(x) \text{ and } F(x) \ominus_{gH} F(x-h)$$

exist and there exists $F^{gH}(x,1) \in \mathcal{F}$ such that

$$\lim_{h \rightarrow 0^+} \frac{F(x+h) \ominus_{gH} F(x)}{h} = \lim_{h \rightarrow 0^+} \frac{F(x) \ominus_{gH} F(x-h)}{h} = F^{gH}(x,1).$$

Moreover, we easily imply that

$$\begin{aligned} -[F(x-h) \ominus_{gH} F(x)]^\alpha &= -([F(x-h)]^\alpha \ominus_{gH} [F(x)]^\alpha) \\ &= [F_{gH}(x)]^\alpha \ominus_{gH} [F(x-h)]^\alpha \end{aligned}$$

for $\alpha \in [0,1]$. So,

$$\begin{aligned} &\lim_{h \rightarrow 0^-} D_H \left(\frac{F(x+h) \ominus_{gH} F(x)}{h}, F^{gH}(x,1) \right) \\ &= \lim_{h \rightarrow 0^+} D_H \left(\frac{F(x-h) \ominus_{gH} F(x)}{-h}, F^{gH}(x,1) \right) \\ &= \lim_{h \rightarrow 0^+} \sup_{\alpha \in [0,1]} d_H \left(\left[\frac{F(x-h) \ominus_{gH} F(x)}{-h} \right]^\alpha, [F^{gH}(x,1)]^\alpha \right) \\ &= \lim_{h \rightarrow 0^+} \sup_{\alpha \in [0,1]} d_H \left(\left[\frac{F(x) \ominus_{gH} F(x-h)}{h} \right]^\alpha, [F^{gH}(x,1)]^\alpha \right) \\ &= \lim_{h \rightarrow 0^+} D_H \left(\frac{F(x) \ominus_{gH} F(x-h)}{h}, F^{gH}(x,1) \right) = 0. \end{aligned}$$

Therefore,

$$\lim_{h \rightarrow 0^-} \frac{F(x+h) \ominus_{gH} F(x)}{h} = \lim_{h \rightarrow 0^+} \frac{F(x+h) \ominus_{gH} F(x)}{h} = F^{gH}(x,1).$$

Hence F is gH -derivable at x , and

$$F^{gH}(x) = F^{gH}(x,1).$$

Sufficiency. If F is gH -differentiable at x , i.e.,

$$\lim_{h \rightarrow 0} \frac{F(x+h) \ominus_{gH} F(x)}{h} = F^{gH}(x) \in \mathcal{F},$$

Then there exists $\delta > 0$ such that $x+h \in (a, b)$ and for any $0 < |h| < \delta$, gH -difference $F(x+h) \ominus_{gH} F(x)$ exists and

$$\lim_{h \rightarrow 0^+} \frac{F(x+h) \ominus_{gH} F(x)}{h} = F^{gH}(x) = F_+^{gH}(x, 1).$$

Moreover, $x-h \in (a, b)$ and gH -difference $F(x+h) \ominus_{gH} F(x)$ exists for any $0 < h < \delta$. So, from Proposition 2.1 and the operation properties of fuzzy number, we can deduce $F(x) \ominus_{gH} F(x-h) = -(F(x+h) \ominus_{gH} F(x))$ and

$$\begin{aligned} \lim_{h \rightarrow 0^+} D_H \left(\frac{F(x) \ominus_{gH} F(x-h)}{h}, F^{gH}(x) \right) &= \lim_{h \rightarrow 0^+} D_H \left(\frac{F(x-h) \ominus_{gH} F(x)}{-h}, F^{gH}(x) \right) \\ &= \lim_{h \rightarrow 0^-} D_H \left(\frac{F(x+h) \ominus_{gH} F(x)}{h}, F^{gH}(x) \right) = 0 \end{aligned}$$

Therefore,

$$\lim_{h \rightarrow 0^+} \frac{F(x) \ominus_{gH} F(x-h)}{h} = F^{gH}(x) = F_-^{gH}(x, 1).$$

Theorem 3.4. Let $F: M \rightarrow \mathcal{F}$ be a fuzzy mapping, and $x^0 = (x_1^0, x_2^0, \dots, x_n^0) \in M$. If $F(x)$ is gH -differentiable in the direction e_i ($i = 1, 2, \dots, n$) at x^0 , then the partial gH -derivative of $F(x)$ exist at x^0 with respect to x_i , and

$$\partial F^{gH} / \partial x_i \Big|_{x=x^0} = F^{gH}(x^0, e_i).$$

Proof. Let $H_i(x_i) = F(x_1^0, \dots, x_{i-1}^0, x_i^0, x_{i+1}^0, \dots, x_n^0)$, then

$$\begin{aligned} \frac{H_i(x_i^0 + h) \ominus_{gH} H_i(x_i^0)}{h} &= \frac{F(x^0 + he_i) \ominus_{gH} F(x^0)}{h}, \\ \frac{H_i(x_i^0) \ominus_{gH} H_i(x_i^0 - h)}{h} &= \frac{F(x^0) \ominus_{gH} F(x^0 - he_i)}{h}. \end{aligned}$$

If $F(x)$ is gH -differentiable in the direction e_i at x^0 , i.e.,

$$\lim_{h \rightarrow 0^+} \frac{F(x^0 + he_i) - F(x^0)}{h} = \lim_{h \rightarrow 0^+} \frac{F(x^0) - F(x^0 - he_i)}{h} = F^{gH}(x^0, e_i).$$

Therefore,

$$\lim_{h \rightarrow 0^+} \frac{H_i(x_i^0 + h) \ominus_{gH} H_i(x_i^0)}{h} = \lim_{h \rightarrow 0^-} \frac{H_i(x_i^0) \ominus_{gH} H_i(x_i^0 - h)}{h} = F_i^{gH}(x^0, e_i).$$

Hence $H_i^{gH}(x_i^0, 1) = F^{gH}(x^0, e_i)$.

From Definition 2.2, we have $H_i(x_i)$ is gH -differentiable at x_i^0 . So by Definition 2.3, the partial gH -derivative of $F(x)$ at x^0 respect to x_i , and denoted as

$$\partial F^{gH} / \partial x_i \Big|_{x=x^0} = F^{gH}(x^0, e_i).$$

Corollary 3.1. Let $F : M \rightarrow \mathcal{F}$ be a fuzzy mapping, and $x^0 = (x_1^0, x_2^0, \dots, x_n^0) \in M$. If all the partial gH -derivatives exist in the direction e_i at x^0 on some neighborhood of x^0 , then F is gH -differentiable at x^0 , and its the gradient

$$\nabla F^{gH}(x^0) = \{F^{gH}(x^0, e_1), \dots, F^{gH}(x^0, e_i), \dots, F^{gH}(x^0, e_n)\}.$$

Proof. If $F^{gH}(x^0, e_i)$ ($i = 1, 2, \dots, n$) exist on some neighborhood of x^0 , then from Theorem 3.4, we have all the partial derivatives $\partial F^{gH}/\partial x_i|_{x=x^0}$ ($i = 1, 2, \dots, n$) exist on some neighborhood of x^0 , and

$$\partial F^{gH}/\partial x_i|_{x=x^0} = F^{gH}(x^0, e_i) \quad (i = 1, 2, \dots, n).$$

Therefore, from Definition 2.3, F is gH -differentiable at x^0 , and the gradient is denoted as

$$\nabla F^{gH}(x^0) = \{F^{gH}(x^0, e_1), \dots, F^{gH}(x^0, e_i), \dots, F^{gH}(x^0, e_n)\}.$$

4. Conclusions

The differentiability of fuzzy mappings is an important concept in fuzzy analysis and plays a very important role in fuzzy optimization theory. In this paper, we discuss the gH -directional differentiability of fuzzy mappings. The concept of gH -directional derivative is proposed, and gH -derivative and gH -partial derivative are described by using gH -directional derivative. These conclusions lay a solid foundation for further discussion on the gH -differentiability, gH -subdifferentiability of fuzzy mappings and their application in fuzzy programming. We will give some examples of corresponding model implementation in the next research work.

Acknowledgments

Inner Mongolia Natural Science Foundation of China (2018MS01010).

References

- [1] M.Puri, D.Ralescu, Differentials of fuzzy functions, *J. Math. Anal. Appl.*, 1983 (91),552-558.
- [2] L.Stefanini, A generalization of Hukuhara difference and division for interval and fuzzy arithmetic, *Fuzzy Sets Syst.*, 2010 (161),1564-1584.
- [3] B.Bede, L.Stefanini, Generalized differentiability of fuzzy-valued functions, *Fuzzy Sets Syst.*, 2013 (230),119-141.
- [4] T.Allahviranloo, Z.Gouyandeh, A.Armand, A.Hasanoglu, On fuzzy solutions for heat equation based on generalized Hukuhara differentiability, *Fuzzy Sets Syst.*, 2015 (265),1-23.
- [5] B. Barnabás, G. Gal, Generalizations of the differentiability of fuzzy-number-valued functions with applications to fuzzy differential equations, *Fuzzy Sets Syst.*, 2015 (151), 581-599.
- [6] L.C. De Barros, F. Santo Pedro, Fuzzy differential equations with interactive derivative, *Fuzzy Sets Syst.*, 2017 (309),64-80.
- [7] G.Zengtai, H.Yang, Ill-posed fuzzy initial-boundary value problems based on generalized differentiability and regularization, *Fuzzy Sets Syst.*, 2016 (295),99-113.

- [8] Y.Chalco-Canoa, R.Rodríguez-Lópezb, M.D.Jiménez-Gameroc, Characterizations of generalized differentiable fuzzy functions, *Fuzzy Sets Syst.*, 2016 (259),37-56.
- [9] H.Shexiang, G.Zengtai, L.Hongxia, Generalized differentiability for n-dimensional fuzzy-number-valued functions and fuzzy optimization, *Inf. Sci.*, 2016 (374),151-163.
- [10] R.Osuna-Gómez, Y.Chalco-Canob, B.Hernández-Jiménezc, I.Aguirre-Cipe, Optimality conditions for fuzzy constrained programming problems, *Fuzzy Sets Syst.*, 2019 (362), 35-54.
- [11] Luciana T. Gomes,Laécio C. Barros,A note on the generalized difference and the generalized differentiability, *Fuzzy Sets Syst.*, 2015 (280),142-145.
- [12] B.Yu-e, B. Eer-dun, Optimality conditions for fuzzy programming problems with differentiable fuzzy objective mappings, *Journal of Information Science and Engineering*, 2019(35), 1311-1327.
- [13] B.Yu-e , Z.Bo , B. Eer-dun, Directional differentiability of interval-valued functions, *J.Math. Computer Sci.*, 2016 (16),507-515.
- [14] Y. R. Syau, Invex and generalized convex fuzzy mappings, *Fuzzy Sets Syst.*, 2000 (115), 455-461.

Structure Optimization of Magnetic Levitation Motor Rotor

Shuyan Yao¹, Bo Wu, Qiang Liu and Kang Xu

Institute of Precision Electromagnetic Equipment and Advanced Measurement Technology, Beijing Institute of Petrochemical Technology, Beijing 102617, China

Abstract. With the development of science and technology, magnetic suspension products are gradually favored by people for the characteristics of no friction and wear, no lubrication and long life. With the increasing consumption of fossil energy, magnetic levitation green energy-saving equipment is gradually studied by researchers. Taking magnetic suspension flywheel (MSMFW) as typical representative, magnetic suspension products in aerospace field have been greatly developed. As the core component of magnetic suspension flywheel, magnetic levitation motor has been widely studied. To obtain the better performance of magnetic levitation motor when it was used in magnetic suspended momentum flywheel, the motor rotor system structure was optimized in this paper. Firstly, the rotor system moment of inertia was calculated and analyzed, and the optimum ratio of polar moment of inertia to equatorial moment of inertia was obtained. Then the basic structure of motor rotor was designed on the basis of the rotor system dynamic analysis. Thirdly, based on the flywheel motor system model, the ANSYS Parametric Design Language (APDL) file was established, and it was applied to optimization software ISIGHT to complete the optimization. In the optimization process, the design variables boundary conditions were given, and the Sequence Quadratic Programming method was used for maintaining the optimization process and the optimization convergence results was obtained. The magnetic flux density as the optimization objective is increased from 0.393 T to 0.53 T through the optimization, which is 34.9% larger than before. It is of great significance for the magnetic levitation motor design, and the engineering application of magnetic levitation motor based on optimization results will be done in the future.

Keywords. Magnetic levitation motor, Optimization design, Moment of inertia, Sequence quadratic programming method

1. Introduction

Momentum flywheel as the main inertial actuators has been used for high accuracy spacecraft attitude control since decades [1-2]. The ball bearing used in momentum flywheel has been considered as one of the main factors which restrict the promotion of control accuracy for the disadvantages of abrasion, friction torque and vibration. Magnetic bearing with the desirable properties of no contact between stator and rotor, low jitter and no need for lubrication, has been widely applied in spacecraft gradually in recent years, and it is used in momentum flywheel, and MSMFW appeared finally.

¹ Corresponding Author, Shuyan Yao, No. 13# Beijing Institute of Petrochemical Technology, Beijing, China; E-mail: 2017520070@bipt.edu.cn

MSMFW with high speed, long life, low noise and high control accuracy gradually become dominant attitude control actuator for spacecraft [3-4].

To obtain the desirable performances of high control accuracy, low power consumption, small volume and high momentum output in the MSMFW, much work has been done by researchers. With the limited of costs and technical level, the early MSMFWs are usually suspended by active magnetic bearings combined with passive magnetic bearings. As early as the 1980s, a large amount of research work on MSMFW was carried out [5-7]. In 1986, France launched the first Earth observation satellite ‘SPOT1’ successfully equipped with a magnetic suspension flywheel as an attitude control device, which opened the prelude to the MSMFW application in space [5]. U. Bichler et al. [6] proposed a 3-DOF actively controlled of MSMFW for attitude control of spacecraft and studied the control method of 1-DOF to 5-DOF active control. K. Yabuuchi et al. [7] raised a 3-DOF actively controlled of MSMFW with a gimbal-capable hybrid bearing supported by a combination of compact permanent magnet and electromagnetic. The above three types of MSMFW with active magnetic bearings and passive magnetic bearings combined have the advantages of low energy consumption and simple structure, which have been widely used in the aerospace field in the early stage. However, these types of MSMFW have low suspension precision, small stability margin and low control precision, which cannot meet the requirements of high performance attitude control. The 5-DOF actively controlled of MSMFW can solve the shortcomings well. Yasushi Horiuchi et al. [8] suggested a MSMFW which uses eight pairs of electromagnets to control the radial translation and deflection, a pair of electromagnet to achieve the axial translation, and 5-DOF actively controlled is realized finally, but the flywheel system consumes too much power. Hideyuki Sawda et al. [9] developed a MSMFW for high-stability attitude control of satellites, the flywheel is suspended and controlled by cone-shaped electromagnets, which effectively reduces the volume of the flywheel system, but the power consumption is too high and there is coupling in the axial and radial control directions.

In order to overcome the shortcomings of high power consumption, a solution for suspension support using a permanent magnet bias hybrid magnetic bearing appeared. A permanent magnet biased axial hybrid magnetic bearing for MSMFW is designed in [10], the performance parameters of magnetic bearing characteristics are analyzed and calculated, which provides a basis for the design and analysis of the MSMFW system. A new type of permanent magnet biased axial hybrid magnetic bearing structure with auxiliary air gap is designed to separate the bias magnetic flux path from the control magnetic flux path, which reduces the magnetic reluctance of the control magnetic circuit and the power consumption of axial magnetic bearings [11]. The prototype test showed that the device has perfect performance and high operational reliability. The dynamic model of the permanent magnet biased radial hybrid magnetic bearing of MSMFW is established in [12], a closed-loop controller that can be linearly controlled is designed through the analysis and calculation. The paper of [13-14] had done a lot of research work to improve the performance of the flywheel system, but all the focus of these works is on the control schemes and magnetic circuits design of magnetic bearing. The rotor system is the key component of the MSMFW system, its structure, mass, dynamic performance and other factors have the direct impact on the performance of the entire MSMFW system, how to realize the optimal mechanical structure of the MSMFW motor rotor is a problem to be solved. Based on the existing MSMFW system model, this paper used the Sequence Quadratic Programming method to optimize the motor rotor, the optimization results demonstrate that the optimization is effective.

2. MSMFW structure

The spacecraft attitude is controlled by MSMFW, which is worked by changing the rotor system angular momentum to realize the momentum exchange. The MSMFW model studied in this paper is shown in figure 1. It mainly consists of a rotor, a pair of radial hybrid magnetic bearings, a pair of axial hybrid magnetic bearings, one integrated radial/axial displacement sensor, one motor, two touchdown bearings, a shaft, a base and so on. The rotor output momentum torque by changing angular momentum. The radial hybrid magnetic bearing is used for controlling the radial translation of rotor and tilting the rotor, and the axial hybrid magnetic bearings are designed for supporting the rotor and controlling the axial translation. The radial and axial magnetic bearings are permanent magnet biased hybrid magnetic bearings, and the biased permanent magnets are used to reduce the consumption of power when the MSMFW works. The rotor displacements and tilting angles are measured by integrated radial/axial displacement sensor. Two touchdown bearings are used to support the rotor when the magnetic bearings are turned off or in case of failure, and allow the rotor spin down from its full operating to zero. This reasonable mechanical structure ensures that the MSMFW can work stably.

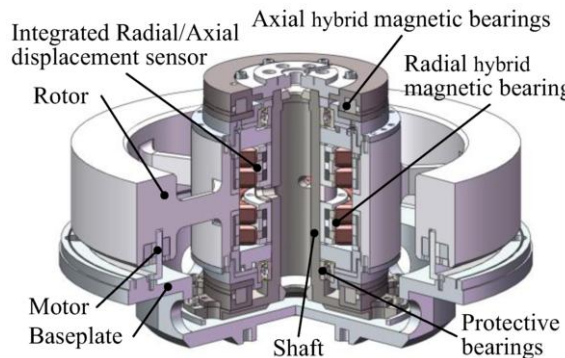


Figure 1. The construction of 15Nms MSMFW.

3. Rotor inertial moment analysis

With the increase of the rotational speed of the MSMFW rotor, precession and nutation modes will have frequency bifurcation under the influence of the strong Gyroscopic Coupling Effect, in which precession frequency is continuously reduced and finally tends to 0, while nutation frequency is constantly rising. This phenomenon brings great difficulty to build the MSMFW control system. Therefore, it is necessary to analysis the precession and nutation mode of the MSMFW rotor.

The gyro rotor is regarded as a rigid rotor, and the rotor centroid is defined as origin, Z-axis as the rotation axis, the inertial coordinate system is established. The 2-DOF gyro rotor dynamic equation can be written

$$\begin{cases} J_x \ddot{\alpha} + H\dot{\beta} = M_x \\ J_y \ddot{\beta} - H\dot{\alpha} = M_y \end{cases} \quad (1)$$

The MSMFW angular momentum and moment of inertia can be expressed

$$\begin{cases} H = J_p \Omega \\ J_x = J_y = J_e \end{cases} \quad (2)$$

Assuming the rotor is supported in a resilient manner, the stiffness of abutment is symmetrical and remains the same, it can be concluded that

$$\begin{cases} M_x = -k_a \alpha \\ M_y = -k_b \beta \\ k_a = k_b = k = C \end{cases} \quad (3)$$

Combing with equation (2), (3), equation (1) can be written

$$\begin{cases} \ddot{\alpha} + \frac{J_p}{J_e} \Omega \dot{\beta} + \frac{k}{J_e} \alpha = 0 \\ \ddot{\beta} - \frac{J_p}{J_e} \Omega \dot{\alpha} + \frac{k}{J_e} \beta = 0 \end{cases} \quad (4)$$

The complex can be used to represent the rotor motions around the X -axis and Y -axis, and the generalized deflection angle can be described as

$$\varphi = \alpha + \beta i \quad (5)$$

Equation (4) can be simplified

$$\ddot{\varphi} - i \frac{J_p}{J_e} \Omega \dot{\varphi} + \frac{k}{J_e} \varphi = 0 \quad (6)$$

It can be seen the motion around the X -axis and Y -axis is periodic vibration from equation (6). The characteristic equation of equation (6) can be obtained

$$\omega^2 - \frac{J_p}{J_e} \Omega \omega + \frac{k}{J_e} = 0 \quad (7)$$

Combing with equation (7), the solution of equation (6) is given

$$\begin{cases} \omega_1 = \frac{1}{2} \left[\frac{J_p}{J_e} \Omega + \sqrt{\left(\frac{J_p}{J_e} \Omega \right)^2 + 4 \left(\frac{k}{J_e} \right)^2} \right] \\ \omega_2 = \frac{1}{2} \left[\frac{J_p}{J_e} \Omega - \sqrt{\left(\frac{J_p}{J_e} \Omega \right)^2 + 4 \left(\frac{k}{J_e} \right)^2} \right] \end{cases} \quad (8)$$

Obviously, the two eddy angular velocities vary as the angular velocity changes of the rotor, and ω_1 and ω_2 are functions of Ω , and J_p/J_e and k/J_e are the parameters which affect the eddy angular velocities. The parameter of k/J_e is kept unchanged, and the influence of the parameter J_p/J_e on ω_1 and ω_2 is studied. Under the undamped condition, the variation of ω_1 , ω_2 with J_p/J_e is shown in figure 2.

It can be concluded that, when $J_p/J_e=1$, the rotor nutation frequency curve and the rotation curve will coincide, which causes the system resonance as the rotor speed increasing. When $J_p/J_e > 1$, the formula $\omega_1 > \Omega$ is always established, and the rotor system does not generate the resonance phenomenon at this time. The curve of precession frequency ω_2 will approach zero in the reverse direction as the rotor speed increasing, the precession frequency will not cause the system resonance in this condition. Considering the actual situation of MSMFW engineering and making the same mass flywheels output large torque as much as possible, the ratio of polar

moment of inertia to equatorial moment of inertia is limited from 1.4 to 2. It can be written as $1.4 \leq J_p/J_e \leq 2$, which is beneficial to the MSMFW engineering stability control.

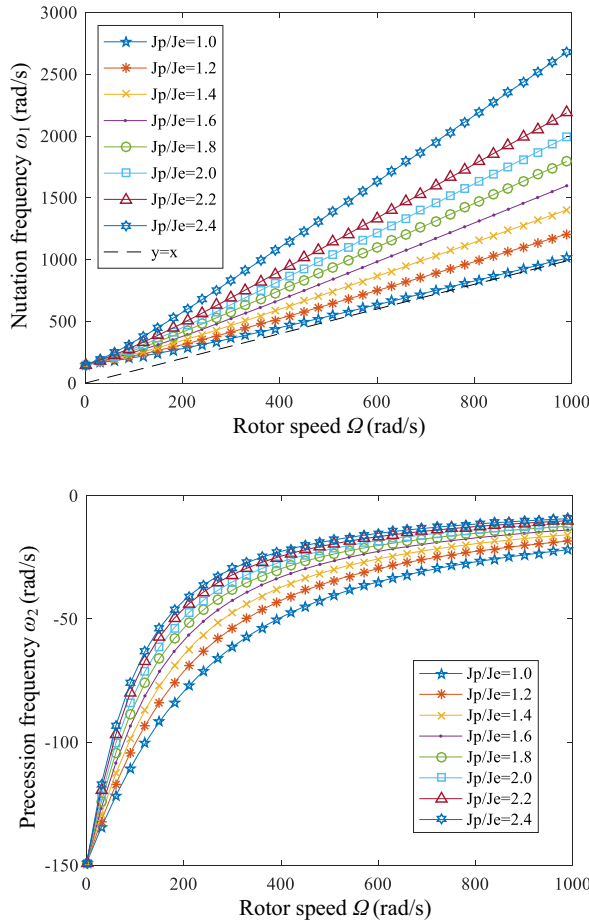


Figure 2. The eddy frequency curve with different ratio of J_p/J_e and Ω

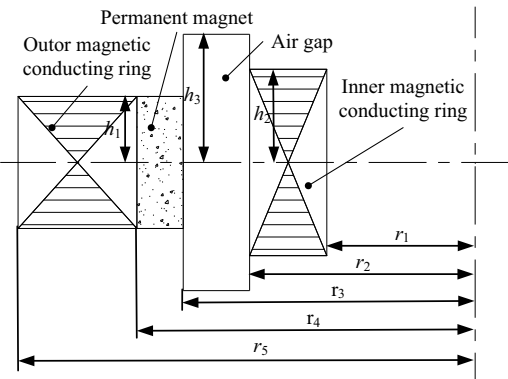


Figure 3. The schematic diagram of motor rotor structure

Based on the analysis above, the basic structure of magnetic levitation motor rotor was designed as shown in figure 3. The air gap size was kept unchanged, and the sizes of magnetic conducting rings and permanent magnet can be optimization.

4. Application of optimization method for MSMFW motor

4.1. Optimization model

Based on the above analysis of the MSMFW system, this paper used the software ANSYS to optimize the motor structural parameters of MSMFW which angular momentum is 15 Nms. The air gap of motor had been determined because of the practical engineering design requirements, only the magnetic conducting rings and permanent magnet of the MSMFW motor system can be optimized.

The design variables are expressed as

$$X = (r_1, r_4, r_5, h_1, h_2)$$

The objective function is established as

$$f_{max} = \max [F(X)] \quad (9)$$

Where

$$F(X) = F(r_1, r_4, r_5, h_1, h_2)$$

In practical engineering applications, it is necessary to ensure that the motor topology model does not change, and the design variables need to be limited to a certain range. According to the actual engineering experience, the design variables' constraints are designed as

$$\begin{cases} 85\text{mm} \leq r_1 \leq 90\text{mm} \\ 100\text{mm} \leq r_4 \leq 105\text{mm} \\ 102\text{mm} \leq r_5 \leq 110\text{mm} \\ 4.4\text{mm} \leq h_1 \leq 6.5\text{mm} \\ 6\text{mm} \leq h_2 \leq 8\text{mm} \end{cases}$$

Based on the above model and boundary conditions, an optimization block diagram was built, and the APDL command file was established. Then the MSMFW motor rotor was optimized.

4.2. Optimization method and results

The relationship among MSMFW motor rotor structural parameters is nonlinear, which increases the system complexity. So the rotor system multi-disciplinary parameter optimization design should be carried out. Firstly, MSMFW motor rotor model was established. Then static and model analyses were calculated, and the Sequential Quadratic Programming method was applied to maintain the optimization process. The MSMFW motor rotor system optimization flow chart is shown in Figure 3.

According to the optimization calculation, the design variables optimization curves were obtained as shown in Figure 4, and the objective function curve were also plotted

in Figure 5. In the first 6 steps, iterative directions of optimization parameters were calculated, and design variables value range were narrowed. Finally, the optimization calculation converges, and the optimal magnetic flux density was obtained through 96 steps iteration. The optimization results are shown in Table 1.

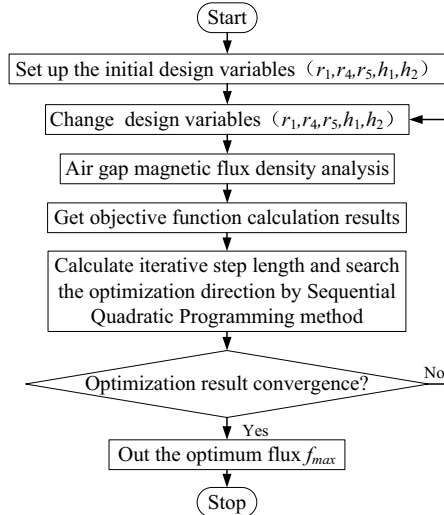


Figure 4. The optimization flow chart.

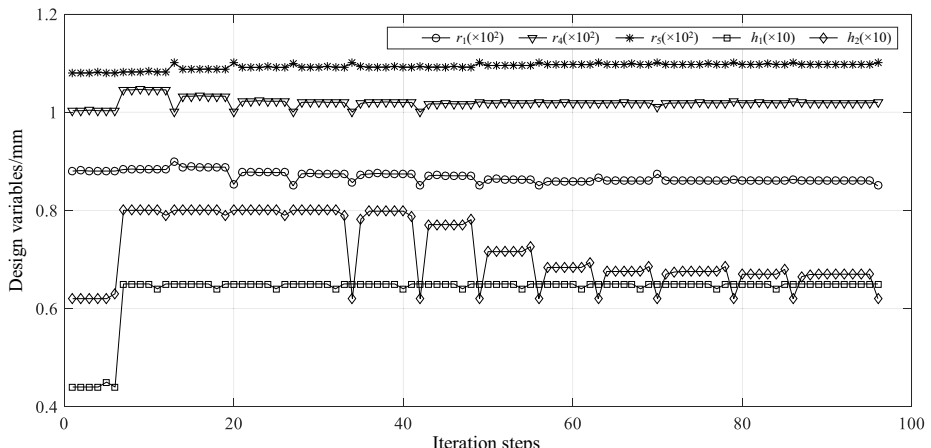


Figure 5. The optimization results of design variables.

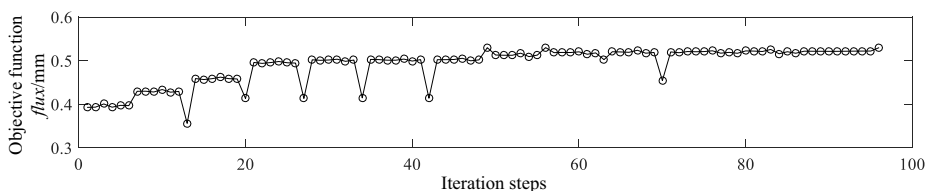


Figure 6. The optimization results of objective function.

Table 1. The results of optimization design

Variables	Before optimization	After optimization
r_1/mm	88	85
r_4/mm	100.3	102
r_5/mm	108	110
h_1/mm	4.4	6.5
h_2/mm	6.2	6.2
f_{\max}/T	0.393	0.53

As shown in Table 1, all the boundary conditions can be satisfied after optimization. The magnetic flux density of air gap as optimization objective was increased from 0.393 T to 0.53 T, which is 34.9% larger than before. The optimization results indicate that the optimization method is effective.

5. Conclusion

This paper concerns a magnetic levitation motor rotor system structure optimization. The rotor dynamics was analyzed, and the optimum ratio of polar moment of inertia to equatorial moment of inertia was obtained, and the basic structure of motor rotor was designed. The Sequence Quadratic Programming method was applied in optimization software to maintain the optimization process, and the maximum magnetic flux density was calculated, and the corresponding motor structure was determined. The prototype of magnetic levitation motor based on the optimization is manufacturing, and further work will be studied in the future.

Acknowledgement

This paper is supported by the Training Funded Project of the Beijing Youth Top-Notch Talents of China (Grant Number: 2017000026833ZK22) and Support Project of High-level Teachers in Beijing Municipal Universities in the Period of 13th Five-year Plan (Grant Number: CIT&TCD201804034).

References

- [1] LH Geng, DY Xiao, Q Wang, et al. Attitude control model identification of on-orbit satellites actuated by reaction wheels[J], *Acta Astronaut.* 66 (5–6), 2010: 714–721.
- [2] LH Yu, JC Fang, C Wu, Magnetically suspended control moment gyro gimbal servo-system using adaptive inverse control during disturbances[J], *Electron Lett.* 41 (17), 2005: 950–951.
- [3] M Kiani, H Salarieh, A Alasty, et al. Hybrid control of a three-pole active magnetic bearing[J], *Mechatronics.* 39, 2016: 28–41
- [4] JC Fang, CE Wang, T Wen, Design and optimization of a radial hybrid magnetic bearing with separate poles for magnetically levitation inertially stabilized platform[J], *IEEE Transactions on Magnetics.* 50(5), 2014: 1–11.
- [5] P Anstett, M Soulaiac, D Gauthier, et al. SPOT: the Very First Satellite to use Magnetic Bearing Wheels[N]. Proceedings of the 33rd Congress of the International Astronautical Federation. Paris, France: 1982

- [6] U Bichler, T Eckardt. A 3(5) degree of freedom electrodynamic bearing wheel for 3-Axis spacecraft attitude control applications[N], in: Proceedings of the 1st International Symposium on Magnetic Bearings, ETH Zurich, Switzerland, 1989.
- [7] K Yabu-Uchi, M Inoue, S Akishita, et al. A compact magnetic bearing for gimballed momentum wheel[N], in: 17th Aerospace Mechanisms Symposium, 1983, 333-342.
- [8] Y Horiuchi, M Inoue, Development of magnetic bearing momentum wheel for ultra-precision spacecraft attitude control[N], in: 7th International Symposium on Magnetic Bearings, 2000, 23-25.
- [9] H Sawada, T Hashimoto, K Ninomiya, High-stability attitude control of satellites by magnetic bearing wheels[J], Transactions of the Japan Society for Aeronautical & Space Sciences. 44 (145), 2001: 133-141.
- [10] JC Fang, JJ Sun, YL Xu, et al. A New Structure for Permanent-Magnet-Biased Axial Hybrid Magnetic Bearings[J]. IEEE Transactions on Magnetics, 2009, 45(12): 5319-5325.
- [11] JJ Sun, JC Fang. A novel structure of permanent-magnet-biased radial hybrid magnetic bearing[J]. Journal of Magnetism & Magnetic Materials, 2011, 323(2): 202-208.
- [12] B Xiang, JC Tang. Suspension and titling of vernier-gimballing magnetically levitation flywheel with conical magnetic bearing and Lorentz magnetic bearing[J]. Mechatronics, 2015, 28: 46-54.
- [13] JQ Tang, B Xiang, CE Wang. Rotor's Suspension for Vernier-gimballing magnetically levitation flywheel with conical magnetic bearing[J]. Isa Transactions, 2015.
- [14] B Gerlach, M Ehinger, HK Raue, et al. Digital Controller for a Gimballing Magnetic Bearing Reaction Wheel[J]. Aiaa Journal, 2005, 606.

Appendix I

C	constant
f_{max}	Maximum magnetic flux density (T)
h_1	half the height of permanent magnet (mm)
h_2	half the height of inner magnetic conducting ring (mm)
H	angular momentum (Nms)
i	imaginary unit
J_e	equatorial moment of inertia (kgm^2)
J_p	polar moment of inertia (kgm^2)
J_x, J_y, J_z	moment of inertia around X -axis, Y -axis and Z -axis (kgm^2)
k	generalized stiffness of gyro rotor to generalized coordinate system
k_α, k_β	support stiffness of magnetic bearing around the X -axis and Y -axis
M_x	torque acting on the rotor around the X -axis (Nm)
M_y	torque acting on the rotor around Y -axis (Nm)
r_1	inner radius of inner magnetic conducting ring (mm)
r_4	outer radius of permanent magnet (mm)
r_5	outer radius of outer magnetic conducting ring (mm)
α	rotor deflection angle around the X -axis (rad)
β	rotor deflection angle around the Y -axis (rad)
ω	eddy angular velocity (rad/s)
ω_1, ω_2	nutation and precession frequency (Hz)
Ω	rotor speed (r/min)
φ	rotor generalized deflection angle (rad)

Assessment of Socio-Economic Efficiency of the Scientific and Educational Complex: Approach and System of Indicators

Alexey SLAVIKOVSKY^{a,1}, Olga VLADIMIROVA^{a,b} and Manon KHUSAINOV^c

^a Siberian Federal University, 79, Svobodny pr., Krasnoyarsk, 660041, Russian Federation

^b Krasnoyarsk State Pedagogical University named after V.P. Astafiev, 82, Ady Lebedevoi str., Krasnoyarsk, 660049, Russian Federation

^c Russian Technological University MIREA, 78, Vernadsky pr., Moscow, 119454, Russian Federation

Abstract. The article is devoted to the current topic of choosing the optimal organizational option of multilateral integration of the scientific and educational sphere, business and the state in the process of globalization of the world economy. The authors justify the format of formation of scientific and educational complex on the basis of network interaction, which allows to obtain the greatest synergistic effect. In order to justify the effective network interaction of the scientific and educational complex, an analysis of existing methods of assessing the efficiency of its functioning was carried out and an author's system of performance indicators and its assessment was proposed in accordance with the general purpose of the integration mechanism and the specific purpose of each interaction subject. The model contains a system of heterogeneous indicators reflecting the principles of formation of a scientific and educational complex on the basis of network interaction, which allows, along with an evaluation task, to determine, using factor models, further directions of inter-network relations of subjects in order to better understand the current processes and identify problem areas of coordination of their innovative activity.

Keywords. Scientific and educational complex, integration, network, socio-economic efficiency, evaluation, innovation

1. Introduction

The post-industrial mode of social reproduction provides for the necessary conditions for socio-economic progress. These include the transfer of scientific results to stimulate innovation in the business environment, and the transformation of R&D results into products and services for sustainable economic growth.

Commercialization of scientific knowledge allows business to significantly reduce the innovation cycle, rationally distribute costs and risks, increase revenues and profitability. This is achieved not only through a linear, unidirectional process of transfer of scientific achievements, but also through active interaction with the

¹ Slavikovsky Alexey Olegovich, 660118, Russia, Krasnoyarsk, N.N. Urvantseva str. 16-82, tel.: 7 (904) 890-41-21, e-mail: slavikovskiy86@mail.ru.

scientific and educational sphere, where the State has a role both in financial support and in creating incentives and the necessary infrastructure for the development and coordination of partnerships among all stakeholders. At the same time, regulatory instruments adapt to changing conditions, such as the transition to the paradigm of “open innovation”, digitalization of activities, and the development of global networks. Today, there are a variety of forms to assist in the above-mentioned tasks. However, the types of coordination of linkages based on vertical subordination and traditional market with price signals have lost their effectiveness in the conditions of the economy of network relations [1]. Therefore, in both scientific and practical terms, the largest number of questions is caused by the formation and functioning of the scientific and educational complex (SEC) using the foundations of network interaction, which unites the spheres of science, education and business into a single whole, for the implementation of educational, research and innovation activities [2].

2. Materials and Methods

Research in the field of integration processes of scientific and educational sphere, business and the state, as well as introduction and commercialization of scientific knowledge is devoted to a rather large volume of foreign works. This issue is most reflected in the scientific works of American (Bailey, Baker, Betz, Carayannis, Frank, Kim, Leslie, Nowotny, Tamacy) [3, 4], English (Ash, Brunch, Pettinger) [5], Canadian (Austin, Chan, Tudiver) [3], Japanese (Kitamura, Moriya) [3], German (Betz, Monks) [6], Netherlands (Bleiklie, Craciunoiu, Henkel) [3], Greek (Grigoroudis) [7] and Romanian (Stăiculescu, Rîchițeanu-Năstase, Dobrea) [8] researchers.

Studies of domestic scientists Boeva [9], Yesina [10], Islakayeva [11], Kartashova [12], Katkova [13], Cleeva [14], Malina [15], Shadoba [13], Shirko [12] are devoted to the problems of choosing the optimal form of interaction between the subjects of the innovative economy at the regional level.

In the scientific works of Akhtenhagen and Ryugg-Sturm [16], Huggins [17] it is noted that in conditions of innovative economy the network method considers social and economic space as a set of interconnected systems. Network connections are a determining condition of interaction, between the same integration subjects, and between subjects with different affiliation to hierarchical systems.

High-tech innovations, which are the basis for the development of the innovative economy, are increasingly being created jointly [18]. Therefore, the mechanism of integration of the scientific and educational sphere and business should be aimed at creating cost-effective conditions for generation of knowledge for their further dissemination and use. However, at a time when highly developed countries are intensifying integration processes that provide synergistic effects, the inconsistency of the goals of the spheres of science and education, as well as the real sector of the economy, leads to a real threat of backwardness, both science and education, and technological development of companies of individual entities and Russia as a whole [10]. Networking is the best way to ensure quality collaboration among actors with different capacities and interests. The network method provides dynamic balance when the combination of entities in the form of SEC, on the one hand, has a sufficiently clear structure, and on the other hand, it has flexibility and openness, which allows for the joint generation of innovations.

3. Theoretical Aspects

The necessity and importance of the NOC is determined by its role in sustainable development and improving Russia's competitiveness in the context of building a model of economic growth based on innovation. The authors propose and justify the principles of formation of SEC on the basis of network interaction of subjects (Figure 1), which include:

1. Common goals – the target principle that determines the degree of coordination of interests of subjects, coordination of their activities, distribution and exchange of resources. Despite the fact that scientists generate new ideas, in most cases they do not have the managerial experience and management abilities necessary to bring R&D to commercial success [19], and according to Isaac Kirzner's business theory entrepreneurs are constantly in search and assessment of new opportunities for business. It is this process, called entrepreneurial discovery, that should be guided by the State, focusing not on sectors, but on activities that can form the basis of a smart specialization strategy [7].
2. Spatial localization – justified by research on national and regional innovation systems [20] and cluster studies [21].
3. Infrastructure – is intended to create conditions for deepening network interactions and developing interactions between actors.
4. Network communication – the SEC is presented as a set of interconnected network nodes between which communication is based. Entry into the complex, on the one hand, is carried out on the basis of the ability of the subject to effective network communication. On the other hand, it guarantees information support to all subjects of interaction. It is on the basis of network communication that information and knowledge are generated in SEC – the main resources for creating innovations.
5. Network inter-firm cooperation – contributes to the formation of a joint competitive advantage, i.e. the network can act as a source of special rent – income, which cannot be obtained within the framework of the operation of an individual entity (the effect of emergence).
6. Resource dependency – determines the legitimacy of borrowed resources and introduces an element of trust, turning external resources for each subject of interaction into internal resources.

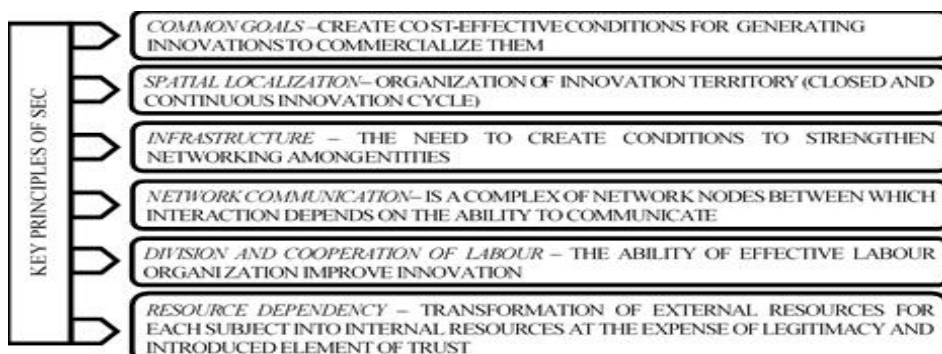


Figure 1. Key principles of SEC based on the network interaction of subjects.

Given that the institutional environment of SEC is a multiple set of interoperable entities based on a network, there is a need for a system of common and private performance indicators and evaluations.

4. Results

The development of a generalized system of indicators is based on the analysis of economic literature and existing methods of assessing the social and economic efficiency of network interaction between subjects [22, 23, 24]. Summarizing the results of the study of the available works of scientists, the following general and private shortcomings of the presented methods can be distinguished:

- do not reflect full diagnostics of problems of network interaction development based on the stages of innovation cycle;
- include only a certain set of effects, largely defined and dependent on the kind and characteristics of network interaction, thus lacking complexity and versatility;
- the implication of the nature of the assessment, without justifying the relationship between the characteristics of the network interaction and the performance of its functioning;
- considers only the educational component of the assessment of the development of the economic space of the region [22];
- considers peculiarities of analysis of efficiency of organizations of associated (network) entrepreneurship [24];
- considers the peculiarities of analysis of network interaction efficiency provided that the university acts as a meta-center [23].

Since none of the considered methods is universal, the authors propose, on the basis of generalization, a list of indicators of socio-economic efficiency of SEC formation and functioning, determined by the general goal of the integration mechanism and the specific goal of each interaction subject (Table 1).

Table 1. Indicators of socio-economic efficiency of the functioning of the SEC.

SEC performance indicators	SEC subject			
	S*	E*	B*	St*
I Economic				
International publication activities, units	K1	W1		
Inventive activity coefficient, units	K2	W2		
Technology exports per researcher, rubles/person	K3			EG1
Number of international patents, units	K4			EG2
Research and development organizations, units	K5			EG3
Research and development costs, rubles	K6			
Number of advanced production technologies created, units	K7			
The share of financial resources of business partners in the university, %		W3		
Increasing revenues from the implementation of educational projects, rubles		W4		
Amount of funds raised, rubles		W5		
Volume of innovative goods and services, rubles			P1	EG4
An export of high-tech products, rubles			P2	EG5
The costs of private business on R&D, rubles			P3	
Business costs for technological innovations, rubles			P4	

SEC performance indicators	SEC subject			
	S*	E*	B*	St*
An innovative activity of business on domestic innovations, units			P5	EG6
Capital participation of companies in the development of SIC infrastructure, %			P6	EG7
The share of innovative products in the total volume of products shipped, %			P7	EG8
The number of used advanced production technologies, units				EG9
Growth rate of average industry profitability, %			P8	EG10
Labor productivity growth, %			P9	EG11
The volume of attracted investments, rubles			P10	
Financing the leading research institutes, rubles				EG12
Growth of tax deductions to the budget, %				EG13
II Social				
An income level per employee, rubles	K8	W6		
Creating direct and indirect infrastructure facilities, units	K9	W7	P11	EG14
The volume of scientific emigration, people	K10			EG15
Number of personnel employed in R&D, people	K11			
Establishing faculties for training in universities, units		W8	P12	
Targets for direct contracts, people			P13	
Creating new jobs, units			P14	EG16
Growth rate of average wages, %			P15	EG17
An employment dynamic in enterprises, %				EG18
The amount of social payments from the integrated structure, rubles				EG19
The influx of young professionals in the scientific and educational sphere, %	K12	W9		EG20

*Legend: S – science, E – education, B – business, St – state.

The model of the scorecard, graphically shown in Figure 2, largely represents the level of integration process, depending on the commonality of goals, division and cooperation of labor, network communication and emerging resource dependency. Accordingly, based on the general and specific purpose of the subjects and the network structure in the form of SEC, it is possible to both add highly specialized indicators and eliminate excess ones.

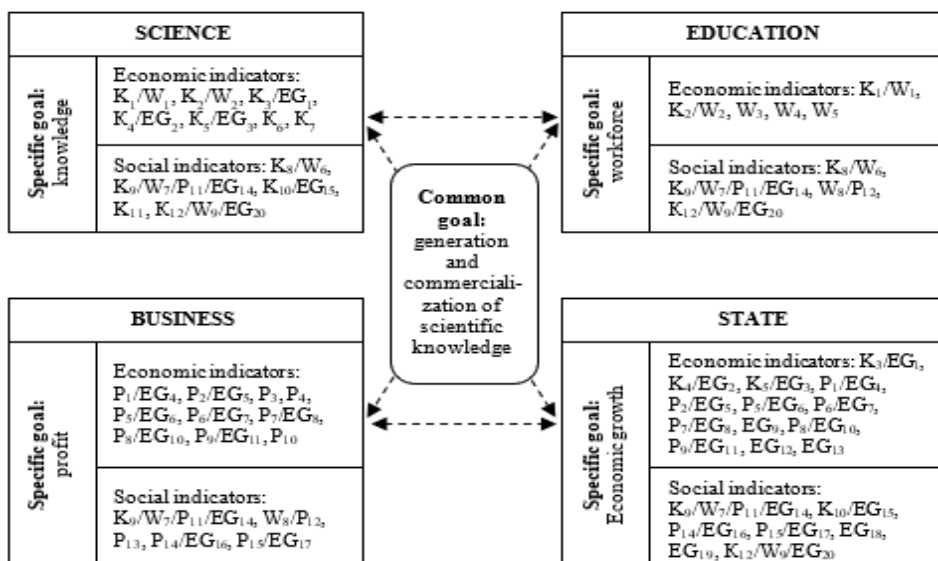


Figure 2. Model of the system of indicators of assessment of socio-economic effectiveness of SEC.

The following indicators of the proposed system of indicators were formed only on the basis of official data sources of the Federal Service of State Statistics of the Russian Federation, the Ministry of Science and Higher Education of the Russian Federation, as well as strategic planning documents, which set targets for interaction between the scientific and educational sphere, business and the State (Table 2).

Table 2. Indicators of socio-economic efficiency of SEC on the example of Krasnoyarsk Krai [25, 26].

SEC performance indicators	SEC subject			
	S	E	B	St
I Economic				
International publication activities, units	734			
Inventive activity coefficient, units	0,99			
Technology exports per researcher, thousands of rubles/person	74			74
Number of international patents, units	15			15
Research and development organizations, units	69			69
Research and development costs, billions of rubles	16,1			
Number of advanced production technologies created, units	31			
The share of financial resources of business partners in the university, %	6,5			
Increasing revenues from the implementation of educational projects, millions of rubles	36			
Amount of funds raised, millions of rubles	27			
Volume of innovative goods and services, billions of rubles		63,1		
An export of high-tech products, millions of rubles		129,49		
The costs of private business on R&D, millions of rubles		760,0		
Business costs for technological innovations, millions of rubles		360,9		
An innovative activity of business on domestic innovations, units		1 110		
Capital participation of companies in the development of SIC infrastructure, %		4,2		
The share of innovative products in the total volume of products shipped, %		3,3		
The number of used advanced production technologies, units			3 787	
Growth rate of average industry profitability, %			90,5	
Labor productivity growth, %			99,8	
The volume of attracted investments, billions of rubles		424,7		
Financing the leading research institutes, millions of rubles			424,0	
Growth of tax deductions to the budget, %			109,8	
II Social				
An income level per employee, thousands of rubles	56,5	38,2		
Creating direct and indirect infrastructure facilities, units			4	
The volume of scientific emigration, people	14			14
Number of personnel employed in R&D, thousands of people	8,1			
Establishing faculties for training in universities, units		3		
Targets for direct contracts, thousands of people			1,5	
Creating new jobs, thousands of units				7,2
Growth rate of average wages, %				106,9
An employment dynamic in enterprises, %				1,4
The amount of social payments from the integrated structure, millions of rubles				230,0
The influx of young professionals in the scientific and educational sphere, %	0,5	0,7		0,2

Testing of the system of indicators of assessment of socio-economic efficiency of SEC on the example of Krasnoyarsk Krai [25, 26] shows their simultaneous heterogeneity (quantitative and qualitative) and commonality for all actors. Consideration of quantitative indicators reflecting the state of SEC resources and qualitative indicators characterizing the efficiency of SEC resources use in dynamics will allow to determine, using factor models, the influence of network characteristics

on the activities of its subjects, further directions of inter-network relations in the form of SEC, to understand in greater depth the current processes and to identify problem areas of interaction.

5. Conclusion

According to the authors, the formation and functioning of an integration structure in the form of an SEC using the foundations of network interaction is an effective way to ensure the growth of the economy through innovation. The network method of building relations between the scientific and educational sphere and business in the form of SEC with the active participation of the state, allows, considering interests, to create conditions for their interaction as equal partners.

The proposed system of indicators for measuring the socio-economic effectiveness of the activity of the SEC is characterized by the identification and structuring of general and specific indicators in relation to the main groups of participants, which allows to obtain the appropriate information base for making a reasonable decision on the participation of the SEC in the sustainable development of the regions of Russia on the following components [27]:

- as a promising sector of the economy, with a high share of employment in enterprises producing knowledge-intensive products;
- as a producer of innovation that increases the competitiveness of enterprises;
- as a factor ensuring growth on the basis of SEC innovative enterprises;
- as a factor of competitiveness, contributing to the inflow of highly skilled labor into the economy.

In addition to the assessment task, further study of the importance of the impact of individual indicators will allow to carry out a reasonable analysis (using factor models) of the reasons that prevented the realization of the potential of the SEC in terms of solving problems of coordination of innovative activity of the scientific and educational sphere and business to ensure the sustainable development of the territory of the region as a whole.

References

- [1] Smorodinskaya NV. The Global Paradigm Shift and the Emanation of a Network Economy. *Economic sociology*. 2012 Sep;13(4):95-115.
- [2] Vladimirova ON, Slavikovsky AO. Questions of methodical support of assessment of socio-economic efficiency of scientific-educational complex. *Russian Journal of Innovation Economics*. 2019 Jul-Sep;9(3):1011-24.
- [3] MinMin V, Petruk GV. Science, Education and Business: Foreign and Domestic Experience of Integration Interaction. *Azimuth of Scientific Research: Economics and Management*. 2017 Apr-Jun;19(2):216-19.
- [4] Pettinger R. The Business of Business: The Context of Organisation and Commercial Development. *Procedia – Social and Behavioral Sciences*. 2016 Jun;221:11-20.
- [5] Bodrunov S. Integration of Manufacturing, Science and Education as a Basis for the Re-Industrialization of Russia. *World Economy and International Relations*. 2015 Oct;59(10):94-104.
- [6] Betz U, Betz F, Kim R. Surveying the future of science, technology and business – A 35 year perspective. *Technological Forecasting and Social Change*. 2019 Jul;144:137-47.
- [7] Carayannis E, Grigoroudis E. Quadruple Innovation Helix and Smart Specialization: Knowledge Production and National Competitiveness. *Foresight and STI Governance*. 2016 Jan-Mar;10(1):31-42.

- [8] Stăiculescu C, Richițeanu-Năstase E-R, Dobrea R. The University and the Business Environment – Partnership for Education. *Procedia – Social and Behavioral Sciences*. 2015 May;180:211-8.
- [9] Boev SG. Integration of Science, Education and Production as the Basis of Innovative Economic Development. *Economist*. 2015 Jul;256(7):58-72.
- [10] Yesina YL, Stepanenkova NM, Agafonov EE. Forms and mechanisms for integration of science, education and the business community under conditions of innovative renovation of the regional economy. *Creative economy*. 2015 Dec;12(9):1491-1508.
- [11] Islakaeva GR. The experience of creating the world scientific and educational centers. *Reports of the University of Bashkortostan*. 2018 Sep-Oct;3(5):519-24.
- [12] Kartashova A, Shirko T, Khomenko I. Educational Activity of National Research Universities as a Basis for Integration of Science, Education and Industry in Regional Research and Educational Complexes. *Procedia – Social and Behavioral Sciences*. 2015 Dec;214:619-27.
- [13] Fetschenko V, Shadoba E, Katkow Y. Management of Innovative Integrated Structures of Education, Business and Science at the Regional Level. *Procedia – Social and Behavioral Sciences*. 2015 Dec;214:243-51.
- [14] Kleeva LP. Development of scientific and educational complexes of Russian regions. *Energy: economics, technology, ecology*. 2015 Oct;(10):2-8.
- [15] Malina SS. The role of subjects of scientific-educational complex in the development of the region innovative economy. *Siberian financial school*. 2015 Jan-Feb;108(1):91-5.
- [16] Ryuegg-Stürm I, Akhtenhagen L. Network organizational and management forms – fashion or necessity? *Problems of management theory and practice*. 2000 Nov-Dec;24(6):53-7.
- [17] Haggins R. The Success and Failure of Policy-Implanted Inter-Firm Network Initiatives: Motivations, Processes and Structure. *Entrepreneurship and Regional Development*. 2000;12:111-35.
- [18] Eisenmann T, Parker G, Van Alstyne M. Platform envelopment. *Strategic Management Journal*. 2011;32(12):1270-85.
- [19] Klyucharyov GA, Mikhaleva MN. Innovative Entrepreneurship and Knowledge-Intensive Production: Ways of Development. In: Gorshkov MK, Arefev AL, Klyucharyov GA, Sheregi FE, editors. *Education and Science in Russia: State and Potential of Development*. Collection of scientific works. Moscow: Center for Sociological Research; 2016. p. 307-38.
- [20] Maskell P, Malmberg A. Localized learning and industrial competitiveness. *Cambridge Journal of Economics*. 1999;23(2):167-86.
- [21] Porter ME. Clusters and New Economics of Competition. *Harvard Business Review*. 1998 Nov-Dec; 76(6):77-90.
- [22] Bolgova EV. Assessment of efficiency of economic functions of the scientific and educational framework of the region. *Economic science and education*. 2010 Nov;72(11):317-20.
- [23] Makoveeva VV. Networking as a mechanism of integration of education, science, production and assessment of its performance: thesis... Candidate of Economic Sciences. Tomsk. Sib. Head of Finance and Banking; 2013. 237 p.
- [24] Neganov SA. Assessment of Efficiency of Regional Network Structures. *Economics and Management: Analysis of Development Trends and Prospects*. 2016;31-1:70-8.
- [25] HSE Statistical Collections [Electronic resource]. Access mode – <https://www.hse.ru/primarydata/> (date of appeal: 12.10.2019).
- [26] Federal State Statistics Service [Electronic resource]. Access mode – <https://www.gks.ru/> (date of appeal: 12.10.2019).
- [27] Slavikovsky AO. Tendency of formation and development of scholarly educational complexes (case of Siberian Federal okrug). *Problems of modern economy*. 2018 Apr-Jun;66(2):253-7.

Classification of Unbalanced Data Based on RSM and Binomial Distribution

LI Rong^{a,1} and ZHOU Wei-bai^a

^a*Guangzhou college of Commerce, China*

Abstract. In the case of extremely unbalanced data, the results of the traditional classification algorithm are very unbalanced, and most samples are often divided into the categories of majority samples, so the accuracy of judgment of the minority classes will be reduced. In this paper, we propose a classification algorithm for unbalanced data based on RSM and binomial undersampling. We use RSM's random part features rather than all each classifier to make each training classifier reduce the dimensions, and dimension reduction makes relatively minority class samples indirectly lift. Using the above characteristics of the RSM to reduce dimension can solve the problem that unbalanced data classification in the minority class samples is too little, and it can also find the important attribute of variables to make the model have the ability of explanation. Experiments show that our algorithm has high classification accuracy and model interpretation ability when classifying unbalanced data.

Keywords. Machine learning; unbalanced data; multi-classifier ensemble; Random subspace method

1. Introduction

When traditional classification algorithms encounter extreme imbalance data, the classification results are very inaccurate, and most samples are divided into the categories of most samples [1-2]. This method reduces the accuracy of judgment of minority classes. However, minority classes are often more valuable than majority classes in real life [3]. In order to deal with the problem about clearly classify minority data, it is very important to study data classification method of unbalanced data sets.

The method to deal with unbalanced data is mainly from two aspects of changing sample proportion of different types data and algorithms [4, 7-8]. The method of changing the proportion of different sample categories of data is mainly to reduce the imbalance degree of data by adding or deleting samples, such as oversampling, under-sampling and under-sampling of negative binomial distribution [5-6].The algorithm includes different categories for different costs, single category learning, or adjustment of probability valuation or threshold value when training the decision tree [9], such as random forest, support vector machine, decision tree, artificial neural network, and nearest neighbor method[9-11].

In previous studies, more researchers used the method of resampling. Although the method of resampling is helpful for solving unbalanced data, it also has some fatal

¹ Corresponding Author: LI Rong, associate professor, Room 1202, No. 8, Wenmei street, Haizhu District, Guangzhou, China; E-mail: 1047161101@qq.com

defects. For example, the method of random oversampling may lead to overfitting [5-6], while the method of random under-sampling may lose some samples containing important data [5, 10-12]. To solve the problem of unbalanced data classification and reduce the defects caused by resampling, we propose an algorithm combining RSM and resampling. The algorithm uses RSM method to train each classifier based on its features of using random partial characteristics instead of all characteristics, which means training sub-classifier with a small number of variables at a time. After training the classifier each time, the dimension of it is lower, so that the number of minority class samples increases. In classifications of unbalanced data, one of the most important problems is that the sample size with a small proportion is too small. It can be solved by taking advantage of the feature of RSM. This feature can also be used to find out importance of variable attributes, to enable the model to have explanatory ability. We use 6 datasets from UCI machine learning database for simulation experiments. Experimental results show that our algorithm can effectively classify unbalanced data and obtain higher classification accuracy.

2. An unbalanced data classification algorithm combining RSM and binomial distribution sampling

Based on RSM, we combine sampling method of binomial distribution. First, our algorithm determines the number of samples needed for the majority sample after undersampling by using binomial distribution, which makes the proportions of the minority class and the majority class similar in new data set. Then use the new data set to train RSM classifier, and get a final classification result by majority vote.

2.1 Binomial distribution sampling

The probability mass function of binomial distribution is shown in formula (1).

$$f(y) = \binom{n}{y} p^y (1-p)^{n-y}, y = 0, 1, \dots, n \quad (1)$$

Where p is the probability of success. n is the total number of experiments. y is the number of successful experiments. Figure 1 shows the distribution of y when $p=0.5$ and $n=10$. we find that the probability of y 's value nearby $n/2$ is the highest.

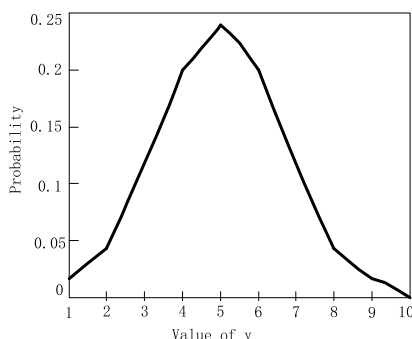


Figure 1. Binomial distribution ($p=0.5$, $n=10$).

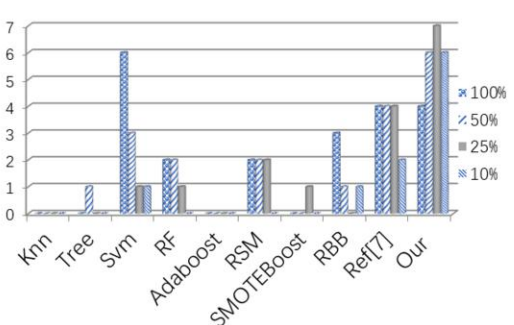


Figure 2. statistical results of G-mean highest number

We set n as 2 times the sample size of the original minority class samples and p as 0.5. The cumulative distribution function of binomial distribution was obtained, as shown in (2).

$$F(y) = \sum_{k=0}^{[y]} \binom{n}{k} p^k (1-p)^{n-k} \quad (2)$$

Where, $F(y)$ is cumulative distribution function. k is the number of successes.

We randomly select a value between 0 and 1 as a probability value, and find out the y value corresponding to probability value. We take this y value as the number of samples after undersampling of the majority class and a new value of minority sample sets $n-y$. After binomial distribution sampling, we can get a new sample which has a similar size with minority class and majority class. We classify this new sample using the RSM classifier and get the final classification result.

2.2 RSM algorithm

RSM algorithm is not like random forest or Adaboost using resampling method to get different training data sets, each time RSM randomly selects a few features in characteristic space and uses these characteristics forming training data set to train classifier. This method improves the stability and efficiency of classifier, and overcomes the problem of small sample in high dimensions. RSM has the advantages of reducing dimensions by using multiple classifiers and feature selection at the same time, so it is very suitable for small sample data classification.

Our method also takes advantages of RSM's feature that uses small variables to build classification models each time to calculate the variable importance of attributes of data set. The calculation formula is shown in (3).

$$w_i = \frac{\sum_{t=1}^{NumT} V_t}{n_i} \quad (3)$$

Where w_i is the variable importance of the i^{th} attribute; V_t is a classification accuracy rate calculated by test set. The test set is formed by the t -th base classifier which do not use majority class samples after previous under-sampling. n_i is the number of times that the i^{th} attribute is selected from all basic classifiers. Accumulate the accuracy of the i^{th} attribute, divided by the number of times. It also uses as variable importance of the attribute.

2.3 Specific algorithm

The steps of our algorithm are as follows:

Input: training data set D in S dimension of N samples;

D is divided into minority class samples D^{pos} and majority class samples D^{neg} ;

D^{pos} and D^{neg} are the sample numbers of minority class and majority class samples respectively;

Set the basic classifier to be used as WeakLearn;

Set the number of training times $NumT$ and the dimension of sampling $NumF$ ($0 < NumF < S$);

For $t = 1, 2, \dots, NumT$

1. Use binomial distribution ($n = 2N^{pos}$, $p = 0.5$) to decide N_t^{neg} and N_t^{pos}
2. Resampling N_t^{neg} majority class samples D_t^{neg} by random under-sampling
3. Sampling N_t^{pos} minority class samples D_t^{pos} by random sampling, which was extracted and not put back (If $N_t^{pos} > N^{pos}$, $D_t^{pos} = D^{pos} +$ randomly selects $(N_t^{pos} - N^{pos})$ minority class samples)
4. Use D_t^{neg} and D_t^{pos} to form a new training sample D'
5. Select the dimension of random sampling from S-dimension training samples
6. Copy dataset D' and retain the data selected in the previous step
7. Train classifier **WeakLearn**
8. Use the original test data set to get the classification category L_t
9. Randomly select $2 \cdot N^{pos}$ samples from the unused D^{neg} as the test set, and calculate the classification accuracy V_t as the variable importance weight of the $NumF$ attributes of the round

Output : 1. The result of $NumT \cdot L_t$ is calculated to the classification of the final result according to the majority vote.

2. Use $NumT \cdot V_t$ to calculate the variable importance of each attribute

3. Experimental results and analysis

3.1 Experimental data

We use 6 sets of unbalanced data from the UCI machine learning database, as shown in Table 1.

Table.1 UCI data sets

data sets	total	majority class	minority class	Proportion of minority	Number of attributes
Pima Indians Diabetes	768	500	268	34.9	8
Blood Transfusion Service Center	748	570	178	23.8	4
Ionosphere	351	225	126	35.9	34
Breast Cancer Wisconsin	569	357	212	37.26	30
Echocardiogram	131	88	43	32.82	7
Statlog	1000	700	300	30	20

3.2 Evaluation indicators

Accuracy is commonly used as evaluation standard in classification problems, which reflects overall classification performance. However, it doesn't reflect the classification of imbalanced data well. We use seven common evaluation indexes to truly judge the quality of the classification results. Including Accuracy, Specificity, Precision, Recall, *F*-measure and *G*-mean. as in (4) to (9).

$$\text{Sensitivity} = \frac{TP}{TP + FN} \quad (4)$$

$$\text{Specificity} = \frac{TN}{TN + FP} \quad (5)$$

$$\text{Precision} = \frac{TP}{TP + FP} \quad (6)$$

$$\text{Recall} = \frac{TP}{TP + FN} \quad (7)$$

$$\text{F-measure} = \frac{2 \times \text{Recall} \times \text{Precision}}{\text{Recall} + \text{Precision}} \quad (8)$$

$$\text{G-mean} = \sqrt{\frac{TP}{TP + FN} \times \frac{TN}{TN + FP}} \quad (9)$$

Where FN is false negative. FP is false positive. TN is true negative. TP is true positive.

Since *F*-measure and *G*-mean comprehensively consider the accuracy of minority classes and majority classes, they have comprehensive comparison ability. In addition, if the classification of the minority samples is wrong, sometimes it will cause more serious losses in the classification of unbalanced data. Therefore, the accuracy of minority class is also an experimental key indicator in this paper.

3.3 Experimental design

In order to prove the superiority of method proposed in this paper, we compared our method and previous classification methods, and observed the influence degree of each method on different degree of data imbalance. In this study, the minority class samples in each data set were randomly undersampling to make sample proportion difference become larger. Minority class samples were undersampling to be 10%, 25% and 50% of the original minority samples. The data set was randomly divided into 5 sub-sets. Four sub-sets were used as the training set and the rest one was used as test set in each experiment. The above steps were repeated. Finally, we get the classification accuracy of five test sets, and the average value was taken as the average accuracy of our method.

We set the nearest neighbor parameter K to 1. The kernel function of SVM classifier is RBF kernel, parameter σ uses the method in reference [3]. Cost function C

choose exponential sequence to search whose scope set as $2^{-12}, 2^{-10}, \dots, 2^{12}$; the parameter $NumT$ of random forest set as 100, and $NumF$ set as the attribute number in data set. Adaboost uses decision tree as its basic classifier and its $NumT$ is 100. The basic classifier of RSM is decision tree and its $NumT$ is 100, $NumF$ is half of the number of attributes in the data set. SMOTEBoost uses a decision tree classifier with $NumT$ setting as 100 and a buffer ratio of 100%. RB Bagging uses a decision tree as its base classifier with $NumT$ setting as 100.

3.4 Experimental results and analysis

3.4.1 Performance comparison

We use six datasets and 4 different proportions of minority classes. The accuracy is shown in table 2 and table 3. We can find that classification accuracy of SVM, RF, RB Bagging, Reference[7] (abbreviated as ref [7] in the table) and our algorithm is better in each data set. With minority class sample ratio decreasing, the accuracy of classification has a small fluctuation. In most data sets, our algorithm's classification accuracy even increased with reducing the proportion of minority class samples. It means that our algorithms can improve the classification results of unbalanced data effectively. Our algorithm performs better when the proportion of minority class samples is small, which indicates that our algorithm is more suitable for classifying data sets in cases where have a small proportion of little samples.

Table.2 performance comparison of correct rate

	Pima Indians Diabetes				Blood Center		Transfusion Service		Ionosphere			
	100 %	50%	25%	10%	100 %	50%	25%	10%	100 %	50%	25%	10%
Knn	0.68	0.73	0.83	0.94	0.70	0.68	0.79	0.89	0.87	0.89	0.92	0.96
Tree	0.69	0.74	0.83	0.91	0.73	0.82	0.87	0.96	0.89	0.97	0.96	0.95
SVM	0.74	0.77	0.77	0.84	0.73	0.71	0.69	0.74	0.95	0.95	0.96	0.98
RF	0.76	0.81	0.88	0.94	0.75	0.84	0.91	0.96	0.93	0.97	0.97	0.97
Adaboost	0.74	0.81	0.88	0.94	0.74	0.82	0.89	0.96	0.90	0.92	0.94	0.94
RSM	0.73	0.80	0.88	0.94	0.78	0.86	0.93	0.97	0.93	0.98	0.97	0.97
SMOTE Boost	0.71	0.79	0.85	0.93	0.73	0.80	0.85	0.94	0.91	0.80	0.95	0.96
RBB	0.75	0.76	0.72	0.74	0.39	0.26	0.16	0.21	0.91	0.92	0.75	0.54
ref [7]	0.74	0.73	0.72	0.75	0.63	0.59	0.64	0.63	0.93	0.95	0.90	0.66
Our	0.74	0.73	0.71	0.76	0.64	0.61	0.63	0.68	0.93	0.95	0.95	0.92

Table.3 performance comparison of correct rate

	Breast Cancer Wisconsin				Echocardiogram				Statlog			
	100%	50%	25%	10%	100%	50%	25%	10%	100%	50%	25%	10%
Knn	0.92	0.94	0.96	0.98	0.52	0.59	0.75	0.75	0.60	0.72	0.83	0.92
Tree	0.92	0.94	0.96	0.97	0.70	0.67	0.81	0.81	0.69	0.75	0.84	0.92
SVM	0.96	0.95	0.96	0.97	0.73	0.67	0.75	0.75	0.68	0.75	0.78	0.76
RF	0.96	0.96	0.98	0.98	0.70	0.75	0.87	0.87	0.77	0.84	0.90	0.96
Adaboost	0.91	0.93	0.96	0.97	0.69	0.73	0.84	0.84	0.75	0.83	0.90	0.96
RSM	0.96	0.96	0.98	0.97	0.66	0.73	0.85	0.85	0.76	0.83	0.90	0.96
SMOTEBoost	0.93	0.94	0.96	0.98	0.67	0.71	0.85	0.85	0.72	0.82	0.89	0.94

	5											
RBB	0.94	0.90	0.9 3	0.87	0.65	0.60	0.56	0.56	0.69	0.67	0.67	0.60
ref [7]	0.96	0.95	0.9 6	0.94	0.65	0.64	0.67	0.67	0.71	0.69	0.69	0.67
Our	0.96	0.94	0.9 5	0.93	0.65	0.69	0.73	0.73	0.71	0.70	0.71	0.69

Table.4 Performance comparison of F-measure

	Pima Indians Diabetes				Blood Transfusion Service Center				Ionosphere			
	100 %	50 %	25 %	10 %	100 %	50 %	25 %	10 %	100 %	50 %	25 %	10 %
Knn	0.55 7	0.3 4	0.2 3	0.2 4	0.39 2	0.2 6	0.1 5	0.1 8	0.78 8	0.6 6	0.5 3	0.2
Tree	0.56 3	0.4 8	0.2 4	0.1 1	0.37 1	0.2 8	0.0 9	0.1 9	0.85 2	0.9 2	0.8 2	0.5
SVM	0.67 6	0.5 1	0.3 3	0.1 1	0.47 1	0.3 5	0.1 3	0.0 3	0.93 9	0.8 9	0.8 3	0.7
RF	0.64 4	0.4 8	0.2 0	0.0 0	0.36 7	0.1 0	0.1 5	0.0 5	0.91 3	0.9 3	0.8 8	0.6
Adaboost	0.62 5	0.4 0	0.3 0	0.0 0	0.38 7	0.1 4	0.1 5	0.0 5	0.86 2	0.8 2	0.7 1	0.4
RSM	0.58 7	0.3 3	0.2 0	0.0 0	0.31 2	0.1 2	0.1 2	0.0 0	0.91 4	0.9 7	0.8 6	0.5
SMOTEBoo st	0.59 8	0.4 2	0.3 6	0.0 8	0.40 0	0.1 0	0.1 3	0.0 3	0.87 7	0.7 0	0.8 3	0.6
RBB	0.68 7	0.5 7	0.3 4	0.2 4	0.30 8	0.1 9	0.0 5	0.0 5	0.87 3	0.8 4	0.4 9	0.0
ref [7]	0.65 4	0.5 8	0.3 3	0.2 6	0.45 6	0.2 9	0.1 6	0.0 6	0.90 9	0.8 9	0.6 9	0.2
Our	0.68 5	0.5 0	0.4 5	0.2 5	0.45 8	0.2 1	0.2 8	0.0 8	0.90 8	0.8 2	0.8 2	0.4

Table.5 Performance comparison of F-measure

	Breast Cancer Wisconsin				Echocardiogram				Statlog			
	100 %	50 %	25 %	10 %	100 %	50 %	25 %	10 %	100 %	50 %	25 %	10 %
Knn	0.89 6	0.8 2	0.8 7	0.7 3	0.34 0	0.0 7	0.0 7	0.0 7	0.36 9	0.1 8	0.1 7	0.0
Tree	0.89 7	0.8 4	0.8 2	0.7 0	0.50 2	0.2 3	0.1 3	0.1 7	0.49 2	0.3 6	0.2 6	0.0
SVM	0.94 0	0.9 7	0.8 7	0.7 2	0.64 3	0.3 2	0.2 3	0.2 3	0.56 6	0.2 1	0.2 2	0.1
RF	0.95 2	0.9 1	0.9 5	0.7 6	0.46 0	0.0 0	0.0 0	0.0 0	0.53 1	0.3 7	0.0 0	0.0
Adaboost	0.88 5	0.8 3	0.8 4	0.7 5	0.49 5	0.0 3	0.1 3	0.1 3	0.50 3	0.2 7	0.0 0	0.0
RSM	0.95 1	0.9 2	0.9 3	0.7 6	0.44 0	0.1 0	0.0 0	0.0 0	0.49 6	0.2 3	0.0 0	0.0
SMOTEBoo st	0.91 7	0.8 2	0.8 7	0.7 4	0.51 0	0.0 0	0.2 0	0.2 0	0.50 9	0.2 9	0.0 9	0.0
RBB	0.93 2	0.8 6	0.7 4	0.4 6	0.56 6	0.3 6	0.2 6	0.2 6	0.59 3	0.4 9	0.2 2	0.1
ref [7]	0.93 9	0.8 7	0.8 3	0.7 9	0.55 9	0.3 9	0.2 9	0.2 9	0.60 5	0.4 1	0.3 3	0.1
Our	0.95 9	0.8 2	0.8 3	0.6 0	0.56 0	0.4 9	0.3 9	0.3 9	0.60 7	0.4 3	0.3 4	0.1

F-measure performance comparison of 6 data sets is shown in Table 4 and table 5. SVM, RBB and our algorithm have better classification effect. With the decrease of the proportion of minority classes samples, our algorithm performance is more stable.

Comparison of G-mean performance of 6 data sets is shown in table 6 and table 7. They indicate that in each data set, SVM, U_RSM, RBB, References[7] and our algorithm all have better effects. In the case of decreasing the proportion of minority samples, the performance of this algorithm is more stable.

Table.6 Performance comparison of G- mean

Pima Indians Diabetes				Blood Transfusion Service Center				Ionosphere				
	100	50	25	10	100	50	25	10	100	50	25	10
	%	%	%	%	%	%	%	%	%	%	%	%
Knn	0.64	0.5	0.4	0.3	0.56	0.4	0.4	0.4	0.80	0.7	0.6	0.2
	5	6	8		9	8	5		3	4	6	
Tree	0.66	0.6	0.5	0.3	0.54	0.4	0.2	0.2	0.88	0.9	0.8	0.6
	1	0	0		0	2	7		4	9	9	
SVM	0.74	0.7	0.5	0.4	0.65	0.6	0.5	0.2	0.94	0.9	0.9	0.8
	4	9	5		0	2	1		2	0	4	
RF	0.72	0.5	0.4	0.0	0.51	0.3	0.2	0.1	0.92	0.9	0.9	0.6
	8	4	0		4	0	0		5	1	2	
Adaboost	0.70	0.5	0.4	0.0	0.54	0.3	0.3	0.1	0.88	0.8	0.7	0.6
	9	5	0		5	2	0		9	9	1	
RSM	0.66	0.5	0.3	0.0	0.45	0.2	0.2	0.0	0.92	0.9	0.9	0.5
	1	4	0		6	0	0		5	2	9	
SMOTEBoo st	0.68	0.6	0.5	0.11	0.56	0.3	0.2	0.1	0.90	0.7	0.8	0.8
	3	2			7	8	0		4	7	0	
RBB	0.75	0.7	0.7	0.7	0.43	0.3	0.2	0.3	0.90	0.9	0.7	0.4
	6	0	7		5	7	6		2	5	9	
ref [7]	0.73	0.7	0.7	0.6	0.63	0.5	0.5	0.4	0.92	0.9	0.9	0.7
	3	1	6		6	7	4		4	0	3	
Our	0.75	0.7	0.7	0.7	0.64	0.5	0.6	0.5	0.92	0.9	0.9	0.8
	5	5	8		8	5	5		4	3	3	

Table.7 Performance comparison of G- mean

Breast Cancer Wisconsin				Echocardiogram				Statlog				
	100	50	25	10	100	50	25	10	100	50	25	10
	%	%	%	%	%	%	%	%	%	%	%	%
Knn	0.91	0.9	0.8	0.8	0.47	0.0	0.1	0.1	0.51	0.3	0.4	0.1
	0	8	6		8	3	3		9	1	6	
Tree	0.92	0.9	0.9	0.8	0.60	0.3	0.2	0.2	0.62	0.5	0.5	0.1
	2	1	4		2	7	7		3	0	9	
SVM	0.95	0.9	0.9	0.9	0.73	0.4	0.4	0.4	0.68	0.4	0.4	0.4
	4	4	1		8	3	3		6	9	6	
RF	0.96	0.9	0.9	0.8	0.57	0.0	0.0	0.0	0.63	0.4	0.1	0.0
	4	3	4		9	0	0		5	5	0	
Adaboost	0.90	0.9	0.9	0.8	0.59	0.0	0.1	0.1	0.61	0.3	0.1	0.0
	0	2	4		9	4	4		7	0	0	
RSM	0.96	0.9	0.9	0.8	0.55	0.2	0.0	0.0	0.60	0.4	0.0	0.0
	4	4	1		7	0	0		0	5	0	
SMOTEBoo st	0.92	0.9	0.9	0.8	0.62	0.0	0.2	0.2	0.62	0.4	0.1	0.11
	1	4	6		9	7	7		5	7		
RBB	0.95	0.9	0.9	0.8	0.65	0.5	0.5	0.5	0.70	0.6	0.6	0.6
	2	2	6		8	6	6		8	7	1	
ref [7]	0.95	0.9	0.9	0.8	0.62	0.4	0.3	0.3	0.00	0.0	0.0	0.0
	3	5	6		8	8	8		0	0	0	
Our	0.96	0.9	0.9	0.9	0.65	0.5	0.7	0.7	0.71	0.7	0.7	0.6
	4	5	4		7	5	5		2	1	5	

The above comparison method is to combine 7 different evaluation indicators to judge the quality of classification results. However, this way can't be used for quantitative comparison. We choose G-mean as a representative from seven evaluation indicators for comparison to find out the highest value in each data set under different

proportion. If the gap between two algorithms was not greater than 0.02, the values are considered the same. The statistical results of the highest number of G-mean are shown in figure 2.

From Figure 2, when the original proportion of minority class samples is classified, SVM algorithm has the best results of 6 data sets. Our algorithm's results of 4 data sets are the second best. However, when the proportion of minority class samples decreases, results of our algorithm are significantly better than others. When the proportion equals to 50%, 25% and 10%, our results are the best, it means that our algorithm can improve classification results of unbalanced data sets effectively. The smaller proportion of minority class samples is, the better classification results we have.

From the experimental results, the SVM algorithm has a better classification effect on the original scale data set, but the classification effect is significantly reduced when the proportion of minority class sample becomes lower. SVM is not suitable for classifying unbalanced data. RB Bagging algorithm has a good classification effect in all six data sets, but its results are unstable. Although it has a high accuracy of minority classes in some data sets, when the accuracy of multiple classes quickly drops at the same time, overall classification effect is bad. Our algorithm has a good classification effect in various data sets and minority class proportions, and it even has a better classification effect when the proportion of minority class samples and majority class samples has a big difference between each other. In original proportions, the classification effect results in 4 data sets are the best; in case of 50% and 10% of minority class samples, 5 results are the best; in case of 25% of minority class samples, all results are the best. This indicates that our algorithm is very suitable for classifying unbalanced data. Moreover, our algorithm is well suitable for unbalanced data classification algorithm.

3.4.2 Importance of variables

Our algorithm calculates the variable importance of each subset. After summing up the variables' importance of 5-fold, the data range is between 0 and 1 through the method of data normalization. Table 8 shows the variables' importance in Pima Indians Diabetes dataset whose value is between 0 and 1. the value is closer to 1, the more important of variable is. From Table 8, the most important variables are attribute 2 and attribute 6.

Table.8 importance of variables for Pima Indians Diabetes data sets

attribute 1	attribute 2	attribute 3	attribute 4	attribute 5	attribute 6	attribute 7	attribute 8
100%	0.18	1.00	0.00	0.15	0.19	0.42	0.28
50%	0.19	1.00	0.12	0.00	0.08	0.48	0.03
25%	0.17	1.00	0.00	0.20	0.03	0.45	0.10
10%	0.06	1.00	0.00	0.10	0.14	0.35	0.04

4. Conclusion

There are unbalanced data problems in many different fields. This target receives much attentions in recent years related to relative issues. The past research mainly combined with a multiple classifier and many people focus on Bagging and Boosting classifier. Few people notice RSM classifier which has not only the advantages of multiple classifier, but also the ability of reducing classification dimension, indirectly promote the minority class sample effect. We use RSM combined with binomial distribution

sampling to propose a binomial random subspace classification algorithm for unbalanced data. This method integrates the concepts of RSM and resampling. Experiments show that our algorithm has a higher, more balanced and more stable classification accuracy when classifying unbalanced data, and it also has the ability of model interpretation.

References

- [1] WANG Canwei, YU Zhilou, ZHANG Huaxiang, New algorithm of AdaBoost for unbalanced datasets, Computer Engineering and Applications. 2011, (28)169-172,175.
- [2] B Yuan, X Ma. Sampling + reweighting: Boosting the performance of AdaBoost on imbalanced datasets// International Joint Conference on Neural Network. Australia: Brisbane 2012, 1-6.
- [3] Li C H, Ho H H, Liu Y L, et al., An automatic method for selecting the parameter of the normalized kernel function to support vector machines. Journal of Information Science and Engineering 2012 (1),1-15.
- [4] XY Liu, J Wu, ZH Zhou, Exploratory under-sampling for class-imbalance learning, IEEE Transactions on Systems Man & Cybernetics Part B Cybernetics A Publication of the IEEE Systems 2009(2), 539-50.
- [5] W Klement, S Wilk, W Michalowski, et al., classifying severely imbalanced data, Germany: Springer Berlin Heidelberg,2011.
- [6] TR Hoens, Q Qian, NV Chawla, et al., Building decision trees for the multi-class imbalance problem, 16th Pacific-Asia Conference on Knowledge Discovery and Data Mining, Malaysia: Kuala Lumpur,2012,122-134
- [7] Gu Yuping, Cheng Longsheng, Classification of unbalanced data based on MTS-AdaBoost, Application Research of Computers 2018(2), 346-353.
- [8] GO Feng, HUANG Hai-yan, Imbalanced Data Classification Method Based on Neighborhood Hybrid Sampling and Dynamic Ensemble, Computer Science 2017 (8),225-229.
- [9] S Hido, H Kashima, Y Takahashi, Roughly balanced bagging for imbalanced data, Statistical Analysis & Data Mining 2010 (2), 412-426.
- [10] MYOUNG J K, DAO K K, HONG B K, Geometric mean based boosting algorithm with over-sampling to resolve data imbalance problem for bankruptcy prediction, Expert Systems with Applications 2015 (42),1074-1082.
- [11] WANG B X, JAPKOWICZ N, Boosting support vector machines for imbalanced data sets, Knowledge and Information Systems 2010 (1),1-20.
- [12] Michael J Procopio, Jane Mulligan, Greg Grudic, Coping with Imbalanced Training Data for Improved Terrain Prediction in Autonomous Outdoor Robot Navigation, 2010 IEEE International Conference on Robotics and Automation Anchorage Convention District ,USA: Anchorage Alaska, 2010, 518-525.

Facial Expression Analysis Based on Fusion Multi-Layer Convolutional Layer Feature Neural Network

Hao Meng^a, Fei Yuan^{a,1} and Tianhao Yan^a

^a*Department of Automation, Harbin Engineering University, China*

Abstract. Concerning the problem that the current facial expression analysis based on convolutional neural network (CNN) only uses the features of the last convolutional layer but the recognition rate is not high, this paper proposes the use of sub-deep convolutional layer features and builds a CNN model which fuses the features of multi-layer convolutional layers. The model uses a CNN for feature extraction and saves the deepest feature vectors and sub-deep feature vectors of the expression images. The sub-deep feature vector is used as the input of the multilayer CNN established in this paper. The processed fourth convolution layer feature is fused with the deepest feature previously saved to perform facial expression analysis. Experiments are performed on FERPLUS dataset, Cohn-Kanade dataset (CK+) and JAFFE dataset. The experimental results show that the improved network structure proposed in this paper can capture richer feature information during facial expression analysis, which greatly improves the accuracy of expression recognition and the stability of the network. Compared with the original CNN-based facial expression analysis using only the last layer of convolution layer features, using multi-layer fusion features on three kinds of datasets can improve the expression recognition rate by 33.3%, 2.3% and 22%, respectively.

Keywords. Convolutional neural network, features of sub-deep convolutional layers, multi-layer convolutional layer Feature fusion, facial expression analysis

1. Introduction

Facial expression analysis refers to the use of computers to analyze human facial expressions and changes through pattern recognition and machine learning algorithms and to judge human psychology and emotions, thereby achieving intelligent human-computer interaction [1]. Deep convolution neural network has the outstanding characteristics of unsupervised feature learning, which has been proved to have the ability to mine the deep potential distributed expression features of data in the fields of image, speech and text. It is very effective when using deeper levels (ie with many layers) to learn features with high level of abstraction [2]. Therefore, in facial expression analysis, CNNs are also often used [3-4], using the powerful learning capabilities of CNNs to learn deep feature representations of expression pictures.

¹ Corresponding Author: Fei Yuan, Harbin Engineering University, China. Email: bohelion@hrbeu.edu.cn

The CNN can be regarded as a combination of feature extraction and classifier, which maps the image layer by layer and the result is the result of feature extraction. Judging from the mapping of its various layers, it is similar to a feature extraction process and features at different levels are extracted. Through continuous interactive mapping and finally mapping to several labels, it has the function of classification. However, the features extracted by the intermediate convolutional layer also include certain information and have a certain expression ability for the image [5]. Ali Mollahosseini [6]et al. proposed a deep neural network architecture to address the facial emotion recognition problem across multiple well-known standard face datasets; Hui Ding [7]et al. proposed a novel idea for training facial expression analysis networks based on static images, because the deep features may contain redundant information from the pre-training domain. These show that the use of intermediate convolutional layer features can improve the feature representation of pictures and then improve the accuracy of deep convolutional network classification. At present, most deep learning models for facial expressions have low accuracy and weak feature representation capabilities.

Based on GoogleNet Inceptionv3 [8] network for facial expression analysis, this paper proposes a fusion neural network structure with multiple convolutional layers to improve the expression recognition rate. The feature of sub-deep convolutional layer using CNN is proposed to ensure that deeper features can be obtained if the original features are relatively complete. The model is based on the GoogleNet Inception v3 network. First save the feature vector of the deepest convolutional layer currently used by the CNN and the feature vector of the sub-deep convolutional layer proposed in this paper; Secondly, the sub-deep high-dimensional feature vector is used as the input of the multilayer CNN established in this paper for training; Finally, the processed convolutional layer 4 features are fused with the deepest feature vector previously saved to perform softmax feature classification.

The rest of the paper is organized as follows. Section II gives an overview of our proposed approach, describing the features of each layer of the CNN and the improved network structure proposed in this paper. It also includes the multi-layer CNN established in this paper. Section III provides experimental results. Section IV concludes the paper.

2. Deep neural network

In CNNs, different convolution kernels have different sizes and the receptive fields are different. CNN can be regarded as the combination of feature extraction and classifier. From the mapping of each layer of CNN, it is similar to a feature extraction process, which extracts different levels of features. The CNN can map the features to different labels, which makes the CNN have the ability of classification. In this study, CNN is regarded as a method of feature extraction. The traditional deep convolution neural network is divided into two parts: feature extraction and final classification. Among the basic CNNs for image classification, the best one is GoogleNet[9-10]. This network structure mainly uses a split-merge idea. First, it splits, makes many branches and each branch does its own convolution pooling, then the results are concatenated to form a better feature channel. Capturing multi-scale features improves multi-scale adaptability and increases the width of the network. This paper uses GoogleNet Inception v3

network for feature extraction. Figure 1 shows the last few layers of the Inceptionv3 structure seen on the tensorboard [11] visualization. Currently the Inception v3 model trained on ImageNet uses the 1×2048 -dimensional vector output from the last layer `pool_3` before softmax classification, but the recognition rate is not good for expression recognition.

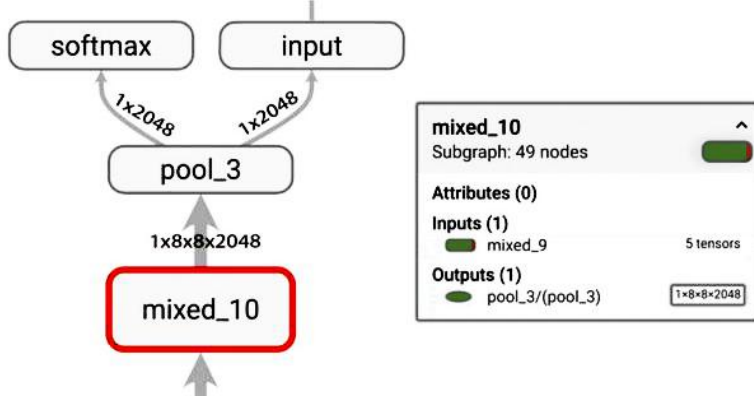


Figure 1. Tensorboard visualization node

The CNN is to map the image layer by layer and the mapping result is the result of feature extraction. How many convolution kernels are there in each convolution layer will get the characteristics of how many channels. After visualizing the convolution layer through feature map [12], we can get the characteristic map of each channel and fuse each channel according to 1:1 to get the fused characteristic map, as shown in Figure 2. Because there are many convolution layers in Inception v3, there are also many convolution kernels in each layer, that is, many channels. Figure 2 only shows the features of the first 25 channels of the first convolution layer and the features after 1: 1 fusion of all channels. Figure 3 shows the convolution feature map of all channels of different convolution layers. Through the visualization of the feature map, it can be seen that the shallow features tend to detect the edge of the image and the detected content is comprehensive. At the same time, there will be key information extracted (such as the bright eyes and mouth of the first convolution layer). With the deepening of the level, the feature image is more and more abstract and the resolution of the image is smaller and smaller. At the same time, a lot of information is ignored. Relatively speaking, the deeper the level is, the more representative the extracted features are. The current CNNs use only the features output by the last convolutional layer for classification and the intermediate feature information also has a certain ability to express images.

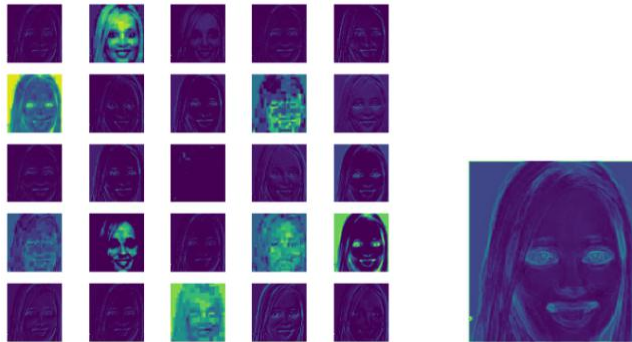


Figure 2. Feature map of the first 25 channels of the convolution layer 1 and the feature map of each channel after 1: 1 fusion



Figure 3. Feature map of each convolutional layer after 1: 1 fusion

This study proposes to use the output vector of the previous convolution layer mixed_10 of the convolution layer pool_3, that is, the input $1 \times 8 \times 8 \times 2048$ of pool_3 as the feature vector and extract the feature vector of the node mixed_10 and save it. The selection of sub-deep features can ensure that deeper features are obtained when the original features are relatively complete. The deeper the number of layers, the higher the level of semantic information and the more sufficient the semantic information is. For the $8 \times 8 \times 2048$ feature vector after extracting the mixed_10 node, this study establishes a CNN structure as shown in Table 1 for training.

Table 1. Multi-layer convolutional network structure

Layer	Input(W*H*D)	Kernel_num	Kernel_size	Stride	Pad	Out(W*H*D)
Conv1	$8 \times 8 \times 2048$	2048	3	1	0	$6 \times 6 \times 2048$
Conv2	$6 \times 6 \times 2048$	2048	3	1	0	$4 \times 4 \times 2048$
Conv3	$4 \times 4 \times 2048$	2048	3	1	0	$2 \times 2 \times 2048$
Conv4	$2 \times 2 \times 2048$	2048	2	1	0	$1 \times 1 \times 2048$
Conv5	$1 \times 1 \times 2048$	1024	1	1	0	$1 \times 1 \times 1024$
Conv6	$1 \times 1 \times 1024$	512	1	1	0	$1 \times 1 \times 512$
Conv6	$1 \times 1 \times 512$	10	1	1	0	$1 \times 1 \times 10$

The network structure designed in this paper is shown in Figure 4. After inputting facial expression pictures, they are sent to the GoogLeNet Inception v3 network for feature extraction and the deepest feature vector and sub-deep feature vector are extracted. The sub-deep features are processed using the multi-layered volume neural network established in this paper (that is, Table 1) and the processed feature vector output from the con4 layer is fused with the deepest feature vector of the original CNN

to obtain a fused feature vector with a size of 1×2048 . Finally, the fused 2048-dimensional feature vector is subjected to softmax classification.

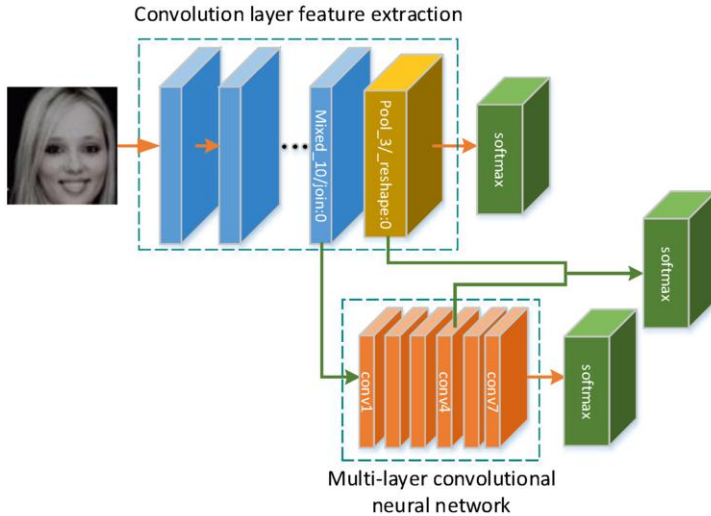


Figure 4. Designed Network Structure

3. Experiment and Results

The experiment is based on the deep learning framework tensorflow of Python3, using the operating system Windows10. Hardware configuration: the CPU is Intel (R) Xeon (R) gold 5122 CPU, the main frequency is 3.60ghz and the memory is 16.0gb; the GPU is NVIDIA geforce RTX 2080 Ti and the video memory is 16GB. This paper uses the FERPLUS dataset [13], the CK+ dataset [14] and the JAFFE dataset [15]. Among them, there are 10 categories of tags in the FERPLUS dataset: neutral, happiness, surprise, sadness, anger, disgust, fear, contempt, unknown, NF. This article removes the unknown and NF, which are a total of 8 expression categories. Both CK+ and JAFFE datasets have 7 expression categories. In this paper, the image is processed into a size of 299 pixels \times 299 pixels and the data set is divided into a training set, a verification set and a test set. The experimental settings train 6000 epochs, the initial learning rate is set to 0.01, the optimizer uses Adam and the batchsize is set to 100.

The experimental steps are as follows:

(1)Send the facial expression data set directly to the Inception v3 network for classification, save the feature 1×2048 -dimensional vector of the bottleneck layer, that is, the feature of the deepest convolutional layer and save the $8 \times 8 \times 2048$ -dimensional feature vector output by the node mixed_10, that is, the feature of the sub-deep convolutional layer, records the final test results;

(2)Extract the $8 \times 8 \times 2048$ -dimensional feature vector output by the mixed_10 node from the network model and save it. Send these $8 \times 8 \times 2048$ -dimensional vectors to the multi-layer convolutional neural network(that is, Table 1)established by us for classification, save the 1×2048 -dimensional feature vectors of the con4 layer and record the final test results;

(3)The feature vectors of the bottleneck layer layer saved in step 1 and the feature vectors of the con4 layer in step 2 are fused and sent to a CNN for classification and the final test results are recorded.

3.1 Experiment on the FERPLUS Dataset

3.1.1 Deepest Feature Training Experiment

The FERPLUS dataset is sent to the inception v3 network for migration learning and the softmax layer was changed from the original 1000 class to 8 class for training classification. Each face expression picture is sent to the network and the features of the bottleneck layer layer, that is, the 1×2048 -dimensional feature vector output by the node pool1_3 are extracted and saved. Each digit is a 32-bit floating point number, which is a total of 35887 pictures, which is $35887 \times 1 \times 2048$. And save the $8 \times 8 \times 2048$ -dimensional feature vector output by node mixed_10. Figure 5 is a graph of accuracy and loss function during training. Figure (a) shows a graph of accuracy of training and verification. Figure (b) shows a graph of loss function of training and verification. Orange represents training and blue represents verification.

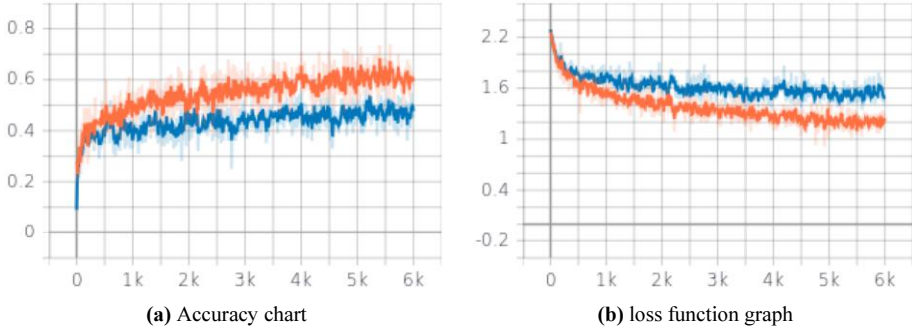


Figure 5. Accuracy curve and loss function of train and validation

It can be seen from Figure 5 that the accuracy rate during training is stable on average at 60% and the loss function value is stable on average at 1.2; the accuracy rate during verification is stable at 46% and the loss function value is stable at 1.5 on average. The accuracy rate is relatively low, the loss function value is relatively large and the curve oscillation is relatively large and unstable.

3.1.2 Sub-deep Feature Training Experiment

In this paper, a multi-layer neural network is designed and the saved sub-deep feature $8 \times 8 \times 2048$ -dimensional feature vector is used as the input of the multi-layer CNN for training and classification. Figure 6 is a graph of accuracy and loss function during training. Figure (a) shows a graph of accuracy of training and verification. Figure (b) shows a graph of loss function of training and verification. Orange represents training and blue represents verification.

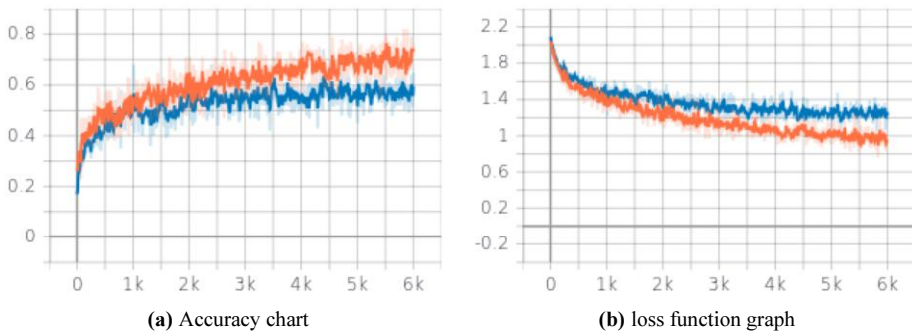


Figure 6. Accuracy curve and loss function of train and validation

It can be seen from Figure 6 that the accuracy rate during training is stable at 66% on average and the loss function value is stable at 1; the accuracy rate during verification is stable at 58% and the loss function value is stable at 1.2 on average. Compared with the traditional method, only the deepest features are used, the accuracy is improved, the value of the loss function is reduced, the amplitude of the oscillation is reduced and the curve is smoother. The effectiveness of using the features of the sub-deep convolutional layer proposed in this paper is proved.

3.1.3 Fusion Feature Training Experiment

The 1×2048 -dimensional features of the conv4 layer processed by the multilayer neural network established in this paper are fused with the 1×2048 -dimensional feature vectors output by the previously saved node pool_3 and the softmax layer is changed to 8 classes for training classification. Figure 7 is a graph of accuracy and loss function during training. Figure (a) shows a graph of accuracy of training and verification. Figure (b) shows a graph of loss function of training and verification. Orange represents training and blue represents verification.

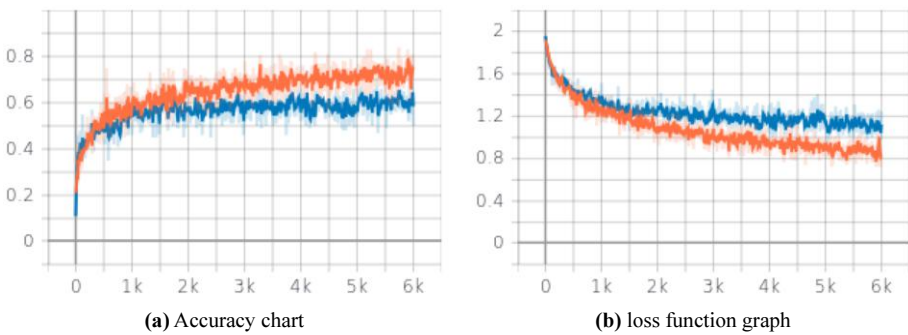


Figure 7. Accuracy curve and loss function of train and validation

It can be seen from Figure 7 that the accuracy rate during training is stable at an average of 70% and the value of the loss function is stable at 0.9; the accuracy rate during verification is stable at an average of 62% and the value of the loss function is stable at 1.1. Compared with using only the sub-deep features proposed in this paper, the accuracy rate has been improved again, the loss function value has been reduced, the oscillation amplitude has become smaller and the curve has been smoother. It is proved that the use of the fused features can further improve the expression recognition

rate and network stability. That is, the effectiveness of the improved convolutional network structure proposed in this paper.

3.2 Final Experimental Results

We obtained three models trained and saved on the FERPLUS dataset through 3.1 and then performed the same experiments on the CK+ dataset and JAFFE dataset to train and save the models according to the above experimental steps. Finally, the test is performed on the test set and the experimental results are shown in the following table.

Table 2. Test Results

Test accuracy (%)	FERPLUS	CK+	JAFFE
Primitive deepest feature	47.7	97.2	61.9
Sub-deep features proposed	59.4	98.9	72.3
Fusion features proposed	63.6	99.4	75.5

It can be concluded that:

Test on the FERPLUS dataset, CK + dataset and JAFFE dataset. The test accuracy of the saved model trained using the original CNN on the final test set is 47.7%, 97.2% and 61.9%, respectively; The accuracy of the model trained and saved using the features of the sub-deep convolutional layer proposed in this paper is 59.4%, 98.9% and 72.3% on the final test set; Using the trained and saved model after fusing two features, the test accuracy on the final test set is 63.6%, 99.4% and 75.5%, respectively. The use of the fused features is 33.3%, 2.3% and 22% higher than using only the deepest features in the original CNN. Compared with the sub-deep features using only the CNN proposed in this paper, it has improved by 26.7%, 1.7% and 16.8%, respectively. It is proved that the convolutional network structure proposed in this paper, which integrates the features of multi-layer convolutional layers, effectively improves the expression recognition rate.

4. Summary and Discussion

The current CNN uses only the last layer of convolutional layer features for facial expression classification, but the effect on expression recognition is not high. This paper proposes a multi-layer convolutional layer feature vector neural network model, which combines the deepest feature vector and sub-deep feature vector of the CNN for facial expression analysis. The experimental results show that the improved network structure proposed in this paper can capture richer feature information, thereby improving the expression recognition rate.

But there are still many parts need to be improved. (1)In this paper, only the deepest feature vector and the penultimate layer feature vector in the CNN are used for feature fusion. According to the use of the features of the convolutional layer by the full CNN, we can also try to use the previous layer or even the first two layers of the sub-deep feature vectors. However, at the same time, the amount of calculation will increase, which needs to be considered comprehensively. (2)Aiming at the problems of low resolution and high error rate of the data set, an expression database can be re-established to improve the expression recognition rate. (3) For the problem of low

discrimination between facial expression classes, the softmax loss function can be researched and changed, so that the CNN is more suitable for facial expression classification.

References

- [1] Haines N, Bell Z, Crowell S, et al. Using automated computer vision and machine learning to code facial expressions of affect and arousal: Implications for emotion dysregulation research[J]. *Development and psychopathology*, 2019, 31(3): 871-886.
- [2] Xin M, Wang Y. Research on image classification model based on deep convolution neural network[J]. *EURASIP Journal on Image and Video Processing*, 2019, 2019(1): 40.
- [3] Liu Q, Zhang J, Xin Y. Face expression recognition based on improved convolutional neural network[C]//Proceedings of the 2nd International Conference on Artificial Intelligence and Pattern Recognition. 2019: 61-65.
- [4] Sun X, Lv M. Facial Expression Recognition Based on a Hybrid Model Combining Deep and Shallow Features[J]. *Cognitive Computation*, 2019, 11(4): 587-597.
- [5] Amin S U, Alsulaiman M, Muhammad G, et al. Multilevel weighted feature fusion using convolutional neural networks for EEG motor imagery classification[J]. *IEEE Access*, 2019, 7: 18940-18950.
- [6] Mollahosseini A, Chan D, Mahoor M H. Going deeper in facial expression recognition using deep neural networks[C]//2016 IEEE Winter conference on applications of computer vision (WACV). IEEE, 2016: 1-10.
- [7] Ding H, Zhou S K, Chellappa R. Facenet2expnet: Regularizing a deep face recognition net for expression recognition[C]//2017 12th IEEE International Conference on Automatic Face & Gesture Recognition (FG 2017). IEEE, 2017: 118-126.
- [8] Szegedy C, Liu W, Jia Y, et al. Going deeper with convolutions[C]//Proceedings of the IEEE conference on computer vision and pattern recognition. IEEE, 2015: 1-9.
- [9] Yoo H J. Deep convolution neural networks in computer vision: a review[J]. *IEIE Transactions on Smart Processing & Computing*, 2015, 4(1): 35-43.
- [10] Al-Qizwini M, Barjasteh I, Al-Qassab H, et al. Deep learning algorithm for autonomous driving using GoogLeNet[C]//2017 IEEE Intelligent Vehicles Symposium (IV). IEEE, 2017: 89-96.
- [11] Nguyen V, Dang T, Jin F. Predict saturated thickness using tensorboard visualization[J]. *Visualization in Environmental Sciences* 2018, 2018.
- [12] Zou J, Rui T, Zhou Y, et al. Convolutional neural network simplification via feature map pruning[J]. *Computers & Electrical Engineering*, 2018, 70: 950-958.
- [13] Tümen V, Söylemez Ö F, Ergen B. Facial emotion recognition on a dataset using convolutional neural network[C]//2017 International Artificial Intelligence and Data Processing Symposium (IDAP). IEEE, 2017: 1-5.
- [14] Lucey P, Cohn J F, Kanade T, et al. The extended cohn-kanade dataset (ck+): A complete dataset for action unit and emotion-specified expression[C]//2010 ieee computer society conference on computer vision and pattern recognition-workshops. IEEE, 2010: 94-101.
- [15] Lyons M J, Akamatsu S, Kamachi M, et al. The Japanese female facial expression (JAFFE) database[C]//Proceedings of third international conference on automatic face and gesture recognition. 1998: 14-16.

Investigation of a Method for EEG Signal De-Noising Based on the DIVA Model

Zhang Shaobai¹, Jiao Lihong and Zhou Ningning

*Computer Department, Nanjing University of Posts and Telecommunications,
Nanjing, Jiangsu 210033, China*

Abstract. The DIVA (Directions Into Velocities of Articulators) model is an adaptive neural network model that is used to control the movement of the analog vocal tract to generate words, syllables, or phonemes. The input signal to the DIVA model is the EEG (electroencephalogram) signal acquired from the human brain. However, due to the influence of power frequency interference and other forms of noise, the input signal can be non-stationary and can also contain a variety of multi-form waveforms in its instantaneous structure. Input of such a signal into the DIVA model affects normal speech processing. Therefore, based on the concept of sparse decomposition, this paper applies and improves an adaptive sparse decomposition model for feature extraction of the general EEG signal structure and then uses the Matching Pursuit algorithm to compute the optimal atom. The original EEG signal can then be represented by atoms in a complete atomic library. This model removes noise from the EEG signal resulting in a better signal than the wavelet transform method. Finally, applies the EEG signal denoised by this model to DIVA model. Simulation results show that the method improves phonetic pronunciation greatly.

Keywords. DIVA model, EEG signal, noise, sparse decomposition

1. Introduction

Research works on various fields (phonetics, control science, robotics, neural physiology) is required in order to accurately simulate and describe functions of brain regions responsible for speech acquisition and production based on neurophysiology and neuroanatomy. A new tool, called the Neuralynx System[1], developed by a team led by Frank Guenther of Boston University, is the most representative and successful among them. The primary feature of this tool is that users only need to think about what they want to express and the speech synthesis system converts their thoughts into speech. The principle is shown in Figure 1.

In Figure 1, black circles and curved arrows represent neurons and axonal projections in the neural circuit for speech motor output, respectively. Signals collected from an electrode implanted in the subject's speech motor cortex are amplified and transmitted wirelessly across the scalp as FM radio signals. The signals are routed to an electrophysiology recording system for further amplification, analog-to-digital

¹ Zhang Shaobai, Nanjing University of Posts and Telecommunications, China; E-mail: adzsb@163.com. This work was supported by the National Natural Science Foundation of China (No. 61271334 & No.61373065)

conversion, and spike sorting. The sorted spikes are sent to a neural decoder which translates them into commands for a speech synthesizer. Audio signals from the synthesizer are fed back to the subject in real time (PrCG represents the precentral gyrus in the brain).

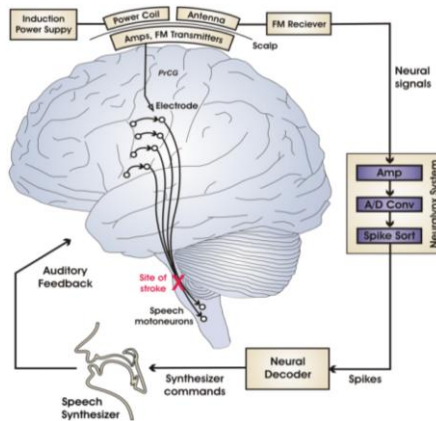


Figure 1. Schematic diagram of Neuralynx System

The Neuralynx System consists of two parts: brain computer interface (BCI) and speech synthesis system DIVA model (Directions Into Velocities of Articulators). BCI is used to achieve communication and control between a human brain and a computer or other electronic device. Input signal is generated from a permanently implanted wireless neural electrode in the cerebral cortex of an aphasia patient that detects generated speech and obtains neural signals from related areas [1, 2]. These signals drive the speech synthesis system to “operate” continuously and provide the patient with real-time speech output. The DIVA model is a biological neural network for generating and obtaining speech [3].

The EEG input signal acquisition process for the DIVA model includes conditioning, sampling, quantization, coding, and transmission. During this process, the EEG signal is non-stationary and can be corrupted by various forms of noise, particularly frequency interference. Input of such an EEG signal into the DIVA model would affect normal speech processing. Therefore, it is necessary to eliminate noise in the original EEG data.

Current de-noising methods include notch filtering, adaptive filtering, and wavelet transform, to name a few. Notch filter leads to EEG waveform distortion [4]. The adaptive filter can automatically track the frequency change for power frequency interference and minimize the loss of useful information, but the frequency tracking range is narrow. The wavelet transform is the most widely used; however, it has drawbacks. For example, the calculation is complex and the choice of wavelet basis and wavelet threshold requires prior knowledge [5-6].

With this in mind, Mallat and Zhang proposed sparse decomposition [7] based on an over-complete dictionary. Based on signal characteristics, sparse signal decomposition can adaptively select the appropriate basis functions to complete signal decomposition. In this process, the over-complete dictionary plays a key role. This paper improves a construction method for an over-complete dictionary by analyzing the structural characteristics of EEG signals and using the matching pursuit algorithm [7, 8] (MP) for sparse decomposition followed by reconstitution. Following this process, the proposed algorithm enhances EEG signal sparsity, performs de-noising, and improves

the speech processing ability of the DIVA model.

2. Diva Model

The DIVA model is an adaptive neural network that describes the processes of speech acquisition and production and generates speech by controlling the simulated voice channel [9,10]. The model is based on behavioral data collected from physical experiments in speech generation and sensory psychology, neuroimaging fMRI data (functional magnetic resonance imaging) and PET (positron emission computed tomography) experiments, and neurophysiology data from motion control experiments in animals. The principle is shown in Figure 2[3].

As shown in Figure 2, the DIVA model consists of a feedforward control subsystem, a feedback control subsystem, and a simulated Maeda vocal tract. By recording the input speech formant frequency during training, the model generates a phonating rate and a time variable sequence that represents positional variations in vocal organs. The model uses this sequence to obtain the required phonations. The feedforward control system is responsible for speech production and the feedback control system is responsible for speech learning. In the feedforward control system, the generation of a phoneme or syllable begins with the activation of a corresponding cell speech map set. Each cell corresponds to a single phoneme or syllable.

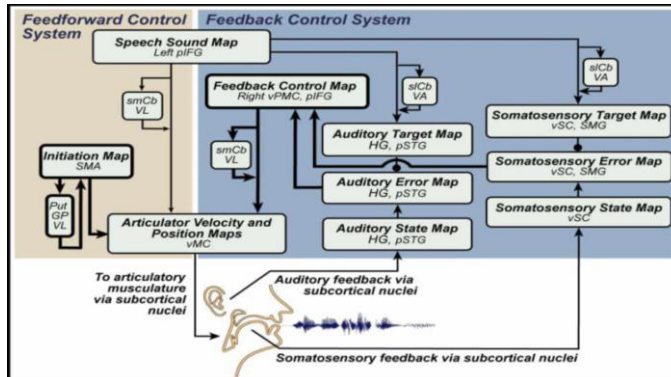


Figure 2. Working wireframes of DIVA model

The DIVA model and fMRI are very closely linked [11]. Various assumptions made by the DIVA model can be tested and demonstrated by applying fMRI experiments. Data obtained from fMRI can also be analyzed and interpreted by the DIVA model. Thus, the DIVA model is a basic framework which can interpret speech neural processes.

3. Sparse Signal Decomposition

The primary aims of signal sparse decomposition are: (1) decompose the signal in the over-complete dictionary, (2) select the base function of the signal adaptively based on signal structural characteristics, and (3) compute correlation coefficients to have only a few non-zero values. Signal sparse decomposition has been successfully applied in many aspects of signal processing, such as signal detection, signal recognition, and

image de-noising. A variety of sparse decomposition algorithms have been developed: MP algorithm (Matching Pursuit) [7,8], BP algorithm (Basis Pursuit)[12], BOB algorithm (Basis Orthogonal Best) [13], and OMP algorithm[14] (Orthogonal Matching Pursuit). BP, and especially MP are the most commonly used.

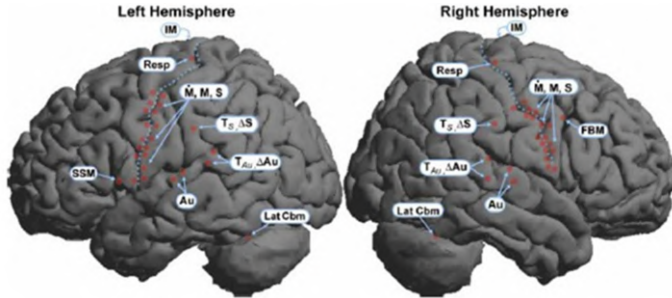


Figure 3. Schematic diagram of neuroanatomy mapping relation to the DIVA model

3.1. MP Algorithm

The Matching Pursuit algorithm (MP) is a signal analysis method that was proposed by Mallet and Zhang in 1993 and belongs to a category of greedy algorithms.

The basic idea is to select the largest component of the correlation coefficients through decomposing the signal in the library (over-complete dictionary). The algorithm gets the sparse representation of the signal through multiple iterative decompositions [15,16]. Implementation of the algorithm can be described as follows:

First, select an over-complete dictionary where $D = \{g_r, r = 1, 2, \dots, M\}$ represents such a collection. Elements of the collection are termed atoms. Each atom can adequately represent the characteristics of the signal. Maintain the over-complete feature amongst the atoms. The so-called overcompleteness is the inner product $\langle g_i, g_j \rangle \neq 0$ between two different atoms g_i and g_j , where $i \neq j$.

The MP algorithm makes the inner product the largest between signal f and the atoms of the over-complete dictionary. This characteristic is regarded as the optimization principle of greedy algorithms [6].

First, select the best atom g_i from dictionary D which satisfies the following condition:

$$|\langle f, g_i \rangle| = \sup_{j \in M} |\langle f, g_j \rangle| \quad (1)$$

where $|\langle f, g_i \rangle|$ is the inner product between signal f and atom g_i .

After selecting g_i , the signal f is decomposed as follows:

$$f = \langle f, g_i \rangle g_i + R^1 f \quad (2)$$

where $\langle f, g_i \rangle$ is the projection of signal f onto the atom g_i , and $R^1 f$ is the residual value after projecting signal f onto g_i (called residual error).

Now, remove the atom g_i from the initial over-complete dictionary because g_i has been used as part of the signal f and will not be used to find the matching atom afterwards; this reduces the amount of computation. Decompose the residual error from

signal f and determine the best atom in the revised over-complete dictionary. The formula can be expressed as follows:

$$R^1 f = \langle R^1 f, g_k \rangle g_k + R^2 f \quad (3)$$

Of course, g_k still needs to be determined as an optimum atom:

$$\langle R^1 f, g_k \rangle = \sup_{j \in M} \langle R^1 f, g_j \rangle \quad (4)$$

After this iterative process, the signal f can be decomposed into:

$$f = \sum_{L=0}^{L-1} \langle R^l f, g_l \rangle g_l + R^L f \quad (5)$$

Mallet proved that the value of $\|R^L f\|$ exponentially converges with increasing L . Thus, the signal f can be approximated by the following decomposition:

$$f \approx \sum_{l=0}^{L-1} \langle R^l f, g_l \rangle g_l \quad (6)$$

The steps above are shown below in Figure 4:

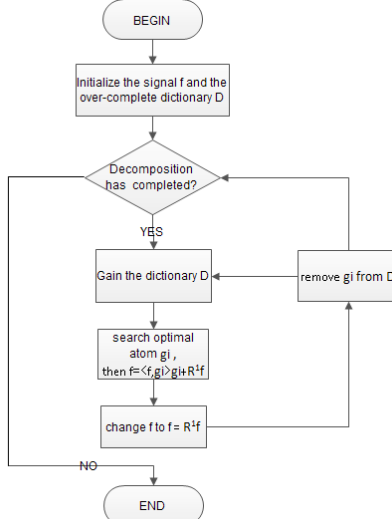


Figure 4. Flow diagram of MP algorithm

3.2. Constructing the Over-complete Dictionary

The Matching Pursuit algorithm decomposes the signal based on a complete library. Constructing the over-complete dictionary is the critical step[17]. This paper constructs a specific over-complete dictionary that would be applicable to EEG signals.

As noted earlier, EEG signals are often corrupted by power frequency interference and other forms of noise during acquisition. This makes the EEG signal non-stationary and yields a variety of multi-form waveforms in its instantaneous structure. Thus, atoms of the single structure type are unable to match the transient EEG waveform effectively. In order to match multi-form waveforms in its instantaneous structure of EEG, the atomic dictionary should contain a variety of structural atoms. In order to extract the feature of EEG signal, reference [18] proposed an SSDM (Structure

Adaptive Sparse Decomposition Model) which is suitable for EEG signal in patients with psychomotor epilepsy. We studies and improves the SSDM model to extract the feature of EEG signal in normal people. The improved SSDM model aims to detect the spike wave automatically. From the view of matching multi-form waveforms in its instantaneous structure of EEG signal, improved SSDM model applies multi-structural atoms to adaptively depose and analyze the general EEG signal which is more suitable for detecting the instantaneous structure of EEG signal. General EEG signal consists of positive phase and negative phase. Small scale Gaussian function can match the single - phase spike wave well and large scale Gaussian function can represent the low frequency component of signal well. Moreover the Gaussian wavelet can match the double-phase spike wave well. We use Gaussian function and its first order derivative as the generating function to design a new multi-component dictionary which differs from the original SSDM model.

$$\begin{aligned}\varphi_r^1(t) &= K_1(r) \exp\left\{-\frac{(t-u)^2}{2s^2}\right\} \\ \varphi_r^2(t) &= K_2(r)\left(\frac{t-u}{s}\right) \exp\left\{-\frac{(t-u)^2}{2s^2}\right\}\end{aligned}\quad (7)$$

where $K_1(r)$, $K_2(r)$ are normalization factors that allow atoms to show the unitized norm, $\varphi_r^1(r)$, $\varphi_r^2(r)$ are Gaussian functions and their first derivatives, and parameter set $r=\{u, s\}$ indicates location and scale characteristics of atoms, respectively. By using transforming methods such as panning and stretching, free variables u and s can be modulated to generate a series of atoms that form a variety of transient and redundant databases which can match the multi-constituent structure.

In reality, free parameters must be sampled to form a discrete atom dictionary in order to sparsely decompose into a discrete digital signal. Discretized atoms may be expressed as:

$$\begin{aligned}\varphi_r^2[n] &= K_1(r) \exp\left\{-\frac{(n-p)^2}{2(a^i)^2}\right\} \\ \varphi_r^2[n] &= K_2(r)\left(\frac{n-p}{a^i}\right) \exp\left\{-\frac{(n-p)^2}{2(a^i)^2}\right\}\end{aligned}\quad (8)$$

where both p and i are integers, $r=\{p, a_i\}$, $p \in [0, N-1]$, $i \in [0, \log_2 N]$ is the discrete set of parameters, and N is the dimension of discrete signals to be decomposed. Generally, $a = 2$ is desired.

The atomic dictionary generated by this improved SSDM is complete and posses the invariance under translation in time and approximate invariance in scale. Moreover the numbers of atomic in improved SSDM are fewer than those in Gabor, which makes the improved SSDM have lower searching complexity and higher sparse decomposing efficiency. This improved SSDM model regard the Gaussian function and Gaussian wavelet as atomic dictionary generating functions which makes the atom structure match the separated instantaneous structure of general EEG signal more closely.

In frequency analysis of the EEG signal, time-frequency structural parameters obtained after sparse decomposition should establish direct contact with the artificial vision analysis criteria. Comparing these time-frequency structural parameters with prior parameters can directly determine whether it is a characteristic EEG signal

waveform. The discrete atomic dictionary designed by this method has explicit morphological structure parameters, such as location, degree, and amplitude.

4. Simulation Experiment

4.1. De-noising Principle

The signal can be separated into the original signal and the noise signal based on whether the correlation coefficient is zero after sparse decomposition. Suppose the original EEG signal with noise is:

$$f = E + N \quad (9)$$

where E is the original signal without noise and N is an independently distributed random noise signal. When applying the MP algorithm in the atomic dictionary, the dictionary is constructed based on the structural characteristics of the EEG signal. Therefore, atom structure must be related to the EEG signal, regardless of noise. The formula can be expressed as:

$$f = \sum_{L=0}^{L-1} \langle R^l f, g_l \rangle g_l + R^L f \quad (10)$$

The first part of the equation is the original EEG signal and the second part is the residual after extracting the EEG signal, i.e., the noise signal. The equation can be compared with the formula:

$$\begin{aligned} E &= \sum_{L=0}^{L-1} \langle R^l f, g_l \rangle g_l \\ N &= R^L f \end{aligned} \quad (11)$$

4.2. Experimental Process and Results Analysis

4.2.1 Experimental Design and Signal Collection

The following experimental data comes from the State Key Laboratory for Cognitive Neuroscience and Learning at Beijing Normal University, which is our collaboration unit.

The subject is a healthy man with experience in EEG acquisition experiments. The experiment uses an electrical scanner and a scanning cap with 128 electrodes to record EEG signals (Figure 5). The sampling frequency of the signal is 1000 Hz. During the process of collecting the EEG signal, the subject's consciousness was clear and he sat on an ordinary chair. The expression of the word “happy” in English was performed 100 times. This experiment was completed in one day.

4.2.2 Experimental Tools

Experimental evaluation uses the EEGLab Toolbox in MATLAB R2010b to read collected EEG signals. The EEGLab Toolbox is a tool for processing EEG data and reading the collected signal waveform.

4.2.3 Pretreating Data

While using the non-invasive acquisition method as described, EOG and muscular movement will degrade the signal. Prior to analyzing the EEG signal, we made use of the ICA (Independent Component Analysis) function in EEGLab to extract the main constituent of effective independence which can remove EOG and muscular movement from the original signal.

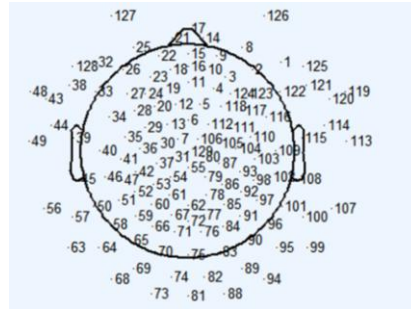


Figure 5. Electrode locations on scanning cap

4.2.4 Construction of SSDM Atom Dictionary and Signal Reconstruction

In sparse decomposition theory, an atomic library has good structure when the following is satisfied: (1) the atomic dictionary contains the most atomic numbers and types possible in order to achieve sparse decomposition and a good sparse decomposition effect and (2) the atomic dictionary doesn't use similar atoms for both storage and computation. When these two criteria are maintained, a good balance is achieved and the structure of the atom dictionary is optimal.

The atom dictionary described above can be used to obtain general atoms for use in sparse decomposition. Figure 6 is a shape schematic for two atoms in which atomic length is 1024. The figure shows concentrated energy in the central region and zero elsewhere. These are representative atoms. Results are consistent with previous work [7].

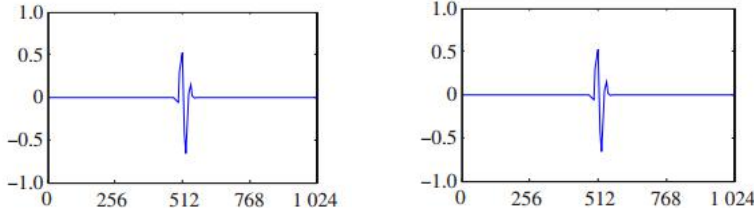
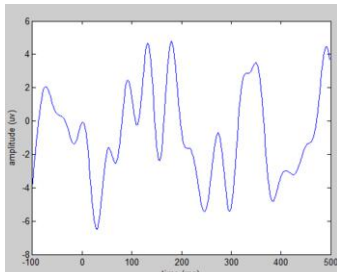
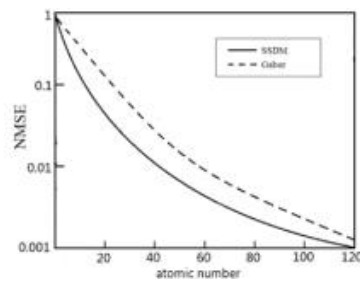
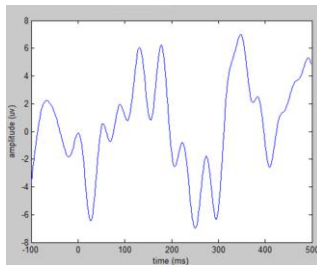
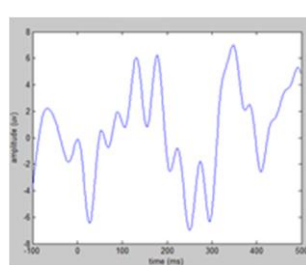
The following verifies the signal reconstruction effect using the SSDM atom dictionary and contrasts it with the Gabor dictionary. First, we intercept the normal EEG signal of the Chinese vowel /a/ after filtering through an EEG database provided by the Brain Research Center at Beijing Normal University.

Figure 7(a) is a normal brain waveform of the Chinese vowel /a/, which is smooth under normal conditions. Figure 7(b) is the waveform graph of the Gabor atom reconstructed vowel /a/ and Figure 7(c) shows the result of the SSDM atom reconstructed vowel /a/. The decomposition and reconstruction of the EEG signal using the SSDM atom dictionary compares well with the Gabor atom dictionary.

Table 1. Time comparison of two dictionaries

Atom dictionary	Gabor	SSDM
Average time /s	218.32	120.76

Since the morphological structure of the atom in SSDM matches each transient structure of the EEG signal more closely, atomic numbers are fewer in SSDM compared with those from the Gabor dictionary. Sparse decomposition efficiency is also improved in SSDM. Table 1 shows the average running time for the signal to reach the optimal result in both methods. Table 1 shows that calculation time is reduced and speed is greatly improved in SSDM.

**Figure 6.** Shapes of two atoms in the SSDM dictionary ($N = 1024$)**Figure 7(a).** Brain waveform of Chinese vowel /a/**Figure 7(b).** Gabor dictionary reconstructed result**Figure 7(c).** SSDM dictionary reconstructed result**Figure 8.** Attenuation graphs of MMSE with an increasing numbers of atoms in the two atom libraries

4.2.5 Comparison of the Matching Pursuit Sparse Approximation Between the SSDM and Gabor

In order to compare the performance of matching pursuit sparse approximation between the SSDM and Gabor, NMSE (normalized mean square error) is used. The formula is:

$$NMSE = \frac{\|s - s'\|_2^2}{\|s\|_2^2} \quad (12)$$

Figure 8 is the attenuation graphs of MMSE with an increasing numbers of atoms in the two atom libraries. It shows that the improved SSDM decays more quickly. Since the improved SSDM consists of multi-structure atoms which can match multi-form waveforms in its instantaneous structure of EEG signal, it owns stronger ability to sparse approximation.

4.2.6 Comparison of the Signal De-noising Effect

Using EEGLab, we can obtain whole pronunciation waveforms during the 2-cycle (Figure 9, provided by the Institute of Cognitive Neuroscience and Learning, Beijing Normal University). We intercept one pronunciation. Since the sampling frequency is 1000 Hz and a pronounced duration is 2 sec, the signal has 2000 sampled points, as shown in Figure 10(a). We now add 50 Hz power frequency interference in which SNR (Signal to Noise Ratio) is 10 dB, 5 dB, -5 dB, and -10 dB, respectively, forming an original signal with noise. Figures 10(b), 10(c) and 10(d) are waveforms processed through the improved SSDM atom library, Gabor atom library and traditional wavelet transform method. It shows that the effect of de-noising based on the two atom libraries is better than wavelet transform method. Moreover the de-noising result of the SSAM is better compared to Gabor atom library. The wavelet transform removes effective constituents as noise.

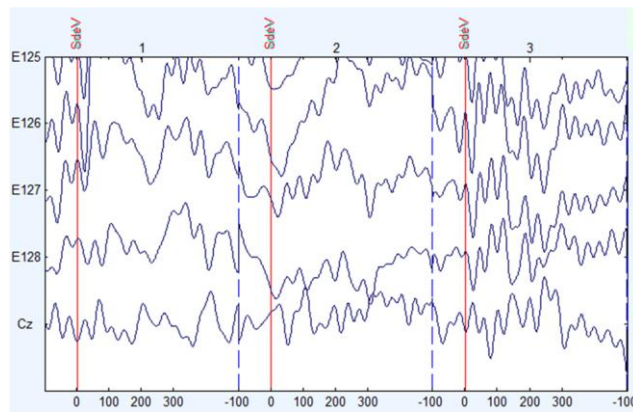


Figure 9. Disposing schematic diagram through EEGLab

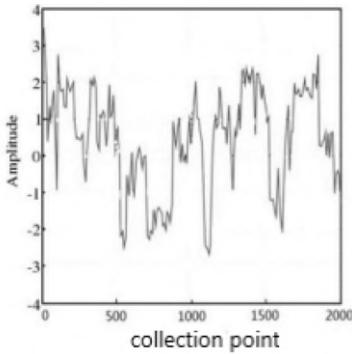


Figure 10(a). Received pronunciation of English word “happy”

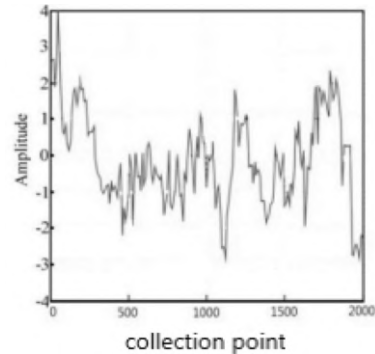


Figure 10(b). SSDM atom library method

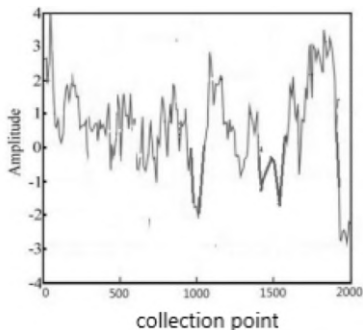


Figure 10(c). Gabor atom library method

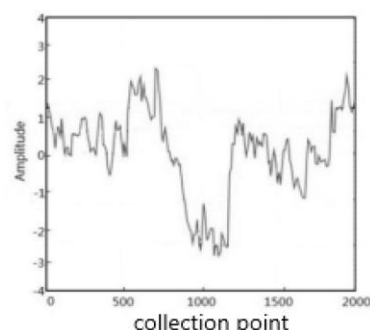


Figure 10(d). Wavelet transform method

The waveform obtained through the SSDM atom library maintains the original waveform component better. In order to assess the three de-noising methods, we evaluate RMSE (Root Mean Square Error) and the effect of SNR. The formula is:

$$RMSE = \sqrt{\frac{1}{N} \sum_{i=1}^N (X_1(n) - X_2(n))^2}$$

$$SNR = 10 \log_{10} \left[\sum_{n=0}^{N-1} \frac{X_1^2(n)}{(X_1(n) - X_2(n))^2} \right] \quad (13)$$

where $X_1(n)$ is the input signal, $X_2(n)$ is the output signal, and N is the dimension of the signal. Table 2 shows the results of the comparison. SNR1 and RMSE1 are the Signal to Noise Ratio and Root Mean Square Error of the SSDM method. SNR2 and RMSE2 are for the Gabor method while SNR3 and RMSE3 are for the wavelet transform method.

Table 2. SNR and RMSE for the SSDM, Gabor and wavelet transform methods.

	SNR1	SNR2	SNR3	RMSE1	RMSE2	RMSE3
10dB	18.9209	15.9281	14.1826	0.0015	0.0103	0.0181
5dB	20.7410	18.2377	15.1293	0.0014	0.0099	0.0192
-5dB	23.3201	22.3230	14.0291	0.0016	0.0143	0.0314
-10dB	18.4029	15.2915	16.1082	0.0025	0.0348	0.0532

Table 2 shows that to different intensity noise, the SNR of SSDM and Gabor improve compared with wavelet method. Furthermore, the RMSE of SSDM reduces

which means that the EEG signal recovered by SSDM is highly similar to the original EEG signal. Overall, the order of de-noising quality is: SSDM>Gabor>wavelet.

4.3. Speech Processing Ability of the Improved DIVA Model

4.3.1 DIVA Model Interface

When applying the DIVA model to evaluate pronunciation function, the system presents a user interface to allow users to control the pronunciation mechanism as shown in Figure 11. The interface can be divided into three parts: control module, acoustic characterization space module, and vocal tract control module.

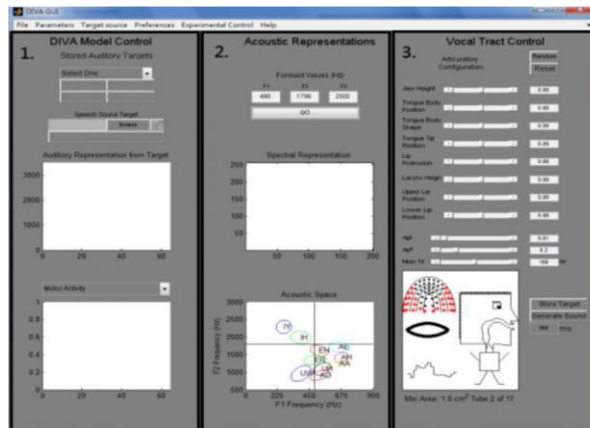


Figure 11. User interface of DIVA model

4.3.2 Flow Chart of DIVA Speech Sound Map Module

Figure 12 shows a flowchart of the DIVA speech sound map module, which is part of the control module section in the DIVA model interface. During a simulation experiment, relevant information must be entered through this module and the input port parameters can be modified.

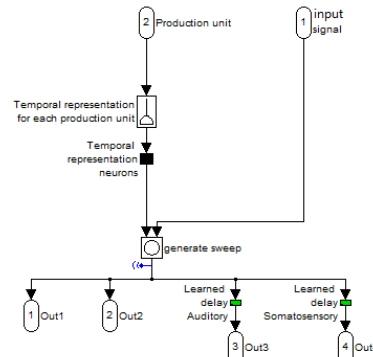


Figure 12. Speech sound map module of DIVA model

4.3.3 Comparison of Result Precision

We input speech learning samples of varying difficulty before de-noising and then enter the de-noised data into the DIVA model. Figure 13 shows comparative results of phonetic pronunciation accuracy in the model. Overall, speech pronunciation accuracy of the DIVA model increases when the de-noised signal is used compared to processing the signal with noise. For example, with normal difficulty speech learning samples containing noise, pronunciation accuracy is about 80% on average, while phonetic pronunciation accuracy can reach 90% after the signal is de-noised. Noise in the EEG signal affects the speech processing ability of the DIVA model.

Besides, the experiment results show that the EEG signal de-noised by Gabor atom dictionary and wavelet can also improve speech pronunciation accuracy of the DIVA model. Since the noise reduction effect by these two methods is less than SSDM, the improved extent in speech pronunciation of the DIVA model is limited compared with the SSDM. Furthermore, atomic numbers are much more in Gabor than in SSDM dictionary which makes the de-noising efficiency based on Gabor dictionary is lower than SSDM dictionary.

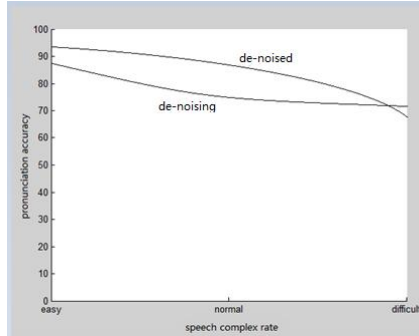


Figure13. Comparative result of speech pronunciation accuracy percent between noisy and de-noised signal

5 Conclusion

This paper studies and improves an adaptive sparse decomposition model (SSDM) which is more suitable for the general EEG signal. Moreover, it applies the EEG signal de-noised by the improved SSDM to DIAV model. Simulation results show that the proposed method removes significant noise and is able to retain active components in the EEG signal. The de-noising effect is better. Meanwhile, the proposed algorithm improves speech pronunciation accuracy of the model by using a de-noised EEG signal for learning samples. This study provides a foundation to improve the speech processing capability of the DIVA model which can better describe and simulate related functions of brain regions involved in speech production and comprehension based on neuroanatomy and neuropsychology.

References

- [1] Guenther, F.H., Brumberg, J.S., Wright, E.J., Nieto-Castañon, A wireless brain-machine interface for real-time speech synthesis[J]. PLoS ONE, 2009, 4 (12), e8218.

- [2] Brumberg, J.S., Nieto-Castanon, A., Kennedy, P.R. and Guenther, F.H. Brain-computer interfaces for speech communication [J]. Speech Communication, 2010, 52 (4), 367-379.
- [3] Tourville, J.T. and Guenther, F.H., The DIVA model: A neural theory of speech acquisition and production[J]. Language and Cognitive Processes. 2011, 25(7):952-981.
- [4] Du Xiaoyan, Li Yingjie, Zhu Yisheng, Ren Qiushi, Zhao Lun. Removal of Artifacts from EEG Signal[J].Journal of Biomedical Engineering, 2008, 25(2). 464-471.
- [5] Poornachandra S. Wavelet-based denoising using subband dependent threshold for ECG signals [J]Digital Signal Processing, 2008, 18(1) : 49-55
- [6] CHEN Ren-xiang, TANG Bao-ping, LV Zhong-liang. De-noising method based on correlation coefficient for EEMD rotor vibration signal[J]. Journal of Vibration, Measurement & Diagnosis, 2012, 32(4):542-546
- [7] Mallat S, Zhang Z. Matching pursuit with time-frequency dictionaries [J]. IEEE Trans on Signal Processing, 1993, 41(12):3397-3415.
- [8] Chen S, Donoho D, Saunders M. Atomic decomposition by basis pursuit[J]. SIAM J Sci Comput, 1999, 20:33-61.
- [9] Zhang shaobai, Ji yanchun.Research on the Mechanism for Phonating Stressed English Syllables Based on DIVA Model[J]. Neurocomputing. 2015, Vol.152(3),11-18.
- [10] Shaobai zhang, Liqin gao, Application of Feedforward and Feedback Control Strategy in the Speech Acquisition and Production Model [J]. Springer, Lecture Notes in Electrical Engineering, Dec.,2011,Vol.123, 489-494.
- [11] Guenther, F.H., Cortical interactions underlying the production of speech sounds [J], Journal of Communication Disorders, 2006, Vol.39(5), 350-365.
- [12] Bohland, J.W., and Guenther, F.H., An fMRI investigation of syllable sequence production [J], NeuroImage, 2006, 32(2), 821-841.
- [13] Coifman R, Wickerhauser M. Wickerhauser, Entropy-based algorithms for best-basis selection[J]. IEEE Transactions on Information Theory, 1992, 38: 713-718.
- [14] Cai T Tony, Wang Lie. Orthogonal matching pursuit for sparse signal recovery with noise [J]. IEEE Transactions on Information Theory, 2011, 57(7):4680-4688.
- [15] Zhang chenmei, Ying zhongke, Xiaomingxia. Over-complete representation and sparse decomposition of signal based on the redundant dictionary had [J]. Chinese Science Bulletin, 2006(6):628-633
- [16] Davis G, Mallat S, Avellaneda M. Adaptive greedy approximation [J]. Constr Approx, 1997, 13(1):57-98
- [17] D Donoho,X Huo. Uncertainty principles and ideal atomic decomposition [J]. Information Theory, IEEE Trans, 2001, 47(7):2845-2862.
- [18] Wu ming, Automatic Detection of Epileptic Characteristics in EEG Signals based on Sparse Representation and the Design of an Application System [D], Doctoral Dissertation : Nanjing University of Science and Technology, 2010.

Origin and Evolution of Conceptual Differences Between Two Measurement Theories

Shi Huisheng^a, Ye Xiaoming^{b1}, Xing Cheng^b, Ding Shijun^b

^aAVIC Changcheng Institute of Metrology & Measurement, Beijing, 100095, China

^bSchool of Geodesy and Geomatics, Wuhan University, Wuhan, Hubei, 430079, China

Abstract. In several published literatures, some new measurement concepts have been proposed to reinterpret measurement theory, which leads to a new interpretation method of measurement theory. By directly comparing the measurement concept differences between the new theory and the traditional theory, this paper reveals that the root of these differences is due to the different understanding of the mathematical concept of random variable, and clarifies the evolution process of other conceptual differences. Also, by reviewing the mathematical concept, it points out that the traditional theory has been gone astray, and the concept of error classification is actually the product of going astray, while the new concept theory should get active attention and research.

Keywords. Measurement; measurement error; random variable; variance; uncertainty

1. Introduction

Traditional measurement theory interprets its measurement concepts according to the logic of error classification, which is showed in various measurement specifications [1][2][3][4][5] and textbooks[6][7][8]. However, in several published literatures, some new measurement concepts have been proposed to reinterpret the measurement theory, which leads to a new interpretation method of measurement theory in which error has no classification[9][10][11][12][13][14]. Reference [9] is the first to criticize the error classification philosophy in a negative way. Reference [10] proposes that there are no systematic and random categories of errors, any error has its variance which is used to evaluate its probability interval, the change of measurement conditions is the source of the dispersion of repeated measured values, and so on. Reference [11] further pointed out that the regularity and randomness of errors are due to different perspectives of observing errors, and both functional model and random model can be used to handle errors. Reference [12] makes a comparative discussion on the explanation of the concept of variance, which proves that the concept of dispersion of measured value in traditional theory is incorrect. References [13][14] provide a relatively complete

¹ Corresponding Author: Ye Xiaoming, School of Geodesy and Geomatics, Wuhan University, Wuhan, Hubei, 430079, China; Email: xmye@sgg.whu.edu.cn

interpretation of measurement theory mathematically based on these new concepts.

However, because the traditional measurement concepts have been deeply rooted in people's minds and many measurement scientists are also difficult to return to the probability theory and rethink the measurement concepts, few people believe that there are conceptual troubles in traditional theories, so that people usually despise these new concepts. Therefore, for the two measurement theories with opposite concepts, it is necessary to dig out the core difference between the two theories and clarify the evolution of the conceptual differences between them, so as to demonstrate which theory is correct.

From the mathematical concept, this paper will conduct a direct comparative study on the source of the basic concepts of the two theories, and show the complete evolution process of the conceptual differences between them, so that readers can have a complete understanding of the formation process of the concept logic of measurement theory. Besides, by reviewing the mathematical concepts, the paper will make readers understand that the traditional theory has been gone astray in the mathematical concept, and the concept of error classification is actually the product of going astray, while the new concept theory should be a new topic that needs active attention and research.

It should be noted that the traditional concepts discussed in this article refer to the mainstream concepts recognized by various measurement standards [1][2][3][4][5]. Although there are actually many literatures that have put forward some concepts beyond the mainstream, because they are not universally recognized and are also different from the new concept theory, this article will not discuss them.

2. Difference in Understanding of the Concepts of Constant and Random Variable

The conceptual differences between the two theories originate from different understandings of mathematical concepts. That is, they have a completely different understanding of the concept of constant and random variable. See Table 1.

Table 1 Different understanding of mathematical concepts in two theories

	Traditional theory	New concept theory
Constant	True value and systematic error	Measured value
Random variable	Random error and measured value	Error and true value

The traditional measurement theory uses Fig 1 to interpret its measurement concepts.

Because people notice that measured values are in a state of random change in repeated measurement, the measured value and random error are considered as random variables, and the variance is assigned to the measured value and random error. Besides, it is noted that the systematic error and the true value are constant in repeated measurement, so the systematic error and the true value are considered as constants and are considered to have no variance (or the variance is zero).

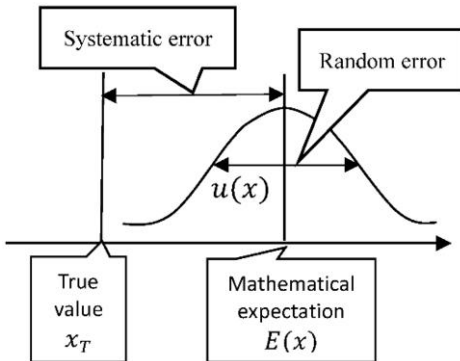


Fig 1. Conceptual sketch of traditional theory

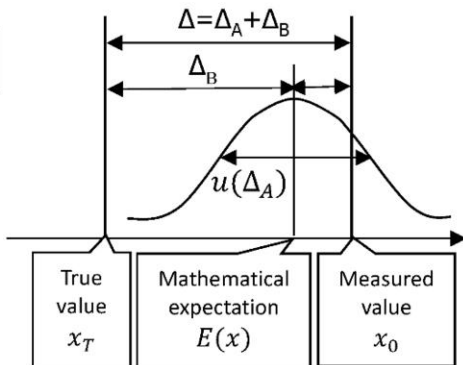


Fig 2. Conceptual sketch of new concept theory

However, this understanding is inconsistent with the concept of probability theory. Therefore, the traditional measurement theory has two troubles in mathematical concepts.

At first, the measured value or observed value in any measurement is expressed by a numerical value, so classifying the measured value or observed value as a random variable actually violates a basic mathematical concept that the variance of a constant is 0.

For example, China National Bureau of Surveying and Mapping announced that the height of Everest is $x = 8844.43m$, and its precision was $u(x) = \pm 0.21m$. However, because equation $x = 8844.43$ clearly indicates that x is a constant 8844.43 instead of a random variable, when we substitute equation $x = 8844.43$ into equation $u(x) = \pm 0.21$, we will find that the equation $u(x) = \pm 0.21$ actually expresses a wrong equation $u(8844.43) = \pm 0.21$. Even though repeated measurements may obtain many other measured values x_1, x_2, \dots , and there can be $x \neq x_1 \neq x_2 \neq \dots$, the equations $x = 8844.43m$ and $u(x) = u(8844.43) = \pm 0.21$ still exist and cannot be explained.

Another example, in Section 5.17 of reference [2] and Section 4.2 of reference [3], a method process is described as follows:

When there are n observed values x_k , the final measured value is

$$\bar{x} = \frac{1}{n} \sum_{k=1}^n x_k \quad (2-1)$$

The variance of each measured value x_k is

$$u^2(x_k) = \frac{1}{n-1} \sum_{j=1}^n (x_j - \bar{x})^2 \quad (2-2)$$

The variance of the final measured value is

$$u^2(\bar{x}) = \frac{u^2(x_k)}{n} \quad (2-3)$$

Similarly, although formula (2-1) has clearly defined that x_k and \bar{x} are numerical values and are constants, formulas (2-2) and (2-3) still assigns them a variance that is not zero.

In probability theory, a constant is a numerical value, such as 20, 300, $x=8844.43$, and so on. Unlike constants, the random variable has no a certain value, but all its possible values (sample space) exist dispersedly within an interval on the number axis. In order to describe and study random variables, people define two parameters: mathematical expectation and variance.

For a random variable $L \in \{L_i\}$, its mathematical expectation is the average of all its possible values $\{L_i\}$. That is:

$$E(L) = \sum_{i=1}^n P_i L_i \quad \text{or} \quad E(L) = \int_{-\infty}^{+\infty} LP(L)dL \quad (2-4)$$

And its variance is the dispersion of all its possible values $\{L_i\}$. That is:

$$u^2(L) = E[L - E(L)]^2 \quad (2-5)$$

The meaning of definitions (2-4) and (2-5) is that although the value of random variable L is unknown, it exists within a probability interval with $E(L)$ as the center and $u^2(L)$ as the width evaluation. In other words, mathematical expectation $E(L)$ and variance $u^2(L)$ are the evaluation values of the probability interval of the random variable L .

Because all possible values of a constant C (a numerical value) are itself, there are $E(C) = C$ and $u^2(C) = 0$. Obviously, it is incorrect that traditional measurement theory assigns a non-zero variance to a numerical value, and its root cause is that the relationship $L \in \{L_i\}$ between the random variable L and the sample L_i is ignored, so that $u^2(L) = E[L - E(L)]^2$ is written as $u^2(L_i) = E[L - E(L)]^2$.

Secondly, according to probability theory, as the numerical description of a random variable, mathematical expectation and variance are two indispensable parameters, and a constant can also be expressed by them. However, the traditional measurement theory cannot give the mathematical expectations of the measured value, systematic error and true value (Shown in Table 2 [13]), which actually means that the probability evaluation of error or true value is not completely described.

Table 2. The conceptual troubles in the traditional theory

	Measured value x	Random error $x - E(x)$	Systematic error $E(x) - x_T$	True value x_T
Mathematical expectation	Absent	0	Absent	Absent
Variance	$u^2(x)$	$u^2(x)$	0	0

Different from the traditional theory, the new concept theory uses Fig. 2 to interpret its measurement concepts.

In this conceptual interpretation, the constant is a known numerical value which represents a unique point on the number axis, but the random variable is an unknown value which exists within an interval on the number axis. Also, the mathematical expectation and variance are the average and dispersion of all possible values of a random variable respectively, express the probability interval in which the value of the

random variable exists, and are the parameters that express the uncertainty of the random variable. In this way, as a numerical value, the measured value x_0 is a constant without dispersion, the random variables are error and true value (Shown in Table 3 [12] [13]). Also, the mathematical expectation and variance of error are the average and dispersion of all possible values of error respectively.

Table 3. The conceptual interpretations in new concept theory

	Measured value x_0	Error Δ	True value x_T
Mathematical expectation	x_0	0	x_0
Variance	0	$u^2(\Delta)$	$u^2(\Delta)$

In this way, the expressions of the above Everest elevation case are $x_0 = 8844.43m$ and $u(\Delta) = \pm 0.21m$, and the formulas (2-2) and (2-3) are proved to be

$$u^2(\Delta x_k) = \frac{1}{n-1} \sum_{j=1}^n (x_j - \bar{x})^2 \quad \text{and} \quad u^2(\bar{\Delta x}) = \frac{u^2(\Delta x_k)}{n}, \quad \text{respectively (where } \Delta x_k = x_k - E(x), \bar{\Delta x} = \bar{x} - E(x)).$$

The keys of this interpretation are that the current measured value x_0 and all possible measured values $\{x_i\}$ are two different concepts. That is, although the current measured value x_0 is a sample within all possible measured values $\{x_i\}$, it is still a constant because it is a numerical value, and only unknown quantities, such as error and true value, need to be expressed with probability. In this way, all possible measured values $\{x_i\}$ are only used to evaluate the error, not need to be used to "evaluate" the current measured value x_0 , and there is no such trouble as equation $u(8844.43) = \pm 0.21$.

3. Difference in Understanding of Error Classification

Because of different understandings for the concepts of the constant and random variable, other conceptual differences arrive one after another. The first conceptual difference is that the traditional theory classifies errors as systematic errors and random errors, but the new concept theory holds that the error has no such classifications.

It can be seen from Fig. 1 that because it is noticed that the measured values are dispersed around the mathematical expectation but the mathematical expectation deviates from the true value, the traditional theory develops its theory according to the conceptual logic of error classification.

Because the random error can be evaluated by the variance, but the systematic error has no variance, people make two concepts of precision and trueness to evaluate them respectively. Because the value of the systematic error is unknown, the trueness can be only a qualitative concept. Besides, because the trueness and precision cannot be combined, as their general name, the accuracy is also a qualitative concept[1][2]. In other words, the total error of a measured value cannot be evaluated quantitatively (as shown in Table 2).

However, from Fig. 3, because the measured value x_0 is a constant, not only the mathematical expectation $E(x)$ deviates from the true value x_T , but also the measured value x_0 deviates from the mathematical expectation $E(x)$. That is, both Δ_A and Δ_B

are unknown deviations. Also, not only Δ_A have all its possible values to obtain its variance, but also Δ_B too, so they are considered to have no systematic/random classifications. Therefore, there is no conceptual difference between the precision and trueness. Only the uncertainty is needed to describe the probability interval of error in error evaluation [10][12][14].

In this way, the conceptual logic of the two theories develops in two completely different directions.

4. The Regularity and Randomness of Error

As we all know, the traditional theory holds that the systematic error has certain regularity, but the random error is random.

However, for the regularity and randomness of errors, the interpretation of the new theory is also different from that of the traditional theory [10][11][12][13][14]. That is, the regularity and randomness come from different perspectives of observing all possible values of error. The regularity refers to the functional relationship between all possible values of error and measurement conditions, but the randomness refers to the density distribution of all possible values of error.

Fig. 3, Fig.4, Fig.5 and Fig.6 are schematic diagrams of the regularity and randomness of four typical errors. In this way, any error has variance to evaluate its probability range. It is all correct to use the function model and the random model to deal with the error [11][14], which completely negates the error classification theory.

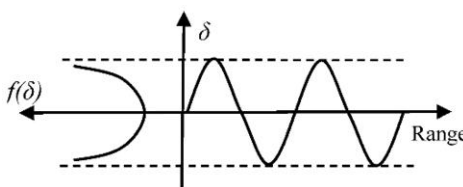


Fig 3. Regularity and randomness of periodic error in geodimeter

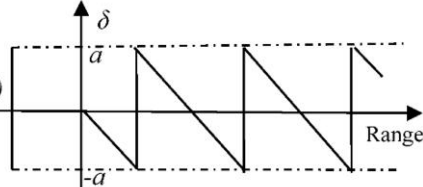


Fig 4. Regularity and randomness of rounding error

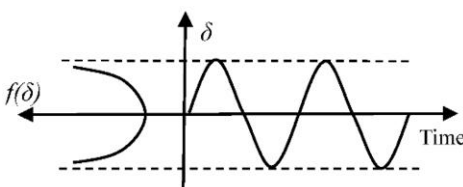


Fig 5. Regularity and randomness of AC interference error in DC voltage measurement

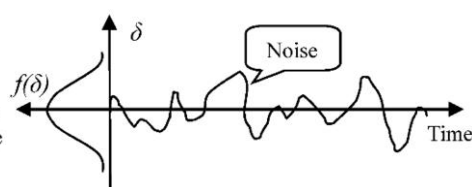


Fig 6. Regularity and randomness of noise error

5. The Principal Interpretation of Deviation, Dispersion and Outlier

The traditional theory holds that the systematic error leads to the deviation, the random error leads to the dispersion, and gross error leads to the outlier. However, on the contrary, the new concept theory also gives a completely different interpretation. [10][11][13][14]

First of all, the new concept theory distinguishes the influence of error on the repeated observed values from that on the final measured value. Because the final measured value is a constant, the influence of any error on it is a deviation.

Secondly, the influence of errors on repeated observations is determined by the change characteristics of measurement conditions, because there are always some changes of measurement conditions in repeated measurements. When the measurement conditions associated with error vary with the repeated measurements, the corresponding error must change and lead to the dispersion; when the measurement conditions associated with error remain unchanged, the corresponding error must also remain unchanged and lead to the deviation; when the measurement conditions associated with error change extremely unbalanced, the corresponding error must change unevenly and lead to the outliers.

We can take the errors in Fig 3 and Fig 4 as examples. If the range condition remains unchanged in the repeated measurements, the two errors must remain constant and contribute to the deviation; if the range conditions vary with the repeated measurements, the two errors will inevitably change and contribute to the dispersion; if the range condition changes unevenly in repeated measurements, the two errors will inevitably change unevenly and contribute to the outliers.

The errors in Fig 5 and Fig 6 can be taken as other examples. If the time remains unchanged in the repeated measurements, the two errors must remain constant and contribute to the deviation; if the time varies with the repeated measurements, the two errors will inevitably change and contribute to the dispersion; if the time changes unevenly in the repeated measurements, the two errors will inevitably change unevenly and can contribute to the outliers.

In addition, there is also a form of influence in which the systematic and random influence coexist. Also, the degree of influence can be divided into strength and weakness, as well as non-influence.

For example, in Fig. 3 and Fig. 5, if the repeated measurements only lead to the phase changes among $0\sim\pi$, these two errors not only cause the dispersion, but also cause the deviation.

Therefore, the reason why the repeated test values in Fig 1 and Fig 2 present density distribution is actually due to the change of repeated measurement conditions, rather than the interpretation of error classification in traditional theory. The most common measurement conditions are: time, range, temperature, instrument, internal working state of the instrument, measuring personnel, instrument placement, route, alignment and so on. There is no "the same condition" for the repeated measurements, and the statistical evaluation of error requires to collect error samples equally under all possible measurement conditions.

6. Covariance Propagation Law

The traditional theory holds that only random errors have the variance and covariance, and the covariance propagation law is interpreted as the propagation relationship between the dispersions of the measured values.

However, according to the new concept theory, the variance is the evaluation value of probability interval of error, which is expressed by the dispersion of all possible values of error. Because any error has all its possible values to obtain its variance, there must be a covariance between any two errors to describe the correlation between all possible values of them. That is, $u(\Delta x_i \Delta x_j) = E(\Delta x_i \Delta x_j)$, which actually comes from the variance of common component contained in two errors.

In this way, for an error sequence $\Delta \mathbf{X} = (\Delta x_1 \quad \Delta x_2 \quad \dots \quad \Delta x_t)^T$, the definition of the variance is

$$\mathbf{U}(\Delta \mathbf{X}) = E(\Delta \mathbf{X})(\Delta \mathbf{X})^T \quad (6-1)$$

In this way, for a linear error propagation equation $\Delta \mathbf{Z} = \mathbf{K} \cdot \Delta \mathbf{X}$, according to the definition of the variance, there is:

$$\mathbf{U}(\Delta \mathbf{Z}) = \mathbf{K} \cdot \mathbf{U}(\Delta \mathbf{X}) \cdot \mathbf{K}^T \quad (6-2)$$

That is, the covariance propagation law is the propagation law of probability intervals between the errors, instead of the propagation law of dispersions between the measured values interpreted by the traditional theory.

7. Uncertainty Concept

Although the concept of uncertainty has been applied to the interpretation of traditional measurement theory [3] [4], it is also defined as the dispersion of the measured values (similar to the precision) because it is derived from analysis of variance. Therefore, the logical relationship between it and other measurement concepts has become a difficult problem.

The concept of uncertainty interpreted by the new concept theory is also completely different from that interpreted by the traditional theory.

In Fig 2, there is $\Delta = \Delta_A + \Delta_B$ (7-1)

According to the covariance propagation law (6-2), there is

$$u^2(\Delta) = u^2(\Delta_A) + u^2(\Delta_B) \quad (7-2)$$

The standard deviation $u(\Delta)$ is the uncertainty of error Δ , which is the evaluation value of probability interval of deviation Δ , and is used to describe the degree we cannot know the value of deviation Δ . Obviously, this uncertainty concept is totally different from the dispersion of measured value interpreted by the traditional measurement theory.

Formula (7-2) is actually a special case of applying the law of covariance propagation to direct repeated measurements. For various indirect measurements, this A/B classification interpretation is not very practical, but it will be simple to use the law of covariance propagation directly [13] (Shown in the case in the next section).

8. Case Comparison

Here, a simple practical case is used to compare the difference between the two theories.

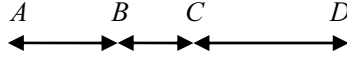


Fig 7. Distances measurement

For example, four points A, B, C and D are located on a straight line, as shown in Fig 7, and the distances obtained by a geodimeter [15] are shown in Table 4. Please solve the final measured values of each baseline and their quality evaluation.

Table 4. Observation values

	Line segment	Observation value
1	AB	x_1
2	BC	x_2
3	CD	x_3
4	AC	x_4
5	BD	x_5
6	AD	x_6

Using y_1 , y_2 and y_3 to express the final measured values of AB, BC and CD respectively, and using k to express the measured value of the additive constant error of geodimeter, the error equations are as follows:

$$\begin{pmatrix} v_1 \\ v_2 \\ v_3 \\ v_4 \\ v_5 \\ v_6 \end{pmatrix} = \begin{pmatrix} x_1 \\ x_2 \\ x_3 \\ x_4 \\ x_5 \\ x_6 \end{pmatrix} - \begin{pmatrix} 1 & 0 & 0 & 1 \\ 0 & 1 & 0 & 1 \\ 0 & 0 & 1 & 1 \\ 1 & 1 & 0 & 1 \\ 0 & 1 & 1 & 1 \\ 1 & 1 & 1 & 1 \end{pmatrix} \begin{pmatrix} y_1 \\ y_2 \\ y_3 \\ k \end{pmatrix} \quad (8-1)$$

According to the least square method, the final measured values are:

$$\begin{aligned} \begin{pmatrix} y_1 \\ y_2 \\ y_3 \\ k \end{pmatrix} &= \left[\begin{pmatrix} 1 & 0 & 0 & 1 & 0 & 1 \\ 0 & 1 & 0 & 1 & 1 & 1 \\ 0 & 0 & 1 & 0 & 1 & 1 \\ 1 & 1 & 1 & 1 & 1 & 1 \end{pmatrix} \begin{pmatrix} 1 & 0 & 0 & 1 \\ 0 & 1 & 0 & 1 \\ 0 & 0 & 1 & 1 \\ 1 & 1 & 0 & 1 \\ 0 & 1 & 1 & 1 \\ 1 & 1 & 1 & 1 \end{pmatrix}^{-1} \begin{pmatrix} 1 & 0 & 0 & 1 & 0 & 1 \\ 0 & 1 & 0 & 1 & 1 & 1 \\ 0 & 0 & 1 & 0 & 1 & 1 \\ 1 & 1 & 1 & 1 & 1 & 1 \end{pmatrix} \right] \begin{pmatrix} x_1 \\ x_2 \\ x_3 \\ x_4 \\ x_5 \\ x_6 \end{pmatrix} \\ &= \frac{1}{4} \times \begin{pmatrix} 1 & -2 & -1 & 1 & -1 & 2 \\ -2 & 1 & -2 & 1 & 1 & 1 \\ -1 & -2 & 1 & -1 & 1 & 2 \\ 2 & 2 & 2 & 0 & 0 & -2 \end{pmatrix} \begin{pmatrix} x_1 \\ x_2 \\ x_3 \\ x_4 \\ x_5 \\ x_6 \end{pmatrix} \end{aligned} \quad (8-2)$$

For the two measurement theories, the above processes are the same, but the difference between them lies in the submission process of the variance.

According to the concept in the traditional theory, the next steps are: 1. the values of each residual v_i are obtained by substituting equation (8-2) into equation (8-1); 2.

$u(x)$ is obtained by using Bessel formula $u(x) = \sqrt{\frac{\sum_{i=1}^n v_i^2}{n-t}}$; 3. the precisions $u(y_1)$, $u(y_2)$ and $u(y_3)$ are calculated by using the covariance propagation law.

However, according to the new concept theory, there are three conceptual troubles in the above process: 1. Bessel formula cannot be used, because the value of freedom degree $n-t$ is too small. 2. The variances of the observed value x_i and the measured value y_j should be zero, because they are all constants. 3. The correlation (covariance) between observation errors is not considered at all.

The variance submission method in the new concept theory is as follows.

Taking total differential of equation (8-2), a complete error propagation equation is:

$$\begin{pmatrix} \Delta y_1 \\ \Delta y_2 \\ \Delta y_3 \\ \Delta k \end{pmatrix} = \frac{1}{4} \times \begin{pmatrix} 1 & -2 & -1 & 1 & -1 & 2 \\ -2 & 1 & -2 & 1 & 1 & 1 \\ -1 & -2 & 1 & -1 & 1 & 2 \\ 2 & 2 & 2 & 0 & 0 & -2 \end{pmatrix} \begin{pmatrix} \Delta x_1 \\ \Delta x_2 \\ \vdots \\ \Delta x_6 \end{pmatrix} \quad (8-3)$$

Applying the law of covariance propagation to equation (8-3), a complete covariance propagation equation is:

$$\begin{pmatrix} u_{\Delta y_1}^2 & u_{\Delta y_1 \Delta y_2} & u_{\Delta y_1 \Delta y_3} & u_{\Delta y_1 \Delta k} \\ u_{\Delta y_1 \Delta y_2} & u_{\Delta y_2}^2 & u_{\Delta y_2 \Delta y_3} & u_{\Delta y_2 \Delta k} \\ u_{\Delta y_1 \Delta y_3} & u_{\Delta y_2 \Delta y_3} & u_{\Delta y_3}^2 & u_{\Delta y_3 \Delta k} \\ u_{\Delta y_1 \Delta k} & u_{\Delta y_2 \Delta k} & u_{\Delta y_3 \Delta k} & u_k^2 \end{pmatrix} = \frac{1}{16} \times \begin{pmatrix} 1 & -2 & -1 & 1 & -1 & 2 \\ -2 & 1 & -2 & 1 & 1 & 1 \\ -1 & -2 & 1 & -1 & 1 & 2 \\ 2 & 2 & 2 & 0 & 0 & -2 \end{pmatrix} \mathbf{U}(\Delta \mathbf{X}) \begin{pmatrix} 1 & -2 & -1 & 2 \\ -2 & 1 & -2 & 2 \\ -1 & -2 & 1 & 2 \\ 1 & 1 & -1 & 0 \\ -1 & 1 & 1 & 0 \\ 2 & 1 & 2 & -2 \end{pmatrix} \quad (8-4)$$

Next, the acquisition method of $\mathbf{U}(\Delta \mathbf{X})$ is as follows.

For the observation x_i , its error Δx_i consists of three components: the additive constant error K , the multiplicative constant error R and the non-uniform indexing error c_i . That is:

$$\Delta x_i = K + R \cdot x_i + c_i \quad (8-5)$$

Its variance is

$$u_{\Delta x_i}^2 = u_K^2 + x_i^2 \cdot u_R^2 + u_c^2 \quad (8-6)$$

Among equation (8-6), the values of u_K , u_R and u_c , which are the dispersions of all possible values of errors K , R and c_i respectively, come from the tolerance standard in the instrument specification or instrument instruction. Further, according to the definition of variance, there is:

$$\begin{aligned}
 \mathbf{U}(\Delta\mathbf{X}) &= E \begin{pmatrix} \Delta x_1 \\ \Delta x_2 \\ \vdots \\ \Delta x_6 \end{pmatrix} (\Delta x_1 \quad \Delta x_2 \quad \cdots \quad \Delta x_6) \\
 &= \begin{pmatrix} u_K^2 + x_1^2 \cdot u_R^2 + u_c^2 & u_K^2 + x_2 x_1 \cdot u_R^2 & \cdots & u_K^2 + x_6 x_1 \cdot u_R^2 \\ u_K^2 + x_1 x_2 \cdot u_R^2 & u_K^2 + x_2^2 \cdot u_R^2 + u_c^2 & \cdots & u_K^2 + x_6 x_2 \cdot u_R^2 \\ \vdots & \vdots & \ddots & \vdots \\ u_K^2 + x_1 x_6 \cdot u_R^2 & u_K^2 + x_2 x_6 \cdot u_R^2 & \cdots & u_K^2 + x_6^2 \cdot u_R^2 + u_c^2 \end{pmatrix} \tag{8-7}
 \end{aligned}$$

Finally, substituting equation (8-7) into equation (8-4), the $\mathbf{U}(\Delta\mathbf{Y})$ is calculated. Among them, the $u(\Delta y_j)$ is called as error's uncertainty, which is the evaluation of probability interval of error Δy_j .

It can be seen that the so-called systematic error without variance does not exist indeed according to the conceptual logic of the new theory. Also, if we adopt the principle of the combination of Type A and Type B uncertainties in the traditional theory, the uncertainty analysis in this case is almost impossible to complete, which is also because the traditional concept of uncertainty has no mathematical logic.

9. Conclusion

Due to the different understanding of concepts of the constant and random variable, the conceptual logic of two measurement error theories has developed in two completely different directions.

Traditional measurement theory pays attention to the dispersion of repeated observations, and thus regards each observation as a random variable, so that the variance is assigned to each specific numerical value, the overall conceptual logic is in a plight, and the quantitative evaluation of error or true value cannot be realized. The traditional theory obviously ignores that the numerical value belongs to a constant, and ignores the conceptual distinction between random variable and sample.

The new concept theory clarifies that the measured value belongs to a constant without the variance, and that the error's variance is the dispersion of all possible values of error (the evaluation of probability interval of error). Recognizing that any error has all its possible values and has its variance, the measurement theory is developed according to the logic that error has no systematic and random category.

By comparison, the traditional theory has obvious deficiency in explaining the concept of probability theory, and other concepts deduced from this are naturally not correct, while the new concept theory is more in line with the concept principle of probability theory and completely solved the issue of quantitative evaluation of error.

In this way, according to the logic of the new concept theory, the error classification concepts such as systematic error, random error, precision, trueness and accuracy will not be needed in measurement practice, and the error evaluation concept is only the uncertainty concept: the evaluation of the probability interval of error (The dispersion of all possible values of the error). Therefore, the revision of metrology terminology and measurement textbooks has become a topic that needs to be discussed

again. Moreover, because the deviation, dispersion and outlier phenomena of repeated observations come from the changing rules of repeated measurement conditions, and especially many outliers are regarded as an unbalanced dispersion instead of gross errors, there is still room for further research on error processing methods.

References

- [1] JCGM 200:2012, International vocabulary of metrology — Basic and general concepts and associated terms (VIM). BIPM, Sèvres, France, 2012.
- [2] JJF1001-2011, General Terms in Metrology and Their Definitions. China Quality Inspection Press, Beijing, China, 2011.
- [3] JCGM 100:2008, Guide to the Expression of Uncertainty in Measurement(GUM). BIPM, Sèvres, France, 2008.
- [4] JJF1059-2012, Evaluation and Expression of Uncertainty in Measurement. China Quality Inspection Press, Beijing, China, 2012.
- [5] GB/T14911-2008, Basic Terms of Surveying and Mapping. China Standard Press, Beijing, China, 2008.
- [6] School of Geodesy and Geomatics, Wuhan University. Error Theory and Foundation of Surveying Adjustment [M]. Wuhan University Press, 2016 6.
- [7] Fei Yetai. Error Theory and Data Processing. Machinery Industry Press, 2016, 3.
- [8] Ye Depei. Understanding, Evaluation and Application of Measurement Uncertainty. China Metrology Publishing House, 2007 10.
- [9] Ye Xiao-ming, Ling Mo, Zhou Qiang, Wang Wei-nong, Xiao Xue-bin. The New Philosophical View about Measurement Error Theory. Acta Metrologica Sinica, 2015, 36(6): 666-670.
- [10] Ye Xiao-ming, Xiao Xue-bin, Shi Jun-bo, Ling Mo. The new concepts of measurement error theory. Measurement, 2016 April, Volume 83, Pages 96-105.
- [11] Ye Xiao-ming, Liu Hai-bo, Ling Mo, Xiao Xue-bin. The new concepts of measurement error's regularities and effect characteristics. Measurement, 2018, October, Volume 126, Pages 65-71.
- [12] Ye Xiao-ming, Ding Shi-jun. Comparison of variance concepts interpreted by two measurement theories. Journal of Nonlinear and Convex Analysis, 2019, Volume 20, Number 7, Pages 1307-1316.
- [13] Shi Huisheng, Ye Xiao-ming, Xing Cheng, Ding Shijun. A New Theoretical Interpretation of Measurement Error and Its Uncertainty. Discrete Dynamics in Nature and Society, Volume 2020, Article ID 3864578, <https://doi.org/10.1155/2020/3864578>
- [14] Ye Xiao-ming. Measurement error theory based on new concepts [M]. Hubei Science and Technology Press, 2017, 11.
- [15] ISO 17123-4:2012,Optics and optical instruments -- Field procedures for testing geodetic and surveying instruments -- Part 4: Electro-optical distance meters (EDM measurements to reflectors), ISO, Geneva, Switzerland, 2012.

Customer Churn Prediction Based on HMM in Telecommunication Industry

Huisheng ZHU^{a,1}, Bin YU^b

^a*School of Mathematics and Information Technology, Jiangsu Second Normal University, China*

^b*Marketing Department, Taizhou Branch of China Telecom, China*

Abstract.

The rapid development of technology and increasing numbers of customers have saturated the communication market. Communication operators must give focused attention to the problem of customer churn. Analyzing the customer's communication behavior and building a prediction model of customer churn can provide the advance evidence for communication operators to minimize churn. This paper describes how to design a HMM to predict customer churn based on communication data. First, we oversample chunders to increase the number of positive samples and establish the relative balance of positive and negative samples. Second, the continuous numerical attributes that affect communication customer churn are relatively discretized and their monthly values are converted into monthly change tendencies. Next, we select the communication features by calculating the information gains and information gain rates of all communication attributes. We then construct and optimize a prediction model of customer churn based on HMM. Finally, we test and evaluate the model by using a Spark cluster and the communication data set of Taizhou Branch of China Telecom. Experimental evaluation provides proof that our prediction model is exceptionally reliable.

Keywords. Customer churn, Prediction, HMM

1. Introduction

The rapid development of technology and increasing numbers of customers have saturated the communication market. With the arrival of 5G era, the communication industry is facing a new round of reshuffle, and the competition among communication operators on customer resources has entered a white-hot stage. A customer will change to a different communication operator when his or her needs are not met, which is called customer churn. The communication operators should pay more and more attention to the problem of customer churn because customer churn is closely related to the profits of communication operators. For communication operators, the cost of acquiring a new customer is approximately six times higher than the cost of retaining an existing customer[1], and reducing 5% customer churn rate will lead to 25%-85% increment of profit [2].

¹Corresponding Author: Huisheng ZHU, Jiangsu Second Normal University, 6 Xinhe West Road, Shiqiu street, Nanjing, China; E-mail: zhs@jssnu.edu.cn.

Communication operators possess massive communication data. How to find the behavior patterns of communication customers hidden in these data by data mining and build a prediction model of communication customer churn has become a research hotspot in industry and academia. Communication operators can identify potential churners in advance and take corresponding measures to retain them by adopting a prediction model of customer churn. Therefore, the research of communication customer churn is of great practical significance for communication operators to adjust their marketing strategies, change their ways of service, expand their market share and enhance their competitiveness.

In this paper, we propose a prediction model of communication customer churn based on HMM (Hidden Markov Model) and evaluate its performances by using a Spark cluster and a real communication data set. The rest of this paper is organized as follows. Section 2 discusses related work. Section 3 introduces our prediction model of communication customer churn. The experiment results for evaluating our prediction model are presented in Section 4, and finally, Section 5 concludes this work.

2. Related work

Since the 1990s, many scholars have focused on the research of communication customer churn prediction and proposed a series of prediction methods. Mozer et al. [3] put forward a prediction model of mobile customer churn based on linear regression, decision tree, neural network and ensemble learning. In [4-6], a prediction model of customer churn based on neural network was proposed. Song et al. [7] designed an algorithm for predicting customer churn by employing a hybrid process neural network based on the Fourier orthogonal basis function. Kisiglu and Topcu [8] proposed an algorithm of customer churn prediction based on Bayesian belief network. In [9][10], the activation diffusion algorithm of psychology was used to calculate the impact of a chunner on other customers in social networks and determine whether a customer will be a chunner or not. Xie et al. [11] applied sampling and cost sensitive learning in a standard random forest and proposed a balanced random forest algorithm for customer churn prediction. In [12][13], a prediction model of customer churn based on decision tree is proposed. In order to settle the problem of imbalance data in customer churn prediction, Li et al. [14] proposed an algorithm of customer churn prediction based on cluster sampling and support vector machine training. Hossam et al. [15] proposed a prediction model of customer churn based on genetic algorithm. In [16-18], three prediction models of customer churn based on the rough set theory were proposed. Huang et al. [19] used linear regression, decision tree, naive Bayes, neural network and support vector machine to predict customer churn and compared the advantages and disadvantages of these methods.

The above research works did not consider the temporal relation among communication data while building their prediction models. In fact, the churn tendency of communication customers are closely related to their historical communication behavior. HMM (Hidden Markov Model) is a probabilistic model of time series data, which describes the process of generating a state sequence from a hidden Markov chain, and then generating an observation sequence from the state sequence. HMM has been widely used in speech recognition [20], biostatistics [21], stock market prediction [22], fault

diagnosis [23], smart home [24] and other fields. However, the application of HMM in communication customer churn prediction is rare. The reason is that the traditional HMM has only one observation attribute, but there are multiple features hidden in the communication data which affect customer churn. How to recognize these features from the communication data and build a HMM based on the observation sequence of these features are the motivations of this paper.

3. Our Prediction Model of Communication Customer Churn

3.1. The framework of communication customer churn prediction

Communication operators usually stop service to the customer who owes for one month and recycle the SIM Card if the customer is in arrears for three months. In this paper, we aim to build a prediction model to identify the communication customer with churn tendency in advance, so a churker is defined as the customer who has not produced any communication data for more than one month.

The framework of communication customer churn prediction as shown in Figure 1 includes samples labelling, attributes discretization, features selection, model training, parameters optimization and model testing.

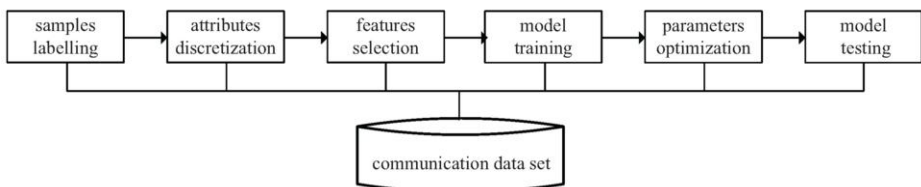


Figure 1. The framework of communication customer churn prediction

3.2. Samples labelling

The average churn rate of communication customers is about 2.2% [25], so the communication data set is an unbalanced data set in scenario of the two classification problem of predicting whether a customer is a churker or not. In the data set, churkers are the minority and are called positive samples, while non-churkers are majority and are called negative samples. The classification model trained directly from these samples will probably lead the prediction result belong to negative class.

Therefore, we oversample churkers to increase the number of positive samples and establish the relative balance of positive and negative samples. As shown in Figure 2, we first label the monthly churkers and non-churkers of the training set composed of N months call data, then copy the data of churkers in $t+2$ and $t+3$ in any month t ($1 \leq t \leq N-3$). Finally, the first $N-3$ months call data will be used as training samples, and the rest data will be used for model optimization.

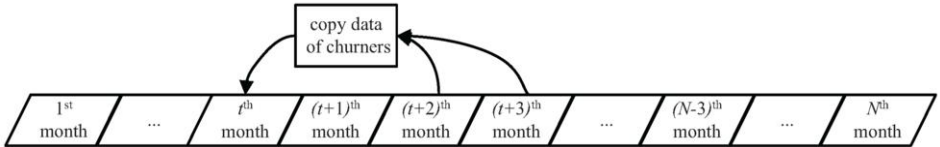


Figure 2. Churners oversampling

3.3. Attributes discretization

Each call record of communication customers has many attributes. Some of these attributes such as switch id, calling area code, calling cell id, etc. are not related to churn tendency of communication customers. The main communication attributes that affect customer churn are some continuous numerical attributes such as call frequency, call duration, call charge, etc. However, the monthly values of these continuous numerical attributes are not directly related to customer churn, instead their monthly change tendencies are most affinitive to customer churn. Therefore, these communication attributes need to be relatively discretized.

Let X_t be the value of communication attribute X of a customer in month t , the change tendency of communication attribute X of the customer in month t compared with month $t-1$ can be calculated by Eq. (1).

$$X'_t = \begin{cases} 0 & X_t = 0 \\ 1 & X_t \neq 0 \wedge X_t - X_{t-1} \leq 0 \\ 2 & X_t \neq 0 \wedge X_t - X_{t-1} = 0 \\ 3 & X_t \neq 0 \wedge X_t - X_{t-1} \geq 0 \end{cases} \quad (1)$$

In Eq. (1), $X'_t = 0$ indicates that the customer did not produce any communication data in month t , $X'_t = 1$ indicates that the value of communication attribute X of the customer in month t is lower than that in month $t-1$, $X'_t = 2$ indicates that the value of communication attribute X of the customers in month t is equal to that in month $t-1$, and $X'_t = 3$ indicates that the value of communication attribute X of the customers in month t is higher than that in month $t-1$.

3.4. Features selection

Different communication attributes have different impacts on churn tendency. Let $IF(X)$ be the impact factor of communication attribute X on churn tendency, its computational procedures are as follows:

1. Calculate the information entropy of customer class set $C = \{\text{churner, non-churner}\}$ by Eq. (2).

$$H(C) = - \sum_{c \in C} p(c) \log_2 p(c) \quad (2)$$

2. Calculate the conditional entropy of customer class set C under the condition of a given communication attribute X by Eq. (3).

$$H(C|X) = \sum_{x \in X} p(x) H(C|X=x) = - \sum_{x \in X} p(x) \sum_{c \in C} p(c|x) \log_2 p(c|x) \quad (3)$$

3. Calculate the information gain of communication attribute X by Eq. (4).

$$IG(X) = H(C) - H(C|X) \quad (4)$$

4. Calculate the information gain rate of communication attribute X , namely the impact factor of attribute X on churn tendency by Eq. (5).

$$IF(X) = \frac{IG(X)}{H(X)} = \frac{IG(X)}{-\sum_{x \in X} p(x) \log_2 p(x)} \quad (5)$$

Let Avg_IG be the average information gain of all communication attributes and Min_IF be the threshold of information gain rate, attribute X is called a communication feature if $IG(X) \geq Avg_IG$ and $IF(X) \geq Min_IF$.

3.5. Model training

HMM is a system embedded with two stochastic processes, one of which is a hidden state transition process (Markov chain), the other is a visible sequence of observation symbols which is related to the state transition process. If the state transition of a HMM depends on its previous n states, such a HMM is called a n -order HMM. The first order HMM is used in this paper.

There are two stochastic processes embedded in the scenario of communication customer churn prediction, one is the visible monthly call data, the other is the hidden states transition. The visible call data is closely related to the hidden state transition, so HMM is suitable for the scenario of communication customer churn prediction, and the prediction model can be trained by determining the following five elements.

1. State set $S = \{S_1=\text{churn}, S_2=\text{non-churn}\}$. A state indicates whether a communication customer has the tendency of churn or not. Let Q_t be the state S_1 or S_2 of the system in month t , the state sequence from the first to the T^{th} month is expressed as $Q = Q_1 Q_2, \dots, Q_T$.
2. Observation symbol set $V = \{V_1, V_2, \dots, V_M\}$. For a traditional HMM, M is the number of all different values of only one observation attribute, and $V_j (1 \leq j \leq M)$ represents a value of the observation attribute. However, for the HMM applied in the scenario of communication customer churn prediction, the observed attributes are K communication features that affect customer churn. Therefore, M in the observation symbol set is equal to 3^K , here 3 indicates that there are three kinds of monthly change tendency of each communication feature (1 is descend, 2 is flat, 3 is ascend), and $V_j (1 \leq j \leq M)$ is a vector composed of the change tendencies of K communication features in the same month. Let O_t be the symbol V_j observed by the system at month t , the observation sequence from the first to the T^{th} month is expressed as $O = O_1 O_2, \dots, O_T$.
3. State transition distribution $A = \{A_{ij}\} = \{P(Q_{t+1}=S_j | Q_t=S_i)\}$. $P(Q_{t+1}=S_j | Q_t=S_i)$ represents the probability that the system is in state S_i at month t and in state S_j at month $t+1$, which is calculated by Eq. (6). Num in Eq. (6) indicates counting values that meets a given condition.

$$A_{ij} = \frac{\sum_{t=1}^{T-1} Num(Q_t=S_i, Q_{t+1}=S_j)}{\sum_{t=1}^{T-1} Num(Q_t=S_i)} \quad (6)$$

4. Observation symbol distribution $B = \{B(V_j|S_i)\} = \{P(O_t=V_j|Q_t=S_i)\}$, where $P(O_t=V_j|Q_t=S_i)$ represents the probability that the system is in state S_i at month t and the observed symbol is V_j , which is calculated by Eq. (7).

$$B(V_j|S_i) = \frac{\sum_{t=1}^{T-1} \text{Num}(Q_t = S_i, O_t = V_j)}{\sum_{t=1}^{T-1} \text{Num}(Q_t = S_i)} \quad (7)$$

5. Initial state distribution $\pi = \{\pi(S_i)\} = \{P(Q_1=S_i)\}$. $P(Q_1=S_i)$ indicates the probability that the system is in state S_i at the first month. If the initial state is a normal uniform distribution, $\pi(S_1)=\pi(S_2)=1/2$.

Obviously, initial state distribution π and state transition distribution A can determine state set S , and observation symbol distribution B can determine observation symbol set V , so a HMM only requires the specifications of A, B and π . For convenience, the whole element set can be denoted by a triple, i.e., $\lambda=(A, B, \pi)$.

3.6. Parameters optimization

Given an initial model $\lambda=(A, B, \pi)$ and an observation sequence $O=O_1O_2, \dots, O_T$, parameter optimization is defined as how to adjust A, B and π to maximize $P(O|\lambda')$, i.e., the probability of the occurrence of O in the new model λ' . We use the following Baum Welch algorithm [20] to optimize an initial model λ .

Step 1, estimate the parameters by model λ and observation sequence O , and a new model $\lambda'=(A', B', \pi')$ is obtained.

Step 2, calculate the probabilities $P(O|\lambda')$ and $P(O|\lambda)$ by λ', λ and O .

Step 3, if $|P(O|\lambda') - P(O|\lambda)| > \varepsilon$, here ε is a very small positive number, let $\lambda = \lambda'$ and goto step 1. Otherwise, optimization is over.

3.7. Model testing

Communication customer churn prediction aims at calculating the churn probability of a customer in month $T+1$ based on the prediction model and the observed change tendency sequence of communication features in the T months of a customer, i.e., $O=O_1O_2, \dots, O_T$ (O_t is an observation vector). The customer whose churn probability is greater than or equal to the churn probability threshold Min_CP is predicted to be a churker, otherwise the customer is predicted to be a non-churker. Obviously, the essence of communication customer churn prediction is seeking the maximum probability of hidden state at time $T+1$, i.e., the maximum $P(Q_{T+1}=S_j|O_1O_2, \dots, O_T)$. $P(Q_{T+1}=S_j|O_1O_2, \dots, O_T)$ can be calculated by Eq. (8).

$$P(Q_{T+1}=S_j|O_1O_2, \dots, O_T) = \sum_i A_{ij} P(Q_T=S_i|O_1O_2, \dots, O_T) \quad (8)$$

$P(Q_T=S_i|O_1O_2, \dots, O_T)$ in Eq. (8) can be calculated by Eq. (9).

$$\begin{aligned} P(Q_T=S_i|O_1O_2, \dots, O_T) \\ = \gamma P(O_T|Q_T=S_i) \sum_j A_{ji} P(Q_{T-1}=S_j|O_1O_2, \dots, O_{T-1}) \end{aligned} \quad (9)$$

In Eq. (9), γ is normalization constant which can ensure that the sum of the probabilities in the two hidden states of churn and non-churn is 1.

4. Experimental Evaluation

Spark is a fast and universal computing engine designed for large-scale data processing. It not only implements the map and reduce methods in MapReduce, but also provides rich components such as Spark Streaming for real-time streaming, MLlib for machine learning, GraphX for large-scale graph processing and Spark SQL for interactive query. Spark supports memory computing and greatly improves the efficiency of iterative algorithm. The experimental environment of this paper is a Spark cluster composed of one master node and four slave nodes. The hardware configuration of each node is 3.60GHz Intel (R) core (TM) i7-7820x CPU, 64GB memory and 2TB hard disk. The software environment is Ubuntu 16.04, Spark 2.3.0, Scala 2.11 and JDK1.8. All the programs are written in Java.

4.1. Data set

The experimental data set is from Taizhou Branch of China Telecom, which stores the call records of all communication customers from January 1 to December 31, 2019. Each call record in the data set includes 146 attributes as shown in Table 1. All call data are compressed by Snappy and stored in the form of plain text on the HDFS of Spark cluster.

Table 1. Attributes of each call record

Attribute	Description
event_id	event id
customer_id	customer id
calling_nbr	calling number
calling_area_code	calling area code
calling_cell_id	calling cell id
calling_op_type	calling operator type
called_nbr	called number
called_area_code	called area code
called_cell_id	called cell id
called_op_type	called operator type
switch_id	switch id
call_frequency	call frequency
call_duration	call duration
basic_charge	basic charge
prepaid_charge	prepaid charge
plan_charge	charge of plan
call_charge	charge out of plan
...	...

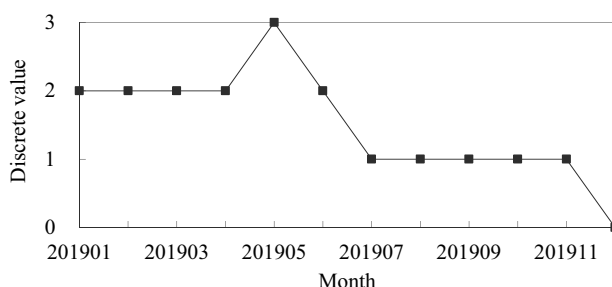
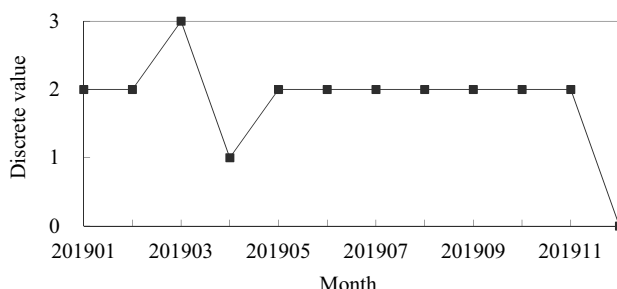
The numbers of churners and non-churners in the data set are shown in Table 2. The ratio of the total number of churners to that of non-churners is about 2%.

Table 2. The numbers of churners and non-churners in the data set

Month	Churner	Non-churner
January 2019	15313	880016
February 2019	20345	895225
March 2019	18466	906232
April 2019	16328	915337
May 2019	11225	923441
June 2019	13532	932105
July 2019	18263	942081
August 2019	21611	956402
September 2019	32829	972033
October 2019	13147	981174
November 2019	16632	989005
December 2019	34206	1005233

4.2. Communication features

We extract a customer who became a churner in December 2019 from the data set and depict the change tendencies of main communication attributes of the customer in Figures 3-8.

**Figure 3.** The change tendency of call_frequency**Figure 4.** The change tendency of basic_charge

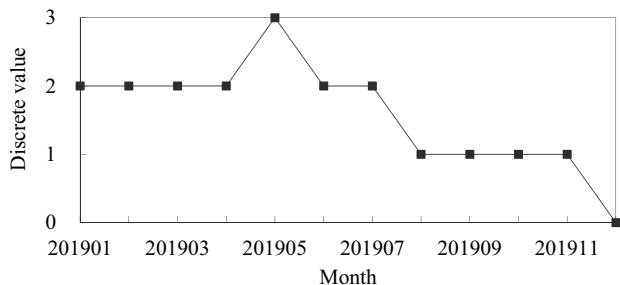


Figure 5. The change tendency of call_duration

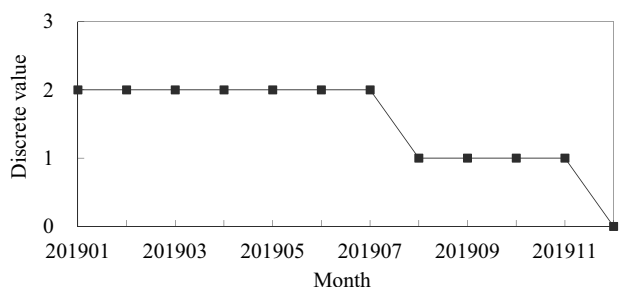


Figure 6. The change tendency of plan_charge

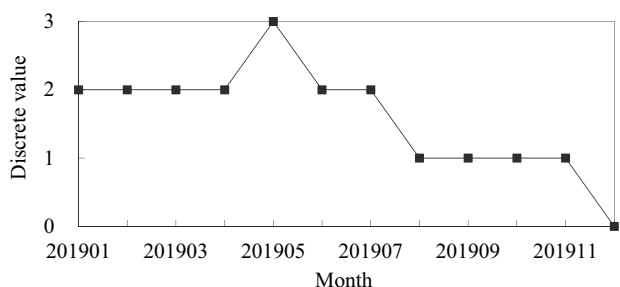


Figure 7. The change tendency of call_charge

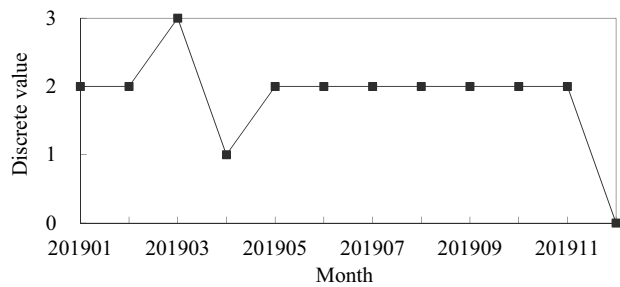


Figure 8. The change tendency of prepaid_charge

For the training set composed of the first 8 months call records in the data set, assume the threshold of information gain rate is 0.02, the communication features calculated from the positive and negative samples of the first 5 months (after samples labelling with the method described in Section 3.2) is shown in Table 3.

Table 3. The communication features in the data set

Communication feature	Impact factor
call_frequency	0.1443
basic_charge	0.1275
call_duration	0.1106
plan_charge	0.0983
call_charge	0.0619
prepaid_charge	0.0238

4.3. Performance evaluation criteria

Customer churn prediction is a problem of classification in two categories, whose confusion matrix is shown in Table 4. The table defines the churners as the positive class, and the non-churners as the negative class.

Table 4. The confusion matrix of customer churn prediction

	Prediction Positive	Prediction Negative
Positive Sample	True Positive (TP)	False Negative (FN)
Negative Sample	False Positive (FP)	True Negative (TN)

We use precision and recall to evaluate the performance of our prediction model. The higher precision and recall, the better the performance. Precision and recall are calculated by Eqs. (10) and (11).

$$Precision = \frac{TP}{TP+FP} \quad (10)$$

$$Recall = \frac{TP}{TP+FN} \quad (11)$$

We also use *AUC* (Area Under *ROC* Curve) [26][27] to evaluate the performance of our prediction model. The larger the *AUC*, the better the performance. *ROC* (Receiver Operating Characteristic) [26][27] refers to the connection of points drawn with FPR (False Positive Rate) as the horizontal axis and TPR (True Positive Rate) as the vertical axis. FPR and TPR are calculated by Eqs. (12) and (13).

$$FPR = \frac{FP}{FP+TN} \quad (12)$$

$$TPR = \frac{TP}{TP+FN} \quad (13)$$

To calculate AUC , we first compute the churn probability of each communication customer by Eq. (9) and sort them in descending order, then we assign the customer with the highest churn probability rank n , the customer with the second highest churn probability rank $n-1$, and so on. In this way AUC can be calculated by Eq. (14).

$$AUC = \frac{\sum_{n \in TP} Rank_n - \frac{TP \times (TP+1)}{2}}{TP \times TN} \quad (14)$$

4.4. Performance evaluation results

Experiment-1 (Performance vs. Size of training set). We choose the first 8 months call records of the data set as the maximum training set. Fixing Min_CP (churn probability threshold) at 0.57, Figures 9-11 depicts how size of training set (in month) affects precision, recall and AUC . From the figures we can notice that precision, recall and AUC increase with size of training set. The reason is that the larger training set, the more balanced the positive and negative samples. We also observe that it needs at least 7 months of training data to make the model have better prediction results.

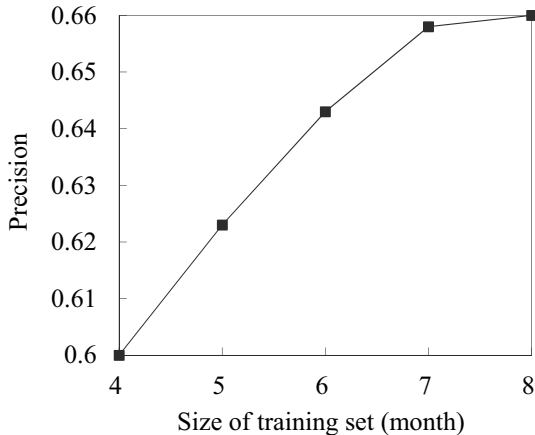
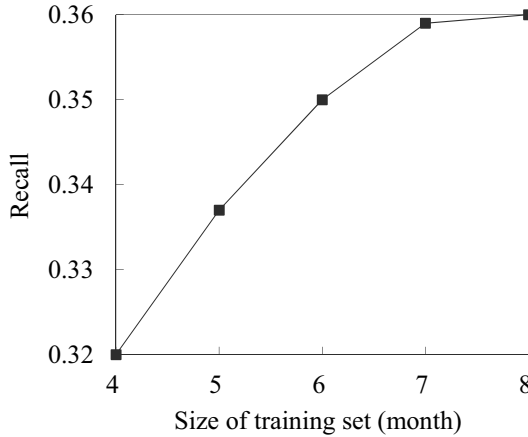
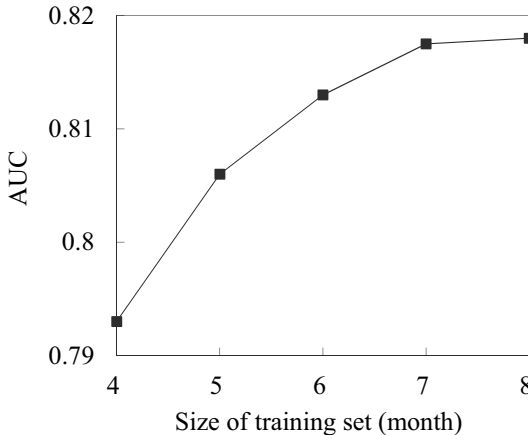


Figure 9. Precision vs. Size of training set

Experiment-2 (Performance vs. Min_CP). In this experiment, we present the performance comparison of our model and *LIBLINEAR* [28] on the real communication data set. *LIBLINEAR* has been a linear model widely used in massive data classification since it received the KDD CUP championship in 2010 [29].

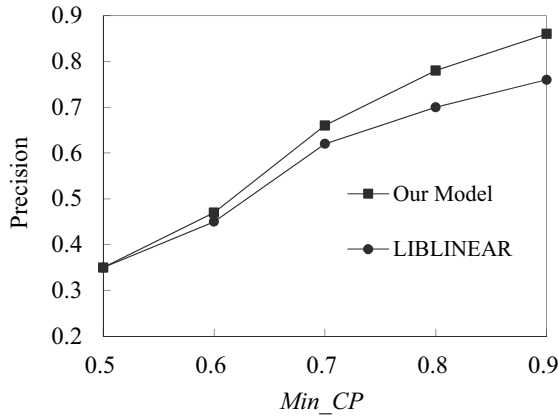
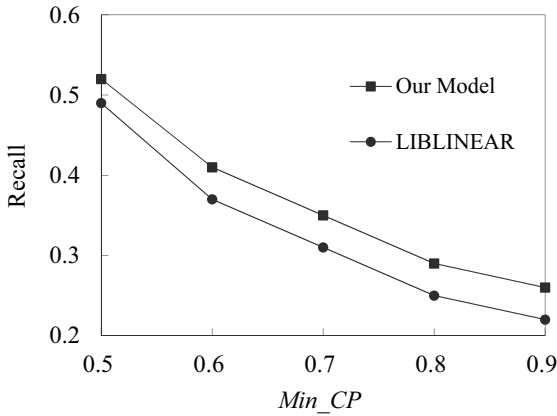
After training our prediction model based on the first 8 months call records of the data set, we predict the average churn probability of all customers in December by their change tendencies of all communication features from September to November. We vary churn probability threshold Min_CP . The precisions and the recalls are shown in Figures 12 and 13. Clearly, the precisions of our model and *LIBLINEAR* increase with Min_CP , but the recalls of our model and *LIBLINEAR* decrease with Min_CP . This is because the

**Figure 10.** Recall vs. Size of training set**Figure 11.** AUC vs. Size of training set

larger the Min_CP , the less false positive and the higher the precision by Eq. (10), the more the false negative and the lower the recall by Eq. (11).

We can also observe that the precision and the recall of our model are higher than those of *LIBLINEAR*. The reason is that our model based on HMM has one more time dimension than *LIBLINEAR*.

Figures 12 and 13 show that $Min_CP = 0.57$ is the intersection of precision curve and recall curve. Therefore, we generally choose $Min_CP = 0.57$ in the actual prediction in order to take into account of precision and recall.

**Figure 12.** Precision vs. *Min_CP***Figure 13.** Recall vs. *Min_CP*

5. Conclusion

In this paper, we design a prediction model of communication customer churn based on HMM and evaluate its performances by using the Spark cluster and the real communication data set. The construction of the model includes samples labelling, attributes discretization, features selection, model training, parameters optimization and model testing. The experimental results shows that our model has better performances than *LIBLINEAR* in the scenario of communication customer churn prediction.

The prediction model designed in this paper only considers call records of communication customers. In the future, we will study on communication customer churn prediction based on call record, message record and network traffic.

Another future research direction is the examination of whether a higher-order HMM can be used to improve the performance of our predicted activities.

6. Acknowledgments

We very appreciate the anonymous reviewers for their valuable comments and suggestions. This research was supported by the National Natural Science Foundation of China grants 61672163, and the Chinese Ministry of Education Foundation for 'Integration of Cloud Computing and Big Data, Innovation of Science and Education' grants 2017B06109.

References

- [1] Alsultanny YA. Database preprocessing and comparison between data mining methods. International Journal of New Computer Architectures and their Applications. 2011 Jan; 1(1):61-73.
- [2] Shin HM, Jeong DH. An application of data mining for marketing in telecommunication. Proceedings of Portland International Conference on Management of Engineering and Technology; 2001 July 29 - August 2; Portland, OR, USA. Wiley: IEEE Press; 2002. p. 247.
- [3] Mozer MC, Wolniewicz R, Grimes DB, Johnson E, Kaushansky H. Predicting subscriber dissatisfaction and improving retention in the wireless telecommunications industry. IEEE Transactions on Neural Networks. 2000 Jan; 11(3):690-6.
- [4] Zhang Y, Liang R, Li Y, Zheng Y, Berry M. Behavior-based telecommunication churn prediction with neural network approach. Proceedings of International Symposium on Computer Science and Society; 2011 July 16-17; Kota Kinabalu, Malaysia. Wiley: IEEE Press; 2011. p. 307-310.
- [5] Yu R, An X, Jin B, et al. Particle classification optimization-based BP network for telecommunication customer churn prediction. Neural Computing and Applications. 2018 Feb; 29(3):707-720.
- [6] Hu J, Zhuang Y, Yang J, et al. pRNN: A recurrent neural network based approach for customer churn prediction in telecommunication sector. Proceedings of IEEE International Conference on Big Data; 2018 December 10-13; Seattle, WA, USA. Wiley: IEEE Press; 2018. p. 4081-5.
- [7] Song G, Yang D, Wu L, Wang T, Tang S. A mixed process neural network and its application to churn prediction in mobile communications. Proceedings of IEEE International Conference on Data Mining Workshops; 2006 December 18-22; Hong Kong, China. Wiley: IEEE Press; 2006. p. 798-802.
- [8] Kisiglu P, Topcu YI. Applying bayesian belief network approach to customer churn analysis: A case study on the telecom industry of Turkey. Expert Systems with Applications. 2011 Jun; 38(6):7151-7.
- [9] Dasgupta K, Singh R, Viswanathan B, et al. Social ties and their relevance to churn in mobile telecom networks. Proceedings of the 11th International Conference on Extending Database Technology; 2008 March 25-29; Nantes, France. ACM Press; 2008. p. 668-677.
- [10] Yossi R, Elad YT, Noam S. Predicting customer churn in mobile networks through analysis of social groups. Proceedings of SIAM International Conference on Data Mining; 2010 April 29 - May 1; Columbus, Ohio, USA. SIAM Press. 2010. p. 732-741.
- [11] Xie T, Li X, Ngai EWT, Ying W. Customer churn prediction using improved balanced random forests. Expert Systems with Applications. 2009 Apr; 36(3):5445-9.
- [12] Wei CP, Chiu TT. Turning telecommunications call details to churn prediction: a data mining approach. Expert Systems with Applications. 2002 Aug; 23(2):103-112.
- [13] Deng W, Deng L, Liu J, Qi J. Sampling method based on improved C4.5 decision tree and its application in prediction of telecom customer churn. International Journal of Information Technology and Management. 2019 Jan; 18(1):93-109.
- [14] Li P, Yu X, Sun B, Huang J. Telecom customer churn prediction based on imbalanced data resampling method. Proceedings of the 2nd International Conference on Measurement, Information and Control; 2013 August 16-18; Harbin, China. Wiley: IEEE Press; 2014. p. 229-233.
- [15] Hossam F, Bashar AS, Nazeem G. A genetic programming based framework for churn prediction in telecommunication industry. Proceedings of the 6th International Conference on Computational Collective Intelligence; 2014 September 24-26; Seoul, Korea. Springer Press; 2014. p. 353-362.
- [16] Amin A, hehzad S, Khan C, Ali I, Anwa S. Churn prediction in telecommunication industry using rough set approach. New Trends in Computational Collective Intelligence. 2015 Jan; 83-95.
- [17] Amin A, Anwar S, Adnan A, et al. Customer churn prediction in the telecommunication sector using a rough set approach. Neurocomputing. 2017 May; 237:242-254.

- [18] Vijaya J, Sivasankar E. Computing efficient features using rough set theory combined with ensemble classification techniques to improve the customer churn prediction in telecommunication sector. *Computing*. 2018 Aug; 100(8):839-860.
- [19] Huang BQ, Kechadi MT, Buckley B. Customer churn prediction in telecommunications. *Expert Systems with Applications*. 2012 Jan; 39(1):1414-1425.
- [20] Rabiner LR. A tutorial on hidden Markov models and selected applications in speech recognition. *Proceedings of the IEEE*. 1989 Feb; 77(2):257-286.
- [21] Liu JS, Neuwald AF, Lawrence CE. Markovian structures in biological sequence alignments. *Journal of the American Statistical Association*. 1999 Mar; 94(445):1-15.
- [22] Hassan MR, Ramamohanarao K, Kamruzzaman J, Rahman M, Hossain MM. A HMM-based adaptive fuzzy inference system for stock market forecasting. *Neurocomputing*. 2013 Mar; 104:10-25.
- [23] Laxman S, Sastry PS, Unnikrishnan KP. Discovering frequent episodes and learning hidden Markov models: a formal connection. *IEEE Transactions on Knowledge and Data Engineering*. 2005 Nov; 17(11):1505-1517.
- [24] Cheng BC, Tsai YA, Liao GT, Byeon ES. HMM machine learning and inference for activities of daily living recognition. *The Journal of Supercomputing*. 2010 Oct; 54(1):29-42.
- [25] Berson A, Thearling K. Building data mining applications for CRM. New York: McGraw-Hill Press; 1999. p. 510.
- [26] T. Fawcett. An introduction to ROC analysis. *Pattern Recognition Letters*. 2006 Jun; 27(8): 861-874.
- [27] J. Davis, M. Goadrich. The relationship between Precision-Recall and ROC curves. *Proceedings of the Twenty-Third International Conference on Machine Learning* 2006 Jun 25-29; Pittsburgh, Pennsylvania, USA, ACM Press; 2006. p. 233-240.
- [28] Fan RE, Chang KW, Hsieh CJ, Wang XR, Lin CJ. LIBLINEAR: A library for large linear classification. *Journal of Machine Learning Research*. 2008 Jul; 9: 1871-1874.
- [29] Yu HF, Lo HY, Hsieh HP, et al. Feature engineering and classifier ensemble for KDD cup 2010. *Proceedings of the JMLR Workshop and Conference*; 2010 July 25-28; Sardinia, Italy. Cambridge: MIT Press; 2010. p. 153-160.

The Diagnosis of Alzheimer's Disease: An Ensemble Approach

Jingyan Qiu^a, Linjian Li^a, Yida Liu^a, Yingjun Ou^a, Yubei Lin^{a,1}

^aSchool of Software Engineering, South China University of Technology, Guangzhou, China

Abstract. Alzheimer's disease (AD) is one of the most common forms of dementia. The early stage of the disease is defined as Mild Cognitive Impairment (MCI). Recent research results have shown the prospect of combining Magnetic Resonance Imaging (MRI) scanning of the brain and deep learning to diagnose AD. However, the CNN deep learning model requires a large scale of samples for training. Transfer learning is the key to enable a model with high accuracy by using limited data for training. In this paper, DenseNet and Inception V4, which were pre-trained on the ImageNet dataset to obtain initialization values of weights, are, respectively, used for the graphic classification task. The ensemble method is employed to enhance the effectiveness and efficiency of the classification models and the result of different models are eventually processed through probability-based fusion. Our experiments were completely conducted on the Alzheimer's Disease Neuroimaging Initiative (ADNI) public dataset. Only the ternary classification is made due to a higher demand for medical detection and diagnosis. The accuracies of AD/MCI/Normal Control (NC) of different models are estimated in this paper. The results of the experiments showed that the accuracies of the method achieved a maximum of 92.65%, which is a remarkable outcome compared with the accuracies of the state-of-the-art methods.

Keywords. Alzheimer's disease, Deep learning, Ensemble learning, Transfer learning, Convolutional Neural Network

1. Introduction

Alzheimer's Disease is the most common cause of dementia [1], with the symptoms of memory loss, difficulty in speaking and execution barrier [2]. The crude prevalence of AD in China has been found to range between 7 per 1000 people to 66 per 1000 individuals and the estimation is that there are 9.5 million patients [3].

These days, deep learning and transfer learning accelerate the development of computer vision, thus boosting the efficiency and effectiveness of the diagnosis of Alzheimer's disease based on MRI images. Glozman et al. [4] used transfer learning that fine-tuned AlexNet architecture. 3D MRI images are essentially a stack of 2D images. Hon et al. [5] used an intelligent method to select slices on each subject's MRI image to select data with an entropy-based mechanism. They employed two

¹ Corresponding Author: Yubei Lin, South China University of Technology, Guangzhou, China;
Email: yupilin@scut.edu.cn

architectures: VGG16 [6] and Inception V4 [7] through transfer learning and compared the performance of the two architectures. Jain R et al. [8] used a similar method to select slices on Alzheimer's Disease Neuroimaging Initiative (ADNI), which is established with the idea of enhancing the prevention and treatment of Alzheimer's disease (AD) [9] and used VGG16 for training analysis. It is worth noting that the previous two research groups ultimately focus on the performance of the models based on slice analysis instead of the analysis of a definite case of an individual, which may cause a test performance being too high.

In our study, unlike Hon et al. [5] and Jain R et al. [8], we divide our data set in the form of medical cases (in .nii format) ahead of pre-processing. This paper is organized as follows: At first, the pre-processing part will be introduced. After that, classification models and a probability-based fusion [10] will be laid out. Following the methodology and algorithm are the experiments conducted respectively on DenseNet [11] and Inception V4, as well as the one on the fusion. We also compare our maximal result with other researchers' results on ternary classification. And eventually, we conclude our work.

2. Methodology and Algorithm

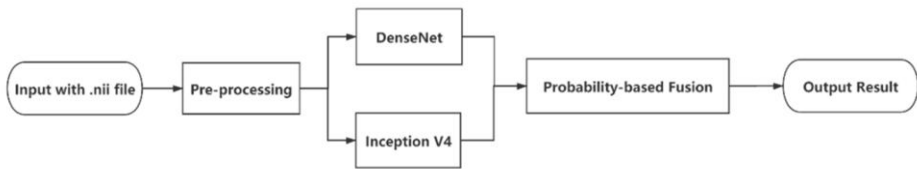


Figure 1. Illustration of the ensemble model

Shown in Fig. 1, at the very beginning, the 3D images are divided into a training set, a validation set, and a test set. Then the 3D images undergo pre-processing through FreeSurfer [12] and are sliced into 256 slices, among which the most informative 32 slices are selected for the following process. The slices will be processed by DenseNet and Inception V4 respectively. During the testing, the judgment given by each base classifier will be passed to the probability-based fusion to figure out the final judgment of the classification.

2.1. Pre-processing and Data Partitioning

In the pre-processing part, we employ a pre-processing model named P_{FS_E} , which is part of the model made by Jain R et al. [8]. In our method, following the 80-20 rule [13], we divide the data set in the ".nii" form into two parts: One is for the training process (80%) and the other is test set (20%). Within the data set for the training process, the data set is again divided into the training set (72%) and validation set (8%). Compared with the paper composed by Jain R et al. [8], their division is based on the slice, which means one person's 32 slices could appear on more than one set. This could be a trick to enhance accuracy, which fails to show the generalization capability of the model.

2.2. Classification Models

2.2.1. DenseNet

In the MRI detection, we select DenseNet instead of VGG16 or Inception V3 because in the experiment given in the next part indicates the higher accuracy and robustness of DenseNet. For DenseNet, the output part from the top layer was removed, and only input layers, dense blocks and transition layers are reserved. The last dense block is connected to the Global Average Pooling, after which the new output layer and fully-connected layers are added. Softmax activates the classification layer and ternary classification is accomplished.

Convolution	112 x 112	7 x 7 conv, stride 2
Pooling	56 x 56	3 x 3 max pool, stride 2
Dense Block (1)	56 x 56	[1 x 1 conv] x 6 [3 x 3 conv]
Transition Layer (1)	56 x 56	1 x 1 conv
	28 x 28	2 x 2 average pool, stride 2
Dense Block (2)	28 x 28	[1 x 1 conv] [3 x 3 conv] x 12
Transition Layer (2)	28 x 28	1 x 1 conv
	14 x 14	2 x 2 average pool, stride 2
Dense Block (3)	14 x 14	[1 x 1 conv] [3 x 3 conv] x 24
Transition Layer (3)	14 x 14	1 x 1 conv
	7 x 7	2 x 2 average pool, stride 2
Dense Block (4)	7 x 7	[1 x 1 conv] [3 x 3 conv] x 16
Classification Layer	1 x 1	7 x 7 global average pool
		3D fully-connected, softmax

Figure 2. Structure of the DenseNet classification model

Softmax in Fig. 2. is a function that takes as input a vector of K real numbers, and normalizes it into a probability distribution consisting of K probabilities proportional to the exponentials of the input numbers. Each component after softmax will be in the interval (0,1), and the components will add up to 1, so that they can be interpreted as probabilities. Softmax is defined as:

$$\sigma(\mathbf{z})_i = \frac{e^{z_i}}{\sum_{j=0}^k e^{z_j}} \text{ for } i = 1 \dots K \text{ and } \mathbf{z} = (z_1, \dots, z_K) \in \mathbb{R}^K \quad (1)$$

The performance of a classifier, the cross-entropy loss, is calculated as:

$$L(y, p) = - \sum_{c=1}^M y_{o,c} \log(p_{o,c}) \quad (2)$$

where y is the actual value, p is the predicted value, M is the class no.

Mini-Batch Gradient Descent is used as the optimization function. The learning rate is set as 0.01. The weight θ used for updating the neuron is calculated as:

$$\theta = \theta - \alpha \nabla_{\theta} J(\theta; x^{i:i+n}; y^{i:i+n}) \quad (3)$$

where α is the learning rate, ∇ is the gradient operand, J is loss function and x, y are sample labels.

Transfer learning is adapted for the size of the data set is so limited. In the model, we employ the DenseNet trained on ImageNet to enhance the classification capability of the model.

After training the model trained on the slice level, majority voting is introduced to accurately classify the case hierarchy. By selecting some specific slices on the sample,

the input model is used to predict the type of the slice, and the category in which the votes are selected by voting is the category of the sample stage.

2.2.2. Inception V4

The Inception architecture is a deep CNN invented by Google. Based on Inception V1, Inception V4 is an architecture brought up by [7]. The Inception V4 discards the fully-connected layer in preference of a global average pooling and connects with a softmax layer to reduce the large parameter number and overfitting [5].

Due to the limitation of the computational devices of our research group, we do not train the whole Inception V4 model by ourselves. Instead, we use the pre-trained model from the internet trained with the dataset from the ImageNet, which contains over 14 million images. The kernel of the pre-trained model can extract the features from general pictures very well, and we do not re-train the convolutional layers and pooling layers of it. Fixing the convolutional layers and pooling layers, we only re-train the last fully-connected layer. This approach can not only facilitate the computation but reserve the generalization capability of the middle convolutional and pooling layers as well.

2.2.3. A Probability-based Fusion

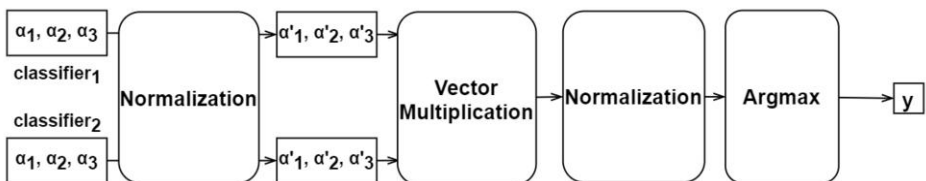


Figure 3. Structure of the probability-based fusion

Shown in Fig. 3., there are 2 classifiers in our model. The classifier₁ is DenseNet and classifier₂ is Inception V4. and α_1 , α_2 , α_3 are three probabilities of a prediction given by a classifier, which indicates the probabilities of AD, MCI and NC respectively when a sample is given. The probabilities have such a relationship, which is $\alpha_1 + \alpha_2 + \alpha_3 = 1$. Each prediction will first be normalized as below:

$$(\alpha'_1, \alpha'_2, \alpha'_3) = \frac{(\alpha_1, \alpha_2, \alpha_3)}{\max(\alpha_1, \alpha_2, \alpha_3)} \quad (4)$$

After normalization, the predictions of different classifiers will be multiplied to vote. Then, the multiplied vectors will be normalized and the argmax is the final prediction of class. The calculation process is shown below:

$$y = \arg \max (\prod_{i=1}^m \alpha_1^i, \prod_{i=1}^m \alpha_2^i, \prod_{i=1}^m \alpha_3^i) \quad (5)$$

3. Experiment

3.1. Ternary Classification of the MRI Slices

We built the model with Keras [14], which is written in Python with TensorFlow [15].

380 medical cases (342 for the training set and 38 for the validation set) were employed for training the model, and 95 cases were used for the test set. Our model for ternary classification was conducted on 12160 slices in a batch size of 16 in 120 epochs. At each epoch, parameter values are updated.

Accuracy is calculated as:

$$\text{Accuracy} = \frac{\sum_{i=1}^n B^i}{n} \quad (6)$$

where n is the number of samples, y_{true}^i is the true class label for i th sample, $y_{predicted}^i$ is the predicted class label for i th sample, and B^i is a Boolean function calculated as:

$$B^i = \begin{cases} 0 & y_{true}^i \neq y_{predicted}^i \\ 1 & y_{true}^i = y_{predicted}^i \end{cases} \quad (7)$$

For further performance evaluation, Precision, Recall, and F1-Score are also presented, which are calculated as:

$$\text{Precision} = \frac{TP}{TP + FP} \quad (8)$$

$$\text{Recall} = \frac{TP}{TP + FN} \quad (9)$$

$$F1 = 2 \times \frac{\text{Precision} \times \text{Recall}}{\text{Precision} + \text{Recall}} \quad (10)$$

where TP is true positive predictions, FP is false positive predictions, and FN is false negative predictions.

3.1.1. Selection of DenseNet

We compared VGG16, DenseNet and Inception V3 on the classification. The confusion matrices are presented in Table 1.

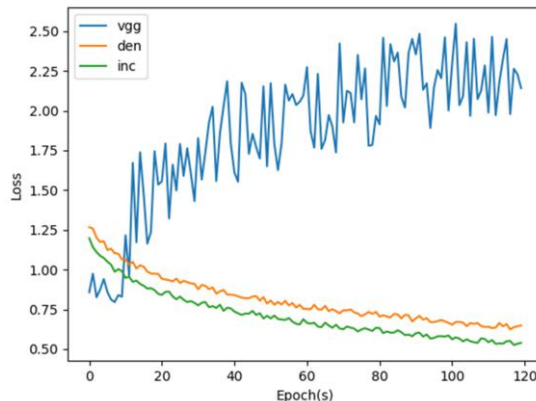


Figure 4. Validation loss of VGG16 (blue line), DenseNet (orange line) and Inception V3 (green line)

From the confusion matrices, we can see DenseNet is more accurate and robust than VGG16. Based on the experiments conducted by Hon and Khan [5], the average accuracy of the leveraged and fine-tuned VGG16 achieved is 0.92296 in the binary classification using 6400 MRI images. Moreover, Fig. 4 also illustrates the loss function of VGG16 does not converge. Therefore, the high accuracy (0.9706) fails to indicate the fabulous performance of VGG16. In contrast, DenseNet could be the most reliable and stable algorithm when it comes to the classification. The connection of the DenseNet guarantees that the overfitting will hardly occur. Shown in Table 2, the accuracy of DenseNet, 0.9118, is still delightful with high accuracy. DenseNet can extract as many features as possible without overfitting. That is why DenseNet is eventually selected as one of the classification models. Obviously, due to the low accuracy of Inception V3 in Table 6, we do not consider it as a selection.

Table 1. Confusion matrix of DenseNet, VGG16 and Inception V3

Actual Value - Prediction	DenseNet	VGG16	Inception V3
AD - AD	0.2059	0.1912	0.1471
AD - MCI	0.0147	0.0294	0.0294
AD - NC	0.0147	0	0.0147
MCI - AD	0.0147	0.0294	0
MCI - MCI	0.3824	0.2941	0.3235
MCI - NC	0.0294	0.0147	0.0735
NC - AD	0.0147	0.0588	0.0882
NC - MCI	0	0.1324	0.0441
NC - NC	0.3235	0.2500	0.2794

Table 2. Performance of DenseNet, VGG16 and Inception V3

Indices	DenseNet	VGG16	Inception V3
Precision of AD	0.8750	1.0000	0.7692
Precision of MCI	0.8966	0.9310	0.8148
Precision of NC	0.9565	1.0000	0.6786
Recall of AD	0.8750	1.0000	0.6250
Recall of MCI	0.9630	1.0000	0.8148
Recall of NC	0.8800	0.9200	0.7600
F1-score of AD	0.8750	1.0000	0.6897
F1-score of MCI	0.9286	0.9643	0.8148
F1-score of NC	0.9167	0.9583	0.7170
Accuracy	0.9118	0.9706	0.7500

3.1.2. Inception V4

We also employ Inception V4 as the enhancement of the classification. Shown in Table 3 and Table 4, the accuracy reaches 0.8235 and the confusion matrix indicates that Inception V4 is comparatively robust.

Table 3. Performance of Inception V4

	Precision	Recall	F1-score
AD	0.8000	0.7500	0.7742
MCI	0.8696	0.8000	0.8333
NC	0.8000	0.8889	0.8421
Accuracy	0.8235		

Table 4. Confusion matrix of Inception V4

Labels	AD	MCI	NC
AD	0.1765	0.0147	0.0294
MCI	0.0294	0.3529	0.0147
NC	0.0147	0.0588	0.2941

3.1.3. The Result after the Fusion

Shown in Table 5 and Table 6, during the fusion process, the performance of our diagnosis model is enhanced and the ensemble model achieves an accuracy of 0.9256.

Table 5. Performance after Fusion

	Precision	Recall	F1-score
AD	1.0000	0.8750	0.9333
MCI	0.9000	1.0000	0.9474
NC	0.9167	0.8800	0.8980
Accuracy		0.9256	

Table 6. Confusion matrix of Fusion

Labels	AD	MCI	NC
AD	0.2059	0	0.0294
MCI	0	0.3971	0
NC	0.0147	0.0441	0.3235

3.2. Comparison with Others' Research

We compared our work with some others' which employed ternary classification. The volume in Table 7 indicates the number of cases instead of the slices.

Table 7. Comparison with Others' Work

Methods	Source	Volume	Accuracy
Gupta A et al. [16]	ADNI	843	0.8500
Payan et al. [17]	ADNI	2265	0.8553
H.A. E et al. [18]	ADNI + CADDementia	210	0.8910
Jain R et al. [8]	ADNI	150	0.9573
This paper	ADNI	475	0.9265

It is worth mentioning again that although Jain R et al. [8], whose method shows high accuracy in Table 7, have already achieved a satisfying accomplishment, our approach to splitting the data set guarantees that nobody's MRI slices can exist in more than one set among the training set, validation set, and test set. Merely based on ADNI, it is delightful that our method reaches a maximum of 0.9265 with such a limited volume of data.

4. Conclusion

In this paper, we proposed an ensemble method that combines DenseNet (transfer learning) with pre-trained Inception V4. In the classification, we reached a maximum of 0.9265 of accuracy in ternary classification with each classification module surpassing 0.8 of accuracy. In our future work, we will continue striving for the enhancement of the probability-based fusion to achieve higher accuracy.

Acknowledgment

This work is supported by Ministry of Education-Microsoft Industry-University Cooperation Project for Educating Teaching Contents and Curriculum System Reform under Grant 201802011006, National Innovation and Entrepreneurship Training Program for College Students under Grant S201910561249, Innovation and Entrepreneurship Training Program of School of Software in South China University of Technology and Student Research Project of South China University of Technology.

References

- [1] A Wilson R S, Segawa E, Boyle P A, et al., The natural history of cognitive decline in Alzheimer's disease[J], *Psychology and aging* (2012), 27(4): 1008.
- [2] Iliffe S, Burns A, Alzheimer's disease, *BMJ* (2009), 338: b158
- [3] Chan KY, Wang W, Wu JJ, et al., Epidemiology of Alzheimer's disease and other forms of dementia in China, 1990–2010: a systematic review and analysis, *Lancet* (2013), 381(9882): 2016–2023.
- [4] Glozman T, Azhari H, A method for characterization of tissue elastic properties combining ultrasonic computed tomography with elastography, *Journal of Ultrasound in Medicine* (2010), 29(3): 387-398.
- [5] Hon M, Khan N M, Towards Alzheimer's disease classification through transfer learning[C], 2017 IEEE International Conference on Bioinformatics and Biomedicine (BIBM) (2017), 1166-1169
- [6] Simonyan K, Zisserman A, Very deep convolutional networks for large-scale image recognition, *International Conference on Learning Representations* (2015)
- [7] Szegedy C, Ioffe S, Vanhoucke V, et al., Inception-v4, inception-resnet and the impact of residual connections on learning, *Thirty-First AAAI Conference on Artificial Intelligence* (2017)
- [8] Jain R, Jain N, Aggarwal A, et al., Convolutional neural network-based Alzheimer's disease classification from magnetic resonance brain images, *Cognitive Systems Research* (2019)
- [9] Fukushima, K., Neocognitron, *Scholarpedia* (2007), 2 (1): 1717.
- [10] G. Wen, Z. Hou, H. Li, D. Li, L. Jiang, E. Xun, Ensemble of deep neural networks with probability-based fusion for facial expression recognition, *Cognit. Comput.* 9 (5) (2017) 597–610.
- [11] Huang G, Liu Z, Van Der Maaten L, et al. Densely connected convolutional networks[C]. Proceedings of the IEEE conference on computer vision and pattern recognition. 2017: 4700-4708.
- [12] Fischl B, FreeSurfer, *Neuroimage* (2012), 62(2): 774-781
- [13] Newman, MEJ, Power laws, Pareto Distributions, and Zipf's law, *Contemporary Physics* (2005). 46 (5): 323–351.
- [14] Chollet, F, et al., Keras(2015)
- [15] Abadi M, Agarwal A, Barham P, et al. TensorFlow: Large-scale machine learning on heterogeneous systems. Software available from tensorflow.org[J]. URL <http://tensorflow.org>, 2015
- [16] Gupta A, Ayhan M, Maida A. Natural image bases to represent neuroimaging data[C]. International conference on machine learning. 2013: 987-994.
- [17] Payan A, Montana G. Predicting Alzheimer's disease: a neuroimaging study with 3D convolutional neural networks[J]. arXiv preprint arXiv:1502.02506, 2015
- [18] Hosseini-Asl E, Gimel'farb G, El-Baz A, Alzheimer's disease diagnostics by a deeply supervised adaptable 3D convolutional network, *Computational and Mathematical Methods in Medicine* (2016)

An Improved Decision Tree Algorithm for Electricity Theft Prediction and Analysis

Chen Xiaofeng, Zhang Lipeng¹, Xu Zhongping, Zhu Feng, Qi Xiaoming

State Grid Information & Telecommunication Accenture Information Technology Co.,
Ltd, Beijing, 100032, China

Abstract. At present, there are many kinds of electricity theft and the corresponding approaches to combat this are insufficient. Manual approaches result in a heavy staff workload and are inefficient. In this paper, the data from an electricity information acquisition system is collected and mined using Python. Based on an understanding of the business and an analysis of the information value (IV) measure, important characteristic indexes are selected and an improved decision tree algorithm is used to construct a model of power theft by users. This method effectively narrows the range of users suspected of power theft, improving the pertinence of audit, and providing strong support for reducing the financial losses of power supply enterprises and ensuring the safety of power grid operation.

Keywords. Electricity Information Acquisition System, Python Platform, Improved Decision Tree Algorithm, Analysis Model of Power Theft, Strong Support

1. Introduction

The theft of electric power seriously disturbs the normal operation of power supply, which not only causes huge economic loss to a country, but also affects the economic benefit of power supply enterprises[1-2]. The traditional detection of power theft mainly relies on manual operation, which not only requires a large amount of human resources and increases the operating cost of power grid companies, but also has low detection efficiency, lagging behind the occurrence of power theft, and has evidence is difficult to obtain[3].

With the development of data mining and other technologies, many anti-theft analysis and prediction methods have emerged[4-6]. Cheng[7] proposed a multi-dimensional characteristic factor correlation model based on the k-means clustering algorithm and parameters taken from the electricity information acquisition system, so as to identify suspected power theft users. Based on the LeNet-5 convolutional neural network model, Zheng[8] modeled and analyzed daily electricity consumption data, selected the abnormal electricity consumption mode, and then used a double-layer deep network to comprehensively analyze user information, line loss in the station area, alarm information, and other data, laying a foundation for the realization of accurate power theft detection. Kangningning[9] adopted FCM clustering

¹ Corresponding Author: Zhang Lipeng, State Grid Information & Telecommunication Accenture Information Technology Co., Ltd, Email: Philip_Zhang@163.com

and an improved SVR model to detect the power consumption behavior of users suspected of stealing electricity. This effectively narrowed the scope of detection, overcame the issue of having only a few samples of theft behavior, and improved the detection efficiency. Based on the Hadoop big data platform, Wu[10] collected data related to the internal customer power consumption behavior patterns of power enterprises, studied the relationship between customer power consumption and power theft, conducted training and modeling on the platform with a neural network, and applied the latest data verification results to prove that it could effectively improve the detection of, and response to, power theft. Through supervised machine learning from core user data such as audit, business expansion, electricity charges, line loss, measurement, and customer service, Cai[11] established a predictive power theft classification model, and assisted in the arrangement of electricity consumption inspection plans, effectively reducing the loss of state-owned assets.

As a new means of data processing, big data and artificial intelligence technologies can perform effective data analysis for a large number of complex scenarios. Based on a variety of user electrical information, this paper makes full use of Python to mine the data, applying logistic regression, random forests, decision trees, and other methods. The decision tree algorithm is made more accurate after business analysis and the application of 50% crossvalidation. The decision tree algorithm will be further improved, so as to more efficiently detect power theft and other abnormal behavior, as well as improving the existing collection system's audit efficiency and power management ability.

2. Principle analysis and algorithm selection

2.1 Analysis of the principle of electricity theft

When considering electricity theft, the user does not steal electrical energy as such, but in some way tampers with the metering device [12], causing a deviation in the reading and thus achieving the goal of paying less money. The expression for a watt-hour meter is as follows:

$$W = Pt = UI \cos \varphi \quad (1)$$

It can be seen from the above equation that the measured electrical energy is mainly related to the power and power consumption time. The metering power is subject to the metering voltage and the current of the watt-hour meter[13], metering voltage, phase-shifting steals electricity[14]. The influence of the three electrical quantities and the change of any factor related to the measurement of electrical energy will interfere with its measurement, thus achieving the purpose of power theft[15]. Various common means of stealing electricity are shown in Figure 1.

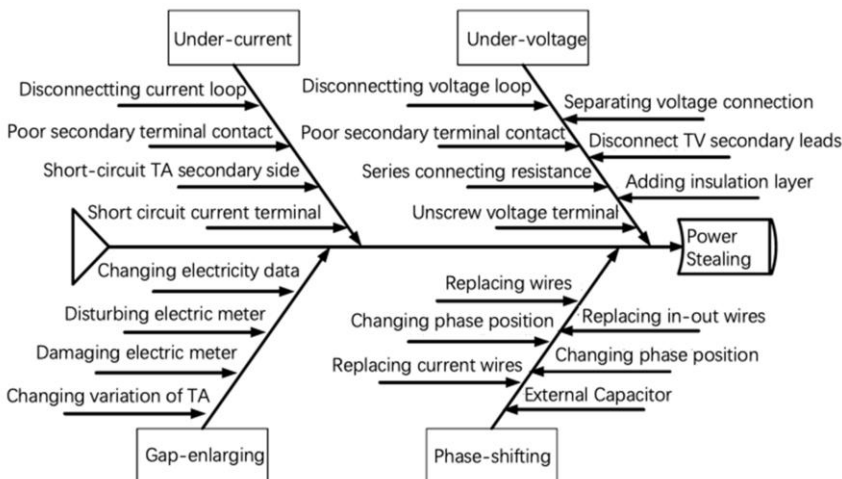


Figure 1. Methods of power theft.

2.2 Algorithm selection

The analysis and automatic recognition of power theft is a classification problem. Logistic regression, CART decision trees, random forests, and other algorithms can be used for this purpose[16]. For each problem, different algorithms have different respective problems with adaptability. A comparison of the advantages and disadvantages of these main algorithms is shown in Table 1.

Table 1. Comparison of algorithms

Algorithm	Advantages	Disadvantages
Logistic Regression	1. Fast analysis and is suitable for dichotomy problems; 2. Has good robustness and will not be affected by slight multicollinearity.	1. Fit accuracy is low; 2. It cannot process data with missing values.
CART decision tree	1. High speed and accuracy, and can handle both continuous and discrete fields 2. There is no limitation on the uniqueness of data attributes; 3. No sensitivity to missing values; 4. Computing efficiency can be improved without remodelling	1. Processing time series data is a heavy workload; 2. Overfitting may occur; 3. Does not work well when dealing with data that is highly correlated.
Random Forest	1. No sensitivity to missing values and outliers; 2. High dimensional data can be processed without characteristic selection; 3. Both discrete and continuous data can be processed.	1. Overfitting may occur; 2. The data processing effect of different attributes is not good.

In order to further improve the performance of the model in predicting unknown data, this article chooses an area with 100 users for the electricity data (50 homes without power theft, 50 homes with power theft). Fifty percent cross validation is introduced to compare the different machine learning algorithms. The logistic regression, decision tree, and random forest models were trained through 50% cross validation[17]. In this environment, the decision tree has the highest accuracy for this data, so this paper focuses on the decision tree algorithm for modeling. The validation results are shown in Figure 2.

Recall rate of Logistic Regression:	0.5337060478199718
Recall rate of Random forests:	0.8382017279485634
Recall rate of Decision tree	0.8432710468153506

Figure 2. Model verification results

2.3 Decision tree algorithm (CART)

Suppose a training set is given $D = (x_1, y_1), (x_2, y_2), \dots, (x_N, y_N)$, $x_i = (x_i^{(1)}, x_i^{(2)}, \dots, x_i^{(n)})^T$, where n is the number of features, $y_i \in 1, 2, \dots, K$ is the number of categories, N is the sample size, $i = 1, 2, \dots, N$. The decision tree model is constructed according to the given training set to achieve the goal of correct classification. The specific method is as follows: the information gain of each feature is calculated. The feature with the maximum value is chosen to be the root node, and the method above is recursively called on each child node to construct the decision tree until the information gain of all features is very small or there is no feature remaining to choose from. Also, in order to prevent overfitting, it is necessary to prune the generated decision tree.

The criterion of feature selection is information gain. Empirical entropy $H(D)$ represents the uncertainty of classifying the data set D , empirical conditional entropy $H(D|A)$ represents the uncertainty of classifying data set D under the conditions given by the feature and $|D|$ represents the sample size. Suppose there are K classes $C_k, k = 1, 2, \dots, K$, and $|C_k|$ is the number of samples belonging to class C_k , $\sum_{k=1}^K |C_k| = |D|$. Let feature A have n different values, $\{a_1, a_2, \dots, a_n\}$; according to the value of feature A , divide D into n subsets D_1, D_2, \dots, D_n , and $|D_i|$ is the number of samples of D_i , $\sum_{i=1}^n |D_i| = |D|$. The sample set belonging to class C_k in subset D_{ik} is denoted as D_i , The information gain is calculated as follows:

$$(1) H(D) = -\sum_{k=1}^K \frac{|C_k|}{|D|} \log_2 \frac{|C_k|}{|D|} \quad (2)$$

$$(2) H(D|A) = \sum_{i=1}^n \frac{|D_i|}{|D|} H(D_i) = -\sum_{i=1}^n \frac{|D_i|}{|D|} \sum_{k=1}^K \frac{|D_{ik}|}{|D_i|} \log_2 \frac{|D_{ik}|}{|D_i|} \quad (3)$$

$$(3) \text{ Calculating the information gain, } g(D, A) = H(D) - H(D|A) \quad (4)$$

In general, the greater the information gain, the greater the "purity enhancement" obtained by this feature for the partition of the data set. However, it has the disadvantage of favoring attributes with more values, so the model established based on this does not have good generality. As a result, the information gain ratio is introduced:

$$g_ratio(D, A) = \frac{g(D, A)}{H_A(D)} \quad (5)$$

$$H_A(D) = -\sum_{i=1}^n \frac{|D_i|}{|D|} \log_2 \frac{|D_i|}{|D|} \quad (6)$$

As the information gain ratio can be less number of desirable properties of preference, we, based on the modified, using the heuristic algorithm, namely from the candidate first find out the information gain above average in attribute, and then choose the highest information gain rate attributes, as the current property root node, in the subsequent also adopt heuristic method of recursive calls to produce the final decision tree.

3. Application scenarios

Based on big data and artificial intelligence, modeling power theft by key users is mainly divided into five parts: data exploration, data cleaning, feature extraction, model construction, and model evaluation. This paper focuses on 4250 power users in a certain area and 112,862 power records for power theft identification.

3.1 Data processing

3.1.1 Data consolidation

For this, the following high voltage power factors were collected: power, current, voltage, and meter code 27 indicators in total. Based on the collected data, using the metering point number and data date as the unique identifier, we will use pandas. This is merged to connect the data in different tables and so form the data table in Table 2.

Table 2. Data after transformation

Category	Name	Description
User	Name of measuring point	The name of the measuring point
	Number of measuring point	The measurement point number of each data item is uniquely identified by the measurement point number
	Date	The date of each data entry
Current	IA	The amplitude of phase A current in one day
	IB	The amplitude of phase B current in one day
	IC	The amplitude of phase C current in one day
	Current	The amplitude of current in one day
	Three-phase current unbalance rate	The magnitude of the three-phase current unbalance rate in one day
Voltage	UA	The amplitude of the phase A voltage in one day
	UB	The amplitude of the phase B voltage in one day
	UC	The amplitude of the phase C voltage in one day
	Voltage	The amplitude of the voltage in one day
	Three-phase voltage unbalance rate	The magnitude of the three-phase voltage unbalance rate
Power	Peak	Peak of total active power in one day
	Valley	Valley of total active power in one day
	Difference	Peak-valley difference for total active power
	Active A	Active power in A direction in three-phase electricity
	Active C	Active power in C direction in three-phase electricity
	Active B	Active power in B direction in three-phase electricity
	Total Active	Active power in three-phase electricity

	Reactive A	Phase A reactive power
	Reactive B	Phase B reactive power
	Reactive C	Phase C reactive power
	Total Reactive	Total phase reactive power
Electricity consumption	Positive active day freezing	The daily electricity consumption
	Power factor	High voltage total power factor
	Phase Angle	The vector angles of the waveforms of any two phases of three-phase electricity differ by 120 degrees at any time, which is called the phase angle of the two waveforms

3.1.2 Data cleaning and conversion

After exploring the formed data set, it was found that the data set contained 467 missing values; this missing data was then filled using an appropriate method[18]. At the same time, the peak-valley difference, forward active power freezing, active power total, three-phase current unbalance, and three-phase voltage unbalance were converted into five categories via Python to achieve the transformation from continuous to discrete values. The remaining continuous variables are divided into five groups, each of which is based on the quantile discretization function pd.qcut in Python. The variables are divided into five groups according to their rank or sample quantiles[19]. The converted data is shown in Table 3 below.

Table 3. Discrete data result

	Power Factor	Phase Angle	IA	IB	IC	Voltage	Active A	Active B	Active C	Peak	Valley
0	0.3549	1.208	0.051	0.0	-0.054	68.741	0.004	0.0	-0.002	0.0056	0.0017
1	0.3297	1.235	0.048	0.0	-0.045	68.643	0.004	0.0	-0.001	0.0092	0.0016
2	0.2650	1.303	0.044	0.0	-0.048	68.526	0.003	0.0	-0.001	0.0040	0.0017
3	0.2450	1.323	0.050	0.0	-0.055	69.592	0.004	0.0	-0.002	0.0043	0.0018
4	0.3014	1.265	0.048	0.0	-0.053	68.866	0.004	0.0	-0.002	0.0057	0.0017

3.2 Feature extraction

Data with strong predictive power were selected from the variables with high collinearity correlation between features. Therefore, we use the information value (IV) to screen features with high correlation and strong predictive power[20].

The calculation of IV is based on WOE[21]:

$$WOE_i = \ln \left(\frac{py_i}{pn_i} \right) = \ln \left(\frac{\#y_i/\#y_T}{\#n_i/\#n_T} \right) = \ln \left(\frac{\#y_i/\#n_i}{\#y_T/\#n_T} \right) \quad (7)$$

When building a classification model, it is often necessary to filter the independent variables. Specific indicators are needed to measure the predictive power of each independent variable, and according to the size of these quantitative indicators, to determine which variables enter the model. The IV measure can be used to assess the predictive power of an independent variable. The formula for calculating IV is:

$$\begin{aligned}
 IV_i &= (py_i - pn_i) * WOE_i = (py_i - pn_i) * \ln\left(\frac{py_i}{pn_i}\right) \\
 &= \left(\frac{\#y_i}{\#y_T} - \frac{\#n_i}{\#n_T}\right) * \ln\left(\frac{\frac{\#y_i}{\#y_T}}{\frac{\#n_i}{\#n_T}}\right)
 \end{aligned} \quad (8)$$

By calculating each characteristic IV quantity, the final result is shown in Figure 3.

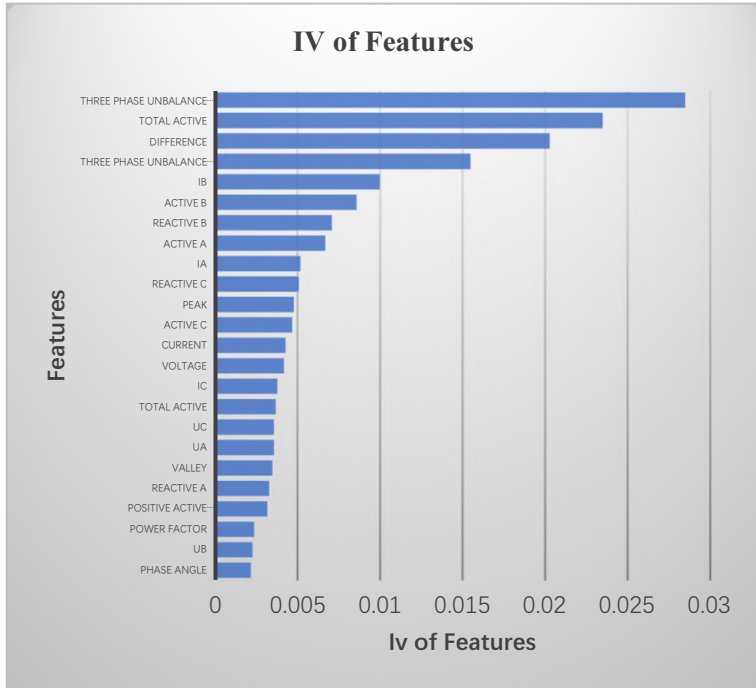


Figure 3. Feature IV.

According to the correlation coefficient and correlation of each index, the P value is used to preliminarily judge the correlation of variables, eliminate highly linear correlated variables, reduce the redundancy of variables, and simplify the input parameters of the model, so as to improve the data quality and improve the accuracy and performance of the model. The correlation between variables is shown in Figure 4.

In order to address the collinearity problem between these features, features with correlation coefficient >0.75 were screened out. Finally, based on the understanding of the business and the judgment of IV measure, 16 important indicators were selected, as shown in Table 4.

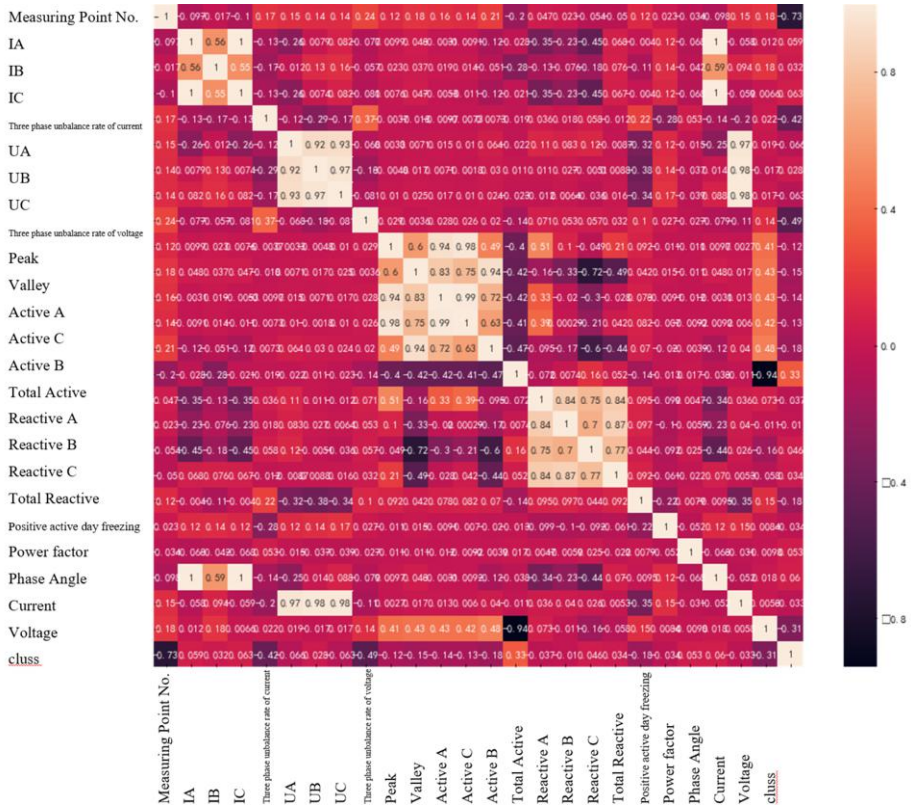


Figure 4. Variable correlation.

Table 4. Effective IV of features

Order Number	Features	IV of Features	Order Number	Features	IV of Features
1	Phase Angle	0.0022	13	Active C	0.0047
2	UB	0.0023	14	Peak	0.0048
3	Power factor	0.0024	15	Reactive C	0.0051
4	Positive active day freezing	0.0032	16	IA	0.0052
5	Reactive A	0.0033	17	Active A	0.0067
6	Valley	0.0035	18	Reactive B	0.0071
7	UA	0.0036	19	Active B	0.0086
8	UC	0.0036	20	IB	0.01
9	Total Active	0.0037	21	Three phase unbalance rate of current	0.0155
10	IC	0.0038	22	Difference	0.0203
11	Voltage	0.0042	23	Total Active	0.0235
12	Current	0.0043	24	Three phase unbalance rate of voltage	0.0285

3.3 Modeling and output

3.3.1 Model building

After processing, the data is divided into a training set and test set, and the optimal partition ratio is shown in Table 5.

Table 5. The accuracy of the model when dividing the test set and training set

Order Number	Split Scale (Test Set : Training Set)	Accuracy
1	4 (test) : 6 (train)	93.5
2	5 (test) : 5 (train)	93.6
3	2 (test) : 8 (train)	94.1
4	3 (test) : 7 (train)	94.5

According to these results, the final partition was achieved using a 7:3 training:test split. The improved decision tree method is used for training using the segmented training set, and the anti-theft model is obtained.

3.3.2 Model output

Python is used to calculate the feature importance for the power theft analysis model. In the model trained by the decision tree, the value of `clf.feature_importances_` (key variable) is extracted as the coefficient of indicator feature importance. The calculation principle is to determine the weight of each index according to the information gain ratio of the dependent variable. The larger the information gain ratio, the higher the index weight. The resulting weights are shown in Figure 5.

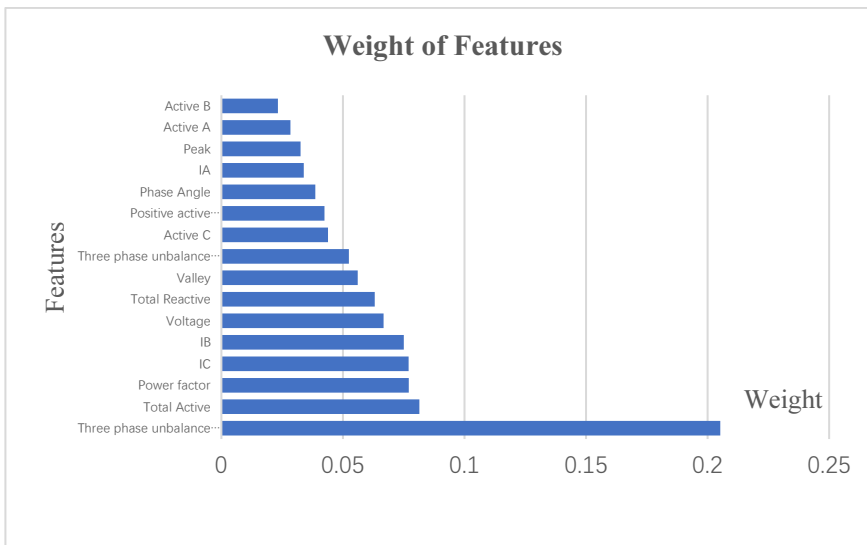


Figure 5. Weight of features.

According to the learned decision tree model, the three-phase voltage unbalance, total active power, power factor, and other factors have a high influence in determining power theft.

After the above data processing and model training, the classification system is established. Whether users steal electricity is the model prediction category, which is divided into users who steal electricity and normal users (1 represents users who steal electricity, 2 represents normal users). The prediction results are shown in Table 6 below.

Table 6. Prediction results

	0	1	2	3	4	5	6	7	8	9	...	3715	3716	3717	3718	3719	3720	3721	3722	3723	3724
test_est	2	2	2	2	2	2	2	2	2	2	...	2	2	2	1	2	2	1	2	2	2

The calculated output of the model includes the number of metering points, data date, suspicion coefficient of power theft, etc., as shown in Table 7.

Table 7. Model calculation result

Measuring Point No.	Date of data	Three phase unbalance rate of current	Three phase unbalance rate of voltage	Positive active day freezing	Phase Angle	Total Reactive	Total Active	Suspected index of stealing electricity
0	20001294867	2015/10/8	0.005548	0.008772	0.00309	-0.009781	0.000329	-0.214651 0.600000
1	24000119881	2017/3/4	-0.149724	-0.062338	0.00309	0.011057	0.013128	0.003330 1.000000
2	68222	2015/11/10	0.005548	0.008772	0.00309	0.003261	0.000329	0.003330 0.250000
3	40606	2018/5/7	0.005548	0.008772	0.00309	-0.009781	0.013128	0.003330 0.714286
4	3158128	2017/7/27	-0.149724	-0.062338	0.00309	-0.009781	-0.017691	0.003330 1.000000

The model is a dichotomy, with a probability for the categories YES and NO. According to the calculated results, if the probability of YES is greater than or equal to 50% and the probability of NO is less than 50% via the suspicion coefficient of electric theft, then the user is classified as stealing power. Through the suspicion coefficient of electric power theft, the users who are stealing power are accurately identified. If the value falls within the range [0.5,0.8] this is determined to be a suspicion of general electric power theft; if it falls within the range [0.8,1] this is considered to be major electric power theft, as shown in Figure 6.

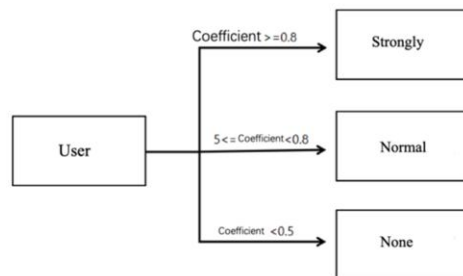


Figure 6. Power theft user division.

The final classification prediction results are shown in Table 8.

Table 8. Anti-theft classification prediction

Measuring Point No.	Date of data	Three-phase unbalance rate of current	Three-phase unbalance rate of voltage	...	Is it stealing electricity	Suspicion of power theft
68222	2015/11/27	0.2215	0.0027	...	Yes	Normal
39826605	2017/8/13	0.9661	1	...	Yes	Strong
107833	2019/3/2	0.0455	0.0043	...	No	None
...

3.4 Evaluation

A true positive TP is where the actual classification in the test set and the predicted result from the model are both that the user is stealing power (i.e. power-theft user); a true negative TN is where both are the normal user category. A false positive FP where the actual classification is a normal user but the predicted result is power theft. A false negative FN is the opposite of this. The formula for precision is: $Precision = \frac{TP}{TP+FP}$, and the formula for recall is: $Recall = \frac{TP}{TP+FN}$. The F_1 score is a harmonic average of the precision and recall, so the larger the F_1 score, the better the model.

$$F_1 = 2 * \frac{precision*recall}{precision+recall} \quad (9)$$

According to the above results, the evaluation of each category is shown in Table 9.

Table 9. Model evaluation

Category	Precision	Recall	F1 score
Power-theft user	88%	83%	85%
Normal user	96%	97%	97%
avg/total	95%	95%	95%

Next, the accuracy of the model is calculated, and the formula is:

$$Accuracy = \frac{TP+TN}{TP+FN+FP+TN} \quad (10)$$

Finally, the model accuracy is 94.1%.

4. Conclusion

In this paper, various behaviors of stealing electricity are analyzed and the fishbone diagram representation is given. Python is used to transform and populate data with missing values, apply IV assessment and an understanding of the business, and filter the important metrics. Based on this, an improved decision tree algorithm is used to construct a power theft prediction model. The validity and correctness of the model are verified by experimentation. The results of this paper show that this is an effective method to improve the efficacy of anti-theft audit.

Reference

- [1] LAI Zhe. Analysis of Anti-stealing Electricity with Big Data Technology[J]. Electronic Test, 2019(16):50-51+38.
- [2] GAO Wei, WEN Tongyang, XU Wei, et al. Analysis of Data Collection Technology and Application of Intelligent Anti Stealing[J]. Science and Technology Innovation Herald, 2019,16(18):32+34.
- [3] XIONG Xia, TAO Xiaofeng, YE Fangbin, et al. Electricity Stealing Detection Method Based on Weighted Algorithm of Station Identification and Correlation Monitoring[J]. Journal of Computer Applications, 2019,39(S2):289-292.
- [4] TANG Liangyi, WANG Kun, LI Hongliu, et al. Analysis on the Application of Big Data Technology in Intelligent Anti Stealing and Line Loss Monitoring[J]. Electrotechnical Application, 2017,36(17):48-53.
- [5] WEI Yao, ZHU Weiyi, GONG Taorong, et al. Abnormal Electric Consumption Analysis System Using Data Mining[J]. Electric Power Information and Communication Technology, 2014,12(05):70-73.
- [6] HOU Dan, LI Gang, ZHAO Wenqing, et al. Application of Big Data Analysis and Visualization Technology in Power Grid Company[J]. Smart Grid, 2015,3(12):1186-1191.
- [7] CHENG Junwen, LI Huijuan, CHAO Zhiqiang. Research on Anti-stealing Based on K-means Clustering Algorithm and Electricity Information Collection System [J] Distribution & Utilization, 2018,36(1):75-80.
- [8] ZHENG Jianning. Detection Method of Electricity Stealing Behavior Based on Deep Learning[J]. Information Technology, 2019(02):156-159.
- [9] Kang Ningning, Li Chuan, Zeng Hu, et al. Electric larceny detectionusing FCM clustering and improved SV R model[J]. Journal of Electronic Measurment and Instrumentation, 2017,31(12):2023-2029.
- [10] WU Yiliang. Research on Prediction Platfrom of Power Stealing Based on Hadoop[J]. Mechanical and Electrical Information, 2017(06):20-21.
- [11] Cai Jiarong, Wang Shunyi, Wu Guangcai. The User's Electric Power Prediction and Electricity Inspection Plan Based on Machine Learning Research on Auxiliary Arrangement[J]. Electronic Test, 2018(02):108-109.
- [12] Zhang Fangfang. Analysis of Anti-Stealing of Intelligent Electric Energy Meter[J]. Electronic Technology & Software Engineering, 2018(15):206.
- [13] LUO Kewei. Analysis of Electric Power Stealing and Anti-Electric Power Stealing Technology in Electric Power Monitoring[J]. New Technology & New Products of China, 2019(24):116-117.
- [14] CHEN Jianliang. Technical Analysis of Anti-Stealing in Power Supply Enterprises[J]. China High-Tech Enterprises, 2013(22):119-120.
- [15] FU Weizhu, ZHANG Pei, GAO Wei, et al. Case Analysis of The Over Differential Stealing of the Telephone Energy Meter by Maliciously Putting Capacitor into Operation[J]. Science and Technology Innovation Herald, 2016,13(08):7+9.
- [16] CUI Hongyan, XU Shuai, Zhang Lifeng, et al. The Key Techniques and Future Vision of Feature Selection in Machine Learning[J]. Journal of Beijing University of Posts and Telecommunications, 2018,41(01):1-12.
- [17] XU Chang, CHEN Jinqiong, ZHOU Wen. Improving unbalanced data classification of unsupervised limit learning machine[J]. Journal of Anhui Normal University (Natural Science), 2018,41(06):544-551.
- [18] FAN Qiao, GUO Ajun. An Improved Solow Residual Method for TFP Calculating under the Framework of Spatial Econometrical Analysis[J]. The Journal of Quantitative & Technical Economics, 2019,36(08):165-181.
- [19] LIU Yun, YUAN Haoheng. Parallel Discretization of Data Preparation Optimization in Data Mining[J]. Journal of Sichuan University(Natural Science Edition), 2018,55(05):993-999.
- [20] Yang Jianfeng, Qiao Peirui, Li Yongmei, A Review of Machine-learning Classification and Algorithms[J]. Statistics & Decision, 2019,35(06):36-40.
- [21] GENG Juncheng, ZHANG Xiaofei, YUAN Shaoguang, et al. Research and Implementation of Users'outage Sensitivity Score Card Basedon Logistic Regression Model[J]. Power Demand Side Management, 2018,20(03):46-50.

Curves Classification by Using a Local Likelihood Function and Its Practical Usefulness for Real Data

Mustapha Rachdi^{a,1}, Ali Laksaci^b, Ali Hamié^a, Jacques Demongeot^a and Idir Ouassou^c

^a Universityé Grenoble Alpes, France

^b Department of Mathematics, College of Science and Statistical Research and Studies Support Unit, King Khalid University, Abha, KSA

^c Université Cadi Ayyad (ENSAM) and Université Mohammed VI Polytechnique (Morocco)

Abstract. We extend the classical approach in supervised classification based on the local likelihood estimation to the functional covariates case. The estimation procedure of the functional parameter (slope parameter) in the linear model when the covariate is of functional kind is investigated. We show, on simulated as well on real data, that classification error rates estimated using test samples, and the estimation procedure by local likelihood seem to lead to better estimators than the classical kernel estimation. In addition, this approach is no longer assuming that the linear predictors have a specific parametric form. However, this approach also has two drawbacks. Indeed, it was more expensive and slower than the kernel regression. Thus, as mentioned earlier, kernels other than the Gaussian kernel can lead to a divergence of the Newton-Raphson algorithm. In contrast, using a Gaussian kernel, 4 to 6 iterations are then sufficient to achieve convergence.

Keywords. Functional data analysis, Logit model, FPCA, Functional discrimination by local likelihood, NIR spectroscopic data, Mass spectroscopic data, Chromatography data, Waveform data

1. Introduction

A regular problem encountered in many scientific fields is the discrimination between curves. Generally, these curves describe the evolution of a quantity over time (monthly totals of precipitation, temperature evolution, patient walk curves with Parkinson's disease, ...) or when there are changes in absorbance depending on the wavelength (e.g., spectra provided by near infrared spectroscopy).

The collected data are in general considered as simple vectors of \mathbb{R}^p , but are curves obtained from observations at discretized random times of continuous functions of time. Traditionally, these observations are dependent on a time index which is a discretization

¹ Corresponding Author: University Grenoble Alpes, UFR SHS, BP. 47, BSHM, 38040 Grenoble Cedex 09, France E-mail: mustapha.rachdi@univ-grenoble-alpes.fr

grid. Thus, for each curve, the times of the grid in which the functions are observed, can be identical or different, uniformly distributed or not. Indeed, these data are in an infinite dimensional space, so they are called *Functional Data*.

In this work, we consider that each curve is associated with a qualitative variable admitting two terms, i.e., each curve is associated with a label. A classic example of label is “sick” or “healthy”, “good” or “bad”, 0 or 1. Therefore, the aim is to calculate the discrimination of curves. In other words, the goal is to explain the value of the label by the values of the curve in its entirety. Thus, another goal is the prediction: once a new curve is obtained, we predict the value that takes its label.

As part of the functional discrimination, most authors make some adaptations to extend the classical statistical models to functional case. We can mention, without being exhaustive, James and Hastie [1] applying the linear discriminant analysis of Fisher in case of functional variables. In 2002, James [2] offered the functional generalized linear model with a solution based on the EM algorithm (Expectation-Maximization) and Ferraty and Vieu [3] also offer non-parametric estimation methods of conditional probabilities based on kernel methods (see also [4], [5], [6], [7], [8], [9], [10], [11], [12], [13], [14], [15], [16], [17], [18], [19] and [20] and references therein). Müller and Stadtmüller [21] propose the functional quasi-likelihood model. Moreover, Escabias *et al.* [22] and [23] offer to perform a logistic regression on principal components. Preda *et al.* [24] provide solutions to the wrong problem, the cover on infinite dimensional data, using partial least squares (PLS), and then, applying a linear analysis discriminant on the PLS components. Recently, Aguilera *et al.* [25] are interested in the same suite of PLS components used by Preda *et al.* [24], then they show that the PLS approach for functional data is equivalent to a multivariate PLS finished by using the coefficients of the approximations in basic functions as a predictor. Note that their method also applies in cases where the dependent variable is binary. Finally, Aguilera *et al.* [26] offer a functional logistic regression with three steps: first, functional data must be smoothed using penalized B-spline bases. Then, the principal components are extracted from the smoothed data. Finally, a logistic model is created using these components.

This paper is organized as follows. The first section presents the procedure of the functional principal components analysis generally used to reduce the dimension, and we recall some generalities about the generalized linear model. Then in Section 2, we briefly describe the approach of Ferraty and Vieu [3], with which we make comparisons to evaluate the performance of our approach. Then, in Section 3, we propose an extended functional version of multidimensional local likelihood. Section 4 focuses on implementation of the proposed method and that of Ferraty and Vieu [3] using real and simulated data.

2. Preliminaries on the eigenfunctions and the generalized linear model

Functional Principal Components Analysis (FPCA)

We consider, in what follows, that the functional variable X and $\mu_X(\cdot) = \mathbb{E}(X)(\cdot)$ exist and belong to $L^2[0, 1]$. The covariance operator is given by

$$\Gamma_X(\eta) = \mathbb{E}[(X - \mu_X) \otimes (X - \mu_X)(\eta)],$$

such that, for all $\eta \in L^2[0, 1]$

$$(X - \mu_X) \otimes (X - \mu_X)(\eta) = \langle X - \mu_X, \eta \rangle (X - \mu_X), \quad (1)$$

where $\langle \cdot, \cdot \rangle$ denotes the usual scalar product on $L^2[0, 1]$.

The principal components analysis of X is based on the Karhunen-Loeve decomposition, breaking down the functional process on the basis of deterministic orthonormal functions. Indeed, there is a positive decreasing sequence $(\lambda_k)_{k \geq 1}$ of eigenvalues of Γ_X , where $\sum_{k=1}^{\infty} \lambda_k < \infty$, and an orthonormal family of functions ψ_1, ψ_2, \dots , such that $\Gamma_X(\psi_k) = \lambda_k \psi_k$, $k = 1, 2, \dots$. This family of functions $\{\psi_k\}_{k \geq 1}$ forms an orthonormal base of functions in $L^2[0, 1]$:

$$X = \mu_X + \sum_{k=1}^{\infty} \theta_k \psi_k, \quad (2)$$

where $\theta_k = \langle X - \mu_X, \psi_k \rangle$, $k = 1, 2, \dots$ are random coordinates (*functional principal component scores*), centered, of variance λ_k and not correlated. We can truncate this decomposition and keep only the $J > 1$ first terms.

3. Functional discrimination by local likelihood

As indicated above, our explanatory variables are assumed to be curves which are observed on all their trajectories. Thus, a natural generalization is obtained by replacing the finite sum by a definite integral on an infinite space [2],

$$g(\mathbb{E}[Y | X]) = \alpha + \int \beta(t) X(t) dt, \quad (3)$$

where $\alpha \in \mathbb{R}$ and where the $\beta(t)$ functions are assumed smooth and square integrable. Thus, the goal is to model the relationship between a curve which corresponds to the functional variable X and a denoted membership to the class Y . We are in the context of an i.i.d. sample $(X_i, Y_i), i = 1, \dots, n$, where $X \in L^2[0, 1]$ and Y is of Bernoulli type.

The linear predictor is given by $\eta_i = \alpha + \int \beta(t) X_i(t) dt$, and accordingly, the generalized linear functional model is written in the form

$$Y_i = g^{-1}(\eta_i) + e_i, \quad i = 1, 2, \dots, n. \quad (4)$$

where $g(\cdot)$ is the link function. The errors e_i are supposed to be independent and of zero mean. To simplify the notations, we set $g^{-1}(\eta_i) = \pi(X_i)$, where π assumed to be smooth enough, and is the inverse of g . So we define as part of a regression model $Y_i = \pi(X_i) + e_i$, $i = 1, \dots, n$. Then it is easy to write that

$$\pi(x) = \mathbb{E}(Y | X = x) = \mathbb{P}(Y = 1 | X = x) \text{ with } 0 \leq \pi(x) \leq 1.$$

In the case of a dichotomous response variable, the likelihood associated with the sample size n is $\prod_{i=1}^n \pi(X_i)^{y_i} (1 - \pi(X_i))^{1-y_i}$. Thus, the *overall log likelihood* is thus written:

$\mathcal{L}(\pi) = \sum_{i=1}^n \ell(y_i, \pi(X_i))$ where $\ell(y, \pi) = y \log \pi + (n-y) \log(1-\pi)$.

Unlike the generalized linear model, the approach of the local likelihood no longer assumes that η has a rigid parametric form. Assuming that η is a smooth function continuously differentiable, the idea is to approximate it locally by a polynomial of order 1 within a viewing window. It follows, via the Taylor expansion around x , that

$$\eta(X_i) \simeq \eta(x) + \langle \beta, X_i - x \rangle,$$

when X_i is located in a neighborhood of x , with $\eta(x)$ scalar noted α , $\beta = \beta(x) \in L^2[0,1]$ and $\langle \cdot, \cdot \rangle$ denoting the scalar product on $L^2[0,1]$. In the same way, the regression function π in X_i is approximated by the local logistic function:

$$\pi(X_i) \approx \frac{e^{\alpha + \langle \beta, X_i - x \rangle}}{1 + e^{\alpha + \langle \beta, X_i - x \rangle}}. \quad (5)$$

Moreover, the transformation logit is written, for $i = 1, \dots, n$, as follows:

$$g(X_i) = \alpha + \langle \beta, X_i - x \rangle = \alpha + \int_{[0,1]} (\beta(t)(X_i(t) - x(t))) dt,$$

In order to estimate the model (6), we choose to adopt the local functional regression by Baflo and Grané [28], whose response variable is scalar. Indeed, our minimization problem is:

$$\sum_{i=1}^n (g(X_i) - (\alpha + \langle \beta, X_i - x \rangle))^2 K\left(\frac{d(X_i, x)}{h}\right) \quad (6)$$

where K is a kernel whose role is to involve the variables X_i which belong to a ball centered at x and of radius h , also called the bandwidth h , and d is a semi-metric defining a measure of proximity between the curves, such that $d(X_i, x) \leq h$. The choice of a semi-metric d is discussed in Benhenni et al. [27], and the section 3.2 is devoted to the choice of the bandwidth h .

3.1. Estimation of the likelihood

In order to reduce the size of the parameter β , Baflo and Grané [28] use an orthonormal basis $\{\phi_j\}_{1 \leq j \leq J}$ of dimension J over $L^2[0,1]$:

$$\beta = \sum_{j=1}^J \beta_j \phi_j \text{ and } X_i - x = \sum_{j=1}^J c_{ij} \phi_j,$$

with $\beta_j = \langle \beta, \phi_j \rangle$ and $c_{ij} = \langle X_i - x, \phi_j \rangle$.

So we choose our base ϕ by calculating the eigenfunctions of the empirical covariance operator (see Barrientos et al. [29]):

$$\frac{1}{|\mathcal{A}|} \sum_{i \in \mathcal{A}} (X_i - \bar{X})^t (X_i - \bar{X}), \text{ where } \mathcal{A} \text{ is the learning sample.}$$

Therefore, for a fixed curve x , the experience planning matrix is written as follows:

$$\mathbf{X}_x = \begin{pmatrix} 1 & c_{11} & \cdots & c_{1J} \\ 1 & c_{21} & \cdots & c_{2J} \\ \vdots & \vdots & & \vdots \\ 1 & c_{n1} & \cdots & c_{nJ} \end{pmatrix}.$$

Now, let's define a *local log-likelihood*. Indeed, the location is carried out via a nonnegative weighting function which depends on the distance between the curves:

$$\mathcal{L}_x(\alpha, \beta) = \sum_{i=1}^n K\left(\frac{d(X_i, x)}{h}\right) \left(Y_i(\alpha + \langle \beta, X_i - x \rangle) - \log(1 + e^{\alpha + \langle \beta, X_i - x \rangle})\right), \quad (7)$$

By passing to the matrix notation, we can write

$$\mathcal{L}_x(\gamma) = \mathbf{W}\ell(Y, \mathbf{X}_x\gamma), \quad (8)$$

where \mathbf{W} is a diagonal matrix ($n \times n$) whose elements are the weights $K\left(\frac{d(X_i, x)}{h}\right)$ for $i = 1, \dots, n$ and $\gamma = (\alpha \ \beta_1 \ \dots \ \beta_J)^T$ is the vector of coefficients.

The solution of (8) is obtained by maximizing the log-likelihood. Generally, this solution is not analytical. Indeed, the optimal solution will be found by iterative methods, the most popular being the algorithms of Newton-Raphson and Fisher. The study of the maximum log-likelihood requires knowledge of derivatives. In the following, the first and second derivative of $\ell(y, \eta)$ with respect to η will be denoted respectively $\dot{\ell}(y, \eta)$ and $\ddot{\ell}(y, \eta)$. So because we are part of a logistic regression, we can write the derivatives as follows:

$$\dot{\ell}(y, \eta) = y - h(\eta), \quad \ddot{\ell}(y, \eta) = -h(\eta)(1 - h(\eta)), \text{ where } h(\eta) = e^\eta / (1 + e^\eta).$$

The estimated parameter vector $\hat{\gamma}$ is therefore a solution for the local log-likelihood equation:

$$\mathbf{X}_x^T \mathbf{W} \dot{\ell}(Y, \mathbf{X}_x\gamma) = 0 \quad (9)$$

To find the local likelihood estimators at x fixed, we numerically solve the equation (9). Note that the system of equations (9) is convex, then it can be solved by the Newton-Raphson algorithm. Therefore, at iteration k , the estimator of Newton-Raphson is updated by the following equation

$$\gamma^{(k+1)} = \gamma^{(k)} + (\mathbf{X}_x^T \mathbf{W} \mathbf{V} \mathbf{X}_x)^{-1} \mathbf{X}_x^T \mathbf{W} \dot{\ell}(Y, \mathbf{X}_x\gamma^{(k)}), \quad (10)$$

where \mathbf{V} is a diagonal matrix whose diagonal elements are $-\dot{\ell}(Y_i, \mathbf{X}_x^T \gamma)$.

Notice that the concavity of $\dot{\ell}(Y_i, \mathbf{X}_x^T \gamma)$ implies that the matrix $\mathbf{X}_x^T \mathbf{W} \mathbf{V} \mathbf{X}_x$ is positive definite, and that the matrix $\mathbf{X}_x^T \mathbf{W}$ is full rank, which therefore causes the uniqueness of $\hat{\gamma}$. Finally, once the parameters have been estimated, the estimator of $\pi(x)$ for x set is calculated using the equation (5):

$$\hat{\pi}(x) \simeq \frac{e^{\hat{\alpha}(x)}}{1 + e^{\hat{\alpha}(x)}} \quad (11)$$

Therefore, the probability for the class $\{Y = 0\}$ is given by:

$$\mathbb{P}(Y = 0|X = x) = 1 - \hat{\pi}(x).$$

Thus, a new curve x is assigned to the class $\{Y = 1\}$ if $\mathbb{P}(Y = 1|X = x) > 0.5$.

We note that, for among existing kernels, we used the Gaussian kernel $K(u) = \frac{1}{\sqrt{2\pi}} \exp\left\{-\frac{u^2}{2}\right\}$. Indeed, other kernels provide smaller neighborhoods. Therefore, it is possible that all curves observed on a neighborhood (window) are from the same membership class. This then causes a divergence of the Newton-Raphson algorithm.

3.2. The bandwidth choice

The bandwidth parameter selection consists in applying a cross-validation procedure on a subset of smoothing parameters calculated from a k nearest neighbors (kNN) estimator. The idea is to consider neighborhoods whose size adapts automatically locally through a single parameter k . In other words, the bandwidth h is replaced by $h_k(x)$. More precisely, if $h_k(x)$ is the quantity associated with exactly k curves x_{i_1}, \dots, x_{i_k} , such as $\text{card}\{i : d(x_i, x) < h_k(x)\} = k$, then $\pi_{g,k}^{(-i)}(x)$ is the leave-out one curve estimator of the local maximum likelihood dependency $h_k(x)$ built using a sample of the observed curves. Therefore, the optimal number k_{opt} of neighbors is defined as follows:

$$k_{opt} = \arg \min_k \sum_i \sum_{g=0}^1 \left(\mathbb{I}_{[Y_i=g]} - \pi_{g,k}^{(-i)}(x) \right)^2 \quad (12)$$

Once the number of neighboring curves is optimized, then the selection process allows us to subsequently evaluate the estimator π in each curve x , by using the best local bandwidth $h(x) := h_{k_{opt}}(x)$.

4. Application on real and simulated data

In this section, we apply our method to three real data sets and a set of simulated data. In this way, we can compare our method with that of Ferraty and Vieu [3].

4.1. NIR spectroscopic data

Data were obtained from the analysis of samples of minced meat by near-infrared spectroscopy (NIR: *Near Infrared Spectroscopy*). Using this technology, the intensity of the absorption of near infrared ray and the wavelength (wavelengths between 850 and 1050 nanometers) have been measured. Thus, the chemical analysis was to evaluate the nutritional quality of meat.

There are 215 spectrometric curves corresponding to absorbance (equal to $-\log 10(\text{transmittance})$ measured by the apparatus) for 100 wavelengths evenly spaced between 850

and 1050 nm, of the corresponding fat. Moreover, these data can be regarded as random functions of the accomplishments: $X_i = \{X_i(\lambda), \lambda \in (850, 1050)\}$, for $i = 1, \dots, 215$.

Meat samples are divided into two classes: those that contain more than 20 % fat and those that contain less than 20 %. Figure 1 represents 20 curves for each class. The statistical discrimination allows avoiding chemical analysis, expensive and time consuming. These data, called Tecator data, and their detailed description are available on the site of StatLib².

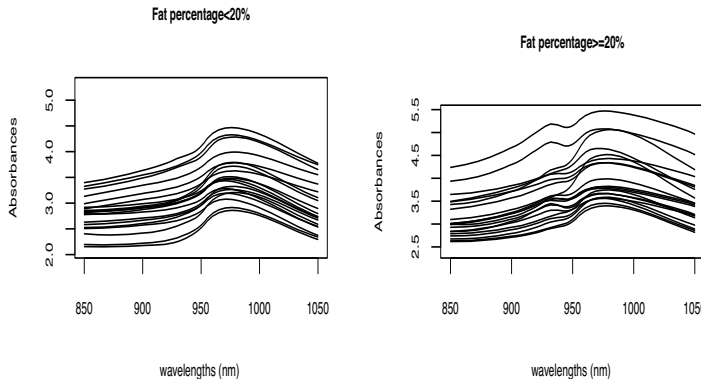


Figure 1. The two classes of data

In order to show the effectiveness of our method of estimation in the context of an anticipation, the sample is randomly divided between a learning subset noted \mathcal{A} with $card(\mathcal{A}) = 160$, and a subset of test \mathcal{T} with $card(\mathcal{T}) = 55$. Thus, the optimal number of neighbors k_{opt} will be calculated using \mathcal{A} , while \mathcal{T} enables us to predict the classes of values \hat{Y}_i , $i \in \mathcal{T}$. Accordingly, the prediction quality is evaluated by the forecasting error (wrong-through rates) defined as follows:

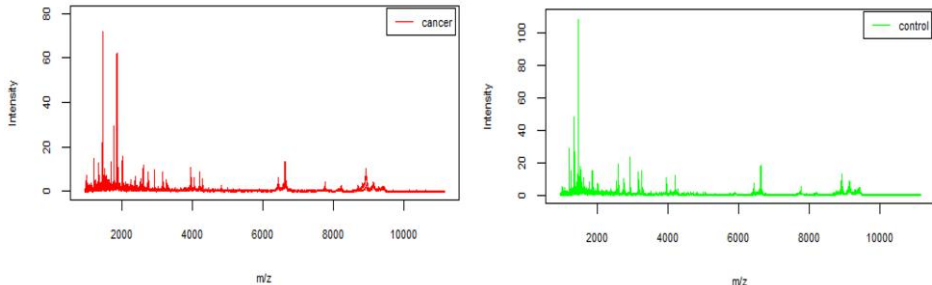
$$\text{Error rate} = \frac{1}{|\mathcal{T}|} \sum_{i \in \mathcal{T}} \mathbb{I}_{[Y_i \neq \hat{Y}_i]}$$

We then apply the two methods, using a semi-metric based on derivatives of order 2 justified by the regular appearance of data. Thus, our method is evaluated on a grid of values of the parameter J representing the basis of size, to optimize within the meaning of the error rate. Therefore, we take $J = 5$ as the number of key components. After the experience of separation repeated 100 times data, the percentage of classification errors and the standard deviation associated to each method are given in Table 1. We will denote by KFV the classical kernel method in Ferraty and Vieu [37], and by LL the Local Likelihood method, showing the superiority of the second method.

4.2. Mass spectroscopic data

We consider a MALDI-TOF mass spectrometry dataset issued from a study on colorectal cancer (see Alexandrov *et al.* [30]). The sample set includes serum profiles of 64 subjects with colorectal cancer and 48 non-cancer control subjects. Each serum profile consists of 16331 recorded intensities corresponding to distinct m/z values.

Method	Mean error rate	Standard deviation
KFV	0.023	0.024
LL	0.018	0.016

Table 1. Tecator data: error rate on 100 test samples.**Figure 2.** Example of spectra for each group coming from colorectal cancer dataset

Method	Mean error rate	Standard deviation
KFV	0.072	0.033
LL	0.060	0.034

Table 2. colorectal cancer: error rate on 100 test samples

The number of major components used to construct the semi-metric and reduce the size of the parameter β equals 4. Thus, Table 2 summarizes the results from 100 iterations, so that at each iteration the data is partitioned randomly into a training set of size 80 and a test set of size 32.

4.3. Chromatography Data derived from HPLC

The data comes from a study seeking to differentiate olive oil from several types of vegetable oils [31] and [32]. These data are composed of 115 oil samples analyzed by high performance liquid chromatography HPLC (*High-performance liquid chromatography*) coupled to an aerosol detector. Thus, the analysis provides 115 spectra of length 4001, also called chromatograms, 71 correspond to the olive oil and 44 are associated with other vegetable oils. The HPLC method provides profiles of triglycerides³, which are a characteristic of different oils. Figure 3 represents 10 curves for each class (olive oil, vegetable oils). These data may be downloaded from the website: <http://www.models.life.ku.dk/oliveoil>. The data separation procedure is repeated 100 times, so that each training set of size 80, and each test set of size 35. Thus, a semi-metric

²<http://lib.stat.cmu.edu/datasets/tecator>

³Triglycerides are molecules belonging to the class of lipids.

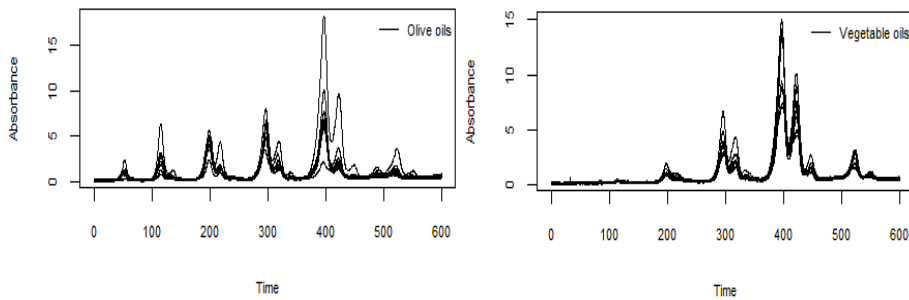


Figure 3. Oils analyzed by HPLC: 10 curves for each class

based on four main components is carried out. Moreover, the dimension J of the space base is also equal to 4. Finally, the results of the predictive performance of the two methods are summarized in the Table 3, showing anew the superiority of the second method.

Method	Mean error rate	Standard deviation
KFV	0.024	0.022
LL	0.008	0.013

Table 3. Data on Oils: error rate on 100 test samples

4.4. Simulated Data: “the waveform data”

As in Preda et al. [24], we plan to implement our method on simulated data, called Breiman *waveform*. This is a two class problem. Each class of curves is generated by linear combination of functions discretized into 101 points uniformly distributed in the interval $[1, 21]$ and generated by the following equations:

$$\text{Class } \{Y = 0\} : X(t) = Uh_1(t) + (1 - U)h_2(t) + \varepsilon(t),$$

$$\text{Class } \{Y = 1\} : X(t) = Uh_1(t) + (1 - U)h_3(t) + \varepsilon(t),$$

where U is a uniform random variable on $[0, 1]$, $\varepsilon(t)$ are independent and identically distributed normal standard variables, $h_1(t) = \max\{6 - |t - 11|, 0\}$, $h_2(t) = h_1(t - 4)$ and $h_3(t) = h_1(t + 4)$. Figure 4 represents 20 curves for each class. The simulated curves are

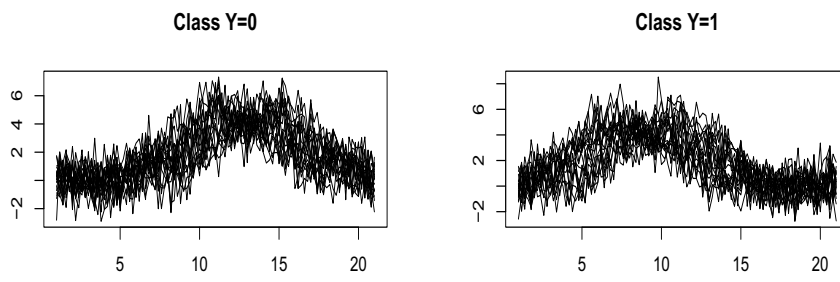


Figure 4. Simulated data: 20 curves for each class

randomly divided into two samples: a sample of 350 curves (175 per class), constituting

Method	Mean error rate	Standard deviation
KFV	0.040	0.022
LL	0.029	0.016

Table 4. Waveform data: error rate for 500 test samples

the learning base and a sample of 150 curves (75 per class) the test database. The optimum number of major components used to construct the semi-metric and the dimension of the projection base ϕ is 3. Thus, Table 4 gives the error rate resulting from the 50 first iterations.

Acknowledgment.

Prof. A. Laksaci extend his appreciation to the Deanship of Scientific Research at King Khalid University for funding this work through General Research Project under grant number: G.R.P-90-41.

References

- [1] G.M. James and T.J. Hastie (2001). Functional linear discriminant analysis for irregularly sampled curves. *Journal of the Royal Statistical Society: Series B (Statistical Methodology)*, Vol. 63, no. 3, Pages 533-550.
- [2] G.M. James (2002). Generalized linear models with functional predictors. *Journal of the Royal Statistical Society: Series B (Statistical Methodology)*, Vol. 64, no. 3, Pages 411-432.
- [3] F. Ferraty and P. Vieu, "Curves discrimination: a nonparametric functional approach," *Computational Statistics & Data Analysis*, vol. 44, no. 1, pp. 161-173, 2003.
- [4] A.M. Almanjahie, Z.C. Elmezouar, A. Laksaci, M. Rachdi (2019). FDA: strong consistency of the kNN local linear estimation of the functional conditional density and mode. *Journal of Nonparametric Statistics*, Vol. 31, no. 1, Pages 175-195.
- [5] A.M. Almanjahie, Z.C. Elmezouar, A. Laksaci, M. Rachdi (2018). kNN local linear estimation of the conditional cumulative function: Dependent functional data case. *C. R. Acad. Sci. Paris, Mathématiques*, Sér. I, Vol. 356, no. 10, Pages 1036-1039.
- [6] B. Altendji, J. Demongeot, A. Laksaci, M. Rachdi (2018). Functional Data Analysis: Estimation of the relative error in functional regression under random left-truncation. *Journal of Nonparametric Statistics*, Vol. 30, no. 2, Pages 472-490.
- [7] F. Awadhi, Z. Kaid, A. Laksaci, I. Ouassou, M. Rachdi (2019). Functional data analysis: local linear estimation of the L1-conditional quantiles. *Statistical Methods & Applications*, Vol. 28, no. 2, Pages 217-240.
- [8] K. Benhenni, S. Hedli-Griche and and M. Rachdi (2017). Regression models with correlated errors based on functional random design. *TEST*, Vol. 26, no. 1, Pages 1-21.
- [9] O. Bouanane, A. Laksaci, M. Rachdi, S. Rahmani (2018). Asymptotic normality of some conditional nonparametric functional parameters in high-dimensional statistics. *Behaviormetrika*, Vol. 46, no. 1, Pages 199-233.
- [10] J. Demongeot, A. Hamié, A. Laksaci, M. Rachdi (2015). Relative-error prediction in nonparametric functional statistics: theory and practice. *Journal of Multivariate Analysis*, Vol. 146, Pages 261-268.
- [11] J. Demongeot, A. Laksaci, F. Madani, M. Rachdi (2011). *A fast functional locally modeled conditional density and mode for functional time-series*. Recent Advances in Functional Data Analysis and Related Topics, Contributions to Statistics, 2011, Pages 85-90, Physica-Verlag/Springer.

- [12] J. Demongeot, A. Laksaci, F. Madani and M. Rachdi (2010). Estimation locale linéaire de la densité conditionnelle pour des données fonctionnelles. *C. R. Acad. Sci. Paris, Sér. I*, 348, No. 15-16, Pages 931-934.
- [13] J. Demongeot, A. Laksaci, A. Naceri and M. Rachdi (2016). Estimation locale linéaire de la fonction de régression pour des variables hilbertiennes *C. R. Mathématiques*, Vol. 354, Issue 8, Pages 847-850.
- [14] J. Demongeot, A. Laksaci, M. Rachdi and S. Rahmani (2014). On the local linear modelization of the conditional distribution for functional data *Sankhyā A: The Indian journal of statistics*, Vol. 76, Issue 2, Pages 328-355.
- [15] M. El Methni and M. Rachdi (2011). Local weighted average estimation of the regression operator for functional data. *Communications in Statistics - Theory and Methods*, Volume 40, Issue 17, Pages 3141-3153.
- [16] S. Dabo-Niang, M. Rachdi and A.-F. Yao (2011). Kernel regression estimation for spatial functional random variables. *Far East Journal of Theoretical Statistics*, Volume 37, Issue 02, Pages 77-113.
- [17] L. Kara-Zaitri, A. Laksaci, M. Rachdi and P. Vieu (2017). Data-driven kNN estimation for various problems involving functional data. *Journal of Multivariate Analysis*, vol. 153, Pages 176-188.
- [18] F. Messaci, N. Nemouchi, I. Ouassou and M. Rachdi (2015). Local polynomial modelling of the conditional quantile for functional data *Statistical Methods & Applications*, vol. 29, no. 1, Pages 597-622.
- [19] I. Ouassou and M. Rachdi (2012). Regression operator estimation by delta-sequences method for functional data and its applications. *AStA Advances in Statistical Analysis*, 2012, vol. 96, Pages 451-465.
- [20] M. Rachdi, A. Laksaci, J. Demongeot, A. Abdali and F. Madani (2014). Theoretical and practical aspects on the quadratique error in the local linear estimation of the conditional density for functional *Computational Statistics & Data Analysis*, Vol. 73, Issue 2, Pages 53-68.
- [21] H.G. Müller and U. Müller, "Generalized functional linear models," *Annals of Statistics*, 774-805, 2005.
- [22] M. Escabias, A. M. Aguilera, and M. J. Valderrama, "Principal component estimation of functional logistic regression: discussion of two different approaches," *Journal of Nonparametric Statistics*, vol. 16, no. 3-4, pp. 365-384, 2004.
- [23] M. Escabias, A. M. Aguilera, and M. J. Valderrama, "Modeling environmental data by functional principal component logistic regression," *Environmetrics*, vol. 16, no. 1, pp. 95-107, 2005.
- [24] C. Preda, G. Saporta, and C. Lévéder, "PLS classification of functional data," *Computational Statistics*, vol. 22, no. 2, pp. 223-235, 2007.
- [25] A. M. Aguilera, M. Escabias, C. Preda, and G. Saporta, "Using basis expansions for estimating functional pls regression: Applications with chemometric data," *Chemometrics and Intelligent Laboratory Systems*, vol. 104, no. 2, pp. 289-305, 2010.
- [26] M. C. Aguilera-Morillo, A. M. Aguilera, M. Escabias, and M. J. Valderrama, "Penalized spline approaches for functional logit regression," *Test*, vol. 22, no. 2, pp. 251-277, 2013.
- [27] K. Benhenni, F. Ferraty, M. Rachdi and P. Vieu, "Local smoothing regression with functional data," *Computational Statistics*, vol. 22, no. 3, pp. 353-369, 2007.
- [28] A. Bafilo and A. Grané, "Local linear regression for functional predictor and scalar response," *Journal of Multivariate Analysis*, vol. 100, no. 1, pp. 102-111, 2009.
- [29] J. Barrientos-Marin, F. Ferraty, and P. Vieu, "Locally modelled regression and functional data," *Journal of Nonparametric Statistics*, vol. 22, no. 5, pp. 617-632, 2010.
- [30] T. Alexandrov, J. Decker, B. Mertens, A. M. Deelder, R. A. Tollenaar, P. Maass, and H. Thiele, "Biomarker discovery in maldi-tof serum protein profiles using discrete wavelet transformation," *Bioinformatics*, vol. 25, no. 5, pp. 643-649, 2009.
- [31] P. De la Mata-Espinosa, J. Bosque-Sendra, R. Bro, and L. Cuadros-Rodríguez, "Olive oil quantification of edible vegetable oil blends using triacylglycerols chromatographic fingerprints and chemometric tools," *Talanta*, vol. 85, no. 1, pp. 177-182, 2011.
- [32] P. De la Mata-Espinosa, J. Bosque-Sendra, R. Bro, and L. Cuadros-Rodríguez, "Discriminating olive and non-olive oils using hplc-cad and chemometrics," *Analytical and bioanalytical chemistry*, vol. 399, no. 6, pp. 2083-2092, 2011.
- [33] K. Chen, S. Guo, Y. Lin and Z. Ying, Least absolute relative error estimation. *J. Am. Statist. Assoc.*, vol. 105, 1104-1112, 2010.
- [34] J. Demongeot, M. Ghassani, I. Ouassou, C. Taramasco and M. Rachdi (2013). Archimedean copula and contagion modelling in epidemiology Networks and Heterogeneous Media, American Institute of Mathematical Science (AIMS), Vol. 08, Issue 01, Pages 149-170.
- [35] J. Demongeot, A. Laksaci, A. Naceri and M. Rachdi (2017). Local linear regression modelization when

- all variables are curves *Statistics & Probability Letters*, Vol. 121, Pages 37-44.
- [36] J. Demongeot, A. Laksaci, F. Madani and M. Rachdi (2013). Functional data: local linear estimation of the conditional density and its application *Statistics*, Vol. 47, Issue 01, Pages 26-44.
 - [37] F. Ferraty and P. Vieu, *Nonparametric functional data analysis: theory and practice*. Springer Science & Business Media, 2006.
 - [38] A. Laksaci, F. Madani and M. Rachdi (2013). Kernel conditional density estimation when the regressor is valued in a semi-metric space. *Communications in Statistics-Theory and Methods*, 2013, vol. 42, no. 19, Pages 3544-3570.
 - [39] P. McCullagh, J.A. Nelder, and P. McCullagh, *Generalized linear models*, vol. 2. Chapman and Hall London, 1989.
 - [40] M. Rachdi, A. Laksaci, A.M. Almanjahie and Z.C. Elmezouar (2020). FDA: Theoretical and practical efficiency of the local linear estimation based on the kNN smoothing of the conditional distribution when there are missing data. *Journal of Statistical Computation and Simulation*, Vol. 90, Issue 8, Pages 1479-1495.
 - [41] M. Rachdi and P. Vieu, "Nonparametric regression for functional data: automatic smoothing parameter selection," *Journal of Statistical Planning and Inference*, vol. 137, no. 9, pp. 2784-2801, 2007.
 - [42] J.O. Ramsay, *Functional data analysis*. Wiley Online Library, 2006.

Application of Grey Prediction in a GA-BP Power Theft Algorithm

Chen Xiaofeng^a, Xu Zhongping^a, Zhang Lipeng^{a,1}, Zhu Feng^a, Qi Xiaoming^a,
Chen Fangzhen^b

^aState Grid Information & Telecommunication Accenture Information Technology Co., Ltd, Beijing, 100032, China

^bPingdingshan Power Supply Company of State Grid Henan Electric Power Company, Pingdingshan, 467000, China

Abstract. Statistics show that power theft is one of the main reasons for the dramatic increase in power grid line loss. In this paper, a genetic algorithm is used to optimize a neural network and establish a power theft prediction model. With the grey prediction model, the predicted values of variables are obtained and then applied to the prediction model of a GA-BP neural network to obtain relatively accurate predictions from limited samples, reducing the absolute error. Through the two levels of prediction and analysis, the model is demonstrated to have good universality in predicting power theft behavior, and is a practical and effective method for power companies to carry out power theft analysis.

Keywords. Genetic Algorithm, Neural Network, Electricity Theft Prediction Model, Grey Model, Electricity Anti-Theft

1. Introduction

Traditional power theft investigation involves the observation of line loss and power consumption data of the area of jurisdiction[1-3]. The staff of the power supply office determine a list of suspects according to their experience and specifications, and determine power theft behavior in combination with on-site investigation.

With the continuous evolution of big, hierarchical data, numerous prediction methods via data analysis have emerged[4-5]. Zheng[6] modeled and analyzed daily electricity consumption data based on the LeNet-5 convolutional neural network, and then used a double-layer deep network to conduct in-depth mining of user information, line loss in the platform area and other data, laying a foundation for accurate anti-power theft. Cai et al.[7] analyzed the correlation of user data and applied a machine learning decision tree method to help staff to determine whether a user has stolen electricity in a time period, and effectively reduce the economic loss. Li et al.[8] studied the potential relationship between electricity consumption behavior and electricity cost risk through big data analysis, so as to accurately locate users who are potentially stealing power. Li et al.[9] constructed a relevant line loss model by using a

¹ Corresponding Author: Zhang Lipeng, State Grid Information & Telecommunication Accenture Information Technology Co., Ltd, Email: Philip_Zhang@163.com

neural network in a data-driven way, and realized the theoretical calculation of line loss and judgment of potential power theft.

With reference to previous studies, we decided to adopt different methods for prediction and then introduce the grey prediction model. The data obtained using the grey prediction model is applied to the GA-BP algorithm, so as to obtain the proposed method of determining suspicion of electricity theft.

2. Theoretical analysis of the GA-BP algorithm

2.1 BP neural networks

The structure of the backpropagation (BP) neural network topology is shown in Figure 1. A BP neural network input variables through the excitation function and adjust each layer connection weights threshold eventually nonlinear mapping to the output variable. In order to make the network output variable consistent with the expected output, learning generally requires several repetitions; the error value tends to zero and ultimately achieve zero[10-12].

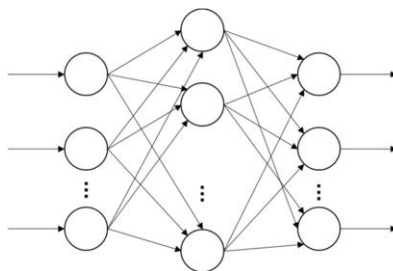


Figure 1: Topological structure of a BP neural network.

The BP neural network algorithm process is as follows:

Suppose the input matrix of the sample is $X = (x_{ij})$, ($i = 1, 2, 3, \dots, m; j = 1, 2, 3, \dots, p$), each row of data represents a group of input samples, and each group of input samples corresponds to a group of output samples, so the actual output samples corresponding to all input samples are $XY = [y_1, y_2, y_3, \dots, y_n]^T$. Each of these columns is an index of the sample, so the input sample I_1 of the input layer is equal to X .

If the hidden layer of the network contains m neurons, weight matrix $W = (w_{ij})$, ($i = 1, 2, 3, \dots, m; j = 1, 2, 3, \dots, p$), threshold matrix $B = [b_1, b_2, \dots, b_m]^T$, the input of the hidden layer is:

$$I_2 = W_{m \times p} X_{p \times n}^T + B_{m \times 1} \text{ones}_{1 \times n} \quad (1)$$

$\text{ones}_{1 \times n}$ is a matrix where all of the elements of the $1 \times n$ vector are 1. The selection of the hidden layer excitation function is a unipolar S function, whose expression is:

$$f(x) = \frac{1}{1+e^{-x}} \quad (2)$$

The output of the hidden layer can be obtained as follows: $O_2 = f(I_2)$. The input

to the output layer is:

$$I_3 = X_{jk}O_2 + B_{jk} + \text{ones}_{1 \times n} \quad (3)$$

Since the transfer function is a linear function, the output of the output layer can be considered to be $O_3 = I_3$. In order to obtain connection weight threshold adjustment between layers, the chain rule is used:

$$\Delta W_{jk} = -\eta \frac{\partial E}{\partial W_{jk}} = -\eta(Y - O_3)O'_2 \quad (4)$$

$$\Delta B_{jk} = -\eta \frac{\partial E}{\partial B_{jk}} = -\eta(Y - O_3)\text{ones}_{n \times 1} \quad (5)$$

Again, $\text{ones}_{1 \times n}$ is a matrix where all of the elements of $1 \times n$ are 1. By formula (2), $f'(x) = f(x)[1 - f(x)]$. The weight threshold adjustment between hidden layers is further calculated as:

$$\Delta W'_{jk} = -\eta W'_{jk}(Y - O_3)O_2(1 - O_2) \quad (6)$$

$$\Delta B'_{jk} = -\eta \frac{\partial E}{\partial B'_{jk}} = -\eta W'_{jk} \quad (7)$$

According to formulae (4) ~ (7) it can be seen that the correct initial threshold can be determined from the second to the first cumulative power threshold; thus, the accuracy of the training is decided by the selection of the initial weight threshold. If the initial threshold selection is not appropriate, it is likely to result in slow convergence and ease of falling into local optimal solutions, so the right choice of initial threshold is important[12].

2.2 BP neural network optimazation with GA

A genetic algorithm (GA) is a global heuristic search algorithm inspired by biological evolution[13]. As a GA is a global search algorithm that can find the global optimal solution, this can address the deficiency of BP neural networks that have a tendency to converge to sub-optimal solutions. Hence, this paper uses a GA to optimize the BP neural network to ensure the accuracy of the model prediction results[14].

2.2.1 Coding and population initialization

The premise of using a genetic algorithm is to encode the solution of a problem into the form of a string. This is achieved using a binary encoding, the simplest coding method [15]. N initial string structures are randomly generated at first, each representing an individual; the N individuals constitute a population. The algorithm begins evolution with this population, initially.

2.2.2 Fitness assessment

Fitness indicates the quality of an individual solution, and the mean squared error between the predicted result and the actual result is taken as the evaluation of individual fitness [16], The calculation is as follows:

$$F = mse(Y - O) = \frac{1}{n} \sum_{i=1}^n (y_i - o_i)^2 \quad (8)$$

where n is the number of inputs to the samples; y_i is the prediction of the network; o_i is the actual result, mse is the mean squared error function.

2.2.3 Model building

Based on the optimization of weights and thresholds of the neural network by the GA, the structure of the neural network is designed, including the selection of the input, output, data processing, the number of hidden layer nodes, and the selection of the activation function.

Step 1: Vector selection Inputting.

The input vector of the mathematical model in this paper is the evaluation of a user's electricity consumption status, including the month, energy efficiency level of the user, monthly electricity consumption, service meter type, line loss rate, three-phase voltage imbalance rate, three-phase current imbalance rate, power factor, single consumption and event record. The internal characteristics of each index intersect, and the index data are correlated and influenced by each other.

Step 2: Selection of output vector.

In order to evaluate the power consumption status of users, the suspected power stealing factor and mode are considered as the output of the network. Here, this is divided into either not electricity-stealing (represented by 0) or suspected electricity-stealing (represented by 1).

2.2.4 Selection Practicing

The selection operator in GAs aims to select individuals with strong adaptability to reproduce in the next generation. This paper adopts the proportional selection strategy; assuming that the total number of individuals in the population is N , then the fitness of individuals n is:

$$p_i = \frac{k/F_i}{\sum_{i=1}^N k/F_i} \quad (k \text{ is the coefficient}) \quad (9)$$

2.2.5 Crossover and mutation

In this paper, some genes were exchanged among chromosomes by single point crossover. For mutation, a simple bit flip approach is used.

3. Application of grey prediction in GA-BP power theft prediction

This section details the GA-BP neural network model for power theft analysis. The evaluation indexes of the power sample data is used as input to the grey model. The output is the suspected behavior: 1 represents unusual behavior, whereas 0 means normal behavior [17].

3.1 Data preprocessing

The test data in this paper are from a power supply company, which is low-voltage non-residential user data. The data of 560 users used. Of these, 10 had stolen electricity,

while the remaining 550 had not.

First of all, it is necessary to determine the evaluation indexes regarding electrical power theft from the power metering data. According to the result of data analysis and measurement of electrical parameter can affect the watt-hour meter and watt-hour meter measurement error to some changes in the electrical parameters, selected the monthly electricity consumption and the area line loss, maximum line loss, power factor, the three-phase imbalance rate and contract constitute the power capacity than the six electrical parameters evaluation index system, and then in order to eliminate the index data and the dimensional difference between the order of magnitude. An index is normalized as follows [18]:

$$x' = b + (a - b) \frac{x - x_{\min}}{x_{\max} - x_{\min}} \quad (10)$$

The data in the electric theft evaluation index system are normalized to the interval $[a, b]$. Here, x' is the normalized data and x is the original data for each index. The maximum value for each index is x_{\max} , and the minimum value is x_{\min} . In this paper, $[0, 1]$ normalization is adopted [19].

3.2 GM(1,1) prediction

The grey prediction model GM(1,1) requires less modeling information, is easy to operate, and has high modeling accuracy. Therefore, it has been widely used in various prediction fields, and is an effective tool to deal with small-sample prediction problems[20]. The following carries out correlation analysis on the data of selected power users. The variation law of the original data system is generated by gray, and a data sequence with strong regularity is generated, so the corresponding differential equation model is established. By the above methods, we obtain the time point of power user data or the predicted value of [21] in the future and its development trend.

3.2.1 Parameter definition

The original data sequence is:

$$x^{(0)} = (x^{(0)}(1), x^{(0)}(2), \dots, x^{(0)}(n)) \quad (11)$$

The new sequence $x^{(1)}$ is generated from the growing sequence of original data:

$$x^{(1)} = (x^{(1)}(1), x^{(1)}(2), \dots, x^{(1)}(n)) \quad (12)$$

The grey derivative is defined as follows:

$$dx^{(1)}(k) = x^{(0)}(k) = x^{(1)}(k) - x^{(1)}(k - 1) \quad (13)$$

Let $z^{(1)}$ approximate the sequence $x^{(1)}$:

$$z^{(1)}(k) = 0.5x^{(1)}(k) + 0.5x^{(1)}(k - 1), (k = 1, 2, \dots, n) \quad (14)$$

$$z^{(1)} = (z^{(1)}(2), z^{(1)}(3), \dots, z^{(1)}(n)) \quad (15)$$

Therefore, the grey differential equation, GM(1,1), is:

$$dx^{(1)}(k) + az^{(1)}(k) = b \quad (16)$$

Let $x^{(0)}(k) + az^{(1)}(k) = b$, $x^{(0)}(k)$ is grey differentiable, then a is uniformly continuous, parameter $z^{(1)}(k)$ is white, b for the grey parameters. Entering the parameter $k = 1, 2, 3, \dots, n$ into

$$x^{(0)}(k) + az^{(1)}(k) = b \quad (17)$$

we obtain:

$$\begin{cases} x^{(0)}(2) + az^{(1)}(2) = b \\ x^{(0)}(3) + az^{(1)}(3) = b \\ \dots \\ x^{(0)}(n) + az^{(1)}(n) = b \end{cases} \quad (18)$$

Let $Y = (x^{(0)}(2), x^{(0)}(3), \dots, x^{(0)}(n))^T$, $u = (a, b)^T$,

$$B = \begin{bmatrix} -z^{(1)}(2), & 1 \\ -z^{(1)}(3), & 1 \\ \vdots & \vdots \\ -z^{(1)}(n), & 1 \end{bmatrix} \quad (19)$$

Y is a data vector, B is a data matrix, where $z^{(1)}(i)$ is the row vector formed by the prediction data obtained from (14) and (15), and u is a parameter vector. Therefore, the GM(1,1) model can be expressed as a matrix equation $Y = Bu$. This can be obtained by the least squares method:

$$\hat{u} = (\hat{a}, \hat{b})^T = (B^T B)^{-1} B^T Y \quad (20)$$

3.2.2 Prediction calculation

By calculating the grey differential equation, we can get the prediction model:

$$\begin{cases} x^{(1)}(k+1) = (x^{(0)}(1) - \frac{u}{a})e^{-ak} + \frac{u}{a} \\ \hat{x}^{(0)}(k+1) = \exp(\hat{x}^{(k)}(k+1) - \hat{x}^{(1)}(k)), \\ k = 1, 2, 3, \dots, n \end{cases} \quad (21)$$

At the same time, the original data sequence is obtained through a dimension reduction calculation:

$$\hat{x}^{(0)}(i) = x^{(1)}(i) - x^{(1)}(i-1) \quad (22)$$

When using the GM(1,1) grey prediction model to carry out analysis of power theft, the sequence is as follows:

$$x^{(i)} = (x^{(i)}(1), x^{(i)}(2), \dots, x^{(i)}(n)) \quad (23)$$

$x^{(i)}$ is defined as the metering value of the electrical energy, so $(x^{(i)}(1), x^{(i)}(2), \dots, x^{(i)}(n))$ is the sequence formed by the influencing factors of electric energy measurement, and i is a time-related variable, so as to achieve time series prediction.

The next part will perform data processing on the influencing factor variables that need to be considered for prediction (as shown in Table 1). The predicted values of these variables are used in the prediction model of the GA-BP neural network.

Table 1: Normalized sample data sheet

Number	Electricity consumption	Maximum line-loss	Line-loss in the platform area	Three phase unbalance rate	Power factor	capacity ratio	Power stealing
1001	0.42412	0.98963	0.99522	0.75942	0.12934	0.82645	0
1002	0.39484	0.98412	0.98373	0.28438	0.23643	0.75244	0
1003	0.21948	0.99762	0.97633	0.26474	0.28233	0.82545	0
1004	0.47283	0.93266	0.99274	0.26154	0.25344	0.71265	0
1005	0.52934	0.97883	0.93744	0.57584	0.17464	0.82514	0
1006	0.54654	0.87354	0.91983	0.43495	0.27544	0.82645	0
1007	0.40285	0.92364	0.91954	0.74387	0.03634	0.87555	0
1008	0.21847	0.89736	0.87625	0.67352	0.12846	0.86456	0
1009	0.08475	0.93764	0.89736	0.83575	0.28746	0.68553	0
1010	0.22847	0.98964	0.91747	0.03754	0.27645	0.67329	0
1011	0.47383	0.97253	0.93865	0.53856	0.12764	0.67454	0
1012	0.68873	0.58373	0.92745	0.83263	0.24675	0.73585	0
1013	0.41847	0.96386	0.92764	0.54925	0.12644	0.97353	0
1014	0.28465	1.00000	0.95274	0.85636	0.37563	0.85347	0
1015	0.58736	0.98363	0.92424	0.74495	0.47563	0.59463	0
1016	0.56285	0.96342	1.00000	0.53956	0.42545	0.73554	0
1017	0.60745	0.91735	0.93856	0.35753	0.24633	0.67833	0
1018	0.57957	0.89622	0.95854	0.66833	0.26496	0.83685	0
1019	0.34756	0.87654	0.93246	0.75554	0.00000	0.68364	0
1020	0.05833	0.96252	0.93654	0.32755	0.27614	0.56533	0
1021	0.00000	0.87226	0.82558	0.02154	0.12755	1.00000	0
1022	0.27445	0.95252	0.85553	0.28564	0.28468	0.38653	0
1023	0.54123	0.93846	0.98365	0.44954	0.28645	0.68365	0
1024	0.72389	0.58323	0.95853	0.22385	0.25385	0.74638	0
1025	0.82745	0.00000	0.85853	0.13587	0.12865	0.65385	1
1026	1.00000	0.07116	0.85255	0.00000	1.00000	0.00000	1
1027	0.97847	0.04001	0.00000	0.04734	0.49766	0.49275	1

3.3 Genetic algorithm optimization

In order to improve the data obtained from the grey prediction model, this article uses the genetic algorithm optimization toolbox[22] from the University of North Carolina. In the genetic algorithm used in this paper, the specific parameter settings are: 100 iterations maximum, the population size is 500, the probability of selection is 0.9, the mutation probability is 0.09, and the crossover probability is 0.5. The changes in the optimal fitness and the average fitness of population individuals are shown in Figure 2.

After this process, the global optimal initial weight threshold can be obtained and used for BP network training. The BP network training parameters are set as follows: six input layer neurons, nine hidden layer neurons, 1 output layer neuron, a unipolar sigmoid function is used as the transfer function, the gradient descent trained function

is used as the corresponding training function, use the largest number of training for 2000 times, the learning rate is 0.1, the target minimum mean variance is 0.003[23].

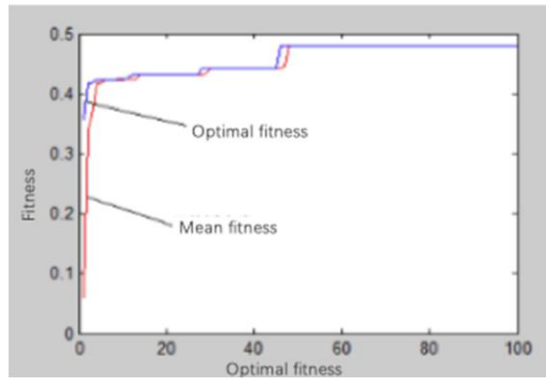


Figure 2. Fitness change over 100 iterations.

3.4 Model testing

The data obtained from the grey prediction model are used by the optimized BP neural network model, and the suspected power theft in the training data could be predicted more accurately. However, the predicted results exhibit overfitting after network optimization, so it is still necessary to use the data in the test samples and further verify the accuracy of the model. The test set data is imported to verify the model, and the predicted results are shown in Figure 3.

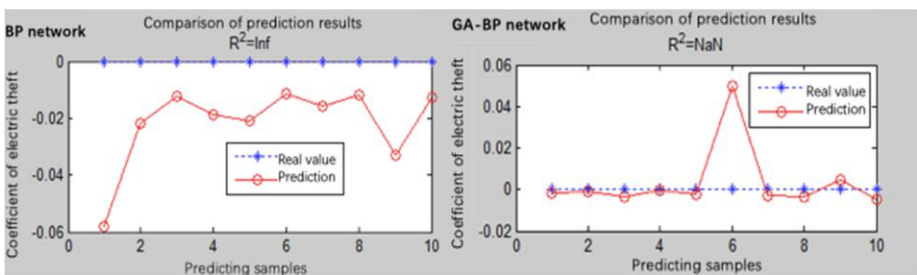


Figure 3. BP and GA-BP model test results.

As can be seen from Figure 3, the predictions of the BP neural network optimized by the GA are closer to the expected values than the unoptimized BP neural network.

4. Conclusion

Using the implementation in this paper, via the grey prediction model, we forecasted data related to power consumption on the time dimension. The prediction after data processing is input to the GA-BP neural network model in order to predict power theft. To a certain extent, the grey prediction model reduced the absolute error of the test data, and provides a long-term and short-term forecast analysis. By combining the grey

prediction model with the neural network analysis, the prediction and analysis on two levels make the model have better universality for the prediction of electric theft behavior, and provide a practical and effective method for related industries to carry out power theft detection. Future work will focus on accessing the large data collected by the information acquisition system and stored in a database, completing the assessment of the power consumption status of a large range of power users, and providing technical support for realizing the intelligent control of the power industry.

Reference

- [1] SHI Yuliang, RONG Yiping, ZHU Weiyi. Stealing Behavior Recognition Method Based on Electricity Characteristics Analysis[J]. Journal of Computer Research and Development, 2018,55(08):1599-1608.
- [2] LAI Zhe. Analysis of Anti-Stealing Electricity with Big Data Technology[J]. Electronic Test, 2019(16):50-51+38.
- [3] ZHANG Yumei. Intelligent Anti-Stealing Data Acquisition Technology and Application Analysis[J]. Technology Innovation and Application, 2017(20):41+43.
- [4] ZHANG Dongxia, MIAO Xin, LIU Liping. Research on Development Strategy for Smart Grid Big Data[J]. Proceedings of the CSEE, 2015,35(01):2-12.
- [5] ZHAI Haini, PANG Xuwei, YOU Mingyu. Analysis and Design of Application Value and Sharing Platform of Power Big Data[J]. Management and Administration, 2017(07):104-108.
- [6] ZHENG Jianning. Detection Method of Electricity Stealing Behavior Based on Deep Learning[J]. Information Technology, 2019(02):156-159.
- [7] CAI Jiarong, WANG Shunyi, WU Guangcai. The User's Electric Power Prediciton and Electricity Inspection Plan Based on Machine Learning Research on Auxiliary Arrangement[J], Electronic Test, 2018(02):108-109.
- [8] LI Jianbin, WU Binbin, ZHU Yakui,et al. Risk Prediction and Prevention and Control of Customer Electricity Charge Based on Big Data Analysis[J]. Power Systems and Big Data, 2019,22(02):1-6. 2018(02):108-109.
- [9] LI Zhipeng, HOU Huiyong, JIANG Sifan,et al. Line Loss Calculation and Electricity Theft Analysis Based on Artificial Neural Network[J]. Southern Power System Technology, 2019,13(02):7-12+50.
- [10] Tianhua Liu,Shoulin Yin. An Improved Particle Swarm Optimization Algorithm Used for BP Neural Network and Multimedia Course-Ware Evaluation[J]. Multimedia Tools and Applications,2017,76(9).
- [11] LIN Jingdong, WU Xinyi, CHAI Yi, et al. Structure Optimization of Convolutional Neural Networks: A survey[J/OL]. Acta Automatica Sinica: 1-14[2020-02-21].<https://doi.org/10.16383/j.aas.c180275>.
- [12] Yilun Shang. Defluant Model of Opinion Formation in One-Dimensional Multiplex Networks[J]. Journal of Physics A: Mathematical and Theoretical,2015,48(39).
- [13] XU Junxing, LI Chuan, LI Yingna. Power Stealing Analysis Based on Genetic Algorithm Optimized BP Neural Network[J]. Computer Engineering & Software, 2017,38(11):18-23.
- [14] Xiaohong Lu,Yongquan Wang,Jie Li,Yang Zhou,Zongjin Ren,Steven Y Liang. Three-dimensional coordinate measurement algorithm by optimizing BP neural network based on GA[J]. Engineering Computations,2019,36(6).
- [15] WANG Zhibin, KONG Yanan, LIU Yongcheng et al. Prediciton of Junction Temperature for High Power LED by Optimizing BP Neural Based on Genetic Algorithm[J]. Journal of optoelectronics· laser, 2014,25(07):1303-1309.
- [16] MIN Jiangtao. Back Analysis Model of BP Neural Network Based on Genetic Algorithm Optimization[J]. Construction Materials & Decoration, 2018(45):296.
- [17] WANG Jingli, LI Liang, YU Lei, et al. Automated Fugl-Meyer Assessment Based on Genetic Algorithm and Extreme Learning Machine[J]. Journal of Computer Applications, 2014,34(03):907-910+914.
- [18] XU Zhi, LI Hongjiao, CHEN Jingjing. Prediciton of User Stealing Behavior Based on Machine Learning[J]. Journal of Shanghai University of Electric Power, 2017,33(04):389-393.
- [19] YE Zhensai, XIAO Hui. Research on Transmission Line Visualization Model Based on Economic Big Data[J]. Power Systems and Big Data, 2019,22(09):28-34.
- [20] Hu Bin, Li Fang, Zhou Hou-Shun. Robustness of Complex Networks under Attack and Repair. 2009, 26(12):128901 (4pp).

- [21] DING Leiming, YANG Xiaolei, HUANG Jinbo, et al. Application of Improved Grey model Based on BP Neural Network Optimization in Electric Quantity Prediction[J]. Mechanical and Electrical Information, 2019(36):36-39.
- [22] SONG Xiuying. Application of GM (1,1) Model based on MATLAB in Economic Analysis[J]. Mathematics Learning and Research, 2011(11):93-95.
- [23] QIAN Guachao, MA Yutang, MA Yi, et al. Application of Genetic Algorithm in Fault Diagnosis of Grounding Grid Corrosion[J]. Yunnan Electric Power, 2016,44(02):113-117+129.

Output Feedback Control Synthesis and Stabilization for Positive Polynomial Fuzzy Systems Under L_1 Performance

Aiwen MENG^{a,1}, Hak-Keung LAM^b Fucai LIU^a, and Ziguang WANG^a

^a*Key Laboratory of Industrial Computer Control Engineering of Hebei Province,
Yanshan University, Qinhuangdao, Hebei 066004, China*

^b*Department of Engineering, King's College London, Strand London WC2R 2LS, U.K*

Abstract. This paper presents the stabilization for positive nonlinear systems using polynomial fuzzy models. To conform better to the practical scenarios that system states are not completely measurable, the static output feedback (SOF) control strategy instead of the state feedback control method is employed to realize the stability and positivity of the positive polynomial fuzzy system (PPFS) with satisfying L_1 -induced performance. However, some troublesome problems in analysis and control design will follow, such as the non-convex problem. Fortunately, by doing mathematical tricks, the non-convex problem is skillfully dealt with. Furthermore, the neglect of external disturbances may lead to a great negative impact on the performance of positive systems. For the sake of guaranteeing the asymptotic stability and positivity under the satisfaction of the optimal performance of the PPFS, it is significant to take the L_1 -induced performance requirement into consideration as well. In addition, a linear co-positive Lyapunov function is chosen so that the positivity can be extracted well and the stability analysis becomes simple. By using the sum of squares (SOS) technique, the convex stability and positivity conditions in the form of SOS are derived. Eventually, for illustrating the advantages of the proposed method, a simulation example is shown in the simulation section.

Keywords. positive polynomial fuzzy system (PPFS), static output feedback (SOF), L_1 performance, stability analysis, sum of squares (SOS)

1. Introduction

As a particular kind of systems, positive systems have attracted ever-increasing researchers to conduct a deep-going research on the stability and positivity analysis. In fact, a great number of practical systems in various disciplines, for instance, physiology [1], communication networks [2] and biology [3] belong to positive systems because the system states maintain in the positive quadrant with the non-negative initial conditions. However, due to the special property of positive systems, a good deal of challenging and

¹Corresponding Author: Aiwen Meng, the Key Laboratory of Industrial Computer Control Engineering of Hebei Province, Yanshan University, Qinhuangdao, Hebei 066004, China; E-mail: 1309494495@qq.com

interesting problems cannot be coped with by employing some mature techniques for general systems [4]. From this point, a series of elegant properties of positive systems are worth studying and digging [5]. Hence, a growing number of researchers have shown great interest in this research topic.

Up to now, many valuable research results have been obtained, which lay a good foundation for future research on positive systems. In [6], the stability analysis for positive linear systems with time-varying delays was carried out. In [7], the authors designed positive filters for positive systems to reduce the influence of the external disturbance. It can be seen that most of existing results are for positive linear systems because the system structures are simple, meanwhile, the controller design is easy to realize. Nevertheless, it is generally acknowledged that a lot of actual systems demonstrate nonlinear characteristics rather than linear ones in practical applications. Because of the complexity of positive nonlinear systems, some current results for positive linear systems cannot be directly employed for positive nonlinear systems. Therefore, it is worth a try to study the control synthesis for positive nonlinear systems.

Fuzzy-model-based control theory offers a systematic way to deal with analysis and control synthesis for nonlinear systems. One of the well-known approaches is through Takagi-Sugeno (T-S) fuzzy model which is in the light of a set of fuzzy rules to express a global nonlinear system [8]. With the further study of fuzzy theory, polynomial fuzzy models have been put forward, comparing with T-S fuzzy models, this kind of fuzzy models have many distinct merits. First of all, more complex and extensive nonlinear systems are able to be handled by polynomial fuzzy models since not only constant terms but also polynomials are permitted in the membership functions (MFs) as well as the system matrices [9]. On the other hand, the imperfect premise matching (IPM) concept and membership-function-dependent (MFD) analysis techniques have been proposed for polynomial fuzzy-model-based control theory [10], which have obvious advantages than parallel distributed compensation (PDC) scheme and membership-function-independent (MFI) analysis technique. For instance, the fuzzy controllers can be designed flexibly and implemented simpler. Besides, MFD analysis techniques are of great help to reduce the conservativeness of the results. For all these reasons, using a polynomial fuzzy model to handle complex nonlinear systems is a better way to facilitate the control synthesis and stability analysis. However, positive polynomial fuzzy systems (PPFSs) have many differences from the general systems, which means some significant results for general polynomial fuzzy systems are difficult to be used for PPFSs [11]. Thereby, the controller design and stabilization for PPFSs is a meaningful but challenging research topic.

In resent literature, a few results corresponding to control synthesis for the positive systems have been provided. It is worth noting that these results are on the basis of state feedback control strategy instead of static output feedback (SOF) control method. Nevertheless, from the practical point of view, it makes more sense to design the SOF controllers for PPFSs because this kind of controllers do not require full state information of PPFSs, meanwhile, it is simple and money-saving to put into practice. In this regard, designing SOF fuzzy controllers for PPFSs is more realistic and reasonable. Unfortunately, some thorny problems will follow, for instance, non-convex terms usually are able to exist in stability and positivity conditions [12]. Although some marture techniques have been provided [13,14], these methods are just appropriate for genneral systems rather than positive polynomial fuzzy systems. Due to this barrier, the obtained results based on SOF control approach for PPFSs are relatively few. Considering the solution of non-

convex problem for positive polynomial fuzzy systems, we have proposed a method to transform non-convex terms into convex ones in [12], but the L_1 -induced performance was not taken into consideration. It is well known that in engineering applications, some practical systems are required to meet the performance requirements. Generally speaking, L_1 performance can better capture the positivity of PPFSs since L_1 -norm represents the sum of the values of the components. Therefore, to accord with the practical scenarios, L_1 performance is considered as well so that the closed-loop PPFSs can satisfy the stability and positivity under L_1 -induced performance requirement. Due to the introduction of L_1 performance, the techniques given in [12] are not suitable for the new non-convex problem in this paper. Looking for an appropriate approach to solve this issue also is an inspiration for us to carry out this work.

2. Preliminaries

2.1. Notation

The monomial in $\mathbf{x}(t) = [x_1(t), \dots, x_n(t)]^T$ is defined as $x_1^{d_1}(t), \dots, x_n^{d_n}(t)$, where $d_k, k \in \{1, \dots, n\}$, is a non-negative integer. The degree of a monomial is defined as $d = \sum_{k=1}^n d_k$. A polynomial $\mathbf{p}(\mathbf{x}(t))$ is shown as finite linear combination of monomials with real coefficients. If a polynomial $\mathbf{p}(\mathbf{x}(t))$ is able to be represented as $\mathbf{p}(\mathbf{x}(t)) = \sum_{j=1}^m \mathbf{q}_j(\mathbf{x}(t))^2$, where m is a non-zero positive integer and $\mathbf{q}_j(\mathbf{x}(t))$ is a polynomial for all j , we can draw a conclusion that $\mathbf{p}(\mathbf{x}(t)) \geq 0$ is a SOS. For a matrix $\mathbf{N} \in \Re^{m \times n}$, where n_{rs} denotes the element located at the r -th row and s -th column. $\mathbf{N} \succeq 0$, $\mathbf{N} \succ 0$, $\mathbf{N} \preceq 0$ and $\mathbf{N} \prec 0$ mean that each element n_{rs} is non-negative, positive, non-positive and negative, respectively. $\mathbf{Q}(\mathbf{x}) = \text{diag}(x_1, \dots, x_n)$ means that $\mathbf{Q}(\mathbf{x})$ is a diagonal matrix with all of the diagonal elements being x_1, \dots, x_n .

2.2. Positive Polynomial Fuzzy Model

A p -rule positive polynomial fuzzy model is shown:

$$\begin{aligned} \text{Rule } i : & \text{ IF } f_1(\mathbf{x}(t)) \text{ is } M_1^i \text{ AND } \dots \text{ AND } f_\Psi(\mathbf{x}(t)) \text{ is } M_\Psi^i \\ \text{THEN } & \begin{cases} \dot{\mathbf{x}}(t) = \mathbf{A}_i(\mathbf{x}(t))\mathbf{x}(t) + \mathbf{B}_i(\mathbf{x}(t))\mathbf{u}(t) + \mathbf{B}_{i\omega}\tilde{\mathbf{w}}(t), \\ \mathbf{z}(t) = \mathbf{C}_i(\mathbf{x}(t))\mathbf{x}(t) + \mathbf{D}_i(\mathbf{x}(t))\mathbf{u}(t) + \mathbf{D}_{i\omega}\tilde{\mathbf{w}}(t), \\ \mathbf{y}(t) = \mathbf{E}\mathbf{x}(t) + \mathbf{E}_\omega\tilde{\mathbf{w}}(t), \end{cases} \end{aligned} \quad (1)$$

where $\mathbf{u}(t) \in \Re^m$, $\tilde{\mathbf{w}}(t) \in \Re^h$, $\mathbf{z}(t) \in \Re^q$ and $\mathbf{y}(t) \in \Re^l$ are the system state vector, the input vector, the disturbance signal, the measurement output and the controlled output, respectively; $\mathbf{A}_i(\mathbf{x}(t))$, $\mathbf{B}_i(\mathbf{x}(t))$, $\mathbf{B}_{i\omega}$, $\mathbf{C}_i(\mathbf{x}(t))$, $\mathbf{D}_i(\mathbf{x}(t))$, $\mathbf{D}_{i\omega}$, \mathbf{E} and \mathbf{E}_ω are the system matrices with appropriate dimensions.

The overall dynamics of the PPFS is introduced:

$$\begin{cases} \dot{\mathbf{x}}(t) = \sum_{i=1}^p w_i(\mathbf{x}(t))(\mathbf{A}_i(\mathbf{x}(t))\mathbf{x}(t) + \mathbf{B}_i(\mathbf{x}(t))\mathbf{u}(t) + \mathbf{B}_{i\omega}\tilde{\mathbf{w}}(t)), \\ \mathbf{z}(t) = \sum_{i=1}^p w_i(\mathbf{x}(t))(\mathbf{C}_i(\mathbf{x}(t))\mathbf{x}(t) + \mathbf{D}_i(\mathbf{x}(t))\mathbf{u}(t) + \mathbf{D}_{i\omega}\tilde{\mathbf{w}}(t)), \\ \mathbf{y}(t) = \mathbf{E}\mathbf{x}(t) + \mathbf{E}_\omega\tilde{\mathbf{w}}(t), \end{cases} \quad (2)$$

where $w_i(\mathbf{x}(t))$ is the normalized grade of membership with satisfying $\sum_{i=1}^p w_i(\mathbf{x}(t)) = 1, w_i(\mathbf{x}(t)) \geq 0 \forall i$.

In order to have a better understanding of positive systems, we give some definitions and lemmas before designing the SOF polynomial fuzzy controller.

Definition 1 [15] A system is called a positive system if the corresponding trajectory $\mathbf{x}(t) \succeq 0$ for all $t \geq 0$ is held under the initial condition $\mathbf{x}(0) = \mathbf{x}_0 \succeq 0$.

Definition 2 [15] If the off-diagonal elements in matrix \mathbf{M} are non-negative: $m_{rs} \succeq 0, r \neq s$, then this matrix is a Metzler matrix.

Lemma 1 [16] System (2) is a positive system if $\mathbf{A}_i(\mathbf{x}(t))$ is a Metzler matrix, $\mathbf{B}_i(\mathbf{x}(t)) \succeq 0, \mathbf{B}_{i\omega} \succeq 0, \mathbf{C}_i(\mathbf{x}(t)) \succeq 0, \mathbf{D}_i(\mathbf{x}(t)) \succeq 0, \mathbf{D}_{i\omega} \succeq 0, \mathbf{E} \succeq 0$ and $\mathbf{E}_\omega \succeq 0$.

2.3. Polynomial Fuzzy Controller Design

By using IPM technique, a c -rule SOF polynomial fuzzy controller is designed:

$$\begin{aligned} \text{Rule } j : & \text{ IF } g_1(\mathbf{y}(t)) \text{ is } N_1^j \text{ AND } \dots \text{ AND } g_\Omega(\mathbf{y}(t)) \text{ is } N_\Omega^j \\ & \text{ THEN } \mathbf{u}(t) = \mathbf{K}_j \mathbf{y}(t), \end{aligned} \quad (3)$$

where $\mathbf{K}_j \in \Re^{m \times l}$ is the SOF gain to be determined.

Through recalling the expression of $\mathbf{y}(t)$, we have:

$$\mathbf{u}(t) = \sum_{j=1}^c m_j(\mathbf{y}(t)) \mathbf{K}_j \mathbf{y}(t) = \sum_{j=1}^c m_j(\mathbf{y}(t)) (\mathbf{K}_j \mathbf{E} \mathbf{x}(t) + \mathbf{K}_j \mathbf{E}_\omega \tilde{\mathbf{w}}(t)), \quad (4)$$

where $m_j(\mathbf{y}(t))$ is the normalized grade of membership with satisfying $\sum_{j=1}^c m_j(\mathbf{y}(t)) = 1, m_j(\mathbf{y}(t)) \geq 0, \forall j$.

Remark 1 It is worth noting that the IPM method is employed to design the SOF controller because it can make the controller design more flexible and the implementation cost more economical.

To simplify, t is omitted in the rest parts, which means $\mathbf{x}(t)$ and $\mathbf{y}(t)$ will be abbreviated as \mathbf{x} and \mathbf{y} , respectively.

3. Stability and Positivity Analysis under L_1 Performance

In this section, we keep our mind on analyzing the stability and positivity for closed-loop PPFSs with satisfying L_1 performance index. A linear co-positive Lyapunov function is chosen to promote the stability and positivity analysis. Meanwhile, convex SOS-based conditions are derived by employing some useful techniques to solve non-convex terms.

3.1. SOF Positive Polynomial Fuzzy Control Systems

In terms of the PPFS (2) and the SOF polynomial fuzzy controller (4), the SOF positive polynomial fuzzy control system is obtained:

$$\begin{cases} \dot{\mathbf{x}} = \sum_{i=1}^p \sum_{j=1}^c w_i(\mathbf{x}) m_j(\mathbf{y}) \left((\mathbf{A}_i(\mathbf{x}) + \mathbf{B}_i(\mathbf{x}) \mathbf{K}_j \mathbf{E}) \mathbf{x} + (\mathbf{B}_{i\omega} + \mathbf{B}_i(\mathbf{x}) \mathbf{K}_j \mathbf{E}_\omega) \tilde{\mathbf{w}} \right) \\ = \sum_{i=1}^p \sum_{j=1}^c w_i(\mathbf{x}) m_j(\mathbf{y}) \left(\tilde{\mathbf{A}}_{ij}(\mathbf{x}) \mathbf{x} + \tilde{\mathbf{B}}_{ij}(\mathbf{x}) \tilde{\mathbf{w}} \right), \\ \mathbf{z} = \sum_{i=1}^p \sum_{j=1}^c w_i(\mathbf{x}) m_j(\mathbf{y}) \left((\mathbf{C}_i(\mathbf{x}) + \mathbf{D}_i(\mathbf{x}) \mathbf{K}_j \mathbf{E}) \mathbf{x} + (\mathbf{D}_{i\omega} + \mathbf{D}_i(\mathbf{x}) \mathbf{K}_j \mathbf{E}_\omega) \tilde{\mathbf{w}} \right) \\ = \sum_{i=1}^p \sum_{j=1}^c w_i(\mathbf{x}) m_j(\mathbf{y}) \left(\tilde{\mathbf{C}}_{ij}(\mathbf{x}) \mathbf{x} + \tilde{\mathbf{D}}_{ij}(\mathbf{x}) \tilde{\mathbf{w}} \right), \\ \mathbf{y} = \mathbf{E} \mathbf{x} + \mathbf{E}_\omega \tilde{\mathbf{w}}. \end{cases} \quad (5)$$

Remark 2 According to Lemma 1, the SOF positive polynomial fuzzy control system (5) is a positive system if $\tilde{\mathbf{A}}_{ij}(\mathbf{x})$ is a Metzler matrix, $\tilde{\mathbf{B}}_{ij}(\mathbf{x}) \succeq 0$, $\tilde{\mathbf{C}}_{ij}(\mathbf{x}) \succeq 0$, $\tilde{\mathbf{D}}_{ij}(\mathbf{x}) \succeq 0$, $\mathbf{E} \succeq 0$, $\mathbf{E}_\omega \succeq 0$, for all i, j .

Next, the L_1 -induced performance is introduced to facilitate the analysis process.

Definition 3 [17] The system (5) can satisfy L_1 -induced performance at the level γ , if the following inequality can be ensured with satisfying zero initial conditions

$$\|\mathbf{z}\|_{L_1} < \gamma \|\tilde{\mathbf{w}}\|_{L_1}, \quad (6)$$

where γ is the optimal level to be determined.

3.2. Stability Analysis of SOF Positive Polynomial Fuzzy Control Systems

In order to better capture the positivity of the SOF positive polynomial fuzzy control system (5), a linear co-positive Lyapunov function candidate [16] is employed to establish some stability and positivity criteria:

$$V(t) = \lambda^T \mathbf{x}, \quad (7)$$

where $\lambda = [\lambda_1, \dots, \lambda_n]^T \succ 0$ is a vector to be determined.

The $\dot{V}(t)$ is given as follows:

$$\dot{V}(t) = \lambda^T \dot{\mathbf{x}} = \sum_{i=1}^p \sum_{j=1}^c w_i(\mathbf{x}) m_j(\mathbf{y}) \lambda^T \left(\tilde{\mathbf{A}}_{ij}(\mathbf{x}) \mathbf{x} + \tilde{\mathbf{B}}_{ij}(\mathbf{x}) \tilde{\mathbf{w}} \right). \quad (8)$$

In the following, by recalling the definition (6), the L_1 performance index is shown:

$$\begin{aligned} J &= \int_0^\infty \|\mathbf{z}\|_{L_1} - \gamma \|\tilde{\mathbf{w}}\|_{L_1} dt = \int_0^\infty \|\mathbf{z}\|_{L_1} - \gamma \|\tilde{\mathbf{w}}\|_{L_1} + \dot{V} - \dot{V} dt \\ &= \int_0^\infty \sum_{k=1}^q \mathbf{z} - \gamma \sum_{k=1}^p \tilde{\mathbf{w}} + \dot{V} dt - V(\infty) + V(0) \\ &= \int_0^\infty \mathbf{I}_1^T \mathbf{z} - \gamma \mathbf{I}_2^T \tilde{\mathbf{w}} + \dot{V} dt - V(\infty) + V(0), \end{aligned} \quad (9)$$

where $V(\infty)$ is equal to 0 when $t \rightarrow \infty$, meanwhile, the unital condition $V(0)$ is zero. $\mathbf{I}_1 \in \Re^q$ and $\mathbf{I}_2 \in \Re^p$ are vectors with all of the elements being 1.

Therefore, taking the expressions of \mathbf{z} and \dot{V} into (9), we have:

$$\begin{aligned}
J &= \int_0^\infty \mathbf{I}_1^T \mathbf{z} - \gamma \mathbf{I}_2^T \tilde{\mathbf{w}} + \dot{V} dt \\
&= \int_0^\infty \mathbf{I}_1^T \left(\sum_{i=1}^p \sum_{j=1}^c w_i(\mathbf{x}) m_j(\mathbf{y}) (\tilde{\mathbf{C}}_{ij}(\mathbf{x}) \mathbf{x} + \tilde{\mathbf{D}}_{ij}(\mathbf{x}) \tilde{\mathbf{w}}) \right) \\
&\quad - \gamma \mathbf{I}_2^T \tilde{\mathbf{w}} + \sum_{i=1}^p \sum_{j=1}^c w_i(\mathbf{x}) m_j(\mathbf{y}) \lambda^T (\tilde{\mathbf{A}}_{ij}(\mathbf{x}) \mathbf{x} + \tilde{\mathbf{B}}_{ij}(\mathbf{x}) \tilde{\mathbf{w}}) dt \\
&= \int_0^\infty \sum_{i=1}^p \sum_{j=1}^c w_i(\mathbf{x}) m_j(\mathbf{y}) \left((\mathbf{I}_1^T \tilde{\mathbf{D}}_{ij}(\mathbf{x}) - \gamma \mathbf{I}_2^T + \lambda^T \tilde{\mathbf{B}}_{ij}(\mathbf{x})) \tilde{\mathbf{w}} \right. \\
&\quad \left. + (\mathbf{I}_1^T \tilde{\mathbf{C}}_{ij}(\mathbf{x}) + \lambda^T \tilde{\mathbf{A}}_{ij}(\mathbf{x})) \mathbf{x} \right) dt. \tag{10}
\end{aligned}$$

In order to make it easier to explain , we define:

$$\begin{aligned}
\mathbf{Q}_{1ij}(\mathbf{x}) &= \mathbf{I}_1^T \tilde{\mathbf{D}}_{ij}(\mathbf{x}) - \gamma \mathbf{I}_2^T + \lambda^T \tilde{\mathbf{B}}_{ij}(\mathbf{x}) \\
&= \mathbf{I}_1^T (\mathbf{D}_{i\omega} + \mathbf{D}_i(\mathbf{x}) \mathbf{K}_j \mathbf{E}_\omega) - \gamma \mathbf{I}_2^T + \lambda^T (\mathbf{B}_{i\omega} + \mathbf{B}_i(\mathbf{x}) \mathbf{K}_j \mathbf{E}_\omega) \\
&= \mathbf{I}_1^T \mathbf{D}_{i\omega} + \lambda^T \mathbf{B}_{i\omega} - \gamma \mathbf{I}_2^T + (\mathbf{I}_1^T \mathbf{D}_i(\mathbf{x}) + \lambda^T \mathbf{B}_i(\mathbf{x})) \mathbf{K}_j \mathbf{E}_\omega, \tag{11}
\end{aligned}$$

$$\begin{aligned}
\mathbf{Q}_{2ij}(\mathbf{x}) &= \mathbf{I}_1^T \tilde{\mathbf{C}}_{ij}(\mathbf{x}) + \lambda^T \tilde{\mathbf{A}}_{ij}(\mathbf{x}) \\
&= \mathbf{I}_1^T (\mathbf{C}_i(\mathbf{x}) + \mathbf{D}_i(\mathbf{x}) \mathbf{K}_j \mathbf{E}) + \lambda^T (\mathbf{A}_i(\mathbf{x}) + \mathbf{B}_i(\mathbf{x}) \mathbf{K}_j \mathbf{E}) \\
&= \mathbf{I}_1^T \mathbf{C}_i(\mathbf{x}) + \lambda^T \mathbf{A}_i(\mathbf{x}) + (\mathbf{I}_1^T \mathbf{D}_i(\mathbf{x}) + \lambda^T \mathbf{B}_i(\mathbf{x})) \mathbf{K}_j \mathbf{E}. \tag{12}
\end{aligned}$$

From (10), it can be seen that $J < 0$ can be guaranteed by $\mathbf{Q}_{1ij}(\mathbf{x}) \prec 0$ and $\mathbf{Q}_{2ij}(\mathbf{x}) \prec 0$ for all i and j . Regrettably, there are non-convex terms $\lambda^T \mathbf{B}_i(\mathbf{x}) \mathbf{K}_j \mathbf{E}_\omega$ and $\lambda^T \mathbf{B}_i(\mathbf{x}) \mathbf{K}_j \mathbf{E}$ in (11) and (12), respectively. Hence, our attention should be focused on transforming the non-convex terms into convex ones in the following.

In accordance with (11) and (12), we find if $\mathbf{I}_1^T \mathbf{D}_i(\mathbf{x}) + \lambda^T \mathbf{B}_i(\mathbf{x}) \succeq \mathbf{I}_m^T$ and $\mathbf{K}_j \prec 0$ are satisfied, the non-convex terms can be dealt with as:

$$(\mathbf{I}_1^T \mathbf{D}_i(\mathbf{x}) + \lambda^T \mathbf{B}_i(\mathbf{x})) \mathbf{K}_j \mathbf{E}_\omega \preceq \mathbf{I}_m^T \mathbf{K}_j \mathbf{E}_\omega, \tag{13}$$

$$(\mathbf{I}_1^T \mathbf{D}_i(\mathbf{x}) + \lambda^T \mathbf{B}_i(\mathbf{x})) \mathbf{K}_j \mathbf{E} \preceq \mathbf{I}_m^T \mathbf{K}_j \mathbf{E}. \tag{14}$$

where $\mathbf{I}_m^T \in \Re^m$ is a column vector with all the elements being 1:

Now, by introducing (13) and (14) into (11) and (12), respectively, the convex stability conditions are derived:

$$\mathbf{Q}_{1ij}(\mathbf{x}) \preceq \mathbf{I}_1^T \mathbf{D}_{i\omega} + \lambda^T \mathbf{B}_{i\omega} - \gamma \mathbf{I}_2^T + \mathbf{I}_m^T \mathbf{K}_j \mathbf{E}_\omega \prec 0, \tag{15}$$

$$\mathbf{Q}_{2ij}(\mathbf{x}) \preceq \mathbf{I}_1^T \mathbf{C}_i(\mathbf{x}) + \lambda^T \mathbf{A}_i(\mathbf{x}) + \mathbf{I}_m^T \mathbf{K}_j \mathbf{E} \prec 0. \tag{16}$$

After the above analysis, the non-convex problem has been addressed well. The next task is to carry out the positivity analysis. By recalling Remark 2, the positivity conditions should be as follows:

$$\begin{aligned} \mathbf{A}_i(\mathbf{x}) + \mathbf{B}_i(\mathbf{x})\mathbf{K}_j\mathbf{E} &\text{ is a Metzler, } \mathbf{B}_{i\omega} + \mathbf{B}_i(\mathbf{x})\mathbf{K}_j\mathbf{E}_\omega \succeq 0, \\ \mathbf{C}_i(\mathbf{x}) + \mathbf{D}_i(\mathbf{x})\mathbf{K}_j\mathbf{E} &\succeq 0, \quad \mathbf{D}_{i\omega} + \mathbf{D}_i(\mathbf{x})\mathbf{K}_j\mathbf{E}_\omega \succeq 0. \end{aligned} \quad (17)$$

In light of (17), it is worth noting that the positivity conditions are convex, therefore, all convex stability and positivity conditions have been established. In the following, the analyzed results are summarized in Theorem 1.

Theorem 1 *Given that the positive polynomial fuzzy model (2) with satisfying Lemma 1 can guarantee the stability and positivity under L_1 -induced performance by the SOF polynomial fuzzy controller (5) if there exist gain matrix $\mathbf{K}_j \in \mathbb{R}^{m \times l}$, vector $\lambda \in \mathbb{R}^n$ and the optimal performance index γ such that the SOS-based positivity and stability conditions are satisfied:*

$$\mathbf{v}^T (a_{irs}(\mathbf{x}) + \mathbf{b}_{ir}(\mathbf{x})\mathbf{K}_j\mathbf{e}_s) \mathbf{v} \text{ is SOS } \forall i, j, r \neq s; \quad (18)$$

$$\mathbf{v}^T (b_{i\omega rs} + \mathbf{b}_{ir}(\mathbf{x})\mathbf{K}_j\mathbf{e}_{\omega s}) \mathbf{v} \text{ is SOS } \forall i, j, r, s; \quad (19)$$

$$\mathbf{v}^T (c_{irs}(\mathbf{x}) + \mathbf{d}_{ir}(\mathbf{x})\mathbf{K}_j\mathbf{e}_s) \mathbf{v} \text{ is SOS } \forall i, j, r, s; \quad (20)$$

$$\mathbf{v}^T (d_{i\omega rs} + \mathbf{d}_{ir}(\mathbf{x})\mathbf{K}_j\mathbf{e}_{\omega s}) \mathbf{v} \text{ is SOS } \forall i, j, r, s; \quad (21)$$

$$\rho^T \left(\text{diag}(\lambda - \varepsilon_1 \mathbf{I}_n) \right) \rho \text{ is SOS}; \quad (22)$$

$$-\sigma^T \left(\text{diag}(\mathbf{I}_1^T \mathbf{D}_{i\omega} + \lambda^T \mathbf{B}_{i\omega} - \gamma \mathbf{I}_2^T + \mathbf{I}_m^T \mathbf{K}_j \mathbf{E}_\omega + \varepsilon_2(\mathbf{x}) \mathbf{I}_h^T) \right) \sigma \text{ is SOS } \forall i, j; \quad (23)$$

$$-\rho^T \left(\text{diag}(\mathbf{I}_1^T \mathbf{C}_i(\mathbf{x}) + \lambda^T \mathbf{A}_i(\mathbf{x}) + \mathbf{I}_m^T \mathbf{K}_j \mathbf{E} + \varepsilon_3(\mathbf{x}) \mathbf{I}_n^T) \right) \rho \text{ is SOS } \forall i, j; \quad (24)$$

$$-\mathbf{v}^T (k_{jrs} + \varepsilon_4) \mathbf{v} \text{ is SOS } \forall j, r, s; \quad (25)$$

$$\mu^T (\mathbf{I}_1^T \mathbf{D}_i(\mathbf{x}) + \lambda^T \mathbf{B}_i(\mathbf{x}) - \mathbf{I}_m^T) \mu \text{ is SOS } \forall i. \quad (26)$$

where γ is the optimal index to be determined. \mathbf{v} is a arbitrary scalar and $\rho \in \mathbb{R}^n$, $\sigma \in \mathbb{R}^h$ and $\mu \in \mathbb{R}^m$ are arbitrary vectors independent of \mathbf{x} and \mathbf{y} ; $\varepsilon_1 > 0$ and $\varepsilon_4 > 0$ are predefined scalars and $\varepsilon_2(\mathbf{x}) > 0$ and $\varepsilon_3(\mathbf{x}) > 0$ for $\mathbf{x} \neq 0$ are predefined scalar polynomials. $a_{irs}(\mathbf{x})$, $b_{i\omega rs}$, $c_{irs}(\mathbf{x})$ and $d_{i\omega rs}$ are the r -th row and s -th column element in $\mathbf{A}_i(\mathbf{x})$, $\mathbf{B}_{i\omega}$, $\mathbf{C}_i(\mathbf{x})$ and $\mathbf{D}_{i\omega}$, respectively. $\mathbf{b}_{ir}(\mathbf{x})$ and $\mathbf{d}_{ir}(\mathbf{x})$ are the r -th row vectors in $\mathbf{B}_i(\mathbf{x})$ and $\mathbf{D}_i(\mathbf{x})$, respectively. \mathbf{e}_s and $\mathbf{e}_{\omega s}$ are the s -th column vectors in \mathbf{E} and \mathbf{E}_ω , respectively. k_{jrs} is the r -th row and s -th column element in \mathbf{K}_j to be determined.

Remark 3 *From (18) to (21), these conditions are able to ensure the positivity of the SOF positive polynomial fuzzy control systems. From (22) to (26), these conditions can guarantee the stability with satisfying the L_1 performance index.*

Corollary 1 *Given that the positive polynomial fuzzy model (2) with satisfying Lemma 1 can guarantee the stability and positivity under L_1 -induced performance by using PDC technique to design the SOF polynomial fuzzy controller (5), if there exist gain matrix $\mathbf{K}_j \in \mathbb{R}^{m \times l}$, vector $\lambda \in \mathbb{R}^n$ and the optimal performance index γ such that the SOS-based positivity and stability conditions are satisfied:*

(22), (25) – (26)

$$v^T (a_{irs}(\mathbf{x}) + \mathbf{b}_{ir}(\mathbf{x}) \mathbf{K}_i \mathbf{e}_s) v \quad \text{is SOS } \forall i, r \neq s; \quad (27)$$

$$v^T (a_{irs}(\mathbf{x}) + \mathbf{b}_{ir}(\mathbf{x}) \mathbf{K}_j \mathbf{e}_s + a_{jrs}(\mathbf{x}) + \mathbf{b}_{jr}(\mathbf{x}) \mathbf{K}_i \mathbf{e}_s) v \quad \text{is SOS } \forall i < j, r \neq s; \quad (28)$$

$$v^T (b_{i\omega rs} + \mathbf{b}_{ir}(\mathbf{x}) \mathbf{K}_i \mathbf{e}_{\omega s}) v \quad \text{is SOS } \forall i, r, s; \quad (29)$$

$$v^T (b_{i\omega rs} + \mathbf{b}_{ir}(\mathbf{x}) \mathbf{K}_j \mathbf{e}_{\omega s} + b_{j\omega rs} + \mathbf{b}_{jr}(\mathbf{x}) \mathbf{K}_i \mathbf{e}_{\omega s}) v \quad \text{is SOS } \forall i < j, r, s; \quad (30)$$

$$v^T (c_{irs}(\mathbf{x}) + \mathbf{d}_{ir}(\mathbf{x}) \mathbf{K}_i \mathbf{e}_s) v \quad \text{is SOS } \forall i, r, s; \quad (31)$$

$$v^T (c_{irs}(\mathbf{x}) + \mathbf{d}_{ir}(\mathbf{x}) \mathbf{K}_j \mathbf{e}_s + c_{jrs}(\mathbf{x}) + \mathbf{d}_{jr}(\mathbf{x}) \mathbf{K}_i \mathbf{e}_s) v \quad \text{is SOS } \forall i < j, r, s; \quad (32)$$

$$v^T (d_{i\omega rs} + \mathbf{d}_{ir}(\mathbf{x}) \mathbf{K}_i \mathbf{e}_{\omega s}) v \quad \text{is SOS } \forall i, r, s; \quad (33)$$

$$v^T (d_{i\omega rs} + \mathbf{d}_{ir}(\mathbf{x}) \mathbf{K}_j \mathbf{e}_{\omega s} + d_{j\omega rs} + \mathbf{d}_{jr}(\mathbf{x}) \mathbf{K}_i \mathbf{e}_{\omega s}) v \quad \text{is SOS } \forall i < j, r, s; \quad (34)$$

$$-\sigma^T \left(\text{diag} (\mathbf{I}_1^T \mathbf{D}_{i\omega} + \lambda^T \mathbf{B}_{i\omega} - \gamma \mathbf{I}_2^T + \mathbf{I}_m^T \mathbf{K}_i \mathbf{E}_{\omega} + \varepsilon_2(\mathbf{x}) \mathbf{I}_h^T) \right) \sigma \quad \text{is SOS } \forall i; \quad (35)$$

$$\begin{aligned} & -\sigma^T \left(\text{diag} (\mathbf{I}_1^T \mathbf{D}_{i\omega} + \lambda^T \mathbf{B}_{i\omega} - \gamma \mathbf{I}_2^T + \mathbf{I}_m^T \mathbf{K}_j \mathbf{E}_{\omega} \right. \\ & \left. + \mathbf{I}_1^T \mathbf{D}_{j\omega} + \lambda^T \mathbf{B}_{j\omega} - \gamma \mathbf{I}_2^T + \mathbf{I}_m^T \mathbf{K}_i \mathbf{E}_{\omega} + \varepsilon_2(\mathbf{x}) \mathbf{I}_h^T) \right) \sigma \quad \text{is SOS } \forall i < j \end{aligned} \quad (36)$$

$$-\rho^T \left(\text{diag} (\mathbf{I}_1^T \mathbf{C}_i(\mathbf{x}) + \lambda^T \mathbf{A}_i(\mathbf{x}) + \mathbf{I}_m^T \mathbf{K}_i \mathbf{E} + \varepsilon_3(\mathbf{x}) \mathbf{I}_n^T) \right) \rho \quad \text{is SOS } \forall i; \quad (37)$$

$$\begin{aligned} & -\rho^T \left(\text{diag} (\mathbf{I}_1^T \mathbf{C}_i(\mathbf{x}) + \lambda^T \mathbf{A}_i(\mathbf{x}) + \mathbf{I}_m^T \mathbf{K}_j \mathbf{E} \right. \\ & \left. + \mathbf{I}_1^T \mathbf{C}_j(\mathbf{x}) + \lambda^T \mathbf{A}_j(\mathbf{x}) + \mathbf{I}_m^T \mathbf{K}_i \mathbf{E} + \varepsilon_3(\mathbf{x}) \mathbf{I}_n^T) \right) \rho \quad \text{is SOS } \forall i < j; \end{aligned} \quad (38)$$

Remark 4 In general, PDC technique is helpful to reduce the conservativeness, but there are some limitations of using this technique. For example, it greatly reduces the flexibility of controller design because PDC technique requires the polynomial fuzzy controller and the polynomial fuzzy system share same fuzzy rules, which means both the number and the type of the MFs should be same. Therefore, when the number and/or the type of the MFs of the polynomial fuzzy system are large and/or complex, it becomes hard to design and implement the polynomial fuzzy controller. Also, the MFI analysis is a source of conservativeness. See [9, 10] for further details of IPM concept and MFD analysis.

4. Simulation Example

4.1. Scenario

A positive polynomial fuzzy model with 3 fuzzy rules is presented:

$$\begin{aligned}\mathbf{A}_1(x_1) &= \begin{bmatrix} 0.03 & 0.45 + 0.08x_1^2 \\ 0.98 & -1.13 - x_1^2 + 0.13x_1 \end{bmatrix}, \mathbf{A}_2(x_1) = \begin{bmatrix} 0.06 & 0.42 + 0.1x_1^2 \\ 0.94 & -1.25 - x_1^2 + 0.26x_1 \end{bmatrix}, \\ \mathbf{A}_3(x_1) &= \begin{bmatrix} 0.08 & 0.39 + 0.16x_1^2 \\ 0.62 & -1.06 - x_1^2 + 0.37x_1 \end{bmatrix}, \mathbf{B}_1 = \begin{bmatrix} 0.36 \\ 0.22 \end{bmatrix}, \mathbf{B}_2 = \begin{bmatrix} 0.37 \\ 0.24 \end{bmatrix}, \mathbf{B}_3 = \begin{bmatrix} 0.36 \\ 0.18 \end{bmatrix}, \\ \mathbf{B}_{1w} &= \begin{bmatrix} 1.12 \\ 1.18 \end{bmatrix}, \mathbf{B}_{2w} = \begin{bmatrix} 1.13 \\ 1.16 \end{bmatrix}, \mathbf{B}_{3w} = \begin{bmatrix} 1.16 \\ 1.14 \end{bmatrix}, \mathbf{x} = [x_1 \quad x_2]^T, \mathbf{E} = [1 \quad 0], \mathbf{E}_\omega = 1, \\ \mathbf{C}_1(x_1) &= [1.07 \quad 1.15 + 0.23x_1^2], \mathbf{C}_2(x_1) = [1.05 \quad 1.18 + 0.15x_1^2], \\ \mathbf{C}_3(x_1) &= [1.14 \quad 1.2 + 0.17x_1^2], \mathbf{D}_1 = [0.35], \mathbf{D}_2 = [0.26], \mathbf{D}_3 = [0.14], \\ \mathbf{D}_{1\omega} &= [1.24], \mathbf{D}_{2\omega} = [1.19], \mathbf{D}_{3\omega} = [1.05].\end{aligned}$$

Recalling the Lemma 1, it can be found that the open-loop PPFS is an positive system since $a_{irs}(x_1)$ is non-negative, for $i \in \{1, 2, 3\}$, $r \neq s$, and all of elements in the rest system matrices are non-negative. The disturbance signal is $\tilde{\mathbf{w}}(t) = \beta e^{-t} |\cos(2t)|$, where $\beta = 1, 2, 3$, respectively.

In order to cut down the complexity of the SOF controller design, we choose 2 fuzzy rules for the SOF controller in this example. The MFs of the PPFS and the SOF controller are same as the ones in [18]. Through setting $\varepsilon_1, \varepsilon_2(x_1), \varepsilon_3(x_1)$ and ε_4 as 0.001, the effectiveness of Theorem 1 is validated.

4.2. Feasibility Analysis

Fig. 1 and Figs. 2 to 4 show the time responses of x_1 and x_2 for the open-loop PPFS and the closed-loop PPFS, repectively. From Fig. 1, we can see that under zero initial condition, the open-loop PPFS is an unstable positive system because the time responses of x_1 and x_2 keep moving in the positive quadrant but do not converge to 0. From Figs. 2 to 4, it can be seen that the closed-loop system becomes an asymptotically stable and positive system since the time responses of x_1 and x_2 keep moving in the positive quadrant and converge to 0. Therefore, it can be concluded that the designed SOF controller can guarantee the unstable PPFS to be stable and positive with satisfying the optimal L_1 performance on the basis of Theorem 1. Meanwhile, the obtained optimal performance is $\gamma = 1.959$, the feedback gains are $\mathbf{K}_1 = -3.0541, \mathbf{K}_2 = -3.0541$. Furthermore, based on the Corollary 1, the obtained optimal performance is $\gamma = 1.956$, the feedback gains are obtained $\mathbf{K}_1 = -3.0571, \mathbf{K}_2 = -3.0231, \mathbf{K}_3 = -3.0098$.

In order to investigate how the disturbance signal influence the stability of the closed-loop PPFS, we obtain different time responses of the states x_1 and x_2 when β is chosen as $\beta = 1, 2, 3$, respectively. In terms of the Figs. 2 to 4, we come to the conclusion that the stronger the disturbance signal, the slower the time response converges and the bigger the amplitude gets.

In order to demonstrate the superiority of the method proposed in this paper, we also compare it with another existing method in [19] and try to figure out the optimal performance index γ . Before making a comparison, we need to set $\mathbf{B}_1 = \mathbf{B}_2 = \mathbf{B}_3 = [0.36; 0.22]$ and keep the rest system matrices the same as the example above. That is because the method proposed in [19] requires the input matrices \mathbf{B}_i to be assumed to be same for all i . The obtained performance indeces are $\gamma = 2.455$ and $\gamma = 1.945$ by using the method in [19] and the method in this paper, respectively, which indicates that the

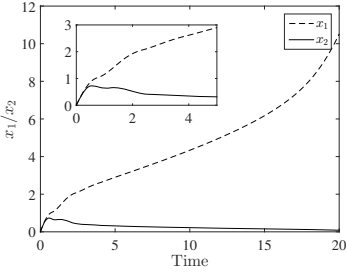


Figure 1. Time responses of the states x_1 and x_2 for the open-loop system.

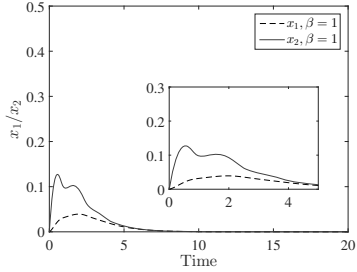


Figure 2. Time responses of the states x_1 and x_2 for the closed-loop system when $\beta = 1$.

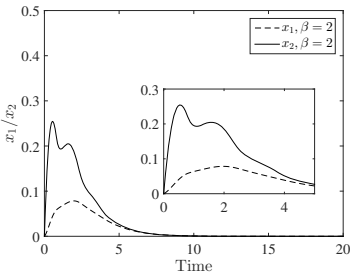


Figure 3. Time responses of the states x_1 and x_2 for the closed-loop system when $\beta = 2$.

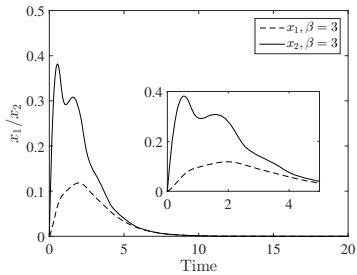


Figure 4. Time responses of the states x_1 and x_2 for the closed-loop system when $\beta = 3$.

method in this paper can provide better performance. In addition, another advantage of the method given in this paper over that one in [19] is that the manually chosen parameter is removed so that the conservativeness of the results can be reduced through eliminating the influence of human intervention.

5. Conclusion

In this paper, the positivity and stability analysis under L_1 -induced performance for SOF PPFSs have been investigated. The SOF control approach has been employed to drive unstable PPFSs to be asymptotically stable and positive. Through introducing some extra constrain conditions, the tricky non-convex problem has been addressed. It is worth noting that this method has some merits than the method proposed in [19] since the manually chosen parameter has been removed which means the relaxation of the results has been improved by removing the human intervention factor. In addition, based on linear co-positive Lyapunov stability theory, the SOS-based stability conditions have been derived. A simulation example has been given to illustrate the reliability and effectiveness of the proposed theorem.

Considering that many dynamical systems are with both discrete and continuous components in real systems [20,21], designing hybrid automata-based controllers for positive systems will be an interesting and challenging research topic for our future work.

6. Acknowledgements

This work is supported in part by the Natural Science Foundation of Hebei Province under Project Number F2019203505; China Scholarship Council and King's College London.

References

- [1] Jerry J, Batzel, Franz K. Time delay in physiological systems: Analyzing and modeling its impact. *Mathematical Biosciences*. 2011 Dec; 234(2):61-74.
- [2] Shorten R, Wirth F, Leith D. A positive systems model of TCP-like congestion control: asymptotic results. *IEEE/ACM Transactions on Networking*. 2006 Jun; 14(3):616-629.
- [3] Arcak M, Sontag, ED. Diagonal stability of a class of cyclic systems and its connection with the secant criterion. *Automatica*. 2006 Sep; 42(9):1531–1537.
- [4] Shen J, Lam J. ℓ_∞/L_∞ -gain analysis for positive linear systems with unbounded time-varying delays. *IEEE Transactions on Automatic Control*. 2015 Mar; 60(3):857-862.
- [5] Zhao X, Liu X, Yin S, Li H. Improved results on stability of continuous-time switched positive linear systems. *Automatica*. 2014 Feb; 50(2):614-621.
- [6] Liu X, Yu W, Wang L. Stability analysis for continuous-time positive systems with time-varying delays. *IEEE Transaction on Automatic Control*. 2010 Apr; 55(4):1024–1028.
- [7] Ren Y, Meng JE, Sun G. Asynchronous ℓ_1 positive filter design for switched positive systems with overlapped detection delay. *IET Control Theory and Application*. 2016 Jan; 11(3):319–328.
- [8] Takagi T, Sugeno M. Fuzzy identification of systems and its applications to modeling and control. *IEEE Transactions on Systems, Man, and Cybernetics*. 1985 Feb; 15(1):116-132.
- [9] Lam HK. A review on stability analysis of continuous-time fuzzy-model-based control systems: From membership-function-independent to membership-function-dependent analysis. *Engineering Applications of Artificial Intelligence*. 2018 Jan; 67:390-408.
- [10] Lam HK. Polynomial Fuzzy model-based control systems: stability analysis and control synthesis using membership function dependent techniques. Switzerland: Springer International Publishing. 2016.
- [11] Steentjes TRV, Doban AI, Lazar M. Feedback stabilization of positive nonlinear systems with applications to biological systems. 2018 European Control Conference. 2018 Nov; 1619-1624.
- [12] Meng A, Lam HK, Yu Y, Li X, Liu F. Static output feedback stabilization of positive polynomial fuzzy systems. *IEEE Transaction on Fuzzy Systems*. 2018 Jun; 26(3):1600-1612.
- [13] Crusius C A R and Trofino A. Sufficient LMI conditions for output feedback control problems. *IEEE Transactions on Automatic Control*. 1999 May; 44(5):1053-1057.
- [14] Chadli M and Guerra T M. LMI solution for robust static output feedback control of discrete Takagi-Sugeno fuzzy models. *IEEE Transactions on Fuzzy Systems*. 2012 Dec; 20(6):1160-1165.
- [15] Rami M A, Tadeo F. Controller synthesis for positive linear systems with bounded controls. *IEEE Transactions on Circuits and Systems II: Express Briefs*. 2007 Feb; 54(2):151-155.
- [16] Zhang J, Han Z, Zhu F, Huang J. Brief paper: Feedback control for switched positive linear systems. *IET Control Theory Application*. 2013 Feb; 7(3):464-469.
- [17] Chen X. Analysis and synthesis of positive systems under ℓ_1 and L_1 performance. Springer Publishing Company. 2016.
- [18] Meng A, Lam H K, Liu F, Zhang C, Qi P. Output feedback and stability analysis of positive polynomial fuzzy systems. *IEEE Transactions on Systems, Man, and Cybernetics: Systems*. 2020, Early Access.
- [19] Meng A, Lam H K, Hu L, Liu F. L_1 -induced static output feedback controller design and stability analysis for positive polynomial fuzzy systems. 19th UK Workshop on Computational Intelligence. 2019 Sep; 1043:41-52.
- [20] Nandi G C, et al. Modeling bipedal locomotion trajectories using hybrid automata. 2016 IEEE region 10 conference (TENCON). 2016; 1013-1018.
- [21] Semwal V B, Nandi G C. Generation of joint trajectories using hybrid automate-based model: a rocking block-based approach. *IEEE Sensors Journal*. 2016 Jul; 16(14):5805-5816.

Distance Metrics of D Numbers

Liguo FEI^{a,1} and Yuqiang FENG^a

^a*School of Management, Harbin Institute of Technology, Harbin 150001, China*

Abstract. Belief function has always played an indispensable role in modeling cognitive uncertainty. As an inherited version, the theory of D numbers has been proposed and developed in a more efficient and robust way. Within the framework of D number theory, two more generalized properties are extended: (1) the elements in the frame of discernment (FOD) of D numbers do not required to be mutually exclusive strictly; (2) the completeness constraint is released. The investigation shows that the distance function is very significant in measuring the difference between two D numbers, especially in information fusion and decision. Modeling methods of uncertainty that incorporate D numbers have become increasingly popular, however, very few approaches have tackled the challenges of distance metrics. In this study, the distance measure of two D numbers is presented in cases, including complete information, incomplete information, and non-exclusive elements.

Keywords. D numbers, Distance metrics, Belief functions

1. Introduction

Belief function, proposed by Dempster [1] and developed by Shafer [2], is crucial in modeling a broad range of uncertainty. In recent years, this avenue of research has been considerable advancements triggered by increasing applications in information fusion [4] and decision making [5]. As an extended version, the D number theory was put forward by Deng [3], which inherits the advantages of the theory of belief function but at the same time had certain expansion mainly reflected in (1) the elements in FOD do not required to be mutually exclusive strictly (2) the completeness constraint is released.

Since D number theory was put forward, it has been widely used in various uncertain modeling problems, such as supplier selection [6], risk assessment [7], etc. In addition, its theory is gradually expanded and perfected [8]. The investigation shows that the distance function is very significant in measuring the difference between two D numbers. Modeling methods of uncertainty that incorporate D numbers have become increasingly popular, however, very few approaches have tackled the challenges of distance metrics. In [9], authors defined a distance function to measure the distance between two D numbers, which is a generalization of the distance measure of belief function. However, this distance function has high computational complexity and is not convenient and flexible to use. As a result, methods with high flexibility and case-by-case processing power are largely unexplored. In this study, the distance measure of two D numbers is presented in cases, including complete information, incomplete information, and non-exclusive elements.

¹Corresponding Author: Liguo Fei, School of Management, Harbin Institute of Technology, Harbin 150001, China; E-mail: feiliguohit@163.com.

2. D numbers

In this section, the basic concept of D numbers is recalled.

Definition 1 [3] Let a finite nonempty set Ω denote the problem domain. D numbers can be denoted as a mapping formulated by

$$D : \Omega \rightarrow [0, 1], \text{with}, D(\emptyset) = 0 \quad \text{and} \quad \sum_{B \subseteq \Omega} D(B) \leq 1 \quad (1)$$

where \emptyset is the empty set and B is a subset of Ω . In addition, for a discrete set $\Omega = \{b_1, b_2, \dots, b_i, \dots, b_n\}$, $b_i \in R$, a special form of D numbers can be expressed by

$$D(\{b_1\}) = v_1, D(\{b_2\}) = v_2, \dots, D(\{b_i\}) = v_i, \dots, D(\{b_n\}) = v_n \quad (2)$$

or simply denoted as $D = \{(b_1, v_1), (b_2, v_2), \dots, (b_i, v_i), \dots, (b_n, v_n)\}$, where $v_i > 0$ and $\sum_{i=1}^n v_i \leq 1$. If $\sum_{B \subseteq \Omega} D(B) = 1$, the information is said to be complete; if $\sum_{B \subseteq \Omega} D(B) < 1$, the information is said to be incomplete.

3. Distance measure between two D numbers

In this section, we shall define the distance of D numbers from three perspectives. First, we consider the case where information is complete and elements in FOD are mutually exclusive. Second, we extend it to the case where information is incomplete. Finally, we discuss the case where elements in FOD are not mutually exclusive.

3.1. The case where the information is complete and the elements in FOD are mutually exclusive

Definition 2 Suppose d_1 and d_2 are two D numbers within the discrete set $\Omega = \{b_1, b_2, \dots, b_i, \dots, b_n\}$, $b_i \in R$, including n mutually exclusive and exhaustive hypotheses, and their information is complete, that is, $\sum_{B \subseteq \Omega} D(B) = 1$. The distance between d_1 and d_2 can be defined as follows.

$$d_{D\text{-number}}(d_1, d_2) = 1 - \frac{\langle \vec{d}_1, \vec{d}_2 \rangle}{|\vec{d}_1| \cdot |\vec{d}_2|} \quad (3)$$

where \vec{d}_1 and \vec{d}_2 are the vector forms of d_1 and d_2 , which can be denoted as $\vec{d}_1 = (v_1^1, v_2^1, \dots, v_n^1)^T$ and $\vec{d}_2 = (v_1^2, v_2^2, \dots, v_n^2)^T$. Therefore, the definition of distance measure in Eq.(3) can also be expressed as

$$d_{D\text{-number}}(d_1, d_2) = 1 - \frac{\sum_{i=1}^n v_i^1 \cdot v_i^2}{(\sum_{i=1}^n (v_i^1)^2)^{1/2} + (\sum_{i=1}^n (v_i^2)^2)^{1/2}} \quad (4)$$

where v_i^1 is the belief of b_i in d_1 and v_i^2 means the belief of b_i in d_2 .

An illustrative example is given to show the calculation of the distance between two D numbers defined above.

Example 1 Let Ω be a FOD with 2 linguistic constants, namely $\Omega = \{\text{Good}, \text{Bad}\}$, and they are mutually exclusive. Given two pairs of D numbers: $d_1(\{\text{Good}\}) = 1$, $d_1(\{\text{Bad}\}) = 0$; $d_2(\{\text{Good}\}) = 0$, $d_2(\{\text{Bad}\}) = 1$. The distance between the two D numbers can be calculated as below:

$$d_{D\text{-number}}(d_1, d_2) = 1 - \frac{1 \times 0 + 0 \times 1}{(1^2 + 0^2)^{1/2} + (0^2 + 1^2)^{1/2}} = 1 \quad (5)$$

Remark 1 From Definition 2 and Example 1, it can be seen some conditions are added to the defined distance measure that the elements in set Ω require mutually exclusive and the completeness is needed, that is, the above definition can work when D numbers is degenerated into D-S theory, but what if these limitations are exceeded? The further discussion will be conducted below.

As shown in Example 1, if the information is complete for the two D numbers, the reasonable result can be obtained, but what if the condition is released? Let's consider the following example.

Example 2 Let Ω be a FOD with 2 linguistic constants, namely $\Omega = \{\text{Good}, \text{Bad}\}$, and they are mutually exclusive. Given two pairs of D numbers: $d_1(\{\text{Good}\}) = 0.4$, $d_1(\{\text{Bad}\}) = 0.6$; $d_2(\{\text{Good}\}) = 0.2$, $d_2(\{\text{Bad}\}) = 0.3$. The distance between the two D numbers can be calculated as below:

$$d_{D\text{-number}}(d_1, d_2) = 1 - \frac{0.4 \times 0.2 + 0.6 \times 0.3}{(0.4^2 + 0.6^2)^{1/2} + (0.2^2 + 0.3^2)^{1/2}} = 0 \quad (6)$$

Apparently, d_1 and d_2 are two different D numbers, but their distance is 0 in above example, which is obviously unreasonable. This case shows that Definition 2 is invalid when information is incomplete for D numbers. To address this issue, the definition of distance measure between two D numbers is improved as follows.

3.2. The case where the information is incomplete and the elements in FOD are mutually exclusive

Definition 3 Suppose d_1 and d_2 are two D numbers within the discrete set $\Omega = \{b_1, b_2, \dots, b_i, \dots, b_n\}$, $b_i \in R$, including n mutually exclusive and exhaustive hypotheses. The distance between d_1 and d_2 can be defined as follows.

$$d_{D\text{-number}}^+(d_1, d_2) = 1 - \frac{\overrightarrow{d_1^+}, \overrightarrow{d_2^+} >}{|\overrightarrow{d_1^+}| \cdot |\overrightarrow{d_2^+}|} \quad (7)$$

where $\overrightarrow{d_1^+}$ and $\overrightarrow{d_2^+}$ are the vector forms of d_1^+ and d_2^+ , which can be denoted as $\overrightarrow{d_1^+} = (v_1^1, v_2^1, \dots, v_n^1, v_{n+1}^1)^T$ and $\overrightarrow{d_2^+} = (v_1^2, v_2^2, \dots, v_n^2, v_{n+1}^2)^T$. v_{n+1}^i represents the belief of the incomplete part in D number d_i , that is, if the information is complete of d_i , $v_{n+1}^i = 0$;

otherwise, $v_{n+1}^i = 1 - \sum_{i=1}^n v_i$. Also, the definition of distance measure in Eq.(7) can also be expressed as

$$d_{D\text{-number}}^+(d_1, d_2) = 1 - \frac{\sum_{i=1}^{n+1} v_i^1 \cdot v_i^2}{(\sum_{i=1}^{n+1} (v_i^1)^2)^{1/2} + (\sum_{i=1}^{n+1} (v_i^2)^2)^{1/2}} \quad (8)$$

An illustrative example, continuing the Example 2, is also given to show the calculation of the distance between two D numbers based on the definition above.

Example 3 (Continued Example 2). Let Ω be a FOD with 2 linguistic constants, namely $\Omega = \{\text{Good}, \text{Bad}\}$, and they are mutually exclusive. Given two pairs of D numbers: $d_1(\{\text{Good}\}) = 0.4$, $d_1(\{\text{Bad}\}) = 0.6$; $d_2(\{\text{Good}\}) = 0.2$, $d_2(\{\text{Bad}\}) = 0.3$. The distance between the two D numbers can be calculated as below: it is obvious the information of d_2 is incomplete, so \vec{d}_1 and \vec{d}_2 should be transformed by $\vec{d}_1^+ = (0.4, 0.6, 0)^T$ and $\vec{d}_2^+ = (0.2, 0.3, 0.5)^T$

$$d_{D\text{-number}}^+(d_1, d_2) = 1 - \frac{0.4 \times 0.2 + 0.6 \times 0.3 + 0 \times 0.5}{(0.4^2 + 0.6^2 + 0^2)^{1/2} + (0.2^2 + 0.3^2 + 0.5^2)^{1/2}} = 0.4151. \quad (9)$$

Compared with the result in Example 2, the distance measure above is obviously more reasonable.

Remark 2 It can be noticed by observing that in Definitions 2 and 3 a constraint is added that elements in the FOD Ω need to be mutually exclusive, which indicates that the distance between two D numbers can only be measured within this condition. However, according to the definition of D number, the elements in set Ω do not require mutually exclusive, so how to measure it in this case?

The following example is given firstly, which is another version of Example 1 by changing a condition.

Example 4 Let Ω be a FOD with 2 linguistic constants, namely $\Omega = \{\text{Good}, \text{Bad}\}$, and their relationship is shown in Fig.1, that means the two linguistic constants are not exclusive (as distinguished from Example 1). Given two pairs of D numbers: $d_1(\{\text{Good}\}) = 1$, $d_1(\{\text{Bad}\}) = 0$; $d_2(\{\text{Good}\}) = 0$, $d_2(\{\text{Bad}\}) = 1$. As the previous definition, the distance between d_1 and d_2 should be 0, however, in this case we consider it unreasonable because there is an intersection between elements Good and Bad, so if the condition elements in Ω are mutually exclusive cannot be satisfied, Definitions 2 and 3 fail to measure the distance between D numbers. To solve this problem, the further definition are developed as follows.

3.3. The case where the elements in FOD are not mutually exclusive

Definition 4 Suppose d_1 and d_2 are two D numbers within the discrete set $\Omega = \{b_1, b_2, \dots, b_i, \dots, b_n\}$, $b_i \in R$. The distance between d_1 and d_2 can be defined as:

$$d_{D\text{-number}}(d_1, d_2) = 1 - \frac{\vec{d}_1 \cdot \underline{D} \cdot \vec{d}_2^T}{|\vec{d}_1| \cdot |\vec{d}_2| + \vec{d}_1 \cdot \underline{D} \cdot \vec{d}_2^T} \quad (10)$$

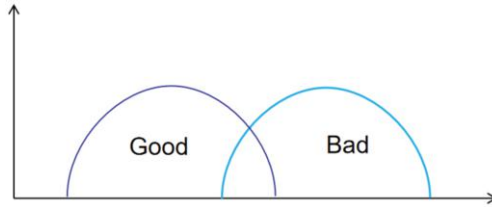


Figure 1. The relationship between two linguistic terms.

where \underline{D} is a $(n \times n)$ -dimensional matrix if the information of d_1 and d_2 is complete ;otherwise, it is a $(n+1) \times (n+1)$ -dimensional matrix whose elements are

$$\underline{D} = \begin{cases} \frac{A \cap B}{A \cup B} & A \neq B \quad A, B \in \Omega / \{\Omega, b_{n+1}\} \\ 1 & A = B \quad A, B \in \Omega / \{\Omega, b_{n+1}\}, \end{cases}$$

and D is also a $(n \times n)$ -dimensional matrix if the information of d_1 and d_2 is complete ;otherwise, it is a $(n+1) \times (n+1)$ -dimensional matrix whose elements are

$$D = \begin{cases} \frac{A \cap B}{A \cup B} & A \neq B \quad A, B \in \Omega / \{\Omega, b_{n+1}\} \\ 0 & A = B \quad A, B \in \Omega / \{\Omega, b_{n+1}\}. \end{cases}$$

if the information of d_1 and d_2 is incomplete, $A, B \in \{b_1, b_2, \dots, b_n, b_{n+1}\}$, which has been introduced in Definition 3.

The above definition considers another special property of D numbers, that is, the elements do not need to be mutually exclusive, which makes the distance measure between D numbers more perfect. To illustrate the calculation process of this definition, the issue proposed in Example 4 will be addressed below.

Example 5 (Continued Example 4). Let Ω be a FOD with 2 linguistic constants, namely $\Omega = \{\text{Good}, \text{Bad}\}$, and their relationship is shown in Fig.1. Given two pairs of D numbers: $d_1(\{\text{Good}\}) = 1, d_1(\{\text{Bad}\}) = 0; d_2(\{\text{Good}\}) = 0, d_2(\{\text{Bad}\}) = 1$. Since elements in Ω do not mutually exclusive, so the distance measure between d_1 and d_2 depends not only on their belief distribution but also on the relationship among the elements. Firstly, matrix \underline{D} and D can be obtained based on the relationship between "Good" and "Bad" in Fig. 1

$$\underline{D} = \begin{bmatrix} 1 & 0.2 \\ 0.2 & 1 \end{bmatrix}, \quad D = \begin{bmatrix} 0 & 0.2 \\ 0.2 & 1 \end{bmatrix}.$$

The distance can be measured based on Definition 4 as

$$d_{D\text{-number}}(d_1, d_2) = 1 - \frac{\begin{bmatrix} 1 & 0 \end{bmatrix} \cdot \begin{bmatrix} 1 & 0.2 \\ 0.2 & 1 \end{bmatrix} \cdot \begin{bmatrix} 0 \\ 1 \end{bmatrix}}{1 + \begin{bmatrix} 1 & 0 \end{bmatrix} \cdot \begin{bmatrix} 0 & 0.2 \\ 0.2 & 1 \end{bmatrix} \cdot \begin{bmatrix} 0 \\ 1 \end{bmatrix}} = 0.8333. \quad (11)$$

It is obvious the above result is more reasonable.

4. Conclusion

In this work, we define the distance function between two D numbers. We employ some examples to demonstrate the use of distance function, and its rationality is illustrated by several cases. Our results show that it is valid and reasonable to define the distance function of D numbers according to different cases. In the following research, we will perfect the definition of the distance function of D numbers and further extend the theoretical results to applications, such as failure mode and effects analysis, risk analysis, multi-sensor data fusion.

References

- [1] Dempster, A.P.: Upper and lower probabilities induced by a multivalued mapping. *The Annals of Mathematical Statistics* **38**(2), 325--339 (1967)
- [2] Shafer, G.: *A mathematical theory of evidence*, vol. 1. Princeton university press Princeton (1976)
- [3] Deng, Y.: D numbers: Theory and applications. *Journal of Information and Computational Science* **9**(9), 2421--2428 (2012)
- [4] Lin, Z., Zhang, Z., Liu, Y., Dezert, J., Pan, Q.: A new pattern classification improvement method with local quality matrix based on K-NN. *Knowledge-based Systems* **164**, 336--347 (2019)
- [5] Thierry, D.: Decision-making with belief functions: A review. *International Journal of Approximate Reasoning* **109**, 87--110 (2019)
- [6] Deng, X., Hu, Y., Deng, Y., Mahadevan, S.: Supplier selection using ahp methodology extended by d numbers. *Expert Systems with Applications* **41**(1), 156--167 (2014)
- [7] Lin, S., Li, C., Xu, F., Liu, D., Liu, J.: Risk identification and analysis for new energy power system in china based on d numbers and decision-making trial and evaluation laboratory (dematel). *Journal of Cleaner Production* **180**, 81--96 (2018)
- [8] Mo, H., Deng, Y.: A new aggregating operator for linguistic information based on d numbers. *International Journal of Uncertainty, Fuzziness and Knowledge-Based Systems* **24**(06), 831-846 (2016)
- [9] Li, M., Hu, Y., Zhang, Q., Deng, Y.: A novel distance function of d numbers and its application in product engineering. *Engineering Applications of Artificial Intelligence* **47**, 61-67 (2016)

Comparison of Two Estimators of the Regression Coefficient Vector Under Pitman's Closeness Criterion

Jibo Wu ¹

*Chongqing Key Laboratory of Complex Data Analysis & Artificial Intelligence,
Chongqing University of Arts and Sciences, Chongqing*

Abstract. Schaffrin and Toutenburg [1] proposed a weighted mixed estimation based on the sample information and the stochastic prior information, and they also show that the weighted mixed estimator is superior to the ordinary least squares estimator under the mean squared error criterion. However, there has no paper to discuss the performance of the two estimators under the Pitman's closeness criterion. This paper presents the comparison of the weighted mixed estimator and the ordinary least squares estimator using the Pitman's closeness criterion. A simulation study is performed to illustrate the performance of the weighted mixed estimator and the ordinary least squares estimator under the Pitman's closeness criterion.

Keywords. Ordinary least squares estimator, Pitman's closeness criterion, Weighted mixed estimator

1. Introduction

In this paper, we discuss the following multiple linear regression model

$$Y = X\beta + \varepsilon \quad (1)$$

where Y shows an $n \times 1$ vector of observation, X denotes an $n \times p$ known matrix of rank p , β shows a $p \times 1$ vector of unknown parameters, ε defines an $n \times 1$ vector of disturbances with $E(\varepsilon) = 0$ and $Cov(\varepsilon) = \sigma^2 I_n$.

By the Gauss-Markov theorem, the classical ordinary least squares (OLS) estimator is given as follows:

$$\hat{\beta}_{OLS} = (X'X)^{-1}X'Y \quad (2)$$

Besides the model (1), we suppose that we have the following stochastic linear restrictions

$$r = R\beta + e, \quad e \sim N(0, \sigma^2 V) \quad (3)$$

¹Corresponding Author: Chongqing Key Laboratory of Complex Data Analysis & Artificial Intelligence, Chongqing University of Arts and Sciences, Chongqing 402160, China. Email:linfen52@126.com

where R shows a $j \times p$ known matrix with $\text{rank}(R) = j$, e shows a $j \times 1$ vector of disturbances with $E(e) = 0$ and $\text{Cov}(e) = \sigma^2 V$, V is assumed to be a known and positive definite matrix, and we suppose that $E(r) = R\beta$. And we also assumed that the random vector ε is stochastically independent of e [2].

Using (1) and (3), Durbin [3], Theil and Goldberger [4] and Theil [5] have presented the mixed estimator (ME):

$$\hat{\beta}_{ME} = (X'X + R'V^{-1}R)^{-1}(X'Y + R'V^{-1}r) \quad (4)$$

When the sample information given by (1) and the prior information depicted by (3) are to be assigned not necessarily equal weights on the basis of some extraneous considerations in the estimation of regression parameters, Schaffrin and Toutenburg [1] introduced a weighted mixed estimator (WME)

$$\hat{\beta}(w) = (X'X + wR'V^{-1}R)^{-1}(X'Y + wR'V^{-1}r), \quad 0 \leq w \leq 1 \quad (5)$$

The weighted mixed estimator is unbiased estimator.

If we put $w = 0$ in (5), the estimator can be written as

$$\hat{\beta}(0) = (X'X)^{-1}X'Y = \hat{\beta}_{OLS}$$

which is the ordinary least squares estimator.

If we put $w = 1$ in (5), the estimator reduces to

$$\hat{\beta}(1) = (X'X + R'V^{-1}R)^{-1}(X'Y + R'V^{-1}r) = \hat{\beta}_{ME}$$

which is the mixed estimator proposed by Durbin [3], Theil and Goldberger [4] and Theil [5]. This estimator give equal weight to sample (1) and prior information (3).

Although mean squared error (MSE) has been regards as the best criterion for comparing different estimators, Pitman's [6] closeness (PC) criterion has got a great deal of attention in recent years. This criterion is to calculate the probability that one estimator is closer than another to an unknown parameter of interest. Although PC is a meaningful alternative criterion to MSE, it never got widespread acceptance among statisticians, since it is difficulties to compute it. Since Keating and Mason [7] and Rao [8], Rao et al. [9], PC criterion has got considerable attention as a method for comparing the estimators [10].

Many authors have compared estimators using PC criterion in linear regression model. For example, Wencheko [11] compared some shrinkage estimator using PC criterion. Reif [12] compared general pre-test estimator with some regression estimator under PC criterion. Yang et al. [13] compared united biased estimators in linear model. Özkal and Kaçırınlar (2008) [10,14] and Li et al. [15] compared $r - k$ class estimator with ordinary least squares estimator under PC criterion. Wu [16] compared the estimators in two normal linear models for some of the identical parameters under Pitman's closeness criterion.

We will compare the weighted mixed estimator to the OLS estimator under the PC criterion in this paper. A simulation study is presented to illustrate that the weighted mixed estimator is always superior to the OLS estimator.

2. Main results

Firstly we list some definitions.

Definition 2.1. Suppose that $\hat{\theta}_1$ and $\hat{\theta}_2$ be two estimators of the unknown p-dimensional vector θ . The PC of $\hat{\theta}_1$ relative to $\hat{\theta}_2$ in estimating θ under a loss function $L(., \theta)$ is defined as $PMC(\hat{\theta}_1, \hat{\theta}_2, \theta) = P_r(\hat{\theta}_1, \hat{\theta}_2, \theta) = P_r(\Delta(\hat{\theta}_1, \hat{\theta}_2) \geq 0)$, where

$$\Delta(\hat{\theta}_1, \hat{\theta}_2) = L(\hat{\theta}_2, \theta) - L(\hat{\theta}_1, \theta) \quad (6)$$

In this paper, we consider the following quadratic loss function $L(\hat{\theta}, \theta) = (\hat{\theta} - \theta)'U(\hat{\theta} - \theta)$, where U is a given positive definite matrix.

Definition 2.2. $\hat{\theta}_1$ is said to be better than $\hat{\theta}_2$ for all $\theta \in \Theta$ in PC if

$$PMC(\hat{\theta}_1, \hat{\theta}_2, \theta) = P_r(\hat{\theta}_1, \hat{\theta}_2, \theta) = P_r(\Delta(\hat{\theta}_1, \hat{\theta}_2) \geq 0) \geq \frac{1}{2}, \text{ for all } \theta \in \Theta \quad (7)$$

Then we give the comparison results of the two estimators.

Theorem 2.1. The PC of $\hat{\beta}(w)$ relative to $\hat{\beta}_{OLS}$ is given by

$$\begin{aligned} & PMC(\hat{\beta}(w), \hat{\beta}_{OLS}, \beta) \\ &= P_r\{\varepsilon_1'[(I_j + wM_j)^{-2} - I_j]\varepsilon_1 + w\varepsilon_1'(I_j + wM_j)^{-2}M_j^{\frac{1}{2}}e_1 \\ &\quad + we_1'(I_j + wM_j)^{-2}M_j^{\frac{1}{2}}\varepsilon_1 + w^2e_1'(I_j + wM_j)^{-2}M_je_1 \leq 0\} \end{aligned} \quad (8)$$

Proof As matrices $X'X$ and $R'V^{-1}R$ are positive definite, they can be diagonalizable simultaneously, that is, there exists a reversible matrix Q such that

$$Q'X'XQ = I_p \quad (9)$$

$$Q'R'V^{-1}RQ = diag(m_1, \dots, m_j, 0, \dots, 0) = M_p \quad (10)$$

where m_1, \dots, m_j denote the positive eigenvalues of matrix $R'V^{-1}R(X'X)^{-1}$.

Denote:

$$Q'X'\varepsilon = \begin{pmatrix} \varepsilon_1 \\ \varepsilon_2 \end{pmatrix} \quad (11)$$

$$M_j = diag(m_1, \dots, m_j) \quad (12)$$

and

$$(M_p^+)^{\frac{1}{2}}Q'R'V^{-1}e = \begin{pmatrix} e_1 \\ 0 \end{pmatrix} \quad (13)$$

where ε_1 and e_1 denote j-dimension column random vector and M_p^+ denotes Moore-Penrose inverse of matrix M_p . Now let $U = X'X$. Thus, we can get:

$$L(\hat{\beta}_{OLS}, \beta) = (\hat{\beta}_{OLS} - \beta)'X'X(\hat{\beta}_{OLS} - \beta) = (Q'X'\varepsilon)'Q'X'\varepsilon \quad (14)$$

and

$$\begin{aligned}
 L(\hat{\beta}(w), \beta) &= (\hat{\beta}(w) - \beta)' X' X (\hat{\beta}(w) - \beta) \\
 &= [(X' X + wR' V^{-1} R)^{-1} (X' Y + wR' V^{-1} r) - \beta]' X' X \\
 &\quad \times [(X' X + wR' V^{-1} R)^{-1} (X' Y + wR' V^{-1} r) - \beta] \\
 &= (Q' X' \varepsilon + wQ' R' V^{-1} e)' (I_p + wM_p)^{-2} (Q' X' \varepsilon + wQ' R' V^{-1} e) \quad (15)
 \end{aligned}$$

Then we can obtain

$$\begin{aligned}
 &PMC(\hat{\beta}(w), \hat{\beta}_{OLS}, \beta) \\
 &= P_r(L(\hat{\beta}(w), \beta) \leq L(\hat{\beta}_{OLS}, \beta)) \\
 &= P_r\{(Q' X' \varepsilon + wQ' R' V^{-1} e)' (I_p + wM_p)^{-2} (Q' X' \varepsilon + wQ' R' V^{-1} e) \\
 &\quad \leq (Q' X' \varepsilon)' Q' X' \varepsilon\} \\
 &= P_r\{(Q' X' \varepsilon)' (I_p + wM_p)^{-2} Q' X' \varepsilon + w(Q' X' \varepsilon)' (I_p + wM_p)^{-2} (Q' R' V^{-1} e) \\
 &\quad + w(Q' R' V^{-1} e)' (I_p + wM_p)^{-2} Q' X' \varepsilon + w^2 (Q' R' V^{-1} e)' (I_p + wM_p)^{-2} \\
 &\quad \times (Q' R' V^{-1} e) \leq (Q' X' \varepsilon)' Q' X' \varepsilon\} \quad (16)
 \end{aligned}$$

Thus, by (11)-(14), we have

$$(Q' X' \varepsilon)' (I_p + wM_p)^{-2} (Q' R' V^{-1} e) = \varepsilon'_1 (I_j + wM_j)^{-2} M_j^{\frac{1}{2}} e_1 \quad (17)$$

$$(Q' R' V^{-1} e)' (I_p + wM_p)^{-2} (Q' R' V^{-1} e) = e'_1 (I_j + wM_j)^{-2} M_j e_1 \quad (18)$$

$$(Q' R' V^{-1} e)' (I_p + wM_p)^{-2} (Q' X' \varepsilon) = e'_1 (I_j + wM_j)^{-2} M_j^{\frac{1}{2}} \varepsilon_1 \quad (19)$$

$$(Q' X' \varepsilon)' [(I_p + wM_p)^{-2} - I_p] (Q' X' \varepsilon) = \varepsilon'_1 [(I_j + wM_j)^{-2} - I_j] \varepsilon_1 \quad (20)$$

Thus put (17)-(20) into (16), we have

$$\begin{aligned}
 &PMC(\hat{\beta}(w), \hat{\beta}_{OLS}, \beta) \\
 &= P_r\{\varepsilon'_1 [(I_j + wM_j)^{-2} - I_j] \varepsilon_1 + w\varepsilon'_1 (I_j + wM_j)^{-2} M_j^{\frac{1}{2}} e_1 \\
 &\quad + w e'_1 (I_j + wM_j)^{-2} M_j^{\frac{1}{2}} \varepsilon_1 + w^2 e'_1 (I_j + wM_j)^{-2} M_j e_1 \leq 0\} \quad (21)
 \end{aligned}$$

Theorem 2.2. $\hat{\beta}(w)$ always dominates $\hat{\beta}_{OLS}$ in the Pitman's closeness criterion for $0 < w < 1$.

Proof By Theorem 2.1, we have

$$\begin{aligned}
 &PMC(\hat{\beta}(w), \hat{\beta}_{OLS}, \beta) \\
 &= P_r\{\varepsilon'_1 [(I_j + wM_j)^{-2} - I_j] \varepsilon_1 + w\varepsilon'_1 (I_j + wM_j)^{-2} M_j^{\frac{1}{2}} e_1
 \end{aligned}$$

$$\begin{aligned}
& +we'_1(I_j + wM_j)^{-2}M_j^{\frac{1}{2}}\varepsilon_1 + w^2e'_1(I_j + wM_j)^{-2}M_j e_1 \leq 0 \\
& = P_r\{-\varepsilon'_1(I_j + wM_j)^{-2}(2wM_j + w^2M_j^2)\varepsilon_1 + w\varepsilon'_1(I_j + wM_j)^{-2}M_j^{\frac{1}{2}}e_1 \\
& \quad + we'_1(I_j + wM_j)^{-2}M_j^{\frac{1}{2}}\varepsilon_1 + w^2e'_1(I_j + wM_j)^{-2}M_j e_1 \leq 0\} \\
& \geq P_r\{-w\varepsilon'_1(I_j + wM_j)^{-2}M_j\varepsilon_1 + \varepsilon'_1(I_j + wM_j)^{-2}M_j^{\frac{1}{2}}e_1 \\
& \quad + e'_1(I_j + wM_j)^{-2}M_j^{\frac{1}{2}}\varepsilon_1 + we'_1(I_j + wM_j)^{-2}M_j e_1 \leq 0\} \tag{22}
\end{aligned}$$

Now we calculate:

$$\begin{aligned}
& P_r\{-w\varepsilon'_1(I_j + wM_j)^{-2}M_j\varepsilon_1 + \varepsilon'_1(I_j + wM_j)^{-2}M_j^{\frac{1}{2}}e_1 \\
& \quad + e'_1(I_j + wM_j)^{-2}M_j^{\frac{1}{2}}\varepsilon_1 + we'_1(I_j + wM_j)^{-2}M_j e_1 \leq 0\} \tag{23}
\end{aligned}$$

Denote $\eta_1 = e_1$ and $\eta_2 = -\varepsilon_1$. Then (23) becomes :

$$\begin{aligned}
& P_r\{-w\eta'_2(I_j + wM_j)^{-2}M_j\eta_2 - \eta'_2(I_j + wM_j)^{-2}M_j^{\frac{1}{2}}\eta_1 \\
& \quad - \eta'_1(I_j + wM_j)^{-2}M_j^{\frac{1}{2}}\eta_2 + w\eta'_1(I_j + wM_j)^{-2}M_j\eta_1 \leq 0\} \tag{24}
\end{aligned}$$

Since $\varepsilon_1 \sim N(0, \sigma^2 I_j)$, $e_1 \sim N(0, \sigma^2 I_j)$, and ε_1 is independent of e_1 . We have: $\eta_1 \sim N(0, \sigma^2 I_j)$, $\eta_2 \sim N(0, \sigma^2 I_j)$, and η_1 is independent of η_2 , thus we can change ε_1 as η_1 and change e_1 as η_2 in (23), we obtain

$$\begin{aligned}
& P_r\{-w\eta'_1(I_j + wM_j)^{-2}M_j\eta_1 + \eta'_1(I_j + wM_j)^{-2}M_j^{\frac{1}{2}}\eta_2 \\
& \quad + \eta'_2(I_j + wM_j)^{-2}M_j^{\frac{1}{2}}\eta_1 + w\eta'_2(I_j + wM_j)^{-2}M_j\eta_2 \leq 0\} \\
& = 1 - P_r\{-w\eta'_2(I_j + wM_j)^{-2}M_j\eta_2 - \eta'_2(I_j + wM_j)^{-2}M_j^{\frac{1}{2}}\eta_1 \\
& \quad - \eta'_1(I_j + wM_j)^{-2}M_j^{\frac{1}{2}}\eta_2 + w\eta'_1(I_j + wM_j)^{-2}M_j\eta_1 \leq 0\} \tag{25}
\end{aligned}$$

On the other hand (24) and (25) is equivalent to (23), we have

$$\begin{aligned}
& P_r\{-w\eta'_1(I_j + wM_j)^{-2}M_j\eta_1 + \eta'_1(I_j + wM_j)^{-2}M_j^{\frac{1}{2}}\eta_2 \\
& \quad + \eta'_2(I_j + wM_j)^{-2}M_j^{\frac{1}{2}}\eta_1 + w\eta'_2(I_j + wM_j)^{-2}M_j\eta_2 \leq 0\} \\
& = P_r\{-w\eta'_2(I_j + wM_j)^{-2}M_j\eta_2 - \eta'_2(I_j + wM_j)^{-2}M_j^{\frac{1}{2}}\eta_1 \\
& \quad - \eta'_1(I_j + wM_j)^{-2}M_j^{\frac{1}{2}}\eta_2 + w\eta'_1(I_j + wM_j)^{-2}M_j\eta_1 \leq 0\} = \frac{1}{2} \tag{26}
\end{aligned}$$

Thus:

$$PMC(\hat{\beta}(w), \hat{\beta}_{OLS}, \beta) \geq \frac{1}{2} \tag{27}$$

Table 1. The PMC of WME relative to OLS when $n = 50$

$\gamma = 0.9$	$w = 0.1$	$w = 0.2$	$w = 0.3$	$w = 0.4$	$w = 0.5$
	0.8084	0.7998	0.7979	0.7896	0.7907
	$w = 0.6$	$w = 0.7$	$w = 0.8$	$w = 0.9$	$w = 1.0$
	0.7793	0.7672	0.7769	0.7687	0.7680
$\gamma = 0.99$	$w = 0.1$	$w = 0.2$	$w = 0.3$	$w = 0.4$	$w = 0.5$
	0.8690	0.8530	0.8468	0.8336	0.8279
	$w = 0.6$	$w = 0.7$	$w = 0.8$	$w = 0.9$	$w = 1.0$
	0.8262	0.8107	0.8130	0.8042	0.8044
$\gamma = 0.999$	$w = 0.1$	$w = 0.2$	$w = 0.3$	$w = 0.4$	$w = 0.5$
	0.8960	0.8849	0.8866	0.8794	0.8805
	$w = 0.6$	$w = 0.7$	$w = 0.8$	$w = 0.9$	$w = 1.0$
	0.8800	0.8771	0.8789	0.8779	0.8728

The proof of Theorem 2.2 is completed.

Remark 2.1. From Theorem 2.2, we can see that the weighted mixed estimator is superior over the OLS estimator in the PC criterion. In fact, these results are easy to be understand. Because by adding the prior information, we have got more information about the unknown regression parameters, and naturally hope that the new estimator may have good accuracy.

3. A simulation study

In this section, we do some simulation to illustrate the performance of the weighted mixed estimator (WME) over the OLS estimator under the PC criterion.

By the methods proposed by Liu [17] and Kibria [18], we have

$$x_{ij} = (1 - \gamma^2)^{1/2} w_{ij} + \gamma w_{ip}, \quad i = 1, 2, \dots, n, \quad j = 1, 2, \dots, 4 \quad (28)$$

and

$$y_i = (1 - \gamma^2)^{1/2} w_i + \gamma w_{i4}, \quad i = 1, 2, \dots, n, \quad j = 1, 2, \dots, 4 \quad (29)$$

where w_{ij} are independent standard normal pseudo-random numbers and the correlation between any two explanatory variables is given by γ^2 . We consider $\gamma = 0.9, 0.99$ and 0.999 , and we choose $n = 50$ and 100 , $\sigma^2 = 1$.

Let us discuss the following restrictions

$$r = R\beta + e, \quad R = (1 \ 1 \ 1 \ 0), \quad r = 1, \quad e \sim N(0, \hat{\sigma}^2) \quad (30)$$

For Tables 1–2, we can see that the PC of WME relative to OLS estimator is greater than 0.5, that is to say the WME is better than the OLS estimator in the PC criterion.

Table 2. The PMC of WME relative to OLS when $n = 100$

$\gamma = 0.9$	$w = 0.1$	$w = 0.2$	$w = 0.3$	$w = 0.4$	$w = 0.5$
	0.8626	0.8670	0.8587	0.8573	0.8547
	$w = 0.6$	$w = 0.7$	$w = 0.8$	$w = 0.9$	$w = 1.0$
	0.8528	0.8528	0.8555	0.8479	0.8469
$\gamma = 0.99$	$w = 0.1$	$w = 0.2$	$w = 0.3$	$w = 0.4$	$w = 0.5$
	0.8362	0.8374	0.8282	0.8196	0.8118
	$w = 0.6$	$w = 0.7$	$w = 0.8$	$w = 0.9$	$w = 1.0$
	0.8095	0.8030	0.7952	0.7937	0.7926
$\gamma = 0.999$	$w = 0.1$	$w = 0.2$	$w = 0.3$	$w = 0.4$	$w = 0.5$
	0.9132	0.8922	0.8899	0.8911	0.8850
	$w = 0.6$	$w = 0.7$	$w = 0.8$	$w = 0.9$	$w = 1.0$
	0.8858	0.8907	0.8872	0.8810	0.8840

4. Conclusion

In this paper, we make the comparison between the weighted mixed estimator and the ordinary least squares estimator in the PC criterion and we show that the weighted mixed estimator is always superior to the ordinary least squares estimator in the PC criterion. A simulation simulation is given to show that the weighted mixed estimator is better than the ordinary least squares estimator in the PC criterion.

Acknowledgements

This work was sponsored by the National Natural Science Foundation of China (Grant No. 11501072), the Natural Science Foundation of Chongqing (Grant No. cstc2019jcyj-msxmX0379) and the Scientific Technological Research Program of Chongqing Municipal Education Commission (Grant No. KJQN201901347).

References

- [1] B. Schaffrin and H. Toutenburg, *Weighted mixed regression*, Zeitschrift fur Angewandte Mathematik und Mechanik, **70**(1990), 735–738.
- [2] C.R. Rao and H. Toutenburg, *Linear models: least squares and alternatives*, Springer, New York, 1995.
- [3] J. Durbin, *A note on regression when there is extraneous information about one of the coefficients*, J Am Stat Assoc. **48** (1985), 799–808.
- [4] H. Theil and A.S. Goldberger, *On pure and mixed statistical estimation in economics*, Int Econ Rev. **2**(1961), 65–78.
- [5] H. Theil, On the use of incomplete prior information in regression analysis, J Am Stat Assoc. **58** (1963), 401–414.
- [6] E.J.G. Pitman, *The closest estimates of statistical parameters*, Proc Cambridge Philosop Soc. **33**(1937), 212–222.
- [7] J. P. Keating and R.L. Mason, *Practical relevance of an alternative criterion in estimation*, Am Stat **39**(1985), 203–205.
- [8] C.R. Rao, *Some comments on the minimum mean square error as a criterion of estimation*, Statistics and related topics. North Holland Amsterdam. 1981, 123–143.
- [9] C. R. Rao, J.P. Keating and R.L. Mason, The Pitman nearness criterion and determination, Commun Statist Theor Meth. **15**(1986), 3173–3191.

- [10] M.R. Özkale and S. Kaçırınlar, Comparisons of the $r - k$ class estimator to the ordinary least squares estimator under the Pitman's closeness criterion, Stat pap 49(2008), 503–512.
- [11] E. Wencheko, *Comparison of regression estimators using Pitman measures of nearness*, Stat. Pap. 42(2001), 375–386.
- [12] J. Reif, *Pitman closeness in classes of general pre-test and regression estimators*, Commun Statist Theor Meth. 35(2006), 263–280.
- [13] H. Yang, W.X. Li and J.W. Xu, *Comparison of Two Estimators of Parameters Under Pitman Nearness Criterion*, Commun Statist Theor Meth. 17(2010), 3081–3094.
- [14] M.R. Özkale and S. Kaçırınlar, *Erratum to: Comparisons of the $r - k$ class estimator to the ordinary least squares estimator under the Pitman's closeness criterion*, Stat pap. 53(2012), 505–505.
- [15] W.X. Li, H. Yang and J.B. Wu, *Some comments on: M. R. Özkale, S. Kaçırınlar: Comparisons of the $r - k$ class estimator to the ordinary least squares estimator under the Pitman's closeness criterion*, Stat pap. 53(2012), 497–503.
- [16] J.B. Wu, *Estimation of the parameters in two linear models with some of the identical parameter vectors under the Pitman's closeness criterion*. Journal of the National Science Foundation of Sri Lanka, 47(2019), 363–368.
- [17] K.J. Liu, *Using Liu-type estimator to combat collinearity*, Commun Stat Theory Methods. 32(2003), 1009–1020.
- [18] B.M.G. Kibria, *Performance of some new ridge regression estimators*, Comm Stat Simul Comput. 32(2003), 2389–2413.

Spatial-Spectral Density Peaks Based Discriminant Projection for Classification of Membranous Nephropathy Hyperspectral Pathological Image¹

Meng LV^a, Wei LI^{a,2} and Ran TAO^a

^a School of Information and Electronics, Beijing Institute of Technology, Beijing, China

Abstract. Microscopic hyperspectral imaging has become an emerging technique for various medical applications. However, high dimensionality of hyperspectral image (HSI) makes image processing and extraction of important diagnostic information challenging. In this paper, a novel dimensionality reduction method named spatial-spectral density peaks based discriminant projection (SSDP) is proposed by considering spatial-spectral density distribution characteristics of immune complexes. The proposed SSDP coupled with support vector machine classifier (SVM) yields high-precision automatic diagnosis of membranous nephropathy (MN). Detailed ex-vivo validation of the proposed method demonstrates the potential clinical value of the system in identifying hepatitis B virus-associated membranous nephropathy (HBV-MN) and primary membranous nephropathy (PMN).

Keywords. Dimensionality reduction, feature extraction, microscopic hyperspectral imaging, membranous nephropathy diagnosis

1. Introduction

Chronic kidney disease (CKD) is a global public health problem [1] with an incidence rate of more than 10%. Early detection and treatment can often keep CKD from getting worse. Among CKDs, one of the most common pathological types of adult nephrotic syndrome is membranous nephropathy (MN) [2] which can be divided into primary membranous nephropathy (PMN) and secondary membranous nephropathy (SMN). Hepatitis B virus-associated membranous nephropathy (HBV-MN) is a popular variety of SMN. In clinical diagnosis, a clear distinction between HBV-MN and PMN is essential for MN identification. The gold standard for MN diagnosis remains tissue biopsy with pathological assessment made by pathologists using visual inspection of stained sections and immunouorescence under the optical microscope, combined with electron microscopy results. However, a certain probability of false positives is exist in the immunouores-

¹This work was supported by the National Natural Science Foundation of China (Grant No.91638201 and No.61421001).

²Corresponding Author: Wei Li, 508 East, Information Science Experiment Building, Beijing Institute of Technology, Beijing; E-mail: liwei089@ieee.org.

cence and the accuracy of MN diagnosis is highly depended on the experience of the pathologists. This technique is considered expensive and time-consuming.

With the rapid development of hyperspectral cameras and artificial intelligence, hyperspectral imaging system has become promising auxiliary diagnostic tool for intelligent medicine. Differ from the bi-dimensionality image acquired by optical microscope which only contains morphological information of samples, HSI possesses abundant spatial-spectral information. Digital pathology, which utilizes the power of slide imaging and computer-aided diagnosis, has proved promising to provide rapid, consistent, and quantitative disease diagnosis from histopathology images [3]. Recently, local fisher discriminant analysis-deep neural network [4] reveals that HBV-MN and PMN have different immune complex components and show subtle spectral differences in hyperspectral images. Previous work also shows that dimensionality reduction (DR) is advantageous for acquiring an optimal reduced subspace with highly separability for features [4,5,6,7], thereby improving the accuracy of computer-based MN automatic clinical diagnosis.

In this paper, we propose a novel DR method based on density peaks (DP) based clustering algorithm [8] to make full use of the spatial-spectral density distribution characteristics of immune complexes. At first, spectral density and spatial density are defined for each pixel based on the density peaks based clustering algorithm. Then, a spatial density scatter matrix is designed to preserve the neighborhood structure in spatial domain and two spectral density scatter matrices are constructed to describe the local discriminant relationship in spectral domain. At last, a spatial-spectral density peaks based discriminant projection (SSDP) method is proposed by compacting the spatial-spectral intra-class scatter while separating the spectral interclass scatter. SSDP efficiently preserves the local intra-class local structure in HSI and enhances the discrimination power of low-dimensional embedding spatial-spectral features.

2. Proposed SSDP Method

The proposed SSDP method consists of three parts: construction of spatial density based scatter matrix, construction of spectral density based scatter matrices and the proposed spatial-spectral discriminant projection model. More details of these parts are described as follows.

2.1. Spatial density based scatter matrix

Let (a_i, b_i) denotes the coordinate of hyperspectral pixel \mathbf{x}_i , the local spatial neighborhood $\Omega(\mathbf{x}_i)$ centered at \mathbf{x}_i is defined as:

$$\Omega(\mathbf{x}_i) = \left\{ \mathbf{x} \leftarrow (a, b) \mid \begin{array}{l} a \in [a_i - q, a_i + q] \\ b \in [b_i - q, b_i + q] \end{array} \right\} \quad (1)$$

where $q = (T - 1)/2$, and the odd number T is the size of spatial neighborhood. $\mathbf{x} \leftarrow (a, b)$ indicates that the sample locate in corresponding coordinate.

Based on the idea of density peaks based clustering algorithm, the spatial density of pixel \mathbf{x}_i is defined as

$$\rho_i^{spatial} = \sum_{\mathbf{x}_j \in \Omega(\mathbf{x}_i)} \chi(l(\mathbf{x}_i) - l(\mathbf{x}_j)) \quad (2)$$

where $\chi(x) = 1$ if $x = 0$ and $\chi(x) = 0$ otherwise, and $l(\mathbf{x}_i)$ is the label of \mathbf{x}_i . Basically, ρ_i is equals to the number of points from $\Omega(\mathbf{x}_i)$ that have the same label with \mathbf{x}_i .

For training sample \mathbf{x}_i , the spatial density weight between \mathbf{x}_i and \mathbf{x}_j is defined as

$$\mathbf{W}_{ij}^{spatial} = \begin{cases} \frac{\rho_i^{spatial} \times \rho_j^{spatial}}{t^{spatial}}, & \text{if } l(\mathbf{x}_i) = l(\mathbf{x}_j) \\ 0, & \text{otherwise.} \end{cases} \quad (3)$$

in which $t^{spatial} = \max_{i,j}(\rho_i^{spatial} \times \rho_j^{spatial})$. The density weight makes the points with lower spatial density not produce larger influence to the embedded space.

The intra-class spatial density based scatter matrix is defined as

$$\mathbf{S}^{sw} = \frac{1}{2} \sum_{i,j=1}^n \mathbf{W}_{ij}^{spatial} (\mathbf{x}_i - \mathbf{x}_j) (\mathbf{x}_i - \mathbf{x}_j)^T \quad (4)$$

2.2. Spectral density based scatter matrices

Based on the idea of density peaks based clustering algorithm, the spectral density of pixel \mathbf{x}_i is defined as same as [8]. That is, $\rho_i^{spectral} = \sum_j \chi(\mathbf{d}_{ij} - d_c)$ where $\mathbf{d}_{ij} = \|\mathbf{x}_i - \mathbf{x}_j\|_2^2$, $\chi(x) = 1$ if $x = 0$ and $\chi(x) = 0$ otherwise.

For training sample \mathbf{x}_i , the spectral density weight between \mathbf{x}_i and \mathbf{x}_j is defined as

$$\mathbf{W}_{ij}^{spectral} = \frac{\rho_i^{spectral} \times \rho_j^{spectral}}{t^{spectral}} \quad (5)$$

in which $t^{spectral} = \max_{i,j}(\rho_i^{spectral} \times \rho_j^{spectral})$. The density weight makes the points with lower spectral density not produce larger influence to the embedded space.

In spectral domain, the inter-class density scatter matrix $\mathbf{S}^{(lb)}$ and the intra-class density scatter matrix $\mathbf{S}^{(lw)}$ are defined as

$$\mathbf{S}^{(lb)} = \frac{1}{2} \sum_{i,j=1}^n \hat{\mathbf{W}}_{ij}^{(lb)} (\mathbf{x}_i - \mathbf{x}_j) (\mathbf{x}_i - \mathbf{x}_j)^T \quad (6)$$

$$\mathbf{S}^{(lw)} = \frac{1}{2} \sum_{i,j=1}^n \hat{\mathbf{W}}_{ij}^{(lw)} (\mathbf{x}_i - \mathbf{x}_j) (\mathbf{x}_i - \mathbf{x}_j)^T \quad (7)$$

where $\hat{\mathbf{W}}^{(lb)}$ and $\hat{\mathbf{W}}^{(lw)}$ are $n \times n$ matrices defined by

$$\hat{\mathbf{W}}_{ij}^{(lb)} = \begin{cases} \mathbf{W}_{ij}^{spectral} / (1/n - 1/n_c), & \text{if } l(\mathbf{x}_i) = l(\mathbf{x}_j) = c \\ 1/n, & \text{otherwise.} \end{cases} \quad (8)$$

$$\hat{\mathbf{W}}_{ij}^{(lw)} = \begin{cases} \mathbf{W}_{ij}^{spectral} / n_c, & \text{if } l(\mathbf{x}_i) = l(\mathbf{x}_j) = c \\ 0, & \text{otherwise.} \end{cases} \quad (9)$$

Here $c \in [1, C]$, C represents the total number of classes and n_c denotes the number of samples belong to class c .

2.3. Spatial-Spectral Density Peaks Based Discriminant Projection

In this section, spatial-spectral density peaks based discriminant projection (SSDP) approach is proposed by minimizing the spatial-spectral intra-class compactness and maximizing spectral inter-class variance in embedded subspace. The intra-class spatial margin , the intra-class spectral margin and the inter-class spectral margin in embedded space can be described by

$$\begin{cases} \frac{1}{2} \sum_{i,j=1}^n \|\mathbf{P}^T \mathbf{x}_i - \mathbf{P}^T \mathbf{x}_j\|_2^2 \mathbf{W}_{ik}^{spatial} = \text{tr}(\mathbf{P}^T \mathbf{S}^{sw} \mathbf{P}) \\ \frac{1}{2} \sum_{i,j=1}^n \|\mathbf{P}^T \mathbf{x}_i - \mathbf{P}^T \mathbf{x}_j\|_2^2 \hat{\mathbf{W}}_{ij}^{(lw)} = \text{tr}(\mathbf{P}^T \mathbf{S}^{lw} \mathbf{P}) \\ \frac{1}{2} \sum_{i,j=1}^n \|\mathbf{P}^T \mathbf{x}_i - \mathbf{P}^T \mathbf{x}_j\|_2^2 \hat{\mathbf{W}}_{ij}^{(lb)} = \text{tr}(\mathbf{P}^T \mathbf{S}^{lb} \mathbf{P}) \end{cases} \quad (10)$$

The model of SSDP is defined as

$$\max_{\mathbf{P}} \frac{\text{tr}(\mathbf{P}^T \mathbf{S}^{lb} \mathbf{P})}{\text{tr}\{\mathbf{P}^T [\alpha \mathbf{S}^{sw} + (1 - \alpha) \mathbf{S}^{lw}] \mathbf{P}\}} \quad (11)$$

where $\alpha \in [0, 1]$ is a tradeoff balancing the contribution of spatial and spectral information in projection process. The solution of the optimizing problem can be translated to solve the generalized eigenvalue problem

$$\mathbf{S}^{lb} \mathbf{p}_i = \lambda_i [\alpha \mathbf{S}^{sw} + (1 - \alpha) \mathbf{S}^{lw}] \mathbf{p}_i \quad (12)$$

where λ_i is an eigenvalue and \mathbf{p}_i represents the corresponding eigenvector. The projected matrix $\mathbf{P} = [\mathbf{p}_1, \mathbf{p}_2, \dots, \mathbf{p}_d] \in \mathbb{R}^{D \times d}$ is constructed by the first d largest eigenvalues.

SSDP makes fully use of spatial-spectral density based properties in hyperspectral images to map the original data into a low-dimensional space, in which not only strengthen the class separability but also preserve the spatial-spectral relationship between pixels as much as possible.

3. Experimental Results and Analysis

In this section, real microscopic hyperspectral dataset is used to evaluate the effectiveness of the proposed approach for MN identification tasks. The dataset consists of 30 HBV-MN images and 24 PMN images, involving 10 HBV-MN patients and 9 PMN patients respectively. The performance of DR can be evaluated with classification applied to the data resulting from DR, and we use SVM due to its popularity. Three objective quality indexes (i.e., each accuracy (EA), overall accuracy (OA), average accuracy (AA)) are used to evaluate the performance of hyperspectral image classification. Throughout, we report results for a variety of state-of-the-art DR methods, comparing SSDP to LFDA [9], EFDC [10], NWFE [11], BCGDA [12] as well as CDME [13].

The identification of HBV-MN and PMN is performed in fully-independent patients, divided across 90 terms. Each term consist of one HBV-MN patient and one PMN patient for training, while testing and validation is performed on remaining patients. Figure 1 shows the average OA of 90 tests. SSDP is the best performing image dimensionality

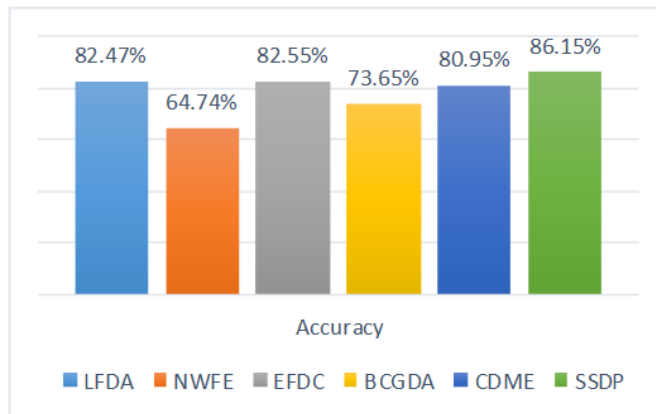


Figure 1. Average over all accuracy of MN identification.

reduction modality with accuracy of 86.15%, which meets the requirement of clinical diagnostic accuracy higher than 85%. Take one term data (one HBV-MN (ID:17472) patient and one PMN (ID:15684) patient are used as training data) as an example, we use visualization techniques to illustrate the effectiveness of SSDP for acquiring a subspace with better separability. Figure 2 shows the distribution of testing sample features before and after different DR methods process, the results confirm the potentiality of SSDP for seeking optimal subspace with high separability for features. In addition, local manifold based DR methods achieve much better performance than reconstruction based DR methods. This indicates that the potential local distribution characteristics of the immune complexes of MN are crucial for improving the discrimination of different diseases.

To further investigate the classification efficiency of the proposed algorithm as compared to other DR approaches, Table 1 and Table 2 tabulate the EA, OA and AA obtained by 1-dimensional data and 10-dimensional data respectively. In order to facilitate identification, the highest accuracy is signed on the bold. Obviously, the improvement effect of SSDP on classification accuracy is significantly better than all other DR methods. Especially, the superiority is also obvious as depicted Table 1, the proposed method still has over 6.4% increase in classification accuracy with limited data dimensionality. In summary, it proves that SSDP has the ability to extract important diagnostic information of medical hyperspectral image of MN, and can compress important diagnostic information in very limit low-dimension data. Our work provides a novel technique for the characterization and distinction of HBV-MN from IMN, especially for cases where the discrimination is not always easy with the optical microscopy, and verifies its nonnegligible potential for further application in medical field.

4. CONCLUSIONS

In this paper, a novel discriminant spatial-spectral dimensionality reduction method was proposed for medical hyperspectral image analysis. By considering the density distribution characteristics of the data, spectral density and spatial density are defined for each pixel based on the density peaks based clustering algorithm. SSDP has been confirmed to be powerful in finding the discriminative embedding space by considering spatial-

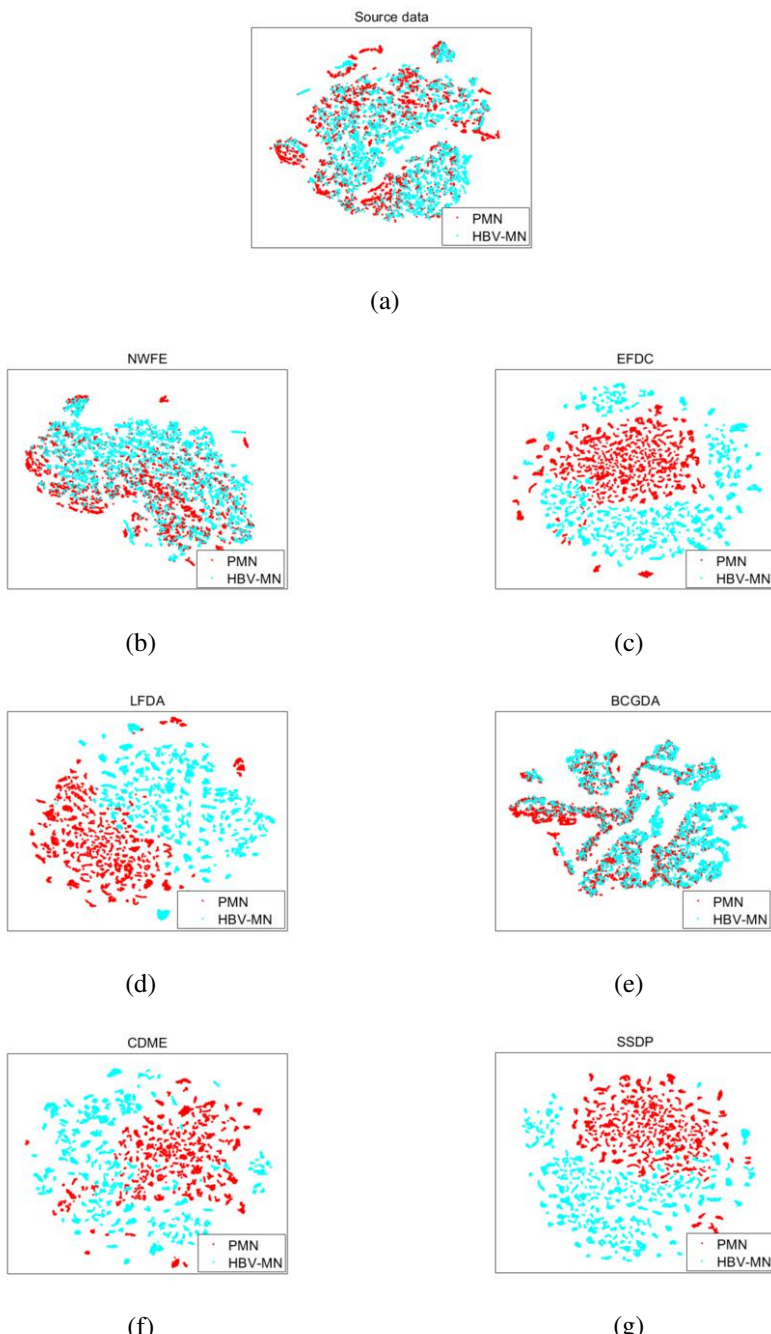


Figure 2. The distribution of (a) source data and low-dimension samples obtained by (b) NWFE, (c) EFDC, (d) LFDA, (e) BCGDA, (f) CDME and (g) SSDP respectively.

Table 1. Classification Accuracy with 1-Dimensional Data

Methods	HBV-MN(%)	PMN(%)	OA(%)	AA(%)
ORG	74.13	85.8	80.43	79.97
LFDA	49.31	44.72	46.83	47.01
EFDC	92.16	92.04	92.09	92.10
BCGDA	65.96	92.02	80.01	77.99
CDME	69.17	81.81	75.99	75.49
SSDP	99.32	97.52	98.49	98.42

Table 2. Classification Accuracy with 10-Dimensional Data

Methods	HBV-MN(%)	PMN(%)	OA(%)	AA(%)
ORG	74.13	85.8	80.43	79.97
LFDA	90.15	97.19	93.95	93.67
EFDC	92.20	95.58	94.02	93.89
BCGDA	71.40	89.95	81.41	80.68
CDME	92.55	95.47	94.13	94.01
SSDP	99.36	97.85	98.66	98.61

spectral intra-class structure and spectral inter-class structure simultaneously. The relative merits of our approach against other existing DR methods are also demonstrated in this paper, highlighting the strengths of our proposed framework in terms of MN identification.

References

- [1] J. Xu, H. Lei, S. Zhang and D. O. Nephrology, Major research advances in chronic kidney disease of 2017, *Clinical Focus*, 2018.
- [2] J. A. J. G. van den Brand, J. M. Hofstra and J. F. M. Wetzels, Low-Molecular-Weight Proteins as Prognostic Markers in Idiopathic Membranous Nephropathy, *Clinical Journal of the American Society of Nephrology Cjasn* **6** (2011), 2846-2853.
- [3] G. Lu, D. Wang, X. Qin and S. Muller, J. V. Little, X. Wang, A. Y. Chen, G. Chen and B. Feis: Histopathology Feature Mining and Association with Hyperspectral Imaging for the Detection of Squamous Neoplasia, *Scientific Reports* **9** (2019), 17863.
- [4] X. Wei, T. Tu, N. Zhang, Y. Yang and W. Li, Membranous Nephropathy Identification Using Hyperspectral Microscopic Images, *Pattern Recognition and Computer Vision - Second Chinese Conference*, Xi'an, China, 2019.
- [5] D. Ravi, H. Fabelo, G. M. Callic and G. Yang, Manifold Embedding and Semantic Segmentation for Intraoperative Guidance With Hyperspectral Brain Imaging, *IEEE Transactions on Medical Imaging* **36** (2017), 1845-1857.
- [6] T. Li and G. Kou and Y. Peng, Improving malicious URLs detection via feature engineering: Linear and nonlinear space transformation methods, *Information Systems* **91** (2020), 101494.
- [7] G. Kou, P. Yang, Y. Peng, F. Xiao, Y. Chen and F. E. Alsaadi, Evaluation of feature selection methods for text classification with small datasets using multiple criteria decision-making methods, *Applied Soft Computing* **86** (2020), 105836.
- [8] A. Rodriguez and A. Laio, Clustering by fast search and find of density peaks, *Science* **344** (2014), 1492-1496.

- [9] W. Li, S. Prasad, J. E. Fowler and L. M. Bruce, Locality-Preserving Dimensionality Reduction and Classification for Hyperspectral Image Analysis, *IEEE Transactions on Geoscience and Remote Sensing* **50** (2012), 1185-1198.
- [10] Q. Gao, J. Liu, H. Zhang, J. Hou and X. Yang, Enhanced fisher discriminant criterion for image recognition, *Pattern Recognition* **45** (2012), 3717-3724.
- [11] B. C. Kuo and D. A. Landgrebe, Nonparametric weighted feature extraction for classification, *IEEE Transactions on Geoscience and Remote Sensing* **42** (2004), 1096 - 1105.
- [12] N. H. Ly, Q. Du and J. E. Fowler, Collaborative Graph-Based Discriminant Analysis for Hyperspectral Imagery, *IEEE Journal of Selected Topics in Applied Earth Observations and Remote Sensing* **7** (2014), 2688-2696.
- [13] M. Lv, Q. Hou and N. Deng and L. Jing, Collaborative Discriminative Manifold Embedding for Hyperspectral Imagery, *IEEE Geoscience and Remote Sensing Letters* **14** (2017), 569 - 573.

Intelligent Identification of Potential Customers for Electricity Substitution

Chen Xiaofeng, Zhao Yadi¹, Wei Zhifeng, Gao Bingqiang

*State Grid Information & Telecommunication Accenture Information Technology Co.,
Ltd, Beijing, 100032, China*

Abstract. This paper proposes an intelligent method for the identification of potential customers for electricity substitution. This is developed on the basis of an original model, where a related indicator system of potential customers is constructed through exploratory analysis, improving the results. At the same time, ANOVA is used to screen the indicators and the XGBoost algorithm is employed to output the index importance score and identify likely electricity substitution customers. This method can accurately identify such customers, accelerate the fundamental transformation of energy development, and adapt to the new strategy of Energy Internet development.

Keywords. Electricity Substitution, Indicator System, XGBoost Algorithm, Accurate Identification

1. Introduction

Energy is the basic guarantee of economic and social development, and energy issues are related to human development, national economy, and people's livelihood [1]. With the rapid development of the global Energy Internet, the State Grid Corporation has proposed the strategic goal of developing an international leading Energy Internet enterprise with Chinese characteristics, as well as promoting the construction of an Energy Big Data Center [2-3]. Guided by both global trends and current strategic objectives, provincial and municipal power companies' in-depth research on commercial value and key technologies under the Energy Internet accelerate the construction of clean, low-carbon, efficient, and safe energy systems[4-6].

Electric energy substitution refers to the use of electric energy instead of coal and fuel energy consumption modes in terminal energy consumption, such as electric heating, agricultural electric irrigation, electric vehicles, etc. [7]. The implementation of electric energy substitution is of great significance for promoting the clean development of energy, and is an important measure to increase the proportion of electricity-coal and reduce air pollution [8]. With the rapid development of information technology and the national development of a new infrastructure strategy, power customers need higher standards and requirements in power products and power supply services [9-10]. Enterprises have begun to explore new methods to improve the efficiency and specialization of power substitution work in enterprises and provide

¹ Corresponding Author: Zhao Yadi, State Grid Information & Telecommunication Accenture Information Technology Co., Ltd, Email: 15510266633@163.com

support for the effective development of energy big data services [11-12].Shan, based on the STIRPAT (Stochastic Impacts by Regression on Population, Affluence, and Technology) ridge-regression model, used the size of the resident population, energy prices, and other factors to fit terminal power substitution, and quantitatively evaluate the role of each factor [13].Using the K-means algorithm²,Tu clustered users who have undergone power substitution, and constructed a power substitution user identification model by a cooperative filtering algorithm [14].Luo proposed to establish a network management system for an electric energy substitution project, which is based on Browser/Server(BS) and combines Hypertext Preprocessor(PHP) and MySQL to realize the whole process, with a multi-angle and diversified management of an power substitution project[15].

This paper introduces an intelligent customer identification method for potential power substitution. We use statistical and data analysis methods to construct customer identification indicators that affect power substitution potential and build models using the XGBoost algorithm. From comparisons with machine learning algorithms, we conclude that the model has strong applicability and expansibility, and can be used in marketing and other related business fields, providing theoretical and methodological guidance for the construction of an Energy Big Data Center.

2.Theoretical Methods

2.1 Variance Analysis

The basic principle of ANOVA is that there are two basic sources of difference between the mean of different processing groups: one is the deviation caused by experimental conditions, A, the other is the deviation caused by random error, B. The mean square error of A and B, MS_b and MS_w, are obtained by dividing by their respective degrees of freedom. If it is a deviation due to random errors within the group,we can establish that each group of samples is from the same population, therefore: $MS_b/MS_w \approx 1$. If it is the error in the processing of the experiment, $MS_b \gg MS_w$. The MS_b/MS_w ratio constitutes the F statistic, and the F value is compared with its critical value to determine whether the difference between the two groups is due to the treatment of the experiment.

In this paper, we can use ANOVA to analyze the difference of the index before and after the substitution, and determine whether the index change comes from the development of electric energy substitution.Finally we can sort the index by F and P values³ to determine the importance of the index.

2.2 XGBoost Algorithm

XGBoost is a kind of boosting algorithm; the main idea of boosting is to integrate many weak classifiers together to form a strong classifier. The strategy of XGBoost is

²K-means algorithm: A clustering method in which similar data members are grouped together.

³P values: An important evidence to determine whether the original hypothesis is correct; the smaller the value, the greater the probability of accepting the original hypothesis, which states that there is a difference between two variables.

to integrate many tree models together to form a strong classifier. The process is to constantly add trees and perform feature splitting to generate a tree. The tree model used in XGBoost is the CART (Classification And Regression Trees) model. We add a tree each time, representing learning a new function to fit the residuals of the last prediction. Each tree will fall into a corresponding leaf node and each leaf node corresponds to a score. Finally, we only need to add each tree corresponding to the score to get the predicted value of the sample.

The regression tree generation algorithm is as follows. Input training data set D , output regression tree $f(x)$. A typical CART regression tree produces an objective function:

$$\sum_{x_i \in R_m} (y_i - f(x_i))^2 \quad (1)$$

In the input space where the training data set is located, a binary decision tree is constructed by recursively dividing each region into two sub-regions and determining the output value for each sub-region:

Select the optimal tangent variable j and the tangent point s , calculate:

$$\min_{j,s} \left[\min_{c_1} \sum_{x_i \in R_1(j,s)} (y_i - c_1)^2 + \min_{c_2} \sum_{x_i \in R_2(j,s)} (y_i - c_2)^2 \right] \quad (2)$$

Traversing variables j , for fixed segmentation variables j , scan the segmentation points s . Select pairs of numbers (j,s) that minimize Formula(2).

Use the selected number pairs (j,s) to divide the region and determine the corresponding output value:

$$R_1(j,s) = \{x | x^{(j)} \leq s\}, \quad R_2(j,s) = \{x | x^{(j)} > s\} \quad (3)$$

$$\hat{c}_m = \frac{1}{N_m} \sum_{x_i \in R_m(j,s)} y_i, \quad x \in R_m, \quad m = 1, 2 \quad (4)$$

Continue to perform steps 1 and 2 for both subregions R_1 and R_2 until the termination condition is satisfied.

Divide the input space into M regions R_1, R_2, \dots, R_M and generate a decision tree:

$$f(x) = \sum_{m=1}^M \hat{c}_m I(x \in R_m) \quad (5)$$

2.3 Error Theory

Using some form of error as an index to evaluate the performance of the model, the main indicators are as follows:

R^2 : The denominator is the degree of discretization⁴ of the original data, and the numerator is the error between the predicted data and the original data.

$$R^2 = 1 - \frac{\sum(Y_{\text{actual}} - Y_{\text{predict}})^2}{\sum(Y_{\text{actual}} - Y_{\text{mean}})^2} \quad (6)$$

Mean Square Error(MSE): The average of the squared errors.

$$\text{MSE} = \frac{1}{n} \sum_{i=1}^n \left(y_i - \hat{y}_i \right)^2 \quad (7)$$

Mean Absolute Error(MAE): The average of the absolute error values.

$$\text{MAE} = \frac{1}{n} \sum_{i=1}^n \left| y_i - \hat{y}_i \right| \quad (8)$$

Mean Absolution Percentage Error(MAPE): Average of relative errors.

$$\text{MAPE} = \frac{1}{n} \sum_{i=1}^n \frac{\left| y_i - \hat{y}_i \right|}{y_i} \quad (9)$$

3. Descriptive Analysis

3.1 Data Preparation

We extracted basic data from power marketing information system, power information collection system and 95598 customer service system etc. in recent three years, as well as data from online platforms and government departments. The data covers three aspects: customer data, electricity use characteristic data, and other factor data.

(1).Customer data: user number, user name, date of establishment, power supply units, contract capacity, industry category, user classification, whether developing electricity substitution, etc.

(2).Electricity use characteristic data: electricity consumption, electricity load, electricity fee, service voltage,etc.

(3).Other factor data: credit value, extent of industry prosperity, business climate index, geographic position,etc.

3.2 Descriptive Statistic Analysis

There are great differences in electricity consumption in different industries, and the potential of electricity substitution is also different. For example, the metal manufacturing industry can transform cupola into electric kilns with large capacity and strong replicability, low-voltage residential areas can adopt electric heating which has

⁴The degree of discretization: The degree of difference between the individual values and the average, measuring the fluctuation of the overall data.

a small transformation capacity and a huge group scale. Therefore, industry categories will play an important role in identifying potential customers.

Table 1. Industry Share

	Industry	Percentage of electricity consumption	Percentage of enterprise number
1	Manufacturing industry	42.52%	35.26%
2	Textile printing and dyeing industry	15.33%	12.78%
3	Business and residential services industry	10.67%	16.03%
4	Agriculture, forestry, and animal husbandry	9.63%	15.67%
5	Public utilities and management organizations	5.08%	6.58%
6	Transport and postal warehousing	4.86%	5.27%
7	Other industries	11.91%	8.46%

According to experience, enterprises with small electricity consumption and high percentage of enterprise number have potential for substitution. Table 1 shows the industry share according to the annual electricity consumption and the proportion of different industries. We can see that the manufacturing industry, textile printing and dyeing industry, and business and residential services industry in this area are more developed, accounting for about 70% of the total, and can be used as the target industries. At the same time, the agriculture, forestry and animal husbandry industry has a small proportion of electricity consumption and a large proportion of the enterprise number, so this can also be used as a target in this research. By carding the standardized data, we preliminarily determine that the enterprises with the characteristics shown in Table 2 are potential customers, and assume that the geographical position, load factor, proportion of valley electricity and other attributes will play an important role in model training.

Table 2. Examples of Important Potential Customer Features

	Indicator Name	Numerical Information		Indicator Name	Numerical Information
Feature 1	Geographical Position	<=20	Feature 2	Geographical Position	>20 and <=30
	Load Factor	3.5%		Load Factor	3.7%
	Proportion of Valley Electricity	>20% and <=35%		Proportion of Valley Electricity	<=20%
	Standard Deviation of E.C.	28-35		Contract Capacity	350-450
				Contamination Index	15-20

The Figure1 shows the 24-hour load curves of enterprises using coal-fired boilers before and after transformation. We can see that the load of the unmodified enterprise from 22:00 to 8:00 the next day is higher than that of the reformed enterprises, and between 8:00 to 22:00 during the day is lower than that of the reformed enterprises. The results show that the load curve of unmodified enterprises is stable all day. However, the load scope of the modified enterprises changes greatly during the entire day, so we can obtain the conclusion that the load index can be used as a key index for the model.



Figure 1. 24-hour Load Curves of Enterprises before and after transformation.

3.3 Indicator System Establishment

According to descriptive statistical analysis, the index system is preliminarily established from basic customer properties, electric characteristics of customers, and other factors as shown in Table 3.

Table 3. Indicator System

Indicator dimensions	Indicator name	Data sources	Indicator description
Basic Customer Properties	Customer Number	Power Marketing Information System	System automatic generation
	Customer Name	Power Marketing Information System	System input
	Household Age	Power Marketing Information System	The opening date until this year
	Power Supply Company	Power Information Acquisition System	System automatic generation
	Contract Capacity	Power Marketing Information System	The user capacity as agreed in the contract.
	Industry Category	Power Marketing Information System	Manufacturing industry/Textile printing and dyeing industry/Business and residential services industry/...
	Customer Classification	Power Marketing Information System	Class I/II/III customers.
	Supply Voltage	Power Marketing Information System	High pressure/Medium pressure/Low pressure.
	Electricity Substitution Implementation	Enterprise Survey	Implemented/Not implemented
Customer Electricity Characteristics	Electricity Type	Power Information Acquisition System	Large Industrial/General Commercial/Domestic/Agricultural
	Electricity Consumption	Power Information Acquisition System	Electricity consumption by day, month, quarter, and year.
	Standard Deviation of Electricity Consumption (E.C.)	Power Information Acquisition System	Standard deviation of electricity consumption by day, month, quarter, and year.
	Peak Electrical Values	Power Information Acquisition System	Average peak value by month, quarter, and year.
	Proportion of Peak Value	Power Information Acquisition System	Frequency of peak values by day, month, quarter, and year.
	Month of Peak Electricity Consumption (E.C.)	Power Information Acquisition System	The month with the highest percentage of electricity consumption.
	Valley Electrical Values	Power Information Acquisition System	Average valley value by month, quarter, and year.
	Proportion of Valley Values	Power Information Acquisition System	Frequency of valley values by day, month, quarter, and year.

Electricity Load	Power Information Acquisition System	Electricity load by day, month, quarter, and year.
Load Factor	Power Information Acquisition System	Ratio of electrical load to maximum load by day, month, quarter, and year.
Electricity Demand Ratio	Power Information Acquisition System	Ratio of actual electricity consumption to maximum requirement by day, month, quarter, and year.
Demand Contract Ratio	Power Information Acquisition System	Ratio of maximum requirement to contract capacity by day, month, quarter, and year.
Electricity Costs	95598 Customer Service System	Average electricity costs by month, quarter, and year.
Standard Deviation of Electricity Costs	95598 Customer Service System	Standard deviation of electricity costs by quarter and year.
Maximum Daily Load Time	Power Information Acquisition System	Maximum load time period in the morning/a.m./p.m./night
Electricity Consumption (E.C.) Growth Rate	Power Information Acquisition System	Electricity consumption growth rate by month, quarter, and year.
Other Factors	Credit Value	95598 Customer Service System Excellent/Good/Qualified/Unqualified
	Industry Prosperity Extent	Power Marketing Information System Volume of electricity for the whole industry compared with the same period of the previous year.
	Geographical Position	Network Map Distance from a central block of a city in a straight line in kilometers.
	Population Density	Regional Statistical Offices Based on the nearby population of two square kilometres.
	Contamination Index	Network Weather Frequency of higher district pollution index in a month.
	Business Climate Index	Power Marketing Information System Comparison of the company electricity volume with that of the same industry.
	Estimated Construction Duration	Enterprise Survey Estimated construction duration for electrical energy substitution.
	Enterprise Economic Benefits	Enterprise Survey The estimated ratio of the gross product of the enterprise to the cost.

4. Model Application

4.1 Model Construction

Taking the manufacturing industry as an example, the index variables are screened by correlation analysis and ANOVA in the enterprise has undergone electric substitution, and the index importance is obtained by finding the changes before and after transformation, so as to achieve a secondary screening of the index. The obtained index importance ranking is shown in Figure 2. We can see that the indexes ranked higher have darker colors, indicating that they have a larger change for before and after energy substitution, which can be screened as the index to enter the model.

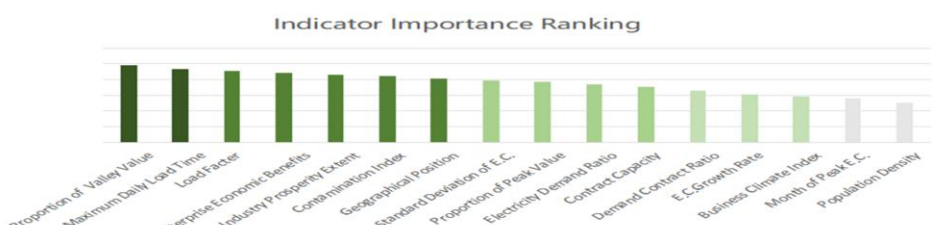


Figure 2. Indicator importance ranking.

In order to compare different data mining algorithms, we introduce five segmentation cross validation to test the generalization ability of the model. We divide the data into five parts, using four groups as training sessions to develop a model, and then using the remaining set as the test set, which requires five training sessions. We use linear SVMs, Random Forests, XGBoost, and derivative algorithm such as LSTM[16], DeepST[17] using the five segmentation cross-validation method; the validation results are shown in Table 4. We can see that the XGBoost algorithm has the least MSE and MAPE which fits the data well as well as faster than others, so we use the XGBoost algorithm to predict potential electricity substitution.

Table 4. Algorithm Evaluation

	Algorithm	R^2	MSE	MAE	MAPE	Calculation times (s)
1	Support Vector Machine (SVM)	0.79	6.314	4.369	0.173	0.560
2	XGBoost	0.95	6.232	4.325	0.098	0.512
3	Random Forests	0.77	6.398	4.483	0.109	0.893
4	LSTM Algorithm	0.83	6.218	4.619	0.204	0.501
5	DeepST	0.91	6.292	4.332	0.126	0.439

We select the top eight indexes for the model, 70% of the estimated enterprise data with electricity substitution potential is extracted as the training set, with 30% as the test set. The model is constructed based on XGBoost to identify potential customers, and at the same time output indicator weights. The potential customer identification output results are shown in Table 5, and the index weight output results are shown in Figure 3. We standardize the output results to the range of 0-100; customers with a score of more than 65 are regarded as potential alternative enterprises represented by the number "1", and the rest by the number "2".

Table 5. Customer Identification Output

Enterprise Serial Number	Load Factor	Maximum Daily Load Time	Proportion of Valley Value	Business Prosperity Index	Geographic Position	Contamination Index	Enterprise Economic Benefits	Standard Deviation of E.C.	Output
1	3.5%	p.m.	29%	75	50	360	41	28	1
2	4.3%	a.m.	41%	46	79	150	26	56	2
3	3.7%	p.m.	42%	51	58	250	21	19	1
4	3.8%	p.m.	28%	80	34	280	37	22	1
5	4.0%	morning	45%	46	19	320	22	61	2
6	3.7%	night	43%	45	65	308	32	26	1
7	3.8%	p.m.	27%	70	28	388	41	31	1
8	4.1%	a.m.	48%	70	22	115	25	51	2
9	4.6%	a.m.	56%	40	26	158	23	53	2
10	4.3%	morning	51%	48	32	133	20	55	2
11	3.6%	p.m.	42%	60	36	105	18	58	2
12	4.0%	p.m.	51%	37	46	428	29	41	1
13	3.7%	p.m.	42%	65	22	288	36	38	1
14	4.3%	a.m.	53%	43	32	110	17	49	2

15	3.8%	p.m.	48%	45	33	335	29	30	1
16	4.1%	night	40%	51	43	156	26	24	1
17	3.3%	p.m.	29%	78	47	350	46	29	1
18	3.5%	p.m.	38%	36	51	320	28	23	1
...
1598	3.7%	p.m.	45%	42	41	332	25	30	1
1599	3.5%	a.m.	36%	62	37	309	38	25	1
1600	3.4%	a.m.	43%	74	39	391	29	25	1

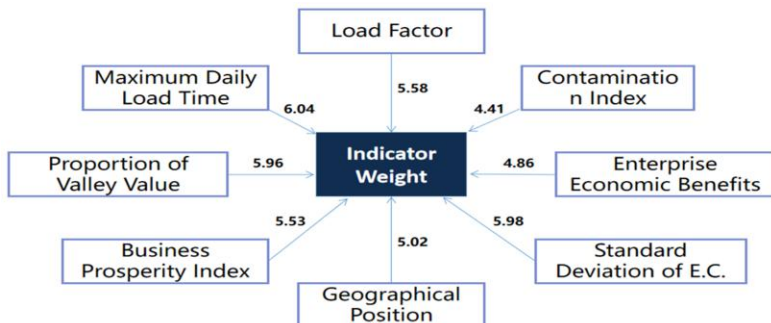


Figure 3. The index weight output results.

We can determine that 1039 of the 1600 companies are predicted as potential replacement customers. At the same time, the weight values of six indexes are greater than 5, which can be regarded as important explanatory variables. We can also derive the conclusion that when the load factor is small, the maximum daily load time is in the night, the business prosperity index is high and the proportion of valley value, the geographical position, and the standard deviation of electricity consumption values are low, we think that the enterprise has a higher likelihood of developing electricity substitution than others.

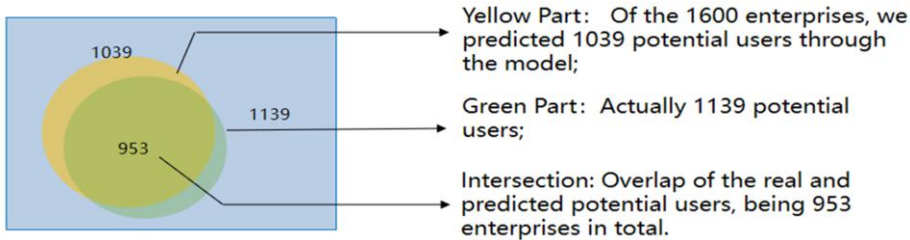
4.2 Model Evaluation

For the evaluation of the classification model, we use performance metrics. The cross matrix between the predicted results of the model and the actual values is shown in Table 6.

Table 6. Forecasting Cross Matrix

		Actual Result	Actual Result
		0	1
Prediction Results	0	True Negative (TN)	False Negative (FN)
	1	False Positive (FP)	True Positive (TP)
Total Number		Negative (N)	Positive (P)

We define Accuracy = $(TP+TN)/(N+P)$, Precision = $TP/(TP+FP)$. The prediction results of the model are shown in Figure 4. We can conclude that the accuracy of the model is 83.00%, the precision is 91.72%, which indicate that the model is accurate and can be applied in practice.

**Figure 4.** Prediction results.

We have also compared the method proposed in this paper with Collaborative Filtering Algorithm in reference[14], SVM, LSTM and DeepST algorithms; the results are shown in Table 7. From this we can see that in the case of equivalent precision, compared with other algorithms, XGBoost has a higher correct rate, which can be extended to more applications.

Table 7. Algorithm Evaluation

	Algorithm	Precision	Accuracy
1	XGBoost	91.72%	83.00%
2	Collaborative Filtering Algorithm	96.23%	68.73%
3	Support Vector Machine (SVM)	87.65%	58.93%
4	LSTM Algorithm	89.31%	64.39%
5	DeepST	85.09%	67.33%

4.3 Business Applications

Technology for identifying customers most likely to adopt electricity substitution can be used in all aspects of enterprise data applications, including intelligent operation of grid enterprises, modernization of government governance, sustainable development of social economy, and so on.

4.3.1 Intelligent Operation of Grid Enterprises

This technology can help the implementation of enterprise label libraries and energy big data center construction. Figure 5 shows the business management process of power substitution; we tap customer demand through data analysis and sharing application, actively propagate power substitution policy to customers with high potential, and improve the company's intelligent operation efficiency.

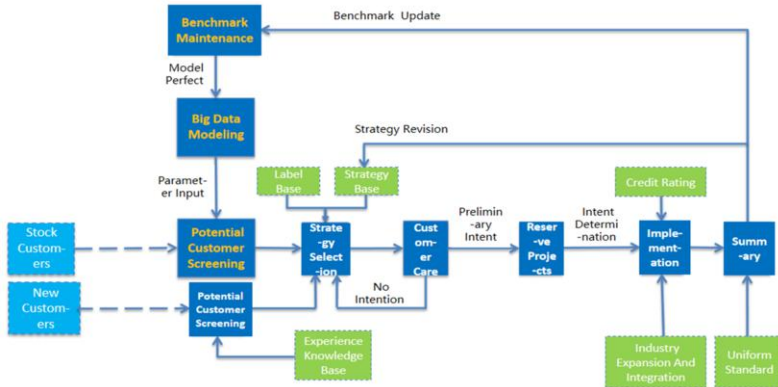


Figure 5. Business management process of power substitution

4.3.2 Modernization of Government Governance

Electric substitution customers identification technology can help the government to implement preferential policies and urge enterprises to transform equipment. We give users economic subsidies to mobilize the enthusiasm of users to use clean energy.

4.3.3 Sustainable Development of Social Economy

The development of electricity substitution identification technology is conducive to improving the level of national electrification and improving the quality of life. At the same time this can cultivate and develop new industries, new forms of business, and new models for the development of the power economy. References[18-19] exploit sophisticated models to capture hidden traffic and environment characteristics from substantial historical mobility data and then makes use of trained models to predict traffic conditions and environmental quality in the future. In the future, we can apply the above research results to this paper ,increase the traffic conditions and environmental quality indicators to make the results more accurate.

5.Conclusion

Based on the XGBoost algorithm, we establish a full set of indicators through descriptive analysis, which makes the calculations quantifiable and accurate; an accuracy of 83% can be achieved. At the same time, compared with other algorithms, it is concluded that the method has good application potential and can be applied to various business areas such as urban computing, follow-up we can enhance further discussion of related work[20-21].

Reference

- [1] WEI Qinglai, SHI Guang, SONG Ruizhuo, et al. Adaptive Dynamic Programming-Based Optimal Control Scheme for Energy Storage Systems With Solar Renewable Energy[J]. IEEE Transactions on Industrial Electronics, 2017, PP(99):1-5478.
- [2] DONG Z, ZHAO J, WEN F, et al. From Smart Grid to Energy Internet: Basic Concept and Research Framework[J]. Dianli Xitong Zidonghua/automation of Electric Power Systems, 2014, 38(15):1-11.
- [3] RAO Wei, JIANG Jing, ZHOU Aihua, et al. Research on Power Big Data Basic Architecture and Standard System for Global Energy Interconnection[J]. Electric Power Information and Communication Technology, 2016(04):21-29.
- [4] TIAN Shiming, LUAN Wenpeng, ZHANG Dongxia, et al. Energy Internet Technology Form and Key Technologies[J]. Proceedings of The Chinese Society for Electrical Engineering, 2015,35(14):3482-3494.
- [5] ZHOU Lin, FU Xueqian, LIU Shuo, et al. Day-Ahead Market Clearing Model of Integrated Energy System for Promoting Renewable Energy Consumption[J]. Electric Power, 2019(11):11-18.
- [6] WU Jielong, YANG Jian, et al. Research on the Current Situation and Development Trend of the Technology of Energy Internet[J].Power System and Clean Energy, 2016,032(003):8-12.
- [7] SUN Yi, ZHOU Shuang, SHAN Baoguo,et al. Analysis of Electric Power Alternative Potential Under Multi-Scenario[J]. Power System Technology, 2017(01):126-131.
- [8] FU Chengran, CHEN Rongjun, HE Yongxiu. Analysis on Electricity Substitution Economics of Multi-Agent Electric Cooker[J]. northeast electric power technology, 2018(04):16-23.
- [9] Li Boyang ,Kisacikoglu M C , Liu Chen , et al. Big Data Analytics for Electric Vehicle Integration in Green Smart Cities[J]. IEEE Communications Magazine, 2017, 55(11):19-25.
- [10] XUE Yusheng, LAI Yening, et al. Integration of Macro Energy Thinking and Big Data Thinking Part One Big Data and Power Big Data[J]. Automation of Electric Power Systems, 2016,40(1):1-8.
- [11] WU Kehe , YAO Peng. Research on Energy Substitution Terminal Energy Application Based on CRITIC Algorithm[C]// 2017 10th International Conference on Intelligent Computation Technology and Automation (ICICTA). IEEE, 2017(10):34-38.
- [12] XIA Huaijian, LIN Haiying, ZHANG Wen, et al. Research on Development Potential of Regional Electric Energy Substitution Based on Multi Model[J]. science and technology management research, 2018(04).
- [13] SHAN Baoguo, ZHAO Jia, JIA Dexiang, et al. Electric Power Substitution Potential Analysis Method Based on STIRPAT-Ridge Regression[J]. Distribution & Utilization, 2018,035(001):68-73.
- [14] TU Ying, LIU Qiang, WANG Qingjuan,et al. Research on Potential User Mining Model of Power Substitution Based on Collaborative Filtering Algorithm[J]. electric power information and communication technology, 2017(12):11-18.
- [15] LUO Jun, DING Canhui, et al. Development of Electric Energy Alternative Information Management System Based on BS Technology[J]. Popular Utilization of Electricity, 2017(03):25-26.
- [16] Essien A, Petrounias I, Sampaio P, et al. A deep-learning model for urban traffic flow prediction with traffic events mined from twitter[J]. World Wide Web, 2020(8):13-38.
- [17] Wang Leye , Geng Xu , Ma Xiaojuan , et al. Cross-City Transfer Learning for Deep Spatio-Temporal Prediction[J]. 2018.
- [18] LIU Lun, Elisabete A.Silva, WU Chunyang, WANG Hui. A machine learning-based method for the large-scale evaluation of the qualities of the urban environment[J]. Computers, Environment and Urban Systems, 2017,65: 113-125.
- [19] LIU Zhidan, LI Zhenjiang, WU Kaishun, LI Mo. Urban Traffic Prediction from Mobility Data Using Deep Learning[J]. IEEE Network,32(4):40-46.
- [20] QI Zhongang, WANG Tianchun, SONG Guojie, et al. Deep Air Learning: Interpolation, Prediction, and Feature Analysis of Fine-Grained Air Quality[J]. IEEE Transactions on Knowledge & Data Engineering, 2018:1-1.
- [21] Gomes E F , Batista F . Classifying Urban Sounds using Time Series Motifs[C]// Security-enriched Urban Computing & Smart Grids. 2015(97):52-57.

A Statistical Analysis of the Social Status of Chinese Women: Data Mining Method Based on MapReduce

Liu Xiangdong¹, Yang Mingzhu and Luo Chengshuai

Department of Statistics, Jinan University, Guangzhou, China

Abstract. By studying the influencing indicators of women's social status, we perform an ordered Logit regression analysis on the data of the China Comprehensive Social Survey in 2012, 2013 and 2015, and then select the assessment of self-social status in the female sample as the dependent variable. Using the impact indicators as independent variables to explore the impact of each variable on women's social status. At the same time, applying k-means clustering analysis based on MapReduce to mine the relationship between employment and education level between different genders. We find out the fact that women have a high level of education does not necessarily result in good employment treatment. Gender discrimination in the Chinese labor market is also persistent.

Keywords. Women's social status; ordered logit regression; MapReduce model;
k-means cluster analysis

1. Introduction

In recent years, China and society have carried out a series of activities to protect women's rights and promote gender equality. The "12th Five Year Plan" of national population development takes promoting gender equality, family harmony and advocating freedom and equality of marriage as the main task, and improves laws and regulations to establish a solid judicial guarantee for gender equality and gender rights and interests.

In February 2019, nine departments, including the Ministry of human resources and social security and the Education Bureau, issued the notice on "further standardizing recruitment and promoting women's employment", which stipulates that discriminatory behaviors such as "asking about women's marriage and childbirth", "limiting gender or gender priority" and "restricting childbearing as employment conditions" are prohibited in the recruitment process, and also expresses the need to strengthen the human resources market supervision, establishment of joint interview mechanism and improvement of judicial relief mechanism to ensure the "zero existence" of gender discrimination in the recruitment process.

But a new report on women's employment published by the United Nations International Labor Organization in 2019 shows that it will take more than 200 years to achieve gender equality in domestic work. The report points out that although the

¹ Liu Xiangdong, Department of Statistics, Jinan University, Guangzhou, China; E-mail: tliuxd@jnu.edu.cn

proportion of women in management is increasing, it is still low. According to the 2018 report of the world economic forum, the overall gender gap has narrowed by 3.6% since 2006, but it will take 108 years to achieve gender equality globally. In 2018, China ranked 103rd in the global gender equality ranking.

It can be seen that although the social status of women is gradually improving with the improvement of the overall awareness of gender equality, the current situation is still not blindly optimistic. While encouraging and supporting the existing policies, it is still necessary to examine the current situation of gender equality through empirical research. By optimizing and refining the indicators for measuring women's social status, improving the methods of horizontal and vertical comparison, we can draw more practical conclusions and make suggestions for the better development of society.

In the study of women's social status, we can find that the issue of employment equality between men and women is crucial. In the research results, researchers have generally reached a consensus that gender discrimination is an important factor causing gender differences. Material resources and social resources reflect the actual status, so we should take the degree of material resources and social resources actually controlled by women as a measure of their social status (Dixon, 1978) [1]. Women's social status is a concept determined by a reference (Chen, 1993) [2]. Therefore, in most of the studies on women's social status, researchers usually understand women's social status from the perspective of gender structure, and take men's social status as the comparative object. We should compare with men from all aspects of society, politics, economy, culture and family life, taking such equality as the measurement standard to measure women's status (Wei, 1999) [3]. We should classify women's social status by the degree of being respected by others and whether they have equal opportunities for survival and development (Ye, 2003; Liu, 2003) [4].

MapReduce programming model has advantages in big data processing, which can greatly shorten the running time, make programming easy to use. It only needs to run on a large number of cheap computer clusters, and the requirements for hardware devices are not high (Liu, 2011) [5]. In the study of graduates' employment, previous researchers found that random forest is the best for the classification accuracy of graduates' employment destination by classifying various training set data. Based on the decision-making system framework of Guruler in 2010 (Guruler, 2010; Istanbullu, 2010) [6], the employment information recommendation department (Tao , 2012, Leting , 2012) [7], and the incremental overall learning model of ADE based on majority voting decision in 2014(Ade , 2014) [8], Qiao Fei and others further proposed that the data in the sample set of students' employment training are basically of label type, and the distribution of attribute values was quite different, so the classical random forest model was no longer applicable, they improved the classification performance of the student employment target data set, and combined the current big data background, proposed a distributed improvement model based on MapReduce (Parmar , 2015; Qiao , 2017) [9,10]. Sun Xiaoyu and others used ordered logit model and marginal effect analysis to study the influence and degree of each factor on women's social status. They also focused on the analysis of the connotation of women's social status, and discussed the indicators to measure women's social status. They further believed that the academic community ignored women's self-recognition and self-evaluation, so they studied the factors affecting women's social status from the social, family and personal levels in the previous research framework(Sun , 2018; Zheng , 2018) [11]. William interviewed employees in the workplace, used OLS regression method to study gender discrimination in the workplace, and hoped to use this method to examine the

effectiveness of various policies in the workplace. They also stressed the seriousness of the idea of gender discrimination at work and pointed out the possibility of tracking and investigating the change of this idea (William ,2019) [12].

Based on the above characteristics, we will carry out the distributed data mining based on MapReduce, classify the employment data of graduates and explore the relationship between the education level and employment destination between different genders.

2 model and method

2.1. logit model

We regard y_i^* as the real social status of the i th interviewee, and as an unobservable potential variable. The ordered logit model can map it to the ordered variable y , and the relationship between the two can be expressed as follows:

$$y_i = \begin{cases} 1, \gamma_0 < y_i^* \leq \gamma_1 \\ 2, \gamma_1 < y_i^* \leq \gamma_2 \\ \vdots \\ j, \gamma_{j-1} < y_i^* \leq \gamma_j \end{cases} \quad (1)$$

Where $\tau = (\gamma_0, \gamma_1, \dots, \gamma_j, \dots, \gamma_J)$ is the set of social status classification points of women, all of which are unknown. At the same time, various factors affecting y are expressed in X , and the expression of the model is constructed as follows:

$$y_i^* = \alpha + BX_i + \varepsilon_i \quad (2)$$

Among $X_i = (x_{i1}, x_{i2}, \dots, x_{ik}, \dots, x_{iK}; i = 1, \dots, N; k = 1, \dots, K)$ are the vectors of the observed values of the influencing factors on women's social status in each valid sample. N is the number of valid samples and K is the number of selected key variables. $B = (\beta_1, \beta_2, \dots, \beta_k, \dots, \beta_K)$ is the influence degree of each variable on the dependent variable, and is also the object which I will explore. ε_i represents the random error term, including the sum of all factors not included in the model or difficult to observe.

2.2 main ideas of MapReduce

Based on MapReduce, there are many algorithms that can be applied, such as clustering, decision tree, naive Bayes and so on. As a unsupervised machine learning method, clustering does not need to use training set. Therefore, based on the purpose of exploring the relationship between gender and employment, combined with the consideration of practicability and operational feasibility, this paper selects K-means clustering algorithm as the parallel algorithm based on MapReduce.

1) Data segmentation stage

According to the size of the data and the computing power of each data node, the clustering task data block is reasonably divided, and these maptasks are allocated to each node.

2) Mapper stage

In this part, the map function is used to decompose the task.

The input data blocks are executed on these nodes by the map function written by the operator, that is, the input key / value pairs are processed, and a new set of key / value pairs is generated. Such new key / value pairs are symmetrical as intermediate results, which are not output and written to the local hard disk.

3) Reducer stage

This part uses the reduce function to merge tasks.

Through network transmission or remote program, the key / value pair from map operation is input to the node where the reduce task is running. Here, the reduce function written by the operator will merge the data sets with the same "key" and store the result output on HDFS. HDFS refers to the distributed file system, which can manage cross computer network storage and is also a sub project of Hadoop.

4) Combiner stage

This part uses the combine function, running between the map function and the reduce function.

Processing key / value pairs from map operations can reduce the intermediate results of map output, thus reducing the network transmission load. The form of combine function is generally the same as that of reduce function. The difference is that the output key / value pair type of combine function should be the key / value pair type of intermediate result, so it can be processed by reduce function.

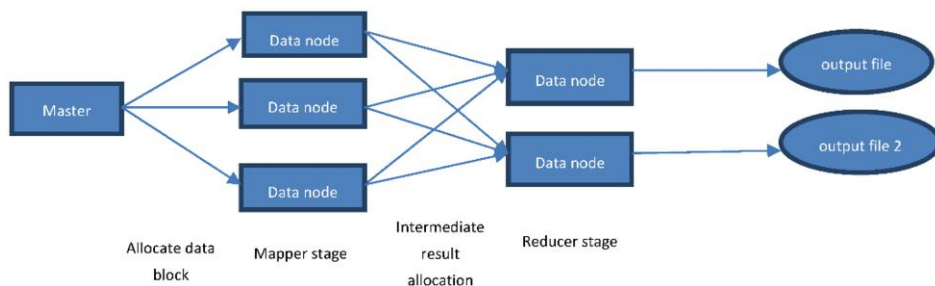


Figure 1. MapReduce calculation framework.

2.2.1 improved k-means clustering model

1)Traditional K-means algorithm

The process of K-means algorithm is to determine the initial center point according to the cluster, calculate the distance between each data point and each center, so as to preliminarily divide the cluster. For each cluster, the average value is re-taken as a new series of centers, and then the distance between each data point and all new centers is calculated, so as to re-divide the cluster, and repeat the process of re-taking the center point to divide the cluster until each cluster no longer changes. The algorithm inputs the database with n data objects, the number of k clusters, and outputs k clusters with the least square error criterion.

2)Canopy clustering algorithm

In the traditional K-means algorithm, it is easy to find that the calculation efficiency is related to the number of processed data, the number of clusters and the number of iterations required. Therefore, in order to improve the efficiency of clustering, the number of iterations must be reduced. On the basis of parallelization, in the face of massive data, canopy algorithm can be used to better determine the value of

K. at the same time, the inaccurate measurement method is used to divide the data points into overlapping areas, so as to generate canopies set and reduce the total amount of calculation.

The canopy clustering algorithm is divided into two stages. In the first stage, the data is divided into overlapping subsets, namely the canopies set mentioned above. In the second stage, we need to use accurate standard clustering method to calculate the distance of canopy as the midpoint. Therefore, canopy algorithm only needs accurate calculation in the second stage, which can reduce the amount of calculation, because the sub datasets divided in the first stage can overlap, so it also increases the fault tolerance of the model.

The process of the algorithm is as follows: first, put all data points into the list m, and select a point n in the list. For each canopy c, if the distance between point n and c is less than the preset threshold T1, it will be classified as canopy c. If the distance is less than the preset threshold T2 ($T1 > T2$), then the point is a strong marker. If there is no strong mark in the process, it need to generate a new canopy. Repeat for all data points. Each canopy will generate a list of center points. Canopy clustering algorithm input point n, preset threshold T1, T2 ($T1 > T2$), output the center point of clustering.

K-means algorithm is based on canopy algorithm. In the first stage, regarding each canopy as the center of the initial clustering, and in the process of repeatedly calculating the distance between data points and the center, only need to calculate the distance between data points and the center in the same canopy.

2.2.2 parallel design of computer cluster

1. Parallel design of canopy algorithm

(1) Design of map stage

This stage focuses on the setting of canopy threshold. Compress the distance formula of strong correlation into the square difference absolute value open root sign, enlarge the distance formula of weak correlation into the square of the square difference absolute value, and calculate the average distance between all sample classifications according to such distance formula. According to the above classification number, it need a total of $(C130)^2$ operations, and take the average value as the average distance AD . According to the theory and experience, AD is much higher than the threshold we need, so we need to use the threshold coefficient to compress. Such coefficient is related to k value, so we use previous research to make the assumption that the sample distance in sample space is uniform, set the threshold coefficient to $k/2$, and set the calculation of threshold to $\frac{AD}{2}$, and modify the threshold through testing.

(2) Reduce stage design

Collect the center points of the output in the Map stage, then merge them according to the key, and the output set of center points is the initial center point in the K-means clustering stage.

2. Parallel design of K-means algorithm

(1) design of map stage

For all the data in the data set, the distance between each data point and the initial clustering center output by canopy algorithm, then calculate and allocate them according to the shortest distance. And the process will continue to iterate until it can no longer be carried out.

(2) design of reduce stage

Combine the intermediate results of map stage with reduce function, and output cluster center and cluster results. A summary of the model framework is shown in Figure 2.

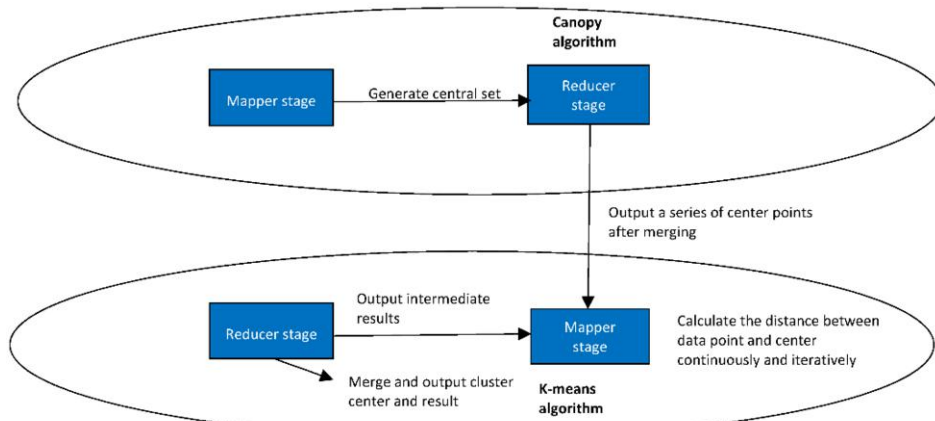


Figure 2. Model framework summary.

3 empirical analysis

3.1 empirical analysis of Logit Model

3.1.1 data source and background

We use the data of China Comprehensive Social Survey (CGSS) in 2012, 2013 and 2015 to analyze women's social status and its related influencing factors, including horizontal analysis and vertical analysis. According to international standards, China's comprehensive social survey has conducted a continuous cross-sectional survey of more than 10000 households in various provinces and autonomous regions of the mainland of China every year since 2003. In principle, these surveys use multi-level stratified random sampling. In the second phase of CGSS, it selects a total of 100 county-level units plus five metropolises, 480 villages / neighborhood committees and 12000 individuals in China, and carries out a follow-up survey. The survey implementation was representative and the data quality was high.

3.1.2 variable description and assumption

In the horizontal analysis, we aim at the evaluation of women's social status and the research purpose of its influencing factors. On the basis of predecessors, it takes the evaluation of women's social status as the dependent variable, and the dependent variable "women's social status" in the questionnaire takes an integer of 1-10 (including 10) as the score, with the score of 1 as the lowest level and the score of 10 as the highest level. The score is divided into three grades: 1-3 (including 3) as the "low" grade; 4-7 (including 7) as the "medium" grade; 8-10 (including 10) as the "high" grade.

At the same time, we take family, society and individual as the three aspects of dependent variable research. Among them, family aspect includes family education background, family burden, husband and wife difference; social aspect includes personal political participation degree, household registration nature and current employment situation; personal aspect includes human capital, self-recognition and gender awareness.

Therefore, in the questionnaire, the education level of the mother, the education level of the father, the number of children born and the number of the elderly in the family, the education level of the husband and the wife, the income difference between the husband and the wife, whether they participate in the election, whether they are non-agricultural registered permanent residence, whether they are employed, the age, the degree of personal education, the total annual income of the individual, whether they are happy, and the social status changes compared with many years ago. The key variables of the study are perception of future social status, self-confidence, gender division of labor, gender advantage, self-concept, gender discrimination and household division of labor.

3.1.3 Data processing and descriptive analysis

Deal with missing values first. After extracting the key variables, because the data volume itself is large but does not have the conditions to give the simulation value, no matter the mean value replacement or multiple replacement of the missing value, it is easy to cause the error and bias of the research results, so I deleted the data with missing value of the key variables in the processing.

Then select the sample. As the social survey is based on households, the survey will ask the interviewees about the subjectivity of the key variables, so the gender of the interviewees is random, then overall is statistically significant. I study the relationship between women's status and various possible influencing factors, so when processing the data, we exclude the male sample and take the subjective status evaluation of the female sample as the dependent variable of the study.

3.1.4 model results

In the process of model analysis, treating the value of income with logarithm, and expressing the degree of income difference between husband and wife by logarithm difference. Using Stata to analyze the data, the results are shown in table 1.

Table 1. Estimation results of ordered logit model for influencing factors of female social status

	Variable name	2012		2013		2015	
		coefficient	Standard error	coefficient	Standard error	coefficient	Standard error
Family education background	Mother's education	0.002	0.027	0.030**	0.0124	0.024*	0.0142
	Father's education	0.060***	0.021	0.010	0.0113	0.0137	0.0125
	Number of children	0.089**	0.035	-0.002	0.0362	0.044	0.029
	Number of the elderly in the family	0.187***	0.050	0.050	0.050	0.051	0.053

	Difference in educational level between husband and wife	0.064***	0.013	0.077***	0.013	0.055***	0.014
Differences between husband and wife	Income difference between husband and wife	0.103***	0.020	0.070***	0.0142	0.056***	0.012
Political participation		0.267***	0.069	-0.057	0.071	0.151**	0.076
Account character		-0.035	0.035	0.008	0.064	0.160***	0.060
Employment		-0.014	0.083	-0.253***	0.087	-0.127	0.089
Personal capital	Age	-0.003	0.004	0.009**	0.004	0.007*	0.004
	My education level	0.097***	0.012	0.090***	0.013	0.084***	0.013
	My total income for the year	0.111***	0.021	0.092***	0.015	0.065***	0.019
Self-recognition	Happiness perception	0.584***	0.052	0.599***	0.054	0.733***	0.059
	Vertical change of social status	0.757***	0.050	0.751***	0.051	0.774***	0.054
	Self-confidence in social status change	-0.135**	0.061	-0.158**	0.063	-0.003	0.066
Gender consciousness	Gender division of labor	-0.002	0.043	0.080*	0.046	0.041	0.049
	Gender advantage	0.039	0.041	-0.082*	0.044	0.022	0.048
	Sense of autonomy	-0.039	0.040	-0.069	0.043	-0.098**	0.046
	Sexual gender discrimination	0.040	0.053	-0.010	0.054	0.113**	0.057
	Division of housework	-0.035	0.050	0.153***	0.050	0.029	0.056
	/cut1	1.979	0.289	1.694	0.263	1.736	0.257
	/cut2	6.728	0.314	6.556	0.290	7.143	0.295

Note: * means significant at 10% significance level, ** means significant at 5% significance level, and *** means significant at 1% significance level.

3.1.5 Overall result analysis

Comparing the 3-year coefficients with the standard errors one by one, and comparing the significance, we can find that the estimated results are basically stable. Under the guarantee of this robustness, I can analyze the following three aspects from family, society and individual.

1) family

We can find that in 2012, family variables have a significant impact on women's social status at a certain level, but in 2013 and 2015, the impact of family burden on women's social status is no longer significant, which is to a certain extent the performance of women's gradually decentralizing the focus of life from family to individual or society. Further analysis shows that there is a positive correlation between parents' education level and women's social status. However, this relationship has been

weakened from 2012 to 2015, which can be seen as the result of the popularization of the Internet, and education no longer relies on family education.

There is also a positive correlation between family burden and dependent variables. We interpret this phenomenon as that the heavier the family burden, the harder the individual in the family needs to work and have more opportunities to participate in social activities, which brings a sense of achievement for women, thus improving their self-evaluation of social status. There is a negative correlation between the number of children born in 2013 and dependent variables, which may be related to gender self-awareness and subjective choice in social reality. Women with higher social status tend to choose fewer and better children.

2) social aspects

The relationship between the degree of political participation and the dependent variables was significantly positive at the level of 1% in 2012 and 5% in 2015, but not significantly negative in 2013. On the whole, the higher the degree of political participation, the more able to voice for their own rights and interests, so as to further promote the improvement of social status, get a better platform for political participation, have more opportunities for political participation, is a process of positive feedback.

In terms of employment, whether women are employed has a negative correlation with their social status, that is, the more unemployed women are, the higher their social status is. This may be because women with stronger self-awareness are more inclined to study and further study, so that they can understand gender equality and clarify their social status. However, in the current human resource market, there may still be sexism. Even if women find jobs, they may not be able to really bring them a sense of self-identity, or their wages are lower than that of men in the same job.

3)Personal aspect

There is a strong positive correlation between education and income and women's social status. Education can help people to set up values, and wealth is the most easily noticed social capital. The more wealth and income, the more able to meet their own desires.

In 2013, the gender division of labor had a significant impact on women's social status at the level of 10%, but in 2015, the impact was no longer significant. It may be because the role orientation of men and women in marriage is no longer a fixed model, but a reasonable distribution according to their strengths. In 2013, gender advantage also showed a significant impact on women's social status. The more women disagree that "men are born stronger than women", the higher their social status. In terms of the concept of self-determination, the more women can pay attention to their own development rather than "whether they marry well", the stronger their self-awareness and social status are. Similarly, the higher the social status of women who can think that housework should be shared equally, and data from 2013 confirm this conclusion.

However, in terms of gender discrimination, the data in 2015 showed that it had a significant impact on women's social status, and the social status of women who had gender discrimination in the workplace was also high. We can explain this by the fact that in the sample of women, many high-level women are still affected by the patriarchal society, and they are still inclined to dismiss women in the economic downturn. This also shows that in the process of eliminating gender discrimination and creating human rights equality, we should not only overcome the prejudice of another group, but also pay attention to the prejudice against compatriots within the group. This requires ideological guidance and education.

On the whole, family is no longer the main factor that affects women's independent development and seeks equal rights, while society and individual have increasingly significant influence on women's social status.

3.2 Gender and employment data mining based on MapReduce

3.2.1 purpose and significance

After exploring the influencing factors of women's social status, it is necessary to analyze the role of gender equality initiatives and policies in all aspects of society in recent years. As one of the four goals of China's macro-economic policy, full employment has always been the focus of research. Whether to achieve equality and non-discrimination in employment is an important measure of gender equality and one of the embodiment of women's social status.

Therefore, combining with the background of big data, using the data mining algorithm based on MapReduce to mine the relationship between employment and education level between different genders and classify the data can not only expand the ideas for the use of this method, but also help us understand the basic situation of employment direction between different genders in the past few years.

3.2.2 data processing

We use the survey data of China Comprehensive Social Survey (CGSS) in 2015, and select gender, education level, employment, nature of work and nature of work unit as the research objects and key variables.

First, merge the information. After merging the information of interviewees with the employment information of their spouses, there are a total of 19749 gender and employment data. Then delete the data. Deleting the samples with missing values of key variables, and screening out the graduates of compulsory education. The number of valid samples after deletion is 7285. Reset and quantify the data. For example, the sample of "labor for the purpose of obtaining economic income" but lack of variables such as the nature of work is identified as "farming". Classifying the working nature, type of working unit and ownership of the sample in a standard way. For gender, men and women are represented by 0 and 1 respectively.

All valid samples were classified by gender. There were 2826 valid samples for women and 4459 valid samples for men. The main reason why the number of effective samples is not equal is that the sample without work is directly deleted. Obviously, the sample of women is more than that of men.

3.2.3 empirical results

In the process of demonstration, using the open-source platform of Hadoop to build the overall environment. The output results are shown in the following figure 3 and figure 4.

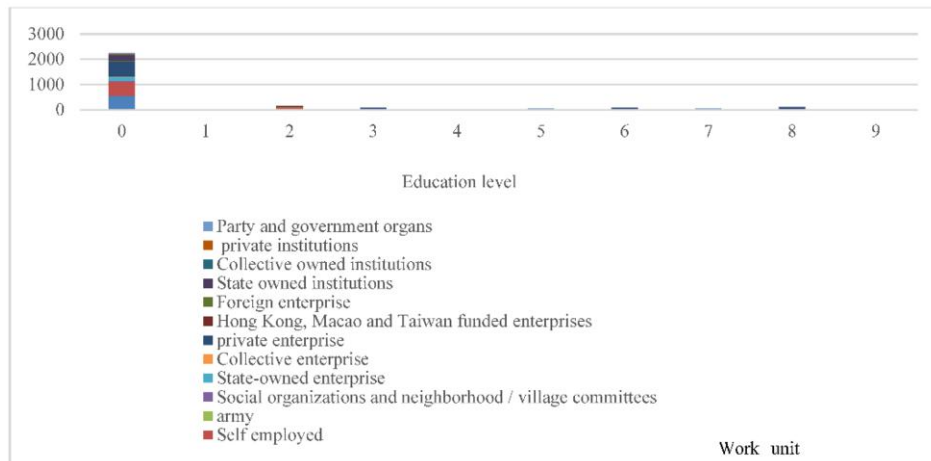


Figure 3. Cluster analysis results of female samples

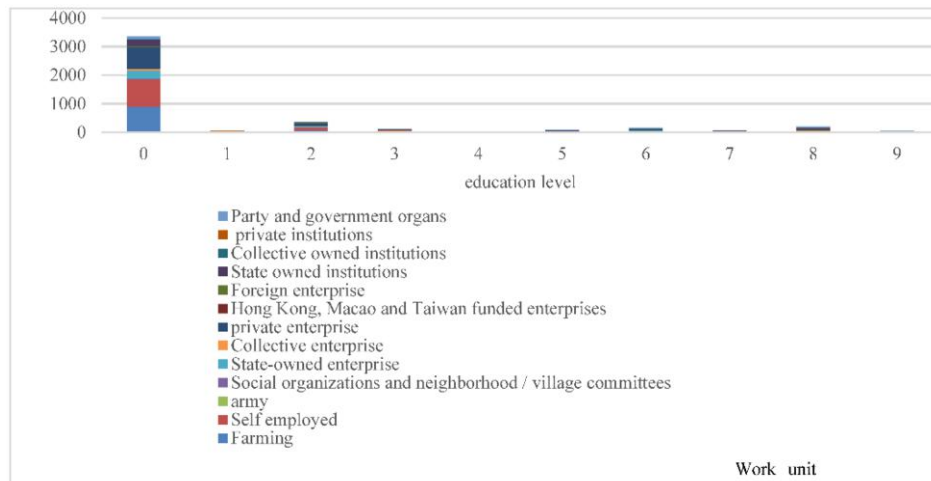


Figure 4. Cluster analysis results of male samples

From Figure 3 and Figure 4, we can see that the number of people employed after the completion of compulsory education accounts for the vast majority of the total number of samples, and this part of the population is widely distributed in all work units, and Agriculture, self-employed and collective enterprises are the most widely distributed. We think it is because some companies will still recruit low-educated people for less knowledgeable jobs. In addition, the number of high school graduates and undergraduate (formal higher education) graduates reached the peak. Therefore, the samples of Higher Education (that is education level = 5, 6, 7, 8) will be analyzed separately. As shown in Figure 5 and Figure 6.

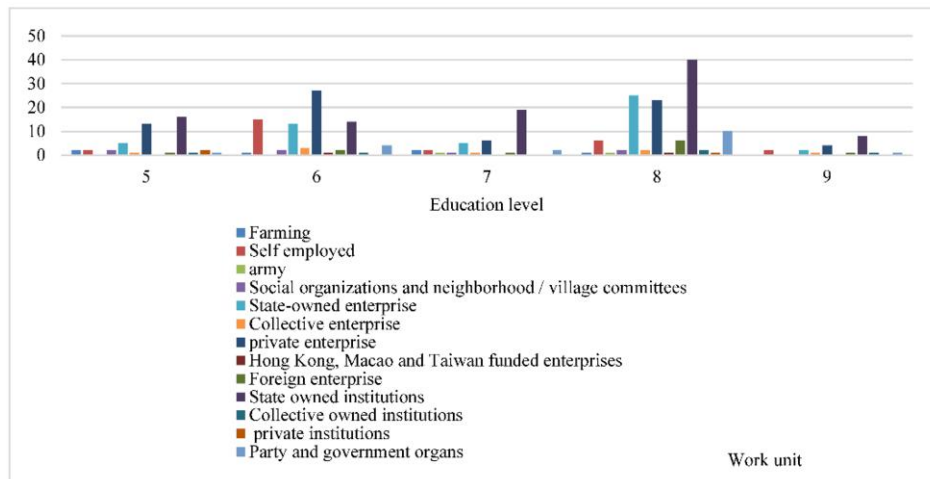


Figure 5. Cluster analysis of female samples in Higher Education

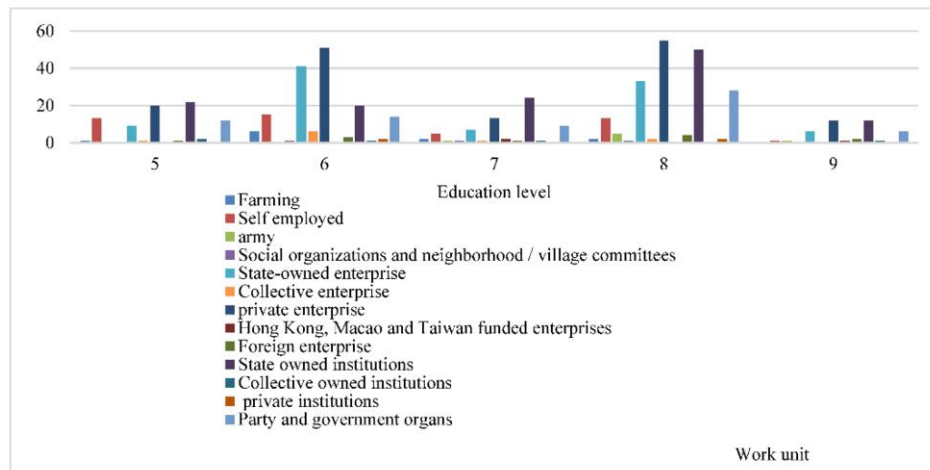


Figure 6. Cluster analysis of male samples in Higher Education

Among the female sample of higher education, more people are destined for state-owned institutions, state-owned enterprises, and private institutions. However, graduates of junior colleges (formal higher education) have outstanding performance in self-employment (including self-employed individuals) after graduation, which is far from other graduates. To a certain extent, this may indicate that women are more willing to go to stable state-owned units, which may be related to overall social expectations and long-term environment and education. Moreover, the graduates of colleges and universities are more adventurous and entrepreneurial, and the distribution of unit types in the other four education levels is basically similar.

In the sample of men with higher education, their employment tends to be more private enterprises, state-owned institutions and state-owned enterprises, but the distribution is more different than the sample of women. For example, the proportion of men of all educational levels who are going to be party and government agencies is

very high, and among college graduates and college graduates, there are many people who start their own businesses or do business. And it can be found that the total number of non-agricultural employment for males in college (formal higher education) and undergraduate (formal higher education) is similar, which is very different from the analysis of female samples. This may explain the tendency: in the long-term labor market, women's education requirements may be higher than men's. In contrast, women's overall employment orientation is relatively single. Under the influence of social culture and social expectation, for decades, women's choice of employment may be constantly restricted by the outside world and themselves, which together lead to the cycle of gender discrimination in work units or self-discrimination within women groups.

4 Conclusion

We divide the study of women's social status and its influence into two parts.

First of all, we use ordered logit model to analyze the rating of women's self-social status and various factors, discuss the factors that may affect women's social status, summarize the nature of the impact and explain it from the perspective of society, family and individual. Through this analysis, we can further understand the social facts shown in the current data. we find that women are more and more isolated from the influence of family, and are more involved in their social roles. At the same time, they pay more attention to their own value and experience. They think that their social status is related to their expectation and optimism, not only the material conditions or whether they are rich or not. But I also find that for high-level women, there is still a part of self-internal sexism.

Secondly, as an exploratory research, based on the background of big data, we conduct data mining on the relationship between education level and employment destination between different genders, which reflects the social status of women in employment. Using the parallel K-means clustering algorithm based on MapReduce. In this process, we improve and optimize the classification algorithm, and finally has better clustering results for the existing gender and work unit data. We find out the different employment situation between men and women, and explain the distribution and phenomenon. we hold that the different employment trends between men and women are based on the long-standing social expectation and cultural influence. The social atmosphere is more expecting women to manage housework, and more expecting men to work. This different pressure on gender makes women more inclined to choose state-owned units no matter what level of education they are in, while men are more likely to germinate the idea of entrepreneurship because of the pressure of earning money. Therefore, the society should gradually form an atmosphere for individuals to choose their own employment, rather than a moral criticism of a gender group. This is also conducive to women and men to explore their self-awareness, while promoting social division of labor equality, family division of labor freedom. At the same time, we also find that gender discrimination in the labor market may exist for a long time, that is, the educational requirements for women may be higher. To some extent, this affects the judgment of women's social status. But with the continuous implementation of the policy, such a phenomenon will inevitably be weakened.

In view of the current situation, the government should pay close attention to the gender dynamics, timely feedback to avoid the disorder of social order, and at the same

time, it should control the improper or cross-border speech in laws and regulations. Social media should be aware of the importance of self-guidance of public opinion and make objective reports and analysis. At present, with the development of network information, the public opinion guidance of various information channels may be tendentious, so that some people who do not have firm self-consciousness and self-worth are guided or even misled by them. Therefore, as a media, we should hold an objective and rational attitude all the time, and should not have strong emotional guidance. Each social platform should improve its own relevant laws and regulations, and abide by the implementation. The social platform should shoulder the huge social responsibility, standardize the use of rules, delete and manage the strong offensive or biased speech.

References:

- [1] Dixon R B. Rural women at work: strategies for development in South Asia. [J]. Baltimore, Maryland, Johns Hopkins University Press for Resources for the Future, 1978, 1978.
- [2] Chen Zaihua. Discussion on Comprehensive Evaluation Indicators of Women's Status [J]. China Population Science, 1993, 39 (6): 38-44.
- [3] Wei Huilan, Yang Yan. Study on evaluation index system of women's status [J]. Journal of Lanzhou University, 1999 (02): 97-103.
- [4] Ye Wenzhen, Liu Jianhua, Du Juan, Xia Yiran. Social status of Chinese women and its influencing factors [J]. Journal of population, 2003 (05): 22-28.
- [5] Liu Na. Application of MapReduce based data mining algorithm in national population system [D]. Capital University of economics and trade, 2011.
- [6] Huseyin Guruler, Ayhan Istanbullu, Mehmet Karahasan. A new student performance analysing system using knowledge discovery in higher educational databases[J]. Computers & Education, 2010, 55(1): 247-254.
- [7] Tao Tan, Leting Tan. Study on Personalization Recommendation System Based on Recruitment Information[J]. Procedia Engineering, 2012, 29: 780-784.
- [8] Ade R, Deshmukh P R. An incremental ensemble of classifiers as a technique for prediction of student's career choice[C]. First International Conference on Networks&Soft Computing (ICNSC), IEEE, 2014.
- [9] Parmar K, Vaghela D, Sharma P. Performance prediction of students using distributed data mining[C]. International Conference on Innovations in Information Embedded and Communication Systems (ICIIECS), 2015: 1-5.
- [10] Qiao Fei, Ge Yanhao, Kong Weichang. Study on the classification model of distributed and improved random forest student employment data based on MapReduce [J]. System engineering theory and practice, 2017 , 37 (05): 1383-1392.
- [11] Sun Xiaoyu, Zheng Yifang, Xu Jiaxian. An Empirical Study on the influencing factors of women's social status based on the comprehensive social survey data of China in 2013 and 2015 [J]. Journal of Shijiazhuang Railway University, 2018, 12 (04): 63-72.
- [12] William J. Scarborough, Danny L. Lambourths, Allyson L. Holbrook. Support of workplace diversity policies: The role of race, gender, and beliefs about inequality[J]. Social Science Research, 2019, 79.

News-Based Research on Forecast of International Natural Gas Price Trend

Tianxiang Li^a, Xiaosong Han^a, Aoqing Wang^a, Hui Li^a, Guosheng Liu^a and Ying Pei^{b,1}

^a*Key Laboratory for Symbol Computation and Knowledge Engineering of National Education Ministry, College of Computer Science and Technology, Jilin University, Changchun 130012, China*

^b*The College of Information Engineering, Changchun University of Finance and Economics, Changchun 130122, China*

Abstract. In this paper, we build a deep learning network to predict the trends of natural gas prices. Given a time series, for each day, the gas price trend is classified as “up” and “down” according to the price compared to the last day. Meanwhile, we collect news articles as experimental materials from some natural gas related websites. Every article was then embedded into vectors by word2vec, weighted with its sentiment score, and labeled with corresponding day’s price trend. A CNN and LSTM fused network was then trained to predict price trend by these news vectors. Finally, the model’s predictive accuracy reached 62.3%, which outperformed most of other traditional classifiers.

Keywords. Natural Gas, Sentiment Analysis, Deep Learning, Price Trend Prediction,

1. Introduction

As the energy supply situation gets tenser, developing and using natural gas efficiently are becoming many countries’ essential method to safeguard energy supply and reduce carbon dioxide emissions [1]. To address this issue, a large number of domestic and foreign scholars have made great efforts to predict the natural gas prices.

With the development of science and technology, more and more data emerged on the Internet. How to collect and manage these data efficiently and extract useful information from the data have become a research focus recently. Now, many scholars have applied big data analysis technology and text mining methods [2] to the study of the operating rules of financial markets. For example, the paper [3] shows that short-term stock price movements can be predicted using financial news. Robert et al.[4] used several kinds of textual representations to train an SVM model for stock prediction. In paper [5], Mark Dras built a character-based neural language model for the stock market of event-based trading. The model finally reached 64.74% accuracy of interday and 61.68% accuracy of intraday stock prediction. Xuerong Li et al.[6] applied deep learning techniques to oil forecasting and extracted hidden patterns within online news media using a CNN. The study also proposed a feature grouping method based on the LDA topic model for distinguishing effects from various online news topics. The

¹ Corresponding Author: Ying Pei, Changchun University of Finance and Economics, China; Email: 1076441579@qq.com

results show that the proposed topic-sentiment synthesis forecasting model performs better than the other benchmark models. Inspired by the above work, we proposed a CNN-LSTM model to predict the natural gas price trend.

2. Data Collecting

The goal of this paper is using natural gas related news and history futures price to predict the trend of the natural gas future price. There are two types of data used in this study: news and gas history futures price data.

2.1. News articles

Among most natural gas related websites, we filtered the ones that update rapidly, contains large amounts of materials and have a reliable source of information [7]. In the end, we chose WorldOil as our news source, which has the fastest update frequency and the most articles. After developing a spider, we have collected 26490 news covering 2274 days. On average, there are about 11 news in one day.

2.2. Natural gas futures price

The natural gas future price was downloaded from Henry Hub, which is recognized as the U.S.'s largest and authoritative natural gas delivery and pricing center.

2.3. Granger causality test

Our initial hypothesis is that the sentiment of news may have an effect on the price trend. Granger causality test [8] is employed to prove that natural gas' futures price is related to the news sentiment score. Granger causality test is a method to analyze the causal relationship between economic variables. The prerequisite for the Granger causality test is that both sequences must be stationary. Thus, ADF tests are performed. The results are as Table 1.

Table 1. ADF test of sentiment score and price.

ADF	NLTK sentiment score	Price
Test Statistic	-3.965393	-3.110797
P-value	0.001603	0.025764
Lags Used	19	16
Number of Observation Used	2254	2257
Critical Value (1%)	-3.433255	-3.433251
Critical Value (5%)	-2.862823	-2.862821
Critical Value (10%)	-2.567453	-0.567452

It can be seen that, individually, two sequences' test statistic values are smaller than critical values (5%), and the p-values are also close to zero. Thus, we reject the null hypothesis and confirm that these two sequences are stationary. After that, two Granger causality tests are performed. The results are as Table 2.

Table 2. Sentiment score - price Granger causality test(Price – sentiment score Granger causality test)

Number of lags 1	Number of lags 2	Number of lags 3	Number of lags 4
Ssr based F test			
F	16.759(0.603)	5.919(0.575)	2.732(1.024)
			2.095(0.794)

P	0.00(0.438)	0.0027(0.563)	0.424(0.381)	0.079(0.529)
Df_denom	2270	2267	2264	2261
Df_num	1	2	3	4
Ssr based chi2 test				
Chi2	16.782(0.604)	11.864(1.153)	8.220(3.080)	8.414(3.188)
p	0.00(0.437)	0.003(0.562)	0.042(0.380)	0.078(0.527)
df	1	2	3	4
Likelihood ratio test				
Chi2	16.720(0.604)	11.833(0.153)	8.205(3.078)	8.399(3.185)
p	0.00(0.437)	0.003(0.562)	0.042(0.380)	0.078(0.527)
df	1	2	3	4
Parameter F test				
F	16.759(0.603)	5.919(0.575)	2.732(1.024)	2.095(0.794)
p	0.00(0.438)	0.003(0.563)	0.042(0.381)	0.079(0.529)
Df_demon	2270	2267	2264	2261
De_num	1	2	3	4

For different inspection methods, the results are examined, and we can draw the conclusion that news sentiment score has a strong Granger causality to natural gas prices. But conversely, the Granger causality of natural gas prices on the emotional value of news is not obvious. So, it can be considered that there is "Granger causality" on the news sentimental value and the price trend.

3. Methodology

There are mainly five steps in our method, data collecting, sentiment analysis, granger causality test, document representation and model building. Firstly, we obtain the news and price data from WorldOil and Henry Hub. Then, sentiment analysis is performed on the news to get the sentiment score of each article. To prove that natural gas related news is correlated to its futures price, we perform granger causality test on the sequence of news' sentiment score and futures price. After that, word2vec and TF-IDF are used to embed the news into vectors. Finally, we build various machine-learning methods to predict the price trend. The total process is shown in Figure 1.

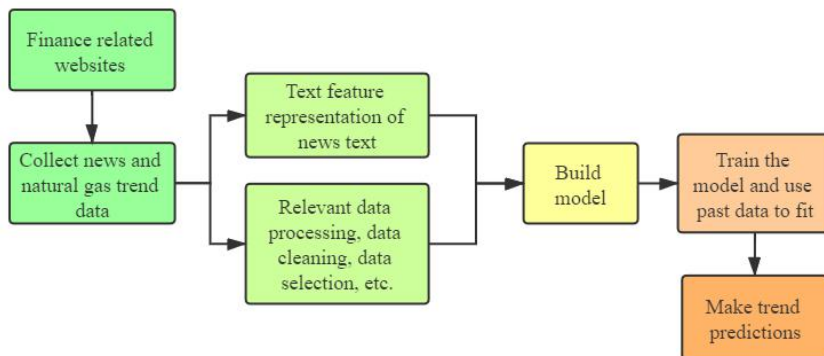


Figure 1. Main workflow

3.1. Sentiment Analysis

Sentiment analysis is a key branch of NLP (Natural Language Processing). NLTK (Natural Langrage Toolkit) [9] is the most popular NLP package. And we use NLTK's

built-in sentiment analyzer to analyze each article's sentiment score. The score is then saved for later use.

After getting the sentiment score and the price data, the two sequences are normalized and denoised, and the resulting trend graph is shown as Figure 2.

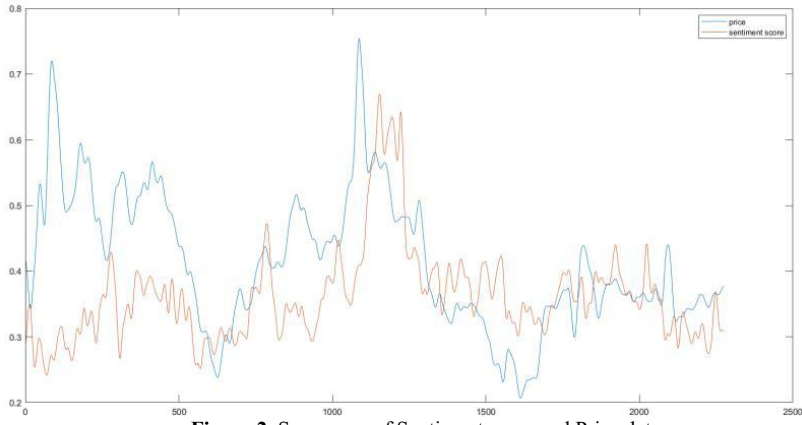


Figure 2. Sequences of Sentiment score and Price data

3.2. Document representation

We use a hybrid approach[10-11] to build article vector in this paper. Firstly, TF-IDF weight is calculated for each word in one article. Later, a Google pre-trained word2vec model is loaded to generate word vectors and the vector is then multiplied with word's corresponding TF-IDF weight. Then, the words' vectors are summed and multiplied by the article's sentiment score to form the article's vector. Since there are often more than one article in one day, the arithmetical average article vectors with the same timestamp is calculated as one day's news vector representation.

3.3. Model Building

In order to capture effective time and spatial field information from the time series sequence, a CNN and LSTM fused network is built [12]. LSTM network is needed to its extract time series features, due to its unique and powerful ability to extract features from pictures and texts, a CNN is also needed to extract features. One-dimensional convolution is performed on the daily news vectors. Then max pooling is followed. In this part, the model allows us to add various layers of different convolution and pooling layers to achieve better convolution performance. However, the optimal results from the experiment is three convolution layers and pooling layers, with convolution kernels of 2, 3, and 4. The multi-day convolution pooling results are entered a LSTM layer. After the fully connected layer, the tensor goes through a Dense layer and output a 128-dimension tensor. The CNN-LSTM network is shown as figure 3.

In order to capture the price's time series feature, another LSTM network is also used to generate a 128-dimension tensor. Then the two tensors are Concatenated and classified into two categories by a Softmax layer. The process is shown in Figure 4. And a detailed description of the network is shown in the Github (<https://github.com/Wangaoqing/natural-gas-price-prediction>).

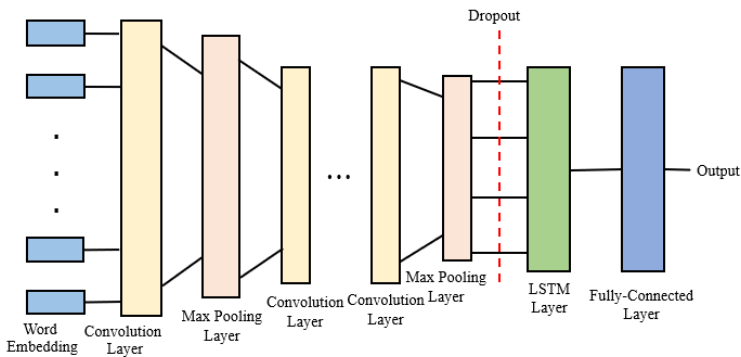


Figure 3. Brief CNN-LSTM network

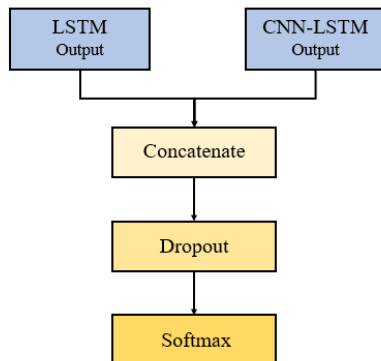


Figure 4. Final Process

4. Experiment

During the experiments, we use 30 day's news to predict next day's gas price trend. With the fused network, we achieved better results, which are shown as Figure 5.

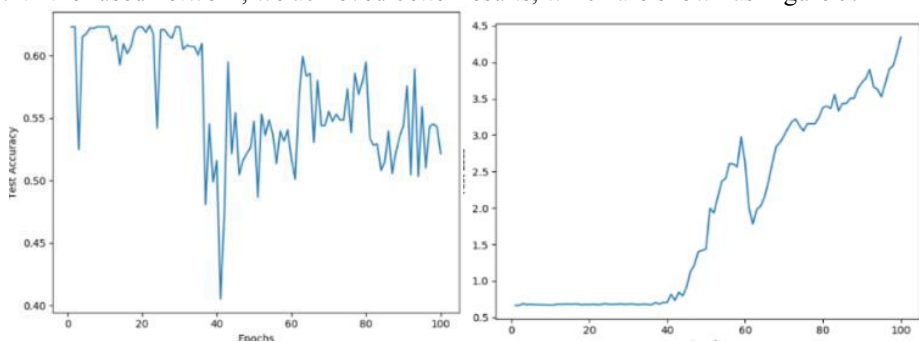


Figure 5. CNN-LSTM model predict results

When the number of iterations is less than 40, the predicted loss value does not rise, the accuracy of the test is 53%-62%, and the optimal accuracy is 62%. When the number of iteration times is greater than 50, the prediction loss rises sharply, and the model enters the over-fitting stage, which can explain the oscillation of the accuracy.

The total number of days we used in this experiment is 2274, and we split 60% of them as a training set and the other 40% as a test set. To verify our model, we also tried several supervised classifiers such as SVM (Support Vector Machines), LightGBM, RF (random forest), and NB (Naïve Bayes). The results are summed up in the Table 3.

Table 3. Results of experiments

	Accuracy
LightGBM	53%
RF	52%
NB	39%
SVM	52%
LSTM	52%
CNN-LSTM	62%

As a comparison, our CNN-LSTM model gives the best result with a 10% percent accuracy promotion, which means the CNN-LSTM network does extract useful features from the news and help predict the natural gas price trends.

5. Conclusion

Based on many NLP techniques and machine learning algorithms, this paper proposed a CNN-LSTM network aiming to predict the future trend of natural gas price trends. After comparison, the CNN-LSTM model performs 10% better than other compared methods. The obtained results suggest that the model works, though the accuracy still has a lot of room for improvement. In future work, we could obtain news text from a larger scale and try some state-of-art classifiers, which may have better performances.

Acknowledgement

The corresponding author is Ying Pei. The authors are grateful to the anonymous reviewers for their insightful comments which have certainly improved this paper. This work was supported in part by the Jilin University provincial science and technology innovation project 2018B2144, and National Science Foundation of China under Grant 61972174.

References

- [1] I. Sutskever, O. Vinyals, and Q. V. Le, “Sequence to sequence learning with neural networks,” in *Advances in neural information processing systems*, 2014, pp. 3104–3112.
- [2] A. Tan, “Text Mining: The state of the art and the challenges,” in *In Proceedings of the PAKDD 1999 Workshop on Knowledge Discovery from Advanced Databases*, 1999, pp. 65–70..
- [3] X. Ding, Y. Zhang, T. Liu, and J. Duan, “Using Structured Events to Predict Stock Price Trend: An Empirical Investigation,” in *Proceedings of the 2014 Conference on Empirical Methods in Natural Language Processing (EMNLP)*, Doha, Qatar, 2014, pp. 1415–1425.

- [4] R. Schumaker and H. Chen, "Textual analysis of stock market prediction using breaking financial news: The AZFin text system," *ACM Trans. Inf. Syst.*, vol. 27, 2009, doi: 10.1145/1462198.1462204.
- [5] L. dos Santos Pinheiro and M. Dras, "Stock Market Prediction with Deep Learning: A Character-based Neural Language Model for Event-based Trading," in *Proceedings of the Australasian Language Technology Association Workshop 2017*, Brisbane, Australia, 2017, pp. 6–15.
- [6] X. Li, W. Shang, and S. Wang, "Text-based crude oil price forecasting: A deep learning approach," *Int. J. Forecast.*, vol. 35, no. 4, pp. 1548–1560, Oct. 2019.
- [7] E. Junqué de Fortuny, T. De Smedt, D. Martens, and W. Daelemans, "Evaluating and understanding text-based stock price prediction models," *Inf. Process. Manag.*, vol. 50, no. 2, pp. 426–441, Mar. 2014.
- [8] C. W. J. Granger, "Investigating Causal Relations by Econometric Models and Cross-Spectral Methods," in *Essays in Econometrics: Collected Papers of Clive W. J. Granger*, USA: Harvard University Press, 2001, pp. 31–47.
- [9] M. S. M. Vohra and J. Teraiya, "A COMPARATIVE STUDY OF SENTIMENT ANALYSIS TECHNIQUES 1," 2013.
- [10] L.-W. Lee and S.-M. Chen, "New Methods for Text Categorization Based on a New Feature Selection Method and a New Similarity Measure Between Documents," in *Advances in Applied Artificial Intelligence*, Berlin, Heidelberg, 2006, pp. 1280–1289.
- [11] A. Graves, "Generating Sequences with Recurrent Neural Networks," *ArXiv13080850 Cs*, Jun. 2014.
- [12] S. Xingjian, Z. Chen, H. Wang, D.-Y. Yeung, W.-K. Wong, and W. Woo, "Convolutional LSTM network: A machine learning approach for precipitation nowcasting," in *Advances in neural information processing systems*, 2015, pp. 802–810.

A Virtual Reality Check: Covid-19 & the Challenges Facing Virtual Reality as an off-the-shelf Mainstream EdTech Solution

Markus Rach^{1,a} and Russell Scott^b

^a*University of Applied Sciences and Arts Northwestern Switzerland*

^b*Cognetic Technologies*

Abstract. Virtual Reality has been much researched as an education technology, particularly under the constructivist perspective of learning environments. Whilst some education institutes have already applied VR within their curriculum, or for marketing purposes, interest has calmed much around the technology. However, since the start of the global Covid-19 pandemic, many educators were faced with the need to distance educate, which sparked a new wave of interest in VR as a potential education technology solution; even to extent of classroom substitution. Whilst the advantages of VR to education have been researched, this paper seeks to address a specific research gap to assist education in the selection of VR as a suitable education technology. Based on qualitative interviews, literature research and the practitioner experience of the authors in the field of education and VR, a technology fit assessment model has been proposed to support education institutes in their VR evaluation process.

Keywords. Virtual Reality, EdTech, Constructivist Learning Theory, Covid-19

1. Introduction

Virtual Reality (VR) gained the attention of educators and academics long before VR became known to the public and portrayed in the media. Although some of the earliest studies of seeing aids in education date back to the 1950s, it was with the birth of modern computing that Virtual Reality sparked a new interest in redesigning learning environments.

Helsel [1] proposed in 1992 how educators portray a natural understanding of VR's learning potential to create virtual learning experience offers for students. McLellan [2] traced early learning concepts back to Airforce studies of 1960s, while Youngblut [3] conducted research into the use of VR in learning environments. His research revealed a wide-spanning field of application cases in almost all areas of education and age groups. However, Youngblut's [3] research suggested the particular usefulness of VR in constructivist learning environments. Constructivist learning theory is based on the experience of learning, the learning environment and the responsibility of learning [4]. The impact of computing technology and particularly virtual technologies has always been closely associated with the development of the

¹ Markus Rach, FHNW, Institute of Competitiveness and Communication, Riggensbachstrasse 16, 4600 Olten, Switzerland; E-mail: markus.rach@fhnw.ch

constructivist learning model [5]. Pantelidis [6] proposed a model to evaluate the use of VR in educational setups by assessing previous literature and research on the topic. It was concluded that VR has specific advantages in experiential based and thus constructivist learning environments. On the detrimental side, cost and learning efforts are mentioned. The model itself is summarized in 10 process steps to guide an educator through the VR selection and design process. Despite of VR's tremendous potential to reshape education and training, it has not found its way into mainstream application, neither in education, professional trainings or even household applications [7]. VR has thus lost some of its glitter and hype, even vanished from the Gartner Hype Cycle Emerging Technology in 2018, whereas in 2017 VR was categorized as a maturing technology [8,9].

Through the emergence of the global Covid-19 pandemic early 2020, VR has found its way back to the media and received a lot of attention as a potential substitute for face to face teaching, learning and even working environments [10]. Exhibitions moved to the virtual spaces [11] and even some universities have adopted virtual learning as part of the solution to substitute physical classroom learning [12]. Through these circumstances and heightened interest in technological solutions to overcome digital barriers, the question of whether VR is the future of learning technologies gained new traction [13, 14].

This paper seeks to evaluate the mainstream readiness of VR for modern education to propose an evaluation model for VR technology selection purposes within constructivist learning environments. Doing so, this paper builds upon the model of Pantelidis [6] by establishing a threshold requirement analysis that expands from subject application to socio-economic and infrastructural aspects.

Since spending on Education Technologies (EdTech) has substantially increased in Australia, through Prime Minister Turnbull's innovation agenda for schools [15], the authors have selected to research exclusively on VR application of Australian educators.

2. Virtual Reality Use Cases

There is plenty of scholarly work on the advantages and disadvantages of VR in educational settings [16, 17, 18], however, a current notion arising out the COVID-19 pandemic is to substitute classrooms through VR. This idea had already received scholarly attention during the boom of online education [19].

As of now, there are various practical examples of educational institutes applying VR as a substitute or add-on technology to deal with the Covid-19 impacts on learning environments. Amongst these institutes is the University of South Wales, which applies VR to teach students crime scene investigation and other specialized subjects [20]. This example is particularly interesting as it focuses on the need to create immersive learning experiences and thus seeks to capitalize upon VR's technology benefit. It also shows how expert knowledge is being built and disseminated across the university to increase the digital or technology literacy of staff in order to create other useful application cases.

The Kellyville Ridge Public School in the North of Sydney applied VR as a teaching technology to have students design a virtual reality neighborhood tour of historic sites [21]. This example is interesting as one of the school's educators details how the technology-facilitated reaching students in a different way. It is noteworthy to mention that over 2 million students worldwide completed a google VR tour [22].

Many schools and universities have followed a similar example and created virtual campus tours, particularly to substitute physical campus visits since the emergence of Covid-19 [23].

Other schools implemented VR to enhance teaching subjects and courses, even in remote appearing domains, such as college football. The University of Michigan's football team applies VR to football training and even player recruiting [24]. The University of British Columbia even integrated VR to give virtual law lectures [25]. VR application cases have emerged in almost all school systems, ranging from primary education [26] to higher education [27].

3. Research Approach

The study is guided by the following research question: What is the readiness of education institutions and homes for deploying Virtual Reality as an EdTech solution?

This research question includes both the readiness to select the appropriate technology for each institutions' respective use case, as well as the readiness to deploy the very technology to maximize the technology's utility. In doing so, the authors investigated aspects ignored by prior research: infrastructural and socio-economic readiness. The underlying notion to this research question is grounded in the practitioners' understanding of the authors, that VR's potential can only be realised if infrastructural and application thresholds are met. The research approach to this paper is outlined in Figure 1.

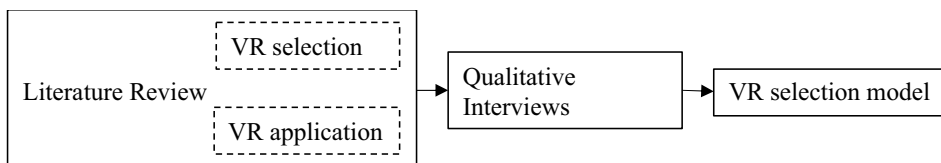


Figure 1. Research Approach

3.1. Literature Review

A literature review was conducted in EBSCO Host, assessing 566 journal publications, ranging from 2010 to 2020 on the abstract based search “Virtual Reality” + “Education”.

Much of the academic research discovered suggests Virtual Reality offers a substantial potential for education and training [28, 29, 30]. Particularly VR's potential to support the constructivist learning approach while motivating student engagement with various subjects has been highlighted as a major technological benefit [31, 32]. There are clear reasons to pursue and deploy VR as an education solution, but aside from the paper of Pantelidis [6], no further scholarly work examining selection bias or selection prerequisites was found. The current relevance of Pantelidis [6] could be seen as questionable, as commercial-grade VR headsets were not available during the study and the technology has moved on significantly since its publication.

3.2. Qualitative Interviews on VR readiness in Australia

There are a number of basic assumptions made when considering VR adoption in schools; a simple example of this is requiring a building with power, or a facility to power up a VR headset, or internet to connect the devices. The literature review found no academic work examining the extent of the assumptions, or the truth of the assumptions being made about the current school ecosystem in the context of VR education. The qualitative interviews, in part, sought to discover the adequacy of the assumptions being made and to further understand the relevancy of these factors to the utilization potential of VR in education.

3.3. Settings and Participants

Interviews were conducted with three digital technologies teachers, covering years 7-12, at three schools in Perth, Western Australia. The respective schools spanned the following three socio-economic categories:

- low socio-economic government school,
- a high socio-economic government school, and
- a high fee private school.

All three schools, regardless of their socio-economic status, are regarded as excellent examples of science, technology, engineering and mathematics (STEM) education, as well as digital technologies teaching. Each school has a VR program, run with the schools' students and each program differs significantly in its implementation.

3.4. Interview Method

Participants were asked seven questions, via teleconferencing methods, with the stated understanding that they may not know or could best guess the answers.

1. What is the ratio of computers to students at the school?
2. What is the ratio of computers to students at home?
3. What percentages of students have computers powerful enough for VR?
4. What percentages of students have VR headsets at home?
5. What percentages of students have mobile devices capable of creating AR or VR?
6. What steps are you taking to achieve digital literacy at home during the Covid19 lock down?
7. What issues do you face implementing at home tech learning?

4. Results

Table 1 provides a brief transcript of each interview. Despite the school's varying socio-economic status, their general advancement in applying VR to their curriculum is likely to reflect outcomes in table 1 as the best-case result scenarios per socio-economic group.

Table 1. Interview Summary

	School 1	School 2	School 3
Q 1	1:6	1:4	1:2 or better
Q 2	1:0.6 (40% have no computer)	1:1	1:1 or better

Q 3	5% at best	5-10% of school	50%
Q 4	0%	0.2% at best	1-5%, maybe?
Q 5	10%	50%?	90+%
Q 6	Sourcing of 90 5+yr old pcs for students to take and use at home. Australian business network provided data packs as many students either had no internet at home or insufficient data. Started crowd funding for further pcs.	We have implemented courses online, but tech courses are not online courses. Often the students have limited video conferencing.	It was difficult transferring lessons to online.
Q 7	Students don't have computers at home, or the whole family relies on a single parent's mobile for connectivity. Adults in the family often have never used or had technology in the home and are therefore unaware how to use it or aid their child in its use. We have had to implement adult tech training. We have had to keep the school open regardless to account for at risk students.	Some teachers have poor home connectivity which makes online delivery even harder. There is a duality of learning intent behind technology lessons. Tech is useful to teach collaboration and communication and teamwork, these are all lost online. Consumption based tech experiences hook the students but don't actually provide useful learning tasks. The vast range of home computer quality means no one approach fits each student	Nil aside from typical online issues.

5. Discussion & VR selection model

It is clear from the interviews conducted that the readiness of the schools to implement VR as a solution is heavily impacted by the social and economic conditions. Particularly infrastructural prerequisites, such as the availability of computing equipment and more specifically, powerful enough computing equipment has shown to be a major bottleneck for the schools interviewed for this paper. This could lead to either increasing the social inequality gap, on both institutional and private levels. Adding to this is the requirement for additional, application ready VR headsets as further hardware requirement. In either school or home setting, this hardware needs to mirror the quantity of parallel users, which poses additional investment needs to be met.

If the hardware conditions are met, there are still narrative-based considerations to be met for VR to be effective [33]. It is unclear how much impact narrative considerations have in VR, however poorly met narrative factors may render the VR learning experience void. Narrative in a VR sense refers to more than a storyline, it refers to the entire environmental setup associated with the VR user experience, the user's familiarity and an array of factors unique to VR. Arguments of efficacy notwithstanding, how does a teacher set digital homework to a class whose cohort is unlikely to have computing available at home? Understanding the consequences of socio-economic disparity encompasses whole fields of research, but in the context of education, it is important to understand that VR adds a unique layer of considerations.

It is, therefore, that the authors propose an alternative selection model, specifically for VR, refer to Figure 2, to the earlier quoted model by Pantelidis [6], which addresses identified gaps in academic literature, but also qualitative findings from conducted interviews. The proposed model strives to achieve the highest VR utility, which is a product of infrastructural and application readiness, as mentioned prior in this paper.

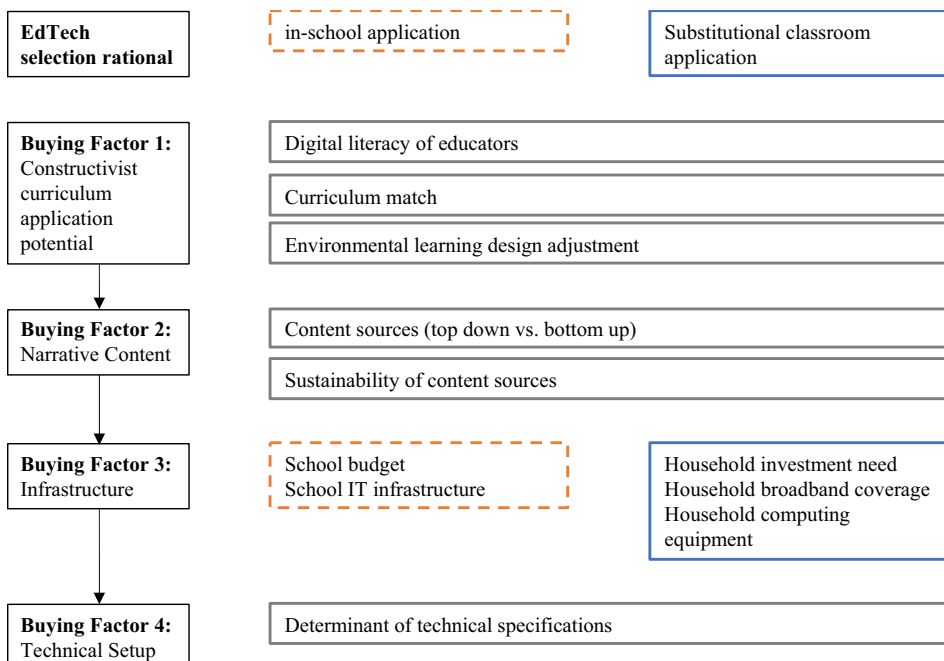


Figure 2. VR Selection Model

The model considers both in-school as well as classroom substitution application fields. In the first instance, the reason to acquire VR as an EdTech solution is a key determinant for the further selection criteria application. This follows the notion of Pantelidis [6], as shown in buying factor 1. Buying factor 2 considers the very narrative requirements of VR to allow for a sustainable hardware application. Only if conditions for buying factor are met, will it make sense to move to buying factor 3 and assess infrastructural prerequisites for VR's mainstream application. As a final step, the model is to create the specification determinants. Therefore, the focus on the maximum investment and thus technology utility is assured. This model therefore fundamentally shifts the experience the authors have with educational institutions to consider hardware before application, while considering relevant application, infrastructural and social-inequality prerequisites.

6. Conclusion.

VR provides the remarkable potential to elevate learning experiences under the constructivist learning theorem. This paper however notes, that VR is not yet an off-the-shelf solution for education institutes.

VR, unlike other technology, requires the consideration of a special environmental and content narrative to realize the full potential of the technology to achieve user immersion. Thus, even if education institutes rightfully select VR on the basis of an application assessment, the potential to have mismatching content and application experience is high. This impact is assumed to be influenced by the degree of digital literacy of VR applying educators.

This paper proposes a model, expanding on previous academic work, to support education institutes in their VR selection process by addressing socio-economic, infrastructural and narrative considerations.

The authors argue, that the proposed model can find a wider application to the assessment of novel EdTech solutions in general.

7. Limitations.

Although the authors have undertaken all reasonable effort to avoid limitations, the following limitations are noted. Due to the authors' technology predisposition, a perspective bias cannot be excluded. Further, since this paper builds on qualitative, non-representative interviews, it requires further quantitative studies to support generalizations.

8. Areas for further research.

Four avenues for further research are identified. First, it is proposed to replicate this study quantitatively to verify findings representatively.

Second, it is proposed to do further fit studies of the proposed model for other technologies, such as Augmented Reality (AR).

Third, the authors propose to research how and when an application mass adoption tipping point emerges for novel EdTech. This is particularly relevant to understand how and when new learning environmental designs emerge to maximize the utility of a given technology.

Fourth, the authors encourage academics to research how the impact of VR as an EdTech solution can be linked to students' learning performance, as the ultimate measure of success, following the constructivist learning theory.

References

- [1] Helsel S. Virtual reality and education. *Educational Technology*. 1992 May 1;32(5):38-42.
- [2] McLellan H. Virtual realities. *Handbook of research for educational communications and technology*. 1996:457-87.
- [3] Youngblut C. Educational uses of virtual reality technology. INSTITUTE FOR DEFENSE ANALYSES ALEXANDRIA VA; 1998 Jan.

- [4] Nugroho KY. Constructivist Learning Paradigm as the Basis on Learning Model Development. *Journal of Education and Learning*. 2017;11(4):410-5.
- [5] Dede C. The evolution of constructivist learning environments: Immersion in distributed, virtual worlds. *Educational technology*. 1995 Sep 1;35(5):46-52.
- [6] Pantelidis VS. Reasons to use virtual reality in education and training courses and a model to determine when to use virtual reality. *Themes in Science and Technology Education*. 2010 Oct 29;2(1-2):59-70.
- [7] Halaweh M. Model of Emerging Technology Adoption (META): Virtual Reality as a Case Study. *Journal of Information & Knowledge Management*. 2019 Jun 30;18(02):1950020.
- [8] Walker M. Hype Cycle for Emerging Technologies, 2017. Available from: <https://www.gartner.com/en/documents/3768572/hype-cycle-for-emerging-technologies-2017> [Accessed 22 May 2020].
- [9] Costello K. Gartner Identifies Five Emerging Technology Trends That Will Blur the Lines Between Human and Machine. Available from: <https://www.gartner.com/en/newsroom/press-releases/2018-08-20-gartner-identifies-five-emerging-technology-trends-that-will-blur-the-lines-between-human-and-machine> [Accessed 22 May 2020]
- [10] De Quetteville H. Coronavirus is offering virtual reality a second life. Available from: <https://www.telegraph.co.uk/technology/2020/03/25/coronavirus-offering-virtual-reality-second-life/> [Accessed 22 May 2020].
- [11] Fink C. VR Takes The Stage As Conferences Cancel. Available from: <https://www.forbes.com/sites/charliefink/2020/03/11/vr-takes-the-stage-as-conferences-cancel/#555d59f11dbe> [Accessed 22 May 2020].
- [12] Murphy K. UNC students are learning in professor's new virtual reality classroom during pandemic. Available from: <https://www.newsobserver.com/news/local/education/article241677001.html> [Accessed 22 May 2020].
- [13] Immersive Learning News. Covid19 — Could Virtual Reality (VR) Solve the Ongoing Crisis in Education? Available from: <https://www.immersivelearning.news/2020/05/05/covid19-could-virtual-reality-vr-solve-the-ongoing-crisis-in-education/> [Accessed 22 May 2020].
- [14] Caffrey M. Is virtual reality the future of online learning? A Temple professor is giving it a try. Available from: <https://www.bizjournals.com/philadelphia/news/2020/03/19/is-virtual-reality-the-future-of-online-learning-a.html> [Accessed 22 May 2020].
- [15] Low ML. Get connected: What to expect from edu-tech in the classroom this year. *Education Technology Solutions*. 2018 Feb(82):60.
- [16] Zender R, Knott AH, Fischer MH, Lucke U. Potentials of Virtual Reality as an Instrument for Research and Education. *i-com*. 2019 Apr 26;18(1):3-15.
- [17] Lei, X., Zhang, A., Wang, B., & Rau, P. L. P. (2018, July). Can Virtual Reality Help Children Learn Mathematics Better? The Application of VR Headset in Children's Discipline Education. In International Conference on Cross-Cultural Design (pp. 60-69). Springer, Cham.
- [18] Collins J, Regenbrecht H, Lanalotz T. Back to the Future: Constructivist Learning in Virtual Reality. In 2018 IEEE International Symposium on Mixed and Augmented Reality Adjunct (ISMAR-Adjunct) 2018 Oct 16 (pp. 45-46). IEEE.
- [19] Hu-Au E, Lee JJ. Virtual reality in education: a tool for learning in the experience age. *International Journal of Innovation in Education*. 2017;4(4):215-26.
- [20] InstaVR. InstaVR Interviews: Meet the VR Practitioners. Available from: <https://www.instavr.co/articles/general/instavr-interviews-dr-dean-whitcombe-university-of-south-wales> [Accessed 22 May 2020].
- [21] Russell D. Virtual reality in the classroom. Available from: <https://www.teachermagazine.com.au/articles/virtual-reality-in-the-classroom> [Accessed 22 May 2020].
- [22] Charara S. Over two million school kids have gone on Google Expeditions. Available from: <https://www.wearable.com/vr/expeditions-two-million-cardboard-6665> [accessed 22 May2020].
- [23] De la Cruz D. How to Choose Colleges With Virtual Tours. Available from: <https://www.nytimes.com/2020/04/30/well/family/coronavirus-virtual-college-tours.html> [accessed 22 May2020].
- [24] Schnell S. Unreal: Virtual reality is changing how college football teams train, recruit. Available from: <https://www.si.com/college/2015/08/05/college-football-virtual-reality-michigan-stanford-recruiting> [accessed 22 May2020].
- [25] Charles P. 'VR Chat' Used to Deliver One of the First University Lectures in Virtual Reality. Available from: <https://www.roadtovr.com/vr-chat-helps-deliver-first-virtual-university-lecture/> [accessed 22 May2020].
- [26] NSW Gov. Virtual reality immersion experiences. Available from: <https://education.nsw.gov.au/teaching-and-learning/school-learning-environments-and-change/virtual-reality-immersion-experiences> [accessed 22 May2020].

- [27] Groves MM, Zemel PC. Instructional technology adoption in higher education: An action research case study. *International Journal of Instructional Media*. 2000;27(1):57.
- [28] Hedberg J, Alexander S. Virtual reality in education: Defining researchable issues. *Educational Media International*. 1994 Dec 1;31(4):214-20.
- [29] Freina L, Ott M. A literature review on immersive virtual reality in education: state of the art and perspectives. InThe International Scientific Conference eLearning and Software for Education 2015 Apr 23 (Vol. 1, No. 133, pp. 10-1007).
- [30] Liu D, Bhagat KK, Gao Y, Chang TW, Huang R. The potentials and trends of virtual reality in education. InVirtual, augmented, and mixed realities in education 2017 (pp. 105-130). Springer, Singapore.
- [31] Wasfy HM, Wasfy TM, Peters JM, Mahfouz RM. Virtual reality enhanced online learning environments as a substitute for classroom instruction. InASME 2011 International Design Engineering Technical Conferences and Computers and Information in Engineering Conference 2011 Jan 1 (pp. 1581-1588). American Society of Mechanical Engineers Digital Collection.
- [32] Roy E, Bakr MM, George R. The need for virtual reality simulators in dental education: A review. *The Saudi dental journal*. 2017 Apr 1;29(2):41-7.
- [33] Rach M, Scott R. The Use of Virtual Reality in Marketing: Exploring the Need for Technology and Language Adaptation to Create High Quality Immersive Experiences. InMarketing and Smart Technologies 2020 (pp. 67-77). Springer, Singapore.

Machine Learning and Statistical Analysis Techniques on Terrorism

Rajesh P^{a,1}, Babitha D^a, Mansoor Alam^b, Mansour Tahernezhadi^b, Monika A^c

^a*K L University, India*

^b*Northern Illinois University, United States*

^c*Sanjivani College of Engineering, Kopargaon*

Abstract. Terrorism is a major issue facing the world today. It has negative impact on the economy of the nation suffering terrorist attacks from which it takes years to recover. Many developing countries are facing threats from terrorist groups and organizations. This paper examines various terrorist factors using data mining from the historical data to predict the terrorist groups most likely to attack a nation. In this paper we focus on sampled data primarily from India for the past two decades and also consider International database. To create meaningful insights, data mining, machine learning techniques and algorithms such as Decision Tree, Naïve Bayes, Support Vector Machine, Ensemble methods, Random Forest Classification are implemented to analyze comparative based classification results. Patterns and predictions are represented in the form of visualizations with the help of Python and Jupyter Notebook. This analysis will help to take appropriate preventive measures to stop Terrorism attacks and to increase investments, to grow the economy and tourism.

Keywords. Data Mining, Classification, Global Terrorism Database (GTD), Machine Learning.

1. Introduction

Terrorism has become a relatively influential factor in the International Politics. A major terrorist cause is an aggrieved organization that resorts to violence for various factors such as political, cultural, religious, etc. This research focuses on the global spread of terrorism as well as in India in the last two decades. From the literature review, it is identified that there are several statistical analyses performed on terrorism database.

Due to terrorism, common people are getting fear, nervousness, and ambiguity on maximum scale of community rather than single individual. According to Statistics on GTD database, 2019 contains 1411 various terrorist attacks have occurred, causing 6362 fatalities, deftly disturbing quality of life of human individuals in society. It is similarly important to understand statics, analyzing terrorist events data, to create awareness, to assist kind of people, take preventive measures not occurring those events in future.

Terrorism attacks has been considered major impact among all nations for decades to identify factors reason to perform of terrorism or to carry out counterterrorism, social

¹ Corresponding Author: RAJESH P, K L University, India. Email: rajesh.pleti@gmail.com

and fiscal effects of terrorism. Due to terrorism complexity of problem in nature, it is difficult to find efficient solution to protect lives of individuals. Classification of terrorist philosophy, forecast of future terrorist attacks have been demonstrated to be of immense importance, time consuming process. We tried to identify interesting insights using machine learning algorithms on GTD database.

This paper is set out as follows. Section 2 illustrates literature review. The pre-processing performed on the Global Terrorism Database, feature selection, analytical tool used for the data mining and the software used for the study was described in detail in Section 3. Section 4 provides a detailed description of results and experimental analysis exploits machine learning algorithms such as Decision Tree, Naïve Bayes, Support Vector Machine and Random Forest Classification to build a classification model. Finally, Section 5 summarizes the insight research findings and future works.

Terrorist attacks got mainly significant imperative issue to all humankind in the world. These kind attacks are more in developing countries like India, Middle East, North Africa, and South Asia. This paper describes insight hidden patterns using machine learning algorithms in GTD Database and how it has grown over time of decades, social impacts, growth of economy and impacts on tourism, and to take proper preventive measures to eradicate the terrorism. It also predicts the region, country, number of terrorist attacks by machine learning approaches.

The Objectives of this paper can be described as follows.

- To perform statistical data analysis on the GTD data to obtain hidden pattern and insights.
- To identify the most terror-prone regions and the weapons mostly used for attack in both India and around the world.
- To identify the most targeted sector and the topmost victim regions in India and the major radical groups behind those attacks in the last two decades.
- To perform several classification techniques for predicting the success or failure of the terrorist attack based on its type and the weapon used for attack.

From the above objectives we can identify a goal of recognizing the patterns and success rate of occurrence of terrorist incidents. These kinds of insight patterns are useful in providing the following benefits.

- To take proper preventive measures to eradicate the terrorism.
- To increase the foreign investments by making the country safe and secure.
- It promotes the growth of economy and develops the tourism.

2. Literature Review

M. Khalifa et. al, presents "Terrorist attacks got mainly significant imperative issue to all humankind in the world". It also employed statistical techniques and association mining algorithms applied to terrorism attacks to identify frequent invisible patterns in database [1].

J. V. Pagán described three classification algorithms (K-Nearest Neighbor, Discriminant Analysis, and Recursive Partitioning) of terrorist attacks database and reduces classification error rate [2].

S. Ray provides Artificial Intelligence has major attention in digital area and described machine learning algorithms merits, demerits of application perception to make decision in selecting suitable learning algorithm to meet explicit requirement of application [3].

K. P. Shroff and H. H. Maheta incorporated comparative study on machine learning classification algorithms performance based on feature selection in high dimensional data [4].

Tarik A. Rashid et. al, presented attack user behaviors of the wicked web mining systems and employed possible solutions for securing web users, organizations, society to prevent attacks. Naïve Bayes approach (NB) and K-Nearest Neighbor (K-NN) algorithms are incorporated to detect terrorist threats in web mining-based approaches [5].

Tarik A. Rashid and Salwa Mohamad described the detection of wicked internet user behaviors in internet forums, Wi-Fi, websites, email accounts, Facebook, etc, using machine learning techniques Random Forest (RF) and Support Vector Machines (SVM) methods [6].

Enrique Lee Huamaní and Alva Mantari, incorporated Terrorist attacks influence confidence, security of citizens, destruction of order and as increase of social networks, terrorist attacks in global are also ongoing. Author employed Artificial Intelligence techniques and classification models to visualize and predict possible terrorist attacks [7].

M. Irfan Uddin and Nazir Zada, address Terrorist Activities and their consequences suppressed physically, emotionally. Five different models on deep neural network (DNN) are incorporated to understand behavior of terrorist activities and presented analytical based results [8].

V. Kumar, M. Mazzara, A. Messina, focused on data mining classification methods and the part of United Nations counterterrorism. It analyzes performance of classifiers (Multilayer Perceptron, Lazy Tree, Naïve Bayes, Multiclass) for detection of trends in terrorist attacks world GTD database [9].

N. Ouassini and A. Verma illustrated association between social, economic, and demographic indices and left-wing intolerance in state of Jharkhand in India [10].

R. Alhamdani, M. Abdullah, exploits deep learning techniques to identify the terrorist attacks behavior and distribution online misinformation using different forms of social media by employing global terrorist database [11].

3. Dataset

The Global Terrorism Database (GTD) [12] is an open-source database from 1970 to 2017, with information on terrorist events around the world. This includes about 1,81,691 terrorist attacks for each scenario, with 135 categories, making it the most detailed unclassified data based on terrorist events in the world. For each terrorist event, the information about the date, location, attack, weapon, target/victim, and perpetrator (the group which carried out the attack) etc. are provided. In this study, we performed analysis on the GTD data during the time 2000 to 2017 [13],[14].

The GTD data was collected from different resources which would cause data inconsistency. Another problem is missing data values which if unhandled causes distortion in the analysis. Therefore, the pre-processing techniques like feature selection, treating the missing values and null values, normalizing the values are

performed to accomplish good analysis. Out of 135 attributes in the original dataset, by performing the Data reduction [15],[16], we selected the features relevant to our study which are described in the Table 1.

Table 1. Selected Attributes for Analysis

Attribute	Description
eventid	ID allotted to the incident occurred.
iyear, imonth, iday	The year, month, and day the incident occurred.
country_txt, provstate, city	Country name, state, city where the incident took place.
latitude, longitude	Location details of the place where the incident occurred.
attacktype1_txt	Type of the attack occurred.
success	Whether the incident was successful.
weaptype1_txt,	Type and subtype of the weapons used in the attack.
weapsubtype1_txt	Information about the type of weapon used in the attack.
weapdetail	
targtype1_txt, targsubtype1_txt	Type and subtype of the target/victim of the attack.
gname	Name of the group that carried out the attack.
nkill, nwound	Number of confirmed fatalities and non-fatal injuries of the incident.

The missing values and the instances with value as unknown of the attribute ‘gname’ have been removed as it is of no use to the analysis if the radical group responsible to the attack is not known. Similarly, the null values in the attributes ‘nkill’, ‘nwound’ have been replaced by the value 0 since we must perform aggregation function on the attribute values. The data is now preprocessed and ready to use for data mining [17],[18].

GTD data extracted for was checked and numerically coded using the Python programming language. The analysis was done purely python based in the Jupyter Notebook. Jupyter notebook is open-source software to perform programming and it is an interactive computational environment. The entire data is split into two sets to construct a classifier model: training data with 80% and testing data with 20% of the dataset [19],[20].

4. Experimental Methodology

In this paper, we conduct the experiments to test the performance of different machine learning models to identify the most suitable algorithm for the GTD database and to identify the interesting insights of the results. Classification models are built using such algorithms as Decision Tree, Naïve Bayes, Support Vector Machine. Naive Bayes belongs to the Bayes family as a probabilistic classifier. Decision Tree induction is an algorithm for the top-down recursive induction of tree [21],[22]. Support Vector Machine transforms the original training data into a higher dimension using a non-linear mapping to figure out the best separating hyper plane.

The classifier's accuracy can be further improved with the use of ensemble approaches such as the Random Forest Classifier. Ensemble Approach is a machine learning method to improve accuracy by studying a series of individual (base) classifier models and integrating them. The performance of the ensemble methods is compared with the base classifier models[23],[24]. To estimate the performance of the classifiers, evaluation metrics like accuracy score, f-measure, Jaccard similarity index, ROC curve are applied on the models developed to find the model with good accuracy [25].

In this section, first we discuss about the visualization of several statistical insights derived and then about the different classifier models developed and their accuracy results.

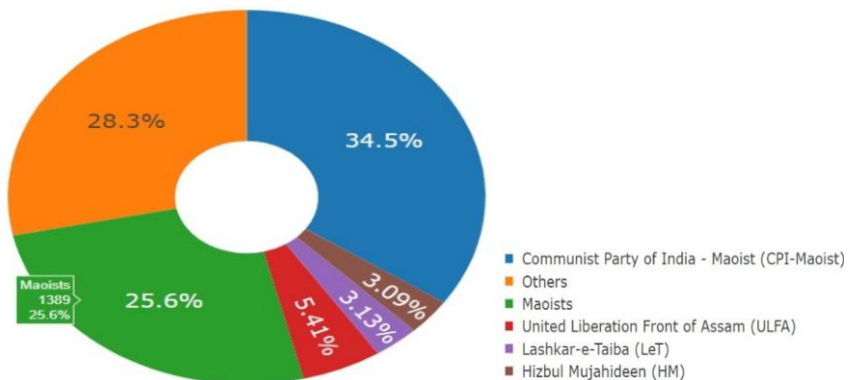


Figure 1. Donut chart showing major radical groups in India.

The donut chart in Figure 1 shows the major radical groups who contributed highest frequency attacks in India. It is evident that highest number of terrorist attacks are done by CPI-Maoist group. In India, most of the terrorist attacks are done by the domestic radical groups compared to the International Terrorist Organizations.

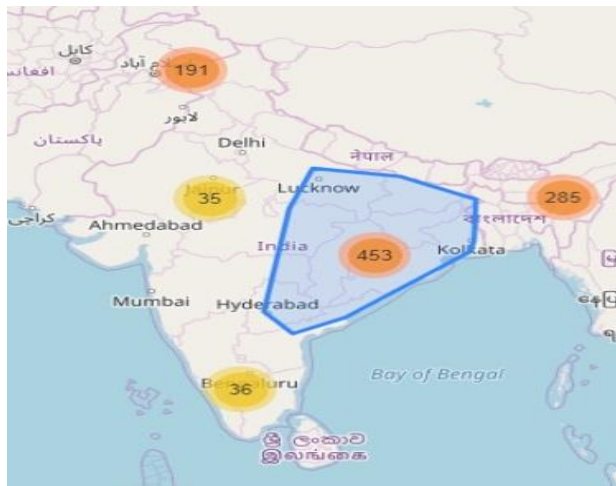


Figure 2. Map view of terrorist attacks in India.

The map in Figure 2 shows that based on several features like the type of attack and the number of fatalities, the data points can be partitioned into several clusters.

Each cluster can be further divided into several sub-clusters. The location details and the number of attacks on each city can be identified; thereby counter measures can be taken to concentrate on the most targeted areas. From the analysis, it is evident that the Middle East region of India is highly prone to terrorist attacks.

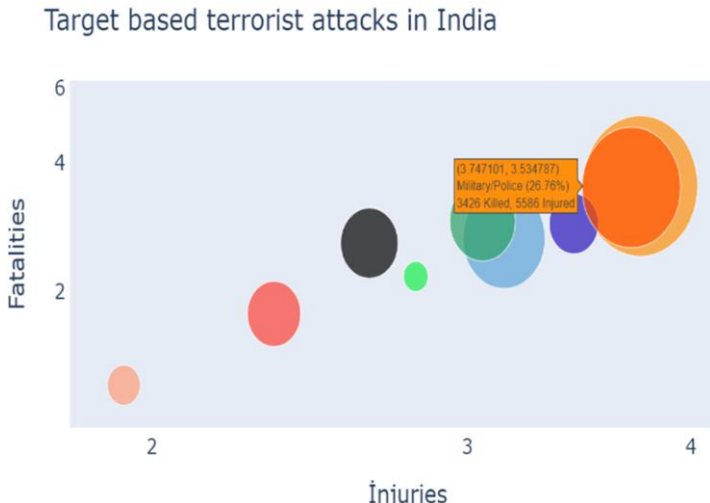


Figure 3. Scatter plot showing target-based attacks in India.

The scatter plot generated as in Figure 3 reveals the hidden information that Military is targeted the most in India with about 27% of all the attacks i.e., 3426 people were killed, and 5586 people were injured. Both the fatalities and injuries are comparatively higher in Military because of the terrorist attacks. Even the Education sector is relatively affected by the terrorism.

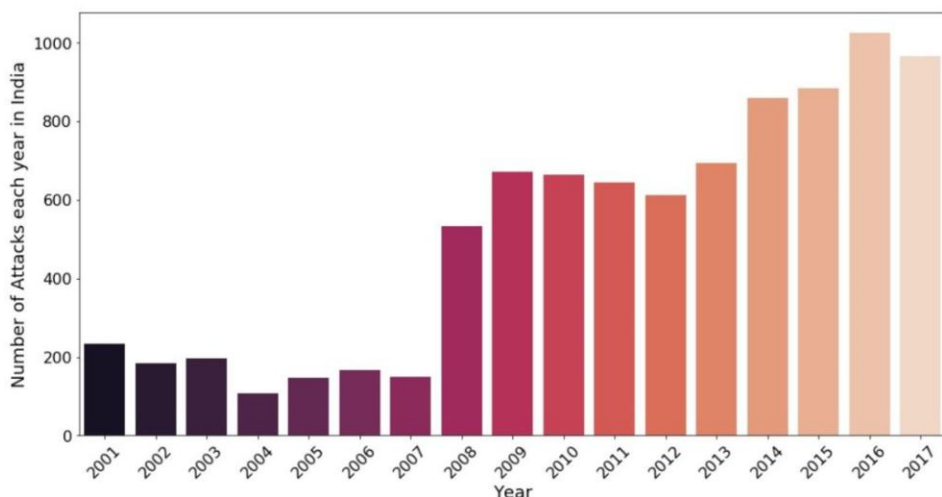


Figure 4. Histogram showing the number of attacks in India.

The histogram plotted in Figure 4 indicates how many terrorist attacks have been committed in India in the last two decades. The rate of attacks gradually increased from the year 2012. However, the attacks occurrence may either be successful or failure.

The Tree map in Figure 5 depicts the top 10 victim regions in India. Out of all the regions in India, terrorist attacks are more frequent in Imphal (34.04%) and Srinagar (22.84%) contributing a major share of greater than 50% out of all the attacks in India.



Figure 5. Tree Map showing the Top 10 victim regions in India.

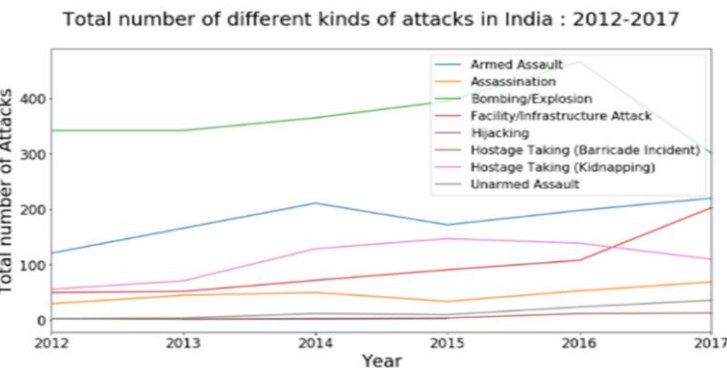


Figure 6. Time-Series graph showing different kinds of attacks in India.

The time-series graph in Figure 6 shows the total number of different types of attacks in India from 2012 to 2017. It shows that Bombing/Explosion is the most frequent method of attack implemented by terrorists in all the years.

The word cloud in Figure 7 shows the states which are highly prone to terrorist attacks. Further protection must be established for Jammu and Kashmir out of all states to prevent terrorist attacks.



Figure 7. Word Cloud showing the states which are mostly attacked.

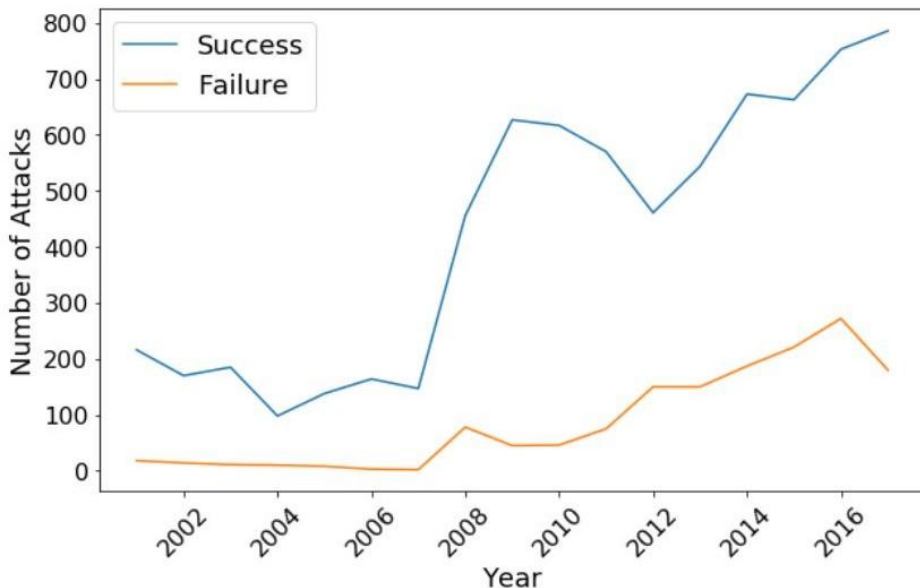


Figure 8. Time-Series graph showing the number of successful and failure events.

Attacks planned by terrorists may either become successful or failure. The time-series graph in Figure 8 describes the summary of the attack's success vs failure during the period 2000 to 2017. This graph depicts that the number of successful attacks increased gradually from the year 2012. Terrorism has seen a drastic increase in the year 2009 when compared to the number of attacks in the year 2007.

The word cloud generated in Figure 9 highlights the most frequent word vocabulary of weapons used for attack in India. Out of all the weapons, explosives, and firearms (portable guns) are used the most in India.



Figure 9. Word Cloud showing the Weapons used for attack.

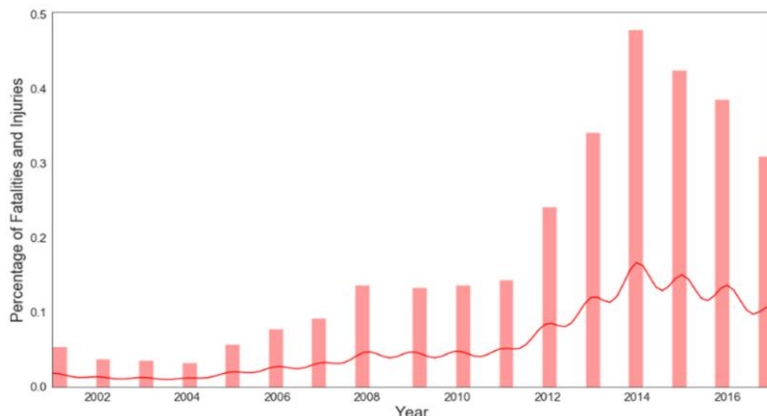


Figure 10. Dist. Plot showing the percentage of fatalities and injuries.

The seaborn dist. plot in Figure 10 shows the density distribution of the total percentage of fatalities and injuries during the time period 2000-2017. It is evident that in the year 2014, the fatalities and injuries are high compared to other years.

Table 2. Classifier Models and Evaluation results

Algorithm	Accuracy Score	F1 Score	Jaccard Similarity
Naive Bayes	0.410755	0.45617	0.410755
Random Forest	0.837529	0.91080	0.837529
Decision tree	0.836957	0.91085	0.836957
SVC	0.834668	0.90988	0.834668

The dataset is divided into training set and test set in the 80:20 split ratio to implement the classification algorithm. The GTD incident is graded into either success or failure based on the type of attack that occurred, and the type of weapon used for the attack. The Table 2 shows the detailed results of the classification algorithms applied. Out of all the individual classifier models developed, Decision Tree Classifier gives the good accuracy. To improve the classification accuracy, ensemble methods like Random Forests classifier is build.

In addition to the standard evaluation metrics applied, ROC curve serves as the metric which can determine the good classifier. Of all the classifiers applied, Random Forest Classifier is the better one as shown in the Figure 11.

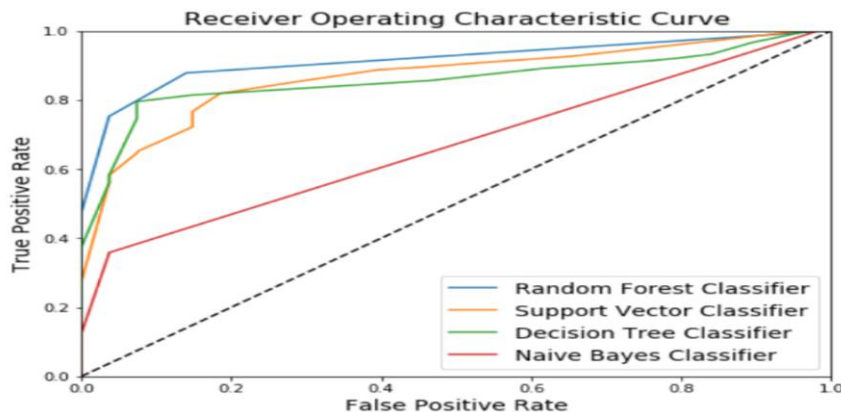


Figure 11. ROC curve showing the accuracy of Classification models.

Several metrics can be calculated from the confusion matrix like the accuracy, sensitivity, and precision etc. The Figure 12 shows the confusion matrix plotted for the Random Forest Classifier.

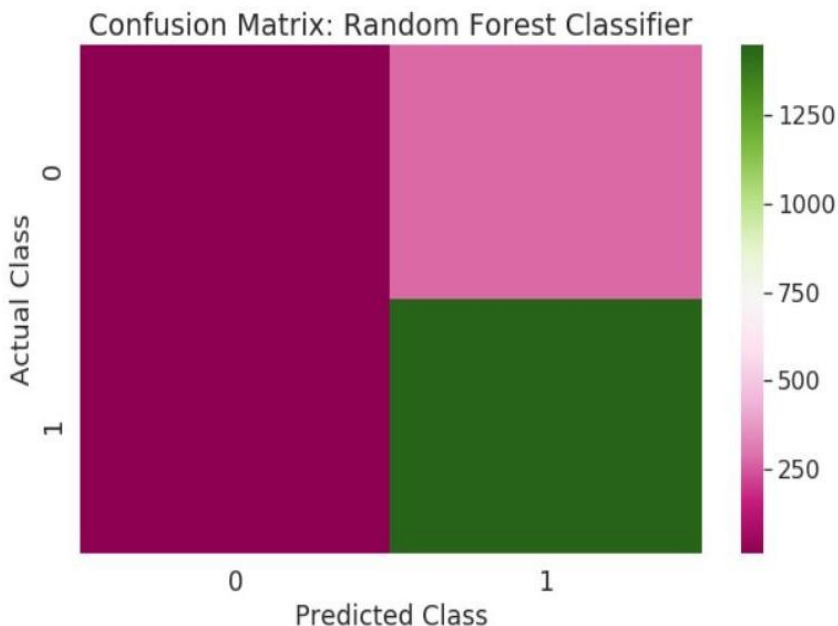


Figure 12. Confusion Matrix of Random Forest Classifier.

The time-series graph in Figure 13 plots the total number of different types of attacks in the world from 2011 to 2017. It shows that Bombing/Explosion is the most frequent method of attack implemented by terrorists in all the years.

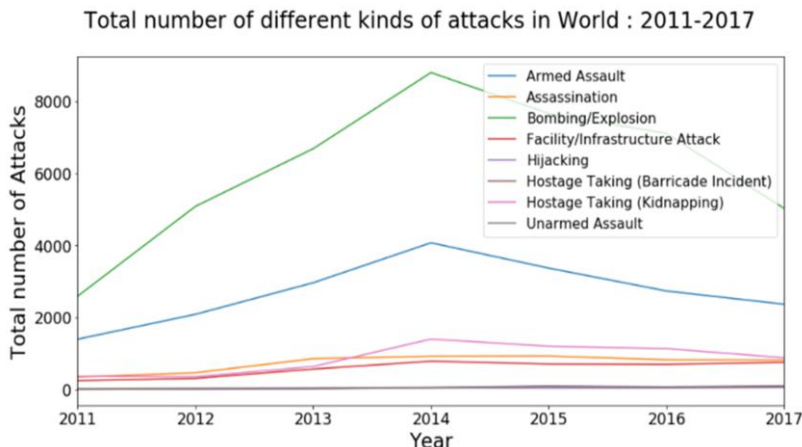


Figure 13. Time-Series graph showing different kinds of attacks in the world.

The map in Figure 14 shows that based on several features like the type of attack and the number of fatalities, the data points can be partitioned into several clusters. Each cluster can be further divided into several sub-clusters. The location details and the number of attacks on each city can be identified; thereby counter measures can be taken to concentrate on the most targeted areas. From the analysis, it is evident that the South-west-Asian region is highly prone to terrorist attacks.

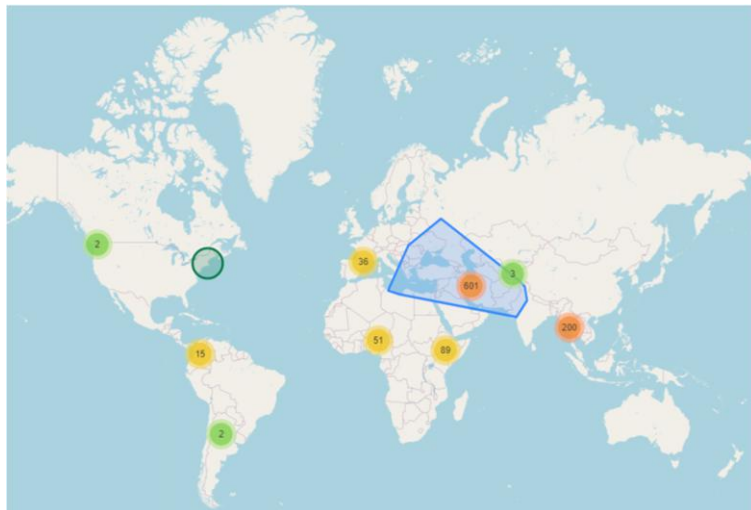


Figure 14. Map view of terrorist attacks in the world.

The scatter plot in Figure 15 reveals the hidden information that Military is targeted the most in the world. Both the fatalities and injuries are comparatively higher in Military because of the terrorist attacks. Even the Education sector is relatively affected by the terrorism.

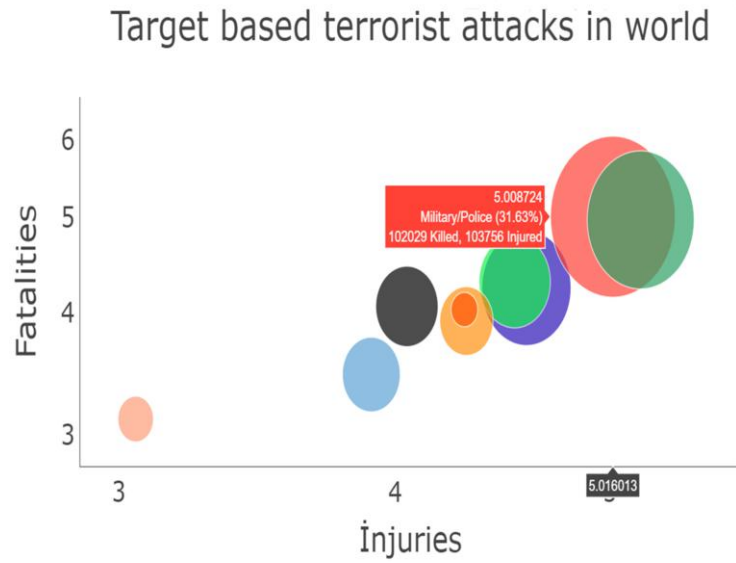


Figure 15. Scatter plot showing target-based attacks in the World.

5. Conclusion and Future Scope

This article has addressed both the worldwide and India's statistical perspectives on terrorism. To develop a model best suited for data analysis, many machine learning algorithms were applied to the GTD data. Classification models such as Decision Tree, Naive Bayes, Random Forest, Support Vector Machine are created. Model evaluation metrics like accuracy score, f-measure, Jaccard similarity index, ROC curve was applied to find the model with good accuracy. The results show that, among all the models, Random Forest Classification algorithm had the highest possible accuracy.

The study disclosed the top 10 victim regions of terrorism in India and predicted the count of fatalities and injuries based on target. The study also revealed the major radical groups responsible for the most frequent attacks in India and identified which states are mostly likely to be attacked. The experimental results suggest that the spread of terrorism in India is mostly due to extreme domestic groups compared with external threats.

An additional direction, innovative based AI solutions can be incorporated by utilizing the comparative based analytical results for progressing future enhancements for decision making on different data sets by considering other aspects like injuries, GPS data, spatial-temporal , video surveillance performance extraction and trajectories data.

References

- [1] Khalifa NEM, Taha MHN, Taha SHN, Hassanien AE. Statistical Insights and Association Mining for Terrorist Attacks in Egypt. In The International Conference on Advanced Machine Learning Technologies and Applications (AMLTA2019) Advances in Intelligent Systems and Computing. 2020, 921: 291-300.
- [2] Pagán JV. Improving the classification of terrorist attacks a study on data pre-processing for mining the Global Terrorism Database. In 2nd International Conference on Software Technology and Engineering, 2010 San Juan, 110:104.
- [3] Ray S. A Quick Review of Machine Learning Algorithms. In International Conference on Machine Learning, Big Data Cloud and Parallel Computing, 2019 Faridabad, p. 35- 39.
- [4] Shroff KP, Maheta HH. A comparative study of various feature selection techniques in highdimensional data set to improve classification accuracy. In International Conference on Computer Communication and Informatics (ICCCI), 2015 Coimbatore, p. 1-6.
- [5] Rashid TA, Rashad DD, Gaznai HM, Shamsaldin AS. A Systematic Web Mining Based Approach for Forecasting Terrorism. In Communications in Computer and Information Science. 2017, Singapore, 752 .
- [6] Rashid TA., Mohamad SO. Enhancement of Detecting Wicked Website Through Intelligent Methods. In Security in Computing and Communications. SSCC 2016 Singapore, 62.
- [7] Enrique Lee H, Alva Mantari A. Machine Learning Techniques to Visualize and Predict Terrorist Attacks Worldwide using the Global Terrorism Database. International Journal of Advanced Computer Science and Applications , 2020 11(4).
- [8] Irfan Uddin M, Nazir Zada. Prediction of Future Terrorist Activities Using Deep Neural Networks. Hindawi Complexity 2020, 20.
- [9] Kumar V, Mazzara M, Messina A, Lee J. A conjoint application of data mining techniques for analysis of global terrorist attacks prevention and prediction for combating terrorism. Advances in Intelligent Systems and Computing, 2019, Berlin, Germany. p.146-158.
- [10] Ouassini N, Verma A. Socio economic inequality or demographic conditions a micro-level analysis of terrorism in Jharkhand.In Journal of Victimology and Victim Justice, 2018, 1(1), p. 63–84.
- [11] Alhamdani R, Abdulla M, Sattar I. Recommender system for global terrorist database based on deep learning. In International Journal of Machine Learning and Computing, 2018, 8, p. 571–576.
- [12] Global Terrorism Database (GTD) <https://www.kaggle.com/START-UMD/gtd>, <https://ourworldindata.org/terrorism>.
- [13] Ben Meskina S. On the effect of data reduction on classification accuracy. In 3rd International Conference on Information Technology and e-Services (ICITEs), 2013 p.1-7.
- [14] Tripathi A, Yadav S, Rajan R. Naive Bayes Classification Model for the Student Performance Prediction. In 2nd International Conference on Intelligent Computing, Instrumentation and Control Technologies (ICICICT) 2019 Kerala, India,p. 1548-1553.
- [15] Rajesh P, Sai Prasanna. A Forensic Approach to Perform Android Device Analysis. In International Women Conference on Technological Innovations. 2019 (7).
- [16] Diao R. Decision Tree-Based Online Voltage Security Assessment Using PMU Measurements. In IEEE Transactions on Power Systems 2009 24(2), p.832-839.
- [17] Suriya Prakash J, Annamalai Vignesh K, Ashok C, Adithyan R. Multi class Support Vector Machines classifier for machine vision application. In International Conference on Machine Vision and Image Processing (MVIP) 2012 Taipei,p. 197-199.
- [18] Rajesh P, Narsimha G. Cerebration Of Privacy Preserving Data Mining Algorithms. International conference on machine learning and data analysis ICMLDA 2014 (2) USA,P:813-817.
- [19] Hasan MK, Alam MA, Das D, Hossain E, Hasan M. Diabetes Prediction Using Ensembling of Different Machine Learning Classifiers. In IEEE Access 2020 (8), p. 76516-7653.
- [20] Huang J, Ling CX. Using AUC and accuracy in evaluating learning algorithms. In IEEE Transactions on Knowledge and Data Engineering 2005 17(3), p.299-310.
- [21] Mrunal k, srinivasu N. support value based fusion matching using iris and sclera features for person authentication in unconstrained environment. In Journal of Engineering Science and Technology 2020 15(4):p. 2595 - 2609.
- [22] Ismail B, Rajesh P. A Machine Learning Classification Technique for Predicting Prostate Cancer.In 20th Annual IEEE International Conference on Electro Information Technology Eit2020 USA.
- [23] Rajesh P, Alam M. A Data Science Approach to Football Team Player Selection. In 20th Annual IEEE International Conference on Electro Information Technology EIT 2020 USA.
- [24] Rajesh P, Narsimha G. Cerebration Of Privacy Preserving Data Mining Algorithms. In International conference on machine learning and data analysis ICMLDA_ 2014 USA.
- [25] Ranjeeth M, Srinivasu N. DES secured k-NN query over secure data in clouds. In Journal of Theoretical and Applied Information Technology 2016. 91(2), p.384-389.

Analysis of the Legal Basis to Mitigate Cyberbullying in Social Networks in Ecuador

Segundo Moisés Toapanta Toapanta^{a,*}, Ingrid Lilibeth Tacuri López^a, Luis Enrique Mafla Gallegos^b

^a*Department Computer Science, Salesian Polytechnic University of Ecuador (UPS), Chambers 227 and June 5, Ecuador*

^b*Faculty of Systems Engineering, National Polytechnic School (EPN), Ladrón de Guevara E11-253, Ecuador*

Abstract. Cyberbullying is a critical issue in society worldwide, however in Ecuador is not given necessary importance to mitigate this cybercrime. It has been proposed to develop an exhaustive analysis of the laws that are currently considered to sanction cyberbullying when denouncing this fact. The deductive method and exploratory research were employed to make the analysis of the information consulted from the various sources that are obtained on the network about the topic discussed. The investigation revealed how cyberbullying cases arise, from which it is obtained that only 0.07% have been reported, with this result it can be deduced that the number of reported cases is very low in relation to the total number of cellphones activated in Ecuador and people who may be victims of this cyber-crime. In addition, a “Criminal Process Diagram” was obtained that determines the sequence of how the judicial process work. The applied method resulted the following: Can be created a law project that battles each type of derived cyberbullying. It was concluded that several institutions in Ecuador work together with organizations to prevent cyberbullying, however, when this happens, the laws are not enough to punish the act.

Keywords. Cyberbullying, risk, social networks, laws, mitigation.

1. Introduction

Digital bullying includes bullying through instant messaging, postings, emails, SMS or creating a website that makes fun of someone through images; also refers to being treated in a hurtful or unpleasant way via mobile phones or online; as well as the appropriation and publication of inappropriate or unflattering photographs [1].

Although social networking websites provide many benefit to users, cyber criminals can use these websites to commit different types of bad behavior and/or aggressive behavior [2], take advantage of the opportunities offered by the information revolution and social networks to communicate and engage in illegal underground activities, such as online fraud, cyberpredation, cyberbullying [3].

* Corresponding Author: Segundo Moisés Toapanta Toapanta,
E-mail: stoapanta@ups.edu.ec

Taking advantage of the accelerated advance of information and communication technologies (ICT), cyberbullying is presented, which is the harassment that a person suffers through messages, photographs, memes, through social networks such as Facebook, Whatsapp, Twitter, Snapchat, becoming viral, every time it reaches a user, multiplying also, the psychological damages that this type of violence causes, that have been the cause of negative effects such as: low self-esteem, poor academic performance, exclusion, depression, and until the victim's death [4].

According to United Nations Children's Fund (UNICEF), more than 175,000 children connect to the Internet every day for the first time, one new child every half-second, becoming the most vulnerable to a range of risks and damages, "including access to harmful content, sexual exploitation and abuse, cyberbullying and misuse of their private information" [5]. The experts say that young people end up feeling the real impact when photographs and online rumors about them spread at their social environment [6].

This starts primarily because people currently have no control over what is posted on the net, most teens post on their social media photos with implicit information that cyber criminals use to stalk virtually, Even parents with no intention of causing discomfort in their children publicly share photos and videos that can generate being targeted by these social attacks. The Internet is within the reach of children and they curiously navigate the Web without limit finding platforms disguised as games that invite them to exchange sensitive information or photos to get a reward or to raise a level in the game turns into manipulation.

How is cyberbullying mitigated on Social Networks in Ecuador?

It's important to reduce the risk of tolerating the different types of harassment that occur via the Internet, for which several public and private companies/organizations have collaborated together through social media campaigns, TV, schools and colleges to prevent more people, mainly children, from falling victim to this social harassment. Internet and social media networks such as Facebook and Twitter have recently made policy and privacy changes to ensure safe user experience. However, the effectiveness of these tools and efforts in curbing abuse and cyberbullying needs constant monitoring and research [7].

Ecuador has laws that contain two articles that were adapt to the crime and allow a complete investigation of cyber bullying so that appropriate measures can be taken in response to this offense. These articles correspond to 173 and 174 stipulated in the Comprehensive Organic Criminal Code (COIP) that contains the existing legislation to protect the rights of individuals and among other articles and news that will be analyzed in the development of this section as a current solution to mitigate the risks of information that freely provided through the internet.

The Government does not have a security policy that protects society from the problems brought about by the advance of technology, insecurity on social networks is becoming more evident, users are easy prey and information can be vulnerable to more constant risks. Public bodies must apply a model that mitigates risks and technological threat and that has a vision of the future of data protection [8].

The information and articles reviewed are:

El ciberacoso es un problema en crecimiento que afecta hasta 1 de cada 10 niños en el mundo [1], Predicting Cyberbullying on Social Media in the Big Data Era Using Machine Learning Algorithms: Review of Literature and Open Challenges [2], Wordnet-Based Criminal Networks Mining for Cybercrime Investigation [3], Cyberbullying: una realidad de intimidación en las unidades [4], Telefónica Movistar: La realidad del ciberacoso en Ecuador y cómo denunciarlo [5], Cómo prevenir el ciberacoso o

ciberbullying [6], Cyberbullying on social media platforms among university students in the United Arab Emirates [7], Impact on the Information Security Management due to the Use of Social Networks in a Public Organization in Ecuador [8], How students react to different cyberbullying events: Past experience, judgment, perceived seriousness, helping behavior and the effect of online disinhibition [9], Exposure to cyberbullying in WhatsApp classmates' groups and classroom climate as predictors of students' sense of belonging: A multi-level analysis of elementary, middle and high schools [10], Investigating the mechanisms of theory of planned behavior on Cyberbullying among Thai adolescents [11], Cyberbullying victimization at work: Social media identity bubble approach [12], Tecnologías de la Información y Comunicaciones [13], Ciberacoso, un dolor de cabeza para los padres [14], Moral disengagement and adolescents' cyberbullying perpetration: Student-student relationship and gender as moderators [15], National Institute of Statistics and Censuses (INEC) [16].

Exploratory research is used in different sources of information and the deductive method to analyze the information found.

It turns out that in Ecuador the laws condemn the fact of having a sexual encounter with a minor through some electronic means but not penalizing the crime of cyberbullying, which are different concepts, but when this happens the legal entities adapt these laws to punish this crime. For this, it is proposed to create a bill that includes articles that penalize the crime of cyberbullying in its different settings.

It can be concluded that the laws in Ecuador are not yet prepared to mitigate cases of cyberbullying in all its scenarios.

2. Materials and Methods

The exploratory research and deductive method used for the development of this article are selected to analyze the information found and obtain results.

2.1. Materials

A web research was carried out, news was consulted in newspapers, scientific journals, digital articles, theses, etc that make references to the topic in question. The information of articles consulted were the following:

Technology has gone considerably beyond the cultural boundaries of communication, has transcended in a globalized way and sometimes even aggressive or violent, we can visualize it online, this leads to the misuse of technology in social media platforms, for this reason it is a priority to review the improper use of users when consuming these sites [2]. A study was conducted through a web page with interviews voluntarily, anonymously and confidentially to evaluate the judgment, behavior and experience of students considering three scenarios: harassment, denigration and exclusion. Results varied by gender, boys were more likely to intimidate and girls recognized the behavior that causes bullying [9]. In Israel today, the most used application is Whatsapp, a large part of children and adolescents occupy this service to establish immediate communication and share content, Part of this content is used to harass another person through this same app and between groups of common friendships generating cyber bullying. This harassment is then taken to the real social environment and can seriously harm the victim [10]. Educational units have an important role in the cultural contribution of the technological development of their target groups so that they

are not victims of cyberbullying, promote clear objectives on the use of social networks that are increasingly used by minors by promoting practices of respect and solidarity, interactive talks among students about cyberbullying and thus prevent computer violence [4]. The behavior of users in the network has a major impact on the development of cyberbullying, so that this does not happen, the family structure is very determinant in this aspect to raise self-esteem, play a leading role and users do not easily descend into intimidation. This should include activities that raise the self-esteem of their leaders and can be managed in an efficient and appropriate manner [11].

In another scenario there is also exists cyberbullying at work that cyberbullying at work adopts aggressive and threatening behaviour including social ostracism. One study analyzed the risks and factors associated with cyberbullying at work, in addition to its impact on well-being. For the study they took surveys of employees of expert organizations and national samples. The results reveal that 13% and 17% respectively of the victims were young people and active users in the bubbles of identity, these showed greater psychological distress, exhaustion and technical stress [12].

Cyberbullying is a type of violence in which people who commit bullying cannot be detected, or whether it is an act of an individual or a group of individuals cannot be determined [11]. Online social networks provide offenders with tools for aggressive actions and networks for committing misconduct. Therefore, methods addressing both aspects (content and network) should be optimized to detect and limit aggressive behavior in complex systems [2].

In Ecuador, there are no exact figures for cyberbullying because the majority of people who are victims of this crime do not report to the Office of the Public Prosecutor, However, United Nations Children's Fund (UNICEF) conducted the NATIONAL SCHOOL BULLYING SURVEY of different groups of people in 2019 to ascertain the status of this problem. From the results of this survey we have obtained data that are relevant to continue the analysis of this topic represented in the following graph:

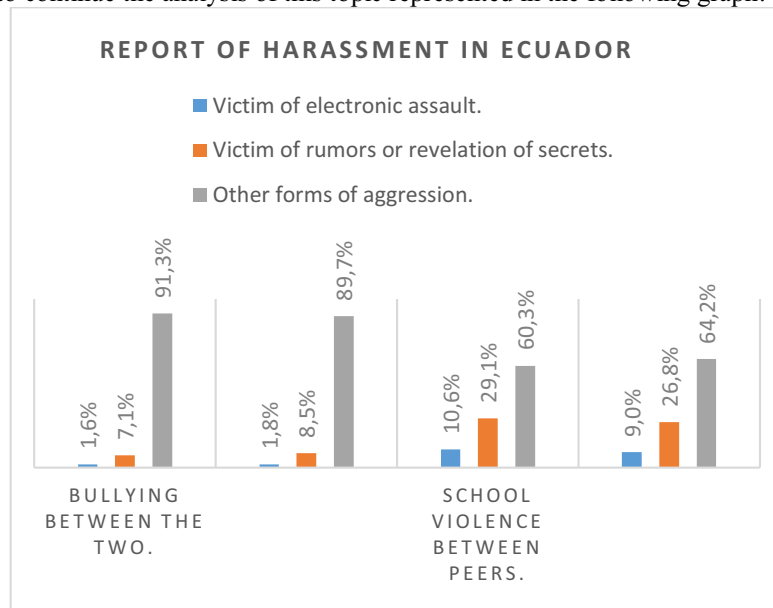


Figure 1. Report on bullying in Ecuador. United Nations Children's Fund (Unicef) – Results of the National Survey of School Bullying in 2020.

National figures published on the page of the National Institute of Statistics and Censuses (INEC) are also analyzed with information related to the subject in question where the percentage of the population that uses the cell phone and social networks can be seen, as well as figures based on the report "Ecuador Digital State" that correspond to the number of users per social network.

The Organic Law for the Prevention, Control and Punishment of Harassment, Intimidation or Violence in the Study Centers of Ecuador (Bullying) was considered to mitigate cyberbullying in social networks.

In Art. 173 and Art. 174 of the Comprehensive Organic Criminal Code (COIP) refer to acts of a sexual nature committed through electronic means, which are punished only when the victims are minors. However, consideration must be given to persons over the age of 18 who are not exempt from such behavior, and who today have been victimized by the commission of such acts and the lack of regulations.

2.2. Methods

Three phases were used to analyze this topic.

The first phase included searching for information in digital newspapers in Ecuador, databases of scientific journals and conference articles indexed to Scopus because it is the database with the largest collection of articles worldwide.

In the second phase we take information in figures that we find in digital newspapers and institutions such as National Statistics and Census Institute (INEC) of people who use the internet, social networks in Ecuador to make a statistical analysis of the current situation, in addition, to the most frequent forms of aggression in the country to focus on aggression by electronic means. Additionally, information related with this topic at the international level was considered for be able to compare the problematic.

The third phase consisted of seeking information on how this fact is mitigated in Ecuador.

To begin our statistical analysis, first analyzed the groups of people who use the internet with the following information provided by National Statistics and Census Institute (INEC) of Ecuador, this institution is the charged of analyzing economic, sociodemographic, and environmental data generated by the obtaining information through censuses, population surveys, and data from other institutions for decision-making in the country through the National Statistical System (SEN):

In addition, until December 2017 the percentage of people who used the internet according to ages are: from 5 to 15 years old is 50.4%; from 16 to 24 years old is 85.2%; from 25 to 34 years old is 73.9%; from 35 to 44 years old is 59.6%; from 45 to 54 years old is 44.0%; from 55 to 64 years old is 27.2%; 65 years old or older is 7.8%. 74.7% of Ecuadorians used the internet for less than once a day [13]. It was deduced that more than 59% of Ecuadorians between 16 and 44 years old accessed and continuously used the internet to obtain information, general communication, education, learning and others [8].

The use of social networks in Ecuador was then analyzed, this analysis was obtained from the figures presented by National Statistics and Census Institute (INEC) on its website. These graphs helped us to know basic and important information to continue with the development of the topic of this article.

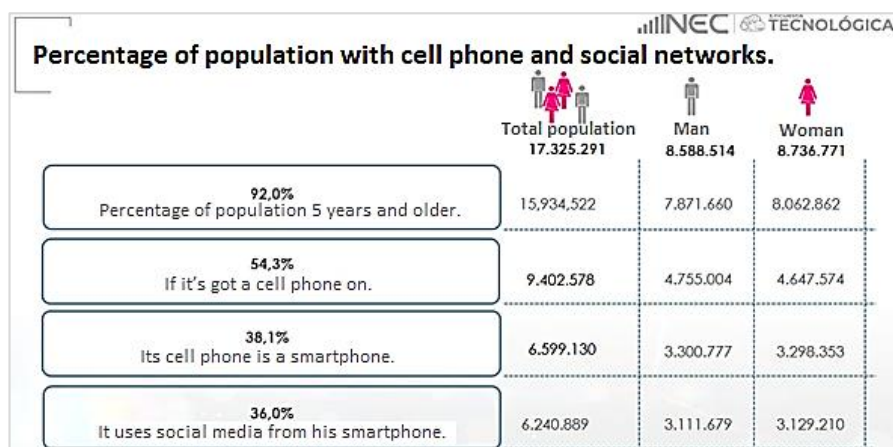


Figure 2. Percentage of population with cell phone and social networks from 2012 to 2018 provided by INEC.

As can be seen from figure 2, according to the figures from 2012 to 2018 given by National Statistics and Census Institute (INEC), the percentage of the population that used social networks is quite high, this percentage took as reference people from 5 years old onwards who made use of social networks from their cell phones, these cell phones in their great majority had internet access at some point in the day. Of the total population surveyed, 17,325,291 people, of whom 92% had cell phones, however, only 38.1% were Smartphones, which means that they have the technology to access the internet, of which 36% made use of social networks, it was possible to interpret that 2.1% did not use social networks either because they did not have access to the internet or because they had no interest in using these social applications.

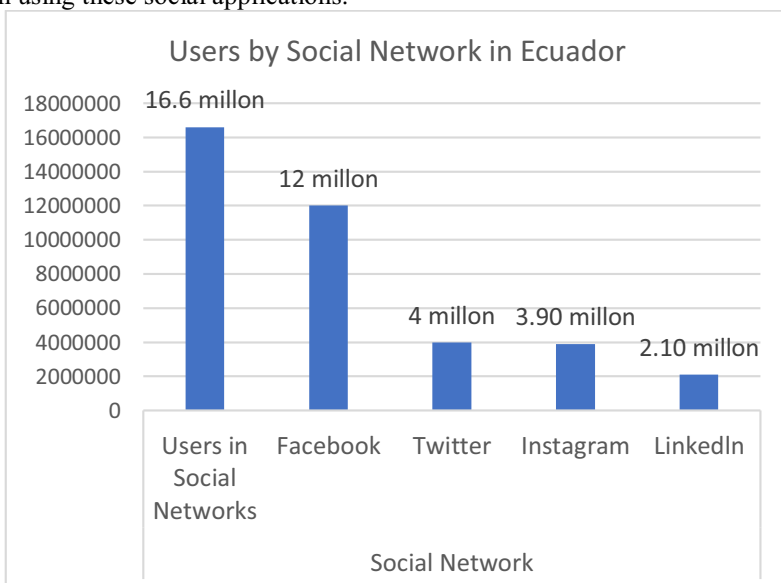


Figure 3. Figures based on the Ecuadorian Digital State report on Ecuador until January 2019.

This figure, compiled with figures based on the report, analyzed the visits of 16.6 million people in Ecuador to the main social networks until January 2019. As could be evidenced until this date there were approximately 12 million users who used Facebook, leading in Ecuador and surpassing notably Twitter and Instagram, this will help us interpret analytical results later.

In the first chart, information presented by National Statistics and Census Institute (INEC) on its web platform was analyzed, the percentage of people who used social networks in their cell phone from 2012 to 2018 was identified, and it was possible to show that this percentage mostly includes minors. Within the range of this percentage, National Statistics and Census Institute (INEC), in its report of the Digital State of Ecuador, compiled a second graph of the figures obtained from social media users with the census of 16.6 million inhabitants until 2019, this information was analyzed in percentages and showed that Facebook leads in Ecuador, being this social network the highest risk in this country because users are of all ages. Whatsapp, the most widely used messaging application in Latin America, has been excluded from these charts.

From this analysis of figures, we obtained the two most commonly used applications in Ecuador, with which we proceeded to investigate in online newspapers all the information related to these apps and cyberbullying. The aim of this research was to find out how it affects the social life of users.

Having knowledge of this information are proceeded to look for laws in Ecuador that mitigate this cybercrime, two articles stipulated in the COIP that currently punish these social cybercrimes with custodial punishment were analyzed.

Article 173 establishes a prison term of one to three years for “a person who, by electronic or telematic means, proposes to arrange a meeting with a person under the age of 18, provided that the proposal is accompanied by material acts aimed at bringing him or her closer together for sexual or erotic purposes”.

Likewise, article 174 sanctions the person who uses or facilitates email, chat, instant messaging, social networks, blogs, photoblogs, network games or any other electronic or telematic means (services and applications that use both computer systems and those of telecommunication) to offer sexual services with minors of eighteen years of age. This will be punished with a custodial sentence of seven to ten years [14].

The general procedure established after the complaint was also known.

The research allowed us to identify the scope of this issue in Ecuador and what needs to be improved.

3. Results

From the research and analysis of the link of Facebook and Whatsapp with cyberbullying obtained from the referenced scientific articles, it was known that social networks users post on the net photos and videos in public form that in a matter of minutes go viral, these publications are accompanied by location, from a known location, user information in the description that the cyber stalker uses to investigate, follow his victim, study it, know the sites he frequently visits, obtain intimate information and ultimately extort or threaten. Unlike Whatsapp where the user consciously sends intimate photos/videos without measuring the consequences.

Making to referring at this first point mentioned, an iterative pattern of how cyberstalkers operate could be evidenced and we have represented it in the following diagram to identify the problem, clarify the actions that originate it and change the result:

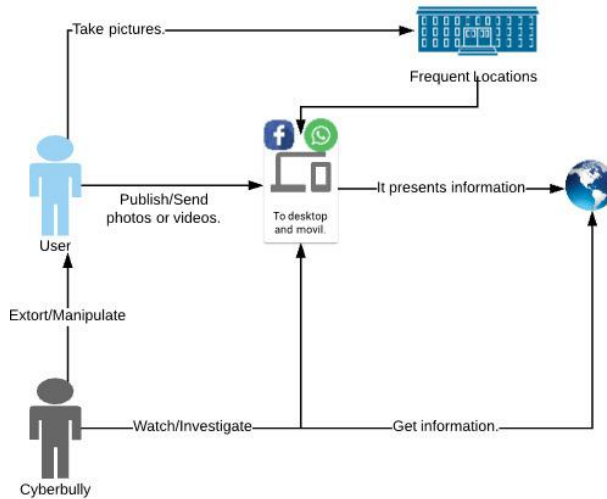


Figure 4. Diagram of how cyberbullying cases arise. Source: The authors.

In addition, research in scientific articles and figures based on the report "Digital State Ecuador" of users by social network in Ecuador indicates that in the country the most used social network is Facebook, unlike other countries, such as in the Emirates United Arab Emirates (EUA) where the highest percentage of users on a social network is concentrated on WhatsApp. After this and also considering the statistical data provided by the INEC in its percentage of population with cellphones and social networks from 2012 to 2018 it is identified that a considerable number of minors have access and use social networks deliberately, being the main victims of this crime.

From the figures collected during the investigation we will take the following:

Ca : People in Ecuador who have their cell phone on. (Figure 2)

Cr : Cases of cyberbullying in Ecuador.

Figures from the National Statistics and Census Institute (INEC) and the United Nations Educational, Scientific and Cultural Organization (Unesco) indicate that 7% of the population has suffered from cyberbullying [15].

$$Cr = \% \text{ Cyberbullying} \times Ca \quad (1)$$

Cme : Cases of harassment by electronic means. (Figure 1)

$$Cme = \% \text{ Victim of assault by electronic means} \times Cr \quad (2)$$

(Figures up to 2018).

$$Ca = 9402578 \quad (3)$$

$$Cr = 658180.46 \quad (4)$$

$$Cme = 151381.51 \quad (5)$$

To estimate a ratio percentage; Inhabitants with cellphone activated - Reported cases of cyberbullying by electronic means will use the following formula:

$$P_{rf} = \frac{Cr \times 100\%}{Cme} \times \frac{Cme \times 100\%}{Ca} = \frac{Cr}{Ca} \quad (6)$$

The result of this formula is 0.07%.

According to the resulting percentage, it can be deduced that in Ecuador the number of cases reported is very low in relation to people who have cell phones activated and who may be victims of cyber-harassment.

This resulting percentage is not reported to citizens in television media, however it is observed daily in digital media and makes us think that it is evident that these cases

are happening frequently and it is important to criminalize the conduct of cyberbullying, Since the commission of the same is more and more unquestionable every day, what makes of it a relevant conduct since it produces threat, with harmful results in the victim difficult to repair generating disastrous consequences for these people.

In order for this conduct to be criminalized, it must be committed through electronic means using social networks, and acts of contempt towards the individual must be committed in order to proceed to report and that legal action process is executed. This process is shown in the following diagram and is successful in some cases:

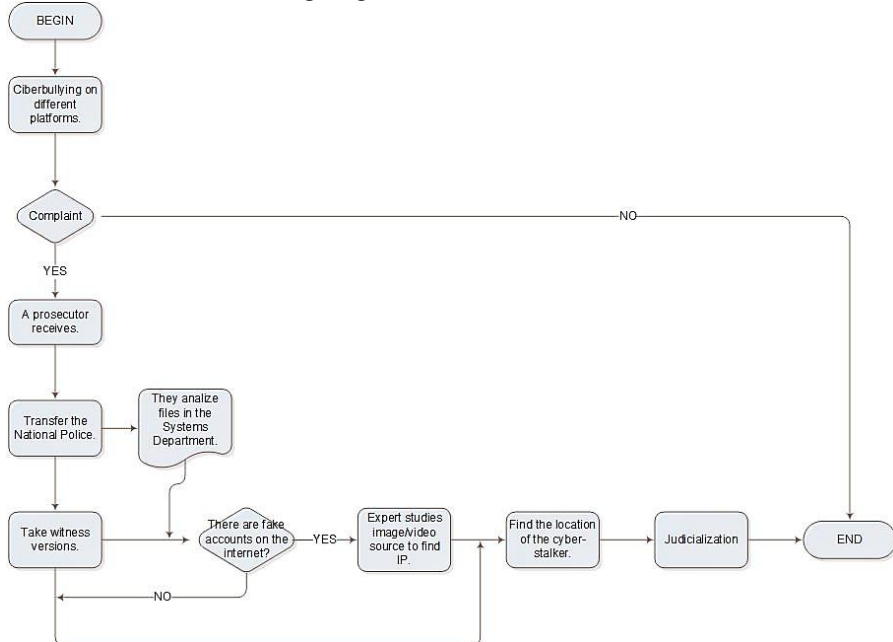


Figure 5. Criminal Process Diagram. Source: The authors.

Within the process of Judicialization it result determinant the reason that entailss to take into consideration articles 173 and 174 stipulated in the COIP to establish what type of computer crime has been committed and subsequently determine the process thereof but not penalized for the crime of cyberbullying in its different scenarios.

Currently there are different concepts associated with cyberbullying, these concepts have been classified by facts that have characteristics in common: cyberbullying, grooming, web beating, flame [16].

In Ecuador there are still no laws that go hand in hand with technological progress and that have a direct impact on these concepts; in the articles presented and analyzed it has been found that their content is very general.

The advance of information on social networks is a crop that cybercriminals often use to carry out illicit activities such as constant cyber-bullying, hacking, blackmail etc., criminal activities that go against the laws of each country. That is why we are constantly working internationally to combat this organized crime and to enforce the law.

4. Discussion

Knowing the results of the investigation and all the information presented during the article, we note that the figures presented by the various institutions responsible for conducting censuses and statistics are far removed from the current situation in Ecuador with reference to the subject under discussion. The government through its ministries supports different organizations to create campaigns that prevent this crime but not to reform laws that help mitigate it, this causes people who are victims of this crime not to report the crime. According to the investigation, the two articles classified in the Comprehensive Organic Criminal Code are very general and allow cases to pass that have been reported, but not resolved by these very limited laws.

5. Future Work and Conclusion

5.1. Futures Works

Comprehensively analyze the laws that refer to computer crimes and harassment, described in the Constitution so that they can be reformed and even incorporated new ones in line with what is currently happening by linking society to technology.

Different types of cyberbullying, such as grooming and sexting, should also be investigated and analyzed, and specifically punished.

5.2. Conclusions

It is concluded after the research and analysis of the topic in question:

- Ecuador works hard and in conjunction with Government Organization (GO)s and Non-Governmental Organization (NGO)s to carry out campaigns to prevent cyberbullying, however, their communication media do not constantly broadcast or support this issue in society for that is examined.
- The lack of laws that mitigate cyberbullying and protect data on social media and other web platforms gives cyberbullies the freedom to commit their acts without clemency and mainly children who tend to keep these facts quiet.
- As cyberbullying is not typified, there is no exact regulation that penalizes the fact, therefore, the rights of the victim are affected, for this problematic it is propose to create a bill that make refers to cyberbullying in its different scenarios so that it is sent to the assembly and thus contrast the present thematic.

Acknowledgments

The authors thank to Universidad Politécnica Salesiana del Ecuador, to the research group of the Guayaquil Headquarters “Computing, Security and Information Technology for a Globalized World” (CSITGW) created according to resolution 142-06-2017-07-19 and Secretaría de Educación Superior Ciencia, Tecnología e Innovación (Senescyt).

References

- [1] «El ciberacoso es un problema en crecimiento que afecta hasta 1 de cada 10 niños en el mundo.,» EcuadorUniversitario.Com, 2019.
- [2] M. ALI AL-GARADI, M. RASHID HUSSAIN, N. KHAN, G. MURTAZA, H. FRIDAY NWEKE, I. ALI, G. MUJTABA, H. CHIROMA, H. ALI KHATTAK y A. GANI, «Predicting Cyberbullying on Social Media in the Big Data Era Using Machine Learning Algorithms: Review of Literature and Open Challenges,» IEEE Access, vol. 7, nº 8720155, pp. 70701-70718, 2019.
- [3] F. IQBAL, B. C. M. FUNG, M. DEBBABI, R. BATTOOL y A. MARRINGTON, «Wordnet-Based Criminal Networks Mining for Cybercrime Investigation,» IEEE Access, vol. 7, nº 8606047, pp. 22740-22755, 2019.
- [4] G. R. Vera Mora y J. V. León Acurio, «CYBERBULLYING: UNA REALIDAD DE INTIMIDACIÓN EN LAS UNIDADES,» Atlante. Cuadernos de Educación y Desarrollo, 2017.
- [5] A. Martinez, «Telefónica Movistar: La realidad del ciberacoso en Ecuador y cómo denunciarlo.,» Metro Ecuador, Quito, 2019.
- [6] «Cómo prevenir el ciberacoso o ciberbullying.,» EL UNIVERSO, Guayaquil, 2019.
- [7] Ghada M. Abaido (2020) Cyberbullying on social media platforms among university students in the United Arab Emirates, International Journal of Adolescence and Youth, 25:1, 407-420, DOI: 10.1080/02673843.2019.1669059..
- [8] S. M. Toapanta Toapanta, F. G. Mendoza Quimi, L. M. Romero Lamboggia y L. E. Mafla Gallegos, «Impact on the Information Security Management due to the Use of Social Networks in a Public Organization in Ecuador,» Smart Innovation, Systems and Technologies, vol. 165, pp. 51-64, 4 Diciembre 2019.
- [9] Huang, C. L., Zhang, S., & Yang, S. C. (2020). How students react to different cyberbullying events: Past experience, judgment, perceived seriousness, helping behavior and the effect of online disinhibition. Computers in Human Behavior, 110 doi:10.1016/j.chb.2020.106338.
- [10] G. Kashy-Rosenbaum y D. Aizenkot, «Exposure to cyberbullying in WhatsApp classmates' groups and classroom climate as predictors of students' sense of belonging: A multi-level analysis of elementary, middle and high schools,» Children and Youth Services Review, vol. 108, nº 104614, pp. 2-10, 2020.
- [11] N. Auemaneeku, A. Powwattana, E. Kiatsiri y N. Thananowan, «Investigating the mechanisms of theory of planned behavior on Cyberbullying among Thai adolescents,» Journal of Health Research, vol. 34, pp. 42-55, 2020.
- [12] Oksanen, A., Oksa, R., Savela, N., Kaakinen, M., & Ellonen, N. (2020). Cyberbullying victimization at work: Social media identity bubble approach. Computers in Human Behavior, 109 doi:10.1016/j.chb.2020.106363.
- [13] INEC, «Tecnologías de la Información y Comunicaciones.,» 2017.
- [14] El Diario.ec, «Ciberacoso, un dolor de cabeza para los padres,» El Dairio.ec, 15 Julio 2018.
- [15] Gao, L., Liu, J., Wang, W., Yang, J., Wang, P., & Wang, X. (2020). Moral disengagement and adolescents' cyberbullying perpetration: Student-student relationship and gender as moderators. Children and Youth Services Review, 116 doi:10.1016/j.childyouth.2020.105119.
- [16] Instituto Nacional de Estadística y Censos, «INEC,» [En línea]. Available: <https://www.ecuadorencifras.gob.ec/objetivos-politicas/>.

Neighborhood Based Multi-Granularity Attribute Reduction: An Acceleration Approach

Jingjing SONG^{a,b,1}, Huili DOU^a, Xiansheng RAO^a, Xiaojing LUO^a and Xuan YAN^c

^a*School of Computer, Jiangsu University of Science and Technology, Zhenjiang,
Jiangsu 212003, China*

^b*Key Laboratory of Data Science and Intelligence Application, Fujian Province
University, Zhangzhou, 363000, China*

^c*School of Economics and Management, Jiangsu University of Science and Technology,
Zhenjiang, Jiangsu 212003, China*

Abstract. As a feature selection technique in rough set theory, attribute reduction has been extensively explored from various viewpoints especially the aspect of granularity, and multi-granularity attribute reduction has attracted much attention. Nevertheless, it should be pointed out that multiple granularities require to be considered simultaneously to evaluate the significance of candidate attribute in the corresponding process of computing reduct, which may result in high elapsed time of searching reduct. To alleviate such a problem, an acceleration strategy for neighborhood based multi-granularity attribute reduction is proposed in this paper, which aims to improve the computational efficiency of searching reduct. Our proposed approach is actually realized through the positive approximation mechanism, and the processes of searching qualified attributes are executed through evaluating candidate attributes over the gradually reduced sample space rather than all samples. The experimental results over 12 UCI data sets demonstrate that the acceleration strategy can provide superior performance to the naive approach of deriving multi-granularity reduct in the elapsed time of computing reduct without generating different reducts.

Keywords. Acceleration approach, attribute reduction, granular computing, multi-granularity, neighborhood rough set

1. Introduction

Attribute reduction [1,2,3,4,5], as a rough set based feature selection technology, has been widely investigated from various perspectives, and it has also been applied to many fields such as pattern recognition [6], decision analysis[7,8,9], data mining [10] and machine learning [11,12,13]. This is mainly because the data collected in real-world applications may contain redundant and irrelative attributes, these attributes may deteriorate the performance of learning algorithms [14,15], attribute reduction can effectively

¹Corresponding Author: Jingjing Song, School of Computer, Jiangsu University of Science and Technology, Zhenjiang, Jiangsu 212003, China; E-mail: songjingjing108@163.com

remove these attributes from data through searching a qualified reduct satisfying the intended constraint, and further reduce the dimensionality of data. Moreover, it is worth mentioning that Rough Set Theory (RST) has its inherent superiority compared with other methods. For instance, it is effective in handling uncertainty without the requirement of prior information.

Notably, the intended constraint defined in attribute reduction is generally constructed over the given measure such as approximation quality [16] or condition entropy [17], and the corresponding derived measure value is highly related to the result of information granulation [18,19,20] over the universe from the standpoint of Granular Computing (GrC) [21,22]. For example, if the neighborhood rough set [23] and measure approximation quality are considered, and given a radius, then the obtained neighborhoods of samples can be regarded as the neighborhood information granules, i.e., the result of information over the universe. Therefore, a smaller size of neighborhood, which indicates the corresponding result of information granulation is finer, may generate higher measure value of approximation quality; contrarily, a greater size of neighborhood, which implies the corresponding result of information granulation is coarser, may lead to lower measure value of approximation quality.

Presently, the concept of granularity has been used for characterizing the level of information granulation in GrC. And the corresponding level of granularity can reflect the discrimination ability related to the result of information granulation. With a careful reviewing of previous research, it is easy to reveal the intended constraint is generally constructed based on one and only one fixed granularity in most attribute reduction approaches, which are referred to as single granularity based attribute reduction in the context of this paper. However, as what has been illustrated in References [24,25,26], there are some inherent limitations in single granularity based attribute reduction. For example, single granularity based attribute reduction may fail to select attributes from multi-level or multi-view [24]; single granularity based attribute reduction may not provide the higher adaptability of the derived reduct for the problem of granularity diversity [26]. Therefore, various definitions of multi-granularity attribute reduction have been proposed for different practical requirements. Notably, Liu et al. [26] not only put forward a general definition for multi-granularity attribute reduction, but also developed the corresponding algorithm of searching reduct.

However, it is worth noting that in multi-granularity attribute reduction, multiple different granularities are required to be considered simultaneously to calculate the measure value, which will be further employed for evaluating the significance of candidate attributes. Immediately, qualified attributes are selected and added into the temporary attribute set until the intended constraints are satisfied. Obviously, such process of searching reduct is time-consuming due to the simultaneous consideration of multiple different granularities especially the size of samples is large. In view of this, to reduce the computational time of obtaining reduct, an acceleration approach is proposed for neighborhood based multi-granularity attribute reduction in neighborhood rough set. Our proposed acceleration approach is mainly designed through the positive approximation mechanism [15]. Specifically, to search the qualified candidate attributes, the significance of candidate attribute can be evaluated over the gradually reduced sample space rather than all samples. Accordingly, the decreasing of sample space may be conducive to the less elapsed time of calculating measure value and selecting attributes. Consequently,

the computations of deriving reduct may be saved along with the time consumption of searching reduct.

The remainder of this paper is organized as follows. The basic notions related to neighborhood rough set and multi-granularity attribute reduction will be briefly reviewed in Section 2. The acceleration approach for neighborhood based multi-granularity attribute reduction will be presented in Section 3. Comparative experiments will be conducted to verify the performance of the proposed acceleration strategy in Section 4. Section 5 will conclude this paper and present future perspectives.

2. Preliminary knowledge

Generally speaking, the obtaining of granularity can be realized through various strategies [26], one of which is the parameter based granularity. Therefore, to simplify our discussion, the neighborhood rough set is employed in the following paper. The main reason can be summarized as the following two points: 1) neighborhood rough set is effective in analysing and handling continuous data and even mixed data; 2) neighborhood rough set intuitively determines the multi-granularity structure based on the concept of neighborhood [23] with considering multiple different radii.

2.1. Neighborhood rough set

From the viewpoint of rough set theory [16], a decision system can be described as a pair such that $DS = \langle U, A \cup \{d\} \rangle$, in which U is the universe, i.e., the nonempty finite set of samples, A is the condition attribute set used for describing the sample, and d is the decision attribute which indicates the true label of sample. Following the label of sample, the equivalence relation for information granulation can be derived, which is denoted as $\text{IND}_d = \{(x, y) \in U \times U : d(x) = d(y)\}$. Based on such equivalence relation, a partition $U/\text{IND}_d = \{X_1, X_2, \dots, X_q\}$ over the universe can be induced, in which $X_p (X_p \in U/\text{IND}_d)$ is the p -th decision class.

It should be noticed that the classical rough set is only useful in analysing and handling nominal data. However, numerical data and mixed data are ubiquitous in real-world applications. Therefore, various generalizations [23,27,28,29,30] of such model have been proposed. Neighborhood rough set has been favoured and employed by many researchers, because it can analyse and handle continuous data and even mixed data directly.

Definition 1 [23] Given a decision system DS and the neighborhood radius δ , $\forall B \subseteq A$, the neighborhood of sample x is:

$$N_B^\delta(x) = \{y \in U : \Delta_B(x, y) \leq \delta\}, \quad (1)$$

in which $\Delta_B(x, y)$ is the distance between samples x and y over the condition attribute set B .

From the viewpoint of GrC, the result of information granulation is actually the neighborhoods of all samples over the universe in neighborhood rough set, i.e., all the neighborhood information granules. Therefore, different scales of neighborhood of sam-

ple can generate different results of information granulation, and then different granularities can be obtained. That is, the granularity can be reflected by the derived neighborhoods or the used neighborhood radius. This is mainly because a smaller radius may generate a smaller size of neighborhood which indicates a finer granularity, while a larger radius may determine a greater size of neighborhood which implies a coarser granularity. From this perspective, a set of different radii can determine a set of different granularities.

Following the definition of neighborhood of sample, the neighborhood relation over the universe can be induced, and it can be denoted as $N_B^\delta = \{(x, y) \in U \times U : \Delta_B(x, y) \leq \delta\}$.

Definition 2 [23] Given a decision system DS and the neighborhood radius δ , $\forall B \subseteq A$, the neighborhood lower and upper approximations of X_p with respect to B are:

$$\underline{N}_B^\delta(X_p) = \{x \in U : N_B^\delta(x) \subseteq X_p\}, \quad (2)$$

$$\overline{N}_B^\delta(X_p) = \{x \in U : N_B^\delta(x) \cap X_p \neq \emptyset\}. \quad (3)$$

The pair $[\underline{N}_B^\delta(X_p), \overline{N}_B^\delta(X_p)]$ is referred to as a neighborhood rough set of X_p with respect to B .

Definition 3 [23] Given a decision system and the neighborhood radius δ , $\forall B \subseteq A$, the approximation quality of d with respect to B is

$$\gamma_B^\delta(U, d) = \frac{|\text{POS}_B^\delta(U, d)|}{|U|}, \quad (4)$$

in which $\text{POS}_B^\delta(U, d) = \bigcup_{p=1}^q \underline{N}_B^\delta(X_p)$ is the positive region of d with respect to B , and $|X|$ indicates the cardinality of the set X .

2.2. Multi-granularity attribute reduction

Multi-granularity attribute reduction implies that multiple granularities are generally considered for the constructing of intended constraints. Accordingly, a general form of definition proposed by Liu et al. [26] is shown as following Definition 4.

Definition 4 [26] Given the decision system DS and a set of granularities $\text{MG} = \{\mathbb{G}_1, \mathbb{G}_2, \dots, \mathbb{G}_n\}$, assuming that C_φ^{MG} is a multi-granularity constraint with regard to measure φ , then $\forall B \subseteq A$, B is a multi-granularity reduct if and only if

1. B satisfies C_φ^{MG} ;
2. $\forall C \subset B$, C does not satisfy C_φ^{MG} .

Following Definition 4, it can be observed that different from the constraint in single granularity based attribute reduction, C_φ^{MG} is a multi-granularity constraint constructed over a set of multiple different granularities with respect to the considered measure φ .

Actually, the multi-granularity constraint C_φ^{MG} shown in Definition 4 is realized based on the derived multi-granularity measure value with respect to the considered

measure φ . For example, higher measure value is expected based on the considered measure φ , such as approximation quality, if the corresponding measure value with regard to B and granularity \mathbb{G}_m is denoted as $\varphi^{\mathbb{G}_m}(B)$, then such multi-granularity measure value $\varphi^{\text{MG}}(B)$ in constraints can be induced through fusing the measure values in $\{\varphi^{\mathbb{G}_1}(B), \varphi^{\mathbb{G}_2}(B), \dots, \varphi^{\mathbb{G}_n}(B)\}$. Immediately, the corresponding constraint can be expressed as “ $\varphi^{\text{MG}}(B) \geq \varphi^{\text{MG}}(A)$ ”.

Note that a set of multiple granularities $\text{MG} = \{\mathbb{G}_1, \mathbb{G}_2, \dots, \mathbb{G}_n\}$ shown in Definition 4 can be intuitively determined by a set of radii $\mathbb{R} = \{\delta_1, \delta_2, \dots, \delta_n\}$, because the granularity is highly correlated with the considered parameter (the neighborhood radius) in neighborhood rough set. Therefore, in neighborhood rough set, if a set of different radii \mathbb{R} and approximation quality are considered, then the multi-granularity constraint C_{φ}^{MG} shown in Definition 4 can be denoted as “ $\gamma_B^{\mathbb{R}}(U, d) \geq \gamma_A^{\mathbb{R}}(U, d)$ ”, where $\gamma_B^{\mathbb{R}}(U, d)$ is a multi-granularity measure value of approximation quality derived by fusing the corresponding measure values related to multiple radii.

Following Definition 4, how to search the corresponding reduct should be immediately addressed. Note that the heuristic searching algorithm has been widely used for the deriving of reduct, and the significance of candidate attribute is generally regarded as the heuristic information in such process. Based on the neighborhood rough set and measure of approximation quality, Algorithm 1 shows the detailed process of computing multi-granularity reduct.

Algorithm 1: The process of computing multi-granularity reduct.

Inputs: Decision system DS , a set of radii \mathbb{R} with ascending order.

Outputs: One multi-granularity reduct B .

1. $\forall \delta_m \in \mathbb{R}$, calculate the measure value $\gamma_A^{\delta_m}(U, d); // 1 \leq m \leq n;$
2. Compute the fused measure value $\gamma_A^{\mathbb{R}}(U, d)$ in terms of the obtained measure values in Step 1;

3. $B \leftarrow \emptyset$;

4. **Repeat**

- 1) $\forall a \in A - B$, calculate the measure value $\phi(B \cup \{a\}) = \gamma_{B \cup \{a\}}^{\delta_1}(U, d) + \gamma_{B \cup \{a\}}^{\delta_n}(U, d);$
- 2) Select a suitable b such that $b = \arg \max \{\phi(B \cup \{a\}) : \forall a \in A - B\};$
- 3) $B \leftarrow B \cup \{b\};$
- 4) Calculate the measure value $\gamma_B^{\mathbb{R}}(U, d);$

Until $\gamma_B^{\mathbb{R}}(U, d) \geq \gamma_A^{\mathbb{R}}(U, d)$

5. **Return** A .

In Algorithm 1, the following two points should be concerned.

1. The fused measure value $\gamma_A^{\mathbb{R}}(U, d)$ is actually obtained by fusing the multiple measure values with regard to a set of radii, and such fusion operation can be realized through various approaches. For instance, if the arithmetic mean is considered to conduct such fusion, then the fused measure value can be denoted as $\gamma_A^{\mathbb{R}}(U, d) = \frac{1}{n} \sum_{m=1}^n \gamma_A^{\delta_m}(U, d)$; if the harmonic mean is considered to perform such fusion, then the fused measure value can be formulated as $\gamma_A^{\mathbb{R}}(U, d) = \left(\frac{1}{n} \sum_{m=1}^n \frac{1}{\gamma_A^{\delta_m}(U, d)}\right)^{-1}$.

2. The selecting of qualified attributes are executed based on the evaluation of attribute significance over the minimal radius and maximal radius simultaneously, and such two radii can determine the finest and coarsest granularities, respectively.

Following Algorithm 1, two representative radii, i.e., the minimal and maximal radii, should be concerned simultaneously in evaluating candidate attributes. Moreover, the deriving of the measure value in the intended constraint requires to fuse measure values of approximation quality over multiple different radii. It follows that the computational cost of obtaining multi-granularity reduct may be expensive if the volume of data is great.

3. Acceleration approach for neighborhood based multi-granularity attribute reduction

From the above discussions, it is trivial to observe that multiple granularities require to be considered in multi-granularity attribute reduction simultaneously, and then the computing of reduct may be a time-consuming process. In view of this, an acceleration approach will be proposed in the following, which aims to improve the computational efficiency of deriving the neighborhood based multi-granularity reduct.

Such acceleration strategy is mainly realized based on the mechanism of positive approximation [15]. Specifically, with the growing of number of used attributes in neighborhood rough set, smaller size of neighborhood will be induced, which may result in greater size of positive region, and this is determined by the monotonicity of neighborhood rough set. Apparently, the size of previously derived positive region is smaller than that of currently obtained positive region, and the former will be contained in the latter in the iterations of searching qualified attributes. Consequently, the samples in previously obtained positive region will not be participated in next iteration for evaluating candidate attributes. That is, the candidate attributes can be evaluated over the reduced sample space rather than all samples. It follows that the computation of deriving reduct may be decreased along with the elapsed time. Algorithm 2 shows the detailed process of quick computing multi-granularity reduct.

Algorithm 2: The process of quick computing multi-granularity reduct.

Inputs: Decision system DS , a set of radii \mathbb{R} with ascending order.

Outputs: One multi-granularity reduct B .

1. $\forall \delta_m \in \mathbb{R}$, calculate the measure value $\gamma_A^{\delta_m}(U, d)$; // $1 \leq m \leq n$
2. Compute the fused measure value $\gamma_A^{\mathbb{R}}(U, d)$ in terms of the obtained measure values in Step 1;

3. $B \leftarrow \emptyset$

4. **Repeat**

- 1) Compute the positive regions $\text{POS}_B^{\delta_1}(U, d)$ and $\text{POS}_B^{\delta_n}(U, d)$ with respect to δ_1 and δ_n , respectively; // $\text{POS}_{\emptyset}^{\delta_m}(U, d) = \emptyset$
- 2) $U_1 \leftarrow U - \text{POS}_B^{\delta_1}(U, d)$, $U_n \leftarrow U - \text{POS}_B^{\delta_n}(U, d)$;
- 3) $\forall a \in A - B$, calculate the measure value $\phi(B \cup \{a\}) = \gamma_{B \cup \{a\}}^{\delta_1}(U_1, d) + \gamma_{B \cup \{a\}}^{\delta_n}(U_n, d)$;

- 4) Select a suitable b such that $b = \arg \max \{\phi(B \cup \{a\}) : \forall a \in A - B\}$;
 - 5) $B \leftarrow B \cup \{b\}$;
 - 6) Calculate the measure value $\gamma_B^R(U, d)$
- Until** $\gamma_B^R(U, d) \geq \gamma_A^R(U, d)$

5. Return A .

In Algorithm 2, it is worth noting that to search the qualified attributes, the selecting of candidate attributes will be executed over the minimal and maximal radii simultaneously. Therefore, the positive regions with respect to such two radii require to be calculated beforehand, respectively, and then the candidate attributes can be evaluated over the reduced sample space.

Moreover, based on the processes of Algorithms 1 and 2, it is easy to know that the sample space of Algorithm 2 is gradually reduced in the iteration of searching qualified attributes, while the sample space of Algorithm 1 is the whole universe in the iteration of searching qualified attributes. Accordingly, compared with the naive process of computing multi-granularity reduct, i.e., Algorithm 1, the redundant computations of deriving multi-granularity reduct may be reduced through the acceleration strategy, i.e., Algorithm 2. Therefore, the time consumption of deriving corresponding reduct may be also decreased.

4. Experiments

4.1. Data sets

To validate the effectiveness of the proposed acceleration approach, 12 public UCI data sets have been used for conducting experiments, the detailed description of data sets is shown in Table 1. All data sets have been normalized by column before conducting experiments.

Table 1. Data sets used in experiments

ID	Data sets	Samples	Attributes	Decision classes
1	Amphetamines	1885	12	7
2	Connectionist Bench	990	13	11
3	Forest Type Mapping	523	27	4
4	Libras Movement	360	90	15
5	Lymphography	98	18	3
6	Optical Recognition of Handwritten Digits	5620	64	10
7	Page-blocks	5473	10	5
8	Statlog (German Credit)	1000	24	2
9	Statlog (Heart)	270	13	2
10	Urban Land Cover	675	147	9
11	Waveform	5000	40	3
12	Wine Quality	4898	11	7

4.2. Experimental setup

In the following experiments, a set of ascending ordered radii \mathbb{R} will be appointed. Note that the same set of radii may be not suitable for all data sets. Therefore, for different data sets, 10 different neighborhood radii has been selected, and the employed set of radii is the same to what has been used in Reference [31], and the details of determining the suitable radii can be observed in the corresponding illustration of References [31]. The detailed values of radii used in our experiments are shown in Table 2.

Table 2. Detailed values of radii for data sets

ID	10 used radii
1	0.021, 0.042, 0.063, 0.084, 0.105, 0.126, 0.147, 0.168, 0.199, 0.210
2	0.021, 0.042, 0.063, 0.084, 0.105, 0.126, 0.147, 0.168, 0.199, 0.210
3	0.025, 0.050, 0.075, 0.100, 0.125, 0.150, 0.175, 0.200, 0.225, 0.250
4	0.054, 0.108, 0.162, 0.216, 0.270, 0.324, 0.378, 0.432, 0.486, 0.540
5	0.037, 0.074, 0.111, 0.148, 0.185, 0.222, 0.259, 0.296, 0.333, 0.370
6	0.047, 0.094, 0.141, 0.188, 0.235, 0.282, 0.329, 0.376, 0.423, 0.470
7	0.014, 0.028, 0.042, 0.056, 0.070, 0.084, 0.098, 0.112, 0.126, 0.140
8	0.041, 0.082, 0.123, 0.164, 0.205, 0.246, 0.287, 0.328, 0.369, 0.410
9	0.045, 0.090, 0.135, 0.180, 0.225, 0.270, 0.315, 0.360, 0.405, 0.450
10	0.035, 0.070, 0.105, 0.140, 0.175, 0.210, 0.245, 0.280, 0.315, 0.350
11	0.047, 0.094, 0.141, 0.188, 0.235, 0.282, 0.329, 0.376, 0.423, 0.470
12	0.011, 0.022, 0.033, 0.044, 0.055, 0.066, 0.077, 0.088, 0.099, 0.110

To test the performance of the derived reduct, 5-fold cross-validation will be used. Note that the comparative experimental results are the average values of 5-fold cross-validation output results in our experiments. Moreover, Euclidean distance has been used in the computing of the distance between arbitrary two samples, and the operator arithmetic mean will be used for realizing the fusion operation in Algorithms 1 and 2. To avoid the constraints in Algorithms 1 and 2 are so strict that redundant attributes may not be removed, the tolerant threshold ϵ has been considered to realize the approximated reduct [32]. Specifically, both the constraints in Algorithms 1 and 2 can be reset to be “ $\gamma_A^{\mathbb{R}}(U, d) - \gamma_B^{\mathbb{R}}(U, d) \leq \epsilon \cdot \gamma_A^{\mathbb{R}}(U, d)$ ”. Two different values of ϵ will be used in the following experiments, and they are 0.05 and 0.10, respectively.

4.3. Comparisons among the time consumption of computing reduct

The computational time for obtaining reduct among Algorithms 1 and 2 will be mainly compared in this experiment. The detailed elapsed time of obtaining multi-granularity reduct is shown in Table 3, where the lower values are highlighted in underline.

Table 3. Time consumption (seconds) for computing multi-granularity reduct

ID	$\epsilon = 0.05$		$\epsilon = 0.10$	
	Algorithm 1	Algorithm 2	Algorithm 1	Algorithm 2
1	7.2617	<u>4.8934</u>	6.7875	<u>4.6246</u>
2	1.8828	<u>1.3655</u>	1.8055	<u>1.2769</u>
3	2.1861	<u>1.5156</u>	1.7224	<u>1.3036</u>
4	3.3829	<u>2.4006</u>	2.4204	<u>1.8659</u>
5	0.0663	<u>0.0639</u>	0.0597	<u>0.0490</u>
6	423.9869	<u>301.8563</u>	400.5364	<u>291.9283</u>
7	31.2085	<u>23.7398</u>	29.3262	<u>23.1574</u>
8	4.6161	<u>2.6439</u>	4.0404	<u>2.5684</u>
9	0.1810	<u>0.1526</u>	0.1629	<u>0.1421</u>
10	16.0863	<u>11.9105</u>	13.9133	<u>10.7305</u>
11	159.1719	<u>135.6123</u>	149.6678	<u>129.4193</u>
12	44.1671	<u>29.1053</u>	40.8465	<u>28.7957</u>

With a careful investigation of Table 3, it is not difficult to observe the following.

1. Compared with Algorithm 1 of computing multi-granularity reduct, the proposed acceleration strategy, i.e., Algorithm 2, can offer the superior performance to Algorithm 1 in the computational time of deriving reduct. From this point of view, the proposed acceleration strategy does help to decrease the time consumption of deriving reduct.
2. If the value of used threshold increases, then the time consumption of deriving multi-granularity reduct may be decreased. This is mainly because when the threshold value increases, then the relevant constraint will become looser, and to search the reduct which satisfies such constraint, fewer qualified attributes may be required. Accordingly, the computational time for obtaining reduct may be saved.

4.4. Comparisons among lengths of the obtained reducts

In this experiments, the lengths of derived multi-granularity reducts in terms of Algorithm 1 and Algorithm 2 will be compared. Note that the compared results of lengths are the mean values of 5-fold cross-validation experimental results. The detailed results are shown in Table 4.

Table 4. Lengths of derived multi-granularity reducts

ID	$\epsilon = 0.05$		$\epsilon = 0.10$	
	Algorithm 1	Algorithm 2	Algorithm 1	Algorithm 2
1	9.0000	9.0000	8.4000	8.4000
2	8.0000	8.0000	7.4000	7.4000
3	16.6000	16.6000	13.2000	13.2000
4	16.2000	16.2000	12.0000	12.0000
5	7.4000	7.4000	6.8000	6.8000
6	12.2000	12.2000	11.6000	11.6000
7	5.0000	5.0000	4.6000	4.6000
8	11.6000	11.6000	10.0000	10.0000
9	10.0000	10.0000	9.0000	9.0000
10	11.6000	11.6000	10.2000	10.2000
11	20.0000	20.0000	18.2000	18.2000
12	9.0000	9.0000	8.4000	8.4000

With a deep investigation of Table 4, it is not difficult to observe the following.

1. Compared with Algorithm 1 of computing multi-granularity reduct, our proposed acceleration approach can generate the same length of reduct. Such observation implies that our proposed acceleration approach may contribute to the deriving of the same reduct as that of Algorithm 1.
2. With the increasing of value of employed threshold, the lengths of the obtained reducts may be reduced. The explanation for such observation result is that when the threshold value increases, the predefined constraint may not be so strict. Accordingly, to derived the qualified multi-granularity reduct, fewer attributes are required. Consequently, the attributes in reduct may be reduced as well as the length of derived reduct. Such reason is consistent with what has been illustrated in previous subsection.

4.5. Comparisons among different reducts in classification performance

The classification performance with respect to the different reducts, which are obtained through Algorithms 1 and 2 will be compared in this experiments. Note that SVM (LIBSVM [33]) classifier is used for estimating the classification performance of reduct over the testing set. Accordingly, the average values of classification accuracies obtained by cross-validation experimental results will be listed, and the detailed results are shown in Table 5.

Table 5. Classification accuracies of multi-granularity reducts

ID	$\epsilon = 0.05$		$\epsilon = 0.10$	
	Algorithm 1	Algorithm 2	Algorithm 1	Algorithm 2
1	0.5194	0.5194	0.5194	0.5194
2	0.5343	0.5343	0.5131	0.5131
3	0.8606	0.8606	0.8567	0.8567
4	0.4556	0.4556	0.4444	0.4444
5	0.8037	0.8037	0.8037	0.8037
6	0.8909	0.8909	0.8794	0.8794
7	0.9357	0.9357	0.9344	0.9344
8	0.7530	0.7530	0.7540	0.7540
9	0.8333	0.8333	0.8074	0.8074
10	0.7763	0.7763	0.7719	0.7719
11	0.8654	0.8654	0.8584	0.8584
12	0.5343	0.5343	0.5300	0.5300

Based on Table 5, it is not difficult to observe the following.

1. The classification accuracies obtained by using Algorithm 2 are same with those obtained through using Algorithm 1. Such result shows that the proposed acceleration strategy may generate the same reduct with Algorithm 1.
2. The increasing of value of threshold may lead to the decreasing of classification accuracy of obtained reduct over most data sets. This is mainly because with the increasing of value of the considered threshold, the related constraint may be looser, and then the derived reduct may contain fewer attributes. Note that the reduct of fewer attributes generally offers the poor classification performance. It follows that the classification accuracies of reducts may be decreased with the increasing of value of the used threshold.

Based on the results shown in Tables 3-5, we can easily conclude that the acceleration approach can provide superior performance to Algorithm 1 in term of the time efficiency of computing multi-granularity reduct, and the generated reducts are the same with those obtained by using Algorithm 1.

5. Conclusions and future perspectives

Multi-granularity attribute reduction is mainly investigated in this paper, and to search the corresponding reduct, multiple different granularities are generally required to be considered simultaneously in the searching of qualified attributes. Accordingly, the produced computational time for obtaining reduct is high if the volume of data is great. Therefore, to decrease the elapsed time of searching multi-granularity reduct, an acceleration approach is proposed in this paper. Our proposed approach is mainly designed based on the mechanism of positive approximation, and then the selecting of qualified attributes are conducted with the gradually reduced sample space instead of the whole universe. Based on neighborhood rough set, the experimental results show us that the proposed acceleration approach can not only generate the same reduct, but also signifi-

cantly reduce the elapsed time of searching reduct compared with the general process of computing multi-granularity reduct. The following topics deserve our further research.

1. Only the measure of approximation quality is considered in this paper, our acceleration strategy will be further investigated by other measure such as information entropy.
2. The main mechanism of our proposed acceleration approach is only realized from the perspective of sample, a novel strategy, which considers the aspects of both sample and attribute, will be further investigated to improve the performance of acceleration approach.

Acknowledgements

This work was supported by the Natural Science Foundation of China (No. 61906078) and the Key Laboratory of Data Science and Intelligence Application, Fujian Province University (No. D1901).

References

- [1] Hongmei Chen, Tianrui Li, Xin Fan, and Chuan Luo. Feature selection for imbalanced data based on neighborhood rough sets. *Information Sciences*, 483:1 – 20, 2019.
- [2] Yan Chen, Keyu Liu, Jingjing Song, Hamido Fujita, Xibei Yang, and Yuhua Qian. Attribute group for attribute reduction. *Information Sciences*, 535:64 – 80, 2020.
- [3] Xiuyi Jia, Lin Shang, Bing Zhou, and Yiyu Yao. Generalized attribute reduct in rough set theory. *Knowledge-Based Systems*, 91:204 – 218, 2016.
- [4] Jingzheng Li, Xibei Yang, Xiaoning Song, Jinhai Li, Pingxin Wang, and Dong-Jun Yu. Neighborhood attribute reduction: a multi-criterion approach. *International Journal of Machine Learning and Cybernetics*, 10:731 – 742, 2019.
- [5] Xiansheng Rao, Xibei Yang, Xin Yang, Xiangjian Chen, Dun Liu, and Yuhua Qian. Quickly calculating reduct: An attribute relationship based approach. *Knowledge-Based Systems*, 200:106014, 2020.
- [6] Roman W. Swiniarski and Andrzej Skowron. Rough set methods in feature selection and recognition. *Pattern Recognition Letters*, 24:833 – 849, 2003.
- [7] Sharma Haresh Kumar, Kumari Kriti, and Kar Samarjit. A rough set approach for forecasting models. *Decision Making: Applications in Management and Engineering*, 3:1 – 21, 2020.
- [8] Stankovic Milan, Gladovic Pavle, and Popovic Vladimir. Determining the importance of the criteria of traffic accessibility using fuzzy ahp and rough ahp method. *Decision Making: Applications in Management and Engineering*, 2:86 – 104, 2019.
- [9] Karavdic Zoran and Projovic Damir. A multi-criteria decision-making (mcdm) model in the security forces operations based on rough sets. *Decision Making: Applications in Management and Engineering*, 1:97 – 120, 2018.
- [10] Hongmei Chen, Tianrui Li, Chuan Luo, Shi-Jinn Horng, and Guoyin Wang. A decision-theoretic rough set approach for dynamic data mining. *IEEE Transactions on Fuzzy Systems*, 23:1958 – 1970, 2015.
- [11] Jie Cai, Jiawei Luo, Shulin Wang, and Sheng Yang. Feature selection in machine learning: A new perspective. *Neurocomputing*, 300:70 – 79, 2018.
- [12] Changzhong Wang, Mingwen Shao, Qiang He, Yuhua Qian, and Yali Qi. Feature subset selection based on fuzzy neighborhood rough sets. *Knowledge-Based Systems*, 111:173 – 179, 2016.
- [13] Suping Xu, Xibei Yang, Hualong Yu, Dong-Jun Yu, Jingyu Yang, and Eric C.C. Tsang. Multi-label learning with label-specific feature reduction. *Knowledge-Based Systems*, 104:52 – 61, 2016.
- [14] Yuhua Qian, Jiye Liang, Deyu Li, Haiyun Zhang, and Chuangyin Dang. Measures for evaluating the decision performance of a decision table in rough set theory. *Information Sciences*, 178:181 – 202, 2008.

- [15] Yuhua Qian, Jiye Liang, Witold Pedrycz, and Chuangyin Dang. Positive approximation: An accelerator for attribute reduction in rough set theory. *Artificial Intelligence*, 174:597 – 618, 2010.
- [16] Zdzisław Pawlak and Andrzej Skowron. Rough sets: Some extensions. *Information Sciences*, 177:28 – 40, 2007.
- [17] Xiao Zhang, Changlin Mei, Degang Chen, and Jinhai Li. Feature selection in mixed data: A method using a novel fuzzy rough set-based information entropy. *Pattern Recognition*, 56:1 – 15, 2016.
- [18] Yuhua Qian, Jiye Liang, and Chuangyin Dang. Knowledge structure, knowledge granulation and knowledge distance in a knowledge base. *International Journal of Approximate Reasoning*, 50:174 – 188, 2009.
- [19] Wei Wei and Jiye Liang. Information fusion in rough set theory : An overview. *Information Fusion*, 48:107 – 118, 2019.
- [20] Yiyu Yao. Information granulation and rough set approximation. *International Journal of Intelligent Systems*, 16:87 – 104, 2001.
- [21] Witold Pedrycz and Wladyslaw Homenda. Building the fundamentals of granular computing: A principle of justifiable granularity. *Applied Soft Computing*, 13:4209 – 4218, 2013.
- [22] Yuhua Qian, Honghong Cheng, Jieting Wang, Jiye Liang, Witold Pedrycz, and Chuangyin Dang. Grouping granular structures in human granulation intelligence. *Information Sciences*, 382-383:150 – 169, 2017.
- [23] Qinghua Hu, Daren Yu, Jinfu Liu, and Congxin Wu. Neighborhood rough set based heterogeneous feature subset selection. *Information Sciences*, 178:3577 – 3594, 2008.
- [24] Yuan Gao, Xiangjian Chen, Xibei Yang, Pingxin Wang, and Jusheng Mi. Ensemble-based neighborhood attribute reduction: A multigranularity view. *Complexity*, 2019:1 – 17, 2019.
- [25] Zehua Jiang, Xibei Yang, Hualong Yu, Dun Liu, Pingxin Wang, and Yuhua Qian. Accelerator for multi-granularity attribute reduction. *Knowledge-Based Systems*, 177:145 – 158, 2019.
- [26] Keyu Liu, Xibei Yang, Hamido Fujita, Dun Liu, Xin Yang, and Yuhua Qian. An efficient selector for multi-granularity attribute reduction. *Information Sciences*, 505:457 – 472, 2019.
- [27] Didier Dubois and Henri Prade. Rough fuzzy sets and fuzzy rough sets. *International Journal of General Systems*, 17:191 – 209, 1990.
- [28] Hengrong Ju, Huaxiong Li, Xibei Yang, Xianzhong Zhou, and Bing Huang. Cost-sensitive rough set: A multi-granulation approach. *Knowledge-Based Systems*, 123:137 – 153, 2017.
- [29] Changzhong Wang, Yunpeng Shi, Xiaodong Fan, and Mingwen Shao. Attribute reduction based on k-nearest neighborhood rough sets. *International Journal of Approximate Reasoning*, 106:18 – 31, 2019.
- [30] Xibei Yang, Shaochen Liang, Hualong Yu, Shang Gao, and Yuhua Qian. Pseudo-label neighborhood rough set: Measures and attribute reductions. *International Journal of Approximate Reasoning*, 105:112 – 129, 2019.
- [31] Xibei Yang and Yiyu Yao. Ensemble selector for attribute reduction. *Applied Soft Computing*, 70:1 – 11, 2018.
- [32] Dominik Slezak. Approximate entropy reducts. *Fundamenta Informaticae*, 53:365 – 390, 2002.
- [33] Chih-Chung Chang and Chih-Jen Lin. Libsvm: A library for support vector machines. *ACM Transactions on Intelligent Systems and Technology*, 2:1 – 27, 2011.

Research on Application of Artificial Intelligence in VR Games

WANG XI^{a,b1}

^a*School of Design and Art, Xijing University, Xi'an, 710123, Shaanxi Province, China*

^b*Keimyung University, Daegu, 42601, South Korea*

Abstract. Purposed to promote the development of artificial intelligence (AI) technology in the game field, this article adopts the literature analysis method and the case study method, analyzes the problems with virtual reality (VR) games and explores several popular VR game cases in China and abroad before summarizing the artistic characteristics of VR games. Artificial intelligence technology has brought a new creative mode to the game industry, while providing more suitable game content for players. Further, artificial intelligence technology can equip VR games with better game experience by analyzing players' physiological and psychological information as well as players' game strategies. Compared with traditional games, VR games can deliver better interactivity, deeper immersion and higher fidelity. However, VR games impose higher requirements on device data and space scale; in other words, they must meet specific requirements to provide better game experience. VR games also have monotonous game types and high prices. In the future, the integration of VR games with artificial intelligence would generate more profound game-player experiences and richer game contents.

Keywords. Artificial Intelligence; VR games; Visual Interaction; Human-computer Interaction; Game Experience Introduction

1. Introduction

This study explores the application of artificial intelligence technology in the field of virtual reality (VR) games and analyzes the artistic characteristics of VR games in terms of interactivity, immersion and fidelity, while researching the problems with VR games in such fields as equipment, space, type and price. With the addition of artificial intelligence, VR games can deliver better development in game creation, user experience and game content. Further, this study will provide research ideas and theoretical bases for the integration of VR games and artificial intelligence technologies. This article also refers to the following three articles: "A Survey of Visual, Mixed, and Augmented Reality Gaming"[1], "Virtual Reality in Multiplayer Carrom Game with Artificial Intelligence"[2], "Artificial Neural Network in Virtual Reality: A Survey"[3]. The above three articles are all researches on VR games or AI algorithms from the field of computer and AI technology. Both the research methods

¹ Corresponding Author: Wang Xi, Xijing University, Chang'an District, Xi'an City, Shaanxi Province, China, 710123. E-mail: 1308573796@qq.com.

and the research steps have strong practicality, but these articles ignore the aesthetics of the game screen. It cannot study the current situation of VR games from an artistic perspective as well as it does not predict the development trend of the combination of VR games and AI technology. The above shortcomings are exactly what this article is about. This article will look at the combination of VR games and AI technology from an artistic perspective, hoping to bring new inspiration to these two fields.

The article adopts the literature analysis method and the case study method. The literature analysis method mainly collects data and materials of game companies for analysis and comparison. The case study method mainly studies the price, equipment, types of a specific game, and gives suggestions on the direction of the game development, as well as provides a theoretical reference for the game industry. This study is divided into four parts. The first part offers an overview of the current development of artificial intelligence technology, the second and third parts describe the characteristics and problems of VR games, and the last part explores the impact of artificial intelligence technology on VR games.

2. Development of artificial intelligence

As a branch of computer science, artificial intelligence attempts to explore the essence of intelligence and develop a new type of intelligent machines that can react in the similar way to human intelligence, covering such fields as robotics, language recognition, image recognition, natural language processing and expert systems. Over recent years, with the development of computer technology, artificial intelligence technology has developed rapidly. Meanwhile, it has spawned a huge industrial development space. Chinese government has also issued a number of policies to support, guide and standardize the artificial intelligence industry. For example, in July 2017, the State Council of China promulgated the "Development Plan for New-Generation Artificial Intelligence", which stated the direction and industrial layout of artificial intelligence in China, so that the application can reach the global advanced level and China can become one of the important centers of global artificial intelligence. [4].

Under this background, VR games have built a novel kind of visual and tactile presentation technology system. With the help of artificial intelligence technology, traditional games can achieve virtual space and strong immersion. As a result, the excellent experience enables VR games to quickly erode some of the territory of traditional game industry, which is encountering the ever-expanding ambitions and aggressive challenges of VR games and brand-new opportunities for industrial development.

3. Features of VR games

Ranging from the simple rock-paper-scissors game and Prisoner's Dilemma to more complex Go games and Blizzard's popular game StarCraft, the most fascinating part of games is that they can always provide some interesting and unknown challenges, because the essence of games lies in how to figure out the next action in a complex scene, so as to achieve the final victory as defined by the games. [5] The game industry

has made tremendous changes so far. For example, game props have evolved from buttons and keyboards to helmets and handles, and game modes have been graded from the simple two-dimensional human-machine interaction to the full-view advanced interactive mode for people currently. Now, VR games have set off another climax for the game industry. Since 2016, VR games have made a rapid growth. According to the "China Game Industry Report" released at the 2019 China Game Industry Annual Conference, "The actual sales revenue of the Chinese game market in 2019 is 230.88 billion yuan, with an increase of 7.7% year-on-year; and the number of game users in China reaches 640 million, with an increase of 2.5% year-on-year. Specifically, AR games' revenue exceeds 70 million yuan, with an increase of 64.3% year-on-year, and its user scale tops about 1.4 million, the year-on-year growth is close to 15%; VR game revenue is 2.67 billion yuan. With a year-on-year growth of 49.3%, VR game users has reached 8.3 million, with an increase of 22% year-on-year." [6] Given the growth rate of VR game users is far greater than that of overall game users, VR games showcase unparalleled advantages over the traditional games.

First, VR games can deliver better fidelity and reduction, because they use various devices to create a 360-degree visible full-view space in users' minds, so as to simulate a real scene, which is different from the two-dimensional plane space generated in traditional video games. In a space with a real sense of depth, players can enjoy scenes at any angle, where players watching the plots can get a more realistic feeling. In addition, VR games can render better light changes, surrounding sounds and better restoration of the information on the objective world. [7]

Second, VR games can achieve better immersion effects. From the users' views, VR games can provide first-person perspective and multiple perspectives. With the help of sound, light, electricity and other technologies, users' physiological and psychological feelings can be integrated into a specific game environment, so that they can experience comprehensive hearing, vision, tactile and even olfactory content. By creating a fascinating and fantasy world, such an environment is almost not affected by external factors, such as light and sound. In the objective world, this technology can give users a better sense of immersion

Third, VR games can realize better interactivity. In traditional games, users make interaction through screens and sounds, which are actually simple signal feedbacks on senses, because such means ignore the interaction between games and players' body movements. [8] Therefore, the game experience is not delicate enough. However, VR games can comprehensively upgrade the interactive system by taking a more advanced method, which can perform different interactions for each change of users and provide them with different game responses in movements, such as position moves, gesture changes and visual transitions. Due to richer and more delicate interactivity, such interactions can render more real and more interesting gaming experiences. **Figure 1** illustrates the interaction process between VR games and players.

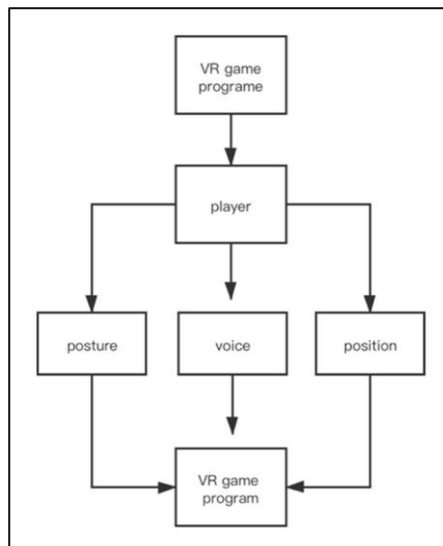


Figure 1. VR games have better interactivity

4. Problems with VR games

While VR games demonstrate a huge advantage in terms of experience compared to traditional games, the following limitations have to be overcome in their further development.

First, device restrictions: VR games require multiple sets of devices to complete the whole game. Especially, heavy requirements are imposed on data transmission, image resolution, somatosensory vibration, etc., thus raising the threshold for VR games' entry. Currently, mainstream VR game devices include Oculus Rift, HTC Vive and Sony PS4-VR. These high-end games also need equipment for positioning, audio, vibration, in addition to VR helmets and gamepads. Compared with the simple devices in traditional video games, the importance of VR game equipment is self-evident. However, too many devices are not easy to deal with, since the game preparation process would be too long and the tedious testing processes of game equipment would also test the patience of gamers who are always eager to dive into games. **Table 1** illustrates the different types of VR equipment and their characteristics. Obviously, the complexity of the device is limiting the development of VR games.

Table 1. Equipment required for VR games.

External VR helmet	The VR display helmet relies on an external computer, host and other equipment to run on the system. The content of the platform has the highest technical content. Representative products: Oculus, HTC VIVE, etc.
All-in-one VR helmet	The VR platform that integrates the content platform and the display device is independent and flat. And the platform strikes a balance between portability and functionality. Representative products: Little Black Spirit Mirror and others.

Smartphone VR glasses	Smart glasses are used as a display device to run the system. The platform has the best portability. But the content technology is at a relatively low level. Representative products: Gear YR, Storm Mirror, etc.
Shooting equipment	Multiple cameras form a seamless 360-degree panoramic virtual reality camera. Representative products: GoPro, Jaunt VR NEO, etc.
Operating equipment	Such platforms include gamepads, steering wheels, and simulated guns operation input devices, among others.
Behavior monitoring equipment	Infrared monitoring cameras, universal treadmills, gesture capturing gloves and other devices used to monitor user behavior.
Others	Headphones, microphones and other supporting equipment.

Source: the 2016 China Virtual Reality (VR) Industry Research Report by iResearch

Second, price restrictions: generally expensive, the devices of VR games affect their expansion to more users. In addition, VR games have a longer production cycle and more complicated manufacturing procedures than traditional video games. Moreover, the resulting game screens are more beautiful in VR games, thus further driving up the price. According to the Steam game website, as of June 2020, the average price of the top ten games listed on the site exceeded 120 yuan. The No.1, Beat Saber, was priced at 90 yuan. The Second half-life, Alyx, was at 163 yuan, and the fifth-ranked game, Tripwire Complete Bundle, is at 568 yuan. As a result, the excessive price weakens the interest of players to a certain extent, thus dwarfing the development of VR games.

Third, space constraints: traditional video games require game consoles or computers, monitors, keyboards, and handles or joysticks to provide players with a higher level of participation. VR games require not only VR headsets, glasses, joysticks, monitors and audio devices, but also require positioning systems, cameras and vibration systems. In order to pursue the realism and immersion for games, some game players even customize special seats, platforms and other equipment. large space is required to accommodate the equipment, a factor that often restricts the development of the VR games. Take the HTC ViveVR device as an example: officially, the game requires a space of 3.5m x 3.5m. For the setting of the scale in the room, the game area must be at least 2m x 1.5m, in order to experience a better virtual game. For example, **Table 2** shows the space required by different brands of VR equipment. For young players, such an environment requirement will limit their desire to purchase VR gaming equipment.

Table 2. Space supported by different brands of VR glasses.

Brand	largest space supported
HTC-Vive Pro	6M*6M
Sony-Play Station	3M*3M
Huawei-NOLO CV1 Air VR	5M*5M
Oculus-Quest VR	3M*3M

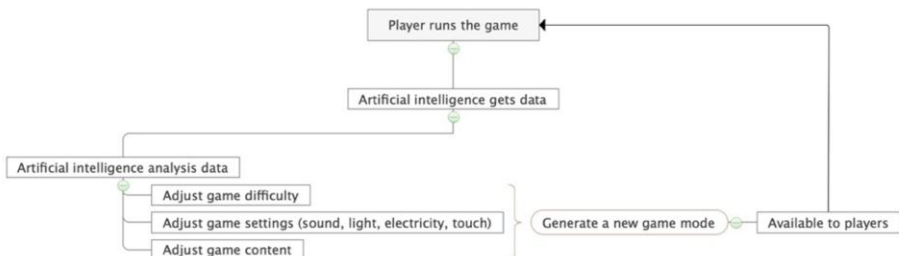
Fourth, the limited types of VR games. The types of VR games are not as rich as the traditional games. VR games are more widely developed for first-perspective games.

Simulated single-player games are less involved in strategy games. Compared with wide selection of the traditional games in game stores, there are not rich types of VR games. As shown on the Steam game website, as of June 2020, although the platform had released more than 3500 VR games, the game types are slightly narrowed, because most of them are first-person ones and there are almost no strategy games available. Few game types raise obstacles to the further development of VR games.

5. The impact of artificial intelligence on VR game

The intervention of artificial intelligence (AI) will transform VR games. First, AI can be used to analyze users' usage habits and separately change the game progresses and rhythms, if VR games utilize artificial intelligence technology to measure game players' physical state, usage habits, etc. Moreover, AI can even test players' responses to game pressures by detecting changes in their breathing and blood pressures. Based on players' physiological and psychological data in the process of VR games, the game programs can match players' physical and psychological fitness better. For example, 18-year-old users and 30-year-old ones would show obvious physiological differences in their personal reaction speeds and stress resistances for the same game. In this case, artificial intelligence may follow the analyzed data and difficulty levels. Tensions and even changes in space and light of games may be re-allocated to maximize the satisfaction of different users. For example, in **Figure 2**, artificial intelligence technology modifies the game program by analyzing player data.

Figure 2. Artificial intelligence changes the course of the game:



Second, artificial intelligence can automatically correct the defects in a game based on the data on game players. By actively learning the wisdom of game players, artificial intelligence may also provide a direction for the development of video games. With Alpha Go developed by Google and artificial intelligence developed by Blizzard, AI players have defeated human professional players. By studying the human thinking mode to explore a thinking process that can defeat humans, a deep simulation of the biological nervous system in the human brain is conducted. Similarly, many organizations are connected to each other through a series of associations, thereby forming a neural network-like processing mode to deal with the faced problems accurately and quickly. [9]. In short, artificial intelligence can learn human game thinking, correct its own defects and develop better game strategies.

Third, artificial intelligence can quickly collect materials based on the content and creativity of games to help with game development. In terms of game production, artificial intelligence can actively search for relevant messages based on the key information provided by the developers as well as the required data, such as pictures, colors, light sources and sounds. Based on the key information available, artificial intelligence technology can independently complete the conversion of styles and scenes. Further, by taking advantage of artificial intelligence technology, designers can configure the characteristics of game scenes in the game development platform. Similarly, based on game development and running procedures, designers can be provided with a good window editing platform. And game test platforms can help game developers complete game development. [10]

Fourth, artificial intelligence technology can improve the performance and size of VR equipment. With the help of high-speed digital technology, VR devices will be able to get rid of heavy computing burdens, store a large amount of data in the clouds for downloading at any time, and reduce the computing tasks of devices. [11] On this basis, the volume and weight of devices can also be cut and the game content can be displayed in a more lightweight way. Then, lightweight equipment can achieve more ergonomic designs and get rid of the heavy and awkward appearance of VR equipment. If full of modern styles, VR equipment will strongly attract young people and play an important role in the development of mixed reality (MR) technology.

6. Conclusion

By integrating artificial intelligence and VR technology in the field of games, the development of the game industry will be accelerating, and the transformation of digital art and technology will be facilitated. With diversified game contents, the forms are becoming more abundant as well, with intelligent game modes appearing. In terms of intrinsic values, the development of artificial intelligence technology meets the requirements of players for higher levels of game art. In terms of extrinsic values, artificial intelligence technology provides a richer production method for VR games. Firstly, VR games, as a new development type in the game industry, have brought new art forms, because they provide a virtual space environment and render more real visual effects and psychological feelings. Relying on the development of artificial intelligence technology, VR games can analyze the habits of game users to adapt the game rhythms to users for more practical game changes. Secondly, the artificial intelligence system in games can acquire game-players' strategies through human-computer interaction and independent learning. Then, it may carry out the corresponding methods to fix the deficiencies in games. Thirdly, artificial intelligence can independently search for the materials needed to help designers develop games. The rapid evolvement of artificial intelligence technology and the integration of VR games with unique AI operation modes will create more attractive game content and promote the further growth of the game industry.

References

- [1] M. Z. Khan, F. Hassan, M. Usman, U. Ansari and S. Noor, "Virtual Reality in Multiplayer Carrom Game with Artificial Intelligence," 2018 12th International Conference on Mathematics, Actuarial Science, Computer Science and Statistics (MACS), Karachi, Pakistan, 2018, pp. 1-5, doi: 10.1109/MACS.2018.8628394.7.
- [2] Thomas, Bruce. (2012). A survey of visual, mixed, and augmented reality gaming. *Comput. Entertain.* 10. 3:1–3:33. 10.1145/2381876.2381879. - Cavazza, M. AI in computer games: Survey and perspectives. *Virtual Reality* 5, 223–235 (2000). <https://doi.org/10.1007/BF01408521>.
- [3] Sharma, Greeshma & Chandra, Sushil & Venkatraman, Saraynya & Mittal, Alok & Singh, Vijander. (2016). Artificial Neural Network in Virtual Reality: A Survey. *International Journal of Virtual Reality.* 15. 44-52. 10.20870/IJVR.2016.15.2.2873.
- [4] Wisdom Bud. Global Pattern of Industrial Intelligence: Future Trends and China's Potential[J]. *Economic Theory and Economic Management*,2019(10):2.
- [5] Alfonsina Pagano, Augusto Palombini, Guido Bozzelli, Maurizio De Nino, Ivana Cerato, Stefano Ricciardi. Arkae Vision VR Game: User Experience Research between Real and Virtual Paestum[J]. *Applied Sciences*,2020,10(9).
- [6] Joe Chen. 2019 China Game Industry Report: VR game revenue 2.67 billion yuan. [EB/OL] VR Home. 2019-12-27 10:59.
- [7] LUCAS Simon, Shen Tianyu, Wang Xiao, Zhang Jie. General artificial intelligence for games based on statistical forward planning algorithm[J]. *Journal of Intelligent Science and Technology*,2019,1(03):219-227.
- [8] Wang Xiaohan. VR game design and implementation analysis[J]. *Digital World*,2020(03):55-56.
- [9] Cao Kunze. Artificial intelligence and its application in the field of games[J]. *Science and Technology Communication*,2020,12(08):143-144.
- [10] Zhao Yue. Design and implementation of 3D game development platform based on artificial intelligence characters[J]. *Computer fan*,2018(05):207.
- [11] He Shucun. Radio and TV game service platform based on cloud computing technology[J]. *Science and Technology Communication*, 2015, 7(10):145-146.

Fuzzy Expert Pricing Systems and Optimization Techniques in Marketing Science

Adeolu DAIRO^{a,1} and Krisztián SZÜCS^b

^{a, b}Faculty of Business and Economics, University of Pecs, Hungary

Abstract. Despite the advancement in the mathematical models for solving and modeling marketing problems, there exists gap between model predictions and market reality. Fuzzy logic bridges this gap by providing marketers with the opportunity of combining robust human experts in the form of linguistic rules to formulate a knowledge-base. These rules are systematically developed into a marketing tool which provides intelligent pricing decision support for marketers in a dynamic and competitive environment. In this paper, these expert pricing systems which are designed and developed to help businesses in pricing decision-making are examined. Price-Strat, FuzzyPrice, and exPrice expert pricing systems are compared and discussed. These three expert pricing systems are explored along with their fuzzy development approach, effectiveness, and attributes in pricing products and services.

Keywords. fuzzy logic, pricing tools, marketing models.

1. Introduction

The advancement and advantages of working with membership function as against crisp values brought to light the importance of fuzzy logic in marketing science [1]. Marketers have a powerful tool when they leverage fuzzy logic in the development of marketing models. The fuzzy logic marketing model is a new way of carrying out marketing analysis by marketers through the emergence of “if-then” rules instead of the crisp value. With this new modeling approach, marketers are now endowed with business tools that are sustainable for driving business performance. Marketers can now respond to the dynamic and sophisticated consumer market, along with competition and other market fluctuations.

Pricing has always been one of the primary issues of every business [2]. Setting the appropriate price has an immediate effect on the company's revenue and profitability. For pricing decision-making, numerous parameters must be taken into consideration. First, the company must decide the strategic aims of its pricing moves. These can be due to the need for survival under intense competition or scarce resources. Also, the need to maximize profit and sales growth can account for the need for a price change. Having the right pricing tools and models helps marketers to respond to the needs of the customers, competition and enhance consumer customer experience toward an acceptable level of profitability [1, 2].

¹ Adeolu Dairo, Faculty of Business and Economics, University of Pecs, Rakoczi 80, Pecs H -7623, Pecs, Hungary; E-mail: dairo.adeolu@pte.hu.

In this study, three Fuzzy Expert knowledge-based pricing systems are discussed. Price-Strat system [3], FuzzyPrice [4], and exPrice expert systems [5] are compared along with their fuzzy development and their focus on solving pricing issues and challenges across different sectors.

2. Literature Review

Many research applications in marketing have emerged using fuzzy logic as modeling techniques [6]. A prominent field of marketing in this regard is customer behavior and customer satisfaction models [7]. Fuzzy expert systems focus and deal with uncertainty by leveraging fuzzy information processing through fuzzy rules. According to Ertay and Kahraman [8], fuzzy logic models offer opportunities in evaluating relations between consumer needs and service attributes. Also, the ability to navigate through the natural language and its statements components has yielded contributions from researchers in the aspects of the product, service with quality evaluation, and group analysis [9, 10, 11]. Customer segmentation is another marketing field that has witnessed the significant application of fuzzy logic [12]. The marketing mix, pricing, and strategy are another prominent area of fuzzy applications in marketing science [13, 14, 15, 16]. In all these applications, marketers have seen an increase in the gathering of marketing analysis because of the use of fuzzy logic in several aspects of marketing science.

Expert systems are considered as part of computer science that leverages the symbolic and non-algorithm approach to solve tasks [6, 7]. These types of computer programs combine techniques and knowledge that are comparable to human experts [17]. Generally, an expert system is comprised of three essential components: the knowledge base, inference engine, and the user interface [18]. The decision-makers are the domain expert, knowledge engineer, and the user. The inference engine generates decisions following its interpretation of the knowledge of experts. The strategic expertise for solving different problems resides with the knowledge engineer who leverages the experience of previously solved problems to address the current issues [19]. Knowledge engineer requires the domain expert to think aloud and explain every step of the decision-making process during the expert system development. Knowledge engineer models the knowledge as soon as he has understood the knowledge structure. Understanding and modeling the experience is a complex task, and at the same time, one of the most critical steps in expert system development [6].

On many occasions, expert system development takes an approach similar to prototype logic [19]. This logic undergoes testing and modification [20, 21]. Also, the second to the n^{th} prototype will be created until an acceptable result is obtained from the expert system. Moreover, expert systems can keep many years of experience of combined marketers in the form of knowledge [7].

3. Methodology

In providing a clear outlook of the importance and advantages of fuzzy logic application and its associated expert systems in marketing science, this study discusses three fuzzy expert pricing tools. These pricing expert systems (Price-Strat, FuzzyPrice, and exPrice)

leverage both descriptive and inference statistics in building the fundamentals of their fuzzy model with details of relevant components of the pricing tools [3, 4, 5].

4. Discussion

During the creation of a typical fuzzy logic model, the first step is the transformation of the linguistic variables within the membership functions with the intention of a clear understanding of the variables in a fuzzy way. In that case, each of the membership functions stands for a linguistic variable with a clear definition of the associated fuzzy set along with the parameter.

4.1 Price-Strat Expert System

Price-Strat [3] stands out as one of the unique pricing expert systems. It is a hybrid expert system that leverages both the historical market data and commercial managers' experiences to arrive at the most appropriate pricing solution for different industries -industry, such as banking, aviation, and telecommunication. The Price-Strat pricing system performs well in reacting to the competitor's move within a competitive environment that is characterized by price wars.

As for the Price-Strat methodology, business goals and objectives for pricing decisions are first determined by the business managers. Afterward, the system generates "what-if" scenarios with regards to possible variations of prices to competitive prices. These scenarios are fed into the system, which creates the knowledge base. An adaptive predictive model is created through historical market data that are fed into the system (see Figure 1). The most appropriate price solution is generated among many proposed solutions through the questioning of the knowledge base. Price-Strat takes into consideration all variable costs, fixed cost, price, and all constraints, such as volume [3, 22].

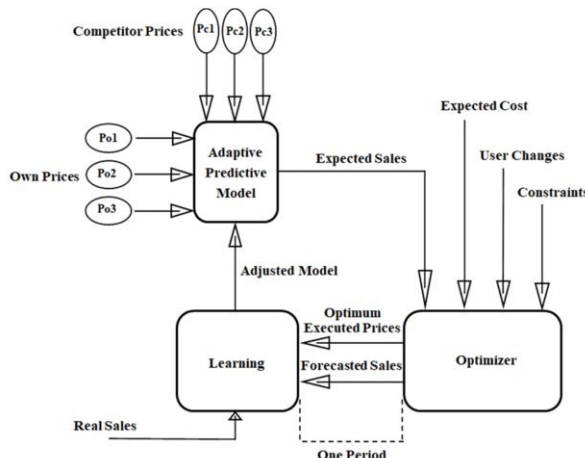


Figure 1. Price-Strat generic system and architecture

4.2 FuzzyPrice Expert System

FuzzyPrice pricing expert system combines fuzzy logic and fuzzy reasoning methods to arrive at the appropriate price combination across the product portfolio of a firm [4]. It does this with a view of aligning with the firm strategic aims while considering the strategic constraints. In this case, the inference follows the price changes of the competitors during the price wars. A unique feature of the FuzzyPrice system is that it is restricted to short and mid-term pricing and cannot be considered for long-term pricing.

FuzzyPrice system is characterized by its operation that follows a fuzzy “what-if” scenarios (see Table 1). The heart of the inference procedure of this system lies in these scenarios. Market predictors are formed from these sets of scenarios. Fuzzy “what-if” scenarios are implemented along with fuzzy rules with the similar structure of the fuzzy “IF-THEN” rules. While managerial decision making, which is coming from human experts, remains the most qualitative knowledge input for the FuzzyPrice system, market research, and historical data are also valuable data sources [4].

Table 1. Characteristic comparison of the expert pricing tools

Attributes	Price-Strat	Fuzzy Price	exPrice
System Type	Hybrid Expert System	Hybrid Expert System	Expert System
Operations	“If-then” rules and price scenarios responses	“What-If” scenarios”	“If-then” production rules
Pricing Application	Multiple industries	Multiple industries	Multiple industries
Unique feature	Easy adaption of variants to different consumer industries	Scenario-oriented along with sensitivity and profit margin analysis	Flexibility and modularity
System Improvements	Large scope for improving profitability for all Price-Strat family of tools	Weighting of each competitor’s actions and extending variable to include variable such as advertisement	Presented as a system open for new production rules extension without modifying the existing ones

4.3 exPrice Expert System

The exPrice expert system is a product and pricing expert system in which four variables were used during the development [5]. The variables are the elasticity of demand in relation to price, market structure, level of business activities, and business goals. Depending on the numerical value of the elasticity coefficient, it can take any of “low,” “significant,” or “high” as a fuzzy variable. Market structure, which is the second variable is a determinant of the number of products and offerings in the market. These offerings can be “high,” “significant,” and “low.” The third variable in the exPrice expert system is the intensity of the firm’s business activities. The most important is the fourth variable, which is the business goal. This determines the strategic intent behind the price move.

The strategic intent behind the price move can be customer retention, acquisition, or response to the competitive landscape and activities. The exPrice expert system can suggest the following pricing move to the business (a) retain existing price, maintain price with promotional activities, equalize price with the competition, or decrease the price by a certain percentage point. It contains production rules (see Table 1), and facts that provide insights and help to marketers in pricing and product management [5, 23].

5. Conclusion

Price-Strat is a knowledge-based and generic pricing tool that takes care of pricing processes. On the other hand, FuzzyPrice and exPrice are hybrid expert systems that contain numbers of fuzzy expert systems layered together in a block and systematic manner [3, 4, 5]. Through the various variants of Price-Strat, experienced and non-experienced marketers across many industries can leverage the pricing tool to determine their price points. The variants of Price-Strat are PriceNet used by gasoline stations, Retail Price Optimizer for retail, TelPrice for the mobile industry, and BankPrice system for the banking industry [22].

During the pricing decision-making process on each of the products of the firm within a market when using the FuzzyPrice system, all the competitor's pricing moves along with all their product mix serve as input to the system [4]. As for the exPrice expert system, pricing decisions are made following the elasticity of demand, market structure, business activity intensity, and the firm business goals and objectives. All the three expert pricing tools that are discussed in this paper have achieved very good results across several vital pricing strategic objectives [5]. However, further improvements in the system can still lead to better accuracy of the recommended price points with a better impact on the customer experience. The systems can achieve this depending on the expert knowledge and historical data availability. This is an exciting area for future work.

One notable limitation in this study is the inability to experiment and evaluate the three pricing tools along their price adjustment performance. This is due to the uniqueness of the expert pricing tools toward specific industry, and perhaps, products and services. However, evaluation and comparison of the pricing tools are measured along their characteristics and development.

References

- [1] Enache IC. Fuzzy logic marketing models for sustainable development. *Bulletin of the Transilvania University of Brasov, Series V: Economic Sciences*. 2015; 8(57).
- [2] Rekettye G, Liu J. *Pricing: The New Frontier*. Transnational Press London; (2018).
- [3] Singh MG, Bennavail JC. Price-Strat: A knowledge support system for profitable decision-making during price wars. *Information and Decision Technologies*. 1993; 19: 227-296.
- [4] Tzafestas SG, Raptis SN, Moschos NA. A hybrid pricing expert system based on fuzzy reasoning. *Foundations of Computing and Decision Sciences*. 1999.
- [5] Bijakšić S, Markić B, Bevanda A. Expert pricing system as part of marketing mix. 2017; 50: 3-4.
- [6] Rhuggenaath J, Akcay A, Zhang Y, Kaymak U. Fuzzy logic-based pricing combined with adaptive search for reserve price optimization in online ad auctions. *IEEE International Conference on Fuzzy Systems Institute of Electrical and Electronics Engineers*. 2019.

- [7] Martinez-Lopez F, Jorge C. Marketing intelligent systems for consumer behavior modeling by a descriptive induction approach based on genetic fuzzy systems. *Industrial Marketing Management*. 2009; 38: 714-731.
- [8] Ektay T, Cengiz K. Evaluation of Design requirements using fuzzy outranking methods. *International Journal of Intelligent Systems*. 2007; 22: 1229-1250.
- [9] Temponi C, John Y, Amos T. House of quality: a fuzzy logic-based requirements analysis. *European Journal of Operational Research*. 1999; 117: 340-354.
- [10] Maruvada DP, Bellamkonda RS. Analyzing the passenger service quality of the Indian Railways using railqual: examining the applicability and technology. 2010; 1: 478-482.
- [11] Yogi K. An empirical and fuzzy logic approach to product quality and purchase intention of customer. *Pacific Science Review, Humanities and Social Sciences*. 2015; 57 -69.
- [12] Razak T, Hashim M, Noor N, Halim I, Shamsul N. Career path recommendation system for UiTM Perlis Students using fuzzy logic. *IEEE*. 2014; 978-1-4799- 4653-2/14.
- [13] Susanto S, Vasant P, Bhattacharya A, Fransiscus RP. Fuzzy LP with a non-linear MF for product-mix solution, a case-based re-modeling and solution. *Proceedings of the 9th joint Conference on Information Science*. 2006.
- [14] Aly S, Ivan V. Fuzzy expert marketing-mix model. *Agricultural Economics*. 2005; 51: 69-79.
- [15] Xiong Y, Li G, Kiran JF. Dynamic pricing model and algorithm for perishable products with fuzzy demand. *Applied Stochastic Models in Business and Industry*. 2010; 26: 758-774.
- [16] Bennouna G, Tkouat M. Fuzzy logic approach applied to credit scoring for microfinance in Morocco. *Procedia Computer Science*. 2018; 127: 274–283.
- [17] Zadeh L. Making computers think like people, *IEEE Spectrum*. 1984; 26-32.
- [18] Ruiz-Mezcua B, Garcia-Crespo A, Lopez-Cuadrado JL, Gonzalez-Carrasco I. An expert system development tool for non-AI experts. *Expert Systems with Applications*. 2011; 38: 597–609.
- [19] Omid M, Lashgari M, Mobli H, Alimardani R, Mohtasebi S, Hesamifard R. Design of fuzzy logic control system incorporating human expert knowledge for combine harvester. *Expert Systems with Applications*. 2010; 37: 7080–7085.
- [20] Tavana M, Hajipour V. A practical review and taxonomy of fuzzy expert systems: methods and applications. *Benchmarking: An International Journal*. 2019; 27: 81-136.
- [21] Thaker S, Nagori V. Analysis of fuzzification process in fuzzy expert system. *Procedia Computer Science*. 2018; 132:1308 -1316.
- [22] Cassaigne N, Singh MG. Intelligent decision support for the pricing of Products and services in competitive consumer markets. *IEEE Transactions on Systems, Man and Cybernetics – Part C: Applications and Reviews*. 2001; 31(1).
- [23] Nan G, Wang S, Li Z, Dou R. A novel pricing strategy for mobile broadband carriers using two-stage Stackelberg model. *Knowledge-based system*. 2018; 142: 45-57.

ClothNet: A Neural Network Based Recommender System

Xing Hao, Han Zhike¹, Shen Yichen

Zhejiang University City College, Hangzhou, Zhejiang, 310015, China

Abstract. The traditional collaborative filtering recommendation systems have many deficiencies, which make them incompetent in the domain of clothing recommendation; we proposed a new ClothNet model based on CNN, RNN, collaborative filtering and the characteristics of the fashion industry. The accuracy and generalization performance of this model are improved compared with traditional systems. The visual information integrated into the ClothNet model enables the recommendation system to alleviate the cold start problem, and new clothes can be added to the recommendation list faster through the visual information. The addition of temporal information enables ClothNet sharply capturing the impact of seasonal and time changes on user preferences. However, because RNN and CNN have the disadvantage of requiring a large amount of data, combining RNN and CNN will make the model more difficult to converge, so we have adopted the LearningToRank training mode and obtained good results.

Keywords. Convolutional Neural Network, Recurrent neural network, Recommend System, LearningToRank, Collaborative filtering

1. Introduction

1.1. Research background

The Internet has gradually become an essential part of people's life which produces uncountable numbers of information. However, there is a problem - information explosion. Tiktok and Kwai are fledging, one of the reasons is that the recommendation system enables users to receive information they want in a closed feed stream. In the shopping software, recommendation systems are vital component. Through recommendation, long tail goods can be mined to exploit users' purchasing power.

In information retrieval, in order to solve the information overload problem, the recommendation system can learn our habits, reduce searching time and improve work efficiency, and at the same time, in the rapid development environment of network and e-commerce, in order to sell more products at a lower cost, recommendation system, as a means of precise marketing, has become increasingly popular.

The entities in the recommendation system fall into two categories: users (users) and recommended items (items). According to how to use these two types of information, recommendation systems can be divided into two types, personalized recommendation system and non-personalized recommendation system.

¹ Corresponding Author, Han Zhike, Zhejiang University City College, Hangzhou, Zhejiang, 310015, China;
E-mail: hanzk@zucc.edu.cn.

Non-personalized recommendation system only considers the information of the item dimension and explored the connection among items, but does not include users' preferences. The most representative traditional methods are association rules and time-sensitive sorting. Since the user's information is not taken into account, there is a lack of targeted recommendations to the user.

The development of the Internet enables us utilizing information more effectively. From this data, we can extract the relationship between users and items, and even the relationship among users, which makes the emergence of personalized recommendation systems possible. CUDA is an accelerator for the development of deep learning, allowing the calculation speed of deep learning surging. In this article, we will introduce some optimization methods for a deep learning-based recommendation system.

Ranking recommendation algorithms can be roughly divided into three categories:

The first category is listwise approach. Listwise approach solves the ranking problem through direct ranking. During the training process, it takes a sorted list of objects (for example, a sorted list of documents in IR) as an example, and trains the ranking function by minimizing the list loss function defined on the list of prediction results and the real list.

The second category is pointwise approach, which looks at a single document at a time in each iteration. They basically take a single document and use it to train a classifier / regressor to predict the correlation between the current query and the real situation.

The third category is the pairwise approach. In the list method, sorting is transformed into sequence classification or sequence regression. The method of pairing is the pairwise sorting loss. For the two pairs of points a and b, if a is sorted before b, we think that the loss is 1, and vice versa.

The first kind of point-pair method is the traditional DEEP FM[1], FM[2], FFM[3],etc.

The second type of paired methods are represented by BPR[4], VBPR[5], etc.

The third type of list method is represented by SoftRank[6], ListNet[7], etc.

The traditional recommendation system and the deep learning-based recommendation algorithm mentioned in the previous section uses a single feature (mainly user, item purchase or rating matrix or a single content-based recommendation), The number of recommendation systems based on multiple content is relatively small.

Besides, the traditional recommendation systems don't exploit the information about the order of purchase time. It only records what items the user purchased, the order of purchasing has been ignored. We will use the recurrent neural network to solve this problem.

1.2. The framework of this article

The main goal of this article is to build a scalable, interpretable, personalized recommendation system with temporal information, which will greatly improve the performance. Our recommendation system can be closer to the changing hobbies of users and communities. Especially in a rapidly mutating field, the relationship between user preferences and time is more encrypted and inseparable; secondly, due to "the long tail" problem and new products are being constantly launched, so we need a cold start solution, we can't rely too much on explicit or implicit user feedback. We can also tap the user's preference for the product from a visual perspective to solve the cold start problem and make more precise recommendations. Our system can extract visual information and

understand the changes in user preferences and fashion preferences in the time dimension. In other words, how fashion is evolving.

At the same time, exploiting visual information can effectively solve the cold start and correctly handle items not co-occur in dataset. This paper proposes a new model--ClothNet, which can effectively extract the corresponding visual information and effectively solve the cold start and non-co-occurrence. Based on the deep neural network model of CNN and RNN, use Pytorch to build and train the model. The loss function is designed using a LearningToRank (sequence learning loss) model [7]. The dataset is the Amazon dataset of women clothing from 2011 to 2017 [8][9][10].

The deep neural network model based on CNN and RNN is the core content of the system. We will introduce the model from the dataset, data preprocessing, model design, training methods and parameters, result comparison and analysis.

2. Related works

Cao[7] et al. have proposed a new approach to LearningToRank, referred to as the listwise approach. In particular, they designed a new and powerful loss function in their work.

Smirnova et al.[11] pointed out that the previous RNN modeling approaches summarize the user state by only considering the sequence of items that the user has interacted with in the past, without taking into account other essential types of context information such as the associated types of user-item interactions, the time gaps between events and the time of day for each interaction. In order to solve this problem, they introduced this context information on the basis of traditional RNN and proposed a new Contextual Recurrent Neural Networks (CRNNs) model.

Rendle [2] proposed the FM (Factorization machines) model in 2010, the purpose is to solve the feature combination problem under sparse data. In traditional machine learning, features are encoded using One-hot, so the feature space is very sparse. In addition, we tend to combine features to create more new features. The FM model can effectively reduce the dimensionality of features. It has the following characteristics:

- The FM model can be trained when the feature space is very sparse.

- The FM model is of linear time complexity.

The FM model is a general model, and its training data feature value can be any real number.

Rendle et al. [4] also investigated the most common scenario with implicit feedback (e.g. clicks, purchases), and provided ideas on how to utilize implicit feedback information, they also presented a generic optimization criterion and learning algorithm for personalized ranking. He et al. [5] proposed a scalable factorization model to incorporate visual signals into predictors of people's opinions, which can be applied to a selection of large, real-world datasets. They made use of visual features extracted from product images using (pre-trained) deep networks, on top of which they learned an additional layer that uncovers the visual dimensions that best explain the variation in people's feedback. This not only leads to significantly more accurate personalized ranking methods, but also helps to solve cold start issues, and qualitatively to analyze the visual dimensions that influence people's opinions. Weston et al. [12], also proposed powerful factorization models which give us great inspiration. These models are used by us as baselines to provide a comparison of the results of our ClothNet model.

Chatfield et al. [13] proposed a new architecture names CNN-F, where F stands for Fast, and this structure has very good training efficiency. It plays a key role as a visual information extractor in the ClothNet model.

In recent years, many interesting research works have emerged in clothing recommendation. Shen et al. [14] proposed the Scenario-Oriented Recommendation. This algorithm requires users to provide special attributes of products, and analyzes the user's purpose to obtain more accurate recommendation results. Tu et al. [15] introduced hierarchical fashion multimedia mining model and developed a refined contour extraction method to build a color tone analysis model. Zhang et al. [16] proposed a neural network for clothing recommendation based on details such as the user's travel destination's weather, scenery and other characteristics, and achieved good results. Liu et al. [17] improved the Collaborative Filtering recommendation algorithm and proposed the Advanced User-based Collaborative Filtering recommendation algorithm. This algorithm introduces a user-item linked list, which can reduce the space complexity of the algorithm. De Barros Costa et al. [18] introduced an approach that recommends items based on fashion and users' body type. Packer et al. [19] proposed an approach that learns users' visual preferences and predicts based on this. Yu et al. [20] pointed out that the traditional clothing recommendation systems did not consider Aesthetic features, and introduced a special neural network for extracting Aesthetic features.

3. Model Design

3.1. Datasets

The Dataset in this study is based on the USCD's AMAZON user shopping and rating dataset [8][9][10]. After cleaning, the fashion category (women's wear) is selected, and the data volume is 100K +. And the main pictures corresponding to the item in the dataset are collected by a web crawler and used as the visual feature.

We use user comment history as implicit feedback, and we filter users who purchase less than five items. The results after processing are shown in Table 1.

Table 1 Dataset introduction (after processing)

Number of users	Number of users	Implicit feedback	Time span
99748	331173	854211	2014.3-2014.7

3.2. Model Architecture

We use a convolutional neural network to extract visual features, a recurrent neural network [21] to obtain time-series related information, and training by LearningToRank (sorted learning loss) method. At the same time, for each time step output of the recurrent neural network, we processed the L2 loss function with the pooling output of the standard picture after CNN.

3.2.1. Problem Definition

We use implicit feedback information, such as purchase history, click history, and ratings. In implicit feedback, there are non-negative feedback and sorted feedback; Our optimization goal is to sort the purchased items so that the items purchased by the user have higher ranks than the items that weren't purchased [4].

Figure 1 shows the architecture of our model. First, we use customer purchase record data to train FM, and compress user preferences to obtain a user matrix. Then we input the image corresponding to the product into the CNN-F module, and get the prediction result through CNN-F and RNN. And compare the output result of CNN and RNN with the result of FM, get the loss value, we use the loss value for back propagation to train the neural network parameters.

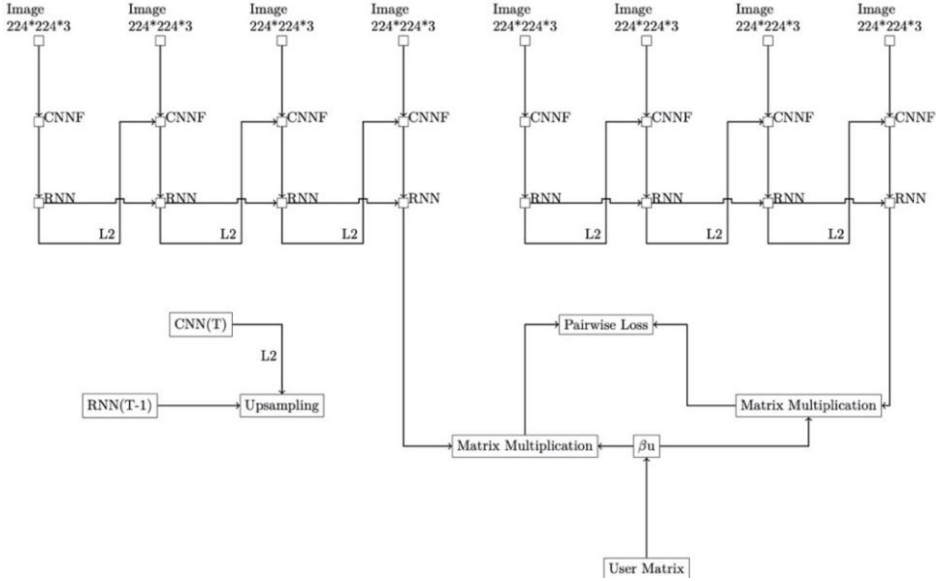


Figure 1. Structure of ClothNet

3.2.2. Preference predictor

We use a factorization machine (FM) to make the final score prediction, which can be regarded as a linear regression model based on matrix factorization initialization [22]. A most basic model for predicting users' commodities can be expressed according to Eqs. (1).

$$x_{u,i} = \alpha + \beta_u + \beta_i \gamma_u^T \gamma_i \quad (1)$$

In the past, the FM models with vision mostly used pre-trained convolutional neural network models (multiplexing backend for other computer vision applications such as target detection, segmentation and other task training models as backend to extract visual information), and use an embedding matrix to map high-dimensional visual information to low-dimensional. [5]

$$x_{u,i} = \alpha + \beta_u + \beta_i + \gamma_u^T \gamma_i + \theta_u^T (\mathbf{E} f_i) \quad (2)$$

Our model is mainly used to solve the problem that the previous models directly using the pre-training model, instead we use the convolutional neural network model trained for the task end2end. In this way, we can directly extract visual features from the image and apply them to our model. At the same time, we exclude the item bias term β_i

and latent user-item preference γ_i compared to the above two models. The improved model is in Eqs. (3).

$$x_{u,i} = \alpha + \beta_u + \boldsymbol{\theta}_u^T \boldsymbol{\phi}(X_i) \quad (3)$$

3.2.3. Visual feature extractor

Our convolutional neural network structure uses [13] as backend, which has very good training efficiency, which is one of the reasons why we choose this structure. The Backend has 8 layers of trainable parameters, 5 layers of convolution layers, and finally three layers of fully connected layers. The input image size is 224 * 224. We use ReLU[23] as activation function. Dropout[24] layer is added to prevent overfitting. BatchNorm[25] layer is used to normalize the input layer by adjusting and scaling the output of the convolutional layer. Table 2 shows the structure of the model.

Table 2 The Structure of CNN-F

Conv1	Conv2	Conv3	Conv4	Conv5	Fc1	Fc2	Fc3
64x11x11 st. 4, pad 0	256x5x5 st. 1, pad 2	256x3x3 st. 1, pad 1	256x3x3 st. 1, pad 1	256x3x3 st. 1, pad 1	4096 Drop 0.5	4096 Drop 0.5	K

3.2.4. Deconvolution (upsampling) layer

Due to our small amount of data, and in order to reduce the pressure of the recurrent neural network training, reduce the number of parameters, and accelerate the convergence of the model, we have performed global maximum pooling on the input data at the channel level. However, since we then have a reconstruction loss with the output of the convolutional neural network, the structures of the inputs are required to be the same, so we can use deconvolution or upsampling to interpolate the data. The traditional upsampling methods include bilinear interpolation, monolinear interpolation, Gaussian interpolation, etc., which we will not introduce here. Let's talk about the principle of deconvolution. Deconvolution is also called transposed convolution. We use the transposition of convolution to restore the dimensionality of the data after dimensionality reduction. Of course, such an operation certainly cannot fully restore the state before convolution, because convolution is not a bijective, but an irreversible dimensionality reduction operation, which is similar to hash functions, the same output may correspond to several inputs. But we can combine it with the convolution operation to transfer the gradient back to the recurrent neural network, so that its parameters can converge.

In practice, we are dealing with a training set with noise, finite dimensions, finite time series, and discrete sampling. However, by expressing the problem as a solution to the Toeplitz matrix and using Levinson recursion, we can estimate the filter with the smallest mean square error relatively quickly. We can also directly perform deconvolution in the frequency domain to obtain similar results. This trick is similar to logistic regression.

3.2.5. Temporal information extractor

In this paper, a variant of the recurrent neural network, Long Short-Term Memory Network (LSTM [26]), is used as the model structure for extracting time series information. Figure 2 shows the structure and propagation of LSTM. As a variant of

recurrent neural network, LSTM allows the previous temporal information to flow to the next step or even later steps through the memory gate and the forgetting, so that the current time step can get the information of the previous step. It is beneficial to the implementation of cold start. At the same time, LSTM provides a two-way flow mode, which allows time steps to not only propagate backwards, but also forwards, which solves the problem of one-way timing and allows the model to extract more information. Eqs. (4)-(8) shows is the principle of LSTM forward propagation:

$$f_t = \sigma_g(W_f x_t + U_f c_{t-1} + b_f) \quad (4)$$

$$i_t = \sigma_g(W_i x_t + U_i c_{t-1} + b_i) \quad (5)$$

$$o_t = \sigma_g(W_o x_t + U_o c_{t-1} + b_o) \quad (6)$$

$$c_t = f_t \circ c_{t-1} + i_t \circ \sigma_c(W_c x_t + b_c) \quad (7)$$

$$h_t = o_t \circ \sigma_h(c_t) \quad (8)$$

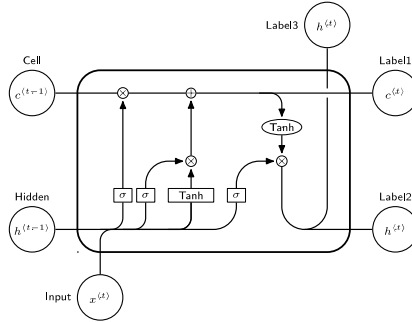


Figure 2. Schematic diagram of LSTM cell unit structure

4. Model loss and training details

4.1. Model loss design

In order to better combine time series information and visual information, we use L2 reconstruction loss [27] to enable time series network to learn time series information. We use pairwise ranking loss to let the model learn the recommendation ability similar to the FM.

4.1.1. L2 reconstruction loss

We adopted the reconstruction loss commonly used in GAN (Generative Adversarial Networks)[28], and made the pointwise mean square error between the output of the convolutional neural network network and the output of the recurrent neural network in the previous time step as our training loss. At the same time, we designed θ as the

attenuation hyperparameter. Since our time series input has the property of padding, we processed the sequence loss function with a long padding sequence, that is, the actual purchase sequence is too short, so that its contribution in the training process is smaller. The calculation formula of MSE is as follows:

$$MSE(\hat{\theta}) = E(\hat{\theta} - \theta)^2 \quad (9)$$

4.1.2. Loss for sorting pairs

In the sequence method, the loss for the sorted pair is transformed into the classification of the sequence or the regression of the sequence. The so-called pair is sorted in pairs. For example, (a, b) indicates that a is in front of b. We don't care how much the ranking pair a (for items observed by the user) is higher than the score for b (for items not observed by the user). As long as the score a is higher than the b score, we truncate the loss 1. Conversely, truncate the loss to 0. During the previous experiment, the model did not converge and eventually collapsed. The main reason for this situation is the large number of parameters of the recurrent neural network, so it requires more training data, and it is more difficult to converge to the best advantage. When we incorporate the convolutional neural network into the RNN, the gradient will be scattered, the model may collapse. The range of pairwise loss is shown below:

$$\begin{cases} 1 & \text{if } a > b \\ 0 & \text{if } a \leq b \end{cases} \quad (10)$$

4.2. Hyperparameters and training details

4.2.1. Dataset processing

We discarded users who purchased less than 5 items, and correspondingly deleted items that had no purchase history. At the same time, we specifically divided the cold start dataset for the cold start problem-commodities purchased less than 5 times were specifically used as the cold start dataset to test the cold start performance of our model.

4.2.2. Training hyperparameter details

The model image input is 224 * 224 * 3, the length of the padding sequence is 10, the weight attenuation coefficient θ is 0.1, the batch-size is 32 (2 * 16), and 50 epochs are trained. The test and training sets are randomly divided according to the user's 3/7 ratio. We use bilinear interpolation to upsample the data.

5. Comparison of model results

5.1. Comparison of model results

Our model compares random results (AUC 0.5), WARP[29], BPR-MF, FM and VBPR. Use AUC as our result evaluation index.

5.1.1. Evaluation index analysis

We use AUC as the result evaluation index, AUC, Area Under Curve, which means the area under the ROC curve. The AUC indicator measures the quality of our results for ranking. The formal representation of the AUC curve is shown in Eqs. (11).

$$AUC = \frac{1}{|U|} \sum_{u \in U} \frac{1}{|\mathcal{D}_u|} \sum_{(i,j) \in \mathcal{D}_u} \xi(x_{u,i} > x_{u,j}) \quad (11)$$

\mathcal{D}_u represents the complete set of users, and $\xi()$ is a Boolean indicator function. If the observed i score is greater than we think of j for the observed item, then we count 1 and vice versa. Accumulate the technology and then get the proportion of correct ordering. This indicator is also the training loss of the traditional BPR model [10].

5.1.2. Detailed explanation of the comparison model

Stochastic model: We use random probability to rank the observed and unobserved items, so the AUC ratio is exactly 0.5. This indicator represents the result of a random recommendation of the user's product, which is the lower limit of the model.

The top K optimized weights approximate matrix decomposition to the ranking loss (WARP) [12]: In order to face the growing dataset and labeling tasks, how to use small-scale datasets for training has become a problem. In the training mode, it aimed at a new ranking method for different score differences. It provides a new online learning mode. Hinge loss is used to cut off the score between different gaps. In order to achieve better optimization results.

Bayesian sorted factorization machine (BPR-MF): It is currently the best implicit user feedback recommendation system based on personal sequences. Use a simple FM and learn the observed priors according to Bayes' theorem as a posterior that can be used in the recommendation system. In this method, we only consider the observed sequence as a sequence of interest to the user. This potential pattern discovery can take advantage of a large amount of implicit feedback in a system. Therefore, the problem of insufficient data amount of the recommendation system is solved.

FM (Factorization Machines) [2]: traditional factorization algorithms. This method is similar to a linear regression model, and uses the second-order term of the vector inner product between items and characters to express the mutual relationship between features. It can be optimized using least squares or stochastic gradient descent.

Bayesian factorization machine with vision (VBPR) [5]: It is currently the best Bayesian sorting algorithm with visual information. It uses pre-trained CNN models to provide visual features. And add the visual information bias item to express the user's preference for visual information, so as to get a visual second-order item similar to the FM, which is our recommendation model more accurate.

5.1.3. Comparison of model results

Table 3 shows the model results, the evaluation index is AUC, and the Dataset is the Amazon Women's Clothing Dataset. Cold start means that our test set contains only goods purchased by less than five people. As we can see, our ClothNet model outperforms many models.

Table 3 Comparison of model results

	RAND	WARP	BPR-MF	FM	VBPR	ClothNet
All	0.5	0.6192	0.6543	0.6678	0.7081	0.7475
Cold Start	0.5	0.3822	0.5196	0.6682	0.6885	0.7268

6. Conclusion

The model we proposed mainly uses convolutional neural networks to extract the visual features of items, and uses LSTM to model the user's purchase dat. Finally, the loss function of pairwise is designed for training based on the LearningToRank method.

At the same time, there are fewer restrictions on the input dimensions based on the RNN. At the same time, we use the FM to decompose the user's implicit feedback (scoring matrix) and use the commodity vector as the initialization of our user matrix.

As for training, the RNN also adds L2 reconstruction loss to allow the model to obtain gradients at every time step, similar to the training method of relay supervision [30], and the relaxation term enables the model with a shorter sequence to converge with long sequences. In the selection of LearningToRank (sequence learning loss) loss functions, we again relaxed the score (the score ranking is only provided by the FM during initialization), and the observed and unobserved samples were truncated so as not to concern about the specific score regression differences, which makes the model easier to train.

For the dataset, we used Amazon women's clothing data as the training set and test set, divided by a ratio of seven to three, filtering users who purchased less than five products, which is convincing.

In terms of results, compared with some existing models, we have improved the accuracy of items by a maximum of 3.7% in the cold start of items (items that are purchased less) (see comparison of experimental results), which proves that our model has a certain ability on cold start.

In terms of future prospects, although our ClothNet model incorporates temporal information, the results when predicting temporal information are not very good, and sometimes even lower than traditional models. The reason is that the amount of training data required by the recurrent neural network is too large, and although we have a large dataset, the timing sequence generated is still very small for the items it contains, so the model is difficult to converge.

Reference

- [1] Guo, H., Tang, R., Ye, Y., Li, Z., & He, X. DeepFM: a factorization-machine based neural network for CTR prediction. arXiv preprint arXiv:1703.04247.2017 Mar;arXiv:1703.04247.
- [2] Rendle, S. Factorization machines. In 2010 IEEE International Conference on Data Mining;2010 Dec 14-17;Sydney, Australia:IEEE;p. 995-1000.
- [3] Juan, Y., Zhuang, Y., Chin, W. S., & Lin, C. J. Field-aware factorization machines for CTR prediction. In Proceedings of the 10th ACM Conference on Recommender Systems;2016 Sept 15-19; Boston,MA.ACM; c2016;p. 43-50.
- [4] Rendle, S., Freudenthaler, C., Gantner, Z., & Schmidt-Thieme, L. (2012). BPR: Bayesian personalized ranking from implicit feedback. arXiv preprint arXiv:1205.2618.2012.
- [5] He, R., & McAuley, J. VBPR: visual bayesian personalized ranking from implicit feedback. In Thirtieth AAAI conference on artificial intelligence.2016 Feb 12-17;Phoenix, Arizona:AAAI;c2016;p.144-150.

- [6] Taylor, M., Guiver, J., Robertson, S., & Minka, T. Sofrank: optimizing non-smooth rank metrics. In Proceedings of the 2008 International Conference on Web Search and Data Mining .2008 Feb 11-12;Palo Alto,CA.ACM;c2008;p. 77-86.
- [7] Cao, Z., Qin, T., Liu, T. Y., Tsai, M. F., & Li, H. Learning to rank: from pairwise approach to listwise approach. In Proceedings of the 24th international conference on Machine learning.2007 Jun 20-24;Corvallis,Oregon.ACM;c2007;p. 129-136.
- [8] He, R., & McAuley, J. Ups and downs: Modeling the visual evolution of fashion trends with one-class collaborative filtering. In proceedings of the 25th international conference on world wide web.2016 Apr 11-15;Montreal,Canada.ACM;c2016;p. 507-517.
- [9] McAuley, Julian, et al. Image-based recommendations on styles and substitutes.In Proceedings of the 38th International ACM SIGIR Conference on Research and Development in Information Retrieval. 2015 Aug 9-13;Santiago,Chile.ACM;c2015;p.43-52.
- [10] Ni, J., Li, J., & McAuley, J. Justifying recommendations using distantly-labeled reviews and fine-grained aspects. In Proceedings of the 2019 Conference on Empirical Methods in Natural Language Processing and the 9th International Joint Conference on Natural Language Processing (EMNLP-IJCNLP).2019 Nov 3-7;Hong Kong,China.Association for Computational Linguistics;c2019;p. 188-197.
- [11] Smirnova, E., & Vasile, F. Contextual sequence modeling for recommendation with recurrent neural networks. In Proceedings of the 2nd Workshop on Deep Learning for Recommender Systems.2017 Aug 27;Como,Italy.ACM;c2017;p. 2-9.
- [12] Weston, J., Bengio, S., & Usunier, N. Wsabie: Scaling up to large vocabulary image annotation. In Twenty-Second International Joint Conference on Artificial Intelligence.2011 Jul 16-22;Barcelona, Catalonia, Spain.IJCAI/AAAI;c2011;p.2764-2770.
- [13] Chatfield, K., Simonyan, K., Vedaldi, A., & Zisserman, A. (2014). Return of the devil in the details: Delving deep into convolutional nets.British Machine Vision Conference, 2014 Sept 1-5,Nottingham, UK.BMVA Press;c2014;
- [14] Shen, E., Lieberman, H., & Lam, F. What am I gonna wear? Scenario-oriented recommendation. In Proceedings of the 12th international conference on Intelligent user interfaces.2007 Jan 28-31;Honolulu,Hawaii.ACM;c2007;p.365-368.
- [15] Tu, Q., & Dong, L. An intelligent personalized fashion recommendation system. In 2010 International Conference on Communications, Circuits and Systems (ICCCAS) .2010 Jul 28-30;Chengdu,China.IEEE;c2010;p. 479-485.
- [16] Zhang, X., Jia, J., Gao, K., Zhang, Y., Zhang, D., Li, J., & Tian, Q. Trip outfits advisor: Location-oriented clothing recommendation. IEEE Transactions on Multimedia. 2017 Apr 24;IEEE;19(11), p.2533-2544.
- [17] Liu, Y., Nie, J., Xu, L., Chen, Y., & Xu, B. Clothing recommendation system based on advanced user-based collaborative filtering algorithm. In International Conference on Signal and Information Processing, Networking and Computers.2017 Dec 19;Springer, Singapore;473,p. 436-443.
- [18] de Barros Costa, E., Rocha, H. J. B., Silva, E. T., Lima, N. C., & Cavalcanti, J. (2017, April). Understanding and personalising clothing recommendation for women. In World Conference on Information Systems and Technologies. 2017 Apr 11-13;Springer, Cham;c2017,569,p.841-850.
- [19] Packer, C., McAuley, J., & Ramisa, A. Visually-aware personalized recommendation using interpretable image representations. arXiv preprint arXiv:1806.09820.
- [20] Yu, W., Zhang, H., He, X., Chen, X., Xiong, L., & Qin, Z. Aesthetic-based clothing recommendation. In Proceedings of the 2018 World Wide Web Conference.2019 Apr 23-27;Lyon,France.ACM;c2018;p. 649-658.
- [21] Pineda, F. J. Generalization of back-propagation to recurrent neural networks. Physical review letters,1987 Nov;59(19), 2229.
- [22] Koren, Y., & Bell, R. Advances in collaborative filtering. In Recommender systems handbook . 2015.Boston,MA:Springer.p. 77-118.
- [23] Glorot, X., Bordes, A., & Bengio, Y. Deep sparse rectifier neural networks. In Proceedings of the fourteenth international conference on artificial intelligence and statistics. 2011 Apr 11-13;Fort Lauderdale, USA.JMLR.org;c2011;p. 315-323.
- [24] Witten, I. H., & Frank, E. Data mining: practical machine learning tools and techniques with Java implementations. 2000 Jan.San Francisco,CA:Morgan Kaufmann.
- [25] Ioffe, S., & Szegedy, C. Batch normalization: Accelerating deep network training by reducing internal covariate shift. In Proceedings of the 32nd International Conference on Machine Learning.2015 Jul 6-11;Lille,France;JMLR.org;c2015;p.448-456.
- [26] Hochreiter, S., & Schmidhuber, J. Long short-term memory. Neural computation,1997 Dec;9(8), 1735-1780.
- [27] Mathieu, M., Couprie, C., & LeCun, Y. Deep multi-scale video prediction beyond mean square error. arXiv preprint arXiv:1511.05440.2015 Nov.

- [28] Goodfellow, I., Pouget-Abadie, J., Mirza, M., Xu, B., Warde-Farley, D., Ozair, S., ... & Bengio, Y.. Generative adversarial nets. In Advances in neural information processing systems.2014 Dec.Montreal Canada.ACMP.p. 2672-2680.
- [29] Weston, J., Bengio, S., & Usunier, N. Large scale image annotation: learning to rank with joint word-image embeddings. Machine learning.2010.Boston,MA:Springer.81(1), p.21-35.
- [30] Wei, S. E., Ramakrishna, V., Kanade, T., & Sheikh, Y. (2016). Convolutional pose machines. In Proceedings of the IEEE conference on Conference on Computer Vision and Pattern Recognition.2016 Jun 27-30;Las Vegas,NV;IEEE Computer Society;c2016;p.4724-4732.

Realistic Face Image Generation System Based on GANs

Han Zhike, Yang Bin¹, Du Yiren, Du Xingyu, Xing Hao and Cheng Qinnan

Zhejiang University City College, Hangzhou, Zhejiang, 310015, China

Abstract. The purpose of this paper is to study the help of generative adversarial networks (GAN) for face generation, and to explore whether the network can have an effect on complex face generation. Training an image translation neural network model based on a generative adversarial network with the help of a large number of real human face data sets. Using the CV2-based face tagging algorithm and the HED-based face edge extraction algorithm to obtain input information, and then based on the translation neural network model Developing a face generation system through Tensorflow, Torch and other frameworks to realize the function of generating real faces through sketches or “changing faces” through existing faces. Finally, this model provides training configuration and training information.

Keywords. Generative Adversarial Network, Face Generation, Face Tag

1. Introduction

Oral memory portrait method is that the investigators describe the characteristics of the criminals or suspects stated by the victims during the detection of the case, and paint the facial portraits of the criminal suspects with a brush. Moreover, the generative adversarial networks-based image generation application can improve the authenticity and Accelerating efficiency can increase the similarity and narrow the criminal search. In addition, a deeper application can achieve a simple textual description of the eyewitness and then depict the face. The past depiction method is obviously not high enough in terms of time efficiency. No matter how powerful a painter can paint a work, it must be faster than a computer. Using technology to describe a face has a great advantage in terms of timeliness. The precise computer resolution band. The accuracy is also self-evident. Solving a case seeks speed. One minute and one second can affect the rate of arrest of criminals. Therefore, this technology can greatly improve the rate and efficiency of criminal investigation. This topic can be extended to the generation of images, such as buildings and animals. With the support of the data set, the demand for generating real pictures by giving sketch outlines can be realized.

In image processing, many problems in computer graphics and computer vision that require image processing can be regarded as “translating” the input image into the corresponding output image. We define graph and graph transformation as the problem of translating a possible scene expression into another and give enough training data. A major difficulty in language translation is that the mapping between languages is rarely

¹ Corresponding Author: Yang Bin, Zhejiang University City College, Hangzhou, Zhejiang, 310015, China; E-mail: sevenyoung7@foxmail.com.

one-to-one. Similarly, the difficulty of most image translations is many-to-one; such as computer vision: images and edges, semantics, semantic labels or one-to-many of computer graphics: labels or the mapping of all user input to real images. These tasks are traditionally separated item by item and processed purposefully, despite the fact that the processing methods are all predicted pixel by pixel. In order to solve this problem, it is proposed to use generative adversarial networks model to effectively apply to this field [1]. Domestic research has proposed a face reduction algorithm based on generative adversarial networks. This algorithm adds a part of supervised learning on the basis of unsupervised learning, called semi-supervised learning (GANs + CNN) [2]. Reference is made to the previously proposed semi-supervised learning ideology [3], and reference to the co-adapted fixed learning rate [4] is used to set the learning rate.

This paper aims to realize the translation of the input contour through a machine learning translation model into a realistic face image. The basic principle is to use generative adversarial networks to achieve machine learning capabilities and meet the conditions for real face generation. Moreover, through the pix2pix translation framework to achieve image translation, the training set required for model training and prediction is processed by the CelebA face database. For users, only the simple operations of mobile terminal or PC terminal for registration; and login, uploading and input can be used to generate the real and touching faces needed.

2. The Problem and Proposed Solution

2.1. Symbol and term definition

Image Domain: The image domain is more inclined to the attributes of the image content, such as the spatial domain of the image, also known as the image space, which is essentially a space composed of image pixels. The variable takes the space as the variable, the horizontal axis is the x axis, and the vertical axis is the y axis.

Discriminant Function: The purpose of setting the concept of discrimination function is to unify the judgment conditions of classification.

Canny Algorithm: The Canny edge detection operator is a multi-level edge detection algorithm developed by John F. Canny in 1986. The edge detection of the traditional canny operator is divided into five steps. First, the Gaussian filter is used to reduce the noise and make the picture smoother. Then the gradient intensity and direction of a given pixel are calculated, and then the obtained data is used. Use non-maximum suppression to eliminate spurious responses, use dual thresholds to detect edges, and finally complete the detection process by suppressing weak edges.

Labeling Method: On the premise of having a face contour, the translation model needs to mark the image features. This algorithm for marking the features of a face image is called a face marking algorithm.

The Table 1 is the relevant symbol definition of GAN. And the Table 2 is the symbol definition of the input and output of the pix2pix framework.

Table 1. The relevant symbol definition of GAN.

real data	data	real data	data
real data distribution	p_{data}	generator output	p_g

real data	data	real data	data
input data (noise) distribution of raw noise	z p_z	generate mapping discriminant mapping	G () D ()

Table 2. The symbol definition of the input and output of the pix2pix framework.

symbol	significance	symbol	significance
G	generator	z	random vector
D	discriminator	D_k^n	Discriminator features of layer n
x	input map	M	total floors
y	output graph	N_n	Number of elements in layer n

2.2. The problem

Area of Research:

Training set: Training a model that generates high-definition images will inevitably require a suitable training set. The training set requires high resolution and a sufficient number.

Edge extraction algorithm: Since the contour of the face needs to be used as both semantic identification and mapping input, it is particularly important to choose an appropriate algorithm to meet these two requirements.

Translation model: In image processing, computer graphics and computer vision, many problems that require image processing can be regarded as "translating" the input image into the corresponding output image. Therefore, a reasonable translation model needs to be selected for training.

System development: After the algorithm design and development are completed, due to the needs of the system user experience. A complete photorealistic image generation system that is convenient for users and meets the basic functions of the system needs to be developed.

Research difficulties:

(1): Training set: using only the open source CelebA face database provided by the Chinese University of Hong Kong is not enough to meet the needs of the project. It needs to be further developed to meet the needs of the project. The specific difficulty is that the pictures in the face library contain Other human parts that are not needed for the subject, thus a large number of pictures need to be edited. In addition, not all the pictures in CelebA meet the requirements of high definition, hence the resolution needs to be adjusted to avoid blurring in the details of the generated image.

(2): Edge extraction: Canny edge extraction is an operator that uses local extreme values to extract edges [5]. The implementation process of the Canny edge detection algorithm mainly includes the following processes: first, Gaussian filtering is used to denoise the image; then the finite difference of the first-order partial derivative is used to calculate the amplitude and direction of the gradient; and finally, it is completed by double thresholds. The algorithm extracts and connects the edges for the first time to obtain the final edge extraction results[6,7,8].The effect of edge extraction using the general Canny algorithm is not very good. It has a problem of many noises and cannot be used as a semantic mark. It needs to be improved to obtain a simpler outline. The idea should focus on semantic segmentation instead of edge extraction. Because after

extraction, the obtained edges are input into the model as corpus. An edge extraction model that better meets the needs of the subject is needed.

(3): Translation model: When generating high-resolution images, the effect of the pix2pix framework is not good. For example, when assigning high-resolution input, it is difficult for the network to generate high-resolution output. This shortcoming is reflected in the generation. The details of the picture are very vague. The feeling is not big enough. Therefore, a deeper network or a larger convolution kernel is needed to obtain a larger feeling field. However, simply increasing the depth or breadth will result in overfitting and requires more GPU memory for training.

(4): System development: Since the user group prefers to use the mobile terminal, cross-platform responsive development is required and a large number of adaptations are needed to ensure that the mobile terminal can also obtain a good user experience when accessing the browser.

According to the research difficulties, the main problems we need to solve are: (1) edit the training set, extract key parts and high-definition images; (2) use the edge extraction technology of the appropriate subject; (3) improve the translation model to ensure that it is suitable for high-resolution input and produces high-resolution output; and (4) the overall structure of the website is responsive layout, modular component development and separation of front and back ends.

2.3. GAN and image translation

GAN is called Generative Adversarial Networks, that generates adversarial networks. It was first proposed by Ian J. Goodfellow et al. in the paper published in October 2014 [9]. This paper proposes a new framework for estimating generative models through an adversarial process, in which two models are trained simultaneously: a generative model G that captures the distribution of data and a discriminant model D that estimates the probability of samples coming from the training data.

Generative adversarial networks are mainly composed of two parts, namely generator and discriminator. The task of the generator is to learn the distribution of the real image to make the generated image more real, and the real image learned through the discriminator test. The task of the discriminator is to judge whether the received picture from the generator is true or false. During the entire training process, the generator continuously makes the generated image more real and the discriminator continuously discriminates whether the image is true or false. This process is similar to a two-player game. During the training, the generator and discriminator continue to confront each other, and finally the two networks approach dynamic equilibrium: the image generated by the generator is close to the real image distribution, and the discriminator could not judge the true and false of the generated image. The probability of being true is infinitely close to 0.5.

real data	data
real data distribution	p_{data}
input data (noise)	z
distribution of raw noise	p_z
generator output	p_g
generate mapping	$G()$
discriminant mapping	$D()$

Figure 1. GAN symbol definition.

G represents a generator, which is a multi-layer perceptron. The parameters of the perceptron are θ_g . The generating function G represents mapping noise to the data space, such as $G(z; \theta_g)$. This means that the generating mapping function maps noise to the corresponding data space, the same as Just like the discriminant function D . As well, it is considered as a multi-layer perceptron with parameters, such as $D(x; \theta_d)$, which outputs a scalar indicating the probability that the input is real data or the probability of generating data.

$$\min_G \max_D V(D, G) = E_{x \sim p_{data}(x)}[\log D(x)] + E_{z \sim p_z(z)}[\log(1 - D(G(z)))] \quad (1)$$

The decoding part consists of another three convolutional layers. However, in this part, it converts the feature vector obtained from the encoding part to restore them to the input size, then we can get the predicted wind speed of each pixel.

The purpose of the discriminator D is to make it possible to distinguish whether the input is a real sample or a generated sample as much as possible, so the goal is to maximize the value of $D(x)$ and minimize the value of $D(G(z))$, which means Maximize $V(D, G)$. For generator G , the goal is that the discriminator cannot distinguish, that is, the value of $D(G(z))$ needs to be maximized, that is, $V(D, G)$ is minimized. Through the confrontation of the two models, the final get a global optimal solution. For generator G , the goal is that the discriminator cannot distinguish, that is, the value of $D(G(z))$ needs to be maximized, that is, $V(D, G)$ is minimized. Through the confrontation of the two models, the final get a global optimal solution.

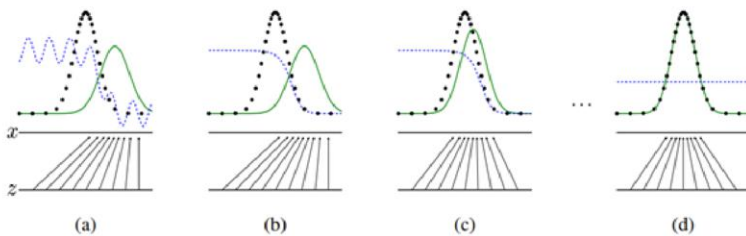
**Figure 2.** Training process [10].

Figure 2 shows the optimization process of the entire confrontation. The black curve corresponds to the true distribution of the samples, while the green curve corresponds to the fake samples generated by the generator. Moreover, the blue curve is the output of the discriminator's judgment on the generated samples. With the

improvement of the detector, the distribution of the generated samples is closer to the real distribution. As well, with the help of the output of the discriminator, the generator is further improved. Therefore, the generated distribution and the real distribution almost overlap. At this time, the discriminator cannot make a judgment, and the output is close to 0.5, reached optimization.

When performing the optimized representation, it needs to be divided into two steps. First, the judge determines whether the input sample is a real sample. The logarithm function belonging to the positive class is in the distribution of $p_{data}(\chi)$, so that the discriminator is in Obtained p_{data} distribution can accurately obtain $D(\chi)=1$, which is the front of the formula:

$$E_{\chi \sim p_{data}(\chi)} [\log D(\chi)] \quad (2)$$

The second step is the discriminator to determine whether the input sample is a generated sample, which is a logarithmic function of the negative class, that is, the rear part of the formula:

$$E_{z \sim p_z(z)} [\log(1 - D(G(z)))] \quad (3)$$

The discriminator needs to maximize the formula. At this time, it is best to judge whether the sample is generated or the real sample. For the generator, it needs to be minimized. The distribution generated at this time is closest to the actual distribution. The entire iterative training process maximizes $V(D, G)$ after the generator outputs, obtains the corresponding D , uses the obtained D and minimizes $V(D, G)$ to obtain a new G . This process can be expressed as:

$$G^* = \operatorname{argmin}_G V(G, D_G^*) \quad (4)$$

When referring to image translation (i.e., image-to-image translation), it is inevitable to first mention the basic encoder-decoder translation model in natural language processing. This model is a description of the framework of a class of models, such as common applications in Chinese and English machines. The most significant feature of translation is the end-to-end learning method of the model, which is mainly two processes of encoding and decoding. This process is required in both Chinese and English translation. The encoding converts the input sequence to a length. The fixed vector and decoding will turn the generated length vector into an output sequence. Such a model is also called seq2seq model, which vividly describes the string sequence that is expected to get semantic translation through a given string sequence.

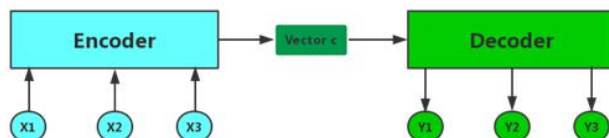


Figure 3. Translation framework.

As shown in Figure 3, the input character sequence X_1, X_2, X_3 is converted into a vector c of fixed length by the encoder, and the decoder converts the vector into a new sequence Y_1, Y_2, Y_3 . The most common neural network used by this model is RNN. The first and second two neural networks serve as encoder and decoder respectively.

Through joint training of these two RNN networks, the input sequence can be the conditional probability is maximized and the output sequence is obtained. As a kind of framework rather than a fixed model, decoding and encoding cannot only deal with text, but more widely such as voice, image, video, etc. The same neural network can be CNN or RNN and many more.

On the basis of Encoder-Decoder, it can naturally be applied to the field of images, but there are still great differences between pictures and text. The first is the two different concepts of image content and image domain. Image content can be understood as the semantics of the corresponding text. Although there is still a big difference between the two.

Next is the concept of the image domain. The image domain is more inclined to the attributes of the image content, such as the image spatial domain, also known as the image space, which is essentially a space composed of image pixels. The variable takes the left side of the space as a variable, sitting is taken as the coordinate origin, the horizontal axis is the x axis and the vertical axis is the y axis, as shown in Figure 4.

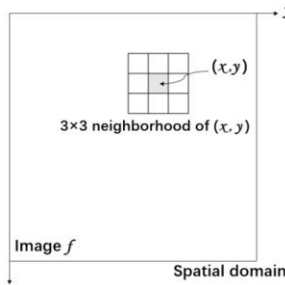


Figure 4. Image domain.

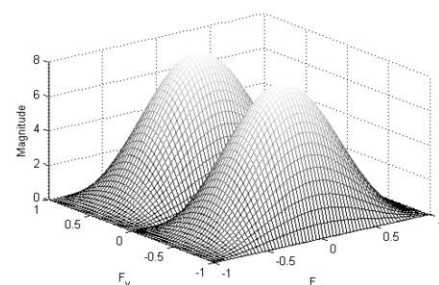


Figure 5. Frequency domain.

The frequency domain is the frequency structure of the signal and the relationship between the frequency and the amplitude of the frequency signal. It often expresses the severity of the grayscale change in the image, that is, the index of the grayscale spatial gradient. For the image, since the edge of the image is abrupt Yes, it belongs to a faster change. Therefore, it appears as a high-frequency component in the frequency domain. As well, the noise in the image represent a high-frequency component in most cases.

Therefore, under the above-mentioned differences, image translation can be understood differently. The first understanding is the translation of the semantics of pictures. The understanding of images is to replace the content of the images, and the specific ones should transform semantic texts into corresponding semantically correct pictures.

In more cases, image translation is understood as the translation of the image domain. One domain α of the image is transformed into another domain β , that is, the original attribute χ of a domain α of the image is removed, and a new attribute δ is given to the domain, namely in the case of $[Y, \chi] \subset \alpha$ and $[Y, \delta] \subset \beta$, a transformation f is obtained. The goal of the transformation f is:

$$f([Y, \chi]) = [Y, \delta] \quad (5)$$

Due to the fierceness of generative adversarial networks, a large number of generative adversarial networks-based image translation methods have appeared, such as pix2pix:

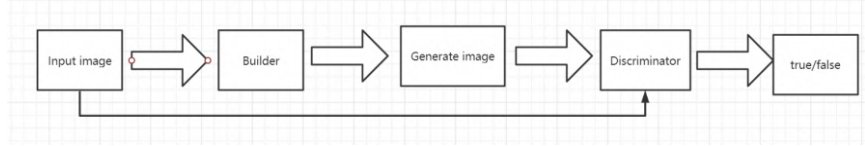


Figure 6. Translation framework pix2pix.

Compared with generative adversarial networks[11], the input to the generator is no longer noise, but an image, which is more biased towards the translation of image semantics. More striking is the improvement of the traditional encoder decoder framework by this model, which uses U-Net [12].

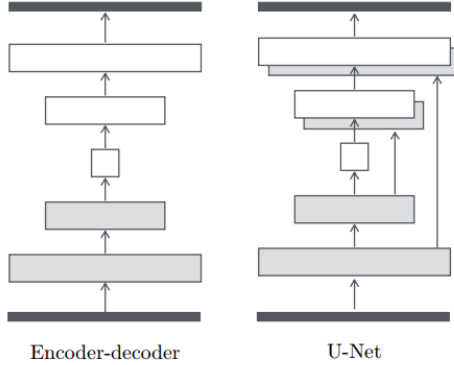


Figure 7. Neural Network U-Net[12].

Compared with the ordinary Encoder-decoder, U-Net in the decoder connects the output before the conv layer with the corresponding mirror layer in the decoder. Through this move, doubling the number of channels will not affect The output dimension of the convolution.

Another translation model, CycleGAN, prefers the conversion of the image domain. The purpose is to convert the images of the two domains with each other, which is different from the traditional generative adversarial networks one-way propagation. As shown in Figure 7, the neural network model is ring-shaped. Two mirror-symmetric generative adversarial networks construct a ring. Each of them has a discriminator. As well, a generator is used to obtain a consistent loss through the loop.

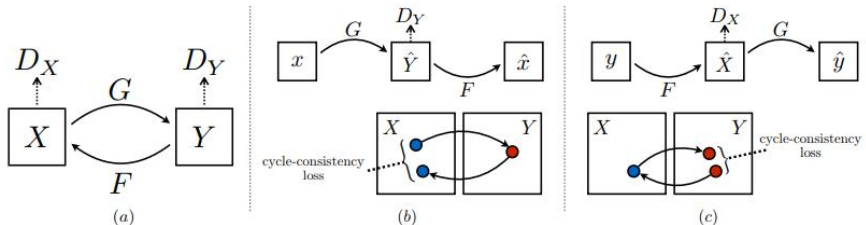


Figure 8. Translation model CycleGAN[11].

3. Experiment and Result

3.1. Face Generation

For user input, two methods are provided. The first is to manually input the contour. Due to the consideration of the two needs of the PC and the mobile, the user needs to implement two methods of manual input and camera shooting, and the manual input method is selected. The way of drawing board, the camera is realized by the front end of the web page.

Canvas is a tag in html that uses scripts to draw graphics, and the specific idea of hand-painting is to use javascript to monitor the mouse. Through the monitoring of mouse events, use the drawcircle method to draw the recorded image. First initialize the canvas, set the function to the brush state, record and display the pressed mouse point, then stop recording when released. For the problem of moving too fast, connect the points to record the line segment. At the back end, cv2 is used to flip the color to meet the needs of the facial feature identification of the translation framework. Based on the principle of image gray value, white to black are divided into multiple gray levels in the form of logarithm. Generally, black is defined as 0 and white is defined as 255. By flipping the gray value of the pixel, the color is flipped. Adjust the resolution of the input image to 1024*1024 pixels that meet the translation framework. Use the dlib face recognition library to perform face recognition on the image, in order to ensure that the input picture meets the facial features and avoids incorrect input.

For the input of a real human face, the file upload function is selected on the pc side. For the mobile side, the camera of the mobile device is first turned on, and the image recorded on the camera is converted into a file and uploaded to the server. Use the dlib face recognition library to perform face recognition on the image to ensure that the input picture meets the facial features and avoids incorrect input. Due to the different resolutions of the uploaded pictures of different cameras, first find the face, intercept the picture, and adjust the resolution of the input image after the interception. According to the original length and width of the image, adjust the length and width to meet the translation frame of 1024 * 1024 pixels.

3.2. Face Tag

Due to the training of machine learning models, a large amount of data is required to form a data set, and the corresponding face translation requires a large number of real faces as a training set. Since the human face has a clear distribution of features, facial features and other features, it is necessary to mark facial features and facial features. Moreover, the edge extraction of human face is divided into two parts: data set and extraction algorithm.

The original data set comes from the celebA face database [13] of the Chinese University of Hong Kong. The face database is open data and contains 202,599 images from 10,177 people at home and abroad. However, these data cannot be directly applied, and preliminary data cleaning is required, as well as the resolution is unified for training. The first step is to perform face detection through the dlib library, determine the position of the face, intercept the picture in proportion, and then transfer it to a 1024*1024 pixel high-definition picture to save it.



Figure 9. Original celebA figure.



Figure 10. HD picture after processing.

After processing, 30,000 faces are obtained as the data set, which is used as the input data of the image translation model.

After having enough initial data, we extract the outline of the picture and initially we use the edge detection of the traditional canny operator, which is divided into five steps. First, the Gaussian filter is used to reduce the noise and make the picture smoother. Next, we calculate the gradient intensity and direction of each pixel. Then we use the obtained data to eliminate the spurious response using non-maximum suppression, we use double thresholds to detect edges, and finally we complete the detection process by suppressing weak edges.



Figure 11. Use canny operator to extract results.

Because the result of using the canny operator [14] is very bad, the training effect is also very poor. Therefore, a lot of noise and discontinuous edges [15] cannot get the ideal results, thus another algorithm is used for edge extraction. The HED [16] network model is based on the structure of the VGG16 network model [17]. The core idea is to use the pooling layer to reduce the constant width of the input image layer by layer at a rate of 1/2, which is a multi-scale. The hierarchical network structure uses CNN to carry out end-to-end edge detection [18]. Based on this algorithm, edge extraction is performed after being reproduced in the Caffe deep learning framework.

As shown in Figure 12, the side back put of the convolution layer adds an output layer to the edge output layer, and depth supervision is performed on the edge output layer to make the generated result close to the edge extraction. With this process, the side output layer gradually becomes smaller, and as the side output layer becomes smaller, the feeling gradually becomes larger. At the end of this process, a weighted fusion algorithm is used to convolve the layer to obtain outputs at different scales. At the same time, it is assumed that there are M-layer edge output layers, each layer is accompanied by a classifier, and the corresponding weight is w , and the objective function is set as:

$$L_{side}(W, w) = \sum_{m=1}^M \alpha_m l_{side}^{(m)}(W, w^{(m)}). \quad (6)$$

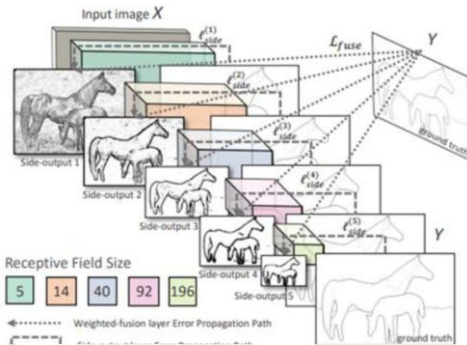


Figure 12. Schematic diagram of network structure.

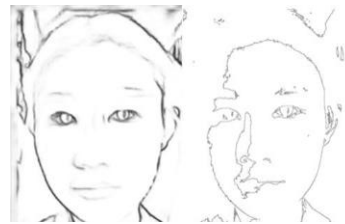


Figure 13. Schematic diagram of network structure.

As shown in Figure 13, compared with the canny operator, a great improvement has been achieved, with extremely continuous edges and less noise.



Figure 14. Extraction process using HED algorithm.

The entire extraction process is represented in Figure 14, and different results obtained by performing different edge detections according to different side outputs as output.

Since the images processed by celebA after preliminary processing did not carry out face annotation, and under the condition that the feasibility of real-life annotation is not large and the annotation information does not meet the requirements of the translation model, the face marking algorithm is designed.

In addition to providing a mature face detection and labeling interface, Dlib provides a trained model for face detection and labeling. The model is used to mark the face contours according to 1-17, 18-22 to mark the left eyebrow, 23-27 to mark Right eyebrow, 28-36 nose, 37-42 left eye, 43-48 right eye, 49-60 lip contour, 61-65 upper lip and 66-68 to mark lower lip. A total of 68 points were marked on the face contour and facial features.



Figure 15. 68 points annotation of face

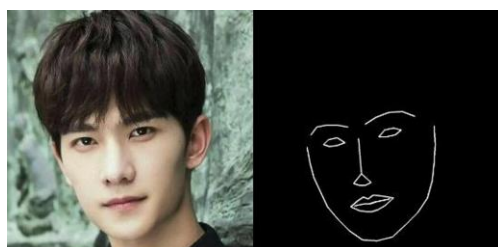


Figure 16. Face feature labeling based on cv2.

Under the premise of having a face contour, the translation model needs to mark the image and the requirements cannot be met only in the form of feature points.

Continuous lines are required to mark the face contour and complete image area for facial features. 68 mark points for further processing. Use cv2 to connect the marked points, and connect the outline, left eyebrow, right eyebrow, left eye, right eye, nose, upper lip and lower lip to obtain the labeled image, as shown in Figure 16.

Due to this labeling method, the distinction between left and right eyebrows, left and right eyes, between eye color patches, lips and nose color patches, is lacking. Therefore, the algorithm is improved by first labeling different parts with different colors, and then eye, nose, upper and lower lips fill in the color blocks to get a new marking method.



Figure 17. facial feature tags before and after improvement

symbol	significance
G	generator
D	discriminator
x	input map
y	output graph
z	random vector

Figure 18. Input and output instructions.

3.3. Face Generation Model Training

The image translation framework uses the pix2pix framework, first defining the input and output.

The output is undoubtedly the image output generated by the generator and the input is not a simple random vector, but a picture. In order to ensure the matching of the output, the discriminator needs some generator characteristics, thus the model loss function is in the generative adversarial networks loss function on the basis of [14] adjusted to:

$$L_{cGAN}(G,D) = E_{x,y}[\log D(x,y)] + E_{x,y}[\log(1-D(G(x,z)))] \quad (7)$$

In order to meet the needs of comparison, generative adversarial networks that only judges the real image is needed, and the loss function of the generative adversarial networks is:

$$L_{GAN}(G,D) = E_y[\log D(y)] + E_{x,z}[\log(1-D(G(x,z)))] \quad (8)$$

For the task of face translation, the input and output of the generator actually share feature information and the side information will affect the similarity. Therefore, the L1 paradigm Loss is added to the original generative adversarial networks loss, in order to ensure the similarity.

$$L_{L1}(G) = E_{x,y,z}[||y - G(x, z)||_1]. \quad (9)$$

In consequence, the aggregate loss function of this model is adjusted to:

$$G^* = \arg \min_D \max_G L_{cGAN}(G, D) + \lambda L_{L1}(G). \quad (10)$$

For contour translation, the resolution of the input contour is adapted, and the noise is added to the input image and then generated by the generator in the trained model. The entire process is represented in Figure 19.

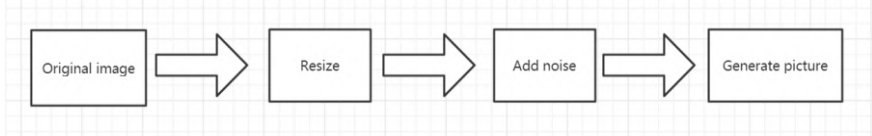


Figure 19. Contour translation process.

Under the premise of satisfying the face identification, there is a better generation situation, as shown in Figure 20.



Figure 20. Contour translation.

For image translation, the resolution of the input contour is adapted. As well, after extracting the face mark, the original image and the mark are input into the generator together, the original image is used as the role of noise, and then generated by the generator in the trained model. The entire process is represented in Figure 21.

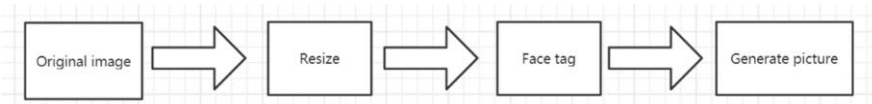


Figure 21. Image translation process.

Under the premise of satisfying the face identification, there is a better generation situation, as shown in Figure 22.



Figure 22. Image translation to generate images.



Figure 23. Generate a comparison chart before and after.

The key to improve the quality of the generated pictures is to enhance the resolution of the pictures. The idea is to gradually increase the training generator and discriminator, starting from low resolution, gradually increase the convolutional layer and gradually improve the image details during the training process [19]. In training,

first obtain the general structure of the image distribution and gradually increase the details, rather than learning all the distributions at the same time. By improving the neural network and training methods, high-resolution images can be obtained more reliably and good results have been achieved, as shown in Figure 23.

In the resolution process performed by the multiplier generator and discriminator (by adding convolution) to smooth the entire process, the neural network is adjusted for the change of α weight, as shown in Figure 24, which is a 16*16. The process of pixel growth regards the processing of higher-resolution convolutional layers as residual blocks (α weights show a linear increase from 0 to 1), correspondingly doubling or halving the nearest neighboring filter and convolution pool. RGB conversion refers to the mutual conversion of vector and RGB color information.

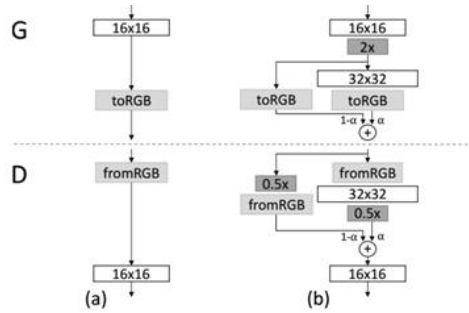


Figure 24. Neural network structure.

At this time, the input sample X is expressed as:

$$X = X_{16\text{pixel}} * (1-\alpha) + X_{32\text{pixel}} * \alpha. \quad (11)$$

The ultimate goal is to achieve the mapping of latent vectors to 1024 pixels. It is difficult to achieve such a mapping network using generative adversarial networks alone, thus procedural training is used, starting with low-quality samples (4*4 pixels), then multiplying the increase of the resolution (4*4 to 8*8 to 16*16, and finally reach 1024*1024) to achieve the detail of the picture. The whole training process is represented in Figure 25.

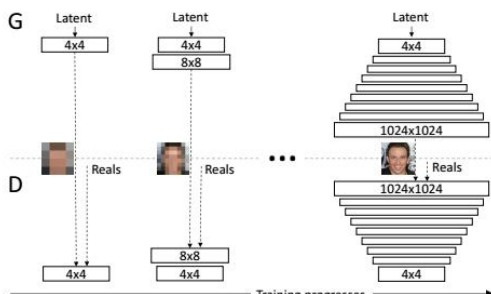


Figure 25. Training process.

symbol	significance
D_k^n	Discriminator features of layer n
M	total floors
N_n	Number of elements in layer n

Figure 26. Symbol Description.

The high resolution requires the discriminator to have a large receptive field, which will lead to overfitting problems and excessive storage space requirements due

to extremely deep networks and extremely large convolution kernels. Therefore, in order to avoid high resolution, the instability brought by the huge receptive field of the residual block uses different discriminators to process images with different resolutions, where these discriminators have the same structure. Suppose there are discriminators D1, D2, D3, D4, then their loss function is expressed as:

$$\min_G \max_{D1,D2,D3,D4} \sum_{n=1,2,3,4} L_{GAN}(G, D_n). \quad (12)$$

At the same time, feature matching is added to stabilize the generation requirements of generators with different resolutions:

$$L_{FM}(G, D_k) = E_{(s,x)} \sum_{n=1}^m \frac{1}{N_n} [||D_k^n(s, x) - D_k^n(s, G(s))||_1]. \quad (13)$$

The objective function of the model at this time is:

$$\min_G (\max_{D1,D2,D3,D4} \sum_{n=1,2,3,4} L_{GAN}(G, D_n)) + \lambda (\sum_{n=1,2,3,4} L_{FM}(G, D_n)). \quad (14)$$

Under the input information, the edges extracted by the HED algorithm are used as the edge distribution and the semantic labels of the labeled faces as the common input, and input to the generation network. After conversion by the encoder, the image data is input, and the edge distribution in the image is matched with the semantic labels. After the matching, a clustering algorithm is used to obtain the feature code of the semantic category. When the model is inferred, a cluster center is randomly selected as the coding feature, matched with the corresponding label map and input to the generator to obtain the generated map.

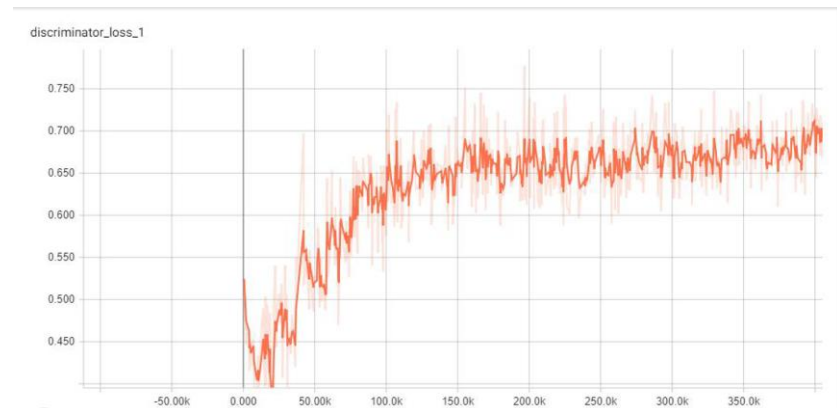
3.4. Training Information and Version Configuration

Sample size	Data round trips	Training time	GPU
5000	20	120 hour	1080TI*1

Figure 27. Model training information.



Figure 28. Generator L1 Loss.

**Figure 29.** Generator Loss**Figure 30.** Discriminator Loss

content	platform	CUDA	Cudnn	Python Version
Edge extraction	Caffe	7.5	5.0	2.7
Face tag	Cv2	7.5	5.0	2.7
Pix2pix model	Tensorflow	9.0	7.0	3.6
HD training	Pytorch	9.0	7.0	3.6

Figure 31. Platform and configuration

4. Conclusion

In this study, the application of image translation in human faces was explored. First, we searched for a suitable data set and cleaned it. In the case of a translation framework, edge extraction and face identification are performed on the face image as a reasonable output of the translation framework. After multiple training and testing of the model, the research method is continuously improved, and then perfected. The method of edge extraction and face identification has improved the neural network structure and training method in the translation framework. After obtaining an effective translation model, the front end, database and back end of the system have been developed and tested. The Face generation system is feasible.

In the research of the subject, although there are certain results, there are also certain problems. First of all, the unfamiliarity with the translation framework, the lack of own experience and the lack of information acquisition channels have caused a lot of useless work that could be avoided. Secondly, due to its own strength, it is not possible to obtain a data set of Asian faces, so there is still a lack of applicability. There are also many areas that can be improved in system development.

However, in the research of the subject, it is found that there is huge room for development on the basis of the traditional translation framework. Only on the basis of the existing framework, there are more fields for translation generation. At the same time, the translation framework is no matter the training efficiency or the generalization. Adaptability and other aspects can be improved and developed.

References

- [1] Phillip Isola. Image-to-Image Translation with Conditional Adversarial Networks[C].CVPR. CVPR2017.Honolulu:CVPR,2017.
- [2] Cao Zhiyi, Niu Shaozhang, Zhang Jiwei. Research on face reduction algorithm based on semi-supervised learning generation adversarial network[J]. Journal of Electronics and Information Technology. 2018, 40(2):323-330. (in Chinese)
- [3] RASMUS A , VALPOLA H, et al. Semisupervised learningwith ladder network[J]. CoRR.2015, 7(2672):1-7.
- [4] Hinton G E , Srivastava N , Krizhevsky A , et al. Improving neural networks by preventing co-adaptation of feature detectors[J]. Computer Science, 2012, 3(4):212-223.
- [5] CANNY J. A compatibility approach to edge detection[J]. Pattern Analysis and Machine Intelligence, 1986, 8(6):679-698.
- [6] Li Junshan, Ma Ying, Zhao Fangzhou, etc. Improved Canny image edge detection algorithm [J]. Acta Photonica Sinica, 2011, 40(1): 55-54. (in Chinese)
- [7] Chen Hongxi. Edge detection of the canny operator based on edge-preserving smooth filtering [J]. Journal of Lanzhou Jiaotong University, 2006, 25 (1): 86-90. (in Chinese)
- [8] Wang Rong, Gao Liqun, Chai Yuhua, etc. Edge detection method combining Canny method and wavelet transform [J]. Journal of Northeastern University, 2005, 26 (12): 1131-1133 (in Chinese)
- [9] GOODFELLOW I J , POUGETABADIE J , MIRZA M, et al. Generative adversarial nets[J]. Advances in Neural Information Processing Systems, 2014, 3: 2672-2680.
- [10] Goodfellow I J. Generative adversarial nets[C].NIPS.NIPS2014.Montreal: NIPS, 2014.
- [11] J Zhu.Unpaired Image-to-Image Translation Using Cycle-Consistent Adversarial Networks [C].ICCV . ICCV2017. Venice: ICCV, 2017.
- [12] Ronneberger O.U-Net Convolutional Networks for Biomedical Image Segmentation[C].MICCAI.MICCAI2015. Munich: MICCAI, 2015.
- [13] Yang S. From Facial Parts Responses to Face Detection A Deep Learning Approach[C].ICCV Santiago: ICCV,2015:3676-3684.
- [14] Xu Xinchao, Fu Chen, Xu Aigong. An improved Canny edge extraction method[J]. Remote Sensing Information. 2016, 31(5): 43-46. (in Chinese)
- [15] Zhang Sheng, Yang Yan. Image Canny edge extraction improvement based on variance between classes[J]. Information Technology.2018,1(1):60-62. (in Chinese)
- [16] Xie S, Tu Z. Holistically-Nested Edge Detection[J]. International Journal of Computer Vision. 2015, 125(1-3):3-18.abs/1701.07875.
- [17] Li Y , Xiao N , Ouyang W . Improved Boundary Equilibrium Generative Adversarial Networks[J]. IEEE Access. 2018,1(1):1-1.
- [18] Lecun Y L , Bottou L , Bengio Y , et al. Gradient-Based Learning Applied to Document Recognition[J]. Proceedings of the IEEE. 1998, 86(11):2278-2324.
- [19] Karras T. Progressive Growing of GANs for Improved Quality, Stability, and Variation[C].ICLR.ICLR2018. Vancouver:ICLR,2018

The Coupling Co-Location Pattern: A New Spatial Pattern for Spatial Data Sets

Shiran Zhou, Lizhen Wang¹ and Pingping Wu

School of Information Science and Engineering, Yunnan University, Yunnan, China

Abstract. There is a variety of interesting knowledge in spatial data sets. Spatial co-location pattern mining can discover sets of different features that are co-located. However, this type of pattern only lists the features that appear together without any consideration of the quantity ratio, which can cause confusion. For example, the co-location pattern {church, restaurants} shows that churches and restaurants are often close to each other, but information such as how many restaurants are near a church is usually not displayed. Also, in real spatial data sets, there is a mutual influence between spatial features, that is, a coupling relationship between different features or the same features. Thus, this paper proposes a novel spatial pattern called a coupling co-location pattern. First, we discuss the properties of the coupling phenomenon between spatial features, and then the concept of coupling co-location patterns is defined formally. Second, the measurement of support and mining framework for coupling co-location patterns are proposed. Finally, we conduct experiments on both real and synthetic data sets, and the results verify the practical significance of coupling co-location patterns.

Keywords. Spatial data mining, Coupling co-location pattern (CCP), Maximal clique

1. Introduction

Co-location pattern mining aims to discover subsets of spatial features that are frequently located together, where a spatial feature represents a type of cataloged object in a space. As an example, snack bar shops and beauty salon shops are often located near each other, which form a co-location pattern. In addition, “located together” usually means located in geographic proximity (e.g., measured by Euclidean distance). With the wide application of spatial positioning services, spatial data sets, which record cataloged objects and their locations (e.g., geographic mapping data or point-of-interest data), are generated very quickly. As a result, spatial co-location pattern mining has been applied in many areas such as mobile commerce, earth science, biology, public health, and transportation [1].

Fig. 1 is an example of a spatial data set, where a triangle, square, and circle represent different spatial features. There are four instances of triangles, circles, and squares, respectively, and each instance uses a number as an identifier. For example, \blacktriangle_1 represents the first instance of the triangle feature. We draw a line to connect two instances if they satisfy the spatial proximity relationship. For the example in Fig. 1, we

¹ Corresponding author: Lizhen Wang, School of Information Science and Engineering, Yunnan University, Dongwaihuan South Road, Kunming, Yunnan 650091, China. E-mail: lzwang@ynu.edu.cn

obtain the four candidate (potential) co-location patterns $\{\blacktriangle, \blacksquare\}$, $\{\blacktriangle, \bullet\}$, $\{\blacksquare, \bullet\}$, and $\{\blacktriangle, \blacksquare, \bullet\}$. When a candidate co-location pattern satisfies the support measure, we say it is a prevalent co-location pattern.

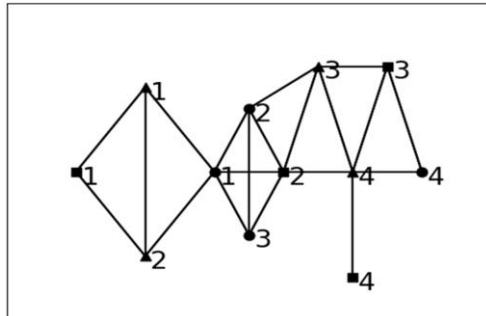


Fig. 1. An example spatial data set.

Several support measures have been proposed, e.g., partitioning-based by S. Shekhar et al [2], construction-based by Y. Morimoto et al [3], enumeration-based by Y. Huang et al [4] and [5] and participation-based by J. S. Yoo [6] and [7]. A partitioning-based measure divides the space into small squares by a set of horizontal lines and vertical lines, counting the number of potential patterns in each small square as the support. Construction-based approaches find candidate patterns heuristically. An enumeration-based measure counts the number of row instances as the support of a pattern, where an instance set of the pattern is said to be a row instance if they are neighbors of each other. For a participation-based measure, the participation rate and participation index are two key indicators. Through the projection of row instances, the participation rates of each feature in a pattern are calculated, and the minimum participation rate of features is considered to be the participation index of the pattern. In addition to this, a new support measurement method called Fraction-Score was proposed by Chen et al [8], where the main idea is to consider instances in row instances as fractional units and then all fractional units are aggregated to form a support of patterns.

A co-location pattern reveals a kind of relationship between spatial features. Consider the following examples: A restaurant in a normal urban area that is located close to a parking area can boost both incomes. If a restaurant is near to a garbage collection station, then the income of the restaurant will be reduced. In nature, the Peony flower and Cosmos are both insect-pollinated flowers. One of them will be pollinated when another attracts insects such as bees, butterflies, moths, and ants to pollinate, if they locate closely. This is a mutually beneficial relationship in nature. That inter-planting beans in a corn field can produce beans without reducing the yield of corn is also an example of this. From these examples, we can see the practical significance of co-location pattern mining.

The co-location relationship of spatial features indicated by co-location patterns looks like a coupling relationship [9]; however, the concept of coupling generally means that there exists a mutual effect between objects, and that this is in a dynamically stable state. Further, there are two aspects of coupling relationships. The first aspect is **intra-coupling**, which means the mutual effect between objects of the same type. For example, consider a restaurant in a certain street and the environmental

factor supporting it is people who order food here daily. If the flow of people can support another restaurant here, the two restaurants will compete for turnover, and this reflects a mutual repulsion relationship. But when people know that they can get food here, this can lead to more customers and the turnover of the two restaurants will increase, which reflects a mutually beneficial relationship. Attaining a balance between promotion and repulsion is a coupling relationship between the same type of objects (intra-coupling). The second aspect is **inter-coupling**, which means the coupling relationship between different objects (features). We need to consider both intra-coupling and inter-coupling.

Let us consider a mutual promotion case for snack bars and beverage shops. Unlike traditional co-location patterns [10], we need to confirm whether two snack bars (intra-coupling) nearby one beverage shop (inter-coupling) are more popular than one snack bar near one beverage shop. We are interested in the proportion of the number of these two instances when the intra-coupling and inter-coupling are balanced, not just knowing that they will appear together. Take a tea shop as another example: imagine that there are many tea shops in a city square mall, and each of them is doing good business. In another city, the number of tea shops may well be different because of the difference in the flow of people, the environment, and other factors. What kind of intra-coupling and inter-coupling of different features are prevalent in a certain city is an interesting question and useful for decision-making. In order to find out the coupling relationships, in this paper we propose a new concept that considers both feature combinations (inter-coupling) and quantity combinations (intra-coupling) simultaneously, namely coupling co-location patterns.

We note that the instances that support coupling co-location patterns have a dynamic stability. Assuming that feature A has two instances and feature B has one instance, if the surrounding could support another instance of feature B, it will appear soon. If the surrounding can only support one instance of feature A, then one instance of A will disappear soon. In spatial data sets, instances satisfying the neighbor relationship form a clique; when a limit is reached of the balance of coupling (intra-coupling and inter-coupling) instances form a maximal clique (or a cluster). From this perspective, when extracting coupling co-location patterns from spatial data sets, we can consider reading candidate patterns from clusters [11]. But a better way is that we should consider maximal cliques as co-location instances that support coupling co-location patterns rather than traditional cliques [12] in co-location pattern mining. Considering the data set in Fig. 1 again, we can see that there are eight supporting instances (maximal cliques): $\{\blacktriangle_1, \blacktriangle_2, \blacksquare_1\}$, $\{\blacktriangle_1, \blacktriangle_2, \bullet_1\}$, $\{\bullet_1, \bullet_2, \bullet_3, \blacksquare_1\}$, $\{\blacktriangle_3, \blacksquare_2, \bullet_2\}$, $\{\blacktriangle_3, \blacktriangle_4, \blacksquare_2\}$, $\{\blacktriangle_3, \blacktriangle_4, \blacksquare_3\}$, $\{\blacktriangle_4, \blacksquare_3, \bullet_4\}$, and $\{\blacktriangle_4, \blacksquare_4\}$. Obviously, co-location patterns $\{\blacktriangle, \blacksquare\}$, $\{\blacktriangle, \bullet\}$, and $\{\blacksquare, \bullet\}$ have the same feature combinations with coupling co-location patterns $\{\blacktriangle^2, \blacksquare\}$, $\{\blacktriangle^2, \bullet\}$ and $\{\blacksquare, \bullet^3\}$, but the latter contain richer information and are more useful for decision-making.

In summary, our main contributions in this paper include: In section 1, a discussion of the coupling relationship of spatial features, and its practical significance; In section 2, the concept of a coupling co-location pattern is defined formally based on maximal cliques over the spatial data set; In section 3, The coupling co-location pattern mining framework is proposed, and a maximal clique generating algorithm is introduced; In section 4, we conduct extensive experiments on both real and synthetic data sets. The results verify that our proposed coupling co-location pattern concept is useful and has practical application. For example, we find that in Beijing, hotels and clinics frequently appear together, and the ratio of their numbers is 2 to 1.

2. Formal definitions

In this section, we define coupling co-location patterns and associated measures. Let F be a set of spatial features and I be a set of instances of spatial features [13], $i \in I$ is an instance and $i.f$ represents the feature of instance i . Let $R(i_1, i_2)$ denote that instances i_1 and i_2 satisfy a spatial neighbor relationship R , and let MC be the set of maximal cliques formed by instances under the neighbor relationship R . $mc \in MC$ is a maximal clique in MC .

Definition 1: *Coupling co-location pattern CCP.* Let F be a set of spatial features, a coupling co-location pattern is a collection of spatial features with numbers, i.e., $c = \{f_1^{n1}, f_2^{n2}, \dots, f_k^{nk}\}$, where ni denotes the number of instances where f_i appears; $f_i \in F, ni \in N^+$. In particular, ni is omitted when ni is 1.

Suppose $F(c/mc)$ returns the set of features in a coupling co-location pattern (CCP) c or returns a set of features contained in a maximal clique mc , and $N_f(c/mc)$ returns the number of instances of feature f in c/mc .

Definition 2: *Row instance and table instance.* We say a maximal clique mc is a row instance of a CCP c if $F(c)$ equals $F(mc)$ and $N_f(mc)$ equals $N_f(c)$ for any $f \in F(mc)$. All row instances of c form the table instance of c , denoted as $table_instance(c)$.

In Fig. 1, let pattern $c = \{\blacktriangle^2, \blacksquare\}$, then the table instance is $table_instance(c) = \{\{\blacktriangle_1, \blacktriangle_2, \blacksquare_1\}, \{\blacktriangle_3, \blacktriangle_4, \blacksquare_2\}, \{\blacktriangle_3, \blacktriangle_4, \blacksquare_3\}\}$.

The next issue is how to quantify the prevalence and stability of a CCP. We consider two basic principles. For a CCP c , the more instances of features in c that participate in its table instance, the higher the prevalence of c ; the more row instances of c , the more stability it has.

Definition 3: *The coupling participation index (CPI).* The coupling participation index of a CCP c is based on the first of the above two basic principles, which is the same as the calculation of the participation index for traditional co-location pattern mining. That is:

$$CPI(c) = \min_{f \in F(c)} \left\{ \frac{|\pi_f(table_instance(c))|}{TN_f} \right\}, \quad (1)$$

where π_f is a projection operation, and TN_f means the total number of instances of feature f .

Note that CPI has a basic property: in its table instance, the more overlapping instances (i.e., an instance appears in multiple row instances), the smaller the value of CPI. For example, in Fig. 1, $\{\blacktriangle_3, \blacktriangle_4, \blacksquare_2\}$ and $\{\blacktriangle_3, \blacktriangle_4, \blacksquare_3\}$ are both row instances of CCP $\{\blacktriangle^2, \blacksquare\}$. There would be four instances of feature \blacktriangle participate in the two row instances if there are no overlapping instances; however, due to the overlapping instances \blacktriangle_3 and \blacktriangle_4 , there are just two instances that participate in the two row instances.

Lemma 1. The CPI value of any CCP c is larger than 0 and smaller than or equal to 1, i.e., $0 < CPI(c) \leq 1$.

Proof: Obviously, $TN_f > 0$, and there is a maximal clique to be a candidate CCP, thus $|\pi_f(table_instance(c))| > 0$. In addition, $|\pi_f(table_instance(c))| \leq TN_f$, so $0 < CPI(c) \leq 1$.

Definition 4: *The coupling stability (CS).* The coupling stability of a CCP c is

based on the second principle mentioned previously. Which is defined as follows:

$$CS(c) = \frac{|table_instance(c)|}{|\Omega|} \quad (2)$$

where Ω is the set of row instances of all CCPs, that is Ω is the set of all maximal cliques in the data set. For example, for $c = \{\blacktriangle^2, \blacksquare\}$ in Fig. 1, $|table_instance(c)| = 3$, $|\Omega| = 8$, thus $CS(c) = 3/8$.

For the coupling stability measure CS , we have the following lemma.

Lemma 2. The value range of CS is greater than 0 and less than or equal to 1, i.e., $0 < CS \leq 1$.

Proof: If c is a CCP, then c has at least one row instance, that is, $|table_instance(c)| > 0$. In general, $|table_instance(c)| < |\Omega|$ thus $0 < CS < 1$. If and only if all maximal cliques are row instances of c , then $|table_instance(c)| = |\Omega|$, $CS = 1$. So, $0 < CS \leq 1$ holds.

In Fig. 1, for $c = \{\blacktriangle^2, \blacksquare\}$, there are three squares and all of them participate in the table instance of c . There are four triangles and three of them participate in the table instance of c , so $CPI(c) = \min\{3/3, 3/4\} = 0.75$. The total number of maximal cliques in Fig. 1 is eight, and three of them are row instances of c , so $CS(c) = 0.375$.

It is worth mentioning that CPI is calculated at the instances level, and CS is calculated at the maximal clique level. The projection operation in CPI considers the number of instances participating in the pattern and chooses the minimum of participation ratio of features in pattern to ensure the frequency. CS considers the number of occurrences of each CCP, and the bigger the number of occurrences, the more stable the CCP is.

Below, a new support measure that considers the participation index and stability simultaneously for a CCP is defined.

Definition 5: The support (Sup). The support of a CCP c is defined as follows:

$$Sup(c) = \alpha * CPI(c) + (1 - \alpha) * CS(c), \quad (3)$$

where α is a weighting factor that balances stability and prevalence, and $0 \leq \alpha \leq 1$.

Lemma 3. The support measure does not satisfy anti-monotonicity.

Proof: From Fig. 1, assuming $\alpha = 0.5$, we can get $Sup(\{\blacktriangle, \blacksquare, \bullet\}) = 0.75$, $Sup(\{\blacktriangle^2, \bullet\}) = 0.625$, $Sup(\{\blacktriangle, \blacksquare\}) = 0.625$, and $Sup(\{\blacktriangle^2, \blacksquare\}) = 0.75$; therefore, at the feature level, we find that $Sup(\{\blacktriangle, \blacksquare, \bullet\}) > Sup(\{\blacktriangle, \blacksquare\})$, at the quantity level, $Sup(\{\blacktriangle^2, \blacksquare\}) > Sup(\{\blacktriangle, \blacksquare\})$.

Lemma 4. The value range of Sup is greater than 0 and less than or equal to 1, i.e., $0 < Sup \leq 1$.

Proof: According to Lemmas 2 and 3, we know that $0 < CPI \leq 1$ and $0 < CS \leq 1$. Thus, $0 < \alpha * CPI \leq \alpha$, $0 < (1 - \alpha) * CS \leq (1 - \alpha)$, then $0 + 0 < \alpha * CPI + (1 - \alpha) * CS \leq \alpha + (1 - \alpha) = 1$.

Definition 6: Strong coupling co-location pattern $S CCP$. A coupling co-location pattern c is called a strong coupling co-location pattern if and only if $Sup(c) \geq min_sup$, where min_sup is a support threshold specified by users.

3. Framework for mining SCCPs

As shown in Fig. 2, the SCCP mining framework [14] involves: (1) finding all the maximal cliques from a spatial data set; then (2) converting all the maximal cliques into candidate SCCPs; and finally (3) obtaining all SCCPs according to Definitions 2-6.

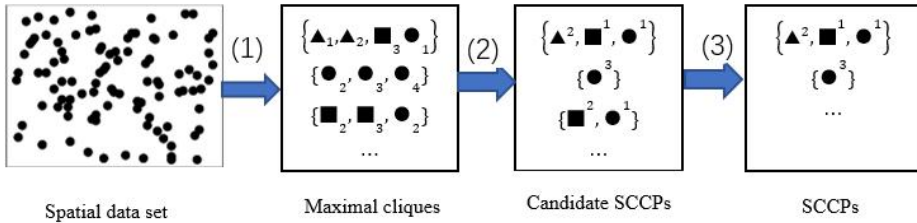


Fig. 2. A framework for SCCP mining

In the first step of SCCP mining, the aim is to enumerate all maximal cliques effectively for a given spatial instance set and a distance threshold. This issue has attracted the attention of some researchers, and we apply the latest work of C. Zhang et al [15] to resolve this issue. The main idea of the algorithm in [15] is turning the enumeration of maximal cliques into an enumeration of convex polygons. First, we assume that the instance set has been sorted based on the x -coordinate values. Second, we select an instance i in order, and enumerate all maximal constraint convex polygons in which i is the leftmost instance. Third, in order to improve the efficiency of the algorithm, pruning considering the geometric properties of the maximal cliques is implemented.

For a finite set of instances in a two-dimensional area, if the instances on the line segment with any two instances as the endpoints belong to the set, then the set is called a **convex set**, and a polygon formed by connecting the outermost instances in a convex set is called a **convex polygon**. The **convex hull** of a point (instance) set S is the minimum convex set containing the set S . The **maximal constraint convex polygon (MCCP)** is a convex polygon such that the distance of any two extreme instances satisfies the distance constraint and cannot be further expanded by adding one more instance without violating the distance constraint.

The basic operation of the algorithm is to find all convex hulls; the well-known Graham's algorithm [16] is briefly introduced in Algorithm 1 for this purpose. First, an anchor instance is selected from the instance set I (Line 1). Then, these instances are sorted according to the polar angle between the instance and i . Instances with the same polar angle are sorted by the distance between the instance and i (Line 2). Finally, the result array Ret is initialized (Lines 3-5) and every instance scanned to check whether it is a convex hull (Lines 6-8). The while loop removes the points found that are not vertices of the convex hull because when traversing the convex hull counter-clockwise we should turn left at each vertex. If the while loop finds that there is no left turn at a vertex, it removes the vertex. Otherwise, it is temporarily added to the result Ret (Line 8).

Algorithm 1: Graham's algorithm (I)

Input: A spatial instance set I
Output: All convex hulls

1. Select a rightmost or leftmost instance i as an anchor instance;
2. Sort these points according to the polar angle of each point relative to i , $I=\{i_1, i_2, i_3, \dots\}$;
3. $j=0$;
4. Push i in $Ret[j++]$
5. Push i_1 in $Ret[j++]$;
6. For each instance i' in I do
 7. while ($\text{multiply}(i', Ret[j], Ret[j-1]) > 0$) $j--$;
 8. $Ret[++j] = i'$;
9. Return Ret

The pseudocode of the maximal cliques mining algorithm is given in Algorithm 2, and Algorithm 3 is a subprocess called in Algorithm 2. Algorithm 2 outlines the framework of the enumeration of the maximal cliques. In Line 1, the instances are sorted based on their x -coordinate values. For each instance i , setting three sets M , C , and E . M is the instances chosen for the current clique, and the initial value is i . C contains the candidate instances for the current clique. The initial value of set C is the neighbors that behind i , that is, the right-side neighbors of i . E is the excluded instances, which contains instances that are close to i and before i (Lines 3-4). Some related information concerning C is calculated for pruning strategies in Lines 5-6. Algorithm 1 is called to calculate the convex hull layer of instances. The subprocess $\text{Enum}(\emptyset, i, C, E)$ is called to find all maximal cliques in which i is the leftmost instance.

Algorithm 2: Enumerate maximal spatial cliques (I, d)

Input: A spatial instance set I , and a distance threshold d
Output: All maximal spatial cliques

1. Sort instances in I based on their x -coordinate value;
2. For each instance i in I do
 3. Put right side neighbors of i in C
 4. Put left side neighbors of i in E
 5. Compute convex layers on $C \cup \{i\}$
 6. Sort instances in C by their polar angles w. r. t i ;
 7. Compute pivot convex polygons;
 8. $\text{Enum}(\emptyset, i, C, E)$;

The time complexity is considered next, where n is the number of instances in I . Sorting (Lines 1, 6) takes $O(n * \log n)$ time. The convex layer calculation (Line 5) takes $O(v * n * \log n)$ time where v is the number of convex layers. The pivot convex polygon calculation takes $O(kn)$ time where k is the number of pivot convex polygons (Line 7).

Algorithm 3: Enum(M, v, C, E)

Input: Instances in the partial solution M , the instance v to be added to M , candidate set C , excluded set E .

Output: All MCCPs and maximal cliques

1. Put v into M ;
2. If v is an outer instance put v into $P(M)$
3. Else put v into $I(M)$
4. Reduce the size of set C
5. If $E = \emptyset$ and $C = \emptyset$ then
 6. $P(M)$ is a maximal constraint convex polygon;
 7. M is a maximal clique;
8. $L = C$
9. Reduce the size of L
10. Sort instances in L by their convex layers;
11. For each $v \in L$ do
 12. $\text{Enum}(M, v, C \cap NB(v), E \cap NB(v))$
13. $E \leftarrow E \setminus \{v\}$

The Enum algorithm is described in Algorithm 3 and is the pseudocode of the enumeration of maximal cliques (represented by Maximal Constraint Convex Polygons, MCCPs) for each anchor point v . Line 1 adds a newly added instance v to M . Lines 2 and 3 determine whether v belongs to the constraint convex polygon set $P(M)$ or the internal instances set $I(M)$. Line 4 is a pruning technique such that if a candidate instance $c \in C$ is contained by the convex polygon $P(M)$, we can move c to $I(M)$. For Lines 5-7, if both E and C are empty, the instances in $P(M)$ are instances of the MCCP and the instances in $P(M) \cup I(M)$ are the corresponding maximal clique. At Line 9, the algorithm reduces the size of set L ; the main idea is that not all instances in C need to be considered, only instances in $C - M$ are checked. Line 10 sorts the instances in L by their convex layers to make sure that the outside instances will be accessed first. Lines 11-13 call the Enum process recursively by choosing an instance from L for the current partial solution M .

The time complexity of the reduction of the size of set C is $O(n)$ (Lines 1-4). The reduction of the size of L takes $O(kn)$ (Line 9) where k is the number of pivot convex layers.

After executing Algorithm 2 on the data set shown in Fig. 1, Table 1 lists all maximal cliques that are obtained. The advantage of this algorithm is that it specifically

solves the problem of maximal clique enumeration in a two-dimensional space. Many pruning strategies in the algorithm are based on geometric properties in two-dimensional space. Therefore, this algorithm cannot be used when the proximity relationship is not Euclidean, which is a disadvantage.

Table 1. All maximal cliques of the data set in Fig. 1

{ $\blacktriangle_1, \blacktriangle_2, \blacksquare_1$ }	{ $\blacktriangle_1, \blacktriangle_2, \bullet_1$ }	{ $\bullet_1, \bullet_2, \bullet_3, \blacksquare_2$ }
{ $\blacktriangle_3, \blacksquare_2, \bullet_1$ }	{ $\blacktriangle_3, \blacktriangle_4, \blacksquare_2$ }	{ $\blacktriangle_3, \blacktriangle_4, \blacksquare_3$ }
{ $\blacktriangle_4, \blacksquare_3, \bullet_4$ }	{ $\blacktriangle_4, \blacksquare_4$ }	

In step (2) of the mining framework in Fig. 2, we extract candidate SCCPs from maximal cliques. Let MC be the set of all maximal cliques. The process of converting MCs to candidate SCCPs is given in Algorithm 4. For each $c \in MC$, all the features it contains are listed and the number of occurrences of each feature is recorded as a superscript. If the pattern has been recorded before, mc need added to the row instances set of the pattern; if not, the pattern needs added as a new item and put mc into the row instance set of the pattern.

Algorithm 4: Convert MCs to candidate SCCPs

Input: A maximal clique set MC

Output: A set of all candidate patterns and their row instances

1. For each $mc \in MC$:
2. Convert mc to candidate pattern p
3. If p has been recorded:
4. Add mc to its row instances set
5. Else:
6. Add a new pattern p , and put mc in its row instances set

The time complexity of Algorithm 4 is related to the data structure used to record patterns. Suppose that there are n maximal cliques that require conversion; for each maximal clique, the conversion process has constant time complexity $O(1)$. Let $t(m)$ be the average time complexity for checking whether a pattern already exists, where m represents the total number of patterns, then the total time complexity is $O(n * t(m))$. If patterns are given an order, the time for each checking process becomes $O(\log_2 m)$, thus it becomes $O(n * \log_2 m)$. If a hash table is used to record patterns, the time complexity of the checking process is $O(1)$, and thus, the total time complexity is $O(n)$. Suppose there are k candidate patterns in total, and the average memory cost for storing a pattern is x bytes, the space complexity will be $O(k * x)$.

Based on the result of Algorithm 4, we can calculate the support for each candidate pattern by Definitions 2-6 in step (3) of the mining framework in Fig. 2, and all SCCPs can be obtained.

4. Experimental Studies

We conducted experimentation with the SCCPs mining algorithm using both real and synthetic data sets on a computer with an Intel i7 3.2 GHz CPU and 16 GB RAM running Windows 10. All code is implemented using Visual Studio Code. The compiler is MingW. The real data set used contains the POIs (point of information) of the city of Beijing. We selected 20493 instances of 20 different features. With a neighboring relationship threshold of 100 meters, 5354 candidate patterns were obtained.

In the results there are many interesting patterns. We have selected four relatively highly supported and interesting patterns in Table 2. The pattern $\{hotel^2, clinic\}$ is interesting because we did not find the pattern $\{hotel, clinic\}$ in the results, which shows that the ratio of hotel and clinic clustered together is not 1:1 but 2:1. This pattern also proves the practical significance of the coupling phenomenon related to the quantity relationship. The pattern $\{hotel^2, bar\}$ is similar to the pattern $\{hotel^2, clinic\}$. The pattern $\{pharmacy^2\}$ is an intra-coupling pattern. We also find patterns such as $\{pharmacy^3\}$, $\{pharmacy^4\}$, and $\{pharmacy^5\}$. This means that pharmacies are stores that have a strong intra-coupling relationship and tend to group together. The pattern $\{hotel^3, pharmacy^2, cinema, laundry^2\}$ is a long pattern that can be used in city planning.

Table 2. Some interesting mined patterns

Pattern	CPI	CS	$\alpha=0.5$
$\{hotel^2, clinic\}$	0.0238441	0.00252071	0.013182405
$\{pharmacy^2\}$	0.0359053	0.00438123	0.020143256
$\{hotel^2, bar\}$	0.0136668	0.0014404	0.0075536
$\{hotel^3, pharmacy^2, cinema, laundry^2\}$	0.000729661	0.000120034	0.000424848

We also use the same data set for mining traditional co-location patterns. After comparing the mining results of the two different algorithms, the following conclusions can be drawn.

(1) For traditional co-location pattern mining, there are patterns with the same feature combination as SCCP. For example, we find a size-2 pattern $\{hotel, clinic\}$ in the results for co-location pattern mining with a support threshold of 0.5. Fig. 3 shows the spatial distribution of instances of hotels and clinics, and Fig. 4 shows the instances of $\{hotel^2, clinic\}$ in SCCP. The difference is that Fig. 3 lists all instances of hotels and clinics, and Fig. 4 lists the instances forming maximal cliques of two hotels and one clinic. The differences of pattern definition and the differences of the way that candidate patterns are selected give us a different view of city planning.

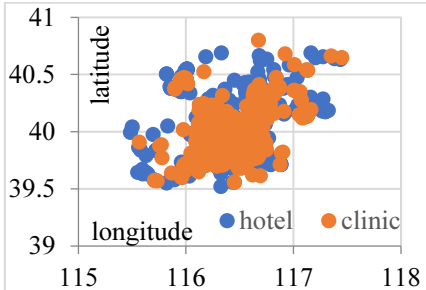
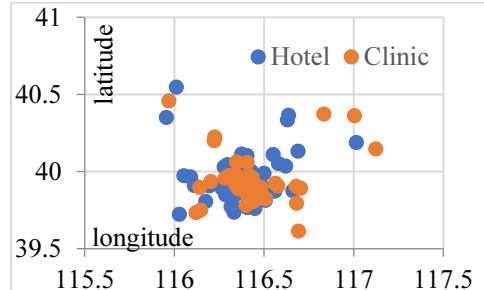


Fig. 3. Instance distribution.

Fig. 4. Support instance of $\{hotel^2, clinic\}$.

(2) The *PI* in traditional co-location pattern mining is a cumulative value, because all instances with the same feature combination in different cliques will be grouped together. However, the *CPI* in SCCP is a non-cumulative value, because instances of the same feature combination are scattered into different maximal cliques. To look deeper into the support, we are interested in knowing how the *CPIs* have been dispersed. We consider two feature combinations $\{clinic, pharmacy\}$; all candidate SCCPs that contain this combination with different quantity combinations are shown in Fig. 5 (where C1P1 means the pattern that contains one clinic and one pharmacy). The y-axis is the number of instances of clinics and pharmacies in patterns that contain $\{clinic, pharmacy\}$. We can see that the support instances of a certain feature have been divided by different patterns.

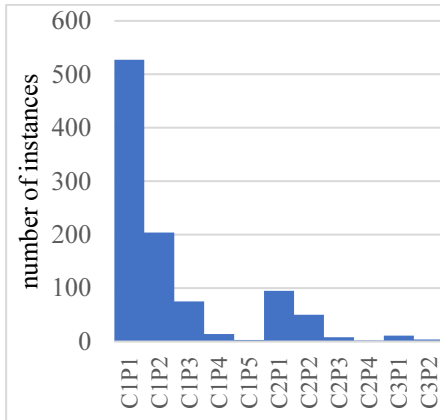


Fig. 5. Number of support instances.

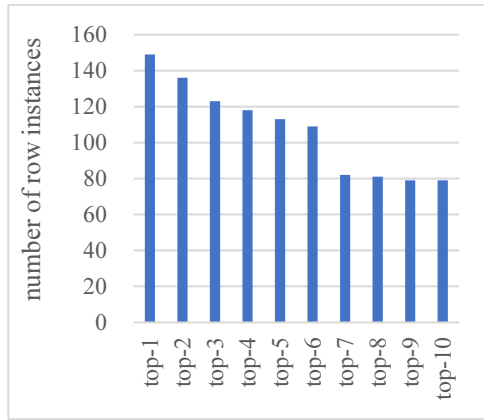


Fig. 6. Number of row instances.

(3) The CS value is a supplementary value that represents the relative frequency at which a pattern repeatedly appears. By Definition 3, the denominator is the number of all maximal cliques in the data set, and the numerator is the number of maximal cliques corresponding to a candidate pattern. Fig. 6 shows the top-10 CS values in the SCCP mining results. We can see that those values are much smaller than the total number of maximal cliques. When considering the frequency, if all values are small, a relatively large value corresponds to a relatively frequent pattern.

(4) The balance factor α can significantly influence the support value. Fig. 7 shows the changes of support value of the top-10 patterns with α . We can see that as

the value of α increases, the weight of CS decreases and the weight of CPI increases. When $\alpha = 0.3$, the biggest support is the support of pattern 1; when $\alpha = 0.7$, the biggest support is the support of pattern 2.

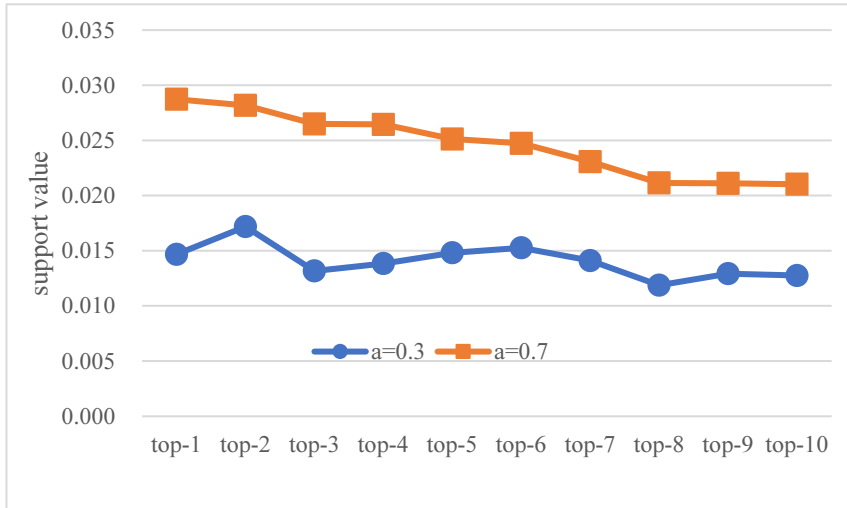


Fig. 7. Support value changes with α .

Table 3. Synthetic data sets

Data size	Distance threshold	Number of maximal cliques
5000	450	17332
12000	450	8860
20000	450	2784

In addition, we tested the maximal clique enumeration algorithm and Algorithm 4 with synthetic data sets. Table 3 shows the related information of the synthetic data sets. We mainly tested the runtime of the algorithm. Fig. 8 is the runtime of the maximal clique enumeration algorithm; the x -axis is the size of the data set, and the y -axis is the runtime (in seconds). Fig. 9 shows the runtime ratio of the two algorithms on the same data sets.

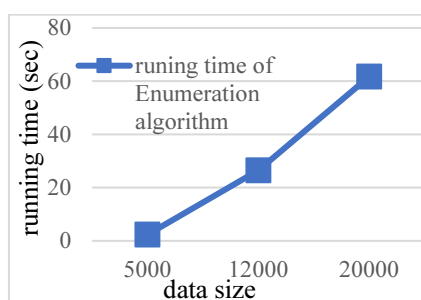


Fig. 8. Runtime.

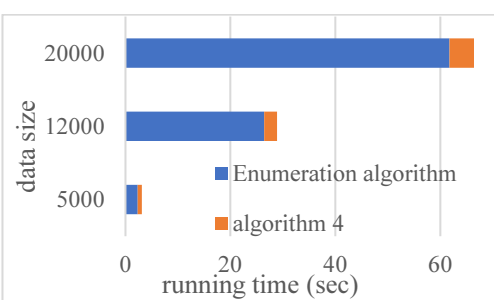


Fig. 9. The runtime ratio.

We can see that the enumeration algorithm used in the paper is a very efficient algorithm. The process of enumerating maximal cliques takes the most of the runtime, and the conversion process takes very little time. Also, experiments show that $\{\text{hotel}, \text{clinic}\}$ is a prevalent pattern and the new pattern tells us the ratio of hotels to clinics is 2:1, which reflects the significance of the proposed pattern.

5. Conclusion

In this paper, we studied the coupling co-location pattern mining problem which considers the coupling relationship (including intra-coupling and inter-coupling) between spatial features. A mining framework for discovering coupling co-location patterns has been developed. We conducted experiments on both real and synthetic data sets, which verified that the proposed coupling co-location pattern has practical meaning. The managerial implication of the new pattern is that it can augment co-location patterns in urban planning and other decision making. One limitation of the proposed pattern is that the support measure does not satisfy anti-monotonicity, which means that it cannot be pruned through the minimum support threshold like co-location patterns. In the future, we plan to design a new support measure approach for coupling co-location patterns and a new maximal clique mining algorithm to improve the efficiency of the mining process.

Acknowledgments

We would like to thank C. Zhang et al. for their outstanding work in maximal clique enumeration. This work is supported by the National Natural Science Foundation of China (61966036, 61662086) and the Project of Innovative Research Team of Yunnan Province (2018HC019).

References

- [1] L. Wang, X. Bao, L. Zhou and H. Chen. Mining maximal sub-prevalent co-location patterns. *World Wide Web*, 2019, 22(5): 1971-1997
- [2] S. Shekhar and Y. Huang. Discovering spatial co-location patterns: a summary of results. SSTD, 2001: 236-256
- [3] Y. Morimoto. Mining frequent neighboring class sets in spatial databases. KDD, ACM, 2001: 353-358.
- [4] Y. Huang, S. Shekhar and H. Xiong. Discovering co-location patterns from spatial data sets: a general approach. *IEEE Trans. Knowl. Data Eng.*, 2004, 16(12): 1472-1385
- [5] Y. Huang, S. Shekhar, H. Xiong and J. Pei. Mining confident co-location rules without a support threshold. In Proceedings, ACM, 2003: 497-501
- [6] J. S. Yoo and S. Shashi. A join-less approach for mining spatial colocation patterns. *IEEE TKDE*, 2006, 18(10): 1323-1337
- [7] J. S. Yoo, S. Shekhar, J. Smith, and J. P. Kumquat. A part join approach for mining co-location patterns. ACM, 2004: 241-249
- [8] H. K. Chan, C. Long, D. Yan, and R. C. Wong. Fraction-score: A new support measure for co-location pattern mining. ICDE 2019, IEEE, 2019: 1514-1525.
- [9] C. Wang, Z. She and L. Cao. Coupled Clustering Ensemble: Incorporating coupling relationships both between base clusterings and objects. ICDE 2013, IEEE, 2013: 374-385.
- [10] P. Yang, L. Wang and X. Wang. A mapreduce approach for spatial co-location pattern mining via ordered-clique-growth. Distribution and Parallel Databases, 2019, 38: 531-560

- [11] Y. Huang and P. Zhang. On the relationships between clustering and spatial co-location pattern mining. IEEE, 2006: 513-522.
- [12] X. Bao and L. Wang. A clique-based approach for co-location pattern mining. Information Sciences, 2019: 244-264
- [13] P. Wu, L. Wang and M. Zou. Vector-degree: A General similarity measure for co-location patterns. IEEE 2019, ICBK, 2019: 281-288
- [14] H. Xiong, S. Shekhar, Y. Huang, V. Kumar, X. Ma and J. S. Yoo. A framework for discovering co-location patterns in data sets with extended spatial objects. SDM, 2004: 1-12.
- [15] C. Zhang, Y. Zhang, W. Zhang et al. Efficient maximal spatial clique enumeration. ICDE 2019, IEEE, 2019: 878-889.
- [16] F. P. Preparata and M. I. Shamos. Computational geometry: an introduction. Springer. 1985.

LAR: A User Behavior Prediction Model in Server Log Based on LSTM-Attention Network and RSC Algorithm

Yingying Shang^{a1}

^a School of Computer Engineering and Science, Shanghai University, Shanghai 200444,
P.R. China

Abstract. Using server log data to predict the URLs that a user is likely to visit is an important research area in user behavior prediction. In this paper, a predictive model (called LAR) based on the long short-term memory (LSTM) attention network and reciprocal-nearest-neighbors supported clustering algorithm (RSC) for predicting the URL is proposed. First, the LSTM-attention network is used to predict the URL categories a user might visit, and the RSC algorithm is then used to cluster users. Subsequently, the URLs belonging to the same category are determined from the user clusters to predict the URLs that the user might visit. The proposed LAR model considers the time sequence of the user access URL, and the relationship between a single user and group users, which effectively improves the prediction accuracy. The experimental results demonstrate that the LAR model is feasible and effective for user behavior prediction. The accuracy of the mean absolute error and root mean square error of the LAR model are better than those of the other models compared in this study.

Keywords. Behavior prediction, LSTM, attention mechanism, cluster, server log

1. Introduction

With the development of the Internet, a massive amount of server log information has become a treasure trove for data mining. The server log not only contains information on the running status of the server, but also contains information related to user behavior. The analysis of valuable information from massive log files and prediction of user behavior is very helpful in balancing the network load, protecting young people from harmful information, and identifying potential customers.

A research direction of web data mining involves the development of predictive models of the access behavior a web user, which can be used to predict the next set of pages that the user might access. The objective of this paper is to predict the user's next access behavior through the historical access records generated by web users in the log. Various models such as fuzzy interference models, support vector machines, artificial neural networks (ANNs), association rule mining, and Markov models have been proposed to address the problem of web page prediction. Among them, the Markov

¹ Corresponding Author: Yingying Shang, Shanghai University, China; Email: yogoshary@163.com

model, which is the most commonly used model, uses the access records to calculate the probability of web page conversion, and predicts the next web page the user is likely to visit. B. Harindra Varma et al. [1] combined the naive Bayesian algorithm with the Markov model to predict the next category of user access. Xing Dongshan et al. [2] proposed a mixed-order Markov tree model. Awad et al. [3] studied several hybrid models combining different classification techniques, such as the Markov model, ANN, and Kth-order Markov model, and solved and predicted problems using Dempster rules. Trinchero et al. [4] analyzed and studied the application of the Markov and All-Kth Markov models for web prediction. Panchal et al. [5] studied the Markov model to predict the browsing behavior of users at the category level, and presented a mining process of web server log files to extract usage patterns for web link prediction with the proposed Markov Model. Pandey et al. [6] integrated a low-order Markov model and clustering to predict user behavior.

However, a predictive model based on the Markov model ignores the influence of long-distance behavior on current behavior. Concurrently, a majority of the user behavior prediction models only consider the access behavior of a single user, while ignoring the relationship between a single user and group users. Therefore, by combining the advantages of the long short-term memory (LSTM) network and attention mechanism, in this paper, a predictive model of user behavior from web logs based on LSTM-attention and reciprocal-nearest-neighbors supported clustering (RSC) (named prediction of web-user behavior based on LSTM-attention and RSC, LAR in short) is proposed. The proposed model incorporates the LSTM network [7], attention mechanism [8], and RSC algorithm [9]. The LSTM network structure can solve the problem ignored by the Markov model, i.e., the influence of short-term and long-term behaviors on current behavior. The attention mechanism can compensate for the limitation of the fixed vector length in the codec of the LSTM structure, and help capture important information in the long input [10]. Basic information on a user's access behavior is used as the feature input, which is then trained by the LSTM-attention network. Concurrently, the user is clustered by the RSC algorithm, and the URL prediction of a single user's expected access behavior is made based on the group users' access record. The experimental data presented in this paper are from the private server of a university campus network, and the proposed model is evaluated and analyzed using real server log datasets. The experimental results show that the LAR model can accurately predict the URL that users might visit in the future. In practice, using the LAR model to predict the online behavior of campus network users, the most concerned information that users pay attention to can be determined, and this information can subsequently be used to improve the campus service.

2. Construction of the LAR Model

2.1. Model Framework

The LAR model is shown in Figure 1.

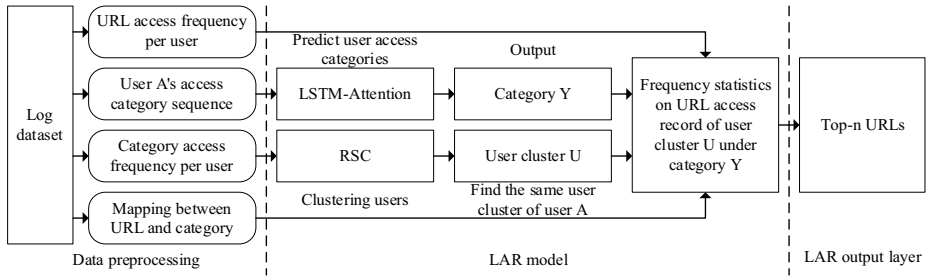


Figure 1. Structure of the LAR model

The proposed model can be divided into three parts, namely the LSTM-attention network, RSC, and section that generates the prediction results. First, the pre-processed data are used as the input to the predictive model. Then, the LSTM-attention model is constructed based on the LSTM network and attention mechanism, and subsequently used to predict the URL category. Concurrently, the RSC algorithm is used to obtain the user clusters. Finally, we use the URL categories predicted by LSTM-attention and the user clusters, combine the mapping relationship between the URL category and URL, and the URL access frequency of each user, to obtain the top N URLs, which is the final result of the LAR model.

The specific steps of the LAR model are: (1) Following normalization, the log data are used as the input to the predictive model. (2) The LSTM-attention network is used to predict the URL category sequence of user A, and the predicted result is category Y. (3) The RSC algorithm is used to cluster users and find the cluster U of user A. (4) Based on the historical access records of user cluster U and mapping relationship between the URL category and URL, the access records with category Y are extracted. Using the frequency statistics of the access records, the top-n URLs with the highest frequency are determined. The top-n URLs constitute the output of the LAR model.

2.2. Model Details

2.2.1 LSTM.

The LSTM network proposed by Hochreiter et al. [7] is an improved model of the recurrent neural network. The LSTM network learns to forget the information from the cell state and updates the information of the cell state via the memory unit. This enables the network to effectively use the long-distance dependent information in the sequence data and solve the problem of vanishing gradient or exploding gradient; thus, this network is mainly used to address time series problems. The structure of each LSTM unit includes a memory cell and three gates. The memory cell is set to record the state of the unit. The input gate and output gate are used to receive the output parameters and modify these parameters, respectively. The forget gate is used to control the forgotten degree of the previous unit state [11]. The structure of the LSTM unit is shown in Figure 2.

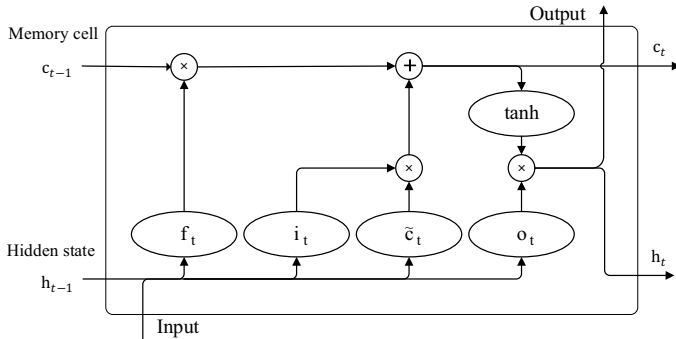


Figure 2. Structure of the LSTM unit

Assuming that the time step is t ($t=1, \dots, n$, where n is the total number of time steps), x_t is the input state of the LSTM, f_t is the forget gate, i_t is the input gate, and o_t is the output gate. Furthermore, c_t is the unit state memory, and h_t is the hidden state output. At the previous time step $t-1$, c_{t-1} represents the memory cell, and h_{t-1} is the hidden state output. The relationships between the variables can be described as:

$$f_t = \text{sigmoid}(W_{fh}h_{t-1} + W_{fx}x_t + b_f) \quad (1)$$

$$i_t = \text{sigmoid}(W_{ih}h_{t-1} + W_{ix}x_t + b_i) \quad (2)$$

$$\tilde{c}_t = \tanh(W_{ch}h_{t-1} + W_{cx}x_t + b_c) \quad (3)$$

$$o_t = \text{sigmoid}(W_{oh}h_{t-1} + W_{ox}x_t + b_o) \quad (4)$$

$$c_t = f_t \otimes c_{t-1} + i_t \otimes \tilde{c}_t \quad (5)$$

$$h_t = o_t \otimes \tanh(c_t) \quad (6)$$

Here, W and b are the training network parameters.

2.2.2. LSTM-Attention Network.

In deep neural networks, two problems might affect the training process. One is that the disappearance of the gradient makes it difficult to achieve neural network convergence, while the other pertains to over-fitting that causes the test set to fail. The LSTM network can effectively solve the gradient disappearance problem, and the dropout layer can alleviate the problem of overfitting by preventing the neurons from co-adapting. Therefore, in the design of the LSTM neural network, a dropout layer is added to optimize the structure of the neural network.

To capture the effective information in the log sequence better and grasp important information, in this paper, an LSTM network structure with the attention mechanism is proposed. This structure overcomes the problem that the standard LSTM model cannot fully learn the details of sequence coding due to the use of the same state vector in each prediction step. The LSTM-attention structure is shown in Figure 3.

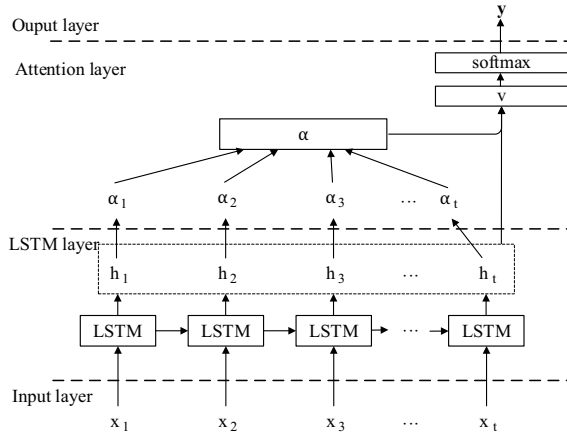


Figure 3. Structure of the LSTM-attention network

In Figure 3, the input sequence (x_1, x_2, \dots, x_t) represents the URL category data obtained in time t. Each item in the input sequence is passed to the LSTM unit to obtain the output (h_1, h_2, \dots, h_t) of the hidden layer. In the hidden layer, the attention mechanism is introduced to calculate the probability distribution values of each input assignment, ($\alpha_1, \alpha_2, \dots, \alpha_t$). The attention mechanism generates the attention weight matrix α and feature representation v. The corresponding equations are given by:

$$u_i = \tanh(W_s h_i + b_s) \quad (7)$$

$$\alpha_i = \exp(u_i^T u_s) / (\sum_{i=1}^t \exp(u_i^T u_s)), \quad \sum_{i=1}^t \alpha_i = 1 \quad (8)$$

$$v = \sum_{i=1}^t \alpha_i h_i \quad (9)$$

Here, W_s is the weight matrix, b_s is the offset, and u_s is the random initial attention matrix. Finally, the softmax function is used to obtain the predictive category y, which can be calculated as:

$$y = \text{softmax}(W_v v + b_v) \quad (10)$$

2.2.3 RSC Clustering Algorithm.

In this study, the RSC algorithm is used to cluster users, find the top-n URLs of each category of similar users, and improve the accuracy of the single user prediction model. The basic idea of the RSC algorithm is that two nearest data points should be placed in a cluster [9]. In the RSC algorithm, data points are connected with their nearest neighbors to build a clustering tree. Each clustering tree has a pair of points that are each other's closest neighbors, which are known as reciprocal nearest neighbors. The midpoints of the reciprocal nearest neighbors represent the center of the cluster, and can be used for a hierarchical aggregation of unclassified data. According to the previous research, tests on standard datasets across multiple domains show that RSC method is much faster and more accurate than the state-of-the-art benchmarks [9].

The RSC algorithm is used to cluster users according to the access frequency of the users in each URL category. The process is as follows: a) Represent user points with vectors. If the access frequency of user A in category c is N_A^c , then each user's access record can be represented by a $1*f$ -dimensional vector $V.V_A = [N_A^0, N_A^1, \dots, N_A^{f-1}]^T$, for $\forall i, 0 \leq i \leq n$, where n is the number of user points, and f is the number of categories. b) Calculate the nearest neighbor points of all users, and direct each user point to its nearest neighbor point. Calculate the Euclidean distance between all users. The point with the smallest distance is the nearest neighbor. If y is the nearest neighbor of x, it is recorded as $x \rightarrow y$. c) Find the members and central points of each user cluster. If $x \rightarrow y$ and $y \rightarrow x$, x and y are the nearest neighbor pairs. The midpoint of the nearest neighbor point pair is the center point of a cluster. The point attached to the nearest neighbor point pair is the member of the cluster. The number of points passed by each member to the nearest neighbor point is the depth of the member. In addition, to avoid the appearance of clusters that are too thin and long, when the depth of the member is greater than the threshold T, the member point is disconnected, and it points to the nearest neighbor point that is not in the current cluster. Let the number of points in this cluster be n, and the threshold T is defined as $T = \lceil \log N + 1 \rceil$.

3. Experiments Results and Analysis

3.1. Setup of the Experiment

3.1.1 Data Collection and Processing.

This paper used the desensitized data on a non-public production server of a university to verify the effectiveness of the proposed model. The size of the original log file is 51 GB, with 80 million lines of data. As an important part of user behavior prediction, the log data records all the information in the network requests, including the pages visited by users, server status information, and other kinds of data. While most lines of the log data have a relatively neat format, there are also many lines with no obvious rules, which need to be collected and cleaned using a web crawler. This paper collected the log data of the fourth week of December 2019 (5 days from Monday to Friday). In total, 398,241 log data items were stored in the database after data cleaning, with 198 users and 26 categories. The standardized data contained 8 columns, as shown in Figure 4.

mysql_id	category	host_ip	user_hash	dst_host	record_time	dst_ip	url
19	IT	10.89.4...	304fcc7f...	cpro.bai...	157698533...	112.122...	cpro.bai...
30	Market...	10.88.2...	4b19612...	www.ge...	157751190...	39.107....	www.ge...
42	Video ...	10.88.2...	8594919...	app.bilib...	157707339...	119.3.6...	app.bilib...
47	Social ...	10.89.7...	8e423dd...	cmshow...	157731748...	122.228...	cmshow...
62	News ...	10.88.1...	b86ea22...	ad-sdk....	157710886...	36.249....	ad-sdk....
86	Cateri...	10.89.2...	023000d...	mobile-p...	157706835...	39.98.2...	mobile-p...
103	Travel ...	10.89.7...	d4d3cd5...	push.12...	157707566...	39.98.7....	push.12...
215	Travel ...	10.95.2...	efd513e...	i0.dtslb...	157729092...	58.215....	i0.dtslb....
226	Search...	10.89.1...	9e3e398...	www.ba...	157753625...	180.101...	www.ba...
241	IT	10.89.1...	e27ae6f...	aod-ima...	157701451...	222.199...	aod-ima...

Figure 4. Sample data obtained after normalization

Among the columns, the ‘mysql_id’ field is a self-increasing field, which is not present in the original data. It was created to avoid the confusion of database sorting caused by the same ‘record_time’ field. The ‘category’ field is the category to which the record belongs. The ‘host_ip’ field is the user’s IP address. The ‘user_hash’ field is the hash value of the user ID that uniquely marks the user. The ‘dst_host’ field is the domain name of the visited site. The ‘record_time’ field is the access time. The ‘dst_ip’ field is the IP address of the site visited. The ‘url’ field is the record of the URL visited by the user.

3.1.2 Experimental Environment.

This experiment was executed in the following environment, CPU: Intel_Core_i3-9100F_3.60GHz; Memory: 16 GB DDR4 dual-channel RAM; Graphics card: NVIDIA RTX2060super 8 GB; Operating system: Windows 10 Professional Edition V1909.

3.1.3 Evaluation Criteria.

In this experiment, to evaluate the performance of the model effectively, the accuracy rate (p), mean absolute error (MAE), and root mean square error (RMSE) were used as the main evaluation criteria [12], which are defined by the following equations:

$$p = (TP)/(TP + FP) \quad (11)$$

$$E_{MAE} = \frac{1}{N} \sum_{i=1}^N |Y_i - \hat{Y}_i| \quad (12)$$

$$E_{RMSE} = \sqrt{\frac{1}{N} \sum_{i=1}^N (|Y_i - \hat{Y}_i|)^2} \quad (13)$$

3.2. Experimental Results and Comparison with Different Models

The RSC user clustering model was constructed and implemented in Java. After repeated experiments, 24 user clusters were stably formed from 198 users. Compared with the K-means clustering algorithm, the RSC clustering algorithm can adaptively form multiple clusters, without any need to manually set the number of clusters. In this model, the RSC algorithm required less time and achieved better performance, and the clustering effect was clearly better than that of the k-means algorithm. Keras, which is a library for deep learning in Python, was used to build the proposed LSTM-attention model. To improve the efficiency of large-scale task training, adaptive moment estimation (Adam) [13] was used to optimize the training process, and the number of iterations was set to 100.

3.2.1. Prediction of URL Categories using the LSTM-Attention Model with Different Steps.

As the length of the input sequence of the LSTM-attention model tends to significantly affect the predicted results, input sequences with different sliding window step-sizes were used to find the best window step. Table 1 shows the results obtained after many

tests.

Table 1. Results obtained with different sliding window steps for the LSTM-attention model

Step	Accuracy	MAE	RMSE
1	0.1803	4.1647	8.9870
3	0.3363	3.9734	6.1037
7	0.3459	3.9293	7.3621
9	0.3391	4.0100	8.8222
11	0.2980	4.4423	9.8545

From Table 1, it can be observed that as the sliding window step increased, the accuracy of the LSTM-attention model initially improved and then degraded. The MAE and RMSE initially decreased and then increased. When the value of the sliding window step was 7, the LSTM-attention model achieved the best performance, and the accuracy for predicting the URL categories was 0.3459. Therefore, the sliding window step size was set to 7, and the predictive result of the URL category obtained with the LSTM-attention model is shown in Figure 5. (the predicted value is shown in yellow, while the true value is depicted in blue)

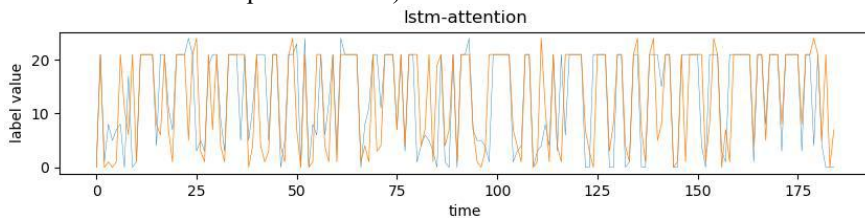


Figure 5. Results of LSTM-attention on the URL categories

(the predicted value of the model is shown in yellow; the true value is depicted in blue)

It can be concluded that with a small increase in the sliding window step, the model can fully learn the time information and the accuracy will increase accordingly. When the sliding window step exceeds 7 and becomes larger, the farther future needs to be predicted. As the model has more forward and backward propagation steps, the training time is longer, and the training curve clearly oscillates. Under such conditions, it will be considerably difficult for the model to predict the correct state of the system, leading to a decline in the performance.

3.2.2 Prediction Results of LSTM and LSTM-Attention on the URL Categories.

The predicted results of LSTM and LSTM-attention on the URL categories were compared to verify whether the attention mechanism improved the performance of the model. A comparison between the results of LSTM and LSTM-attention is shown in Table 2.

Table 2. Comparison between the results of LSTM and LSTM-attention on the URL categories

Method	Accuracy	MAE	RMSE
LSTM-Attention	0.3459	3.9293	7.3621
LSTM	0.2958	4.8764	9.8723

It can be observed that the predicted results of the LSTM and LSTM-attention models are similar to the URL category actually accessed by the users. Furthermore, the accuracy of the LSTM-attention model is slightly higher than that of the LSTM model. Therefore, the attention mechanism can effectively improve the model performance. In addition, the LSTM-attention model can reduce the network complexity and enhance

the generalization of the model.

3.2.3 Predicted Results of LSTM-Attention and Other Models on the URL Categories.

To verify the performance of the LSTM-attention model in predicting the URL categories, the LSTM-attention model was compared with the hidden Markov model (HMM) and BP neural network. The predicted results of different models on the same data set are shown in Figure 6, and the corresponding prediction errors are shown in Table 3.

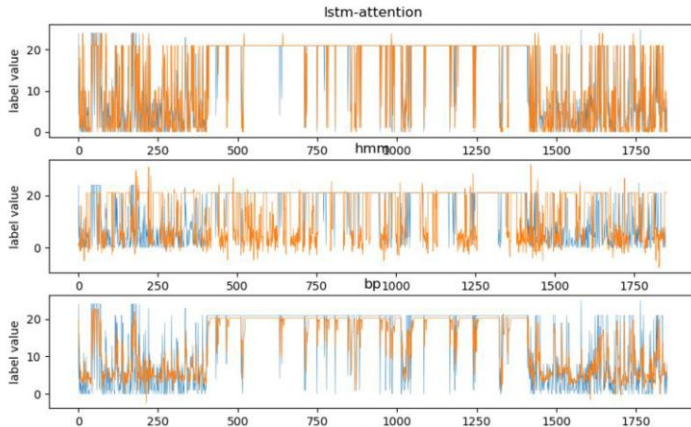


Figure 6. Results of LSTM-attention and other models on the URL categories
(the predicted value of each model is shown in yellow; the true value is shown in blue)

Table 3. Comparison between LSTM and LSTM-attention on the URL categories

Method	Accuracy	MAE	RMSE
LSTM-attention	0.3459	3.9293	7.3621
HMM	0.2839	9.1528	12.4451
BP	0.2644	3.5057	5.6620

It can be observed from Figure 6 that, for the same data set, the prediction ability of the LSTM-attention model for the trend derived from the data is not as good as that of the BP neural network model. However, the accuracy of the LSTM-attention model is slightly higher than that of the HMM and BP neural network models, as shown in Table 3. The BP neural network has the highest predictive ability for the trend revealed from the data, with the trend with a small amplitude being the most sensitive.

3.2.4 Predicted Results of the LAR Model and Other Models on the Top-n URLs.

In the LSTM-attention model, the relationship between the URL category and frequency stems from a user's historical records. In the LAR model, the relationship between the URL category and frequency is established based on the group users' historical records generated after RSC clustering. The relationship between the URL category and frequency in the LSTM-attention + K-means model stems from the group users' historical records generated after K-means clustering. The accuracy of the top-n

URLs predicted by each model is shown in Table 4.

Table 4. Accuracy of the top-n URLs predicted by each model

Model	TOP 1	TOP 2	TOP 3	TOP 5	TOP 10
LSTM-attention	0.1010	0.1010	0.1263	0.2289	0.2310
LAR model	0.1010	0.1250	0.1466	0.2446	0.2501
LSTM-attention + K-means	0.1010	0.1105	0.1324	0.2295	0.2336

According to Table 4, when the value of N was 1, each model achieved a similar accuracy. When the value of N was 2, the accuracy of the LAR model was slightly higher than that of the LSTM-attention and LSTM-attention + K-means models. With increase in N, the performance of the proposed model gradually improved through using the historical records of the group users clustered by the RSC algorithm. It can thus be inferred that the RSC clustering algorithm significantly improved the accuracy of the model for URL prediction.

4. Conclusion

In this paper, a predictive model of user behavior from web log data based on the LSTM-attention network and RSC algorithm (called LAR) was proposed, which was used to classify and predict the web pages visited by users via the log data. In the proposed model, the LSTM-attention network was used to predict the category of the next URL that users might visit, and the RSC algorithm was used to cluster users. By using LSTM-attention to predict the URL category and the RSC algorithm to cluster users, combined with the URL category and URL mapping relationship, the prediction results of the LAR model provided the top-n URLs the users were likely to visit.

Through the experiments detailed in this paper, it can be concluded that the LSTM-attention network is slightly sensitive to different sliding window steps, and an improved performance is achieved when a moderate step value is used (in this study, the best value was determined to be 7). The accuracy of the predicted results for the URL categories by the LSTM-attention model was slightly higher than those of the HMM and BP neural network models. Furthermore, the RSC algorithm improved the predictive accuracy of the final URL. In summary, the LAR model is viable and effective for predicting a user's future access URL.

There are still some deficiencies in LAR model, which does not consider the influence of URL classification on the prediction results. In the future, we will consider using URL text as a direct input to the prediction model, eliminating aside the influence of classification. The predictive model proposed in this paper can be used for load balancing of servers or pre-caching of pages by browsers to achieve faster access. In addition, based on the predicted data, relevant data for public opinion surveys and early warning of abnormal and other applications can be obtained.

References

- [1] B.Harindra Varma, K. Ashok Reddy, Web User Behavior Analysis Using Improved Naïve Bayes Prediction Algorithm. *international journal of computer trends & technology* 5.2 (2013).
- [2] Dongshan X, Junyi S, A new Markov model for Web access prediction, *Computing in ence & engineering*, 4.6 (2002),34-39.
- [3] Awad M, Khalil I, Prediction of User's Web-Browsing Behavior: Application of Markov Model, *IEEE*

- transactions on systems, man, and cybernetics. Part B, Cybernetics: a publication of the IEEE Systems, Man, and Cybernetics Society*, 42.4(2012), 1131-1142.
- [4] D Trinchero, R Stefanelli, L Cisoni, Integrating Markov Model with KNN Classification for Web Page Prediction, *International Journal of Computer Applications*, (2013).
 - [5] Panchal P S, Agrawat U D, Hybrid technique for user's web page access prediction based on Markov model, *2013 Fourth International Conference on Computing, Communications and Networking Technologies (ICCCNT)*, (2013).
 - [6] Pandey, Trilok, Ranjita et al, Merging Data Mining Techniques for Web Page Access Prediction: Integrating Markov Model with Clustering, *International Journal of Computer Science Issues*, (2012).
 - [7] Hochreiter S and Schmidhuber J, Long Short-Term Memory, *Neural computation*, 9(1997), 1735-1780.
 - [8] Bahdanau D, Cho K, Bengio Y, Neural machine translation by jointly learning to align and translate, *computer science*, (2014).
 - [9] Xie W B, Lee Y L, Wang C et al, Hierarchical Clustering Supported by Reciprocal Nearest Neighbors, *Information Sciences*, 7(2020), 279-292.
 - [10] Cho, Kyunghyun et al, On the Properties of Neural Machine Translation: Encoder-Decoder Approaches, *Computer Science*, (2014).
 - [11] Greff K, Srivastava R K, Jan Koutník et al, LSTM: A Search Space Odyssey, *Neural Networks and Learning Systems*, 28.10(2017), 2222-2232.
 - [12] C. J. Willmott, and K. Matsuura, Advantages of the mean absolute error (MAE) over the root mean square error (RMSE) in assessing average model performance, *Climate Research* 30.1(2005),79-82.
 - [13] Kingma D, Ba J, Adam: A Method for Stochastic Optimization, *Computer Science*, (2014).

The Improved Algorithm of Sample Adaptive Offset Based on Visual Saliency

Nana Shan^{a,1}, Wei Zhou^b and Zhemin Duan^b

^aSchool of Information Science and Technology, Taishan University

^bDepartment of Electronics and Information, Northwestern Polytechnical University

Abstract. Sample Adaptive Offset (SAO) in High Efficient Video Coding (HEVC) is a new technic to improve the quality of videos. It categories the pixels and choices the best way by adding some offsets to the reconstructed video. So, it causes a dramatically increased computational complexity. According to the dependency of sample adaptive offset and visual saliency map, an improved SAO method is proposed in order to minimize the coding time of SAO by skipping some RD cost calculation. Experimental result shows that the proposed method reduces 27.02% SAO encoding time with negligible performance loss.

Keywords. visual saliency, sample adaptive offset, high efficiency video coding, rate distortion optimization

1. Introduction

Sample Adaptive Offset (SAO) is a new coding tool of High Efficiency Video Coding (HEVC). It is an in-loop filter to reduce ringing effect and the distortion after the process of prediction coding and quantization. SAO can produce better coding efficiency and improve the quality of the videos [1]. Extreme correction (EXC) and band correction (BDC) were proposed to reduce the distortion based on the pixel classification in 2010 at the first meeting of JCT-VC [2]. Both techniques are effective to reduce the distortion as well as to improve the subjective quality. MediaTek's proposed each picture can be divided into multi-level quadtree partitions, and each leaf partition can be enhanced by band offset (BO) or edge offset (EO). Both BO and EO classify pixels of a partition into groups, and one offset is derived for each group [3]. SAO is located after deblocking and divides a picture into LCU (Largest Coding Unit)-aligned regions. Each region can be enhanced by either BO or EO with a localized parameter set. The statistical information for deriving offsets is collected, and the decision of all SAO parameters can be made right after the information collection by using fast distortion estimation [4]. Choi explore various SAO encoding policies including complexity reduction in the SAO parameter estimation and efforts to remove inefficiency caused by its implementation in a pipelined manner through numerous experimental tests [5]. In Yang's paper, the human visual characteristics represented by a JND (Just Noticeable Difference) model are introduced into the SAO optimization process for the first time [6].

¹ Shan Nana: School of Information Science and Technology, Taishan University. E-mail: helensnn@hotmail.com.

Most of those methods are based on pixels and lead to inefficient coding problems. This paper proposed a new SAO process by introduce visual saliency map to analysis the region of human visual attention. This proposed method will skip lots of useless calculation and improve coding efficiency with this strategy.

2. Sample Adaptive Offset

Figure 1 shows the ringing effect in the signal processing. The distortion is mainly caused by the loss of high frequencies of the original samples [7].

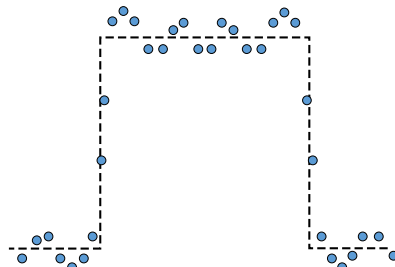


Figure 1. ringing effect

2.1. Types of SAO

SAO adapted in a 64×64 coding units and use different offsets in a region depending on the sample classification with three types including Edge Offset (EO), Band Offset (BO) and Merge [8].

a. edge offset

EO adapts four directional patterns for EO sample classification: 0° horizontal, 90° vertical, 135° diagonal, and 45° diagonal as shown in Figure 2 and named with EO_0, EO_1, EO_2, EO_3 separately.

Every sample will be classified into one of the five categories for the given EO class. And the roles are summarized in Table 1.

The meanings of edge offset are explained in Figure 3. Positive offsets for category 1 and category 2, while negative offsets for category 3 and category 4.

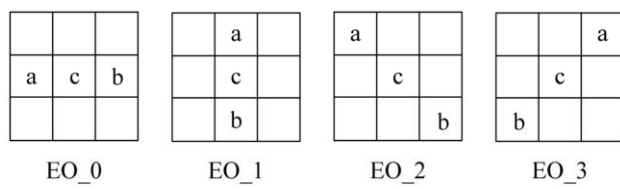
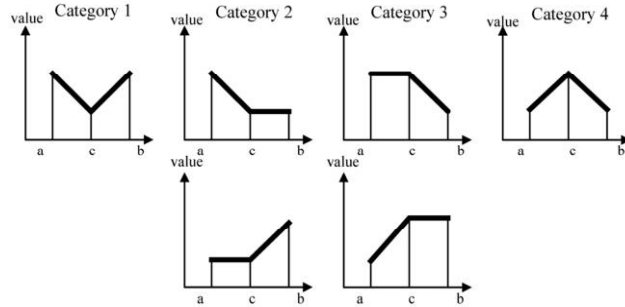


Figure 2. Edge Offset

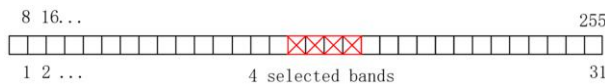
Table 1. Category of Edge Offset

Category	Condition
1	$c < a \& \& c < b$
2	$(c < a \& \& c == b) (c == a \& \& c < b)$
3	$(c > a \& \& c == b) (c == a \& \& c > b)$
4	$c > a \& \& c > b$
0	Others

**Figure 3.** Offsets relations of Edge Offset

b. band offset

The sample value is equally divided into 32 bands in the band offset mode as Figure 4 shows. For 8-bit samples changing from 0 to 255, and the width of a band is 8, so the sample value from $8k$ to $8k+7$ belongs to band k. The value of band offset could be positive or negative. Four consecutive band are signaled to the decoder.

**Figure 4.** Band Offset

c. Merge

SAO also could use the parameters of their neighbor and transmit it with the syntax element to reduce the coding time. There are three options of them: reusing SAO parameters of the left CTU, reusing SAO parameters of the above CTU, or sending a new SAO parameters [9].

2.2. Process of SAO

As we mentioned before, the types of SAO are EO_0, EO_1, EO_2, EO_3, merge_left, merge_above and OFF. When the SAO processing is starting, the SAO parameter will be chosen among those eight types [10].

(x, y) represents the position of a certain pixel, $s(x, y)$ represents the value of the original pixels, $u(x, y)$ represents the value of the reconstructed pixels, and m represents the value of the offsets, c represents the range of the pixels, the distortion between the original pixels and the reconstructed pixels will be presented as:

$$D_{\text{pre}} = \sum_{(x,y) \in c} (s(x, y) - u(x, y))^2 \quad (1)$$

And the distortion between the original pixels and the reconstructed pixels after SAO will be presented as:

$$D_{\text{post}} = \sum_{(x,y) \in c} (s(x,y) - (u(x,y) + m))^2 \quad (2)$$

So, the difference of them is:

$$\Delta D = D_{\text{post}} - D_{\text{pre}} = Nm^2 - 2mE \quad (3)$$

N represent the number of pixels, E is the summation of the difference between the original pixels and the reconstructed pixels.

$$E = \sum_{(x,y) \in c} (s(x,y) - u(x,y)) \quad (4)$$

The delta rate distortion cost is defined in the following equation:

$$\Delta J = \Delta D + \lambda R \quad (5)$$

λ is the Lagrange multiplier, R represents the number of bits to encoding the SAO parameters.

3. Visual Saliency

Visual saliency can describe the most important factors in visual attention of human. An infrared small target detection algorithm based on visual saliency improved by spatial distance is proposed by Yang Linna [11]. The gray value of target is weighted by the ratio of the target pixel block and its surrounding blocks through saliency map. A new algorithm based on multi-scale fusion of the image high frequency information is proposed by Yang Xuye [12].

Seo presents a bottom-up approach and computes local regression kernels. Then the framework results in a saliency map where each pixel indicates the statistical likelihood of saliency of a feature matrix given its surrounding feature matrices [13].

They define saliency at pixel position x_i as a posterior probability as follows:

$$S_i = P_r(y_i = 1 | F) \quad (6)$$

F_i contains a set of feature vectors in a local neighborhood and $F_i = (f_i^1, \dots, f_i^L)$. $F = (F_1, \dots, F_N)$ is a matrix containing features not only from the center, but also a surrounding region. If x_i is salient, y_i equals 1, otherwise y_i equals 0. Using Bayes' theorem, it could be written as:

$$S_i = P_r(y_i = 1 | F) = \frac{p(F | y_i = 1) P_r(y_i = 1)}{p(F)} \quad (7)$$

They adapted a locally data-adaptive kernel density estimator as follows:

$$S_i = \hat{P}(F | y_i = 1) = \frac{G_i(\bar{F}_i - \bar{F}_i)}{\sum_{j=1}^N G_j(\bar{F}_i - \bar{F}_j)} \quad (8)$$

G is weight function and can be computed as follows:

$$G_i(\overline{F}_i - \overline{F}_j) = \exp\left(\frac{-\|\overline{F}_i - \overline{F}_j\|_F^2}{2\sigma^2}\right) = \exp\left(\frac{-1 + \rho(F_i, F_j)}{\sigma^2}\right) \quad (9)$$

The matrix cosine similarity can be written as a weighted sum of the vector cosine similarities.

$$\rho_i = \sum_{l=1}^L \rho(f'_i, f'_j) \frac{\|f'_i\| \|f'_j\|}{\|F_i\|_F \|F_j\|_F} \quad (10)$$

Then, the saliency map from color channels can be analogously defined as follows:

$$S_i = \frac{1}{\sum_{j=1}^N \exp\left(\frac{-1 + \rho(F_i, F_j)}{\sigma^2}\right)} \quad (11)$$

4. Proposed Method

SAO have several directional modes as we mentioned before. In combination of the perceiving characteristics if human eyes for brightness, chroma, contrast and moving targets, an objective assessment method of video quality based on contrast sensitivity characteristics of human visual system was proposed by Yao Juncai [14]. Li proposed a visual attention-based bit allocation strategy to detect interesting regions in video [15]. There are two bottlenecks for the processing of SAO, one is the huge number of pixels at the statistic stage. The other is the high complexity in calculating the rate-distortion cost. An improved SAO algorithm that based on the visual saliency will be proposed in this paper to save the encoding time of SAO process.

4.1. Determination of SAO with visual saliency

As shown in figure 5, using visual saliency algorithm in [13] to generate visual saliency maps for the sequence BasketballPass (416x240, frame rate 50f/s). For the natural image, the bright region is more salient than the dark region. Red values in saliency map images represent higher saliency, while blue values mean lower saliency as we know.



Figure 5. Image in a video and visual saliency map

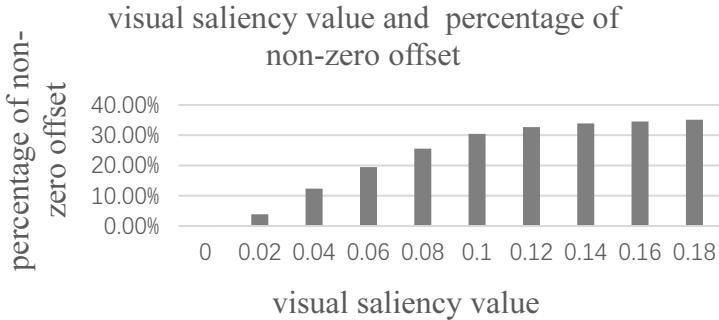


Figure 6. visual saliency value and percentage of non-zero offset in CTU

Figure 6 shows the statistics results of visual saliency average values and the sample adaptive offset which equals zero in a CTU of sequence BasketballDrive (1920x1080, 50f/s). It is important to note that in the regions with lower visual saliency, the sample adaptive offset has a very good chance to be zero, although with a series bitrate optimal calculation. It could be divided into many kinds of regions by their visual saliency values to skip some zero offset.

4.2. The processing of proposed algorithm

In the stand SAO algorithm, every pixel (with one luma value and two chroma value) will go through every kind of mode, including edge offset, band offset and merge. And it will be calculated in different categories. Those method leads to the problem of huge calculation complexity. We notice that the visual saliency statistics can be used as an important measurement for SAO. The proposed algorithm generates the visual saliency value of the pixels according to the visual saliency maps. And the average of visual saliency value will be calculated for every coding units. Then the coding units will be categorized by the average visual saliency values. For the regions with higher saliency, it attracts human visual attentions and is like to be a non-zero offset. On the contrary, for the regions with lower saliency, we can make early decision to stop the SAO process.

As shown in figure 6, there are about 30.42% non-zero offset values when visual saliency reaching 0.10, while the increasing process is getting slower. So, we set 0.10 as the SAO threshold.

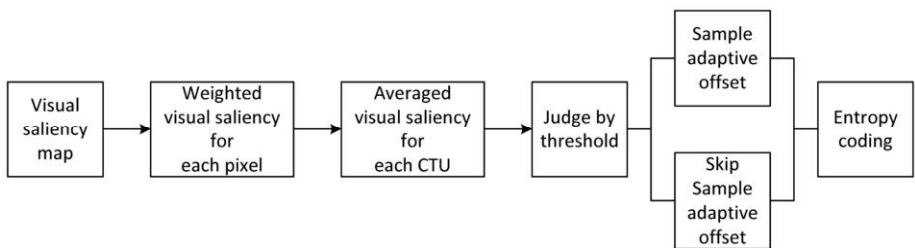


Figure 7. flow chart of proposed algorithm

Figure 7 shows the flowchart of the proposed method, it is explained in several stages as follows:

- Visual saliency map
- Weighted visual saliency for each pixel
- Averaged visual saliency for each CTU
- Judge by threshold: calculate sample adaptive offset or skip it
- Entropy coding

5. Experimental Results

This section presents experimental results to illustrate the benefits of proposed method.

5.1. Test Conditions

Those experiments were conducted using the HEVC test model version 16.0

- Five classes of test sequences
- 12 test sequences
- set quantization parameter with 22, 27, 32, 37
- using all intra configuration

5.2. Simulation Results

Table 2 shows the change of time, BD-rate and PSNR of the proposed SAO algorithm. It achieves about 27.02% encoding time saving only with 0.02 BD_rate and 0.0019 PSNR degradation.

Table 2. the result of proposed algorithm

Class	Size	Name	Δ PSNR/dB	Δ BR/%	Δ TIME/%
Class A	2560×1600	Traffic	-0.0007	0.01	-41.84
		Kimono	-0.0013	0.01	-36.53
Class B	1920×1080	BQTerrace	-0.0011	0.01	-33.44
		BasketballDrive	-0.0010	0.01	-32.09
Class C	832×480	RaceHorsesC	-0.0013	0.01	-26.45
		BQMall	-0.0019	0.01	-29.31
Class D	416×240	BasketballDrill	-0.0021	0.01	-26.29
		BasketballPass	-0.0034	0.03	-21.08
Class E	1280×720	BQSquare	-0.0025	0.02	-16.29
		Vidyo1	-0.0036	0.03	-21.60
		Vidyo3	-0.0011	0.02	-15.79
		Vidyo4	-0.0026	0.02	-23.53
Average			-0.0019	0.02	-27.02

5.3. Types of SAO

Figure 8 shows the pictures of a certain frame for both original HM algorithm and the proposed algorithm. From these pictures, we can see the proposed algorithm does not cause any notable visual distortions.



Figure 8. result of HM and proposed algorithm

6. Conclusion

In this paper, a relationship between SAO and visual saliency feature of the coding units is established by analyzing the SAO processing. Instead of calculate the SAO parameter one by one, the necessity will be attained by their visual saliency maps. The proposed method reduces SAO encoding time to average 27.02% only with trivial BD_rate and PSNR loss.

References

- [1] Sullivan G J, Ohm J, Han W J, et al. Overview of the High Efficiency Video Coding(HEVC) Standard[J]. IEEE Transactions on Circuits and Systems for Video Technology, 2012, 22(12): 1649-1668.
- [2] McCann K, Han W J, Kim I K, et al. Samsung's Response to the Call for Proposals on Video Compression Technology[C]// Proc. of ITU-T SG16 WP3 and ISO/ IEC JTC1/ SC29/ WG11, Dresden, German: JCT-VC, 2010: 1-3.
- [3] Fu Chihming, Chen Ching-Yeh, Huang Yuwen, et al. Picture Quadtree Adaptive Offset[C]// Proc. of ITU-T SG16 WP3 and ISO/ IEC JTC1/ SC29/ WG11, Daegu, Korea: JCT-VC, 2011: 1-10.
- [4] Fu ChihMing, Chen ChingYeh, C.Y. Tsai, Y.W. Huang, et al. Sample Adaptive Offset with LCU-Independent Decoding[C]// Proc. of ITU-T SG16 WP3 and ISO/ IEC JTC1/ SC29/ WG11, Geneva, Switzerland: JCT-VC, 2011: 1-6.
- [5] Choi Y, Joo J. Exploration of Practical HEVC/H.265 Sample Adaptive Offset Encoding Policies[J]. IEEE Signal Processing Letters, 2015, 22(4): 465-468.
- [6] Yang Kaifang, Wan Shuai, Gong Yanchao, et al. Perceptual Based SAO Rate-distortion Optimization Method with a Simplified JND Model for H.265/HEVC[J]. Signal Processing Image Communication, 2015, 31:10-24.
- [7] Fu Chih-Ming, Alshina E, Alshin A, et al. Sample Adaptive Offset in the HEVC Standard[J]. IEEE Transactions on Circuits & Systems for Video Technology, 2012, 22(12): 1755-1764.
- [8] Benjamin B, Han Woo-Jin, Ohm J R, et al. High Efficiency Video Coding Test Model 10 (HM10) Encoder Descriptions[C]// Proc. of ITU-T SG16 WP3 and ISO/ IEC JTC1/ SC29/ WG11, Geneva, Switzerland: JCT-VC, 2013: 1-310.
- [9] Joo J, Choi Y, Lee K. Fast Sample Adaptive Offset Encoding Algorithm for HEVC Based on Intra Prediction Mode[C]// Proceedings of the 3rd IEEE International Conference on Consumer Electronics. Washington D. C., USA: IEEE Press, 2013: 50-53.
- [10] Eun-kyung R, Jung-hak N, Lee S, et al. Sample Adaptive Offset Parallelism in HEVC[J]. Multimedia and Ubiquitous Engineering, 2013, 240: 1113-1119.

- [11] Yang Linna, An Wei, Lin Zaiping, *et al.*. Small Target Detection Based on Visual Saliency Improved by Spatial Distance[J]. *Acta Optica Sinica*, 2015(7):246-251.
- [12] Yang Xuye, Li Xuewei, Zhang Libao, *et al.*. Saliency Region Detection of Remote Sensing Image Based on Multi-Scale Frequency Analyses[J]. *Acta Optica Sinica*, 2014(13):111-115.
- [13] Seo H J, Milanfar P. Static and space-time visual saliency detection by self-resemblance[J]. *Journal of Vision*, 2009, 9(12):1-27.
- [14] Yao Juncai, Liu Guizhong. Video quality objective assessment combined contrast sensitivity characteristics of human visual system[J]. *Optics and Precision Engineering*, 2016, 24(03):659-667.
- [15] Li Z, Qin S, Itti L. Visual attention guided bit allocation in video compression[J]. *Image & Vision Computing*, 2011, 29(1):1-14.

The Overview of Genetic Algorithm with Tree Chromosome Structure to Identify Functions

Mitsukuni MATAYOSHI^{a,1}

^a*Department of Industry and Information Science, Japan*

Abstract. This paper is a collection of previous studies for function identification by simple genetic algorithm (GA) [1] with tree chromosome structure which has been proposed in [2]-[7], and gives the details more than survey paper. This paper also aims to introduce the studies which were written in Japanese. In this paper, there are five main points. First, a tree chromosome structure, which is the core idea of the studies, is introduced. The tree chromosome structure makes GA succeed in function identification called symbolic regression. Second, the proposed GA with tree chromosome structure succeeded in identifying the target functions from the observed data are shown indeed. The target functions are algebraic functions, primary transcendental functions, time series functions including chaos function, and user-defined one-variable functions. Third, to find function represented with some parentheses, a hierarchical tree chromosome structure is introduced. Forth, some local search methods to aim at the improvement for identification success rate and shortening identification time are introduced. In the end of this paper, the proposed tree and hierarchical tree chromosome structure can be adapted for identifying Boolean functions are laid out.

Keywords. Genetic Algorithm, Evolutionary Algorithm, Function Identification, Symbolic Regression, Local Search, Time Series Function, Boolean Function

1. Introduction

The scientist finds natural laws from observed data. It has long been human's dream to automate this process. One such attempt is Genetic Programming (GP) [8]-[12], which treat structural representations of functions directly as gene code using computer language LISP. It can search for a target function by applying basic operators of genetic algorithm to the concept tree coded in LISP. However, in real experiments, the high number of initial groups needed to maintain the variety of a graph causes the huge amount of calculation necessary, that is the big problem in GP. And, by crossover and/or mutation of genetic manipulation approach, a profitable partial tree structure may be destroyed. Thereby the search process is not steady, and much time is needed in many cases.

However, in 1998, a unique approach using simple GA [2], which can find the laws from the observed data in a very short time, has been proposed. Subsequently, its local

¹Corresponding Author: Mitsukuni Matayoshi, Okinawa International University, 2-6-1 Ginowan Ginowan-shi Okinawa, Japan; E-mail: matayosi@okiu.ac.jp

search methods and a modified chromosome structure to find Boolean function have been also proposed [3]-[7]. Nevertheless, the approach is unknown to researchers who are engaged in studying of genetic algorithms. Even though the evolutionary computing research area becomes wide, and recently there are so many applied research areas such as [13]-[15]. Presumably, the reason is that the study and some related studies were written in Japanese. Therefore, the aim of this paper is to introduce the studies in English.

In this paper, first of all, a sophisticated chromosome structure for a simple genetic algorithm [2] to identify function from observed data is introduced, and that is required for understanding the studies, which have been proposed by Matayoshi [2]-[7]. The proposed GA-based function identification methods with tree chromosome structure can, for example, identify $f(r, x, m) = r \cdot \tan(x) + m$ (obtaining the height of a point from its elevations viewed from another point) in a few minutes even when Pentium 350MHz computer is used. After that, some local search methods for the previous study are introduced in English because the original paper is only written in Japanese. In the rest of this paper, Boolean function identification by using tree chromosome structure in GA is described and shown the results.

2. Function Identification

The purpose of symbolic regression is to obtain a function's form, in many cases, with coefficients from the observed data. Before the proposed GA approach with sophisticated chromosome structure, automatic identification of unknown functions was a monopoly of GP. The method introduced in this paper allows symbolic regression and various identifications by the implementation of the tree structure as a chromosome, which is called Tree Chromosome Structure (TCS), of GA based approach. Three chromosome structure consists of function chromosome, pointer chromosome, constant chromosome, and operator chromosome. These are shown below.

3. Tree Chromosome Structure

One of the main points of the study is the unique chromosome structure (refer to Figure 1). GA can find the form of the target function by using it as a chromosome. For example, in Figure 1, when the fourth gene of the function chromosome is $Fm[4] = 2$, and the corresponding gene of the pointer chromosome is $Pm[4] = 4$, then the operator “÷” which is division symbol is selected as the gene of the operator chromosome. That is the “divide” operation is set.

$$f(x) = \begin{cases} \text{odd} & (\text{Refer to variable chromosome or constant chromosome set}) \\ \text{even} & (\text{Refer to operator chromosome}) \end{cases} \quad (1)$$

$$F_m[f] = \begin{cases} 0 & (f : \text{odd}, \text{Refer to variable chromosome}) \\ 1 & (f : \text{odd}, \text{Refer to constant chromosome}) \\ 2 & (f : \text{even}, \text{Refer to operator chromosome}) \end{cases} \quad (2)$$

$$P_m[f] = \begin{cases} \in V_c & (f : \text{odd}, V_c \in \text{Positive integer}) \\ \in C_c & (f : \text{odd}, C_c \in \text{Positive integer}) \\ \in O_p & (f : \text{even}, 0 \leq O_p \leq 5) \end{cases} \quad (3)$$

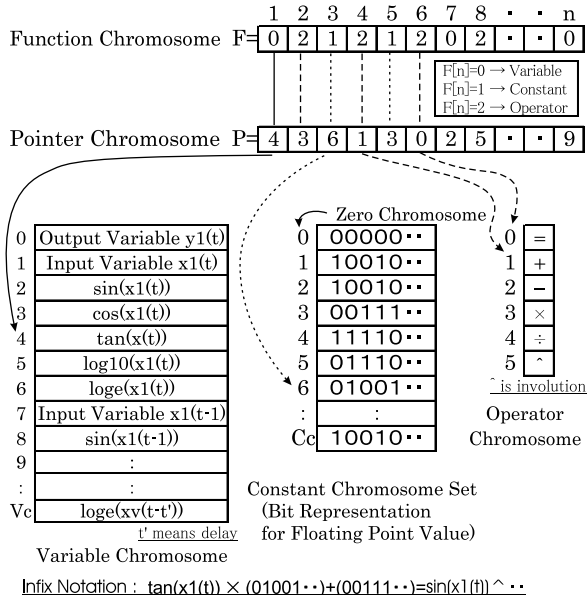


Figure 1. The tree chromosome structure.

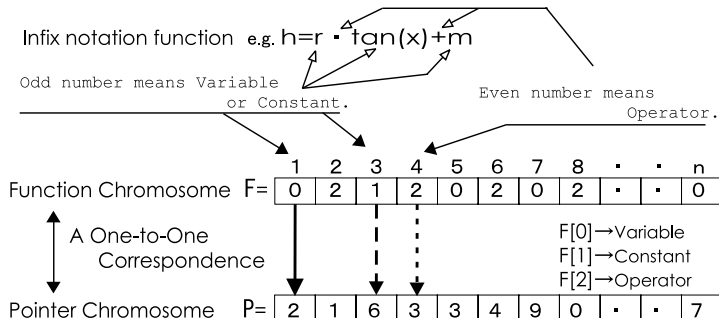


Figure 2. The Function Chromosome and Pointer Chromosome.

Here, $m \in$ natural number, $n \in$ positive odd number, V_c : variable chromosome length, C_c : number of representable constants, O_p : operator chromosome length.

The basic operators of GA are applied to the function chromosome, the pointer chromosome, and the constant chromosome set.

3.1. Function chromosome and pointer chromosome

The function chromosome is described by infix notation without parentheses (refer to Section 6). The pointer chromosome and the function chromosome have a one-to-one correspondence. The correspondence by the function chromosome and the pointer chromosome makes a form of function (see Figure 1, Figure 2).

3.2. Variable Chromosome

The variable chromosome is a fixed length chromosome and does not itself undergo GA operations. It is generated according to the observed data.

3.3. Operator Chromosome

Tree-Chromosome structure has one operator chromosome that cannot allow GA's operators such as selection. The operator chromosome has six genes including “=” and that is an irrevocably fixed chromosome (refer to Figure 1). Here “ \wedge ” means power function. The operators are defined to be left-associative, and each gene of operator chromosome takes mathematical operation priority as follows: $+,-,<,\times,\div,<^<=$.

3.4. Structure of constant chromosome set

The structure of the constant chromosome set is a two-dimensional array. Rows in this array represents different constant floating-point value (refer to Figure 3). This chromosome is manipulated by GA operators to get the appropriate constant value.

$$\text{Chromosome: } \underbrace{0 + \dots + 1}_{\substack{i=m \\ \text{Integer part: } m \text{ bits}}} + \underbrace{0 + 1 + \dots + 0}_{\substack{i=0 \\ j=1 \\ j=2 \\ \text{Floating point part: } n \text{ bits}}} + \dots + \underbrace{0}_{j=n}.$$

The decimal notation: $0 \cdot 2^m + \dots + 1 \cdot 2^1 + 0 \cdot 2^0 + 0 \cdot 2^{-1} + 1 \cdot 2^{-2} + \dots + 0 \cdot 2^{-n}$.
 Here, $m, n \in$ natural number.

Figure 3. Representation of constant chromosome with decimal notation.

4. The genetic operators and the fitness function

To find appropriate function, the proposed method applies the simple well-known basic GA operators (selection, crossover, and mutation) to the function chromosome, pointer chromosome, and the constant chromosome sets. The three basic operators on each chromosome adopt the following methods consistently:

Crossover method: One point crossover.

Mutation method: Compulsory conversion of gene.

Selection method: Elite preservation method.

Here, the function chromosome and the pointer chromosome have a one-to-one correspondence. Therefore, the crossover point is made the same. GA operators are repeated until the end condition, such as an iteration is set in advance or the convergence condition calculated by the fitness function given in (4), is satisfied. The elite solution survives reliably into the next generation by the fitness. Then, there is no change effected by GA operators because the elite solution's function chromosome,

$$\text{Fitness} = \sum_{i=0}^n \frac{1.0}{(|R_i - \text{Observed_data}_i| + 1.0)} \quad (4)$$

(R : output of a chromosome, n : number of observed data)

5. Experiment

5.1. Experimental function

The test function and observed data used for the experiments are as follows:

- (a) $Y = \frac{1}{2}gt^2$. (the law of free fall, $g = 9.8$)
 - (b) $r^2 = x^2 + y^2$. (circle at origin)
 - (c) $h = r \cdot \tan(x) + m$. (refer to Section 1 and Section 3)
 - (d) $Y = x_1 \cdot x_2 \cdot x_3 - x_4 \cdot x_5 \cdot x_6$. (two-box problem [10])
 - (e) $Y = (x+z)^{(x-z)}$. (calculation with parentheses)
 - (f) $Y = x + (w-z)f(x)$. (user-defined function: $f(x) = (x + \frac{1}{x})(x^2 + \ln(x))$, $x \neq 0$)
 - (g) $a_{n+2} = a_{n+1} + a_n$. ($n \in$ positive integer, $a_0 = 1, a_1 = 1$: Fibonacci sequence)
 - (h) $a_{n+1} = \alpha \cdot a_n(1 - a_n)$.
- ($n \in$ positive integer, $0 < a_0 < 1.0, 3.57 < \alpha \leq 4.0$: chaos phenomenon in logistic map)

Table 1. Restrictions for Test Functions.

Function	Observed variable	Unknown variable	Noise	Note
(a)	Y, t	$\frac{1}{2}, g$	$Y \pm 1 \sim 5\%$	$0 \leq t \leq 24(s)$ $g : 9.8(m/s^2)$
(b)	r, x, y		$r \pm 1 \sim 5\%$	$r : \text{radius}$ $ x, y \leq 10$
(c)	h, r, x	m	$h \pm 1 \sim 5\%$	$x : \text{elevation}$ $0 \leq r \leq 10$ $m : 1.5 \text{ view height}$
(d)	$Y, x_{1 \sim 6}$		$Y \pm 1 \sim 5\%$	$0 \leq x_{1 \sim 6} \leq 10$
(e)	Y, x, z		$Y \pm 1 \sim 5\%$	$-5 \leq z - x \leq 10$
(f)	Y, x, z		$Y \pm 1 \sim 5\%$	$0 \leq x \leq 10$ $0 \leq z \leq 10$
(g)	a_n		$a_n \pm 1 \sim 5\%$ Here, $2 \leq n$	$n = 0 \sim 24$ $a_0 = 1.0$ $a_1 = 1.0$
(h)	a_n	α	$a_n \pm 1 \sim 5\%$ Here, $2 \leq n$	$\alpha = 3.8$ $a_0 = 0.2$ $n = 0 \sim 24$

Note: An unknown variable means the data which cannot be observed independently.

5.2. Objectives

Function identification succeeds when the following objectives are achieved (see Section 5.1):

- (a): Obtain the law and unknown constant value.
- (b): Obtain a complete solution when both positive and negative one-time solutions are given as input.
- (c): Obtain a complete solution which contains the transcendental function and unknown constant value (view height).
- (d): Obtain the complete solution when there are a lot of observation variables.

- (e): Obtain the approximation solution of factorized functions.
- (f): Obtain a complete solution of the function which contains the user-defined function.
- (g): Obtain a complete solution of the Fibonacci sequence (time series function).
- (h): Obtain a complete solution and the constant value (= 3.8 for a fixed chaotic behavior) of the logistic map.

5.3. Experimental conditions

In all experiments, the upper bound of generations is 5000. Each mutation rate of the function chromosome, the pointer chromosome, and constant chromosome is 10%. The number of individuals in the function chromosome and pointer chromosome are $F_m = P_m = 500$. The number of constant chromosome individuals is $C_c = 200$. The constant chromosome length is $T = 10$ (5 bits for integer part, 5 bits for after the decimal point). Then experimental runs were executed for each problem in Table 1. The number of input data was 25 sets of the observed data. The experiment ends when the iteration reaches the upper bound or the absolute error value of Eq.(4) is $|R_i - Observed_data_i| < 0.05$.

5.4. Experimental results: No noise

Experimental results are indicated in Table 2; the proposed method identifies the target functions at very high speed (Pentium II 350 MHz). In (a) and (c), the approximate value of unknown constant $\frac{1}{2} \cdot g$ and, in consideration of the end condition, accurate value of m are obtained.

Table 2. Results, (No Noise in Observation Data).

Func.	The best detected solution			Average of detected solutions (include approximation solutions)			
	Detected Function	Time (s)	Detected generation	Number of times detected	Error	Time (s)	Detected generation
(a)	$t \cdot 19.96/4.062 \cdot t$	155.0	574	$1 + 8^* + 1^\sharp$	0.112	432.8	1558.3
(b)	$x \cdot x + y \cdot y$	1.84	18	10	0	6.9	59.7
(c)	$r \cdot \tan(x) + 1.531$	494.96	2682	$1 + 6^* + 3^\sharp$	0.024	270.2	1430.4
(d)	$x_1 \cdot x_2 \cdot x_3 - x_4 \cdot x_5 \cdot x_6$	11.04	119	$6 + 3^\sharp$	0.005	103.9	919.4
(e)	—	—	—	—	—	—	—
(f)	$x + w \cdot f(x) - z \cdot f(x)$	30.25	721	10	0	75.7	1681.5
(g)	$a_{n+1} + a_n$	0.14	0	$9 + 1^\sharp$	0	0.6	2.8
(h)	—	—	—	—	—	—	—

Note: * is a solution when the rounding error is considered. # is an approximate solution.

The proposed method with tree chromosome structure has succeeded in calculating values of constants with high accuracy (although this is difficult in GP). However, the identification both of (e) and (h) have failed. All detected functions in (h) are oscillatory functions (e.g., $a_{n+1} = a_n^{4.875}$). Indeed, the logistic map oscillates in the range $1 + \sqrt{6} < \alpha \leq \alpha_*(\simeq 3.57)$. The reason why the method could not find it is later mentioned (refer to Section 5.6). In regard to (e), the method is insufficient to solve it. To get the solution of factorized functions, a sensible approach has been also proposed (refer to Section 6).

5.5. Experimental results: Noise

Experimental results when the observed data contains noise are shown in Table 3. The proposed method identifies functions (a), (b), (c), (f), and (g), and succeeds in obtaining of constant values with high accuracy. In the real world, noise is often included in the observed data. In such cases, this method obtains reasonable results.

Incidentally, a solution of the form $x_1 \cdot x_2 \cdot x_3 - x_4 \cdot x_5 \cdot x_6 + \beta$ appeared in all experiments in (d). Because the error value ($\cong 5.02$) is small, β is a kind of an extra expression which absorbs and/or represents noise term.

Table 3. Results, (Noise in Observation Data).

Func.	The best detected solution			Average of detected solutions (include approximation solutions)		
	Detected Function	Error	Time (s)	Number of times detected	Error	Time (s)
(a)	$t/10.250 \cdot 28.219/9.875 \cdot t - t \cdot t/3.031$	35.16	1408.32	7* + 3 [#]	35.36	1425.03
(b)	$x \cdot x + y \cdot y + y/19.562 \cdot y$	1.06	912.67	9*	1.41	915.72
(c)	$r \cdot \tan(x) + 1.5$	0.97	609.34	3 + 4* + 3 [#]	0.99	581.37
(d)	—	—	—	10 [#]	5.02	581.599
(e)	—	—	—	—	—	—
(f)	$1.688 + w \cdot f(x) - z \cdot f(x) + x$	55.99	238.59	4* + 4 [#]	56.23	219.10
(g)	$0.906 \cdot a_n + a_{n+1}/27.031/30.906 + a_{n+1}$	463.14	1229.66	3* + 5 [#]	434.17	1235.948
(h)	—	—	—	—	—	—

Note: * is a solution when the rounding error is considered. # is an approximate solution.

5.6. Logistic map experiment

In Sections 5.4 and 5.5, the identification of the logistic map failed. This indicates falling into local solution, however, that is not so far from original function, of a wide search space. Two results were as follows:

No noise: $a_{n+1} = 3.938 \cdot a_n - 3.962 \cdot a_n \cdot a_n$ (detecting rate 10%, error: 0.017).

Noise: $a_{n+1} = 3.969 \cdot a_n - 4.031 \cdot a_n \cdot a_n$ (detecting rate 10%, error: 0.044).

Here, variable numbers are rounded off to four decimal places.

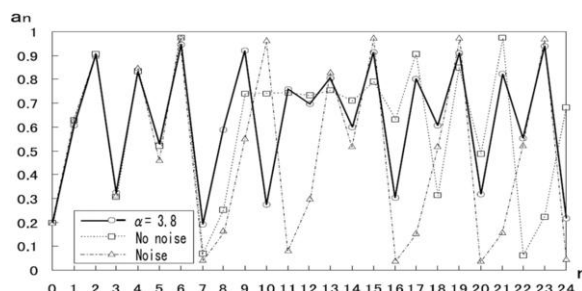


Figure 4. Comparison of Predicted and Actual Values for Test Function(h), The Logistic Mapping.

However, the obtained value for α , which determines the chaotic behavior, is not 3.8 exactly. The butterfly effect makes prediction difficult. In original paper, the constant chromosome cannot make constant value $\alpha = 3.8$ because five bits for decimal value has been assigned unfortunately. Hence, in this experiment, $\alpha = 0.813$ or $\alpha = 0.781$ should have been assigned.

6. Hierarchical Tree Chromosome Structure

The tree chromosome structure identified functions (f) and (h) in their expanded forms. However, the identification of (e) failed because its expansion was not possible. In order to identify general expressions in their factorized form, the tree chromosome structure needs to be expanded.

6.1. Hierarchical tree chromosome

The function chromosome shown in Section 3 is without parentheses. When one function chromosome is regarded as a formula in a pair of parentheses, that is, it is factorized form, the general expression can be obtained by connecting the factorized forms with operators. Thus, a new chromosome called HTCSF (Hierarchical Tree Chromosome Structure for Function) has been designed and proposed (see Figure 5). This method can represent a complex form function by hierarchizing.

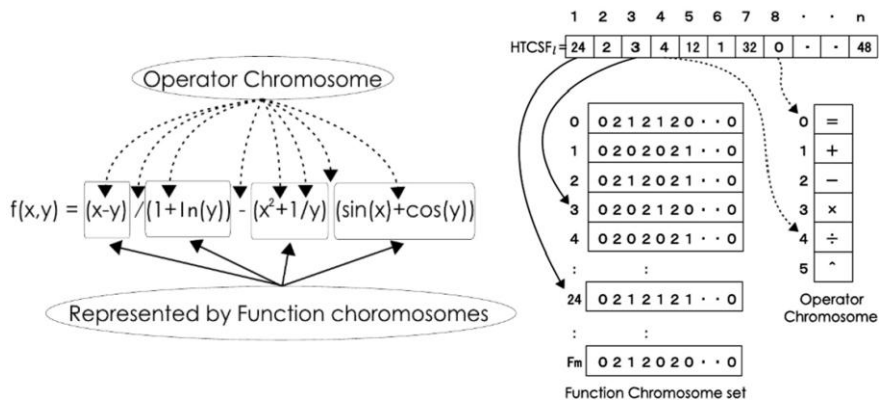


Figure 5. Representation of the hierarchical tree chromosome structure for factorized function chromosomes.

6.2. Experiments using HTCSF

The experimental results for using HTCSF are shown in Table 4. Reliable identification of (5) is seen; however, the identification of expandable functions failed. To get appropriate function formula in reasonable time, local search method might be efficient. In next Section 7, the proposed method with some local search methods get good results are shown.

Table 4. Results for Identification of Factored Expressions. Using HTCSF.

Func.	The best detected solution				Average of detected solutions			
	Detected Function	Error	Time (s)	Detected generation	Number of times detected	Error	Time (s)	Detected generation
(e)	$(x+y)^{(x-y)}$	0.0	1.21	5	10	0.0	3100.69	1085.8
(f)	—	—	—	—	—	—	—	—
(h)	—	—	—	—	—	—	—	—

7. Local search methods to Identify function

Tree Chromosome Structure succeeds in function identifications. However, there are not exact solution in the results. For example, in Table 2 the results of target function (c) are one exact solution, six solutions with rounding error, and three approximate solutions. Thus, to get more sophisticated form of target function, some local search methods have been proposed [7] (written in Japanese). Of course, the proposed local search methods also aim at the identification success rate improvement and shortening identification time.

7.1. Local search methods

Three different Local Search Methods for Tree Chromosome Structure (LSMs-TCS) have been proposed in [7]. And each LSMs-TCS takes two moving strategies. Therefore, in total, there are six different approaches to find good solution. In other words, six methods to avoid trapping into local solution are given. LSMs-TCS is the method which can change variable, constant value, or operator compulsory. The first method changes variable or constant value to another variable. Second method switches an operator to an another operator including power operator. The last one exchanges variable or constant value for ZERO. Here, the behavior of LSMs-TCS is shown in as follows:

- Compulsory changing procedure for variable and/or constant to variable
This local search method changes variable and/or constant to another variable compulsorily, and simultaneously changes the related gene of the pointer chromosome to a gene of variable chromosome so that one-to-one correspondence is kept.
e.g., when $f(x, y) = x \cdot y + y \cdot y$ is found during function identification, this local search method is able to change the y of $x \cdot y$ to x and get the right form of circle at origin function $f(x, y) = x \cdot x + y \cdot y$.
- Compulsory changing procedure for variable and/or constant to ZERO
The behavior of this local search method is to replace the target variable and/or constant by ZERO. This is a special case of method mentioned above.
e.g., when $f(x, r, m) = m \cdot r + \tan(x) + x - 1/x^2$ is obtained by the process of function identification, $f(x, r, m) = m \cdot r + \tan(x) + 0.0 - 0.0/x^2$ is made by this local search method by replacing x and 1 with 0.0 respectively.
- Compulsory changing procedure for operator
This local search method changes operator to another operator. However, if the value of right side of the target operator is near ZERO, then the target operator

never changes to division operator because of to avoid dividing by ZERO.

e.g., when $f(x, r, m) = m \cdot r + \tan(x) + x \cdot 0.0$ was gotten by during function identification, the local search method could obtain the right function formula by changing the multiplication operator of $m \cdot r$ to addition operator, and the addition operator of $r + \tan(x)$ to multiplication operator. Thereby, the found function expression finally becomes $f(x, r, m) = m + r \cdot \tan(x) + x \cdot 0.0$. The found function formula has a redundant part which is multiplied by ZERO in this case. Incidentally, the multiplication operator of this redundant part is never exchanged by division operator. Here, when m is the height of another point, r is the distance from the another point to the point directly underneath of the objective point, and x is the angle of elevation from another point. Then, the found function gets the height of an objective point from its elevations viewed from another point.

Each LSMs-TCS can take two moving strategies. The one of moving strategy is Fast Admissible Move Strategy (FAMS) which changes the solution to another good solution immediately when a better fitness individual is gotten by applying the local search method. The other strategy called the Best Admissible Move Strategy (BAMS) takes the Best solution from the neighborhood solution sets. The both strategies are repeated until there is nothing of exchangeable object in neighborhood.

In original paper [7], the six approaches are described in detail but are written in Japanese. However, hereinto, for want of space, the essence of two strategies are given instead of the detailed description of each six approaches. The essence of local search methods with moving strategies are shown as follows:

Step1: Take an individual at random from the population.

Step2: Take a genetic locus on the function chromosome and apply LMS. Simultaneously, change the gene of pointer chromosome because of one-to-one correspondence.

Step3: Calculate the fitness.

In FAMS;

Step4: If the fitness is improved, then the alteration is fixed, and back to Step 2.

Step5: If there is no good individual in neighborhoods, then quit the FAMS operation.

In BAMS;

Step4: If an improved fitness is obtained, then the altered individual is copied as the best so far.

Step5: Restore to the previous individual, and back to Step 2.

Step6: If there is no good individual in neighborhoods, then quit the BAMS operation.

Step7: Replace the best as a new individual to the previous individual.

7.2. New fitness

Differences of fitness function make some interesting differences for obtained solutions, which were reported and cleared in [7]. Specifically, when the identification system uses the original fitness function (4), undesirable approximate solutions are obtained in many cases (refer to Table 2, Table 3). Hereupon next two fitnesses have been tested.

$$\text{Fitness_2} = \frac{1}{n} \sum_{i=1}^n \frac{|input(i) - output(i)|}{|input(i)|} * 100. \quad (5)$$

$$\text{New_fitness} = \max \left(\frac{|input(i) - output(i)|}{|input(i)|} * 100 \right). \quad (6)$$

($input(i)$: i -th observed datum, $output(i)$: i -th output datum obtained by the system)

As a result, a new very simple fitness function (6) has been introduced in [7]. In formula (4) and (5), it is cleared that more observed data are given, the more averaging fitness is obtained because the fitness is divided by the total number of observations n . In other words, it is reasonable to assume that approximate solutions might be brought instead of the right solution.

Table 5. Testing results when the fitness value functions are different.

Obtained function	Fitness function	
	(6)	(5)
$Y = \frac{1}{2}gt^2$	47	22
$Y = \frac{1}{2}gt^2 \pm \beta t$	1	14
$Y = \frac{1}{2}gt^2 \pm \beta$	0	4
$Y = \frac{1}{2}gt^2 \pm \beta t + \gamma$	0	9
Don't find	2	1

β, γ : constant value

7.3. Experimental conditions

In all experiments, the limited time is 5 minutes. Therefore, the upper bound of generations does not set. The evaluation of convergence is $New_fitness < 5\%$. The number of individuals in the function chromosome and pointer chromosome are $F_m = P_m = 100$. The number of constant chromosome individuals is $C_c = 50$. The initial length of function chromosome and pointer chromosome is 31. The constant chromosome length is $T = 10$ (5 bits for integer part, 5 bits for after the decimal point). The length of operator chromosome is 6 including equal operator. Each mutation rate of the function chromosome, the pointer chromosome, and constant chromosome is 30%. The rate of crossover for function chromosome and pointer chromosome, and constant chromosome is around 70% because of excluding mutated chromosomes. To keep diversity of population, the most of chromosomes excluded the elite take gene manipulation in each generation. The proposed method has three exception processes are shown as follows:

- Multiple power operator prohibition: e.g. $f(x) = x^{3^5}$
- Overflow prevention: e.g. $f(x) = x \cdot 100^{1000}$
- Zero-divide prevention: e.g. $f(x) = x \cdot (1/100)^{1000}$

7.4. Selection from LSMs-TCS

It is necessary for the proposed GA-based identification system to take one of LSMs-TCS in each generation. However, it is not known in advance which LSM is the best one

to get good solution at the moment. Therefore, the experiments (W), (F), and (B) were performed in [7]. Here, (W) means with no LSMs and is for the verification experiment, (F) uses local search method with FAMS, and (B) uses local search method with BAMS. In the experiments, the only elite chromosome is chosen for manipulation by LSMs-TCS because many “0.0” gene were frequently appeared in the population in preliminary experiments. Even under such conditions, “0.0” gene were often made in the experiment. For example, the “0.0” gene appearance frequency of function identification for (b) were 3/69 in (W), 44/73 in (F), and 57/80 in (B) (refer to Table 6).

7.5. Target functions for experiments

The target functions of identification are composed of (a)-(h) excluding (e) in Section 5. And a new famous natural law called Kepler’s the third law, that is $T = k \cdot a^{2/3}$, $k \cong 1$, is added as (e).

7.6. Experiment using local search methods

The experimental results using proposed local search methods are shown in Table 6 and Table 7. Table 6 and Table 7 show better results in comparison with original identification method ((W) in tables) in Table 2, 3, and 4. Table 6 shows that LSMs-TCS gets good results in many cases excluding identification for function (c). Table 7 shows LSMs-TCS gets good improvement rate in finding time and the good results of statistical test. Here, +, * symbols in Table 7 are the results of Wilcoxon rank-sum test which is a Non-parametric test of mean difference. (F)-imp. and (B)-imp. are the improvement rate.

Table 6. Number of successes and improvement rate.

Func.	(W)	(F)	(B)	(F)-imp. (%)	(B)-imp. (%)
(a)	88	94	94	6.8	6.8
(b)	69	73	80	5.7	15.9
(c)	28	26	17	-7.1	-39.2
(d)	82	82	78	0.0	-4.8
(e)	95	99	100	4.2	5.2
(f)	0	1	2	-	-
(g)	53	59	68	11.3	28.3
(h)	0	0	0	-	-

Table 7. Average times(sec.) and improvement rate.

Func.	(W)	(F)	(B)	(F)-imp. (%)	(B)-imp. (%)
(a)	11.60	8.76*	8.75**	24.4	24.5
(b)	30.71	10.41**	11.72**	66.1	61.8
(c)	163.71	146.28	124.05	10.6	24.2
(d)	53.43	71.19 ⁺⁺	88.95 ⁺⁺	-33.2	-66.4
(e)	15.48	16.86	19.61	-8.9	-26.6
(f)	-	90.68	275.77	-	-
(g)	1.16	0.89	0.64**	23.2	44.8
(h)	-	-	-	-	-

*,+ / **,++: significance level 5%/1%(two-tailed test).

Table 8. Average length of expression of successfully identified functions.

Func.	ML	(W)	(F)	(B)	(F)-imp. (%)	(B)-imp. (%)
(a)	5	6.63	6.51	7.23	1.8	-9.0
(b)	7	9.17	11.57	12.30	-26.1	-34.1
(c)	5	8.42	8.23	9.47	2.2	-12.4
(d)	11	11.17	11.75	12.15	-5.1	-8.7
(e)	3	4.43	4.49	4.86	-1.3	-9.7
(f)	9	-	27.0	11.0	-	-
(g)	3	4.01	4.32	5.23	-7.7	-30.4
(h)	9	-	-	-	-	-

ML:Minimum Length of function.

Table 8 shows that when LSMs-TCS is used, the length of found function become longer. For example, in the meaning of function, both function $f(x, r, m) = m \cdot r + \tan(x)$ and $f(x, r, m) = m \cdot r + \tan(x) + 0.0 - 0.0/x^2$ are the same. However, the length of former function is 5, but the later one becomes 13. It is certain that the found function has some 0.0 term more than expected when zeroizing method of LMSs is used.

8. Boolean function identification

The target Boolean functions have single output and single/multi variable input. The identification of a Boolean function is different from function identification through symbolic regression in the following respect: Abbreviated forms of Boolean function are critical when constructing circuits, and one aim of the proposed method is to produce the most efficient Boolean representation. To find Boolean function by the proposed approach, Tree Chromosome Structure and Hierarchical Tree Chromosome Structure described above have to be modified for Boolean function identification.

8.1. Tree chromosome structure for identifying Boolean function

Figure 6 shows that the modified chromosome structure has one function chromosome and one pointer chromosome of one-to-one correspondence, one variable chromosome, and one operator chromosome. The variable chromosome is composed only of the variable and its negative form. The operator chromosome has (NAND, NOR, AND, OR, =). Here, Boolean operators are defined to be left-associative, and their order of priority is as follows: $\uparrow, \downarrow < \cap, \cup < =$. The factors and function chromosome is shown in Figure 7. Figure 8 is the HTCSF for Boolean function.

8.2. Fitness for identifying Boolean function

The fitness is calculated by the following two target functions. Here, *Fitness.b1* means the fitness until GA detects a complete form. Only when the derived expression is a complete form, is *Fitness.b2* used. In the Boolean function identification, the aspired goal is a complete expression and length minimization. The former is essential as an existence of error in a detected Boolean function is fatal. One the other hand, the latter is also an important concept when considering the manufacturing costs for an actual electric circuit.

$$Fitness_b1 = \frac{1}{n} \sum_{i=1}^n \frac{1.0}{1.0 + \alpha \cdot |R_i - Truth_table_i|} \quad (7)$$

$$Fitness_b2 = (7) + \frac{1.0}{(LDF + 1.0)} \quad (8)$$

(n : Truth table, R : Output of detected function, α : constant > 0 , LDF : Length of Detected function)

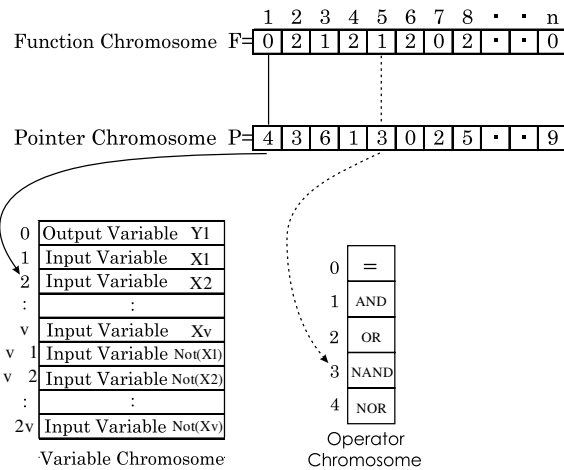


Figure 6. TCS for Boolean function identification.

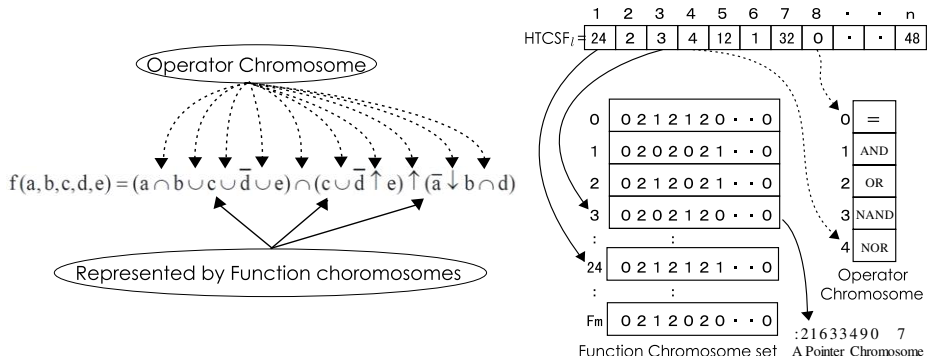


Figure 7. Factors and function chromosome.

Figure 8. Representation of the HTCSF for Boolean function.

8.3. Experiments

The test functions used for the experiments in the paper are as follows:

- (A) $f = a \oplus b$ (Exclusive - OR)
- (B) $f = \bar{b} \cap \bar{c} \cup a$
- (C) $f = (a \cup \bar{b}) \cap (a \cup \bar{c})$
- (D) $f = (a \uparrow b \downarrow c \cup d)$
- (E) $f = (a \cap b \cup c \cup \bar{d} \cup e) \cap (c \cup \bar{d} \uparrow e) \uparrow (\bar{a} \downarrow b \cap d)$
- (F) $f = (a \cap b \cup c \cup \bar{d} \cup e) \cap (c \cup \bar{d} \uparrow b) \uparrow (\bar{a} \downarrow b \cap d)$
- (G) $f = (a \cap b \cup c \cup \bar{d} \cup e) \cap (c \cup \bar{d} \uparrow d \cap e) \uparrow (\bar{a} \downarrow b \cap d)$

Where (B) and (C) have the same truth tables; (B) is the disjunctive canonical form, and (C) is the conjunctive canonical form. (D), (E), (F), and (G) are Boolean functions prepared for experiment, possible abbreviations for which are unknown. The truth tables of the above functions act as the input observation data for the identification system.

8.4. Condition and results

Conditions are indicated in Table 9. In all experiments, the upper bound of generations is 1000. Mutation rates of both the function chromosome and the pointer chromosome are 10%. The number of individuals in the function chromosome and the pointer chromosome are $F_m = P_m = 500$. Further, each chromosome length is 31, and $\alpha = 5.0$. Ten experimental runs were executed for each problem in Table 9. The number of input data varied with the size of the relevant truth table. The experiment ends when the generation reaches the upper bound or the value of *Fitness_b2* equal or exceeds 1.1. Here, ‘Rate of [1](%)’ means the appearance rate of output 1 in each truth table, and ‘Variables’ means the total number of variables (the sum of input and output variables).

Table 9. Experimental Examination Conditions for Three Chromosome Structure.

Function	(A)	(B)	(C)	(D)	(E)	(F)	(G)
Variables	3	4	4	5	6	6	6
Rate of [1](%)	50.0	62.5	62.5	6.25	81.25	78.125	87.5

Table 10 indicates that the proposed method succeeds in the identification of abbreviated forms of Boolean functions. However, functions (E) could not be identified, despite function (E) being very similar in form to (F) and (G) (refer to Section 8.3).

Table 10. Results for identification of factored expression of Boolean functions. : Using HTCSF.

Number	The best detected function				Average of detected functions		
	Function	Length	Generation	Time(s)	Length	Generation	Time(s)
(A)	$a \downarrow b \downarrow a \cap b$	7	5	0.19	8.0	38.8	1.27
(B)	$\bar{a} \uparrow c \cup b$	5	0	0.06	6.4	36.6	2.1
(C)	$\bar{b} \cap \bar{c} \cup a$	5	1	0.11	6.6	36.0	2.06
(D)	$\bar{d} \uparrow b \downarrow c \cup \bar{a}$	7	0	0.10	7.6	127.4	13.34
(E)	—	—	—	—	—	—	—
(F)	$\bar{e} \uparrow \bar{c} \downarrow e \cup \bar{d} \downarrow \bar{a} \uparrow \bar{b}$	11	10^3	198.2	19.4	10^3	199.1
(G)	$d \downarrow \bar{e} \uparrow a$	5	0	0.20	6.0	61.8	12.6

9. Conclusion and future work

This paper introduces the studies of function identification by simple GA with Tree Chromosome Structure, and also aims to show and to make understand some directly related studies written in Japanese. The unique point of the introduced GA-based identification approach is the Tree Chromosome Structure. By using the chromosome structure, GA can identify algebraic functions, primary transcendental functions, time series functions including chaos function, user-defined one-variable functions, and Boolean functions. The results show good performances in each function identification, so that it is not too much to say that the introduced approaches are so powerful.

An eventual research topic is to detect concealed laws from observed raw data such as empirical data of engineering, psychological, social research, and so on, by the use of the introduced methods that still remains to be done as a future work.

References

- [1] D. E. Goldberg. *Genetic Algorithms in Search, Optimization, and Machine Learning*: Boston, MA: Addison-Wesley; 1989. 372 p.
- [2] Mitsukuni Matayoshi. A Method for Function Identification using a Genetic Algorithm. IEICE Technical Report. 1998;98(199):25-31. (in Japanese)
- [3] Mitsukuni Matayoshi. Three Chromosome Structure in a Genetic Algorithm to Identify Functions. IEICE. 1999 Nov; J82-D-I:1327-1335. (in Japanese)
- [4] Mitsukuni Matayoshi. Boolean function identification in GA with Tree-chromosome structure. Proceedings of the 13th Annual Conference of JSAI: 1999 Jun 16-18; JSAI; p. 248-250. (in Japanese)
- [5] Mitsukuni Matayoshi. Three Chromosome Structure in a Genetic Algorithm to Identify Functions. Systems and Computers in Japan. 2000; 31(10): 32-40.
- [6] Mitsukuni Matayoshi. Boolean function identification in GA with Tree-chromosome structure. The Journal of General Industrial Research. 2002 Mar;10;1-8.
- [7] Mitsukuni Matayoshi, et al. Local Search Methods for Tree Chromosome Structure in a GA to Identify Functions. IEEJ Transactions on Electrical and Electronic Engineering. 2006 Jan;C126(1):123-131. (in Japanese)
- [8] Koza, J. R. *Genetic Programming: On the Programming of Computers by Means of Natural Selection and Genetics*. Cambridge. MA: MIT Press; 1992.
- [9] Hitoshi, Iba et al. System Identification based on structured genetic algorithms. Proceedings 5th International Conference on Genetic Algorithms (ICGA 93); 1993 Jun; Urbana-Champaign, IL. p. 279-286.
- [10] Hitoshi, Iba et al. System Identification Approach to Genetic Programming; Journal of Japanese Society for Artificial Intelligence (JSAI). 1995 Jul;10(4):590-600. (in Japanese)
- [11] Hitoshi, Iba et al. Temporal Data Processing Using Genetic Programming. Proceedings 6th International Conference on Genetic Algorithms (ICGA 95); 1995 Jul; San Francisco, CA. p. 279-286.
- [12] Les M. H and Donna J. D'Angelo. The GA-P: A Genetic Algorithm and Genetic Programming Hybrid. IEEE Intelligent Systems. 1995 Jun; 10(3):11-15.
- [13] Gudar J. Ibrahim, Tarik A. Rashid, Ahmed T. Sadiq. Evolutionary DNA Computing Algorithm for Job Scheduling Problem. IETE Journal of Research. 2018 May; 64(4):514-527.
- [14] J. M. Abdullah and T. Ahme. Fitness Dependent Optimizer: Inspired by the Bee Swarming Reproductive Process. IEEE Access. 2019;7:43473-43486.
- [15] Ahmed S. Shamsaldin, Tarik A. Rashid, Rawan A. Al-Rashid Agha, Nawzad K. Al-Salihi, Mokhtar Mohammadi. Donkey and smuggler optimization algorithm: A collaborative working approach to path finding. Journal of Computational Design and Engineering. 2019 Oct;6(4):562-583.

A Pipeline Abnormal Signal Detection Method Based on 1D-Faster R-CNN

Zhen Zhang^a and Weiguo Lin^{a,1}

^a College of Information Science and Technology, Beijing University of Chemical Technology, Beijing 100029, China

Abstract. Aimed at the detection difficulty of local abnormal signals during pipeline operation, this paper takes the local abnormal signals as the detected targets, and proposes a new method based on target detection to extract abnormal signals with different amplitude and shape; and for the case where there are few actual leak samples, combined with the characteristics that the training samples of each module of the model itself are derivative samples of the original sample, so as to realize the small sample training of the model. Finally, a new pipeline leak detection and location method is proposed by combining the 1D-faster R-CNN with the cross-correlation location method based on signal matching. The experimental results show that the proposed method effectively extracts local abnormal signals, accurately alarms leak signals, and eliminates the false alarms caused by the recognition errors of normal signals.

Keywords. target detection, local abnormal signal extraction, small sample, pipeline leak detection

1. Introduction

Pipeline is an important infrastructure in petroleum transportation. Due to pipeline aging, corrosion and third-party damage, pipeline leak accidents often occur [1-3], which can lead to serious safety accidents [4], especially for the transportation of some dangerous substances, such as liquid chlorine and hydrogen. Therefore, the monitoring of pipeline leak is critical, for which domestic and foreign scholars have conducted a large number of studies [5-8].

In recent years, deep learning has been widely used in image processing, natural language processing and other fields [9-10]. For pipeline leak detection, Kang et al. [11] proposed one-dimensional convolutional neural network and support vector machine (1D-CNN-SVM) model to classify leak and normal signals of water supply pipelines; Zhou et al. [12] proposed a classification model based on improved spline-local mean decomposition (ISLMD) and CNN, and identified leak signals with different leak apertures. Wang et al. [13] utilized time domain statistical features of normal samples to establish a diagnosis model based on support vector data description (SVDD) and implemented pipeline leak diagnosis. But it cannot extract the local abnormal information of an abnormal signal, and is hard to avoid false and missing alarm after long continuous running.

¹ Corresponding Author: Weiguo Lin, College of Information Science and Technology, Beijing University of Chemical Technology, Beijing 100029, China ; Email: linwg@mail.buct.edu.cn

And existing pipeline leak detection methods take a whole signal as the detection object, and fail to provide its local abnormal information, such as the number of local abnormal signals and their positions in a whole signal. However, in practical applications, the local abnormal information is vital to accurately locate and eliminate false and missing alarms. Wang et al. [14] proposed a model-free abnormal signal separation method, which realized the detection of local abnormal signals. However, it is based on the signal-to-noise ratio (SNR) increment of interval sub-signals, which is likely to cause the missing detection of relatively obvious abnormal signals.

In image processing, the target detection method can give the specific location of the target in the image and is suitable for multi-scale object detection. Girshick et al. proposed region-based convolutional neural networks (R-CNN) [15] and Fast R-CNN [16] successively, which greatly improved the accuracy of image target recognition. Subsequently, Ren et al. [17] proposed Faster R-CNN, making progress again in detection speed and identification accuracy. In addition, since the training samples of each module in the Faster R-CNN model are derivative samples of the original samples, and the number of which is much larger than original samples, it is very suitable for model training under the condition of small samples. Based on the faster detection speed, accurate target recognition, and small sample modeling of Faster R-CNN, and combined with the characteristics of fewer pipeline leak samples, this paper proposes an abnormal signal detection method based on 1D-Faster R-CNN. This method takes leak signals and interfering signals as training samples to establish a local abnormal signal extraction model, which reduces the dependence of model training on the number of samples. The position and number of local abnormal signals detected quickly and accurately are very beneficial for reducing false and missing alarms, and improving the accuracy of leak location.

The rest of the paper is organized as follows. Section 2 introduces the abnormal signal extraction methods based on 1D-Faster R-CNN from five aspects: data preprocessing, anchor point and boundary interval regression for one-dimensional signals, model structure, derivative samples and model training. Experimental results are presented in Section 3. And this paper is summarized and concluded in Section 4.

2. Local abnormal signal detection method based on 1D-Faster R-CNN

2.1. Data preprocessing

Deep neural network usually needs to normalize data, and commonly used data normalization methods are maximum minimum normalization and z-score standardization. And z-score standardization is more sensitive to outliers. According to the purpose of extracting abnormal signals, this paper uses z-score standardization to preprocess the data. The calculation of z-score standardization is:

$$x^* = \frac{x - \bar{x}}{\sigma} \quad (1)$$

Where x is the signal amplitude, \bar{x} is the signal mean, σ is the standard deviation of a signal, and x^* is the signal amplitude after z-score standardization.

Since the actual leak samples are difficult to obtain and deep learning requires a large number of samples, samples need to be expanded. In this paper, each abnormal

signal is regarded as an independent target, so the time sequence of the abnormal signal does not affect its detection. Based on this, this paper uses Eq. (2) to carry out symmetric transformation of the input sample to realize the expansion of the training dataset. That is, the signal is symmetrically flipped along the axis of symmetry to double the size of the dataset.

$$\begin{cases} x_{length-i} = x_i \\ 1 \leq i \leq length \end{cases} \quad (2)$$

Where $length$ is the length of the signal, and x is the amplitude of the signal.

Generally, infrasound signals of pipeline need to be filtered to improve the SNR. However, the boundary effect of filtering sometimes brings serious outliers at the signal boundary, which affects the detection of local abnormal signals. Additionally, the filtered signal becomes smoother, which affects the convergence of the model and easily lead to the overfitting of the model. Therefore, the original signal is not filtered in this paper.

2.2. Anchor, candidate interval and boundary interval regression

In one-dimensional signals, the position of each feature point extracted from the original signal is called anchor, and each anchor is associated with k candidate intervals of different sizes and scales. Referring to the method of literature [17], this paper proposes a candidate interval generation method for one-dimensional signals, and utilizes Eq. (3) to generate 9 candidate intervals at each anchor point.

$$\begin{cases} base_size = 16 \\ anchor_size = [8, 16, 32] \\ ratio = [0.5, 1, 2] \\ x_1 = \frac{1}{2} base_size - anchor_size_i * ratio_{j0} + x_0 \\ x_2 = \frac{1}{2} base_size + anchor_size_i * ratio_j + x_0 \end{cases} \quad (3)$$

Where $base_size$ is the base size of the candidate interval, $anchor_size$ is the additional amount above the base size, $ratio$ is the scale of $anchor_size$, x_1 and x_2 are the starting and end coordinate of the candidate interval, j_0 is the fixed subscript calculated each iteration, and x_0 is the anchor coordinate.

When the anchor coordinate is 0, for example, the 9 candidate intervals generated at the anchor are [4, 12], [4, 16], [4, 24], [0, 16], [0, 24], [0, 40], [-8, 24], [-8, 40], [-8, 40], [-8, 72]. All anchor coordinates of a signal are [0, 16, 32, 48..., 2976, 2992]. Hence, 1683 candidate intervals can be generated from a signal. Figure 1 shows the position relationship between the 9 candidate intervals associated with an anchor point and a local abnormal signal.

For boundary interval regression, this paper adopts two position transformation parameters [15]. The proposed and predicted intervals are $P = \{P_x, P_w\}$ and the $G = \{G_x, G_w\}$, where P_x, P_w, G_x, G_w are the starting coordinates and interval widths of the proposed interval and predicted interval respectively. And the transformation from P to G is:

$$\begin{cases} G_x = P_x + P_w * d_x \\ G_w = P_w * \exp(d_w) \end{cases} \quad (4)$$

And the position transformation parameter $d^* = \{d_x, d_w\}$ is:

$$\begin{cases} d_x = (G_x - P_x)/P_w \\ d_w = \log(G_w/P_w) \end{cases} \quad (5)$$

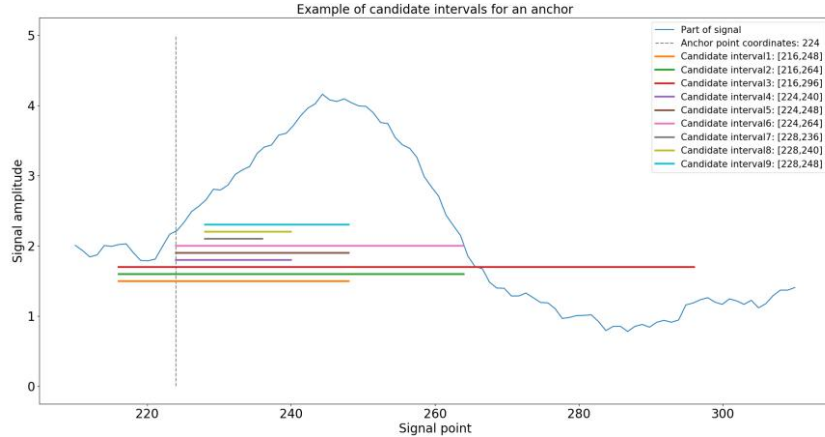


Figure 1. Example of candidate intervals for an anchor.

2.3. Model structure

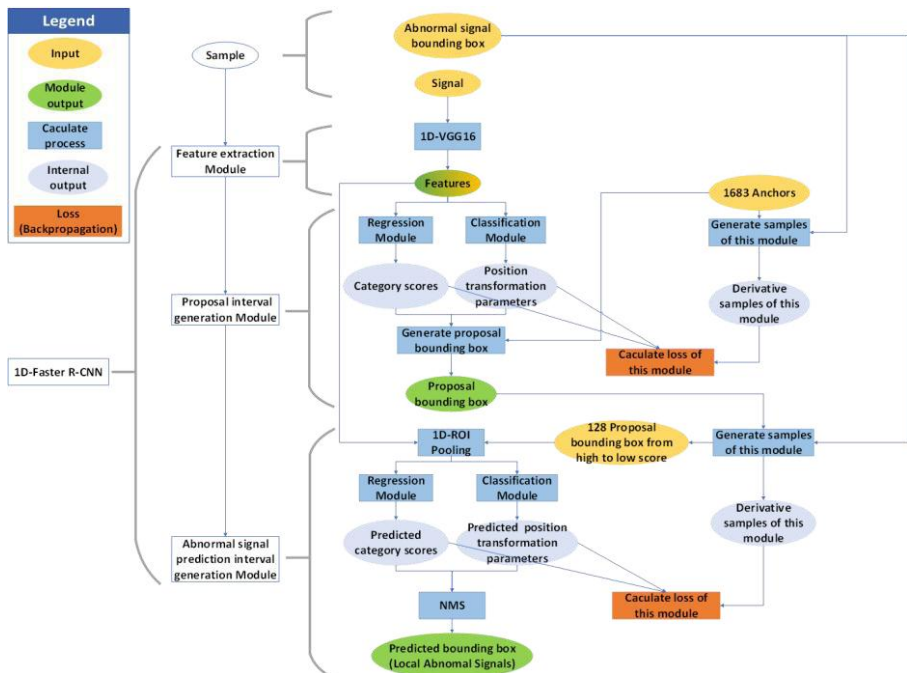


Figure 2. Model structure.

1D-Faster R-CNN is composed of three modules: feature extraction module, proposal interval generation module, and abnormal signal prediction interval generation module. Figure 2 shows the overall structure of the model.

(1)The feature extraction module is used to extract the features of a signal, which can be realized with the full convolution calculation of visual geometry group network 16 (VGG16). In this paper, the length of a signal to be processed is 3000 points. And after the feature extraction module, the feature of 512 channels is obtained, and the number of feature elements in each channel is 187. Figure 3 shows some features extracted from normal and leak signals.

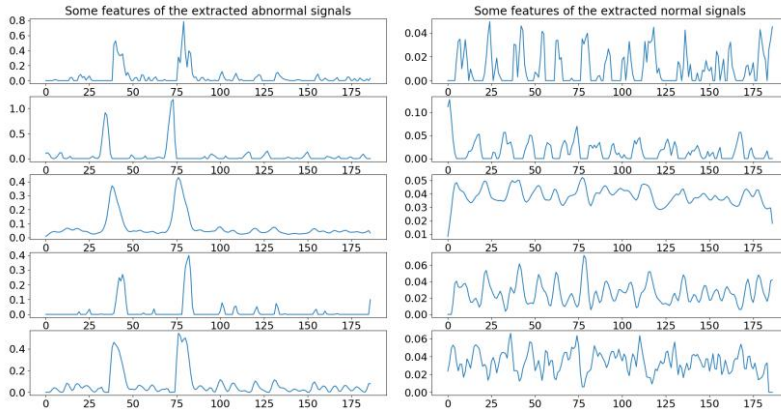


Figure 3. Some features extracted from normal and leak signals.

(2) The proposal interval generation module is to generate the proposal interval of the local abnormal signal to be detected. And it contains two models (classification and regression) and outputs the proposal intervals for abnormal signal identification. At the beginning of the module, a convolution layer is added to map the extracted features and further expand the feeling of the characteristic vector field. The receptive field size is 228. After the activation transformation (Rectified linear unit, ReLU), 512 feature vectors with length 187 are obtained, which are the input of the classification and regression models in this module.

The classification and the regression models are each composed of a convolution layer with a convolution kernel size of 1, step size 1, and 18 channels. They obtain the normal and abnormal signal category scores, and the two position transformation parameters of all candidate intervals, respectively. The position of each candidate interval is corrected according to the position transformation parameters obtained by regression. And the duplicate candidate intervals are deleted by non-maximum suppression (NMS) based on the abnormal signal category score of each candidate interval. When calculating NMS, the threshold of the intersection over union (IOU) is set to 0.7. Finally, the 200 candidate intervals with the highest abnormal signal category scores are used as the final proposal intervals.

(3)Abnormal signal prediction interval generation module is to further realize the classification and interval position correction of local abnormal signal. It also includes classification and regression models. The 200 proposal intervals need further classification and position correction to obtain the final abnormal signal prediction interval. Firstly, each proposal interval is mapped to the feature extracted by feature extraction module to obtain the feature of corresponding interval. Then, by global

maximum pooling, the features of the corresponding interval are divided into feature vector with the same length, and the obtained features are used as the input of the classification and regression models in this module.

The classification and regression models consist of a fully connected layer with 2 and 4 nodes, respectively. The classification and regression models obtain category scores and position transformation parameters of the normal and abnormal signal for all proposal intervals, respectively. Combining the results of the classification and regression models in this module, if there is an abnormal signal prediction interval, NMS is used to delete the repeated revised proposal interval to obtain the final abnormal signal prediction interval; if there is no abnormal signal prediction interval, the module has no output.

2.4. Derivative samples

The training samples are signal sequences marked with category labels and boundary intervals. The proposal interval generation module generates derivative samples for their own training through these samples and candidate intervals. Each sample is composed of position transformation parameters and category labels, and the number of derivative samples is much larger than training samples of the overall model. The process of generating derivative samples is:

- (1) Compute the IOU between the elements in sets A and B, where A contains all the candidate intervals and the known boundary intervals of the signal sample, and B contains boundary intervals of the signal sample;
- (2) Set the elements in set A larger than the positive threshold IOU as positive sample, and others as negative sample, and discard the remaining samples. Since $B \subset A$, at least one positive sample exists. In this paper, the positive and negative thresholds of this IOU are set as 0.7 and 0.3 respectively.
- (3) If the number of positive samples is larger than the set number of positive samples, part of the positive samples will be discarded at random; the same processing is performed on the negative samples.

The training samples of abnormal signal prediction interval generation module are also derivative samples of the model training samples. And their generation process is:

- (1) Compute the IOU between the elements in sets A (all the proposal intervals) and B (the boundary intervals of the signal samples themselves);
- (2) Through the IOU calculated in Step 1, the corresponding true boundary interval of each proposed interval can be obtained, and the IOU corresponding to the true boundary interval of each element in set A constitutes set C;
- (3) By comparing all elements of set C with the set IOU threshold, the ones larger than the IOU threshold are positive samples, while the others are set as negative samples. If there are too many positive samples, some of them will be discarded randomly, thus generating the label of positive and negative samples. Set the IOU threshold used here to 0.5 in this paper;
- (4) Calculate the position transformation parameters of the real boundary interval corresponding to the sample of the generated label.

2.5. Model training

The principle of labeling the boundary of the local abnormal signal in a signal is: the mean value of a signal is taken as the dividing line, the position of the abnormal signal

that begins to cross dividing line as the starting point, and the position when it crosses the dividing line as the end point. Since the signal is not filtered, there may be some signals that fluctuate near the dividing line.

In the model training, the loss function of the proposal interval generation module is the sum of the losses of the classification and regression models, as shown in Eq. (6).

$$L_{rpn}(\{p_i\}, \{t_i\}) = \frac{1}{N_{cls}} \sum_i L_{cls}(p_i, p_i^*) + \frac{1}{N_{reg}} \sum_i p_i^* L_{reg}(t_i, t_i^*) \quad (6)$$

Where i is the index of the proposal interval, p_i is the probability that the i^{th} sample is predicted as an abnormal signal, p_i^* is the true label corresponding to the i^{th} sample, and $t_i = \{t_x, t_w\}$ are two prediction regression interval transformation parameters, t_i^* are the transformation parameters of two proposal interval of positive samples, L_{cls} is the Cross-Entropy loss function used in the classification model, L_{reg} is the Smooth L1 loss function used in the regression model, N_{cls} is the number of classification samples, and N_{reg} is the regression samples number. In this article, N_{cls} is 256, and N_{reg} is 200.

The loss function of the abnormal signal prediction interval generation module is also represented in Eq. (6). The difference is that N_{cls} is 128 and N_{reg} is 128.

The loss function of 1D-Faster R-CNN is the sum of the loss function of proposal interval generation module and abnormal signal prediction interval generation module, which is shown in Eq. (7).

$$L_{1D-faster-rcnn} = L_{rpn} + L_{roi} \quad (7)$$

In this paper, Adaptive moment estimation (Adam) algorithm [18], whose two super parameters are set as follows: $\beta_1 = 0.9$, $\beta_2 = 0.999$, is used to train the model. Set the initial learning rate to 0.0001. During the training process, each batch contains one sample, and 1000 iterations of training are performed. After each iteration of training, calculated the average precision of the test dataset. The loss curve and the average precision curve of the training process of a certain batch of samples are shown in Figure 4.

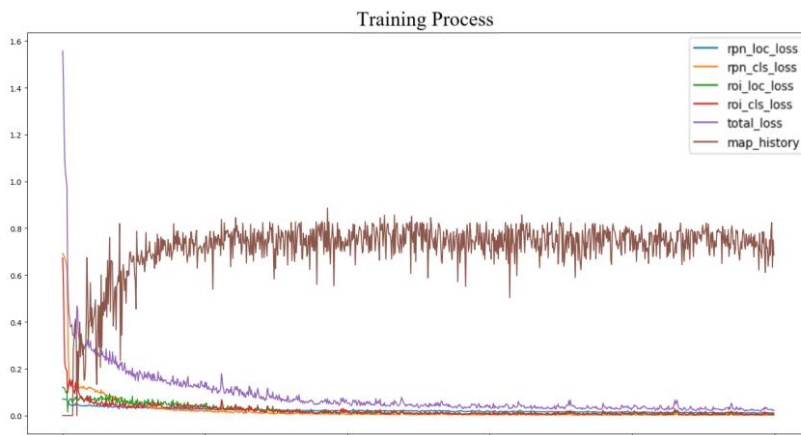


Figure 4. Training process.

It can be seen from the Figure 3 that the model tends to be stable at about the 500th iteration, and the training model, when the best average precision value is saved during the training process, is 0.877 at this time. Figure 5 shows the extraction effect of abnormal signals from leak signals.

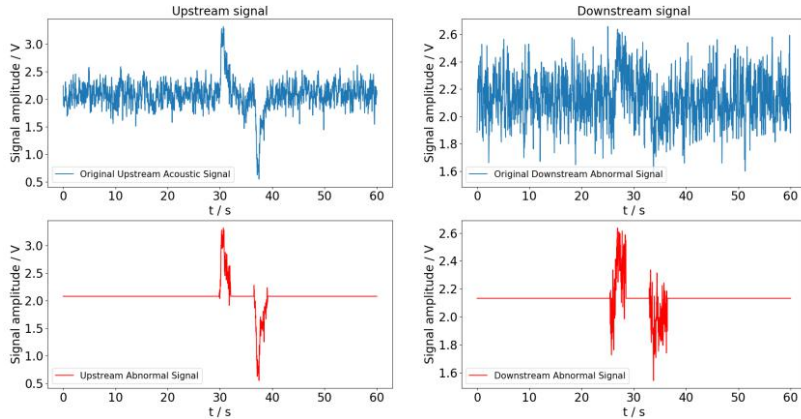


Figure 5. Extraction effect of abnormal signals from leak signals.

3. Validity test of method

The effectiveness of the abnormal signal detection method proposed in this paper is verified experimentally with a naphtha transmission pipeline as the experimental platform. The pipeline parameters and operating conditions are the same as literature [14]. Acoustic signal transmitters are installed in the upstream and downstream stations and the acoustic signal is collected synchronously. Among them, on November 20 and 21, 2013, a total of 15 burst leak simulation experiments were carried out on the naphtha transmission pipeline at a distance of 9.476 km from the upstream.

3.1. Modeling

Two leak signals, four station operation signals and four random interference signals are selected as the training dataset, and 10 samples are randomly selected from the known signals containing local abnormal signals as the test dataset. Using the method in Section 2.5 for modeling, the average precision of the upstream and downstream models on their respective verification datasets is 0.82 and 0.87, respectively. Combined with the cross-correlation localization method based on signal matching in literature [14], it is used as a complete leak detection and localization algorithm.

3.2. Comparative experiment

In the historical data collected from November 3, 2013 to December 17, 2013 of the naphtha pipeline, there were a total of 53,006 valid signal samples, and the above signal samples are used as diagnostic objects. This paper compares the local abnormal signal extraction algorithm with the model-free abnormal signal extraction algorithm

proposed in literature [14] from four aspects: false alarming, missing alarming, location errors and average sample detection time. The method in literature [14] is implemented by Matlab2019b and the proposed method is implemented by python3.6.5 and pytorch1.2. Compare from the perspectives of false alarm, missing alarm, location error and average sample detection time. The hardware platform required for the algorithm to run is shown in Table 1, and Table 2 shows the comparison results.

From the experimental results in Table 2, it can be seen that both methods have not missing alarm, but both caused false alarms. False alarms of the abnormal signal extraction method of 1D-Faster R-CNN are mainly the operation of the stations that cause false alarms due to inaccurate location (3 false alarms), and non-homologous interference signals (11 false alarms). In addition to the above two reasons, there are 16 false alarms that diagnose normal signals as abnormal signals. From the perspective of abnormal signal recognition and real-time, the proposed method in this paper has high accuracy and fast calculation speed, which meets the requirements of practical applications.

Table 1. Related parameters of hardware experiment platform

Parameters	Value/Unit
Memory	8G
Video Memory	6G
CPU	Intel Core i7-9750H
GPU	NVIDIA RTX 2060

Table 2. Comparison results

Method	Number of Alarms		Largest Location Error(m)	Average detection time(s)
	False	Missing		
This paper	14(0.026%)	0(0%)	167(1.08%)	0.032
Model-free	23(0.043%)	0(0%)	85(0.5496%)	0.017

3.3. Experiment on the effect of local abnormal signal extraction

Construct the dataset to compare the extraction effects of the method in this paper and the method of model-free abnormal signal extraction. When constructing the dataset, in order to eliminate the subjective factors of artificially judging whether the signal is abnormal, the following principles are used to construct the dataset:

- Select the signal frame containing obvious local abnormal and non-controversial parts;
- Select the signal frame with known operation;
- Select the signal frame where there is obviously no local abnormal signal;
- Record continuous outliers in a frame signal as one local abnormal signal.

According to the above four principles, 400 signal frames are selected to form the dataset. Among them, there are 200 signal frames containing local abnormal signals and 200 signal frames containing no local abnormal signals. A total of 290 local abnormal signals are included.

Compare the two methods from the perspectives of the accuracy of local abnormal signal detection and the accuracy of whether the signal frame contains local abnormal signals. The experimental results are shown in Table 3.

The experimental results show that the proposed method is superior to the comparison method in terms of the detection accuracy of local abnormal signals and whether the signal frame contains local abnormal signals. Moreover, the accuracy of

the constructed dataset can reach more than 95%, so the method proposed in this paper is effective in the aspect of local abnormal signal extraction.

Table 3. Experimental results of local abnormal signal extraction

Method	Accuracy of local abnormal signal detection	Classification accuracy
This paper	95.2% (276/290)	99.5% (398/400)
Model-free	75.2% (218/290)	81.8% (327/400)

4. Conclusion

This paper proposes a local abnormal signal extraction method for pipeline leak detection based on 1D-faster R-CNN. It can detect local abnormal signals of different amplitude, shape and time-frequency domain characteristics by the application of target detection to one-dimensional signal processing. From the perspective of signal preprocessing, this paper only highlights the abnormal part of the signal through z-score standardization. While avoiding the influence of filtering boundary effect on the signal in the traditional method, it also realizes the detection of small leak. In terms of the model, this paper proposes a method for generating candidate intervals related to anchors for one-dimensional signals, which effectively realizes the coverage of multi-scale candidate intervals on the whole frame signal. In addition, based on the characteristics of the derived samples in 1D-Faster R-CNN, it overcomes the problem of fewer leaking samples in the actual pipeline, and realizes the modeling of small samples, which reduces the dependence of the modeling on a large number of samples. Finally, the combination of the abnormal signal extraction method and the cross-correlation location method based on signal matching in this paper realizes a new type pipeline leak real-time monitoring method, which can effectively reduce false alarms while achieving accurate detection of pipeline leaks.

References

- [1]. Lu Z, She Y, Loewen M.. A Sensitivity Analysis of a Computer Model-Based Leak Detection System for Oil Pipelines. Energies, 2017, 10, 1226.
- [2]. He G, Liang Y, Li Y, Wu M, Sun L, Xie C, et al.. A method for simulating the entire leaking process and calculating the liquid leakage volume of a damaged pressurized pipeline. Journal of Hazardous Materials, 2017, 332: 19-32.
- [3]. Wang X, Ghidaoui M. Processing S.. Identification of multiple leaks in pipeline: Linearized model, maximum likelihood, and super-resolution localization. Mechanical Systems and Signal Processing, 2018,107.
- [4]. Qu Z, Wang Y, Yue H, An Y, Wu L, Zhou W, et al.. Study on the natural gas pipeline safety monitoring technique and the time-frequency signal analysis method. Journal of Loss Prevention in the Process Industries, 2017, 47.
- [5]. Lang x, Li P, Hu Z, Ren H, Li Y.. Leak Detection and Location of Pipelines Based on LMD and Least Squares Twin Support Vector Machine. IEEE Access, 2017, PP:1-1.
- [6]. Ranginkaman M, Haghghi A, Mohammad Vali Samani H.. INVERSE FREQUENCY RESPONSE ANALYSIS FOR PIPELINES LEAK DETECTION USING THE PARTICLE SWARM OPTIMIZATION. INTERNATIONAL JOURNAL OF OPTIMIZATION IN CIVIL ENGINEERING, 2016, 6:1-12.
- [7]. Wang C, Zhang Y, Song J, Liu Q, Dong H.. A novel optimized SVM algorithm based on PSO with saturation and mixed time-delays for classification of oil pipeline leak detection. Systems Science & Control Engineering, 2019, 7:75-88.
- [8]. Xiao R, Hu Q, Li J. Leak detection of gas pipelines using acoustic signals based on wavelet transform and Support Vector Machine. Measurement, 2019, 146:479-89.

- [9]. Hori T, Watanabe S, Zhang Y, Chan W. Advances in Joint CTC-Attention based End-to-End Speech Recognition with a Deep CNN Encoder and RNN-LM. 2017.
- [10]. Kiranyaz S, Ince T, Gabbouj M.. Real-Time Patient-Specific ECG Classification by 1D Convolutional Neural Networks. IEEE transactions on bio-medical engineering, 2015, 63.
- [11]. Kang J, Park Y-J, Lee J, Wang S-H, Eom D-S.. Novel Leakage Detection by Ensemble CNN-SVM and Graph-Based Localization in Water Distribution Systems. IEEE Transactions on Industrial Electronics, 2017, PP:1-1.
- [12]. Zhou M, Pan Z, Liu Y, Zhang Q, Cai Y, Pan H.. Leak Detection and Location Based on ISLMD and CNN in a Pipeline. IEEE Access, 2019, PP:1-1.
- [13]. Wang F, Lin W, Liu Z, Wu S, Qiu X.. Pipeline Leak Detection by Using Time-Domain Statistical Features. IEEE Sensors Journal, 2017, PP:1-1.
- [14]. Wang F, Lin W, Liu Z, Qiu X.. Pipeline Leak Detection and Location Based on Model-Free Isolation of Abnormal Acoustic Signals. Energies, 2019, 12:3172.
- [15]. Girshick R, Donahue J, Darrell T, Malik J. Rich feature hierarchies for accurate object detection and semantic segmentation. Proceedings of the IEEE Computer Society Conference on Computer Vision and Pattern Recognition, 2013, 2014.81
- [16]. Girshick R.. Fast r-cnn. ICCV. 2015, 2015.169
- [17]. Ren S, He K, Girshick R, Sun J. Faster R-CNN: Towards Real-Time Object Detection with Region Proposal Networks. IEEE Transactions on Pattern Analysis and Machine Intelligence, 2015,39.
- [18]. Kingma D, Ba J., Adam: A Method for Stochastic Optimization. International Conference on Learning Representations. 2014.

Research on Characteristics of Chinese Herbal Medicine Compounds Based on Bisecting k-Means Algorithm

Yushu Wu^{a*}, Fenfen Xie^{a,*}, Lu Wang^{a,1}, Shoude Zhang^b, Lei Zhang^c and Xiaoying Wang^a

^a*Department of Computer Technology and Applications, Qinghai University, Xining, 810016, China*

^b*State Key Laboratory of Plateau Ecology and Agriculture, Qinghai University, Xining, 810016, China*

^c*College of Computer Science, Information Management Center, Sichuan University, Chengdu 610065, China*

Abstract. The properties of Chinese Herbal Medicine (CHM) are determined to some extent by the properties of their molecular compounds, so it is of great significance to study CHM from the perspective of molecular compounds. In this paper, the clustering algorithm in data mining is used to study the relationship between the properties of CHM and its chemical components. Firstly, the molecular data are collected from the Traditional Chinese Medicine Systems Pharmacology Database and Analysis Platform, and the data set is preprocessed to extract the key molecular descriptors of chemical components. Secondly, the k-means algorithm and the Bisecting k-means algorithm are used to cluster the chemical components based on the CHM molecular descriptors, and the representative molecular features of the cold and hot CHM are extracted; finally, through experimental comparison, it is found that the clustering results obtained by Bisecting k-means algorithm are better. The clustering results show that the average values of molecular composition descriptors and charge descriptors in cold CHM are significantly higher than those in hot CHM. Therefore, the properties of CHM may be affected by molecular structure and molecular charge properties.

Keywords. bisecting k-means, Chinese Herbal Medicine, compounds, descriptors

1. Introduction

Chinese Herbal Medicine (CHM) has a long history of development. It is not only a bright pearl in Chinese culture, but also an important part of Chinese medicine and health. In recent years, the development of CHM has attracted more and more attention from all walks of life, and the research of CHM has also received widespread attention [1]. The properties of CHM are summarized by the predecessors through thousands of years of observation and long-term practice, and they are an important part of the

* These two authors contributed equally to this work.

¹ Corresponding Author, Department of Computer Technology and Applications, Qinghai University, Xining, 810016, China; E-mail: wlgqgl@126.com.

whole CHM theoretical system. The four characters of CHM properties refer to the four properties of cold, hot, warm and cool [2-3]. For different patients with different diseases, traditional Chinese medicine practitioners often decide the CHM to be used by CHM properties [4]. Therefore, the study of the properties of CHM is of great significance for guiding the use of CHM.

In recent years, data mining technology has been widely used in the research of CHM properties. Liu Jingliang et al. used the ancient and modern literature as the basic data, and used the association rule algorithm to analyze the internal relationship between the properties and active ingredients of CHM. The research results show that there is a certain correlation between the efficacy of CHM and the properties [5]. Fu Xianjun et al. analyzed the molecular descriptors of the main components of CHM by using association rule algorithm, and found that the drug properties of CHM have a certain correlation with the molecular structure of the main components of CHM. The properties of CHM may be related to the molecular energy state of the main effective components of CHM [6]. Based on the records of “Chinese Pharmacopoeia”, “Chinese Medicine”, “Chinese Materia Medica Selected”, “Chinese Medicine Pharmacology” and “New Chinese Medicine Journal”, Wang Zhe analyzed the property, taste, meridian tropism, function and main treatment of CHM by frequency statistics and association rules, and found that “cold-bitter-lung-detoxification-sore throat” has the closest relationship [7].

However, up to now, there are still many problems and challenges in the research of CHM molecules. Firstly, there are few studies on the properties of CHM from a molecular perspective, and it is still in its infancy; secondly, the relationship between CHM properties and CHM molecules is not clear, and there is a serious disconnection between CHM and its chemical components. Thirdly, the traditional drug molecular research methods are tedious and time-consuming. Therefore, it is an urgent problem to explore new methods to explain the properties of CHM from the molecular perspective.

The purpose of this paper is to explore the relationship between the properties of CHM and its chemical components by data mining technology, and to find out the potential laws of properties. Firstly, the descriptors of CHM molecules were calculated, and then the binary k-means algorithm was used to cluster the CHM molecules. The results showed that the average values of component descriptors and charge descriptors in cold CHM were significantly higher than those in hot CHM. Therefore, the properties of CHM may be affected by molecular structure and molecular charge properties.

2. Research Methods

2.1. Molecular Descriptors

Molecular descriptors are a measure of the properties of a molecule in a certain aspect, and the molecular descriptors can describe the characteristics of a molecule from various aspects. Molecular descriptors can be roughly divided into: composition descriptors, topology descriptors, continuity descriptors, kappa descriptors, charge descriptors, molecular property descriptors, space descriptors, and so on. Because there are many kinds of molecular descriptors, this experiment screened out the molecular descriptors which have great influence on CHM properties in the data preprocessing stage [9].

2.2. K-means Clustering Algorithm

The K-means algorithm is an iterative algorithm. At the beginning of the algorithm, k-objects are randomly selected as clustering centers, and then the distance from each object to the cluster center is calculated, and the object is assigned to the nearest cluster center. A cluster center and objects belonging to it are collectively called a cluster. Every time an assignment is made, the cluster center will be recalculated according to the existing assignment objects, and the process of recalculation will continue until no objects are assigned to the new cluster, or the cluster center will not change, and the process will be terminated [10].

2.3. Bisecting k-means Algorithm

However, the k-means algorithm is sensitive to the initial clustering center, and the difference in clustering center often leads to a large volatility of clustering results [11].

To avoid that the initial clustering center will be on the same class, which will cause the algorithm to fall into the state of local optimal solution, this paper introduced another clustering algorithm: The Bisecting k-means Algorithm. The main idea of Bisecting k-means: first, all points are regarded as a cluster, and then the cluster is divided into two parts. Then a cluster with small sum of error squares is added to the cluster list, and the cluster with the largest sum of error squares is divided into two clusters [12]. This continues until the number of clusters is equal to the number k-given by the user. The square sum of clustering error is an index to measure the quality of clustering results. The smaller the value is, the closer the data points are to their centroids, indicating the better the clustering effect. So, the cluster with the largest sum of error squares should be divided first [13]. It can be seen that the main feature of this algorithm is to make up for the shortcomings of k-means algorithm. K-means algorithm cannot recalculate particles distribution between clusters very well when the clustering center is relatively far away, and this can give rise to a poor clustering result. The specific algorithm is described as follows:

Input: Data: Is data set; k: Is Number of clusters;

Output: LowestSSE: sum of the squares of the minimum errors;

```

1:      Select a cluster from the cluster table
2:      while centList < k          do\when the number of clusters is less than k-
3:          LowestSSE → +∞\Initialization minimum error
4:          for i = 0 → centList - 1   do
5:              Get data set samples belonging to cluster I
6:              k-means clustering of the cluster
7:              Get the sum of the errors after the cluster classification
8:              Get the sum of the error of the sample set that does not
belong to the cluster
9:              if sseSplit + sseNotSplit < LowestSSE      then
10:                 bestCentToSplit ← i\Save best cluster
center
11:                 LowestSSE sseSplit + sseNotSplit\Save
the sum of the squares of the minimum
errors
12:             end if
```

```

13:      end for
14:       $centList \leftarrow centList + 1 \backslash \backslash \text{Number of clusters plus 1}$ 
15: end while

```

3. Data preprocessing

3.1. CHM Molecular Data Set

The data of this study comes from the Traditional Chinese Medicine Systems Pharmacology Database and Analysis Platform. 22 kinds of CHM were selected from the cold CHM in the database, and 33 kinds of CHM were selected from the hot CHM. Then 1419 different compounds were extracted from cold CHM, 2153 different compounds were extracted from hot CHM, 3199 compounds in total.

3.2. Calculation of Molecular Descriptors

We used the ChemoPy package of Python to calculate the molecular descriptors [14]. This paper focused on six kinds of descriptors, including molecular composition descriptors, topological structure descriptors, connectivity descriptors, kappa descriptors, charge descriptors and molecular property descriptors.

4. Experiment design

4.1. Algorithm Comparison

4.1.1. Comparison of Data Performance Indicators

The k-means algorithm and the Bisecting k-means algorithm were used to cluster all the data sets of cold CHMs. The distance formula was the European distance formula, and the number of clusters is 2~10 clusters.

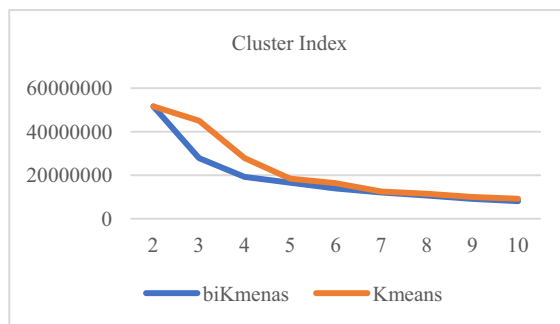


Figure 1. The change of the sum of squared errors of two algorithms for cold CHM

It can be seen intuitively from Figure 1 that Bisecting k-means algorithm has a smaller sum of squared errors for each cluster than the k-means algorithm for the cold CHM data set. Therefore, Bisecting k-means algorithm was more suitable for cold CHM data set [15]. The line graph of the Bisecting k-means algorithm slowed down

significantly after the fourth cluster. Meanwhile, the k-means algorithm line graph slowed down at the fifth cluster. Therefore, 4 clusters were the best for the clustering result of Bisecting k-means, and 5 clusters were the best for the result of k-means algorithm.

Next, all data sets of hot CHM were clustered using the same way as cold CHM data.

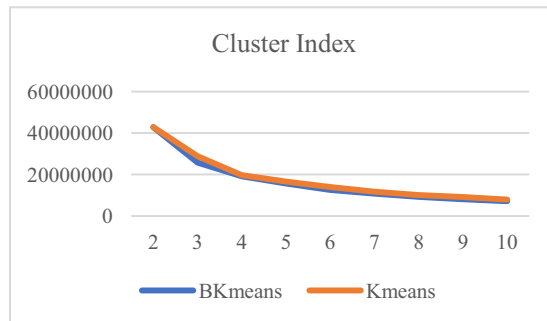


Figure 2. The change of the sum of squared errors of two algorithms for hot CHM

It can be seen from Figure 2, the Bisecting k-means algorithm was more suitable for hot CHMs. 3 clusters were the best for the clustering result of Bisecting k-means, meanwhile the result of k-means algorithm showed 4 clusters was the best.

4.1.2. Comparison of clustering results

As for the clustering of cold CHM data set, the fourth cluster result calculated by the Bisecting K-means algorithm and the third cluster result calculated by the K-means algorithm have the same number of compounds. The clustering results are shown in the following tables:

Table 1. The fourth cluster of compounds using the Bisecting k-means algorithm for cold CHM

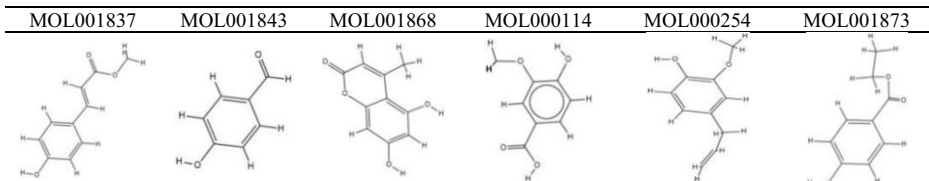
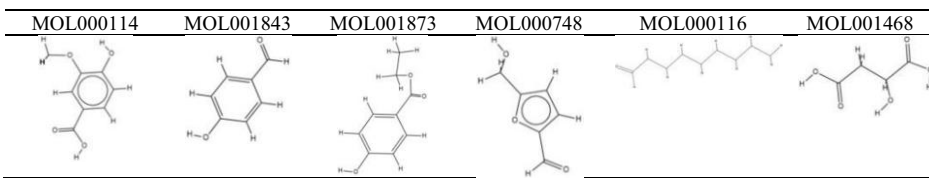


Table 2. The third cluster compounds by using k-means for cold CHM



Further observation of these two clusters of other elements showed that the element similarity of the fourth cluster calculated by the Bisecting k-means algorithm was very high, which basically has the characteristics of ring, double bond and oxygen atom, while the third cluster calculated by the k-means algorithm appeared the chain

like compound as shown in Figure 3. Thus, the clustering effect of the Bisecting k-means algorithm was better than that of the k-means algorithm [16].

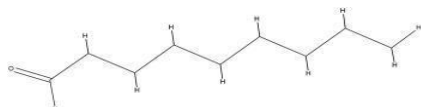


Figure 3. The third cluster compounds have low similarity with others calculated by the k-means algorithm

5. Clustering

5.1. Clustering Analysis

The representative molecules of each molecular descriptor in each cluster were found out through the median, which was calculated by the different molecular descriptors for each cluster. Additionally, if the value in the molecular descriptor is not the same as the median, then the numerator corresponding to the two closest values greater than and less than the median is taken. Finally, the sdf format of the compound was imported into the chemical draw software to visualize the compound [17].

Table 3. The representative compounds of each cluster in cold CHM calculated by Bisecting k-means

MOL008239	MOL001965	MOL003008	MOL001873

Table 4. The representative compounds of each cluster in cold CHM calculated by Bisecting k-means

MOL000303	MOL002764	MOL001278

As can be seen from the results, it turns out that the compounds in cold CHM mostly contained benzene rings. Additionally, the compound structure of cold CHM was more complex than hot CHM. Specifically, hot CHM have more chain structures.

The results of the parameters showed that the values of the important molecular descriptor parameters of cold CHM were almost higher than that of hot CHM.

Table 5. Comparison of the average value of molecular descriptor parameters of compounds in cold and hot CHM

Molecular descriptors	Cold property	Hot property
EWeight	500.4971602	375.7607915
nring	3.916804242	2.978081874
naccr	8.418577528	5.577138326
nsb	29.97761745	20.89608456
nta	73.03398545	56.35364337
TIAC	99.09199099	73.58934786

TPSA	145.1813007	91.48157419
FTPSA	145.1813007	91.48157419

Table 6. Comparison of the average value of the molecular descriptor parameters of each cluster of compounds in cold CHM

Molecular descriptors	Cluster 1	Cluster 2	Cluster 3	Cluster 4
EWeight	335.9508055	520.1070516	977.4764605	168.4543232
nring	2.484760522	4.351351351	7.710526316	1.120578776
naccr	3.956458636	8.071253071	19.51315789	2.133440514
nsb	17.93613933	30.14250614	64.17105263	7.660771704
nta	52.78955007	75.87714988	137.7763158	25.69292605
TIAC	65.49813788	101.8535971	195.7446711	33.27155788
TPSA	65.87849057	138.5108354	334.2089474	42.12692926
FTPSA	65.87849057	138.5108354	334.2089474	42.12692926

Table 7. Comparison of the average value of the molecular descriptor parameters of each cluster of compounds in hot CHM

Molecular descriptors	Cluster 1	Cluster 2	Cluster 3
EWeight	174.9042918	603.1325541	349.2455286
nring	1.23852459	5.026229508	2.669491525
naccr	1.106557377	11.82295082	3.80190678
nsb	9.577459016	33.60655738	19.50423729
nta	30.59344262	82.52786885	55.93961864
TIAC	34.20304877	117.7405213	68.82447352
TPSA	19.37276639	193.9616066	61.11034958
FTPSA	19.37276639	193.9616066	61.11034958

As can be seen from Table 6 and Table 7, it could be seen that the sorting results were basically the same if the value of each molecular descriptor is sorted between clusters, no matter it is a cold CHM or a hot CHM. For example, the numerical value of each molecular descriptor of the third cluster in cold drugs was basically the largest in each cluster, and the numerical value of each molecular descriptor of the second cluster in thermal drugs was basically the largest in each cluster.

Indicated from the above analysis results, the molecular weight-related descriptors have a great impact on the clustering results, and the average values of the molecular composition descriptors and charge descriptors in cold drugs are higher than those in hot drugs. It can be inferred that the medicinal properties of CHM may be affected by the charge properties and molecular structure.

5.2. Clustering discussion

There are some limitations of this research. The first is about the properties of molecular descriptors in the data set. The types of molecular descriptors in the data set used in this study are not comprehensive, and the number of compositions descriptors take up higher percentages, leading to the majority of conclusions is obtained from the point of view of atoms and molecular weight. Therefore, the conclusion is relatively one dimensional.

The second limitation refers to the algorithm used in this study. Although the Bisecting k-means algorithm overcomes the problem of the k-means algorithm converging to a local minimum, the algorithm considers that the attributes of the analyzed samples contribute uniformly to the clustering result, and does not consider the weighting of attributes. This may make the result less accurate [18-19].

6. Conclusions

This paper was based on the cluster analysis of molecular descriptors of CHM molecular compounds. Furthermore, it turns out that the Bisecting k-means algorithm could better seek and explore the characteristics of the compound in hot and cold CHM through the comparison of the application results of two clustering methods of k-means and Bisecting k-means. In addition, the algorithm found that EWeight (average molecular weight), nta (number of all atoms), TIAC (total information index of atomic composition), TPSA (Topological Polar Surface Area), FTPSA (Topological Surface Area Based on Fragmentation), the numerical values of compounds in cold CHM were significantly higher than those in hot CHM.

This research, where combined data mining technology and adopted new research ideas and methods to explore the medicinal properties of CHM, has great theoretical value and profound significance in promoting the modernization of CHM and the development of related industries.

There will be further improve for the algorithm, such as considering the contribution of attributes, and deeply discover the characteristics of cold and hot CHM. Finally, we still need to further explore the relationship and orderliness between the properties of CHM and chemical components.

Funding

This research was supported in part by the Applied Basic Research Programs of Science and Technology Department of Sichuan Province under grant number 2019YJ0110, in part by the Science and Technology Service Industry Demonstration Programs of Sichuan Province under grant number 2019GFW167, in part by the National Natural Science Foundation of China under grant number 61762074, in part by the Scientific Research Cooperation Project under grant number IPP-ZC-19071806, and in part by the Second Class Course Construction of Qinghai University in 2019 under grant number FL192002.

References

- [1] Wu X. Data mining in the analysis of four properties for traditional Chinese medicine. Jinan University, Guangzhou, 2012;1-56.
- [2] Chen L. Analysis on the theory of the rising and falling of traditional Chinese medicine. *Guangxi Tradit. Chinese Med.* 2020;43(02):44-7.
- [3] Wang CY, Wang P, Wang ZG. Origin and development of Chinese medicine four-nature theory. *Guangxi Tradit Chinese Med.* 2009;33(01):8-10.
- [4] Zheng BY. Study on the theory of traditional Chinese medicine based on its pharmacological action. *Electron J Clin Med Lit.* 2015;2(18):3718.
- [5] Zhang LJ, Pei L, Li Y, Shi L. A study on association rules of Chinese herbal properties and the effective components in diuresis efficacy based on data mining. *Chinese J Libr Inf Sci Tradit Chinese Med* 2014;38(5):9-12.
- [6] Fu XJ, Wang ZG, Li XB. Study on relationship between nature and multidimensional structure descriptor of main compounds from Chinese medicinal herbs. *World Sci Technol Tradit Chinese Med* 2017;19(04):549-55.
- [7] Wang Z, Zhang PJ. Associated research on the traditional Chinese medicine nature. *World Sci. Technol. Tradit. Chinese Med.* 2013;30(08):859-63.

- [8] Chen ZK, Song X, Gao J, Zhang JL, Li P. Research progress in the data mining-based TCM diagnoses. Chinese J. Tradit. Chinese Med. 2020;1-15.
- [9] Cao DS. Chemopy: A software package of QSAR / QSPR molecular descriptor calculation based on Python. China Chemical Society. Abstracts of papers of the 11th National Conference of Computer Chemistry. China Chemical Society: China Chemical Society 2011;1.
- [10] Kant S, Ansari IA. An improved k-means clustering with Atk-inson index to classify liver patient dataset. Int J Syst Assur Eng Manag. 2016;7(1).
- [11] Wu XB, Guo Q, Zhang LB, Liang YZ, Liu JG. Multidimensional data clustering based on network community detection method. Int J Syst Assur Eng Manag. 2020;37(02):421-3.
- [12] Liu GC, Huang TT, Chen HN. Improved Bisecting K-means clustering algorithm. Comput. Appl Res. 2015;32(02):261-3.
- [13] Wang JY, Wan QYn, Yan TW. Improved Bisecting k-means algorithm based on hadoop. Comput. Appl Softw. 2016;(9):4-8.
- [14] Zhang L. Study on the drug-likeness of Chinese herbal medicine based on molecular descriptors and application. Harbin University of Commerce, Harbin, 2019;62.
- [15] Li YK. Analysis and comparison of three typical clustering algorithms in data mining. Comput Knowl Technol. 2020;16(15):52-6.
- [16] Yang L, Peng LF, Feng BH. Component analysis of traditional Chinese medicine based on Data Mining—Application of cluster analysis in the determination of ginsenosides in Panax ginseng by HPLC. Softw Guid. 2009;(08):169-171.
- [17] Peng T, Sun LY, Zhou JJ. Hierarchical clustering of traditional Chinese medicine database based on Molecular Fingerprint. Softw Guid. 2013;30(06):575-581.
- [18] Liu WW. The research on varying weight k-means and its application. Xiamen University, Xiamen, 2017;(07):64.
- [19] Wu B. Improvement and application of correlation weighted k-means algorithm. Jiangxi University of Science and Technology, Nanchang, 2018;(07):58.

Keyword Extraction from TV Program Viewers' Tweet Based on Neural Embedding Model

Taiga KIRIHARA^{a,1}, Kazuyuki MATSUMOTO^b, Minoru YOSHIDA^b, Kenji KITA^b

^a*Graduate Schools of Science and Technology for Innovation Division of Science and Technology, Tokushima University, Japan*

^b*Graduate School of Technology, Industrial and Social Sciences, Tokushima University, Japan*

Abstract. In recent years, young people have not been watching television (TV) as much as they used to. This is mainly because a number of TV programs are very long and/or have limited viewing times. Recently, individuals have been actively posting live-action tweets on Twitter to comment on TV content while watching programs in real time. In this study, we propose a method for extracting key phrases related to the event scenes of TV programs using live tweets, and we propose a scene search system that aims at efficient TV program viewing. The experimental results indicated that the program contents were estimated with an error of approximately 5% to 10% with respect to the program time. In addition, the extracted key phrases were visualized for each event scene category using the t-SNE algorithm.

Keywords. Natural Language Processing, TV Program, Key Phrase Extraction, Twitter Analysis

1. Introduction

The number of people who watch television (TV) programs by recording them has increased in recent years due to the diversification of TV viewing methods. The main reasons in regard to why a person records TV programs are the following: preferring to watch at a favorite time, not wanting to be tied to the broadcast time, and wanting to use time effectively. Even if there is a TV program that an individual does want to watch, it may be difficult to watch in real time if the program is long or has limited available viewing times; therefore, the number of people who record TV programs to watch them at a later time is increasing.

With the spread of social networking sites (SNS) such as Twitter in recent years, individuals are actively posting live-text tweets, which are tweets sent in real time while the person watches TV programs. These live tweets contain information on the TV program's events and content as well as the poster's impressions and opinions on the program. When a person posts to Twitter in real time in regard to the TV program

¹ Graduate Schools of Science and Technology for Innovation Division of Science and Technology, Tokushima University. E-mail: c612035024@tokushima-u.ac.jp.

they are currently viewing, the title and the name of the performer are included in hash tags. We refer to this as the act of performing a live TV program on Twitter.

In this research, we propose an event scene retrieval method for supporting the viewing of TV programs by focusing on live TV program tweets on Twitter. We expected that the detection of a specific scene in a TV program could be automated by collecting tweets for a specific TV program and extracting information about the program in the tweet text. We propose a method for extracting key phrases related to event scenes of TV programs using tweets. In addition, we consider the possibility of scene retrieval by comparing the categorization of the scene with the extracted keywords.

2. Related research

2.1. Detection and labeling of significant scenes from a TV program based on Twitter analysis

In Nakazawa et al.'s [1] study, the researchers were able to automatically detect an important scene by collecting data on the fluctuation of the number of tweets about a TV program. The tweet contents were used to determine the main character involved and the event contents in the TV scene, and the result was taken as the scene. They proposed a method that included adding a label. In Shamma et al. [2], the researchers detected essential scenes, and TF-IDF was used to ascertain the main character in the important scene. These authors aimed to develop a system that is able to search all the scenes in a program to determine which ones are important scenes rather than focusing on the peak number of tweets.

2.2. A scene explorer for TV programs based on Twitter emotion analysis

In Yamauchi et al. [3], the authors collected data on tweeted sentences for specific TV programs from Twitter, analyzed the tweets, estimated the viewer's feelings on the recorded program, and visualized the data to search for a program. They proposed a support method. Yamauchi et al. used the emotion analysis method and adopted Plutchik's Wheel of Emotions[4]. In addition, the researchers identified the emotions for emoticons and are used as an index of emotions.

In our research, keywords were extracted based on the specific content of the event scene as described in the tweet texts, rather than using sensitizing information such as how the viewer felt.

3. Proposed method

The present study followed these steps: first, we collected data on the tweets about a TV program; next, the tweets were vectorized to extract the important expressions that directly illustrated the scene content of the program. We refer to the expression that represents the scene content of the program for each tweet as a key phrase, and we searched the event scenes based on these key phrases. In addition, we classified the scenes via categorizing the key phrases.

3.1. Tweet collection and time division

We used Twitter's API to collect data on the tweets. The hash tag ("#[program name]") was used as a specific search keyword when collecting the data. After collecting the tweets, the tweet set for each program was divided into one-minute units. Taking this step allowed us to search for programs in one-minute units. We separated by one-minute units based on this present study's purpose, which was to search TV program scenes.

Conducting these time-divided scene searches made it easier to compare errors with actual scenes and extracted key phrases. We used the one-minute mark since there were a sufficient number of tweets to perform.

3.2. Vectorization

We vectorized the tweet sentence sets that were divided into one-minute units using the bidirectional encoder representations from transformers (BERT) method[5]. BERT is a deep learning model for natural language processing that was first announced by Google in 2018. BERT has 12 stages of transformers and can be used to understand the context.

The BERT used in this study is a pre-learned model based on the Japanese Wikipedia article corpus[6]. We did not use the pre-learned model that is based on the SNS text because we expected that many of the important keywords that characterize the program scenes were Wikipedia-registered words. Wikipedia offers rich resources, which allowed us to collect accurate information, such as events that occur in TV programs and character names. On the other hand, such information may be missing in SNS-based models, increasing the possibility that incorrect information would be obtained. Therefore, this study used the Wikipedia-based BERT model.

In addition, BERT requires a large-scale, high-quality dataset to learn the distributed expressions. Since the tweet data collected in the present study are biased and small, this dataset was not suitable for fine tuning with BERT. Therefore, we did not train the BERT model using my own dataset as fine tuning, and we use a pre-trained BERT model.

3.3. Key phrase extraction

Regarding key phrase extraction, there were many sentences in the live-action tweets that included a "noun + adjective" part-of-speech pattern. For example, many collected tweets included the following: "Pikachu cute" and "Pennywise scary." There was such a thing. We argue that such tweets characterize the TV program scene; therefore, we used the EmbedRank algorithm[7] to extract key phrases by combining proper nouns and adjectives. Among the nouns, proper nouns often characterize the TV program, while adjectives are closely related to the content of the scene. In addition, the adjectives can represent the emotions of the person.

EmbedRank is an algorithm that extracts important key phrases that do not require training data. In this study, we obtained a distributed expression vector for candidate phrases and entire sentences (a set of tweets per unit time) that were extracted based on a part-of-speech pattern. The important key phrases were decided based on the degree of similarity. The Japanese morphological analyzer MeCab[8] and the morphological analysis dictionary NEologd[9] were used for part-of-speech determination. The figure

below shows the following: “The giant Snorlax will appear in the next week's Anipoke!” (Raishu no Anipoke wa Kabigon kyodaika desu.). This flow is explained using a concrete example of this tweeted sentence. In this case, the proper nouns are “Anipoke” and “Snorlax” (Kabigon, with “Anipoke” indicating Pokémon anime. Fig.1 shows the flow of keyphrase extraction.

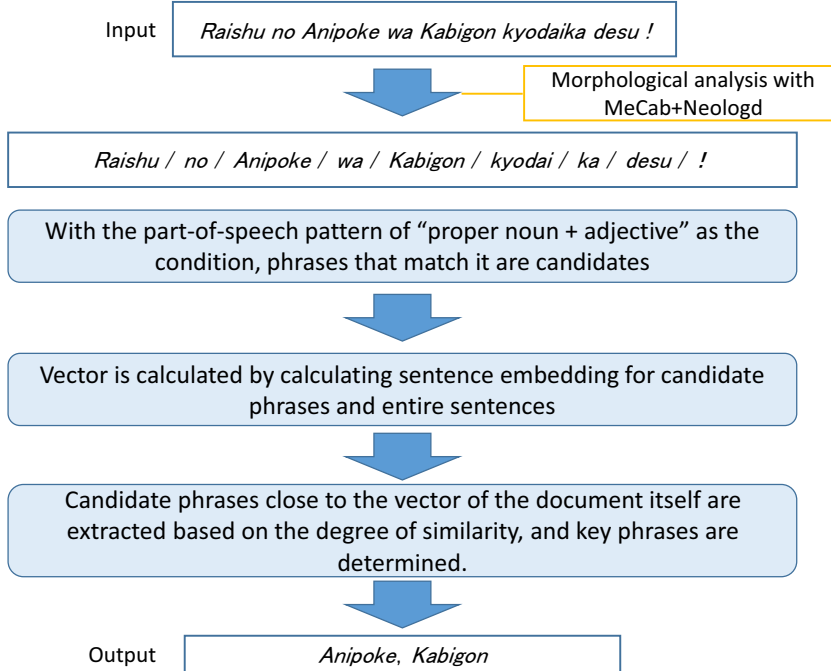


Figure 1. Flow of key phrase extraction

By simply extracting key phrases based on the degree of similarity, we were able to avoid including redundant expressions with similar meanings by calculating the maximal marginal relevance (MMR). Equation (1) shows the MMR calculation formula.

$$MMR := \arg_{D_i \in R \setminus S} \max [\lambda \cdot \text{Sim}_1(D_i, Q) - (1 - \lambda) \max_{D_j \in S} \text{Sim}_2(D_i, D_j)] \quad (1)$$

Using the MMR equation allowed us to exclude expressions with similar meanings and extract more important key phrases. We assumed that this would improve the accuracy of scene retrieval.

3.4. Difference between this method and conventional method

Aside from the EmbedRank and MMR methods used in the present study, there are several other methods that can be used to extract important words. The TF-IDF has been used in previous research and is considered to be a general method. This method calculates a word's importance according to the frequency with which the word appears. The TF-IDF formula is shown as Equation (2).

$$tfidf(t_i, d_j) = tf(t_i, d_j) \cdot idf(t_i) = \frac{f(t_i, d_j)}{\sum_{t_k \in d_j} f(t_k, d_j)} \cdot \log\left(\frac{N}{df(t_i)} + 1\right) \quad (2)$$

The disadvantage of the TF-IDF method is that the term frequency (TF) value increases as the number of words in the document decrease (and vice versa). Since the total number of words in a document is calculated during the TF value estimation process, the difference in the number of words in each document affects the importance of words. As explained previously, we divided the tweet set every minute. When the set of tweets is divided by time, we can assume that the number of tweets in time increases in a scene that is live on a TV program, and that the number of tweets decreases during other parts of the program. In fact, even in the tweet data used in the present study, there was a difference in the number of tweets for each time period. When we used TF-IDF, we observed that the difference in tweets in each time zone had a large effect on the extraction of key phrases. Therefore, we extracted the key phrases using the BERT and EmbedRank algorithms and MMR.

3.5. Classification of key phrases by scene category

In this step, we manually classified the scenes into categories. We expected that using the relationship between key phrases and scene categories would lead to a rough visualization of similar event scenes. In this study, the following six categories were defined:

- People: Scenes in which people appear
- Action: A scene in which a person takes action
- Emotion: A scene in which a person shows emotion
- Summary: Rough description of a scene without humans
- Scenery: A scene where the location and time of day can be observed
- Conversion: A change of scene from the main program to other images (e.g., a commercial)

4. Evaluation experiment

In order to observe how the TV program genre may lead to differences in the results, we targeted the following program types: "variety," "animation," and "movie." In this experiment, we evaluated the scene search performance by searching the event scene based on the extracted key phrases and calculating the error from the actual time zone. In addition, we verified the effectiveness by comparing cases in which the MMR method was used for key phrase extraction to cases in which it was not used.

4.1. Data

In this section, we describe the collected data—the TV programs and the related tweets. Three programs in total were recorded—“Getsuyou Kara Yofukashi” (Yofukashi) that

was broadcast on the “Nihon TV” series on October 14, 2019, “Friday Road SHOW – It” (Friday) that was broadcast on the “Nihon TV” series on November 8, 2019, and “Pokémon” (Pokémon) that was broadcast on the “TV Tokyo” series on December 8, 2019. In addition, we collected live tweets posted by viewers in each time zone based on hashtags using the Twitter API. We collected a total of 37,804 tweets. All three programs were programs of the broadcasting station that was on the same net as the production station. This is because the event scene search uses the time slot in which the live tweet was posted as the search result. We assumed that it was necessary to post the tweet in the same time zone regardless of where (i.e., which region) the program was viewed.

For evaluation, we created a key with the correct answers for each program. Including multiple keywords for each scene, this data describes the time zone in which the event scene occurred, the category that the scene belongs to, the character who appeared in the event scene, what happened in the scene, etc. For this step, we used the keyword of the correct answer data as the search query. The time zone of the event scene was estimated based on the similarity to the key phrase that was automatically extracted from the live tweet in each scene. The time zone was outputted as the search result. Table 1 shows the number of scenes by category in each program.

Table 1. Number of scenes in each program category

Category	Yofukashi	Friday	Pokemon	Total
Person	5	13	7	25
Action	8	70	4	82
Emotion	1	1	1	3
Summary	7	2	0	9
Scenery	2	19	2	23
Conversion	26	17	9	52
Total	49	122	23	194

4.2. Result

In this section, the experimental results are presented. By investigating the error between the output time zone and the correct answer time zone, we compare the search performance with and without MMR and confirm the difference depending on the program genre. Furthermore, by visualizing the vector of the key phrases in the two-dimensional coordinate space, the similarity between scenes is roughly determined.

4.2.1. Event scene search results

Table 2 shows the average error when the smallest error is selected from the top five search results.

Table 2. Average error of each program

	With MMR	Without MMR
Yofukashi	9 min. 41 sec.	14 min. 43 sec.
Friday	11 min. 3 sec.	16 min. 3 sec.
Pokemon	3 min. 33 sec.	5 min. 38 sec.

As a result, there was an error of approximately 5% to 10% with respect to the broadcast time of each program. The error was smaller when MMR was used than

when it was not used. This is considered to be the result of MMR being able to suppress the duplication of similar key phrases. The difference between the correct answer data and the tweet is considered to be the cause of the error. For example, even though the correct answer data says "XX (person name) appeared," the tweet text was written as "XX Kita" using Japanese slang. The context is important for vectorization by BERT to absorb the notational fluctuation of such expressions. There is a difference in the amount of information between the key phrase vector and the sentence vector, and it is considered that there is a large difference between the two in the obtained vector. In addition, we used the Wikipedia-based pre-learning model this time, but this model did not handle the internet slang words such as "Kita" (come out) well. In addition, since the correct answer data itself is a different type of expression (keyword rather than phrase) from the tweeted sentence, it is necessary to improve the method by converting a search query into a key phrase and reviewing the experimental setting itself.

4.2.2. Key phrase visualization for each scene category

Figures 1 to 6 represent two-dimensional coordinates obtained by dimensionally compressing the BERT vector of the key phrase extracted per unit time for each scene category of the program "Friday Road SHOW" using t-distributed stochastic neighbor embedding (t-SNE) [10]. This is visualized in space.

In the correct data created this time, most event scenes are classified as "action." Generally, in an event scene related to a motion, when a live tweet about how a viewer feels about the motion of a character, an adjective and a proper noun (personal name that is used to indicate a person) are often included in the tweet. For this reason, the key phrases include not only motions but also various types, such as emotional expressions and person names. In addition, a number of key phrases extracted in the "feelings" and "summary" scenes (of which relatively few were classified) were found to match the emotions and summaries; however, in this method, proper nouns and adjectives were used. Since the combination of was used as a key phrase candidate, the verbs, adverbs, and general nouns that are necessary to express emotions and abstract scenes could not be extracted. Thus, we assume that the divergence from the search query was large.

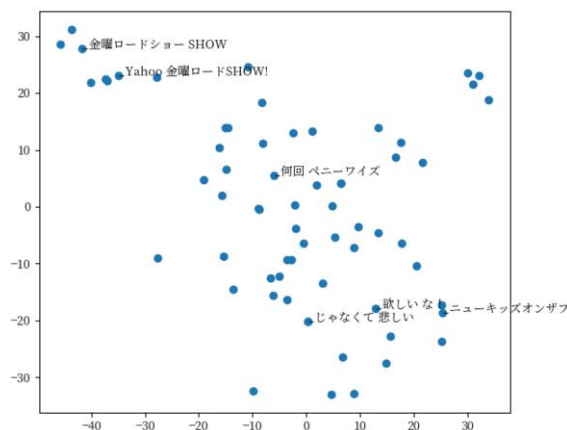


Figure 2. Key phrases in the “person” scene

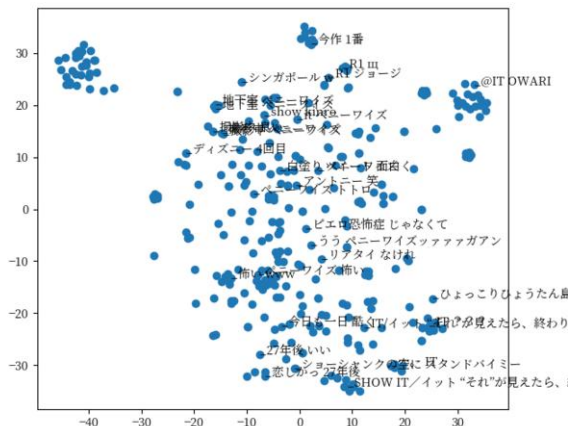


Figure 3. Key phrases in the “action” scene

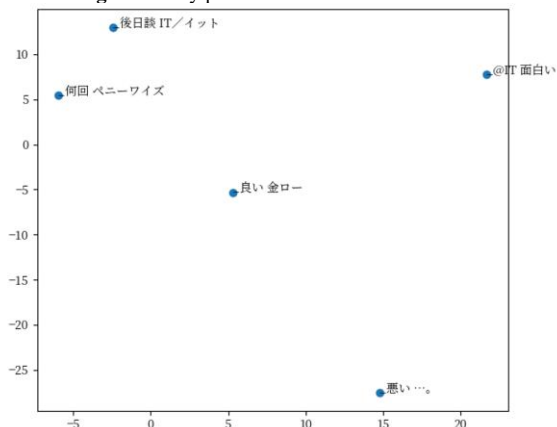


Figure 4. Key phrases in the “emotion” scene

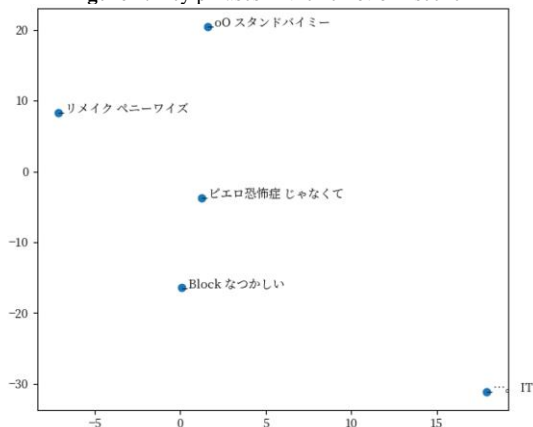


Figure 5. Key phrases in the “summary” scene

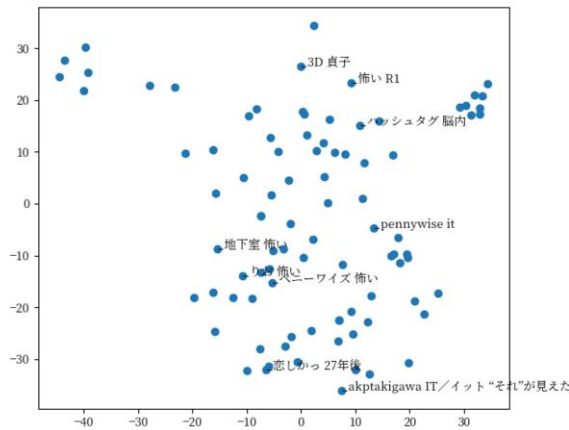


Figure 6. Key phrases in the “scenery” scene

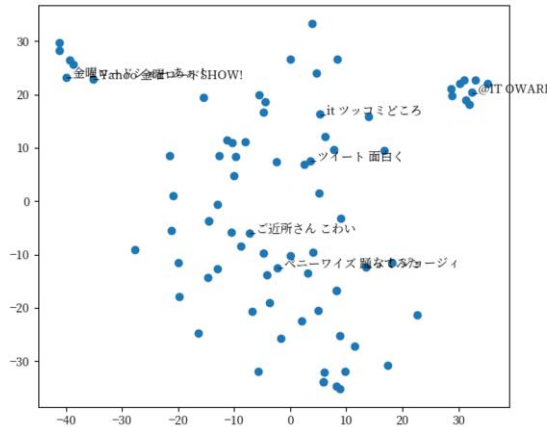


Figure 7. Key phrases in the “conversion” scene

5. Conclusions

In this research, we focused on TV program live tweets and devised a system that retrieves and classifies the scenes by extracting the key phrases that represent the event scenes of the program from the tweeted sentences. As a result, approximately 5% to 10% of the total error that was observed in the performance evaluation was due to the time zone error.

We also succeeded in extracting more important key phrases by mining these phrases based on the vector using the EmbedRank algorithm and MMR. In addition, we simultaneously extracted key phrases with part-of-speech patterns (e.g., proper nouns and adjectives), "scene estimation," and "emotion estimation." Conventional research has extracted these separately. We expect that it will be easier to provide feedback on the results (e.g., the type of influence it has on the viewers) and to more simply provide scene information when deploying services using this method. Furthermore, previous research has manually determined the emotional polarity value (an index of emotion)

for each emotional word. However, we succeeded in significantly reducing the required human labor by integrating emotional words as adjectives.

On the other hand, we determined whether the outline of the scene could be confirmed by scene classification and visualization of the key phrase; however, in each category, there was a tendency for many key phrases to be extracted that did not describe the characteristics of the scene well. Therefore, it was found that the key phrase extraction condition needs to be improved in order to use the visualization of the key phrases to confirm the general tendency of the scene.

In the future, in order to improve the accuracy of key phrase extraction, we plan to use the BERT pre-learned model based on SNS. We also plan to improve it so that the context can be properly acquired, and we intend to examine the conversion method from the input query to the key phrase. In addition, we aim to construct a TV program event scene search system from more intuitive keyword input by examining the weighting of key phrases corresponding to the frequency of the occurrence of words, and we hope to expand key phrase candidates by optimizing the part-of-speech conditions.

Acknowledgments

This work was supported by JSPS KAKENHI Grant Numbers JP20K12027, JP18K11549.

References

- [1] Masami Nakazawa, Keiichiro Hoshida, Chihiro Ono: Detection and Labeling of Significant Scenes from TV program based on Twitter Analysis. DEIM Forum 2011 F5-6.
- [2] David A. Shamma, Lyndon Kennedy, Elizabeth F. Churchill: Tweet the Debates: Understanding Community Annotation of Uncollected Sources, In *Proceedings of the first SIGMM workshop on Social media*, pp. 3-10, 2009.
- [3] Takashi Yamauchi, Yukiko Nakano: A Scene Explorer for TV Programs based on Twitter Emotion Analysis, In *Proceedings of The 26th Annual Conference of the Japanese Society for Artificial Intelligence*, 2012
- [4] Plutchik, R: The Emotions, University Press of America, Lanham, 1991.
- [5] Jacob Devlin, Ming-Wei Chang, Kenton Lee, Kristina Toutanova: BERT: Pre-training of Deep Bidirectional Transformers for Language Understanding, In *Proceedings of the 2019 Conference of the North American Chapter of the Association for Computational Linguistics: Human Language Technologies*, Vol. 1, pp. 4171–4186, 2019.
- [6] <https://github.com/yohheikikuta/bert-japanese>. Last viewed date: 2020/2/5
- [7] Kamil Bennani-Smires, Claudiu Musat, Andreea Hossmann, Michael Baeriswyl, Martin Jaggi: Simple Unsupervised Keyphrase Extraction using Sentence Embeddings, In *Proceedings of the 22nd Conference on Computational Natural Language Learning*, pp. 221–229, 2018.
- [8] MeCab: Yet Another Part-of-Speech and Morphological Analyzer, <https://taku910.github.io/mecab/>. Last viewed date: 2020/2/5
- [9] Neologism dictionary for MeCab, <https://github.com/neologd/mecab-ipadic-neologd>. Last viewed date: 2020/2/5.
- [10] Laurens van der Maaten, Geoffrey Hinton: Visualizing Data using t-SNE, *Journal of Machine Learning Research*, Vol. 9, pp. 2579–2605, 2008.

Water Quality Data Outlier Detection Method Based on Spatial Series Features

Jianzhuo Yan^{a,b}, Ya Gao^{a,b,1}, and Yongchuan Yu^{a,b}

^a*Faculty of Information Technology, Beijing University of Technology, Beijing 100124,
China*

^b*Engineering Research Center of Digital Community, Beijing University of Technology,
Beijing 100124, China*

Abstract. Outlier detection is one of the major branch in data mining which has been applied in different fields. Researchers have focused on the outlier detection in time series, but rarely spatial series. In this paper, we propose a new outlier detection method based on k-nearest neighbour (KNN) and Mahalanobis distance, which is first applied to the water field. Experimental results verify that the algorithm has good accuracy and effectiveness in outlier detection for water quality spatial series dataset.

Keywords. outlier detection, spatial series data, Mahalanobis distance, k-nearest neighbour

1. Introduction

One of the basic features of spatial data analysis is that it involves not only spatial attributes such as latitude, longitude and altitude, but also related non-spatial attributes. The spatial relation among the points in the spatial data set is established by an adjacency matrix which can be expressed as the adjacent distance relation. Due to the characteristics of spatial data mining, the detection of spatial outliers needs to find a specific data instance, whose non-spatial attribute values are obviously different from the size of adjacent points. Most of the existing spatial outlier detection algorithms focus on identifying single attribute outliers and may misclassify normal items as outliers, while the real spatial outliers exist in their neighborhood. Notably, many practical applications involve multiple non-spatial attributes that should be incorporated into outlier detection. Because the definition of neighborhood is crucial for determining spatial outliers, in addition, compared with the aggregated distribution of attribute values on all adjacent data, statistical methods are needed to characterize the distribution of attribute values at various locations. Therefore, the detection of spatial outliers is still a great challenge.

In this paper, for the spatial attributes and multivariable characteristics of water quality data, a new outlier detection method based on KNN(k-Nearest Neighbour) and Mahalanobis distance, is presented in this paper, Which first utilize KNN to find the neighboring function points of each data point, and then use the watershed as a

¹ Ya Gao, Corresponding author, Faculty of Information Technology, Beijing University of Technology, Beijing 100124, China; E-mail: gy@emails.bjut.edu.cn

comparison function under weight adjustment and the Mahalanobis distance suitable for multivariable as a threshold function to perform outlier detection on water quality data with spatial feature attributes. Results show that the method can detect outliers of water quality data well, with good accuracy and high sensitivity.

2. Related Work

Multivariate time series have been widely used in various fields, such as traffic data analysis [1],[2], livestock [3], finance [4], and others [5][6][7], etc. In recent years, there have been many researches devoted to predicting water quality, for instance, Liu et al.[8][9] forecast the water quality of a station over the next few hours from a data-driven perspective and present a multi-task multi-view learning method to fuse those multiple datasets from different domains into an unified learning model. However, there are few methods to study the outlier detection for water quality spatial data. Liu et al. [10] proposed an outlier detection algorithm for spatial sequence data sets based on the SOM neural network. Martínez Torres et al. put forward to use the depth function to curve the gas emissions with time, and obtain the outliers by comparing the curves instead of vectors [11][12]. Then, Blasi put the function depth function applied to spatial outlier detection of water quality data of different automatic monitoring stations in the Mino River Basin in Spain to detect spatial outliers [13]. Google Earth Engine methodology [14] and improved Z-score test [15] are used to detect spatial data. Ramaswamy et al. proposed a partition-based method that uses the k-th nearest neighbor to determine outliers [16]. Chen et al. demonstrated a neighborhood-based method [17] in 2010, which distinguishes outliers by the sum of all attribute distances of neighbors, but its rules are too inflexible to accurately detect outliers. Yu et al. proposed k local outlier factors and used k-walk similarity to create a new LOF-based metric [18], which improved the accuracy of outlier detection. Araki et al. used LUR and regression kriging to model the spatial distribution of the annual mean [19], and then generated a concentration map based on the predicted method of observation, that can clearly detect the content of PM2.5 and NO₂ in air pollutants. However, the water quality data cannot fit the data into a concentration map, this method cannot be well applied to the detection of spatial outliers in water quality data. Harris et al. proposed a geographic weighting algorithm [20] for high-dimensional data. The geographic weighted PCA was used to calculate the score distance, orthogonal distance, and component distance, and the three scores were compared with the theoretical quantile. This method mainly uses PCA to reduce the dimensionality of high-dimensional data, but the correlation and interpretability of data variables in dimensionality reduction will be reduced, so it is not suitable for the detection of water affairs data.

3. Methodology

3.1. Mahalanobis Distance

Mahalanobis distance is a statistical distance proposed by Indian statistician Mahalanobis in 1936 [21]. This method considers the correlation between feature quantities and is not affected by the feature quantity scale [22]. Mahalanobis distance provides a suitable method to identify points far away from other points in multi-

dimensional space, it is widely used in discriminant analysis, clustering, and principle analysis. When dealing with multivariate data, it has many advantages over Euclidean distance. It is not affected by the dimension that the Mahalanobis distance between two points has nothing to do with the unit of measurement of the original data. It takes into account the connections between various characteristics, and excludes the interference of the correlation between variables.

If the density function of the multivariate normal random variable (x_1, x_2, \dots, x_n) is as follows:

$$f(x_1, x_2, \dots, x_n) = \frac{|\Sigma|^{-1/2} e^{-1/2(x-\mu)' \Sigma^{-1} (x-\mu)}}{(2\pi)^{-n/2}} \quad (1)$$

Where μ is the mean vector of the sample population and Σ is the covariance matrix of the sample population. Mahalanobis distance is defined as Eq.(2).

$$d(M) = \sqrt{(X - \mu)' \Sigma^{-1} (X - \mu)} \quad (2)$$

Where X is a feature vector composed of all feature quantities of sample point x .

If $\Sigma = LL'$, transform Eq.(2) as follows:

$$d(M) = \sqrt{(L^{-1}(X - \mu)' L^{-1}(X - \mu))} \quad (3)$$

where u has the same function as the Euclidean distance, which is the average of each feature; L has the function of normalizing and decorrelating each feature. From a geometric point of view, it can be regarded as the Euclidean distance after converting the original feature quantity into standardized uncorrelated data through L , in other words, the Euclidean distance is the equal weight operation of each feature quantity, and the Mahalanobis distance adjusts the sample feature weight by L Value to obtain a better distance. The Mahalanobis distance is based on the overall distribution characteristics of various samples. The feature quantity consistent with the overall correlation of the sample, the Mahalanobis distance is given a smaller weight, and the calculated distance is small, otherwise, a larger weight is given, and the calculated distance is larger.

3.2. K-Nearest Neighbour Algorithm

KNN algorithm is one of the most basic and simplest algorithms in machine learning algorithms. It can be used for both classification and regression. The idea of the KNN algorithm is very simple: for any n-dimensional input vector, corresponding to a point in the feature space, the output is the category label or a predicted value corresponding to the feature vector. The following are the steps of the KNN algorithm:

- Step 1: Calculate the distance between the test data and each training data.
- Step 2: Sort according to the increasing relationship of distance.
- Step 3: Pick K points with the smallest distance.
- Step 4: Determine the frequency of the first K points in the category.
- Step 5: Return the most frequent category of the first K points as the predicted classification of test data.

3.3. Outlier Detection Algorithm based on Mahalanobis distance and KNN

Assuming that x for spatial object data points has $q (\geq 1)$ attribute values, use a to represent the vector of these q values at x . The attribute value of a given set of spatial points X is $X=\{X_1, X_2, X_3, \dots, X_n\}$, with $p (\geq 1)$ spatial points, and the attribute function $f(x)$ is the attribute vector of each spatial point a . $NNk(x_i)$ represents the k nearest neighbors of x_i , where $i=1,2,3,\dots,n$, $k=k(x_i)$, and the neighborhood function $g(x)$ is the return attribute function of the function of the k nearest neighbors of $f(x)$. To detect spatial outliers, all attribute values of x should be compared with the corresponding quantities from the nearest neighbors of x .

We choose g as the vector of neighboring points, and each component represents the degree of influence of the neighboring points on the point. Then we calculate the difference between f and g , let $h(x)=f(x)-g(x)$, where $h(x)$ is the comparison function. Next, check the Mahalanobis distance from each point to that point, and the point whose distance is greater than the predetermined threshold will be returned as an outlier.

For samples $h(x_1), h(x_2), h(x_3), \dots, h(x_n)$ and n spatially referenced objects $x_1, x_2, x_3, \dots, x_n$. MCD is the sample mean μ_J^* and covariance matrix Σ_J^* under sample s , is defined as the following formula:

$$MCD = (\mu_J^*, \Sigma_J^*) \quad (4)$$

$$J = \{|\Sigma_J^*| \leq |\Sigma_M^*|, \forall M \text{ s.t. } |M| = s\} \quad (5)$$

$$\mu_J^* = \frac{1}{s} \sum_{i \in J} h(x_i) \quad (6)$$

$$\Sigma_M^* = \frac{1}{s} \sum_{i \in J} [h(x_i) - \mu_J^*][h(x_i) - \mu_J^*]^T \quad (7)$$

The specific algorithm steps are as follows:

Step 1: For each spatial point x_i , calculate k nearest neighbor sets $NNk(x_i)$.

Step 2: For each spatial point x_i , calculate the attribute function $f(x_i)$ and the neighborhood function $g(x_i)$.

Step 3: Calculate the comparison function $h(x_i)=f(x_i)-g(x_i)$.

Step 4: Assuming that the distribution of $h(x)$ is $Nq(\mu, \Sigma)$, it means that the q -dimensional vector $h(x)$ follows a multivariate normal distribution with mean vector μ and covariance matrix Σ . Use μ^* and Σ^* to simulate the real parameter mean vector μ and covariance matrix Σ . Then, calculate the μ^* and Σ^* of the comparison functions $h(x_1), h(x_2), h(x_3), \dots, h(x_n)$.

Step 5: To check whether the distance reaches the requirement of the abnormal value, a predetermined threshold is needed.

If $d(x) = [(h(x) - \mu_J^*)^T (\Sigma^*)^{-1} (h(x) - \mu_J^*)]^{\frac{1}{2}}$, $\frac{c(m-1+1)}{qm} d^2(x)$ is an approximate distribution, which is an F distribution with q and $(m-q+1)$ degrees of freedom, and the parameters m and c can be calculated from the asymptotic formula. Therefore, $\frac{c(m-q+1)}{qm} d^2(x) > F_{q,m-q+1}(a)$, which is the probability that $h(x)$ satisfies a . $F_{q,m-q+1}(a)$ is a percentage of the F distribution with q and $m-q+1$ degrees of freedom.

Step 6: Calculate the $d(x)$ in each spatial point x_i , where $d(x_i) = [(h(x_i) - \mu_J^*)^T(\Sigma^*)^{-1}(h(x_i) - \mu_J^*)]^{\frac{1}{2}}$.

Step 7: If $d^2((x_i)) > \frac{qm}{c(m-q+1)}F_{q,m-q+1}(a)$, return as an outlier.

3.4. Evaluation of Performance

To evaluate the performance of the method we proposed, the following evaluation indicators are applied, while the calculation formulas are as follows:

(1) Accuracy

Accuracy rate measures the overall effectiveness of the classification model, which is the proportion of the number of correctly classified samples in the total number of samples. The formula can be obtained as follows:

$$\text{Accuracy} = \frac{TP+TN}{TP+TN+FP+FN} \quad (8)$$

(2) Sensitivity

Sensitivity represents the proportion of pairs among all positive examples, and measures the classifier's recognition ability of positive examples. The formula is as follows:

$$\text{Sensitivity} = \frac{TP}{TP+FN} \quad (9)$$

(3) Specificity

Specificity refers to the ratio of pairs among all negative cases, and measures the classifier's ability to recognize negative cases. The formula is as follows:

$$\text{Specificity} = \frac{TN}{TN+FP} \quad (10)$$

(4) F value

F value is the comprehensive evaluation standard of precision rate and recall rate. The formula has the following form:

$$F\text{ value} = \frac{2 \times \text{Precision} \times \text{Recall}}{\text{Precision} + \text{Recall}} \quad (11)$$

Where Precision and Recall can be given by Eqs. (12) and (13).

$$\text{Precision} = \frac{TP}{TP+FP} \quad (12)$$

$$\text{Recall} = \frac{TP}{TP+FN} \quad (13)$$

Where, TP represents the case that the sample which belongs to a positive class is also recognized as a positive class, while FP represents the case where the sample that belongs to a negative class is identified as a positive class; TN represents the case that

the negative class is identified as the negative class, while FN represents the case that the positive class is identified as negative.

4. Results and Discussion

In this paper, the water quality data of the eleven sewage treatment plant stations in Beijing is selected as this experiment's data, coming from Beijing Municipal Water Affairs Bureau. These stations include Tuanjiehu, Gaobeidian, Qijiahuozi, Zhangfang, Songlin Gate, Longtan Gate, Sanjadian, Xiahui, Zhangjiafen, Shidu, Hot Springs. We select four variable indicators as ammonia nitrogen (NH_4N), Nitrate (NO_3N) dissolved oxygen (DO) and permanganate index (CODMn). The time interval of data is from January 1, 2010, to January 1, 2011, a total of 1760 data. Each sewage treatment plant has 160 pieces of data at the same time. The outlier samples with labels are shown in Figure 1.

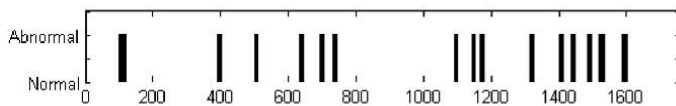


Figure 1. Normal value and outliers of real data.

This experimental algorithm is implemented by the matlab2018 platform. Since four attributes are used in the experiment, the parameter $q = 4$. Through the implementation of the FAST MCD algorithm in the Matlab toolbox LIBRA to generate a robust mean and covariance matrix estimate, calculate the parameters m and c , $m = 352.365$ and $c = 0.469$. In this algorithm, we take the parameters of each sewage treatment plant watershed as -1 to 1, indicating the correlation between the plants in the watershed.

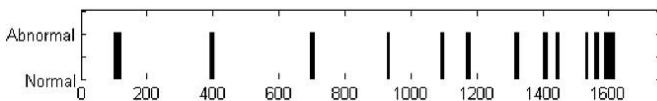


Figure 2. Normal value and outliers detected by the algorithm

The final detected outliers are shown in Figure 2. It can be seen that the algorithm detects most of the outliers in real data, and the detected error outliers are very few, which can meet the requirements of water quality data outlier detection algorithm. Table 1 illustrates the specific indicators of outlier detection of each sewage treatment plant.

Table 1. Comparison of classification indicators of each plant

Sewage treatment plants	Accuracy	Sensitivity	Specificity	F value
Tuanjiehu	0.8232	0.902	0.9862	0.9267
Gaobeidian	0.8597	0.9789	0.8898	0.9783
Qijiahuozi	0.8864	0.9932	0.9168	0.9219
Zhangfang	0.8794	0.9168	0.9378	0.8453
Songlin Gate	0.8657	0.8465	0.9634	0.9267
Longtan Gate	0.9425	0.9689	0.9265	0.9436
Sanjadian	0.9347	0.8668	0.9767	0.9523

Xiahui	0.9689	0.9399	0.8864	0.9094
Zhangjiafen	0.8986	0.9648	0.9263	0.9812
Shidu	0.9279	0.8367	0.9459	0.9098
Hot Spring	0.9386	0.9124	0.9398	0.9764
Average value	0.902	0.9206	0.936	0.934

As shown in Table 1, the accuracy, sensitivity, specificity, and F value of each factory are almost above 0.9, and only a few indicators are around 0.85. Whether it is the index of each factory or the average index, it meets the classification index requirements for detecting outliers, indicating that the model can detect spatial outliers well and has a good effect.

In order to prove the effectiveness and better performance of our method, we compare the proposed algorithm with the K-nearest neighbor algorithm based on Manhattan distance(MD-KNN) and the weighted distance based outlier detection (WDBOD). As can be seen from the performance indicators in Table 2, compared with the MD-KNN and WDBOD, our proposed algorithm shows better results that precision increased from 0.8426, 0.8524 to 0.9949, recall increased from 0.8302, 0.8357 to 0.9021, and F value increased from 0.8399, 0.8440 to 0.9462.

Table 2. Comparison of classification indicators for outlier detection

Method	Precision	Recall	F value
MD-KNN	0.8426	0.8302	0.8399
WDBOD	0.8524	0.8357	0.8440
Our method	0.9949	0.9021	0.9462

5. Conclusion

Outlier detection for spatial series dataset is a very meaningful and challenging task. Facing the multidimensional dataset containing outliers, we propose an algorithm based on KNN and Mahalanobis distance, results illustrate that the method gets better results as compare to the existing technique, providing a new idea for detecting spatial outliers. At the same time, it provides good research value for data outlier detection with similar data features in other fields. In future research, we will collect more water quality spatial data and optimize the method to improve performance in outlier detection.

References

- [1] Yu JC, Ju PH, Jia DH, Yue W, Zhang X. Spatial-temporal traffic outlier detection by coupling road level of service. *IET Intelligent Transport Systems*. 2019 June; 13(6):1016-1022.
- [2] Pu J, Wang Y, Liu X, Zhang X. STLP-OD: Spatial and Temporal Label Propagation for Traffic Outlier Detection. *IEEE Access*. 2019 May; 7:63036-63044.
- [3] Ismail ZH, Chun AKK, Shapirai Razak MI. Efficient Herd – Outlier Detection in Livestock Monitoring System Based on Density – Based Spatial Clustering. *IEEE Access*. 2019; 7:175062-175070.
- [4] Cheng SH, Chen SM, Jian WS. A Novel Fuzzy time series forecasting based on fuzzy logical relationships and similarity measures. *Proceedings of the 2015 IEEE International Conference on Systems, Man, and Cybernetics*; 2015 Oct 9-12; Kowloon, China; c2015. p. 2250-2254.
- [5] Heydari G, Vali MA, Gharaveisi AA. Chaotic time series prediction via artificial neural square fuzzy inference system. *Expert Systems with Applications*. 2016 Aug; 55:461-468.
- [6] Heydari A, Tavakoli M, Salim N. Detection of fake opinions using time series. *Expert Systems with Applications*. 2016 Oct; 58:83-92
- [7] Lingras P, Haider F, Triff M. Granular meta-clustering based on hierarchical, network, and temporal connections. *Granular Computing*. 2016; 1(1):71-92.

- [8] Liu Y, Zheng Y, Liang YX, Liu SM. Urban water quality prediction based on multi-task multi-view learning. Proceedings of the Twenty-Fifth International Joint Conference on Artificial Intelligence; 2016 July 9-15; New York, USA; c2015.p.2576-2582.
- [9] Liu Y, Liang Y, Ouyang K, Liu S, Rosenblum D, Zheng Y. Predicting Urban Water Quality with Ubiquitous Data - A Data-driven Approach. IEEE Transactions on Big Data. 2020; p.1-1.
- [10] Liu Y, Lu H. Outlier detection algorithm based on SOM neural network for spatial series dataset. Proceedings of the 2018 Tenth International Conference on Advanced Computational Intelligence (ICACI); 2018 Mar 29-31; Xiamen, China; c2018. p. 162-168.
- [11] Martínez Torres J, Nieto PJG, Alejano L. Detection of outliers in gas emissions from urban areas using functional data analysis. Journal of Hazardous Materials. 2011; 186(1):144-149.
- [12] Martínez J, García-Nieto PJ, Piñeiro JI, Iglesias C, Taboada J. Air quality parameters outliers detection using functional data analysis in the Langreo urban area (Northern Spain). Applied Mathematics and Computation. 2014 Aug; 241:1-10.
- [13] Blasi JIPD, Torres JM, Nieto PJG. Analysis and detection of functional outliers in water quality parameters from different automated monitoring stations in the Nalón River Basin (Northern Spain). Environ Sci Pollut Res Int. 2015; 22(1):387-396.
- [14] Peter BG, Messina JP. Errors in Time-Series Remote Sensing and an Open Access Application for Detecting and Visualizing Spatial Data Outliers Using Google Earth Engine. IEEE Journal of Selected Topics in Applied Earth Observations and Remote Sensing. 2019 Apr; 12(4):1165-1174.
- [15] Aggarwal V, Gupta V, Singh P, Sharma K, Sharma N. Detection of Spatial Outlier by Using Improved Z-Score Test. Proceeding of the 2019 3rd International Conference on Trends in Electronics and Informatics (ICOEI); 2019 Apr 23-25; Tirunelveli, India; c2019. p.788-790.
- [16] Ramaswamy, Sridhar, Rastogi, Rajeev, Shim. Efficient Algorithms for Mining Outliers from Large Data Sets. 2000.
- [17] Chen Y, Miao D, Zhang H. Neighborhood outlier detection. Expert Systems with Applications. 2010; 37(12):8745-8749.
- [18] Yu JX, Qian W, Lu H. Finding centric local outliers in categorical/numerical spaces. Knowledge & Information Systems. 2006; 9(3):309-338.
- [19] Araki S, Shimadera H, Yamamoto K. Effect of spatial outliers on the regression modelling of air pollutant concentrations: A case study in Japan. Atmospheric Environment. 2017 Mar; 153:83-99.
- [20] Harris P, Brunsdon C, Charlton M. Multivariate Spatial Outlier Detection Using Robust Geographically Weighted Methods. Mathematical Geosciences. 2014 Sept; 46(1):1-31.
- [21] Mahalanobis PC. On the generalized distance in statistics. Proceedings of the National Institute of Sciences of India. 1936; 12(1):49-55.
- [22] Ömer NG, Dogan GE. Power-quality event analysis using higher order cumulants and quadratic classifiers. IEEE Transactions on Power Delivery. 2006 Mar; 21(2):883-889.

Security and Privacy in Information Management in a Distributed Environment for Public Organizations

Segundo Moisés Toapanta Toapanta^{1*}, Yaritza Julieth Terán Terranova¹, Bertha Alice Naranjo Sánchez¹, Luis Enrique Mafla Gallegos²

¹ Computer Science Department, Salesian Polytechnic University of Ecuador (UPS), Chambers 227 and June, Ecuador

² Faculty of Systems Engineering, National Polytechnic School (EPN), Ladrón the Guevara E11-253, Ecuador

Abstract: Security and privacy problems in information management are evident in public organizations. The objective of this research is the analysis risks that these organizations run, since computer attacks have increased along with both internal and external threats. Causing information and database thefts, there are risk analysis methodologies which are oriented to the objective for the preservation of guaranteeing the security and privacy of the information. Were used the deductive method and exploratory research to analyze the articles in the references and in the information available online and MAGERIT methodology what protects the information in its integrity, confidentiality and availability guaranteeing the security of the system and processes of public organizations. It turned out a Control of Security and Privacy factors, Threat Probability, Risk Assessment Formula, Prototype of Risk Management for Public Organizations and Privacy and security factor formula. It was concluded that MAGERIT is an alternative what allow mitigate the vulnerabilities, threat and risks its processes in public organizations for protecting their information.

Keywords: Management, Distributed Environment, Public Organizations, Privacy and Security.

1. Introduction

Information security represents a great challenge to all organizations, as information is required to be confidential. This research is made on public organizations that currently present information risk problems due computer attacks and internal and external threats. It has been allowed in public organizations, that false and useless information enters with no protection and cause damage and hacking of information and databases. This is why they give higher priority to the protection of their information assets to generate confidence in the citizens, in their environment and in turn prevents them from having risks of computer vulnerabilities [1].

Public organizations face many threats that can affect them. It has been suggested that if the organizations knew and apply the methodology they would not be questioned. The security and privacy of their information and their database would be protected. This is why this article will reveal the help provided by this methodology, it

* Corresponding Author: Segundo Moisés Toapanta Toapanta, Salesian Polytechnic University of Ecuador (UPS), Ecuador; Email:stoapanta@ups.edu.ec

is important to take into account the recommendations on this model since it is considered a timely way to help when public organizations faces risks that affect them. Methodology to ensure information security in a distributed architecture for a public organization of Ecuador [2], Hyperledger technology in public organizations in Ecuador [3], Study of the evolution of information security in Colombia: 2000-2018[4], Information security methods to protect rest web services communication and data in http requests using json web token and keycloak red hat single sign on[5], El rol de la seguridad informática en el ámbito académico y los sistemas de información asociados[6], Security of networks and information systems in the European Union: A comprehensive approach? [7], WSN security applied to smart metering systems based on cryptography techniques [8], The reduction of number of parliamentary members and the modification of remuneration schemes for deputies in autonomous community [9], A new data protection law [10], From «computing freedom» towards the constitutionalization of new digital rights (1978-2018) [11], Securing the human: Broadening diversity in cybersecurity[12], Intruder attacks on wireless sensor networks: A soft decision and prevention mechanism[13], Transposition of EU network and information security directive into national law[14] and An Approach to Optimize the Management of Information Security in Public Organizations of Ecuador [15].

The projects implemented in regards to ISO information security and privacy management system, ensure the information assets of public organizations, therefore it is necessary not only the use of methodologies but also of experts who can manage them as it is not rare to see, that these problems harm the security of information on such organizations. Therefore, after the analysis, correct decisions on confidentiality, integrity and availability will be taken. This guarantees improvements in the information security and privacy managing. Looking to optimize it public organizations[15].The MAGERIT methodology finds inconsistency in the organization system, which hasn't been detected before and for a long time, they did not know of their existence. To arrive to the conclusion analysis, we compared with the investigations. This methodology helps to public organizations to have greater control of threats. As a result, security measures were taken, so that they can have a guarantee and that their processes could be manageable, using risk assessment and threat probability formula, a risk management prototype for public organizations and a privacy and security factor formula.

2. Materials and Methods

The procedures used are supported by the reviews of references and articles. It is presented in sequence so to give logical results.

2.1 Materials

The methodology that was used, allowed the correct use of risk analysis, ensuring and protecting the information security and privacy in public organizations with the aim of protecting the database and information within organizations. This is why the MAGERIT methodology was analized; being a risk analysis and management methodology for information systems, known in the European Information Network Security Agency; the methodology used the impacts organizations normally have when security breaches occur and identified the threats that affected these organizations.

Once the vulnerabilities were identified, they could be used to set clear and corrective measures. Technology moves constantly, that is why this methodology helped and will help because it minimize the associated risks, making use of confidentiality, integrity and availability systems that generate trust. This methodology was widely used, without dismissing CRAMM methodology. This analysis and central computer and telecommunications risk control methodology also identified and reduced the attacks that organizations faced. Such methodology relied on the management tool which makes organizations have a clearer vision and be effective acting when facing the threats, previously mentioned [1]. These methodologies were analyzed, approved and were taken into account based on the risk analysis. They found vulnerabilities, threats and risks, allowing better results and providing information security and privacy in public organizations. Risks were analyzed, this being a management tool for decision-making that corrected risks, for improvements and prevention of active analyzes that were factors of the computer systems that support the mission of public organizations, that were threatened causing them damage.

2.2 Methods

The deductive method was used, including criteria applications of the Information Management System (ISMS) that corresponds to ISO / IEC 2700, and risk analysis studied by the research.

2.2.1 Risk Analysis

The security and privacy of the information risks affected entirely to the public organizations. As this methodology determined the threats to which they were exposed, it proved to be effective against these risks that impacted them. Having these factors exposed to threats caused some impact degradation with a certain probability of risks. In fact, this analysis identifies relevant assets such as information data, computer equipment, information support, communication networks and services. It depended on these types to be able to safeguard threats.

The information system updates constantly, and it also faces more threats. We look to protect the information assets by implementing security control measures, which allow to manage and reduce risks, to achieve the major goal, which is to protect it from threats and risks.

Carrying out the analysis we have the types of risks and threats, in the threats we have of intentional and unintentional types; in the case of the intentional ones in the public organizations the production of damages is tried like the robbery of the information applying the trashing, the malicious codes, impersonation on the other hand in the unintentional ones it is where the actions or omissions take place that if we realize they do not look for to exploit a vulnerability, but that they put in risk the assets of information that this produces a damage like threats related to the natural phenomena. Public organizations should bear in mind that these threats are a warning that damage is imminent, or that damage is occurring or has occurred. Among the risks we have when working in computers without antivirus is possible to have a malware through USB memory most of these are computer viruses, trojans and worms, opening suspicious emails because cybercriminals take advantage of this way in public organizations through users for the theft of information, introduce infected USB flash

drives that is also a risk because possibly someone can collect information, passwords and can collect information from users and confidential information.

2.2.2 Risk management process

Risk management is structured with an ISO standard and we show the following picture

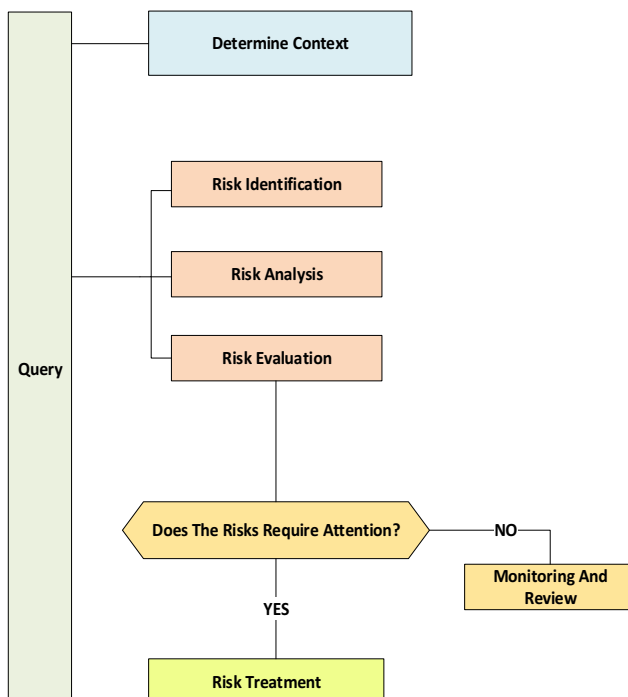


Figure 1. Risk management process

In figure 1, the context is determined, looking for parameters, whether internal or external. We also identify the risks and dangering positions. If they are not identified, they remain hidden. When analyzing the risk it is important to have a vision to which we want to reach and focus on the important risks, executing an evaluation and a treatment represented by analyzed options. At the end, a follow-up and review take place and the incidents are acted on accordingly to observe the continuous improvement in the environment by means of experiences.

With 2 essential things, information that it handles and the services that public organizations provide. Setting requirements for security and privacy of the information in management of the organizations, which are being analyzed, in order to come to an agreement and a stable methodology to avoid that the threats grow but rather minimize them.

2.2.3 Probability of threats and risks

Table 1: Risks

High risks	Medium Risks	Low Risks
(12-16)	(8-9)	(1-6)
4	8	12
3	6	9
2	4	6
1	2	3
LIKELIHOOD OF THREATS		
EXTENT OF DAMAGE		

Table 1 indicates the probability of damage and risk, this being the most used method in risk analysis. We have values as: 1 = Insignificant, 2 = Low, 3 = Medium and 4 = High.

Observing the risk table, the instances it handles and the measure of damage they can cause, the changes that must be made for the best way of handling information are determined. In this process, when analyzing the risks, it is important to have in mind the characteristics of these risks, being those, dynamic and unsteady (perform an interaction between threats and vulnerability), separated by different letters, not always is perceived in the same way between public organizations, so it can produce inadequate results. This method was applied in different public organizations. The higher the probability of threat and magnitude of damage is, the greater the risk and danger to information security and privacy, which means it is mandatory to implement the information security and privacy protection measure.

2.2.4 Risk analysis methodology

One of the factors that was taken into account in the organizations, was information privacy and security due the many times some active incidents put them at risk. That is why it is urgent to have variables for the analysis of information security risks.

Table 2: Variables applied to risk analysis

Assets	Threats	Vulnerabilities
Servers	Hacker	Unnecessary open ports
Database	Loss of information	Backup not active
Antivirus	Virus	No antivirus update
Switch	Electric shock	Without preventive maintenance
Firewall Technological equipments	Lack of update Hardware damage	Lack of updates No preventive maintenance

3. Results

The result turns out into a control of security and privacy factors, a risk and probability evaluation formula, a risk management prototype in public organizations and a privacy and security factor formula with the corresponding equations by which it was made known through the analysis provided. The analysis of risk determined by its probabilities allows to have a risk evaluation, to make a global analysis of the risks that need to be prioritized, thus facilitating the decision of the organization to treat and implement the variables related to the analysis of risks.

a) Control of Security and Privacy Factors

It is important to do not lose the sense of the organizational information related to the privacy and security of the given action. To demonstrate this, we convert it in a simple way into graphics. The data shown below has been processed and displayed; it includes details and technical knowledge that perform the main work within the ISMS, to help to make decisions and the necessary adjustments to achieve the aforementioned objectives.

Table 3. Control of Privacy and Security Factors.

Incidents	11
Violations	17
nonconformities	20

In table 3. Description of Privacy control and security factors, giving an referential value to which each one of them can reach. Below, you will find a table and a graphic with indicator data.

Table 4. Monthly privacy and security control

MONTHS	Incidents	Violations	Nonconformities
January	1	3	1
February	2	5	4
March		1	
April	1		
May	3	4	3
June			2
July		2	1
August	1		
September	2		5
October		2	3
November	1		
December			1

In table 4. Monthly Description of the control taken over the privacy and security factors, indicating the incidents, violations and non-conformities that are recorded every month. The monthly control for organizations was presented initially

through measurements and indicators. For information security, we took into account an annual control. In this way through public organizations, the actions taken on information security and privacy were made known.

Table 5. Experimental data of business

BUSINESS	YEAR	USERS
AOL	2006	6.5
DPE	2007	3.2
HPS	2008	134

In the table 5 shows the risk and threat attacks that public organizations had in 3 years, where millions of records were lost by which users are affected.

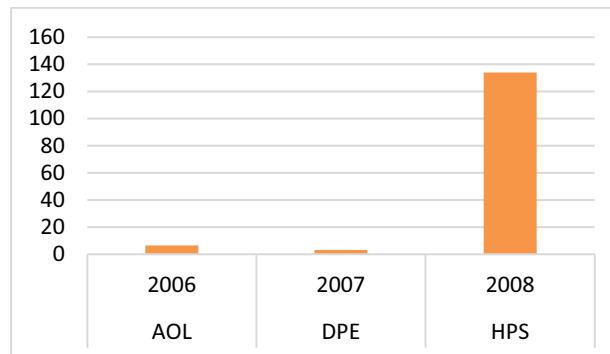


Figure 2. Experimental Data

In figure 2, we have internal attacks, the incidents of information security being these since 2007 in organization DPE (Public Defender's Office of Ecuador) specifying that more than 3.2 million records of clients were stolen in which they include the banking data and the credit cards with personal data the ministry of telecommunications realized the analysis of which they realized the leak of data, on August 6, 2006 there was an attack to AOL, 6.5 million users were affected because their bank details were filled with purchases on a web page, without leaving behind the 2008 attack on the Heartland Payment Systems database, 134 million credit and debit cards were exposed, which resulted in the theft of identity information and money[6].

b) Threat Probability and Risk Assessment Formula

There are several methods of how to assess a risk, many times they are difficult to specify, but it was developed using a mathematical formula.

Values

1 = insignificant, 2 = Low, 3 = Medium y 4 = High

R = Risk, PA = Probability of threats y MD = Magnitude of damage

$$R = PA - MD \quad (1)$$

To represent the risk result, we use the graphic detailed in Table 1, in which the x-axis (Probability of threats), and the y-axis (magnitude of damage) can be between 1 Insignificant and 4 High. Facilitating spreadsheets, specifying or estimating the

conditions of the values, providing a risk analysis that allows to give them a position and learn the influence these factors can have in a negative or positive way. To establish the risks in the information security, we did a comparison between the risk probability analysis and its impact. It presents a way to measure the risks according its level of impact and the probabilities established, in the risk zones, presenting also the way to handle that risk.

3.1 Prototype of Risk Management in Public Organizations

The following prototype displayed in the flow chart, show the process steps used to identify risks, in public organizations in order to improve whether internal or externally, preventing or reducing the risks known within the organization, reviewing the need being this, a previously analyzed planning. It gives an alternative to reduce risks on the information security and to improve the management of it. This is why the public organizations take into account the identification of risk to take measures, to supply the necessary resources and implement actions so that after the verifications, the risk management improves, due to the measures taken to improve the security and privacy of information.

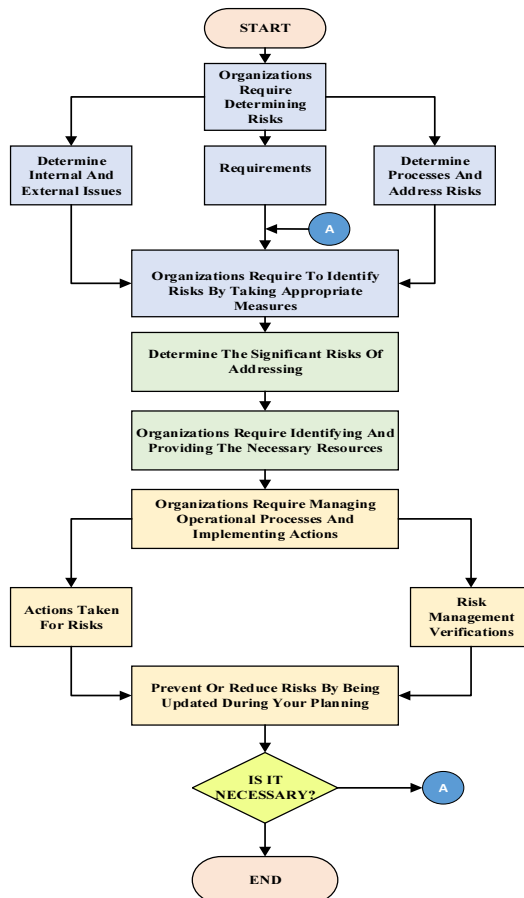


Figure 3. Risk Management Prototype

In figure 3 the risks in the organizations are determined, questioning internally and externally having requirements by which it determines the processes and treats the risks or threats, the public organizations identify the risks taking measures on the analysis that is carried out to be able to do so. Addressing, identifying and providing necessary resources, the operational processes manages and implements actions, whether these are taken for risks, since it prevents and reduces them, being updated during their planning, if it is not necessary to return to identify the processes, but if it is, it ends.

3.2 Privacy and security factor formula

In order to get this results, the factors were taken into account, to help to define clearly the weekly, monthly, quarterly, annually intervals. For this you must; K = Total of factors to evaluate and k = How many are met.

$$\frac{k}{K} = \frac{7}{10} = 0.7 = 70\% \quad (2)$$

Referring to an example of 10 predetermined factors, 7 are met. using values **Table 3**.

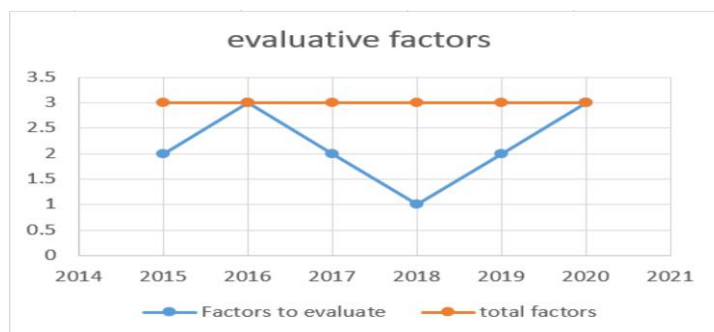


Figure 4. Evaluative factors

In Figure 4 we learn about the factors that need to be evaluated in the last 5 years, remembering that these factors are incidents, violations and non-conformities that exist within public organizations, so good security has not been maintained.

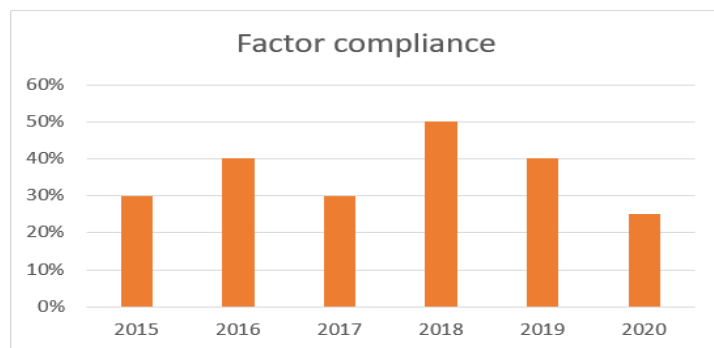


Figure 5. Factor compliance

In figure 5 we have the percentage of compliance of the last 5 years given with the interval formula using K y k.

Table 6. Qualitative Comparisons of proposals

Investigation	Proposition	Factors	Conclusions
[1]	MAGERIT	Confidentiality, integrity and availability	Better results to avoid risks and threats
[3]	Hyperledyer	Advances in technologies	Innovations through open source.
[3]	Blockchain	Organizational Verification	Transparency
[13]	Antivirus	Protection	Prevents damage to the base and protects security.
[15]	ISO	Optimize security management	Information security

Table 6 presents a comparison describing all the analysis carried out and presenting proposals for the security and privacy of the information, making the analysis available and effective.

4. Discussion

It is important that with this research, public organizations have received correct information so that they can follow the methodology and adapt it. It also helped solving information security problems. The methodology should have been taken into account despite the fact, the former methodology didn't stop threats or risks to damage the information in the database. For this reason, the MAGERIT methodologies analyzed and helped in a qualitative and quantitative way, based in elements such as confidentiality, integrity and availability.

It is then considered that this methodology is the correct and effective alternative to handle information privacy and security in public organizations, without forgetting the ISMS contribution in showing the associated security controls and benefits, determining the main risks and approaches for risk management, which were adjusted to the privacy and security requirements for public organizations.

The results obtained are directly linked to other researches regarding; that for each El rol de la seguridad informática en el ámbito académico y los sistemas de información asociados[6] and An Approach to Optimize the Management of Information Security in Public Organizations of Ecuador [15].

Any prototype based on a methodology must be considered as an alternative for the security and privacy of information in public organizations

5. Future Work and Conclusion

The organization that considers the Prototype Conceptual Model of Security and Privacy of information; it must carry out the analysis of organizations to improve security using the MAGERIT methodology. Organizations that consider the risk

management prototype in public organizations must determine internal and external risks by identifying and taking the correct measures.

It was concluded that MAGERIT is an alternative what allow mitigate the vulnerability, threat and risks its processes in public organizations for protecting their information.

It was concluded that MAGERIT is a security measure that mitigates the vulnerability, threat and risks of its processes in public organizations to protect information.

The Risk Management prototype and the threat probability and risk assessment formula presented as results are an alternative that improves the security and privacy of information in public organizations.

Acknowledgments

The authors thank to Universidad Politécnica Salesiana del Ecuador, to the research group of the Guayaquil Headquarters “Computing, Security and Information Technology for a Globalized World” (CSITGW) created according to resolution 142-06-2017-07-19 and Secretaría de Educación Superior Ciencia, Tecnología e Innovación (Senescyt).

References

- [1] M. A. Tejena-Macías, “Análisis de riesgos en seguridad de la información,” *Polo del Conoc.*, vol. 3, no. 4, p. 230, Apr. 2018, doi: 10.23857/pc.v3i4.809.
- [2] S. M. T. Toapanta, F. G. M. Quimi, K. E. O. Pazmiño, R. M. Arrellano, and L. E. M. Gallegos, “Methodology to ensure information security in a distributed architecture for a public organization of Ecuador,” in *Frontiers in Artificial Intelligence and Applications*, Oct. 2019, vol. 320, pp. 933–944, doi: 10.3233/FAIA190267.
- [3] S. M. Toapanta Toapanta, T. F. Prado Quintana, M. R. Maciel Arellano, and L. E. Mafla Gallegos, “Hyperledger technology in public organizations in Ecuador,” in *Proceedings - 3rd International Conference on Information and Computer Technologies, ICICT 2020*, Mar. 2020, pp. 294–301, doi: 10.1109/ICICT50521.2020.00052.
- [4] J. J. Cano M. and A. Almanza, “Study of the evolution of information security in Colombia: 2000–2018,” *RISTI - Rev. Iber. Sist. e Tecnol. Inf.*, vol. 2020, no. E27, pp. 470–483, Mar. 2020.
- [5] C. Muyón and F. Montaluisa, “Information security methods to protect rest web services communication and data in http requests using json web token and keycloak red hat single sign on,” *RISTI - Rev. Iber. Sist. e Tecnol. Inf.*, vol. 2020, no. E29, pp. 198–213, May 2020.
- [6] A. Bogantes, “El rol de la seguridad informática en el ámbito académico y los sistemas de información asociados,” in *CICIC 2020 - Decima Conferencia Iberoamericana de Complejidad, Informatica y Cibernetica, Memorias*, 2020, vol. 1, pp. 57–62.
- [7] M. Robles Carrillo, “Security of networks and information systems in the European Union: A comprehensive approach?,” *Rev. Derecho Comunitario Eur.*, no. 60, pp. 563–600, May 2018, doi: 10.18042/cepc/rdce.60.03.
- [8] L. Valencia, T. Guarda, G. P. L. Arias, and G. N. Quiña, “WSN security applied to smart metering systems based on cryptography techniques,” *RISTI - Rev. Iber. Sist. e Tecnol. Inf.*, no. E17, pp. 393–406, Jan. 2019.
- [9] R. S. Cristóbal, “The reduction of number of parliamentary members and the modification of remuneration schemes for deputies in autonomous community,” *Rev. Derecho Polit.*, vol. 92, pp. 73–118, 2015.
- [10] A. Rallo Lombarte, “A new data protection law,” *Rev. Esp. Derecho Const.*, vol. 2019, no. 116, pp. 45–74, 2019, doi: 10.18042/cepc/redc.116.02.
- [11] A. R. Lombarte, “From «computing freedom» towards the constitutionalization of new digital rights (1978–2018),” *Revista de Derecho Político*, no. 100. Universidad Nacional de Educacion a Distancia, pp. 639–669, Sep. 01, 2017.

- [12] M. Azhar *et al.*, “Securing the human: Broadening diversity in cybersecurity,” in *Annual Conference on Innovation and Technology in Computer Science Education, ITiCSE*, Jul. 2019, pp. 251–252, doi: 10.1145/3304221.3325537.
- [13] I. Hussain, S. Zahra, A. Hussain, H. D. Bedru, S. Haider, and D. Gumzhacheva, “Intruder attacks on wireless sensor networks: A soft decision and prevention mechanism,” *Int. J. Adv. Comput. Sci. Appl.*, vol. 10, no. 5, pp. 609–617, 2019, doi: 10.14569/ijacsa.2019.0100578.
- [14] T. Katulic, “Transposition of EU network and information security directive into national law,” in *2018 41st International Convention on Information and Communication Technology, Electronics and Microelectronics, MIPRO 2018 - Proceedings*, Jun. 2018, pp. 1143–1148, doi: 10.23919/MIPRO.2018.8400208.
- [15] S. Moisés Toapanta Toapanta and L. Enrique Mafla Gallegos, “An Approach to Optimize the Management of Information Security in Public Organizations of Ecuador,” in *Fault Detection, Diagnosis and Prognosis*, IntechOpen, 2020.

Exploring the Potential of GPT-2 for Generating Fake Reviews of Research Papers

Alberto BARTOLI^{a,1} and Eric MEDVET^a

^aDepartment of Engineering and Architecture, University of Trieste, Italy

Abstract. Modern tools for natural language generation may enable novel forms of scholarly fraud based on the *automatic* generation of *fake review reports* for academic papers, i.e., of a few sentences broadly related to the textual content of a submission and written with the style of an anonymous reviewer. A tool capable of generating such reports automatically and for free could enable various forms of unethical behavior by publishers and researchers. In this work we experiment with a simple heuristic that makes use of widely available and easy to use tools for natural language generation, including the *Generative Pretrained Transformer 2 (GPT-2)*, in order to craft fake reviews automatically. We also perform a small user study for assessing the credibility of those reviews. Our analysis suggests that academic frauds based on fake reviews may indeed be feasible and ready to be deployed in the wild.

Keywords. academic fraud, artificial intelligence, bibliometry, language models, natural language generation, natural language processing.

Introduction

Peer review of research papers is a cornerstone of scholarly publishing and is widely believed a crucial element for ensuring quality of published research. Peer review must be done by experts in the specific field and must be fair, accurate, and timely. Satisfying these essential requirements is becoming more and more difficult [1,2,3], which could encourage certain publishers to not perform stringent peer reviews in order to expand their customer base and attract more submissions from authors. Indeed, the incentives that drive the behaviors of the many actors involved in scholarly publishing—authors, publishing companies, conference organizers, editors, reviewers, research institutions—do not necessarily lead to an overall scientific progress and have often resulted in various forms of questionable behavior if not plain fraud.

In this work we explore the feasibility of a novel form of scholarly fraud based on the automatic generation of fake review reports for academic papers, i.e., of a few sentences with just some generic criticisms or recommendations broadly related to the textual content of a submission and written with the style of an anonymous reviewer. A tool capable of generating such reports automatically and for free could enable various forms

¹Corresponding Author. E-mail: bartoli.alberto@units.it.

of unethical behavior by publishers and researchers. A journal or conference could return one or more fake review reports to authors in order to simulate an accurate vetting procedure, while busy researchers asked to review a paper could return fake review reports for justifying their presence in boards and committees. We are aware of only one prior attempt at generating fake reviews for scientific papers automatically, proposed by our research group [4]. The proposal was based on a template system constructed from a small set of existing reviews and specialized with terms specific of the paper being reviewed. The generated reviews were thus severely limited in the richness and diversity of text, but were considered credible by several readers (please refer to the cited work for full details). In this work we explore the usage of modern neural language models, such as the *Generative Pretrained Transformer 2 (GPT-2)* [5,6], that were not available at the time the cited proposal was developed. Indeed, recent developments in “artificial intelligence” have enabled various applications able to emulate the behavior of a human to an extent that appeared not possible just a few years ago.

1. Our Framework

1.1. Natural Language Generation

At the core of our framework there is the GPT-2 language model developed by the OpenAI research institute. GPT-2 has been constructed in an unsupervised way from a large corpus of 8 million web pages [5,6]. The training objective consisted in predicting the next word given all the previous words in the stream. The typical usage of GPT-2 consists in generating synthetic text samples in response to a textual input. The generated text follows the style and content of the input, which in principle allows generating realistic continuations about any topic inserted as input. GPT-2 is available in several versions depending on the number of parameters in the model, that range from 124 millions (“small”), to 1.5 billions (“extra large”). The two smallest versions of GPT-2 can be fine-tuned on a selected input text in order to make the text generated by the fine-tuned model “more typical” of the domain associated with that text. Naturally, given the large amount of model parameters, such a fine-tuning cannot eliminate any bias included in the original training corpus and a fairly large amount of additional text is required, in the order of several millions of characters.

We fine-tuned the “medium” version of GPT-2 (355 million parameters) with a 55 MB textual corpus of review reports. We constructed this corpus based on a dataset of peer reviews of scientific papers that has publicly made available recently². This dataset, called *PeerRead*, contains reviews from several conferences in machine learning and the authors demonstrated its usage for predicting acceptance/rejection and numerical scores [7]. We extracted from PeerRead only the textual reports and discarded all the scores. We used also the reports from NIPS conferences 2018 and 2019, not included in PeerRead. We chose to fine-tune a single language model on the full set of review reports available rather than, e.g., fine-tuning a model on positive reviews and another model on negative reviews. We used the resulting language model, *GPT-2-ReviewGenerator*, as described in the next section. We performed fine-tuning and text generation based on a publicly available Colaboratory Notebook [8].

²<https://github.com/allenai/PeerRead>

1.2. *Fake reviews generation*

We experimented with a simple procedure for fake reviews generation, designed to minimize human intervention and, most importantly, amenable to be implemented with skills at the level of an editorial assistant. The actual implementation of our experiments required some manual steps but, as will be evident, these steps can be automated easily.

Practical usage of GPT-2 involves several parameters, in particular: p (*prefix*), the textual input for conditioning the generated text; n_{samples} the number of different textual outputs to be randomly generated (*samples*), all conditioned by the same input p ; len , the desired length for the samples; *temperature* and top_k , two numerical values which control the degree of randomness in the generation of the words for the samples (please refer to [8] for details).

Our procedure takes title and abstract of the paper as input, along with a short and possibly incomplete sentence biased toward the desired outcome for the review, e.g., “This is a solid work and should be accepted because”, “The experimental section is flawed and I cannot recommend acceptance” or something alike. The procedure is as follows.

1. Use an automatic summarization service for constructing a summary of the paper based on abstract and introduction. The length of the summary, denoted by s , should be 80–100 words.
2. If the summary contains any sentence in active voice, rephrase the sentence in passive voice, e.g., “We propose an algorithm” should become “An algorithm is proposed”.
3. Write the beginning of a short sentence biased toward the desired outcome for the review, as indicated above. Let this *driving sentence* be denoted as d .
4. Concatenate s and d and use the resulting string as input prefix p to GPT-2-ReviewGenerator. For the other parameters we used $n_{\text{samples}} = 10$, $len = 800$ words, *temperature* = 0.7 (default value) and $top_k = 40$ (default value).
5. Analyze the generated samples and choose a single, contiguous snippet that satisfies these requirements: (a) it has adequate length (between 150 and 300 words); it is coherent with the desired outcome (accept vs. reject); (b) it is internally coherent (e.g., it does not provide both strongly positive and strongly negative comments); (c) it does not contain elements that might be totally unrelated to the paper being reviewed (e.g., references to prior publications, acronyms of algorithms and alike); (d) it looks natural (this requirement obviously requires human judgement). The chosen snippet constitutes the output of our procedure, i.e., the fake review report.

Regarding step 5, the choice of the snippet from the generated samples took no more than 5 minutes for each paper. Several samples could be discarded immediately because after a more or less creative beginning, the generated text started to repeat itself. The requirements at step 5 could be modified or extended in several ways. We do not elaborate on this point for brevity.

All the steps of the procedure could be automated, either in full or in part, with the only exception of step 5-(d). The automatic summarization at step 1 can be done with one of the many techniques and services for automatic summarization that exist. According to our early experimentation, the relative length of abstract, introduction, and summary makes the summary not very dependent on the specific summarization technique used.

We chose the target length for a review report (i.e., requirement (a) above) based on the length of the many thousands of reports in our (augmented) PeerRead dataset: for two of the conferences of the dataset, it is reported a mean of 531 and 346 words and a standard deviation of 323 and 213 words. While a longer report could be, in principle, more credible, obtaining a long, coherent text from GPT-2 tends to be difficult.

We emphasize that we strive for simplicity, in particular, with respect to the actions required by human operators. In this respect, we remark that we select a *single* snippet as review report, rather than a text obtained from the samples in a more elaborated way, e.g., by merging a number of different snippets. For example, it would be easy to greatly improve the “quality” of generated reviews by simply concatenating a few selected snippets, even without any modification to those snippets. We preferred to not explore more elaborated options, not only for keeping the procedure as simple as possible but also for a better assessment of the power of modern tools for natural language generation in our domain of interest.

2. Assessment

Several metrics exist for assessing the quality of a natural language generator tool, e.g., lexical richness, syntactic complexity, complexity, and diversity [9,10,11]. In our opinion such metrics are not adequate for our fake reviews tool: they would assess more the GPT-2 (fine-tuned) model than the fake review generator; and, they would not address the real issue of the credibility and usefulness of the generated reviews. It would be necessary to insert those reviews in a real reviewing process and verify their actual impact, which would depend on the target of the fraud. A busy researcher asked to review a paper could return a fake review, in which case we should assess whether the journal editor or conference program committee are actually able to detect the fraud. Conversely, and perhaps most interestingly, a journal or conference could return one or more fake reviews to authors in order to simulate an accurate vetting procedure, in which case we should assess whether the fraud may be detected by authors (assuming that authors are indeed interested in having their papers actually reviewed, rather than only in having their papers published). We are not able to perform this kind of assessment and thus performed a small user study, described below.

For our assessment we selected three papers published by our research group [12, 13,14], in venues different from those of the dataset that we used for fine-tuning GPT-2. For each paper we selected a real review that recommended acceptance and generated two fake reviews, one recommending acceptance, and another recommending rejection. All the real reviews were, in our opinion, of good quality. The resulting set of 9 reviews is available on line, in the “Data and tools” section of the web site of our laboratory³. We provide two fake reviews in Table 1 for completeness.

Then, we constructed a form containing, for each paper, title, abstract, and the three reviews. Each review consisted of the recommendation (accept vs. reject) and the textual report. The order of the three kinds of reviews was different for each paper. The form asked to rate each report as “Very useful”, “Useful”, “Useless”, “Completely useless”. We circulated the form between some of our academic contacts, by asking collaboration for a generic “research on the quality of peer reviews” and *without* specifying that some

³<https://machinelearning.inginf.units.it/>

Regex golf has recently emerged as a specific kind of code golf, i.e., unstructured and informal programming competitions aimed at writing the shortest code solving a particular problem. A problem in regex golf usually consists in writing the shortest regular expression which matches all the strings in a given list and does not match any of the strings in another given list. In this paper, a methodology based on Genetic Programming for generating solutions to regex golf problems is proposed—a regex golf player. A population of candidate regular expressions represented as trees and constructed with carefully selected regular expression operators and constants is generated.

This paper is solid work that should definitely be accepted because it shows an ability to generate solutions for the regex golf problem. The authors have done a good job in developing the scheme and the general idea of the paper. The authors have also shown a clear connection between the concept of Genetic Programming and the solution to the regex golf problem. I think this is a good result. The paper is written well and the authors have done a good job in developing their scheme. However, some issues remain. The paper is not clear about the significance of the tree structure. Does it reflect the fact that the tree structure is only used to encode the solutions to the problem? Is it the case that this structure is only used to encode the solutions to the problem? If so, then it is unclear what happens to the solution when a new tree is created? What happens to the solution when the current tree is deleted?

The experimental section is unclear because the paper does not present any data in the experiment. The proposed approach is difficult to evaluate, as the paper presents results only when an operator is used and does not describe the number of operators or the number of operators. The experiment is also unclear because the experiment was performed on a different machine than the one used to evaluate the results presented in the paper. The results are not convincing, as performance on the machine was limited by the number of operators used, not by the number of regular expressions used.

The paper is not clear as to whether it is possible to use a subset of operators in the same regular expression, thus, there are no guarantees that performance will be comparable to that of a single operator. The experiment is also not convincing because it is unclear whether the proposed approach will work on other kinds of regular expressions. The results are not convincing, because performance on the machine was limited by the number of operators used, not by the number of regular expressions used. The paper is not clear as to whether it is possible to use a subset of operators in the same regular expression, thus, there are no guarantees that performance will be comparable to that of a single operator.

Table 1. Fake reviews for [12], recommending acceptance (up) and rejection (down). These correspond to 1-fake-accept and 1-fake-reject, respectively, in Table 1

of the reviews were fake. Users accessed the form anonymously and were asked to self-assess their research experience and their knowledge on the topics of the papers.

We obtained 16 responses from 12 “Experienced researchers”, 3 “Junior researchers”, and 1 “Student (undergrad/PhD)”, corresponding to 75.5 %, 18.8 %, 6.2 % respectively. The self-assessed familiarity with the research topic of the papers was 2 “High”, 6 “Medium”, and 8 “Low”, 12.5 %, 37.5 %, 50.0 % respectively. The corresponding results are in Figure 1.

In order to interpret these results one should determine the minimum acceptable rating for a fake review. In this respect we observe that the real review of paper 1 was rated “Useless” by a significant fraction of users. If we consider this rating as the minimum acceptable one, then the experiment has been highly successful: only a small percentage of answers rated fake reviews as “Completely Useless”. Even if we consider the much more challenging baseline corresponding to at least “Useful”, though, it seems fair to claim that the experiment has proven the potential relevance of fake reviews: approximately 75 %, 30 %, and 25 % of the answers for the three papers, respectively, has satisfied this baseline. Interestingly, for paper 1, the fake reviews were deemed more useful overall than the real one.

Some of the optional comments provided by users were quite interesting. Only one of them (experienced researcher, low familiarity) mentioned the possibility that some reviews might have been generated automatically, yet the corresponding ratings for fake

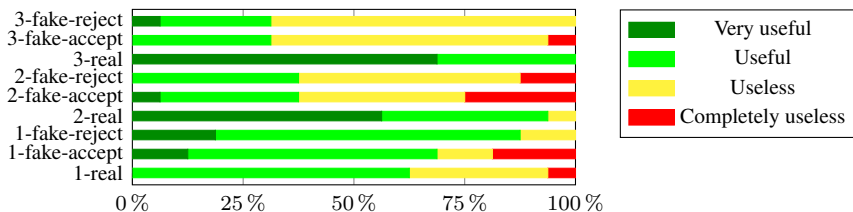


Figure 1. Summary of user study (see the text for a description)

reviews were 1 “Very Useful”, 3 “Useful”, 2 “Useless” without any “Completely Useless” rating. Another user (experienced researcher, medium familiarity) commented that although he/she provided 3 “Useless” ratings, all reviews should be rated at least “Useful” because “they all provide at least some reasons (even vague ones) to accept/reject and specific elements to clarify/explain; real reviews often lack that very basics.”. It is unclear whether the mention of “real reviews” implies that this user realized that some reviews were generated automatically, but this comment is quite interesting anyway.

3. Discussion and concluding remarks

Modern tools for natural language processing and natural language generation may enable novel forms of scholarly fraud based on the automatic generation of fake review reports for academic papers. Although our small user study cannot certainly be conclusive, we have shown that a simple heuristic based on widely available and easy to use tools may be remarkably effective. Such heuristics may be improved in a variety of ways and, most importantly, the power of the language generation engine may be boosted by a new language model much more powerful than GPT-2 that has been recently announced [15]. This new model, called GPT-3, consists of 175 billion parameters in its larger version—two orders of magnitude bigger than GPT-2. GPT-3 will be made available as a paid cloud-based service and is currently available to a small set of researchers in a wait list.

Our analysis thus indicates that academic frauds based on fake reviews could indeed be feasible and ready to be deployed in the wild. We suggest that journal publishers and conference organizing committees could occasionally inject fake reviews in the reviewing process, in a carefully controlled way, to make sure that these reviews are indeed spotted and discarded. We believe that procedures of this kind could consolidate the quality of a publishing venue and be useful for the scientific community as a whole.

References

- [1] Charles W Fox. Difficulty of recruiting reviewers predicts review scores and editorial decisions at six journals of ecology and evolution. *Scientometrics*, 113(1):465–477, 2017.
- [2] Charles W Fox, Arianne YK Albert, and Timothy H Vines. Recruitment of reviewers is becoming harder at some journals: A test of the influence of reviewer fatigue at six journals in ecology and evolution. *Research Integrity and Peer Review*, 2(1):3, 2017.
- [3] Sameer B Raniga. Decline to Review a Manuscript: Insight and Implications for AJR Reviewers, Authors, and Editorial Staff. *American Journal of Roentgenology*, 214(4):723–726, 2020.

- [4] Alberto Bartoli, Andrea De Lorenzo, Eric Medvet, and Fabiano Tarlao. Your paper has been accepted, rejected, or whatever: Automatic generation of scientific paper reviews. In *Availability, Reliability, and Security in Information Systems*, pages 19–28, Cham, 2016. Springer International Publishing.
- [5] Alec Radford, Jeffrey Wu, Rewon Child, David Luan, Dario Amodei, and Ilya Sutskever. Language Models are Unsupervised Multitask Learners. 2019.
- [6] Alec Radford. Better language models and their implications. <https://openai.com/blog/better-language-models/>, February 2019. Accessed: 2020-7-8.
- [7] Dongyeop Kang, Waleed Ammar, Bhavana Dalvi, Madeleine van Zuylen, Sebastian Kohlmeier, Eduard Hovy, and Roy Schwartz. A Dataset of Peer Reviews (PeerRead): Collection, Insights and NLP Applications. In *Meeting of the North American Chapter of the Association for Computational Linguistics (NAACL)*, New Orleans, USA, June 2018.
- [8] Max Woolf. How to make custom AI-Generated text with GPT-2. <https://minimaxir.com/2019/09/howto-gpt2/>, September 2019. Accessed: 2020-7-8.
- [9] Ondřej Dušek, Jekaterina Novikova, and Verena Rieser. Evaluating the state-of-the-art of End-to-End natural language generation: The E2E NLG challenge. *Comput. Speech Lang.*, 59:123–156, January 2020.
- [10] Dimitra Gkatzia and Saad Mahamood. A snapshot of NLG evaluation practices 2005–2014. In *Proceedings of the 15th European Workshop on Natural Language Generation (ENLG)*, pages 57–60, 2015.
- [11] Chris Van Der Lee, Albert Gatt, Emiel Van Miltenburg, Sander Wubben, and Emiel Krahmer. Best practices for the human evaluation of automatically generated text. In *Proceedings of the 12th International Conference on Natural Language Generation*, pages 355–368, 2019.
- [12] Alberto Bartoli, Andrea De Lorenzo, Eric Medvet, and Fabiano Tarlao. Playing regex golf with genetic programming. In *Proceedings of the 2014 conference on Genetic and evolutionary computation*, pages 1063–1070. ACM, 2014.
- [13] Alberto Bartoli, Andrea De Lorenzo, Eric Medvet, and Fabiano Tarlao. Syntactical similarity learning by means of grammatical evolution. In *International Conference on Parallel Problem Solving from Nature*, pages 260–269. Springer, 2016.
- [14] Alberto Bartoli, Andrea De Lorenzo, Eric Medvet, and Fabiano Tarlao. Active learning of regular expressions for entity extraction. *IEEE transactions on cybernetics*, 48(3):1067–1080, 2017.
- [15] Tom B Brown, Benjamin Mann, Nick Ryder, Melanie Subbiah, Jared Kaplan, Prafulla Dhariwal, Arvind Neelakantan, Pranav Shyam, Girish Sastry, Amanda Askell, et al. Language models are few-shot learners. *arXiv preprint arXiv:2005.14165*, 2020.

Development of IoT Based Fresh Food Delivery Tracking System Using GPS

Man-Ching YUEN^{a,1}, Yip-Hin CHOI^b, Tsun-Hin NG^c, Chun-Tung POON^c and Kin-Chung FUNG^d

^a*Centre for Applied Data Science, Department of Journalism and Communication,
Hong Kong Shue Yan University, Hong Kong, China*

^b*School of Science and Technology, The Open University of Hong Kong,
Hong Kong, China*

^c*Department of Computer Science, Hong Kong Baptist University, Hong Kong, China*

^d*Department of Information Technology, Hong Kong Institute of Vocational Education
(Tsing Yi), Hong Kong, China*

Abstract. Home delivery service is an essential service for online shopping. The need for reliable delivery system to ensure freshness of foods is challenging with consumers' busy schedule and heavy traffic. An efficient fresh food delivery tracking system is designed and implemented for tracking the fresh food delivery ordered on an online shopping system. The proposed system made use of Internet of Things (IoT) technology, Global Positioning System (GPS) and a smart online shopping system. Using this GPS system, consumers are able to track their delivery and arrival of their grocery to ensure the freshness of products. To create the user-friendly access website, we have included four functions in this website: Online shopping cart, system to support various payment methods, GPS food tracking system, and members' easily access account data system. Since the cost of this fresh food delivery tracking system is low, it is suitable for online shop of start-ups.

Keywords. Internet of things; IoT; Global Positioning System; GPS; delivery tracking

1. Introduction

Continuous progress in technologies has led the development of new tools and programs for improving the quality of consumers' needs and satisfaction. Many enterprises keep their data at a cloud database that runs on a cloud computing platform and can be accessed at anytime at anywhere. Since the cloud technology offers pay-as-you-go payment policy, the cloud storage can be expanded as needed and enterprises can reduce costs on infrastructure. However, the security issue of data stored in the cloud is a big concern, especially for customers' personal information such as payment details. Therefore, many new payment methods, such as digital wallets, are launched, and customers have a lot of choices on e-payment methods. With rapid evolving

¹ Corresponding Author, Man-Ching YUEN, Centre for Applied Data Science, Department of Journalism and Communication. Hong Kong Shue Yan University, Hong Kong, China; E-mail: mcyuen@hksyu.edu.

technologies, newer technologies (e.g., Internet of Things, robots) and business models (e.g., member's subscription) emerged to embrace customers' consumption decisions [1]. The Internet of Things (IoT) describes the network of physical objects, which are embedded with sensors, software, and other technologies. By using different types of sensors, IoT devices can collect different real-time data, such as locations of sensors, temperatures, humidity, and occurrences of triggered events. With big data and predictive analytics, retailers can now offer better appealing offers, better target their customers, and develop better tools to encourage consumers to make purchase decisions. Meanwhile, consumers are receiving more beneficial offers to enable them to make more informed decisions [2].

Many factors that affect consumers' purchase decision. One concept, known as the "holistic customer experience" indicated that customer's cognitive, affective, emotional, social, and physical responses to the retailer is the success of a retailer among its competitors [3]. With technologies, retailers are progressing to meet the evolving consumer behaviors. These include using Internet of Things, virtual or augmented reality, robots, and artificial intelligence to help consumers to make good decisions and increase their satisfaction to purchase [4-5].

Online shopping has been shown to provide more satisfaction to consumers who seek for convenience and speed [6]. It is convenience because it opens 24 hours per day, and 7 days per week. Consumers are able to access the online shop at their convenient time as long as they can access the Internet. Although the customers rarely have a chance to touch and feel the product, they are able to get product information from website and products' reviews by other customers before making their purchase decision. This gives customers more chances to compare price from different websites and to find the product with a lower price than buying from local retailing stores. It also save time as customers do not have to stuck in the traffic, look for a parking spot, or wait in checkout lines [7]. Meanwhile, there are some factors that impede consumers from online shopping, such as unsecured payment, slow shipping, intangibility of online product, competition with branded products, and lack of social contact [8-11]. Hence, retailer should continue to improve or create effective online shopping tools that could ease the customers concerns to persuade customer to use their online shopping system [12].

The basic purpose of a low-cost fresh food delivery tracking system is to track a specific target fresh food ordered on an online shopping system. The vehicle for fresh food delivery has a tracking device which uses Global Positioning System (GPS) module to get its current location and inform the customers by updating the information in the database of the online shopping system. The tracking device is a type of IoT device. The Global Positioning System (GPS) is a satellite-based navigation system made up of at least 24 satellites, which is owned by the United States government. The satellites constantly send out signals, while the receiver in a GPS module listens for these signals. Once the receiver in a GPS module calculates its distance from four or more GPS satellites, it can figure out the location of the GPS module. In this way, GPS can effectively get the real-time location information from satellites in the form of latitude, and it is commonly used in many vehicle tracking systems. By using GPS, our online shopping system can give confident to customers on the fresh food delivery process. As the cost of this fresh food delivery tracking system is low, it is suitable for online shop of start-ups. The proposed vehicle tracking system connecting with an online system is not only suitable for fresh food delivery, but it has many applications, such as agricultural farming monitoring system to monitor automatic tasks done by

robots. Since the cost of hardware is low, it is very suitable for start-ups to develop their own system. The fresh food delivery tracking system proposed in the paper has the following objectives:

- To obtain geographic location of vehicle carrying target fresh food in real-time using the GPS module
- To transmit the geographic location of vehicle carrying target fresh food to the web server after a specified time interval using the mobile network signal
- To design a database to store and manage received vehicles' location information
- To allow customers to view the location of vehicle on Google map when he sends out a request on the online shopping system
- To allow customers to get the estimated delivery time of ordered fresh food

2. Related Works

2.1. Vehicle Tracking Systems

Vehicle tracking systems attracted much attention in the past years [13], such as anti-theft tracking system [14-15], vehicle detection and tracking system [16], bus tracking system [17] and web-based vehicle tracking system [18].

2.1.1. Anti-theft tracking system

Maurya et al. [14] proposed an anti-theft vehicle tracking system. It is used for tracking and positioning of any vehicle by using GPS and GSM technology. The system continuously monitors a moving vehicle and reports the status of the vehicle on demand. The system can automatically send a reply to the requesters on indicating the position of the vehicle in terms of latitude and longitude in real time. Liu et al. [15] proposed a vehicle anti-theft tracking system which is controlled by an RFID model to switch on and off. When the car is stolen, the sensors mounted inside the vehicles are triggered, and the system will send the location information collected by the GPS module to the owner's mobile phone. The owner can track the position of the stolen car.

2.1.2. Vehicle detection and tracking system

Li [16] proposed a moving vehicle detection and tracking system, which consists of road detection, vehicle detection and vehicle tracking. The road detection algorithm can detect either well-structured or unstructured roads, so the system works well at outdoor environment in real-time mode.

2.1.3. Bus tracking system

Eken and Sayar [17] proposed a smart bus tracking system that allows passengers to use scan QR placed at bus stop to view estimated bus arrival times and buses' current locations and bus routes on a map.

2.1.4. Web-based vehicle tracking system

Salim and Idrees [18] proposed a web-based vehicle tracking system enables enterprises owners to check and track the present and past position recorded of the target vehicles on Google Map in a specified website. It is a challenge and opportunity to develop a website of specified application which can make good use of vehicle tracking system by using GPS technology.

2.2. Fresh Food Delivery Systems

There exist a number of previous works on fresh food delivery systems [19-22]. Hsu et al. [19] proposed a solution for the vehicle routing problem which is to minimize not only the fixed costs for dispatching vehicles, but also the transportation costs for violating time-windows. They suggested that the solution is suitable for the perishable food delivery. Nakandala et al. [20] developed an intelligence total cost model that includes various costs incurred during transportation from farms to retailers by using genetic algorithms and fuzzy genetic algorithms. Wang and Yin [21] proposed a model for optimal route selection, temperature control and the average speed of vehicle for fresh food delivery. Chen et al. [22] proposed a model for optimal route selection for minimizing emission of carbon dioxide. However, all existing work are evaluated by simulation experiments or mathematical model, and do not consider the way on how to inform the customers' updated information as soon as possible. One of the main contributions of our work is to develop a prototype of online shopping system which allows consumers to get the latest information of fresh food delivery by using IoT devices and GPS technology.

3. Methodology Implemented

3.1. Project Scope

The HKMall online shopping system is designed for 4 main users: Administrator, Staff, Member and Visitor. The administrators have the full access to the system. The staff can manage the foods information and assist customers to handle their requests or questions. The visitors/members can browse the website and make their purchase decision. Figure 1 shows the system overview.

Our online shopping system has 4 parts:

- Online shopping cart – Members add their favorite items to the shopping cart system for purchase.
- Support new generation of payment methods – When members making purchases on our online shopping system in Safari on their iPhone, iPad, or Mac, they can use Apple Pay without having to create an account or fill out lengthy forms. Additionally, with Touch ID on MacBook Pro, making payment transaction is quicker, easier, and more secure with this system.
- Track Arrival for ordered goods by GPS – When the order was paid, members can go to the ‘Personal’ page to review the purchase progress. We also provide GPS tracking system to track the real-time location of the ordered goods to make sure the goods can be delivered within a reasonable time to ensure the freshness of

goods. By using Google Map API, the GPS tracking system also show a suggested route offered by Google Map API.

- Ease of accessing user data – Members can access their data easily. These data include their purchase histories and account information



Figure 1. System overview

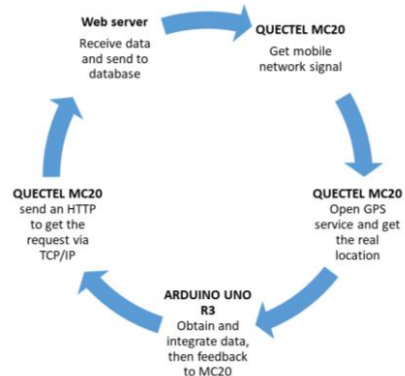


Figure 2. GPS tracking system

3.2. GPS Tracking System

Figure 2 shows the GPS structure of the HKMall system. QUECTEL MC20 is the core of our GPS system. It provides GPS service to obtain real-time location via mobile network signal. When the location data (i.e., latitude and longitude) was obtained and integrated, data will feedback to the QUECTEL MC20. Then, QUECTEL MC20 will send HTTP to get the request via TCP/IP. Finally, the data will be sent to Web server and uploaded to our database. An illustrative example is shown in Figure 3.

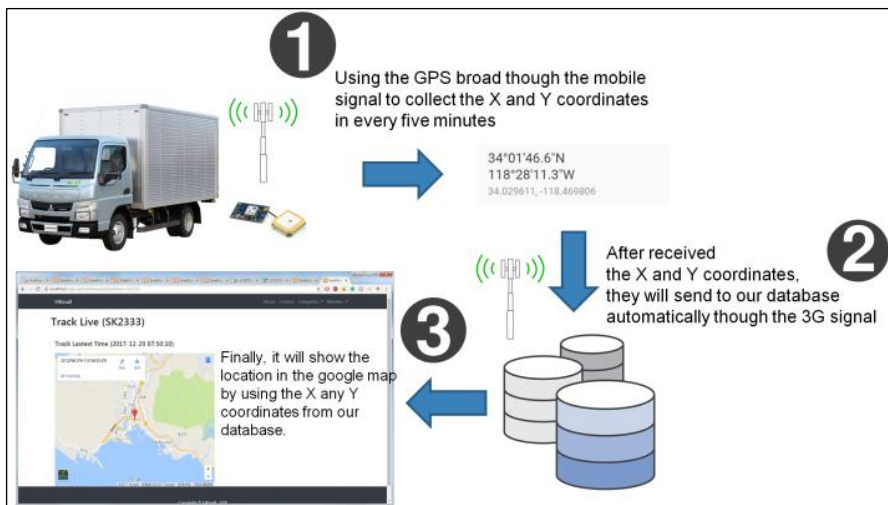


Figure 3. An illustrative example for our GPS tracking system

3.3. System requirements

For software requirement, we use the following software during our system development:

- PHP - it is used for webpage design
- PHPMyAdmin - it is used for database administration
- NetBeans - it is used for web development tool
- Arduino IDE - it is used to develop our tracking system (as shown in Figure 4)

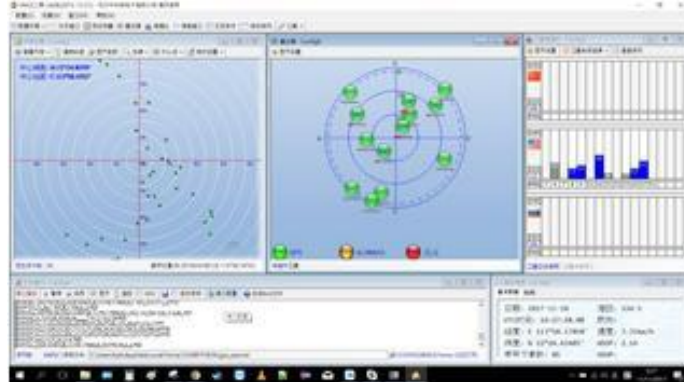


Figure 4. Coding for tracking system in Arduino IDE

For hardware requirement, we used low-cost hardware for our system development for cost effectiveness. They are:

· QUECTEL MC20 sensor (Figure 5) - It is a high-performance GPS positioning module and it's in tiny size. It works with AT command and includes Bluetooth 3.0 to support SIM and USIM card.

· ARDUINO UNO R3 motherboard (Figure 6) - A microcontroller board based on the ATmega328P. It has 14 digital input/output pins, 6 analog inputs, a 16 MHz quartz crystal, a USB connection, a power jack, an ICSP header and a reset button.



Figure 5. QUECTEL MC20 sensor



Figure 6. ARDUINO UNO R3 motherboard

4. Result

In the online shopping system, after customers selecting target product (Figure 7) and choose the payment method (Figure 8), they can check the purchase record. After the order was shipped, the GPS function will start at the same time and customers can click the “More Details” (Figure 9). The consumer can track the location of their product by

clicking on the “Click me to check real-time tracking” (Figure 10). The location will be updated automatically every 5 minutes (Figure 11).

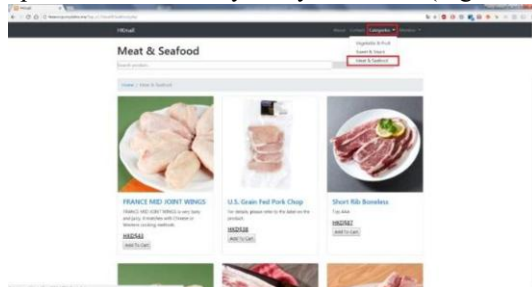


Figure 7. Features of the food categories

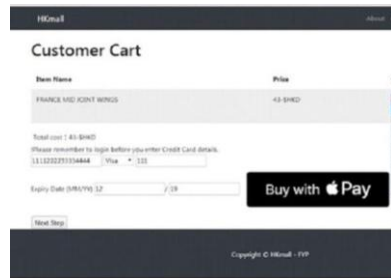


Figure 8. Payment page



Figure 9. Checking on shipment

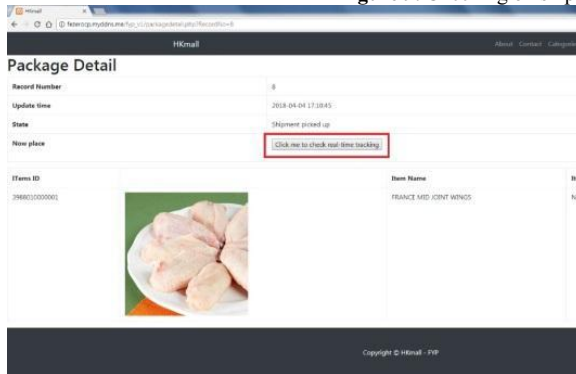


Figure 10. Tracking system

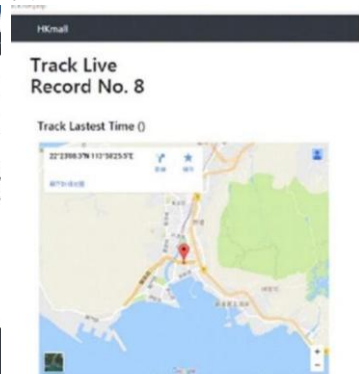


Figure 11. Real-time GPS tracking system

5. Conclusion and Future Work

In this paper, we have proposed a low-cost fresh food delivery tracking system by using GPS technology. The tracking device can rely on information concerning the current location of the vehicle and update the information in the database of the online shopping system. Consumers can track the delivery and arrival of their grocery products to ensure the freshness of products. Additionally, the GPS system allows the consumers to manage their schedule more efficiently as they do not need to stay at home to wait for the package arrival after ordering their goods. As the cost of this fresh food delivery tracking system is low, it is suitable for online shop of start-ups. As huge amount of data on food purchase and delivery is collected, we can use these data to analyze and obtain an optimized schedule and route for food delivery. In the future

work, we will investigate route selection for food delivery, especially for the case that we have a lot of bookings but not enough means for delivery.

References

- [1] Grewal D, Roggeveen AL & Nordfält, J (2017), The Future of Retailing. *Journal of Retailing* 93, 1-6.
- [2] Inman JJ & Nikolova H (2017), Shopper-Facing Retail Technology: A Retailer Adoption Decision Framework Incorporating Shopper Attitudes and Privacy Concerns. *Journal of Retailing* 93, 7-28.
- [3] Verhoef PC, Lemon KN, Parasuraman A, Roggeveen A, Tsilos M & Schlesinger LA (2009), Customer Experience Creation: Determinants, Dynamics and Management Strategies. *Journal of Retailing* 85, 31-41.
- [4] Deloitte (2016), Retail Trends in 2016, (accessed October 11, 2018), <https://www2.deloitte.com/qa/en/pages/consumer-business/articles/retail-trends-2016.html>
- [5] Salman A, Abdullah MYH, Aziz J, Ahmad AL & Kee CP (2013), Utilising information and communication technologies (ICT) for development: What research contributes. *Journal of Asian Pacific Communication* 23, 239-251.
- [6] Yu T & Wu G (2007), Determinants of internet shopping behaviour: an application of reasoned behaviour theory. *International Journal of Management* 24, 744-762.
- [7] Childers TL, Carr CL, Peck J & Carson S (2001), Hedonic and utilitarian motivations for online retail shopping behavior. *Journal of Retailing* 77, 511-535.
- [8] Abd. Mukti N (2017), Barriers to putting businesses on the internet in Malaysia. *The Electronic Journal of Information Systems in Developing Countries* 2, 1-6.
- [9] Katawetawarks C & Wang CL (2011), Online Shopper Behavior: Influences of Online Shopping Decision. *Asian Journal of Business Research* 1, 66-74.
- [10] Shah Alam S & Mohd. Yasin N (2010), The antecedents of online brand trust: Malaysian evidence, *Journal of Business Economics and Management* 11, 210-226.
- [11] Omar NA, Shah Alam S, Abdul Aziz N & Nazri MA (2011), Retail Loyalty Programs in Malaysia: The Relationship of Equity, Value, Satisfaction, Trust, and Loyalty among Cardholders, *Journal of Business Economics and Management* 12, 332-352.
- [12] Shah MH, Peikari HR & Mohd. Yasin N (2014), The determinants of individuals' perceived e-security: Evidence from Malaysia. *International Journal of Information Management* 34, 48-57.
- [13] Dukare, S. S., Patil, D. A., & Rane, K. P. (2015). Vehicle tracking, monitoring and alerting system: a review. *International Journal of Computer Applications*, 119(10).
- [14] Maurya, K., Singh, M., & Jain, N. (2012). Real time vehicle tracking system using GSM and GPS technology-an anti-theft tracking system. *International Journal of Electronics and Computer Science Engineering*. ISSN, 22771956, V1N3-1103.
- [15] Liu, Z., Zhang, A., & Li, S. (2013, July). Vehicle anti-theft tracking system based on Internet of things. In Proceedings of 2013 IEEE International Conference on Vehicular Electronics and Safety (pp. 48-52). IEEE.
- [16] Li, X., Yao, X., Murphey, Y. L., Karlsen, R., & Gerhart, G. (2004, August). A real-time vehicle detection and tracking system in outdoor traffic scenes. In Proceedings of the 17th International Conference on Pattern Recognition, 2004. ICPR 2004. (Vol. 2, pp. 761-764). IEEE.
- [17] Eken, S., & Sayar, A. (2014, June). A smart bus tracking system based on location-aware services and QR codes. In 2014 IEEE International Symposium on Innovations in Intelligent Systems and Applications (INISTA) Proceedings (pp. 299-303). IEEE.
- [18] Salim, K. A., & Idrees, I. M. (2013). Design and implementation of web-based GPS-GPRS vehicle tracking system. *International Journal of Science, Engineering and Computer Technology*, 3(12), 443.
- [19] Hsu, C.I., Hung, S.F. and Li, H.C., 2007. Vehicle routing problem with time-windows for perishable food delivery. *Journal of food engineering*, 80(2), pp.465-475.
- [20] Nakandala, D., Lau, H. and Zhang, J., 2016. Cost-optimization modelling for fresh food quality and transportation. *Industrial Management & Data Systems*.
- [21] Wang, Y.M. and Yin, H.L., 2018. Cost-optimization problem with a soft time window based on an improved fuzzy genetic algorithm for fresh food distribution. *Mathematical Problems in Engineering*, 2018.
- [22] Chen, J., Gui, P., Ding, T., Na, S. and Zhou, Y., 2019. Optimization of Transportation Routing Problem for Fresh Food by Improved Ant Colony Algorithm Based on Tabu Search. *Sustainability*, 11(23), p.6584.

Consistency-Check Edge Refinement for Deep Stereo Matching

Fangrui Wu, Menglong Yang ¹

*School of Aeronautics and Astronautics, Sichuan University
Chengdu, Sichuan, PR China*

Abstract. Recent end-to-end CNN-based stereo matching algorithms obtain disparities through regression from a cost volume, which is formed by concatenating the features of stereo pairs. Some downsampling steps are often embedded in constructing cost volume for global information aggregation and computational efficiency. However, many edge details are hard to recover due to the imprudent upsampling process and ambiguous boundary predictions. To tackle this problem without training another edge prediction sub-network, we developed a novel tightly-coupled edge refinement pipeline composed of two modules. The first module implements a gentle upsampling process by a cascaded cost volume filtering method, aggregating global information without losing many details. On this basis, the second module concentrates on generating a disparity residual map for boundary pixels by sub-pixel disparity consistency check, to further recover the edge details. The experimental results on public datasets demonstrate the effectiveness of the proposed method.

Keywords. Cascaded cost volume filtering, Deep learning, Edge refinement, Stereo matching, Sub-pixel consistency check

1. Introduction

Recently stereo matching has become a research hotspot, aiming at finding corresponding pixels for stereo pairs. And it has been widely applied to autonomous driving, robotics, 3D object detection, computational photography, virtual and augmented reality [1]. For traditional stereo matching methods, a typical four-step framework has been established and widely used, composed of matching cost calculation, cost aggregation, optimization and final disparity refinement, respectively.

This paper proposes a novel tightly-coupled edge refinement pipeline composed of two modules, to gently upsample cost volumes and effectively recover edge details. The main contributions of this paper are listed as follows:

- We propose a tightly-coupled edge refinement pipeline to effectively recover edge details.
- We design a cascaded cost volume filtering module, to aggregate sufficient global context information without losing many details.

¹Corresponding Author; E-mail: steinbeck@163.com.

- We design a sub-pixel disparity consistency refinement module to effectively refine the disparity prediction for boundary pixels.
- Our model achieves state of the art on SceneFlow benchmark [2], and comparable performance on KITTI benchmark [3][4].

2. Related Work

CNN have been widely adopted in deep learning stereo matching algorithms. J. Zbontar and Y. LeCun [5] pioneered a CNNs-based siamese network for stereo matching. Pang *et al.* [6] proposed a cascaded CNN architecture, to refine disparity by learning multi-scale residuals. Godard *et al.* [7] fused the left-right disparity consistency check loss into its loss function to train a better monocular depth estimation network. Zhang *et al.* [8] supervised thier network through calculating the pixel intensity difference between the original input image and reconstruction of input image generated by left-right disparity consistency mechanism. Enlightened by [8], we perform a sub-pixel left-right consistency check on groundtruth disparity of the stereo pair, to acquire a fine-grained inconsistent map consists of boundary pixels. And we supervise the disparity residual with the inconsistent map to effectively improve the refinement performance.

3. Approach

The proposed architecture is mainly composed of four modules: multi-resolution feature extraction, multi-resolution cost volumes, cascaded cost volume filtering and sub-pixel disparity consistency refinement, as shown in Figure. 1.

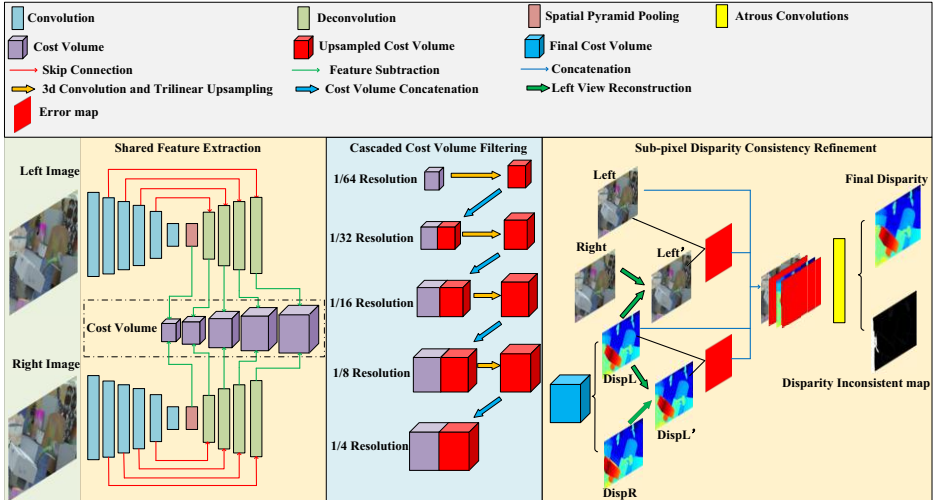


Figure 1. The architecture of our proposed network.

3.1. Multi-resolution Feature Extraction

Inspired by several multi-scale feature extraction methods, such as ASPP [9], 4P [10] and image pyramid [11], we propose a multi-resolution feature extraction architecture. The architecture is composed of a weight-share siamese network with hourglass structure and skip connections, as shown in Figure. 1, to encode local and global contextual information for stereo pairs.

3.2. Multi-resolution Cost Volumes

Multi-resolution cost volumes are directly generated by multi-resolution features extracted in the previous step. There are three typical approaches for cost volume construction, including dot products [2], concatenation [12] and absolute difference [13] between features. To aggregate sufficient context information, we construct cost volumes by the way of simply calculating absolute difference.

3.3. Cascaded Cost Volume Filtering

Different from [14], we propose a cascaded cost volume filtering method. Instead of upsampling and refining the initial disparity map of low resolution, we directly upsample cost volumes formed in the previous step. We perform four 3D convolutions with $3 \times 3 \times 3$, as shown in Fig. 1. filter and stride of 1, to obtain a new cost volume,

3.4. Disparity Regression

For disparity regression, we use soft argmin operation proposed in [8],

$$D = \sum_{d=0}^{D_{max}} d \times P(d) \quad (1)$$

where D is the estimated disparity map, and $P(d)$ is the softmax operation to the filtered cost along the disparity dimension.

3.5. Sub-pixel Disparity Consistency Refinement

This module aims at effectively recovering edge details for initial disparity prediction. We implement a simple addition between initial left disparity and disparity residual map. A ReLu activation is followed to keep all disparity values greater than 0:

$$D_{\hat{a}} = \sigma \times D_b + (1 - \sigma) \times D_c \quad (2)$$

$$\Phi = \{a | D_a - D_{\hat{a}} > 1\} \quad (3)$$

where D denotes disparity, and Φ is a set for inconsistent pixels, which form our inconsistent groundtruth. Note that, we choose pixels whose original disparity is one-pixel distance larger than the reprojection one as our inconsistent map. We do not choose pixels whose reprojection disparity is larger, for the purpose of avoiding joining occluded pixels in our inconsistent map, as shown in Fig. 2.

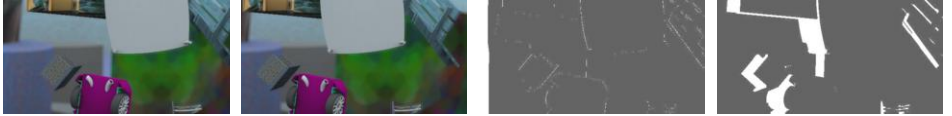


Figure 2. Examples of different groundtruth disparity inconsistent map, from left to right: left input images, right input images, edge-aware inconsistent map without occluded pixels, inconsistent map with occluded pixels. (Better zoom in to view)

3.6. Loss

We train our model with supervised learning using both groundtruth disparity data and disparity inconsistent map generated by the aforementioned method ,

$$\begin{aligned} L_1 = \alpha \times & \left(\frac{1}{N} \sum_{i=1}^N \text{smooth}_{L_1}(\hat{l}_i - l_i) + \frac{1}{N} \sum_{i=1}^N \text{smooth}_{L_1}(\hat{r}_i - r_i) \right) \\ & + \beta \times \left(\frac{1}{N} \left(\sum_{i=1}^N \text{smooth}_{L_1}(\hat{l}_i - l_i) \right) \right) \end{aligned} \quad (4)$$

in which

$$\text{smooth}_{L_1}(x) = \begin{cases} 0.5x^2, & \text{if } |x| < 1 \\ |x| - 0.5, & \text{otherwise} \end{cases}, \quad (5)$$

where N is the total number of pixels in a single input image, l_i and r_i are left and right groundtruth disparity value of pixel i respectively. \hat{l}_i and \hat{r}_i are the initial left and right prediction disparity value of pixel i respectively. And \hat{l}_i is the final left prediction disparity value of pixel i .

We utilize the second term to supervise the disparity inconsistent prediction, the loss is defined as:

$$L_2 = \frac{1}{N} \sum_{i=1}^N (-p_i \log(1 - \hat{p}_i) - (1 - p_i) \log \hat{p}_i) \quad (6)$$

where p_i and \hat{p}_i are groundtruth and prediction of disparity inconsistent value for pixel i , respectively.

Finally, we train the model using an end-to-end supervised learning mechanism with following joint loss function:

$$\mathcal{L} = L_1 + \gamma * L_2 \quad (7)$$

4. Experiment

4.1. Datasets and Implementation

Datasets: We test the proposed architecture on Sceneflow and KITTI datasets in this work.

Implementation: We implemented the proposed architecture by using Pytorch, and we trained the whole network with the stochastic optimization algorithm of Adam [15], where $\beta_1 = 0.9$, $\beta_2 = 0.999$ and $\varepsilon = 10^{-8}$. We firstly trained our network with a batch size of 12 on two Titan RTX GPUs using 256×512 randomly cropped stereo pairs from SceneFlow training set. We set the max disparity to 192. We performed color normalization on the whole datasets before training. We set the initial learning rate to 0.001, and kept it unchanged for the first 10 epochs, and halved for the following 4 epochs, finally we fixed the learning rate to 0.0001 to the end (25 epochs). We retrained the model on KITTI dataset for an extra 600 epochs, with learning rate of 0.001 for the first 300 epochs and 0.0001 for the last 300 epochs. And we set $\alpha = 1$, $\beta = 1.2$ and $\gamma = 0.4$ in Eq. (4) and Eq. (7) respectively.

4.2. Ablation Study

In this section, we demonstrate the effectiveness of the proposed modules by presenting several ablation experiment results on SceneFlow. The experiment results are shown in Table 1. And we also test the performance of proposed model trained with different α , β and γ on SceneFlow, as shown in Table 2.

Table 1. Ablation study of different network architecture settings on SceneFlow. CR represents the resolution of final cost volume, and BI represents upsampling operation by simple bilinear interpolation.

CR	Network Architecture					SceneFlow	
	Upsampling method			Edge refinement		EPE	time
	BI	CDF	CCVF	TDRA	SDCR		
1/8	✓					2.01	0.05s
1/8		✓				1.65	0.06s
1/8			✓			1.12	0.08s
1/8			✓	✓		1.05	0.09s
1/8			✓		✓	0.88	0.09s
1/4			✓	✓		0.93	0.27s
1/4			✓		✓	0.81	0.28s

Table 2. Comparing results of proposed model trained with different combinations of loss weight on SceneFlow testing datasets.

Parameters			EPE
α	β	γ	
0.8	1.0	-	1.07
1.0	1.2	-	0.98
1.2	1.4	-	1.04
1.0	1.2	0.2	0.88
1.0	1.2	0.4	0.81
1.0	1.2	0.6	0.85

Our cascaded cost volume filtering module and sub-pixel disparity consistency refinement module are abbreviated to CCVF and SDCR respectively in Table 1, and other annotations are listed as follows:

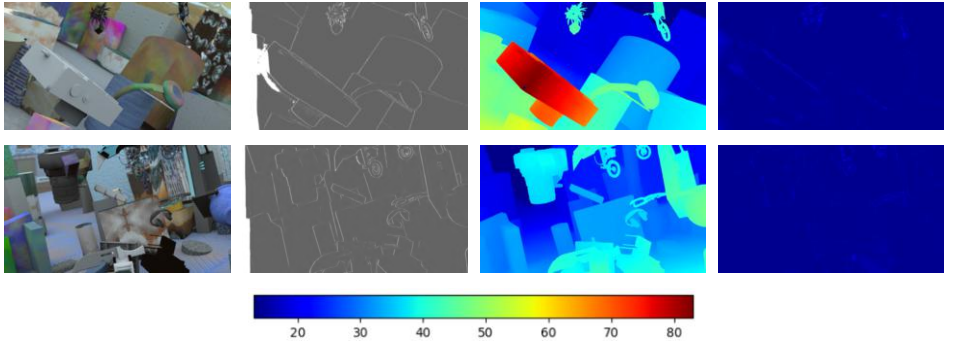


Figure 3. Qualitative results of SceneFlow testing set. From left to right: left input image, inconsistent prediction, disparity prediction and error map. The last row is the color bar for error maps. (Better zoom in to view)

End Point Error (EPE). The average absolute difference between disparity prediction and groundtruth for testing pixels.

Cascaded Disparity refinement (CDF). This module bilinearly upsamples the disparity map, then downsamples the input to the same resolution, and implements several atrous convolutions to obtain the disparity residual level by level.

Training Disparity Residual Alone (TDRA). This module outputs disparity residual map by implementing several atrous convolutions on an input volume, which concatenates original left input image and disparity prediction of full resolution.

4.3. Comparison With Other Methods

We trained two models $\frac{1}{8}$ and $\frac{1}{4}$ resolution of cost volumes, and we compared the EPE on Sceneflow testing datasets with other state-of-the-art methods, The evaluation results is shown in Table 3.

Table 3. Comparing results of stereo matching algorithms on the SceneFlow testing datasets.

Non-Real-Time	GC-Net [8]	SegStereo [16]	PSMNet [17]	DeepPruner(Best) [18]	Proposed(Best)
EPE	2.51	1.45	1.09	0.86	0.81
time	900ms	600ms	410ms	200ms	280ms
Real-Time	DispNetC [2]	StereoNet [14]	DeepPruner(Fast) [18]	Proposed(Fast)	
EPE	1.68	1.10	0.97	0.88	
time	60ms	17ms	62ms	90ms	

To prove the effectiveness of the proposed method on boundary and occluded pixels, we performed another evaluation on these pixels of Sceneflow testing datasets , respectively. And we compared the testing results with PSMNet [17] and DeepPruner(best) [18], and the result is presented in Table 4.

Then we evaluate our best version model on KITTI. We compare the error rates of our model with several published compelling algorithms on KITTI 2012 and KITTI 2015 datasets respectively. And the comparing results are shown in Table 5 and Table 6.

Our method achieves the three-pixel error rate of 2.18% in KITTI 2012 and 2.50% in KITTI2015, which is better than EdgeStereo [19]. And our method significantly outperforms these algorithms and achieves state-of-the-art performance on SceneFlow.

Table 4. Comparing results of boundary and occluded pixels on the SceneFlow testing datasets.

Method	EPE (boundary)	EPE (boundary + pixels)	EPE (all pixels)	Runtime
PSMNet [17]	3.96	2.92	1.09	0.41 s
DeepPruner(best) [18]	3.81	2.74	0.86	0.2 s
Proposed	3.73	2.66	0.81	0.28 s

Table 5. Testing results of KITTI 2012 [3].

Method	Out-Noc	Out-All	Avg-Noc	Avg-All	Runtime
PSMNet [17]	1.49 %	1.89 %	0.5 px	0.6 px	0.41 s
EdgeStereo [19]	1.73 %	2.18 %	0.5 px	0.6 px	0.48 s
GC-NET [8]	1.77 %	2.30 %	0.6 px	0.7 px	0.9 s
Proposed	1.80 %	2.30 %	0.5 px	0.6 px	0.28 s

Table 6. Testing results on KITTI 2015 [1].

Method	D1-bg	D1-fg	D1-all	Time
DeepPruner [18]	1.87 %	3.56 %	2.15 %	0.28 s
PSMNet [17]	1.86 %	4.62 %	2.32 %	0.41 s
EdgeStereo [19]	2.27 %	4.18 %	2.59 %	0.27 s
Proposed	2.11 %	4.46 %	2.50 %	0.28 s

5. Conclusion

In this paper, we propose a novel end-to-end deep learning architecture, aiming at effectively giving consideration to both global and local areas for stereo matching. To achieve this goal, we developed a cascaded cost volume filtering module to aggregate sufficient global information without losing many details. Besides, we designed a sub-pixel disparity consistency refinement module to further recover edge details for local areas.

6. Acknowledgements

This work is supported by the National Natural Science Foundation of China (Grant No. U1933134, U1833128), National Key R&D Program of China (Grant No. 2018YFC0809500), Sichuan Science and Technology Program (Grant No. 2018JY0602, 2018GZDZX0024, 2020YFG0134), and the funding from Sichuan University (Grant No. 2018SCUH0042).

References

- [1] Menze M, Geiger A. Object scene flow for autonomous vehicles. Proceedings of the IEEE Conference on Computer Vision and Pattern Recognition; 2015; p. 3061-70.
- [2] Mayer N, Ilg E, Hausser P, Fischer P, Cremers D, Dosovitskiy A, Brox T. A large dataset to train convolutional networks for disparity, optical flow, and scene flow estimation. Proceedings of the IEEE Conference on Computer Vision and Pattern Recognition; 2016; p. 4040-8.
- [3] Geiger A, Lenz P, Urtasun R. Are we ready for autonomous driving? the kitti vision benchmark suite. Proceedings of the IEEE Conference on Computer Vision and Pattern Recognition; 2012; p. 3354-61.
- [4] Menze M, Geiger A. Object scene flow for autonomous vehicles. Proceedings of the IEEE Conference on Computer Vision and Pattern Recognition; 2015; p. 3061-70.

- [5] Zbontar J, LeCun Y. Computing the stereo matching cost with a convolutional neural network. Proceedings of the IEEE Conference on Computer Vision and Pattern Recognition; 2015; p. 1592-9.
- [6] Pang J, Sun W, Ren JS, Yang C, Yan Q. Cascade residual learning: A two-stage convolutional neural network for stereo matching. Proceedings of the IEEE International Conference on Computer Vision Workshops; 2017; p. 887-95.
- [7] Godard C, Mac Aodha O, Brostow GJ. Unsupervised monocular depth estimation with left-right consistency. Proceedings of the IEEE Conference on Computer Vision and Pattern Recognition; 2017; p. 270-9.
- [8] Zhang Y, Khamis S, Rhemann C, Valentin J, Kowdle A, Tankovich V, Schoenberg M, Izadi S, Funkhouser T, Fanello S. Activestereonet: End-to-end self-supervised learning for active stereo systems. Proceedings of the European Conference on Computer Vision; 2018, p. 784-801.
- [9] Chen LC, Papandreou G, Kokkinos I, Murphy K, Yuille AL. Deeplab: Semantic image segmentation with deep convolutional nets, atrous convolution, and fully connected crfs. IEEE Transactions on Pattern Analysis and Machine Intelligence. 2017;40(4):834-48.
- [10] Park H, Lee KM. Look wider to match image patches with convolutional neural networks. IEEE Signal Processing Letters. 2016;24(12):1788-92.
- [11] Choudhary BK, Sinha NK, Shanker P. Pyramid method in image processing. Journal of Information Systems and Communication. 2012;3(1):269.
- [12] Kendall A, Martirosyan H, Dasgupta S, Henry P, Kennedy R, Bachrach A, Bry A. End-to-end learning of geometry and context for deep stereo regression. Proceedings of the IEEE International Conference on Computer Vision; 2017; p. 66-75.
- [13] Yang G, Manela J, Happold M, Ramanan D. Hierarchical deep stereo matching on high-resolution images. Proceedings of the IEEE Conference on Computer Vision and Pattern Recognition; 2019; p. 5515-24.
- [14] Khamis S, Fanello S, Rhemann C, Kowdle A, Valentin J, Izadi S. Stereonet: Guided hierarchical refinement for real-time edge-aware depth prediction. Proceedings of the European Conference on Computer Vision; 2018; p. 573-90.
- [15] Kingma DP, Ba J. Adam: A method for stochastic optimization. Proceedings of the International Conference for Learning Representations; 2015.
- [16] Yang G, Zhao H, Shi J, Deng Z, Jia J. Segstereo: Exploiting semantic information for disparity estimation. Proceedings of the European Conference on Computer Vision; 2018; p. 636-51.
- [17] Chang JR, Chen YS. Pyramid Stereo Matching Network. Proceedings of the IEEE Conference on Computer Vision and Pattern Recognition; 2018; p. 5410-8.
- [18] Duggal S, Wang S, Ma WC, Hu R, Urtasun R. Deeppruner: Learning efficient stereo matching via differentiable patchmatch. Proceedings of the IEEE International Conference on Computer Vision; 2019; p. 4284-93.
- [19] Song X, Zhao X, Hu H, Fang L. Edgestereo: A context integrated residual pyramid network for stereo matching. Proceedings of the Asian Conference on Computer Vision; 2018; p. 20-35.

The Design of ERP Intelligent Sales Management System

Jianghui Liu^{a,1}, Qiuyi Chen^b and Yuexing Qiu^c

^a*Network and Information Center, Experimental Teaching Center, Guangdong University of Foreign Studies, China*

^b*School of Business, Guangdong University of Foreign Studies, China*

^c*School of Economics and Trade, Guangdong University of Foreign Studies, China*

Abstract. With the popularization of informatization, most companies have their own information management systems. However, faced with massive amounts of data, most companies cannot integrate and utilize its potential value. When traditional companies make sales forecasts, they usually purchase data completion, connect multiple data source channels, and then judge the future sales situation perceptually. This lack of data accumulation and analysis, and it is impossible to display the intrinsic value of the massive data in the system. Some companies will also build professional data analysis teams or seek help from third-party companies. But this will cause high expenses and greatly reduce sales expenses. This study combines artificial intelligence technology with ERP sales management system. We apply artificial intelligence, machine learning, cloud computing to the design and construction of intelligent ERP sales management system. It solves the core problems of enterprise product sales through the deep learning function of the sales system. It may predict enterprise sales and rationally allocate enterprise resources, increase product sales effectively, and help enterprises build effective modern management systems.

Keywords. ERP, Sales Management, Artificial Intelligence, Deep Learning

1 Preface

Enterprises should effectively use the huge amount of accumulated data. Enterprises may explore the value behind the data. This study will help enterprises improve the traditional ERP system. The study integrates big data, cloud computing, artificial intelligence into the traditional ERP system. And the new system may make sales forecasts for the enterprise. It will reduce inventory costs and improve business efficiency.

How do companies keep up with the development of technologies to improve the sales management? This study may give enterprises some enlightenment.

¹ Corresponding Author: Jianghui Liu, Network and Information Center, Experimental Teaching Center, Guangdong University of Foreign Studies, China; Email: maggyliu1978@163.com

2 Studies review

2.1 Background

In China, small and medium-sized enterprises have small production scales, weak technological research, development capabilities and weak anti-risk capabilities. The impact of the corona virus alone has caused many small and medium enterprises to close down. For such small and medium-sized enterprises, how to adapt to the ever-changing customer needs under the inherent background and how to keep up with the speed of economic globalization are all issues that worth considering. With the trend of economic globalization, the advantage of China's cheap labor is not existing. A large number of enterprises withdraw from my China, which has brought a rapid withdrawal of capital and technology. In response to its impact, China has begun to improve the competitiveness of enterprises through technological innovations and lower operating costs.

At present, managers only make some decisions based on former experience and decision makers' intuition, rather than based on information-rich data in the database. Meanwhile, it is difficult for traditional forecasting methods to take into account the information brought by complex and diverse data. Therefore, traditional forecasting methods have no way to meet the increasing requirements of enterprises for sales demand. The accuracy of traditional sales forecasting of enterprises is becoming lower and lower.

ERP intelligent sales forecast is only in its infancy in China, especially for small and medium-sized enterprises that have not yet had the concept of intelligent ERP. At present, companies have an urgent need for intelligent ERP to achieve accurate sales forecasts and enhance their competitiveness. The ERP intelligent sales system helps companies find reliable forecasting information from a large amount of historical data, analyze the correlation between products and customers, and analyze the correlation between products and suppliers, and then use machine learning to train the model to improve accuracy.

2.2 Development status and shortcomings of ERP sales system at home and abroad

The development of artificial intelligence is rapid in recent years. The demand of enterprises in the application of artificial intelligence and cloud platforms is becoming more and more popular. PwC's 22nd Annual Global CEO Survey shows that 85% of CEOs believe that artificial intelligence will have a significant impact on companies and their business models in the next five years. However, the scope of application of artificial intelligence in enterprise management is still limited so far. Less than one-tenth of the CEO said that artificial intelligence is being widely used. In addition, according to a report released by Panorama Consulting in early 2020, only 33% of suppliers use cloud services or provide cloud-based services. About 67% of companies still use local ERP systems. It shows that companies should use cloud-based ERP and it can take the lead in artificial intelligence. [1]

Both artificial intelligence and ERP can provide good services to enterprises. It can optimize and improve management decision-making. It can also improve the sales efficiency of enterprises. Therefore, the combination of the two will have broad development prospects. Cloud service providers have applied and promoted big data technologies, such as block chain and cloud computing at the same time. It uses

machine learning to process massive amounts of data information. It has increased the efficiency of cloud sharing and the level of user demand for cloud sharing services. [2]

The previous research and project applications were mainly in the fields of financial management, salary management, warehouse management and so on. The previous research has less involved in sales management. With the continuous improvement of the market mechanism, the amount of relevant data information continues to grow rapidly. The importance of sales information management in the enterprise continues to increase. It is becoming one of the core tasks of the enterprises [3]. However, the sales management system still has some problems of single development means, such as its limited system service items and low technical content. It makes the overall application effect of the system and the actual business needs a large gap.

This study discusses the design of the ERP sales management system based on artificial intelligence technology. It uses the latest artificial intelligence, big data processing and analysis technology, cloud computing, blockchain to build an artificial intelligence-based sales management system in the ERP environment. It also solves the core problems of enterprise product sales. And it helps enterprises build an effective way of modern management system and realize the leapfrog development from relying on experience to make sales forecasts to technology.

3 Theory and related technology

3.1 Artificial Intelligence

Artificial intelligence completes identification, understanding, analysis, and decision-making through replacing humans with the development of human-related theories, technologies, and application systems. The popularity of mobile Internet, the rise of supercomputing and big data has brought the research of artificial intelligence into a new stage. The related applications have gradually penetrated into various fields of social life that play a role in assisting human work. [4]

The core of artificial intelligence research is machine learning. Computer derives laws can predict unknown new data by studying existing data. The computer has the ability to learn as intelligently as a person. Among them, machine learning is mainly divided into two categories: supervised learning and unsupervised learning. Supervised learning is mainly aimed at classification and regression problems. It finds rules in the data information given corresponding feature labels. Unsupervised learning is mainly oriented to cluster analysis and data dimensionality reduction [5]. It requires the computer to actively determine the characteristics of the data by looking for the rules in the data.

Artificial intelligence is widely used in sales. It has applications in personalized content, product recommendations, conversational artificial intelligence, predictive analysis and insights, and social listening and sentiment analysis. The application of artificial intelligence can only predict the total sales amount at present. It cannot predict the consumption quota of a single user. Also, there are problems that the massive data is difficult to manage and the data is redundant. It is difficult for enterprises to obtain intuitive results from the massive data. This project will focus on researching issues such as consumption forecasting [6]. This project can also realize functions such as

workflow automation and consumption forecasting. It aims to help companies improve sales performance.

3.2 Demand analysis of commodity sales management system

Cloud computing technology is to simplify computer equipment. Various application software and their computing capabilities simplify the complicated work by providing services on the Internet. The rapid and widespread use of network technology makes the application environment of commercial software systems become very dependent in all walks of life on the Internet. Under the protection of the Internet, people only need to use a computer or mobile device. And they can access the Internet to use the application system anytime and anywhere. This breaks the shortcomings of the local system application limitations. It is also significantly saving the time for users to use the system to process work. Improve work efficiency. [7]

The combined application of ERP sales system and cloud service can greatly save the cost of enterprise system construction. It can improve the efficiency of system use and make enterprise management more systematic and intelligent.

4 Demand analysis of commodity sales management system

4.1 Business needs

The interface of the sales information management system needs to implement the concept of intelligent and personalized design. So that users can complete the management of related merchandise sales information by performing simple operations. The intelligent sales management system should have the economic feasibility of making the system work for a long time. It should also have the feasibility of the merchants using the system for actual operation. [8]

In addition to the corresponding basic functions, the intelligent sales management system also needs to have the function of sales forecasting. Therefore, the background production resources can be reasonably allocated to effectively solve the sales problems such as the disadvantage of hot-selling commodities and the backlog of unpopular commodities, which can reduce production costs and maximize the profits of enterprises [9]. The demand for sales forecasting function is to conduct deep learning on the law of historical sales data and scientifically predict the future sales of different products. Then it should find potential customers and ensure product sales through pushing advertisements. Finally, it should formulate corresponding production plans to allocate enterprises reasonably resources to increase sales.

4.2 System design goals

The general goals of the commodity sales management system design is shown in Figure 1.

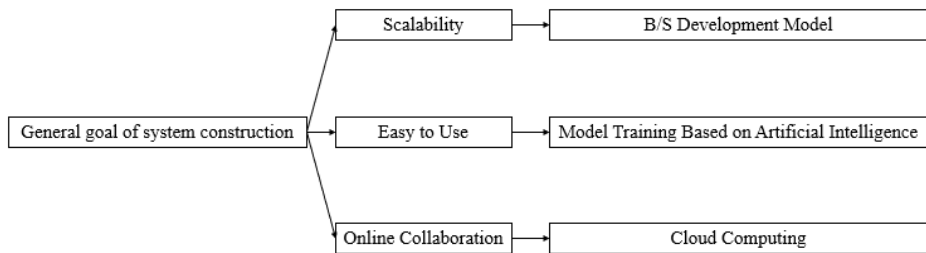


Figure 1. The overall goal of system construction

The system is optimized and rebuilt on the basis of the relevant technology of the original ERP system of the enterprise. Eventually, it will meet the needs of business and management. The goals of system construction are as follows: (1) To integrate the data of the original database of the enterprise, introduce data mining technology and make full use of the data accumulated by the enterprise to bring new profit growth points for the enterprise. (2) Using data mining technology and highly automated analysis of the original data of the enterprise to make inductive reasoning, mining potential patterns, predicting customer behavior, helping enterprise decision makers adjust market strategies and reducing risks. (3) Adopting the B/S internal and external network combination mode to enable the system to realize the function of one-key prediction based on various dimensions.

5 Design of commodity sales management system based on artificial intelligence

Based on the above analysis of the sales system, this study divides the intelligent sales management system into multiple core modules for design. And it sorts out the core functions of each link in the specific division process, as is shown in Figure 2.

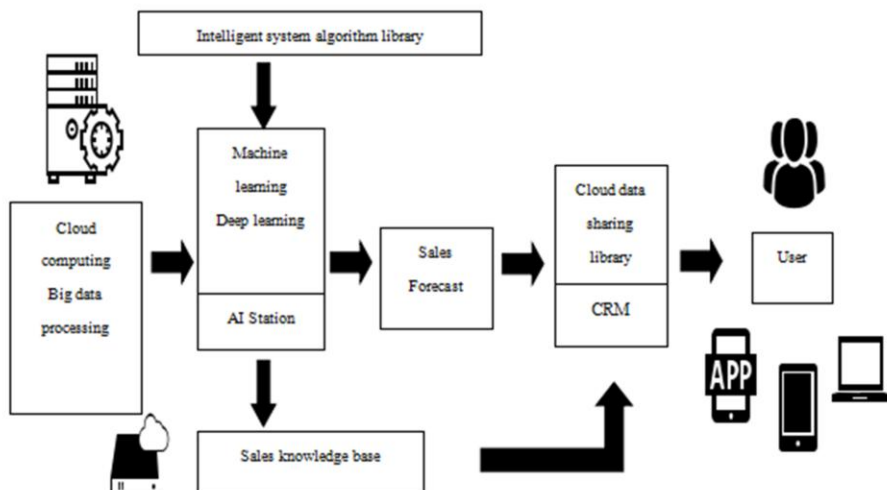


Figure 2 ERP intelligent sales system architecture

- To support the application of large-scale artificial intelligence, we realize the application of data processing, model analysis, application reasoning and other functions through the operation of machine learning and deep learning. For data, we will first perform the following three steps: data preparation, mining operations, result expression and interpretation. In the data preparation stage, we call the data in the database and perform integrated operations on the data, which is to merge the data in the multi-file or multi-database operating environment, explain the semantic ambiguity, deal with the future in the data, and clear the dirty data. Then select the data, narrow the processing range, and improve the quality. After the data preprocessing operation, the data mining is in the procedure. In this process, we first decide how to generate hypotheses, then select the appropriate tools to explore the data, and finally verify the knowledge found. We use the model and continuously train the model to form in the mode of continuous optimization. The final process is to visualize and explain the results.
- We build a rich and diverse deep learning system architecture and machine learning algorithm library environment, such as Torch, CNTK, Cafe-MPI and TensorFlow. It can provide users with a full range of services.
- Through the implementation of cloud service resource management platform, deep learning management AI Station platform and application analysis tool Teye, the implementation of enterprise data information is effectively summarized, changed, adjusted, arranged and analyzed.
- Distribute differentiated computing resources based on the computing characteristics of machine learning, deep learning models and the related resource requirements are required. Taking the CPU cluster required for data preprocessing as an example, in order to complete the rapid preprocessing of model data, Nvidia P40 high-density GPU cluster can be used to complete rapid training for large-scale big data models for deep learning with inference recognition function. Moreover, we provide FPGA cluster to meet the requirements of high throughput and low latency processing. The cloud platform system as a whole provides high-speed cloud services with large capacity, high bandwidth, and low resource storage delay.
- Forecast product sales is based on machine learning. Firstly, we explore and confirm the distribution of product data and missing information through data analysis. Secondly, we use feature engineering to split columns containing complex data information into time nodes of day, week, month, and year, and clearly sell products through visualization technology. The amount of the forecast has the greatest impact on the characteristics. Through the algorithm to predict the sales situation of the seller in the next six months, the key data features are more intuitively displayed in a graphical arrangement. The performance of different single models in predicting customer consumption is compared horizontally. Finally, the models are combined linearly. And the linear combination model with the highest accuracy is selected from them.
- Predict product sales is based on BP network prediction algorithm. Neural network is a non-linear adaptive system that can self-find the internal connection of sales data through machine learning to achieve prediction.

The algorithm is as follows:

The output of the i-th neuron in the hidden layer is:

$$al_i = f_1(\sum_{j=1}^r wl_{ij}p_j + bl_i) \quad (1)$$

The output of the kth neuron in the output layer is:

$$ak_2 = f_2(\sum_{i=1}^{s1} w2_{ki}al_i + b2_k) \quad (2)$$

The defined error function is:

$$e = \frac{1}{2} \sum_{k=1}^{s2} (t_k - a2_k)^2 \quad (3)$$

Since the algorithm has an error between the actual output and the ideal in actual operation, the algorithm converges. Therefore, the algorithm is optimized, and the correlation analysis can be used to analyze the factors that most affect sales forecasts. The data of these factors and historical real data are analyzed again. If the correlation is high, the original sales model is proved to be feasible. Then the correlation coefficient will be further optimized until the predicted data is consistent with the real data (here the agreement refers to more than 95%).

Performing correlation analysis on the algorithm and then adjusting and optimizing:

The adjustment formulas for the weight and threshold of the output layer can be expressed as:

$$w2_{ki}(t+1) = w2_{kj}(t) + \sigma \sum_{m=1}^Q \lambda2_{km} al_{im} \quad (4)$$

$$b2_{ki}(t+1) = b2_k(t) + \sigma \sum_{m=1}^Q \lambda2_{km} \quad (5)$$

The adjustment formulas of the hidden layer weight and threshold are respectively expressed as:

$$wl_{ij}(t+1) = wl_{ij}(t) + \sigma \sum_{m=1}^Q \lambda1_{im} p_{jm} \quad (6)$$

$$bl_{ij}(t+1) = bl_{ij}(t) + \sigma \sum_{m=1}^Q \lambda1_{im} \quad (7)$$

Where P is the input sample; Q is the number of input samples; t_k is the expected output of the network; σ is the learning step size, $0 < \sigma < 1$, $\lambda1$ is the hidden layer error transmission term; $\lambda2$ is the output layer error transmission term.

Finally, enterprises can use cloud sharing as a data sharing library. Employees can obtain these materials through the mobile APP. The sharing tool provides a simple way to centrally manage file materials. It can authorize different user groups to view different materials. It frees people from the tedious work of making paper materials.

6 Experimental results

This experiment takes a company's product A as an example. It compares the sales of the product within six months when using the intelligent sales system and the traditional sales system. It verifies the improvement effect of the intelligent sales system on product sales.

Firstly, we enter the sales data for the first six months of product A and make preparations for forecasting. The result is shown in Figure 3.

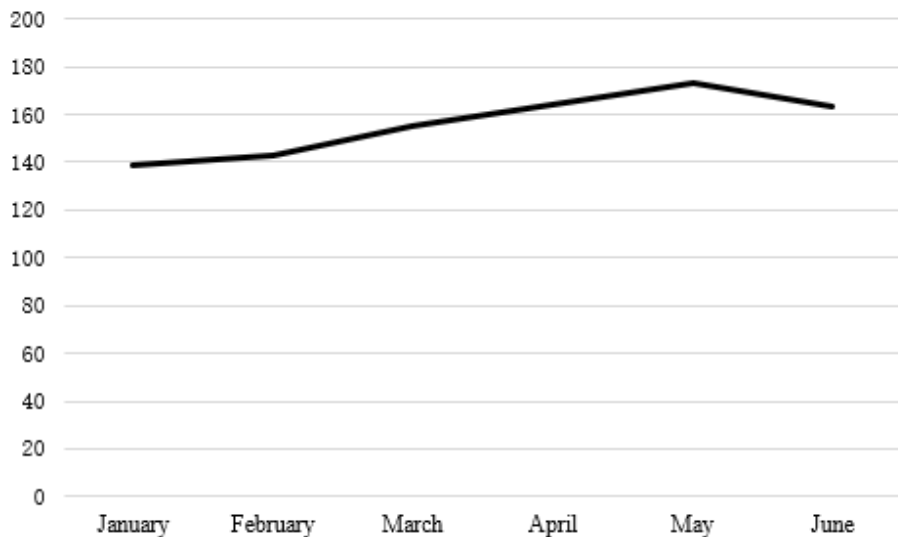


Figure 3 A company's sales of A products

From July to December, the intelligent sales system and the traditional sales system were used to observe the difference in product sales when applying two different systems. In the first six months of using the traditional sales system, the monthly sales volume of product A was between 139 and 173. The overall sales volume was low. In the second half of the year, in the control group, the traditional sales system was used. The result is shown in Figure 4.

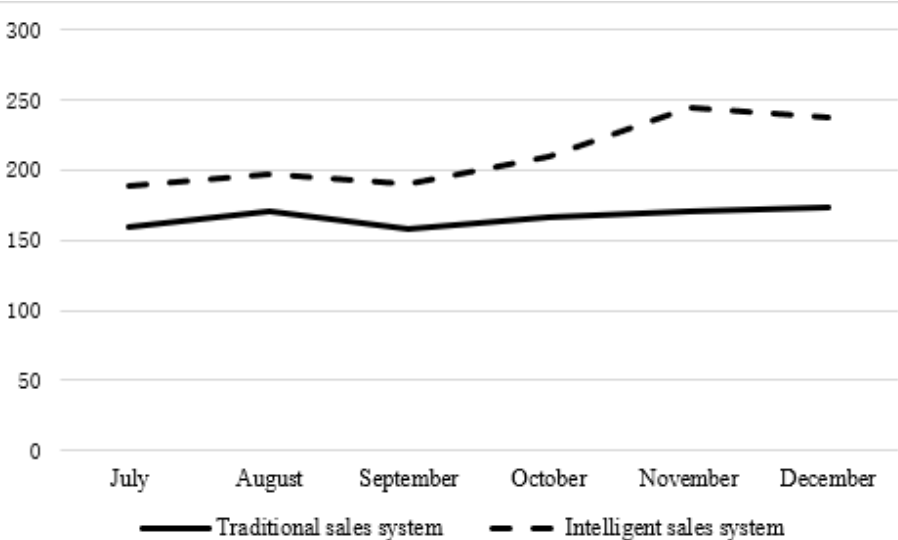


Figure 4 Comparison of sales of traditional and intelligent ERP sales systems

The sales volume of the product remained the same as that of the previous June with an average of 166 products sold per month. After using the intelligent sales system, the sales volume of the modified products has been greatly increased. The use of the intelligent sales system improves customer satisfaction. Through sales forecasting, we understand customer needs and provide corresponding services in a timely manner. And we also reduce the loss of sales and increase customer loyalty. The use of intelligent sales system also allows companies to arrange production more effectively, and the improvement of the forecast level will directly determine the effectiveness of the production plan, and it can reduce inventory and safety stock. Sales forecasts would reduce inventory backlogs, and directly reduce safety stocks, improve inventory management. It would effectively increase sales to an average of 211 products sold per month, and improve corporate operating efficiency.

7 Conclusion

This study designs the ERP intelligent sales management system based on artificial intelligence technology. Through the analysis of the demand of the commodity sales system, it clarifies the sales forecasting functions that the intelligent sales management system should have, and then discusses the specific implementation technology and introduces the sales forecasting model. It determines the system architecture of the commodity sales information management platform. In the process of designing this system, the following conclusions are obtained: (1) Through the investigation of various enterprise sales department, we can fully understand the sales pain points. Then we summarize the actual needs of the enterprise and optimize the ERP sales system. Finally, we improve the efficiency of business operations. (2) When designing the architecture, the most important design part is to integrate artificial intelligence and cloud computing into the ERP sales management system, and build the system through BP algorithm, machine learning optimization model, cloud computing collaborative work and other methods. (3) Use .NET related technology to develop the company's sales information system and realize seamless connection of various departments, and the core modules of the system have reserved interface fields which are extensible. Experiments have proved that the intelligent ERP sales system effectively improves the efficiency of product sales management, simplifies sales communication links through deep learning, discovers potential customers, and effectively increases sales by pushing advertisements to them.

In the design process, although certain results have been achieved, but this study still has shortcomings. The intelligent ERP sales management system did not apply artificial intelligence to all aspects of the sales system.

Acknowledgement

This study was financially supported by the Undergraduate Innovation Training Project of Guangdong University of Foreign Studies in 2020.

References

- [1] Hicham A, Yassine T, Elyacoubi A, Lamia H. Forecasting Fuzzy Delphi and Hybrid intelligent system for ERP Architecture through the Scientific Private Cloud. International Journal of Computer Applications. 2018 April; 179(36):22-28.
- [2] Motokane YI, Fukuda H, Ueda K. Creating an In-group Relation between Humans and Agents. Transactions of the Japanese Society for Artificial Intelligence. 2016 November; 31(6):AI30-J-1-10.
- [3] Sahoo N, Dellarocas C, Srinivasan S. The Impact of Online Product Reviews on Product Returns. Information Systems Research. 2018 June; 29(3): DOI: 10.1287/isre.2017.0736.
- [4] Deepak Alur, Dan Malks, John Crupi, Grady Booch, Martin Fowler. Core J2EE Patterns (Core Design Series): Best Practices and Design Strategies. Sun Microsystems, Inc. 2003.
- [5] Cai, J. , Luo, J. , Wang, S. , & Yang, S. . Feature selection in machine learning: a new perspective. NEUROCOMPUTING, 2018 July; 300:70-79.
- [6] Avi Goldfarb, Daniel Trefler. Artificial Intelligence and International Trade. NBER Chapters, in: The Economics of Artificial Intelligence: An Agenda, National Bureau of Economic Research, Inc. 2018. 463-492.
- [7] Christidis, K., Devetsikiotis, M.. Blockchains and smart contracts for the Internet of Things. IEEE Access 4. 2016 January; 2292-2303.
- [8] Yoo M., Won Y. Study on Smart Automated Sales System with Blockchain-Based Data Storage and Management. In: Park J., Loia V., Yi G., Sung Y. (eds) Advances in Computer Science and Ubiquitous Computing. CUTE 2017, CSA 2017. Lecture Notes in Electrical Engineering, Singapore. Springer Press, 2017 December; 474:734-740.
- [9] Yu Q., Wang K., Strandhagen J.O., Wang Y. Application of Long Short-Term Memory Neural Network to Sales Forecasting in Retail—A Case Study. In: Wang K., Wang Y., Strandhagen J., Yu T. (eds) Advanced Manufacturing and Automation VII. IWAMA 2017. Lecture Notes in Electrical Engineering, Springer Press, 2018 February; Singapore. 451:11-17.

Federated Learning in Big Data Application and Sharing

Yang Jing¹, Zhang Quan, Liu Kunpeng, Jin Peng, Zhao Guoyi

Customer Service Center of the State Grid Corporation of China

Abstract: In recent years, electricity big data has extensive applications in the grid companies across the provinces. However, certain problems are encountered including, the inability to generate an ideal model using the isolated data possessed by each company, and the priority concerns for data privacy and safety during big data application and sharing. In this pursuit, the present research envisaged the application of federated learning to protect the local data, and to build a uniform model for different companies affiliated to the State Grid. Federated learning can serve as an essential means for realizing the grid-wide promotion of the achievements of big data applications, while ensuring the data safety.

Keywords: Federated learning, big data application, blockchain, data sharing

1. Introduction

Electricity big data is known to possess widespread applications at companies under the State Grid in recent years, including the evaluation of electricity charge collection risk[1]-[5], electricity theft identification[6]-[8], overload of distribution transformer[9]-[10], and electric vehicle layout optimization[11]-[12]. For each grid company across the country, the model is trained, based on the already possessed business data. Currently, different companies in different provinces work in an isolated manner. In the era of big data, the urgent issues faced include the means to break data barriers and to perform collaborative modeling across the companies. Collaborative modeling across the companies can help to overcome the problems like low data quality and small sample size at each grid company, and also promote the grid-wide big data applications.

Federated machine learning provides a framework for machine learning, which facilitates the data use and development of models in machine learning across the institutions under the premise of users' privacy and data safety protection, and compliance to laws and regulations. Federated learning was initially proposed by Google[13] in 2016 and started to attract a lot of interest in the academic and industrial circles by 2019. At present, federated learning has become a hot technology in the field of artificial intelligence research and application. At present, two major difficulties need to be overcome in big data applications: (1) Data-related problems: In actual applications, the problems of limited data volume and low data quality are common, especially in the specialized fields. For example, electricity theft analysis, severe overload in the distribution transformer, customer complaint forecast, and big customer

¹ Corresponding Author, Yang Jing, Customer Service Center of the State Grid Corporation of China, Tianjin, China ,E-mail: zjuyangjing@126.com.

loss. In these fields, the annotated data is hardly enough to support model training. (2) Problems of privacy protection: Worldwide consensus has been reached as to data privacy and safety, and concerted efforts have been made to protect the data privacy and safety. In May 2018, the European Union (EU) published the General Data Protection Regulation (GDPR), which consists the regulations imposing the constraints on data acquisition, transmission, retention, and processing. Requirements on data privacy and safety protection have added to the difficulties in data acquisition, sharing, and exchange and brought an unprecedented challenge for the realization of many artificial intelligence technologies and applications.

Literature [14]-[18] shows the research and practice of confidential data protection during the model training process. In this study, we propose a uniform federate learning platform, which can be used for the sharing of a uniform model without data exchange across the companies under the State Grid. A particular emphasis was laid upon the application of the horizontal federated learning across the companies under the State Grid.

The advantages and features of federated learning used across the companies under the State Grid via a uniform platform are as follows: (1) The model is trained separately by using local data of each company, which satisfies the requirements for users' privacy and data safety protection; (2) The model algorithm is trained by grid-wide data with iterative optimization, thereby solving the problems of limited sample volume and difficult annotation; (3) All participants enjoy an equal status and are engaged in fair cooperation. In this way, the encrypted exchange of information and model parameters can be achieved, while safeguarding the independence of participants. Moreover, all participants could grow synchronously.

2. Federated learning

Federated learning defines the machine learning architecture, under which collaboration among the parties possessing different data is achieved through the design of a virtual model, without incurring the need for data exchange. The virtual model is an optimal model for pooling the data from different parties, where the local objectives are served in different regions according to the model. With federated learning, it is essential that the modeling results should be infinitely close to those of the conventional model. That is, the data from different parties are pooled together for the modeling. Under the federated mechanism where all participants enjoy equality of identity and status, it is possible to build a shared data strategy. As there is no data transfer, there will be no privacy leak or violation of the data norm. Therefore, the requirements for data privacy protection and legal compliance gets satisfied.

Federated learning has three major components: data source, federated learning system, and users. The relationships between the three components is illustrated in Figure 1. In a federated learning system, data from all sources are pre-processed. The learning model is built collaboratively, and the output is the feedback to the users.

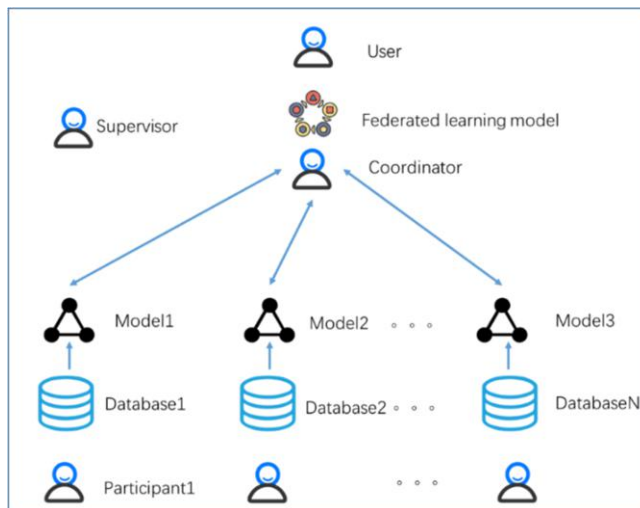


Figure. 1 Components of federated learning

The Customer Service Center of the State Grid Corporation of China has developed the supermarket for big data application sharing as a part of the exploration in federated learning applications. Based on the features of the State Grid Corporation of China, this supermarket offers a federated learning system along with the coordination and organization services. All companies under the State Grid Corporation of China are the participants and users of federated learning.

2.1 Vertical federated learning

This method employs two datasets that have many overlaps in users, but not in user features. The data are vertically partitioned (i.e., feature dimension), and the portions of data that share the same users but not the user features between the two datasets are selected and used for training. This method is known as vertical federated learning.

For example: Collaborative construction of an electricity charge overdue model is carried out between the grid company and the cooperative enterprise. The grid company possesses data Y, including the label data and overdue records. These data may be sufficient for building a good model. However, we may want to obtain more data, such as the label data and profile data of the cooperative party, in order to improve the performance and stability of the risk control model.

The problem with the conventional model is as follows: The cooperative enterprise cannot build the model independently due to the lack of data Y. It needs the grid company to bring data Y into the production environment of the cooperative enterprise for modeling. However, given the national laws on data protection and the strict regulations laid down by enterprises on their own data, the data X obtained from the grid company cannot be transmitted in full volume to the cooperative enterprise.

This problem can be addressed through vertical federated learning. As shown by the right side of the above figure, the data in both two parties share the same ID, though the features are different. The features lacking in one party can be made up by using the features from the other party.

Table 1 Vertical federated learning

Cooperative enterprise (bank)				Companies under the State Grid		
ID ID number	X1 Account receivable age	X2 Monthly profit	X3 Grade	ID ID number	X4 Monthly electricity consumption	Y Electricity charge overdue
u1	7	100	A1	u1	7	1
u2	8	200	A2	u2	8	1
u3	9	400	A1	u3	9	0
u4	10	500	A3	u4	10	0
u5	12	100	A4	u5	12	0

2.2 Horizontal federated learning

This method employs the two datasets that have many overlaps in user features, but not in users. The data are horizontally partitioned (i.e., user dimension), and the portions of data that share the same features, but not the same users between the two datasets are selected and used for training. This method is known as horizontal federated learning.

For example: The grid company in province A and the grid company in grid B collaboratively build an electricity theft model for the purpose of optimizing the electricity theft identification model. The need for collaborative modeling arises from the failure of the electricity theft models built separately by each party to meet the actual requirements for performance and stability. The federated learning mechanism can be utilized to make advantage of anti-electricity-theft samples from multiple parties to build a very expansive model without sample leak. Now with horizontal federated learning, the grid companies in both province A and B have (X, Y).

Table 2 Horizontal federated learning

Company in province A				
ID ID number	X1 Daily electricity consumption of user	X2 Voltage	X3 Current	Suspected electricity theft
u1	20	220	10	0
u2	30	220	20	0
u3	30	220	20	0
u4	40	220	20	0
u5	50	000	10	1
Company in province B				
ID ID number	X1 Daily electricity consumption of user	X2 Voltage	X3 Current	Suspected electricity theft
u6	20	220	0	1
u7	30	220	0	1
u8	30	220	0	1
u9	40	220	20	0
u10	50	000	10	1

3. Building a uniform grid-wide model through horizontal federated learning

The grid companies in different provinces share the same business-related need for the evaluation of electricity charge collection risk, electricity theft identification, overload of distribution transformer, work and production resumption analysis, and electric vehicle layout optimization. The model is trained separately by each company based on their own business data. At present, such work is done in an isolated manner. However, the State Grid Corporation of China faces an urgent need to build an effective uniform model for nationwide popularization by promoting a collaboration among the companies.

3.1 A brief introduction to the business scenarios

For the business scenarios of electricity theft and electricity charge collection risk, the following problems exist when the grid companies undertake the modeling work separately:

- (1) Electricity theft is a small probability event, and the sample size of electricity theft is small. After eliminating the poor quality, the sample size gets even smaller.
- (2) There are currently two pathways for the exploration of data sharing and data application sharing. The first is to pool the data from different parties. The second is to promote the wider use of mature model developed by a company in a certain province. However, there may be a problem of the data leak, and a general model is hardly possible due to the differentiation of businesses across the companies.

By forming an alliance for federated learning, different companies reach the federated protocol for multiparty cooperation. Without the need for sharing data across the parties, the federated big data ecosystem can be built to achieve the collaborative updates and optimization of the machine learning model. Thus, federated learning is very important in the optimization and integration of big data resources.

3.2 Architecture of horizontal federated learning

A typical architecture of horizontal federated learning is presented in the Figure 2. In this system, k participants sharing the same data structure are engaged in the collaborative learning of the machine learning model through parameters or cloud server. A typical hypothesis is that the participants are honest, while the server is honest and curious. Therefore, no participant is allowed to leak information to the server.

The training process of this system usually consists of the following four steps:

Step 1: The participants calculate the training gradients locally and mask the gradients through encryption, differential privacy or secret sharing technology. The masked results are sent to the server.

Step 2: The server implements secure pooling, without knowing about the information of the participants.

Step 3: The server sends the pooled results to the participants.

Step 4: The participants update their respective models using the deciphered gradients.

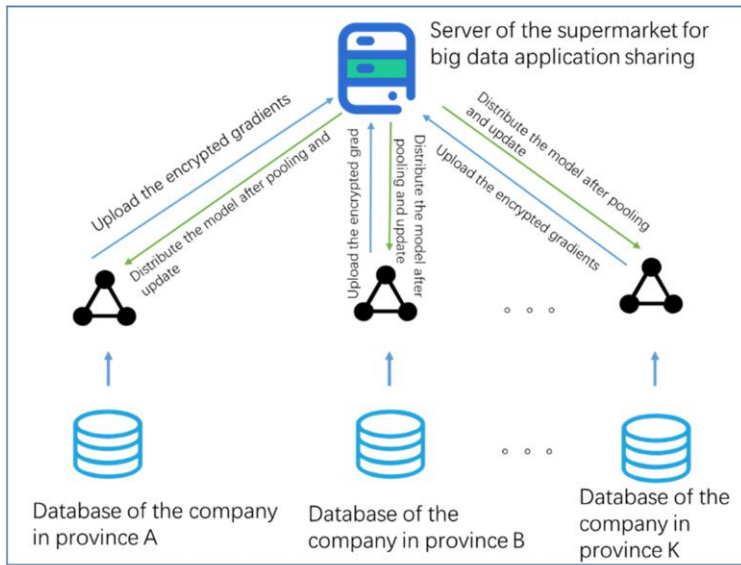


Figure. 2 Architecture of horizontal federated learning

The above steps are iterated until the convergence of the loss function, leading to the end of the entire training process. The above-described structure is independent of the type of machine learning algorithm used (eg., logistic regression or DNN). All participants share the final model parameters.

Safety analysis: If the gradient pooling is done by SMC or homomorphic encryption, it is usually indicated that the above-mentioned structure can protect a data leak from the influence of the semi-honest server. However, this structure can be vulnerable to the attack from an another safe mode. That is, the generative adversarial network (GAN) obtained by training in the collaborative learning process by the malicious participants.

The protocol developed by WeBank is used as a reference. The homomorphic encryption technology is used in this protocol, and the central parameter server has no way to know the parameters and models after pooling (this requirement can be loosened sometimes). In this way, the privacy of the participants is protected to the maximal extent. Moreover, the central parameter server is usually not involved in the training. Its only role is the pooling and distribution of the encrypted parameters.

3.3 Homomorphic encryption

Homomorphic encryption is a special encryption scheme, which allows the third parties to operate the encrypted data without a prior decryption, and the result of decryption is consistent with that of the plain text. Hence, the homomorphic encryption is an effective technology to protect the privacy of the users. The training process employs the homomorphic encryption to ensure that the intermediate training parameters have the same training effect with or without encryption. The data owner does not upload the model and data, hence, the other participants are unable to use the intermediate parameters to infer the content of source data.

Considering a logistic regression model as an example [19]:

$$(x_i, y_i) , i = 1, 2, 3, \dots, n$$

where, $x_i \in R^m$, $y_i \in \{1, 0\}$. (1)

Logistic maximizes the likelihood estimator as shown in Equation (2).

$$\prod_{i=1}^n P_r(y_i / x_i) = \prod_{i=1}^n \frac{1}{1 + \exp(-y_i(1, x_i)^T \beta)} \quad (2)$$

where, $\beta \in R^{m+1}$, Starting from an initial β_0 , the gradient descent method at each step t updates the regression parameters using Equation (3).

$$\beta^{(t+1)} \leftarrow \beta^{(t)} + \frac{\alpha_t}{n} \sum_{i=1}^n \sigma(-z_i^T \beta^{(t)}) \cdot z_i \quad (3)$$

where, α_t is learning rate at step t ,

and $z_i = y_i \cdot (1, x_i)$, $i = 1, 2, 3, \dots, n$

The HEAAN scheme proposed by Cheon [20] [21] is adopted in this case. The HEAAN scheme supports the approximate arithmetic of the encrypted messages, so that the size of the parameters do not increase too much. Furthermore, it reduces a certain precision and greatly improves the efficiency. The Heaan scheme supports the key generation, encryption, decryption, addition and multiplication. At the same time, the scheme supports message packaging. If the encryption function is H, then the encryption gradient of each provincial company is shown by Equation (4).

$$G(u, t) = H\left(\frac{\alpha_t}{n} \sum_{i=1}^n \sigma(-z_i^T \beta^{(t)})\right) \quad (4)$$

where, $G(u, t)$ is the Step t iterative encryption gradient for u -Th provincial company.

3.4 Technological realization

FATE, an open source program first maintained by WeBank, provides a secure computation platform to support the federated learning algorithms. FATE realizes the secure computation protocol based on homomorphic encryption and multiparty computation. It supports the secure computation in the federated learning framework and machine learning, including the typical machine learning algorithms as logistic regression and gradient boosted regression trees, and also in deep learning, transfer learning and other frontier algorithms. FATE not only provides a framework, but also runs some classical algorithms, including the linear regression, gradient boosted regression trees and other classifiers. It has been sufficiently verified in practice that FATE can be readily applied to the industrial field. If the developers are not willing to construct the federated learning model from scratch, they can borrow from the mature ones or make certain modifications on this basis.

The architecture of FATE[22] is illustrated in Figure 3.

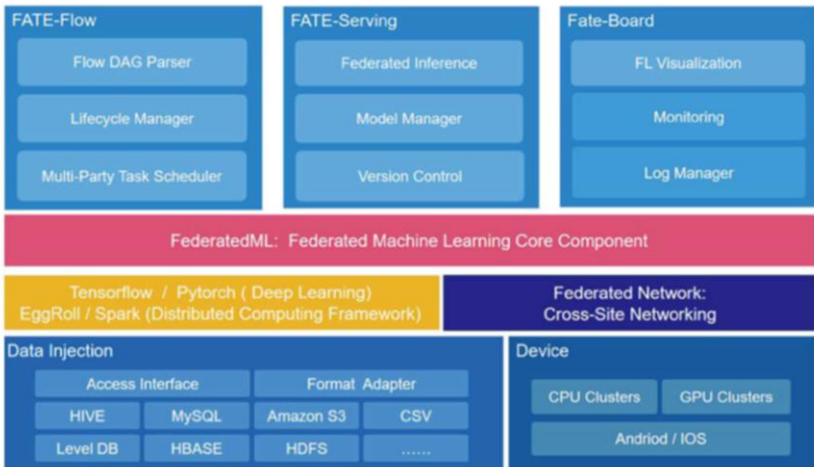


Figure. 3 Architecture of horizontal federated learning

Furthermore, FATE offers a set of friendly, cross-domain mutual information management protocols, which solves the difficulty of information security audit in federated learning. A simple, easy-to-use open source tool platform enables a multiparty data collaboration while protecting users' privacy and data safety and conforming to government regulations.

3.5 Applications of federated learning in the supermarket for big data application sharing

Federated learning is not only a technical standard, but also a business model. The Customer Service Center of the State Grid Corporation of China sets up a special space for federated learning in the supermarket for big data sharing, which can serve as a mutual benefit and collaboration platform for different companies under the State Grid. Stage 1. Model training: The sensitive data can be shared through the training model to the party needing these data. That is, the party needing the data, uploads the model to the sharing platform, from which the data provider downloads the model and trains it with its own data. After the training is done, the updated model is uploaded to the sharing platform. In this way, only the trained model is made available for the party needing the data, which allows for data sharing without the leak of sensitive data.

This method is further illustrated through the example of electricity theft identification. To this goal, the data on the users' daily electricity consumption, three-phase voltage, three-phase current, distribution transformer number, and user profiles are usually needed. The target variable is suspected electricity theft, to which the value of 1 or 0 is assigned.

The training process of the horizontal federated learning model can be summarized as follows: Initially, the initiator of federated learning for electricity theft identification uploads the original model to the supermarket for big data application sharing as the initial sharing model. Each participant downloads this model and independently calculates the gradient according to their respective data. Initially, the gradient is encrypted and sent to the server of the big data sharing supermarket. The federated

model of the big data sharing supermarket (server) implements weighted averaging of the models uploaded to the cloud without accessing the data from any client terminal. Thus a new sharing model is obtained. Later, the computation results are returned to each participant. Finally, the client terminals update their respective models using the deciphered gradients.

Let the encryption function of HEAAN scheme be H . Equation (5) can be deduced as:

$$G(u, t) = H\left(\frac{\alpha_t}{n} \sum_{i=1}^n \sigma(-z_i^T \beta^{(t)})\right) \quad (5)$$

In step t, the gradient values of provincial companies are $G(u_1, t), G(u_2, t), \dots, G(u_m, t)$, which are uploaded to the server of federal learning management system. The server carries out weighted average as given by Equation (6).

$$\bar{G}_t = \sum_{i=1}^n p_i G(u_i, t) \quad (6)$$

The server is unable to decrypt G and also the model parameters. It only knows the homomorphic encryption domain, but it is unable to decrypt without the private key. The client downloads the parameters, decrypts it with its own private key, and then updates its own model.

Operational logic:

Step 1: $t=1$, Provincial companies get the provincial model gradient based on local data

$$g(u_i, t) = \frac{\alpha_t}{n} \sum_{i=1}^n \sigma(-z_i^T \beta^{(t)}) \quad (7)$$

Step 2: Gradient encryption

$$G(u_i, t) = H(g(u_i, t)) \quad (8)$$

Step 3: Upload to the server of federal learning management system

Step 4: The server carries out weighted average

$$\bar{G}_t = \sum_{i=1}^n p_i G(u_i, t) \quad (9)$$

Step 5: The server sends it to the provincial company, provincial company get Decryption gradient,

$$g(u_i, t+1) = D(\bar{G}_t) \quad (10)$$

Step 6: Proceed to the next iteration

$$t = t + 1 \quad (11)$$

Step 7: When the overall loss function is less than the threshold value, the iteration is stopped

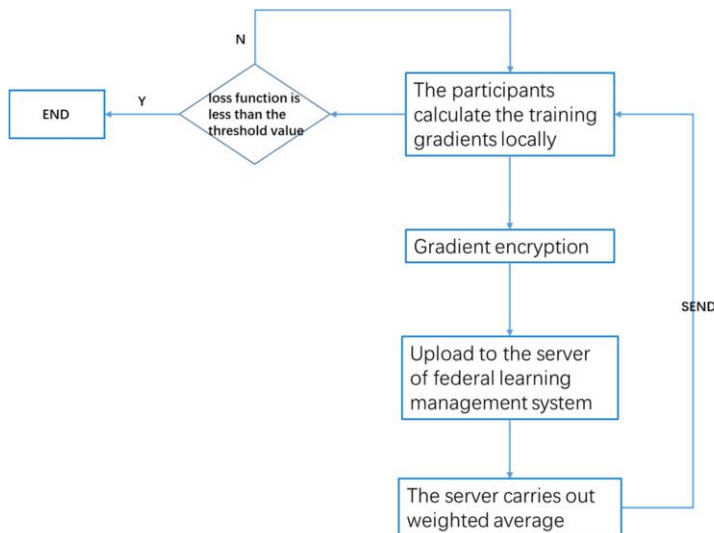


Figure. 4 Horizontal federated learning Operational logic

Stage 2. Application of a common model: The common model is shared through a remote technology. The data users can have a direct access to the big data application products by uploading the data or by processing the data with the middle platform. Application products are usually related to specific business scenarios, including the whole process of data processing and integration, computation, analysis and display. These products have a strong specificity for businesses, and can be shared via the remote technology. The party needing the data can use the application products according to the instruction manual. The data processing can be performed according to the use workflow for the application products.

The process of common model sharing can be summarized as follows: The cooperative party of the federated learning uploads the common model to the big data application platform, which can developed into the abnormal electricity consumption identification products for the use of grid companies in other provinces. This cooperative party will get credits as a reward, so as to facilitate the popularization of the achievements of big data applications.

Practical application: Five provincial companies participate in the federal study of electricity theft identification. The data format of provincial companies collects and processes electricity charge data, voltage data and current data according to the same standard, and marks electricity stealing situation, the data standards is shown in the Table 3.

Table 3 Data standards

Customers data				
Customer id	Tariff data set	Voltage data set	Current data set	Suspected electricity theft
id1	T1	V1	C1	1
id2	T2	V2	C2	1
id3	T3	V3	C3	1
id4	T4	V4	C4	0
.....

The application effect is shown in the Table 4.

Table 4 Model effect

Model effect			
Model	Sample size	Prediction accuracy (%)	Recall (%)
Provincial companies independently identify the electricity theft (Logistic)	10000(avg)	30.4(avg)	50%(avg)
Provincial companies use the federal learning model (Logistic)	10000(avg) 50000(total)	70.5(avg)	60%(avg)

4. Conclusion and Future Work

Through the practical application of federal learning in the analysis of electricity theft in five provincial companies, it can be seen that the effect of federal learning is better than that of individual provincial companies.

We have discussed the multiparty collaboration and application of horizontal federated learning within the State Grid. The electricity businesses across the companies in different provinces have considerable overlaps horizontally, and the federated learning enables the trans-party model training. However, a cross-domain collaboration may be needed for the construction of the electricity big data application sharing ecosystem. For example, the collaboration between the banks and internet companies. Vertical federated learning is a good way to expand the knowledge of the attributes of electricity users in the financial and Internet fields. These features, if pooled in an encrypted state, can be used to promote the performance of the sharing model and in the construction of the electricity big data application ecosystem. In the future, the application of vertical Federation learning is the focus of our research and exploration.

References

- [1] Li Jianbin, Wu Binbin, Zhu Yakui, Wang Yue, an Yagang, Zhao Shasha. Risk prediction and control of customer electricity tariff based on big data analysis [J]. Power Systems and Big Data ,2019, 22 (2):1-6.
- [2] He Rong, Zhang Xiangdong, Qiu Lin, Chen libing, Zhou Qian, Zhang Yan. Electricity tariff risk prevention and control based on clustering and logistic regression [J]. Power Systems and Big Data ,2019,22(12): 42-49.
- [3] Zhao Hong, Shen Jianzhong, Wang Jun, Zhang Cheng, Qu Qing. Risk prediction model of electricity charge recovery based on customer portrait and machine learning algorithm and its application [J]. Microcomputer Applications,2020, 36(2):93-96.
- [4] Wang Zongwei, Zhao Guoqi, Jin Peng, Yang Jing, Wang Hailong, Zhang Zuobin. Research on the risk identification model of electricity tariff based on customer credit system [J].Machine Design and Manufacturing Engineering ,2019 ,48(10): 99-104.
- [5] Xie Ying, Wang Zheng, Zhao Yongliang. Research on risk identification model of customer electricity consumption behavior [J]. Zhejiang Electric Power, 2017,36(12):53-56
- [6] Qiang Hao, Dai Qiaoyun, Wu Ke, Du Jian, Yin Xinbo, Chen Chen. Research on anti stealing technology of variable structure BP neural network based on big data [J].Journal Of Jiangsu University Of Technology,2019,25(2):10-14
- [7] Li Zhi Peng, Hou Huiyong, Jiang Si fan, Wan can, Zheng Ruimin. Line loss calculation and power stealing analysis based on artificial neural network [J]. Southern Power System Technology , 2019,13(2):8-12
- [8] Li Bo, Cao min, Zhu Yuanjing, Li Shilin, Zhang Linshan, Lin Cong, Wang Xianpei. A joint power stealing detection method based on network characteristics and user behavior analysis [J]. Engineering Journal of Wuhan Universit,2019, 52 (12) :1121-1128
- [9] Qiu xiaogeng, Dong Xiangyu, Zhang Peng, Liang Wei, Guo Jun, Bai Kaifeng, Liang Zhixian, Feng Chao. Analysis of distribution transformer overload warning based on big data [J]. POWER SYSTEMS AND BIG DATA 2018,21(10):38-42
- [10] He Jianzhang, Wang Haibo, Ji Zhixiang, Meng Xiangjun, Zhang Tao. Heavy overload prediction of distribution transformer based on Stochastic Forest theory [J] . Power System Technology, 2018,21(10):38-42
- [11] Xie Yuande, Zhang Lin, Deng Shali, he jiemeng. Study on optimization network layout of electric vehicle charging facilities [J]. Practice and understanding of Mathematics, 2020,50(10):168-176
- [12] Sun Yue, Jiang Cheng, Wang Zhizhi, Tang chunsen. Optimal layout of dynamic wireless power supply system for electric vehicles based on PSGA [J]. Power system automation, 2019, 43 (9) : 125-131
- [13] McMahan H B ,Moore E , Ramage D , etal . Communication-efficient learning of deep networksfrom decentralized data[C]/Proceedings of the 20th International Conference on Artificial Intelligence and Statistics (AISTATS) 2017. JMLR : W&CP volume 54.
- [14] Jia Yanyan, Zhang Zhao, Feng Jian, Wang Chunkai Applications of federated learning models in the processing of confidential data [J]. Journal of China Academy of Electronics and Information Technology, 2020, 15 (1):43-49.
- [15] Wang Chunkai, Feng Jian. A study on the applications of federated learning in the insurance industry [J]. Journal of Insurance Professional College (Bimonthly), 2020, 34 (1):13-17.
- [16] Wang Yashen. A review of the technological development of federated learning oriented towards data sharing and exchange [J]. Unmanned Systems Technology, 2019, 2(6): 58-62.
- [17] Pan Rusheng, Han Dongming et al. Visualization of federated learning: challenges and architecture [J]. Journal of Computer-Aided Design & Computer Graphics, 2020 (32):1-6.
- [18] Liu Junxu, Meng Xiaofeng. A review of the privacy protection studies in machine learning [J]. Journal of Computer Research and Development, 2020, 57 (2): 346 – 362.
- [19] CHENH, GILAD-BACHRACHR, HAN K,etal. Logistic regression overencrypted datafrom fully homomorphic encryption[J]. BMC Medical Genomics, 2018, 11(S4): 3–12. [DOI: 10.1186/s12920-018-0397-z]
- [20] CHEON J H, KIM A, KIM M, et al. Homomorphic encryption for arithmetic of approximate numbers[C]. In:Advances in Cryptology—ASIACRYPT 2017, Part I. Springer Cham, 2017: 409–437. [DOI: 10.1007/978-3-319-70694-8_15]

- [21] CHEON J H, HAN K, KIM A, et al. Bootstrapping for approximate homomorphic encryption[J]. IACR Cryptology ePrint Archive, 2018: 2018/153. <https://eprint.iacr.org/2018/153>
- [22] Artificial Intelligence Department of Weizhong bank, et al. Federal learning white paper[M].2020.4

Exploration on the Construction of Sharing Platform of Power Big Data Application

Yang Jing¹, Zhang Quan, Gong Lihua, Zhu Longzhu, Liu Kunpeng
Customer Service Center, State Grid Corporation of China

Abstract. Big data application sharing supermarket is a big data application sharing portal. The first, one or more enterprise users can share and use the same big data application product. This product comes from the contribution of enterprise users of a certain sharing supermarket. In this way, we can solve the problem of unbalanced development of big data capabilities, and avoid repeated construction and repeated investment in the same kind of big data applications; the second. Through such a sharing platform, many enterprises carry out cooperation such as federal learning to jointly create big data application products.

Keywords. big data, platform, sharing, block-chain, federated learning

1. Introduction

At present, the application of big data has made great development and is widely used in various industries, Kuo, Y. H., & Kusiak, A.[1], The review of the literature suggests that production research enabled by data has shifted from that based on analytical models to data-driven. Manufacturing and data envelopment analysis have been the most popular application areas of data-driven methodologies. The research published to date indicates that data mining is becoming a dominant methodology in production research. Future trends and opportunities for data-driven production research are presented. Lu, Y., & Xu, X.[2], focus on how to ensure efficient synchronization of the mobile health record in unreliable mobile environments. The proposed middleware is a software-as-a-service (SaaS) layer which enables the mobile health record. Zhang, Y., Zhang, R., Wang, Y., Guo, H., Zhong, R. Y., Qu, T., & Li, Z.[3], the composition of big data service layer is described in detail, and a sales predicting method based on neural network is introduced. The salability of products is divided, and the qualitative economic production volume mechanism is finally given. Based on the framework, an intelligent service system for enterprises with the characteristics of mass production is implemented. Experimental results show that the big data service framework can support chemical enterprises to make decisions to reduce costs, and provides an effective method for Smart Product Service System (PSS).

Some experts introduce the application of big data technology and framework in manufacturing industry. A. Papacharalampopoulos, J. Stavridis, P. Stavropoulos, G. Chryssolouris[4], The current study addresses the challenges, associated with the framework of the thermal oriented processes, having holistic (digital) modelling as a

¹ Corresponding Author, Yang Jing, Customer Service Center of the State Grid Corporation of China, Tianjin, China, E-mail: zjuyangjing@126.com.

main objective. Herein two different case studies are performed; numerical examples regarding big data impact on manufacturing and simulation-based paradigms of control design taking into account communications. Implementation of the aforementioned takes into account the controller's complexity.D. Mourtzis, E. Vlachou, N. Milas, N. Tapoglou, J. Mehnert[5], proposes a Cloud-based, knowledge-enriched framework for machining efficiency based on machine tool monitoring. More precisely, it focuses on the optimization of the machining parameters and moves through an event-driven optimization algorithm, utilizing the existing machining knowledge captured by the monitoring system.

In China, there are many provincial companies under the State Grid Corporation of China. In recent years, they have produced a large number of big data application results based on power business scenarios. These big data application results belong to different provincial companies of State Grid Corporation, and have the promotional value in other internal units, such as distribution transformer overload influence factor mining and prediction service[6]-[7], optimized layout of electric vehicle charging facilities [8]-[9], electricity charge risk forecast and other big data analysis models [10]-[14].

An attempt is made in this paper to explore different issues such as, how to share big data applications faster, avoid repeated investment from the perspective of State Grid Corporation, shorten the development cycle from the perspective of power companies, and in turn save human and material resources. For example, if a provincial company A has the product of electricity stealing analysis then other provincial companies such as B-E can use the products of the provincial company A by mere sharing the platform of big data application. Therefore, the provincial companies B-E need not invest separately in power stealing analysis and thus, can save both manpower and precious material resources.

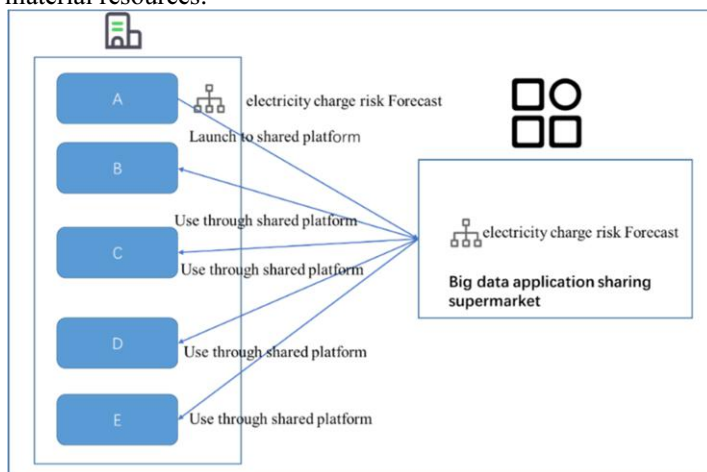


Figure 1 Big data application product sharing

At present, the power industry only realizes data level achievement sharing, but the sharing of model, algorithm, tool and product achievements have not yet been realized. The power big data platform is positioned as the energy big data sharing and operation service platform, focusing on the data sharing service function, data mining analysis function, data product development function and data product operation function [15]. The present paper focuses on the data sharing function of the platform where users can

develop new data products and excavate data value based on data sharing and platform capability. The data sharing is an important means to solve the unbalanced distribution of big data resources and realize its reasonable allocation [16]. We introduce a data sharing platform OpenEI created by non-governmental organizations in the United States, share their own energy related data and data modeling tools for different organizations and institutions on this website for other users to download, analyze and model. The data, on this data sharing platform, is mostly in the form of small examples, such as 24-hour power load data. In addition, the paper mentioned the design of power big data sharing platform, mainly from the management, service, exchange and monitoring of power data. The key point is the sharing of power data.

This paper explores the construction of big data application sharing supermarket to realize the sharing of big data application results. Big data application achievements include models, algorithms, tools, etc., but they are not just limited to themselves. But they are the application of big data technology in a certain business scenario, such as electricity tariff risk prediction, electricity theft analysis, optimized layout of electric vehicles, heavy overload of station area, etc.

2. Design of data application sharing platform

2.1 Platform positioning

The platform of the big data application sharing supermarket is positioned from the following four aspects. First, the big data product trading platform, which provides three types of big data products, namely, data services, tool models and applications. Second, the mutual benefit cooperation platform, which integrates and shares the data resources, technical resources and business resources of relevant parties between ecosystems and within the big data commercialization service ecosystems so as to promote the transaction matchmaking between supply and demand sides and multiple parties to achieve profit sharing and mutual benefits. Third, the innovation driven platform of big data application, which realizes online selection and assignment of big data topics, realizes objective evaluation of the value of big data results through the real feedback of the market and users, and conducts targeted promotion of excellent big data results according to key work points in relevant stage. And finally, the big data technology exchange platform which encompasses online technology exchange forum and offline training, special competition, achievement exchange, technology salon, etc., in which personnel training can be promoted and innovation ability is enhanced.

2.2 Division of cooperation relationship of big data application sharing supermarket

From the perspective of cooperation, the platform is divided into the supplier and demander of on-shelf products and the operator of the sharing supermarket. Suppliers of on-shelf products mainly refer to the enterprises or units that provide big data on-shelf products to the sharing supermarket, which can be subdivided into data service, tool model and product application suppliers according to the supply function. The demand side of the on-shelf products mainly refers to the enterprises or units that have actual business requirements for big data on-shelf products. The operator of the sharing supermarket is the operating unit entrusted by the company. Whereas, the internal units

mainly include directly affiliated units, provincial (municipal) companies, industrial units and scientific research institutes.

From the users' point of view, it can be divided into subscribers, publishers and operators as follows:

The subscriber can log in the big data application sharing supermarket as a member, order and use the required big data products through the sharing supermarket.

The publisher can log in the big data application sharing supermarket as a member, release its own products through the sharing supermarket, and promote the products.

The operator engages in the operation and management side of the big data application sharing supermarket.

Members of the big data application sharing supermarket can have multiple identities i. e., they can be both subscribers as well as publishers and can publish their own excellent products to other members to meet their own business needs.

2.3 On-shelf product design of big data application sharing supermarket

Based on the application characteristics, the supermarket products can be divided into data products, application products and tool products. The data products refer to the on-shelf products that provide data resources or data processing and desensitization result sets directly for users under the premise of compliance with laws and regulations. The application products refer to the big data applications with UI interfaces that can directly provide analysis and prediction results to the end users. The tool products refer to the big data model and algorithm, which can be used only when integrated into the program code or the training platform.

2.4 Internal business model design

Mainly the internal partners of the State Grid Corporation trade in the virtual mode of points. The initial score of each unit is 500 points. The on-shelf products are divided into 10—50 points according to the classification and scale. The suppliers of the on-shelf products can set such points by themselves with different charging standards by times, weeks, months and years. The demanders of the on-shelf products can use the points to purchase the products according to the different charging standards of the products. On successful completion of the transaction, corresponding fee of the buyer is deducted, the operating party of the sharing supermarket withdraws the service fee from each transaction at a rate of 6%, and the supplier of the on-shelf product gets the remaining 94% transaction fee.

2.5 Design of product sharing mode

Data products can be shared through downloading, internal data interface of the company, and federated learning, specifically as follows:

(1) The documents that do not involve sensitive detailed data (like the industry analysis report, general standard training set, etc.) can be directly shared through downloading and internal interface of the company.

(2) The data involving sensitive information is shared in the way of model training for the demander. The specific implementation method is that when the demander, who needs the data training model, uploads his model to the sharing platform, the data side downloads the model and uses its own data for the training. After completion of the

training, only the trained model is provided to the data demander, which can realize data sharing thereby, avoiding the sensitive data leakage.

Application products are remotely shared and used, where users directly use big data application products by uploading data or processing data in the middle platform. The application products involve specific business scenarios, including data processing, integration, calculation, analysis and display, with strong business context. These are shared and used remotely. The user needs to process the data according to the application product instructions.

Tool products are shared and used by downloading or remote calling, and users can directly use big data application products by uploading data or processing data in the middle platform. The demand side of tool products can download the model for direct use, perform further training based on the current model, and remotely use the product after processing according to the tool product instructions.

3. Design of big data application sharing platform

3.1 Business framework of big data application sharing supermarket

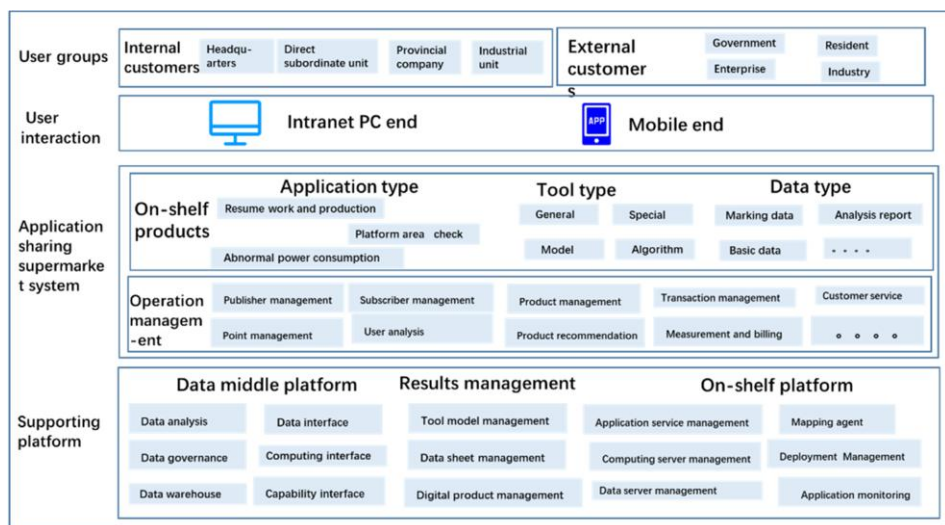


Figure 2 Business framework of big data application sharing supermarket

The business architecture of shared supermarket is divided into four parts: supporting platform, application sharing supermarket system, user interaction and user group.

The supporting platform includes data middle platform, achievement management function and on-shelf platform, which provides source data, data processing ability and product shelf management for the products on the shelves of shared supermarkets.

The application sharing supermarket system includes products on the shelf and operation management of the shared supermarket. Similar to online shopping mall, users can select and purchase big data application products, including application class, tool class and data class. Through the operation function, the management of on-shelf and off-shelf approval, product iterative update management, transaction management

and shared supermarket operation management include: user operation, product operation and transaction operation.

User interaction can be done by provincial company users through the web PC terminal and mobile app end for sharing supermarket.

The current users are the company headquarters, directly affiliated institutions and provincial companies, and the future users can further be expanded to the government, enterprises and residents.

3.2 Framework of arrangement of big data application sharing supermarket

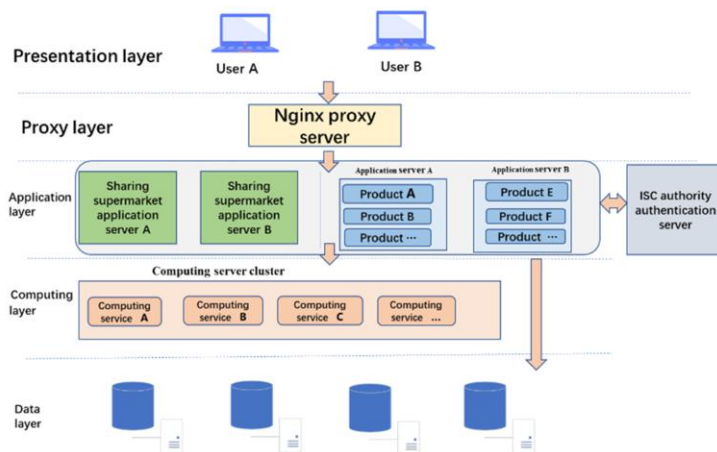


Figure 3 Arrangement framework of big data application sharing supermarket

The deployment architecture of shared supermarket is divided into data layer, computing layer, application layer, agent layer and presentation layer.

The data layer includes business source data, index processing and result data. Source data and result data are stored in Oracle, and indicators are processed in hive Library of big data platform.

The calculation layer supports the model operation of the application products on the shelf, and outputs the results based on the intermediate result table of the data layer. In order to reduce the impact of data computing model on the application server, the application service is separated from the computing model as far as possible, and a unified computing server is planned. Virtualenv or Anaconda is installed on the computing server, and the python environment for different application products is established, and the application service makes remote calls.

The application layer includes the application of shared supermarket and the application service of products on the shelf, including web application service, middleware service and message service.

The agent layer uses nginx proxy to map the servers and port addresses of shared supermarkets and products on shelves to nginx servers, so as to realize unified IP port access and reduce the security risks brought by the opening permissions of IP ports of all servers.

The presentation layer is open to users through the web page scheme. Users log in to the sharing supermarket through the web page to order and use the products.

3.3 Property rights protection of big data application products

The sharing supermarket protects the property rights of big data application products through blockchain technology. JI Lusheng [17] proposed an anonymous address technology scheme based on block chain to use resource services to process encrypted addresses for personal data rather than sending them directly to the third-party services. WANG Jingwei [18] proposed a blockchain based data marketplace framework demonstration system to verify its feasibility and security, and providing reference solutions for building practical data marketplaces in the future. YAN Shu [19] introduced the characteristics of blockchain technology to expound the main ideas of transforming the authorized storage link, data traceability and the realization of smart contract by using blockchain to comb the overall framework of data circulation. In view of this, an attempt is made in this work to give the application examples of data circulation using blockchain in foreign countries, and introduce some other numbers according to the circulation of new technology.

In the blockchain mode, the complete authorization and authentication process of big data application sharing supermarket is shown in Figure 4. The put-on-shelf side signs the electronic agreement and authorizes corresponding authority to share supermarket. Firstly, the shared supermarket, stores the evidence locally through the application system, and then uploads the authorization information to the authorization information chain. The application system executes the code on the chain, initiates the query on the chain, and records the authorization information to the block. When the demand side submits the product requirements, the authentication transaction is initiated on the chain to confirm the validation of the authorized user. Then, the verification node on the chain returns the authorization information. If it is authorized, corresponding big data product will be returned. The blockchain model avoids the defects of the traditional model. Any node can record the authorization information which cannot be changed. Multiple sides can share the authorization records in real time, so the query efficiency is high. In addition, the authorization is decoupled from the business, and can be added and exited at any time.

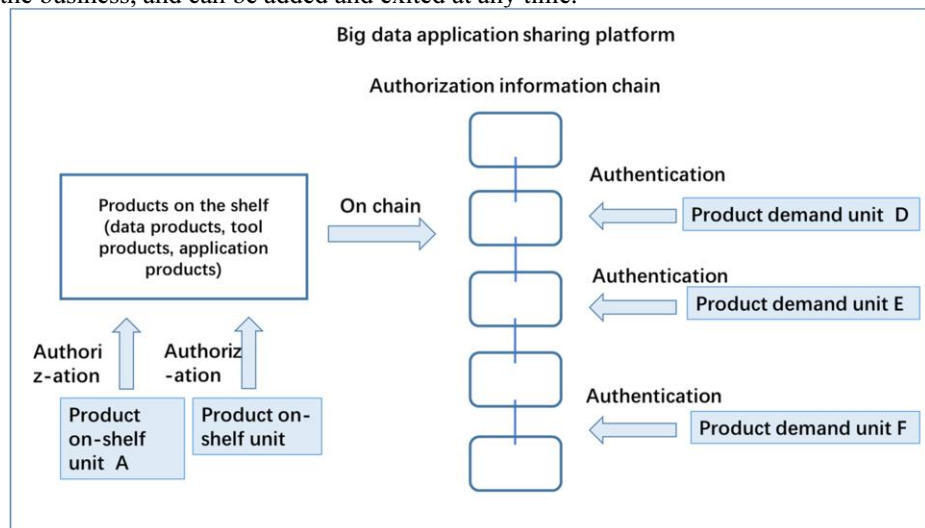


Figure 4 Big data application sharing supported by blockchain

Following three aspects are explored in this paper:

- 1) Blockchain-based data product certification: The blockchain characteristics like distributed storage, multi-node consensus synchronization and hash encryption storage of files are used to provide certification for data products released by the product publisher to prevent tampering, subjective change, malicious deletion and other operations brought by the network security threats, and effectively guarantee the reliability and authenticity of network security data.
- 2) Blockchain-based tool and model certification: The blockchain characteristics like distributed storage, multi-node consensus synchronization and hash encryption storage of the files are used to provide certification for the models and tools released by the product publisher. For other users, certification is provided for the results of continuing training based on the current model. The intellectual property rights and sharing of partners in federated learning are recorded.
- 3) Certification for process behavior involved in the purchase and use of products: The process and behavior involved in the order and use are recorded in the chain, so as to ensure the authenticity and traceability of detailed information such as the time and content of the behavior of each side, and prompt handling of abnormal behavior, if any, and other information.

The work is carried out in the following order:

- 1) Data, tool, application and other product certification: The platform is a blockchain-based electronic data certification system. The system makes full use of the characteristics of the blockchain like decentralization and non-tampering, anchoring the product information on the blockchain, controlling the access of different users to the electronic data, and effectively solving the security problem of certification storage of the electronic data. It provides users with services like data upload, download, query, use and authorization. At the same time, distributed storage technology and access control mechanism are introduced to increase the reliability of the system.
- 2) Certification for ordering and using process of sharing supermarket products: For products on the shelf in this system, the enterprise users or individual users can register as system users of the platform. After successful registration, users must first conduct real name authentication, and then they can provide certification for the electronic data in cloud forensics system. Users can put all kinds of big data application products on the shelves. In order to protect the privacy of data and tool products, users can choose whether to encrypt or not.

3.4 Joint construction of big data application products based on Federated learning

Federated learning is a new basic technology of artificial intelligence. Google first proposed the concept of federated learning in 2016 [20]. Its main idea is to build a machine learning model based on data sets on multiple devices and preventing data leakage at the same time. Subsequently, scholars have further studied more secured and personalized federated learning mechanism, and optimized the data distribution imbalance, user management mechanism and other directions.

The big data application sharing supermarket brings together the internal units to update the model through federated learning. The model publisher publishes the model that needs further training to the sharing supermarket for collecting federated learning partners. After downloading the model, the partner uses the data of the unit to optimize and improve the model, and then uploads it. The updated model is immediately aggregated with the updates of other users to improve the sharing model.

The federated learning zone is built for users based on the following three aspects:

- (1) Secure multi-party computation: The security model involves multiple participants, and each participant needs to provide the security evidence of the simulation platform to ensure that each participant cannot obtain additional information except input and output. However, the ideal model needs a complex computing framework, and the effectiveness of its implementation is limited. In some scenarios, some knowledge disclosure can be considered and data disclosure with security guarantee can be accepted.

(2) Differential privacy: The differential privacy or anonymous technology is used to protect data privacy and conceals some sensitive attributes by adding noise to the data or using generalization method, so that the third party cannot distinguish the subjects. However, the specific implementation still requires data transmission to other places, which involves data authenticity and privacy issues.

(3) Homomorphic encryption: Privacy protection is realized by parameter exchange of machine learning under the encryption mechanism. The data and models themselves are not transmitted.

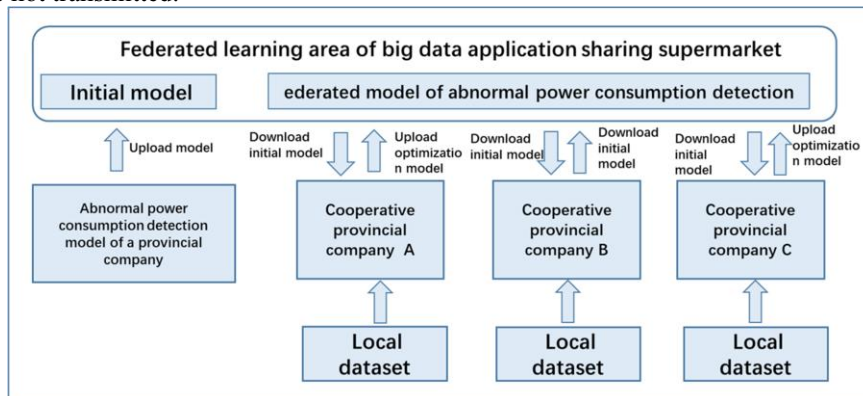


Figure 5 Federated learning zone of big data application sharing supermarket

Taking the forward propagation method of convolutional neural network as an example,

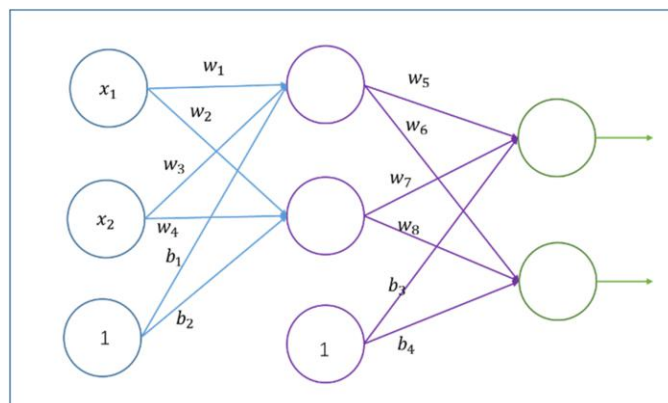


Figure 6 Schematic diagram of three-layer neural network

The communication scheme of federal learning privacy protection proposed in reference [21] is adopted; different TLS / SSL security channels are established between trainers and the parameter servers. The classical Advanced Encryption Standard (AES) encryption algorithm is used among the trainees to encrypt the public key PK and the private key sk of homomorphic encryption algorithm, the structural parameters of deep neural network model, the selected optimization algorithm and its learning rate.

If t is the number of iteration steps and $t=1$, the provincial companies get the provincial model gradient based on the local data, $J(\omega)$ is loss function, and ω is the parameter, then Gradient encryption is given by,

$$g(u_i, t) = \frac{\partial (J(\omega))}{\partial \omega} \quad (1)$$

H is a homomorphic encryption function

$$G(u_i, t) = H(g(u_i, t)) \quad (2)$$

Upload to the server of federal learning management system

The server carries out the weighted average:

$$\bar{G}_t = \sum_{i=1}^n p_i G(u_i, t) \quad (3)$$

The server sends it to the provincial company, and the provincial company gets the Decryption gradient, and D is the decryption function:

$$g(u_i, t + 1) = D(\bar{G}_t) \quad (4)$$

Proceed to the next iteration

$$t = t + 1 \quad (5)$$

Effect of federal learning

Table 1 Model effect

Model effect			
Model	Sample size	Prediction accuracy (%)	Recall (%)
Provincial companies independently identify the electricity theft (Neural network)	10000 (avg)	55.5(avg)	57.8 (avg)
Provincial companies use the federal learning model (Neural network)	10000 (avg) 50000 (avg)	80.6 (avg)	64.3 (avg)

4. Application effect

Table 2 shows the application of products and provincial usage on the shelves in the sharing supermarket.

Table 2 Big data products and usage

Big data products and usage				
ID	Product name	Number of provincial companies using products	Saving investment	
1	Electricity stealing identification	20	19	
2	Risk prediction of electricity charge	20	19	
3	Layout optimization of electric vehicles	10	9	
4	Customer service panoramic view	5	4	
5	Efficiency evaluation of business hall	16	15	
6	Customer portrait	27	26	
7	Identification of abnormal power consumption	29	28	
8	Overload prediction of distribution transformer	10	9	
9	Customer service efficiency analysis	5	4	
10	Power index monitoring for resumption of work and production	27	26	
11	Power marketing data service sharing	20	19	
12	Intelligent identification of abnormal electricity price	15	14	
13	Traffic prediction analysis	6	5	

5. Conclusions

Big data application sharing supermarket is an effective means of big data application sharing. In power application, it can achieve the purpose of providing services to many provincial companies by matured products of any provincial company. At the same time, as a sharing platform, it can help provincial companies to create new big data application products through federal learning.

6. Future work

At present, the big data application sharing supermarket is used by the internal users of the State Grid of China. How to cooperate with the external units and build the big data application sharing ecosystem are the key topics to be researched in the future.

At present, the planning for the external units is as follows: Firstly, leading Internet enterprises such as Alibaba, Huawei, Baidu and Tencent mainly rely on their advanced Internet thinking, creation, technical capabilities, large ecosystem, and reliable service resource capacity; secondly, the external research institutions mostly rely on their extensive research on theoretical basis, scientific research strength and talent advantages in their professional fields; thirdly, the government agencies, enterprises and institutions have actual demand for power data and application scenarios that can be applied to the industrial data.

The external key business planning of big data application sharing supermarket includes: first to carry out the transaction of big data on-shelf products with the support of supermarket construction; second, to understand the value-added realization of data through transaction and settlement; third, to gather partners, suppliers and demanders through sharing supermarket, and make use of platform advantages to facilitate multilateral transactions and product crowdfunding to enable transaction growth and enhance value-added realization of the data; fourth, to carry out the operation of sharing supermarket, expand the data commercialization service ecosystem, attract more ecological partners to participate, enrich the on-shelf products, and promote big data innovation by trading; and fifth, to carry out optimization iteration of sharing supermarket, constantly expand functions, consolidate data service capacity, and improve data security.

References

- [1] Kuo, Y. H., & Kusiak, A. From data to big data in production research: the past and future trends. *International Journal of Production Research*.2019, 57(15-16):4828-4853.
- [2] Lu, Y., & Xu, X. Cloud-based manufacturing equipment and big data analytics to enable on-demand manufacturing services. *Robotics and Computer-Integrated Manufacturing*.2019,57:92-102.
- [3] Zhang, Y., Zhang, R., Wang, Y., Guo, H., Zhong, R. Y., Qu, T., & Li, Z. Big data driven decision-making for batch-based production systems. *Procedia CIRP*.2019,83:814-818.
- [4] A. Papacharalampopoulos, J. Stavridis, P. Stavropoulos, G. Chryssolouris, Cloud-based Control of Thermal Based Manufacturing Processes. *Procedia CIRP*, 5th CIRP Global Web Conference-Research and Innovation for Future Production .2016, 55:254-259.
- [5] D. Mourtzis, E. Vlachou, N. Milas, N. Tapoglou, J. Mehnen, A cloud-based knowledge enriched framework for machining efficiency based on machine tool monitoring, *Journal of Engineering Manufacturing, IMECE Part B*, Accepted for publication.2017,233:278-292.

- [6] Qiu xiaogeng, Dong Xiangyu, Zhang Peng, Liang Wei, Guo Jun, Bai Kaifeng, Liang Zhixian, Feng Chao. Analysis of distribution transformer overload warning based on big data [J]. POWER SYSTEMS AND BIG DATA 2018, 21(10):38-42.
- [7] He Jianzhang, Wang Haibo, Ji Zhixiang, Meng Xiangjun, Zhang Tao. Heavy overload prediction of distribution transformer based on Stochastic Forest theory [J]. Power System Technology, 2018, 21(10):38-42.
- [8] Xie Yuande, Zhang Lin, Deng Shali, he jiemeng. Study on optimization network layout of electric vehicle charging facilities [J]. Practice and understanding of Mathematics, 2020,50(10):168-176.
- [9] Sun Yue, Jiang Cheng, Wang Zhizhi, Tang chunsen. Optimal layout of dynamic wireless power supply system for electric vehicles based on PSGA [J]. Power system automation, 2019, 43(9):125-131.
- [10] Li Jianbin, Wu Binbin, Zhu Yakui, Wang Yue, and Yagang, Zhao Shasha. Risk prediction and control of customer electricity tariff based on big data analysis [J]. Power Systems and Big Data ,2019, 22 (2):1-6.
- [11] He Rong, Zhang Xiangdong, Qiu Lin, Chen libing, Zhou Qian, Zhang Yan. Electricity tariff risk prevention and control based on clustering and logistic regression [J]. Power Systems and Big Data, 2019, 22(12): 42-49.
- [12] Zhao Hong, Shen Jianzhong, Wang Jun, Zhang Cheng, Qu Qing. Risk prediction model of electricity charge recovery based on customer portrait and machine learning algorithm and its application [J]. Microcomputer Applications, 2020, 36(2):93-96.
- [13] Wang Zongwei, Zhao Guoqi, Jin Peng, Yang Jing, Wang Hailong, Zhang Zuobin. Research on the risk identification model of electricity tariff based on customer credit system [J].Machine Design and Manufacturing Engineering , 2019, 48(10): 99-104.
- [14] Xie Ying, Wang Zheng, Zhao Yongliang. Research on risk identification model of customer electricity consumption behavior [J]. Zhejiang Electric Power, 2017,36(12):53-56.
- [15] Li J, Xu Z P, Zhou C L, Kang C T. Application architecture design of energy big data sharing and operation service platform [J]. Power and Energy, 2019, 40 (5): 568-571.
- [16] Qu H N, Pang X W, et al. Application value of power big data and analysis and design of its sharing platform. Management and Administration[J], 2017 (7):104-108.
- [17] JI Lusheng ,ZHANG Guiling ,YANG Jiarun. The protection scheme of personal data under the chain based on block chain, Computer Engineering[J], 2020,<https://doi.org/10.19678/j.issn.1000-3428.00.EC0057024>.
- [18] WANG Jingwei, ZHENG Zhenzhe, WU Fan, CHEN Guihai. Block chain based data marketplaces[J]. Big Data Research. <http://kns.cnki.net/kcms/detail/10.1321.g2.20200311.1050.004.html>.
- [19] YAN Shu, QING Sude, WEI Kai. Application of block chain in data circulation[J]. BIG DATA RESEARCH,2018 (1):3-12.
- [20] McMahan H B, Moore E, Ramage D, et al. Communication-efficient learning of deep networks from decentralized data[C]/Proceedings of the 20th International Conference on Artificial Intelligence and Statistics (AISTATS) .2017. JMLR: W&CP volume 54:1273-1282.
- [21] Phong L T, Aono Y, Hayashi T, Wang L H.Privacy-preserving deep learning via additively homomorphic encryption. IEEE Transactions on Information Forensics and Security. 2017, 13(5):1333-1345.

Estimating Observation Error Statistics Using a Robust Filter Method for Data Assimilation

Yue Wang^a, Yulong Bai^{a,1}

^a*College of Physics and Electrical Engineering, Northwest Normal University, Lanzhou
730070, China*

Abstract. For the data assimilation algorithms, the observation error covariance plays an important role, because they control the weight that is given to the model forecast and to the observation in the solution, i.e., the analysis. In order to easily calculate, we often assume observation to be a diagonal matrix, however, the observation errors are correlated to the state and have a certain dependence on time, such as certain observing types which are remotely sensed. In this work, we obtain the time-dependent and correlated observation error by the method of observation error estimation in the data assimilation system. We combine the ensemble time-local H-infinity filter (EnTLHF) with an estimate of observation error covariance matrix, named ensemble time-local H-infinity filter with observation error covariance estimation (EnTLHF-R). In the experiment, a classical nonlinear Lorenz-96 model to evaluate the performance of new method is used. The results show that the robust filtering with observation error estimation is more accurate, more robust, and the filtering is more stable.

Keyword: Robust filtering; Observation error covariance; Lorenz-96 model;
Robustness

1. Introduction

Data assimilation is a statistical process that combines numerical models with systematic observations to estimate the state of spatiotemporal dynamic systems. With the complexity and requirements of the actual situation, Evensen[1] used the idea of ensemble for Kalman filtering, and proposed the ensemble Kalman filter (EnKF) to solve the limitations imposed by dynamic models for complex nonlinear systems. However, the Kalman filtering-based method normally takes the error statistics as Gaussian distributions. For nonlinear, this assumption is often false. To address the issue of non-Gaussian error statistics, robust filtering is used to solve this limitation in the assimilation system[2]. Compared to Kalman filtering, robust filtering can guarantee that the error growth rate is bounded, and does not require certain assumptions about the model and observation system, Luo and Hoteit [3] apply the idea of ensemble to robust filtering to form ensemble time-localized robust filtering(EnTLHF). The observation error in the data assimilation usually includes two

¹ Corresponding author address: Yulong Bai, College of Physics and Electrical Engineering, Northwest Normal University, Lanzhou Gansu, 730070, China. E-mail: yulongbai@gmail.com

parts, instrument error and representation error. We often only consider the instrument error and assume it is an unit diagonal array, however recent literatures indicate that representation errors are correlated and have a certain dependence on the time and state [4][5][6]. And recent literatures indicate that observation errors are correlated and have a certain dependence on time and state [7][8][9]. Many scholars [10][11] have demonstrated that a rough approximation of the observed error covariance matrix may also provide significant benefits. And Desroziers et al [12] introduced a method based on two type innovations in the observation space to obtain the estimation of observation error covariance. So we will apply the estimating method into robust filtering and proposed a new method named robust filtering with observation error estimation (EnTLHF-R), and we will estimate observation error by DBCP method, the estimated observation error obtained is time-dependent and is related to the background and state of the previous moment.

In the work, we use typical Lorenz-96 chaotic system to compare the robustness and accuracy of robust filtering method with observation covariance estimation and robust filtering method, the results show considering estimation of observation error in the assimilation could improve accuracy and robustness.

In this paper. Section 2 presents the robust filtering method and how to apply the method of observation error covariance to the robust filtering. In the Section 3, we access the effectiveness of the new method to estimate observation error covariance and show the robustness of robust filtering with observation error covariance estimation. Concluding remarks are followed in summary.

2. Theoretical Background

2.1. Time-local H -infinity Filter (TLHF).

HF[2] is one of the robust filters involving the properties of the model and the observation system. Luo and Hoteit[3] applied the objective function in HF to Kalman filtering and proposed a new filtering method named time-localized H_∞ filtering (TLHF). The local cost function of TLHF is written as follows:

$$J_{x,i}^{HF} = \frac{\|x_i - x_i^a\|_{S_i}^2}{\|x_i - x_i^b\|_{(\Delta_i^b)^{-1}}^2 + \sum_{i=0}^N \|u_i\|_{Q_i^{-1}}^2 + \sum_{i=0}^N \|v_i\|_{R_i^{-1}}^2} \quad (1)$$

$$\frac{1}{\lambda} > \frac{1}{\lambda^*} \equiv \inf_{x_i^a} \sup_{x_i, u_i, v_i} J_{x,i}^{HF} \quad (2)$$

Where v_i , u_i represent process noise and measurement noise respectively. The subscript Q_i^{-1} , $(\Delta_i^b)^{-1}$, R_i^{-1} is called the information matrix. x_i and x_i^a are truth and estimating value of system. Equation (2) is the minimum and maximum criterion, where \sup represent the *supremum* of the cost function $J_{x,i}^{HF}$, relating to variables x_i, u_i, v_i .

x_i, u_i, v_i ; $\inf_{x_i^a}$ is the *infimum* responding to x_i^a . λ^* ensures that there is a value λ that meets the minimum and maximum criteria^[2].

Concretely, let $x_i^b = \{x_{i,j}^b : x_{i,j}^b = M_{i,i-1}(x_{i-1,j}^a), j = 1, \dots, n\}$ be the n-member background ensemble, deriving from the prediction of the analysis ensemble $x_{i-1}^a = \{x_{i-1,j}^a, j = 1, \dots, n\}$ at the previous cycle.

The prediction step of the EnTLHF:

$$\bar{x}_i^b = \text{mean}(x_i^b) \quad (3)$$

$$\hat{\Delta}_i^b = \text{cov}(x_i^b) + Q_i \quad (4)$$

The filtering step of the EnTLHF:

$$\bar{x}_i^a = \bar{x}_i^b + G_i(y_i - H_i(\bar{x}_i^b)) \quad (5)$$

$$(\Delta_i^a)^{-1} = (\Delta_i^b)^{-1} + (H_i)^T(R_i)^{-1}H_i - \lambda_i S_i = (P_i^a)^{-1} \quad (6)$$

$$\hat{G}_i = \hat{\Delta}_i^a(H_i)^T(R_i)^{-1} \quad (7)$$

Subject to the constraints:

$$(\Delta_i^a)^{-1} = (\Delta_i^b)^{-1} + (H_i)^T(R_i)^{-1}H_i - \lambda_i S_i = (P_i^a)^{-1} - \lambda_i S_i \geq 0 \quad (8)$$

Here Δ_i represents the uncertainty matrix, similar with the P_i^a in the KF, and G_i is the gain matrix. The symbol " ≥ 0 " means that the matrix is a semi-positive definite matrix. For Equation (6), the condition satisfying the semi-positive definite matrix is related to the value of variables R_i , λ_i , S_i . At the same time, we know that the value of λ_i is related to R_i , Q_i , S_i . In Equation (1), the value of R_i, Q_i, S_i is usually chosen freely by the designer[3][13], which motivates us to improve this algorithm in this article.

In Equation (6), we make some formula transformation:

$$\lambda_i S_i = c[(\Delta_i^b)^{-1} + (H_i)^T(R_i)^{-1}H_i] = c(P_i^a)^{-1} \quad 0 < c < 1 \quad (9)$$

C is the local performance level, and S_i is the information matrix that can be chosen by designer, so we consider the specific term of $\lambda_i S_i$, building the relation between $\lambda_i S_i$ and P_i^a . By inflating covariance, so we named an uncertainty inflation technique.

So the analysis error covariance becomes:

$$(\Delta_i^a)^{-1} = (1 - c)(P_i^a)^{-1} \quad (10)$$

Where the c called the performance level coefficient, which is related to the λ_i value.

2.2. Method of Estimating Observation Error

The DBCP method is based on the two types of innovation statistics between observations, forecasts and analysis. $d^b = y - H(x^f)$ named the background innovation and $d^a = y - H(x^a)$ named the analysis innovation. Taking their statistical expectation, then could obtain observation error covariance matrix.

$$E[d^a(d^b)^T] \approx R \quad (11)$$

2.3. Observation Error Covariance Matrix

The observation error includes two parts, instrument error and representation error:

$$R^T = R^I + R^H = \sigma_D^2 \varepsilon^I + \sigma_C^2 \varepsilon^H \quad (12)$$

$$\varepsilon^H(r) = (1 + |r|/L) \exp(-|r|/L) \quad (13)$$

Where R^T represents the true observation covariance matrix, R^I represents the instrument error covariance matrix, and R^H represents the correlated representative error covariance matrix. σ_D^2 is the uncorrelated error variance, ε^I is the instrument error, and σ_C^2 is the correlated error variance. ε^H is the correlation between two points separated by distance[6].

2.4. The Robust Filtering with Observation Error Estimation (EnTLHF-R)

In general, the robust filtering with observation error estimation consist four parts: initialization, running EnTLHF steps, computing innovations and estimating observation. The schematic diagram of robust filtering with observation error estimation is show in Table 1.

Table 1 Description of the ensemble time-local filter with observation error covariance estimation

Algorithm: EnTLHF-R

Initialization: Generate initial ensemble members $\{x_0^{a,i}\}, i=1, \dots, N$, observation vectors y_i , Initial background covariance matrix P_0^f , Determine the number of DBCP diagnostic samples N_s , Assume that the initial observation error covariance is R_{input} .

For $i=1$:assimilation step($i = 2N_s$)

ENTLHF: $x_i^f = \{x_{i,j}^f : x_{i,j}^f = M_j(x_{i-1,j}^a) \text{ j}=1, \dots, n\}$

If $i \leq N_s$

$R_i = R_{input}$

```

else
     $R_{t+1} = E[d^a(d^b)^T]$ 
end if
Prediction step:  $\bar{x}_i^b = \bar{x}_i^f = \text{mean}(x_i^f)$ 
 $\Delta_i^b = \text{cov}(x_i^b) + Q_i$ 
Obtain background innovation:  $d_i^b = y_i - H(\bar{x}_i^b)$ 
Filtering step:  $[p_i^a, K_i] = ETKF(X_i^b, Q_i, H_i)$ 
 $G_i = (I_m - \lambda_i P_i^a S_i)^{-1} K_i$ 
 $x_i^a = \bar{x}_i^b + G_i [y_i - H(\bar{x}_i^b)]$ 
Obtain analysis innovation:  $d_i^a = y_i - H(\bar{x}_i^a)$ 
If  $(\Delta_i^a)^{-1} = (p_i^a)^{-1} - \lambda_i S_i \geq 0$ 
Return  $\lambda_i$ 
Else
End for

```

3. Numerical Experiment

3.1. The Lorenz-96 Model.

The Lorenz-96 model is defined by ordinary differential equations (ODEs) defined over a periodic domain of variables indexed by $n=0\dots N_x - 1$ where $N_x = 40$

$$\frac{dx_n}{dt} = (x_{n+1} - x_{n-2})x_{n-1} - x_n + F \quad (14)$$

This model is an idealized for state estimation problems. For computational stability, a time step of 0.05 units is adopted. In the experiment, the value of the forcing term F can be changed, representing different degrees of model error and the solution of the Lorenz-96 equation is obtained by using the classic fourth-order Runge-Kutta. The total length of the iteration is 1500 steps.

3.2. Performance Comparison of two Robust Filtering Methods.

In this section, we show the performance of traditional robust filtering (EnTLHF) and new method (EnTLHF-R) on the Lorenz96 model. The results show the RMSE mean of EnTLHF and EnTLHF-R when observation error is RT.

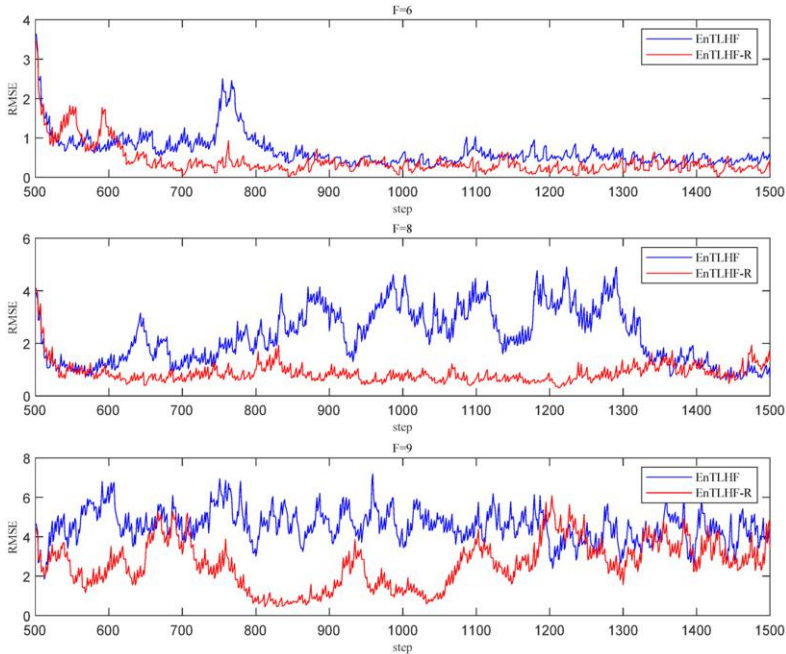


Figure 1. When forcing parameter $F=6, 8, 9$, the RMSE mean of EnTLHF and EnTLHF-R algorithm in the Lorenz-96 model

The results show: (1) the robust filtering with observation error estimation (EnTLHF-R) has lower Root Mean Squared Errors (RMSE) when the force parameter changes. (2) As force parameter increases the model error increase correspondingly, the RMSE of EnTLHF and EnTLHF-R increase, however the RMSE of EnTLHF-R is always lower EnTLHF. The larger the forcing parameter is, the more obvious the effect will be. Overall, the robust filtering with observation error estimation (EnTLHF-R) is more robust when model error is changing; this indicates that the new method improves the performance; the estimation of observation error covariance in the data assimilation may provide benefit.

3.3. Estimation of Observation Error Covariance

In this section, we access the ability of new method to accurately estimate R . In the experiment, we set the RT as the reference observation error covariance. The above Figure 2 (a) represents the covariance of the observation error obtained in the first estimation (the 126th assimilation), and the figure 2 (b) represents the estimated covariance of the observation error obtained in the 250th assimilation.

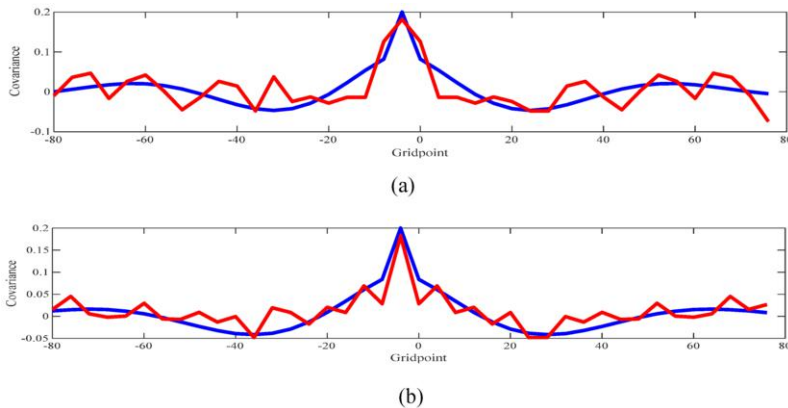


Figure 2. The blue line represents the true covariance matrix, and the red line represents the estimated covariance matrix. (a) Obtaining R using the first 125 innovations. (b) Obtaining covariance using the last 125 innovations

The results show: (1) when taking into account the spatial error correlations, the Desroziers diagnostic is useful to estimate off-diagonal term of observation. (2) The last estimating of R is more fitting RT; it also suggests that estimating method could obtain a time-dependent estimate of correlate observation.

4. Summary

This paper introduces traditional robust filtering method and new robust filtering method. In particular, the diagnostic method is coupled to obtain the time-varying observation error, in the simulation experiments; we compare the performance of robust filtering with observation error estimation and original robust filtering with Lorenz-96 model. In addition, we access the observation error estimation method; the results prove taking correlated observation into account in data assimilation is more benefit.

Acknowledgement

This work is funded by the NSFC (National Natural Science Foundation of China) project (grant number: 41861047 and 41461078), also based on Northwest Normal University young teachers' scientific research capability upgrading program (NWNU-LKQN-17-6).

References

- [1] Evensen G. Sequential data assimilation with a nonlinear quasi-geostrophic model using Monte Carlo methods to forecast error statistics. *Journal of Geophysical Research* 1994;99:10143-10162
- [2] Simon, D. *Optimal State Estimation: Kalman, H_{infinity}, and Nonlinear Approaches*. John Wiley & Sons, Inc.: Hoboken, New Jersey and Canada; 2006. pp 333- 365
- [3] Luo XD, Hoteit I. Robust ensemble filtering and its relation to covariance inflation in the ensemble Kalman filter. *Month Weather Review*. 2011 Jul; 139: 3938–3953.
- [4] Stewart LM. Correlated Observation Errors in Data Assimilation. PhD Thesis, University of Reading. 2010

- [5] Weston P. Progress towards the implementation of correlated observation errors in 4d-var. Technical report, Met Office, UK. Forecasting Research Technical Report.2011; 560.
- [6] Waller JA, Dance SL, Lawless AS, and Nichols NK. (2014) Estimating correlated observation error statistics using an ensemble transform Kalman filter. Tellus A: Dynamic Meteorology and Oceanography.2014 Set; 66:1, 23294
- [7] Janjic and Cohn SE. Treatment of observation error due to unresolved scales in atmospheric data assimilation. Month Weather Review, 2006 Feb; 134: 2900–2915.
- [8] Bormann N and Bauer P. Estimates of spatial and inter channel observation-error characteristics for current sounder radiances for numerical weather prediction. I: methods and application to ATOVS data. Quarterly Journal of Royal Meteorological Society. 2010 Apr; 136, 1036-1050.
- [9] Liu W. State estimation for discrete-time Markov jump linear systems with time-correlated measurement noise. Automatica. 2017, 76:266-276.
- [10] Stewart LM, Dance SL, and Nichols NK. Data assimilation with correlated observation errors: experiments with a 1-D shallow water model. Tellus A. Dynamic Meteorology and Oceanography. 2013 Apr; 65:1, 9546.
- [11] Healy SB, and White AA. Use of discrete Fourier transforms in the 1D-Var retrieval problem. Quarterly Journal of Royal Meteorological Society.2005; 131, 63-72
- [12] Desroziers G, Berre L, Chapnik B. and Poli P. Diagnosis of observation, background and analysis-error statistics in observation space. Quarterly Journal of Royal Meteorological Society. 2005 Oct; 131: 3385-3396
- [13] Bai YL, Zhang ZH. Inflating transform matrices to mitigate assimilation errors with robust filtering based ensemble Kalman filters. Atmospheric science letters.2016 Jul; 17: 470-478.

Community Detection, Pattern Recognition, and Hypergraph-Based Learning: Approaches Using Metric Geometry and Persistent Homology

Dong Quan Ngoc NGUYEN^{a,1}, Lin XING^a, and Lizhen LIN^a

^a*Department of Applied and Computational Mathematics and Statistics,*

University of Notre Dame,

Notre Dame, Indiana 46556 USA

Abstract. Hypergraph data appear and are hidden in many places in the modern age. They are data structure that can be used to model many real data examples since their structures contain information about higher order relations among data points. One of the main contributions of our paper is to introduce a new topological structure to hypergraph data which bears a resemblance to a usual metric space structure. Using this new topological space structure of hypergraph data, we propose several approaches to study community detection problem, detecting persistent features arising from homological structure of hypergraph data. Also based on the topological space structure of hypergraph data introduced in our paper, we introduce a modified nearest neighbors methods which is a generalization of the classical nearest neighbors methods from machine learning. Our modified nearest neighbors methods have an advantage of being very flexible and applicable even for discrete structures as in hypergraphs. We then apply our modified nearest neighbors methods to study sign prediction problem in hypergraph data constructed using our method.

Keywords. Distance matrices; Hypergraphs; Metric geometry; Metric spaces; Nearest Neighborhoods; Persistent homology;

1. Introduction

One of the challenges in the modern age is to classify data arising from many resources; for example, following the rapid developments of several areas in mathematics, a large number of publications in mathematics creates a tremendous amount of data, which signifies useful information such as relationships (or collaborations) among authors and their publications, and their influences on development of mathematics. It is often the case that analyzing such data is not straightforward, and very difficult task because of the extremely fast growth of relations among data, and of data itself.

¹Corresponding Author: Department of Applied and Computational Mathematics and Statistics, University of Notre Dame, Notre Dame, Indiana 46556 USA; E-mail: dongquan.ngoc.nguyen@nd.edu

In this paper, we propose several methods to analyze *hypergraph data*. Recall that a hypergraph X is a pair $(\mathcal{V}(X), \mathcal{E}(X))$, where $\mathcal{V}(X)$ is the set of data points (called vertices of X), and $\mathcal{E}(X)$ is a subset of the power set of $\mathcal{V}(X)$ which represents relations among data points. Each element in $\mathcal{E}(X)$ is called a *hyperedge*. Note that by abuse of notation, we sometime use the same symbol for X and its set of vertices.

A standard example of a hypergraph is a collaboration network in which the set of vertices consists of mathematicians, and a group of mathematicians (not necessarily only two) forms a hyperedge if they have at least one joint publication. Many real data can be modeled as a hypergraph. Applications of hypergraph data are diverse such as in protein function prediction (see [1]), and other areas (for example, see [2], [3], [4], [5]).

The aim of this paper is to propose several approaches to studying community detection, pattern recognition, and sign prediction problem. Our approaches use main tools from metric geometry (see, for example, [6]), combined with techniques from geometric and topological inference, to adapt classical techniques such as nearest neighbors methods into the hypergraph settings. More precise, for a given hypergraph data, we introduce a class of metrics modulo certain equivalence relations (for a precise definition, see Section 2) to equip such hypergraph with a metric space structure. Using these structures, we propose several approaches to detect features from hypergraphs; for example, only using distance matrix approach, we provide a way to approach to community detection problem. Based on the metric space structure, we apply tools from algebraic topology to propose a method for detecting *persistent features* arising from homological structures hidden in a hypergraph. Such approach has an advantage of visualization of the space structure of data which provides a visual insight into the topological structure of hypergraph data. Also based on the metric space structure of hypergraph data, we introduce a modified nearest neighbors method which is a generalization of the classical nearest neighbors method from machine learning. Using our modified nearest neighbors methods, we apply to sign prediction problem on hypergraph data constructed by our method.

One of the novel and main features in our paper is that we propose a new type of hypergraph data (which we coin the term “*congruence hypergraph data*”) which are very easy to construct and implement, and very flexible for testing our theories.

The structure of our paper is as follows. In Section 2, we introduce several notions and our main metric on hypergraphs that will be used throughout the paper. In Section 3, we introduce congruence hypergraph data, and several methods for analyzing hypergraph data including the distance matrix approach, homology-based learning, and modified nearest neighbors methods. Several examples will be performed on congruence hypergraph data which we introduce in Subsection 3.2.

2. Basic notions

2.1. Metrics modulo equivalence relations

Let X be a set. An *equivalence relation*, denoted by \cong , on X is a subset of $X \times X$ such that the following conditions are true:

- (i) (**Reflexivity**) $(a, a) \in \cong$ for every $a \in X$.
- (ii) (**Symmetry**) $(a, b) \in \cong$ if and only if $(b, a) \in \cong$.
- (iii) (**Transitivity**) if $(a, b) \in \cong$ and $(b, c) \in \cong$ then $(a, c) \in \cong$.

When $(a, b) \in \cong$, we say that a is \cong -equivalent to b . Throughout this paper, in order to signify this relation, we write $a \cong b$ whenever $(a, b) \in \cong$.

For a given high order network (which is another terminology for hypergraph data), one of the problems that we address in this paper is concerned with *distinguishing communities* in the network. It is clear that there are many examples of networks in which several communities are viewed as identical communities with respect to certain properties that one wants to know about these networks. So if we view a given high order network X as a hypergraph, in order to use a metric geometry approach to the community detection problem, it is natural to introduce a metric (or distance) on X modulo a certain equivalence relation which will be explicitly introduced depending on the structure of X . Before making it clear what exactly we mean by this point of view, using an example of high order collaboration network, we first introduce the notion of a metric modulo an equivalence relation.

Definition 2.1 Let X be a set, and let \cong be an equivalence relation on X . A mapping $d : X \times X \rightarrow \mathbb{R}$ is said to be a metric on X modulo the equivalence relation \cong if the following conditions are satisfied:

- (i) $d(a, b) \geq 0$ for all $a, b \in X$.
- (ii) $d(a, b) = 0$ if and only if $a \cong b$.
- (iii) (**Symmetry**) $d(a, b) = d(b, a)$ for all $a, b \in X$.
- (iv) (**Triangle inequality**) for any $a, b, c \in X$,

$$d(a, b) \leq d(a, c) + d(c, b).$$

A set X equipped with a metric modulo an equivalence relation \cong , say $d : X \times X \rightarrow \mathbb{R}$ is called a metric space modulo \cong . In notation, we write (X, d) to indicate this metric space modulo \cong .

2.2. Hypergraphs equipped with intrinsic properties

Let X be a set. In order to create a *hypergraph* structure on X , we view the set of all points in X as the set of vertices $\mathcal{V}(X)$, and one needs to identify the relations among points in X , which one can view as the set of hyperedges of X , denoted as $\mathcal{E}(X)$. A hyperedge having exactly ℓ vertices is called an ℓ -hyperedge. The way which one identifies hyperedges in X , signifies certain properties pertained to the set X that we want to study. For example, let X be a set of mathematicians. In order to study how collaborative the mathematicians in X are, we introduce a hypergraph structure on X as follows. The set of vertices of X simply consists of all mathematicians in X . A group of mathematicians, say m_1, \dots, m_ℓ in X forms an ℓ -hyperedge if they have at least one joint publication. In this way, the set X becomes a hypergraph in which the construction of hyperedges signifies the collaboration among mathematicians in X .

In many real data examples, one is not only interested in the hypergraph structure of X , but also in knowing certain properties attached to such structure but hidden in the hyperedge data. For example, in the collaboration network just described, in order to study in which areas of mathematics the mathematicians in X have joint publications, we can associate to each hyperedge the *main area of mathematics* in which the joint publication of the hyperedge belongs. If an ℓ -hyperedge e is formed out of the joint paper,

say P , of ℓ mathematicians m_1, \dots, m_ℓ , and the paper P is mainly concerned about number theory, then one can define $\Gamma(\epsilon) = \text{number theory}$. Hence one obtains a mapping Γ from the set of hyperedges of X to the set of all areas in mathematics. Studying such a map Γ provides insight into the relationships between joint publications of mathematicians in X and their contributions to certain fields in mathematics. Motivated by this example in mind, we introduce a notion of hypergraphs equipped with certain properties.

Definition 2.2 Let $X = (\mathcal{V}(X), \mathcal{E}(X))$ be a hypergraph, and let \mathcal{P} be a nonempty set. The hypergraph X is called a hypergraph equipped with properties \mathcal{P} if there is a map $\Gamma : \mathcal{E}(X) \rightarrow \mathcal{P}$ which associates each hyperedge in X to a unique element in \mathcal{P} .

In notation, we write $\{X, \mathcal{P}\}_\Gamma$ to indicate X is a hypergraph equipped with properties \mathcal{P} , where the subscript Γ is a map from $\mathcal{E}(X)$ to \mathcal{P} .

In this subsection, for each hypergraph equipped with properties \mathcal{P} , say $\{X, \mathcal{P}\}_\Gamma$, we introduce a metric space structure on X , which provides a way to distinguishing communities in X . We begin by defining a notion of neighborhood of a vertex which is more suitable for defining a metric on the hypergraph X .

Definition 2.3 Let $X = (\mathcal{V}(X), \mathcal{E}(X))$ be a hypergraph. Let a be a vertex in X . The neighborhood of a , denoted by $\mathcal{N}(a)$, is defined by

$$\mathcal{N}(a) = \{a\} \cup \{b \in \mathcal{V}(X) \mid \exists \epsilon \in \mathcal{E}(X) \text{ such that } \{a, b\} \subset \epsilon\}.$$

The next result is clear from the above definition.

Proposition 2.4 Let X be a hypergraph whose set of vertices consists of a_1, \dots, a_n . Then X can be decomposed into n neighborhoods, say $\mathcal{N}(a_1), \dots, \mathcal{N}(a_n)$ of the form

$$X = \mathcal{N}(a_1) \cup \dots \cup \mathcal{N}(a_n).$$

Remark 2.5 For the community detection problem, the proposition above plays a key role. Indeed, by communities in X , we mean neighborhoods of each vertex. And thus in order to point out differences among communities, we are interested in finding out the exact differences among the populations of hyperedges with specific properties in \mathcal{P} , contained in these neighborhoods; more precisely, letting a property P range over the set \mathcal{P} , the differences between the neighborhoods of a_i and a_j are reflected in terms of the differences between the numbers of hyperedges contained in the neighborhoods of a_i and a_j whose values under the map Γ is exactly P , i.e., they share the same property P . Because of this observation and the proposition above, we want to study neighborhoods of vertices in X instead of the vertices themselves, and thus one views X as a space whose points are neighborhoods $\mathcal{N}(a_i)$. So each neighborhood is in fact viewed as a single point in the space X .

The metric geometry approach we use in this paper is that we want to construct a metric d on such a space X which should incorporate information about the number of hyperedges in X with specific properties P . And once such a metric is established for the space X , two neighborhoods $\mathcal{N}(a_i), \mathcal{N}(a_j)$ (i.e., two points in X) are different if and only if $d(\mathcal{N}(a_i), \mathcal{N}(a_j))$ is nonzero. And this is our first method for distinguishing communities in hypergraphs.

Let $\{X, \mathcal{P}\}_\Gamma$ be a hypergraph equipped with properties \mathcal{P} . Suppose that the set of vertices in X consists of a_1, \dots, a_n , and the largest size of hyperedges in X is ℓ . Let $1 \leq i \leq n$ be an integer. For each property $P \in \mathcal{P}$, let $\mathfrak{C}_P^1(a_i)$ be the number of 1-hyperedges in $\mathcal{N}(a_i)$ whose value under the map Γ is P . In a similar manner, let $\mathfrak{C}_P^2(a_i)$ be the number of 2-hyperedges in $\mathcal{N}(a_i)$ whose value under the map Γ is P . In general, for any integer $1 \leq m \leq \ell$, let $\mathfrak{C}_P^m(a_i)$ be the number of m -hyperedges in $\mathcal{N}(a_i)$ whose value under the map Γ is P . Thus one obtains a unique double sequence $((\mathfrak{C}_P^m(a_i))_{1 \leq m \leq \ell})_{P \in \mathcal{P}}$ of non-negative real numbers for each neighborhood $\mathcal{N}(a_i)$.

We introduce an equivalence relation on the space X which allows to identify certain points in X . Note that if two points, say $\mathcal{N}(a_i)$ and $\mathcal{N}(a_j)$ have the same double sequence $((\mathfrak{C}_P^m(a_i))_{1 \leq m \leq \ell})_{P \in \mathcal{P}} = ((\mathfrak{C}_P^m(a_j))_{1 \leq m \leq \ell})_{P \in \mathcal{P}}$, then it is natural to view both of them as *identical points* in X since their hyperedge structures are exactly the same with respect to the map Γ and the properties \mathcal{P} . Hence it is natural to define a binary relation on X as follows: *two points $\mathcal{N}(a_i)$ and $\mathcal{N}(a_j)$ are equivalent, denoted by $\mathcal{N}(a_i) \cong \mathcal{N}(a_j)$ if their associated sequences $((\mathfrak{C}_P^m(a_i))_{1 \leq m \leq \ell})_{P \in \mathcal{P}}, ((\mathfrak{C}_P^m(a_j))_{1 \leq m \leq \ell})_{P \in \mathcal{P}}$ are identical, i.e., $\mathfrak{C}_P^m(a_i) = \mathfrak{C}_P^m(a_j)$ for all $1 \leq m \leq \ell$ and all $P \in \mathcal{P}$.* One obtains the following.

Proposition 2.6 *The binary relation “ \cong ” is an equivalence relation.*

For the rest of this paper, whenever we use the symbol \cong on hypergraphs, we mean the equivalence relation “ \cong ” in the proposition above.

Now we define a mapping $\mathcal{D} : X \times X \rightarrow \mathbb{R}_{\geq 0}$ as follows. For $1 \leq i, j \leq n$, define

$$\mathcal{D}(\mathcal{N}(a_i), \mathcal{N}(a_j)) := \sum_{P \in \mathcal{P}} \sum_{m=1}^{\ell} |\mathfrak{C}_P^m(a_i) - \mathfrak{C}_P^m(a_j)|.$$

From the above definition, we obtain the following.

Theorem 2.7 *The mapping \mathcal{D} defined above is a metric on X modulo the equivalence relation \cong .*

The proof of the above theorem will be given in the appendix.

Remark 2.8 *In [7, Definition 7, p.1060], Leontjeva et al. constructed a distance function (or metric) between hypergraphs which uses the sizes of hyperedges in hypergraphs, in contrast to our construction using the number of hyperedges of each size. Note that in [7], Leontjeva et al. claimed their metric is the metric in the usual sense which is not correct. It is in fact a metric modulo an equivalence relation.*

3. Analysis for hypergraph data

In this section, we propose several methods for analyzing hypergraph data. Instead of using real data examples as in most papers studying data structures in literature, we introduce in this paper a new type of data which is inspired from elementary number theory (or more precisely from the theory of congruences in number theory), and is extremely easy to construct. There are many advantages of using such data which can also

be viewed as hypergraphs. For simplicity, we call such data *congruence hypergraph data*. Firstly, these data are very easy to construct, simply using congruences in the ring of integers \mathbb{Z} . Secondly, congruence hypergraph data are very *diverse* and *random*, which provide a reasonably fine data to immediately test theory without referring to other data resources which in turn take a huge amount of time to build. The *randomness* of congruence hypergraph data allows to justify with high probability that any theory used to successfully test on such data can be also applied to real data examples. Lastly, for congruence hypergraph data, we can easily control the size of data. On letting the data size go to infinity, one can detect patterns hidden in the data which are often not available and straightforward if the data size is only limited to be finite.

3.1. Congruence hypergraph data

We now describe congruence hypergraph data which relies on the theory of congruences in the ring of integers \mathbb{Z} .

Let n be a positive integer, and $\{m_1, \dots, m_n\}$ be a collection of positive integers. Take n collections of integers, say $\{a_{i,1}, \dots, a_{i,m_i}\}$ for each $1 \leq i \leq n$ such that

$$\{a_{i,1}, \dots, a_{i,m_i}\} \cap \{a_{j,1}, \dots, a_{j,m_j}\} = \emptyset$$

for any $i \neq j$.

Consider n sets of integers, say $V_i = \{a_{i,1}, \dots, a_{i,m_i}\}$ for each $1 \leq i \leq n$ so that $\#V_i = m_i$. We want to introduce a hypergraph structure on each V_i , and thus the set $X = V_1 \cup V_2 \cup \dots \cup V_n$ becomes a hypergraph which is a disjoint union of subhypergraphs V_i .

Now take an integer $1 \leq i \leq n$. Let s_i be an integer such that $2 \leq s_i \leq m_i$. We want to introduce a hypergraph structure on V_i such that the largest size of hyperedges in V_i is s_i .

Let $\{p_{2,i}, \dots, p_{s_i,i}\}$ be a sequence of integers such that the $p_{j,i}$ are ≥ 2 and not necessarily distinct. Correspondingly we choose a sequence of finite sets of integers $\{S_{2,i}, \dots, S_{s_i,i}\}$ for each $1 \leq i \leq r$.

Let k be an integer such that $2 \leq k \leq s_i$. A k -tuple of integers $\{\alpha_1, \dots, \alpha_k\}$ in V_i forms a k -hyperedge if the following conditions are satisfied:

- (i) $\alpha_s - \alpha_r \equiv 0 \pmod{p_{k,i}}$ for any $1 \leq s, r \leq k$.
- (ii) $\alpha_s \pmod{p_{k,i}}$ belongs in $S_{k,i}$ for any $1 \leq s \leq k$.

So we have obtained a subhypergraph structure for each of the V_i , and thus $X = \cup_{i=1}^n V_i$ is a hypergraph which splits into disjoint subhypergraphs. Note that X has exactly $m_1 + m_2 + \dots + m_n$ vertices.

3.2. Main example

The hypergraph data we use to test our proposed methods in this paper is motivated from the construction of congruence hypergraph data in Subsection 3.1. We now describe two hypergraphs that we use throughout this work.

3.2.1. First example

Let $X = \{1, \dots, 1000\}$. We introduce a hypergraph structure on X as follows. A pair $\{a, b\}$ in X forms a 2-hyperedge if and only if either $a, b \equiv 1 \pmod{2}$ or $a, b \equiv 0 \pmod{2}$. In other words, a, b have the same parity. Now for each $3 \leq n \leq 9$, an n -tuple $\{a_1, \dots, a_n\}$ forms an n -hyperedge if and only if

$$a_i \pmod{n} = \begin{cases} 0 & \text{if } n \equiv 0 \pmod{3} \\ 1 & \text{if } n \equiv 1 \pmod{3} \\ 2 & \text{if } n \equiv 2 \pmod{3} \end{cases}$$

for every $1 \leq i \leq n$.

Since this data is about integers, we are interested in properties regarding integers such as divisibility. For this reason, we study, for example, the divisibility by 11 of each vertex in a hyperedge in X . So it is natural to define a map $\Gamma : \mathcal{E}(X) \rightarrow \{0, 1\}$ by letting, for each n -hyperedge $\{a_1, \dots, a_n\}$ in $\mathcal{E}(X)$,

$$\Gamma(\{a_1, \dots, a_n\}) = 1$$

if

$$a_i \equiv 0 \pmod{11} \quad (1)$$

for every $1 \leq i \leq n$, and

$$\Gamma(\{a_1, \dots, a_n\}) = 0$$

if condition (1) is not satisfied.

The hypergraph X above has very large number of hyperedges. Up to our knowledge, comparing with real data examples in literature, the hypergraph data X above contains the *largest* number of hyperedges which is very suitable for testing theories. For example, the number of hyperedges in the neighborhood (or community) of the vertex 1 is approximately 2.3685×10^{11} .

3.2.2. Second example

Let X be a set of integers obtained by randomly selecting 5000 positive integers. The sizes of hyperedges range from 2 to 9. We randomly select 8 integers, say $\{\alpha_2, \dots, \alpha_9\}$, such that any two of them have no common divisors. The set of vertices X are sorted in increasing order. For each $2 \leq n \leq 9$, we divide X into n subsets. The first subset, say X_1 , contains vertices a in X such that $\min(X) \leq a \leq p_1$, where $\min(X)$ is the minimum value of X and p_1 is the $1/n$ -th percentile of X . For each $2 \leq j \leq n$, the j -th subset, say X_j , contains vertices a in X such that $p_j < a \leq p_{j+1}$, where p_j is the j/n -th percentile of X . An n -tuple $\{a_1, \dots, a_n\}$ forms an n -hyperedge if and only if

$$a_j \equiv 1 \pmod{\alpha_n} \text{ and } a_j \in X_j$$

for every $1 \leq j \leq n$.

Then we randomly select an odd prime number β that does not divide any elements in $\{\alpha_2, \dots, \alpha_9\}$. The congruence classes modulo β are divided into two sets, the first of which consists of $\{-(\beta-1)/2, -(\beta-1)/2+1, \dots, -1, 0\}$, and the second of which consists of $\{1, 2, \dots, (\beta-1)/2\}$. Set

$$S_\beta^- = \{-(\beta-1)/2, -(\beta-1)/2+1, \dots, -1, 0\},$$

and

$$S_\beta^+ = \{1, 2, \dots, (\beta-1)/2\}.$$

The properties of hyperedges are defined as follows. For each n -hyperedge $\{a_1, \dots, a_n\}$ in $\mathcal{E}(X)$,

$$\Gamma(\{a_1, \dots, a_n\}) = -1$$

if every a_i modulo β belongs to S_β^- , and

$$\Gamma(\{a_1, \dots, a_n\}) = 1$$

otherwise.

3.3. Using patterns from the distance matrices to recognize patterns in hypergraph data

In this subsection, we describe a simple but useful approach to detecting communities in hypergraphs. Using this approach, one can identify which communities in a hypergraph are the same with respect to the equivalence relation “ \cong ” and the metric \mathcal{D} in Subsection 2.2. On the other hand, one can also find patterns among vertices whose neighborhoods (i.e., communities) are identified as the same.

Let $\{X, \mathcal{P}\}_\Gamma$ be a hypergraph equipped with properties \mathcal{P} . Assume that the set of vertices in X consists of a_1, \dots, a_n . Hence there are exactly n neighborhoods (or communities), say $\mathcal{N}(a_1), \dots, \mathcal{N}(a_n)$ which as remarked in Remark 2.5 can be viewed as points in the space X . Using the metric \mathcal{D} , we equipped X with a metric space structure in which each community $\mathcal{N}(a_i)$ is a point of the metric space X . Since there are exactly n points $\mathcal{N}(a_1), \dots, \mathcal{N}(a_n)$ in the metric space, one obtains the *distance matrix* of the finite metric space X , say \mathcal{M}_X of dimensions $n \times n$ of the form

$$\mathcal{M}_X = (\mathcal{D}(\mathcal{N}(a_i), \mathcal{N}(a_j)))_{1 \leq i, j \leq n},$$

where the (i, j) -entry in this matrix is the value $\mathcal{D}(\mathcal{N}(a_i), \mathcal{N}(a_j))$.

In order to identify which communities are the same in the hypergraph X , we identify all zero entries in \mathcal{M}_X except the diagonal. More precisely, let $1 \leq i \leq n$, and consider the i -th column in \mathcal{M}_X . Define

$$Z_i = \{1 \leq j \leq n \mid j \neq i \text{ and } \mathcal{D}(\mathcal{N}(a_i), \mathcal{N}(a_j)) = 0\}.$$

Then the set Z_i consists of all vertices j whose communities $\mathcal{N}(a_j)$ are considered to be the same as the community $\mathcal{N}(a_i)$. It is often the case that one can find patterns to describe Z_i .

We use the hypergraph data in section 3.2.1. In this case X is a hypergraph whose vertices are $1, 2, \dots, 1000$. Thus the distance matrix \mathcal{M}_X is of dimensions 1000×1000 . For example, considering the 1st column of \mathcal{M}_X , we see that Z_1 contains exactly the following vertices: 29, 43, 71, 85, 113, 155, 169, 211, 239, 253, 281, 295, 323, 365, 379, 421, 449, 463, 491, 505, 533, 575, 589, 631, 659, 673, 701, 715, 743, 785, 799, 841, 869, 883, 911, 925, 953, 995. And thus the communities (or neighborhoods) of these vertices are viewed as the same as that of the vertex 1.

From the list of vertices in Z_1 , one can recognize the patterns shared by the vertices in Z_1 . Indeed all vertices j in Z_1 satisfy the following four conditions: (i) $j \not\equiv 0 \pmod{3}$; (ii) $j \not\equiv 2 \pmod{5}$; (iii) $j \equiv \pm 1 \pmod{4}$; and (iv) $j \equiv 1 \pmod{7}$.

From the distance matrix \mathcal{M}_X , one also can identify the set of all distinct communities in X consisting of the neighborhoods of 1, 2, 3, 4, 5, 6, 7, 8, 12, 15, 22, 27, 36, 57, 127, and 162 such that every community in X is equal to exactly one of these neighborhoods.

3.4. Homology-based learning using the metric \mathcal{D}

In this subsection, we use the *persistent homology* of filtrations of simplicial complexes arising from a finite metric space modulo an equivalence relation $\cong X$ to study the community detection problem. For simplicity, in this subsection, we simply call X a metric space instead of a metric space modulo \cong . Let $\mathcal{V} = \{a_1, \dots, a_n\}$ be a finite set. A *simplcial complex* X with vertex set \mathcal{V} is a set of finite subsets of \mathcal{V} satisfying the following conditions:

- (i) every element in \mathcal{V} belongs to X ;
- (ii) if $\tau \in X$ and $\sigma \subseteq \tau$, then $\sigma \in X$.

The elements of X are called the *simplices* of X . If a simplex σ has exactly $k+1$ elements, the *dimension* of σ is k , and we call σ a k -simplex.

To each simplicial complex X one can associate a unique sequence of *homology groups* $(H_k(X))_{k \geq 0}$ which contains information about topological and geometric properties of X . (See, for example, [8] or [9] for a notion of homology groups and their properties.)

Now we describe how to use homology groups to identify distinct communities in hypergraphs. Let $\{X, \mathcal{P}\}_\Gamma$ be a hypergraph equipped with properties \mathcal{P} , and suppose that the set of vertices of X consists of the vertices a_1, \dots, a_n . We equip X with the metric \mathcal{D} in Subsection 2.2.

We introduce a method to attach to the finite metric space X a collection of simplexes which one in turn can obtain the corresponding *persistent homology sequences* and their *barcodes* (see [10], [11], [12], [13], [14] for persistent homology and barcodes.) We first recall a notion of Vietoris–Rips complex.

Definition 3.1 Let $\varepsilon > 0$, and let X be a finite metric space with metric \mathcal{D} . The Vietoris–Rip complex, denoted by $\mathcal{VR}(X, \varepsilon)$ is defined by the following condition: a $k+1$ -tuple $\{x_0, \dots, x_k\}$ forms a k -simplex in $\mathcal{VR}(X, \varepsilon)$ if and only if $\mathcal{D}(x_i, x_j) \leq \varepsilon$ for all i, j .

Let h be a sufficiently large positive integer, and let $1 \leq n_1 < n_2 < \dots < n_h = n$ be a collection of positive integers. For each $1 \leq k \leq h$, define

$$X_k = \{a_1, \dots, a_{n_k}\}.$$

Note that $X_k \subset X$ for all $1 \leq k \leq h$, and thus each X_k is a metric space with the same metric \mathcal{D} . We have a filtration of metric spaces

$$X_1 \subset X_2 \subset \dots \subset X_h = X.$$

For each finite metric space X_k , one obtains a filtration of Vietoris–Rip complexes $\mathcal{VR}(X_k)$ from which one obtains the *barcode* containing the topological and geometric information about X_k . The key observation using homology-based learning is that when k ranges from 1 to h , the barcodes of dimension 0 will stabilize to have exactly m bars, which signifies that *there are exactly m distinct communities* in the hypergraph X . Furthermore when considering the barcodes of dimension 1, they will stabilize to have very similar forms when k approaches to h .

We illustrate the above method by testing this theory on sub-hypergraph datasets of the congruence hypergraphs defined in the first and second examples in Subsections 3.2.1 and 3.2.2. Note that for computing barcodes, we use the package **TDAstats** in *R* (see [15]). For the first example, let $h = 3$, and for each $0 \leq k \leq h$, set

$$X_k = \{1, \dots, (2k+1)100\},$$

and $X_3 = \{1, \dots, 700\}$. One obtains exactly 4 barcodes, each of which corresponds to exactly one X_k .

In the barcode of X_0 (see Fig. 1a), we observe that the barcodes of dimension 0 (the blue barcodes) have exactly 13 bars; so there are 13 distinct communities in X_0 . For the barcodes of X_1 , X_2 , X_3 (see Fig. 1b, 1c, 1d), we note that all barcodes of dimension 0 have exactly 15 bars (which is stabilized), and thus since X_3 is the last finite metric space in the filtration

$$X_0 \subset X_1 \subset X_2 \subset X_3,$$

we deduce that there are exactly 15 distinct communities. This result agrees with the one in Subsection 3.3.

On the other hand, note that in the barcode of dimension 0 of X_0 , there are 13 bars, and in the barcode of dimension 0 of X_1 , there are 15 bars. Since $X_0 = \{1, \dots, 100\}$, and $X_1 = \{1, \dots, 300\}$, we conclude that out of 15 distinct communities in X_3 , 13 of them are communities of vertices in X_0 , and 2 of them belong to the communities in X_1 .

Note that one can also study barcodes of dimension 1 of the metric spaces X_k , and observe that the barcodes of dimension 1 of X_1 , X_2 and X_3 have exactly 5 important bars, and the remaining bars are *noises*. All these 5 bars have similar patterns although the number of vertices in X_k changes when k varies from 0 to 3. Using persistent homology, one can also realize geometric properties of each X_k , for example, how *connected* these spaces are.

For the second example, we choose the 8 integers $\alpha_2, \dots, \alpha_9$ to be 3, 4, 5, 7, 11, 13, 17, 19, respectively, and the prime number $\beta = 23$. We randomly select 700 integers

from $\{1, \dots, 1000\}$ and sorted in increasing order, denoted as Y_3 . Let $h = 3$, for each $0 \leq k < h$, set Y_k to be the first $(2k+1)100$ integers in Y_3 . Thus we have a filtration of metric spaces

$$Y_0 \subset Y_1 \subset Y_2 \subset Y_3.$$

Fig. 2 presents the 4 barcodes, each of which corresponds to one Y_k . Note that the barcodes of Y_0 to Y_3 have similar patterns in both of dimension 0 and dimension 1. As the number of vertices increases, the barcodes become stabilized.

An important remark is that when comparing the barcodes of the X and Y , for example, in dimension 0, the barcodes of the Y is very connected, which indicates that communities in Y are closely related to each other. This can be seen by observing that each integer can fall into congruence classes of different moduli 3, 4, 5, 7, 11, 13, 17, 19. In contrast, in order to define hyperedges of X in the first example, the conditions depend on certain congruence classes modulo 3, and thus the communities of X are decomposed into distinct connected components which are related to congruence classes modulo 3 in some way.

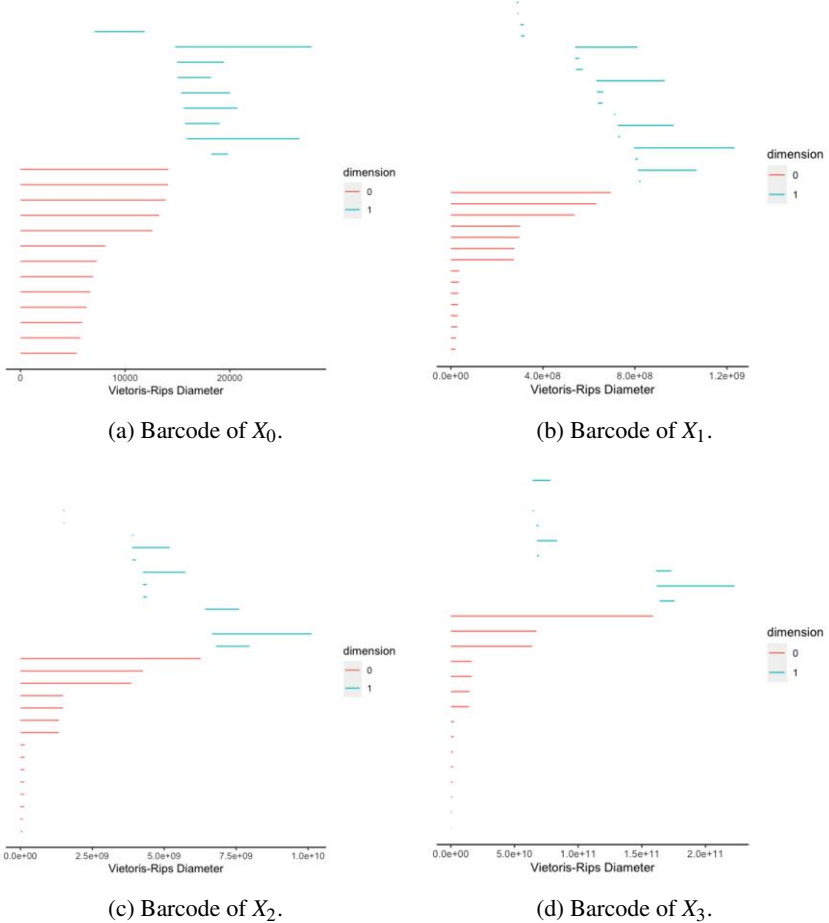
3.5. Hypergraph-based learning using the metric \mathcal{D} and nearest neighborhoods

In hypergraph-based learning, for a given hypergraph, the aim is to find the correct labels for the unlabeled vertices of the test set in the hypergraph under the assumption that one knows the correct labels for the training set. In this subsection, we introduce a modification of the nearest neighbors methods to learn the objective function for a hypergraph. (for the classical nearest neighbors methods, see, for example, in [16].)

Let $\{X, \mathcal{P}\}_\Gamma$ be a hypergraph equipped with properties \mathcal{P} . We equipped X with the metric \mathcal{D} in Subsection 2.2 so that X becomes a finite metric space under the metric \mathcal{D} . Suppose that the set of vertices in X consists of a_1, \dots, a_n . Let $f : \mathcal{V}(X) \rightarrow \{-1, 1\}$ be the objective function of labels to be learned such that it sends each vertex to exactly one of the values -1 or 1 . The values of f are also called *signs* of vertices. Let $T = \{(\alpha_i, \beta_i) \mid 1 \leq i \leq m\}$ for some positive integer $1 \leq m < n$. Here the α_i are vertices in X , and $\beta_i \in \{-1, 1\}$ are the correct label of α_i , i.e., $\beta_i = f(\alpha_i)$ for each $1 \leq i \leq m$. Our aim is to find all values of $\mathcal{V}(X) \setminus \{\alpha_1, \dots, \alpha_m\}$ under the objective function f , based on the training set T . The set $\mathcal{V}(X) \setminus \{\alpha_1, \dots, \alpha_m\}$ is called the *test set*. For this purpose, we use the modified nearest neighbors to find a *predictive model* f_{NN} for f . Fix a positive integer $k \geq 1$. For each vertex a in X , we define the following two sets attached to k , denoted as $\text{kNN}_1(a)$ and $\text{kNN}_{\text{all}}(a)$ as follows.

- (i) $\text{kNN}_1(a)$ is the set of k -th *nearest neighbors* of a in the training set T according to the metric \mathcal{D} . Note that if there are more than one vertex, say x, y in T such that $\mathcal{D}(a, x) = \mathcal{D}(a, y)$ and x, y are k -th nearest neighbors, then one picks up randomly exactly one such vertex to include in $\text{kNN}_1(a)$.
- (ii) $\text{kNN}_{\text{all}}(a)$ is the set of k -th *nearest neighbors* of a in the training set T according to the metric \mathcal{D} . Note that in this set, one includes all vertices x in T such that x is a k -th nearest neighbor of a .

Using the above two sets $\text{kNN}_1(\cdot)$ and $\text{kNN}_{\text{all}}(\cdot)$, we propose two predictive models for f , denoted as f_{kNN_1} and $f_{\text{kNN}_{\text{all}}}$, respectively. We define

**Figure 1.** Barcodes of the first example.

- (i) $f_{k\text{NN}_1}(a) = \text{sign}(\sum_{\alpha \in k\text{NN}_1(a)} f(\alpha))$ for each a in the test set.
- (ii) $f_{k\text{NN}_{\text{all}}}(a) = \text{sign}(\sum_{\alpha \in k\text{NN}_{\text{all}}(a)} f(\alpha))$ for each a in the test set.

Here the sign function is defined by

$$\text{sign}(a) = \begin{cases} 1 & \text{if } a \geq 0 \\ -1 & \text{if } a < 0 \end{cases}$$

We illustrate our method by testing on the hypergraph datasets defined in Subsections 3.2.1 and 3.2.2. Here we define the objective function $f : \mathcal{V}(X) \rightarrow \{-1, 1\}$ as follows: $f(a) = 1$ if $a \equiv 0, 1 \pmod{3}$, and $f(a) = -1$ if $a \equiv -1 \pmod{3}$.

Table 1 contains the results of kNN using the congruence hypergraph defined in the first example, and we set $X_{2000} = \{1, \dots, 2000\}$. The value of k for kNN are set to be 1 to 5. In each time, we randomly select 70% vertices from X to be the training set, and we repeat the computation 10 times for each k . Each element in the table presents an

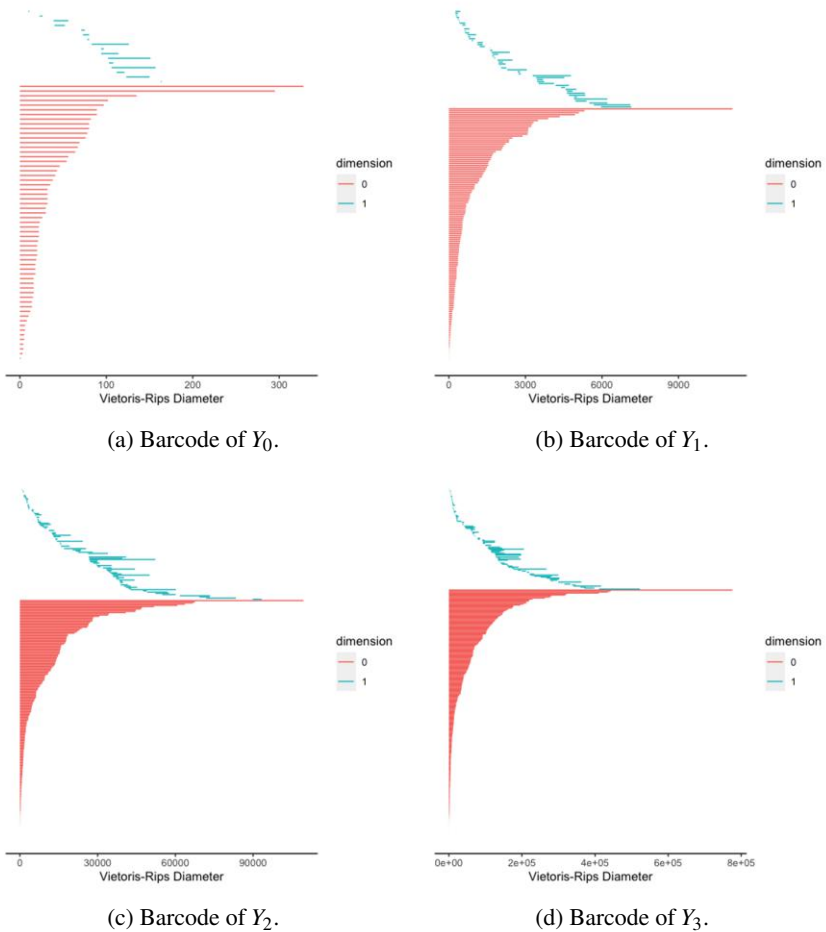


Figure 2. Barcodes of the second example.

error rate which is computed by the percentage of incorrect predictions. According to the average error rates in Table 1, we obtain the smallest average error rate 0.2841 at $k = 3$ when using kNN_{all} method and 0.2641 at $k = 2$ when using kNN₁ method. Figure 3 presents the curve comparison for the predicted and true signs for the method kNN_{all}. In this figure, the error rates of $f_{k\text{NN}_{\text{all}}}$ are from the ninth row in Table 1. According to the figure, most of vertices with label 1 are predicted correctly. One of the reasons that cause this result is that the number of vertices with positive sign are much larger than the number of vertices with negative sign according to the way we define the objective function.

Table 2 contains the results of kNN using the congruence hypergraph defined in the second example. We randomly select 5000 vertices from $\{1, \dots, 8000\}$, the values of $\{\alpha_2, \dots, \alpha_9\}$ and β are the same as described in section 3.4. Using the kNN_{all} method, the smallest average error rate is 0.3463 at $k = 5$. Using the kNN₁ method, the smallest average error rate is 0.3419 at $k = 2$. According to the results in Table 1 and 2, the kNN_{all} method performs slightly better than kNN₁.

Table 1. Error rates of KNN using the first example

Error rate	Error rate of $f_{kNN_{all}}$					Error rate of f_{kNN_1}				
	K=1	K=2	K=3	K=4	K=5	K=1	K=2	K=3	K=4	K=5
1	0.3263	0.3200	0.3200	0.3200	0.3200	0.4762	0.2700	0.4012	0.2800	0.3775
2	0.3187	0.4613	0.1887	0.3925	0.4463	0.4712	0.2837	0.4712	0.2700	0.4225
3	0.2800	0.3163	0.2987	0.3888	0.3050	0.5100	0.2913	0.4975	0.3337	0.4525
4	0.3762	0.3225	0.3313	0.1850	0.1775	0.4087	0.2213	0.2813	0.1900	0.3075
5	0.3013	0.2925	0.2925	0.2925	0.3850	0.4225	0.2650	0.3812	0.2450	0.3800
6	0.4400	0.2538	0.3938	0.3775	0.4150	0.4437	0.2163	0.3888	0.2875	0.3938
7	0.1562	0.2675	0.2675	0.4225	0.3063	0.4587	0.2562	0.3975	0.2850	0.3800
8	0.3137	0.2762	0.2712	0.2712	0.2850	0.4625	0.2450	0.4050	0.2750	0.3938
9	0.4250	0.2638	0.1125	0.2438	0.2825	0.4675	0.2312	0.4663	0.2937	0.4287
10	0.4350	0.3900	0.3650	0.3275	0.3550	0.5075	0.2688	0.4525	0.3363	0.4300
Average	0.3372	0.3164	0.2841	0.3221	0.3278	0.4626	0.2641	0.4098	0.2866	0.3946

Table 2. Error rates of KNN using the second example

Error rate	Error rate of $f_{kNN_{all}}$					Error rate of f_{kNN_1}				
	K=1	K=2	K=3	K=4	K=5	K=1	K=2	K=3	K=4	K=5
1	0.3527	0.3447	0.3447	0.3440	0.3433	0.3713	0.3347	0.3687	0.3260	0.3500
2	0.3567	0.3413	0.3487	0.3347	0.3360	0.3493	0.3367	0.3660	0.3453	0.3527
3	0.3793	0.3693	0.3633	0.3433	0.3480	0.3913	0.3473	0.3933	0.3413	0.3540
4	0.3733	0.3580	0.3540	0.3500	0.3460	0.3707	0.3487	0.3813	0.3433	0.3580
5	0.4000	0.3660	0.3607	0.3627	0.3593	0.3960	0.3540	0.3807	0.3573	0.3780
6	0.3853	0.3580	0.3653	0.3453	0.3460	0.3873	0.3380	0.3893	0.3447	0.3680
7	0.3520	0.3347	0.3373	0.3493	0.3453	0.3680	0.3333	0.3720	0.3420	0.3520
8	0.3773	0.3587	0.3687	0.3547	0.3540	0.3627	0.3513	0.3847	0.3500	0.3567
9	0.3707	0.3500	0.3653	0.3453	0.3467	0.3807	0.3527	0.3800	0.3493	0.3640
10	0.3633	0.3427	0.3473	0.3360	0.3380	0.3707	0.3227	0.3613	0.3333	0.3540
Average	0.3715	0.3523	0.3555	0.3465	0.3463	0.3748	0.3419	0.3777	0.3460	0.3587

4. Conclusions

Our main contributions in this paper can be summarized as follows:

- (i) Introducing a natural metric space structure modulo certain equivalence relations on a general hypergraph data which bears a resemblance to a usual metric space structure;
- (ii) Using the metric space modulo certain equivalence relation structure introduced, we emphasize that this topological space structure on hypographs is very natural and suitable for studying several problems in machine learning;
- (iii) Proposing a distance matrix approach using the metric space structure introduced in this paper to study community detection problem in hypographs;

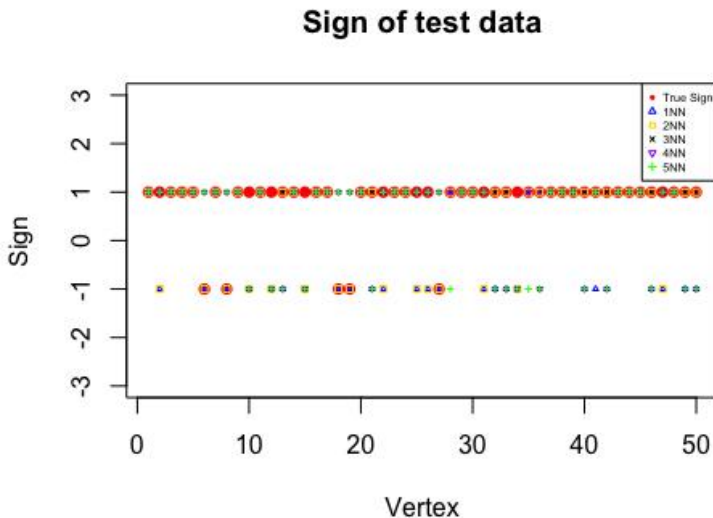


Figure 3. Predicted and true signs of test data for kNN_{all}.

- (iv) Proposing a modified homology-based learning to study topological structures of hypergraphs which in turn can be used to detect persistent homological features; this method can also be used to study community detection problem;
- (v) Proposing modified nearest neighbors methods for studying sign prediction problem on general hypergraph data; such methods have advantages that they can be applied even to hypergraphs which do not contain an embedding into a Euclidean space, or do not carry a Euclidean space structure.
- (vi) One of our main contributions is to propose a new way to construct hypergraph data which are very easy to implement and test theories from machine learning which we coin the term “*congruence hypergraph data*”.
- (vii) Experimental analysis are performed on congruence hypergraph data which are simulated by our methods.

5. Acknowledgements

Lizhen Lin would like to acknowledge the support of NSF grant DMS CAREER 1654579.

6. Appendix

In this Appendix, we give a proof of Theorem 2.7

For the sake of simplicity, let $\alpha_i = \mathcal{N}(\alpha_i)$ for each $1 \leq i \leq n$.

Suppose that $\mathcal{D}(\alpha_i, \alpha_j) = 0$ for some $1 \leq i, j \leq n$. By definition, we know that

$$\mathcal{D}(\alpha_i, \alpha_j) = \sum_{P \in \mathcal{P}} \sum_{m=1}^{\ell} |\mathfrak{C}_P^m(a_i) - \mathfrak{C}_P^m(a_j)| = 0,$$

which implies that

$$\mathfrak{C}_P^m(a_i) - \mathfrak{C}_P^m(a_j) = 0$$

for all $m \geq 1$ and $P \in \mathcal{P}$. Thus $\mathfrak{C}_P^m(a_i) = \mathfrak{C}_P^m(a_j)$ for all $m \geq 1$ and $P \in \mathcal{P}$, and hence $\alpha_i = \mathcal{N}(a_i) \cong \alpha_j = \mathcal{N}(a_j)$.

It is obvious that $\mathcal{D}(\alpha_i, \alpha_j) = \mathcal{D}(\alpha_j, \alpha_i)$ for all $1 \leq i, j \leq n$, which proves that \mathcal{D} is symmetric.

We now show that \mathcal{D} satisfies the triangle inequality. Indeed, we see that

$$\begin{aligned} \mathcal{D}(\alpha_i, \alpha_j) &= \sum_{P \in \mathcal{P}} \sum_{m=1}^{\ell} |\mathfrak{C}_P^m(a_i) - \mathfrak{C}_P^m(a_j)| \\ &= \sum_{P \in \mathcal{P}} \sum_{m=1}^{\ell} |(\mathfrak{C}_P^m(a_i) - \mathfrak{C}_P^m(a_k)) + (\mathfrak{C}_P^m(a_k) - \mathfrak{C}_P^m(a_j))| \\ &\leq \sum_{P \in \mathcal{P}} \sum_{m=1}^{\ell} |\mathfrak{C}_P^m(a_i) - \mathfrak{C}_P^m(a_k)| + \sum_{P \in \mathcal{P}} \sum_{m=1}^{\ell} |\mathfrak{C}_P^m(a_k) - \mathfrak{C}_P^m(a_j)| \\ &= \mathcal{D}(\alpha_i, \alpha_k) + \mathcal{D}(\alpha_k, \alpha_j) \end{aligned}$$

for any $1 \leq i, j, k \leq n$. Thus \mathcal{D} satisfies the triangle inequality, and therefore \mathcal{D} is a metric on X modulo the equivalent relation \cong .

References

- [1] Tian Z, Hwang T, Kuang R. A hypergraph-based learning algorithm for classifying gene expression and arrayCGH data with prior knowledge. *Bioinformatics*. 2009 Nov 1;25(21):2831–8.
- [2] Levene M, Poulovassilis A. An object-oriented data model formalised through hypergraphs. *Data & Knowledge Engineering*. 1991 May 1;6(3):205–24.
- [3] Goertzel B. Patterns, hypergraphs and embodied general intelligence. In: The 2006 IEEE international joint conference on neural network proceedings; 2006 Jul 16; pp. 451–458.
- [4] Klamt S, Haus UU, Theis F. Hypergraphs and cellular networks. *PLoS Comput Biol*. 2009 May 29;5(5):e1000385.
- [5] Kok S, Domingos P. Learning Markov logic network structure via hypergraph lifting. In: Proceedings of the 26th annual international conference on machine learning; 2009 Jun 14; p. 505–512.
- [6] Burago D, Burago Y, Ivanov S. A course in metric geometry. American Mathematical Soc.; 2001.
- [7] Leontjeva A, Konstantin T, Vilo J, Tamkivi T. Fraud Detection: Methods of Analysis for Hypergraph Data. In: The 2012 IEEE/ACM International Conference on Advances in Social Networks Analysis and Mining; August 2012; pp. 1060–1064.
- [8] Edelsbrunner H, Harer J. Computational topology: an introduction. American Mathematical Soc.; 2010.
- [9] Zhu X. Persistent homology: An introduction and a new text representation for natural language processing. In: IJCAI; 2013 Aug 3; p. 1953–1959.
- [10] Boissonnat JD, Chazal F, Yvinec M. Geometric and topological inference. Cambridge University Press; 2018 Sep 27.
- [11] Carlsson G. Topology and data. *Bulletin of the American Mathematical Society*. 2009;46(2):255–308.

- [12] Carlsson G, Zomorodian A, Collins A, Guibas LJ. Persistence barcodes for shapes. International Journal of Shape Modeling. 2005 Dec;11(02):149-87.
- [13] Collins A, Zomorodian A, Carlsson G, Guibas LJ. A barcode shape descriptor for curve point cloud data. Computers & Graphics. 2004 Dec 1;28(6):881-94.
- [14] Zomorodian A, Carlsson G. Computing persistent homology. Discrete & Computational Geometry. 2005 Feb 1;33(2):249-74.
- [15] Wadhwa RR, Williamson DF, Dhawan A, Scott JG. TDAstats: R pipeline for computing persistent homology in topological data analysis. Journal of open source software. 2018 Aug 8;3(28):860.
- [16] Friedman J, Hastie T, Tibshirani R. The elements of statistical learning. New York: Springer series in statistics; 2001.

A Classification for Electronic Nose Based on Broad Learning System

Yu Wang^a, Xiaoyan Peng^b, Hao Cui^b, Pengfei Jia^{b,1}

^a*College of Electronic and Information Engineering, Southwest University, Chongqing,
China*

^b*College of Artificial Intelligence, Southwest University, Chongqing, China*

Abstract. The odor of citrus juice changes during the storing process. We use an electronic nose (E-nose) to detect the volatile odors released by citrus juice and use the detect results to classify citrus juices from different storage periods. In this article, a novel classifier of E-nose, namely broad learning system (BLS) is introduced. BLS is different from traditional classifier. It has a simple network model, which can greatly reduce the training time of the model. BLS can effectively combine feature extraction and classification recognition to make the model more efficient. We apply BLS to the analysis of valencia citrus juice data. The experimental results show that BLS can effectively identify the current stage of the stored valencia citrus juice. Compared with traditional classifier such as radical basis function neural network (RBFNN) and linear discriminant analysis (LDA), the results show that BLS has better performance for the storage period classification of valencia citrus juice.

Keywords. Citrus juice, Electronic nose, Broad learning system, Classifier

1. Introduction

Due to the improvement of people's living standards, citrus juice is loved by consumers in their daily life. However, the storage of citrus juice is a serious problem. We need to detect citrus juice at all times to ensure the quality of citrus juice. Because citrus juice emits some volatile odors, we can determine the storage period of citrus juice by detecting volatile gases, and thus determine the quality of citrus juice. In this article, we use the electronic nose (E-nose) for the quality identification of juice. At present, the feasibility of the identification of juice quality by the E-nose has been verified [1, 2].

E-nose is an intelligent system composed of sensor arrays and pattern recognition algorithm. It can be used to simulate human olfactory organs to identify odors or gases [3, 4]. In the current research, E-nose has been widely used in the detection of gas or odor, and it also has certain advantages compared with traditional methods such as human olfactory analysis and precision instrument analysis. Compared with traditional methods, E-nose has the following advantages. Firstly, it can work stably for a long time. Secondly, it is less affected by external factors during the detection process. Finally, it can make accurate quantitative analysis of the target gas or odor. At present,

¹ Corresponding Author, Pengfei Jia, College of Artificial Intelligence, Southwest University, Chongqing, China; E-mail: jiapengfei200609@126.com

it has been widely used in explosive detection [5, 6], environmental monitoring [7, 8], Food storage [9] and disease diagnosis [10].

In traditional pattern recognition algorithms, feature extraction and classification recognition are divided into two independent steps. The first step of processing the raw response data of the sensor is feature extraction. Then, we use the data after feature extraction to build a classifier model. Feature extraction will influence the recognition rate of the final classification, but the target requirements of the two stages may be different, which will lead to unsatisfactory results. It is assumed that the combination of feature extraction and classification recognition unifies the requirements of the two stages, and whether the final classification accuracy can be improved. Therefore, it is necessary to find an algorithm that integrates feature extraction and classification recognition.

Broad learning system (BLS) is a simple flat network, proposed in 2018 by C. L. Philip Chen [11, 12]. BLS uses a random mapping method to convert the original data into mapped features and enhanced features, and then connects the two horizontally to form the actual input of the model. Through random mapping, effective feature is extracted from the original data. Therefore, no other feature extraction methods are needed to process the raw data. In addition, high-dimensional (or even infinite-dimensional) data can be processed by random mapping. Finally, the simple network structure of BLS can shorten the time to train the model. Compared with traditional classifier, when BLS processes large samples, the training time required for the model is shorter. BLS perfectly combines feature extraction and classification recognition. The advantage of doing so is that it can uniformly set parameters and modify the model according to the accuracy of the final classification recognition. So far, it has been applied to time series prediction [13], drift compensation [14], image classification [15] and so on.

In this article, we apply BLS to solve the classification problem of E-nose. In the other parts of the article, we first introduce the experimental platform and sample collection in Section 2, then, overview of BLS will be introduced in Section 3, the results and discussion are presented in Section 4, finally, the conclusion of this article is in Section 5.

2. Materials and methods

2.1. Experimental setup

In this section, we introduce the self-made E-nose system. The detailed structure of the self-made electronic nose system is shown in Figure 1. The self-made E-nose system is composed of E-nose, PC, gas flow meter, a temperature-humidity controlled chamber and air pump. The E-nose has two ports, port 1 is for injecting target gas into the air chamber, and port 2 is for injecting clean air into the air chamber. When the target gas is injected into the gas chamber to make full contact, the sensors will respond and use the analog-digital converter (A/D) to convert the response signal of the sensor into a digital signal, and use a joint test action group (JTAG) to save data to PC.

According to paper [16], we can find that valencia citrus juice is composed of hydrocarbons, alcohols, aldehydes, ketones, esters and other chemical components. The E-nose has a sensor array composed of 15 gas sensors, which ensures that the odor components emitted by valencia citrus juice can be fully detected, and these sensors

used have the advantages of cost-effective, low energy consumption and high measurement accuracy.

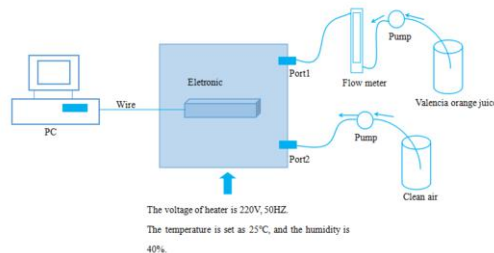


Figure 1. System diagram of self-made E-nose system

2.2. Sampling experiments

Firstly, we adjust the temperature and humidity of the air chamber, and set the temperature and humidity to 25°C and 40% respectively. Then start the sampling experiment, and one single sampling steps are as follows:

- Step 1: Restore the baseline of the sensor, inject clean air into the air chamber, and fully contact the sensor array for 5 min to obtain its baseline value.
- Step 2: Data sampling, inject the target gas into the gas chamber 7 min to obtain the response value of the sensor.
- Step 3: Cleaning phase, clean air is injected into the air chamber to fully contact the sensor array for 5 minutes to restore the sensor to the baseline value.

The response curve of the sensor array during one single sampling is shown in Figure 2.

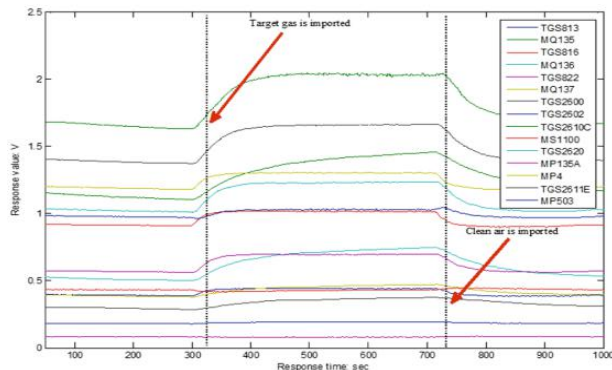


Figure 2. Response of sensor array

As shown in Figure 2, we can learn that the first 5 min is to process the sensor array to return to the baseline value, 5 min to 12 min to make the sensor array response stage, 12 min to 17 min is to inject clean air, clean the sensor array to return to the baseline value.

3. Broad learning system

BLS has a very simple network structure, which makes its training time shorter. The structure of BLS is shown in Figure 3, BLS generates mapping features from the original input data X through a random mapping method, and saves them in feature nodes Z , and generates enhancement nodes H through random mapping of feature nodes to broaden the network horizontally. Then the generated feature nodes and enhancement node are connected horizontally as the input of the model, and after input the data, get the output of the network. Finally, the ridge regression algorithm is used to calculate the connection weight between the network input and output. The detailed derivation process is as follows.

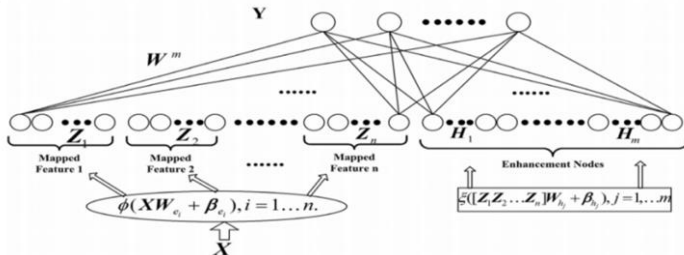


Figure 3. Structure of BLS

Assuming that the input original data is X , the i -th mapping feature Z_i is generated as follow:

$$Z_i = \phi_i(XW_{ei} + \beta_{ei}) \quad (1)$$

where W_{ei} and β_{ei} are randomly generate weights and biases respectively, ϕ_i is the linear mapping function. Mark as $Z^i = [Z_1, Z_2, \dots, Z_i]$, which means that there are i group of mapping features for horizontal connection. The way to generate the j -th group of enhancement nodes is as follows:

$$H_j = \xi_j(Z^i W_{hj} + \beta_{hj}) \quad (2)$$

where W_{hj} and β_{hj} are weights and biases respectively, ξ_j is the nonlinear mapping function. Mark as $H^j = [H_1, H_2, \dots, H_j]$, which means that there are j group of enhancement features for horizontal connection. The values of i and j are determined by the complexity of the modeling task.

In order to obtain better classification results, it is necessary to have a good input feature representation. In the process of random mapping, weights and biases are randomly generated, but the randomness is unpredictable. In order to overcome the nature of randomness, by fine-tuning W_{ei} and β_{ei} through the sparse autoencoder method, more essential features can be explored. Assuming that m feature nodes and n enhancement nodes are generated, all nodes are horizontally connected to form the input of the model, namely $A = [Z^m | H^n]$. Therefore, the input Y of the BLS model can be expressed as:

$$Y = AW \quad (3)$$

where W is the connection weight of the broad network. And W can be calculated by a simple method, which can be expressed as $W = A^+Y$, where A^+ is pseudo-inverse matrix of BLS mapping matrix A . Then, the solution of the matrix pseudo-inverse problem is transformed into l_2 norm regularized BLS, which can be expressed as the following convex optimization problem:

$$\arg \min_W \|AW - Y\|^2 + \lambda \|W\|^2 \quad (4)$$

where the second term in the above formula further restricts the weight W , λ is the regularization coefficient.

Therefore, We can use formula (5) to calculate W :

$$W = (\lambda I + AA^T)^{-1} A^T Y \quad (5)$$

Specifically

$$A^+ = \lim_{\lambda \rightarrow 0} (\lambda I + AA^T)^{-1} A^T \quad (6)$$

where I represents the identity matrix.

BLS extracts important features through random mapping. Simultaneously, the output result of the model is compared with the actual label to obtain the classification accuracy. Consequently, the BLS model perfectly combines feature extraction and classification recognition, so that parameter settings and model modifications can be unified through the obtained accuracy of classification, making the model more efficient.

4. Results and discussion

We will briefly introduce the process of sample sampling in this section. The citrus juice data set used in this article is composed of data collected in 5 storage stages of citrus juice through the sensor array in the E-nose. Each stage is sampled for 24 times, and a total of 120 sampling experiments in 5 stages, 400 points which are selected from each response curve of sensors are input into BLS, 75% of samples are used as training samples, and the rest are used as test samples. As shown in Figure 4, it is the data obtained in one sampling. The data in the boxes are randomly selected. There are a total of 400 boxes, which represent the response scatter points of 400 sensing matrices are selected.

In order to prove the availability of BLS, we compare BLS with LDA and RNFNN, and make the correct rate of the training set and the test set as indicators to evaluate its performance. Each program runs 10 times, and then takes the average as the final result. The final accuracy of classification are shown in Table 1.

From Table 1, we know that the classification accuracy of BLS training data set and test data set are higher than LDA and RBFNN, which shows that BLS has good performance in classification recognition.

$$\begin{bmatrix} x_{11} & x_{12} & x_{13} & \cdots & x_{1N} \\ x_{21} & x_{22} & x_{23} & \cdots & x_{2N} \\ \vdots & \vdots & \vdots & \ddots & \vdots \\ x_{15,1} & x_{15,2} & x_{15,3} & \cdots & x_{15,N} \end{bmatrix}$$

Figure 4. Schematic diagram of obtaining input BLS data in one sampling.

Table 1. Classification recognition rate of different classifiers (%)

	LDA	RBFNN	BLS
Training set	77.58	80.24	99.96
Test set	51.67	60.00	95.11

We also explored the training time of BLS and compared it with the training time of LDA and RBFNN. Each program runs 10 times, and then takes the average as the final result. The final results are shown in Table 2.

Table 2. Running time of different classifiers

Classification algorithm	Running time
LDA	0.5616
RBFNN	171.5596
BLS	8.7371

Table 2 lists the results of running time of the LDA, RBFNN and BLS. We can find that the running time of LDA is the shortest, while the running time of RBFNN is the longest. Though the running time of BLS is longer than LDA, but much shorter than RBFNN.

Combining Table 1 and Table 2, we can conclude that the BLS classifier has a greater improvement in recognition accuracy than LDA and RBFNN, and the running time of BLS is much less than RBFNN, just slightly longer than LDA with the higher recognition accuracy. Therefore, BLS has a better advantage in classification recognition.

5. Conclusion

In this paper, we propose a novel classifier based on BLS to improve the classification accuracy of the E-nose for different storage periods of citrus juice. BLS has some advantages that traditional classifier do not have. On the one hand, BLS has a simple flat network structure. The simple structure means that the model training time is short. On the other hand, BLS effectively combines feature extraction and classification recognition. The two-stage requirements can be unified, and the parameters and structure of the model can be uniformly adjusted from the final classification results, thereby further improving the classification recognition rate. Comparing BLS with LDA and RBFNN, we can find that BLS has a greater improvement in the classification accuracy of orange juice storage period, and the training time is shorter. Through the research in this article, we believe that BLS is a good classifier of E-nose.

This article proposes a better classification method to deepen the theory of broad learning system and expand its application range. For our citrus data, it can better classify the different storage periods of citrus, and promote the practical application of E-nose in the field of citrus. However, the weight matrix in the BLS model is generated

randomly and has a strong uncertainty. Therefore, we can optimize the weight matrix assignment method to further improve the accuracy in future work.

Acknowledgments

This work is supported by National Natural Science Foundation of China (61906160, 61804127), Fundamental Science and Advanced Technology Research Foundation of Chongqing (Grant No. cstc2018jcyjA0867, Grant No. cstc2018jcyjAX0261), Fundamental Science on Nuclear Wastes and Environmental safety Laboratory (Grant No. 19kfhk03), Open Research Fund Program of Data Recovery Key Laboratory of Sichuan Province (Grant No. DRN19015), and the Fundamental Research Funds for the Central Universities (XDJK2020C040).

References

- [1] Cao H, Jia P, Xu D, Jiang Y, Qiao S. Feature extraction of citrus juice during storage for electronic nose based on cellular neural network. *IEEE Sensors Journal*. 2020 Apr;20(7):3803-3812.
- [2] Jiang X, Jia P, Qiao S, Duan S. Odor change of citrus juice during storage based on electronic nose technology. International conference on neural information processing. 2017 Nov 14-18; Guangzhou, China; p. 317-326.
- [3] Pearce T C. Computational parallels between the biological olfactory pathway and its analogue 'the electronic nose': Part II. Sensor-based machine olfaction. *BioSystems*, 1997 Jan;41(2):69-90.
- [4] Bahraminejad B, Basri S, Isa M M, Hambali Z. Application of a sensor array based on capillary-attached conductive gas sensors for odor identification. *Measurement Science and Technology*. 2010 Aug;21(8):085204(17pp).
- [5] Sukhvir K, Arvind K, Kaur RJ, Priya A, Harminder S. SnO₂-glycine functionalized carbon nanotubes based electronic nose for detection of explosive materials. *Sensor Letters*, 2016 Jul;14(7):733-739.
- [6] Brudzewski K, Osowski S, Pawłowski W. Metal oxide sensor arrays for detection of explosive at sub-parts-per million concentration levels by the differential electronic nose. *Sens. Actuators B Chem.* 2012 Jan;161(1):528-533.
- [7] Galang GM, Zarra T, Naddeo V, Belgioro V, Florencio JB. Artificial neural network in the measurement of environmental odours by E-nose. *Chemical engineering transactions*. 2018 Jan;68:247-252.
- [8] Pan L, Yang SX. An electronic nose network system for online monitoring of livestock farm odors. *IEEE-ASME Transactions on Mechatronics*, 2009 Jun;14(3):371-376.
- [9] Pang L, Wang J, Lu X, Yu H. Discrimination of storage age for wheat by E-nose. *Transactions of the ASABE*. 2008 Sep/Oct;51(5):1707-1712.
- [10] Saidi T, Zaim O, Moufid M, Bari NE, Ionescu R, Bouchikhi B. Exhaled breath analysis using electronic nose and gas chromatography-mass spectrometry for non-invasive diagnosis of chronic kidney disease, diabetes mellitus and healthy subjects. *Sens. Actuators B chem.* 2018 Mar;257:178-188.
- [11] Chen CL, Liu Z, Feng S. Universal approximation capability of broad learning system and its structural variations. *IEEE Transactions on Neural Networks*, 2019 Apr;30(4):1191-1204.
- [12] Chen CL, Liu Z. Broad Learning System: An effective and efficient incremental learning system without the need for deep architecture. *IEEE Transactions on Neural Networks*. 2018 Jan;29(1):10-24.
- [13] Xu M, Han M, Chen CL, Qiu T. Recurrent broad learning systems for time series prediction. *IEEE Transaction on Cybernetics*, 2020 Feb;50(4):1405-1417.
- [14] Liu B, Zeng X, Tian F, Zhang S, Zhao L. Domain transfer broad learning system for long-term drift compensation in electronic nose systems. *IEEE Access*. 2019 Sep;7:143947-143959.
- [15] Fan J, Wang X, Wang X, Zhao J, Liu X. Incremental wishart broad learning system for fast polaris image classification. *IEEE Geoscience and Remote Sensing Letters*. 2019 Dec;16(12):1854-1858.
- [16] Moshonas MG, Shaw PE. Quantitative determination of 46 volatile constituents in fresh unpasteurized orange juice using dynamic headspace gas chromatography. *J. Agric. Food Chem.* 1994 Jul;42(7):1525-1528.

3D Single Person Pose Estimation Method Based on Deep Learning

Xinrui Yuan¹, Hairong Wang, Jun Wang

North Minzu University, Yinchuan, China

Abstract. In view of the significant effects of deep learning in graphics and image processing, research on human pose estimation methods using deep learning has attracted much attention, and many method models have been produced one after another. On the basis of tracking and in-depth study of domestic and foreign research results, this paper concentrates on 3D single person pose estimation methods, contrasts and analyzes three methods of end-to-end, staged and hybrid network models, and summarizes the characteristics of the methods. For evaluating method performance, set up an experimental environment, and utilize the Human3.6M data set to test several mainstream methods. The test results indicate that the hybrid network model method has a better performance in the field of human pose estimation.

Keywords. Human pose estimation, deep learning, end-to-end, staged, hybrid network

1. Introduction

Human posture is an important feature of living beings and has been widely used in application scenarios such as behavior recognition [1], interactive analysis [2], video surveillance [3], entertainment [4], virtual reality [5], animation[6], etc. Through human pose estimation, it can assist in judging other people's behaviors, actions, and identification. In recent years, researchers have discovered that the human pose estimation method based on deep learning can effectively develop the accuracy of the estimation [7], resulting in a large number of research achievements. Chen Y et al. [8] gave a method for estimating human pose using structure-aware convolutional networks. The training of three sub-networks optimized the problems of joint occlusion and overlap. Chou CJ et al. [9] learn the structure and configuration of human body parts through confrontation training to achieve human pose estimation. Great achievements have been made in 2D single person pose estimation [10], but due to the single data set and the division of key points, the accuracy cannot be greatly improved. For the past few years, a breakthrough has been made in 3D single person pose estimation. Zhou X et al. [11] integrated the kinematics object model into deep learning and performed effective 3D single person pose estimation. Tekin B et al. [12] presented a novel deep learning regression architecture that combines an autoencoder with CNN to improve the prediction accuracy between various parts of the human body. These two methods belong to the end-to-end 3D single person pose estimation method [13].

¹ Corresponding Author, Hairong Wang, North Minzu University, Yinchuan, China; E-mail: bmdwhr@163.com.

Due to the constraints of the 3D human annotation data set, they can not be applied to more complex networks. In order to deal with complex and changeable scenes more accurately, researchers began to use the increasingly accurate 2D human pose estimation method as an aid to produce a staged 3D human pose estimation method. Zhou X et al. [14] combined a 2D part regressor based on deep learning and a sparse-driven 3D reconstruction method to design a 3D human pose estimation framework. Tome D et al. [15] presented a associated method, in order to estimate the human pose, combining the image appearance-based prediction offered by the 2D landmark detector with the geometric 3D skeletal information encoded in the new pre-trained model of the 3D human pose. Chen CH et al. [16] proposed a simple method for 3D human pose estimation by performing 2D pose estimation and then matching 3D examples. Moreno-Noguer F[17] formulated the 3D human pose estimation problem as a regression between the matrix encoding the 2D and 3D joint distances, and solved the problem of 3D human pose estimation from a single image. Martinez J et al. [18] established a system combining 2d joint positions to predict 3d positions, which greatly improves the previous results from 2D to 3D pose estimation. Pavlakos G et al. [19] used two separate networks to solve the problem of 3D human pose estimation from a single color image. With the development of the research process, the ambiguity problem in the process of 2D to 3D plane projection has appeared. Even if the deep learning network structure is optimized, it cannot be solved. Therefore, research scholars have begun to study the 3D single human pose estimation based on the hybrid network model. Zhou X et al. [20] extended the most advanced 2D pose estimation sub-network through the 3D deep regression sub-network. According to the correlation between the 2D pose and the depth estimation sub-task, the network was trained end-to-end, and 3D geometric constraints are introduced to predict the 3D human pose, which can better perform human pose estimation in the wild environment. Zhou X et al. [21] proposed a framework called MonoCap, which consists of a 2D part regression based on deep learning, a sparse-driven 3D reconstruction method and 3D temporal smoothness. Pavlakos G et al. [22] proposed a solution that can train end-to-end ConvNets for 3D human pose estimation in the absence of accurate 3D ground truth by using weaker supervision signals. Yang W et al. [23] came up with an adversarial learning framework to transform the 3D human pose structure learned from a fully noted data into a field image with only 2D pose annotations, and designed a original discriminator is used to enhance the generalization ability of of the 3D pose estimator. Pavllo D et al. [24] proved that a complete convolution model using time convolution of 2D keypoints can effectively estimate the 3D poses in the video. An ordinary and resultful semi-supervised training way is also introduced. It uses unlabeled video data to predict the 2D key points of the unlabeled video, then estimate the 3D pose, in the end input it into the 2D key points for back projection. Li C et al. [25] proposed a novel method with multiple feasible hypotheses to generate 3D poses from 2D joints. Experiments have shown that the 3D pose estimated by this method from 2D joint input is consistent in 2D reprojection.

In summary, although 2D single person pose estimation has achieved great accuracy, there are problems such as inaccurate recognition when the human pose is occluded or the data set is missing. 3D single person pose estimation uses 3D human skeletons to describe the human body pose. Through the improvement of the network model, the deep-level features can be effectively obtained from the image, which has gradually become the mainstream method. This article will review the 3D single person estimation methods using neural networks in the next section. In the third section, the

verification of the 3D single person estimation method based on neural network is carried out. A unified public data set is used to compare and analyze several mainstream methods, and some methods are evaluated by comparing experimental results. Finally, summarize the work done in this article and put forward prospects for the next research work.

2. 3D Single person pose estimation method

The current research on 3D single person pose estimation using deep learning neural networks can be classified through different training methods of 3D single person pose models, which are generally summarized in three types: end-to-end network model, staged network model and hybrid network model.

2.1. End-to-end 3D human pose estimation

An end-to-end network is a type of neural network. For a task, the input to the network is the original data, and the final output is what the task expects data. In the image classification task, the original picture is input of the neural network, and the output is the given image prediction category identification. As shown in figure 1, this method is an improved end-to-end CNN method. RGB images or videos are input to the neural network, and the output is the 3D coordinate position information of all human joint points corresponding to it. The end-to-end network actually uses a network structure to process the input content, there is no other data in the process of processing. Therefore, for this type of method, data preprocessing and network structure design are particularly important.

Tekin B et al. [12] generated a 3D pose from the input image through regression. By using the mapping obtained by the auto encoder and the output of the regular CNN, the dependencies can finally be encoded more effectively. In the paper, the regression architecture is used to analyze the structure, two high-dimensional embedded mappings are introduced, and the final pose estimation is completed after further adjustment of the network.

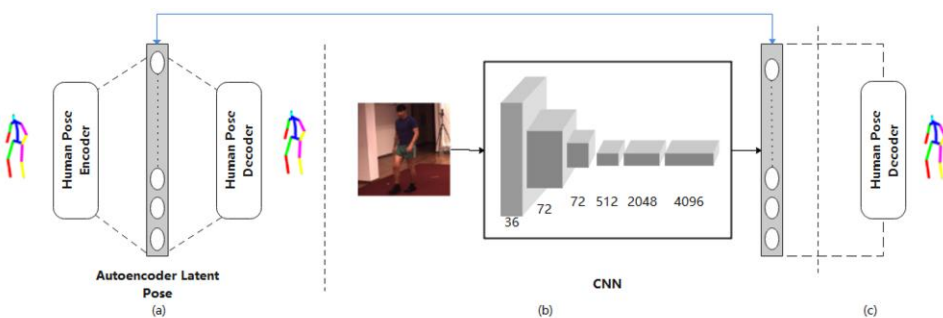


Figure 1. Structure diagram of the improved end-to-end CNN method.

Figure 1 shows a 3D human pose estimation architecture based on structured prediction. (a) It is a designed automatic encoder, in which the size of the hidden layer is larger than the size of its input and output layers. During the practice, adopt the CNN in (b) to map to the latent representation learned by the autoencoder in (a). (c) Use the decoder to map the latent representation back to the original pose space. This improved

end-to-end CNN structure combines traditional CNN networks with autoencoders for structured learning, which can resolve dependencies and improve the performance of pose estimation.

The data set applied to the human pose estimation by the end-to-end network is generally not constrained by the 3D human pose annotation data set, and therefore more complex networks cannot be realized. In order to perform more accurate and precise 3D single person pose estimation, the network structure must be able to cope with more complex and changeable scenes. 2D human pose estimation methods have become more and more accurate after recent years of development. Under such demand, researchers have begun to study the combined application of 2D human pose estimation methods and 3D human pose estimation methods.

2.2. Staged 3D human pose estimation

The staged 3D human pose estimation is a heterogeneous method proposed by researchers in order to solve the problem that the amount of labeled data encountered when using end-to-end network for 3D human pose estimation does not match the network scale. The staged method is similar to the end-to-end method in that 2D pose data is used. The difference is that the phased 3D human pose estimation method combines 2D data with 3D data. When acquiring data, a 2D human pose estimation method is needed for assistance, that is, a 2D human pose estimation model is used to obtain 2D human pose data from the original image data. Assuming that the generated 2D human pose is accurate, the 2D human pose is used as input, and the 3D human pose regression network is used to improve the dimensionality of the 2D data.

Martinez J et al. [18] designed a concise neural network as shown in Figure 2 below, which uses a linear layer to perform batch normalization in the network, and adds random dropout and ReLU activation functions twice. Input an array of 2D joint positions into system, and obtain a battery of 3D human joint positions through network operations.

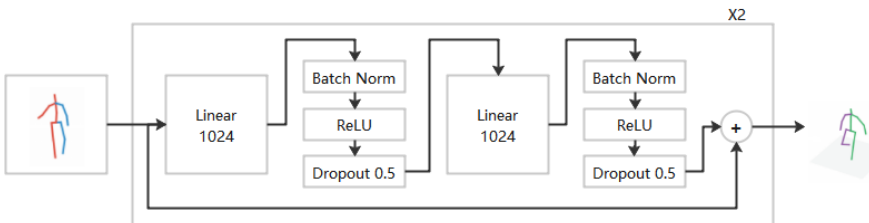


Figure 2. Improved staged neural network.

Based on the staged 3D human pose estimation, it is established on the 2D human pose estimation method. It uses 2D human pose as input to estimates the 3D human pose. Because 2D human pose can be considered as 3D human pose on a plane from a certain angle of view, there may be multiple different 3D human poses in the same projection. This is an ambiguity problem that cannot be solved by optimizing the deep learning network structure. At this time, more information needs to be introduced into the network to eliminate this ambiguity. Therefore some researchers began to research 3D human pose estimation of the hybrid network model.

2.3. 3D human pose estimation of the hybrid network model

Different from the end-to-end and staged 3D human pose estimation, the 3D human pose estimation of the hybrid network model adds additional image information and geometric constraints on the basis of pre-estimated 3D human pose. Then use these information to train a network model that promotes a 2D pose to 3D. The 3D human pose estimation of the hybrid network model uses accurate 2D human pose estimation methods while introducing more additional information including human joint points and motion characteristics. The network trained with this information can relieve the problem of 2D to a certain extent. The ambiguity problem of posture projection calculation of 3D human posture can also reduce the overfitting problem of end-to-end network.

At present, the more successful 3D human pose estimation method of hybrid network model is proposed by Pavllo D [24], which performs 3D human pose from video with convolution and semi-supervised training. A semi-supervised training means is introduced to boost the precision in the usability setting of annotated 3D ground truth pose data. The unlabeled video is combined with a ready-made 2D keypoint detector to develop the supervisory loss function with the back projection loss term. The designed encoder estimates the 3D pose through the 2D joint coordinates, and the decoder maps the 3D pose back to the 2D joint coordinates to solve the problem of automatic encoding of unlabeled data. As shown in Figure 3, the model takes a series of 2D poses that may be predicted as input, uses regression methods to obtain the 3D trajectory of the human pose, and adds soft constraints to make the average bone length of the unlabeled prediction and the average bone length of the labeled prediction match.

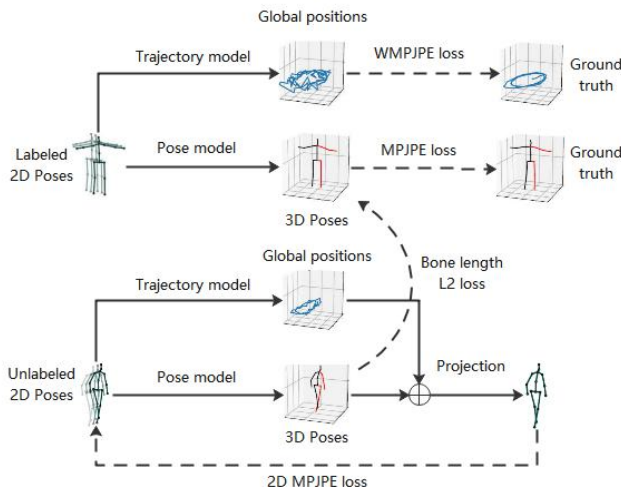


Figure 3. Semi-supervised training using 3D hybrid network model.

This chapter introduces the 3D single person pose estimation methods of three neural networks, gives the definition of different means, and illustrates merit and demerit of each estimation method through the method model in the paper. Among the three methods, using a hybrid network model to estimate the pose of a 3D single person is the best, and the second best is to use a staged method. With the development of technology, the end-to-end method will no longer be used alone. Hybrid network

models usually combine the end-to-end network with other methods to improve the accuracy of estimation. In the next chapter, we will verify the conclusions of this chapter through comparative experiments.

3. Method validation and comparative analysis

3.1. Dataset

The data set used in the human pose estimation method is usually divided into a 2D human pose estimation data set and a 3D human pose estimation data set.

Most of the data in the 2D human pose data set derived from image data online media, and these data are manually annotated. Since 3D human pose estimation is more complicated than 2D human pose estimation, the 3D human pose data set used in this article is also more complicated than the 2D human pose data set in the data acquisition and processing stage. Most of the data sets used in 2D human pose estimation are collected in natural environments, and the acquisition method of manual annotation is relatively simple. In contrast, the 3D human pose acquisition process requires a large number of cameras and sensors. Synchronous acquisition of multiple perspectives requires camera parameters. Therefore, many 3D human pose data sets are collected in laboratory environments. The final 3D human pose annotation data sets are far lower than the 2D human pose data sets in terms of diversity and quantity.

At present, common 3D human pose annotation data sets include HumanEva[26], Human3.6M[27], CMU Panoptic dataset[28], MPI-INF-3DHP[29], etc[30]. The following is a detailed introduction to these commonly used annotation data sets, and summarized in Table 1.

HumanEva data set[26]. The HumanEva data set [26] consists of two sub-data sets, HumanEva-I and HumanEva-II. The two data sets were captured using ViconPeak's commercial MoCap system and annotated with ground truth. The HumanEva-I data set has a total of 13.5GB, which contains 7 verified view video sequences synchronized with 3D human poses, including 4 grayscales and 3 colors. These 3D human posture marker data are collected through a motion capture system. In the 3m x 2m capture area, the bodies of four objects are tagged and six common movements such as walking, gesturing, throwing and catching, boxing and combination are performed. The HumanEva-II data set has a total of 4.54GB and contains only 2 objects. Its ground truth motion capture data is also obtained using ViconPeak's system.

Human3.6M data set[27]. The collection of Human3.6M data set [27] is carried out in the laboratory. The collection system is a precise MoCap system based on tags. There are 11 occupational actors wearing well-fitting clothes in the laboratory, including 5 women and 6 men. Collect 17 activities, including posing, discussing, smoking, taking pictures, making phone calls, etc. It has a total of approximately 127GB, containing 3.6 million 3D human poses, each of which corresponds to 4 images with diverse perspectives. The main capture equipment includes 4 digital cameras, 1 time-of-flight sensor, and 10 synchronized motion cameras. The capture area is approximately 4m x 3m. Figure 4 below is a schematic diagram of the motion capture system used by Human3.6M. In order to evaluate, it is divided into three protocols according to diverse training and test data: protocol 1, protocol 2, and protocol 3. There are two commonly used division criteria. The first is to use 1, 5, 6, 7, 8 as the training set, and 9, 11 as the test set. The second is to use 1, 5, 6, 7, 8, 9 as the

training set, and 11 as the test set. In this article, we mainly use the first protocol in Human3.6M to conduct comparative experiments on each model.

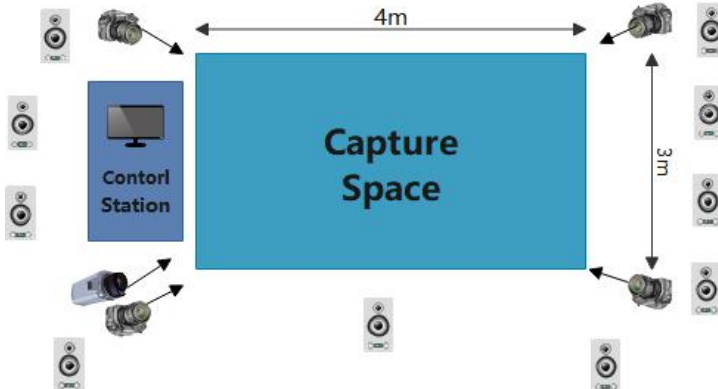


Figure 4. Human3.6M motion capture system schematic diagram.

CMU Panoptic dataset[28]. The CMU Panoptic dataset [28] is produced by CMU and is captured using a multi-view system with unmarked motion capture. The system has 480 VGA camera views, 31 HD views, 10 RGBD sensors and hardware synchronization system. The annotations include 3D key points, cloud points, optical flow, etc. The total size is about 41GB.

MPI-INF-3DHP data set[29]. The MPI-INF-3DHP dataset [29] was collected using an unmarked multi-camera MoCap system in indoor and outdoor sites. It contains 1.3 million frames from 14 different views. Eight subjects (4 women and 4 men) were noted to perform 8 events (such as walking, standing, exercising, sitting, squatting, stretching, exercising, etc.).

Table 1. Summary of commonly used data sets

Data Set Name	Scale	Collection Scene	Number Of People Collected	Number Of Samples	Capture Method
HumanEva[26]	18G	Indoor	4	~8	Motion capture
Human3.6M[27]	127GB	Indoor	11	360	Motion capture
CMU Panoptic dataset[28]	41GB	Indoor	Multiplayer	unknown	Motion capture
MPI-INF-3DHP[29]	unknown	Indoor and Outdoor	8	> 130	Motion capture, Image synthesis

3.2. Evaluation index

Human3.6M dataset is currently the most widely used 3D human pose annotation dataset. There are three evaluation methods mentioned in the paper, namely MPJPE, MPJAE and MPJLE.

MPJPE is the mean per joint position error. It is currently the most widely used measure for performance evaluation of 3D attitude estimation. It calculates the Euclidean distance (in millimeters) from the estimated 3D joint to the real condition of the ground, and then compares the results with the real value. The position of each joint point is represented in a 3D coordinate system. If it is used for 2D data, the unit used is pixel.

MPJAE is the mean per joint angle error. The function returns the joint angle instead of the joint position. It is also an MPJPE in nature, but some too small joint position errors are filtered and the errors are normalized.

MPJLE is the mean per joint localization error. MPJPE and MPJAE have two shortcomings. The first problem is that they do not have sufficient robust stability. Mispredicted joints will affect the error of the entire data set. The second disadvantage is that the final result may overemphasize errors that are hard for humans to detect. MPJLE is proposed to solve some of these problems.

The error evaluation method used in this article is the most commonly used MPJPE in 3D pose estimation. The calculation formula is as follows:

$$E_{MPJPE}(f, S) = \frac{1}{N_S} \sum_{i=1}^{N_S} \|m_{F,S}^{(f)}(i) - m_{gt,S}^{(f)}(i)\|_2 \quad (1)$$

Where f represents the frame, S represents the skeleton, N_S represents the quantity of nodes in the skeleton S, F represents the estimation result, gt represents the true value, and m represents a function, the input is the node number i, $\|\cdot\|_2$ which represents 2 norm.

3.3. Comparative Test

Aiming at the three different human pose estimation methods listed in the previous chapter, this section uses the python programming language with the deep learning open source framework Tensorflow. Corresponding experimental environment was built on the Ubuntu system, and several models were verified and compared. The Human3.6M data set is used as the verification set for model verification. The verification set contains a total of 15 different human daily activity scenes of 11 different people. When dividing the training set and the verification set, consider the generalization ability of the human pose difference for the training model. It is not possible to put all 11 people in the training set, so division rules are formed for the training set and the verification set. This article uses protocol 1, which uses S1, S5, S6, S7, and S8 of the 17 joint bones as the training set and S9 and S11 as the test set. The evaluation method used in quantitative analysis is the average joint point position error MPJPE. After aligning the depth of the root joint (usually the pelvic joint), use the trained model to perform MPJPE calculation on the scene in the verification set, and then compare with the current method using the same data set, and finally summarize the experimental contrast results, as shown in the following Table 2 below.

Table 2. Estimated and verified results of each network model on the Human3.6M test set (MPJPE(mm))

Method	Directions	Discussion	Eating	Greeting	Phoning	Photo	Posing	Purchases
Zhou X[11]	91.83	102.41	96.95	98.72	113.35	125.22	90.04	93.84
Tome D[15]	64.98	73.47	76.82	86.43	86.28	110.67	68.93	74.49
Chen C[16]	71.63	66.60	74.74	79.09	70.05	93.26	67.56	89.30
Moreno[17]	67.48	79.01	76.48	83.12	97.43	100.37	74.58	71.96
Martinez[18]	51.8	56.2	58.1	59.0	69.5	78.4	55.2	58.1
Zhou X[20]	54.82	60.70	58.22	71.41	62.03	65.53	53.83	55.58
Pavlakos[22]	48.5	54.4	54.4	52.0	59.4	65.3	49.9	52.9
Li C[25]	43.8	48.6	49.1	49.8	57.6	61.5	45.9	48.3
Pavllo[24]	45.2	46.7	43.3	45.6	48.1	55.1	44.6	44.3

Method	Sitting	Sitting Down	Smoking	Waiting	Walk Dog	Walkin g	Walk Together	Average
Zhou X[11]	132.16	158.97	106.97	94.41	126.04	79.02	98.96	107.26
Tome D[15]	110.19	173.91	84.95	85.78	86.26	71.36	73.14	88.39
Chen C[16]	90.74	195.62	83.46	71.15	85.86	55.74	62.51	82.72
Moreno[17]	102.40	116.68	87.70	94.57	82.72	75.21	74.92	85.64
Martinez[18]	74.0	94.6	62.3	59.1	65.1	49.5	52.4	62.9
Zhou X[20]	75.20	111.59	64.15	66.05	51.43	63.22	55.33	64.90
Pavlakos[22]	65.8	71.1	56.6	52.9	60.9	44.7	47.8	56.2
Li C[25]	62.0	73.4	54.8	50.6	56.0	43.4	45.5	52.7
Pavllo[24]	57.3	65.8	47.1	44.0	49.0	32.8	33.9	46.8

According to Table 2, it is concluded that for the data obtained by experiments of the models in some papers in the Human3.6M data set, the phased 3D human pose estimation method is better than the end-to-end human pose estimation method. For the average MPJPE of all scenarios in the test set, the average MPJPE of Martinez et al. [18] is about 40mm lower than that of Zhou X et al. [11]. Moreover, the 3D human pose estimation method of the hybrid network model is also better than staged 3D human pose estimation method. In the chart, the average MPJPE of the method of Pavllo et al. [24] is 16.1 mm lower than that of the method of Martinez et al. [18].

In summary, in the 3D single person pose estimation method, the constantly evolving neural network model is combined with the data information of the 2D human pose joints and the geometric structural characteristics of the human pose structure itself to optimize the method performance of the model. This kind of mixed and matched network model greatly improves the accuracy of human pose estimation, and at the same time increases the possibility of application in more different complex scenes.

4. Summary

This article reviews the development of 3D single person pose estimation methods using neural networks, describes in detail the important method models, and compares the better theoretical models in previous studies, and gives the comparative experimental results. Make a summary of it.

The existing 3D single person pose estimation methods based on neural networks are relatively mature, but the accuracy of pose estimation in complex scenes needs to be improved. The current 3D single person pose estimation method based on neural networks cannot achieve satisfactory results in the case of multiple poses, which points out specific directions for future research work. In addition, a plenty of commonly used data sets are collected indoors, and there are too few types of human postures. Therefore, the way of generating data will be an immense challenge.

Acknowledgments

This work has been supported by the Natural science foundation of Ningxia province (No. 2020AAC03 218), and the North Minzu University key research project (No. 2019KJ26) and the National Innovation and Entrepreneurship Project under Grant (No. S2020-11407-010G).

References

- [1] Wang K, Lin L, Jiang C, et al. 3D human pose machines with self-supervised learning[J]. IEEE Transactions on Pattern Analysis and Machine Intelligence, 2019, 42(5): 1069-1082.
- [2] Véges M, Varga V, Lörincz A. 3d human pose estimation with siamese equivariant embedding[J]. Neurocomputing, 2019, 339: 194-201.
- [3] Cheng Y, Yang B, Wang B, et al. Occlusion-aware networks for 3d human pose estimation in video[C]//Proceedings of the IEEE International Conference on Computer Vision. 2019: 723-732.
- [4] Hwang D H, Kim S, Monet N, et al. Lightweight 3D Human Pose Estimation Network Training Using Teacher-Student Learning[C]//The IEEE Winter Conference on Applications of Computer Vision. 2020: 479-488.
- [5] Huang F, Zeng A, Liu M, et al. DeepFuse: An IMU-Aware Network for Real-Time 3D Human Pose Estimation from Multi-View Image[C]//The IEEE Winter Conference on Applications of Computer Vision. 2020: 429-438.
- [6] Mehta D, Sotnychenko O, Mueller F, et al. Xnect: Real-time multi-person 3d human pose estimation with a single rgb camera[J]. arXiv preprint arXiv:1907.00837, 2019.
- [7] Soonchan Park,Sang-baek Lee,Jinah Park. Data augmentation method for improving the accuracy of human pose estimation with cropped images[J]. Pattern Recognition Letters,2020,136.
- [8] Chen Y, Shen C, Wei X S, et al. Adversarial posenet: A structure-aware convolutional network for human pose estimation[C]//Proceedings of the IEEE International Conference on Computer Vision. 2017: 1212-1221.
- [9] Chou C J, Chien J T, Chen H T. Self adversarial training for human pose estimation[C]//2018 Asia-Pacific Signal and Information Processing Association Annual Summit and Conference (APSIPA ASC). IEEE, 2018: 17-30.
- [10] Sun K, Xiao B, Liu D, et al. Deep high-resolution representation learning for human pose estimation[C]//Proceedings of the IEEE conference on computer vision and pattern recognition. 2019: 5693-5703.
- [11] Zhou X, Sun X, Zhang W, et al. Deep kinematic pose regression[C]//European Conference on Computer Vision. Springer, Cham, 2016: 186-201.
- [12] Tekin B, Katircioglu I, Salzmann M, et al. Structured prediction of 3d human pose with deep neural networks[J]. arXiv preprint arXiv:1605.05180, 2016.
- [13] Long J, Shelhamer E, Darrell T. Fully convolutional networks for semantic segmentation[C]//Proceedings of the IEEE conference on computer vision and pattern recognition. 2015: 3431-3440.
- [14] Zhou X, Zhu M, Leonardos S, et al. Sparseness meets deepness: 3d human pose estimation from monocular video[C]//Proceedings of the IEEE conference on computer vision and pattern recognition. 2016: 4966-4975.
- [15] Tome D, Russell C, Agapito L. Lifting from the deep: Convolutional 3d pose estimation from a single image[C]//Proceedings of the IEEE Conference on Computer Vision and Pattern Recognition. 2017: 2500-2509.
- [16] Chen C H, Ramanan D. 3d human pose estimation= 2d pose estimation+ matching[C]//Proceedings of the IEEE Conference on Computer Vision and Pattern Recognition. 2017: 7035-7043.
- [17] Moreno-Noguer F. 3d human pose estimation from a single image via distance matrix regression[C]//Proceedings of the IEEE Conference on Computer Vision and Pattern Recognition. 2017: 2823-2832.
- [18] Martinez J, Hossain R, Romero J, et al. A simple yet effective baseline for 3d human pose estimation[C]//Proceedings of the IEEE International Conference on Computer Vision. 2017: 2640-2649.
- [19] Pavlakos G, Zhou X, Derpanis K G, et al. Coarse-to-fine volumetric prediction for single-image 3D human pose[C]//Proceedings of the IEEE Conference on Computer Vision and Pattern Recognition. 2017: 7025-7034.
- [20] Zhou X, Huang Q, Sun X, et al. Towards 3d human pose estimation in the wild: a weakly-supervised approach[C]//Proceedings of the IEEE International Conference on Computer Vision. 2017: 398-407.
- [21] Zhou X, Zhu M, Pavlakos G, et al. Monocap: Monocular human motion capture using a cnn coupled with a geometric prior[J]. IEEE transactions on pattern analysis and machine intelligence, 2018, 41(4): 901-914.
- [22] Pavlakos G, Zhou X, Daniilidis K. Ordinal depth supervision for 3d human pose estimation[C]//Proceedings of the IEEE Conference on Computer Vision and Pattern Recognition. 2018: 7307-7316.

- [23] Yang W, Ouyang W, Wang X, et al. 3d human pose estimation in the wild by adversarial learning[C]//Proceedings of the IEEE Conference on Computer Vision and Pattern Recognition. 2018: 5255-5264.
- [24] Pavllo D, Feichtenhofer C, Grangier D, et al. 3d human pose estimation in video with temporal convolutions and semi-supervised training[C]//Proceedings of the IEEE Conference on Computer Vision and Pattern Recognition. 2019: 7753-7762.
- [25] Li C, Lee G H. Generating multiple hypotheses for 3d human pose estimation with mixture density network[C]//Proceedings of the IEEE Conference on Computer Vision and Pattern Recognition. 2019: 9887-9895.
- [26] Sigal L, Balan A O, Black M J. HumanEva: Synchronized video and motion capture dataset and baseline algorithm for evaluation of articulated human motion[J]. International journal of computer vision, 2010, 87(1-2): 4.
- [27] Ionescu C, Papava D, Olaru V, et al. Human3. 6m: Large scale datasets and predictive methods for 3d human sensing in natural environments[J]. IEEE transactions on pattern analysis and machine intelligence, 2013, 36(7): 1325-1339.
- [28] Joo H, Liu H, Tan L, et al. Panoptic studio: A massively multiview system for social motion capture[C]//Proceedings of the IEEE International Conference on Computer Vision. 2015: 3334-3342.
- [29] Mehta D, Rhodin H, Casas D, et al. Monocular 3d human pose estimation in the wild using improved cnn supervision[C]//2017 international conference on 3D vision (3DV). IEEE, 2017: 506-516.
- [30] Chen Y, Tian Y, He M. Monocular human pose estimation: A survey of deep learning-based methods[J]. Computer Vision and Image Understanding, 2020, 192: 102897.

A Review of Inference Methods Based on Knowledge Graph

Dexiang Zhang¹, Hairong Wang, Yudan Ding
North Minzu University, China

Abstract. With the development of Internet and big data technology, the scale of data is growing exponentially, and these data contain a lot of valuable information. As the most intuitive way of knowledge expression, knowledge map can effectively organize and express data. As an important means of knowledge map completion, knowledge inference aims to deduce new knowledge or identify wrong knowledge based on existing knowledge in the knowledge map. Different from traditional knowledge inference methods, knowledge inference methods based on knowledge graphs are also diversified according to their simple, intuitive, flexible and rich knowledge expression forms. According to the types of reasoning methods, knowledge reasoning methods based on knowledge graph can be divided into single-step reasoning and multi-step reasoning. According to the different methods adopted for each type, each type also includes reasoning based on distributed representation; reasoning based on neural network and mixed reasoning. These methods are summarized in detail, and the future research direction and prospect of knowledge inference based on knowledge map are discussed and prospected.

Keywords. Knowledge mapping, knowledge inference, distributed representation, neural networks, hybrid networks

1. Introduction

A formalized representation method of the knowledge graph is to use fact triples [1] to record various things and their interrelationships. It transforms human knowledge into a form understandable and usable by machines. It can be represented by the "head entity" and "tail entity" in the above triples, and the relationship between things is represented by the "relationship" in the triples [2]. At present, because most of the open knowledge graphs, such as DBpedia [3], Freebase [4], are constructed manually or semi-automatically, these knowledge.

The knowledge map is relatively sparse, and the hidden relationships among a large number of entities have not been fully explored. According to statistics in 2014, in the Freebase knowledge base, 71% of people have no exact date of birth, and 75% have no nationality information [5]. The incompleteness of the knowledge graph seriously restricts the development of the field of artificial intelligence. How to complete the knowledge graph has become one of the important issues in the field of knowledge graph research.

¹ Corresponding Author, Hairong Wang, North Minzu University, China; E-mail: bmdwhr@163.com. This work has been supported by the Natural science foundation of Ningxia province (No. 2020AAC03218), and the North Minzu University key research project (No.2019KJ26) and the North Minzu University Graduate innovation program (No. S2020-11407-039G)

ch. Knowledge Graph Completion (KGC) [6] technology was born to deal with the above problems. The knowledge graph completion technology adopts the method of knowledge reasoning, using the existing explicit knowledge in the knowledge graph to predict the tacit knowledge that has not been stored in the graph, and gradually complete the knowledge graph [7].

Traditional knowledge reasoning mainly includes logical reasoning and non-logical reasoning. The process of logical reasoning includes strict constraints and reasoning process, while the process of non-logical reasoning is relatively fuzzy. Logical reasoning is mainly divided into two categories according to the different ways of reasoning: deductive reasoning [8] and inductive reasoning [9]. Among them, inductive reasoning includes abductive reasoning [10] and analogical reasoning [11]. In recent years, the knowledge graph has continued to develop. The number of examples in the graph has gradually increased, and the content covered has become more and more extensive, and a large number of logical rules are required. Therefore, whether it is at the instance level or the abstract concept level, traditional reasoning methods are faced with complexity Problems such as difficulty in solving instantiation problems. In the face of situations where traditional reasoning methods cannot meet the needs, on the basis of significant progress in distributed representation and neural network technology, reasoning based on knowledge graphs has evolved its unique reasoning method.

Compared with traditional knowledge reasoning methods, knowledge reasoning based on knowledge graphs is dominated by the knowledge graph itself, not limited to abstract reasoning at the main conceptual level of the ontology, and can have more specific reasoning methods [12]. There are mainly distributed representation-based methods, neural network-based methods and a mixture of multiple methods. Knowledge reasoning technology is affected by the development of knowledge graphs, and has received wide attention as the main means of knowledge graph completion and knowledge graph denoising.

2. Reasoning based on knowledge graph

The reasoning based on the knowledge graph mainly revolves around the reasoning of the relationship, inferring unknown facts or relationships from the facts or relationships that already exist in the knowledge graph [13], generally focusing on the three aspects of the feature information of entities, relationships and graph structure. Figure 1 shows the reasoning of the character relationship graph, using reasoning to get new facts and rules. In general, reasoning oriented to knowledge graphs can mainly assist in reasoning new facts, new relationships, new axioms, and new rules.

Specifically, the knowledge graph usually uses triples containing head entities, relationships, and tail entities to express the attributes of things and the semantic relationships between things. Among them, the entities in the triples are composed of transactions and attribute values, and the relationship in the triple is composed of attributes and relationships. Knowledge graph completion [14] is actually given any two elements in the triplet, the other missing element is obtained through the inference algorithm. That is, given the head entity and the relationship or the relationship and the tail entity, find the tail entity or head entity of the matching triple. This process is called entity prediction [15]. In the same way, relationship prediction is to find out the relationship of matching triples under the premise of given head entity and tail entity in the triple. Regardless of entity prediction or relationship prediction, it will be transformed into entities or relati

onships that are more likely to form a valid triple under the premise of a given element as the prediction result, and the effectiveness of the entity can be obtained by calculating the score function of a specific hypothesis.

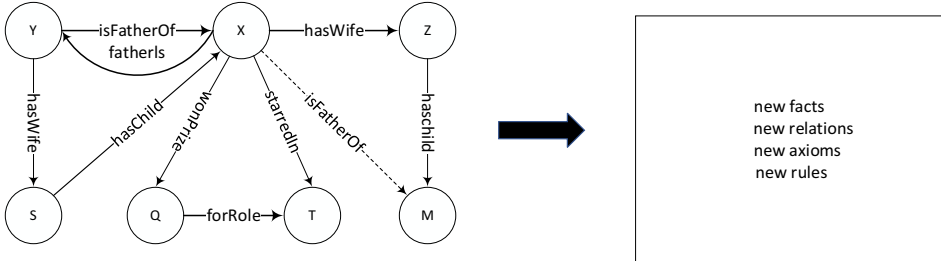


Figure 1 Character diagram reasoning

Since there are thousands of knowledge in the real world, it is very difficult to cover all knowledge, which will lead to the incompleteness of the knowledge map. Therefore, it is very necessary to complete the knowledge map. In the process of completion, Link test is a very typical reasoning task. The triples in the knowledge graph can be obtained through manual definition or text extraction. Due to the limitations of artificial knowledge and the uncertainty of algorithms, there may be conflicting or incorrect information in the knowledge graph. Therefore, inconsistency detection is also an important reasoning task in the knowledge graph. The large amount of information stored in the knowledge graph can provide good knowledge services and provide correct relevant knowledge information for related queries. However, the vagueness of the query and the rich semantic information of the knowledge graph make the query difficult, and knowledge reasoning can help query rewriting. Effectively improve the quality of query results.

By summarizing the reasoning methods based on the knowledge graph, according to the reasoning type, the current reasoning methods are divided into two categories: single-step reasoning and multi-step reasoning. According to the different methods used in each category, further division and explanation of knowledge reasoning methods are made.

3 Single-step reasoning

Single-step reasoning refers to the method of learning and reasoning using the fact tuples stored in the knowledge graph. Its main feature is that it does not consider path characteristics. According to the different methods used, it can be divided into reasoning based on distributed representation, reasoning based on neural network and hybrid reasoning [12].

3.1 Distributed Representation Reasoning

Distributed knowledge representation refers to the transformation of entities and relationships in triples into dense low-dimensional real-valued vectors. Distributed knowledge representation includes two types of vectors: entity vector and relationship

vector, where the entity vector can represent either the head entity or the tail entity. The two entities in the knowledge graph and the relationship between them are represented by triples in the form of (h, r, t) , where h is the head entity vector, r is the tail entity vector, and t is the relationship vector. Single-step reasoning based on distributed representation refers to a direct reasoning process based on distributed knowledge representation. Among them, the most typical is representational reasoning based on translation. The idea of this method is inspired by the experimental results of word2vec. Mikolov et al. proposed a word2vec word representation learning model and toolkit [16], on the basis of which they found that there is a phenomenon of translation invariance between the trained word vectors, and found through analogy inference experiments that this translation invariant. The phenomenon generally exists in the semantic relationship of words.

TransE: Based on the knowledge of hierarchical knowledge and natural transfer representation of knowledge base, Bordes [17] et al. proposed the first transfer-based representation model TransE. The main idea is: if the triple is established, the head entity vector h The sum of the relation vector r is close to the tail entity vector t , otherwise the three will be far away.

The score function is obtained from the above basic assumptions:

$$f(h, t) = \|r + h - t\|L1/L2 \quad (1)$$

Where L_1 or L_2 represents the norm, and the norm is used to measure the distance. The learning process replaces the head entity or the tail entity to get a negative example, similar to a support vector machine, which minimizes the loss function based on Margin. The score of the positive example is at least one Margin higher than the score of the negative example. In reasoning, the candidate entity or relationship with a large score function is the reasoning result. TransE defines the loss function by defining the maximum interval:

$$L = \sum_{(h, r, t) \in S} \sum_{(h', r', t') \in S'} [\gamma + d(h + r, t) - d(h' + r', t')] + \quad (2)$$

The $[\gamma + d(h + r, t) - d(h' + r', t')] +$ means $\max(a, x)$; γ is a constant, which means the distance between positive and negative samples.

Compared with the previous model, the TransE model has fewer parameters, low computational complexity, and significantly improved performance. However, for different types of relationships, all entity vectors are represented the same; this leads to the TransE model being effective when solving one-to-one relationships, but not applicable when dealing with complex relationships.

TransR: Both TransE and TransH models put entities and relationships in the same semantic space, which limits the expressive ability of the model. In response to this problem, Lin et al. proposed the TransR model [18], which established entity vectors and relationship vectors in independent entity space and relationship space. First, the entities are projected from the entity space to the corresponding relationship space, and then the relationship between the projected entities is translated. The main idea of the TransR model is: Given a triple (h, r, t) , project the head entity and tail entity vectors into the relationship space to get:

$$h_r == M_r h, t_r = M_r t \quad (3)$$

Among them, is the projection matrix from the entity space to the relational space; is the entity space; is the relational space.

The potential energy function of the TransR model is:

$$f_r(h, t) = \|h_r + r - t_r\| L_n \quad (4)$$

The TransR algorithm maps entities and relationships into two spaces respectively, and then transfers the entities in the entity space to the relationship space through the transition matrix M_r for vector representation. In the TransR algorithm, the entity vector of each triple is set as a k -dimensional vector, the relationship vector is set to a d -dimensional vector, but k may not be equal to d , and the mapping matrix is a $k \times d$ matrix, so that after transferring from the entity space to the relationship space, each head entity and tail entity all become vector representations of the relational space. Since the relationships in the graph are usually different, the TransR model learns a unique vector for each relationship. Therefore, the TransR model is not enough to represent all entity pairs under the relationship.

TransD: The TransD model uses two vectors to represent entities and relationships, one is used to represent the meaning of the entity, and the other is used to dynamically construct a mapping matrix [19]. Compared with TransR and CtransR [18], the TransD model not only considers the diversity of relationships but also the diversity of entities. TransD has few parameters and does not require matrix vector multiplication. The main idea of the TransD model is: for a given triple (h, r, t) , its vectors are h, h_p, r, r_p, t, t_p , and the subscript p represents the projection vector, defining two projections .

The matrix maps entities from physical space to relational space:

$$M_{rh} = r_p h_p^T + I^{m \times n}, M_{rt} = r_p t_p^T + I^{m \times n} \quad (5)$$

Among them: $h, h_p, t, t_p \in R_n$, $r, r_p \in R_n$, $M_{rh}, M_{rt} \in R_{mn}$. Therefore, the mapping matrix is determined by the entity and the relationship. This operation enables the two projection vectors to interact well with each other Function, because each element of them can satisfy each element from another vector. When we initialize each mapping matrix, we will add it to M_{rh} and M_{rt} . Using the mapping matrix, we define the projection vector as follows:

$$h_\perp = M_{rh}, t_\perp = M_{rt} \quad (6)$$

Compared with the TransR model, TransD sets up projection matrices for the head entity and tail entity. In addition, notice that there is no matrix-vector multiplication operation after the formula is expanded in TransD. This reduces the computational complexity compared to the TransR model and is more suitable for Calculation of large-scale knowledge graph. In addition to the representation learning methods mentioned so far, there are many other representation learning methods, such as pure neural network methods NTN, ConvE.[20], etc.

From the current analysis of related technologies, the research work of the TransE series of transfer-based representation reasoning methods is relatively comprehensive. However, when modeling, only the constraints of the knowledge graph fact tuple are usually considered, and the deeper combination of semantic information is not considered, and the reasoning ability is limited. The TransE method has the characteristics of simplicity, effectiveness, and high computational efficiency. This has also attracted widespread attention. Many researchers have gone deep into it, and a series of methods have emerged to form the Trans series. However, the TransE series model has been developed for many years, and the development space is trending. Because of saturation, the development potential is small. In addition, the problem-based improvement development route of the Trans series is not suitable for this type of method. More innovative methods, such as methods in the field of mathematics, and modeling spatial distribution are needed.

3.2 Neural Network Reasoning

In single-step reasoning, neural network-based reasoning uses the neural network to directly model the knowledge graph fact tuple, and obtain the vector representation of the fact tuple element for further reasoning. In this method, the entire network constitutes a score function, and the output value of the neural network is used as the score value of the score function. Typical single-step neural network inference models include neural tensor network NTN (neural tensor network), and shared variable neural network model ProjE.

NTN: In order to be able to discover and mine the implicit relationship between different entities in the knowledge graph, Socher et al.[21] proposed a neural tensor network (NeuralTensorNetwork, NTN) method, which uses a bilinear tensor layer to replace the traditional standard linear neural Network layer. By representing each entity in the database as a vector to obtain the facts about the entity and the probability that it belongs to a certain relationship, each relationship is defined by the parameters of the neural tensor network, and the relationship is expressed as a third-order Zhang It can accurately predict other facts under the condition of using the existing database. The advantage of expressing the relationship as a tensor is that each slice can correspond to a different semantic type, that is, a relationship has multiple slices, which can better model the different semantic connections between different entities under the relationship. The score of the possibility that two entities are in a certain relationship is defined by the following function:

$$g(e_1, R, e_2) = u_R^T f \left(e_1^T W_R^{[1:k]} e_2 + V_R \begin{bmatrix} e_1 \\ e_2 \end{bmatrix} + b_R \right) \quad (7)$$

Where f is a standard nonlinear function, $W_R^{[1:k]} \in R^{d \times d \times k}$ Is a tensor, $e_1^T W_R^{[1:k]} e_2$ Is the bilinear tensor product, The result is $h \in R^k$, Each h_i represents a tensor $cuth_i = e_1^T W_R^{[1:k]} e_2$, Other parameters related to R refer to the standard neural network: $V_R \in R^{k \times 2d}$, $U \in R^k$, $b_R \in R^k$, $g(e_1, R, e_2)$ the higher the function score, It shows that the relationship between e_1 and e_2 the entity and R is higher.

The NTN model fully retains the entity semantics implicit in the long tail entity by expressing the long tail entity as the average value of the word vector. In the absence of text description information, the NTN model can still be used to disassemble the entity name. Get entity description information.

Although the NTN model can dig out implicit relationships and entity semantics, it also needs to link the discovered new entities outside the knowledge base to the knowledge base. In this regard, Chen[22] et al. improved the NTN model based on the NTN neural tensor network. The improved model discovers new entities outside the knowledge base by predicting additional real relationships between entities and links them to the knowledge In the library, realize the expansion and completion of the knowledge base. The model uses word vectors in the unsupervised text corpus to initialize the entity representation. At the same time, the model uses a method similar to the long-tail entity representation in the NTN model, using subunits separating entity names with spaces to capture grammatical and semantic information, thereby detecting whether entities outside the database are in a specific relationship. The improvement of the NTN model does not require manual design rules nor additional analysis of other text resources. However, the NTN model is based on the tensor decomposition method. Because this method does not consider the characteristics of the multi-path structure in the knowledge graph, the NTN model can only be used for single-step reasoning and

can only predict the relationship between directly connected entities, And can't mine the deep-level relationship information passed between entities through paths.

ProjE: with the development of knowledge graphs, the amount of information stored in the knowledge base continues to increase, the model feature space of knowledge reasoning is becoming increasingly complex, and the parameter scale is also growing. In order to reduce the parameters, Shi [23] et al. proposed a projection embedding model (Embedding Projection, ProjE) with better effect and smaller parameter scale by simplifying the underlying model architecture. The main method is to treat entity prediction as a multi-candidate ranking problem. Among them, the candidate with the highest ranking score is the entity prediction result, as shown in Figure 2.

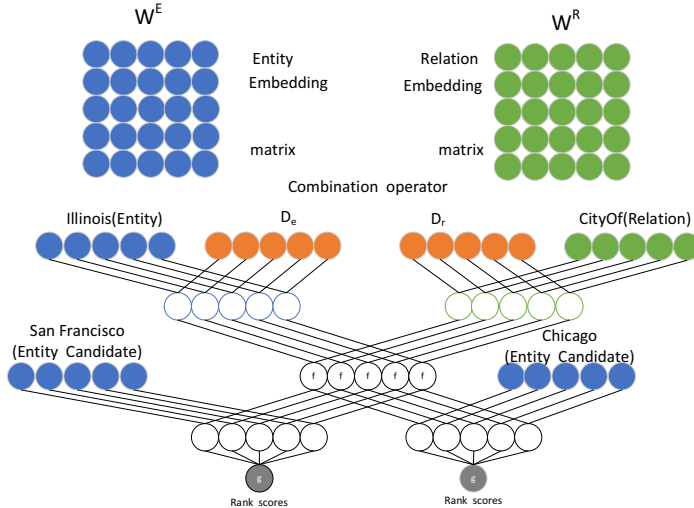


Figure 2. ProjE model

In order to generate the ranking list, this method projects each candidate object onto a target vector generated by the input vector through a predefined combination operator, and calculates the projection similarity. The combination operator is defined as follows:

$$e \oplus r = D_e e + D_r r + b_c \quad (8)$$

The sum is the diagonal matrix, which is the weight of the entity and the relationship respectively, and is the combined deviation. The model defines the embedded projection function as:

$$h(e, r) = g(W^c f(e \oplus r) + b_p) \quad (9)$$

Among them, f and g use sigmoid and tanh as activation functions, respectively, which are the matrix of candidate entities and the projection deviation. Represents the ranking score vector, where each element represents the similarity between a certain candidate entity in the combined input embedding.

From the perspective of the number of parameters, compared with other transfer matrix methods, the number of parameters in the ProjE model is greatly reduced in the process of using combined operations. This model can not only perform entity prediction tasks, but also perform relationship prediction tasks by changing the input. However, because the ProjE model processes the entity and relationship embedding vectors through the combination operator to generate the output vector, the quality of

the word vector preprocessing has a great influence on the combination operation. Not only that, the ProjE model does not use semantic information such as entity descriptions and relationship paths, and the interpretability of the reasoning results is still lacking.

All in all, single-step reasoning based on neural networks attempts to use the powerful learning capabilities of neural networks to model knowledge graph fact tuples, and obtain good reasoning and generalization capabilities. However, the inherent interpretability problems of neural networks still exist. How to properly explain in the application of knowledge graph

The reasoning ability of neural networks is a big difficulty. At present, there are relatively few researches on single-step reasoning based on neural networks, but the high expressive ability of neural networks and its application in other fields, including image processing, text processing, and knowledge The outstanding performance and high performance of graph structure data fields such as social networks with similar graph structures make the research prospects in this direction broad. How to extend more neural network-based methods in other fields to the field of knowledge graphs has become a subject to be studied in depth in the future Question. General graph structure data, such as the representation and reasoning of social networks, are nodes, while the representation and reasoning of knowledge graphs focus on nodes (entities) and edges (relationships). Therefore, from general graph structure data based on neural networks, the transfer of methods to the knowledge graph will be a relatively simple breakthrough. At the same time, the research on the interpretability of neural networks needs to be further developed.

3.3 Confluent reasoning

ILP: In the process of rule discovery assisted by distributed representation, the discovery of reasoning rules in the earlier reasoning method of combining rules and distributed is realized by calculating the distributed similarity between relations, and the relationship is represented as the feature vector of corresponding instance. However, the earlier methods do not consider the specific context information, and use an independent method to model the relationship, which ignores the dependency between relationships. In view of the above two problems, Han[24] et al. proposed a context sensitive reasoning rule discovery method. To adopt this method, you need to first build a relationship graph (as shown in Figure 5), and use abstract relationship tuples (such as A buy B) and instantiated features (such as A=Facebook and B=WhatsApp) as the nodes in the relationship graph. The edge in represents the co-occurrence of the abstract relationship tuple and the instantiation feature (such as the edge between A buy B and A=Facebook) or the semantic dependency between the abstract relationship tuple (Such as the connection between A buy B and A purchase B). Then, learn the relationship representation of a specific context based on the relationship graph (as shown in Figure 3, the relationship acquire on the specific context (Google, YouTube) and (children, skill) will be different), and the abstract relationship tuple is related to the corresponding feature context sensitively. The sex score is visualized as a splicing vector, and the correlation score is calculated by restarting random walks from the relation tuple to the feature. Finally, the similarity between the relation vectors is calculated, and the relation pair and the corresponding context larger than the threshold are used as inference rules.

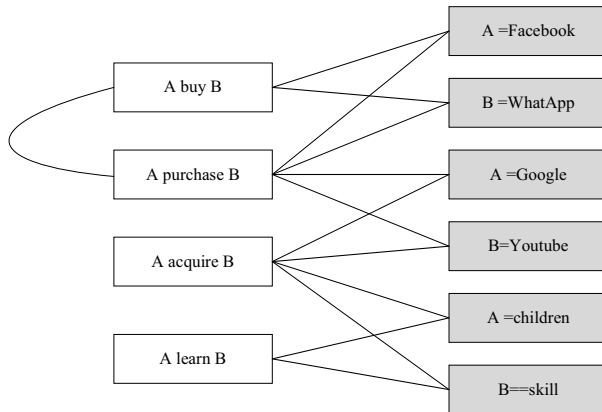


Figure 3 Example of relationship diagram

In the aspect of rule assisted reasoning based on distributed representation, Wang [25] et al. seamlessly embedded logical rules and physical rules in the representation model, formalizing the reasoning method into an integer linear programming problem (ILP). Physical rules include the restriction of entity type and the number of entities. In general logic rules, if another relationship R_2 can be deduced through relationship R_1 , then the two entities connected by relationship R_1 are also connected by relationship R_2 , and the model and rules are integrated by ILP. The objective function is based on the score function of the triple, and any of the above can be used to represent the score function of the model, and each rule is formalized as a condition to be satisfied.

Although this method can improve the reasoning accuracy to a certain extent, the rules in these methods need to be instantiated at a high cost.

DKRL: There are two hybrid models in the hybrid reasoning method of neural network and distributed representation: the first is to use the neural network method to model the external information such as the related external text and entity description, and use the representation model to model the triples in the knowledge map; the second method is to use the neural network method to model the knowledge map and get the output Value is applied to the representation model. Xie[26] et al. thought that the description information of an entity can help to improve the accuracy of entity representation, so a description embedded knowledge representation learning (DKRL) model was proposed, which used the entity description in the knowledge map to predict the entity and relationship. The model uses two kinds of encoders, including continuous bag of words (CBOW) and deep convolution neural network. By learning the description content, this method can not only obtain the structure information in the triple, but also the keywords in the entity description and the text information hidden in the word order. The energy function e of DKRL model is defined as:

$$E = E_S + E_D \quad (10)$$

Where, is the energy function based on structure representation, which is the same as the energy function of model TransE:

$$E_S = \| h_s + r - t_s \| \quad (11)$$

E_D is an energy function based on description representation, which is defined as:

$$E_D = E_{DD} + E_{DS} + E_{SD} \quad (12)$$

E_{DD} is defined as:

$$E_{DD} = \| h_d + r - t_d \| \quad (13)$$

The head and tail entities are all based on description. EDS and ESD are defined as:

$$E_{DS} = \| h_d + r - t_s \| \quad (14)$$

$$E_{SD} = \| h_s + r - t_d \| \quad (15)$$

One of the head and tail entities is a description based representation, and the other is a structure based representation. The training goal of DKRL model is to minimize the marginal based score function L:

$$L = \sum_{(h,r,t) \in S} \sum_{(h',r',t') \in S'} [\gamma + d(h+r, t) - d(h'+r', t')] + \quad (16)$$

Among them, S is the set of positive case triples, which is the set of negative cases. The negative example means that one of H, R and T in the triple (h, R, t) is replaced by another entity or relationship with the wrong triple. γ is the marginal super parameter, which represents the minimum distance margin between positive and negative examples, and D () represents the calculation distance.

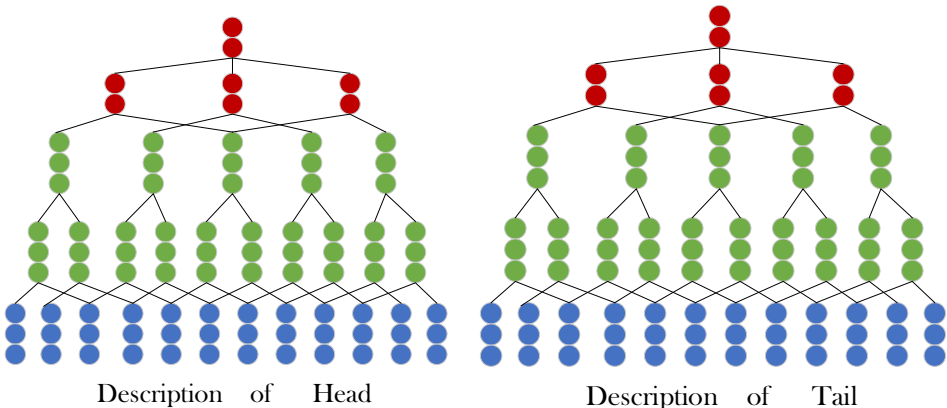


Figure. 4 DKRL model deep convolution neural network framework

The advantage of DKRL model is that it combines the text description information of entity in the process of entity representation, but the disadvantage is that the word vector needs to be preprocessed. The model is sensitive to noise data and needs to be eliminated manually. Moreover, the model is only compared with the TransE model, so it is not referential.

Generally speaking, the hybrid reasoning in the single-step reasoning method is to use a variety of different single-step reasoning methods to achieve complementary advantages. At present, the hybrid single-step reasoning method still stays in the shallow mixing of one method as the main method and the other as the auxiliary method. The hybrid reasoning method is different from other specific methods. It is more like a strategy. It is mainly based on the thorough analysis of various methods to find and mix the methods with complementary advantages. The development lies in the selection of several methods for integration and the mode of integration. Among them, one method is used as the main method and the other as the auxiliary strategy in the hybrid method of rule and distributed representation. There are two main ideas in the hybrid one-step reasoning of neural network and distributed representation: one is to use the existing representation model to learn the triples of knowledge map, and the other is to directly use neural network to model knowledge map and integrate the

learning model. In view of the outstanding performance of neural network in various aspects, it will become a hot spot in future research.

4 Multi step reasoning

The multi-step reasoning method is based on the direct relationship modeling by single-step reasoning, which is a deeper indirect relationship modeling, namely multi-step relationship. Multi step relation is a kind of transitive constraint. For example, there is relationship R_1 between entity A and entity B and relationship R_2 between entity B and entity C. The direct relationship corresponding to these two-step paths is the relationship R_3 between entity A and entity C. Through the introduction of multi-step relationship, more information can be modeled, so the effect of multi-step reasoning method is generally better than that of single-step reasoning method. According to different reasoning methods, multi-step reasoning can also be divided into distributed representation based reasoning, neural network-based reasoning and hybrid reasoning.

4.1 Reasoning for distributed representation

The multi-step distributed representation reasoning method also infers through the vectorized knowledge map. Different from the single-step reasoning method, multi-step relation constraints are introduced in the process of learning vector representation. The introduction of multi-step relationship can make the learned vector representation more helpful to the inference and prediction of entities and relationships. For the case of multiple paths between entities, the contribution difference of paths is not distinguished in the TransE model, and these paths are treated equally no matter how important the practical significance is. In this way, some paths with little practical significance are considered more, which increases the complexity of the model. In view of the above situation, the academia has made a series of improvements.

PTransE: For the drawbacks of unified treatment of paths in the TransE model, Lin et al. [27] proposed the PTransE model, which deals with different paths between entities. PTransE model adds relationship path constraint on the basis of TransE, and models the path through the combination operation of relationship. As shown in Figure 5, the paths pass through the relationships BornInCity, CityInState and StateInCountry in turn. Through the combination operation modeling of relations, the combination operation can be in the form of addition and multiplication of relations on the path, and then the combined path is regarded as the transition between the head entity Steve Jobs and the tail entity UnitedState. For multiple paths between entities, the weight of relational paths is weighed by path constrained resource allocation algorithm [14], which is used to weight the path modeling results.

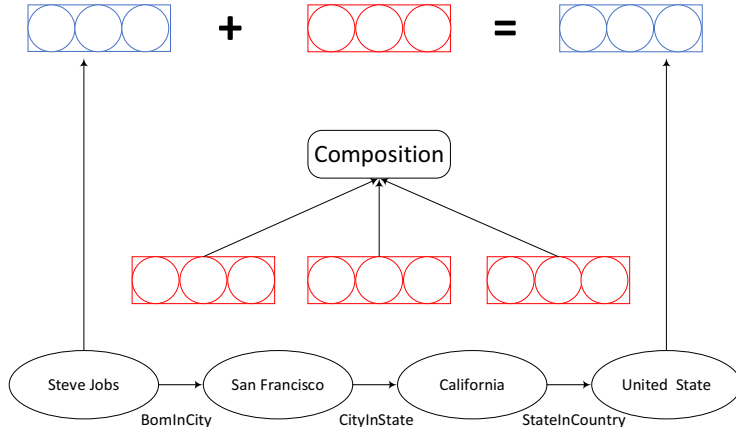


Figure 5. PTransE Path modeling

Specifically, for a relation path $p = (r_1, \dots, r_l)p = (r_1, \dots, r_l)$. We define a semantic composition operation and obtain the relational path representation $p = r_1, \dots, r_l$.

For a multi-step path triple (h, P, t) , we can define its energy function simply by referring to the TransE.

$$(h, p, t) = ||p - (t - h)|| = ||p - r|| \quad (17)$$

When the relation path P and relation R are consistent, the energy function has a lower score, and does not need to consider the vector information of the entity:

$$L(S) = \sum_{(h,r,t) \in S} [L(h, r, t) + \frac{1}{Z} \sum_{p \in P(h,t)} R(p|h, t)L(p, r)] \quad (18)$$

L is the energy function, Z is the normalization factor, and R is the reliability for the entity (h, t) relation path P.

Although PTransE model increases the relationship path constraints and reduces the parameters of combination operation, PTransE model can't deal with some complex relationship forms, such as reasoning from Queen to female, so it can be used as first-order logic to code this reasoning.

GAKE: At present, most of the knowledge representation methods deal with triples separately and PTransE model only introduces multi hop relation information. In this regard, Feng et al. [28] proposed a graph aware knowledge embedding (GAKE), which uses the structural information in the knowledge map to learn the vector representation of entities and relationships.

The GAKE model introduces three kinds of graph context information: neighbor context, path context and edge context. It reflects knowledge attributes from different angles. Meanwhile, it designs the attention mechanism, that is, weight learning of entities and relationships to learn entities or relationships with representative capabilities. Among them, the neighbor context reflects the triple relationship, the neighbor context of an entity is the relationship and tail entity pair in all triples with the entity as the head entity, the neighbor context of the relationship is the head entity and tail entity pair in all triples corresponding to the relationship, and the path context is the entity and relationship on the multi-step path. The edge context of an entity is all the relationships connected with the entity, and the edge context of a relationship is all the entities connected by the relationship. The objective function of each context is the sum

of probability functions of entities or relationships in a given context. Finally, the GAKE model maximizes the weighted sum of the above three kinds of objective functions.

In general, multi-step reasoning based on distributed representation is mainly based on the single-step reasoning based on distributed representation to add multi-step relationship modeling, using supplementary modeling or joint modeling. The method of supplementary modeling is Single-step relationship is the main, multi-step relationship assists learning, used to adjust the empty space

In general, multi-step reasoning based on distributed representation is mainly based on the single-step reasoning based on distributed representation to add multi-step relationship modeling, using supplementary modeling or joint modeling. The method of supplementary modeling is as follows: The single-step relationship is the main, and the multi-step relationship auxiliary learning is used to adjust the position of the vector in the space. The method of co-modeling treats the direct relationship and the indirect relationship equally to obtain a better vector representation, but may introduce cascading errors, that is, the errors caused by the relationship modeling of the intermediate steps on the path will be transmitted Accumulate to the final result. For the common modeling approach, some of the high-quality paths and the corresponding direct relationships actually constitute transitive rules. In this case, multi-step reasoning based on distributed representation can be used to a certain extent It can be seen that while modeling the triples in the knowledge graph, the transitive rules are additionally modeled in the form of vector operations that are convenient for calculation, and the reasoning performance is improved. This requires determining whether the multi-step path and the corresponding direct relationship have a strong correlation. However, PTransE only generally calculates the reliability of multi-step paths in the entire knowledge graph. In fact, a certain path may be an unreliable path for the predicted relationship r_1 , but it is a decisive path for the predicted relationship r_2 . Therefore, considering the reliability of the path and the corresponding direct relationship, more likely and effective transitive rules will be obtained, and the modeling on this basis will further improve the effect. This will also become a small research point.

4.2 Reasoning based on Neural Network

RNN+PRA classifier-b: The fact triples in the knowledge map are not isolated from each other. Many triples have connection relations. The tail entity of one triplet may be the head entity of another. Such two triples can form a five tuple path, and there may be some relationship between the head and tail entities of the five tuples. For example, if there are triples (*a*, father, *b*) and (*B*, father, *c*), you know that there should be a triple (*a*, grandfather, *c*). In order to predict the relationship between the first and last entities of a multi group path, Arvind et al. [29] proposed a multi hop relationship reasoning method, which uses recurrent neural network (RNN) to combine the implied semantics of relationships in paths of any length. In the combination step of each path, the embedding vector of the next hop relation and the vector representing the multi hop path from the beginning to the present entity are combined into an output vector as the input of the next step. After using the multi hop path, RNN outputs a relation vector between the first entity and the last entity of the path, which contains all the information of the relationships in the whole path.

In the combination step of each path, this method uses the embedded vector of the next hop relationship and the vector representing the multi-hop path from the beginning

to the current entity to form an output vector (representing the extended path so far), As input for the next step. After using the multi-hop path, RNN outputs a relationship vector between the first entity and the last entity of the path, which contains the information of all the relationships on the entire path. As shown in Figure 6, after combining all the relationship vectors along the tuple path "Microsoft (IsBasedIn) Seattle (StateLocatedIn) Washington (CountryLocatedIn) USA" in turn, the above method sets the head entity "Microsoft" and the tail entity "USA" Produce a vector very close to the "CountryOfHeadquarters" relationship.

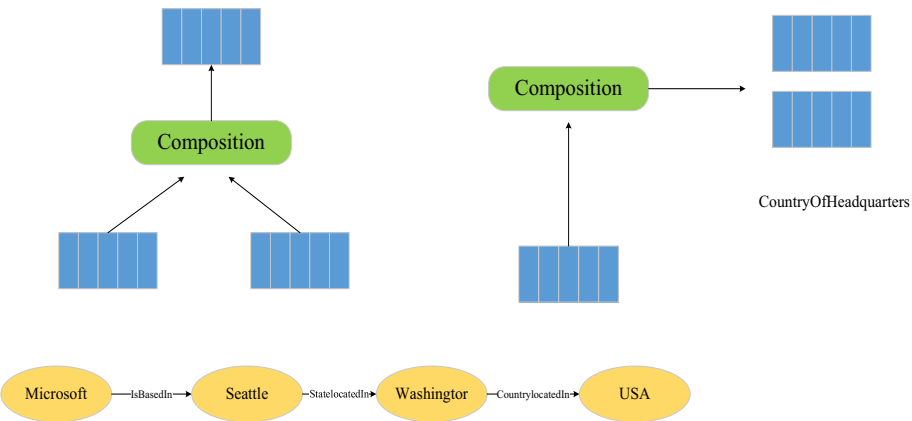


Figure 6 Multiple jump relation inference method

In other words, this method uses all the relationship information in the multi group, combines them in turn and generates the final merging relationship between the head and tail entities. However, considering that a large number of multiple groups in the knowledge map do not necessarily have sequential semantic association, it is difficult to explain the combination reasoning only by using the relationship information on the path of multiple groups, and it is easy to be misled by the semantic differences of different types of relationships on the path in the calculation, resulting in meaningless or unexplained reasoning results.

Path-RNN: In other words, there may be multiple paths between the first and the last entities of a multi-component group formed by multiple triples in the knowledge map. In other words, there may be multiple paths between the first and last entities. The previous multi hop relation reasoning method only uses the single path information of the multivariate group, that is, the probability score is calculated by the combination of the relationship vectors on the path, and other paths are not considered, and the entity on the path is not modeled, but only the "merge" relationship is deduced. In order to improve the above method, Das et al. [30] combined rich symbolic logic reasoning with neural network with strong generalization ability to train a single high-capacity *RNN*. This model alleviates the common problems of Path Ranking Algorithm (*PRA*) that cannot share parameters and a large amount of parameters. It allows the sharing of parameters across multiple relationship types for reasoning. It uses the intermediate paths that exist between entity pairs. Information about entities, and express them as annotated functions to alleviate the issue of entity transparency. Top-k, average and LogSumExp methods are used to add weight to the similarity score of each path. In this

way, the information contained in each path is considered, not just the one with the highest score. However, this method is not suitable for dealing with long text features.

The Path-RNN model is a high-capacity RNN model that allows inference chains across multiple relationship types. It utilizes the information of intermediate entities existing in the path between entity pairs, and alleviates the problem of invisible entities by representing entities as functions of their annotation types. In addition, the author of the article proposes that gathering evidence across multiple paths can improve training speed and accuracy, and shows significant performance improvements through multitasking.

In summary, the multi-step reasoning process based on neural network is a process of directly modeling multi-step path or reasoning. Compared with the single-step reasoning based on neural network, the research work is richer, the interpretability is stronger, and the effect is better. Good. However, the interpretability needs to be further enhanced. Among them, the way of directly modeling the multi-step path, because the multi-step path can be regarded as a relationship or a sequence of relations and entities, it is mainly modeled by RNN. In view of this direction, the research space is relatively small and has related work, and its continued development space is relatively small. The method of directly modeling the reasoning process can simulate the learning and reasoning process of humans, and people have strong learning and reasoning capabilities, so this will be a very popular The direction of research. Moreover, the process of human learning and reasoning is relatively complex, making it a very challenging problem. Based on existing models, further research on how to better model the reasoning process will become a need for future efforts Problems solved.

4.3 Confluent reasoning

In multi-step reasoning, hybrid reasoning is realized by mixing different multi-step methods. Neural network is usually used to mix with other methods because of its strong learning ability and generalization ability. The hybrid reasoning in multi-step reasoning mainly includes path sorting and embedding method, and rule and neural network hybrid reasoning.

RL reinforcement learning method: In order to deal with the problem that it is impossible to find a clear answer in complex query problems; the intelligent algorithm must be able to infer the existing resources and learn to deduce the location of the answer. Specifically, in a large-scale knowledge map, when faced with multi hop reasoning relationship, it is necessary to learn the formula of display reasoning.

Aiming at the above problems, Xiong[31] and others proposed a new controllable multi hop reasoning method, which constructed the path learning process as reinforcement learning. Compared with PRA model, this method uses translation based knowledge-based embedding method to encode RL agent into continuous space, and RL agent conducts reasoning in vector space of knowledge map. The agent extends its path by sampling a relationship, thus taking incremental steps. In order to better guide RL agent learning relationship path, the method also uses strategy gradient training and a new reward function, which jointly encourages accuracy, diversity and efficiency.

The specific task of relational reasoning is to find reliable prediction paths between entity pairs [29]. In this method, the path finding problem is described as a sequential decision problem that can be solved by RL agent. RL system consists of two parts. The

first part is the external environment, which specifies the dynamic interaction between agent and knowledge map. The environment is modeled as a Markov decision process.

The second part of the system is the RL agent, which is represented as the policy network [32], which maps the state vector into the random policy. The parameters of neural network are updated by stochastic gradient descent. Compared with DQN, the RL method based on policy is more suitable for the scenario of knowledge map. One reason is the path finding process of the knowledge map, and the behavior space may be very large because of the complexity of the relationship diagram. This may lead to poor convergence of DQN. In addition, the strategy network can learn the gradient strategy, prevent the agent from falling into some intermediate state, and avoid the problems of value-based methods such as DQN in learning strategy gradient.

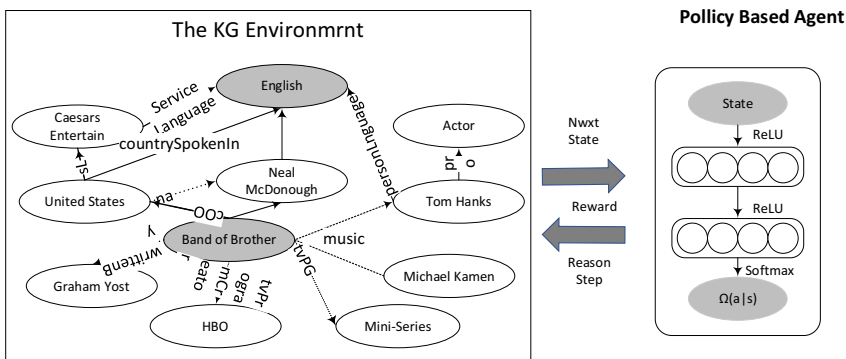


Figure 7 RL system diagram

For the setting of the environment, the number of operations that an agent can perform can be very large, because there are many more wrong sequential decisions than the correct macro volume. To solve the problem of large number of operations, the first reward function is added in RL model.

$$r_{GLOBAL} = \begin{cases} +1, & \text{if the path reaches } e_{target} \\ -1, & \text{otherwise} \end{cases} \quad (19)$$

The purpose of reward function is that when agent R reaches the target after performing a series of behaviors, an offline positive reward + 1 will be given.

In relational reasoning tasks, the short path contains more reliable reasoning evidence than the long path. Short relation chain can also improve the efficiency of reasoning by limiting the length of interaction between RL and environment. Efficient reward is defined as:

$$r_{EFFICIENCY} = \frac{1}{length(p)} \quad (20)$$

The path P is defined as a sequence of relations.

The RL agent is trained to find the path of positive samples for each relationship. These training samples (resources, etargets) have similar state representation in vector space, and RL agents tend to find paths with similar syntax and semantics. These paths usually contain redundant information because some of them may be relevant. In order to encourage agents to find diverse paths, we use the cosine similarity between the current path and the existing path to define a diversity reward function.

$$r_{DIVERSITY} = -\frac{1}{|F|} \sum_{i=1}^{|F|} \cos(p, p_i) \quad (21)$$

Where $p = \sum_{i=1}^n r_i$ is the embedding path $r_1 \rightarrow r_2 \rightarrow \dots \rightarrow r_n$ of the relation chain. Unlike previous random walk based pathfinding models, RL model allows us to control the attributes of the paths we find. In many path based reasoning methods, these effective paths can also be used as a substitute for PRA.

This model uses a reinforcement learning framework to improve the performance of relational reasoning in KGs. Specifically the author trains an RL agent to find a reasoning path in the knowledge base. Unlike previous pathfinding models based on random walking, the RL model allows us to control the properties of the path found. In many path-based reasoning methods, these effective paths can also be used as a substitute for PRA. For the two standard reasoning tasks, the RL path is used as the reasoning formula, which is usually better than other methods.

In future research, the model can introduce adversarial learning to provide the possibility of better rewards with the human-defined reward function used in the model. Instead of designing rewards based on path characteristics, a discriminant model can be trained to give rewards. In addition, in order to solve when KG does not have enough reasoning paths, we can apply the RL framework to joint reasoning based on KG triples and text mentions.

Neural LP: The reasoning of hybrid rule and neural network mainly transforms the rule into vector operation, which is applied to the neural network method with strong learning ability to realize a differentiable model. Yang et al. [32] proposed a fully differentiable system. For the first time, we learned an end-to-end differentiable model Neural LP (Neural logic programming) by combining the parameters and structures of first-order logic rules. In NeuralLP, each entity is associated with a fixed one hot vector, and each relationship is associated with a fixed $\{0,1\}$ operation matrix. The logic rule reasoning is formalized as matrix multiplication. The score function of the entity is weighted and correlated with the confidence degree of the product of the relational operation matrices on all corresponding paths. Neural LP designs a neural controller system with attention mechanism and storage. The learning process combines the differentiable operations used in TensorLog in sequence. The parameters to be learned are rule set and its corresponding confidence degree. Since each confidence level is associated with a specific rule, enumerating rules is a discrete task, and direct learning is difficult to formalize into a differentiable process.

In order to solve this problem, the multiplication and addition operations of the score function are exchanged, that is, add first and then multiply. Firstly, the confidence weighted sum of operation matrices is carried out from the perspective of relationship, and then multiplied. However, the resulting paths are all the same length, related to the number of multiplications. Therefore, the auxiliary storage vector, storage attention vector and operation attention vector are introduced, and the learning is carried out in the form of circulation. Among them, the auxiliary storage vector is initialized to the given entity, followed by the intermediate reasoning results obtained by each step; the storage attention vector stores the weight of each step until the current step; the operation attention vector stores the weight of each TensorLog operation. Finally, the model calculates a weighted average of all storage vectors, and the weight is the storage attention vector. In this way, use attention to select the appropriate rule length. The whole process is implemented by LSTM. In each step of reasoning, the attention mechanism is used to select the subset of TensorLog operation, and then the

content is selected from the storage. The result of operation is the storage vector of the step and added to the storage.

The model treats the KGC task as a sorting problem, and puts the candidate entities on a combined embedding vector representing the known part of the input triples, and arranges the ranking score vector in descending order. In order to improve the prediction performance, the author uses a list The ProjE mutation of the formula optimizes the collective ranking score vector. In the training process, only the direct connection and the length of 1 path are used, which has a relatively simple 2-layer structure, but is better than complex models with richer parameters or feature sets. Compared with other models, the current work of this model does not require any pre-trained embeddings and has much fewer parameters than related models. Finally, the author proves that ProjE performs better than existing methods in fact checking tasks. In the future development, the model can use the embedded projection model proposed in this paper to adapt to more complex neural network models, such as RNN and CNN. But this will inevitably add additional complexity. How to reduce complexity is the focus of future research.

In general, hybrid multi-step reasoning is richer in content than hybrid single-step reasoning. In addition, after recent years of development, distributed reasoning methods have more effective hybrid modes. However, the current hybrid reasoning is still limited to the mixture of the two methods. Among various hybrid methods, the reasoning of hybrid rules and neural networks has a lot of room for development, the high accuracy and interpretability of the rule method and the strong strength of the neural network method Learning and high generalization capabilities enable the combination of the two to obtain a high-accuracy differentiable model, avoiding the computational problems of traditional rule methods, and to a certain extent, increasing the interpretability of neural network methods. In the future, mixed rules Reasoning with neural networks will be worthy of more in-depth research, which can be further studied from the perspective of hybrid modes and the specific manifestations of rules and neural networks.

5 Comparison of experiments and methods

5.1 Data set and evaluation index

In order to compare the quality of the model, this article selects the FB15K-237 dataset and the WN18 dataset. The FB15K-237 dataset is a subset of Freebase and contains 237 relationships and 14K entities. The WN18 dataset contains 18 relationships and 40K species of entities. The results of fact prediction and link prediction are used as evaluation indicators to compare some knowledge reasoning methods. The subtasks of link prediction include entity prediction and relationship prediction, the purpose of which is to predict the missing part of the triple.

Entity forecast: Entity prediction is to predict the missing entities in triples. The specific test methods are as follows:

1) Extract the triad $\langle h, R, t \rangle$ from the test set;

2) The head entity and tail entity in the dataset are replaced respectively, and the triplet $\langle e_n, R, t \rangle$, n is the number of entities in the dataset;

3) The newly replaced triples are scored and sorted from high to low reliability, and the lower the score, the better;

4) Repeat the first three steps until all triples in the test set are tested.

There are two evaluation indexes: Meanrank and evaluation index hits@10. Meanrank is the average rank of all test triples in the test dataset; hits@10 is the probability of the top 10 triples in the test dataset. A good link prediction method should have a lower mean rank and a higher link prediction method hits@10.

In addition, it should be noted that if a triple knowledge map constructed during the test exists, that is, the triple is actually correct, it is reasonable to rank it before the test triples $\langle h, R, t \rangle$. In order to eliminate the influence of this problem, the correct triples existing in training set, verification set and test set are eliminated before ranking each test triplet. It is no doubt that the evaluation result of "filter" is more important than "raw".

Relationship prediction: The method of relation prediction is similar to entity prediction, except that the target of replacement is changed from entity to relation. Due to the small number of relationships in the knowledge map, hits@10, it is difficult to compare the advantages and disadvantages of different methods hits@1 Instead hits@10.

5.2 Comparative analysis of experimental results

When training the model, the learning rate α is set to $\{0.01, 0.1, 1\}$, the spacing l is set to $\{0.25, 0.5, 1\}$, the vector dimension d is set to $\{20, 50, 100\}$, the balance rate between the models is set to η It is $\{0.01, 0.1, 1, 10\}$, and the nearest neighbor structure order n is set to $\{1, 2, 3\}$. After many experiments, the optimal parameter configuration is as follows: On the FB15K data set, $\alpha = 0.01$, $l = 1$, $d = 50$, $\eta = 0.1$, $n = 2$; on the WN18 data set, $\alpha = 0.01$, $l = 2$, $d = 20$, $\eta = 0.1$, $n = 2$. The experimental results are as follows:

Table 1: entity prediction results on FB15k-237

Method	MeanRank		Hits@10(%)	
	Raw	Filter	Raw	Filter
TransE	243	125	34.9	47.1
TransD	194	91	53.4	77.3
TransR	198	77	48.2	68.7
PTransE	200	54	51.8	83.4
ProjE	124	34	54.7	88.4
DKRL	200	113	44.3	57.6

Table 2: entity prediction results on WN18.

Method	MeanRank		Hits@10(%)	
	Raw	Filter	Raw	Filter
TransE	263	251	75.4	89.2
TransD	224	212	79.6	92.2
TransR	238	225	79.8	92.0
PtransE	242	92	50.6	82.2
ProjE	152	56	79.7	92.3
DKRL	212	125	54.3	87.6

From the experimental data in the table, whether it is in the FB15K data set or the WN18 data set, each model has its own outstanding side and certain defects. Among them, the ProjE model performs on both Raw and filter. It's the best. In the Trans series model, the PTransE model performs better, slightly worse on Raw, and best on filter. The reason for this result is that some correct triples interfere during sorting, but in the filter process. It is to deal with this interference.

When there are not enough paths between entities, RL model and PRA model may give bad results. For example, for the FilmWrittenBy relationship, the RL model only finds four unique inference paths, which means that there is not enough reasoning evidence in the knowledge map. Another observation is that RL achieves better performance on Nell datasets. By analyzing the paths found from the map, we find that Nell dataset has more short paths than FB15k-237, and some of them are just synonyms of reasoning relations.

Table 3: Number of reasoning paths used by PRA and RL model

Tasks	#of Reasoning Paths	
	PRA	RL
worksFor	247	25
teamplaySports	113	27
TeamPlaysInLeague	69	21
...		
Average	137.2	20.3

Table 3 shows some comparisons of the number of inference paths. From the data in the table, it can be found that compared with PRA model, RL agents with pre-defined reward functions can select better paths, and filter out similar or unrelated paths, so as to enhance the reasoning strength.

Next, we provide quantitative results supporting our claim that modeling the entities along a KB path can improve reasoning performance. The last section of Table 4 lists the performance gain obtained by injecting information about entities. We achieve the best performance when we represent entities as a function of their annotated types in Freebase (Single-Model + Types) ($p < 0.005$).

Table 4: Model performance comparison

model	Performance (%MAP)
ILP	51.13
PRA	64.43
Path-RNN	68.43
RNN+PRA classifier-b	61.17
RL	65.41
Neural LP	73.28

Table 4 compares the performance of the six model methods. When training all paths, NeuralLP performed significantly ($p < 0.005$) better than other models. The accuracy of NeuralLP model is as high as 73.28%, the accuracy of RL reinforcement learning model is 65.41%, and the accuracy of Path-RNN model is 68.43%.

From the comparative analysis of the above experimental results, it can be found that the mixed model is better than the single model in terms of accuracy and model complexity.

6 Summary

Generally speaking, the single-step reasoning method is based on the fact tuples in the knowledge map, while the multi-step reasoning method adds the multi-step path constraints on the basis of the single-step reasoning modeling method. The expression ability of the multi-step reasoning method is generally stronger than that of the single-step reasoning method, and the inference prediction effect is relatively better. The spatial distribution characteristics of knowledge map are fully considered in the modeling of single-step reasoning method based on distributed representation. The spatial distribution of knowledge map is modeled by fine-grained method, which has stronger expression and reasoning ability. The research on this kind of methods is still relatively small, and it needs to further explore the spatial distribution characteristics of knowledge map, explore more modeling methods, and expand to multi-step reasoning. Among the subclasses of single-step reasoning and multi-step reasoning, neural network-based reasoning and hybrid reasoning are relatively good methods. With the continuous development of neural network, more in-depth research still needs to be carried out. Further enhancing the interpretability of neural network for the task of reasoning is also a major difficulty. Hybrid reasoning attempts to use the advantages of various reasoning methods to obtain better reasoning performance. Generally, the effect of ensemble learning is better than that of single model. However, the current hybrid reasoning is limited to the mixing of the two methods. How to mix multiple complementary methods to further improve the reasoning ability needs further research.

References

- [1] Wang YZ,Jia YT,Liu DW,Jin XL,Cheng XQ.Open Web knowledge aided information search and data mining.Journal of Computer Reseach and Development,2015,52(2):456-474.
- [2] Jin XL,Wah BW,Cheng XQ,Wang YZ.Significance and challenges of big data research.Big Data Research,2015,2(2):59-64.
- [3] Auer S,Bizer C,Kobilarov G,Lehmann J,Cyganiak R,IvesZ,DBpedia:A nucleus for a Web of open data.In: Proc.of the 6th Int'l Semantic Web Conf.Berlin,Heidelberg:Springer-Verlag,2007.722-735.
- [4] Bollacker K,Evans C,Paritosh P,Sturge T,Taylor J.Freebase:A collaboratively created graph database for structuring human knowledge.In:Proc.of the 2008 ACM SIGMOD Int' l Conf.on Management of Data.New York:ACM Press,2008.1247-1250
- [5] Ding Jianhui, Jia Weijia. Overview of Knowledge Graph Completion Algorithms[J]. Information and Communication Technology, 2018 (1): 57-62.
- [6] Xu ZL,Sheng YP,He LR,Wang YF. Review on knowledge graph techniques. Journal of University of Electronic Science and Technology of China, 2016,45(4):589–606.
- [7] Gardner, Matt, and Tom Mitchell. "Efficient and expressive knowledge base completion using subgraph feature extraction." Proceedings of the 2015 Conference on Empirical Methods in Natural Language Processing, 2015.
- [8] Clark,Herbert.Linguistic Processes in Deductive Reasoning.Psychological Review,1969,76(4)387.
- [9] Arthur W Brian.Inductive Reasoning and Bounded Rationality.The American Economic Review,1994,84 (2):406-411.
- [10] van Hoek, Remko, et al. "Abductive reasoning in logistics research." International journal of physical distribution & logistics management (2005).
- [11] Gentner Dedre.Structure-mapping:Atheoretical Framework for Analogy.Cognitive Science,1983,7(2):15 5-170.
- [12] Guan Saiping, Jin Xiaolong, Jia Yantao, et al. Research progress of knowledge reasoning oriented to knowledge graph[J].Journal of Software,2018,29(10):74-102.
- [13] Pearl Judea,Azaria Paz.Graphoids:A Graph-Based Logic for Reasoning about Relevance Relation ECAI, 1985:357-363.

- [14] Rudolf Kadlec,Ondrej Bajgar,Jann Kleindienst Knowledge Base Completion:Baselines Strike Back.AC L2017,69-74.
- [15] Zhang Youmin,Liu Li,Fu Shun,et al.Entity Alignment Across Knowledge Graphs Based on Representative eRelations Selection.ICSAI 2018,2018:1056-1061.
- [16] Tomas Mikolov,Kai Chen,Greg Corrado, and Jeffrey Dean.(2013).
- [17] Bordes A,Usunier N,Garcia-Duran A,Weston J,Yakhnenko O.Translating embeddings for modeling multi-relational data.In:Proc.of the Advances in Neural Information Processing Systems.Red Hook:Curran AssociatesInc.,2013.2787-2795.
- [18] Lin Y,Liu Z,Sun M,Liu Y,Zhu X. Learning entity and relation embeddings for knowledge graph completion. In: Proc. of the 29th AAAI Conf. on Artificial Intelligence. Menlo Park: AAAI, 2015. 2181 – 2187.
- [19] Ji G,He S,Xu L,Liu K,Zhao J.Knowledge graph embedding via dynamic mapping matrix. In: Proc. of the 53rd Annual Meeting of the Association for Computational Linguistics, Vol.1. Stroudsburg: ACL, 2015. 68 7–696.
- [20] Tim Dettmers,Pasquale Minervini,Pontus Stenetorp,et al.Convolutional 2D Knowledge Graph Embeddings.AAAI,2018:1811-1818.
- [21] Socher R,Chen D,Manning CD,Ng A.Reasoning with neural tensor networks for knowledge base completion.In:Proc.of the Advances in Neural Information Processing Systems.Red Hook:CurranAssociatesInc.,2013.926-34.
- [22] Chen Danqi, Socher R, Manning C D, et al.Learning new facts from knowledge bases with neural tensor networks and semantic word vectors[J].Computer Science,2013.11(1):392-399.
- [23] Shi, Baoxu, and Tim Weninger. "ProjE: Embedding projection for knowledge graph completion." Thirty-Fifth AAAI Conference on Artificial Intelligence. 2017.
- [24] Han X,Le S.Context-Sensitive inference rule discovery:A graph-based method.In:Proc.of the 26th Int'l Conf.on Computational Linguistics.Stroudsburg:ACL,2016.2902-2911.
- [25] Wang Q,Wang B,Guo L.Knowledge base completion using embeddings and rules.In:Proc.of the 24th Int'l Joint Conf.on Artificial Intelligence.San Francisco:Morgan Kaufmann Publishers,2015.1859-1866.
- [26] Xie R,Liu Z,Jia J,Luan H,Sun M.Representation learning of knowledge graphs with entity descriptions.In:Proc.of the 30th AAAI Conf.on Artificial Intelligence.Menlo Park:AAAI,2016.2659-2665.
- [27] Lin Y,Liu Z,Luan H,Sun M,Rao S,Liu S. Modeling relation paths for representation learning of knowledge bases. arXiv Preprint arXiv: 150600379, 2015
- [28] Feng J,Huang M,Yang Y,Zhu X.GAKE:Graph aware knowledge embedding.In:Proc.of the 26th Int'l Conf.on Computational Linguistics.Stroudsburg:ACL,2016.641-651.
- [29] Neelakantan A,Roth B,Mccallum A.Compositional vector space models for knowledge base completion [J].Computer Science,2015:1-16.
- [30] Das R,Neelakantan A,Belanger D,McCallum A. Chains of reasoning over entities, relations, and text using recurrent neural networks. arXiv Preprint arXiv: 160701426, 2016.
- [31] Xiong W,Hoang T,Wang W Y,et al.DeepPath:A Reinforcement Learning Method for Knowledge Graph Reasoning[C].empirical methods in natural language processing,2017:564-573.
- [32] Yang F,Yang Z,Cohen WW.Differentiable learning of logical rules for knowledge base reasoning.arXiv Preprint arXiv:170208367,2017.

Recommendation Based on Java Code Analysis and Search

Shanqing FU^a, Bing LI^a, Yi CAI^a, Zhuang LIU^b, Junxia GUO^{a,1}

^a*College of Information Science and Technology, Beijing University of Chemical Technology, Beijing 100029, China*

^b*China Beijing Environment Sanitation Engineering Group Co, Beijing 100101, China*

Abstract. How to improve the efficiency and quality of software development is an ongoing concern in the field of software engineering. As a useful auxiliary function, code recommendation is embedded in almost all integrated development environments. There has been increasing interest and research in the area of code recommendation in recent years due to its convenience for project development. Existing research has made a lot of contributions to this field, but there are still many issues that need further study. One of the key points is the low success rate of recommendation. Focusing on this problem, this paper proposes a method to recommend Java source code after parsing massive amounts of source code information. We propose a new source code analysis algorithm for the scraped source code data. A source file is parsed into classes, methods, and attributes as recommendation objects. At the same time, the annotation information is bound to the annotated objects. Finally, the parsed information is indexed at the project, class, and method levels for code recommendations in a hierarchical recommendation manner. A code recommendation system is implemented by combining this with full-text retrieval technology for class library, class, and method level recommendation. The experimental results show that the method proposed in this paper has better performance in recommendation accuracy than existing code recommendation engines.

Keywords. code search, code analysis, static code recommendation

1. Introduction

The Integrated Development Environment (IDE) is an essential tool for programmers, especially when developers are starting to work with a new code base. The main existing main IDEs provide practical code recommendations or completion of auxiliary functions. In actual project development, the code recommendation function provides recommendations such as methods, attributes and parameter lists, which can shorten development time and improve development efficiency. Moreover, research shows that code recommendation is favored by Java developers [1].

¹ Corresponding Author: Junxia GUO, Beijing University of Chemical Technology, Beijing 100029, China. E-mail: gjxia@mail.buct.edu.cn

The work described in this paper is supported by the National Natural Science Foundation of China under Grant No.61702029, No.61872026 and No.61672085

In the 1970s and 1980s, the style of software development was still to write most of the code by oneself. Today, with the rapid development of the Internet, this situation has been greatly changed [2]. Much research has shown that software and code reuse improves software development efficiency [3]. The lack of experience of software developers, or skilled developers, hoping to find the existing software or code to help them save development time means that, a lot of time is spent searching the Internet. Therefore, how to lessen the amount of search to meet their code requirements deserves further study.

Many code search engines (e.g., Krugle [4]) have large common codebases, where programmers can obtain relevant code through searching. However, these engines only provide keyword search functions. Typically, keyword matching does not mean that there are any similarities in software functionality. Lv [5] established an index domain of method entities by extracting code text, descriptive names, API calls, and other features, but this method ignores the correlation between code-related feature information outside the method and method entities, such as comments and class names. HILL [6] considered a variety of code characteristics of the program; however they didn't distinguish between classes and methods in the program comments. Therefore, to consider more code-related information and to make class and method distinctions, this paper considers code recommendation from a new perspective by, selecting projects, classes, and methods as recommended objects, and proposes a new program analysis method and index structure. For different recommended objects (projects, classes, methods), the code characteristics we considered are different, and we establish different indexes according to the parsed relevant information. Also, the annotation information is bound to its object for improving the accuracy of code recommendation.

2. Related Work

2.1. Program Analysis

For the recommendation of Java static language, the recommended class, method and other information are included in the Java source file. This is not structured data, so code analysis should be completed first. Most of the existing code recommendation methods are based on program static analysis [7]. For example, Grechanik [8] analyzed API calls and their description information in the program, and recommended them to programmers by searching for keywords matching the API information. Li et al. [9] used a program static analysis tool to process the source code. This identifies method calls and the variable define use and other dependencies, confirm the annotation passing path, and extracts the text from the annotation before method definitions. These methods provide a large number of references and have their own characteristics and advantages. However, they are not perfect. The problem is that the amount of feature information extracted by the above methods is insufficient, and the correlation between the recommended object and the feature information under a variety of feature information is not considered.

2.2. Code Recommendation Based on Search

The goal of recommendation system is to recommend information or products that users are interested in according to their information needs and interests. At present,

such systems have been widely used in various fields [10][11][12]. Most search-based code recommendation systems are based on information retrieval technology, which can quickly retrieve large-scale codebases. In the field of code search, the engines are mainly based on keywords [13], input and output [14], and interface [15]. Wu et al. [16] found that the methods retrieved by programmers cannot directly meet their needs, and the changes made by programmers to the methods also reflect their needs. Therefore, starting from the possible intention of programmers to alter methods after retrieval, the aim is to predict this possibility, and use it for query expansion, so as to improve the accuracy of recommendation. LV [5] extracted features through a parsing program, established an index field of method entities, and constructed a Boolean logic query expression through query statements and the related API to help improve the accuracy of code search.

3. Code Parsing and Index Creation

This section introduces the processing of massive amounts of source code and the Java code recommendation model. The framework is shown in Figure 1, which mainly includes data crawling, code parsing, and hierarchical recommendation. First, we construct the codebase which contains a lot of source code. This paper constructs a crawler system to provide source code data for the whole recommendation process. Second, we parse the crawled source code and convert it into class, method, attribute, and other recommended objects; then we segment its words and establish a hierarchical index. When a user enters a query statement, the recommendation system will carry out full-text retrieval according to the keywords and filter conditions in the query statement and score the relevance of the retrieval results. Finally, the system recommends the corresponding project name, class, or method that can realize the relevant functions to the user.

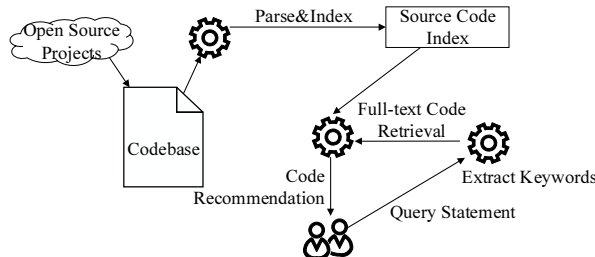


Figure 1. The framework of our code recommendation model

3.1. Code Analysis

Each structure of a Java program has its own rules. For example, a ".java" file can contain the following structures: a package declaration, multiple import declarations, multiple multiline/single-line comments inserted anywhere, multiple annotations using enum types, interfaces, classes, annotations, the definition of multiple enums, annotation structure, etc. Each structure in a Java program has its own characteristics which are different to others, and its own syntax rules. All structures form code blocks independently and do not interfere with other structures.

Based on the above ideas, aiming at the characteristics of Java source code, Algorithm 1 is proposed to analyze the various structures in Java source files mentioned above. Before parsing the code, it is necessary to make clear the information contained in various structures and the criteria for judging each structure. Taking the class structure as an example, each class structure of a Java file can contain information such as static/non-static member variables, method definitions, general comments, Javadoc annotations, usage of annotations, internal classes, interfaces, annotation definitions, enum type definitions, static/non-static code blocks, etc. The criterion for judging the current code as a class is that when a '{' is first detected, the character before it contains the 'class' keyword which is not part of another string.

Based on a clear understanding of the information and criteria that each structure of the Java code file contains, the Java source file is traversed. When a character or string that can indicate a structure (such as enum, class, method, etc.) is identified, it is processed recursively in the processing function of the structure and the information contained in the structure is obtained. When the structure is resolved, the processing continues by tracing back to the structure that recursively calls the method. This is repeated until all the structures of the entire file are parsed. With this algorithm, Java code files can be fully parsed into structured data. Based on this data, full-text retrieval indexes are constructed and data support is provided for implementing hierarchical recommendations.

Algorithm 1 Java program parsing algorithm

Input: Java program file

Output: The feature information of the program

```

1: packInfo=getPackage(JavaFile)
2: impoInfo=getImport(JavaFile)
3: P←JavaFile.readlines()
4: while P != null do
5:   If type(P) == enum then
6:     enumMembers=enumProcessor(P)
7:   else if type(P) == interface then
8:     interMembers=interProcessor(P)
9:   else if type(P) == class then
10:    classMembers=classProcessor(P)
11:   else if type(P) == method then
12:    methodMembers=methodProcessor(P)
13:   else if type(P) == annotation then
14:    annotMembers=annotationProcessor(P)
15:   end if
16:   P=P.next()
17: end while
18: return(packInfo,impoInfo,enumMembers,iterMembers,classMembers,annotMerbers)
```

The annotation information of the program is very important for code search. When the algorithm recurses downward, it can transfer the annotation information that has been resolved by the parent structure of the current structure, and attach the recently generated annotation information (not attached to other structures) to the structure.

3.2. Index Creation

After parsing the source code, the extracted information becomes a new kind of representation of the code. Due to the different information of projects, classes and methods, in order to achieve hierarchical recommendation, the extracted information is divided into project domains, class domains, and method domains, and we establish the index respectively.

Elasticsearch [17], as a commonly used full-text retrieval tool, and is an open-source real-time search and distribution engine based on Lucene [18]. Based on Elasticsearch, we establish different indexes for different recommended objects (project, classes, methods).

Table 1. The keywords contained in classname and description fields

Class number	Field	Keywords
1	Classname	Set
	Description	collection,contains, duplicate,elements
2	ClassName	List
	Description	Ordered,Collection

Table 2. The classes corresponding to keywords

Field	Keywords	Class number
Classname	Set	1
	List	2
	Collection	1,2
	Contains	1
Description	Duplicate	1
	Elements	1
	Ordered	2

In the Java language, all methods belong to a specific class in the program. For each method there is the corresponding method-name, class, annotation, method body, and other information. In this paper, each project, class, and method are regarded as recommendation objects, denoted as documents (the objects stored in the indexes in the Lucene framework). Each document will be divided into multiple fields according to different code characteristics. Similarly, for projects and classes, different index fields are constructed. We list the index fields of method level, class level and item level respectively at <https://github.com/fushanqing/CodeTip/tree/master/Index>.

When users search through query statements, our recommendation system gets a series of keywords token. An inverted index is used to find the project, class, or method containing it through keywords. We create an inverted index for each field. As shown in Table 1 and Table 2, the relationship between the classname field and the description field in the two classes is simply represented.

4. Experimentation and Analysis

To evaluate the effectiveness of the proposed method, a complete code recommendation system is designed. The code for our system is released at <https://github.com/fushanqing/CodeTip>. The recommendation system uses Elastic Search (ES) as a tool for full-text retrieval. ES provides search services for other services in the form of RESTful APIs. Other services can store documents in ES and send the DSL statements to query matching documents.

4.1. Experimental Settings

This paper chooses the Ali Maven Mirror Warehouse [19] source code dataset as the data source with a total size of 1Gb. In the Maven project, users can uniquely identify a

project for a Maven mirror warehouse by groupId, artifactId, and version. Considering that there are a large number of related methods and research in the field of code recommendation, this experimentation uses 32 query statements, which is listed at <https://github.com/fushanqing/CodeTip/tree/master/Query>, based on previous studies [20][21].

In order to provide a better evaluation of this work, two research questions are raised.

Question 1: What is the accuracy of our method?

To answer this question, 32 queries are used in the experimentation, in which the first 15 query statements are the same with as Krugle [4] searches for comparison.

Question 2: What is the recommendation performance of our method in graded recommendation?

To answer this question, the experiment analyze the query-related recommendations at the higher-ranked project, class, and method levels to determine the accuracy of recommendations at these levels.

4.2. Measurement and Evaluation

In the information retrieval system, there are a series of indicators that can be used to evaluate the questions raised in the previous section comprehensively and accurately. The common indicators are: precision of the first N results (Precision@N), mean reorder reciprocal(MRR), precision-recall, mean average precision (MAP), etc.

We analyzed these evaluation indicators and considered that the objective of this study is to achieve high precision code recommendation, so Precision@N and MRR are selected as the evaluation indicators here.

4.3. Experimental Results

In order to reduce the impact of human subjective judgment on the experimental results, we use the comprehensive judgment of two programmers for the evaluation of the recommended results. Only when both programmers think that the recommended results are related to the query will the recommendations be recorded as correct.

In order to answer Question 1, the first 15 query statements are tested against Krugle to compare the correlation of the recommended method code. As can be seen from Table 3, in the experimental comparison of the first 15 query statements, our method results in an overall improvement over Krugle in sorting the related results, which indicates that our method has a higher recommendation precision. Among the query statements used for the experimentation, some are highly relevant to the recommended results, such as ‘how to split a string into words’, but there are still individual query statements that are not recommended as well, such as ‘how to Deserialize an XML document’. The reason for this is that there is no code base associated with the query statement in the code depository.

A summary of 32 selected query statements is shown in Table 4. It can be seen that each index value decreases with the increase of search sentences, but the above two experimental results show that this method is effective in improving the search accuracy. The experimental results for each query statement are shown at http://github.com/fushanqing/CodeTip/tRee/master/experiment_Results.

Table 3. The comparison of experimental results

Indicators	Our method	Krugle	Improvement
Precision@1	73.3%	70%	3.3%
Precision@5	57.3%	29.4%	27.9%
MRR	81.3%	60%	21.3%

In order to answer Question 2, the experimentation also uses all the query statements to compare the recommendation at project and class level with the recommendation directly. The experimenter can choose a specific project (or class) to judge the correlation between the method code recommended in the project(or class) and the query statement. The experimental results are shown in Table 5.

Table 4. Experimental results for all query statements

Indicators	Our method
Precision@1	68.8%
Precision@5	55%
MRR	77.7%

Table 5. Experimental results at different levels

Indicators	Project	Class	Method
Precision@1	53.3%	60%	73.3%
Precision@5	34.7%	42.7%	57.3%

As can be seen in Table 5, our method can recommend code related to query statements at the project and class levels. The recommended accuracy for a specific class is higher than that for a specific project, and the two levels of recommendation have slightly less precision than that of direct method level recommendation. The above results show that the code recommendations methods at the project, class, and method levels in this paper are valid.

5. Conclusion

In order to address the problem of low accuracy in the current code recommendation field, this paper proposed a Java code recommendation method based on full-text retrieval. After obtaining the Java source code information through the Java source code parsing algorithm designed in this paper, we established a hierarchical index for this information, and recommend projects, classes, and methods to users according to query statements. The experimental results show that our method improves the accuracy of the recommendation results.

References

- [1] Murphy GC, Kersten M, Findlater L. How Are Java Software Developers Using the Eclipse IDE?. IEEE Software. 2006, 23(4):76-83.
- [2] Grechanik M, Fu C, Xie Q, McMillan C, Poshyvanyk D, Cumby C. A search engine for finding highly relevant applications. In: 2010 ACM/IEEE 32nd International Conference on Software Engineering, Cape Town; 2010, p. 475-484 .
- [3] Andrew JK, Brad AM, Michael JC, Htet HA. An Exploratory Study of How Developers Seek, Relate, and Collect Relevant Information during Software Maintenance Tasks. IEEE Trans. Softw. Eng, 2006, 32(12):971–987.
- [4] Krugler K, Krugle Code Search Architecture. In: Sim S.E., Gallardo-Valencia R.E. (eds) Finding Source Code on the Web for Remix and Reuse. Springer; 2013, p. 103-120.
- [5] Fei L, Hongyu Z, Jian-guang L, Shaowei W, Dongmei Z, Jianjun Z. CodeHow: effective code search based on API understanding and extended boolean model. In: Proceedings of the 30th IEEE/ACM International Conference on Automated Software Engineering (ASE '15). IEEE Press, 2015, p. 260–270.

- [6] Emily H, Lori P, Vijay-Shanker K. Improving source code search with natural language phrasal representations of method signatures. In: Proceedings of the 2011 26th IEEE/ACM International Conference on Automated Software Engineering (ASE'11). IEEE Computer Society, USA; 2011, p. 524–527.
- [7] Kirkov R, Agre G. Source code analysis-an overview. Bulgarian Acad Sci. 2010, 10: 60-77.
- [8] Grechanik M, Fu C, Xie Q, McMillan C, Poshyvanyk D, Cumby C. A search engine for finding highly relevant applications. In: ACM/IEEE 32nd International Conference on Software Engineering, Cape Town, 2010, p. 475-484.
- [9] Li B, Li F, Huang X, He X, Xu L. Transferring Java Comments Based on Program Static Analysis. 2019,638-643.
- [10] H. Li, Y. Liu, N. Mamoulis and D. S. Rosenblum. Translation-Based Sequential Recommendation for Complex Users on Sparse Data. In: IEEE Transactions on Knowledge and Data Engineering, 2020, vol. 32, no. 8, pp. 1639-1651.
- [11] X. Chen, X. Liu, Z. Huang and H. Sun, RegionKNN: A Scalable Hybrid Collaborative Filtering Algorithm for Personalized Web Service Recommendation. In: 2010 IEEE International Conference on Web Services, Miami, FL, 2010, pp. 9-16.
- [12] Wanigasekara N , Liang Y , Goh S T , et al. Learning Multi-Objective Rewards and User Utility Function in Contextual Bandits for Personalized Ranking. In: Twenty-Eighth International Joint Conference on Artificial Intelligence IJCAI-19. 2019.
- [13] Fafalios P, Tzitzikas Y. Post-analysis of keyword-based search results using entity mining, linked data, and link analysis at query time. In: IEEE International Conference on Semantic Computing, Newport Beach, CA; 2014, p. 36-43.
- [14] Stolee KT, Elbaum S, Dobos D. Solving the Search for Source Code. Acm Transactions on Software Engineering & Methodology. 2014, 23(3):1-45.
- [15] Mukund R, Yi W, Youssef H. SWIM: synthesizing what i mean: code search and idiomatic snippet synthesis. In Proceedings of the 38th International Conference on Software Engineering (ICSE '16). Association for Computing Machinery, New York, NY, USA;2016, p. 357–367.
- [16] Wu H, Yang Y. Code search based on alteration intent. IEEE Access. 2019, 7: 56796-56802.
- [17] <https://www.elastich.co/cn/>
- [18] Gospodnetic O, Hatcher E, Cutting D. Lucene in action. Manning, 2005.
- [19] <https://maven.aliyun.com/mvn/view>
- [20] Lemos O A L , Paula A C D , Sajnani H , et al. Can the use of types and query expansion help improve large-scale code search? In: IEEE 15th International Working Conference on Source Code Analysis and Manipulation (SCAM), Bremen; 2015, p. 41-50.
- [21] Sushil KB, Joel Ossher, and Cristina V. Lopes. Leveraging usage similarity for effective retrieval of examples in code repositories. In Proceedings of the eighteenth ACM SIGSOFT international symposium on Foundations of software engineering (FSE '10). Association for Computing Machinery, New York, NY, USA; 2010. 157–166.

Research Progress and Advantage Analysis of Big Data Application in Chinese Academic Journals

Qin WU^{a,b,1} and Hui WU^c

^a*Editorial Department of Journal, Shandong Jianzhu University, Jinan, China*

^b*School of Art, Shandong Jianzhu University, Jinan, China*

^c*Longquan Primary School in Tai'an high-tech Industrial Development Zone,
Tai'an, China*

Abstract. The mining and application of big data in academic journals can accelerate the construction of data journals, enhance journal's influence, and promote the sharing and dissemination of scientific data in academic journals worldwide. This paper uses bibliometric method to retrieve published articles with the theme of big data and journal in CNKI database, analyzes the academic achievements of the development of academic journals with the application of big data in the recent five years using quantitative visualization analysis, expounds the research progress of academic journals in big data field, and discusses the advantages of big data application in periodical industry. The results show that: study on the application of big data in academic journals are gradually deepening and scientific, and the relevant research still needs more financial fund from the state and social units, big data has prominent advantages such as accuracy, scientificity and value maximization in the workflows of academic journals. The mining and application of massive data is very important for promoting the development of high-quality academic journals and optimizing the supply-demand relationship of knowledge services of academic journals.

Keywords. big data, academic journals, bibliometric method, advantages analysis

1. Introduction

Big data is not simply a huge amount of data, but a data collection that greatly exceeds the capabilities of traditional database software tools. It has four characteristics: massive data scale, fast data flow, diverse data types and low value density [1]. The feature of big data lies in the distributed data mining, analysis and processing of massive data, so that people can make more scientific and well founded decisions. As another disruptive technological revolution after cloud computing and internet of things, big data has been widespread used in various research fields of natural science and social science, providing a new research paradigm and quantitative method for various disciplines [2]. The effective application of big data will be the core of the common

¹Qin Wu, Editorial Department of Journal/School of Art, Shandong Jianzhu University, Jinan 250101 China; E-mail:1063983400@qq.com

competition of all industries. The mining and application of massive data is entering and deeply affecting every industry, organization and unit.

Academic journals are the windows to reflect the level of scientific and technical innovation of a country, and the sci-tech carrier to spread new discoveries and new knowledge [3]. In the process of knowledge dissemination and service, it is necessary for academic journals to make full use of big data to mine its potential value [4]. As an organic part of the national independent innovation system, academic journals are closely related to scientific research and play an important role in sci-tech support. Big data is both a challenge and an opportunity for the development of Chinese academic journals [5]. However, at present, the general progress of the research on the relationship between the development of academic journals and big data is not clear, resulting in a lack of profound grasp of the application and necessity of big data in journal industry, under the background of the fast development of big data, academic journals, such as some university journals and local trade sci-tech journals, are also faced with the problems of limited data resources, lower accuracy of information, and lower value of data reuse. Therefore, the establishment of organic integration and effective collaboration between academic journals and big data technology is a problem in need of immediate solutions in the information dissemination of academic journals in big data era.

This paper uses bibliometric method to retrieve published articles with the theme of big data and journal in China national knowledge infrastructure (CNKI) database, analyzes the retrieved documents through quantitative visualization analysis, so as to understand the research situation of big data application in Chinese academic journals, illustrates the application advantages of big data in academic journals. It is helpful to promote the efficient application of big data and the technology, optimize the allocation of academic journal resources, improve the accuracy, scientificity and value-added of journal publishing process, and enhance the frontier and creativity of knowledge and information dissemination of Chinese academic journals. This study may have theoretical guidance and reference significance for the related School of Art as well as primary school education.

2. Research progress of big data and the development of academic journals

2.1. Data sources

All data in this paper are from CNKI database.

2.2. Research methods

Log in to CNKI database and use advanced search functions to retrieve published articles with the theme of big data and journal. The time of publication is limited to January 1, 2015 to December 31, 2019. The retrieval time in this study is July 30, 2020. The retrieved literature is preliminarily screened, and some non-paper literature is removed, and the effective literature related to the subject is retained and analyzed visually; the retrieved data is imported into Excel to be analyzed.

3. Results and analysis

3.1. Numbers of published articles

A total of 189 relevant literatures were retrieved in CNKI database from 2015 to 2019. 186 effective literatures related to the theme were retained after removing some non-paper literatures. The numbers of published articles from 2015-2019 is shown in Figure 1. As can be seen from Figure 1, published articles about journal big data in recent five years showed a trend of first increasing and then decreasing. The year with the most published articles is 2016, with 53 articles, which is probably related to the high popularity of big data research and the rapid increase of attention in the periodical industry. From the data of the past three years from 2017 to 2019, the numbers of published articles shows a small decline, which may be due to the more rational and in-depth research on big data in periodical industry, which leads to the reduction of literature output. It is believed that with the in-depth study of big data research in various industries, the promotion and application of big data will lead to a new round of research boom in the quality improvement, communication mode, digital upgrading and personalized service of academic journals.

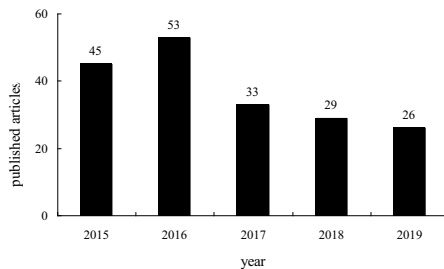


Figure 1.The numbers of published articles with the theme of big data and journal from 2015 to 2019

In 2020, The higher frequency of keyword co-occur network of articles on big data research is data technology and artificial intelligence in academic journals, which indicates that big data research has penetrated into all work links of academic journals [6-7], and has played a great role in promoting their brand building [8].

3.2. Resource type distribution

The academic literatures retrieved in this study are mainly periodical articles, accounting for 88.2%, then of academic articles in newspapers, accounting for 4.8%. The distribution of other resource types is shown in Figure 2. As can be seen from Figure 2, articles about journal big data research published in periodicals are the main resource type, indicating that the journal industry is closely related to big data research. Among the periodicals articles cited more frequently, Xia dengwu reconstructed the effective way of data cognition and value reconstruction of academic journals from the perspective of data [9], Wu Meiyings research show that big data research in academic

journals has changed from exploring the causal relationship between the data to revealing its correlation [10].

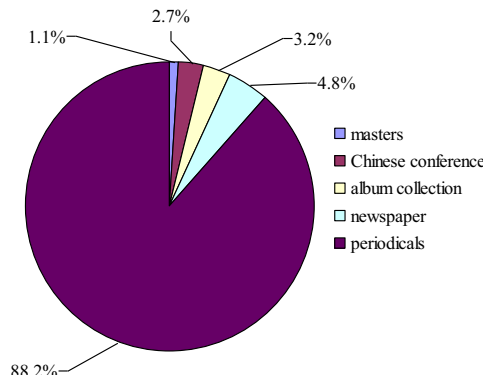


Figure 2. Distribution of resource types of published articles

3.3 Fund distribution

In fund distribution, published articles about journal big data research received less funding; only 3.8% of them were funded by the National Social Science Foundation, followed by educational research projects, accounting for 3.3%. Other fund distribution is shown in Figure 3. It shows that more financial fund from the state and relevant departments is needed to support the research of journal big data.

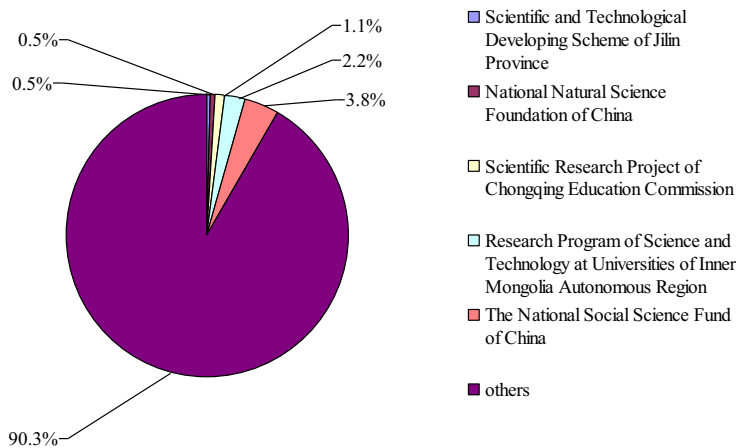


Figure 3. Fund distribution of published articles

4. Advantage analysis of big data application in academic journals

With the coming big data era, the living environment of academic journals has undergone essential changes. Although the printed journals have certain vitality based on their authority, reliability and reality accumulated over the years, but in the era of big data, compared with the characteristics of printed academic journals, data journals have unprecedented huge advantages. These advantages are mostly reflected in the following aspects.

Accuracy. In big data era, knowledge and information are in a state of data. From the macroscopic view, by collecting and statistical analysis the academic data, academic journals can fully utilize the information provided by big data, grasp the academic development direction and scientific hot spot to enhance their influence [11]; from the micro view, using big data analysis to predict the audience group, academic journals can understand the personalized needs of authors and readers, and realize the intelligent matching between the knowledge service of academic journals and the personalized needs of the audience [12]. With the support of big data analysis, academic journals can timely obtain information feedback from users, accurately evaluate the dissemination effect of academic information, guide the direction of journal content integration, and realize the accurate positioning of academic guidance and knowledge service.

Scientificity. This advantage is mainly reflected in the evaluation function and mechanism of academic journals. At present, most comprehensive academic journals adopt the qualitative evaluation method of peer review, but this evaluation method is subjective. Big data analysis and application can provide an objective quantitative standard for this qualitative evaluation. On the basis of peer review, the influence and innovation of journals are quantified, and the combination of qualitative evaluation and quantitative evaluation ensures the evaluation index and evaluation method of academic journals more scientific [13-14].

Value maximization. In big data era, journal industry and data technology are deeply integrated. Through the cooperation with network database, academic journals deeply mine the knowledge information and academic resources using the big data analysis ability of open data platform, and excavate valuable data for future trends and predictive pattern analysis of academic journals [15]. Through big data analysis, the value of information resources of academic journal can be deeply excavated to produce more derivatives, and to maximize the value of knowledge services of academic journals.

5. Conclusion and discussion

This paper uses bibliometric method to retrieve published articles with the theme of big data and journal in CNKI database, and analyzes the retrieved literature through quantitative visualization analysis. The results show that the researches on the development of academic journals and the application of big data are more in-depth and scientific, but such researches lack the support of scientific research funds from the state and social units, which is consistent with that of Guo Yi's result [16]. In the future, the funding for big data research in academic journals should be increased. Big data has outstanding advantages in the accuracy, scientificity and value maximization of academic journals.

The data age creates more opportunities and challenges for periodical industry. Relying on big data and intelligent terminal technology platform, academic journals always adhere to high-quality content construction, enhance the core competitiveness, and strengthen the authority, reliability and credibility of journal content in big data era. The mining and application of massive data is of great significance in accelerating the prosperity of high-quality academic journals and optimizing the supply-demand relationship of knowledge services of academic journals, so as to better serve the progress of national science and economic.

Acknowledgement

This work was funded by Social Science Innovation and Development Research Project of Shandong Province (No.2019SSD014)

References

- [1] Chen ZQ .The necessity of journals using big data. Journalism Tide. 2020 Jan; 1:62-64.
- [2] Wu HJ, Sun HF, Sun T, Tian C. Frontier evolution of international BigData in knowledge cluster perspective. Information Science. 2019 May; 37(5):173-177.
- [3] Yan XM .The path to improve the communication power of sci-tech journals in the era of big data. China Publishing Journal. 2019 Jun; 12:64-65.
- [4] Huang F. Research on operation practice of WeChat public account and big data of university science and technology journal. Communication and Copyright. 2019 Oct; 8:103-107.
- [5] Guan LL, Ma HQ, Wang CL. Practice and thoughts on establishing international data journals: A case study of Big Earth Data. Chinese Journal of Scientific and Technical Periodicals. 2020 Jan; 31(1):56-62.
- [6] Tan XJ. Application of big data and artificial intelligence in editing of comprehensive academic journals. Public Communication of Science and Technology. 2020 Mar; 3:11-13.
- [7] Jiang XD, Tu P, Yin LX. Topic selection planning of scientific journals from the perspective of data mining and intelligent screening. Publishing Journal. 2020 Jan; 28(1):36-41.
- [8] Yang YJ. The role of big data technology in promoting the brand building of academic journals. Media Forum. 2020 Jul; 3(17):85-86.
- [9] Xia DW. Content optimization and value reconstruction of academic journals in the data era. Chinese Journal of Scientific and Technical Periodicals. 2016 Mar; 27(3):264-268.
- [10] Wu MY. Academic journal editors' quality reconstruction and capacity improvement in the era of big data. Publishing Journal. 2017 Jan; 25(1):47-51.
- [11] Zhou J. Thought and practice on optimizing publishing process of scientific journals by big data. Chinese Journal of Scientific and Technical Periodicals. 2018 Feb; 29(2):144-147.
- [12] Zhou X, Qin Q. Knowledge management innovation and international influence promotion of academic journals under the background of big data. View on Publishing. 2018 Apr; 5:12-15.
- [13] Zhao Y, Kong Q. Statistics and analysis of evaluation indexes of Chinese science and technology periodicals in the big data era. Journal of Qingdao University(Engineering & Technology Edition). 2019 Nov; 34(4):98-102.
- [14] Jiao B. Comprehensive academic journals under the background of big data. Chinese Social Sciences today. 2016-07-12. http://www.cssn.cn/zx/201607/t20160712_3117419.shtml
- [15] Wu H, Chen XF, Wang F, Huang JX. Study on global OA journal publishing monitoring method. Journal of Modern Information. 2019 Feb; 39(2):145-151.
- [16] Guo Y, Chi L, He XG. Overview of big data and the development of Chinese sci-tech journal. Development and Orientation of Sci-tech Periodicals. 2018 Jul; 11:45-50.

The Mechanism Analysis of the Accelerator for Support Vector Regression Based on Data Partition

Yunsheng SONG^{a,1}, Fangyi LI^a, Jianyu LIU^a and Juao ZHANG^a

^aSchool of Information Science and Engineering, Shandong Agricultural University,
Tai'an, 271018, Shandong, China

Abstract. Support vector regression is an important algorithm in machine learning, and it is widely used in real life for its good performance, such as house price forecast, disease prediction, weather forecast, and so on. However, it cannot efficiently process large-scale data, because it has a high time complexity in the training process. Data partition as an important solution to solve the large-scale learning problem mainly focuses on the classification task, it trains the classifiers over the divided subsets produced by data partition and obtain the final classifier by combining those classifiers. Meanwhile, the most existing method rarely study the influence of data partition on the regressor performance, so that it is difficult to keep its generation ability. To solve this problem, we obtain the estimation of the difference in objective function before and after the data partition. Mini-Batch K-Means clustering is adopted to largely reduce this difference, and an improved algorithm is proposed. This proposed algorithm includes training stage and prediction stage. In training stag, it uses Mini-Batch K-Means clustering to divide the input space into some disjoint sub-regions of equal sample size, then it trains the regressor on each divided sub-region using support vector regression algorithm. In the prediction stage, the regressor merely offers the predicted label for the unlabeled instances that are in the same sub-region. Experiment results on real datasets illustrate that the proposed algorithm obtains the similar generation ability as the original algorithm, but it has less execution time than other acceleration algorithms.

Keywords. Machine learning, Large-scale data, Data partition, Support vector regression, Generation ability

1. Introduction

As the volume of data becomes increasingly large, it takes a revolutionary change for training support vector regression (SVR) model for its time complexity and space complexity. Lots of improved algorithms are proposed to accelerate the training process and minimize losses on the generalization performance. The proposed algorithms are classified into reduction algorithms and decomposition algorithms [1]. The main style of reduction algorithms is that the training samples nearby the hyperplane have a large con-

¹Corresponding Author: Yunsheng Song, Shandong Agricultural University, Tai'an, Shandong, China; E-mail: sys_sd@126.com

tribution to SVR model than others [2–6]. In this way, these proposed algorithms seeks the critical samples to form a new subset instead of the training set, where the size of the selected subset tends to be smaller than the original training set. Therefore, the regressor trained over the selected subset has a high training efficiency. In fact, the reduction algorithms want to find the support vectors to keep the prediction performance. However, the support vectors are determined by the regressor, and it is difficult to obtain before training the model. Meanwhile, the reduction algorithms usually requires to read the entire training data several times, so that they needs lots of time to get the final result [7–10]. Decomposition algorithms train the SVR model with all the training instances rather than some of them. The existing decomposition algorithms focus on how to obtain the approximate performance as the original SVR using optimization strategy, while they still deal with all the data once or more [11–13]. Therefore, these algorithms could not handle the big data well.

2. Related Concept

Let $T = \{(x_1, y_1), (x_2, y_2), \dots, (x_N, y_N)\}$ mark the training set, where each instance x_i is expressed with m attributes, $y_i \in R$ is its output, and N is the number of labeled instances. The main task in training a SVR model over T is to solve the following quadratic optimization problem:

$$\min_{\theta, \rho \in R^N} \psi(\theta, \rho) \text{ s.t. } 0 \leq \theta, \rho \leq C, e^T(\theta - \rho) = 0 \quad (1)$$

where the objective function $\psi(\theta, \rho) = \{\frac{1}{2}(\theta - \rho)^T \mathbb{K}(\theta - \rho) + \varepsilon e^T(\theta + \rho) - Y^T(\theta - \rho)\}$, $\theta = (\theta_1, \theta_2, \dots, \theta_N)^T \in R^N$ and $\rho = (\rho_1, \rho_2, \dots, \rho_N)^T \in R^N$ are the vectors of dual variables; \mathbb{K} is an $N \times N$ matrix with $\mathbb{K}_{ij} = K(x_i, x_j)$, and $K(x_i, x_j)$ is the kernel function; C is the balancing parameter between loss and regularization in the SVR primal problem; e_N is the vector of all ones, and ε is the relaxation factor; $Y = (y_1, y_2, \dots, y_N)$ is the output vector of the training set. Let $\theta^* = (\theta_1^*, \theta_2^*, \dots, \theta_N^*)$ and $\rho^* = (\rho_1^*, \rho_2^*, \dots, \rho_N^*)$ denote the optimal solution of the problem (1), the predicted value for a test data x can be computed by the decision function $g(x) = \sum_{i=1}^N (\theta_i^* - \rho_i^*) K(x, x_i) + b$, where the bias term $b = 0$, because any improvement in test accuracy is not observed by it in this paper.

The main idea behind accelerating the process of training SVR based on data partition is to divide the training set into smaller disjoint subsets, and then each model can be trained independently and efficiently over each subset. Suppose the training dataset T can be decomposed into n sets $T_l (l = 1, 2, \dots, n)$, $\bigcup_{l=1}^n T_l = T$ and $T_l \cap T_k = \emptyset$, where n is prefixed by the user. Then each subproblem over each divided subset T_l is that

$$\min_{\theta_{(l)}, \rho_{(l)}} \psi_l(\theta_{(l)}, \rho_{(l)}) \text{ s.t. } 0 \leq \theta_{(l)}, \rho_{(l)} \leq C, e_{(l)}^T(\theta_{(l)} - \rho_{(l)}) = 0 \quad (2)$$

where $\psi_l(\theta_{(l)}, \rho_{(l)}) = \{\frac{1}{2}(\theta_{(l)} - \rho_{(l)})^T \mathbb{K}_{l \times l} (\theta_{(l)} - \rho_{(l)}) + \varepsilon e^T (\theta_{(l)} + \rho_{(l)}) - Y_{(l)}^T (\theta_{(l)} - \rho_{(l)})\}$, $\theta_{(l)}, \rho_{(l)}$ denote the subvector $\{\theta_i | (x_i, y_i) \in T_l\}$ and the subvector $\{\rho_i | (x_i, y_i) \in T_l\}$ respectively, $\mathbb{K}_{l \times l}$ is the submatrix of \mathbb{K} with row and column indexes T_l , and $Y_{(l)}$ is the output vector of the instances over the subset T_l , $0 \leq \theta_{(l)}, \rho_{(l)} \leq C, e^T (\theta_{(l)} - \rho_{(l)}) = 0$. In this way, the optimal problem (1) is approximately divided into n subproblems. Then the optimal solutions of all the subproblems are combined to initialize a coordinate descent solver for the original problem. Let $\hat{\theta}_{(l)}, \hat{\rho}_{(l)}$ are the optimal solution of the subproblem $\min_{\theta_{(l)}, \rho_{(l)} \in R^N} f_l(\theta_{(l)}, \rho_{(l)})$. Then we could concatenate all the subproblem solutions to form an approximate solution $\hat{\theta}$ and $\hat{\rho}$ for the whole problem, where $\hat{\theta} = [\hat{\theta}_{(1)}, \hat{\theta}_{(2)}, \hat{\theta}_{(3)}, \dots, \hat{\theta}_{(n)}]$ and $\hat{\rho} = [\hat{\rho}_{(1)}, \hat{\rho}_{(2)}, \hat{\rho}_{(3)}, \dots, \hat{\rho}_{(n)}]$.

3. MK-SVR algorithm

In this section, we discuss the relationship between the raw problem (1) and the divided subproblems (2). A kernel function $\hat{K}(x_i, x_j) = I_{t(x_i), v(x_j)} K(x_i, x_j)$ is defined, $\hat{K}(x_i, x_j) = I_{t(x_i), v(x_j)} K(x_i, x_j)$, where $t(x_i)$ is the divided subset that the instance x_i belongs to; $I_{t(x_i), t(x_j)} = 1$ iff $t(x_i) = t(x_j)$, otherwise $I_{t(x_i), v(x_j)} = 0$.

Lemma 1. *The vector pair $[\hat{\theta}, \hat{\rho}]$ could be the solution of the optimization problem (1) with kernel function $K(\cdot, \cdot)$ replaced by $\hat{K}(\cdot, \cdot)$, where the objective function of this optimization problem is $\hat{\psi}(\theta, \rho) = \{\frac{1}{2}(\theta - \rho)^T \hat{\mathbb{K}}(\theta - \rho) + \varepsilon e^T (\theta + \rho) - Y^T (\theta - \rho)\}$, $\hat{\mathbb{K}}$ is a $n \times n$ kernel matrix with each element $\hat{\mathbb{K}}_{ij} = \hat{K}(x_i, x_j)$.*

Proof. According to its definition of $\hat{K}(\cdot, \cdot)$, $\hat{K}(x_i, x_j) = 0$ if $t(x_i) \neq t(x_j)$, and $\hat{K}(x_i, x_j) = K(x_i, x_j)$ if $t(x_i) = t(x_j)$. Then the function $\hat{f}(\theta, \rho)$ can be decomposed into the sum of several functions.

$$\begin{aligned} \hat{\psi}(\theta, \rho) &= \frac{1}{2}(\theta - \rho)^T \hat{\mathbb{K}}(\theta - \rho) + \varepsilon e^T (\theta + \rho) - Y^T (\theta - \rho) \\ &= \frac{1}{2} \sum_{t(x_i)=t(x_j)} (\theta_i - \rho_i) \hat{K}(x_i, x_j) (\theta_j - \rho_j) + \frac{1}{2} \sum_{t(x_i) \neq t(x_j)} (\theta_i - \rho_i) \hat{K}(x_i, x_j) (\theta_j - \rho_j) \\ &\quad + \sum_{i=1}^N \{\varepsilon(\theta_i + \rho_i) - y_i(\theta_i - \rho_i)\} \\ &= \frac{1}{2} \sum_{t(x_i)=t(x_j)} (\theta_i - \rho_i) \hat{K}(x_i, x_j) (\theta_j - \rho_j) + \sum_{i=1}^N \{\varepsilon(\theta_i + \rho_i) - y_i(\theta_i - \rho_i)\} \\ &= \sum_{l=1}^n \left\{ \frac{1}{2}(\theta_{(l)} - \rho_{(l)})^T \mathbb{K}_{l \times l} (\theta_{(l)} - \rho_{(l)}) + \varepsilon e^T (\theta_{(l)} + \rho_{(l)}) - Y_{(l)}^T (\theta_{(l)} - \rho_{(l)}) \right\} \\ &= \sum_{l=1}^n \hat{f}_l(\theta_{(l)}, \rho_{(l)}). \end{aligned} \tag{3}$$

From Eq. (3), the problem $\min_{\theta, \rho \in R^N} \hat{f}(\theta, \rho)$ is divided into n subproblems (2) and these subproblems are independent. As the subvector pair $[\hat{\theta}_{(l)}, \hat{\rho}_{(l)}]$ could be the solution of the optimal subproblem ($l = 1, 2, \dots, n$), the vector pair $[\hat{\theta}, \hat{\rho}]$ must be the solution of the original problem $\min_{\theta, \rho} \hat{f}(\theta, \rho)$. Furthermore, $e^T (\hat{\theta} - \hat{\rho}) = \sum_{l=1}^n e_{(l)}^T (\hat{\theta}_{(l)} - \hat{\rho}_{(l)}) = 0$,

each element h of the vector $\widehat{\theta}_{(l)}$ satisfies the condition $0 \leq h \leq C$, and each element of the vector $\widehat{\rho}_{(l)}$ also satisfies this condition. Therefore, the vector pair $[\widehat{\theta}, \widehat{\rho}]$ satisfies the restrictions of the problem (1). \square

From the **Lemma 1**, we can find that the accelerating SVR algorithm using the divide-and-conquer strategy is equivalent to solve the problem $\min_{\theta, \rho \in R^N} \widehat{f}(\theta, \rho)$. Now we discuss the difference between $f(\widehat{\theta}, \widehat{\rho})$ and $f(\theta^*, \rho^*)$, so as to study the effect of data partition to the generation ability of this algorithm.

Theorem 1.

$$0 \leq \psi(\widehat{\theta}, \widehat{\rho}) - \psi(\theta^*, \rho^*) \leq (1/2)C^2D(v)$$

$$\text{where } D(\tau) = \sum_{i,j:\tau(x_i) \neq \tau(x_j)} |K(x_i, x_j)|.$$

Proof. Based on the mathematical notation, we can get

$$\begin{aligned} \widehat{\psi}(\theta^*, \rho^*) &= \frac{1}{2}(\theta^* - \rho^*)^T \widehat{\mathbb{K}}(\theta^* - \rho^*) + \varepsilon e^T(\theta^* + \rho^*) - Y^T(\theta^* - \rho^*) \\ &= \frac{1}{2} \sum_{i,j:\tau(x_i) = \tau(x_j)} (\alpha_i^* - \beta_i^*) K(x_i, x_j) (\alpha_j^* - \beta_j^*) + \varepsilon e^T(\alpha^* + \beta^*) - Y^T(\alpha^* - \beta^*) \\ &= \psi(\alpha^*, \beta^*) - \frac{1}{2} \sum_{i,j:\tau(x_i) \neq \tau(x_j)} (\alpha_i^* - \beta_i^*) K(x_i, x_j) (\alpha_j^* - \beta_j^*) \end{aligned} \quad (4)$$

$$\widehat{\psi}(\widehat{\theta}, \widehat{\rho}) = \psi(\widehat{\theta}, \widehat{\rho}) - \frac{1}{2} \sum_{i,j:\tau(x_i) \neq \tau(x_j)} (\widehat{\theta}_i - \widehat{\rho}_i) K(x_i, x_j) (\widehat{\theta}_j - \widehat{\rho}_j) \quad (5)$$

Furthermore, $\widehat{\psi}(\widehat{\theta}, \widehat{\rho}) \leq \widehat{\psi}(\theta^*, \rho^*)$, because the vector pair $[\widehat{\theta}, \widehat{\rho}]$ is the optimal solution of the problem (2). Combining with Eqs.(4) and (5), and $0 \leq \theta_i^*, \rho_i^*, \widehat{\theta}_i, \widehat{\rho}_i \leq C$ for all i , then

$$\begin{aligned} \psi(\widehat{\theta}, \widehat{\rho}) &= \widehat{\psi}(\widehat{\theta}, \widehat{\rho}) + \frac{1}{2} \sum_{i,j:\tau(x_i) \neq \tau(x_j)} (\widehat{\theta}_i - \widehat{\rho}_i) K(x_i, x_j) (\widehat{\theta}_j - \widehat{\rho}_j) \\ &\leq \widehat{\psi}(\theta^*, \rho^*) + \frac{1}{2} \sum_{i,j:\tau(x_i) \neq \tau(x_j)} (\widehat{\theta}_i - \widehat{\rho}_i) K(x_i, x_j) (\widehat{\theta}_j - \widehat{\rho}_j) \\ &= \psi(\theta^*, \rho^*) + \frac{1}{2} \sum_{i,j:\tau(x_i) \neq \tau(x_j)} [(\widehat{\theta}_i - \widehat{\rho}_i) - (\theta_i^* - \rho_i^*)] K(x_i, x_j) [(\widehat{\theta}_j - \widehat{\rho}_j) - (\theta_j^* - \rho_j^*)] \\ &\leq \psi(\theta^*, \rho^*) + \frac{1}{2} C^2 D(\tau) \end{aligned} \quad (6)$$

\square

In order to minimize the difference between $\psi(\widehat{\theta}, \widehat{\rho})$ and $\psi(\theta^*, \rho^*)$, we need a data partition algorithm with small $D(v)$. This kernel function is one kind of similarity measure according to its definition. When the kernel function is the radical basis function, the value of $K(x_i, x_j)$ is proportional to the Euclidean distance of the instances x_i and x_j . In this way, $D(\tau) = \sum_{i,j:\tau(x_i) \neq \tau(x_j)} K(x_i, x_j)$, and it is the sum of the similarity between

instances in different divided subsets. Min-Batch K-Means clustering algorithm that is one is one kind of improved algorithm can obtain small $D(v)$ using Euclidean distance. It produces the subset subsets of approximately equal size for large-scale data, because it inherits the uniformity effect of K-Means clustering algorithm.

As the dataset T can be decomposed into n disjoint divided sets $T_i (\bigcup_{l=1}^n T_l = T, T_i \cap T_j = \emptyset)$ using Min-Batch K-Means clustering algorithm, and the input space χ is also divided into n disjoint region χ_l , where $l = 1, 2, \dots, n$. The SVR regressor $\hat{g}_l(x)$ trained over the divided subset T_l only uses the information of the divided region χ_l , so it could effectively predict the instances within the the divided region χ_l rather than the instances not in other regions. In this way, the final regressor $\hat{g}(x)$ is that

$$\hat{g}(x) = \sum_{i=1}^l I_{x,\chi_l} \hat{g}_l(x) \quad (7)$$

where $I_{x,\chi_l} = 1$ if and only if $x \in \chi_l$ and $I_{x,\chi_l} = 0$ otherwise, and the region which the instance x belongs to can be computed by finding the nearest cluster center. Therefore, the predicting process firstly searches the nearest cluster which the given unlabeled instance x_0 belongs to, and uses the regressor obtained by data within that cluster to compute its predicted value.

3.1. Time complexion analysis

The time complexion is very important for the algorithms for large-scale data. The proposed algorithm includes the data partition and training the regressors on the divided subsets. The first process has a time complexion of $O(N)$, and the time complexion of the second process is $O(s^3)$, where n and s are the training instances number and the size of the maximum divided subsets. Then the time complexion of our proposed algorithm is $O(N + s^3)$. So the size of divided subsets is inversely proportional to the time complexion. On the other hand, the difference $D(\tau)$ could be small as the large size of divided subsets, the proposed algorithm with the largely divided subsets has a better generation ability than one with the small divided subsets.

4. Experiment

4.1. Data Information and Related Setup

Nine representative real datasets are chosen for their characteristic from the LIBSVM datasets [14] and UCI datasets [15]. The information of the selected datasets is shown in Table 1, where the size of each dataset is larger than 10000.

Table 1 Information of nine datasets

Datasets	Size	Features
ailerons	13750	40
cada	20640	8
california	20640	8
house	22784	16
mv	40768	10
pole	14998	26
Aggregates	200000	4
sgemm	241600	10
YearMSD	515345	90

Two typical algorithms for accelerating SVR algorithm are chosen in this paper: LIBSVM and SVR based on random data partition (RP-SVR). Mean square error (MSE), coefficient of determination (R^2), and execution time (ET) in seconds are chosen for evaluating their performance, and the first two indicators evaluate the prediction ability [16]. All the measurement results is computed using 10-fold cross-validation method, and $n = N^{0.3}$ [17].

4.2. Prediction Ability

Table 2 shows the prediction ability evaluated by MSE and R^2 of three algorithms.

Table 2 Prediction performance on nine datasets

Datasets	MK-SVR		RP-SVR		LIBSVM	
	MSE	R^2	MSE	R^2	MSE	R^2
ailerons	0.735	0.003	0.685	0.004	0.821	0.002
cadata	0.664	0.02	0.609	0.023	0.663	0.02
california	0.367	8.81E+09	-0.066	1.48E+10	-0.064	1.48E+10
house	0.07	2.83E+09	-0.105	3.36E+09	-0.105	3.36E+09
mv	0.977	2.362	0.774	23.417	0.989	1.112
pole	0.415	1.05E+03	-0.478	2.66E+03	-0.343	2.41E+03
Aggregates	0.767	1.68E+04	0.437	40514.548	0.778	1.60E+04
sgemm	0.182	1.10E+05	0.022	1.31E+05	0.364	8.55E+04
YearMSD	0.214	114.417	0.1826	105.56	0.22	117.625
Mean	0.488	1.29E+09	0.229	2.02E+09	0.369	2.02E+09
Median	0.415	1.05E+03	0.1826	2.66E+03	0.364	2.41E+03

On the whole, the average values of MSE for three algorithms are 1.29E+09, 2.02E+09 and 2.02E+09, as well as the medians of MSE are 1.05E+03, 2.66E+03 and 2.41E+03 from **Table 2**. So it indicts that the MK-SVR algorithm obtains a similar prediction accuracy as LIBSVM algorithm, but better than the RP-SVR algorithm. This significant result is shown on datasets california, house and pole. For another prediction performance measurement R^2 , the average values of R^2 for three algorithms are 0.488, 0.229, 0.369, as well as the medians of R^2 are 0.415, 0.183, and 0.364. In conclusion, MK-SVR algorithm has a better prediction performance than the RP-SVR algorithm, similar to LIBSVM algorithm.

4.3. The execution time

Table 3 lists the execution time (in seconds) of these three algorithms. *ET* of MK-SVR is much smaller than that of the other two algorithms on most of the datasets .

Table 3 *ET* of three algorithms on nine datasets

Dataset	MK-SVR	RP-SVR	LIBSVM
ailerons	0.086	0.123	0.416
cadata	0.39	0.563	4.827
california	0.888	1.306	13.232
house	1.446	2.149	20
mv	1.495	4.852	40.556
pole	1.053	1.663	38.122
Aggregates	30.869	84.437	2365.737
sgemm	57.184	146.269	4396.376
YearMSD	138.547	156.325	48714.719
Mean	231.958	397.687	55594.167
Median	1.446	2.149	38.122

The average values of *ET* for three algorithms are 231.958, 397.687 and 55594.167, as well as the medians of *ET* are 1.446, 2.149, 38.122. Then MK-SVR has less training time both than RP-SVR algorithm and LIBSVM algorithm. Meanwhile, the training time of MK-SVR algorithm is also less than other algorithms on each dataset from **Table 3**. Compared with other algorithms, MK-SVR algorithm is very efficient in processing large-scale data. The reason for this issue is that they have different training process and data partition strategy.

5. Conclusion

This paper analyzes the influence of data partition on the performance of SVR model, and finds that Mini-Batch K-Means clustering could largely reduce this effect. Therefore, we have given an improved SVR algorithm using the Mini-Batch K-Means clustering. In the training process, the input space spanned by the training instances is divided into several disjoint regions, and each SVR model is trained using the instances within each divided region independently. In the prediction process, the SVR model over the divided region gives the predicted outputs of the unlabeled instances within that region. Analysis and experiment results show that our algorithm can obtain a good performance as the original SVR algorithm, but better than another representative algorithm. In the future, we will consider how to adaptively determinate the number of divided subsets for different datasets.

Acknowledgements

This work is supported by the Major Scientific and Technological Innovation Project of Shandong Province (No.2019JZZY01071).

References

- [1] Song Y, Liang J, Wang F. An accelerator for support vector machines based on the local geometrical information and data partition. International Journal of Machine Learning and Cybernetics. 2018;10(9):2389-2400.
- [2] Cachin C. Pedagogical pattern selection strategies. Neural Networks. 1994;7(1):175-181.
- [3] Foody G. The significance of border training patterns in classification by a feedforward neural network using back propagation learning. International Journal of Remote Sensing. 1999;20(18):3549-3562.
- [4] Zhang, C., Li, D. and Liang, J., 2020. Multi-granularity three-way decisions with adjustable hesitant fuzzy linguistic multigranulation decision-theoretic rough sets over two universes. Information Sciences, 507, pp.665-683.
- [5] Adnan, R., Liang, Z., Heddam, S., Zounemat-Kermani, M., Kisi, O. and Li, B., 2020. Least square support vector machine and multivariate adaptive regression splines for streamflow prediction in mountainous basin using hydro-meteorological data as inputs. Journal of Hydrology, 586, p.124371.
- [6] Yang, L. and Dong, H., 2019. Robust support vector machine with generalized quantile loss for classification and regression. Applied Soft Computing, 81, p.105483.
- [7] Han X, Clemmensen L. On Weighted Support Vector Regression. Quality and Reliability Engineering International. 2014;30(6):891-903.
- [8] Guo G, Zhang J. Reducing examples to accelerate support vector regression. Pattern Recognition Letters. 2007;28(16):2173-2183.
- [9] Pan X, Yang Z, Xu Y, Wang L. Safe screening rules for accelerating twin support vector machine classification. IEEE Transactions on Neural Networks and Learning Systems. 2018; 29(5):1876-1887.
- [10] Pan X, Pang X, Wang H, Xu Y. A safe screening based framework for support vector regression. Neurocomputing, 2018; 287:163-172.
- [11] Ho C, Lin C. Large-scale linear support vector regression. Journal of Machine Learning Research. 2012; 13(1): 3323-3348.
- [12] JimenezAlex S, Aviles A, Galn L, Flores A, Matovelle C, Vintimilla, C. Support vector regression to downscaling climate big data: an application for precipitation and temperature future projection assessment. In: Conference on Information Technologies and Communication of Ecuador. 2019 Nov 27-29 ; Cuenca, Ecuador: Springer Press, c2019. p. 182-193.
- [13] Wang K, Pei H, Ding X, Zhong P. Robust Proximal Support Vector Regression Based on Maximum Correntropy Criterion. Scientific Programming. 2019;2019:1-11.
- [14] Chang CC, Lin CJ. Libsvm: a library for support vector machines. ACM Transactions on Intelligent Systems and Technology. 2011; 2(3):27-66.
- [15] UCI Machine Learning Repository [Internet]. Archive.ics.uci.edu. 2020 [cited 13 August 2020]. Available from: <http://archive.ics.uci.edu/ml/index.php>
- [16] Han J, Kamber M, Pei J. Data mining. Burlington: Elsevier Science; 2012.
- [17] Kleiner A, Talwalkar A, Sarkar P, Jordan MI. A scalable bootstrap for massive data. Journal of the Royal Statistical Society: Series B (Statistical Methodology). 2014; 76(4):795-816

Focused Crawler Strategy Based on Improved Energy Landscape Paving Algorithm

Jingfa Liu^{a,b}, Wei Zhang^{a,b¹}, Zhihe Yang^{a,b}, Ziang Liu^c

^a *Guangzhou Key Laboratory of Multilingual Intelligent Processing, Guangdong University of Foreign Studies, Guangzhou 510006, China*

^b *School of Information Science and Technology, Guangdong University of Foreign Studies, Guangzhou 510006, China*

^c *Faculty of Science, University of Alberta, Edmonton T6G2H6, Canada*

Abstract. The traditional crawlers have difficulty in implementing semantic analysis. Therefore, the focused crawler technologies with topic preference characteristics have received many attentions in the recent years. To increase the precision of focused crawlers and prevent “topic drifting”, this paper adopts the comprehensive relevancy evaluation (CRE) of hyperlinks based on the combination of web content and link structure. In addition, the improved version of the energy landscape paving (ELP) algorithm that is a class of metropolis-sampling-based global optimization method is proposed to avoid the focused crawler falling into local optima. By incorporating the CRE strategy into the improved ELP, a novel focused crawler strategy denoted by IEELP is proposed. The experimental results on rainstorm disasters domain show that the precision of the proposed focused crawler is obviously promoted compared to other focused crawlers in literature, illustrating the ability of the IEELP to retrieve topic-related web pages.

Keywords. focused crawler, energy landscape paving, rainstorm disasters, link evaluation

1. Introduction

Due to the huge data resources, the Internet has become an important channel for obtaining specific domain knowledge. At present, the scale of web pages on the Internet is massive and growing, while the content of web pages is highly dynamic and complex. Web pages related to specific domain knowledge are very sparse and have the characteristics of big data. Traditional search engines (such as Google, Baidu) and web crawlers (such as Scrapy, Pyspider) face very challenges in accuracy rate of information retrieval. Unlike these methods, focused crawlers filter web pages based on the topic-relevant values of web pages on the Internet. For specific search topic of users, the results returned by focused crawlers are more streamlined and more accurate. Therefore, the development of the focused crawler has become an inevitable

¹ Corresponding Author, Wei Zhang, Guangdong University of Foreign Studies, Guangzhou 510006, China; E-mail: westrive@qq.com.

trend and attracted attentions of an increasing number of scholars.

Generally, focused crawlers are different in topic-relevancy calculation and search strategies. Among the existing crawlers, topic-relevancy calculation methods are mainly divided into link-based evaluation methods and content-based evaluation methods. The link-based evaluation methods focus on the authority of the structure itself. This type of methods ignores the relevancy between the web pages content and the topic, which is likely to lead to “topic drifting” [1] and obtain massive web pages of irrelevant topics by the crawlers, such as the hyperlink-induced topic search (HITS) algorithm [2] and the PageRank[3]. On the other hand, the evaluation methods based on web content analysis evaluate links by calculating and analyzing the relevancy of the web content, the anchor text, the anchor text context, such as the shark-search algorithm [4], probability model based on Bayes algorithm [5] and topic-focused crawlers based on semantic similarity [6]. In searching strategies, the breadth first search (BFS)[7] and the optimal priority search (OPS)[8] are employed mostly. This sort of methods has better performance for crawling a small number of web pages and searching near the relevant ones. However, it ignores some structural features existing between pages themselves, and the design of crawler system in this way will lead to a lack of loyalty mostly. BFS is an omission-free search algorithm, which is widely used in traditional web crawlers. Nevertheless, when used in the focused crawler, the accuracy is not high. With the increase of crawling web pages, a large number of irrelevant web pages will be downloaded, which increase the waste of system resources. For example, the design of the MySQL-based news search engine in [9]. OPS gives priority to visit web pages with high-valued links and extend the best web pages according to a certain priority strategy. Obviously, OPS is a sort of greedy algorithm and is prone to fall into local optima. In order to improve global optimization ability of focused crawlers, in recent years some researchers introduce some global optimization algorithms into the focused crawler, such as genetic algorithm [10], ant colony algorithm [11]. Regrettably, due to the incomplete application of some operation operators (such as crossover and mutation) in this type of methods, they only repeat the selection operation and do not generate new links, so the effects are often not good enough.

The rest of this article is organized as follows. The second section gives the comprehensive topic-relevancy evaluation of the unvisited hyperlinks based on the combination of web page content and link structure. The third section proposes a focused crawler strategy based on the improved energy landscape paving algorithm. The proposed crawler allows sub-optimal hyperlinks to be visited so as to discover web pages with greater potential value and to improve the global search performance of the crawler. The fourth section conducted a controlled experiment, and the fifth section summarizes the work of this article.

2. Comprehensive Topic-Relevancy Calculation

Based on the semantic similarity analysis, the calculation of the topic relevancy of the web page text and the anchor text are first described. Then, the comprehensive topic-relevancy evaluation of the unvisited hyperlink is given to direct the search of the focused crawler.

2.1. Topic-Relevancy Calculation of Web Pages

This paper takes "rainstorm disaster" as the topic and describes it in the form of a topic word set. According to the experience of experts in this field, we set the topic-relevant term set as $TK=\{\text{rainstorm, disaster, rainfall, weather, meteorology}\}$ in experiments, and assign corresponding semantic weight $W_{TK}(0.8, 0.5, 0.3, 0.1, 0.1)$ to this group of topic words. Most of the web pages on the Internet are represented in a form of HTML files. Different topic words extracted from different labels have different influences on the topic-relevancy of the whole web page. According to an analysis of label structures in large amounts of web page texts, this paper divides the main labels into five groups, as shown in Table 1, and assigns different weights ($w_1, w_2, \dots, w_5=(2, 1.5, 1.2, 1.0, 0.2)$) to different labels, respectively.

After segmenting the web page and counting the term frequency (TF) of each topic word, we map a web page text into a feature vector $\{tf_i, tf_2, \dots, tf_n\}$, where tf_i denotes the TF of the i -th topic word in the web page, and n is the number of topic words. Considering that the topic words occurring in different positions within the web page text hold different weights, the feature vector of a web text can be expressed as a TF vector $D_{TF}=\{(tf_{i1}, \dots, tf_{ij}, \dots, tf_{in}), \dots, (tf_{i1}, \dots, tf_{ij}, \dots, tf_{in}), \dots, (tf_{j1}, \dots, tf_{jj}, \dots, tf_{jn})\}$. Here $J=5$ represents the group number into which labels are divided, and tf_{ij} represents the term frequency of the j -th topic word in the i -th group of the labels within the web page. To calculate the weight w_{dk_i} of the i -th topic word in the web page feature set $DK=\{dk_1, dk_2, \dots, dk_n\}$, this paper uses the improved TF-IDF model [12]:

$$w_{dk_i} = \sum_{j=1}^J \left(\frac{tf_{i,j}}{\max(tf_{i,j})} \times w_j \right) \quad (1)$$

Here $\max(tf_{i,j})$ represents the maximum TF of the i -th topic word occurring at all positions within the web page text; w_j represents the weight of the j -th web page label. This paper uses the vector space model (VSM) [13] to calculate the topic relevancy of the web page text:

$$R(P) = \frac{W_{TK} \times W_{DK}}{\|W_{TK}\| \times \|W_{DK}\|} \quad (2)$$

Here $R(P)$ represents the topic relevancy of the web page P ; W_{TK} represents the semantic weight vector of topic words; W_{DK} represents the feature weight vector of the web page text. $0 < R(P) < 1$ and the topic relevancy is higher if $R(P)$ is closer to 1.

Table 1. Division of labels and their weights

Groups	Labels	Meanings	Weights(wj)
Group1	<title>, <keyword>, <h1>	title, keyword, first-level headline	2
Group2	<h2>, <h3>	second-level headline, third-level headline	1.5
Group3	<h4>, <h5>, 	fourth-level headline, fifth-level headline, Bold text	1.2
Group4	<p>, <td>, 	body information	1.0
Group5	Other labels	non-body information	0.2

2.2. Comprehensive Relevancy Calculation of Links

By filtering out links with low relevancy, the crawler is enabled to select high-quality web pages. The three indicators to measure the relevancy of links are the topic relevancy of the anchor text, the topic relevancy of the web page where the link is located, and PageRank value of the page to which the link points.

Hyperlinks enable interconnection between the web pages. The anchor text information of the hyperlink is often one of the important basis for people to judge whether the web pages will be visited. The short anchor text information is like the title of an article, which often points directly to the topic. The topic relevancy of the anchor text is therefore an important basis to identify whether the link is relevant to the topic in the design of focused crawler system. An anchor text is short in most cases, so this paper adopts an improved Term Frequency \times Inverse Document Frequency algorithm to calculate the feature weight of the anchor text AR_i :

$$w_{AR_i} = \frac{f_i}{\sum_{j=1}^n f_j} \times \log_a \left(\frac{N}{N_i} + 0.01 \right) \quad (3)$$

Here f_i represents the term frequency of the i -the topic word in the anchor text; N represents the total number of the crawled web pages; N_i represents the number of the crawled web pages containing the i -th topic word and $a > 1$. After calculating the feature weight vector $W_{AR} = \{ w_{AR_1}, \dots, w_{AR_i}, \dots, w_{AR_n} \}$ of the anchor text, we calculate the cosine of the weight vector W_{TK} of topic words and the feature weight vector W_{AR} to obtain the topic relevancy $R(AR_i)$ of the anchor text AR_i of hyperlink $link_i$ by equation (2).

PageRank (PR) value is generally used to evaluate the importance of a web pages, and web pages with high PageRank value are often more reliable. The core idea of PageRank algorithm is to determine the importance of links through cross-reference relations among pages. The PR value of a web page generally depends on the number of its in-links and their average PageRank value. Although it reflects the reliability of a web page, it cannot tell whether the link is relevant to the topic, so the crawler may visit some pages with high PR value but low topic relevancy. Different from traditional PageRank algorithm, this paper gives an improved calculation method of PR value by integrating the topic relevancy of the in-link anchor text into the calculating process of PageRank algorithm. Suppose that P_{next} is the web page pointed to by the hyperlink $link_i$. The PR value of P_{next} is computed by equation (4).

$$PR(P_{next}) = (1 - d) + d \times \sum_{i=1}^U \left[\frac{PR(P_i)}{S(P_i)} \times (1 + \lambda \times R(AR_i)) \right] \quad (4)$$

Here d represents the damping coefficient, and λ is the adjustment factor to adjust the influence of anchor text's topic relevancy on PR of the web page P_i . U is the total number of all in-links of P_{next} in the crawled web pages. $PR(P_i)$ is the PR value of the i -th in-link web page of the web page P_{next} . $S(P_i)$ denotes the total number of out-links of the web page P_i . $R(AR_i)$ represents the topic relevancy of the anchor text AR_i of the i -th in-link of P_{next} .

According to the above analysis, a comprehensive relevancy evaluation function of unvisited hyperlink $link_i$ is given as follows:

$$E(link_i) = \alpha \times R(AR_i) + \beta \times R(P_i) + \chi \times PR(P_{next}) \quad (5)$$

Here α , β , and χ represent weight factors. Considering the fact that an anchor text can characterize the target contents from links well, this paper sets α to 0.7, β to 0.2 and χ to 0.1. $R(AR_i)$ denotes the topic relevancy of the anchor text AR_i of the hyperlink $link_i$. $R(P_i)$ denotes the topic relevancy of the web page where the hyperlink $link_i$ is located. $PR(P_{next})$ denotes the PageRank value of the web page pointed to by the hyperlink $link_i$. To avoid visiting irrelevant web pages as much as possible when the focused crawler is crawling, this paper sets a threshold of the comprehensive relevancy of links. Links below this threshold are discarded and those above it are inserted into the waiting queue according to the comprehensive relevancy, thus ensuring that the comprehensive relevancy of links in the queue waiting for access is arranged in descending order.

3. Focused Crawler Based on Improved Energy Landscape Paving Strategy

In this section, we first introduce the energy landscape paving (ELP) algorithm, then design an improved energy landscape paving algorithm, and finally propose a focused crawler strategy based on the improved energy landscape paving algorithm.

3.1. Energy Landscape Paving algorithm

The ELP algorithm [14] is a class of Monte-Carlo-based optimization algorithm put forward by Hansmann etc. in 2002, which combines energy landscape deforming algorithm and Taboo Search. In the solution process, the ELP algorithm usually starts from an initial state X . If X is sampled at time t , its corresponding energy function $E(X, t)$ will be modified by the formula $\tilde{E}(X, t) = E(X, t) - k \times H(X, t)$, which leads to lower probability for state X to be sampled next time. Here k is a constant and the penalty term $H(X, t)$ denotes the frequency histogram function that represents the frequency of being sampled in this state. The frequency histogram will be updated during each Monte-Carlo step. The statistical weight for a state X is defined as $\exp(\tilde{E}(X, t)/(k_b \times T))$, where $k_b T$ is the thermal energy at the temperature T , and k_b is Boltzmann constant. During the ELP's search, as the number that the ELP visits to certain a local minimum increases, the penalty term $H(X, t)$ also increases, which leads to the modified energy value of the state X reduces. As a result, the recently visited repeatedly region will be avoided during searching, which is conducive for the ELP to jump out of the local minimum, search a wider space, and finally may obtain the global optimum state of the problem.

In the focused crawler designing, we use the comprehensive relevancy of hyperlink as its energy value, and the number of times the web page is downloaded as its frequency value of the histogram function. The focused crawler based on the ELP is prevented from repeatedly visiting the web pages that locate at local minima via the influence of punitive frequency histogram. On the other hand, the method of Metropolis sampling is adopted to make it possible for the sub-optimal link to be accessed in advance. This "non-greedy" link selection strategy improves the network coverage of the focused crawler, thus effectively avoiding local optimization of the crawler.

3.2. Focused Crawler Based on IELP

In the original ELP method, there is a technical defect that after the current state X_1 tries to visit the new state X_2 , X_2 is accepted only if $\text{random}[0,1] < \exp((\tilde{E}(X_2, t) - \tilde{E}(X_1, t))/(k_b \times T))$ is satisfied. Due to the existence of a punitive frequency histogram function, it may miss the higher energy around X_1 . Liu et al. [15] made an improvement on the original ELP algorithm: when $E(X_1, t) < E(X_2, t)$, accepted X_2 unconditionally, and when $E(X_1, t) \geq E(X_2, t)$, if X_2 satisfies $\text{random}[0,1] < \exp((\tilde{E}(X_2, t) - \tilde{E}(X_1, t))/(k_b \times T))$, receives X_2 , otherwise does not receive X_2 . In the original ELP algorithm and the improved version [15], the frequency histogram function $H(X, t)$ is updated in each Monte Carlo process. That is to say, for a new link, although it is not accepted, its frequency histogram function will be updated. Due to the increase of the frequency histogram function, these links may be difficult to be accepted in subsequent simulations, and some high-quality links will be missed. In response to this defect, we propose a new frequency histogram update strategy based on the improved version [15]: the frequency histogram is updated only when the newly generated link is accepted. On the other hand, the original ELP adds all sub-links to the waiting queue, while the improved ELP (IELP) filters the sub-links. Only keep sub-links whose comprehensive relevance is higher than the threshold of links' comprehensive relevancy " r_2 ", thereby effectively reducing access to low-quality web pages. This strategy is more helpful for crawlers to retrieve high-quality web pages.

The focused crawler based on IELP algorithm starts from the initial seeds. It downloads the corresponding web pages, extracts all the links whose comprehensive relevancy is higher than the set threshold and adds them into the waiting queue, and then selects the next link in the waiting queue by using the IELP algorithm. The specific process of the focused crawler based on the IELP is as follows:

Step 1: Initialize the waiting queue of links, the threshold of web page relevancy " r_1 " and the threshold of link relevancy " r_2 ". Initialize k and let $t=1$.

Step 2: Rank the waiting queue of links in descending order according to their comprehensive relevancy, and pick out the head link, signed as the current link.

Step 3: Analyze the corresponding web page Phead of the link "head". Calculate the topic relevancy $R(Phead)$ of this page by formula (2), and save this page into a downloaded web page set termed PageDown. If $R(Phead) > r_1$, save this page into the topic-relevant web pages set termed PageSave.

Step 4: If the number of pages downloaded in the PageDown reaches 15,000, stop the algorithm; otherwise go to Step 5.

Step 5: Keep all the sub-links obtained in the current web page into set SubLink, and calculate the comprehensive relevancy $E(link_i)$ of every sub-link $link_i$ in the SubLink by formula (5). If $E(link_i) > r_2$, it will be inserted into the waiting queue; otherwise it will be discarded.

Step 6: Take the comprehensive relevancy of link "head" at the time as its energy $E(head, t)$, and the number of downloads of the current link's corresponding page as its frequency histogram function $H(head, t)$. Calculate $\tilde{E}(head, t) = E(head, t) - k \times H(head, t)$.

Step 7: Pick out the next link termed "next" from the sub-links with equal probability. Calculate this link's energy value $E(next, t)$, frequency histogram function $H(next, t)$ and the value of $\tilde{E}(next, t)$.

Step 8: If $E(\text{head}, t) < E(\text{next}, t)$, then accept next , i.e., let $\text{head}=\text{next}$, $E(\text{head}, t)=E(\text{next}, t)$, $t=t+1$, and go to Step3; otherwise, go to Step 9.

Step 9: If $\text{random}[0,1] < \exp((\tilde{E}(\text{next}, t) - \tilde{E}(\text{head}, t))/(k_b \times T))$, then accept next , i.e., let $\text{head}=\text{next}$, $E(\text{head}, t)=E(\text{next}, t)$, $t=t+1$, and go to Step3; otherwise, do not accept next and restore head as current link, let $t=t+1$, and go to step10.

Step 10: If all the sub-links in SubLink have already been extracted, but still not any "next" link is accepted, then empty SubLink and go to Step2; else go to Step 7.

4. Experimental Results and Analysis

We have implemented IELP algorithm on the Intel Core(TM) i7-4710 computer using Java language. Some important parameters such as r_2 , r_1 , T have great impact on experimental results. In fact, if the threshold of links' comprehensive relevancy r_2 is set too high, few links may meet the requirement and there will be not enough links in the waiting queue. Crawlers will run to a dead end and may miss some topic-relevant web pages. On the other hand, if the threshold is set too low, some web pages that are not relevant to the topic obviously may be crawled, leading to a lower precision. This paper performs simulation experiments on different values between $0.1 \sim 0.3$ of r_2 , respectively. The results show that crawlers work best when r_2 is set to 0.12, so we define $r_2=0.12$ in this paper. Other parameters are set in a similar way. Here $T=2 \times 10^{21} \text{K}$, and r_1 to 0.62.

4.1. Algorithm Evaluating Indicators

Evaluating indicators for the effectiveness of focused crawlers are generally accuracy and recall. Accuracy refers to the ratio of the crawled relevant web pages number LG among the total number DG of the crawled web pages; recall refers to the ratio of the crawled relevant web pages number LG among the total number TG of the relevant web pages within the whole network. Given that it is difficult to count the total number of web pages relevant to a particular topic on the Internet, and that web resources are constantly updated, the recall is hard to calculate scientifically. As a result, this paper adopts precision as the indicator to compare crawlers' performance. On the other hand, this paper uses the average topic relevancy AR of web pages downloaded (see formula (6)) to analyze the proposed IELP algorithm's performance.

$$AR = \frac{1}{DG} \times \sum_{i=1}^{DG} R(P_i) \quad (6)$$

Here $R(P_i)$ represents the topic relevancy of web page P_i .

4.2. Experimental Results and Analysis

To test the effectiveness of the proposed focused crawler, we run the IELP algorithm, the BFS[7], the OPS[8], the FCSA[16], and the ELP algorithm, respectively. Table 2 lists the results of LG, accuracy, AR, and computational time (s) by five different algorithms when DG reaches 15,000. It is not hard to see that the proposed IELP crawler overmatches the three algorithms (BFS, OPS, FCSA) in literature and the

origin ELP algorithm in terms of LG, accuracy and AR, while the BFS and OPS algorithms have a slightly shorter retrieval time. Figure 1 shows the comparison of results of LG by the above five algorithms where the horizontal axis represents the total number of crawled web pages and the vertical axis represents the number of relevant web pages crawled by each method. As the number of crawled web pages increases, the number of relevant web pages crawled by OPS, FCSA, ELP and IELP algorithms increases rapidly, while that by the BFS algorithm grows at a relatively slow speed. IELP is better than the other four algorithms when the number of crawled web pages is larger than 4,000.

Table 2. Comparison of experimental results obtained by five different algorithms when DG reaches 15,000

algorithm	LG	Accuracy	AR	Computational time/s
BFS	1899	0.1265	0.3951	6896
OPS	9053	0.6035	0.5692	7212
FCSA	10596	0.7064	0.6392	7833
ELP	10026	0.6684	0.6212	7742
IELP	11976	0.7984	0.6812	8579

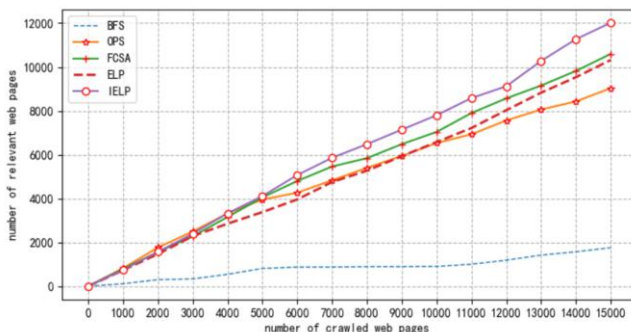


Figure 1. Comparison of the results of the number of crawled relevant web pages for five algorithms

Figure 2 shows the comparison of results on the accuracy of five algorithms where the horizontal axis represents the total number of crawled web pages and the vertical axis represents the precision of each method. As can be seen from Figure 2, the IELP algorithm has the highest precision and tends to be stable when the number of crawled web pages is more than 4,000. Precision of IELP closes to 80%, FCSA 71%, ELP 68%, OPS 60% and BFS around 13% when the number of crawled web pages reaches 15,000. Figure 3 shows the comparison of results on the average topic relevancy of web pages crawled by above five algorithms. The average topic relevancy under the IELP algorithm keeps relatively high values during the whole crawling process and reaches about 0.67, when the number of crawled web pages reaches 15,000. In general, the BFS algorithm has a low precision during the whole crawling process because it does not predict the topic relevancy of web pages during the search process and then visits a large number of irrelevant web pages. The OPS algorithm, which adopts the greedy strategy, downloads the most relevant web pages every time, so its precision is relatively high in the early crawling stage. However, as the number of crawled web pages increases, the greedy strategy adopted by the OPS algorithm leads to the local optimum in the late stage and cannot crawl more

high-quality web pages. The FCSA algorithm selects and receives sub-optimal links with a certain probability, which can improve crawlers' shortcoming in falling into the local optimum, and has the advantages of global search. However, this algorithm is not specially designed to solve above problems and it is still likely to repeatedly visit links that have already been searched, which may affect the searching results. The IELP algorithm makes it possible for the sub-optimal links to be visited in advance by means of Metropolis sampling, and on the other hand, it enables focused crawlers to obtain a similar nature to the Taboo Search algorithm by updating frequency histogram, thus avoiding circuitous search by crawlers. This "non-greedy" link selection strategy raises the network coverage rate of focused crawlers, thus effectively avoiding falling into local optimization and improving the crawler's ability to search relevant web pages.

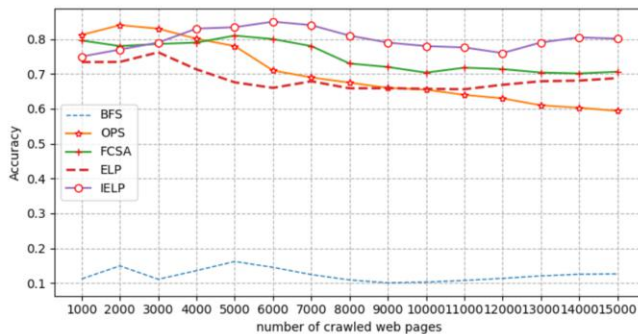


Figure 2. Comparison of the results of accuracy for five algorithms

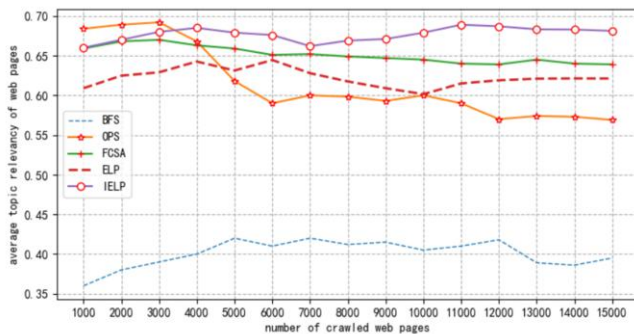


Figure 3. Comparison of the average topic related results of web pages with five algorithms

5. Conclusions

This paper designs a focused crawler based on the improved version of the energy landscape paving (IELP) algorithm that can download relevant web pages on the topic of rainstorm disasters as much as possible. It uses a set of topic words with semantic weight to describe the topic, and designs a method to evaluate the comprehensive relevancy of links in the aspect of the priority of hyperlinks to be visited. Additionally, this paper combines the link search strategy with IELP algorithm to prevent the crawler from falling into local optimization, thus enhancing the precision of focused

crawlers. Experiments suggest that the method proposed in this paper is non-greedy and is not limited to current optimum and it also considers future returns, which effectively improves the precision to crawl relevant web pages. Distributed focused crawlers will be studied in the next stage, for improving the speed of crawlers to visit and download web pages in a distributed form.

Acknowledgments

This work is supported by the Special Foundation of Guangzhou Key Laboratory of Multilingual Intelligent Processing, China (Grant No. 201905010008), the Major Program of the National Social Science Foundation of China (Grant No. 16ZDA047), and the Program of Science and Technology of Guangzhou, China (Grant No. 202002030238).

References

- [1] Seyfi A, Patel A, Junior JC. Empirical evaluation of the link and content-based focused Treasure-Crawler. Computer standards & interfaces, 2016, 44:54-62.
- [2] Liu H, Hong Y, Yao L, et al. HITS-based optimization method for bilingual corpus mining. Journal of Chinese Information Processing, 2017, 31(2): 25-35.
- [3] Wang C, Ji XH. Improved PageRank algorithm based on user interest and topic. Computer Science, 2016, 43(3): 275-278.
- [4] Prakash J, Kumar R. Web Crawling through Shark-Search using PageRank. Procedia Computer Science, 2015, 48: 210-216.
- [5] Zhang W, Chen Y. Bayes topic prediction model for focused crawling of vertical search engine //Proceeding of the 2015 Computing Communications & It Applications Conference. Piscataway: IEEE, 2015: 295-300.
- [6] Du Y, Liu W, Lv X, et al. An improved focused crawler based on semantic similarity vector space model. Applied Soft Computing, 2015, 36: 392-407.
- [7] Li L, Zhang GY, Li ZW. Research on focused crawling technology based on SVM. Computer Science, 2015, 42 (2): 118-122.
- [8] Rawat S, Patil DR. Efficient focused crawling based on best first search //2013 IEEE International Advance Computing Conference. Washington D C: IEEE press, 2013: 908-911.
- [9] Chen J. Design and implementation of news search engine based on MySQL. Fudan University, 2013.
- [10] Jing WP, Wang YJ, Dong WW. Research on adaptive genetic algorithm in application of focused crawler search strategy. Computer Science, 2016, 43(8):254-257.
- [11] Zheng S. Genetic and ant algorithms based focused crawler design// Proceeding of the 2011 International Conference on Innovations in Bio-Inspired Computing & Applications. Piscataway: IEEE, 2011:374-378.
- [12] Wu YL, Zhao SL, Li CJ, etc. Text classification method based on TF-IDF and cosine similarity. Journal of Chinese Information processing, 2017, 31(5): 138-145.
- [13] Turney PD, Pantel P. From Frequency to Meaning: Vector space models of semantics. Journal of Artificial Intelligence Research, 2010, 37(1):141-188.
- [14] Hansmann UHE, Wille LT. Global optimization by energy landscape paving. Physical Review Letters, 2002, 88(6): 068105
- [15] Liu JF, Li G. Basin filling algorithm for the circular packing problem with equilibrium behavioral constraints. Science China: Information Sciences, 2010, 53(5): 885-895.
- [16] Liu JF, Li F, Jiang SY. Focused crawler for rainstorm disaster based on host information and simulated annealing algorithm with comprehensive priority evaluation strategy. Computer Science, 2019, 46(02): 215-222.

Mapping Property of Bilateration and Its Application to Human-Following Robot

Heungju AHN^a, Van Chien DANG^b, Hyeon Cheol SEO^b, and Sang C. LEE^{b,1}

^a*College of Transdisciplinary, DGIST, Daegu, 42988, Rep. of Korea*

^b*IO Lab, Division of Intelligent Robot, Convergence Research Institute, DGIST, Daegu, 42988, Rep. of Korea*

Abstract. Objective of this paper is twofold. The first one is to study the mapping property and unified form of the component equations of the unknown node in bilateration, and the second one is to introduce the concept model for human-following robot based on bilateration. Bilateration needs only two known nodes and two distances' data. Because of the simple sensor arrangement in bilateration, it needs less computation and uses less number of unavoidable erroneous distances compared to the trilateration.

Keywords. trilateration, bilateration, human-following, mapping property, hyperbola

1. Introduction

The Internet of Things (IoT) is a system that connects different '*things*' to provide ubiquitous connectivity and enhanced services [1] and has an extensive set of applications in view of consumer, commercial, industrial, and infrastructure spaces [2]. Up to now, the technology of IoT has been evolved focused on sensing, collection of information, and communication [3]. In this situation, if the position information is added to each IoT, then IoT can provide much wider range of services [1].

The purpose of this paper is twofold; the first objective is to reveal several mathematical properties of the bilateration method; the second one is to propose a bilateration method based on moving frame for the concept model of the human-following robot.

The trilateration in two dimensional geometry, i.e., in \mathbb{R}^2 is most well-known method to determine the unknown node from three different *known nodes*² [4]. Bilateration in \mathbb{R}^2 is a method to determine the coordinates of a movable or stationary point (which will be called *unknown node*) using two measured distances between two distinct known node and unknown node. However, as shown in **Figure 1a**, two measured distances in bilateration do not give the exact coordinates of the unknown node, but fortunately, there

¹Corresponding Author (E-mail:sclee@dgist.ac.kr)

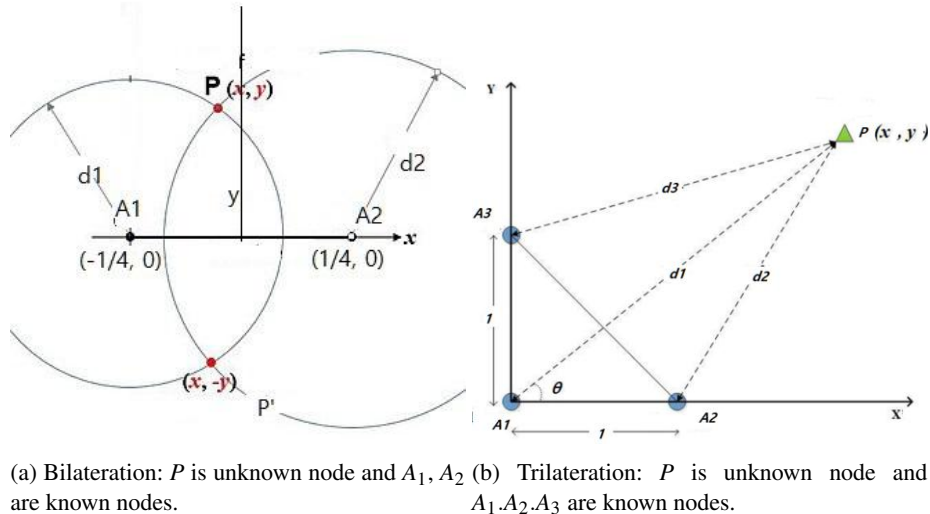
This work was partly supported by DGIST R&D program of the Ministry of Science, ICT, and Future Planning of KOREA (20-IT-03) and Korea Institute of Energy Technology Evaluation and Planning (KETEP) grant funded by the Korea government (MOTIE) (2019-3010032490, Development of 25kW modular fuel cell power conversion system)

²Different terminology is 'stations' or 'anchor'

are finitely many (two except the points on the x -axis) candidates. To choose the desired one from two candidates, we suggest the bilateration, which is acting on the moving robot (see **Figure 3b**).

So far, Heron-bilateration method [5,6,7] has been proposed by many researchers. Unlike our bilateration method mounted on the mobile robot, they all ask somehow *a priori* knowledge about the unknown node.

The bilateration has more advantages compared to trilateration in the following sense: to reduce the number of required known nodes, to require less computation and time to response, and also to provide better position accuracy, since it uses less number of inaccurate distance in computation [5,6,7].



(a) Bilateration: P is unknown node and A_1, A_2 are known nodes.
(b) Trilateration: P is unknown node and A_1, A_2, A_3 are known nodes.

Figure 1. Bilateration and Trilateration

2. Properties of Bilateralation

In this section we prove that the bilateralation is the most efficient method among the multilateration in \mathbb{R}^2 if we have a method to choose the exact coordinates of the unknown node among two candidates. Actually, trilateration method is the following: bilateration gives information to narrow the possible positions down to two candidates, and then another distance measurement from a known node that is different from two known nodes in bilateration determines the exact position.

As we shall see it in §3, there is another way of choosing the exact position by moving the one of the two known nodes. In this case, bilateration has more advantage compared to the trilateration, since we have only two measurement errors and the process for the additional information contains no more numerical error.

Also, as a main contribution of this paper, we study the mapping properties of the bilateralation and show the x - and y -components of the coordinates of the unknown node obtained from the bilateralation method have similar forms as trilateration under the suitable change of variables.

2.1. Generalized Geometry Problem

Let \mathbb{R}^2 be two dimensional Euclidean space equipped with the Cartesian coordinate system. Let $A_1, A_2, \dots, A_n \in \mathbb{R}^2$ be n -distinct nodes in the plane whose coordinates are known and $P \in \mathbb{R}^2$, an unknown node. Further, assume that non-negative scalar-valued numbers d_1, d_2, \dots, d_n are given, where each d_k ($k = 1, 2, \dots, n$) is obtained from the information³ between A_k and P . The generalized geometry problem is to determine the coordinates of the unknown node P from known nodes A_1, A_2, \dots, A_n using measurement data d_1, d_2, \dots, d_n .

Since the space filling curve can not be one-to-one, one known node $A = A_1$ and one measured datum $d = d_1$ can not uniquely determine every position in \mathbb{R}^2 . It is possible to approximate the position in \mathbb{R}^2 instead of filling it. This kind of localization corresponds to the empirical method to match the information from the unknown location with a sufficiently large data of known locations.

2.2. Bilateration

In this section, we explain the bilateration method using the distance data. For the simplicity of notations, let $A_1 = (-1/4, 0)$, $A_2 = (1/4, 0)$ be two known nodes, and $P = (x, y)$, unknown node to be determined using d_1 and d_2 (recall d_1 is the distance between A_1 and P , and d_2 is the distance between A_2 and P).

Simple observation (see **Figure 1a**) gives

$$(x + 1/4)^2 + y^2 = d_1^2, \quad (1)$$

$$(x - 1/4)^2 + y^2 = d_2^2. \quad (2)$$

Subtracting (2) from (1), we have

$$x = d_1^2 - d_2^2, \quad (3)$$

and plugging (3) into (1) and arranging the terms, we obtain

$$y^2 = d_1^2 - (d_1^2 - d_2^2 + 1/4)^2. \quad (4)$$

Theorem 2.1. *The function $(d_1, d_2) \mapsto (x(d_1, d_2), y(d_1, d_2))$, which will be called a bilateration mapping, defined by (3) and (4)*

$$\begin{aligned} x(d_1, d_2) &= d_1^2 - d_2^2 \\ y(d_1, d_2) &= \sqrt{d_1^2 - (d_1^2 - d_2^2 + 1/4)^2} \end{aligned}$$

is a bijective mapping from the domain $S = \{(x, y) \in \mathbb{R}^2 : d_1 + d_2 \geq 1/2, d_2 \leq d_1 + 1/2, d_2 \geq d_1 - 1/2\}$ to the upper half plane set $H = \{(x, y) \in \mathbb{R}^2 : x \in \mathbb{R}, y \geq 0\}$. Also, the function x, y are differentiable in the interior of S , and preserves the boundary.

³The most typical information is the Euclidean measured distance d_k between A_k and P using sensors.

Proof. Since three points A_1, A_2 , and P form a triangle, and the length of the line segment $\overline{A_1A_2}$ is exactly $(1/2)$, we have the first restriction equation

$$d_1 + d_2 \geq 1/2. \quad (5)$$

Next, note that $y^2 = d_1^2 - (d_1^2 - d_2^2 + 1/4)^2 \geq 0$. Solving this inequality, we have two more equations

$$\begin{aligned} 0 &\leq d_1 - (d_1^2 - d_2^2 + 1/4) = d_2^2 - (d_1 - 1/2)^2, \quad \text{and} \\ 0 &\leq d_1 + (d_1^2 - d_2^2 + 1/4) = (d_1 + 1/2)^2 - d_2^2. \end{aligned}$$

Solving the above inequalities simultaneously and noticing that d_1, d_2 are non-negative real numbers, we obtain the restrictions

$$d_1 - 1/2 \leq d_2 \leq d_1 + 1/2$$

that define the domain S .

Finally, we have to check how the bilateration mapping maps the boundary of S onto that of H . The boundary of S is composed of three parts: $d_1 + d_2 = 1/2$ ($0 \leq d_1, d_2 \leq 1/2$); $d_2 = d_1 - 1/2$ ($1/2 \leq d_1$), and $d_2 = d_1 + 1/2$ ($0 \leq d_1$). From the equality $d_2 = d_1 - 1/2$, the straightforward calculation shows

$$\begin{aligned} x(d_1, d_2) &= d_1^2 - d_2^2 = d_1 - 1/4 \quad (0 \leq d_1 \leq 1/2) \\ y(d_1, d_2)^2 &= d_1^2 - (d_1^2 - d_2^2 + 1/4)^2 = d_1^2 - (d_1^2 - (d_1 - 1/2)^2 + 1/4)^2 = 0. \end{aligned}$$

Hence one line segment of the boundary of S is mapped to the line segment $-1/4 \leq x \leq 1/4$ of the boundary H (see **Figure 2**). Similarly, from the other equations, we see the boundary behaviour by the bilateration mapping.

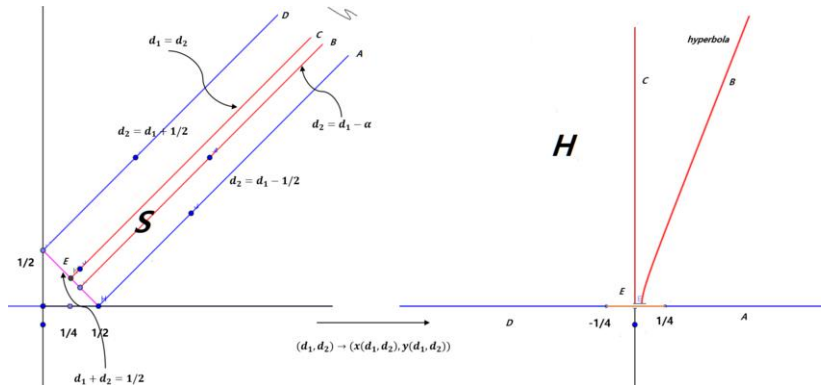


Figure 2. Bilateration Mapping

□

Note. The lines $d_2 = d_1 - \alpha$ ($0 \leq \alpha \leq 1/2$) in S are mapped to the hyperbolas (see the red lines in **Figure 2**), since $d_1 - d_2 = \alpha$ (constant) defines one piece in the right half plane of hyperbola (note that it define a hyperbola if the difference of the distance $\overline{PA_1}$, $\overline{PA_2}$ two known nodes A_1, A_2 is constant).

Theorem 2.2. *The bilateration mapping $(d_1, d_2) \mapsto (x, \pm y)$ of **Theorem 2.1** exactly gives the localization mapping from $S \times \{+1, -1\}$ to \mathbb{R}^2 .*

Next section (§ 3), we give a practical way how to choose ± 1 (upper half plane, or lower half plane).

Proof. By (3) and (4), the function $(d_1, d_2) \mapsto (x(d_1, d_2), +y(d_1, d_2))$ maps S to the upper half plane (see the proof of **Theorem 2.1** and **Figure 2**). Also, $(d_1, d_2) \mapsto (x(d_1, d_2), -y(d_1, d_2))$ maps S to the lower half plane, since the lower half plane is the mirror reflection of the upper half plane with respect to the x -axis, and the y -component has negative values in lower half plane, \square

2.3. Change of Variables: New Expression

In trilateration method (see **Figure 1b**), it is known [8,9] that the coordinates of the unknown node is represented by the following hyperbolic equation

$$x = (d_1^2 - d_2^2 + 1)/2, \quad y = (d_1^2 - d_3^2 + 1)/2.$$

Similarly, up to change of variables, we have also hyperbolic equations in bilateration.

Theorem 2.3. *By almost linear change of variables, that is, squared mapping $t \mapsto t^2$ and linear transformation (including rotation translation), we have*

$$\begin{aligned} x(d_1, d_2) &= (d_1 + d_2)(d_1 - d_2) \rightsquigarrow \sqrt{(u_1^2 - u_2^2)/2} \\ y(d_1, d_2) &= \left[d_1^2 - (d_1^2 - d_2^2 + 1/4)^2 \right]^{1/2} \rightsquigarrow \sqrt{(v_1^2 - v_2^2)/2} \end{aligned}$$

Proof. Let $s = d_1 + d_2$, and $t = d_1 - d_2$, and $\tilde{u}_1 = s^2, \tilde{u}_2 = t^2$. Then, rotating the curve by $(-\pi/4)$ around the origin,

$$\begin{aligned} x^2 &= (d_1^2 - d_2^2) = (d_1 + d_2)^2(d_1 - d_2)^2 \\ &= s^2 t^2 = \tilde{u}_1 \tilde{u}_2 \rightsquigarrow (u_1^2 - u_2^2)/2. \end{aligned}$$

Next, consider the equation of y -component. By factoring the term $y^2 = d_1^2 - (d_1^2 - d_2^2 + 1/4)^2$, we have

$$\begin{aligned} y^2 &= (d_1 - (d_1^2 - d_2^2 + 1/4)) (d_1 + (d_1^2 - d_2^2 + 1/4)) \\ &= -((d_1 - 1/2)^2 - d_2^2) ((d_1 + 1/2)^2 - d_2^2) \\ &= -(d_1 - 1/2 - d_2)(d_1 - 1/2 + d_2)(d_1 + 1/2 - d_2)(d_1 + 1/2 + d_2) \\ &= -[(d_1 + d_2)^2 - (1/2)^2][(d_1 - d_2)^2 - (1/2)^2] \end{aligned}$$

Letting $s = d_1 + d_2$, and $t = d_1 - d_2$, and again $\tilde{v}_1 = s^2 - 1/4$, and $\tilde{v}_2 = t^2 - 1/4$,

$$y^2 = -(s^2 - 1/4)(t^2 - 1/4) = -(\tilde{v}_1 \tilde{v}_2) \rightsquigarrow (\tilde{v}_1^2 - v_2^2)/2$$

by $(\pi/4)$ -rotation. \square

3. Application of Bilateration to the human-following robot

Let C be a curve in the plane. Now, assume the *moving frame* on \mathbb{R}^2 along the curve C , which just means the Cartesian coordinate system⁴ of the Euclidean plane \mathbb{R}^2 that moves with the observer along C (see **Figure 3a**).

To develop human-following robot based on the position of leading human, it is necessary to consider only the relative position of human with respect to the robot. Equivalently, from the following robot's view point, it is better to consider the moving coordinate system mounted on the robot, since the robot follows it as human is moving along C . In this case, by rotating the robot fixing the origin O , we can determine the right solution from the two candidates coordinates in **Theorem 2.2** of the human, which are calculated by the proposed bilateration. It is known [10] that the human-following robot based on the position has fundamental advantages compared to the vision-based one [11].

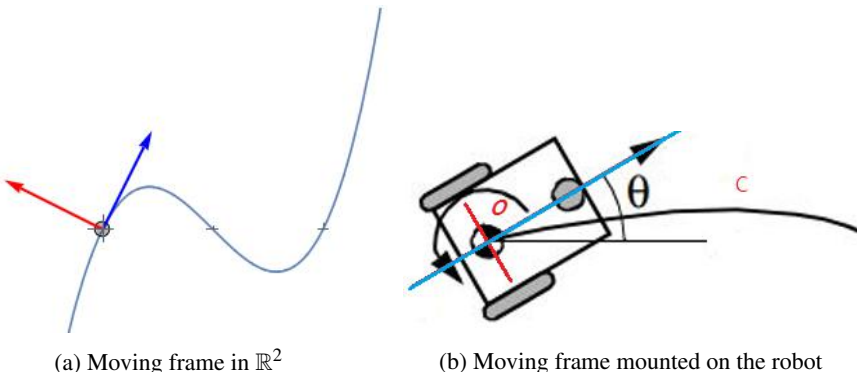


Figure 3. Bilateration based on moving frame for the human-following robot

4. Conclusion

In this paper we have studied the mapping properties of the bilateration method and proposed the bilateration for the concept model of the human-following robot, since the relative position of the leading human with respect to the robot is easily obtained and the bilateration needs only two sensor nodes mounted on the robot, which results in very simple robot's architecture.

With regard to the mapping property of the bilateration, first, we showed how two measured distances maps into the position of the unknown node (**Theorem 2.1** and **The-**

⁴orthonormal frame

orem 2.2). Second, we proved that the coordinates functions of the unknown node by the bilateration essentially have the same hyperbolic equation as the trilateration after changing almost linear change of variables (**Theorem 2.3**).

In general, though the bilateration has one more ambiguous coordinates for the unknown node, we can overcome this disadvantage by mounting the sensors on the mobile robot and moving (or rotating) the robot or sensors.

The proposed bilateration has more advantages compared to other localization techniques like multilateration, since we have only two measurement errors in bilateration, from which the number of the required nodes, computation time, and the response time can be reduced and hence better positioning accuracy is expected.

References

- [1] Zafari F, Gkelias A, Leung KK. A Survey of Indoor Localization System and Technologies. *IEEE Comm. Surveys & Tutorials*. 2019; 21(3): 2568-2509.
- [2] Perera, C.; Liu, C. H.; Jayawardena, S. (December 2015). The Emerging Internet of Things Marketplace From an Industrial Perspective: A Survey. *IEEE Transactions on Emerging Topics in Computing*. 2015 Dec; 3(4): 585-598.
- [3] Want, R; Schilit, BN.; Jenson, S. Enabling the Internet of Things. *Computer*. 2015 Dec; 48: 28-35.
- [4] Safavi S, Khan UA, Kar S, Moura JMF. Distributed Localization: A Linear Theory. *Proc of IEEE*. 2018 July; 106(7): 1204-1223
- [5] Cota-Ruiz J, Rosiles JG, Sifuentes E, Rivas-Perea P. A Low-Complexity Geometric Bilateration Method for Localization in Wireless Sensor Networks and Its Comparison with Least-Squares Methods, *Sensors*. 2012 Dec; 839-862
- [6] Li X, Hua B, Shang Y, Xiong Y. A robust localization algorithm in wireless sensor networks, *Front. Comput. Sci. China* 2008; 2(4): 438-450
- [7] Tiwari S, Jain VK. Heron-Bilateration based Location Estimation Technique for Indoor WLAN, In: Proceeding of the 31st International Conference on Information Networking (ICOIN 2017); 2017 Jan 11-13; Da Nang, Vietnam: IEEE PDF eXpress; p. 13-17
- [8] Lee SC, Rizal S, Ahn H. Anchor Placement Design for a Decoupled Simple Trilateration Algorithm. *Journal of Nonlinear and Convex Analysis*. 2019; 20(7); 1327-1339
- [9] Lee SC, Ahn H., A New Mobile Real-Time Localization System for a Following Robot Application, *Journal of Nonlinear and Convex Analysis*. 2020; 21(7); 1477-1485
- [10] Feng T, Yu Y, Wu L, Bai Y, Xiao Z, Lu Z. A Human-Tracking Robot Using Ultra Wideband Technology. *IEEE Access*. 2018; 6: 42541-42550
- [11] Gupta M, Kumar S, Behera L, Subramanian VK. A Novel Vision-Based Tracking Algorithm for a Human-Following Mobile Robot. *IEEE Trans on Systems*. 2017 July; 47(7): 1415-1427

Construction of Cloud ERP Security Evaluation Index System Based on Text Mining

Ying GAO^a, Qin SU^{a,1}, Yue FANG^a and Pinyan LAI^a

^aSchool of Management, Xi'an Jiaotong University, Xi'an, China

Abstract. The aim of this study is to investigate and discuss the potential security issues arising from the deployment of the Cloud Enterprise Resource Planning system, and to propose a perfect and standard set of security evaluation index system for Cloud ERP security issues. Considering the issues which may be inherent in the conventional Enterprise Resource Planning systems and new ones brought by Cloud Computing, Cloud Platform, Cloud ERP, we use text mining technology to mine the related standard files in this paper. Since the standard literature is based on the comprehensive results of technology, science and practice, its characteristics of standardization, objectivity and validity also ensure the effectiveness and applicability of indicators. By using NLP methods, we construct a Cloud ERP security evaluation index system consisting of five parts: evaluation method security, information access security, data security, management security and others. The entropy method is used to assign weights for the Cloud ERP security evaluation index system, which is more scientific and rational and the method moderates the lack of objectivity caused by traditional evaluation methods which over-rely on evaluators. By analyzing cases of Cloud ERP collected in various application reports and research papers, we improve our system and find that compared to other evaluation systems, our system can evaluate the security of Cloud ERP more comprehensively.

Keywords. Cloud ERP, security evaluation index, text mining

1. Introduction

With the development of Internet technology and digital information technology, as well as the higher requirements for data processing speed, cloud computing has come into. According to a survey in 2011, 43% of IT executives said they would use cloud services to replace current systems. Global Industry Analysts, a research firm, estimates the global market for cloud computing services is on the verge of reaching \$127 billion[1].

Cloud ERP introduces cloud computing to ERP software and makes it possible for enterprises to run ERP software on the cloud computing platform of suppliers, which further promotes the development of enterprises. With this technology, companies can safely provide services on a global scale, regardless of geographic location. This may address some of the risks and challenges of ERP, for example, it eliminates implementation

¹Corresponding Author: No. 28, Xianning West Road, Xi'an, Shaanxi Province 710049, China. E-mail address: qinsu@mail.xjtu.edu.cn (Q. Su).

time and cost, reduces hardware investment and maintenance, and enhances security[2]. However, cloud computing also has security issues, including governance, data management, architecture, application, and assurance[3]. It will bring huge losses, if the cloud ERP system encounters problems such as confidentiality of important business data, loss of personal information, malicious attacks, etc. Therefore, it is very important to ensure the information security of ERP system. The current literature on cloud ERP only puts forward security as a problem, but does not clearly point out what the security problems of cloud ERP are. Due to the limited resources for cloud ERP security issues, this article analyzes the security standard literatures relating to traditional ERP system, cloud computing and cloud platform, uses text mining methods to extract the evaluation indicators from text databases, screens and improves the indicators through qualitative and quantitative analysis, and finally builds and tests the cloud ERP security standard evaluation indicator system.

On the theoretical level, this research adopts text mining based on cloud ERP security standard documents. On the one hand, it puts forward the important role of security standards in enterprise practice. On the other hand, the text mining method provides a certain objective basis for the establishment of cloud ERP evaluation system. On the practical level, the cloud ERP security evaluation system proposed in this study provides a certain sense of reference value for the security management practices of enterprises (ERP users) and suppliers. Through this evaluation system, enterprises can measure the cloud ERP security level more efficiently and conveniently, and put forward relevant measures and suggestions based on the specific evaluation results to improve the security management level of the cloud ERP system.

2. Related literature

Traditional ERP systems have limited capabilities in terms of multi-user access, performance and resource availability. The complex structure behind ERP has caused security problems and maintenance difficulties[4], so the traditional ERP has always focused on internal controls to limit user's behavior and privileges[5]. For example, faulty or incomplete access enforcement conditions can cause information resource access security problems[6].

Cyber security incidents or threats on China's cloud platforms have further intensified in the first half of 2019 compared to 2018, according to the Internet Security Situation in China in the first half of 2019[7]. At the same time, CNCERT also pointed out in the report that cloud service providers and cloud users should work together to improve the defense capability of cloud platform network security.

Data security and trust problems of users's lack of relying on the cloud to provide IT infrastructure are the priorities of cloud computing security research. For example, Feng[8] proposed cloud computing security standards and an assessment system with data security and privacy protection as the main target, security objectives verification and security service level evaluation as the core. Xu[9] classified the security framework of cloud computing platform based on data confidentiality, integrity, non-repudiation, availability and reliability.

3. Construction of cloud ERP security evaluation index system

3.1. Text sources

Standard literature has both the function of general scientific and technological literature and the legal effect to ensure that the products or services developed by different subjects can have the same quality. Therefore, in order to ensure the effectiveness and applicability of the indicators, a total of 39 standard literatures are adopted in this study, including national standards, industry/local standards and international standards. The standard literatures are all from the official website of ISO and the Open Standards Website of China. See appendix for details.

3.2. Text preprocessing

Since the original file format is an image-type PDF, the file format needs to be converted firstly to facilitate text analysis. 39 PDF standard literatures in picture format are extracted by Python. And then the API interface of picture and text recognition in Baidu intelligent cloud platform is used to extract all the words in each picture. Finally a TXT format text file of each standard literature is obtained.

In order to better identify the keywords of the whole text, we extract all the headings of the text, including the first level headings and sub-headings of other levels.

3.3. Natural language processing

3.3.1. Chinese word segmentation

The precise mode of Python's jieba library[10] is used to segment the text, at the same time, some special words are imported to the custom dictionary and refer to it when we are doing the word segmentation. In this paper, both the standard full-text text and the standard title text are divided. The standard full-text refers to a text file summarizing the content of all standard literatures, while the standard title text refers to a text file summarizing the title part of all standard literatures.

3.3.2. Word frequency statistics

The word frequency of each word after word segmentation is counted, and the word with higher word frequency is found as our keyword, because the higher frequency a word appears in the text, the better it can reflect the central content of the text. At the same time, we also need to remove some stop words. Finally, the top 30 words of standard full-text and standard title frequency are selected respectively, as shown in table 1.

3.3.3. Keyword filtering

After counting the top 30 words in the frequency of standard full-text text and standard title text respectively, taking its 23 common words as our text keywords.

TF-IDF is a commonly used weighting technique for text mining and information retrieval, which is used to evaluate the importance of words to one of the documents in the file base. In order to filter out the keywords with a high degree of differentiation, this study calculates the IDF value of all keywords, and sorts them from small to large.

Table 1. Word frequency statistics

Word frequency of title (30)				Word frequency of text (30)			
evaluation	925	control	78	security	4320	platform	1244
requirement	858	access control	69	requirement	3448	user	1211
method	704	technology	68	certificate	2510	strategy	1166
security	525	information assurance	67	service	2090	visit	1112
management	231	identify	67	data	1884	property	1111
certificate	151	user	64	cloud service	1814	personnel	1083
data	140	protection	64	information	1767	document	1070
information	132	environment	64	system	1740	audit	1044
service	117	visit	62	evaluation	1589	function	1043
audit	115	platform	61	management	1486	extension	1043
extension	112	strategy	61	cloud-computing	1474	public key	1007
cloud service	111	test	59	client	1450	resource	997
resource	104	client	56	check	1432	method	979
cloud-computing	101	function	55	cloud service providers	1406	business	949
property	96	system	53	component	1375	technology	923

The results are shown in Table 2. Words with IDF value less than 0.05 are selected as the final keywords. Finally, a total of 15 keywords are selected, namely security, management, information, user, technology, requirement, data, system, access, evaluation, service, function, audit, method and cloud computing.

Table 2. IDF value of keywords

IDF value					
security	0	access	0.011899	strategy	0.07684
management	0	evaluation	0.024134	paltform	0.09108
information	0	service	0.024134	cloud service	0.105804
user	0	function	0.024134	customer	0.18799
technology	0	audit	0.036723	extension	0.18799
requirement	0.011899	method	0.049688	property	0.422074
data	0.011899	cloud computing	0.049688	certificate	0.526809
system	0.011899	resource	0.063052		

3.4. Indicators extraction

3.4.1. Clustering analysis

In order to further analyze and classify keywords, keywords need to be quantified. In this paper, TF value is taken as the quantized data of keywords, and TF value of each keyword in each standard is calculated and normalized. Then, the quantified data are imported into SPSS, and the Pearson correlation is used as the measurement standard of the interval for systematic clustering analysis of the data.

At the distance of 20, 15 keywords can be divided into five groups. In view of the common characteristics of each group of keywords, the common characteristics of each group are summarized to form the first-level index of the cloud ERP security evaluation index system. The first group is the security of evaluation method; the second group is

information security; the third group is data security; the fourth group is management security and the fifth group is other security.

3.4.2. Analysis of paragraph contribution

After the construction of the first-level index, this paper adopts the method of piecewise review of the text, gives priority to the extraction of the second-level index and the third-level index from the important, valuable and highly relevant paragraphs, so as to improve the accuracy of the index extraction.

Firstly, each standard literature is divided into paragraphs according to its first-level title to form several paragraphs-ending documents. Then the contribution of keywords is calculated for each paragraph. Each paragraph has 15 contribution values. The calculation method of contribution degree is keyword word frequency multiplied by keyword position weight. When a keyword appears in a first-level title, other levels or the text, a position weight of 10,5,1 is assigned respectively.

According to the previous literatures [11,12,13], we find that for convenience of users' practical construction, usually they are willing to have different levels for management concern. So we construct an evaluation system consisting of 5 first-level indexes, 21 second-level indexes and 105 third-level indexes.

4. Index weight

Due to the limitation of subjective weighting method and objective condition limitation, entropy value method is used to assign weights to each index in this study. We extract the keywords of the third-level index included in n=21 second-level index from m=39 standard literatures. Matrix is obtained by text mining.

$$(1) \text{Standardize the data: } x'_{ij} = \frac{x_{ij} - \min\{x_{1j}, \dots, x_{nj}\}}{\max\{x_{1j}, \dots, x_{nj}\} - \min\{x_{1j}, \dots, x_{nj}\}}$$

(2) Quantify the indicators in the same degree, the proportion of the i_{th} sample value of the j_{th} index in this index:

$$p_{ij} = \frac{x_{ij}}{\sum_{i=1}^n x_{ij}}, i = 1, \dots, n \quad j = 1, \dots, m$$

(3) The entropy value of the j_{th} index:

$$e_j = -k \sum_{i=1}^n p_{ij} \ln(p_{ij}), j = 1, \dots, m \quad k = \frac{1}{\ln(n)} > 1$$

(4) The coefficient of difference of the j_{th} index: $d_j = 1 - e_j, \quad j = 1, \dots, m$

$$(5) \text{The weight of each index: } w_j = \frac{d_j}{\sum_{j=1}^m d_j}, \quad j = 1, \dots, m$$

5. The empirical analysis

5.1. Data collection

In this paper, security-related contents in various cloud ERP software application reports and research papers on cloud ERP are collected at home and aboard. In order to improve

the accuracy of data extraction and reduce the deviation caused by subjective factors, the Delphi method[14] is adopted to consult the selected expert group members for investigation and 68 pieces of security data are finally summarized.

Through the case data segmentation and word frequency statistics, as shown in Table 3, we find that data, management, access, personnel security and other words are more important. This is also consistent with our index system.

Table 3. word frequency statistics

data	43	information	10	record	7	document	6
user	27	application	10	management	7	staff	6
system	21	service	10	backups	7	specific	6
access	21	authorization	9	client	6	event	5
security	14	organization	8	business	6	segregation	5
ERP	12	organization	8	storage	6	sensitivity	5
permission	10	log	8	law	6	supplier	5

5.2. Case evaluation

According to the cloud ERP security evaluation index system proposed in this paper and the weight of each index obtained by entropy method, the security evaluation score of this case is calculated as 46.7. In order to verify the effectiveness of the security evaluation index system, we adopt another cloud computing security evaluation model[13] for appraisement. This model is based on the evaluation requirements of information security level protection in China. And the security evaluation score of this case is 44.6.

The calculation shows that the evaluation model proposed in this paper has completed the quantification of the security level of the cloud ERP security example, and the evaluation result is consistent with the comprehensive conclusion obtained through the evaluation of the other schemes, what proves the feasibility and effectiveness of the evaluation system to a large extent.

5.3. Perfection of the system

Through case evaluation and comparison with cloud computing security evaluation model[13], we further improve the index system accordingly, and finally obtain a quantifiable cloud ERP security three-level evaluation index system, as shown in Table 4.

6. Conclusion

In this paper, based on the method of text mining, we have realized the representativeness and objectivity of index extraction, and obtained the specific and applicable cloud ERP security evaluation index. On the one hand, it affirms the significance and value of the standard literature, on the other hand, it provides relevant supporting basis for the extraction of evaluation index.

Compared with the traditional ERP security evaluation system[5,6,15,16], the characteristics of multi-tenancy and scalable of cloud ERP determine that the cloud ERP

Table 4. Cloud ERP security evaluation index system

First-level index	Second-level index	Third-level index
A1. Evaluation method security (0.2055)	B1. Evaluation method (0.1062)	whether the evaluation method is objective and impartial whether the evaluation method is reusable whether the evaluation method is flexible Whether the evaluation method has little impact on it operation
	B2. Evaluation results (0.066)	Whether the evaluation method includes interview, examination, etc Whether the evaluation results are reproducible whether the evaluation results are supported by evidence
	B3. Evaluation organization 0.0333	whether the evaluation organization has a high level of confidentiality
A2. Information access security (0.1043)	B4. Resource access control (0.0365)	Whether the information flow control strategy is established Whether to have a remote access policy Whether there is an identification strategy Whether to use technical measures to restrict the address range of the access terminal
	B5. Resource access authorization (0.0387)	Whether access to information resources conforms to the minimum authorization principle Whether access to information resources conforms to the separation of duties principle Whether there is an authentication authorization verification mechanism
	B6. Information security incidents (0.0291)	Whether all user's information can be protected Whether to provide corresponding strength security protection for different types of information Whether it can respond to information security incidents quickly, effectively and orderly Whether there is a documented procedure consistent with information security incident response Whether there is a document that provides users with the relevant information security events Whether it can monitor and warn information security events in real time
A3. Data security (0.3294)	B7. Data transmission (0.0405)	Whether to take effective measures to guarantee the confidentiality of data transmission process Whether to take effective measures to ensure the integrity of the data transmission process Whether it can detect the data transmission process is damaging and take recovery measures Whether effective measures can be taken to prevent electromagnetic leakage of data transmission medium Whether the reliability of transmission network can be guaranteed
	B8. Data storage (0.0314)	Whether effective measures are taken to safeguard the confidentiality of data stored procedures Whether effective measures are taken to ensure the integrity of data stored procedures Whether to provide an effective virtual machine image file loading protection mechanism Whether data with different security levels is stored in different Spaces Whether an effective method of disk protection or data fragmentation storage is provided Whether to take effective measures to ensure the environmental security of data storage equipment and media
	B9. Data usage (0.06)	Whether data usage is authorized and validated Whether the use of sensitive data is audited and an audit log is formed
	B10. Data backup and recovery (0.0434)	Whether to provide data backup and restore function Whether automatic and manual backup of data is supported Whether to support local and remote backup of data Whether there is a disaster recovery policy Whether there is a disaster backup and recovery center
	B11. Data isolation (0.0444)	Whether to take effective measures to isolate data from different users Whether to take effective measures to isolate different business application data Whether to take effective measures to isolate different levels of security data Whether to partition different data security domains
	B12. Data migration(0.0472)	Whether it can ensure that data migration does not affect business continuity Whether to establish a data migration plan Whether to establish a risk control strategy for data migration Whether to use a distributed migration strategy Whether to monitor the data migration Whether there are effective measures to guarantee the confidentiality of the data migration process Whether there are effective measures in place to ensure the integrity of the data migration process Whether there are measures for data backup and recovery during data migration
	B13. Data disposal (0.0625)	Whether it can clear all legacy data and data copies Whether to take effective measures to prohibit the recovery of destroyed data Whether data destruction generates appropriate logging Whether it is possible to ensure that all data is completely cleared before the storage space is reallocated Whether the storage device or media should be cleaned up before being discarded
	B14. Security management policy (0.0582)	Whether there is the daily management procedure Whether there is a comprehensive information security management system Whether to check and revise the safety management system regularly Whether the security management system is issued in a formal and effective manner Whether to establish safety management system for all kinds of management contents in safety management activities
	B15. Personnel management (0.0518)	Whether to establish a functional department of information security management Whether to set up a leading group to manage information security work Whether the responsibilities of each department and position of the safety management organization are clearly defined Whether to conduct regular safety review and skill assessment for personnel Whether to provide safety awareness education and relevant training to personnel regularly Whether the safety education and training are documented
	B16. System management (0.0276)	Whether there is a clear system boundary and security protection level Whether to select basic security measures according to the security protection level of the system Whether there is a master plan for information security construction Whether it can grade the system regularly Whether the rating is evaluated in time when the system changes Whether to maintain the system according to the operation manual
A4. Management security (0.182)	B17. Operations management (0.0444)	Whether to establish the asset safety management system Whether to establish media safety management system Whether to establish supporting facilities, software and hardware maintenance management system Whether each device has a detailed operation log Whether to establish network security management system Whether the network system is regularly scanned for vulnerabilities Whether to exercise the emergency plan on a regular basis Whether to assess the potential risk to the machine room Whether to implement strict access control to the machine room Whether to maintain and manage the machine room facilities regularly Whether it can provide enough space and capacity to meet the needs of facility expansion Whether it can reasonably divide the physical area of the computer room and arrange the information system components Whether the data use and system management meet the requirements of local laws and regulations

A5. Others (0.1788)	B18. Network security (0.0402)	Whether to draw the network topology diagram that is consistent with the current operation Whether the business processing capacity of key network equipment is guaranteed to have redundant space Whether there are different subnets, segments, or security groups Whether to deploy access control devices at network or segment boundaries Whether to limit the maximum number of network traffic and network connections Whether the network boundary can be realized inspection
	B19. Host security (0.0463)	Whether each group of hosts has implemented the security protection system Whether to monitor important servers Whether to install anti-malicious code software Whether the security audit can cover every operating system user and database user Whether the operating system can follow minimum installation principles
	B20. Application security (0.051)	Whether it can severely restrict user access to the application Whether the permissions for applications to call each other are strictly limited Whether the audit scope covers significant events in the user's application
	B21. Virtualized security (0.0413)	Whether isolation between virtual machines is supported Whether it has the ability to identify and deal with malicious attacks on the virtual machine Whether to provide a virtual network structure map that matches the current health Whether virtual network critical logs are monitored and audited Whether to monitor the virtual machine's running state, resource occupancy and other information Whether it has the ability to spot vulnerabilities in the virtualization platform

evaluation system constructed in this paper pays more attention to user authentication and access control security in the cloud environment, such as data isolation, data backup and data recovery. Compared with the cloud computing security evaluation index system[13,17], the cloud ERP system designed in this paper focuses on physical security, namely the security of the storage media data center, such as the security of the computer room, on the basis of virtual security.

In short, this cloud ERP security evaluation index system not only provides theoretical reference for cloud ERP security evaluation and directions for strengthening cloud ERP security, but also provides method reference for the practical application of text mining technology in the evaluation.

In further research, we will modify the index system, so that the evaluation system can be adjusted continuously as the cloud ERP software structure and application changes, and enhance the automation function of the evaluation process.

7. Acknowledgement

The work was funded by the National Key R & D Program of China (No. 2019YFB1704103).

References

- [1] Trend Micro. Despite security concerns, businesses moving to the cloud(Op/Ed). <https://blog.trendmicro.com/despite-security-concerns-businesses-moving-to-the-cloud/>. November 30,2011.
- [2] Torbacki, Witold. SaaS-direction of technology development in ERP/MRP systems. Archives of Materials Science and Engineering.2008(32).
- [3] II John, Alhamdani Wasim. Who can you trust in the cloud? A review of security issues within cloud computing. Proceedings of the 2011 Information Security Curriculum Development Conference.2011(9).
- [4] Brehm Nico, Gómez Jorge. Secure Web service-based resource sharing in ERP Networks. Journal of Information Privacy and Security.2005(1):29-48.
- [5] Shen Shen. ERP Security Status and Solutions [J]. Network Security Technology and Application.2005(05):16-17.
- [6] Elisabeth J Umble, Ronald R Haft, M.Michael Umble,Enterprise resource planning: Implementation procedures and critical success factors.European Journal of Operational Research.2003(146):241-257.

- [7] National Internet Emergency Response Center. China's Internet Network Security Situation in the First Half of 2019.August 13, 2019.
- [8] Feng Dengguo, Zhang Min, Zhang Yan, Xu Zhen. Research on cloud computing security [J].Journal of software.2011(22):71-83.
- [9] Xu Xiaoping. The Application of trusted Computing Technology in Cloud Computing Security [J]. Computer Nerd.2016(01):26-27.
- [10] <https://pypi.org/project/jieba>.
- [11] Yang Aimin, Gao Fang, Bian Minhua, Yang Shulei. Cloud computing security evaluation and counter-measure based on AHP-fuzzy comprehensive evaluation[J]. Journal on Communications.2016,(37):104-110.
- [12] Zheng Jinghua, Li Kun, Zhao Yonggang. Research on cloud system security evaluation index [J]. Shandong Industrial Technology.2015(09):188-189.
- [13] Jiang Zhengwei, Zhao Wenrui, Liu Yu, Liu Baoxu. Cloud computing security assessment model based on hierarchical protection [J]. Computer science.2013(40):151-156.
- [14] <https://en.wikipedia.org/wiki/Delphi-method>.
- [15] Cheng Naiwei. Study on Safety Risk Assessment Methods of ERP Systems [A]. Proceedings of 2010(Shenyang) International Colloquium on Safety Science and Technology[C].Northeastern University: Center for Safety Engineering, Northeastern University,2010(4):50-53.
- [16] Zheng Ziqiu, Zhang Weidong, Liu Ning, Fu Qixuan, Yin Xingkang, He Hongmei. Application of Information Security Technology in enterprise ERP system [J]. Science and Technology Innovation and Application.2019(18):174-176.
- [17] Sengupta Shubhashis, Kaulgud Vikrant,Sharma Vibhu Saujanya. Cloud Computing Security–Trends and Research Directions. Proceedings - 2011 IEEE World Congress on Services, SERVICES 2011(20):524-531.

Appendix

Standard number	Standard name
1 ISO/IEC 19086-4:2019	Cloud computing-Service level agreement (SLA) framework-Part 4: Components of security and of protection of PII
2 ISO/IEC 27009:2016	Information technology-Security techniques-Sector-specific application of ISO/IEC 27001-Requirements
3 ISO/IEC 27017:2015	Information technology-Security techniques-Code of practice for information security controls based on ISO/IEC 27002 for cloud services
4 ISO/IEC 27018:2019	Information technology-Security techniques-Code of practice for protection of personally identifiable information (PII) in public clouds acting as PII processors
5 ISO/IEC 27036-4:2016	Information technology-Security techniques-Information security for supplier relationships-Part 4: Guidelines for security of cloud services
6 ISO/IEC TR 23108:2018	Information technology-Cloud computing-Framework of trust for processing of multi-sourced data
7 ISO/IEC 9594-8:2017	Information technology-Open Systems Interconnection-The Directory-Part 8: Public-key and attribute certificate frameworks
8 ISO 22381:2018	Security and resilience-Authenticity, integrity and trust for products and documents-Guidelines for establishing interoperability among object identification systems to deter counterfeiting and illicit trade
9 GA/T 1345-2017	Information security technology-Security technical requirements for cloud computing network intrusion prevention system
10 GA/T 1346-2-17	Information security technology-Security technical requirements for cloud operating system
11 GA/T 1347-2017	Information security technology-Security technical requirements for cloud storage system
12 GA/T 1348-2017	Information security technology-Security technical requirements for desktop cloud system
13 GA/T 1393-2017	Information security technology-General requirements for classified protection of cyber security-Part 2: Special security requirements for cloud computing
14 GA/T 1527-2018	Information security technology-Security technical requirements for cloud computing security comprehensive defense products
15 GB/T 31167-2014	Information security technology-Security guide of cloud computing services
16 GB/T 31168-2014	Information security technology-Security capability requirements of cloud computing services
17 GB/T 34080.1-2017	Security specification of electronic government common platform based on cloud computing-Part 1: General requirements
18 GB/T 34080.2-2017	Security specification of electronic government common platform based on cloud computing-Part 2: Information resources security
19 GB/T 34942-2017	Information security technology-The assessment method for security capability of cloud computing service
20 GB/T 34982-2017	Cloud computing data center basic requirement
21 GB/T 35279-2017	Information security technology-Security reference architecture of cloud computing
22 GB/T 35301-2017	Information technology-Cloud computing-Platform as Service(PaaS)j reference architecture
23 GB/T 36326-2018	Information technology-Cloud computing-General operational requirements of cloud service
24 GB/T 37739-2019	Information technology-Cloud computing-Platform as a service deployment requirements
25 GB/T 37740-2019	Information technology-Cloud computing-Guide for applications and data migration between cloud platforms
26 GB/T 37950-2019	Information security technology-Security technical requirements for desktop cloud
27 GB/T 37956-2019	Information security technology-Technology requirement for website security cloud protection platform
28 GB/T 37972-2019	Information security technology-Operation supervision framework of cloud computing service
29 GB/T 38249-2019	Information security technology-Security guide of cloud computing services for government website
30 GB/T 26327-2010	Implementation guide for enterprise informatization system integration
31 DB13/T 3000-2019	Information security technology-E-government cloud security protection technology and management norms
32 DB37/T 3304-2018	Information security technology-Cloud computing operation and maintenance security management specifications
33 DB44/T 1342-2014	Information security technology-Cloud computing operation and maintenance security management specifications
34 JR/T 1167-2018	Information security technology-Cloud computing operation and maintenance security management specifications
35 SJ/T11293&T2003	Technical specifications for enterprise informatization-Part 1: Enterprise resource Planning system (ERP) specifications
36 YDB 156-2015	Security baseline requirement of cloud computing
37 YD/T 3148-2016	Security framework for cloud computing
38 YD/T 3157-2016	Security protection requirements for public cloud service
39 YD/T 3158-2016	Security protection test requirements for public cloud service

Personalized Mobile Information Recommendation Based on Fine-Grained User Behaviors

YILEI WANG ^a, XUEQIN CHEN ^{a,1,2}

^a*College of Mathematics and Computer Science, Fuzhou University, Fuzhou
350108, China*

Abstract. At present, the enthusiasm of users to score actively in mobile information recommendation system is generally poor. Moreover, the existing research works rarely start with the analysis of fine-grained reading behaviors of mobile terminal users, but mostly based on the analysis of reading content and the improvement of model. It is difficult to find out the objective, short-term and local behavioral preferences of users. To solve the above problems, we propose six kinds of explicit fine-grained reading behaviors and integrate them into the user reading interest model to form the SVR-ALL model. The effectiveness of these six fine-grained behaviors is verified by ablative experiments. On the basis of SVR-ALL model, four implicit fine-grained reading behaviors are further mined by considering the difference of user reading habits, and then propose the user reading preference model called F-AFC. The updating mechanism for user preference designed in F-AFC can fully reflect the changes of users' reading habits in different periods. Experiments show that the accuracy of the user interest model considering user's reading preference and its update can be improved to some extent.

Keywords. fine-grained reading behavior, user reading interest model, user reading behavior preference model

1. Introduction

At present, the service mode of the information push application is centered on the mobile Internet. And the intelligent mobile terminal device is the main carrier of information in the mobile Internet environment[1]. However, the traditional user personalized information acquisition method in the Internet era cannot be directly transplanted to the mobile terminal[2,3].

Meng Xiangwu et al. [4] proposed that the disadvantages of mobile devices lie in poor input ability and small screen size, and the explicit scoring method adopted by users in the process of reading has a certain impact on user experience. Therefore, the implicit

¹Corresponding Author: Xueqin Chen, College of Mathematics and Computer Science, Fuzhou University, Fuzhou 350108, China; E-mail: 714867833@qq.com.

²Fund Project: Project supported by the Natural Science Foundation of Fujian Province, China(Grant No. 2018J01799). Personalized mobile information recommendation integrating fine-grained user behavior and privacy protection.

scoring method should be adopted in the acquisition, that is, there is no need for users to make additional operations for scoring. Xu Hailing et al. [5] proposed that the acquisition of users' reading behavior can be obtained from the frequency of users' reading pages, explicit score and the time stayed on the page. By introducing more detailed object characteristics and more precise user preferences, the accuracy of predicting user ratings would also be higher. Ming Z et al. [6] analyzed the diversified purchasing behaviors of users before online shopping and confirmed the critical shopping behaviors that determine the precursors of purchases by adopting the 5-fold cross verification method. Meng W et al. [7] proposed a novel session-based recommendation(SR) model MKM-SR, which incorporates user micro-behaviors and item knowledge into multi-task learning for SR, thus improving the recommendation accuracy. The above researches fully demonstrate that the discussion of more detailed and precise behaviors of users can effectively improve the accuracy of recommendation. "Fine-grained" is often used to represent further subdivision of an object[8,9,10], we use the term to refer to more granular user behaviors.

Due to the rapid development of machine learning, most scholars tend to focus on the modeling of complex models and the mining of users' implicit behaviors. Zhou C et al. [11] proposed an attention based user behavior modeling framework called ATRank, which is dedicated to modeling heterogeneous user behaviors with Multi-headed attention. Feng Y et al. [12] proposed a new framework named Adaptive Target-Behavior Relational Graph network(ATBRG) to effectively capture structural relations of target user-item pairs over knowledge graph. Minh-Duc Nguyen et al. [13] proposed a mixture model based on variational autoencoder, which is dedicated to mining users' hidden interests and discovering users' invisible behaviors. Although these studies have indeed improved the performance and accuracy of recommendation, they neglected to explore the fine-grained behavior of users.

Claypool M et al. [14] proposed that when acquiring user interest can according to the length of time that user browsing a certain page and the time spended on dragging the page with mouse. [15] showed that the user's accurate points of interest can be obtained by getting the user's average reading speed and time. But none of the above documents showed how to quantify users' reading interest based on various types of behavior data. Teng Y et al. [16] calculated users' interest based on the statistical relationship between the user's average active rating and operation behavior. This method has a better effect than others, but its accuracy is still poor. Claypool M et al. [14] took into account the influences of different reading behaviors of users, and proposed a model calculating users' interest based on their behaviors. But it is only applicable to the calculation and analysis of users' web browsing behaviors on the desktop computer.

The operation mode of the mobile terminal is completely different from that of the computer. There are also big differences in the format of the information and how the page is displayed. As a result, the users' reading behaviors on the mobile terminal and on the computer terminal are quite different[17]. Therefore, the existed analysis of the users' reading behaviors cannot be directly used in the mobile-side recommendation system.

We aim to study a personalized mobile information recommendation model based on fine-grained user behaviors. The main contributions of this paper are summarized as follow:

In order to explore the objective short-term and local behavioral preferences of users, we propose six kinds of explicit fine-grained reading behaviors and integrate them into

the user reading interest model to form the SVR-ALL model. The effectiveness of the proposed six explicit fine-grained user reading behaviors is proved by ablation experiments. Based on the users' reading interest model and considering the different reading habits of different users, four implicit fine-grained user reading behaviors are further explored. A user reading behavior preference model named F-AFC is established. We also design a reasonable updating mechanism for the user's reading preference model, and further improves the accuracy of the model through continuous iteration in the updating process.

The remainder of this paper is organized as follows. In Section 2 the related work is presented. Section 3 illustrates the proposed user reading interest model and user reading behavior preference model. The experimental studies are presented in Section 4. Finally, Section 5 concludes the paper.

2. Related Works

2.1. Support Vector Regression Model(SVR)

The basic idea of regression is to determine a function that accurately approximates the target values using the input value[18]. Support Vector Regression(SVR) model is obtained by introducing loss function in Support Vector Machine(SVM) and expanding it[19]. There are two major training strategies for SVR. One is ε -SVR, which employs an ε -insensitive loss function to solve the quadratic optimization problem. Another training strategy is called v -SVR[20], and the parameter v can effectively control the number of support vectors. In this paper, we adopt the first strategy ε -SVR for the subsequent related work.

2.2. Volatility of Reading Behavior

In order to avoid the burden of frequent updating of the model, we propose the Volatility of Reading Behavior(VRB). VRB refers to the change of a certain behavior b_j of user u_i in a certain period of time compared with its historical state. The formula is as follows:

$$VRB_{i,j,T} = \frac{1}{n_{i,j,T}} \sum_{t \in T} \frac{|X(u_i, b_j, t) - \overline{X}(u_i, b_j)|}{X(u_i, b_j)}, 1 \leq j \leq m \quad (1)$$

Where T is the update time window of model; $VRB_{i,j,T}$ represents the volatility of behavior b_j of user u_i in time period T; $n_{i,j,T}$ represents the actual times that behavior b_j of user u_i happened in time period T; $\overline{X}(u_i, b_j)$ is the average b_j behavior of user u_i calculated based on historical data, and the statistical cut-off is the last global update; $X(u_i, b_j, t)$ is the behavior value of b_j uploaded by user u_i at time t.

2.3. Coulomb's Law

In the early days, Marin L et al. [21] innovatively introduced a physical concept - Coulomb's law in user preference parameter learning. Recently, Haixin Z et al. [22] proposed a new method to calculate the fractal dimension of complex networks. Lai Y et

al. [23] proposed the concept of coulomb's law of urban traffic to model the relationship between urban taxis and passengers, and on this basis proposed a path recommendation scheme for taxis and passengers as positive and negative charges. Inspired by the above research, we introduce Coulomb's law into the F-AFC model for weight updating, and the details will be explained in the section 3.2.2.

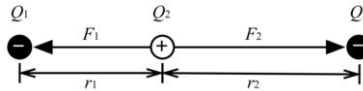


Figure 1. Coulomb's law diagram

Figure 1 shows the distribution of charges at three fixed points on a straight line in a vacuum environment. The charges are represented by Q_1, Q_2, Q_3 , and the corresponding electric quantities of them are represented by q_1, q_2, q_3 . The following formula can be used when calculating the resultant force of charges:

$$F_e = F_1 - F_2 = k_e \frac{q_1 q_2}{r_1^2} - k_e \frac{q_1 q_2}{r_2^2} \quad (2)$$

k_e in Eq.(2) represents the Coulomb constant[24].

3. The Proposed Method

3.1. User Reading Interest Model

Taking the user reading on the mobile terminal as the research background, the reading behaviors is generated under the guidance of user interest preferences[25]. Therefore, the users' reading behaviors can make the most direct reflection on the their information needs and reading preferences, and also reflect the users' reading interest to a large extent.

3.1.1. Mobile Fine-grained User Reading Behavior Data Acquisition

Compared with the computer, the amount of user behavior generated by mobile devices is much larger. Fine-grained behavior means that more reasonable and scientific behavior objects can be generated by subdividing user behavior objects. For example, the scrolling behavior that superficially displays the users' browsing information can form a series of objects after the scrolling behavior is subdivided. Including the scrolling displacement and the scrolling duration. This behavior can directly express the user's reading preferences.

After analysis, we mainly collected and pre-processed fifteen kinds of fine-grained user behaviors of mobile terminals. Some of them are shown in Table 1.

Table 1. Fine-grained user behaviors collected

Symbol	Meaning
<i>readCmp</i>	Page read completeness
<i>dragCnt</i>	Number of effective page drags
<i>meanV(msg)</i>	User's average reading speed on a page
<i>meanV(u)</i>	User's average reading speed
<i>scrollPt</i>	The point in time when the page first scrolled
<i>loadedPt</i>	The point in time at which the page is loaded
<i>slContentOffset</i>	The displacement of a page generated by one slide

(1) User reading time

User reading time is a key content to measure user interest and it can't be equal to the time user staying on the page. Therefore, we consider the following factors when calculating this item:

1) Starting point for reading time

In addition to the text content, the page of mobile terminals often has objects such as pictures or emoticons. Due to the differences in the hardware and software configuration of each mobile device, there will inevitably be differences in the loading speed of each page. And most users have already started reading the content of the page without loading all the content. So, accumulating immediately after the user enters the page is improper.

Generally, comparing the height of the information content with the height of the reading area of the mobile terminal screen. When the former is higher than the latter ($contentHt > readZoneHt$), the user-generated page scrolling behavior indicates that the user has read part of the content and continues reading. So the starting point of reading time set to be the time that first scrolling behavior happened minus the time spent scrolling the page. When $readZoneHt > contentHt$, we use the first two formulas in Eq.(3) to compute the starting point of reading time:

$$startPt = \begin{cases} 0.5, & contentHt \leq readZoneHt \text{ and } u \text{ is a new user} \\ meanPt(u), & contentHt \leq readZoneHt \text{ and } u \text{ is not a new user} \\ scrollPt - Time(scroll), & contentHt > readZoneHt \end{cases} \quad (3)$$

Where $Time(scroll)$ represents the time required for page scrolling and $meanPt(u)$ represents the average value of the starting point of reading time of user u on each page.

2) Reading time pause

The user may has a sudden state during actual reading and the reading page is shelved for a long period of time. When the system detects that the user has not operated the terminal screen for more than a certain period of time, the user is deemed to have suspended reading, and the length of time before the user resumes reading should not be counted as the user's reading time. The timeout threshold is set to the average time the user u needs to read text at the height of $readzoneHt$:

$$threshold(msg) = readzoneHt(msg)/meanV(u) \quad (4)$$

Where $readzoneHt$ represents the height of the reading area of the mobile terminal screen, $meanV(u)$ represents the average reading speed of the user.

(2) Page reading completeness

Whether a user has read a certain page completely can reflect the user's level of interest. This parameter can be obtained simply by determining whether the page is scrolled to the bottom. In the case that the $contentHt(P)$ of the page height is less than the height of the readable area $readHt$ that can be displayed on the screen, if the user's reading duration $t(P)$ reaches the operation timeout threshold $ths(P)$, the page reading completeness set to be "1". However, in the vast majority of mobile information push systems, the tail of most pages contains extended reading and advertisements. In this case, the page may not be scrolled to the end. Therefore, so long as the page is scrolled to reaches a certain page ratio, the user is considered to have read it completely.

(3) Effective number of page drags

Due to the large screen size of traditional desktop computers, users only need to swipe a few times to read the entire content. Therefore, in the process of calculating users' Web page reading time, the impact of sliding/dragging pages is generally ignored. At present, most pages of the mobile terminal are in the form of "scroll", which is limited by the screen size. The user needs to drag the finger on the page multiple times when reading on the mobile device.

Users' behaviors of scrolling the page includes dragging and sliding. Dragging means the pages will stop rolling after the finger leave screen. Sliding means pages will keep rolling for one to two seconds after the finger leave screen. The former action reflects the user's slow reading speed or high concentration, while the latter reflects the user is browsing the page hastily.

We record the drag behavior generated by the page, including the start time of the behavior, the displacement $drContentOffset$ generated by the page during the drag, and the end time $drEndTime$ of the behavior. The meaningful drag behavior of the page should be close to the average reading speed of the user, so the actual drag time is obtained by using the ratio between the average reading time of the user and the displacement of the content information. So, if the time interval between the two dragging actions before and after the dragging threshold is lower than the dragging threshold, they can be combined into one "effective dragging operation":

$$scrollThs_i = drContentOffset_{2i+1}/meanV(u), \quad i = 1, \dots, n \quad (5)$$

Where $scrollThs_i$ means that the i -th group continuous page dragging behavior produces a corresponding drag threshold. Using Eq.(5), the user's drag time series is corrected to obtain the number of effective drag operations during the user's reading process.

(4) Effective number of page slides

Taking the iOS operating system as an example. When acquiring the user's sliding page behavior, determine whether the page is a decelerated sliding based on the parameter $decelerate$ generated by the user's finger touching and leaving the screen. We collect and use the following data: sliding page start time $slStartTime$, information page displacement distance $slContentOffset$ and sliding page end

time $slEndTime$. The calculation of the number of slides is similar to the drag operation, and the "effective operation" must also be judged.

(5) Number of user reviews

The retrospective behavior means that the user adopts the reverse continuous mode when quickly dragging the page, so that the page can be scrolled to a certain position that has been read in the shortest time. The number of reviews can intuitively indicate the user's preference for information. We find the following rules by analyzing the drag behavior and sliding behavior. During the user's search for the location, multiple drag behavior and sliding behavior will be generated. The above mentioned continuous behavior does not have any meaning and is regarded as an "effective operation". However, the information that the user sees during the review process is the information that has been browsed, so all the content of the information before reaching the target position is not meaningful. So after analyzing a large number of test data, we set 0.45s as the threshold of review time.

(6) Average reading speed

We divide the average reading speed into the average speed of reading page and average reading speed of user.

1) Average speed of reading page

The average speed of reading page $meanV(msg)$ represents the average speed of a user reading a page. The same user will have different average speeds on different pages. In Eq.(6), when the height of the reading area is greater than the height of the information, the average speed of the reading page is the ratio of the height of the information to the total length of the time the user use in reading the information; while when the height of the reading area is less than the height of the information, the user must have a drag or slide operation. The average speed of the "effective operation" generated by the user's continuous forward reading is summed, and the average value is further calculated as the average speed of reading the page.

$$meanV(msg) = \begin{cases} \frac{contentHt(msg)}{readTime(msg)}, & contentHt \leq readZoneHt \\ \frac{1}{n} \sum_{i=1}^n \frac{contentOffset_i}{Time(contentOffset_i)}, & contentHt > readZoneHt \end{cases} \quad (6)$$

Among them, n represents the number of "effective operations" generated by continuous forward reading, $contentOffset_i$ represents the actual page scrolling displacement distance in the i -th "effective operation", and $Time(contentOffset_i)$ represents the time required for the i -th "effective operation" to scroll the page.

2) Average reading speed of user

This parameter is expressed by $meanV(u)$, which refers to the average value of all $meanV(msg)$ sums generated by user u in all the content read. It can be calculated by Eq.(7):

$$meanV(u) = \frac{1}{m} \sum_{i=1}^m meanV(msg_i) \quad (7)$$

Where m represents the amount of all reading information of user u .

3.1.2. User Reading Interest Modeling

We conduct a statistical analysis of fine-grained user reading behavior and find that there is a linear relationship between multiple fine-grained reading behavior and the user's reading interest score. Considering the sample distribution characteristics of the regression model, data approximation accuracy and limited sample optimization issues. Therefore, support vector regression model (SVR) is used for subsequent experiments.

After all the sample sets are trained, SVR can calculate the predicted value by Eq.(8):

$$f(x) \equiv \sum_{i=1}^n \omega_i \phi(x, x_i) + b \quad (8)$$

In this paper, the values of all support vector regression models are calculated separately, and the average value is calculated after completion. This can make the generated values more reliable:

$$\begin{aligned} b = & \frac{1}{N_{SVR}} \left\{ \sum_{0 < \alpha_i < C} \left[y_i - \sum_{x_j \in SVR} (\alpha_j - \alpha_j^*) x_j \cdot x_i - \varepsilon \right] \right. \\ & \left. + \sum_{0 < \alpha_i^* < C} \left[y_i - \sum_{x_j \in SVR} (\alpha_j - \alpha_j^*) x_j \cdot x_i + \varepsilon \right] \right\} \end{aligned} \quad (9)$$

N_{SVR} in Eq.(9) is the number of support vector models.

3.2. User Reading Behavior Preference Model

The definition of the user reading behavior preference represents the personalized operation behavior and habits of the user when reading. Analysis of the current user behavior data obtained through normalization processing shows that different users have different reading behavior preferences.

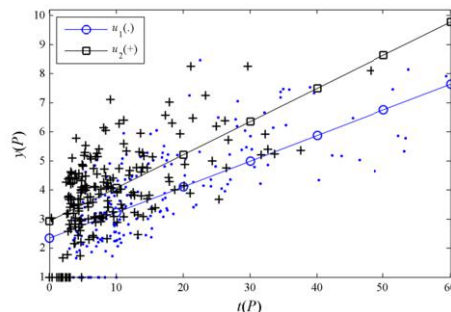


Figure 2. Differences in the linear relationship between reading time and interest score of two users

Figure 2 shows that in a short and same period of time, different users have different reading behavior preferences. For example, under the same $t(p)$, the score corresponding

to user u_1 is significantly lower than the score of user u_2 . The larger $t(p)$ is, the more gradually the rating gap between the two users increases. So, using the same regression equation to calculate the reading interest of different users is less effective. Therefore, considering different reading preferences of users and establishing corresponding preference models can further improve the accuracy of calculating user interest.

3.2.1. Establishment of User Reading Behavior Preference Model

(1) Representation of the preference model

We use Eq.(10) to express user reading behavior preference[26,27]:

$$\{(behavior_1, weight_1), (behavior_2, weight_2), \dots, (behavior_m, weight_m)\} \quad (10)$$

Where $behavior_j (1 \leq j \leq m)$ represents the user's reading behavior, m represents the specific number of behavior types, and $weight_j (1 \leq j \leq m)$ represents the preference weight corresponding to the behavior $behavior_j (1 \leq j \leq m)$.

Use the multivariate group in Eq.(11) to represent the user reading behavior preference model.

$$M = \{u_i, B, W\} \quad (11)$$

Where u_i represents user, $B = \{behavior_1, behavior_2, \dots, behavior_m\}$, which is the fine-grained user reading behavior vector, and $W = \{weight_1, weight_2, \dots, weight_m\}$ represents the preference weight vector corresponding to the reading behavior in B .

After calculation, the reading interest degree $\hat{y}(P)$ generated on page P is obtained. The formula is as follows:

$$\hat{y}(P) = X^{(P)} \cdot W \quad (12)$$

Where $X^{(P)} = (x_1^{(P)}, x_2^{(P)}, \dots, x_m^{(P)})$ represents the corresponding vector of each fine-grained user reading behavior value generated on page P .

(2) Determination of implicit behavior

We divides fine-grained user behavior into two categories, explicit and implicit, according to the relationship between the user's reading interest and reading behavior. If the user's reading interest score and some fine-grained user behaviors show a significant or less obvious potential relationship, they are classified as explicit behaviors, such as the six explicit behaviors mentioned in Section 3.1.1. Otherwise, it is implicit behavior.

Based on experimental verification and data analysis, we propose four implicit fine-grained reading behaviors: delete page operation(del), page repeat reading(rp), page collection(cl), and page content copy(cp) and add to user reading behavior preference model. The fine-grained user reading behavior vector after adding these four implicit behaviors can be expressed as:

$$B = (\text{readTime}, \text{readHt}, \text{meanV}, \text{dragCnt}, \text{slideCnt}, \text{reviewCnt}, \text{del}, \text{cl}, \text{rp}, \text{cp}) \quad (13)$$

(3) Establishment of preference model

The establishment of the user reading behavior preference model M means that after the behavior vector B is determined, the initial value corresponding to the preference weight vector is selected. In the process of calculating the implicit user reading behavior preference weight, we use the establishment of a linear regression model to determine the residuals of the support vector regression model. Using this regression model, the behavior preference weights of all users are set to a uniform initial value. In the process of continuously updating the user model, each parameter corresponding to the reading preference model of different users will increasingly reflect the user's own real reading habits.

Eq.(14) represents the quaternary linear regression model composed of the residuals and $\{del, cl, rp, cp\}$ in the support vector regression model. The linear regression model uses the residuals corresponding to each set of data in subsequent support vector regression experiments as its dependent variable.

$$r_{R-4}(P) = a_5 \cdot del + a_6 \cdot cl + a_7 \cdot rp + a_8 \cdot cp + \delta \quad (14)$$

3.2.2. User Reading Behavior Preference Model Update

The update of the user reading behavior preference model is to make the model fully reflect the change of the user's reading habits under the change of time, and make the model more accurate in predicting the user's reading interest.

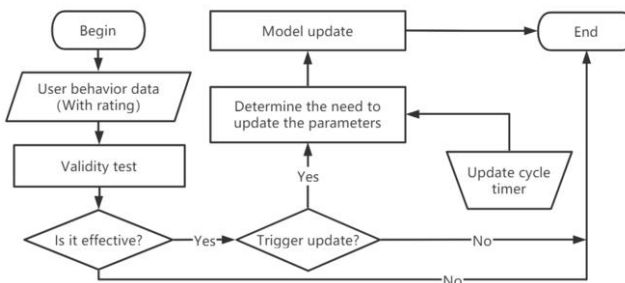


Figure 3. Flowchart of updating user reading behavior preference model

In this paper, the two strategies of system global update and update time window are applied to the update of the preference model at the same time. The update method is shown in Figure 3. When the newly added effective data reaches a certain amount, the user reading interest model based on the support vector regression model is rerun, and the user preference model is reanalyzed and adjusted based on the data generated by the model. Considering that a large number of users in the recommendation system are accustomed not to submit reading scores actively for a long time, the preference model adds a periodic timer in updating process to start mandatory updates. This avoids that the model cannot be updated effectively for a long time.

(1) Trigger condition for update

In this paper, the trigger conditions for model update are set as follows. For all users, when the error value $|\hat{y}(P) - y(P)|$ reaches a certain range compared with

the mean $\bar{r}_{SVR-ALL}$ of the residual value of the historical support vector regression model, the model update can be triggered. The formula is shown below:

$$|\hat{y}(P) - y(P)| \geq \alpha \cdot \bar{r}_{SVR-ALL} \quad (15)$$

Where the α is set to 1.3 on the basis of the experiment; $\bar{r}_{SVR-ALL} = \frac{1}{n} \sum_{i=1}^n |r_i|$, r_i represents the residual of each group of data in the SVR model experiment.

(2) Determine update parameters

The change of user reading behavior preference lies in the overall change or the change of a certain behavior habit. Both of the above cases need to evaluate all the behavior parameters one by one and judge whether they need to be adjusted to effectively update the model. For the change of the corresponding user preference model caused by time changes, Shi Yancui et al. [28] proposes a new concept, called behavior volatility, which is used to quantify the change of user behavior.

Changes in user behavior habits will increase the volatility. When it exceeds a certain threshold, the user preference model should be updated. We set the volatility threshold $VRB_{j,ths}$ for all fine-grained user behaviors. If $VRB_{i,j,T} > VRB_{j,ths}$, that is, the behavior b_j of the user u_i has changed greatly, resulting in the volatility corresponding to the behavior exceeding the threshold. At this time, the weight ω_j corresponding to the behavior b_j should be updated. The setting of $VRB_{j,ths}$ is related to factors such as system load, operating capacity, and computing power. For example, the system configuration is low and the computing resources are insufficient. In this case, the volatility threshold corresponding to certain behaviors can be slightly increased to reduce the frequency of model updates and ensure the normal operation of the system.

(3) Law of behavioral forgetting

Usually the speed of human forgetting is proportional to time, and after a certain period of time, only a small part of memory remains. Although the characteristics of human behavior habits and human memory content are not exactly the same, they also have the law of forgetting[29,30,31,32]. Ming-Sheng S et al. [33] proposes a human behavior dynamics model.

In order to better achieve the simulation of the forgetting rules of user reading behavior preference, we make appropriate modifications to the model based on the characteristics of the mobile information recommendation system based on the theory of [33]. The formula is shown as Eq.(16):

$$w'_j(t') = \frac{\alpha}{\beta + (t' - t)} w_j(t) \quad (16)$$

Where $w'_j(t')$ represents the new preference weight updated at time t' , $w_j(t)$ represents the value generated by updating the weight at time t , or the corresponding preference weight value may be generated according to the initial settings, and α and β are forgetting parameters, respectively.

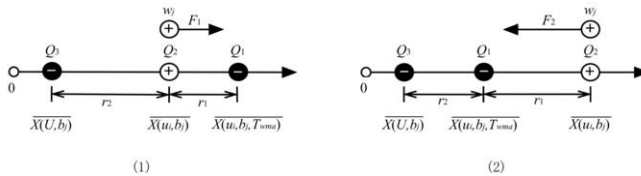


Figure 4. Schematic diagram of the relationship between Coulomb's law and user behavior

(4) Weight update function

As shown in Figure 4, we refer to Coulomb's law and regards the average value $\bar{X}(u_i, b_j, T_{wma})$ of the behavior b_j of the user u_i in the time window T_{wma} of the preference model update as the charge Q_1 . The historical average value $\bar{X}(u_i, b_j)$ of the behavior b_j of the user u_i as the charge Q_2 . The charge Q_3 is the average $\bar{X}(U, b_j)$ of b_j behavior of all users. The "resultant force" received by "charge" is mapped to the preference weight value ω_j corresponding to the b_j behavior of user u_i , showing the update mode used by ω_j .

A large change in the "resultant force F_e " experienced by the charge Q_2 means that the user has a large deviation in behavior preference within the model update time window T_{wma} , and the credibility of this change is low. In this case, preference weights should not be adjusted significantly. The small drift of preference will result in a small change in the resultant force. In this case, the credibility of the change is higher. Therefore, we divide the user's behavior change into two "directions". "Forward" means getting closer to the average of all users' behavior, and "reverse" means moving away from the average. When users change their behavior habits in the "forward" direction, we believe that the adjustment range of their behavior preferences should be greater than the "reverse" situation.

3.2.3. F-AFC Model Based on the Forgetting Law of User Behavior Preference

Based on the above analysis, we propose a user reading behavior preference update model named F-AFC based on the user behavior preference forgetting law.

$$\begin{aligned} \omega'_{i,j} &= f_{AFC}(u_i, b_j, \omega_j, t_{trig}, t_j) \\ &= f(t_{trig}, t_j) \cdot \omega_j - (1 - f(t_{trig}, t_j)) \cdot k(b_j) \cdot \left(\frac{d_1}{r_1^2(b_j)} - \frac{d_2}{r_2^2(b_j)} \right) \end{aligned} \quad (17)$$

Where ω_j is the preference weight corresponding to the behavior b_j of the user u_i, t_j is the previous update time of ω_j , $\omega'_{i,j}$ is the updated value of $\omega_j, t_{\text{trig}}$ is the time when the update is triggered in the model update window T_{wma} , and $f(t_{\text{trig}}, t_j) = \frac{\alpha}{\beta + (t_{\text{trig}} - t_j)}$ is the forgetting function. $k(b_j)$ is the weight coefficient corresponding to behavior b_j . d_1 and d_2 are the behavior fluctuation proportion coefficient, which are used to adjust the behavior fluctuation relationship to determine the weight update direction. And set the upper limit $r_{\max 1}(b_j), r_{\max 2}(b_j)$ and the lower limit $r_{\min 1}(b_j), r_{\min 2}(b_j)$ in $r_1(b_j)$ and $r_2(b_j)$ to avoid small fluctuations in behaviors that result in large-scale updating of behavioral weights, or behavioral weights cannot be effectively updated after substantial changes in behaviors.

We use the following six-tuple to represent the user reading behavior preference update model F-AFC considering the user's fine-grained behavior forgetting laws.

$$F - AFC = \{u_i, B, W, \bar{X}, T, f_{AFC}\} \quad (18)$$

Where B is the behavior vector of user u_i , W is the preference weight corresponding to each behavior in B , $\bar{X} = (\bar{x}_j : \bar{x}_j = \bar{X}(u_i, b_j) \wedge 1 \leq j \leq m)$ is the historical average value of each behavior in B , $T = (t_1, t_2, \dots, t_m)$ is the update time corresponding to each behavior preference weight in $F - AFC$ model, and f_{AFC} is the preference weight update function in Eq.(17).

4. Experiments and Analysis

4.1. User Reading Interest Modeling

4.1.1. Experimental Data and Environment

The real fine-grained data of user reading behavior is used as the data in the experiment to ensure that the experimental results are accurate and effective. A total of 1537 pieces of information are selected, and the number of users is 116. The number of fine-grained reading behaviors with explicit reading interest rating of users is 18013. Set up the experimental environment: Intel Core™ i5-4570 CPU 3.20 GHz processor; 8 GB memory. Table 2 lists the data format information of some users' fine-grained behaviors.

Table 2. User behavior data table

Symbol	user 1	user 2	user 3
<i>topicID</i>	1	2	3
<i>readTime(s)</i>	23.65	47.82	12.10
<i>readCmp</i>	1	0.3	1
<i>meanV(row/min)</i>	20.13	28.34	5.49
<i>dragCnt(time)</i>	4	8	5
<i>slideCnt(time)</i>	6	12	7
<i>reviewCnt(time)</i>	1	2	0
<i>rating</i>	5	8	5.5

4.1.2. Experimental Results and Analysis

We propose a variety of explicit fine-grained reading behaviors of different mobile terminals, including user reading time, page reading completeness, effective number of page drags, effective number of page slides, number of user reviews and average reading speed. In this paper, by selecting two, three, four and six independent variables from six different explanatory variables, the corresponding binary model (SVR-2), ternary model (SVR-3), quaternary model (SVR-4) and six-metamodel (SVR-ALL) are established. Based on three indicators: average absolute error (MAE), goodness of fit (R^2) and accuracy (precision), the regression models using partial fine-grained user reading behavior and all fine-grained user reading behavior are compared.

Figure 5 shows the experimental results of four support vector regression models under the evaluation of goodness of fit R^2 . After considering more fine-grained reading behaviors, the regression model's goodness of fit R^2 is even better. What's more, it can be seen that the results of the goodness of fit R^2 of the four support vector regression models are all higher than 0.7. In particular, the R^2 of SVR-ALL, which takes into account all fine-grained reading behavior, is closer to 0.8, which fully reflects the advantages of the model in representing the relationship between user's reading interest and fine-grained reading behaviors.

Figure 6 shows the MAE results of four different support vector regression models. Under the four vector regression models, the results are all less than 0.9. The optimal one is the SVR-ALL curve, whose final MAE value is close to 0.6.

The accuracy rate curve shown in Figure 7 shows an upward trend, and the absolute error has the highest accuracy when $\epsilon = 1$. Keep other conditions invariant, with the continuous introduction of six kinds of explicit fine-grained reading behaviors (from SVR-2 to SVR-ALL), the accuracy of the model is also constantly improving. The experimental results fully demonstrate the effectiveness of the six behaviors. It also shows that the regression analysis can explain the functional relationship between user reading interest and fine-grained reading behaviors.

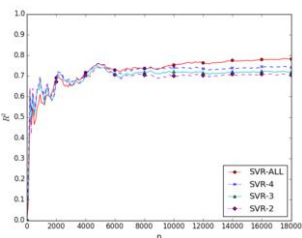


Figure 5. Goodness of fit of SVR model at Multiple data scales

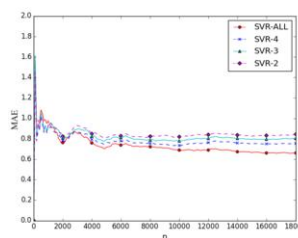


Figure 6. The average absolute error of the SVR model at various data scales

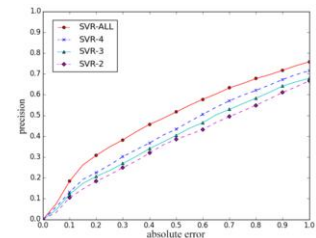


Figure 7. Accuracy of SVR model under different absolute errors

4.2. User Reading Behavior Preference Model

4.2.1. Experimental Data and Environment

This section uses the same experimental conditions as 4.1 above, and the source of the user reading behavior data is also the same. The F-AFC model is trained according to the training set, and a personalized user reading behavior preference model is generated for all users. During training, the SVR-ALL experimental data is compared and analyzed, and then the test set is used to verify the validity of the F-AFC model.

In the process of training the F-AFC model, first initialize the user reading behavior preference model. Then set the global update cycle for ten days and run the F-AFC model. During the system operation, the user's reading preference model can be automatically updated to make the model more in line with the user's personalized characteristics. On the basis of the model obtained in the previous step, the test set is used to calculate the users' reading interest. The actual scores of users are compared, and the changes of accuracy and average absolute error are analyzed. Meanwhile, the experimental results displayed by SVR-ALL model are compared and analyzed.

4.2.2. Preference Model Parameter Setting

Table 3 lists the initial weight values of the implicit behavior preference model.

Table 3. Initial weight table of implicit fine-grained behavior preferences

	Page Delete	Page Collection	Page Repetition	Page Content Copy
Symbol	$del(P)$	$cl(P)$	$rp(P)$	$cp(P)$
Weight	-1.0936	2.0105	1.7087	1.3263

After a lot of experiments in this paper, the parameters of the F-AFC model are obtained. $\alpha = 25.5, \beta = 28.1, d_1 = 0.142, d_2 = 0.105$, The remaining parameters are shown in Table 4-7.

Table 4. Explicit fine-grained behavior volatility threshold table

b_j	b_1	b_2	b_3	b_4	b_5	b_6
Corresponding Behavior Name	Page Reading Time	Page Reading Completeness	Page Drag Times	Page Swiping Times	Review Times	Average Page Reading Speed
$VRB_{j,ths}$	0.06	0.026	0.12	0.083	0.054	0.023

Table 5. Implicit fine-grained behavior volatility threshold table

	b_1	b_2	b_3	b_4	b_5	b_6
$k(b_j)$	0.15	0.0014	0.0016	0.00093	0.0036	0.0279
$r_{\min 1}(b_j)$	0.18	0.08	0.32	0.28	0.14	0.36
$r_{\max 1}(b_j)$	1.5	0.2	1.1	2.2	0.26	1.03
$r_{\min 2}(b_j)$	0.18	0.05	0.23	0.31	0.15	0.28
$r_{\max 2}(b_j)$	2.0	0.15	1.2	2.2	0.28	1.15

Table 6. Corresponding parameters of explicit behavior in the F-AFC model

	b_1	b_2	b_3	b_4	b_5	b_6
$k(b_j)$	0.15	0.0014	0.0016	0.00093	0.0036	0.0279
$r_{\min 1}(b_j)$	0.18	0.08	0.32	0.28	0.14	0.36
$r_{\max 1}(b_j)$	1.5	0.2	1.1	2.2	0.26	1.03
$r_{\min 2}(b_j)$	0.18	0.05	0.23	0.31	0.15	0.28
$r_{\max 2}(b_j)$	2.0	0.15	1.2	2.2	0.28	1.15

Table 7. Corresponding parameters of implicit behavior in F-AFC model

	b_7	b_8	b_9	b_{10}
$k(b_j)$	0.0091	0.027	0.021	0.016
$r_{\min 1}(b_j)$	0.06	0.08	0.08	0.05
$r_{\max 1}(b_j)$	0.11	0.15	1.3	1.6
$r_{\min 2}(b_j)$	0.06	0.08	0.09	0.06
$r_{\max 2}(b_j)$	0.11	0.15	1.2	1.9

4.2.3. Experimental Results and Analysis

The experiment compares two models: SVR-ALL model and F-AFC model. Figure 8 shows the average absolute error of them. It can be clearly seen from the figure that when the data volume rises to 600 groups, the fitting error is significantly reduced. When the data volume rises to 3600 groups, the value tends to be stable, around 0.6 and the overall performance is more stable. Which indicate that the F-AFC model has a certain effect on improving the accuracy of the user's reading preference model.

Figure 9 compares the accuracy of the above two models in calculating user reading interest. The experimental results show that after running the F-AFC model, the accuracy is significantly increased. When the absolute error δ_{prc} is set to 0.5, the accuracy rate increases from approximately 0.4 to 0.5. When δ_{prc} is set to 1, the accuracy rate is improved from 0.71 to 0.88 .

The model is further tested by using the test data set. Figure 10 shows the average absolute error value before and after the F-AFC model is run. The results also show that the F-AFC model has certain advantages. Figure 11 shows the accuracy rate curve of the user's reading interest before and after the F-AFC model is run. It can be seen from the figure that after the F-AFC model is run and the accuracy of the predicted value also rises significantly. When the value of δ_{prc} is 0.5, the accuracy rate can reach 0.49. If the limit of δ_{prc} is relaxed to 1, the accuracy rate is about 0.86. The experimental results show that based on the SVR-ALL model, the four implicit fine-grained user reading behaviors are effective in improving the accuracy of user reading interest prediction. Moreover, on the basis of the former, the F-AFC model considering the updating mechanism of user preference has a certain improvement in recommendation performance and accuracy compared with the SVR-ALL model.

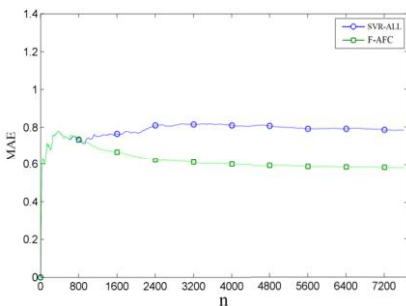


Figure 8. Comparison of average absolute error under two models

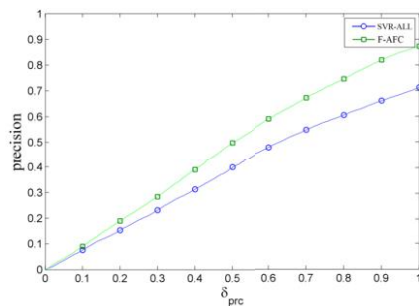


Figure 9. Comparison of accuracy under two models

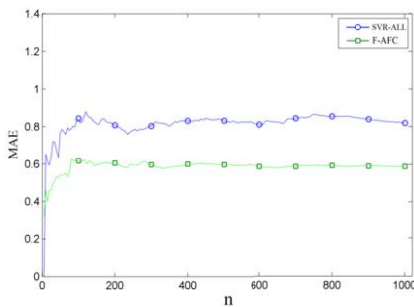


Figure 10. Comparison of MAE under test data

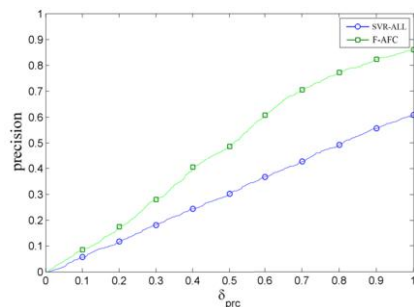


Figure 11. Comparison of accuracy under test data

5. Conclusions

In this paper, the normalization method of user's fine-grained behavior acquisition and preprocessing is studied for mobile information push system, which can carry out unified normalization and quantification of fine-grained user behavior. A support vector regression model is introduced to model the fine-grained user's reading behavior, and the relationship between fine-grained user reading behavior and user reading interest is successfully established. And the validity of the proposed six explicit fine-grained behaviors is verified by ablation experiments. On this basis, considering the different reading habits of different users, four implicit fine-grained behaviors are introduced and the corresponding updating mechanism is designed to establish and update the user reading behavior preference model. Experiments show that the change of the user's reading interest can be explained by the user's fine-grained reading behavior. The proposed preference modeling and updating method have a certain improvement effect on the accuracy of reading interest calculation of users.

References

- [1] Kwok R. Personal technology: Phoning in data. *Nature*, 2009, 458(7241): 959.
- [2] Roitman H, Carmel D, Mass Y, et al. Modeling the uniqueness of the user preferences for recommendation systems. In: Proceedings of the 36th international ACM SIGIR conference on Research and development in information retrieval. New York: ACM, 2013. 777-780.
- [3] Said A, Jain B J, Narr S, et al. Estimating the magic barrier of recommender systems: a user study. In: Proceedings of the 35th international ACM SIGIR conference on Research and development in information retrieval. New York: ACM, 2012. 1061-1062.
- [4] Meng X W , Hu X , Wang L C , et al. Mobile Recommender Systems and Their Applications. *Journal of Software*, 2014, 24(1):91-108.
- [5] Hai-Ling X U , Xiao W U , Xiao-Dong L I , et al. Comparison Study of Internet Recommendation System. *Journal of Software*, 2009, 20(2):350-362.
- [6] Zeng M, Cao H, Chen M, et al. User behaviour modeling, recommendations, and purchase prediction during shopping festivals. *Electronic Markets*, 2019, 29(2): 263-274.
- [7] Meng W, Yang D, Xiao Y. Incorporating user micro-behaviors and item knowledge into multi-task learning for session-based recommendation. In: Proceedings of the 43rd International ACM SIGIR Conference on Research and Development in Information Retrieval. 2020: 1091-1100.
- [8] Ma Q J, Ng C W W, Mašin D, et al. An approach for modelling volume change of fine-grained soil subjected to thermal cycles. *Canadian Geotechnical Journal*, 2017, 54(6): 896-901.

- [9] He X, Peng Y, Zhao J. Fast fine-grained image classification via weakly supervised discriminative localization. *IEEE Transactions on Circuits and Systems for Video Technology*, 2018, 29(5): 1394-1407.
- [10] Huang F, Wu W, Yang M, et al. A fine-grained permission control mechanism for external storage of android. *IEEE International Conference on Systems, Man, and Cybernetics (SMC)*. IEEE, 2016: 002911-002916.
- [11] Zhou C, Bai J, Song J, et al. Atrank: An attention-based user behavior modeling framework for recommendation. *arXiv preprint arXiv:1711.06632*, 2017.
- [12] Feng Y, Hu B, Lv F, et al. ATBRG: Adaptive Target-Behavior Relational Graph Network for Effective Recommendation. In: *Proceedings of the 43rd International ACM SIGIR Conference on Research and Development in Information Retrieval*. 2020: 2231-2240.
- [13] Nguyen M D, Cho Y S. A Variational Autoencoder Mixture Model for Online Behavior Recommendation. *IEEE Access*, 2020, 8: 132736-132747.
- [14] Claypool M, Le P, Wased M, et al. Implicit interest indicators. In: *Proceedings of the 6th international conference on Intelligent user interfaces*. New York: ACM, 2001. 33-40.
- [15] Liang T P, Lai H J. Discovering user interests from web browsing behavior: An application to internet news services. In: *Proceedings of the 35th annual Hawaii international conference on system sciences*. IEEE, 2002: 2718-2727.
- [16] Teng Y, He L. Rating prediction algorithm and recommendation based on user behavior in IPTV. In: *2012 2nd International Conference on Consumer Electronics, Communications and Networks (CEC-Net)*. Yichang: IEEE, 2012. 3373-3378.
- [17] Song Y, Ma H, Wang H, et al. Exploring and exploiting user search behavior on mobile and tablet devices to improve search relevance. In: *Proceedings of the 22nd international conference on World Wide Web*. 2013: 1201-1212.
- [18] Rho S, Han B, Hwang E. SVR-based music mood classification and context-based music recommendation. In: *Proceedings of the 17th ACM international conference on Multimedia*. 2009: 713-716.
- [19] Vohr, Hans-Werner. *Systemic Vascular Resistance (SVR)*. Springer Berlin Heidelberg, 2005.
- [20] Hao P Y. New support vector algorithms with parametric insensitive/margin model. *Neural Networks*, 2010, 23(1): 60-73.
- [21] Marin L, Isern D, Moreno A. Dynamic adaptation of numerical attributes in a user profile. *Applied intelligence*, 2013, 39(2): 421-437.
- [22] Zhang H, Wei D, Hu Y, et al. Modeling the self-similarity in complex networks based on Coulomb's law. *Communications in Nonlinear Science and Numerical Simulation*, 2016, 35: 97-104.
- [23] Lai Y, Lv Z, Li K C, et al. Urban traffic coulomb's law: A new approach for taxi route recommendation. *IEEE Transactions on Intelligent Transportation Systems*, 2018, 20(8): 3024-3037.
- [24] Nichols D M. Implicit Rating and Filtering. In: *Proceedings of the Fifth Delos Workshop on Filtering and Collaborative Filtering*, 1997:31-36.
- [25] Bu J, Tan S, Chen C, et al. Music recommendation by unified hypergraph: combining social media information and music content. In: *Proceedings of the 18th ACM international conference on Multimedia*. 2010: 391-400.
- [26] Salton G, Wong A, Yang C S. A vector space model for automatic indexing. *Communications of the ACM*, 1975, 18(11): 613-620.
- [27] Lin Hongfei, Yang Yuansheng. Representation and update mechanism of user interest model. *Computer Research and Development*, 2002, 39 (7): 843-847.
- [28] Shi Yancui, Meng Xiangwu, Zhang Yujie, etc. An adaptive learning method for contextual mobile user preferences. *Journal of Computers*, 2012, 23 (10): 2533-2549.
- [29] Matuszyk P, Vinagre J, Spiliopoulou M, et al. Forgetting techniques for stream-based matrix factorization in recommender systems. *Knowledge and Information Systems*, 2018, 55(2): 275-304.
- [30] Barabasi A L. The origin of bursts and heavy tails in human dynamics. *Nature*, 2005, 435(7039): 207-211.
- [31] Fan Chao, Guo Jinli, Han Xiaopu, etc. A review of studies on human behavior dynamics. *Complex Systems and Complexity Science*, 2011, 8 (2): 1-17.
- [32] Vazquez A. Impact of memory on human dynamics. *Physica A: Statistical Mechanics and its Applications*, 2007, 373: 747-752.
- [33] Ming-Sheng S, Guan-Xiong C, Shuang-Xing D, et al. Interest-driven model for human dynamics. *Chinese Physics Letters*, 2010, 27(4): 250-252.

Research on the Construction of Cloud ERP Ecosystem Security Evaluation Index System

Zhujun WANG, Qin SU¹, Yue FANG

School of Management, Xi'an Jiaotong University, Xi'an, China

Abstract. Cloud ERP system realizes the functions of ERP in the way of cloud service, which greatly improves the service level of ERP and reduces the cost for enterprise to use ERP. Cloud ERP system has the characteristics of open ecology, therefore the interactions between users increase, which brings data security risks to the cloud ERP platform. This paper discusses the security of cloud ERP system from the perspective of ecosystem, and puts forward the concept and connotation of cloud ERP ecosystem. The LDA method is used to analyze the literature related to the security of ecosystem and cloud ERP open ecology, based on which seven main themes are summarized. It mainly focuses on system risk assessment, information security management and platform ecosystem construction. Based on LDA analysis results, this paper constructs a cloud ERP ecosystem security evaluation system using expert interviews from three dimensions: developer ecosystem security, user ecosystem security and device-system-user ecosystem security.

Keywords. Cloud ERP, ecosystem, text analysis, Cloud ERP ecosystem security evaluation system

1. Introduction

Cloud ERP system is the most commonly used cloud computing system in enterprises. Compared with the traditional ERP system, the cloud ERP system is more convenient. It breaks through the geographical restrictions and meets the needs of enterprises to move and work anytime and anywhere. However, due to the particularity of its environment and the architectural characteristics of its products, the security of cloud ERP has become a concern. According to the survey, 80% of users consider security as the primary indicator for whether to migrate their business to ERP cloud platform. It can be seen that security has become the bottleneck affecting the promotion of ERP cloud product. There is urgent demand for rational analysis of the mechanism of cloud ERP system security problems, as well as scientific assessment of the security risks of cloud ERP system.

Compared with the traditional ERP system, the cloud ERP system has more information transmission and more interaction between users and the system, which makes the system dynamic and open. By referring to the competitive and cooperative process of population and community in the ecosystem, the interaction among developers,

¹ Corresponding Author: Qin SU, School of Management, Xi'an Jiaotong University, Xi'an, China.
Email:qinsu@mail.xjtu.edu.cn

systems and users in the cloud ERP system can better reflect the dynamic, ecological and open nature of cloud ERP system.

2. Literature review

2.1. Cloud ERP and security literature review

Cloud ERP system eliminates the bottleneck of traditional ERP, such as high investment cost, low success rate of implementation, and great difficulty in operation and maintenance. However, the interaction of cloud ERP system poses a threat to the user information and data security of the platform[1]. GUPTA et al.[2] and some other researchers pointed out that security risk is the biggest threat to the adoption of cloud ERP for both small and medium-sized enterprises and large enterprises. Erdal Cayirci1 et al.[3] proposed a cloud adoption risk assessment model, providing automatic analysis of the risks of representative cloud service providers from the aspects of security, trust and guarantee registration of cloud security alliance, so as to help select the cloud service providers with the lowest risk in configuration. Chandramohan.D et al.[4] proposed hybrid authentication technology to protect user data privacy. LEWANDOWSKI et al.[5] pointed that the information-based enterprise has a significant impact on the adoption of SaaS ERP. The adoption of cloud ERP can be realized smoothly only if the enterprise has certain capital, technology and management foundation in informatization. Customers with higher awareness on informatization can make better use of their own advantages and appropriately adopt cloud ERP according to their own needs.

2.2. Ecosphere and security literature review

The concept of biosphere in biology has been gradually applied to study various fields. Lu Yibo et al.[6] studied the driving role of universities in open innovation ecosystem. With the concept of ecosystem, Tong Yuqing et al.[7] focused on the core business of e-commerce in the business system of Alibaba Group and the financial business supporting the e-commerce system. They study a business ecosystem that integrates local living, health and recreation. Qian Xiaocong[8] proposed the concept of big data industry ecosystem, and studied and analyzed the composition of the big data industry from the perspective of with the tools of system, community, population and so on, trying to interpret the division and relationship of each part of the industry from the perspective of length and breadth.

2.3. Cloud service security evaluation index system literature review

Xue Shan[9] outlined the cloud service business and security management requirements of small and medium-sized financial enterprises, and according to the security risks they are faced with, a cloud service security management framework was built. Then, the cloud service security management evaluation system is formed. Xuexiu Chen et al.[10] proposed a complete set of cloud security assessment indicators based on classification and gradation. And a comprehensive evaluation method including positive evaluation

and feedback evaluation is proposed to verify the rationality and effectiveness of the cloud security evaluation index system.

To sum up, previous studies pointed out the advantages of cloud ERP system and security threats to cloud ERP systems have attracted extensive attention. Current research focuses on the analysis and description of security issues and ignores the impact of cloud ERP ecosystem's ecological openness on system security. This paper proposes the concept of cloud ERP ecosystem from the perspective of open innovation ecosystem, and discusses the relationship between cloud ERP ecological openness characteristics and information security of system. The existing evaluation indicator system in the field of cloud service is oriented towards the whole cloud service. But there is no system for evaluation indicator specified for the security of cloud ERP. Moreover, most of the studies are based on the analysis and improvement of existing evaluation indicators, or subjective extraction of indicators from existing studies and standards. This paper utilizes the method of text analysis to sort out papers related to ecosystem security and openness of cloud ERP ecology, and summarizes specific topics. Based on the concept of cloud ERP ecosystem and the system of evaluation indicator, the security evaluation system of cloud ERP ecosystem is constructed to help improve the information security level of cloud ERP system.

3. Construction of cloud ERP ecosystem

Traitler H et al[11] proposed the concept of open innovation ecosystem to study the change of innovation paradigm; Yu Yao[12] proposed the concept of e-commerce ecosphere and studied the collaborative mechanism of e-commerce ecosphere; Tong Yuqing et al.[13] proposed the concept of business ecosphere to study the collaboration of Internet technology and service terminals in the business system of Alibaba Group; Qian Xiaocong[14] proposed the concept of big data industry ecosystem to analyze the composition of big data industry. This paper draws on the concept of ecosphere in various fields. Based on the concepts of system, community and population in ecology, the concept of cloud ERP ecosystem was further analyzed. Cloud ERP ecosystem is a dynamic and organic system composed of developers, users and software systems with cloud ERP system at its core. Cloud ERP ecosystem contains three levels of meaning: developers constitute the ecosystem, the ecosystem of users and developers, users and cloud ERP system.

3.1. Developer ecosystem

The ecosystem composed of developers is mainly oriented towards the service functions of the system. One of the core ideas of cloud computing is to reduce the processing burden on the user end by continuously improving the processing capacity of the cloud. The user end is reduced to a single input-output device, and enjoys the powerful computing capability of the cloud as needed. Cloud ERP represents the integration of the advantages of cloud computing and traditional ERP system. At present, the projects of technical research and exchanges in open source mode have covered various fields such as big data architecture, data query, data processing, workflow coordination, statistical tools, machine learning and cloud computing. System developers jointly constitute the

development ecosystem to realize the sharing of technology, platform and data, and jointly improve the service functions of the system.

3.2. User ecosystem

The ecosystem composed of cloud ERP users is mainly the application object of the system. For an enterprise, the users of the cloud ERP system are distributed in a pyramid structure, as shown in Figure 1. It includes three main groups. First, procurement, production, inventory, sales or finance worker, who is responsible for the data entry system. The second is the data analyst, who monitors and analyzes the data in the system to generate periodic reports for decision-making. On the top is the management level of the enterprise. Through the data retained by the system, the management level identifies risks faced by the enterprise and carries out macro control over the enterprise.



Figure 1. Pyramid structure of user ecosystem within an enterprise.

All system users in the enterprise together constitute the user ecosystem. From the perspective of industry distribution, cloud ERP system is widely used, and users came from many enterprises in the fields of government, energy, telecommunications, manufacturing and medical care, which together constitute the user ecosystem.

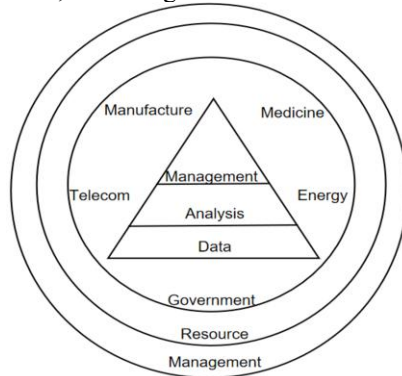


Figure 2. User ecosystem.

3.3. Developer-system-user ecosystem

Cloud ERP system developers, users and the cloud ERP system interact with each other and form an organic dynamic ecosystem. Cloud ERP system developers complete the construction of the cloud ERP system and realize system's various service functions;

Cloud ERP platform is Shared by many users, and business data of enterprises are retained on the system side to achieve data centralization. It optimized the process of enterprise data input, storage and management, improved the system efficiency among various departments of the enterprise, and reduced the labor cost. System developers and many users interweave and influence each other through the cloud ERP system, forming a collaborative ecosystem together, as shown in the figure below.

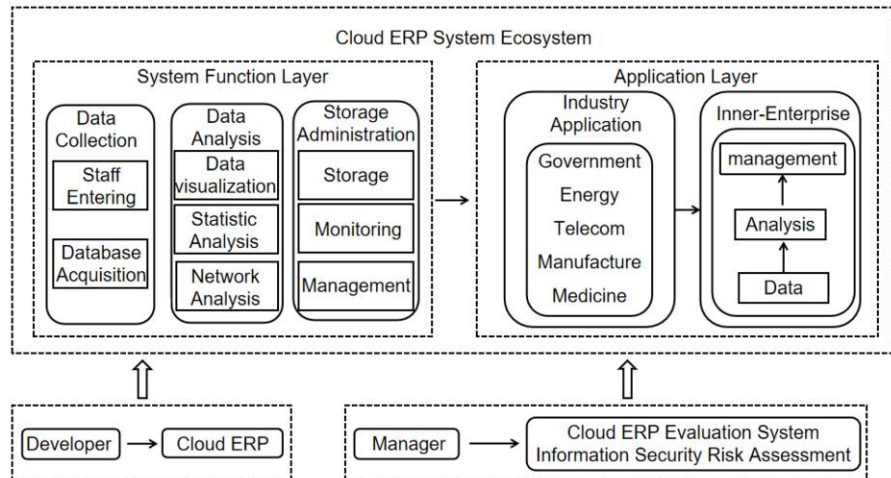


Figure 3. Cloud ERP system ecosystem.

4. Text analysis based on LDA

At present, most researches on the evaluation index system of cloud security are based on the analysis and improvement of existing evaluation indexes, or subjective extraction of indexes from existing researches and standards, which make the evaluation index system become less scientific and applied. Therefore, in view of this deficiency, LDA method is adopted in this study to analyze the documents related to the ecological opening characteristics of ecosphere, security and cloud ERP, and summarize the characteristic literature to obtain the research topic[15], which provides the basis for the construction of cloud ERP ecosystem security evaluation system.

4.1. The topics of ecosphere and security field

The security of ecosphere is the focus of scholars' attention. LDA is used to analyze the document set related to the ecosystem and ecosystem safety, as shown in Table 1.

Table 1. Most relevant term frequencies for the biosphere and biosphere security.

#	Term	Frequency	#	Term	Frequency
1	Technology	998	16	Market	601
2	Data	976	17	Organization	595
3	Ecosystem	956	18	Institution	584
4	Develop	903	19	Value	570
5	Business	878	20	Relationship	554
6	Innovation	865	21	Resource	543
7	Platform	843	22	Process	453
8	Service	801	23	Change	403

9	Information	769	24	Product	389
10	Manage	745	25	Different	367
11	Govern	721	26	Study	348
12	System	698	27	Need	278
13	Platform	667	28	Provide	256
14	Company	657	29	Work	221
15	Knowledge	642	30	Process	201

In table 1, Technology, Data, Ecosystem, Develop words have the highest frequency. It can be seen that big data ecosystem and platform ecosystem are highly concerned at present. By summarizing and combing feature literature[16]-[17], the following topics can be obtained: (1). The development and innovation of platforms are shifting competition among enterprises to competition among platform-centric ecosystems. (2).The interaction between the platform ecosystem and the environment as well as between each ecosystem affects the utilization of market resources. The current research focuses on the design of the platform ecosystem management system.

4.2. The topics of open ecological characteristics of cloud ERP system

LDA method is used to analyze the literature collection in the field of open ecological characteristics of cloud ERP system, and the results are shown in Table 2.

Table 2. Most relevant term frequencies for the open and ecological characteristics of cloud ERP system.

#	Term	Frequency	#	Term	Frequency
1	Cloud	1443	16	Process	652
2	ERP	1201	17	Implement	601
3	Information	1025	18	System	598
4	Data	977	19	Adopt	576
5	Security	945	20	Research	541
6	Application	920	21	Quality	487
7	Risk	899	22	Technology	432
8	Service	875	23	Digit	387
9	Manage	846	24	Content	352
10	Govern	832	25	Behavior	321
11	Model	820	26	Space	298
12	Computing	798	27	Activity	274
13	Business	765	28	Work	251
14	Use	742	29	Control	229
15	Enterprise	731	30	Software	201

In table 2, ERP, Data, Risk, Security, Application, Information words have the highest frequency. It can be seen that scholars pay more attention to the data security of cloud ERP system. By summarizing and combing feature literature[18]-[19], the following topics can be obtained: (1).Cloud ERP is an open service platform, and developers should adapt to a wider range of users with a more agile development cycle. (2).The cloud ERP system and users together constitute the cloud ecosystem, in which the data are huge and complex and users face data risks. 3.The information system in the cloud ERP system is the core of cloud services, realizing the integration of information. Distinguishing the information quality dimensions in the information management process can provide a deeper understanding of end-user satisfaction and the outcome performance of the workspace.

5. Construction of cloud ERP ecosystem security evaluation system

Based on the analysis results of LDA and the concept of cloud ERP ecosystem, this paper constructs the cloud ERP ecosystem security evaluation system by expert interview.

The scientific and reasonable construction of the index system needs to go through the solicitation of expert opinions. This paper adopts the method of expert interview to conduct the first round of expert opinion survey. By investigating and sorting out the opinions of a research expert in the field of information security, a research expert in the field of cloud ERP and a research expert in the field of platform ecosystem, the evaluation index system initially established was modified and improved, and the index system was finally determined as shown in Table 3 .

Table 3. Security evaluation index system of cloud ERP ecosystem

Cloud ERP Ecosystem Security Evaluation Index System		
I level Indicators	II level Indicators	III level Indicators
A1 Developer ecosystem security	B1 Interaction security during development	<p>The development environment protects confidential data from attack and theft.</p> <p>Developers on different projects communicate to ensure that information is not leaked.</p>
	B2 Security technical guarantee for login and exit and password modification	<p>Malicious users cannot obtain sensitive information such as user's account and password through network monitoring.</p> <p>An account can only be logged in on one device at a time</p> <p>When the user does not log out, make sure that the malicious user cannot get the user's session ID by sniffing or other means.</p> <p>When the user changes the password, the system verifies the original password in the background database.</p>
	B3 Security and technical guarantee of data analysis	<p>In the process of analysis, the content with higher confidentiality level shall be protected by data blur or encryption.</p> <p>There is no possibility of information leakage in the process of data submission to the next analysis link.</p>
	B4 The security technical guarantee of data storage management	<p>SQL injection vulnerability will not occur in the business system and will not cause information disclosure or modification.</p> <p>The business system will not leak information due to constant POST requests submitted by the plug-in software.</p>
	B5 User interaction security	<p>The information confirmation button is returned at the end of the input.</p> <p>Keep the trace of information analysis and automatically save the analysis report.</p> <p>Data entry personnel, data analysts and managers all sign confidentiality agreements.</p>
	B6 User interaction security between companies	<p>There is a shield between the enterprise isolation, will not cause data leakage.</p> <p>The system sets different encryption methods for the data of each enterprise.</p>
A2 User ecosystem security	B7 Management of ecosystem risk assessment	<p>The ecosystem has a risk assessment capability that alerts people when the risk is high.</p> <p>The risk assessment of the ecosystem is universal.</p>
	B8 Information security management of ecosystem	<p>Categorize and manage all information in the ecosystem.</p> <p>When the information surface in the ecosystem is high risk, the system should be quickly feedback to the background and front end, and developers should timely maintain it.</p>
A3 Developer-Platform-User ecosystem security		

In the security evaluation index system of cloud ERP ecosystem, equal weight is adopted[20] to give weight to each three-level index. In other words, each three-level index is given the same weight, the one that meets the three-level index conditions is 1,

and the one that does not is zero. The number of each cloud ERP ecosystem satisfying the three-level index was comprehensively calculated, that is, the security degree of the ecosystem.

6. Conclusion

Cloud ERP system is more convenient and flexible than traditional ERP system. At the same time, it provides enterprises with a modern enterprise management mode with less input cost, but can meet all kinds of requirements at any time, which is the general trend of ERP development in the future under the big data environment. The ecological and open features of cloud ERP increase system interaction and bring information security risks to enterprises, and their information security threats are of great concern to enterprises. Based on the research in the fields of big data, commerce and e-commerce, this paper proposes the cloud ERP ecosystem, and analyzes the influence mechanism of the ecological openness of the cloud ERP system on the information security of the system. In this paper, the evaluation index is objectively extracted from the text database by text analysis, and the security evaluation index system of cloud ERP ecosystem is finally constructed by expert review, and the security of cloud ERP system is standardized from the ecological open perspective of cloud ERP ecosystem, so as to provide guarantee for the efficient and safe development of cloud ERP.

On the theoretical level, this research adopts the text mining based on the ecological opening characteristics of ecosphere, security and cloud ERP. On the one hand, it points out the significance of solving the cloud ERP security problem for the development of cloud ERP, and demonstrates the applicability of the concept of cloud ERP ecosystem to the research of cloud ERP security problem. On the other hand, text mining method is used to provide objective basis for the establishment of cloud ERP ecosystem security evaluation system. On the basis of practice, the concept of cloud ERP ecosystem proposed in this paper emphasizes the characteristics of cloud ERP system's ecological openness. The interaction and feedback information among developers, systems and users in the ecosystem is an important basis for cloud ERP service providers to optimize and improve system functions. In addition, the cloud ERP ecosystem security evaluation system provides reference for the information security management practice of the cloud ERP platform. Through the evaluation system, cloud ERP service providers can measure the security level of cloud ERP platform more efficiently and conveniently, and put forward relevant measures and suggestions to improve their own cloud service security management level according to the evaluation results.

Acknowledgement

The work was funded by the National Key R &D Program of China (No.2019YFB1704103).

References

- [1] Zhu Zonggan, Jia Yiwu. Exploratory Research on influencing Factors of Cloud ERP Service Model Classification [J]. Journal of management,2016,13(8):233-1240.

- [2] GUPTA S,MISRA S C,SINGH A, et al. Identification of challenges and their ranking in the implementation of cloud ERP : a comparative study for SMEs and large organizations[J]. International Journal of Quality & Reliability Management,2017,34(7):1056 -1072.
- [3] Erdal Cayircil, Alexandr Garaga, et al. A risk assessment model for selecting cloud service providers [J]. Journal of Cloud Computing: Advances, Systems and Applications, 2016, (5),14.
- [4] Chandramohan.D, Vengattaraman.T, Rajaguru.D, Baskaran.R, and Dhavachelvan.P, "Hybrid Authentication Technique to Preserve User Privacy and Protection as an End Point Lock for the Cloud Service Digital Information".[J].IEEE-International Conference on Green High Performance Computing,2013,(40):1-4.
- [5] LEWANDOWSKI J,SALAKO A O, GRACIAPEREZ A. SaaS enterprise resource planning systems: challenges of their adoption in SMEs[C] / IEEE 10th International Conference on e - Business Engineering. Coventry:IEEE,2013:56-61.
- [6] Lyu Yibo, Han Shaojie, Su Jingqin and Wang Shujuan. Research on the Construction of University-driven Open Innovation Ecosystem[J].Management Review,2017,29(4):68-82.
- [7] Tong Yuqing, Yang Yaojun .Research on Operation Mode of Ali Business Ecosystem and Platform [J].Science and Technology Management Research,2019,11:254-260.
- [8] Qian Xiaocong.Study on Big Data Industry Ecology Atlas[J]. Informatization Research ,2013,39(6):49-52.
- [9] Shan Xue.Research on design and Evaluation of cloud Service Security Management Framework for small and medium-sized financial enterprises[D].Hefei: Hefei University of Technology, 2018.
- [10] Xuexiu Chen, Chi Chen, Yuan Tao, et al. A Cloud Security Assessment System Based on Classifying and Grading[J]. IEEE Cloud Computing, 2015,2(2):58-67.
- [11] Traitler H, Watzke H.J, Saguy I.S. Reinventing R&D in an Open Innovation Ecosystem[J]. Journal of Food Science,2011,76(2):62-68.
- [12] YU Yao. A Research on Construction Logic and Synergistic Mechanism of E-commerce Ecosystem in the Era of Big Data[J]. Journal of North University of Water Resources and Electric Power (Social Science Edition),2016,32(4):35-37.
- [13] Tong Yuqing, Yang Yaojun. Research on Operation Mode of Ali Business Ecosystem and Platform [J].Science and Technology Management Research,2019,11:254-260.
- [14] Qian Xiaocong. Study on Big Data Industry Ecology Atlas[J]. Informatization Research ,2013,39(6):49-52.
- [15] Sérgio Moro, Paulo Cortez, Paulo Rita. Business intelligence in banking: A literature analysis from 2002 to 2013 using text mining and latent Dirichlet allocation [J]. Expert Systems with Applications, 2015,42:1314–1324.
- [16] Amrit Tiwana, et al. Platform Evolution: Coevolution of Platform Architecture, Governance, and Environmental Dynamics[J] Information Systems Research,2010,21(4):675-687.
- [17] Sahar Mohammed,Osman Hegazy,Ehab E. Hassanein. A Novel Approach for Handling Security in Cloud Computing Services[J]. International Journal of Computer Applications,2013,69(5):9-14.
- [18] Shivam Gupta, Subhas C Misra. Compliance, network, security and the people related factors in cloud ERP implementation [J]. International Journal of communication systems,2016,29:1395–1419.
- [19] Sven Laumer,Christian Maier,Tim Weitzel. Information quality, user satisfaction, and the manifestation of workarounds: a qualitative and quantitative study of enterprise content management system users [J]. European Journal of Information Systems,2017,26:333-360.
- [20] Zhao Jin-xu, Zheng Yue-ping. Research on privacy Protection of E-government in China -- Based on 70 Investigation on "Privacy Statement" of government websites in large and medium-sized cities [J]. E-government,2016(7):81-93.

Interval Observer Design for Metzlerian Takagi-Sugeno Systems

Dušan KROKAVEC and Anna FILASOVÁ

Technical University of Košice, Slovakia

Abstract. The generalized interval observer design conditions for continuous-time Metzlerian Takagi-Sugeno systems are presented in the paper. Attention is focused on the analysis and design guaranteeing the asymptotic convergence of the interval observer error and positivity of interval observer state. The relationship between the nonnegativity of the observer gains and the corresponding positive observer state attractiveness is also shown. The method presented extends and generalizes the results that recently appeared in the literature.

Keywords. interval observers, Metzlerian Takagi-Sugeno fuzzy systems, diagonal stabilization, convex optimization, linear matrix inequalities

1. Introduction

the type of fuzzy inference systems. The study of state observers is a topic of great importance in effective control concepts and system fault diagnosis applications. Because the Takagi-Sugeno (T-S) fuzzy approach addresses fuzzy implication of local dynamics by linear models [1], excellent unifications of state observer design for sector-bounded nonlinear systems are related with T-S fuzzy models [2], [3]. Since using Takagi-Sugeno method the consequents are the crisp functions of inputs, nonlinear control theories prefer T-S fuzzy approach with relation to state-space representation of systems, although there exist other fuzzy inference systems [4], [5]. The design algorithm turns out to be feasible utilizing the linear matrix inequalities (LMI) technique [6], [7].

Restricting attention to positive linear systems, maintaining given features whenever the system states are nonnegative [8], [9], concepts in this field prioritize in analysis and design the theory of matrices of Metzler structure [10], [11]. In order to reflect large number of constraints, an excellent unification is an LMI-based design strategy for linear positive (Metzlerian) systems [12].

Based on nominal system models, the state observers in general asymptotically estimate unknown system state. Counterpart of this approach is outlined in [13] to provide, for given system matrix bounds, the system state estimation in projected intervals. In addition to the above, reference [14] presents a cooperative observer error approach for exact analysis of interval observers with grasp of the Metzler matrix details. Interval observer algorithms, with LMI projection of interval bounds, for uncertain Metzlerian systems are analyzed in [15].

Adapting the above results in synthesis of T-S fuzzy observers and interval observers for uncertain Metzlerian systems and reflecting [16], the paper extend the latter

approaches to design interval observer for Metzlerian Takagi-Sugeno systems. Preferring LMI formulation for solving the problem, the interval observer stability proofs use standard arguments and reflect the concept of diagonal stabilization that is in keeping with the structure of Metzler matrices. Working along these lines to establish the observer design conditions, the newly presented theoretical aspect gives relationships between system parametric constraints, the LMIs feasibility and the observer state attractiveness guaranty. Because only a set of LMIs defines conditions, practical aspects are standard.

The paper is organized as follows. In Sec. 2 the essential properties of Metzlerian Takagi-Sugeno fuzzy models are adduced and Sec. 3 outlines problems with Metzlerian observer design for given class of strictly Metzlerian T-S systems. The set of LMIs, describing the design conditions for Metzlerian Takagi-Sugeno interval observer, and its solution is the theme of Sec. 4 and an example to implement the algorithm is included into Sec. 5. Within the underlying concept, Sec. 6 draws conclusions and the topics of the research activity in the future.

Throughout the paper, the following notations are used: x^T , X^T denotes the transpose of the vector x , and the matrix X , respectively, $\text{diag}[\cdot]$ marks a (block) diagonal matrix, for a square symmetric matrix $X \prec 0$ means that X is negative definite matrix, the symbol I_n indicates the n -th order unit matrix, \mathbb{R}_+ , \mathbb{R}_+^n qualify the sets of nonnegative real numbers and n -dimensional real vectors, $\mathbb{R}_+^{n \times n}$ refers to the set of nonnegative real matrices and $\mathbb{R}_{-+}^{n \times n}$ covers the set of Metzler matrices.

2. Metzlerian Takagi-Sugeno Fuzzy Model

The used systems are multi-input and multi-output (MIMO) Metzlerian continuous-time dynamic systems, represented in T-S form as

$$\dot{q}(t) = \sum_{i=1}^s h_i(\vartheta(t))(A_i q(t) + B_i u(t)), \quad (1)$$

$$y(t) = Cq(t), \quad (2)$$

where $q(t) \in \mathbb{R}_+^n$, $u(t) \in \mathbb{R}^r$, $y(t) \in \mathbb{R}_+^m$, are vectors of the state, input, and output variables and $A \in \mathbb{M}_{-+}^{n \times n}$, $B \in \mathbb{R}_+^{m \times r}$, $C \in \mathbb{R}_+^{m \times n}$. Moreover, $h_i(\theta(t))$ is averaging weight for the i -th rule, representing the normalized grade of membership, where

$$0 \leq h_i(\vartheta(t)) \leq 1, \quad \sum_{i=1}^s h_i(\vartheta(t)) = 1 \quad \text{for all } i \in \langle 1, s \rangle, \quad (3)$$

while s is the number fuzzy rules (linear sub-models) and

$$\vartheta(t) = [\theta_1(t) \ \theta_2(t) \ \cdots \ \theta_q(t)] \quad (4)$$

is q -dimensional vector of premise variables. More details can be found, e.g., in [6], [12].

Within the above model, there are considered nonnegative matrices $B_i \in \mathbb{R}_+^{n \times r}$, $C \in \mathbb{R}_+^m$ and a strictly Metzler $A_i \in \mathbb{R}_{-+}^{n \times n}$, where strictly Metzler A_i means that all its off diagonal elements are greater than zero and all its diagonal elements are negative. Such above given system is noted as strictly Metzlerian T-S system. In general, a Metzler matrix is so confronted with n^2 boundaries implying from the structural constraints

$$a_{lh} < 0, \quad l = h, \quad a_{lh} > 0, \quad l \neq h, \quad \forall l, h \in \langle 1, n \rangle. \quad (5)$$

This just means in consequence that continuous-time strictly Metzlerian systems are diagonally stabilizable. To respect diagonal structures the following are reflected.

Definition 1. [17] A square matrix $L_p \in \mathbb{R}^{n \times n}$ is permutation matrix if exactly one element in each column and each row is equal to 1 and all others are equal to 0.

Definition 2. [17] Let $L \in \mathbb{R}_+^{n \times n}$ be a permutation matrix. L is called circulant if

$$L = \begin{bmatrix} 0^T & 1 \\ I_{n-1} & 0 \end{bmatrix}. \quad (6)$$

Moreover, the following remark can be easily checked applying the circulant permutation matrix representstion.

Remark 1. If $X \in \mathbb{R}^{n \times n}$ is a diagonal matrix then, consequently,

$$L^T \text{diag} [x_1 \ x_2 \ \cdots \ x_n] L = \text{diag} [x_2 \ \cdots \ x_n \ x_1]. \quad (7)$$

In the case when only a matrix $A_i \in \mathbb{R}_{-+}^{n \times n}$ is analyzed and structural constraints (65) are represented as a set of n LMIs, then

Lemma 1. [12] $A_i \in \mathbb{R}_{-+}^{n \times n}$ is Metzler and Hurwitz if and only if there exists a positive definite diagonal matrix $P \in \mathbb{R}_+^{n \times n}$ such that

$$P \succ 0, \quad (8)$$

$$PA_i(p, p)_\Delta \prec 0, \quad (9)$$

$$PL^h A_i(p+h, p)_\Delta L^{hT} \succ 0, \quad (10)$$

$$A_i^T P + PA_i \prec 0, \quad (11)$$

for $i = 1, 2, \dots, s$, $h = 1, 2, \dots, n-1$, $p = 1, 2, \dots, n$, where

$$A_i(p+h, p)_\Delta = \text{diag} [a_{i,1+h,1} \ \cdots \ a_{i,n,n-h} \ a_{i,1,n-h+1} \ \cdots \ a_{i,hn}], \quad (12)$$

$$\Delta = (1 \leftrightarrow n)/n. \quad (13)$$

Note, with the matrix P thus defined, the set of LMIs (9), (10) reflects (65) and the Lyapunov inequality (11) guaranties that A_i is Hurwitz.

3. Strictly Metzlerian Takagi-Sugeno Fuzzy Observer

The state estimation assumes the observer to strictly Metzlerian Takagi-Sugeno fuzzy system (1), (2) in the form

$$\dot{q}_e(t) = \sum_{i=1}^s h_i(\theta(t))(A_i q_e(t) + B_i u(t) + J_i(y(t) - y_e(t))), \quad (14)$$

$$y_e(t) = C q_e(t), \quad (15)$$

where $q_e(t) \in \mathbb{R}_+^n$ is the estimation of the system state vector, $J_i \in \mathbb{R}_+^{n \times m}$, $i = 1, 2, \dots, s$ is the set of the positive observer gain matrices and forms of the parameters are

$$A_i = \begin{bmatrix} a_{i11} \cdots a_{i1n} \\ \vdots \\ a_{in1} \cdots a_{inn} \end{bmatrix}, \quad C = \begin{bmatrix} c_1^T \\ \vdots \\ c_m^T \end{bmatrix}, \quad c_k^T = [c_{k1} \cdots c_{kn}], \quad J_i = [j_{i1} \cdots j_{im}], \quad j_{ik} = \begin{bmatrix} j_{i1k} \\ \vdots \\ j_{ink} \end{bmatrix}, \quad (16)$$

$$J_{dik} = \text{diag} [j_{i1k} \cdots j_{ink}], \quad C_{dk} = \text{diag} [c_{1k} \cdots c_{nk}]. \quad (17)$$

Then the structural constraints problem for strictly Metzler $A_{ei} \in \mathbb{R}_{-+}^{n \times n}$ is formable as

$$A_{ei} = A_i - J_i C = A_i - \sum_{k=1}^m j_{ik} c_k^T = A_i - \sum_{k=1}^m J_{dikl} l^T C_{dk}, \quad (18)$$

where

$$l^T = [1 \ 1 \ \cdots \ 1], \quad (19)$$

$$a_{elh} - \sum_{k=1}^m j_{ihk} c_{kl} < 0, \quad h = l, \quad a_{ilh} - \sum_{k=1}^m j_{ihk} c_{kl} > 0, \quad h \neq l, \quad \forall h, l \in \{1, \dots, n\}. \quad (20)$$

Having in mind constraints (20) it is not hard to establish the following:

Theorem 1. *The observer (14), (15) is stable if there exist positive definite diagonal matrices $P, R_{ik} \in \mathbb{R}_+^{n \times n}$ such that*

$$P \succ 0, \quad R_i \succ 0, \quad (21)$$

$$PA_i(p, p)_\Delta - \sum_{k=1}^m R_{ik} C_{dk} \prec 0, \quad (22)$$

$$PL^h A_i(p+h, p)_\Delta L^{hT} - \sum_{k=1}^m R_{ik} L^h C_{dk} L^{hT} \succ 0, \quad (23)$$

$$PA_i + A_i^T P - \sum_{k=1}^m R_{ik} l^T C_{dk} - \sum_{k=1}^m C_{dk} l^T R_{ik} \prec 0. \quad (24)$$

for $i = 1, 2, \dots, s$, $p = 1, 2, \dots, n$, $h = 1, 2, \dots, n-1$, $k = 1, 2, \dots, m$.

When the above conditions hold, the set of J_{ik} is given by

$$J_{dik} = P^{-1} R_{ik}, \quad j_{ik} = J_{dik} l, \quad J_i = [j_{i1} \ \cdots \ j_{im}]. \quad (25)$$

Proof. Writing A_{ei} from (18) as follows

$$A_{ei} = \begin{bmatrix} a_{i11} & a_{i12} & \cdots & a_{i1n} \\ a_{i21} & a_{i22} & \cdots & a_{i2n} \\ \ddots & & & \\ a_{in1} & a_{in2} & \cdots & a_{inn} \end{bmatrix} - \sum_{k=1}^m \begin{bmatrix} j_{i1k} \\ j_{i2k} \\ \vdots \\ j_{ink} \end{bmatrix} [c_{k1} \ c_{k2} \ \cdots \ c_{kn}], \quad (26)$$

it can see that the diagonal elements of (26) satisfy the first set of conditions from (20) if

$$A_i(p, p)_\Delta - \sum_{k=1}^m J_{idk} C_{dk} \prec 0, \quad (27)$$

where

$$A_i(p, p)_\Delta = \text{diag} [a_{i11} \ a_{i22} \ \cdots \ a_{inn}]. \quad (28)$$

Therefore, multiplying the left side by a positive definite diagonal matrix $P \in \mathbb{R}_+^{n \times n}$ then (27) implies

$$PA_i(p, p)_\Delta - \sum_{k=1}^m PJ_{idk} C_{dk} \prec 0, \quad (29)$$

and with the notation

$$R_{ik} = PJ_{idk} \quad (30)$$

(29) implies (22) and (30) forces (25).

Rewriting (26) in the circular shifted structures to cover other sets of algebraic constraints then

$$L^{hT} A_{ei} = \begin{bmatrix} a_{i,h+1,1} & a_{i,h+1,2} & \cdots & a_{i,h+1,n} \\ \vdots & & & \\ a_{in1} & a_{in2} & \cdots & a_{inn} \\ a_{i11} & a_{i12} & \cdots & a_{i1n} \\ \vdots & & & \\ a_{ih1} & a_{ih2} & \cdots & a_{ihn} \end{bmatrix} - \sum_{k=1}^m \begin{bmatrix} j_{i,h+1,k} \\ \vdots \\ j_{ink} \\ j_{i1k} \\ \vdots \\ j_{ihk} \end{bmatrix} [c_{k1} \ c_{k2} \ \cdots \ c_{kn}] \quad (31)$$

and it can see that the diagonal elements of (31) force the set (18) for fixed h if

$$A_i(p+h, p)_\Delta - \sum_{k=1}^m J_{dikch} C_{dk} \succ 0, \quad (32)$$

where $A_i(p+h, p)_\Delta$ is defined in (12) and J_{dikch} is derived from the diagonal matrix J_{idk} by h circular shifts of its diagonal elements applying circulant L from (6).

Since, it yields for $h = 1, 2, \dots, n-1$,

$$J_{idk} = L^h J_{dikch} T^{hT}, \quad (33)$$

pre-multiplying the left side by T^h and post-multiplying the right side by T^{hT} then (32) can be represented as

$$T^h A_i(p+h, p)_\Delta T^{hT} - \sum_{k=1}^m T^h J_{dkch} T^{hT} T^h C_{dk} T^{hT} \succ 0, \quad (34)$$

$$T^h A(i+h, i)_\Delta T^{hT} - \sum_{k=1}^m J_{dk} T^h C_{dk} T^{hT} \succ 0, \quad (35)$$

respectively. Thus, multiplying the left side by positive definite diagonal matrix $P \in \mathbb{R}_+^{n \times n}$ and using (33) then (35) implies (23).

Introducing the error in system state observations as

$$e(t) = q(t) - q_e(t) \quad (36)$$

and performing the time derivative then, exploiting (1) and (14), it is obtained

$$\dot{e}(t) = \sum_{i=1}^s h_i(\theta(t))(A_i(q(t) - q_e(t)) - J_i(y(t) - y_e(t))), \quad (37)$$

which can be written using (2), (18) as follows

$$\dot{e}(t) = \sum_{i=1}^s h_i(\theta(t))A_{ei}e(t). \quad (38)$$

Defining the Lyapunov function

$$v(e(t)) = e^T(t)Pe(t) > 0, \quad (39)$$

where $P \in \mathbb{R}_+^{n \times n}$ is positive definite diagonal matrix, then (39) implies

$$\dot{v}(e(t)) = \dot{e}(t)Pe(t) + e^T(t)P\dot{e}(t). \quad (40)$$

Substituting (38) into (40) gives

$$\dot{v}(e(t)) = e^T(t) \sum_{i=1}^s h_i(\theta(t))(PA_{ei} + A_{ei}^T P)e(t), \quad (41)$$

which results with (18) to

$$P(A_i - \sum_{k=1}^m J_{dik}ll^TC_{dk}) + (A_i - \sum_{k=1}^m J_{dik}ll^TC_{dk})^TP \prec 0 \quad \forall i. \quad (42)$$

Therefore, using (30), then (42) implies (24). This concludes the proof. \square

4. Metzlerian Takagi-Sugeno Fuzzy Interval Observer

Consider (1), (2), where (A_i, C) and $q(0)$ are unknown but bounded and for all $i \in \langle 1, s \rangle$ the known constant bounds satisfy elementwise

$$\underline{q}(0) \leq q(0) \leq \bar{q}(0), \quad \underline{A}_i \leq A_i \leq \bar{A}_i, \quad \underline{C} \leq C \leq \bar{C}. \quad (43)$$

The aforementioned problem can be turned to construction of the (strictly) Metzlerian T-S fuzzy interval observer, defined as the couple of the algorithms

$$\dot{\underline{q}}_e(t) = \sum_{i=1}^s h_i(\vartheta(t)) (\bar{A}_i \bar{q}_e(t) + B_i u(t) + J_i \underline{C}(q(t) - \bar{q}_e(t))), \quad (44)$$

$$\dot{\bar{q}}_e(t) = \sum_{i=1}^s h_i(\vartheta(t)) (\underline{A}_i \underline{q}_e(t) + B_i u(t) + J_i \bar{C}(q(t) - \underline{q}_e(t))), \quad (45)$$

where the design objective constraints can be stated as

$$0 \leq \underline{q}_e(t) \leq q(t) \leq \bar{q}_e(t) \quad (46)$$

for all $t \geq 0$ if $\bar{q}_e(0) = \bar{q}(0)$, $\underline{q}_e(0) = \underline{q}(0)$. It is the problem that is reformulated in the following definition.

Definition 3. The set of equations (44), (45) give stable observer for uncertain Metzlerian Takagi-Sugeno fuzzy plant (1), (2) if both the lower estimation error $\underline{e}(t)$ and the upper estimation error $\bar{e}(t)$ converge to the equilibrium.

Assumption 1. Supposing that it is possible to force equilibrium convergence of errors

$$\bar{e}(t) = q(t) - \bar{q}_e(t), \quad \underline{e}(t) = q(t) - \underline{q}_e(t). \quad (47)$$

If (1), (2), (44), (45) are rearranged as

$$\dot{\bar{e}}(t) = \sum_{i=1}^s h_i(\vartheta(t)) (\bar{A}_i - J_i \underline{C}) \bar{e}(t) = \sum_{i=1}^s h_i(\vartheta(t)) \bar{A}_{ei} \bar{e}(t), \quad (48)$$

$$\dot{\underline{e}}(t) = \sum_{i=1}^s h_i(\vartheta(t)) (\underline{A}_i - J_i \bar{C}) \underline{e}(t) = \sum_{i=1}^s h_i(\vartheta(t)) \underline{A}_{ei} \underline{e}(t) \quad (49)$$

trajectories (48), (49) are asymptotically stable if for given set $(\underline{A}_i, \bar{A}_i, \underline{C}, \bar{C}, i \in \langle 1, s \rangle)$ satisfying (43), and nonnegative $\bar{e}(0)$, $\underline{e}(0)$, all matrices \bar{A}_{ei} , \underline{A}_{ei} are Metzler and Hurwitz.

Corollary 1. By performing an inner adjustment for (49)

$$\dot{q}(t) - \dot{\underline{q}}_e(t) = \sum_{i=1}^s h_i(\vartheta(t)) \underline{A}_{ei} (q(t) - \underline{q}_e(t)), \quad (50)$$

it then follows from (50)

$$\dot{\underline{q}}_e(t) = (\dot{q}(t) - \sum_{i=1}^s h_i(\vartheta(t)) \underline{A}_{ei} q(t)) + \sum_{i=1}^s h_i(\vartheta(t)) \underline{A}_{ei} \underline{q}_e(t) \quad (51)$$

and considering the autonomous part of (1)

$$\begin{aligned} \dot{\underline{q}}_e(t) &= \sum_{i=1}^s h_i(\vartheta(t)) (A_i - (\underline{A}_i - J_i \bar{C})) q(t) + \underline{A}_{ei} \underline{q}_e(t) \\ &= \sum_{i=1}^s h_i(\vartheta(t)) \underline{A}_{ei} \underline{q}_e(t) + \sum_{i=1}^s h_i(\vartheta(t)) J_i \bar{C} q(t) + \sum_{i=1}^s h_i(\vartheta(t)) (A_i - \underline{A}_i) q(t). \end{aligned} \quad (52)$$

Thus, for $\bar{C} \in \mathbb{R}_+^{m \times n}$, $q(t) \in \mathbb{R}_+^n$ the lower state estimate is nonnegative if $J_i \in \mathbb{R}_+^{n \times m}$ is nonnegative and all \underline{A}_{ei} are (strictly) Metzler and Hurwitz.

With the above facts in mind, Theorem 1 is adapted to obtain \bar{A}_{ei} , $\underline{A}_{ei} \in \mathbb{R}_{-+}^{n \times n}$.

Theorem 2. *Using algorithms (44), (45) in state estimation of uncertain strictly Metzlerian Takagi-Sugeno fuzzy system (1), (2), then matrices \bar{A}_{ei} , $\underline{A}_{ei} \in \mathbb{R}_{-+}^{n \times n}$ for all $i \in \langle 1, s \rangle$ are strictly Metzler and Hurwitz if for given strictly Metzler matrices $\bar{A}_i, \underline{A}_i \in \mathbb{R}_{-+}^{n \times n}$, $i \in \langle 1, s \rangle$ and non-negative matrices $\bar{C}, \underline{C} \in \mathbb{R}_{+}^{m \times n}$ there exist positive definite diagonal matrices $P, R_{ik} \in \mathbb{R}_{+}^{n \times n}$ such that*

$$P \succ 0, \quad R_{ik} \succ 0, \quad (53)$$

$$P\bar{A}_i(p, p)_\Delta - \sum_{k=1}^m R_{ik}\underline{C}_{dk} \prec 0, \quad (54)$$

$$P\underline{A}_i(p, p)_\Delta - \sum_{k=1}^m R_{ik}\bar{C}_{dk} \prec 0, \quad (55)$$

$$PL^h\bar{A}_i(p+h, p)_\Delta L^{hT} - \sum_{k=1}^m R_{ik}L^h\underline{C}_{dk}L^{hT} \succ 0, \quad (56)$$

$$PL^h\underline{A}_i(p+h, p)_\Delta L^{hT} - \sum_{k=1}^m R_{ik}L^h\bar{C}_{dk}L^{hT} \succ 0, \quad (57)$$

$$P\bar{A}_i + \bar{A}_i^T P - \sum_{k=1}^m R_{ik}ll^T\underline{C}_{dk} - \sum_{k=1}^m \underline{C}_{dk}ll^TR_{ik} \prec 0, \quad (58)$$

$$P\underline{A}_i + \underline{A}_i^T P - \sum_{k=1}^m R_{ik}ll^T\bar{C}_{dk} - \sum_{k=1}^m \bar{C}_{dk}ll^TR_{ik} \prec 0, \quad (59)$$

for $i = 1, 2, \dots, s$, $h = 1, 2, \dots, n-1$, $p = 1, 2, \dots, n$, where L , l^T are predefined and

$$\bar{A}_i(p+h, p)_\Delta = \text{diag} [\bar{a}_{i,1+h,1} \dots \bar{a}_{i,n,n-h} \bar{a}_{i,1,n-h+1} \dots \bar{a}_{i,hn}], \quad (60)$$

$$\underline{A}_i(p+h, p)_\Delta = \text{diag} [\underline{a}_{i,1+h,1} \dots \underline{a}_{i,n,n-h} \underline{a}_{i,1,n-h+1} \dots \underline{a}_{i,hn}], \quad (61)$$

$$\bar{C}_{dk} = \text{diag} [\bar{c}_{k1} \bar{c}_{k2} \dots \bar{c}_{kn}], \quad \underline{C}_{dk} = \text{diag} [\underline{c}_{k1} \underline{c}_{k2} \dots \underline{c}_{kn}]. \quad (62)$$

When these conditions are successfully met, (25) defines the rule to compute a set of strictly positive gain matrices $J_i \in \mathbb{R}_{+}^{n \times m}$.

Proof. Adequately adapting (26) then \underline{A}_{ei} takes its open structure

$$\underline{A}_{ei} = \begin{bmatrix} \underline{a}_{i11} & \underline{a}_{i12} & \dots & \underline{a}_{i1n} \\ \underline{a}_{i21} & \underline{a}_{i22} & \dots & \underline{a}_{i2n} \\ \ddots & & & \\ \underline{a}_{in1} & \underline{a}_{in2} & \dots & \underline{a}_{inn} \end{bmatrix} - \sum_{k=1}^r \begin{bmatrix} j_{i1k} \\ j_{i2k} \\ \vdots \\ j_{ink} \end{bmatrix} [\bar{c}_{k1} \bar{c}_{k2} \dots \bar{c}_{kn}] \quad (63)$$

and the constraints on the diagonal elements of (63), if $J_i \in \mathbb{R}_{+}^{n \times m}$ is strictly positive for all i , are by definition

$$\underline{A}_i(p, p)_\Delta - \sum_{k=1}^r J_{dik}\bar{C}_{dk} \prec 0, \quad (64)$$

where J_{dik} is defined in (17) and (61) for $h = 0$ implies

$$\underline{A}_i(p, p)_\Delta = \text{diag} [\underline{a}_{i11} \underline{a}_{i22} \dots \underline{a}_{inn}]. \quad (65)$$

Multiplying the left side by a positive definite diagonal matrix $P \in \mathbb{R}_{+}^{n \times n}$ and using (30) then (64) implies (55). Quite analogously, it can be applied to \bar{A}_{ei} and derived (54).

The condition (31) can be reformulated to \underline{A}_{ei} in the analogous way as

$$L^{hT} \underline{A}_{ei} = \begin{bmatrix} \underline{a}_{i,h+1,1} & \underline{a}_{i,h+1,2} & \cdots & \underline{a}_{i,h+1,n} \\ & \vdots & & \\ \underline{a}_{in1} & \underline{a}_{in2} & \cdots & \underline{a}_{inn} \\ \underline{a}_{i11} & \underline{a}_{i12} & \cdots & \underline{a}_{i1n} \\ & \vdots & & \\ \underline{a}_{ih1} & \underline{a}_{ih2} & \cdots & \underline{a}_{ihn} \end{bmatrix} - \sum_{k=1}^m \begin{bmatrix} j_{i,h+1,k} \\ \vdots \\ j_{ink} \\ j_{1lk} \\ \vdots \\ j_{ihk} \end{bmatrix} \begin{bmatrix} \bar{c}_{k1} & \bar{c}_{k2} & \cdots & \bar{c}_{kn} \end{bmatrix}, \quad (66)$$

while the diagonal elements of (66) for fixed h implies

$$\underline{A}_i(p+h, p)_\Delta - \sum_{k=1}^m J_{dikch} \bar{C}_{dk} \succ 0, \quad (67)$$

where $\underline{A}_i(p+h, p)_\Delta$ is defined in (61) and J_{dikch} is related to J_{dik} in (33).

Pre-multiplying the left side by PL^h and post-multiplying the right side by L^{hT} with $P \in \mathbb{R}_+^{n \times n}$ defined as above, (67) with (33) gives

$$PL^h \underline{A}(p+1, p)_\Delta L^{hT} - \sum_{k=1}^r P J_{ik} L^h \bar{C}_{dk} L^{hT} \succ 0 \quad (68)$$

and applying (30) then (68) implies (57).

Constructing a positive Lyapunov function candidate

$$v(\underline{\epsilon}(t)) = \underline{\epsilon}^T(t) P \underline{\epsilon}(t) > 0, \quad (69)$$

using the same P as above, then solving for

$$\dot{v}(\underline{\epsilon}(t)) = \underline{\epsilon}^T(t) \sum_{i=1}^s h_i(\theta(t)) (\underline{A}_{ei}^T P + P \underline{A}_{ei}) \underline{\epsilon}(t) < 0, \quad (70)$$

which corresponds to the conditions writable for $i \in \langle 1, s \rangle$ in the set of LMIs

$$\underline{A}_{ei}^T P + P \underline{A}_{ei} \prec 0 \quad (71)$$

and results in

$$P \left(A_i - \sum_{k=1}^m J_{dik} l^T C_{dk} \right) + \left(A_i - \sum_{k=1}^m J_{dik} l l^T C_{dk} \right)^T P \prec 0 \quad \forall i. \quad (72)$$

Thus, for $k = 1, \dots, m$, $i = 1, \dots, s$ and with (30) then (72) implies (59), and analogously, (58), (59) guaranty required stability. This completes the proof. \square

To apply for uncertain non-strictly Metzlerian Takagi-Sugeno fuzzy system the principle of structured matrix variables [18] can be adapted, with the following procedure, excluding cases that both the column of \bar{C} and \underline{C} indexed by β are zero column vectors.

Corollary 2. Let for given $\alpha, \beta \in \langle 1, n \rangle$ the off-diagonal element $\bar{a}_{i\alpha\beta}$ of \bar{A}_i as well as the off-diagonal element $\underline{a}_{i\alpha\beta}$ of \underline{A}_i are zero. Then R_{ik} must be structured so that

$$R_{ik} = \text{diag} [r_{ik1} \cdots r_{ik,\alpha-1} r_{ik\alpha} r_{ik,\alpha+1} \cdots r_{ikn}], \quad (73)$$

where

$$r_{ik\alpha} = 0, \quad r_{ik\gamma} > 0 \text{ for } \gamma \neq \alpha, \gamma = 1, \dots, n. \quad (74)$$

If columns \bar{c}_β , \underline{c}_β of \bar{C} , \underline{C} are strictly positive, (73), (74) must be satisfied for all $k = 1, \dots, m$, $i = 1, \dots, p$. Otherwise, for i, k related to positive elements in nonnegative \bar{c}_β , \underline{c}_β .

The proposed design conditions have no tuning parameters with relation to (58), (59). This problem can be redefined using the approaches proposed in [19].

5. Illustrative Example

The system is represented by the Metzlerian Takagi-Sugeno equations (1), (2), where

$$\begin{aligned}\underline{A}_1 &= \begin{bmatrix} -0.272 & 1.940 & 1.450 \\ 0.058 & -3.960 & 0 \\ 0.100 & 0 & -2.910 \end{bmatrix}, \quad \underline{A}_2 = \begin{bmatrix} -0.272 & 1.940 & 1.450 \\ 0.058 & -3.960 & 0.100 \\ 0.100 & 0 & -2.910 \end{bmatrix}, \\ \underline{A}_3 &= \begin{bmatrix} -0.272 & 1.940 & 1.450 \\ 0.058 & -3.960 & 0 \\ 0.100 & 0.080 & -2.910 \end{bmatrix}, \quad \underline{A}_4 = \begin{bmatrix} -0.272 & 1.940 & 1.450 \\ 0.058 & -3.960 & 0.100 \\ 0.100 & 0.080 & -2.910 \end{bmatrix}, \\ \bar{A}_1 &= \begin{bmatrix} -0.258 & 2.060 & 1.550 \\ 0.142 & -3.640 & 0 \\ 0.200 & 0 & -2.550 \end{bmatrix}, \quad \bar{A}_2 = \begin{bmatrix} -0.258 & 2.060 & 1.550 \\ 0.142 & -3.640 & 0.100 \\ 0.200 & 0 & -2.550 \end{bmatrix}, \\ \bar{A}_3 &= \begin{bmatrix} -0.258 & 2.060 & 1.550 \\ 0.142 & -3.640 & 0 \\ 0.200 & 0.080 & -2.550 \end{bmatrix}, \quad \bar{A}_4 = \begin{bmatrix} -0.258 & 2.060 & 1.550 \\ 0.142 & -3.640 & 0.100 \\ 0.200 & 0.080 & -2.550 \end{bmatrix}, \\ B &= \begin{bmatrix} 0.50 & 1.00 \\ 1.00 & 0.90 \\ 0.70 & 1.10 \end{bmatrix}, \quad \underline{C} = \begin{bmatrix} 0.9 & 0 & 0 \\ 0 & 1.2 & 0 \end{bmatrix}, \quad \bar{C} = \begin{bmatrix} 1.1 & 0 & 0 \\ 0 & 1.5 & 0 \end{bmatrix},\end{aligned}$$

while, for all i , $B_i = B$.

It is not hard to attest that \bar{A}_i , \underline{A}_i are Metzler and Hurwitz for all i , $\underline{A}_i \leq \bar{A}_i$, $\underline{C} \leq \bar{C}$, B is positive matrix and \underline{C} , \bar{C} are nonnegative matrices.

For the vector of premise variables and the sector bounds

$$\vartheta(t) = [\theta_1(t) \ \theta_2(t)] = [q_1(t) \ q_2(t)],$$

$$d_1 = \max(q_1) = 1, \ d_2 = \min(q_1) = 0, \ e_1 = \max(q_2) = 1, \ e_2 = \min(q_2) = 0,$$

the sector functions are given as

$$w_{11}(q_1(t)) = \frac{d_1 - q_1(t)}{d_1 - d_2}, \quad w_{12}(q_1(t)) = \frac{q_1(t) - d_2}{d_1 - d_2} = 1 - w_{11}(q_1(t)),$$

$$w_{21}(q_2(t)) = \frac{e_1 - q_2(t)}{e_1 - e_2}, \quad w_{22}(q_2(t)) = \frac{q_2(t) - e_2}{e_1 - e_2} = 1 - w_{21}(q_2(t))$$

and the set of membership functions is aggregated as

$$h_1(\theta(t)) = w_{12}(q_1(t))w_{22}(q_2(t)), \quad h_2(\theta(t)) = w_{12}(q_1(t))w_{21}(q_2(t)),$$

$$h_3(\theta(t)) = w_{11}(q_1(t))w_{22}(q_2(t)), \quad h_4(\theta(t)) = w_{11}(q_1(t))w_{21}(q_2(t)).$$

It is evident that some from the matrices \underline{A}_i , \bar{A}_i are not strictly Metzler and a certain structuring of the diagonal matrix variables R_{dk} is necessary. Since the third column of \underline{C} as well as \bar{C} is zero vector, it is not necessary to define zero elements of the structured diagonal matrix variables R_{dk} in the lower right corner position for $k = 1, 2$ and so the problem with zero elements \underline{a}_{i23} , \bar{a}_{i23} for $i = 1, 3$ is solved in general. Conversely, since c_{22} , \bar{c}_{22} are not equal to zero, it is necessary to choose zero elements $r_{i2} = 0$ in structured diagonal matrix variables R_{i2} , $i = 1, 2$. Summarising,

$$R_{ik} = \text{diag} [r_{ik1} \ r_{ik2} \ r_{ik3}] \succ 0 \text{ for } (k = 1, i = 1, 2, 3, 4) \text{ and } (k = 2, i = 3, 4),$$

$$R_{ik} = \text{diag} [r_{ik1} \ r_{ik2} \ 0] \succeq 0 \text{ for } k = 2, i = 1, 2.$$

To reflect diagonal LMIs structures, the representations of \underline{C} , \bar{C} are given as

$$\underline{C}_{d1} = \text{diag} [0.9 \ 0 \ 0], \underline{C}_{d2} = \text{diag} [0 \ 0.2 \ 0], \bar{C}_{d1} = \text{diag} [1.1 \ 0 \ 0], \bar{C}_{d2} = \text{diag} [0 \ 0.5 \ 0]$$

and with modulo n summation operator $\Delta = (1 \leftrightarrow 3)/3$, for example the representations of \underline{A}_1 are

$$\underline{A}_1(p, p)_\Delta = \underline{A}_i(p, p)_\Delta = \text{diag} [-0.272 \ -3.960 \ -2.910] \quad \forall i \in \langle 1, 4 \rangle,$$

$$\underline{A}_1(p+1, p)_\Delta = \text{diag} [0.058 \ 0 \ 1.450], \underline{A}_1(p+2, p)_\Delta = \text{diag} [0.100 \ 1.940 \ 0].$$

The remaining matrices \underline{A}_i , \bar{A}_i are parameterized analogously.

By applying Theorem 2 for solving by toolbox SeDuMi [20], the feasible solution is obtained as follows

$$J_1 = \begin{bmatrix} 1.1667 & 0.7376 \\ 0.0210 & 0.6443 \\ 0.0286 & 0 \end{bmatrix}, \quad J_2 = \begin{bmatrix} 1.1679 & 0.7389 \\ 0.0210 & 0.6449 \\ 0.0286 & 0 \end{bmatrix},$$

$$J_3 = \begin{bmatrix} 1.1812 & 0.7476 \\ 0.0198 & 0.6491 \\ 0.0270 & 0.0181 \end{bmatrix}, \quad J_4 = \begin{bmatrix} 1.1812 & 0.7476 \\ 0.0198 & 0.6491 \\ 0.0270 & 0.0181 \end{bmatrix},$$

guaranteing Metzler and Hurwitz local system matrices of the interval observer

$$\underline{A}_{e1} = \begin{bmatrix} -1.5553 & 0.8336 & 1.450 \\ 0.0349 & -4.9265 & 0 \\ 0.0686 & 0 & -2.910 \end{bmatrix}, \quad \underline{A}_{e2} = \begin{bmatrix} -1.5567 & 0.8317 & 1.450 \\ 0.0349 & -4.9274 & 0.100 \\ 0.0685 & 0 & -2.910 \end{bmatrix},$$

$$\underline{A}_{e3} = \begin{bmatrix} -1.5713 & 0.8186 & 1.450 \\ 0.0362 & -4.9337 & 0 \\ 0.0703 & 0.0528 & -2.910 \end{bmatrix}, \quad \underline{A}_{e4} = \begin{bmatrix} -1.5727 & 0.8170 & 1.450 \\ 0.0362 & -4.9339 & 0.100 \\ 0.0702 & 0.0527 & -2.910 \end{bmatrix},$$

$$\bar{A}_{e1} = \begin{bmatrix} -1.3080 & 1.1749 & 1.550 \\ 0.1231 & -4.4132 & 0 \\ 0.1743 & 0 & -2.550 \end{bmatrix}, \quad \bar{A}_{e2} = \begin{bmatrix} -1.3091 & 1.1733 & 1.550 \\ 0.1231 & -4.4139 & 0.100 \\ 0.1742 & 0 & -2.550 \end{bmatrix},$$

$$\bar{A}_{e3} = \begin{bmatrix} -1.3080 & 1.1749 & 1.550 \\ 0.1231 & -4.4132 & 0 \\ 0.1743 & 0 & -2.550 \end{bmatrix}, \quad \bar{A}_{e4} = \begin{bmatrix} -1.3091 & 1.1733 & 1.550 \\ 0.1231 & -4.4139 & 0.100 \\ 0.1742 & 0 & -2.550 \end{bmatrix}.$$

Having in mind (43) it is not hard to verify that the condition $\underline{A}_{ei} \leq \bar{A}_{ei}$ is satisfied for all $i \in \langle 1, 4 \rangle$.

Note, feasibility of the presented set of LMIs can be checked also by using the LMI toolbox of MATLAB[®].

Based on the structured matrix variable properties, defined in (73), (74), it is verified that conditions (53)-(59) allows the existence of nonnegative J_i for $i \in \langle 1, 4 \rangle$ such that Lyapunov function (69) establishes asymptotic stability of the interval observer equilibrium. Moreover, set of nonnegative J_i for $i \in \langle 1, 4 \rangle$ for nonnegative initial state of Metzlerian Takagi-Sugeno system guaranties that the lower observer estimate is nonnegative in the sense of (52).

Involving additional inequality constraints the problem of interval observer design is transformed to equivalent linear time invariant forms and make the design problem standard.

6. Concluding Remarks

The key observation is that it can obtain a finite number of linear matrix inequalities to account in design for Metzler and Hurwitz interval observer system matrices and non-negative interval observer gains. Therefore, to obtain a solution, the design method can be applied yielding feasibility of the set of linear matrix inequalities. Moreover, the condition extensions take into account the fact that certain elements of bounds can to equal zero and so reflect also non strictly Metzler matrix structures. The novelty lies in strictly LMI representation of interval bounds, parametric constraints and stability. The example, demonstrating how one can formulate design task, also indicates that defined LMI design conditions are necessary in synthesis of interval observers for uncertain Metzlerian Takagi-Sugeno multidimensional systems.

Presented version prefers standard LMI numerical procedures to manipulate the interval observer stability and structural properties and is guided in the direction of the second Lyapunov method, which guarantees convergence to equilibria of the estimation errors. It seems to be significant to extend the approach for uncertain Metzlerian Takagi-Sugeno continuous-time systems with external disturbances.

Since interval estimation of switched Takagi-Sugeno systems is connected with Metzler system matrices, further future research is naturally focused on this application field. A similar trend can be expected in the positive control of agent systems in the case when additional criteria are found for design of nonnegative gains for agents whose system matrices are not Metzler. Hence it is apparent that exactly the same methods of solution can carry potentially through to fractional fuzzy inference systems.

Acknowledgements

The work presented in the paper was supported by VEGA, the Grant Agency of the Ministry of Education and the Academy of Science of Slovak Republic, under Grant No. 1/0463/21. This support is very gratefully acknowledged.

References

- [1] Takagi T, Sugeno M. Fuzzy identification of systems and its applications to modeling and control IEEE Transactions on Systems, Man, and Cybernetics. 1985; 15(1):116–32.
- [2] Ichalal D, Marx B, Ragot J, Maquin D. Design of observers for Takagi-Sugeno discrete-time systems with unmeasurable premise variables. In: Proceedings of the 5th Workshop on Advanced Control and Diagnosis ACD 2007; 2007 Nov 15-16; Grenoble, France: p. 1-7.
- [3] Gao Z, Shi X, Ding SX. Fuzzy state/disturbance observer design for T-S fuzzy systems with application to sensor fault estimation. IEEE Transactions on Systems, Man, and Cybernetics, Part B: Cybernetics. 2008; 38(3):875-80.
- [4] Rutkowski L. Flexible Neuro-Fuzzy Systems. Structures, Learning and Performance Evaluation. Boston: Kluwer Academic Publishers; 2004. 279 p.
- [5] Mazandarani M, Li X. Fractional fuzzy inference system. The new generation of fuzzy inference systems. IEEE Access. 2020; 8:126066-82.
- [6] Tanaka K, Wang, HO. (2001) Fuzzy Control Systems Design and Analysis. A Linear Matrix Inequality Approach. New York: John Wiley & Sons; 2001. 305 p.
- [7] Wang Y, Karimi HR, Lam HK, Shen H. An improved result on exponential stabilization of sampled-data fuzzy systems. IEEE Transactions on Fuzzy Systems. 2018; 26(6):3875-83.

- [8] Nikaido H. Convex Structures and Economic Theory. New York: Academic Press; 1968. 422 p.
- [9] Smith HL. Monotone Dynamical Systems. An Introduction to the Theory of Competitive and Cooperative Systems. Providence: American Mathematical Society; 1995. 174 p.
- [10] Berman A, Neumann M, Stern R. Nonnegative Matrices in Dynamic Systems. New York: John Wiley & Sons; 1989. 167 p.
- [11] Carnicer JM, Pena JM, Zalik RA. Strictly totally positive systems. *Journal of Approximation Theory*. 1998; 92:411-41.
- [12] Krokavec d, Filasová A. LMI based principles in strictly Metzlerian systems control design. *Mathematical Problems in Engineering*. 2018; 2018:1-14.
- [13] Gouzé JL, Rapaport A, Hadj-Sadok MZ. Interval observers for uncertain biological systems. *Ecological modelling*. 2000; 133(1):45-56.
- [14] Mazenc F, Bernard O. Interval observers for linear time-invariant systems with disturbances. *Automatica*. 2011; 47(1):140-7.
- [15] Krokavec D, Filasová A. Interval observer design for uncertain linear continuous-time Metzlerian systems. In: Proceedings of the 28th Mediterranean Conference on Control and Automation MED '20; 2020 Sep 16-18; Saint-Raphaël, France: p. 1051-6.
- [16] Ito H, Dinh TN. An approach to interval observers for Takagi-Sugeno systems with attractiveness guarantees. In: Proceedings of the 58th Annual Conference of the Society of Instrument and Control Engineers of Japan; 2019 Sep 10-13; Hiroshima, Japan: p. 1268-73.
- [17] Horn RA, Johnson CR. Matrix Analysis. New York: Cambridge University Press; 1985. 643 p.
- [18] Krokavec D, Filasová A. H_∞ norm principle in residual filter design for discrete-time linear positive systems. *European Journal of Control*. 2019; 45:17-29.
- [19] Krokavec D, Filasová A. On observer design methods for a class of Takagi-Sugeno fuzzy systems. *Computer Science & Information Technology*. 2014; 4(11):279-90.
- [20] Peaucelle D, Henrion D, Labit Y, Taitz K. User's Guide for SeDuMi Interface 1.04. Toulouse: LAAS-CNRS; 2002. 37 p.

A Cognitive Robotic System for a Human-Following Robot

Chien Van DANG^a, Heungju AHN^b, Hyeyon C. SEO^a, and Sang C. LEE^{a,1}

^a IO Lab, Division of Intelligent Robot, Convergence Research Institute, DGIST, Daegu,
42988, Rep. of Korea

^b College of Transdisciplinary, DGIST, Daegu, 42988, Rep. of Korea

Abstract. In this paper we propose a cognitive robotic system that utilizes computational psychology (the Soar cognitive architecture) and an obstacle avoidance method (modified dynamic window approach) in ROS (Robot Operating System) platform for controlling a mobile robot. This system is applied to perform a task of human-following, aiming to help the robot navigate itself to the target person avoiding collision. A cognitive agent based on Soar cognitive architecture is created to reason its current situation and make decisions on movement direction such as go-straight, turn-left or turn-right, whereas the dynamic window approach is modified to avoid collision by computing appropriate velocities for driving the robot motors. To the end, a part of implementation is presented to describes how the system works.

Keywords. Cognitive robotic system, obstacle avoidance, following mobile robot

1. Introduction

The problem of human-following for mobile robots has been attracted by world-wide researchers over twenty years. There are two main major issues: firstly, detecting and determining distance from the robot to the target person; secondly, navigating the robot to the target user. In order to achieve such problem, there are a number of different approaches. In particular, we can mention approaches that are using vision based techniques [1,2], non-vision based ones [3,4], transmitter-receiver based ones [5,6], intelligent space techniques [7], and multi-modal approaches [8,9].

This research belongs to multi-modal approach. In order to determine distance from the robot to the target, we use a local positioning system with ultra wideband sensors: a transmitter carried by the target person transmits ultra wave signals, two receivers mounted on the robot receive the signals [10]. However, as the second issue, on which this paper focuses, the robot navigating to the target person needs more attention in unstructured environments. A cognitive robotic system, which associates computational

¹Corresponding Author (E-mail:scline@dgist.ac.kr)

This work was partly supported by DGIST R&D program of the Ministry of Science, ICT, and Future Planning of KOREA (20-IT-03) and Korea Institute of Energy Technology Evaluation and Planning (KETEP) grant funded by the Korea government (MOTIE) (2019-3010032490, Development of 25kW modular fuel cell power conversion system)

psychology based on Soar cognitive architecture with ROS platform, is utilized. Possessing effective knowledge representations with both short-term and long-term knowledge for accessing memory, learning and decision-making, the architecture aims to human-like intelligence [11,12]. On the other hand, ROS platform supports mechanisms for the system to be able to communicate easily with devices. A Soar based agent illustrates how the robot should behave heading to the human target. Besides, a modified dynamic window approach is also proposed as a local controller for the robot.

The rest of this paper is organized as follows. Section 2 describes hardware architecture of a testbed robot and its motion equations with differential drive. Section 3 presents our cognitive robotic system which contains a Soar cognitive agent and a local controller using modified dynamic window approach. A data graph of the system is presented as well. And we wrap-up with discussion and further work in section 4.

2. Robot hardware architecture and motion equations

2.1. Robot hardware architecture

A testbed robot used in this research includes an embedded motor driver board, an embedded control board, three ultra wideband sensors (two on robot, one is carried by a human user), and an RGB-D camera as shown in **Figure 1**. The motor driver board has multiple input and output capabilities, including direct current motors, encoders, and a serial port. The control board, UP squared, with an Intel Atom x7-E3950 2.0GHz processor and 4GB of RAM using the Linux Ubuntu operating system is used to communicate with the motor driver board and several sensors. Working on ROS platform, driver nodes of these devices can be able to easily exchange information. A Soar package is also built on this control board for creating an agent to control the system. Ultra wideband (UWB) sensors are Decawave DWM1001 modules which are claimed to measure distance with a 10cm degree of accuracy [13]. For measuring distance from the robot to the target user, two UWB modules are mounted on the top front left and right of the robot, and one UWB module is carried by the user. An RGB-D camera is an Intel Realsense D435 depth camera which is used to sense obstacles in surrounding environment.

In addition, other hardware components include a DC-DC regulator which converts the battery power 24 voltages to 5 voltages to power the UP board. A monitor screen is also included for monitoring during the debugging process.

2.2. Motion equations for a differential robot

The mobile robot used in this research is equipped with differential drive. That means that the direction of motion is controlled by separately controlling speeds v_l and v_r of the left and right wheels respectively. Starting from the pose $[x, y, \theta]$ at the time t , this motion modeling determines the new pose $[x', y', \theta']$ at the time $(t + \delta t)$ given the control v_l and v_r .

First of all, when the robot is moving in a curve, there exists a center of that curve at that moment, known as the Instantaneous Center of Curvature (ICC). Let R be the radius of the curve, and L be the distance between the two wheels. Then the rate of rotation ω around the ICC is related to the velocity of the robot by equations:

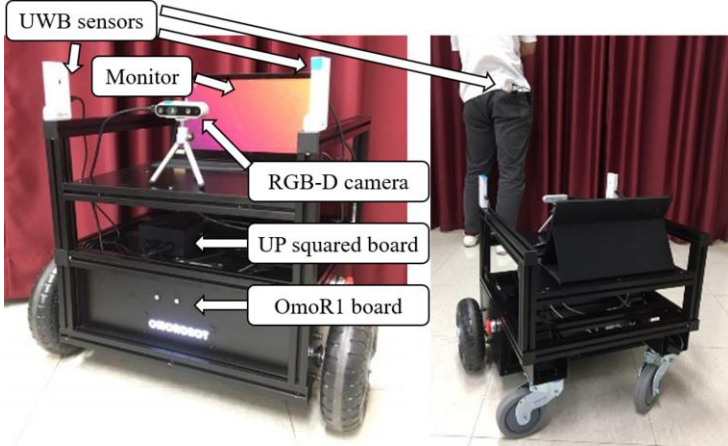


Figure 1. A testbed robot and its components

$$\omega \left(R + \frac{L}{2} \right) = v_r, \quad \text{and} \quad \omega \left(R - \frac{L}{2} \right) = v_l \quad (1)$$

These equations give values of R and ω :

$$\omega = \frac{v_r - v_l}{L}, \quad \text{and} \quad R = \frac{L \cdot (v_r + v_l)}{2(v_r - v_l)} \quad (2)$$

The angle that the robot rotates with angular velocity ω in period of time δt is expressed as follows:

$$\omega \delta t = \frac{(v_r - v_l) \delta t}{L} \quad (3)$$

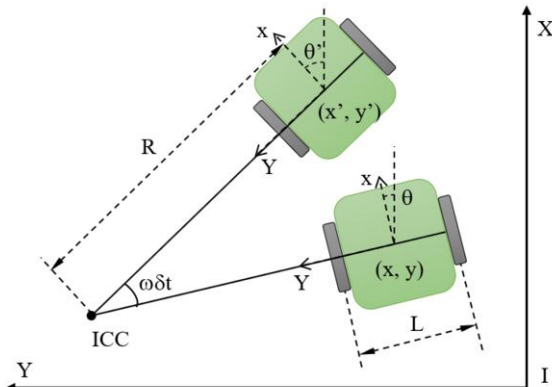


Figure 2. The robot rotating around ICC

We will present the pose of the robot a vector $[x, y, \theta]^T$, where (x, y) is a coordinates of the position of the robot in the xy -plane, θ is the heading which points in the forward

direction of the robot. **Figure 2** illustrates relative position between the current pose and the next pose of the robot. To retrieve the next pose, the robot performs a consequent steps: start at the initial frame, translate out to the current position (${}^I T_c$); rotate to the current orientation (${}^c R_c$); translate to the ICC position (${}^c T_{icc}$); rotate around the ICC to the new angle $\omega\delta t$; finally, translate out to the new position. These steps are described by the equation:

$${}^I T_N = {}^I T_c \cdot {}^c T_{c\theta} \cdot {}^{c\theta} T_{icc} \cdot {}^{icc} T_{\omega\delta t} \cdot {}^{\omega\delta t} T_N \quad (4)$$

Equivalently

$${}^I T_N = \begin{bmatrix} 1 & 0 & 0 & x \\ 0 & 1 & 0 & y \\ 0 & 0 & 1 & 0 \\ 0 & 0 & 0 & 1 \end{bmatrix} \cdot \begin{bmatrix} \cos \theta & -\sin \theta & 0 & 0 \\ \sin \theta & \cos \theta & 0 & 0 \\ 0 & 0 & 1 & \theta \\ 0 & 0 & 0 & 1 \end{bmatrix} \cdot \begin{bmatrix} 1 & 0 & 0 & 0 \\ 0 & 1 & 0 & R \\ 0 & 0 & 1 & 0 \\ 0 & 0 & 0 & 1 \end{bmatrix} \cdot \begin{bmatrix} \cos \omega\delta t & -\sin \omega\delta t & 0 & 0 \\ \sin \omega\delta t & \cos \omega\delta t & 0 & 0 \\ 0 & 0 & 1 & \omega\delta t \\ 0 & 0 & 0 & 1 \end{bmatrix} \cdot \begin{bmatrix} 1 & 0 & 0 & 0 \\ 0 & 1 & 0 & -R \\ 0 & 0 & 1 & 0 \\ 0 & 0 & 0 & 1 \end{bmatrix}$$

Equation (4) results a set of new pose of the robot as follows:

$$\begin{bmatrix} x' \\ y' \\ \theta' \end{bmatrix} = \begin{bmatrix} R\cos \theta \sin \omega\delta t + R\sin \theta \cos \omega\delta t + x - R\sin \theta \\ R\sin \theta \sin \omega\delta t - R\cos \theta \cos \omega\delta t + y + R\cos \theta \\ \theta + \omega\delta t \end{bmatrix} \quad (5)$$

After getting motion mode of the robot, we start to implement a controller on the robot as presented in the next section.

3. Cognitive robotic system

3.1. Cognitive agent

In our cognitive robotic system, a cognitive agent based on Soar cognitive architecture is implemented. A Soar agent attempts to use its knowledge in form of symbol representations about its current state, after applying operation, which will be changed into next state in an effort to reach its goal. The current state which includes the state of the agent and its environment is stored in working memory, that can be regarded as a short-term memory. In the agent, long-term knowledge is encoded as production rules. These rules consist of elaborations and operators to add information and make changes to working memory. Detail information about Soar can be found in [11].

As production rules, operators can be organized into problem spaces that are relevant to specific problem. In this research, the agent has a problem space called avoid-obstacle, in which operators describe how it should move if an obstacle is sensed.

Figure 3 shows a symbol graph of working memory in our following agent. The graph represents relation between the mobile robot, the user and obstacle, as well as their property characteristics. Labels in circles (S1, O1, R1, U1, P1, P2) are called identifiers. Words preceded by a character ^ (robot, user, obstacle, so on) are called attributes. “Combo”, “David”, “Obs1”, and numbers in float type are values that are constant, whereas U1 is the value associated with the character ^ preceding attribute, but is an identifier instead of a constant.

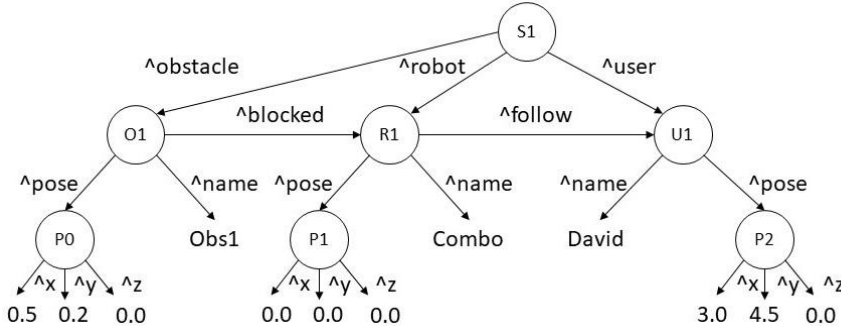


Figure 3. A part of working memory in our cognitive agent

A production rule for creating an operator can be briefly written as follows: If the agent is blocked by an obstacle, the obstacle is on the right direction, then an operator of action turn-left is proposed. After that, another production rule will apply the operator of turn-left and make changes to working memory. A number of actions are used for the agent to make change to the environment such as go-straight, turn-left, turn-right. These actions are then executed by a local controller using a modified version of dynamic window approach which is presented in the next section.

3.2. Modified dynamic window approach

Algorithm 1 MDWA(robot, configure, goal, obstacle, direction)

```

1: allowable_V  $\leftarrow$  generateWindow(robot, configure, direction)
2: allowable_W  $\leftarrow$  generateWindow(robot, configure, direction)
3: for each v in allowable_V do
4:   for each w in allowable_W do
5:     trajectory  $\leftarrow$  predictTrajectory(v, w)
6:     heading  $\leftarrow$  headingCost(trajectory, goal)
7:     clearance  $\leftarrow$  clearanceCost(trajectory, obstacle)
8:     speed  $\leftarrow$  speedCost(v)
9:     cost  $\leftarrow$  costFunction(heading, clearance, speed)
10:    if cost > optimal then
11:      best_v  $\leftarrow$  v
12:      best_w  $\leftarrow$  w
13:      optimal  $\leftarrow$  cost
14:    end if
15:  end for
16: end for
17: velocity_command  $\leftarrow$  (best_v, best_w)

```

Obstacle avoidance controller plays an important role to help the robot tackle current situation while operating in real environment. In this research, a modified dynamic window approach (MDWA) algorithm is utilized for the robot to avoid both static and dynamic obstacles. Pseudo code of the MDWA is described above.

This modified version of dynamic window approach differs from the original version at a point that the movement direction to goal is decided by a cognitive agent. Directions commanded from the agent is converted into a window of velocities in form of $[V_{\min}, V_{\max}, W_{\min}, W_{\max}]$, where V_{\min}, V_{\max} are minimum and maximum translational velocities, W_{\min}, W_{\max} are minimum and maximum angular velocities respectively. For example, turn-left direction refers to a velocity window of $[0, V_{\max}, 0, W_{\max}]$. This window is added to generate velocity window to specify a possible set of velocities for the robot.

3.3. Data flow of the system

During execution of the robot, the following five ROS nodes are concurrently running:

- (1) Detect and determine distance from the robot to the target,
- (2) Measure distance from the robot to its surroundings,
- (3) Acquire motor states,
- (4) Interface with Soar and send output commands for control robot behaviors,
- (5) Compute translational and angular velocities to drive motors.

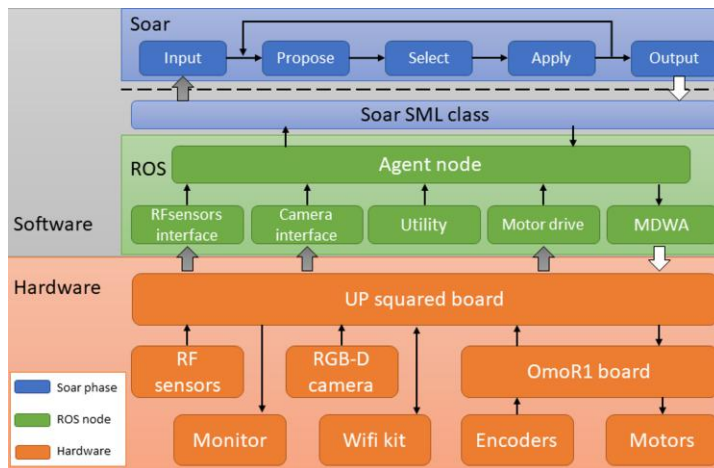


Figure 4. Data flow graph between software and hardware

Figure 4 shows the data flow between hardware devices and software components in the system. The hardware is shown on the bottom layer including an UP squared board, an OmoR1 board, and several devices: ultra wideband sensor, RGB-D camera, motors with encoders. The software in the CRS has primarily two parts: Soar, ROS. The main node, agent node, coordinates communication between five other nodes, all in ROS environment: RFsensor interface node, camera interface node, utility node, motor drive node, and MDWA node. The RFsensor node is a program that activates two UWB sensor modules at the same time, receives measured distance values, then computes relative position and angular direction of the target, and finally sends them to the main node for further processing. The camera node subscribes images from the depth camera, and publishes 3-dimensional coordinates of obstacle.

Besides, the motor drive node is activated to bring-up the robot. Last but not least, the MDWA node is the modified dynamic window approach in order for the robot to be able to avoid static and dynamic obstacles. The agent node is a node that subscribes sensor data, sends them to Soar agent via input links, receives behavior commands from the agent via output links, then publishes commands to the MDWA node to activate the robot.

4. Discussion and future work

This paper introduces a cognitive robotic system which associates Soar cognitive architecture with an obstacle avoidance method in ROS platform in order to operate a mobile robot following the human user. Two main parts including a cognitive agent and a obstacle avoidance controller are described. The agent attempts to reason its current situation, and make decisions on direction of movement, whereas the controller using a modified version of dynamic window approach computes a set of translational and angular velocities to drive the robot motors. Then data flow of the system is presented to show how the system works. Among general approaches to accomplish a human-following robot, this approach of using cognitive robotic system is newly proposed offering the robot abilities of reasoning and decision making like humans to avoid obstacle while following the human user. In additions to local positioning problem, we also have to deal with knowledge representations which should be further studied in the future.

References

- [1] Dixon W.E., Dawson D.M., Zergeroglu E., Behal A. Adaptive tracking control of a wheeled mobile robot via an uncalibrated camera system. *IEEE Transactions on Systems, Man, and Cybernetics, Part B (Cybernetics)*. 2001 Jun; vol. 31(3): p. 341-352.
- [2] Emina P., Adrian L., Danijela R.D., Vlastimir N. Stereo vision-based human tracking for robotic follower. *International Journal of Advanced Robotic Systems*; 2013 Feb; vol 10(5).
- [3] Kawarazaki N., Kuwae L.T., Yoshidome T. Development of human following mobile robot system using laser range scanner. *Procedia Computer Science*. 2015; vol 76: p. 455-460.
- [4] Peng W., Wang J., Chen W. Tracking control of human-following robot with sonar sensors. *Intelligent autonomous systems*. 2016 Feb. vol 531: p. 301-313.
- [5] Akihisa O., Yousuke N., Youhei G. Intelligent escort robot moving together with human – Methods for human position recognition. 2002 Jan.
- [6] Tao F., Yao Y., Lin W., Yanru B., Ziang X., Zhen L. A human-tracking robot using ultra wideband technology. *IEEE Access*. 2018 July; vol. 6: p. 42541-42550.
- [7] Morioka K., Lee J-H., Hashimoto H. Human-following mobile robot in a distributed intelligent sensor network. *IEEE Transactions on Industrial Electronics*. 2004 Feb. vol 51(1): p. 229-237.
- [8] Algabri R., Choi M-T. Deep-learning-based indoor human following of mobile robot using color feature. *Sensors*. 2020 May; vol 20: p. 2699-2718.
- [9] Sebastian L., Marcus K., Sascha H., Jannik F., Gernot A.F., Gerhard S. Providing the basis for human-robot-interaction: a multi-modal attention system for a mobile robot. In *Proceedings of the 5th International conference on Multimodal interfaces (ICMI '03)*. 2003 Nov. p. 28-35.
- [10] Sang C.L., Syamsul R., Heungju A. Anchor placement design for a decoupled simple trilateration algorithm. *Journal of Nonlinear and Convex analysis*. 2019 July; vol 20(7): p. 1327-1339.
- [11] Laird J. The Soar cognitive architecture. The MIT Press. 2012.
- [12] Laird J. et al. "Cognitive robotics using the Soar cognitive architecture. CogRob@AAAI. 2012.
- [13] Decawave DWM1001 development module website: <https://www.decawave.com/product/dwm1001-development-board/> (available on 30th Aug. 2020).

ASCII Art Classification Model by Transfer Learning and Data Augmentation

Akira Fujisawa^{a,1}, Kazuyuki Matsumoto^b, Kazuki Ohta^c, Minoru Yoshida^b,
Kenji Kita^b

^a *Aomori University, Japan*

^b *Graduate School of Technology, Industrial and Social Sciences, Tokushima University,
Japan*

^c *Faculty of Engineering, Tokushima University, Japan*

Abstract. In this study, we propose an ASCII art category classification method based on transfer learning and data augmentation. ASCII art is a form of nonverbal expression that visually expresses emotions and intentions. While there are similar expressions such as emoticons and pictograms, most are either represented by a single character or are embedded in the statement as an inline expression. ASCII art is expressed in various styles, including dot art illustration and line art illustration. Basically, ASCII art can represent almost any object, and therefore the category of ASCII art is very diverse. Many existing image classification algorithms use color information; however, since most ASCII art is written in character sets, there is no color information available for categorization. We created an ASCII art category classifier using the grayscale edge image and the ASCII art image transformed from the image as a training image set. We also used VGG16, ResNet-50, Inception v3, and Xception's pre-trained networks to fine-tune our categorization. As a result of the experiment of fine tuning by VGG16 and data augmentation, an accuracy rate of 80% or more was obtained in the "human" category.

Keywords. ASCII art, transfer learning, fine tuning, data augmentation

1. Introduction

In recent years, so-called net framing, whereby critical comments have increased explosively due to comments and behaviors on the Web, has become a problem. From the viewpoint of risk management, the use of social media is often prohibited or censored by persons belonging to organizations such as companies. On the Web, on the other hand, electronic bulletin boards have existed as an online culture that flourished before the development of social media. In particular, anonymous bulletin boards allow users to avoid the risk of spreading personal information about themselves and they are easy to use because they allow users to write their intentions easily. As a result, the number of anonymous bulletin board users has exploded with the spread of the Internet.

The disadvantage of being anonymous, however, is that it leaves users prone to crime notifications, online bullying, and profanity. For example, bulletin boards often have users who engage in trolling on the Internet and they are often confusing. On the

¹ Corresponding Author: Akira Fujisawa, Faculty of Software and Information Technology, Aomori University. E-mail: fujisawa@aomori-u.ac.jp

operation side, it is costly to delete harmful write monitors such as net patrol settings. Therefore, although it may be possible to deal with this issue by filtering writing using stop words, doing so is often delayed until the problem becomes serious.

Some online trolls use ASCII art copy and paste. Since ASCII art contains visual information rather than regular text, it has a strong impact and can be said to have a powerful effect on first-time users.

In this research, we grasp the visual representation of ASCII art as an image rather than text information, and classify objects drawn in ASCII art into categories. Most ASCII art is unrestricted in its use and it rarely occurs in typical real-world scenes; therefore, it is rarely treated as a target for image processing. For this reason, there is no large-scale data set of ASCII art, and it is difficult to secure a sufficient amount of data for machine learning such as deep learning. Therefore, this study uses a deep learning model trained on various objects and tasks for transfer learning and the learning data are enriched. Instead of simply processing and padding the training data, it is recommended to use different kinds of image corpus and use more diverse images as training data.

By this research, the ASCII Art classification model by using DCNN would become easier to generate. These methods become to help to judge that text which appeared in Internet are trolls or not.

2. Related Research

2.1. Studies on ASCII arts

ASCII art research includes text extraction, automatic generation, and content classification. Suzuki [1] proposed a method that uses the REL (Run Length Encoding) algorithm to regard ASCII art, which comprises text data, as data of a specific length, and to extract ASCII art from text.

Fujisawa et al. [2] proposed a method of using image features to recognize pictograms or ASCII art that has more information than pictograms. Matsumoto et al. [3] proposed a method to classify input ASCII art by work category by focusing on the types and numbers of characters that appear in ASCII art and extracting each as a feature.

In a previous study, Fujisawa et al. [4] also proposed how to process a regular photo image and treat it as training data for ASCII art classification to create a deep learning classifier for ASCII art.

2.2. Transfer Learning

Transfer learning is a method of applying a model trained to solve a specific task to solve a task that differs from the original target. If we do not have sufficient training data to perform deep learning, our goal is to supplement the missing training data by applying a model created on the basis of sufficient training data for various tasks. Nakayama [5] evaluated the effectiveness of transfer learning aimed at compensating for the lack of data, and in particular the diversity of deep learning models created using ImageNet [6].

In transfer learning, the weights of the original model are used as they are by adjusting only the final output layer of the pre-trained model; however, by adding another training data and retraining, the learning model can be expanded. There is also a method called fine adjustment of fine tuning, which allows us to obtain more accurate output for unknown input data that were not supported by the original model by using the data that correspond to the new task for training.

Hetsugi et al. [7] created a classifier using CNN (convolutional neural network) to classify excavated stone tools. To extend the learning model, they performed transfer learning based on an existing learning model created using ImageNet. This is a fine-tuning using existing high-performance classification models, similar to the classification problem built into this study. As in this study, we are studying data expansion at the same time as transfer learning, and are studying the methods necessary to create an efficient classifier for classification objects that do not have a large data set.

Another study that uses fine-tuned transfer learning is Yamada et al., [8] which aims to identify artifact areas from landscape images. In their research, the model that is the basis of the fine adjustment uses ImageNet data, while the model created based on ImageNet in the field of image processing using CNN is a reliable and effective way to recognize an object.

2.3. Domain Adaptation

Domain adaptation is a kind of transfer learning method. When we create a classification model in CNN, we need training and test data, which are also called source and target domains, respectively. In a real classification task, the source and target domains rarely have the same environmental data, and the classification performance varies from domain to domain. Domain adaptation aims to improve the classification performance of the generated model by processing the source domains and reducing the differences between domains.

Ishii et al. [9] realized domain adaptation by executing conversion processing when extracting features from the source domain. Suzuki et al. [10] proposed a method for domain adaptation by simplifying the domain and reducing the image in the source domain. This study also proposes a way to treat the source domain to mimic the ASCII art of the target domain when creating a classifier based on different source domains for adaptive learning.

3. Proposed Method

3.1. Data Augmentation

In this research, data expansion is performed from the following two viewpoints:

1. Add processed data by adding rotation etc. to the original training data.
2. From the material that differs from the original training data, add the processed data like the original training data.

In both cases, the original image set is required. This study classifies ASCII art using a dataset that collects ASCII art by category. In step 1, the training data auto-expansion feature is used to increase the number of images by three for each image. The transformation parameters (such as rotation angle) are random, and each experiment performs different expansions.

In step 2, since data are added from image datasets with different characteristics, learning efficiency may be reduced depending on the data collection method, which may adversely affect accuracy. To keep the selection criteria consistent, we used the same search engine (such as Google search) to collect data for deployment and the same operator selected the image.

3.2. Fine Tuning with the Pre-trained Model

This study used four pre-trained deep learning models: VGG16 [11], ResNet-50 [12], Inception-v3 [13], and Xception [14].

VGG16 is a kind of deep convolutional neural network consisting of 13 layers of convolution and 3 layers of total connections. We achieved high performance in the 2014 ILSVRC (ImageNet Large Scale Visual Recognition Challenge) image classification task. ResNet-50 is a network consisting of 50 layers, which has a structure called shortcut connection (residual module) and which uses the output of residuals to avoid the problem that the gradient disappears when the layers become deeper.

Inception v3 is a convolutional neural network trained using over 1 million images in the ImageNet database. It has a structure called Inception module, which is a stack of small networks with a depth of 48 layers. Xception outperformed Inception v3 in the ImageNet image recognition task. A structure called separable convolution (spatial and channel convolution to reduce the number of parameters) is used.

By using the weights of the learned network as they are, it is possible to create a classifier with a certain level of performance, without additional learning of a large amount of data from the beginning, by additional learning of a small amount of data. For this reason, in this study, performing a transfer learning using a trained model and performing fine adjustment, which is a method of re-learning the layers near the output layer, cause overlearning and a decrease in accuracy due to lack of training data.

4. Evaluation experiment

4.1. Experimental Data

The image data used in the experiment comprised a web search engine for each of the five categories of “car,” “cat,” “fish,” “flower,” and “human.” Data were collected manually and there are four types of image data: “ASCII art (AA),” “photo/illustration (image),” and “images converted from pictures or illustrations to ASCII art using the automatic conversion tool (ImgToAA).” Table 1 shows an example. Of these, only ASCII art is classified in this study, while others are used as training data.

Table 2 shows a breakdown of the collected data. For learning, preprocessing involves cropping into squares with short sides, and for photos/illustrations, grayscale conversion and conversion to edge images.

4.2. Transfer Learning and Fine Tuning

In this study, the weights of the pre-trained network are used as they are, but the transfer characteristics are learned and fine-tuned because it is necessary to match the property and category type of data to the task of ASCII art classification.

Instead of removing the output layer of the trained network, we added a 2D Global Average Pooling (GAP) Layer, 256 units of fully connected layer, and a fully connected layer (using Softmax function as an activated function) into five categories as a new output layer. Here, in the case of transfer learning, the weights just before the GAP layer were not updated in learning. For fine tuning, the layer immediately before the GAP layer was updated.

Table 1. Example of Dataset

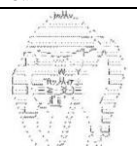
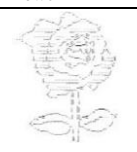
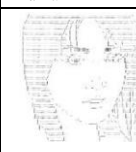
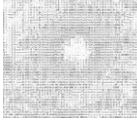
Category	Car	Cat	Fish	Flower	Human
AA					
Image					
Image to AA					

Table 2 Breakdown of Collected Image Dataset

Category	AA	Image	ImgToAA	Total
Car	200	200	200	600
Cat	200	200	200	600
Fish	200	200	200	600
Flower	200	200	200	600
Human	200	200	200	600
Total	1000	1000	1000	3000

We used TensorFlow's Keras module (version 2.2.0) to train and evaluate the model. We implemented RMSprop as an optimization method, set the learning rate to 0.001, and implemented early stop, which stops learning when the loss value of the loss function becomes less than 0.1.

4.3. Evaluation Method

In this experiment, four types of pre-training network were used to train the ASCII art category classification model by combining the seven types of training data shown in

Table 3 to evaluate performance. In addition, the data were randomly sorted by category and created in five parts. Cross-validation of the five parts calculates and evaluates Accuracy, Recall, Precision, and mean F-score. The equations for Accuracy, Recall, Precision, and F-score are shown in Equations 1 - 4. In this formula, M is the number of categories, C_i is the number of successful classifications of ASCII art for categories i , N_i is the number of ASCII arts in category I , and O_i is the number of ASCII arts classified as category i by the classifier.

$$\text{Accuracy}(\%) = \frac{\text{Number of Correct AA}}{\text{Total number of AA}} \times 100 \quad (1)$$

$$\text{Recall}(\%) = 100 \times \frac{1}{M} \sum_{i=1}^M \frac{C_i}{N_i} \quad (2)$$

$$\text{Precision}(\%) = 100 \times \frac{1}{M} \sum_{i=1}^M \frac{C_i}{O_i} \quad (3)$$

$$\text{F-score} = \frac{\text{Recall} \times \text{Precision} \times 2}{\text{Recall} + \text{Precision}} \quad (4)$$

Table 3 Combination of Training Data

No.	Combination of Training Data
1	AA
2	AA, Image, ImgToAA
3	AA, Image
4	AA, ImgToAA
5	Image
6	ImgToAA
7	Image, ImgToAA

5. Results and Discussion

5.1. Experimental Results

The experimental results (correct answer rate, F value) by transfer learning are shown in Tables 4 - 7, and the experimental results (correct answer rate, F value) by fine adjustment are shown in Tables 8 - 11. Bold number means a best score of accuracy and f-measure in each category.

Table 4 Experimental Result (Transfer Learning: VGG16)

Combination	1	2	3	4	5	6	7
Accuracy	78.0	76.1	79.6	75.8	36.3	31.5	35.0
F	Car	89.6	88.6	87.1	88.6	30.1	11.4
	Cat	62.3	58.4	66.7	59.5	2.9	25.4
	Fish	72.6	71.5	75.5	70.3	21.7	1.0
	Flower	72.7	72.5	76.6	69.7	51.8	36.0
	Human	91.9	88.2	91.0	90.2	46.0	46.7

Table 5 Experimental Result (Transfer Learning: ResNet-50)

Combination	1	2	3	4	5	6	7	
Accuracy	59.2	52.1	53.8	57.9	28.7	23.2	31.5	
F	Car	76.9	73.4	77.6	76.8	40.3	26.3	48.7
	Cat	42.6	29.1	15.7	28.5	8.1	2.8	11.7
	Fish	53.5	42.2	42.3	45.8	21.8	2.0	9.5
	Flower	47.3	45.3	52.3	55.3	33.0	34.3	34.5
	Human	71.0	65.4	62.3	67.3	34.4	26.9	38.1

Table 6 Experimental Result (Transfer Learning: Inception v3)

Combination	1	2	3	4	5	6	7	
Accuracy	71.7	68.6	69.7	69.6	41.8	29.2	42.4	
F	Car	81.2	81.3	80.8	81.4	52.6	19.7	42.9
	Cat	54.2	47.8	51.7	48.8	14.4	5.2	9.9
	Fish	67.8	62.7	67.0	65.4	32.0	19.0	39.2
	Flower	69.6	67.0	66.1	68.0	43.4	42.2	50.4
	Human	84.9	80.6	81.2	81.9	51.5	36.2	52.8

Table 7 Experimental Result (Transfer Learning: Xception)

Combination	1	2	3	4	5	6	7	
Accuracy	73	68.6	70.2	69.4	44.1	31.6	42.8	
F	Car	84.9	80.1	82.0	80.7	53.9	21.3	46.5
	Cat	55.2	48.9	48.9	50.4	15.7	4.0	5.4
	Fish	66.7	63.9	65.4	66.3	36.7	19.1	39.0
	Flower	72.4	68.0	69.4	66.3	46.7	43.5	50.1
	Human	84.4	79.1	82.4	80.4	53.7	42.7	53.5

Table 8 Experimental Result (Fine Tuning: VGG16)

Combination	1	2	3	4	5	6	7	
Accuracy	73.8	59.4	74.8	75.2	42.3	31.4	46.1	
F	Car	71.5	69.3	67.4	68.0	69.6	65.4	66.4
	Cat	46.6	44.8	43.5	43.3	44.1	41.7	41.7
	Fish	55.1	53.2	51.5	52.1	52.9	49.9	50.2
	Flower	57.6	56.2	55.0	55.5	56.1	53.3	54.5
	Human	71.8	69.7	68.4	68.8	68.8	66.8	67.5

Table 9 Experimental Result (Fine Tuning: ResNet-50)

Combination	1	2	3	4	5	6	7	
Accuracy	40.1	40.2	49.4	42.8	32.1	24.9	35.1	
F	Car	56.7	55.4	54.1	54.1	55.6	52.3	53.3
	Cat	23.7	23.6	21.7	22.1	22.4	21.1	21.1
	Fish	37.6	36.9	35.3	35.9	36.1	34.5	35.2
	Flower	42.7	41.8	41.9	40.9	42.3	41.4	41.2
	Human	38.9	41.6	38.7	39.6	38.4	37.3	39.4

Table 10 Experimental Result (Fine Tuning: Inception v3)

Combination	1	2	3	4	5	6	7	
Accuracy	57.4	47.1	57.5	59.7	38.4	23.4	35.9	
F	Car	58.0	56.3	55.2	55.1	56.6	53.7	53.2
	Cat	34.4	33.3	32.6	32.7	33.1	31.6	31.6
	Fish	47.3	46.3	45.3	45.4	46.6	44.1	44.5
	Flower	47.5	46.8	45.9	46.3	46.7	45.0	45.6
	Human	53.9	52.3	50.8	51.2	52.4	49.2	50.2

Table 11 Experimental Result (Fine Tuning: Xception)

Combination	1	2	3	4	5	6	7
Accuracy	58.9	45.4	57.3	53.4	33.6	29.9	30.1
F	Car	57.5	54.7	54.8	54.2	55.9	52.6
	Cat	31.6	30.3	29.3	28.5	29.9	28.3
	Fish	40.2	37.9	37.9	37.0	38.4	35.8
	Flower	43.8	43.4	43.1	43.4	42.4	43.0
	Human	54.5	52.6	52.7	51.8	52.7	51.6

In the transfer learning results, the maximum correct answer rate was 79.6% when the combination of VGG16 and learning data (3:AA, Image) was obtained. As a result of fine tuning, the correct answer rate and F value were lower than those of transfer learning.

When fine tuning was performed, the combination of learning data with VGG16 (4:AA, ImgToAA) gave the highest correct answer rate. In both transfer learning and fine tuning, the combination of learning data (7: Image, ImgToAA) shows the lowest correct answer rate, while the correct answer rate is the same when using Image and ImgToAA individually as the learning data.

Furthermore, the F-values of “human” and “cars” tended to be high. One cause of this may be that the dataset contained many similar pieces of ASCII art in the automobile category.

5.2. Discussion

Comparing all the results, regardless of the model used, the F value is the lowest value for cat ASCII art in all five categories. This is because most of the AA used as learning data were deformed. When we expanded the data, it was difficult to find common points in the learning data and feature extraction failed. Figure 1 is an example of a deformed “cat” AA.

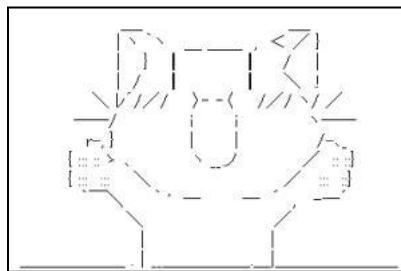


Figure. 1 Deformed cat's ASCII art

This time, the image was converted to ASCII art for domain adaptation. Many of the original images included the background, and when converted to ASCII art, the background information was also included in the conversion.

Figure 2 shows an example of an image before and after conversion of the category “flower.” In this example, the background of the original image (pot clay and shadow) is also represented as a component of ASCII art, so the converted ASCII art itself has a large amount of information.



Figure 2 Photo of flower and Image, which converted into AA from the photo of a flower

Figure 3 shows an example of the image before and after the conversion of the category “car.” In this example, the original image has a solid background, so converting it to ASCII art will only properly convert the target object to ASCII art. As a result of the experiment, many images with a composition with little background were seen even among “human” with high F values on average. Therefore, when converting an image to ASCII art, it is considered that the classification performance is greatly affected by the influence of the background. Therefore, when transforming the original image for domain adaptation, in addition to monochromatization by grayscale conversion, preprocessing and region extraction are performed, and only the target object is extracted to determine the matching rate between domains.

5.3. Visualizations

To explore how the learning network used in the experiment extracts features, we used UMAP to visualize in two dimensions [15]. Figure 4 shows the result of inputting ASCII art into VGG16 and visualizing the output of the GAP layer. Categories are displayed in color. From this figure, it can be seen that the ASCII art features are not grouped into categories and have a wide distribution.



Figure 3 Photo of a car and Image which converted into AA from the photo of a car

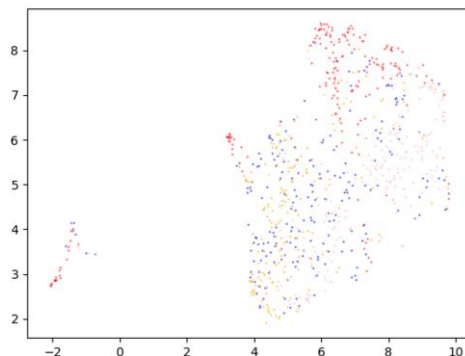


Figure 4 Visualization by UMAP (AA, VGG16)

After tweaking and learning only the ASCII art, these features can be visualized in UMAP as shown in Figure 5.

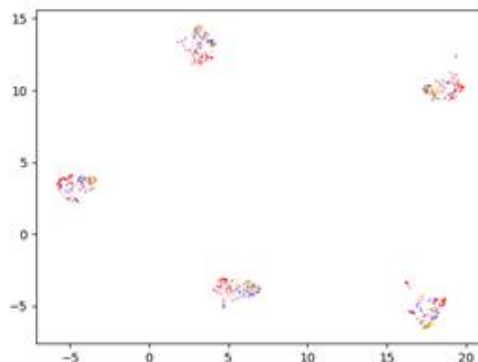


Figure 5 Visualization by UMAP (Fine Tuned)

From this result, it can be seen that a highly accurate classifier cannot be learned. This is because the ASCII ART data set collected in this study may have been over-learned due to lack of diversity and lack of data only by data expansion. In fact, there was a problem that the value of verification loss in cross validation did not decrease even if learning progressed.

For these reasons, expansion of the amount of learning data is vital, while the edge feature is important for ASCII art that does not have color information. Therefore, both training and evaluation perform edge enhancement and preprocessing. It may be necessary to clarify the shade to improve accuracy.

6. Conclusion

This study (1) data expansion and (2) trained models to compensate for the lack of training data for ASCII art categorization. In data expansion, the volume of ASCII art data collected is small, so in addition to conventional data expansion methods such as rotation, the same processing as ASCII art is performed from image corpora (photos, illustrations) that have different characteristics from ASCII. We also proposed a method to increase learning data by applying art.

We used multiple neural network architectures as trained models. As a result of the evaluation experiment, transfer learning and fine adjustment was performed. When transfer learning was performed by including ASCII art in the learning data, a high F value was obtained as a whole. The highest correct answer rate (79.6%) was obtained when using the learning images obtained by converting images and illustrations into edge images in addition to ASCII art.

Furthermore, most of the ASCII art in the dataset created this time contained many modified images. However, the illustrations other than the photos that were added when the data were developed were almost untransformed and realistic. This difference in data quality may have affected the loss of accuracy. To improve the classification accuracy, it is necessary not only to prepare all kinds of image data but also to select an image according to the tendency of the ASCII art to be classified.

In future work, we will perform object detection to the training image as preliminary preparation. By this, we try to remove the evil effect of background of test data. By using the test image that were removed background as training data, we would become able to generate the good performance ASCII Art classification model.

Acknowledgments

This work was supported by JSPS KAKENHI Grant Numbers JP20K12027, JP18K11549.

References

- [1] Tetsuya Suzuki: Introduction of N-gram into a run-length encoding based ASCII art extraction method, Proceedings of 15th International Conference on Current Trends in Web Engineering, ICWE 2015 Workshops NLPIT, PEWET, SoWEMine, Lecture Notes in Computer Science, 9396, pp. 28-39, 2015.
- [2] Akira Fujisawa, Kazuyuki Matsumoto, Noriyuki Okumura, Minoru Yoshida, and Kenji Kita : Challenge to ASCII Art – An Image Feature-Based Approach –, Journal of JSAI, 32(3), pp.364-371, 2017.
- [3] Kazuyuki Matsumoto, Akira Fujisawa, Minoru Yoshida and Kenji Kita: ASCII Art Classification based on Deep Neural Networks Using Image Feature of Characters, Journal of Software, Vol.13, No.10, pp. 559-572, 2018.
- [4] Akira Fujisawa, Kazuyuki Matsumoto, Kazuki Ohta, Minoru Yoshida and Kenji Kita: ASCII Art Category Classification based on Deep Convolutional Neural Networks, Proceedings of the 5th IEEE International Conference on Cloud Computing and Intelligence Systems (CCIS), pp.345-349, 2018.
- [5] Hideki Nakayama, Image Feature Extraction and Transfer Learning Using Deep Convolutional Neural Networks, IEICE Technical Report, vol. 115, no. 146, SP2015-45, pp. 55-59, 2015.
- [6] ImageNet: <http://www.image-net.org/> (accessed 2020-07-13).
- [7] Michihiro Hetsugi, and Fumihiro Yamagushi, Excavator Classification model by CNN and Data Augmentation about training model., Proc.82nd National Convention of IPSJ, 2020, 1, pp.553-554, 2020.
- [8] Sohei Yamada, and Yuko Osana, Improving Accuracy of Artifact Region Identification using Convolutional Neural Networks with Fine Turing, Proc.82nd National Convention of IPSJ, 2020, 1, pp.295-296, 2020.
- [9] Masato Ishii, and Atsushi Sato, Joint Optimization of Feature Transform and Instance Weighting for Domain Adaptation, The 30th Annual Conference of the Japanese Society for Artificial Intelligence, 2016, 4K1-1in2, pp.1-4, 2016.
- [10] Ryosuke Suzuki, Tadachika Ozono, and Toramatsu Shintani, On a Domain Adaptation Method Based on Image Simplification for Machine Learning with Synthetic Data, The 34th Annual Conference of the Japanese Society for Artificial Intelligence, 2020 , 2H5-GS-13-03, pp.1-2, 2020.
- [11] Karen Simonyan and Andrew Zisserman: Very Deep Convolutional Networks for Large-Scale Image Recognition, Proceedings of ICLR 2015.
- [12] Kaiming He, Xiangyu Zhang, Shaoqing Ren and Jian Sun: Deep Residual Learning for Image Recognition, Proceedings of 2016 IEEE Conference on Computer Vision and Pattern Recognition (CVPR), 2016.
- [13] Christian Szegedy, Vincent Vanhoucke, Sergey Ioffe, Jonathon Shlens, Zbigniew Wojna: Rethinking the Inception Architecture for Computer Vision, Proceedings of IEEE Conference on Computer Vision and Pattern Recognition, 2016.
- [14] François Fleuret: Xception: Deep Learning with Depthwise Separable Convolutions, Proceedings of 2017 IEEE Conference on Computer Vision and Pattern Recognition (CVPR), 2017.
- [15] Leland McInnes, John Healy, James Melville: UMAP: Uniform Manifold Approximation and Projection for Dimension Reduction, The Journal of Open Source Software Vol. 3, No. 29, 861, 2018.

The Efficiency of Employment Relationship: Through Data Envelopment Analysis

Wang Kunyi¹, Liu Ping, Liu Yujiang
Sichuan University, Chengdu, China

Abstract. Employment relationship (ER) is a social exchange relationship in nature with uncertainty and incongruence during the exchange process. Previous studies has been stuck on regression-based methods, examining and exploring related issue by studying the exchanges of both parties and even more stakeholders, but the nature of the exchange process itself is ignored. This study jumps out of the causality study represented by the regression analysis method, and uses the FCE that reflects the essence of object better and the Data Envelopment Analysis(DEA) to measure the efficiency of the exchange process, which can help enterprises to improve the evaluation of ER. DEA is used to evaluate the technical effectiveness of decision units (DMUs) with the same type of inputs and outputs. The result suggests that the phenomenon of inefficient exchange is still widespread. We make the importance ranking of selected inducement and find that labors in China attach importance to the correctness of management process rather than the additional benefits. For the first time, the quantitative efficiency value replaces the simple description “uncertainty” in research of the exchange process. Meanwhile, the framework independently measures the input of enterprises and the output of employees which has high adaptability. It can adjust, modify and accurately evaluate the exchange efficiency of two parties according to the actual exchange situation.

Keywords. Employment relationship, Social exchange, Data envelopment analysis, Work engagement

1. Introduction

ER, a social exchange relationship [1], is the most basic social relationship as one of the foundations for the development of economy. The tangible or intangible resources owned by the enterprise are exchanged with employees' performance; the company provides employees with guarantees or incentives in exchange for positive returns such as organizational commitment and high performance [2].

Regrettably, studies have shown that the exchange may not be fully efficient: the inputs of the enterprises have not been fully transformed into the expected returns from its employees [3]. The level of policy implementation of the organization may differ from the perception of employees [4], resulting in a disagreement between the two parties in most enterprises, and the employee's performance factors are not fully invested in the work [5]. The existence of this difference leads to the inefficiency of

¹ Corresponding Author: Wang Kunyi, Sichuan University, Chengdu, China. Email: 31788400@qq.com

enterprise management, which brings unnecessary heavy burden to the normal operation of the enterprise. At the same time, enterprises are caught in the blind area of management, unable to effectively deal with various problems arising from ER management, and burying hidden dangers for the overall human resources management and strategic development. As a result, how organizations can identify better-performing projects from a wide range of alternative management tools, and improving the efficiency of ER exchange process to achieve higher levels of employee engagement and performance has become an important topic. This study introduces data envelopment analysis (DEA) to evaluate the exchange efficiency between enterprise input and employee returns in the process of ER exchange, verifies the following problems: (1) Whether the exchange process in ER is efficient; (2) Sorting the contribution of various factors invested by the enterprise to the efficiency of the exchange process and identifying inefficient inputs.

2. Theoretical Framework and Propositions

This model conceptualized employment relationship as an exchange relationship where employees provide contributions in exchange for inducements from organization [6][7]. The studies of perceived organizational support (POS) and leader-member exchange (LMX) hold similar view of inducements with Foa and Foa's[8] prediction. Hence, the validity of inducements through the theory of POS and LMX rely on the validity of the theory of proximity [9][10][11].

Hard inducements, or known as transactional [12][13], are measurable and tangible in employment relationships. For organization (as an anthropomorphic "employer"), the process of exchange differs from it between individuals (view the direct supervisor as "employer") and mostly its inducements are in the form of resources and management in order to build long-term trust with employee and stabilize the exchange in employment relationship. Therefore, the inducements contain HRM practices and management policies that protect employees' basic rights and economic relations (hard inducements) within the framework of labor laws. The evaluation system above can accurately and objectively reflect the employer's input level of inducements, and proposes the following propositions:

Proposition I: The hard inducements from organization can be measured by compliance in the employment relationship. **Proposition II:** The soft inducements from organization can be measured by competition in the employment relationship.

Work engagement (WE) is closely related with employee performance [14] and business operation [15]and it refers to the state in which organization members bring themselves into the role of work through self-management [16]. For a variety of reasons, in the process of exchange of employment relationship, the expectation of one party to the other party's obligations may be different from the other's own perception, which is called (obligation) fulfillment incongruence [17].

Proposition III: The contribution from employees can be measured by the level of their work engagement. **Proposition IV:** The exchange in employment relationship is inefficiency due to the incongruence in employees' and organization's perceptions of obligations.

3. Methodology

In this study, 45 enterprises were selected from China, including field research and online surveys. Refer to Maas and Hox's study of the sample size requirement of cross-level models [18], removing sample enterprises that didn't archive this requirement and resulted in 38 valid enterprises with 2,711 valid surveys. Based on Liu and Duan's ER evaluation system [19], the level of inducements was measured by professional teams which contain professors and third-party HR managers through field research. The questionnaire used a seven-level short form UWES of nine items proposed by Schaufeli et al [20]. The collected data was calculated by fuzzy comprehensive evaluation (FCE) based on entropy weight method. The original DEA model was named the CCR model by the initials of Charnes [21], assuming that the scale returns were unchanged. For an DEA model which n stands for the quantity of DMUs, and m stands for the inputs x_i , each with a weight v_i while q stands for the outputs y_r , each with a weight u_r . The model indicates that the efficiency value of each DMU is maximized in the case where the scale return is constant and the efficiency value does not exceed 1. The linear programming model is

$$\begin{aligned}
 & \min \sum_{i=1}^m v_i x_{ik} \\
 \text{s.t. } & \sum_{r=1}^s u_r y_{rj} - \sum_{i=1}^m v_i x_{ij} \leq 0 \\
 & \sum_{r=1}^q u_r y_{rk} = 1 \\
 & v \geq 0; u \geq 0 \\
 & i = 1, 2, \dots, m; r = 1, 2, \dots, q; j = 1, 2, \dots, n
 \end{aligned} \tag{1}$$

The weight of all 13 input indicators including compliance and competition have been reflected in its full score. The output is calculated to one indicator thus the weight is 100%. Therefore, the ER efficiency linear programming model of DMU_k ($k = 1, 2, \dots, 43$) in any of the 43 companies in this study is

$$\begin{aligned}
 & \min \sum_{i=1}^{11} x_{ik} \\
 \text{s.t. } & WE_j - \sum_{i=1}^{11} x_{ij} \leq 0 \\
 & WE_j = 1 \\
 & j = 1, 2, \dots, 43
 \end{aligned} \tag{2}$$

which x_{ij} stands for the i th inducements input indicator in the j th sample enterprise ($k=1, 2, \dots, 43; i=1, 2, \dots, 11$). WE_j stands for the contribution output indicator from employees in the j th sample enterprise ($j=1, 2, \dots, 43$).

4. Results

Among the valid samples, there are 5 pharmaceutical industry enterprises, 8 IT enterprises, 11 service industry enterprises, 11 manufacturing enterprises, and 3 enterprises from other industries. Among the employee data, there are 49.6% males and 50.4% are females, ranged from 15 to 60 years old. The maximum length of service is 38 years and the average is 4.8 years.

This research results in the percentile system which the highest score is 96.46 points and the lowest is 72.29 points, in average 88.25 points. For five competitive indicators results in the percentage system which the highest score is 88.64 points and the lowest is 40.00 points, in average 62.21 points.

The results are shown in Table 1.

Table 1. CFA Test for UWES-9

	λ^2	df	CFI	TLI	RMSEA (90% C.I.)	SRMR
Single-factor Model	507.010	27	0.933	0.911	0.082 (0.076, 0.088)	0.025
Three-factor Model	461.005	24	0.939	0.909	0.083 (0.077, 0.090)	0.025

It can be seen from Table 1 that there is no significant difference in the goodness of fit indexes between the single factor model and the three factor model.

4.1 The level of employee contribution

$$A_{WE} = [0.117 \quad 0.068 \quad 0.101 \quad 0.106 \quad 0.147 \quad 0.130 \quad 0.089 \quad 0.133 \quad 0.109] \quad (3)$$

Then the discriminant matrix of each enterprise is constructed. Take a pharmaceutical industry enterprise with code A2 as an example. The enterprise has a total of 62 valid employee data, and the frequency of each item at the seven evaluation levels is shown in Table 2.

Table 2. Frequency of item choosing in A2

	1 (=strongly disagree)	2	3	4	5	6	7 (=strongly agree)
WE1	1	2	0	9	12	15	23
WE2	1	2	0	4	6	18	31
WE3	1	2	0	8	10	16	25
WE4	1	2	1	6	12	17	23
WE5	1	1	0	16	8	15	21
WE6	1	1	0	11	13	16	20
WE7	1	1	0	5	8	22	25
WE8	1	1	0	10	10	20	20
WE9	1	1	0	10	8	19	23

Therefore, its evaluation matrix is (4), Using the $M(\wedge, \vee)$ operator, the FCE result of A2 is(5)

$$R_{A2} = \begin{bmatrix} 0.016 & 0.032 & 0.000 & 0.145 & 0.194 & 0.242 & 0.371 \\ 0.016 & 0.032 & 0.000 & 0.065 & 0.097 & 0.290 & 0.500 \\ 0.016 & 0.032 & 0.000 & 0.129 & 0.161 & 0.258 & 0.403 \\ 0.016 & 0.032 & 0.016 & 0.097 & 0.194 & 0.274 & 0.371 \\ 0.016 & 0.016 & 0.000 & 0.258 & 0.129 & 0.242 & 0.339 \\ 0.016 & 0.016 & 0.000 & 0.177 & 0.210 & 0.258 & 0.323 \\ 0.016 & 0.016 & 0.000 & 0.081 & 0.129 & 0.355 & 0.403 \\ 0.016 & 0.016 & 0.000 & 0.161 & 0.161 & 0.323 & 0.323 \\ 0.016 & 0.016 & 0.000 & 0.161 & 0.129 & 0.306 & 0.371 \end{bmatrix} \quad (4)$$

$$B_{A2} = A_{WE} \circ R_{A2} = [0.016 \quad 0.032 \quad 0.016 \quad 0.147 \quad 0.133 \quad 0.147 \quad 0.147] \quad (5)$$

$$V = [1 \quad 2 \quad 3 \quad 4 \quad 5 \quad 6 \quad 7] \quad (6)$$

$$B'_{A2} = [0.025 \quad 0.050 \quad 0.025 \quad 0.230 \quad 0.209 \quad 0.230 \quad 0.230] \quad (7)$$

$$WE_{A2} = B'_{A2} \cdot V^T = 5.158 \quad (8)$$

The FCE is used to calculate the employee work engagement scores of each researched enterprise. The full score is 7, the highest score of the sample enterprises is 6.20 points and the lowest is 4.60 points, with an average score of 5.33 points.

4.2 The DEA efficiency of ER

The result is shown in Table 3.

Table 3. DEA efficiency θ

Code ^a	θ	Code	θ	Code	θ	Code	θ
A1	1	B6	1	C8	0.96	D7	0.86
A2	0.87	B7	0.97	C9	1	D8	0.91
A3	1	B8	0.89	C10	1	D9	0.86
A4	0.92	C1	1	C11	1	D10	0.96
A5	1	C2	1	D1	1	D11	0.89
B1	1	C3	0.99	D2	1	O1	0.99
B2		C4	1	D3	0.95	O2	0.83
B3	0.99	C5	1	D4	0.93	O3	0.93
B4	0.96	C6	1	D5	0.96		
B5	0.95	C7	0.93	D6	0.96		

a: Code A stands for pharmaceutical industry, B stands for IT enterprises, C stands for service industry, D stands for manufacturing enterprises, and O stands for enterprises from other industries

As can be seen from Table 3, 16 enterprises have achieved DEA effective ($\text{efficiency} = 1$), accounting for 42.11% of the total. The enterprises that does not reach DEA effective have efficiency value up to 0.99 and the lowest is 0.83. In terms of industries, 72.73% of enterprises in service industry reached DEA efficient ER, ranking first in the four categories. Followed by pharmaceutical industry, reaching 60.00% and IT industry was 37.50%. Manufacturing was the lowest. It can be seen that the exchange of ER between organizations and employees is still inefficient.

4.3 Importance of different inducements

In order to identify the low efficient, or invalid indicators in the inducements, this study uses the back-off method [22] to further evaluate the importance of various indicators

in this research. In the analysis of all enterprises, the importance ranking of compliance indicators is female and juvenile protection (0.191), wages (0.152), training (0.127), labor contract management (0.071), social security (0.055), working hours (0.016). Consistent with previous studies, wages remain the most important part of hard incentives [23][24][25][26]. The importance ranking of competitive indicators is democratic negotiation (0.318), labor dispute handling (0.103), employment stability (0.082), employee care (0.051), welfare system (0.035).

5. Discussion

The analysis results show that the phenomenon of inefficient exchange between inducements from organization and contribution from employees is widespread but with some difference. Employers should correctly treat the phenomenon of incomplete exchange and do not think about the management of ER only in terms of laws and regulations. Compared with competitive indicators, the inducing-contributing exchange process with the compliance indicators clearly limited by laws and regulations is inefficient. In terms of industries, the manufacturing industry in the four major categories showed obvious insufficient with serious ER inefficiency. According to the evaluation of specific indicators, the female and juvenile protection, wages, training, democratic negotiation and labor dispute handling are the most important indicators in the inducements. It should be noted that the DEA efficiency does not represent the absolute value.

6. Conclusion

Through the lens of social exchange theory, this study uses the DEA method to quantitatively evaluate the efficiency of exchange process in ER, and further ranks the importance of each inducements indicator. Compared with competitive indicators, the inducing-contributing exchange process with the compliance indicators clearly limited by laws and regulations is inefficient. In the competitive indicators, employees pay more attention to the democratic and fairness in the management process (democratic negotiation, labor disputes), followed by a sense of work safety (employment stability), which verifies the view how social comparison influence the obligation perceive in exchange relations [27]. In terms of industries, the manufacturing industry in the four major categories showed obvious insufficient with serious ER inefficiency.

According to the evaluation of specific indicators, this study believes that the female and juvenile protection, democratic negotiation have improved the sense of fairness of employees, and the wages, training, and labor disputes handling have improved the employees' sense of work safety. Both of them are important factors in social exchange research, which are in line with the conclusions of previous studies. Future research can operate further empirical tests on these points.

It should be noted that the DEA efficiency does not represent the absolute value. While paying attention to the efficiency of exchange, enterprises should not neglect the actual level of investment to balance the high quality and efficiency of ER. In addition, as a study of the exchange process, its impact on organizational performance and stability is inevitably one of the topics of continuing research. Therefore, in the future,

variable causality research based on exchange efficiency can be further developed to more fully understand ER through the process of social exchange.

The contributions are as follows, for the first time, the quantitative efficiency value replaces the simple description “uncertainty” in research of the exchange process. Meanwhile, the framework used in this study independently measures the input of enterprises and the output of employees which has high adaptability. It can adjust, modify and accurately evaluate the exchange efficiency of two parties according to the actual exchange situation. The limitation of this study is that the research method is based on the cognitive assumption that the two groups, organization and employees, are anthropomorphized as “individuals”.

References

- [1] Efendiev, A., Gogoleva, A., & Balabanova, E.. Social exchange concept as a methodological framework for employment relations analysis. Higher School of Economics Research Paper No. WP BRP, 2014, 18.
- [2] Yu, M.-C., Mai, Q., Tsai, S.-B., & Dai, Y.. An Empirical Study on the Organizational Trust, Employee-Organization Relationship and Innovative Behavior from the Integrated Perspective of Social Exchange and Organizational Sustainability. *Sustainability*, 2018, 10(3), 864–14.
- [3] Tsui, A. S., Pearce, J. L., Porter, L. W., & Tripoli, A. M.. Alternative approaches to the employee-organization relationship: does investment in employees pay off?. *The Academy of Management Journal*, 1997, 40(5), 1089-1121.
- [4] Gerhart, B., Wright, P. M., Mahan, G. C. M., & Snell, S. A.. Measurement error in research on human resources and firm performance: how much error is there and how does it influence effect size estimates?. *Personnel Psychology*, 2000, 53(4), 803-834.
- [5] Gebauer, J., Lowman, D., & Gordon, J. *Closing the engagement gap: How great companies unlock employee potential for superior results*. Penguin. 2008.
- [6] Hannah, D., & Iverson, R. Employment relationships in context: Implications for policy and practice. In Coyle-Shapiro, Jacqueline A-M., Shore, L., Taylor, M. S. and Tetrick, L. (Eds.), *The employment relationship: Examining psychological and contextual perspectives: 2004*, 332-350, New York, NY: Oxford University Press.
- [7] Rousseau, D. M., & McLean Parks, J.. *The contracts of individuals and organizations. Research in organizational behavior*, 1993, 15, 1-1.
- [8] Festinger, L.. (1954b). A theory of social comparison processes. *Human Relations*, 1954, 7, 117-140.
- [9] Coyle-Shapiro, Jacqueline A-M., & Conway, N. The employment relationship through the lens of social exchange. In Coyle-Shapiro, Jacqueline A-M., Shore, L., Taylor, M. S. and Tetrick, L. (Eds.), *The employment relationship: Examining psychological and contextual perspectives: 2004*, 5-28, New York, NY: Oxford University Press.
- [10] Coyle-Shapiro, Jacqueline A-M., & Conway, N.). Exchange relationships: Examining psychological contracts and perceived organizational support. *Journal of applied psychology*, 2005, 90(4), 774.
- [11] Coyle-Shapiro, Jacqueline A-M., & Kessler, I.. Exploring reciprocity through the lens of the psychological contract: Employee and employer perspectives. *European journal of work and organizational psychology*, 2002, 11(1), 69-86.
- [12] Robinson, S. L., & Morrison, E. W.. Psychological contracts and OCB: The effect of unfulfilled obligations on civic virtue behavior. *Journal of organizational behavior*, 1995, 16(3), 289-298.
- [13] Sapienza, H. J., Korsgaard, M. A., & Schweiger, D. M.. procedural justice and changes in psychological contracts: a longitudinal study of reengineering planning. in academy of management proceedings. 1997, August,(Vol. 1997, No. 1, pp. 354-358). Briarcliff Manor, NY 10510: Academy of Management.
- [14] Xi, m., liu, y.y., xu, y.f., cao, m. & xu, z.j. A Study on Employee Engagement in Multiple Employment Relationship Modes: From the Perspective of Social Exchange Theory. *Chinese Journal of Management*, 2018, 15(08), 1144-1152.
- [15] Schneider, B., Macey, W. H., Barbera, K. M., & Martin, N. Driving customer satisfaction and financial success through employee engagement. *People and Strategy*, 2009, 32(2), 22.
- [16] Kahn, W. A.. Psychological conditions of personal engagement and disengagement at work. *The Academy of Management Journal*, 1990, 33(4), 692-724.

- [17] Morrison, E. W., & Robinson, S. L.. The employment relationship from two sides: Incongruence in employees' and employers' perceptions of obligations. In Coyle-Shapiro. 2004.
- [18] Maas, C. J., & Hox, J. J. Sufficient sample sizes for multilevel modeling. *Methodology*, 2005, 1(3), 86-92.
- [19] Liu, P., & Duan, W.P.. Research on Evaluation System of Harmonious Labor Relations: Based on Entropy Method and AHP. *Innovation, Entrepreneurship and Strategy in the Era of Internet – Proceedings of 2016 International Conference on Strategic Management*. Schaufeli, W. B., Salanova, M., González-Romá, V., & Bakker, A. B. (2002). The measurement of engagement and burnout: A two sample confirmatory factor analytic approach. *Journal of Happiness studies*, 2016, 3(1), 71-92.
- [20] Schneider, B., Macey, W. H., Barbera, K. M., & Martin, N.. Driving customer satisfaction and financial success through employee engagement. *People and Strategy*, 2009, 32(2), 22.
- [21] Charnes, A., Cooper, W. W., & Rhodes, E.. Measuring the efficiency of decision making units. *European journal of operational research*, 1978, 2(6), 429-444.
- [22] LOU, D. H., YI, H. G., & YU, H.. studies of selecting variables about synthesize evaluation of performance with data envelopment analysis. *Modern Preventive Medicine*, 2009, 9.
- [23] Simon, H. A.. A formal theory of the employment relationship. *Econometrica*, 1951, 19(3), 293-305.
- [24] Lawler, E. E., & Lawlor, E. E.. Pay and organization development. 1981,(Vol. 268). Reading, MA: Addison-Wesley.
- [25] Blau, P. Exchange and power in social life. NY: John Wiley & Sons. 1964.
- [26] Lee, C., Liu, J., Rousseau, D. M., Hui, C., & Chen, Z. X.. Inducements, contributions, and fulfillment in new employee psychological contracts. *Human Resource Management*, 2011, 50(2), 201-226.
- [27] Morrison, E. W., & Robinson, S. L.. The employment relationship from two sides: Incongruence in employees' and employers' perceptions of obligations. In Coyle-Shapiro, Jacqueline A-M., Shore, L., Taylor, M. S. and Tetrick, L. (Eds.), *The employment relationship: Examining psychological and contextual perspectives*: 2004, 161-180, New York, NY: Oxford University Press.

An Intelligent Marshalling Model for Enterprise Station Freight Railway

Junxia GUO^a, Gang LU^{a,1}, Zili Xie^b, Jiawei WEN^c, Nanshan XU^a

^aCollege of Information Science and Technology, Beijing University of Chemical Technology, Beijing 100029, China

^bResearch and Development Center for Science & Technology, SINOPEC Pipeline Storage & Transportation Company limited, Xuzhou 221008, China

^cChina Science and Technology Museum, Beijing 100029, China

Abstract. Railway marshalling and transportation is an important component of the production supply chain for large and medium-sized enterprises in China. Traditional inefficient manual-made marshalling plans usually are not optimal in time or energy consuming. An efficient method needs to be developed to find the optimal marshalling plans automatically. This paper mainly studies the railway train automatic marshalling in large and medium-sized enterprises in China. Based on the investigation at the train station of a certain enterprise, according to the railway track information, carriage information, and production task information, this paper designs the abstracted railway state definitions of the station. Then based on the state definitions, the scheduling rules, and the objective function of time cost and economic cost, this paper converts abstract scheduling instructions into a general railway automatic marshalling model which can be executed by computers. By introducing the greedy strategies into different situations to optimize the algorithm of tracks occupation, carriages selection and train path selection in the model, the planning efficiency can be improved while ensuring the economic benefits of the enterprises and the quality of the formation plan. The experimental results show that the proposed model can generate fewer marshalling plans and find the optimal one faster in most cases, which proves the feasibility and availability of the model.

Keywords. enterprise station railway, scheduling methods and constraint sets, automatic marshalling model

1. Introduction

As the source of freight railway transportation, railway marshalling is the first step to ensure the normal operation of railway stations. The railway stations in China mainly serve large and medium-sized industrial areas such as mining, petroleum, petrochemical plants, and metallurgical processing industries. With the development of the national economy, the railway freight volume of stations is increasing, the marshalling time is more compact, and the dispatching operation is more complicated. A marshalling operation scheduling includes freight train arrival, dispatch, and marshalling operations. There are always some constraints for a good train marshalling plan, such as the number of hooking or unhooking operations or moving distance of the carriages should be as less

¹ Corresponding Author: Gang LU, College of Information Science and Technology, Beijing University of Chemical Technology, Beijing 100029, China; E-mail: lugang@mail.buct.edu.cn

The work described in this paper is supported by the National Natural Science Foundation of China under Grant No.61702029.

as possible, or there are some rules of using the tracks and carriages because of their different functions. For example, carriages loading chemicals A must not be connected with carriages loading chemicals B because it's dangerous. Also, maybe some tracks can be only used for carriages storage but not moving them, or vice versa. All those constraints make us have to consider the availability of the marshalling plans as well as their time and energy consuming. However, making marshalling plans under complex constraints manually usually is slow and inefficient. Optimized plans cannot be guaranteed by manually-made plans in respect of the time and energy consuming of the plans.

Train scheduling and marshalling problem is a typical NP problem [1]. In the field of mathematical modeling, Dessouky [2] regarded the railway freight route as a network with different scales, the route planning problem as the core of the train scheduling research, the minimum delay as the evaluation indicator, and adopted different heuristic algorithms to optimize the scheduling route in the large and medium-sized networks. Krasemann [3] and He [4] respectively apply the greedy algorithm to reduce data interference and avoid train interference, so as to implement rapid rescheduling of trains. Pathania et. al [5] proposed a greedy strategy for multi-core scheduling, which is based on dynamic programming scheduling problems to reduce scheduling overhead in space searching and data filtering. Katsavounis [6] used the graph theory to model the production scheduling problems, and greedy strategy to solve the allocation problems of limited resources in the network with topology structure. Ribas et. al [7] applied the improved iterative greedy algorithm to the scheduling optimization of pipeline jobs. By introducing a genetic algorithm, He et. al [8] solved the fuzzy scheduling problem in the railway management system. Chuntian Zhang et. al [9] propose a joint optimization model for a railway network with double-track, where the upstream and downstream trains are independent and a maintenance task on a section cannot be split or disrupted. A heuristic algorithm using Lagrangian relaxation is developed in their paper. Due to the large number of constraints, they used a dynamic constraint-generation technique in the iterations of the sub-gradient optimization procedure. In [10], Chuntian Zhang et. al researched integrated optimization of train scheduling and maintenance planning on high-speed railway corridors. They used some linearization techniques to formulate a mixed integer linear programming model to identify the operation modes and the timetable of SDSA-trains, by integrating the time window selection of regular maintenances on high-speed railways. They introduced state variables to indicate whether a train is running on high-speed railway or not. That made it convenient to express the selection of operation modes.

In the field of computer intelligent marshalling, most of the research takes national railway stations [11] or metro lines [12] as the research object. The research and application on medium and large-scale enterprise stations are weak. The existing intelligent dispatching system cannot be directly applied to station railways for those enterprise stations because that most of those researches focus on the multi-trains dispatching between stations instead of multi-track scheduling in one station for multi-functional carriages. Therefore, it is necessary to research and develop automatic marshalling models suitable for large and medium-sized enterprise station railways in one station with complex constraints of tracks and carriages.

The common goal of an automatic marshalling model is to organize a new train as soon as possible and prepare for departure at the minimum cost on the premise of meeting the planning requirements. Because the train scheduling process involves a large number of variables and multiple rules, which should be transformed into constraints of

the model, the train marshalling scheduling problem is essentially a large-scale combinatorial optimization problem. This paper mainly studies the following problems:

(1) Designing the state definition of stations. By analyzing the specific content and process of operational railway dispatching, design the state information of the station.

(2) Designing the automatic train marshalling model. According to the real-time states of the station, the model can automatically compile the scheduling scheme by scheduling constraints, which meet the planning requirements.

(3) Aiming at the problem of marshalling time cost and economic benefit of enterprises, different greedy strategies are introduced to optimize the general marshalling model so that the marshalling time of the obtained scheduling scheme is the shortest and the launching revenue is the largest.

2. Station State Definitions

Before solving the railway marshalling problem, it is necessary to define the variables that affect the marshalling planning. The station state information is defined from three aspects, which are railway carriages, tracks, and marshalling tasks. The state space is represented by $U = \langle C, P, A \rangle$, where C is the carriage state, P is the track state, and A is the marshalling task state. U can represent all the carriages and tracks in the station railway at a certain time, as well as the marshalling task information of the station.

1) Carriages State

The state of railway carriages in the station is composed of four types of information: basic information, position of the carriage, availability of the carriage, and the working state, as shown in Table 1. C_v refers to the availability state of the carriage. $C_v \in \{1,0\}$ indicates whether there is any follow-up plan for the carriage. C_o represents the carriage's working state. $C_o \in \{1,2,3\}$ respectively represent the three working states of railway carriages in the station during the stage planning cycle. When $C_o = 1$, the carriage is in the free state, which means that the carriage has completed all the previous tasks and is placed on the respective track, which can be directly invoked. When $C_o = 2$, the carriage is in the waiting loading and unloading state. For example, the carriage has arrived at the station, and is waiting for the unloading operation after the disassembly. When $C_o = 3$, the carriage is in running state, which means the carriage is about to arrive at the station as planned and has been registered on the dispatch schedule.

Table 1. Symbol description of carriage state

Type	Symbol	Definition
Basic information	C	Carriage set
	C_n	Wagon number of carriage
	C_k	Kind of carriage kind
	C_c	Commodity of carriage
	C_a	Carriage attribution
	C_w	Carriage load
	C_m	Carriage charges
Position state	C_t	Parking track of carriage
	C_l	Carriage positioning on track
Availability state	C_v	Availability of carriage
Working state	C_o	Working state of carriage

2) Track State

There are m tracks in the station, denoted by $P = \{p_1, p_2, \dots, p_m\}$. If p_i has j connected track, then all states of track p_i are expressed as: $p_i = \langle P_t, PC_w, PF_i, L \rangle$, where $L = \{< p_1, L_{t1} >, < p_2, L_{t2} >, \dots, < p_j, L_{tj} >\}$. $PF_i \in \{1,2,3,4,5\}$ is the track function set of the station, representing the five types of functions in the station's track. PF_1 means the track is an

arrival-marshalling line, which means trains can be marshalled, disassembled, dispatched and temporarily parked on it. PF_2 means the track is a preparatory emergency task line, and this track only performs the marshalling and dispatching of emergency priority trains. PF_3 means the track is a parking traction line, which is used for parking existing carriages that have been loaded and unloaded or temporarily parking carriages. PF_4 means the track is a loading line, while PF_5 means the track is an unloading line. Those two kinds of tracks are respectively used for different specific commodity loading and unloading. Table 2 lists the symbol descriptions of track state.

Table 2. Symbol descriptions of track state

Type	Symbol	Definition
Track basic information	P	Track set
	P_t	Track name
	PC_w	Track carriage capacity
	PF_i	Track function
Adjacent track information	L	Adjacent tracks set
	L_t	Trains run time between adjacent tracks

3) Marshalling Task

The preparation of the marshalling plan requires information of the production tasks in a certain period, such as the number of marshalling and the type of carriages. The involved symbols and their description are shown in Table 3.

Table 3. Symbol description of marshalling task

Symbol	Definition
A	Production task set
A_n	Task number
A_d	Task destination
A_k	Task type
A_c	Task commodity
A_a	Task Quantity
A_t	Task requires carriages number
A_p	Task quotation
T_D	Production task cycle

In this paper, three types of tasks are defined, which are denoted as $A_k \in \{1,2,3\}$. They respectively represent product delivery task, empty vehicle returning task, and urgent priority task. The arrival and departure marshalling tracks can be used for product delivery and empty vehicle returning tasks. Emergency priority tasks are grouped separately on the preparatory emergency task tracks. They are not subject to the lower limit of starting load, which means as soon as the marshalling completes, the train can apply for starting.

3. Construction of Marshalling Model

The automatic marshalling model mainly considers three issues: the selection of marshalling carriages, the occupation of marshalling tracks and temporary dispatching tracks, and the operation of carriages.

Basing on the definitions in Section 2, two assumptions are made as follows:

Assumption 1: the time spent on hooking and unhooking is ignored;

Assumption 2: carriages move with uniform speed.

3.1. Selection of Marshalling Carriages

1) Rule of Selecting Carriage

When selecting carriages, three issues should be considered: the corresponding commodity, availability state of the carriages, and the number of carriages required. The carriages selection algorithm is shown in Algorithm 1.

Algorithm 1: selectcarriages

```

Input:  $a_0$ : Production task;  $C$ : Carriage set  $C = \{c_1, c_2, \dots, c_n\}$ 
Output: fitting carriages set selectcarriages
1 selectcarriages  $\leftarrow <\emptyset, \emptyset>$  //< $C$ : carriage ,  $C_w$ : carriage load>
2 carriages  $\leftarrow <\emptyset, \emptyset>$  //< $C$ : carriage ,  $C_w$ : carriage load>
3  $U = a_0 \cdot A_a$  // Task Quantity
4 for  $c_i$  in  $C$  do
5   if  $c_i.C_v = a_0 \cdot A_c$  then
6     carriages.C.append( $c_i$ )
7     carriages.Cw = carriages.Cw +  $c_i.C_w$ 
8   if carriages.Cw  $\geq U$  then
9     selectcarriages.Cw = selectcarriages.Cw +  $c_i.C_w$ 
10    selectcarriages.C.append( $c_i$ )
11    selectcarriages.Cw = selectcarriages.Cw +  $c_i.C_w$ 
12  end if
13  if  $U > selectcarriages.C_w$  then
14    selectcarriages  $\leftarrow$  carriages
15  end if
16 return selectcarriages
17 else
18 Output : There are not enough carriages at the station for marshalling
  
```

2) Rules for Grouping Carriages

The basic operations of railway dispatching are hooking and unhooking. Too many hooking or unhooking operations not only reduce the efficiency of station dispatching operation, but also lead to increased wear and tear of equipment and workload. A good marshalling scheme should take hooking and unhooking operations as less as possible to form a carriage group by combining carriages with the same state.

By this rule, after selecting marshalling carriages, all the suitable carriages parking on the same track will be interconnected into one carriage group. All the carriages groups in the station will be recorded, including their numbers and total load. The symbol descriptions of carriage groups are listed in Table 4.

Table 4. Symbol Description of Carriage Group

Symbol	Description
G	Carriage group set
G_n	Carriage group number
G_c	Carriage group category
G_w	Carriage group load
G_l	Carriage amount of carriage group
G_t	Parking track of carriage group

If there are n groups of carriages in the station, the set of them is denoted by $G = \{g_1, g_2, \dots, g_n\}$. A certain carriage group g_i contains m carriages, where $g_i = \{c_1, c_2, \dots, c_m\}$. In addition, carriage group information is expressed as $g_i = \{G_n, G_c, G_w, G_l, G_t\}$.

3.2. Parking Rule of Disassembling Train

Before disassembling or marshalling a train, it is necessary to decide the operating track. In order to ensure the transportation safety of station, different traction lines are usually preset for different functions, such as train disassembling, product delivery, or empty carriage storage, and so on. At the same time, during disassembling, traffic distribution, or other operations, it is often necessary to temporarily move away the carriages those do not participate in the subsequent operations. Only the arrival and departure marshalling

traction lines and the carriage storage traction lines can be temporarily assigned for parking the trains.

3.3. General Marshalling Model

The general marshalling model is proposed by summarizing the actual marshalling planning process and constraints. Basing on state space searching, exhaustive method is applied here to find the optimal solution. In order to avoid invalid state searching, constraints are introduced into the searching progress to prune the invalid states. The general marshalling model is as follows.

Step 1: Initialize station status, including station track, carriage status information, and production task.

Step 2: Select the marshalling carriage. According to the requirements of production task, and the method of scheduling and carriage selection in the constraint set, enumerate all the suitable carriages and carriage groups, and then decide the information such as load and position.

Step 3: Generate the following marshalling plan:

(1) Deciding the tracks to use: decide the operation tracks for different production tasks, the temporary scheduling tracks may be involved, and the target group tracks.

(2) Generating train scheduling plan: simulate the scheduling plan by moving the selected carriage groups to the target tracks, and calculate the time cost and economic cost. Meanwhile, the train position and working status are updated.

Step 4: Select optimal marshalling scheme. By comparing the generated marshalling schemes by Step 3 in their time cost and economic cost, the optimal marshalling scheme can be selected.

Step 5: Successively generate marshalling plans. If there are more than one production and transportation tasks, take the current state of the station after previous optimal marshalling plan as the initial state of the next plan, and then execute Step 1 to Step 4 again.

3.4. Optimized Marshalling Model by Greedy Strategies

General marshalling model proposed in Section 3.3 can find the optimal solution by exhaustive searching under constraints. However, when the number or types of carriages becomes larger, or the topology of the tracks becomes complex, the state space will expand rapidly. That will make general marshalling model inefficient. There are some NP problems involved in the general marshalling model, such as the backpack problem in selecting the trains and carriages for capacity, the routing problem in selecting the trains' running route and the temporarily parking track, etc.. As a result, greedy strategy is introduced into those parts to try to improve the model. Although greedy strategy may not provide the exact optimal solution, it still helps to approach to the optimal solution, as well as to improve the efficiency.

Concretely, greedy strategy is introduced in three parts: 1) choosing the best carriage groups based on the biggest capacity and the best position; 2) getting the shortest working time T_c ; 3) optimizing the running path based on trains' running time minimization. Based on those greedy strategies, the optimized marshalling model is designed to prepare the optimal marshalling plan in a shorter time by generating less marshalling plans. The process steps are similar with the general marshalling model, except the using of above greedy strategies.

4. Experiment and Performance Analysis

This paper uses the railway station of a certain supply and marketing department of a company in China as the experimental example. The railway line of this station is Class I Railroad. Its allowable speed is 30km/h. The layout of the tracks is shown in Figure 1. The text in the figure indicates the code name of the station track. This station is an internal marshalling station of the enterprise, which mainly handles the dissembling of freight trains and the dispatch of product trains. There are 28 tracks, 84 carriages, 7 marshalling tasks, and 1 available train in the experimental environment.

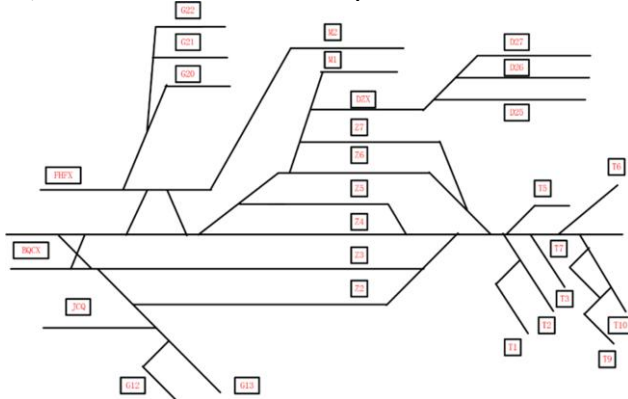


Figure 1. Layout of the tracks in the railway station of supply and Marketing Department

The marshalling tasks received by the station on a certain working day are taken as the test data. The state of the station at that time is taken as the initial environments. The general marshalling model and the optimized marshalling model are compared on the experimental environments. The experimental results are shown in Table 5.

Table 5. Comparative Experimental Results

Tasks	General marshalling model		Optimized marshalling model by greedy strategies	
	# of marshalling plans generated in one task	Optimal marshalling time (min)	# of marshalling plans generated in one task	Optimal marshalling time (min)
Task 1	4	35	1	35
Task 2	2	75	1	75
Task 3	7	35	1	35
Task 4	2	40	2	40
Task 5	13	30	2	45
Task 6	762	70	15	70
Task 7	63	45	3	45

In Table 5, it can be found that both the two automatic marshalling models designed in this paper can effectively obtain the optimal marshalling plan of stations, which proves the correctness of state descriptions designed in this paper. According to the experimental comparison between the general marshalling model and the optimized model, the optimized model needs to generate less plans than the general model in order to find the optimal marshalling plan with shortest time. Along with the increasing number of carriages in different working states in the station, the general marshalling model using exhaustive method needs to explore significantly increasing number of plans. In that case, the advantage of the optimized model is more distinct in generating

much less plans. For example, the general model need to explore all the 2 plans for Task 2, while the optimized model generates 1 plans with the same marshalling time of 75 minutes. In contrast with Task 2, the general model needs to generate all the 762 plans for Task 6, and the optimal plan takes 70 minutes for marshalling. However, by the optimized model, only 15 plans are generated to find the optimal one with the same 70 minutes of marshalling time. Task 5 is an exception. Although the optimized marshalling model generates only 2 plans for it, but the optimal plan takes 45 minutes, which is more than 30 minutes for the one found by general marshalling model. That is because for Task 5, the optimized marshalling model finds the locally optimal solution, but not the globally optimal one.

The output of the model is the marshalling steps of the generated plans. According to the requirements in real work, as well as the defined symbols in Section 2 and Section 3, the information of output can be organized and formatted into readable form. For example, it can be as:

- Step 1: unhook carriage C_0 ;
- Step 2: move carriage C_0 to Track T_2 .

5. Conclusions

Based on the railway carriage information, track information, and marshalling task information, this paper constructs the state definitions which can fully express the real-time state information of railway stations, and abstract the marshalling problem into state space searching problem. A general marshalling model is built with the exhaustive method, which can be applied directly or be ground truth. Furthermore, greedy strategies are introduced to find the optimal solution more efficiently, which is verified by the experimental results, proving the feasibility and availability of the model.

Future work includes trying other searching and optimizing method such as evolutionary computation and multi-objective optimization for more complex constraints and states. In addition, researching on generating successive marshalling plans is under consideration. Implementing the models into standardized programs with standard inputs and outputs which can be easily used will be interesting, too.

References

- [1] E. Dahlhaus, P. Horak, M. Miller, and J. F. Ryan, "The train marshalling problem," *Discrete Applied Mathematics*, 2000, vol. 103, no. 1–3, pp. 41–54.
- [2] Dessouky M. Scheduling freight trains traveling on complex networks [J]. *Transportation Research Part B*, 2011, 45(7):0-1123.
- [3] Krasemann J. T. Greedy algorithm for railway traffic re-scheduling during disturbances: A Swedish case [J]. *IET Intelligent Transport Systems*, 2010, 4(4):375-0.
- [4] He Z. Research on Improved Greedy Algorithm for Train Rescheduling[C]// Seventh International Conference on Computational Intelligence & Security; 2011; Hainan, China: IEEE; p. 1197-1200.
- [5] Pathania A , Venkataraman V , Shafique M , et al. Optimal Greedy Algorithm for Many-Core Scheduling[J]. *IEEE Transactions on Computer-Aided Design of Integrated Circuits and Systems*, 2016:1-1.
- [6] Katsavounis S. A greedy algorithm for scheduling tasks on production lines[J]. *Operational Research*, 2001, 1(3):285-298.
- [7] Ribas I, Companys R, Tort-Martorell X. An iterated greedy algorithm for the flowshop scheduling problem with blocking [J]. *Omega*, 2011, 39(3):293-301.
- [8] Shi-Wei HE, Rui S , Fang L U, et al. Fuzzy Scheduling Problem with Multi-Processors Using Genetic Algorithm for Railway Management[J]. *Journal of Beijing University of Aeronautics and Astronautics (Social Sciences Edition)*, 2000, 13(4):4-10.

- [9] Chuntian Zhang, Yuan Gao, Lixing Yang, et al. Joint optimization of train scheduling and maintenance planning in a railway network: A heuristic algorithm using Lagrangian relaxation[J]. *Transportation Research Part B*, 2020, 134(4): 64–92.
- [10] Chuntian Zhang, Yuan Gao, Lixing Yang, et al. Integrated optimization of train scheduling and maintenance planning on high-speed railway corridors [J]. *Omega*, 2019, 87(6):86–104.
- [11] Abels D., Jordi J., Ostrowski M., Schaub T., Toletti A., Wanko P. Train Scheduling with Hybrid ASP [C]. Logic Programming and Nonmonotonic Reasoning. LPNMR 2019. LNCS, (2019) vol 11481.
- [12] Liu R, Li S, Yang L. Collaborative optimization for metro train scheduling and train connections combined with passenger flow control strategy[J]. *Omega*, 2020, 90: 101990.

Fault Diagnosis of Coal Mining Machinery Based on State Parameters

Dong Song¹

*Taiyuan Research Institute of China Coal Technology & Engineering Group,
Taiyuan, China*

Abstract. The reliable operation of coal mining machinery acts as an important guarantee for safe productions in underground coal mines. The status monitoring and fault diagnosis of traditional coal mining machinery mainly rely on threshold judgments. However, a single judgment condition and a long fault propagation chain can be found in the method of threshold judgments, which make it difficult to accurately seek the fault type. By using the data analysis of state parameters for coal mining machinery, fault parameters and propagation paths can be analyzed effectively. This paper takes the cutting unit of a certain type of bolter miners as an example, a static and dynamic numerical analysis method of the cutting unit of bolter miners are established by virtue of FTA-Petri net models and BP-Firefly neural networks, which can provide a new perspective for fault diagnosis of coal mining machinery.

Keywords. FTA-Petri net models; BP-Firefly neural networks; fault diagnosis; cutting part

1. Introduction

Coal is the main source of energy in this day and age. Because the coal mine accidents happen frequently in some countries, how to improve the safety and reliability of coal mining machinery equipments becomes a universal attention question. The condition monitoring and fault diagnosis methods of traditional coal mining machinery are mainly based on on-line threshold judgments, which may be confronted with some limitations when using intelligent fault diagnosis methods. Currently, the online threshold method relies on the over-limit alarm based on motors and currents to judge the fault type. In addition, the online threshold fault diagnosis is usually a post-judgment method, which is based on local data analysis when the equipment is stopped. This method owns a single judgment condition and a long fault propagation chain, and it is difficult to accurately determine the fault type. What is worse, the maintenance cost is high by using the above-stated traditional methods [1-2]. By introducing the data analysis of state parameters for coal mining machinery, the failure propagation path can be effectively analyzed and the failure point can be accurately judged, which can enhance the performance of fault diagnosis of coal mining machinery from the aspect of costs, efficiencies, and accurate predictions [3-5].

¹ Corresponding Author: Dong Song, Taiyuan Research Institute of China Coal Technology & Engineering Group, Taiyuan, China; Email: tymkysd@126.com

Since coal mining equipments, such as bolter miners or roadheaders, act as complex heavy electromechanical systems, and the working environment and conditions of them are complicated and harsh. Therefore, intelligent fault diagnosis methods based on state parameters for coal mining machinery may face many challenges, such as insufficient detection approaches, more data interference factors, difficult data collections, etc. Nowadays, the fault diagnosis of coal mining machinery still relies on information threshold discrimination [6-8]. Recently, some scholars begin to use data mining-based methods to seek fault types for mining machinery such as artificial intelligence approaches including genetic algorithms and artificial neural networks, which allow employing the non-iterative methods, where one only needs to enter input parameters as the considered parameters of the process are generated as an answer to the input data set. Moreover, artificial neural networks have the ability to reproduce the process from training samples and specific knowledge of the process is not essential. Krzywanski et al. [9] introduced genetic algorithms and artificial neural networks approach for the optimization study of a hydrogen concentration in syngas via CaO Sorption. Yang et al. [10] established a fault tree along with a diagnosis expert system by establishing fuzzy expert systems to realize the on-line fault diagnosis and the fault interpretation of roadheaders.

In light of the above literature review, it is necessary to study data mining-based methods to seek fault types for mining machinery. In the current paper, we aim to obtain a satisfactory fault diagnosis conclusion by taking advantages of FTA-Petri net models and BP-Firefly neural networks within the background of bolter miners. To the best of our knowledge, there are no reports on model research of fault diagnosis of bolter miners by using FTA-Petri net models and BP-Firefly neural networks. Thus, we first revisit some basic knowledge on FTA-Petri net models and BP-Firefly neural networks, then an experiment analysis is made to show the merit of the hybrid method.

2. FTA-Petri net models

Fault Tree Analysis (FTA) is an efficient data-mining method which is used to evaluate the safety and reliability for diverse systems. It mainly uses the causality diagram and takes the top event as the analysis object. Various hardware, software, environment and other factors are used as sub-events, and the relative logical relationship is determined according to the causality of each sub-event that leads to the occurrence of the top event. Then, the iterative calculation will stop until the basic event that causes the target event is found [11-12]. In what follows, we summarize the main notions of FTA-Petri net models.

(1) The occurrence probability of top events

Suppose the failure probability of the bottom event x_i is q_i , n represents the number of bottom events, and the failure probability of minimum cut sets is provided as:

$$P = P(x_1 \text{ I } x_2 \text{ I } \dots \text{ I } x_m) = \prod_{i=1}^m q_i,$$

in the above formulae, m represents the number of minimum cut sets. Let the minimum cut set be F_1, F_2, K, F_m , the occurrence probability of fault tree top events provided as:

$$P_T = \sum_{j=1}^m \left(\left(\prod_{i \in K_j} F_i(t) \right) \right),$$

the above formulae indicates the probability of top events is equal to the sum of the probability of minimum cut sets.

(2) Let $\Sigma = (P, T, F, K, W, Z, M_0)$ be a faulty petri net, $P = \{p_1, p_2, \dots, p_m\}$ and $T = \{t_1, t_2, \dots, t_n\}$, then the structure of faulty petri nets can be represented by a matrix (m rows and n columns) as follows:

$$A = \begin{matrix} & t_1 & t_2 & t_3 & t_4 \\ \begin{matrix} p_1 \\ p_2 \\ p_3 \\ p_4 \end{matrix} & \begin{bmatrix} w_{11} & & & \\ & \ddots & & \\ & & O & \\ & & & w_{mn} \end{bmatrix} \end{matrix}.$$

(3) The state equation of faulty Petri nets is

$$M_K = M_{K-1} + A \oplus Z_K,$$

where M_K and M_{K-1} represent state identification sets of faulty networks at time k and $k-1$, A is the correlation matrix, Z_K represents the sequence of the transition for faulty petri networks at time k , and the operation \oplus represents the logical ‘or’ relationship.

3. BP-Firefly neural networks

The learning principle of BP neural networks involves the forward propagation of signals and the backward propagation of errors. After repeated iterative calculations, an artificial neural networks model is established to process nonlinear and unknowable complex information. In addition, BP neural networks mainly include an input layer, a hidden layer, and an output layer. The neurons in each layer are not connected, whereas the neurons in different layers are completely interconnected. Since BP neural networks own the limitations of slow convergence speed in learning processes, low robustness, and poor network performances, it is noted that the firefly algorithm can simulate cooperative group behaviors of fireflies’ movements through lights and life habits such as foraging and mate selections. As a result, the firefly algorithm owns the advantage of simple structures, few adjustment parameters, and fast convergence speeds [13-15].

The motivation of using the firefly algorithm to optimize BP neural networks is listed below: we first use the firefly algorithm to train weights and thresholds of BP neural networks for solving the randomness of initial weights and threshold selections, that is, we make full use of the global optimization and heuristics optimization features of the firefly algorithm. Next, we use the BP neural network algorithm to get the final neural network structure. The fundamental steps of the optimization algorithm are shown as follows:

Step 1. Create a BP neural network, set network parameters, initialize weights and thresholds.

Step 2. Set the parameters of the firefly algorithm, including the number of fireflies n , the light absorption intensity coefficient γ , the step size factor α , the maximum attraction β_0 , the maximum number of iterations $\max t$, and the adaptation threshold.

Step 3. Randomly initialize all positions of firefly within a feasible region.

Step 4. Calculate the fitness value of the firefly, that is, calculate the objective function value. The process of BP network's training is that when the error value during iterative calculations, that is, when the mean square error is less than the set error threshold, the learning is considered to be completed, and the calculation is stopped, the result is the output. Since the firefly algorithm finds the maximum value, it is necessary to convert the minimum value into the maximum value. The fitness function is the reciprocal of the mean square error function of the BP neural network, that is,

$$f = \frac{1}{E}, \text{ where } E = \frac{1}{N} \sum_{i=1}^n (D_i - Y_i)^2. \text{ In the above formulae, } f \text{ is the objective}$$

function value, E is the mean square error of the BP neural network, N is the number of output nodes, D_i is the target value of the i th output node, and Y_i is the actual value of the i th output node.

Step 5. Calculate relative brightness and attractiveness, and determine the direction of movement. The relative fluorescent brightness of fireflies is $I = I_0 e^{-\gamma r_{ij}}$. In the above formulae, I_0 is the maximum fluorescence brightness of the firefly, γ is the light intensity absorption coefficient, and r_{ij} is the spatial distance between the firefly i and the firefly j . The attraction of fireflies is $\beta = \beta_0 e^{-\gamma r_{ij}^2}$. In the above formulae, β_0 is the maximum attraction, that is, the attraction at the light source.

Step 6. Randomly disturb the firefly in the best position, and then update the position of the firefly. The position update formula for the firefly i moving to the firefly j because of its attraction is $x_i = x_i + \beta(x_j - x_i) + \alpha(rand - 1/2)$. In the above formulae, α is the step factor, $rand$ is a uniformly distributed random number on $[0, 1]$.

Step 7. Check whether the updated position of the firefly is out of the feasible range, and if it exceeds the range, use the boundary value as the updated position of the firefly.

Step 8. Increase the number of iterations by 1 to judge whether the termination condition is satisfied. The iteration is stopped if it is satisfied, and the weight and threshold are output. Otherwise, go to Step 4.

Step 9. Use the weights and thresholds output in Step 8 to train the neural network.

4. Experimental analysis

The cutting part of bolter miner mainly consists of cutting motor, cutting reducer, cutting drums, cutting lifting cylinders, sump cylinders and other devices. After analyzing common faults and their causes, a fault tree model of the cutting part for bolter miners is established, which is shown in Figure 1 as below.

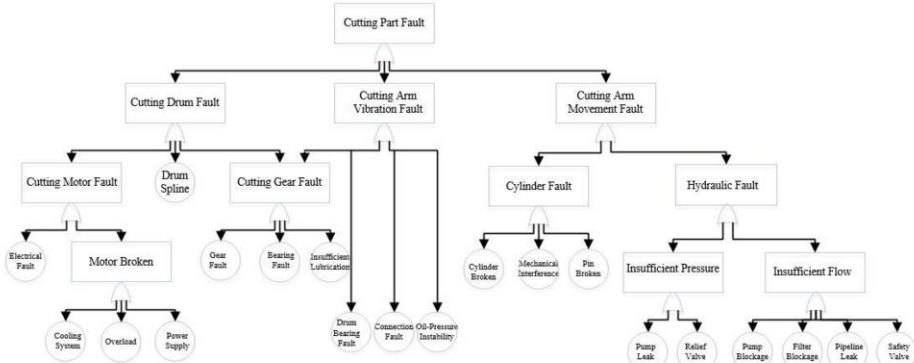


Figure 1. The fault tree model of cutting part of bolter miner

Due to the large scale of the fault tree model, the probability of occurrence of each fault can be judged based on expert scoring methods, and then the fault diagnosis can be performed through the top event probability calculation method. According to the weight of each fault event and the importance of each event, the optimal fault source search route is derived when the system owns problems, which provides a basis for fault diagnosis and saves time for fault diagnosis. However, the hierarchical analysis of the fault tree model is complex and the calculation process is lengthy, which make it difficult to perform quantitative analysis quickly. Based on FTA-Petri net models, the fault tree model can be greatly simplified, and hierarchical calculations can be transformed into matrix calculations. By establishing the faulty FTA-Petri net models, all the failure modes of bolter miners can be summed up.

Taking a cutting cylinder failure in a bolter miner in Shanxi Province, China as an example, the designed neural network adopts a three-layer structure, the number of input layer nodes is determined as 5, the number of output layer nodes is determined as 3 according to the features of a fault tree model of the cutting unit for bolter miners as shown in Figure 1. Moreover, we select the activation function as the Sigmoid function, the learning step length is set to 0.1, the error factor is 0.0001, the training function is traingd. After a trial-and-error procedure, we set the hidden neurons as 15 and the hidden layer as 1. The parameters of the firefly BP neural networks are set as follows: the population number is 30, the initial population of the firefly neural network is 30, $\beta_0 = 1$, $\gamma = 1$, and $\alpha = 0.2$.

In the above-stated case, the input variables are symptoms of failures, and there are 5 in total. They are x_1 : temperature of the emission pipe; x_2 : pressure of the scavenging box; x_3 : pressure of the maximum breakout; x_4 : outlet temperature of the compressor rotor; x_5 : temperature of the scavenging box. The output variable is the cause of the failure, that is, the failure mode. There are 3 in total, namely y_1 : cylinder broken; y_2 : technical interface; y_3 : pin broken. There are 48 sets of training samples for the neural network, each with 12 sets of training samples for each type of fault. Some of the training samples are extracted and normalized as shown in Table 1. After the fault diagnosis procedure, we can obtain the output result as shown in Table 2.

Table 1 The training samples

Samples	Input model (Fault symptom set)				
	x_1	x_2	x_3	x_4	x_5
1	0.568	-0.702	-0.752	0.065	0.088
2	0.411	0.520	0.412	0.365	-0.062
3	0.236	-0.185	-0.396	-0.366	0.114

Table 2 The sample output of BP-Firefly neural networks

Samples	Diagnostic sample output		
	y_1	y_2	y_3
1	1.0521	-0.0121	-0.1012
2	0.6588	1.0358	0.0015
3	-0.3656	0.2565	0.8525

It is easy to see from Table 2 that the fault types corresponding to sample 1, sample 2 and sample 3 are y_1 , y_2 and y_3 respectively.

In order to compare the performance of the network, 50 simulation tests were performed on the conventional BP neural networks and the BP neural network was optimized by the firefly algorithm. Under the same environment and parameter settings, the maximum and minimum average variances of the test sample network output are calculated respectively. The network performances are shown in Table 3.

Table 3 The network performances

Training method	Average time/s	Output maximum average variance	Output maximum average variance
conventional BP	52.1251	0.0265	0.0025
BP-Firefly	3.0235	9.52×10^{-5}	5.62×10^{-7}

It can be seen from Table 3 that the BP neural network that is optimized by the firefly algorithm has higher accuracies in fault diagnosis of bolter miners and better network performances.

5. Conclusions

In this paper, the characteristic values that are selected from the cutting cylinder of bolter miners are used as the input vector of BP neural networks. By setting the neural network structure and initial parameters, the performance of the networks are tested, which can effectively explain the fault type of cutting cylinders of bolter miners in different working states. Through the establishment of bolter miner fault tree models, it can provide a guidance for quantitative analysis of the fault cause of bolter miners. The improved fault tree diagnosis method based on petri nets overcomes the conflicts, collisions, deadlocks and other phenomena of resources in traditional petri nets, and establishes theoretical reasoning process through matrix operations which provides a mathematical theoretical basis for the realization of intelligent diagnosis. In conclusion, FTA-Petri net models and the BP-Firefly algorithm provide new methods for fault diagnosis of coal mining machinery such as bolter miners and roadheaders. In the future, we can combine more convincing genetic algorithms to propose intelligent fault

diagnosis rules. Moreover, we can also introduce granular-computing approaches, such as rough sets and three-way decisions, to explore related fault diagnosis approaches.

Acknowledgements

This work is supported by the Major Research and Development Project of Shanxi Province (No.201803D121121) and Science and Technology Innovation Project of China Coal Technology & Engineering Group (No.2020-TD-ZD009).

References

- [1] M. Bhuiyan, L. Parvez, M. Islam, et al. Heavy metal pollution of coal mine-affected agricultural soils in the northern part of Bangladesh. *Journal of Hazardous Materials*, 2010, 173(1-3): 384-392
- [2] K. Ozgen, P. Warwick. Assessment of coal mine methane (CMM) and abandoned mine methane (AMM) resource potential of longwall mine panels: Example from Northern Appalachian Basin, USA. *International Journal of Coal Geology*, 2019, 208: 37-53
- [3] C. Zhang, D. Li, Y. Mu, et al. A pythagorean fuzzy multigranulation probabilistic model for mine ventilator fault diagnosis. *Complexity*, 2018, 2018: 1-19
- [4] C. Zhang, D. Li, J. Liang. Multi-granularity three-way decisions with adjustable hesitant fuzzy linguistic multigranulation decision-theoretic rough sets over two universes. *Information Sciences*, 2020, 507: 665-683
- [5] L. Zou, Y. Li, F. Xu. An adversarial denoising convolutional neural network for fault diagnosis of rotating machinery under noisy environment and limited sample size case. *Neurocomputing*, 2020, 407: 105-120
- [6] Y. Hu, B. Ping, D. Zeng, et al. Research on fault diagnosis of coal mill system based on the simulated typical fault samples. *Measurement*, 2020, 161: 107864
- [7] V. Agrawal, B. Panigrahi, P. Subbarao. Review of control and fault diagnosis methods applied to coal mills. *Journal of Process Control*, 2015, 32: 138-153
- [8] X. Chen, W. Li, X. Yan. Analysis on rock burst danger when fully-mechanized caving coal face passed fault with deep mining. *Safety Science*, 2012, 50(4): 645-648
- [9] J. Krzywanski, H. Fan, Y. Feng, et al. Genetic algorithms and neural networks in optimization of sorbent enhanced H₂ production in FB and CFB gasifiers. *Energy Conversion and Management*, 2018, 171: 1651-1661
- [10] B. Yang, D. Lim, A. Tan. VIBEX: an expert system for vibration fault diagnosis of rotating machinery using decision tree and decision table. *Expert Systems with Applications*, 2005, 28(4): 735-742
- [11] M. Talebberrouane, F. Khan, Z. Lounis. Availability analysis of safety critical systems using advanced fault tree and stochastic Petri net formalisms. *Journal of Loss Prevention in the Process Industries*, 2016, 44: 193-203
- [12] J. Wu, S. Yan, L. Xie. Reliability analysis method of a solar array by using fault tree analysis and fuzzy reasoning Petri net. *Acta Astronautica*, 2011, 69(11-12): 960-968
- [13] B. Amiri, L. Hossain, J. Crawford, et al. Community detection in complex networks: Multi-objective enhanced firefly algorithm. *Knowledge-Based Systems*, 2013, 46: 1-11
- [14] D. Biu, T. Nguyen, T. Ngo, et al. An artificial neural network (ANN) expert system enhanced with the electromagnetism-based firefly algorithm (EFA) for predicting the energy consumption in buildings. *Energy*, 2020, 190: 116370
- [15] A. Hammid, M. Sulaiman, O. Awad. A robust firefly algorithm with backpropagation neural networks for solving hydrogeneration prediction. *Electrical Engineering*, 2018, 100: 3617-2633

Hierarchies and Uncertainty Measures on Pythagorean Fuzzy Approximation Spaces

Xiaojing LUO^a, Jingjing SONG^{a,b,1}, Huili DOU^a, Xibei YANG^a, Taihua XU^a

^a*School of Computer Science, Jiangsu University of Science and Technology,
Zhenjiang, Jiangsu 212100, P. R. China*

^b*Key Laboratory of Data Science and Intelligence Application, Fujian Province
University, Zhangzhou, 363000, P. R. China*

Abstract. In Granular Computing, the hierarchies and uncertainty measures are two important concepts to investigate the granular structures and uncertainty of approximation spaces. In this paper, hierarchies and uncertainty measures on pythagorean fuzzy approximation spaces will be researched. Firstly, the introduction and operations of pythagorean fuzzy granular structures are given, and three hierarchies and a lattice structure on pythagorean fuzzy approximation spaces are examined. The hierarchies are characterized by three order relations, the first order relation is defined on the inclusion relation of pythagorean fuzzy information granules, the second one is defined on the cardinality of pythagorean fuzzy information granules, and the third one is defined on the sum of the cardinality of pythagorean fuzzy information granules. The lattice structure is constructed on the first order relation on pythagorean fuzzy approximation spaces. Fuzzy information granularity and fuzzy information entropy are extended to describe the uncertainty of pythagorean fuzzy granular structures, and the relationship between the uncertainty measures and hierarchies are discussed. The examples show that hierarchies are effective to analyze the relationships among all granular structures on pythagorean fuzzy approximation spaces.

Keywords. Granular Computing, hierarchies, pythagorean fuzzy set, uncertainty measures

1. Introduction

Granular Computing(GrC), which was initiated by Zadeh [1,2], is an emerging computing paradigm of information processing. It is an effective way to simulate human being's thinking and divide the complex problem into a series of relatively simple problems to facilitate the information processing. In GrC, a collection of objects cluster with indivisibility, similarity, proximity, and functionality is called information granule [1]. All of these information granules together lead to an information granulation, which provide a visible underlying framework for problem solving. The information granulation of all objects in the universe results in a set of granules called a granular structure [1].

¹Corresponding Author. E-mail: songjingjing108@163.com

Different information granulations lead to different levels of abstraction and may present different granular views of our comprehension of a real world problem. GrC is searching for some suitable information granules so that a complex concept is able to approximate effectively at a specific level of granulation [1]. Up to now, GrC research is progressing rapidly [3,4,5], the results show that GrC is becoming the mainstream of computer science.

After constructing all the granular structures on the approximation spaces, the hierarchies of the approximation spaces can be used to analyze the relationship among all the granular structures on approximate spaces [6]. Many scholars researched the hierarchies on various granular structures. For example, Yao [7] recommended to use hierarchical granulations to research of hierarchical rough set approximations. Zhang et al. [8] constructed the hierarchies of fuzzy quotient space by constructing the normalized isosceles distance function. Wang et al. [9] studied hierarchies knowledge space chain based on different knowledge granulation levels. In order to explore the finer or coarser relationships among multigranulation spaces, Yang et al. [10] have conducted three different hierarchies on the multigranulation rough set models. Song et al. [11] introduced knowledge distance [12,13] to fuzzy environment, and proposed the local knowledge distance and global knowledge distance, such two knowledge distances are used to construct algebraic lattices, which are useful in characterizing the hierarchies on fuzzy information granulations. Huang et al. [14] investigated the hierarchies and a lattice structure of intuitionistic fuzzy set, and then further researched the uncertainty measures of intuitionistic fuzzy set. Some order relations were used to characterize the hierarchies on hesitant fuzzy approximation spaces by Tsang et al. [15].

In GrC, a granular structure's uncertainty measure is a significant problem. Two main representations of uncertainty measure in different approximation spaces are information entropy and information granularity. An information granularity shows the discernibility of an information granule in a granular structure. If a granular structure is to be more recognizability, the smaller information granularity of granular structure is required [16]. Based on the different goals, the calculation of information granularity of granular structure is always a significant problem [17]. Granular structure entropy proposed by Shannon is an effective method to describe the information content of granular structure. Partition probability is used to define Shannon entropy, so the uncertainty of granular structure can not be described by Shannon entropy. Thus, the uncertainty of generalized granular structures are expressed by information entropy, which is obtained by extending Shannon entropy to different generalized granular structures [18,19].

Fuzzy set, which was first put forward by Zadeh [20], deals with the uncertainty problems has achieved great success in many fields. Many different extend fuzzy set methods have been proposed by researchers to deal with more inaccurate information in practical applications, among which the intuitionistic fuzzy set proposed by Atanassov is one classic model [21]. Intuitionistic fuzzy set gives each element a membership degree and a nonmembership degree, and requests the sum of membership degree and nonmembership degree must less than or equal to 1. It should be noted that sometimes the sum of membership degree and nonmembership degree is greater than 1, which can not be dealed with intuitionistic fuzzy set. To address this problem, Yager [22,31,32,33] proposed pythagorean fuzzy set, which is obtained when the sum of squares of its membership degree and nonmembership degree is less than or equal to 1. Therefore, pythagorean fuzzy set is one extension of fuzzy set, which is a direct promotion of intuitionistic fuzzy

set. The pythagorean fuzzy set not only retains the advantages of the intuitionistic fuzzy set in processing uncertain information, but also broadens the application range of intuitionistic fuzzy set. Pythagorean fuzzy set has attracted by many scholars [26]- [30], but the hierarchy of pythagorean fuzzy approximation spaces has been rarely discussed, so the relationship among all the granular structures on pythagorean fuzzy approximation spaces can not be characterized.

Based on the descriptions above, there are three points to consider in GrC: information granulation, hierarchies and information granularity. Information granulation aims at granulating the objects in the universe of discourse into information granulation structure. Hierarchies with the purpose of sorting the information granulation structures on the approximation spaces. And the information granularity is used for measuring the granulation degree of an information granular structure [14]. As far as we know, there is no unified framework for these three developments, which is also important for the study of the pythagorean fuzzy granular structure. That is what drives our research. The motivation of this paper is to research the hierarchies and uncertainty measures of pythagorean fuzzy approximation spaces. To characterize the hierarchies on pythagorean fuzzy approximation spaces, three order relations on pythagorean fuzzy approximation spaces are proposed and some operations are defined on them, and then their lattice structures are given. Furthermore, the information granularity and information entropy to pythagorean fuzzy approximation spaces are extended to describe the uncertainty measures of pythagorean fuzzy approximation spaces. At last, the relationships between uncertainty measures and hierarchies of pythagorean fuzzy approximation spaces are discussed [14].

The rest of this study is organized as follows. Several basic notions are reviewed in Section 2, such as the notions of fuzzy set, fuzzy granular structure and the order relations on fuzzy granular structures. On this basis, the pythagorean fuzzy set and pythagorean fuzzy approximation spaces are represented naturally. In Section 3, three order relations on pythagorean fuzzy approximation spaces are discussed. Furthermore, a lattice structure of pythagorean fuzzy approximation spaces, which based on the first order relation is investigated. The uncertainty measures of pythagorean fuzzy approximation spaces are discussed by using pythagorean fuzzy information granularity and pythagorean fuzzy information entropy in Section 4, and then the relationships among hierarchies and the uncertainty measures are established. The conclusions and the future perspectives of this study will be shown in Section 5.

2. Preliminary knowledge

This section introduces some basic concepts of fuzzy set and three order relations of fuzzy information granulation, then the pythagorean fuzzy set and the pythagorean fuzzy approximation spaces are also introduced.

2.1. Fuzzy Set

Definition 1 [20] Let $U = \{x_1, x_2, \dots, x_n\}$ be a nonempty set, which is called the universe of discourse. Assuming that $\hat{A} : U \rightarrow [0, 1]$ such that $\mu_{\hat{A}}(x_i) \in [0, 1]$ for each $x_i \in U$, then $\hat{A} = \{\frac{\mu_{\hat{A}}(x_i)}{x_i} | 1 \leq i \leq n\}$ is called a fuzzy set over U where $\mu_{\hat{A}}(x_i)$ is the membership degree of element x_i . Furthermore, a fuzzy relation over U is a fuzzy set such that $\hat{R} : U \times U \rightarrow [0, 1]$.

Definition 2 [19] Let U be the universe of discourse, a fuzzy granular structure over U is defined as

$$F(\hat{R}) = (S_{\hat{R}}(x_1), S_{\hat{R}}(x_2), \dots, S_{\hat{R}}(x_n)),$$

where $S_{\hat{R}}(x_i) = \{\frac{r_{ij}}{x_j} \mid 1 \leq j \leq n\} (1 \leq i \leq n)$ is a fuzzy information granule induced by the element x_i and the fuzzy relation \hat{R} .

The cardinality of $S_{\hat{R}}(x_i)$ is presented as $|S_{\hat{R}}(x_i)| = \sum_{j=1}^n r_{ij} (1 \leq i \leq n)$. According to Definition 2, the group of all fuzzy granular structures over U is presented by $F(U, \hat{\Omega})$, which is denoted as a fuzzy approximation space, where $\hat{\Omega}$ represents the set of all fuzzy relations over U .

2.2. Three Order Relations on Fuzzy Granular Structures

Since order relation is a widely used method to characterize the hierarchies of granular structure, thus three order relations on fuzzy granular structures will be reviewed.

Definition 3 [19] Let $F(\hat{P}), F(\hat{Q}) \in F(U, \hat{\Omega})$, $F(\hat{P}) = (S_{\hat{P}}(x_1), S_{\hat{P}}(x_2), \dots, S_{\hat{P}}(x_n))$, $F(\hat{Q}) = (S_{\hat{Q}}(x_1), S_{\hat{Q}}(x_2), \dots, S_{\hat{Q}}(x_n))$. The first order relation \leq_1 is defined as

$$F(\hat{P}) \leq_1 F(\hat{Q}) \iff S_{\hat{P}}(x_i) \subseteq S_{\hat{Q}}(x_i) (1 \leq i \leq n)$$

where $S_{\hat{P}}(x_i) \subseteq S_{\hat{Q}}(x_i) (1 \leq i \leq n)$ means that each membership of the elements in $S_{\hat{P}}$ is less than or equal to that in $S_{\hat{Q}}$, that is, $p_{ij} \leq q_{ij} (1 \leq i \leq n)$ for each element x_i .

Definition 4 [11] Let $F(\hat{P}), F(\hat{Q}) \in F(U, \hat{\Omega})$, $F(\hat{P}) = (S_{\hat{P}}(x_1), S_{\hat{P}}(x_2), \dots, S_{\hat{P}}(x_n))$, $F(\hat{Q}) = (S_{\hat{Q}}(x_1), S_{\hat{Q}}(x_2), \dots, S_{\hat{Q}}(x_n))$. The second order relation \leq_2 is defined as

$$F(\hat{P}) \leq_2 F(\hat{Q}) \iff |S_{\hat{P}}(x_i)| \leq |S_{\hat{Q}}(x_i)| (1 \leq i \leq n)$$

Definition 5 [11] Let $F(\hat{P}), F(\hat{Q}) \in F(U, \hat{\Omega})$, $F(\hat{P}) = (S_{\hat{P}}(x_1), S_{\hat{P}}(x_2), \dots, S_{\hat{P}}(x_n))$, $F(\hat{Q}) = (S_{\hat{Q}}(x_1), S_{\hat{Q}}(x_2), \dots, S_{\hat{Q}}(x_n))$. The third order relation \leq_3 is defined as

$$F(\hat{P}) \leq_3 F(\hat{Q}) \iff \left| \sum_{x_i \in U} S_{\hat{P}}(x_i) \right| \leq \left| \sum_{x_i \in U} S_{\hat{Q}}(x_i) \right| (1 \leq i \leq n)$$

2.3. Pythagorean Fuzzy Set

Definition 6 [22] Let U be the universe of discourse, a pythagorean fuzzy set P in U is denoted by $P = \{\frac{<\mu_P(x_i), v_P(x_i)>}{x_i} \mid 1 \leq i \leq n\}$, where $\mu_P(x_i) : U \rightarrow [0, 1]$ is the degree of membership of element x_i , $v_P(x_i) : U \rightarrow [0, 1]$ is the degree of nonmembership of element x_i , and $0 \leq \mu_P(x_i)^2 + v_P(x_i)^2 \leq 1$. Furthermore, the hesitancy degree of x_i to P is denoted by $h_P(x_i) = \sqrt{1 - \mu_P(x_i)^2 - v_P(x_i)^2}$.

For the sake of convenience, Zhang and Xu [25] called $(\mu_P(x_i), v_P(x_i))$ a pythagorean fuzzy number denoted by $p = (\mu_P(x_i), v_P(x_i))$.

Remark 1 Specially, if the membership degree $\mu_P(x_i)$ and nonmembership degree $v_P(x_i)$ of element x_i in pythagorean fuzzy set P satisfy the condition that $0 \leq \mu_P(x_i) + v_P(x_i) \leq 1$, then the pythagorean fuzzy set P is an intuitionistic fuzzy set [21]. The classical fuzzy set can be regarded as a special intuitionistic fuzzy set of the form $P = \{\frac{<\mu_P(x_i), 1 - \mu_P(x_i)>}{x_i} | 1 \leq i \leq n\}$.

Definition 7 [23] Let $A = \{\frac{<\mu_A(x_i), v_A(x_i)>}{x_i} | 1 \leq i \leq n\}$ and $B = \{\frac{<\mu_B(x_i), v_B(x_i)>}{x_i} | 1 \leq i \leq n\}$ be two pythagorean fuzzy sets over the universe of discourse U , some operators, i.e., intersection \cap , union \cup , complement \setminus , equation $=$ on A and B , and the inclusion relation between pythagorean fuzzy granular structures A and B can be defined as follows

1. $A \cap B = \left\{ \frac{\min\{\mu_A(x_i), \mu_B(x_i)\}, \max\{v_A(x_i), v_B(x_i)\}}{x_i} | 1 \leq i \leq n \right\},$
2. $A \cup B = \left\{ \frac{\max\{\mu_A(x_i), \mu_B(x_i)\}, \min\{v_A(x_i), v_B(x_i)\}}{x_i} | 1 \leq i \leq n \right\},$
3. $\setminus A = \left\{ \frac{<\nu_A(x_i), \mu_A(x_i)>}{x_i} | 1 \leq i \leq n \right\}$ is the supplementary of A ,
4. $A = B \iff \mu_A(x_i) = \mu_B(x_i) \wedge \nu_A(x_i) = \nu_B(x_i) (1 \leq i \leq n),$
5. $A \subseteq B \iff \mu_A(x_i) \leq \mu_B(x_i) \wedge \nu_A(x_i) \geq \nu_B(x_i) (1 \leq i \leq n).$

Let U be the universe of discourse, the pythagorean fuzzy relation R over U can be represented by $n \times n$ matrix

$$M_R = \begin{pmatrix} \langle \mu_R(x_1, x_1), \nu_R(x_1, x_1) \rangle & \langle \mu_R(x_1, x_2), \nu_R(x_1, x_2) \rangle & \cdots & \langle \mu_R(x_1, x_n), \nu_R(x_1, x_n) \rangle \\ \langle \mu_R(x_2, x_1), \nu_R(x_2, x_1) \rangle & \langle \mu_R(x_2, x_2), \nu_R(x_2, x_2) \rangle & \cdots & \langle \mu_R(x_2, x_n), \nu_R(x_2, x_n) \rangle \\ \vdots & \vdots & \vdots & \vdots \\ \langle \mu_R(x_n, x_1), \nu_R(x_n, x_1) \rangle & \langle \mu_R(x_n, x_2), \nu_R(x_n, x_2) \rangle & \cdots & \langle \mu_R(x_n, x_n), \nu_R(x_n, x_n) \rangle \end{pmatrix},$$

where $\mu_R(x_i, x_j), \nu_R(x_i, x_j) \in [0, 1]$ and $0 \leq \mu_R^2(x_i, x_j) + \nu_R^2(x_i, x_j) \leq 1 (1 \leq i, j \leq n)$.

We suppose that all pythagorean fuzzy relations in this paper are reflexive in the universe of discourse U , because reflexive is significant to characterize the similarity between objects, i.e., $\mu_R(x_i, x_i) = 1, \nu_R(x_i, x_i) = 0 (1 \leq i \leq n)$ in M_R .

The group of pythagorean fuzzy relations over U are denoted as $PFAS = (U, \Omega)$, which is called the pythagorean fuzzy approximation space over U , where Ω represents the set of pythagorean fuzzy relations over U .

3. Hierarchies of Pythagorean Fuzzy Approximation Spaces

Granular structure is a fundamental term in GrC, and new granular structures can be generated by using several operators on granular structure. Four operators extended to fuzzy granular structures by Qian et al. [19]. In this section, the pythagorean granular structure is constructed and all objects are granulated into pythagorean fuzzy information granules. We also extend four operators of Qian on fuzzy granular space into pythagorean fuzzy granular space and then give three order relations on pythagorean fuzzy granular space, which constitute the hierarchies on pythagorean fuzzy approximation spaces. In the end, the lattice structure of the pythagorean approximation spaces is discussed.

3.1. Pythagorean Fuzzy Granular Structure

Definition 8 A pythagorean fuzzy granular structure determined by pythagorean fuzzy relation R in PFAS is defined as

$$P(R) = (S_R(x_1), S_R(x_2), \dots, S_R(x_n)),$$

where $S_R(x_i) = \left\{ \frac{<r_{ij}^+, r_{ij}^->}{x_j} \mid 1 \leq j \leq n \right\} (1 \leq i \leq n)$, $S_R(x_i)$ is the pythagorean fuzzy information granule induced by element x_i and pythagorean fuzzy relation R ; r_{ij}^+ is the similarity between elements x_i and x_j , and r_{ij}^- is the dissimilarity between elements x_i and x_j .

The collection of all pythagorean fuzzy granular structures over the universe U can be represented by $PF(U, \Omega)$. As is known to all, there is a 1-1 relationship between pythagorean fuzzy approximation space and pythagorean fuzzy granular structure space, thus, we do not distinguish the pythagorean fuzzy relation and pythagorean fuzzy granular structure between (U, Ω) and $PF(U, \Omega)$.

The fuzzy set's cardinality is important for investigating the information granulation and its measure of uncertainty, so is the pythagorean fuzzy set. The new cardinality of pythagorean fuzzy set is defined in Definition 9.

Definition 9 Let $P(R) = (S_R(x_1), S_R(x_2), \dots, S_R(x_n))$, where $S_R(x_i) = \left\{ \frac{<r_{ij}^+, r_{ij}^->}{x_j} \mid 1 \leq j \leq n \right\} (1 \leq i \leq n)$. The cardinality of $S_R(x_i)$ is regarded as

$$|S_R(x_i)| = \frac{1}{2} \sum_{j=1}^n (1 + (r_{ij}^+)^2 - (r_{ij}^-)^2).$$

Accordingly, the cardinality of pythagorean fuzzy relation matrix is denoted by $|M_R(x_i)| = \frac{1}{2} \sum_{j=1}^n (1 + (\mu_R(x_i, x_j))^2 - (v_R(x_i, x_j))^2)$.

By employing this cardinality of pythagorean fuzzy information granule, we can construct the hierarchies and uncertainty measures on pythagorean fuzzy approximation spaces in this paper.

Definition 10 Let $P(L), P(Q) \in PF(U, \Omega)$, and $P(L) = (S_L(x_1), S_L(x_2), \dots, S_L(x_n)), P(Q) = (S_Q(x_1), S_Q(x_2), \dots, S_Q(x_n))$, where $S_L(x_i) = \left\{ \frac{<l_{ij}^+, l_{ij}^->}{x_j} \mid 1 \leq j \leq n \right\} (1 \leq i \leq n), S_Q(x_i) = \left\{ \frac{<q_{ij}^+, q_{ij}^->}{x_j} \mid 1 \leq j \leq n \right\} (1 \leq i \leq n)$. Some operators, i.e., intersection \cap , union \cup , minus $-$, complement \complement , equation $=$ and inequation \neq on $P(L)$ and $P(Q)$ can be defined as follows

1. $P(L) \cap P(Q) = \{S_{L \cap Q}(x_i) \mid S_{L \cap Q}(x_i) = S_L(x_i) \cap S_Q(x_i), 1 \leq i \leq n\},$
2. $P(L) \cup P(Q) = \{S_{L \cup Q}(x_i) \mid S_{L \cup Q}(x_i) = S_L(x_i) \cup S_Q(x_i), 1 \leq i \leq n\},$
3. $P(L) - P(Q) = \{S_{L-Q}(x_i) \mid S_{L-Q}(x_i) = S_L(x_i) \cap \complement S_Q(x_i), 1 \leq i \leq n\},$
4. $\complement P(L) = \{\complement S_L(x_i) \mid 1 \leq i \leq n\},$
5. $P(L) = P(Q) \iff S_L(x_i) = S_Q(x_i) \iff l_{ij}^+ = q_{ij}^+ \wedge l_{ij}^- = q_{ij}^-, 1 \leq i, j \leq n\}$
6. $P(L) \neq P(Q) \iff S_L(x_i) \neq S_Q(x_i) \iff l_{ij}^+ \neq q_{ij}^+ \wedge l_{ij}^- \neq q_{ij}^-, 1 \leq i, j \leq n\}$

where $S_{L \cap Q} = \left\{ \frac{\min\{l_{ij}^+, q_{ij}^+\}, \max\{l_{ij}^-, q_{ij}^-\}}{x_j} \mid 1 \leq j \leq n \right\}$, $S_{L \cup Q} = \left\{ \frac{\max\{l_{ij}^+, q_{ij}^+\}, \min\{l_{ij}^-, q_{ij}^-\}}{x_j} \mid 1 \leq j \leq n \right\}$, $\delta_L(x_i) = \left\{ \frac{l_{ij}^-, l_{ij}^+}{x_j} \mid 1 \leq j \leq n \text{ and } j \neq i \right\} (1 \leq i \leq n)$.

Proposition 1 Let $P(L), P(Q), P(R), P(\mathcal{U})$ and $P(\varphi) \in PF(U, \Omega)$, $P(\mathcal{U}) = (S_{\mathcal{U}}(x_1), S_{\mathcal{U}}(x_2), \dots, S_{\mathcal{U}}(x_n))$, if $S_{\mathcal{U}}(x_i) = \left\{ \frac{<1,0>}{x_j} \mid 1 \leq i, j \leq n \right\}$, then \mathcal{U} is the pythagorean fuzzy universal relation over U , $P(\mathcal{U})$ is the maximal pythagorean fuzzy granular structure; $P(\varphi) = (S_{\varphi}(x_1), S_{\varphi}(x_2), \dots, S_{\varphi}(x_n))$, if $S_{\varphi}(x_i) = \left\{ \frac{<0,1>}{x_j} \mid 1 \leq j, i \leq n, j \neq i \right\}$, and $S_{\varphi}(x_i) = \left\{ \frac{<1,0>}{x_j} \mid 1 \leq j = i \leq n \right\}$, then φ is the pythagorean fuzzy identical relation over U , $P(\varphi)$ is the minimal pythagorean fuzzy granular structure. The operators, i.e., intersection \cap , union \cup , and complement \complement on $PF(U, \Omega)$ satisfy the following properties.

1. Identity law: $P(L) \cap P(\mathcal{U}) = P(L)$ and $P(L) \cup P(\varphi) = P(L)$.
2. Zero law: $P(L) \cup P(\mathcal{U}) = P(\mathcal{U})$ and $P(L) \cap P(\varphi) = P(\varphi)$.
3. Commutative law: $P(L) \cap P(Q) = P(Q) \cap P(L)$, $P(L) \cup P(Q) = P(Q) \cup P(L)$.
4. Association law: $(P(L) \cap P(Q)) \cap P(R) = P(L) \cap ((P(Q) \cap P(R)), (P(L) \cup P(Q)) \cup P(R) = P(L) \cup ((P(Q) \cup P(R))$.
5. Distributive law: $P(L) \cap (P(Q) \cup P(R)) = (P(L) \cap (P(Q)) \cup (P(L) \cap P(R))$, $P(L) \cup (P(Q) \cap P(R)) = (P(L) \cup P(Q)) \cap (P(L) \cup P(R))$.
6. Absorption law: $P(L) \cap (P(L) \cup P(Q)) = P(L)$, $P(L) \cup (P(L) \cap P(Q)) = P(L)$.
7. De Morgan law: $\complement(P(L) \cap P(Q)) = \complement P(L) \cup \complement P(Q)$, $\complement(P(L) \cup P(Q)) = \complement P(L) \cap \complement P(Q)$.

3.2. Three Order Relations on Pythagorean Fuzzy Approximation Spaces

In this section, we give three order relations to characterize the hierarchies on different pythagorean fuzzy granular structures.

Definition 11 Let $P(L), P(Q) \in PF(U, \Omega)$, $P(L) = (S_L(x_1), S_L(x_2), \dots, S_L(x_n))$, $P(Q) = (S_Q(x_1), S_Q(x_2), \dots, S_Q(x_n))$, the first order relation \preceq_1 is defined as follows

$$P(L) \preceq_1 P(Q) \iff S_L(x_i) \subseteq S_Q(x_i) \text{ for any } 1 \leq i \leq n.$$

$$P(L) \prec_1 P(Q) \iff P(L) \preceq_1 P(Q) \wedge P(L) \neq P(Q).$$

$$P(L) \approx_1 P(Q) \iff S_L(x_i) = S_Q(x_i),$$

where $S_L(x_i) \subseteq S_Q(x_i)$ means that $\forall 1 \leq i, j \leq n$, we have $l_{ij}^+ \leq q_{ij}^+ \wedge l_{ij}^- \geq q_{ij}^-$.

Example 1 Let U be the universe of discourse, L, Q, S and T are four pythagorean fuzzy relations over U , which are denoted by the following matrices, respectively.

$$M_L = \begin{pmatrix} <1.0, 0.0> <0.3, 0.8> <0.4, 0.7> <0.3, 0.7> <0.4, 0.5> \\ <0.3, 0.8> <1.0, 0.0> <0.6, 0.7> <0.4, 0.8> <0.5, 0.6> \\ <0.4, 0.7> <0.6, 0.7> <1.0, 0.0> <0.3, 0.8> <0.6, 0.5> \\ <0.3, 0.7> <0.4, 0.8> <0.3, 0.8> <1.0, 0.0> <0.4, 0.6> \\ <0.4, 0.5> <0.5, 0.6> <0.6, 0.5> <0.4, 0.6> <1.0, 0.0> \end{pmatrix}$$

$$M_Q = \begin{pmatrix} < 1.0, 0.0 > < 0.5, 0.7 > < 0.6, 0.6 > < 0.5, 0.6 > < 0.6, 0.4 > \\ < 0.5, 0.7 > < 1.0, 0.0 > < 0.7, 0.4 > < 0.6, 0.5 > < 0.7, 0.4 > \\ < 0.6, 0.6 > < 0.7, 0.4 > < 1.0, 0.0 > < 0.7, 0.5 > < 0.8, 0.4 > \\ < 0.5, 0.6 > < 0.6, 0.5 > < 0.7, 0.5 > < 1.0, 0.0 > < 0.6, 0.4 > \\ < 0.6, 0.4 > < 0.7, 0.4 > < 0.8, 0.4 > < 0.6, 0.4 > < 1.0, 0.0 > \end{pmatrix}$$

$$M_S = \begin{pmatrix} < 1.0, 0.0 > < 0.4, 0.8 > < 0.7, 0.4 > < 0.5, 0.6 > < 0.8, 0.5 > \\ < 0.5, 0.8 > < 1.0, 0.0 > < 0.8, 0.3 > < 0.6, 0.5 > < 0.7, 0.4 > \\ < 0.7, 0.4 > < 0.8, 0.3 > < 1.0, 0.0 > < 0.7, 0.5 > < 0.8, 0.4 > \\ < 0.5, 0.4 > < 0.7, 0.4 > < 0.7, 0.5 > < 1.0, 0.0 > < 0.6, 0.4 > \\ < 0.8, 0.5 > < 0.7, 0.4 > < 0.8, 0.4 > < 0.6, 0.4 > < 1.0, 0.0 > \end{pmatrix}$$

$$M_T = \begin{pmatrix} < 1.0, 0.0 > < 0.3, 0.7 > < 0.8, 0.4 > < 0.5, 0.6 > < 0.9, 0.2 > \\ < 0.3, 0.7 > < 1.0, 0.0 > < 0.8, 0.2 > < 0.6, 0.5 > < 0.7, 0.4 > \\ < 0.8, 0.4 > < 0.8, 0.2 > < 1.0, 0.0 > < 0.7, 0.5 > < 0.8, 0.4 > \\ < 0.5, 0.6 > < 0.6, 0.5 > < 0.7, 0.5 > < 1.0, 0.0 > < 0.6, 0.4 > \\ < 0.9, 0.2 > < 0.7, 0.4 > < 0.8, 0.4 > < 0.6, 0.4 > < 1.0, 0.0 > \end{pmatrix}$$

We can observe that $\forall 1 \leq i, j \leq n$, we have $l_{ij}^+ < q_{ij}^+$ and $l_{ij}^- > q_{ij}^-$, which means that $S_L(x_i) \subseteq S_Q(x_i)$, thus $P(L) \prec_1 P(Q)$ obtained. Then the pythagorean fuzzy granular structure $P(L)$ is finer than pythagorean fuzzy granular structure $P(Q)$, the order relation \preceq_1 can well differentiate the granularity between pythagorean fuzzy granular structures $P(L)$ and $P(Q)$.

We can observe that neither $S_Q(x_1) \subseteq S_S(x_1)$ nor $S_S(x_1) \subseteq S_Q(x_1)$ satisfies, which means the order relation \preceq_1 can not differentiate the granularity between the two pythagorean fuzzy granular structures $P(Q)$ and $P(S)$. To further distinguish their difference, a new finer criterion \preceq_2 will be proposed in Definition 12.

Definition 12 Let $P(L), P(Q) \in PF(U, \Omega)$, $P(L) = (S_L(x_1), S_L(x_2), \dots, S_L(x_n))$, $P(Q) = (S_Q(x_1), S_Q(x_2), \dots, S_Q(x_n))$, the second order relation \preceq_2 is defined as follows

$$P(L) \preceq_2 P(Q) \iff |S_L(x_i)| \leq |S_Q(x_i)| \text{ for any } 1 \leq i \leq n.$$

$$P(L) \prec_2 P(Q) \iff P(L) \preceq_2 P(Q) \wedge P(L) \neq P(Q).$$

$$P(L) \approx_2 P(Q) \iff |S_L(x_i)| = |S_Q(x_i)| \text{ for any } 1 \leq i \leq n.$$

Continued from Example 1, we can easily verify that $|M_Q(x_i)| < |M_S(x_i)|$ for $i = 1, 2, 3, 4, 5$, which means $|S_Q(x_i)| < |S_S(x_i)|$, thus $P(Q) \prec_2 P(S)$ obtained. Then the pythagorean fuzzy granular structure $P(Q)$ is finer than pythagorean fuzzy granular structure $P(S)$, the order relation \preceq_2 can well differentiate the granularity between pythagorean fuzzy granular structures $P(Q)$ and $P(S)$.

By computing, we have $|M_S(x_1)| = 3.065$, $|M_S(x_4)| = 3.430$, $|M_T(x_1)| = 3.370$, $|M_T(x_4)| = 3.220$, then $|M_S(x_1)| < |M_T(x_1)|$ and $|M_S(x_4)| > |M_T(x_4)|$ exist, neither $|S_S(x_i)| < |S_T(x_i)|$ nor $|S_T(x_i)| < |S_S(x_i)|$ satisfies. Thus, the order relation \preceq_2 can not differentiate the granularity between the two granular structures $P(S)$ and $P(T)$. To further reveal their difference, a new finer criterion \preceq_3 will be introduced in Definition 13.

Definition 13 Let $P(L), P(Q) \in PF(U, \Omega)$, $P(L) = (S_L(x_1), S_L(x_2), \dots, S_L(x_n))$, $P(Q) = (S_Q(x_1), S_Q(x_2), \dots, S_Q(x_n))$, the third order relation \preceq_3 is defined as follows

$$P(L) \preceq_3 P(Q) \iff |\sum_{x_i \in U} S_P(x_i)| \leq |\sum_{x_i \in U} S_Q(x_i)| \quad (1 \leq i \leq n).$$

$$P(L) \prec_3 P(Q) \iff P(L) \preceq_3 P(Q) \wedge P(L) \neq P(Q).$$

$$P(L) \approx_3 P(Q) \iff |\sum_{x_i \in U} S_P(x_i)| = |\sum_{x_i \in U} S_Q(x_i)| \quad (1 \leq i \leq n).$$

Continued from Example 1, by computing, we can verify that $|\sum_{x_i \in U} S_S(x_i)| = 17.295$, $|\sum_{x_i \in U} S_T(x_i)| = 17.700$, thus we have $|\sum_{x_i \in U} S_S(x_i)| < |\sum_{x_i \in U} S_T(x_i)|$ for $i = 1, 2, 3, 4, 5$, which implies $P(S) \prec_3 P(T)$. Thus the pythagorean fuzzy granular structure $P(S)$ is finer than pythagorean fuzzy granular structure $P(T)$, the order relation \preceq_3 can well differentiate the granularity between pythagorean fuzzy granular structures $P(S)$ and $P(T)$.

Proposition 2 The order relation \preceq_i is a special case of the order relation \preceq_{i+1} ($i = 1, 2$).

The first order relation \preceq_1 is defined on the basis of pythagorean fuzzy inclusion relation between two pythagorean fuzzy granular structures, thus \preceq_1 is a partial order relation, however \preceq_2, \preceq_3 are not necessarily antisymmetric, thus they are quasi-order relations. The three order relations provide different criterias to discriminate the granularity of pythagorean fuzzy granular structures at multiple levels.

3.3. Lattice Structure of Pythagorean Fuzzy Approximation Spaces

Yang et al. [24] used a lattice structure from set distance to study the hierarchies of granular structures on a crisp approximate space. In this subsection, we will study the lattice structure of pythagorean fuzzy approximate spaces based on partial order relation \preceq_1 .

Definition 14 Let (L, \leq) be a poset, if there exist two operators \wedge and \vee on $L : L^2 \rightarrow L$, $\forall a, b, c \in L$, such that

1. $a \wedge b = b \wedge a, a \vee b = b \vee a;$
2. $(a \wedge b) \wedge c = a \wedge (b \wedge c), (a \vee b) \vee c = a \vee (b \vee c);$
3. $a \wedge b = b \iff b \leq a, a \vee b = b \iff a \leq b.$

We then call (L, \leq) is a lattice.

Furthermore, we call (L, \leq) a distributive lattice, if $a \wedge (b \vee c) = (a \wedge b) \vee (a \wedge c)$, $a \vee (b \wedge c) = (a \vee b) \wedge (a \vee c)$ is satisfied.

We call (L, \leq) a complemented lattice, if $\forall a \in L$, there exists a^{-1} such that $(a^{-1})^{-1} = a$ and $a \leq b \iff b^{-1} \leq a^{-1}$. If there exist $0, 1 \in L$ such that $0 \leq a \leq 1, \forall a \in L$, then we call 0 and 1 its minimal and maximal elements, respectively.

Theorem 1 Let \cap, \cup and \wr be defined on $PF(U, \Omega)$ as Definition 10, then $(PF(U, \Omega), \preceq_1, \cap, \cup, \wr)$ is a complemented distributive lattice.

Proof Based on Definitions 10, 14 and Proposition 1, it is straightforward.

In the complemented distributive lattice $(PF(U, \Omega), \preceq_1, \cap, \cup, \wr, P(\varphi))$ and $P(\mathcal{U})$ defined in Proposition 1 are the minimal and maximal elements in $(PF(U, \Omega), \preceq_1)$, respectively.

4. Uncertainty Measures for Pythagorean Fuzzy Approximation Spaces

Two main uncertainty measures: granularity and information entropy, are important for an approximation space. In this section, we extend two measures, i.e., granularity and information entropy, to pythagorean fuzzy approximation spaces, and then analyze the relationships among the proposed order relationships and the two uncertainty measures.

4.1. Granularity of Pythagorean Fuzzy Granular Structure

Definition 15 [32] Let $F(\hat{R}) = (S_{\hat{R}}(x_1), S_{\hat{R}}(x_2), \dots, S_{\hat{R}}(x_n))$ be a fuzzy granular structure, where $S_{\hat{R}}(x_i) = \{\frac{r_{ij}^+}{x_j} | 1 \leq j \leq n\} (1 \leq i \leq n)$. The granularity of $F(\hat{R})$ is defined as follows

$$GF(\hat{R}) = \frac{1}{n} \sum_{i=1}^n \frac{|S_{\hat{R}}(x_i)|}{n} = \frac{1}{n^2} \sum_{i=1}^n \sum_{j=1}^n r_{ij}$$

Definition 16 Let $P(R) \in PF(U, \Omega)$, and $P(R) = (S_R(x_1), S_R(x_2), \dots, S_R(x_n))$, where $S_R(x_i) = \{\frac{<r_{ij}^+, r_{ij}^->}{x_j} | 1 \leq j \leq n\} (1 \leq i \leq n)$. The granularity of pythagorean fuzzy granular structure $P(R)$ is defined as follows

$$GP(R) = \frac{1}{n} \sum_{i=1}^n \frac{|S_R(x_i)|}{n}$$

Theorem 2 Let $P(L), P(Q) \in PF(U, \Omega)$, then,

1. $P(L) \preceq_1 P(Q) \implies GP(L) \leq GP(Q)$.
2. $P(L) \preceq_2 P(Q) \implies GP(L) \leq GP(Q)$.
3. $P(L) \preceq_3 P(Q) \implies GP(L) \leq GP(Q)$.

Proof Based on Definitions 11, 12, 13 and Definition 16, it is obvious.

Example 2 Continued from Example 1.

The pythagorean fuzzy granularity of $P(L)$ is computed as follows

$|S_P(x_1)| = 2.3150, |S_P(x_2)| = 2.3650, |S_P(x_3)| = 2.5500, |S_P(x_4)| = 2.1850, |S_P(x_5)| = 2.8550$, then $GP(L) = 0.4906$.

The pythagorean fuzzy granularity of $P(Q)$ is computed as follows

$|S_Q(x_1)| = 2.9250, |S_Q(x_2)| = 3.2650, |S_Q(x_3)| = 3.5250, |S_Q(x_4)| = 3.2200, |S_Q(x_5)| = 3.6850$, then $GP(Q) = 0.6648$.

The pythagorean fuzzy granularity of $P(S)$ is computed as follows

$|S_S(x_1)| = 3.0650, |S_S(x_2)| = 3.3000, |S_S(x_3)| = 3.8000, |S_S(x_4)| = 3.4300, |S_S(x_5)| = 3.7000$, then $GP(S) = 0.6918$.

The pythagorean fuzzy granularity of $P(T)$ is computed as follows

$|S_T(x_1)| = 3.3700, |S_T(x_2)| = 3.3200, |S_T(x_3)| = 3.9000, |S_T(x_4)| = 3.2200, |S_T(x_5)| = 3.8900$, then $GP(T) = 0.7080$.

The results verify the Theorem 2.

4.2. Information Entropy of Pythagorean Fuzzy Granular Structure

Definition 17 [19] Let $F(\hat{P}) = \{S_{\hat{P}}(x_1), S_{\hat{P}}(x_2), \dots, S_{\hat{P}}(x_n)\}$ be a fuzzy granular structure. The fuzzy information entropy of $F(\hat{P})$ is defined as follows:

$$EF(\hat{P}) = \frac{1}{n} \sum_{i=1}^n \left(1 - \frac{|S_{\hat{P}}(x_i)|}{n}\right)$$

Definition 18 Let $P(R) \in PF(U, \Omega)$, and $P(R) = (S_R(x_1), S_R(x_2), \dots, S_R(x_n))$, the pythagorean fuzzy information entropy of $P(R)$ is defined as follows

$$EP(R) = \frac{1}{n} \sum_{i=1}^n \left(1 - \frac{|S_R(x_i)|}{n}\right)$$

Theorem 3 Let $P(L), P(Q) \in PF(U, \Omega)$, then

1. $P(L) \preceq_1 P(Q) \implies EP(L) \geq EP(Q)$.
2. $P(L) \preceq_2 P(Q) \implies EP(L) \geq EP(Q)$.
3. $P(L) \preceq_3 P(Q) \implies EP(L) \geq EP(Q)$.

Proof Based on Definitions 11, 12, 13 and Definition 18, it is obvious.

Example 3 Continue from Example 1.

By computing, $|S_P(x_1)| = 2.3150, |S_P(x_2)| = 2.3650, |S_P(x_3)| = 2.5500, |S_P(x_4)| = 2.1850, |S_P(x_5)| = 2.8550$ obtained, then the pythagorean fuzzy information entropy of $P(L)$ is $EP(L) = 0.5094$.

By computing, $|S_Q(x_1)| = 2.9250, |S_Q(x_2)| = 3.2650, |S_Q(x_3)| = 3.5250, |S_Q(x_4)| = 3.2200, |S_Q(x_5)| = 3.6850$ obtained, then the pythagorean fuzzy information entropy of $P(Q)$ is $EP(Q) = 0.3352$.

By computing, $|S_S(x_1)| = 3.0650, |S_S(x_2)| = 3.3000, |S_S(x_3)| = 3.8000, |S_S(x_4)| = 3.4300, |S_S(x_5)| = 3.7000$ obtained, then the pythagorean fuzzy information entropy of $P(S)$ is $EP(S) = 0.3082$.

By computing, $|S_T(x_1)| = 3.3700, |S_T(x_2)| = 3.3200, |S_T(x_3)| = 3.9000, |S_T(x_4)| = 3.2200, |S_T(x_5)| = 3.8900$ obtained, then the pythagorean fuzzy information entropy of $P(T)$ is $EP(T) = 0.2920$.

The results verify the Theorem 3.

5. Conclusion

Hierarchies and uncertainty measures are two key issues in the theory of GrC. The contributions in this paper are listed as follows

1. Three order relations on pythagorean fuzzy approximation spaces are discussed. On the basis of the first order relation, the lattice structure of pythagorean fuzzy approximation spaces is given.
2. The pythagorean fuzzy information granularity and pythagorean fuzzy information entropy are employed to characterize the uncertainty measures on pythagorean fuzzy approximation spaces.

3. The relationships between the order relations and uncertainty measures are also discussed.

The followings topics deserve our further investigations.

1. We have only researched the hierarchies on pythagorean fuzzy approximation spaces by considering the degree of membership and nonmembership, did not take the hesitancy degree into account.
2. We have only characterized the uncertainty on pythagorean fuzzy approximation spaces with pythagorean fuzzy granularity and pythagorean fuzzy information entropy, some other uncertainty measures such as rough entropy and information Shannon entropy will be explored further.
3. This paper only mentioned the hierarchies and uncertainty measures of pythagorean fuzzy set, but does not apply it to specific practice, such as medical diagnosis, group decision making and other fields. We will continue to explore its applications in the future work.

Acknowledgements

This work was supported by the Natural Science Foundation of China (Nos. 61906078, 62076111, 62006099) and the Key Laboratory of Data Science and Intelligence Application, Fujian Province University (No. D1901).

References

- [1] L. A. Zadeh. Towards a theory of fuzzy information granulation and its centrality in human reasoning and fuzzy logic. *Fuzzy Sets and Systems*, 1997, 19:111-127.
- [2] L. A. Zadeh. Some reflections on soft computing, granular computing and their roles in the conception, design and utilization of information/intelligent systems. *Soft Computing*, 1998, 2:23-25.
- [3] Xin Yang, Tianrui Li, Dun Liu, H. Fujita. A multilevel neighborhood sequential decision approach of three-way granular computing. *Information Sciences*, 2020, 538:119-141.
- [4] Y. Y. Yao. Three-way granular computing, rough sets, and formal concept analysis. *International Journal of Approximate Reasoning*, 2020, 116:106-125.
- [5] Shuyin Xia, Yunsheng Liu, Xin Ding, Guoyin Wang, Hong Yu, Yuoguo Luo. Granular ball computing classifiers for efficient, scalable and robust learning. *Information Sciences*, 2019, 483:136-152.
- [6] P. Lingras, A. Elagamy, A. Ammar, Z. Elouedi. Iterative meta-clustering through granular hierarchy of supermarket customers and products. *Information Sciences*, 2014, 257:14-31.
- [7] Y. Y. Yao. Information granulation and rough set approximation. *International Journal of Intelligent Systems*, 2001, 16:87-104.
- [8] Qinghua Zhang, Guoyin Wang, Xianquan Liu. Hierarchical structure analysis of fuzzy quotient space. *Pattern Recognition and Artificial Intelligence*, 2008, 5:627-634.
- [9] Guoyin Wang, Qinghua Zhang. Uncertainty of rough sets in different knowledge granularities: uncertainty of rough sets in different knowledge granularities. *Chinese Journal of Computers*, 2009, 31:1588-1598.
- [10] Xibei Yang, Yuhua Qian, Jingyu Yang. Hierarchical structures on multigranulation spaces. *Journal of Computer Science and Technology*, 2012, 27:1169-1183.
- [11] Jingjing Song, Xibei Yang, Xiaoning Song, Hualong Yu, Jingyu Yang. Hierarchies on fuzzy information granulations: a knowledge distance based lattice approach. 2014, 27:1107-1117.
- [12] Yuhua Qian, Jiye Liang, Chuangyin Dang. Knowledge structure, knowledge granulation and knowledge distance in a knowledge base. *International Journal of Approximate Reasoning*, 2009, 50:174-188.

- [13] Jiye Liang, Ru Li, Yuhua Qian. Distance: A more comprehensible perspective for measures in rough set theory. *Knowledge-Based Systems*, 2012, 27:126-136.
- [14] Bing Huang, Chunxiang Guo, Huaxiong Li, Guofu Feng, Xianzhong Zhou. Hierarchical structures and uncertainty measures for intuitionistic fuzzy approximation space. *Information Sciences*, 2016, 336:92-114.
- [15] Eric C. C. Tsang, Jingjing Song, Degang Chen, Xibei Yang. Order based hierarchies on hesitant fuzzy approximation space. *International Journal of Machine Learning and Cybernetics*, 2019, 10:1407-1422.
- [16] Jianmin Ma, Wenxiu Zhang, Yee Leung, Xiaoxue Song. Granular computing and dual Galois connection. *Information Sciences*, 2007, 177:5365-5377.
- [17] Bingzhen Sun, Weimin Ma, Degang Chen. Rough approximation of a fuzzy concept on a hybrid attribute information system and its uncertainty measure. *Information Sciences*, 2014, 284:60-80.
- [18] C. E. Shannon. A mathematical theory of communication. *The Bell System Technical Journal*, 1948, 27:379-423.
- [19] Yuhua Qian, Jiye Liang, Weizhi Wu, Chuangyin Dang. Information granularity in fuzzy binary GrC model. *IEEE Transactions on Fuzzy Systems*, 2011, 19:253-264.
- [20] L. A. Zadeh. Fuzzy sets. *Information AND Control*, 1965, 8:338-353.
- [21] K. T. Atanassov. Intuitionistic fuzzy sets. *Fuzzy Sets and Systems*, 1986, 20:87-96.
- [22] R. R. Yager. Pythagorean fuzzy subsets[C] 2013 Joint IFSA World Congress and NAFIPS Annual Meeting, Canada, 2013, 57-61.
- [23] Xindong Peng, Huiyong Yuan, Yong Yang. Pythagorean fuzzy information measures and their applications. *International Journal of Intelligent Systems*, 2017, 32:991-1029.
- [24] Xibei Yang, Yuhua Qian, Jingyu Yang. On characterizing hierarchies of granulation structures via distances. *Fundamenta Informaticae*, 2013, 123: 365-380.
- [25] Xiaolu Zhang, Zeshui Xu. Extension of TOPSIS to multiple criteria decision making with pythagorean fuzzy sets. *International Journal of Intelligent Systems*, 2014, 29:1061-1078.
- [26] Guangming Lang, Duoqian Miao, H. Fujita. Three-way group conflict analysis based on pythagorean fuzzy set theory. *IEEE Transactions on Fuzzy Systems*, 2020, 28:447-461.
- [27] Anhui Tan, Suwei Shi, Weizhi Wu, Jinjin Li, W. Pedrycz. Granularity and entropy of intuitionistic fuzzy information and their applications. *IEEE Transactions on Cybernetics*, DOI: 10.1109/TCYB.2020.2973379
- [28] Decui Liang, Yinrunjie Zhang, Zeshui Xu, Adam Jamaldeen. Pythagorean fuzzy VIKOR approaches based on TODIM for evaluating internet banking website quality of Ghanaian banking industry. *Applied Soft Computing*, 2019, 78: 583-594.
- [29] Fuyuan Xiao, Weiping Ding. Divergence measure of pythagorean fuzzy sets and its application in medical diagnosis. *Applied Soft Computing*, 2019, 79:254-267.
- [30] Decui Liang, Zeshui Xu, Dun Liu, Yao Wu. Method for three-way decisions using ideal TOPSIS solutions at Pythagorean fuzzy information. *Information Sciences*, 2018, 435:282-295.
- [31] R. R. Yager. Pythagorean Membership Grades in Multicriteria Decision Making. *IEEE Transactions on Fuzzy Systems*, 2014, 22(4):958-965.
- [32] Qinghua Hu, Daren Yu, Zongxia Xie, Jinfu Liu. Fuzzy probabilistic approximation spaces and their information measures. *IEEE Transactions on Fuzzy Systems*, 2006, 14:191-201.
- [33] Jiye Liang, Zhongzhi Shi, D.Y. Li, M. J. Wierman. The information entropy, rough entropy and knowledge granulation in incomplete information system. *International Journal of General Systems*, 2006, 35:641-654.

Data-Driven Modeling of Mechanical Properties of Cast Iron Using Fuzzy Logic

He TAN^{a,1}, Vladimir TARASOV^a and Vasileios FOURLAKIDIS^b and
Attila DIOSZEGI^b

^a*Department of Computer Science and Informatics, School of Engineering, Jönköping University, Sweden*

^b*Department of Materials & Manufacturing, School of Engineering, Jönköping University, Sweden*

Abstract. For many industries, an understanding of the fatigue behavior of cast iron is important but this topic is still under extensive research in materials science. This paper offers fuzzy logic as a data-driven approach to address the challenge of predicting casting performance. However, data scarcity is an issue when applying a data-driven approach in this field; the presented study tackled this problem. Four fuzzy logic systems were constructed and compared in the study, two based solely upon experimental data and the others combining the same experimental data with data drawn from relevant literature. The study showed that the latter demonstrated a higher accuracy for the prediction of the ultimate tensile strength for cast iron.

Keywords. Fuzzy logic system, Data scarcity, Fatigue related properties prediction, Cast iron components

1. Introduction

Casting is essential to many industries. The ability to predict the performance of a cast component helps to produce near-net shape cast components and provides greater freedom for manufacturing design. There are two categories of approach to casting performance prediction: model-based and data-driven. The model-based approach attempts to develop mechanism models to explain observed phenomena, e.g. the Griffith and Hall-Petch equations, and their adopted versions. However, the mechanical properties of a cast component can be affected by many parameters. Melt treatment and the casting process both display stochastic behavior. The assumptions and simplifications of the mechanism models limit the performance of this approach.

Data-driven techniques utilize experimental data for prediction. Such techniques have been proposed to deal with uncertainty and imprecision when predicting the mechanical properties of cast components or when relating the mechanical properties to the parameters of the casting process, and include: regression methods, machine learning methods, neural networks, and fuzzy logic. In our previous work [1] two fuzzy logic systems (FLS) were built to predict yield strength (YS) for two Al-Si-Mg alloys. The re-

¹Corresponding Author: He Tan, E-mail: he.tan@ju.se.

sults showed high accuracy of prediction. When compared with several machine learning methods, the prediction accuracies of the two constructed FLS were at the same level as or slightly better than the machine learning methods. The advantage of the FLS approach over machine learning methods is that the former provides a highly interpretable model. This is important for industrial applications. The interpretability of fuzzy logic method was appreciated by the industry partners in the research project where the work in [1] where the work on Al-Si-Mg alloy yield strength was conducted.

The current work investigated the use of fuzzy logic to address the problem of predicting the ultimate tensile strength (UTS) of a particular form of cast iron morphology – Lamellar Graphite Iron (LGI). LGI is the most used casting material nowadays and is especially important in the automotive industry. For example, cylinder heads and cylinder blocks for diesel truck engines are mostly manufactured with LGI. The UTS is one of the main factors that affect the performance and fuel consumption of these engines.

One challenge posed by the application of data-driven approach in material science is data scarcity. This is caused by an unusually high data acquisition cost in the field compared to other domains where any data-driven approach has proven useful. The current work examined using data published in literature to deal with this challenge. The data from literature together with the current experimental data provided a larger set of training data to construct FLS. The results showed that the constructed FLS provided a high accuracy of prediction, which was not be achieved by the FLS constructed only from the experimental data.

The paper is structured as follows. Related work is given in Section 2. Section 3 presents the data collected from experimental work and the data derived from literature. The method to design and build FLS and the evaluation results are presented in Section 4. The conclusions are drawn in Section 5.

2. Related Work

Although the attempts to apply fuzzy logic in the casting industry are found to be limited, studies have shown that fuzzy logic models of mechanical properties of die casts and metallic materials can achieve desired performance. In [2] fuzzy logic was applied to estimate surface roughness of die casting alloys. A FLS was constructed to map the presence of additives and machining parameters to surface roughness. The percentage error of the FLS is 5.4%. The authors of [3] showed that fuzzy expert system was efficient to optimize the parameters in the milling process and predict the performance measures. The fuzzy logic model built in [4] predicted surface hardness of aluminium alloy with TiN (titanium nitride). The percentage error and accuracy of the model are 6.09 and 96.142%, respectively. In our previous work [1], two FLS were constructed to predict YS for Al-Si-Mg alloys. The prediction errors of the models are 3.53% for the first and 3.19% for the second alloy. In the presented work we applied fuzzy logic to predict the UTS for LGI. The purpose is to evaluate the applicability of fuzzy logic as a data-driven approach to address the problem of understanding fatigue behavior of cast iron. The latter is a challenge in the field of materials science.

Data-driven approach is a new paradigm in materials science. It is extremely expensive to generate data in the field. The community also lacks a unified approach to reusing and sharing materials data [5]. To the best of the authors' knowledge, none of the previ-

ously published works utilizes published data sets for modeling of mechanical properties of cast components. The current paper presented a study to utilize data set published in literature together with experimental data during construction of fuzzy logic models to address the data scarcity.

3. Data Collection

This section presents the data sets that were used to design, built and evaluate the FLS in Sect. 4. The first data set was generated from the experimental work. The second data set is a combination of the experimental data and the data found in the published literature.

3.1. Experimental Data

This section describes the experimental work and the data collected during the experiment. For more details the reader is referred to [6]. Four hypoeutectic lamellar graphite iron heats with varying chemical composition were produced. The four samples were labeled individually with C13-4, C13-B, C13-C and C13-D. The carbon content of the samples is 3.62, 3.34, 3.05 and 2.8, respectively. The experimental mould contained three cylindrical cavities. Each was surrounded by a different material, i.e. steel, sand or isolation, to provide the different cooling rates of 3.5°C/s (high), 0.8 °C/s (medium) and 0.2 °C/s (low), respectively.

The microstructure was examined using an optical microscope. Secondary dendrite arm spacing (SDAS) was measured by a linear intercept method. The eutectic cell (EC) size was calculated as the average diameter of the 5–10 biggest eutectic cells. The obtained microstructure is fully pearlitic (>95% pearlite) for all the cooling conditions.

Uniaxial tensile testing was performed on one sample machined from each cylindrical casting. The tests were conducted on a Lloyd EZ50 testing machine, at a strain rate of 0.035 mm/s and at room temperature. Tensile strength was measured using dog-bone shaped bars according to VOLVO standard 5C25.

Table 1 presents the data collected during the experiment. In total 12 data points were generated from the experiment. The value of ECEL was not collected during the experiment for the sample C13-D when cooling rate is high.

3.2. Literature data

A number of papers are published concerning the prediction of UTS and they contain relevant experimental data (e.g. [6,7,8]). The investigation data from [7] together with the current experiment data were employed in this work (see Table 2). The experimental procedure from [7] involves the production of 11 fully LGI with varying N content and inoculation addition aimed to provide material with difference in microstructure and mechanical properties. Contrary to the current experiment, the work in [7] utilized similar carbon content but constant cooling rates for all the castings.

4. Fuzzy Modeling of Ultimate Tensile Strength

In the presented work, the FLS were constructed as multiple-input-single-output mamdani-type models. Each FLS has two inputs. The inputs are considered to be the

Table 1. Data collected during the experimental work.

Sample	Cooling rate	σ_{UTS} [MPa]	ECEL [μm]	SDAS [μm]
C13-A	High	363	423	25.0
	Medium	195	1153	55.9
	low	154	1977	92.2
C13-B	High	368	330	25.0
	Medium	254	1072	63.9
	low	211	1583	87.0
C13-C	High	440	263	30.0
	Medium	286	965	56.4
	low	250	1454	95.0
C13-D	High	447	-	29.0
	Medium	337	899	63.2
	low	289	1380	101.0

Table 2. The combination of the data collected from [7] (see the first 11 rows) and the experimental data when the cooling rate is 0.2°C/s , i.e. Low (see the last 4 rows)

Sample	Carbon content	σ_{UTS} [MPa]	ECEL [μm]	SDAS [μm]
W1	3.36	335	185	30
W2	3.41	288	332	28
W3	3.36	318	193	28
W4	3.41	323	181	27
W5	3.42	323	285	26
W6	3.36	345	224	26
W7	3.4	358	176	28
W8	3.28	347	307	28
W9	3.3	373	165	30
W10	3.3	393	140	27
W11	3.36	357	179	27
C13-A	3.62	154	1977	92.2
C13-B	3.34	211	1583	87.0
C13-C	3.05	250	1454	95.0
C13-D	2.8	289	1380	101.0

most important input variables to predict the output by the experts in the field of materials science. The input variables also have high correlation coefficient with the output. The first input is "Carbon content" that represents the percentage of C in the iron cast alloy. The second input concerns microstructure. It is either "SDAS", representing microstructure coarseness, or "ECEL", representing the eutectic cell size. The output is the resulting ultimate tensile strength, i.e. "UTS". The systems were implemented using Scikit-Fuzzy².

²<https://pythonhosted.org/scikit-fuzzy/>

As described in Sect. 3, two data sets were collected. Each data set was divided into a training data set and a test data set. The training data sets were used to build the FLS, i.e. to define the parameters for membership functions (Sect. 4.1) and to learn fuzzy inference rules (Sect. 4.2). The first data set has 12 data points. 8 data points constituted the training data. The rest were used for test (4 data points when the second input is SDAS, or 3 data points when the second input is ECEL). The second data set contains 15 data points. 11 data points constitutes the training data set, the rest were used for test.

4.1. Linguistic variables and membership functions

The membership functions for both input and output variables are Gaussian functions, because Gaussian function was considered to be the most adequate by the experts in materials science. For each membership function the standard deviation σ and mean c were determined by manual examination of the training data sets.

The examination were carried out as follows: 1) compiling the values of an input/output into a list, sorting it and determining the range of the variable; 2) partitioning the values in the list into segments to determine the number of memberships functions (linguistic labels) for an input/output variable and the σ and c for each membership function. The size of each partition was chosen to encompass several values. Finally, *max* was used for the aggregation and *centroid* was the defuzzification method.

4.2. Fuzzy inference rules

A set of two-input one-output inference rules were produced for each fuzzy logic system. The rules were first determined to be "and" rules (i.e., logical conjunction) by a knowledge engineer. Then the rules were learned from the training data using the method adapted from [9]. The method consists of three steps:

1) Generate a rule for each input-output data pair $(x_1, x_2; y)$ in training data:

IF x_1^i is A and x_2^i is B , THEN y^i is C , where x_1 and x_2 are the two inputs, y is the output, $\mu_A(x_1^i)$, $\mu_B(x_2^i)$, and $\mu_C(y^i)$ are membership functions with the maximum membership degree for each respective value.

2) Calculate a degree for each rule: $D(\text{rule}^i) = \mu_A(x_1^i) \times \mu_B(x_2^i) \times \mu_C(y^i)$

3) Generate the final list of rules. If there is more than one rule with the same antecedent, the rule that has the maximum degree is selected for the final list.

This is a general and straightforward method for learning rules from data. The method was implemented in Python. The performance of the method was evaluated in [10] which showed that the rules generated using the presented method were identical to the rules manually created by a knowledge engineer.

4.3. Evaluation Results

The prediction accuracy of the constructed FLS was measured using Mean Absolute Percentage Error (MAPE) [11] (see Fig. 1). The percentage prediction errors are also depicted in Fig. 1. The results show that the prediction accuracy of the two fuzzy logic systems for the second data set is satisfactory and also at the same level as reported in the related work described in Sect 2. The prediction accuracise of the two FLS are very similar, despite different sets of input variables were used.

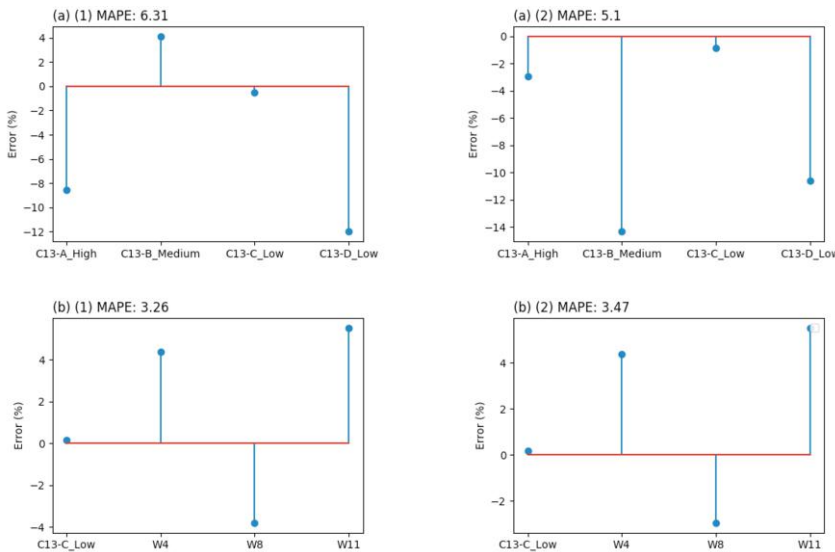


Figure 1. Percentage prediction errors plotted as stems for the UTS value in each data point: (a) present the results for the first data set and (b) are the result for the second data set. (1) show the results when the input variables are "Carbon content" and "ECEL"; (2) give the results when the input variables are "Carbon content" and "SDAS".

The two FLS for the second data set showed better MAPE than the systems for the first data set. The accuracy of the prediction of the UTS of the alloy samples with the low cooling rate is much better and stable for the FLS for the second data set than for the FLS for the first data set. The prediction accuracy of the two FLS for the first data set is not satisfactory. Moreover, the two FLS performed very differently when the different input variables were applied.

5. Conclusion

The presented work contributes a data-driven approach using fuzzy logic to address the lack of understanding of the fatigue behavior of cast irons. In addition, the study investigated the utilization of data published in literature to address data scarcity in the field of materials science when applying a data-driven approach. The study showed that the data derived from the related literature together with experimental data provided a larger set of data to support the construction of a FLS. This FLS constructed using combined data presented a high accuracy of prediction. Compared to the FLS constructed only from the experimental data, the former FLS performed better and was more stable.

For future work, we are considering three lines of activity. Firstly, we would like to apply fractional fuzzy inference systems [12] to the UTS problem addressed in this paper. We expect an FLS of this new type to deliver even better predictive performance. We will also broaden our FLS approach to investigate the mapping of other fatigue-related properties to chemical composition and the various microstructure properties of cast components. Finally, to address the data scarcity in this field, we are considering the establishment of an online infrastructure to collect, host and provide such materials data in support of further research and production-focused investigations.

References

- [1] Vladimir Tarasov, He Tan, Anders EW Jarfors, and Salem Seifeddine. Fuzzy logic-based modelling of yield strength of as-cast A356 alloy. *Neural Computing and Applications*, pages 1–12, 2019.
- [2] Mohsen Marani Barzani, Erfan Zalnezhad, Ahmed A.D. Sarhan, Saeed Farahany, and Singh Ramesh. Fuzzy logic based model for predicting surface roughness of machined Al-Si-Cu-Fe die casting alloy using different additives-turning. *Measurement*, 61(Supplement C):150–161, 2015.
- [3] Asif Iqbal, Ning He, Liang Li, and Naeem Ullah Dar. A fuzzy expert system for optimizing parameters and predicting performance measures in hard-milling process. *Expert Systems with Applications*, 32(4):1020–1027, 2007.
- [4] E. Zalnezhad, Ahmed A. D. Sarhan, and M. Hamdi. A fuzzy logic based model to predict surface hardness of thin film TiN coating on aerospace AL7075-T6 alloy. *The International Journal of Advanced Manufacturing Technology*, 68(1):415–423, Sep 2013.
- [5] Lauri Himanen, Amber Geurts, Adam Stuart Foster, and Patrick Rinke. Data-driven materials science: Status, challenges, and perspectives. *Advanced Science*, 6(21):1900808, 2019.
- [6] Vasilios Fourlakidis and Attila Diószegi. A generic model to predict the ultimate tensile strength in pearlitic lamellar graphite iron. *Materials Science and Engineering: A*, 618:161–167, 2014.
- [7] Fredrik Wilberfors and Ingvar L Svensson. The effect of nitrogen and inoculation on the tensile properties and microstructure of cast iron with lamellar graphite. In *Key Engineering Materials*, volume 457, pages 114–119. Trans Tech Publ, 2011.
- [8] Torsten Sjögren and Henrik Svensson. Study of the eutectoid transformation in grey cast irons and its effect on mechanical properties. In *Key Engineering Materials*, volume 457, pages 157–162. Trans Tech Publ, 2011.
- [9] L-X Wang and Jerry M Mendel. Generating fuzzy rules by learning from examples. *IEEE Transactions on systems, man, and cybernetics*, 22(6):1414–1427, 1992.
- [10] He Tan, Vladimir Tarasov, Anders EW Jarfors, and Salem Seifeddine. Fuzzy logic based modelling of cast component properties. *IFAC-PapersOnLine*, 52(13):1132–1137, 2019.
- [11] Arnaud de Myttenaere, Boris Golden, Béatrice Le Grand, and Fabrice Rossi. Mean absolute percentage error for regression models. *Neurocomputing*, 192:38–48, 2016. Advances in artificial neural networks, machine learning and computational intelligence.
- [12] M. Mazandarani and X. Li. Fractional fuzzy inference system: The new generation of fuzzy inference systems. *IEEE Access*, 8:126066–126082, 2020.

Reward-Free Reinforcement Learning Algorithm Using Prediction Network

Zhen Yu^{a,b,1}, Yimin Feng^a and Lijun Liu^{a,b}

^aSchool of Aerospace Engineering, Xiamen University, Xiamen 361005, China

^bShenzhen Research Institute of Xiamen University, Shenzhen 518000, China

Abstract. In general reinforcement learning tasks, the formulation of reward functions is a very important step in reinforcement learning. The reward function is not easy to formulate in a large number of systems. The network training effect is sensitive to the reward function, and different reward value functions will get different results. For a class of systems that meet specific conditions, the traditional reinforcement learning method is improved. A state quantity function is designed to replace the reward function, which is more efficient than the traditional reward function. At the same time, the predictive network link is designed so that the network can learn the value of the general state by using the special state. The overall structure of the network will be improved based on the Deep Deterministic Policy Gradient (DDPG) algorithm. Finally, the algorithm was successfully applied in the environment of FrozenLake, and achieved good performance. The experiment proves the effectiveness of the algorithm and realizes rewardless reinforcement learning in a class of systems.

Keywords. Reinforcement learning, no reward value, prediction network, RFPG

1. Introduction

Reinforcement learning is an important machine learning method that has many applications in the fields of intelligent control, robotics, analysis, and prediction [1]. Such as using fuzzy reinforcement learning approach for efficient and reliable solution to the unit commitment problem [2], using fuzzy reinforcement learning propose an efficient solution to the Economic thermal power dispatch [3], using fuzzy reinforcement learning to increase efficiency of the traffic light control system [4]. Reinforcement learning overlaps with many disciplines. Compared with traditional machine learning, it has the following advantages: Firstly, because it does not require a sample labeling process, it can solve special control problems more effectively; Secondly, the entire system as a whole can enhance its robustness; thirdly, reinforcement learning can relatively easily learn some tasks that cannot be completed by traditional control methods [5]. Therefore, as a new type of control method, reinforcement learning can play its unique role in many fields.

Deep reinforcement learning [6] (DRL) is a kind of reinforcement learning using deep learning [7] methods, such as DQN algorithm. However, DQN has certain limitations which can only deal with discrete problems [8], and most of the systems that

¹ Corresponding Author: LiJun Liu, Room 485, Aerospace Building, Xiang'an Campus of Xiamen University, Xiamen, Fujian, China; E-mail: liulijun@xmu.edu.cn.

need to be controlled are high-dimensional continuous and must output continuous control quantities. The discretization of continuous quantities will cause the problem of dimensional explosion [9]. In response to this situation, the DeepMind team proposed the deep deterministic strategy gradient algorithm DDPG in 2015 [10-11]. Traditional reinforcement learning algorithms have a common drawback, which relies too much on artificially designing reward functions. For the agent in an unknown environment, the reward function can provide a goal and an improvement direction for the reinforcement learning algorithm [12]. If the system has too many state variables, the reward value function will be very complicated [13]. The artificially designed reward value function may deviate from human intuition value, resulting in the inconsistent direction of Agent learning and people's cognition [14-15]. This drawback limits the application scenarios of reinforcement learning. Inverse reinforcement learning [16] is an exploration of the reinforcement learning algorithm with no reward value function, which uses human expert data to reverse the reward value function. However, the workload of expert data collection is large, which is not suitable for a wide range of applications.

Based on the above situation, this paper proposes an algorithm model without reward function. Design a new evaluation function by defining the characteristics of a class of controlled systems. In a system that satisfies these characteristics, an algorithm without reward value function is proposed. This method can avoid the design of reward value function and reduce the design workload. In order to evaluate the effectiveness of the algorithm, Gym [17] is used to build a simulation environment. Use Tensorflow [18] to build an algorithm environment. This paper defines the concept of state quantity, and designs the Reward Free Policy Gradient (Reward Free Policy Gradient) RFPG algorithm using predictive network learning state transition relations. The algorithm performed well in various experiments and proved its effectiveness.

2. Reinforcement learning model

The basic structure of reinforcement learning includes the controlled object Agent, environment, state, reward, and action [19]. The purpose of reinforcement learning is to learn certain strategies so that Agent can reach the target state. The tasks of reinforcement learning are usually described by Markov processes [20]. We abstractly represent the trajectory of a Markov process as $(s_1, a_1, r_1, s_2, a_2, r_2)$. The reward at s_t is $r_t = R(s)$, $R(s)$ is the reward function. The expression is as equation (1):

$$r_t = R(s_t) = \sum_{i=0}^n b_i \|x_{ti} - x_{gi}\|_m \quad (1)$$

Where $s_t = (x_{t1}, x_{t2}, \dots, x_{tn})$ is the current state, $s_g = (x_{g1}, x_{g2}, \dots, x_{gn})$ is the target state, b_i is the empirical parameter, and m is a certain norm. The reward function is very critical in reinforcement learning. The cumulative reward value V_t is expressed as:

$$V_t = r_{t+1} + \gamma r_{t+2} + \gamma^2 r_{t+3} + \dots = \sum_{k=0}^{\infty} \gamma^k r_{t+k+1} \quad (2)$$

Where γ is the reward discount value, Agent and the goal of adopting strategies are to maximize the cumulative reward value V_t . From this, the value-based method represented by Q-learning [21] and the strategy-based method represented by strategy gradient were born. The DDPG algorithm combines the advantages of the two.

DDPG is mainly composed of strategy network, action network and experience pool. The strategy network is responsible for outputting actions, and the evaluation network is responsible for estimating value. And the two groups of networks have an online network and a target network, respectively, and these four networks are denoted as Actor-online, Actor-target, Critic-online, Critic-target. The experience pool is a data structure that can store basic units. The four networks interact to update the parameters. The DDPG algorithm also relies on the reward function design.

3. RFPG Algorithm

3.1. First-class application scenarios

In reinforcement learning algorithms such as DQN and DDPG, we use the reward value provided by the environment as the basis for the correction of the evaluation network and the optimization goal of the strategy network. Researches have found that certain reinforcement learning scenarios do not require specific reward value functions. Summarizing such conditions into the following two, this paper is dedicated to solving the control problems of this type of system: (1) The purpose of Agent is to achieve a certain target state. (2) Agent has a probability to reach the target state when outputting random actions. The set of target states is recorded as I . The state that is not allowed to exist is called the failure state, and the failure state is recorded as E . The environments that meet the above conditions include FrozenLake, etc.

3.2. RFPG algorithm design

This paper designs a reinforcement learning algorithm with no reward value called RFPG (Reward Free Policy Gradient) algorithm. The RFPG algorithm includes three networks: prediction network P, action network A, and value network G. Value network: divided into online value network G-online and target value network G-target, where the role of online value network is to fit the value of each state; the role of target value network is to provide value targets for online action network. Action network: divided into online action network A-online and target action network A-target, where the role of online action network is to output action values during the training phase; the role of target action network is to provide action output for the prediction network. Prediction network: The prediction network represents the Agent's understanding of the external environment, and its role is to predict the next state obtained by the action under the action.

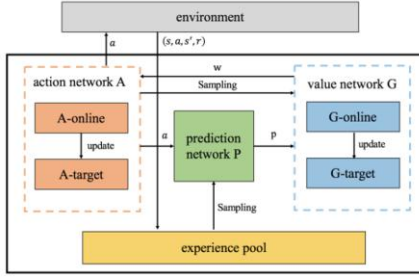


Figure 1. RFPG basic structure

A basic experience unit in DDPG is (s, a, s', r) , where r is the reward value among them. This reward value is usually a customized function of human expert experience. The RFPG algorithm replaces the reward value r with a simpler state quantity w . The definition of w is shown in equation (3), which is simpler than equation (1).

$$w_s = W(s) = \begin{cases} 1 & s \in I \\ 0 & s \notin I \cup E \\ -1 & s \in E \end{cases} \quad (3)$$

In the definition of observation w , the state quantity function $W(s)$ is different from the value function $R(s)$, which only defines the target state I and the failure state E . The ideal value of other general conditions w is 0, and its value is learned by the G network, not provided by the environment. The basic experience unit of the RFPG experience pool is (s, a, s', r) . This process avoids the design of traditional reward functions. State quantity w is simpler, intuitive and easier to use than traditional reward functions, reducing design workload. The relationship between the various networks is shown in Figure 2.

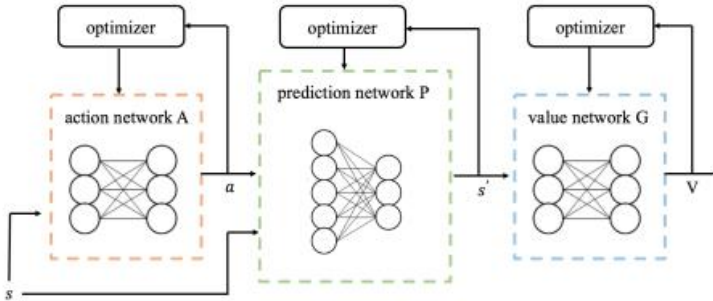


Figure 2. RFPG network relationships

Each network parameter is indicated by θ , θ_G is a G network parameter, θ_u is an A network parameter, and θ_p is a G network parameter.

The purpose of the A -online output action is to maximize value, so the action network loss function is equation (4). A -target obtains parameter values from A -online in soft update mode.

$$(4) \quad loss_a = J(\theta_\mu) = -\frac{1}{m} \sum_{j=1}^m G(p_i | \theta_\mu)$$

The value network G is the learning of the value function. The value of the G network is obtained through learning. The objective function of fitting is equation (5).

$$(5) \quad V_t = \begin{cases} 1 & s_t \in I \\ \gamma V_{t+1} & s_t \notin I \cup E \\ -1 & s_t \in E \end{cases}$$

Where γ is the attenuation coefficient, which is generally around 0.9. The loss function of G -online is shown in equation (6), which p_i is the output of the prediction network. G -target obtains parameter values from G -online in soft update mode.

$$(6) \quad loss_g = J(\theta_G) = \frac{1}{m} \sum_{j=1}^m (w_i - \gamma G(p_i, \theta_G))^2$$

The function of the prediction function is based on s, a to predict the next state s' . The samples s' in the sample can be regarded as labels to do training to minimize the mean square error. The loss function corresponds to equation (7).

$$(7) \quad loss_p = J(\theta_P) = \frac{1}{m} \sum_{j=1}^m (s_{i+1} - P(s_i, a_i))^2$$

In practical applications, the network infrastructure of each part is a typical double-layer neural network. The network hyperparameters can be adjusted according to the application scenario. The algorithm steps are shown in Algorithm 1 and the flowchart of RFPG are shown in Figure 3.

Table 1. RFPG algorithm flow

Algorithm 1 RFPG algorithm flow

1. Initialize action network A, predict network P, evaluate network G, and assign random weights $\theta_u, \theta_p, \theta_G$
2. Initialize the target network $\theta_{G'} \leftarrow \theta_G, \theta_{\mu'} \leftarrow \theta_\mu$, initialize the experience pool R.
3. **for** $j = 1$ to M **do**
4. Randomly initialize the environment to get the initial state S
5. **for** $t = 1$ to T **do**
6. Use the ϵ -greedy strategy to output action a
7. Agent performs action a and obtains sample (s, a, s', r) and deposit into experience pool
8. Take n samples (s_i, a_i, s'_i, r_i) from the experience pool, forecasting p_i with prediction network
9. Update the value network with minimized variance G :

$$Lg = \frac{1}{n} \sum (w_i - \gamma G(p_i, \theta_g))^2$$

10. Update the action network with a strategy gradient A.

$$La = -\frac{1}{n} \sum G(p_i, \theta_\mu)$$

-
11. Train prediction network using state transition P

$$Lp = \frac{1}{n} \sum (S_{i+1} - P(S_i - a_i))^2$$
 12. Use soft update to update the target network :

$$\theta_G' \leftarrow \tau \theta_G + (1 - \tau) \theta_G'$$

$$\theta_\mu' \leftarrow \tau \theta_\mu + (1 - \tau) \theta_\mu'$$
 13. **end for**
 - 14.**end for**
-

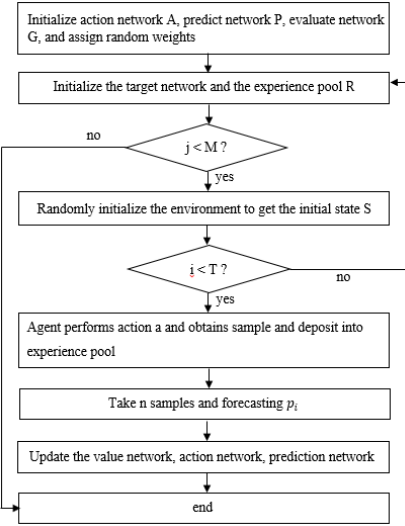


Figure 3 flowchart of RFPG

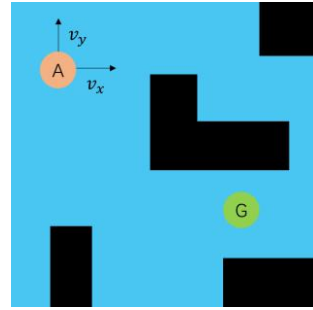


Figure 4 FrozenLake environment

Compared with a series of traditional reinforcement learning methods such as DDPG, the RFPG algorithm has the following improvements: (1) The design of the reward value function is eliminated, and the workload is reduced. (2) Avoid situations where the network is sensitive to reward value functions. (3) Reduced dependence on the experience pool.

4. Simulation study

The purpose of this chapter is to verify the effectiveness of the algorithm and compare the performance of the DDPG algorithm. The main indicator is the average return value. From the previous analysis, it can be seen that the larger the average return value, the better the control performance. The following content analyzes the experimental results of FrozenLake and CartPole in detail. All networks in the experiment are fully connected neural networks.

4.1 Environmental introduction

As shown in Figure 4, the environment is a continued state version of FrozenLake in Gym. The environment is a square ice surface with side length n , Agent glides on the ice surface. The starting point of the agent is marked A, and the target point is marked G.

Dangerous areas exist on the ice, which are represented as black areas in the figure. Entering the black area indicates that the operation failed. Agent has position x, y on the horizontal and vertical coordinates, so the state value dimension is 2. The action output is speed v_x, v_y , and the action value dimension is 2. There is random interference in the environment, and there is a 10% chance that the action performed by the Agent cannot be executed smoothly, and the direction command is a random

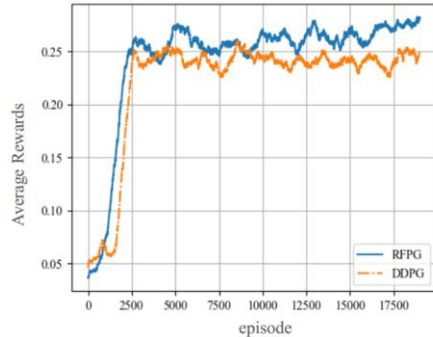


Figure 5 Frozen Lake training process

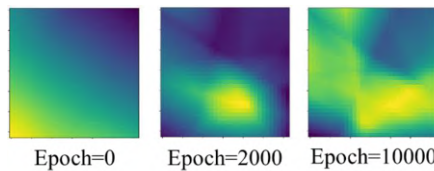


Figure 6 Value network learning results

4.2 Experimental analysis

The experiment first needs to define the state quantity w . The target state is the G position, which w is 1 at this time; the failure state is the black area, which w is -1 at this time, and the subtraction factor γ is 0.9.

Figure 5 shows the trend of average returns in the Frozen Lake environment. The performance of the RFPG algorithm in the Frozen Lake environment is superior to the DDPG algorithm. It shows that the RFPG algorithm can still perform quite well without return value

For the environment in Figure 4, the learning results of the value network are shown in Figure 6. The colors in the figure represent the value learned. The brighter the color, the higher the value. It can be seen that the value area is basically consistent with the environmental characteristics. Explain that the value network has learned the characteristics of the environment.

5. Conclusion

Aiming at a class of reinforcement learning problems defined in Chapter 3, this paper designs a reinforcement learning algorithm RFPG with no reward value. This method uses state quantities to provide learning directions for the network. The state quantity can distinguish the target state, failure state and general state of the agent. Experiments in various environments, the experimental results show that in an environment that meets certain conditions, the reinforcement learning method without reward value can still achieve control of the system. In the future, the application scenarios can be further expanded in the research. The RFPG algorithm is not only used for solving fixed target problems, but also for solving optimal state problems.

Acknowledgement

This work was supported by the National Natural Science Foundation of China under Grant 61304110, the Guangdong Natural Science Foundation under Grant 2018A030313124, the Natural Science Foundation of Shanghai under Grant 18ZR1443200, the Basic Research Program of Science and Technology of Shenzhen JCYJ20190809163009630, and the Open Foundation of Key Laboratory of Marine Navigation and Control Technology under Grant 202005.

References

- [1] Rubo Zhang, et al. Reinforcement learning theory, Algorithm and application[J]. Theory and Applications. 2000, 17(5):637-642.
- [2] Navin N K , Sharma R . A fuzzy reinforcement learning approach to thermal unit commitment problem[J]. Neural Computing and Applications, 2017.
- [3] Nandan Kumar Navin, Rajneesh Sharma, H. Malik. Solving nonconvex economic thermal power dispatch problem with multiple fuel system and valve point loading effect using fuzzy reinforcement learning. 2018, 35(5):4921-4931.
- [4] Kumar N , Rahman S S , Dhakad N . Fuzzy Inference Enabled Deep Reinforcement Learning-Based Traffic Light Control for Intelligent Transportation System[J]. IEEE Transactions on Intelligent Transportation Systems, 2020, PP(99):1-10.
- [5] Guoyan Xu, Xiaopeng Zhong, Guizhen Yu, et al. Research on intelligent Obstacle Avoidance Method of Unmanned Vehicle based on DDPG[J]. Automotive Engineering. 2019, 41(02):90-96.
- [6] Mnih V, Kavukcuoglu K, Silver D, et al. Playing atari with deep reinforcement learning[J]. arXiv preprint arXiv:1312.5602, 2013.
- [7] Yujian Li. Introduction to Deep Learning and Case Study [M]. China Machinery Industry Press, 2016.
- [8] Šemrov D, Marsetić R, Žura M, et al. Reinforcement learn-ing approach for train rescheduling on a single-track rail-way[J]. Transportation Research Part B: Methodological, 2016, 86: 250-267.
- [9] Heess N, Wayne G, Silver D, et al. Learning continuous control policies by stochastic value gradients[C]// Advances in Neural Information Processing Systems. 2015: 2944-2952.
- [10] Lillicrap T P, Hunt J J, Pritzel A, et al. Continuous control with deep reinforcement learning[J]. arXiv preprint arXiv:1509.02971, 2015.
- [11] Lin L J. Reinforcement learning for robots using neural networks[R]. Carnegie-Mellon Univ Pittsburgh PA School of Computer Science, 1993.
- [12] Sutton R S, Barto A G. Reinforcement learning: An intro-duction[M]. MIT press, 2018.
- [13] Christiano P F, Leike J, Brown T, et al. Deep reinforcement learning from human preferences[C]//Advances in Neural Information Processing Systems. 2017: 4299-4307.
- [14] Bostrom N . Superintelligence[J]. Computer Science, 2016.
- [15] Amodei D, Olah C, Steinhardt J, et al. Concrete problems in AI safety[J]. arXiv preprint arXiv:1606.06565, 2016.
- [16] Ng A Y, Russell S J. Algorithms for inverse reinforcement learning[C]//Icml. 2000, 1: 2.
- [17] Brockman G, Cheung V, Pettersson L, et al. Openai gym[J]. arXiv preprint arXiv:1606.01540, 2016.
- [18] Abadi M, Agarwal A, Barham P, et al. Tensorflow: Large-scale machine learning on heterogeneous distributed systems[J]. arXiv preprint arXiv:1603.04467, 2016.
- [19] Quan Liu, Jianwei Zhai, Zongchang Zong, et al. Review of Deep Reinforcement learning [J].Journal of Computer Science, 2018, 41(1): 1-27.
- [20] Yin Luo, Wenhui Qin, Jinfeng Zhai. Research on Vehicle Low-speed tracking Behavior Decision Based on improved DDPG Algorithm [J].Measurement and Control Technology, 2019 (9): 4.
- [21] Watkins C J C H. Learning from delayed rewards[J]. 1989.

Differential Privacy Trajectory Data Protection Algorithm Based on Polar Coordinate Transformation

Zhenzhen ZHANG, Jianping CAI, Lan SUN, Yongyi GUO, Yubing QIU, Yingjie WU¹

College of Mathematics and Computer Science, Fuzhou University, Fuzhou 350108, China

Abstract. Differential privacy technology has been widely used in the issue of trajectory data release. Improving the availability of data release under the premise of ensuring privacy and security is one of its basic research goals. At present, most trajectory data release methods use a rectangular coordinate system to represent location information. Research has shown that the availability of published data cannot be optimized through the rectangular coordinate system. In order to improve the effect of trajectory data release, this paper proposes a differential privacy trajectory data protection algorithm based on polar coordinates. First, the stay point detection method is used to find frequent stay points in the trajectory and the key location points related to personal privacy are detected by the type of location points. Then, this paper converts the rectangular coordinate system representation of the key position points to the polar coordinate system representation, and implement differential privacy trajectory data release by adding noise to the key position points represented by the polar coordinates. Experiments show that the algorithm proposed in this paper effectively improves the usability of trajectory data on real data sets.

Keywords. Trajectory data protection, Differential privacy, Polar coordinates, Position type

1. Introduction

In recent years, with the development of smartphones and the popularization of location-based services (LBS), the location information continuously uploaded by mobile objects has formed trajectory big data. The release of trajectory data enables people to analyze and mine it, and provide strong support for government departments in urban planning and commercial organizations in decision-making. However, if these trajectory data is directly released without protection, malicious attack reasoning will pose a serious threat to individual privacy. For example, Strava [1], a popular movement in Europe and the United States in 2017, released a "heat map" of user activities in the world, and netizens unearthed the location of military bases, training time, home addresses and real identities of individual users. Therefore, protecting the privacy of user identity while taking into account the high availability of data and

¹ Corresponding Author: Yingjie WU, College of Mathematics and Computer Science, Fuzhou University, Fuzhou 350108, China; E-mail: yjwu@fzu.edu.cn.

achieving the secure release of trajectory data has become the core content of current trajectory data release research.

Nowadays, more and more people pay attention to privacy data protection, and some researchers [2-3] have conducted in-depth studies on privacy date protection in many fields. To realize an effective personal privacy protection scheme in the process of data release, in 2006 Dwork [4] and others proposed a differential privacy protection model, which is currently recognized as a model for strict privacy protection, mainly through the original data, original data add appropriate noise to the conversion or statistical results to achieve privacy protection. Compared with other trajectory protection methods such as suppression [5], it theoretically guarantees that no matter what background knowledge the attacker has, any record in the original database cannot be identified [6].

Differential privacy protection was originally applied in the field of statistical database security, aiming to protect the private information of individuals in the database when statistical information is released. In 2012, Chen et al. [7] proposed the use of differential privacy to protect trajectory data. By adding Laplace noise to the location data to ensure that the mining results meet the differential privacy requirements, the trajectory privacy protection of transportation information can be realized. The differential privacy mechanism has since been used for trajectory privacy protection. Subsequently, many researchers researched this field and achieved a series of results. The PriLocation [8] algorithm consists of three operations: location clustering, weight interference, and location selection. Since the number of clusters is much smaller than the number of locations, the number of times of adding noise is drastically reduced, thereby reducing the amount of noise. Literature [9] believes that the generated random and unbounded noise cannot completely realize differential privacy, so it proposes a bounded noise generation algorithm and a trajectory merging algorithm, which effectively improves the efficiency of privacy protection. Literature [10] proposed a method of dividing the trajectory into shorter new trajectories, which is suitable for processing longer trajectory data. Literature [11] divides the entire plane location area into several hexagons, and at the same time geographic indistinguishability technology is used to reduce the loss of privacy budget by publishing the location of the centroid of each hexagon.

When protecting the trajectory data set, the existing trajectory data protection algorithms directly add noise to the longitude and latitude of the position indicated in the rectangular coordinate system. And most of them are only based on the distance measurement to identify the location, which is difficult to distinguish a certain location belongs to what type of building. Though personal privacy is protected, the availability of data is low [12]. At the same time, during the privacy protection of trajectory data, if all trajectory data sets are directly disturbed to protect personal privacy, serious loss of data information will become unusable. Therefore, finding key location points in the trajectory data set that will leak personal privacy is a major problem at present. And Literature [13] proposed a method to protect important location points of the trajectory based on the k-anonymity model. It innovatively models and process semantic trajectories which greatly improve data availability. But the k-anonymity model cannot provide an effective and strict method to prove its level of privacy protection. In order to solve the above problems, Baidu Map Application Programming Interface (API) technology is utilized to mine the Point of Information (POI) of frequently staying points to obtain the types of location points, thereby determining the key location points for protection and subsequent experiments prove that the rectangular coordinate

representation of longitude and latitude is converted into extremes. Coordinate representation and differential privacy protection can greatly improve the availability of trajectory data.

In summary, this paper has made the following innovations.

- In order to provide stronger support for government departments in urban planning and decision-making by commercial institutions, Baidu Map API technology is utilized to get the POI of the location point to obtain the location type. Then according to whether the location type leak privacy, the location points are divided into key location points and non-critical locations, and key location points which are easy to reveal personal privacy are protected. Make the protected data more realistic.
- This paper innovatively proposes that converting the rectangular coordinate representation of the private location point into polar coordinate representation. Then the differential privacy protection mechanism is used to protect the polar coordinate of the sensitive location point. Experiments on the real data set prove that the data conversion can greatly improve the availability of data.

2. Basic Knowledge and Definitions

The differential privacy protection model is currently recognized as a model that provides strict privacy protection. It mainly implements privacy protection by adding appropriate noise to the original data, the conversion of the original data, or the statistical results.

Definition 1 (ε - Differential Privacy [4]) Given data sets D_1 and D_2 that differ by only one record, i.e. $|D_1 \Delta D_2 \leq 1|$. Given a privacy algorithm A , $Rang(A)$ is the range of A . If the output result O ($O \in Rang(A)$) of algorithm A on data set D_1 and D_2 satisfies Eq. (1), then A satisfies ε - differential privacy.

$$\Pr[A(D_1) = O] \leq e^\varepsilon \times \Pr[A(D_2) = O] \quad (1)$$

Privacy budget parameter ε represents the degree of privacy protection. The smaller the ε value, the higher the degree of privacy protection and the greater the noise added. And the Laplacian mechanism [14] is a commonly used noise adding mechanism, which realizes differential privacy by adding a noise value satisfying the Laplacian distribution to the query result.

Definition 2 (Trajectory Data Set [15]) A trajectory is a chronological sequence of the position information of a moving object. A trajectory can be expressed as $T = \{(x_1, y_1, t_1), (x_2, y_2, t_2), \dots, (x_n, y_n, t_n)\}$, where (x_i, y_i, t_i) represents the user's position point at time t_i , x_i represents latitude, and y_i represents longitude. $T[i]$ represents the i -th element of the trajectory T , $|T| = n$ represents the length of the trajectory T . The trajectory data set is a set of multiple trajectories.

In order to realize the safe release of the trajectory data set, literature [16] uses the definition of differential privacy to propose a Geo-indistinguishability model (Geo-Indistinguishability). Based on the reality of location privacy protection, this model

believes that small changes in the user's location should have little impact on the query results, but when the user's location changes greatly, the query results can have large changes, so it can be based on the degree of user location changes. Set the corresponding privacy protection level.

Definition 3 (Geo-Indistinguishability [16]) Suppose that X represents the set of possible locations for users and Z represents the set of possible locations for publishing, $d(\cdot, \cdot)$ is the Euclidean distance, For any two positions $x_1, x_2 \in X$, $z \in Z$ and $d(x_1, x_2) \leq r$, if the algorithm K satisfies Eq. (2), it is said that K satisfies ε -inseparable region within the radius r .

$$\Pr[K(x_1) = z] \leq \exp(\varepsilon \cdot d(x_1, x_2)) \cdot \Pr[K(x_2) = z] \quad (2)$$

The parameter ε represents the privacy protection level per unit distance. Geo-Indistinguishability can be achieved by adding two-dimensional Laplace noise to the user's real location. The geographical indistinguishability model proposes a practical mechanism for the application of differential privacy in location privacy protection, which becomes the basis of some follow-up studies.

Literature [17] proposes that if Geo-Indistinguishability is independently applied to each location, the amount of noise generated will be unacceptable. Since certain behavior patterns and habits of users can be obtained by digging the location points or areas where the user stays for a long time, these location points and areas are protected.

Definition 4 (Stop point detection [18]) A cluster whose distance is less than a certain threshold and whose time difference is greater than a certain threshold is regarded as a stopping area. If the requirement of Eq.(3) is satisfied, the trace sequence from (x_i, y_i, t_i) to (x_j, y_j, t_j) is the stay region. The average position point of latitude and longitude of the trajectory sequence of the stop area is the stop point.

$$\begin{aligned} Dis tan ce((x_i, y_i), (x_j, y_j)) &\leq \Delta S \\ \cap Dis tan ce((x_i, y_i), (x_{j+1}, y_{j+1})) &\succ \Delta S \cap t_j - t_i \geq \Delta T \end{aligned} \quad (3)$$

Because Dynamic Time Warping (DTW) distance allows time series to be scaled locally to minimize the distance between two sequences, it can better match the characteristics of time series, which makes it widely adopted [19]. Therefore, this paper adopts DTW distance to measure data availability.

Definition 5 (Dynamic Time Warping (DTW) distance [20]) Suppose there are two tracks $A = \{(x_1, y_1, t_1), (x_2, y_2, t_2), \dots, (x_n, y_n, t_n)\}$ and $B = \{(x_1, y_1, t_1), (x_2, y_2, t_2), \dots, (x_m, y_m, t_m)\}$, is the DTW distance between two trajectories as follows:

$$\begin{aligned} DTW(A, B) &= dist(A_1, B_1) + \\ &\min(DTW(Re st(A), B), DTW(A, Re st(B)), DTW(Re st(A), Re st(B))) \end{aligned} \quad (4)$$

where $dist(A_1, B_1) = |A_1 - B_1|$, $Rest(T)$ is the child track after the first position point of the track is removed.

3. Differential Privacy Trajectory Data Protection Algorithm Based on Polar Coordinate Transformation

To achieve the high availability of the trajectory data set, and security, this paper proposes a differential privacy trajectory data protection algorithm based on polar coordinate transformation, the algorithm includes two steps. First step, find frequent stops, and then Baidu Map API technology is used to get the POI for the position type, so as to determine the key location points which easily leak privacy. Second step, Transform the rectangular coordinate system representation of the privacy position points into the polar coordinate system representation. Then, using the differential privacy protection mechanism to add noise to the key location points in the polar coordinate representation. Finally generate the trajectory data after user privacy protection. Each of these processes is described below.

3.1. Find Key Location Points

When the privacy of trajectory data is protected, if all the position points are directly protected by noise, the data will become unusable. Moreover, not all points can reveal personal privacy, so it is a big problem to find the key points in the trajectory data set that can reveal personal privacy.

3.1.1. Frequent Stop Points Detection

Literature [21] points out that users' frequent stop points are the easiest to infer personal privacy information. If the occurrence times of a stop location point are greater than the frequency threshold ΔQ , the stop point is a frequent stop point. And Literature [17] adds noise to the frequent stop points of the trajectory to achieve personal privacy protection, and the experimental results showed that the availability of data was greatly improved. Therefore, based on this work, this paper further improves the availability of data. This process is mainly to find the frequent stop points in the user's trajectory data set. The key is to calculate the trajectory set whose stay time is greater than a certain time threshold, but whose distance is limited within a certain distance threshold, and then traverse to find the stop points whose occurrence frequency is greater than the frequency threshold, which are frequent stop points. In this paper, the time threshold and distance threshold of the stop point refers to the stop point analysis of Baidu Map API, and the time threshold is set as 10 minutes, the distance threshold is 20m. And the frequency threshold ΔQ is analyzed in the experimental part.

3.1.2. Identify Key Location Points

Baidu Map API technology is a set of application interfaces based on Baidu Map service which is provided for developers for free. It provides a basic map display, reverses geocoding services, and other functions. The reverse geocoding service can provide the POI for the corresponding location based on the longitude and latitude of the requested location point, where the POI contains the type of the location point. A partial display of Baidu Map as shown in Figure 1. For each location, in addition to the name information, there are icons of the type to which the location belongs, such as Brownings Grove Park belongs to the type of tourist attractions in Figure 1.



Figure 1. A Part of Baidu Map.

Literature [22] found that by disturbing the location points in the continuous positions, the user's trajectory privacy can also be obtained by restricting the attacker's association. Therefore, it is important to select key location points in the trajectory data set that is likely to leak user privacy.

In order to make the track data released safely can better provide strong support for the urban planning of government departments and the decision-making of commercial organizations. Baidu Map API technology is used to connect the trajectory with reality, and requests the types of frequent stop points from Baidu Map API. The types are set as non-key location points according to whether the location points are public entertainment and not easy to reveal personal privacy. In this paper, shopping, tourist attractions and life services are set as non-key location points. And the other point types that leak personal privacy are set as the key location points, then protect these points. This paper roughly classifies whether the location is critical, and a follow-up investigation is needed to determine whether the point type is a key point type that is prone to divulging personal privacy.

The process begins by setting the appropriate API's Uniform Resource Location (URL) with the latitude and longitude of frequent stop points. Then, a request is sent to the Baidu Map API, and the POI of the location point represented by the Extensible Markup Language (XML) file is returned, and the location type is extracted by using the regular expression. Finally, determining if the type of point contains the name of the above key point types. If yes, setting the point as the key location point which is saved to the critical location point set $G = \{(x_1, y_1), (x_2, y_2), \dots, (x_m, y_m)\}$ for privacy protection in the next step.

3.2. Add Noise to Key Location Points Based on Polar Coordinate

If the key location points that are likely to leak personal privacy are published without personal privacy protection, it may damage personal reputation, property, physical and mental health or discriminatory treatment [23]. Because Geo-indistinguishability can be achieved by adding two-dimensional Laplace noise to a user's real location. Therefore, for the attacker cannot obtain personal sensitive information from the published trajectory information, traditional differential privacy trajectory data protection algorithms directly noise the longitude and latitude which expressed by the rectangular coordinate system. In this paper, the rectangular coordinate representation of latitude and longitude is creatively converted into polar coordinate representation, and then noise protection is carried out. After data transformation, the position points in spatial coordinates can be expressed in the same way, but the availability of data can be greatly improved.

The process starts with the data transformation of the set of key location points obtained in the previous step $G = \{(x_1, y_1), (x_2, y_2), \dots, (x_m, y_m)\}$, convert the rectangular coordinate system representation of latitude and longitude of each location point to polar coordinate system representation $JG = \{(\rho_1, \theta_1), (\rho_2, \theta_2), \dots, (\rho_m, \theta_m)\}$. Then $2m$ random noises obeying Laplace distribution are generated, and the noises were successively added to the polar coordinates ρ_i and θ_i in the JG data set. Finally, the polar coordinate system is converted back to the longitude and latitude coordinate system, and the original position points are replaced. The algorithm steps are shown in algorithm 1.

Algorithm 1 Data conversion and add noise

Input: Key location points set $G = \{(x_1, y_1), (x_2, y_2), \dots, (x_m, y_m)\}$;

Output: $PG = \{(\dot{x}_1, \dot{y}_1), (\dot{x}_2, \dot{y}_2), \dots, (\dot{x}_m, \dot{y}_m)\}$ as the points set after differential privacy protection;

1: Converts the set G to a polar representation $JG = \{(\rho_1, \theta_1), (\rho_2, \theta_2), \dots, (\rho_m, \theta_m)\}$;

2: Generate $Lap(1/\epsilon)$ noise sets $L = \{(z\rho_1, z\theta_1), (z\rho_2, z\theta_2), \dots, (z\rho_m, z\theta_m)\}$;

3: For S in JG

4: $\rho_i = \rho_i + z\rho_i$; $\theta_i = \theta_i + z\theta_i$;

5: End for;

6: Converts a JG set to a set PG represented by rectangular coordinates

In order to verify that the conversion of the rectangular coordinate system representation of the location point to the polar coordinate representation can improve the usability of the data, the frequent stay points with and without data conversion are compared and analyzed. Figure 2 randomly selects all trajectory data sets of three users in a year as examples, but the complete experimental results are consistent with the distribution of the sample trajectory results. Among them, the PC method represents the method of adding noise to the position indicated by the polar coordinate system which use a five-pointed star to mark the point; RC represents the method of adding noise to the position expressed by the rectangular coordinate system which use a triangle to mark the point. Different users are represented by different colors. It can be seen from Figure 2 that for each user, the PC method has less distortion than the IR method. And when the value of ϵ is smaller which represent the degree of privacy protection is higher, the less distortion of the PC method than the IR method becomes more obvious. It is verified that data conversion can greatly improve the usability of trajectory data.

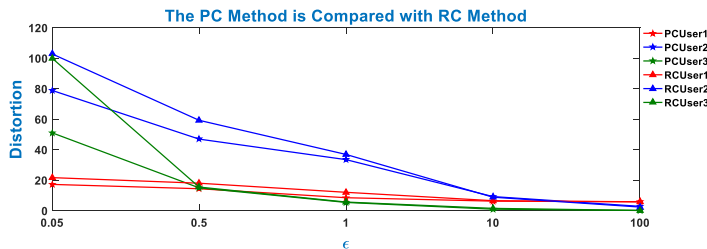


Figure 2. The PC Method is Compared with RC Method.

4. Experimental Analysis

For fair comparisons, all experiments are implemented on MATLAB and GeoLife GPS Trajectories [24-26] dataset provided by Microsoft Research Asia. The dataset was completed by 182 users in more than 5 years. There are 17621 trajectories, each represented by a series of timestamps points, and each timestamp point contains latitude, longitude, and time information. Most of the data is created every 1 to 5 seconds or every 5 to 10 meters in Beijing, China. Since the location points of the trajectory data set are collected intensively, this article reads the original trajectory data every 5 minutes to simplify the data set.

4.1. Evaluation Criteria

In the data release research for trajectory privacy protection, data utility and privacy protection degree are two main evaluation indicators.

- **Data utility.** Since DTW distance [16] allows time series to be locally scaled to minimize the distance between the two series, it can better match the characteristics of the time series, which makes it widely adopted. Therefore, this paper uses DTW to determine the deviation from the original trajectory and measure the utility of the data. The DTW distance represents the degree of distortion after trajectory data protection. The smaller the trajectory distortion, the greater the similarity to the original trajectory, and the higher the availability of processed data. The greater the trajectory distortion, the smaller the similarity to the original trajectory, and the lower the availability of processed data.
- **Degree of privacy protection.** According to the definition of differential privacy, the privacy budget parameter ε represents the degree of privacy protection. The smaller the ε value, the greater the noise added to the original trajectory and the higher the degree of privacy protection; the larger the ε value, the smaller the noise added to the original trajectory. The lower the degree of privacy protection.

4.2. Parameter Analysis

In summary, this paper has two parameters, the frequency threshold ΔQ of the stay point and the privacy protection degree ε of the differential privacy protection mechanism. This section analyzes and discusses the different values of ΔQ and ε for studying the influence of the setting of these two parameters on the performance of the algorithm.

In this paper, the stay points where a certain stay point appears more than the frequency threshold ΔQ are called frequent stay points. Considering the accuracy of the actual latitude and longitude which have six decimal places, and the stay points are obtained as the average of multiple points, so when searching frequent stay point, this paper set the actual tolerance of 1 meter. Figure 3 randomly selects all trajectory data sets of 5 users in a year for display, and analyzes the influence of different frequency threshold ΔQ on distortion when $\varepsilon = 0.5$. Different colors indicate different users, the abscissa indicates the frequency threshold ΔQ , and the ordinate indicates the distortion

represented by the DTW distance. It can be seen from Figure 3 that as the frequency threshold ΔQ increases, the distortion shows a downward trend. The reason is that the greater the frequency threshold ΔQ , the stricter the conditions for forming key location points which making fewer key location points. So that the disturbance location points become less when adding noise which leads to the less distortion. And due to the randomness of noise, some data fluctuate slightly in a certain interval.

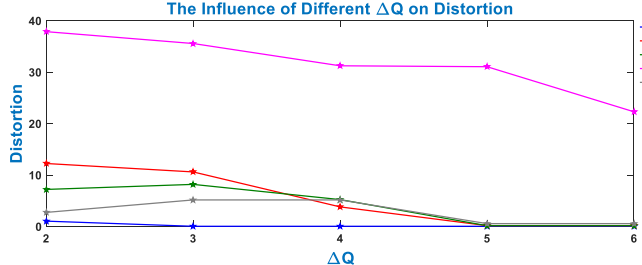


Figure 3. The Influence of Different ΔQ on Distortion.

Figure 4 also randomly selects all trajectory data sets of 5 users in a year for display, and analyzes the influence of different privacy protection degrees ε on distortion when $\Delta Q = 2$. Among them, different colors represent different users, the abscissa represents the frequency threshold ΔQ , and the ordinate represents the distortion represented by the DTW distance. It can be seen from Figure 4 that as the degree of privacy protection ε increases, the distortion degree shows a downward trend. This is because of the larger the ε value, the lower the degree of privacy protection, the smaller the added noise, and the smaller the distortion. Due to the randomness of noise, some data fluctuate slightly in a certain interval.

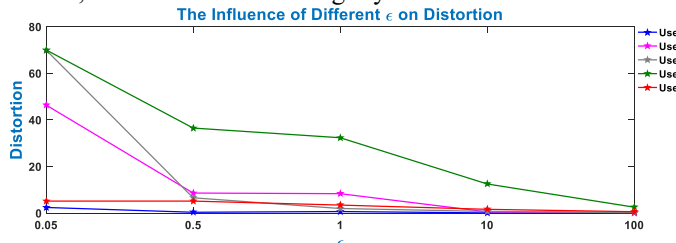


Figure 4. The Influence of Different ε on Distortion.

4.3. Experimental Comparison and Analysis

In 2019, literature [17] proposed the Interest Region (IR) method which is the frontier method in this direction. And it also protects the sensitive location points of the trajectory based differential privacy technology. So the IR method is used as a baseline method to demonstrate the effectiveness of the proposed method in this paper. In this section, this paper compares and analyzes the PT algorithm which is proposed in this paper and IR algorithms. This experiment use real data sets and set $\Delta Q = 2$. Figure 5 randomly selects all trajectory data sets of three users in one year for example, but the complete experimental results are consistent with the distribution of the sample trajectory results. The algorithm PT algorithm uses five-pointed stars for punctuation;

the IR algorithm uses circular punctuation. Different users are represented by different colors. It can be seen from Figure 5 that for each user, the PT algorithm which is proposed in this paper has less distortion than the IR algorithm. And when the value ϵ is smaller which means the degree of privacy protection is higher, the less distortion of the PT algorithm than the IR algorithm becomes more obvious. It is verified that the algorithm in this paper can greatly improve the usability of trajectory data in the process of safely publishing trajectory data.

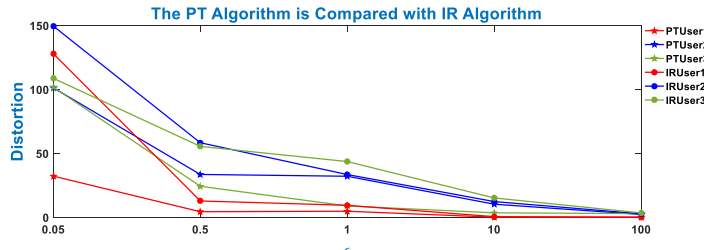


Figure 5. The PT Algorithm is Compared with IR Algorithm.

5. Conclusion

For the release of the trajectory data set, this paper connects the position with reality, and proposes a differential privacy trajectory data protection algorithm based on polar coordinate conversion. The algorithm uses Baidu Map API technology to obtain POI which contain point types. Then determining key location points that are likely to leak personal privacy, thereby provide stronger support for government departments in urban planning and commercial organizations in decision-making. Besides, the rectangular coordinate system representation of the key location points is converted to the polar coordinate system representation, and then the differential privacy protection mechanism is used to protect the key location points represented by the polar coordinate system. Experiments show that this data conversion greatly improves the availability of data. However, the trajectory also contains a lot of other real information, such as speed, transportation, etc. Combining this real information to set different privacy protection levels can make the protected data more realistic and improve the usability of the data. Therefore, how to use other realistic information to achieve better trajectory data privacy protection and release is the next research direction.

References

- [1] Lu YL. An American fitness APP leaked information about military bases, 2018. https://www.guancha.cn/america/2018_01_29_445035_s.shtml
- [2] D.Chandramohan, Rajaguru.D, Vengattaraman.T, Dhavachelvan.P, "A COORDINATOR - SPECIFIC PRIVACY - PRESERVING MODEL FOR E - HEALTH MONITORING USING ARTIFICIAL BEE COLONY APPROACH", Security and Privacy. (2018). <https://doi.org/10.1002/spy2.32>.
- [3] Chandramohan.D, Vengattaraman.T, Rajaguru.D, Baskaran.R and Dhavachelvan.P, "EMPPC-An Evolutionary Model Based Privacy Preserving Technique for Cloud Digital Data Storage Service", 3rd IEEE International Advance Computing Conference, INDIA, 2013, 6, pp.89-95. ISBN: 978-1-4673-4528.

- [4] Dwork C. Differential privacy. Proceedings of the 33rd international conference on Automata, Languages and Programming - Volume Part II. Springer, Berlin, Heidelberg, 2006. 26(2):1-12.
- [5] Komishani EG, Abadi M, Deldar F. PPTD: Preserving personalized privacy in trajectory data publishing by sensitive attribute generalization and trajectory local suppression. Knowledge-Based Systems, 2016, 94(Feb.15):43–59.
- [6] Zhang XJ, Meng XF. Differential privacy in data publication and analysis. Chinese Journal of Computers, 2014(4):927-949.
- [7] Chen R, et al. Differentially private transit data publication: a case study on the montreal transportation system. Proceedings of the18th ACM SIGKDD international conference on Knowledge discovery and data mining, Beijing, China, August 12-16.New York, NY, USA: ACM, 2012: 213-221.
- [8] Xiong P, Zhu TQ, Pan L, et al. Privacy preserving in location data release: A differential privacy approach. In: Pham DN and Park SB, Eds, PRICAI 2014: Trends in Artificial Intelligence, Springer, Berlin, 183-195.
- [9] Li M, Zhu L, Zhang Z, et al. Achieving differential privacy of trajectory data publishing in participatory sensing. Information Sciences, 2017, s 400–401:1-13.
- [10] Terrovitis M, Poulis G, Mamoulis N, et al. Local suppression and splitting techniques for privacy preserving publication of trajectories. IEEE Transactions on Knowledge and Data Engineering, 2017, 29(7):1466-1479.
- [11] Hua JY, Tong W, Xu FY. A geo-Indistinguishable location perturbation mechanism for location-based services supporting frequent queries. IEEE Transactions on Information Forensics and Security, 2017:1-1.
- [12] Wang B, Zhang L, Zhang GY. A gradual sensitive indistinguishable based location privacy protection scheme. Journal of Computer Research and Development, 2020, 57(3):616-630.
- [13] Tan R , Tao Y , Si W , et al. Privacy preserving semantic trajectory data publishing for mobile location-based services[J]. Wireless Networks, 2019(1).
- [14] Dwork C, McSherry F, Nissim K, et al. Calibrating noise to sensitivity in private data analysis. Proceedings of theory of Cryptography Conference. Springer, Berlin, Heidelberg, 2006:265-284.
- [15] Huo Z, Meng X F. A survey of trajectory privacy-preserving techniques. Chinese Journal of Computers, 2011, 34(10):1820-1830.
- [16] Miguel E. Andrés NE. Bordenabe CK. Geo-Indistinguishability: Differential privacy for location-based systems. Proceedings of the 2013 ACM SIGSAC Conference on Computer & Communications Security, Berlin, 4-8 November 2013, 901-914.
- [17] Lan W, Lin Y, Bao LY, et al. A Trajectory-differential privacy-protection method with interest region. Journal of Frontiers of Computer Science and Technology,2020,14(1):59-72.
- [18] Fu ZL, Tian ZS, Xu YQ, et al. A two-step clustering approach to extract locations from individual GPS trajectory data. ISPRS International Journal of Geo-Information, 2016, 5 (10):166.
- [19] Liu Y , Chen J, Wu S , et al. Incremental fuzzy C me-doids clustering of time series data using dynamic time warping distance. PLoS ONE, 2018, 13(5):1-25.
- [20] Sharma A, Sundaram S. On the exploration of Information from the DTW cost matrix for online signature verification. IEEE Transactions on Cybernetics, 2017, 48(2):611-624.
- [21] Feng DG, Zhang M, Ye YT. Research on differentially private trajectory data publishing. Journal of Electronics & Information Technology, 2020, 042(001):74-88.
- [22] Fei F, Li S, Dai H, et al. A K-anonymity based schema for location privacy preservation. IEEE Transactions on Sustainable Computing, 2019, 4(2): 156-167.
- [23] Research report on Personal Information Protection of Internet + Industry. China Academy of Information and Communications Technology, 2020. http://www.caict.ac.cn/kxyj/qwfb/bps/202003/t20200301_275474.htm
- [24] Zheng Y, Zhang LZ, Xie X, et al. Mining interesting locations and travel sequences from GPS trajectories. Proceedings of International conference on World Wild Web (WWW 2009), Madrid Spain. ACM Press, 2009: 791-800.
- [25] Zheng Y, Li QN, Chen YK, et al. Understanding mobility based on GPS data. Proceedings of ACM conference on Ubiquitous Computing (UbiComp 2008), Seoul, Korea. ACM Press: 312-321.
- [26] Zheng Y, Xie Y, Ma WY. GeoLife: A collaborative social networking service among user, location and trajectory. IEEE Data Engineering Bulletin. 2010, 33, 2, pp. 32-40.

Visualization of the Artist Relations Using Twitter User Profiles

Minoru YOSHIDA^{a,1}, Shogo KOHNO^a and Kazuyuki MATSUMOTO^a and
Kenji KITA^a

^a*Tokushima University*

Abstract. We propose a new music artist recommendation algorithm using *Twitter profile texts*. Today, *music recommendation* is provided in many music streaming services. In this paper, we propose a new recommendation algorithm for this music recommendation task. Our idea is to use *Twitter profile texts* to find appropriate artist names to recommend. We obtained word embedding vectors for each artist name by applying word2vec algorithm to the corpus obtained by collecting such user profile texts, resulting in vectors that reflect artist co-occurrence in the profile texts.

Keywords. music recommendation, Twitter profiles

1. Introduction

We propose a new music artist recommendation algorithm using *Twitter profile texts*.

Today, many songs can be accessed on the Internet. In many cases, users access to these songs by the artist names, e.g., search for songs by inputting the artist name as keyword to a search box. In this scenario, users can access only to songs performed by the artist input to the system. This approach has its merits such as users can access to desired songs with high certainty (i.e., high accuracy), but its demerits such as the user is unlikely to find unpredicted but good (i.e., fit to the user's taste) songs. To cover the latter demerits of simple keyword search, *music recommendation* is provided in many music streaming services. Typically, such recommendation provides a list of songs that are similar to the song currently listened to by the user.

In this paper, we propose a new recommendation algorithm for this music recommendation task. Our idea is to use *Twitter profile texts* to find appropriate artist names to recommend. We assume that many Twitter users list their favorite things in their social networking services (SNS) profile texts and we can thus find the artist who is likely to be preferred by the fans of artist a by looking at the Twitter profile text of the fans of a .

We obtain word embedding vectors for each artist name by applying word2vec algorithm to the corpus obtained by collecting the user profile texts, resulting in vectors that reflect artist co-occurrence in the profile texts. Our recommendation system also has potential to assist the simple artist name search approach, e.g., even if the user does not know the artist name of the song s/he is searching for, s/he can guess the (potentially

¹Tokushima University; E-mail: mino@is.tokushima-u.ac.jp

wrong) artist name from the song's flavor or mood and input it to the system, then the system can suggest the list of artists which may include the correct artist name.

2. Related Work

Music recommendation research has been mainly studied by audio or music-IR research communities [1]. Traditional approaches to music recommendation are to use collaborative filtering approach, which makes a user-item matrix (where each entry e_{ij} represents the user-i's rating on item-j) and calculate item-item similarity based on the obtained matrix [2]. In another approach, Moling et al. [3] proposed to use a user's listening behavior on radio channels to train the agent for music recommendation. Another line of approaches is content-based recommendation using music features [2] [4]. For example, Hijikata et al. [5] used content-based filtering for music recommendation. Musical features such as tempo, rhythm, codes, timbres, keys, etc. from musical instrument digital interface (MIDI) files and used to construct music vectors, which were used to calculate similarity between songs.

On the other hand, music recommendation using texts found on SNS have been investigated by several researchers recently. Mimura et al.[6] selected 20 music artists and collected followers of the official Twitter accounts for these artists. Tweets of these users are collected as text sets, and they applied Latent Dirichlet Allocation (LDA) to extract topics. Finally, artist similarity was defined as the topic distribution similarity. Sasai [7] proposed *ArtistVector* which is embedding vectors for music artists. He collected texts for artists from Wikipedia articles and web texts written by fans of artists, and applied several algorithms including word2vec to the texts to obtain document embedding vectors. The resulting document vectors were used as artist embeddings to visualize artist similarity. Hirota et al. [8] collected texts from Web dictionary and curation sites for each artist, and obtained artist vectors by counting the number of each word. The extracted context words were used to provide the interface to select desired contexts to be used for recommendation. Hyung et al. [9] extracted texts from song requests in radio and recommended artists based on the extracted texts.

Compared to these previous approaches, we propose a new method to obtain artist vectors that uses *Twitter profile texts*. Recently, several researchers have used Twitter user profiles for automatic labeling of Twitter users. For example, [10] used Twitter profile texts to classify users' political affiliations into "Democrats", "Republicans" or "Unknown". However, approaches that use user profiles as general text corpus have not been studied actively [11].

2.1. Word2vec

Word2vec is a standard tool to obtain word embedding in low (typically 50-500) dimensions. Skip-gram with Negative Sampling (SGNS) approach is frequently used to obtain such vectors. It maximizes the sum of the plausibility scores

$$\log \sigma(v'_{w_O} \cdot v_{w_I}) + \sum_{k=1}^K \log \sigma(-v'_{w_k} \cdot v_{w_I})$$

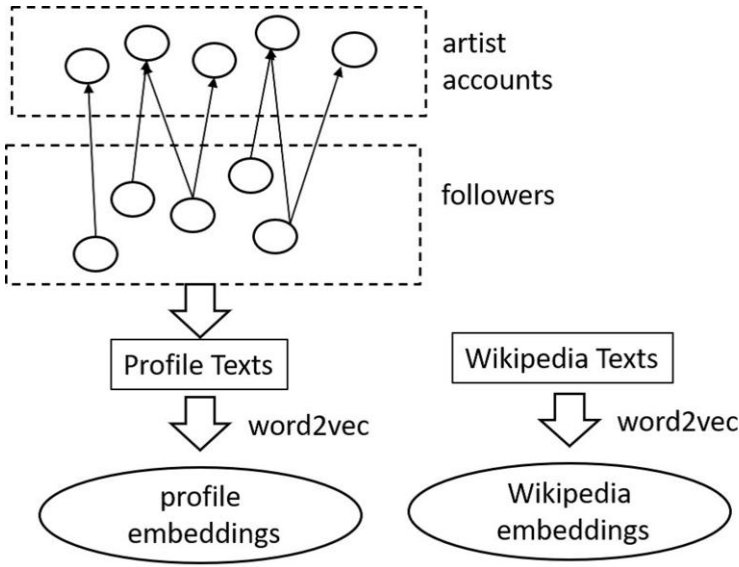


Figure 1. System Workflow of Our Method

of predicting the “output word” w_O given the “input word” w_I , where w_O and w_I appears in the same *context* i.e., in text window of the pre-defined size. Here, K is the number of negative samples, v_w and v'_w are two types of vectors called the “input” and “output” vectors, respectively, and σ is the sigmoid function. Negative samples w_k are selected randomly in each learning step.

This approach is based on the *distributional hypothesis* that assumes *words in similar meaning appear in the similar contexts* where *contexts* is the words that appear around the target word.

3. Problem Setting

We assume a user gives one or two artist names to the system. The system returns the names of other artists *similar* to the query artists. We consider two types of similarities: document-based similarity calculated with *Wikipedia vectors* and profile-based similarity calculated with *profile vectors* described later.

To make the corpus balanced and comprehensive, we selected 6 artist categories: “J-POP”, “Idols”, “Rock”, “Alternative Pops”, “Anime”, and “Others” and collected equal amounts of texts from each category.

4. Proposed Method

We observed that many users wrote two or more artist names in their profiles (e.g., a user who writes one rock artist name in his/her profile tend to write another rock artist in his/her profile,) and in many cases these names were in near positions in the text. This means that we can obtain co-occurrence statistics for artist names found in the profile

texts. Our idea is to obtain the artist embeddings by running word2vec on these profile texts because word2vec learn embedding vectors using word co-occurrences in limited-size windows.

4.1. Corpus

Figure 1 shows an overview of our method. We selected twitter users who show strong interest in some music artists (i.e., we collected fans of some music artists.) More concretely, we selected users who follow one or more music artists or music events. We used TwitterAPI to obtain Twitter profiles and main texts (i.e., tweets) for the selected users.

We selected the 50 Twitter accounts of artists or events related to the above-mentioned categories. We call these selected accounts “artist accounts”. We collected around 1,000 followers for each artist account and extracted their profiles. As a result, we obtained around 50,000 accounts without considering overlapping. All profile texts from them were concatenated into one file, resulting in a 262,280-lines text². However, we found overlap between these lines because the same person may follow two or more artist accounts. After removing overlap, we obtained the final profile texts that consisted of 32,781 lines.

The collected profile texts looks like as follows.³

I'm AKB48 fan living in Tokyo. I also love SKE48 and NMB48!

We obtained *artist embeddings* learned by running word2vec on the obtained texts.

4.2. Implementation Issues

Profile texts were separated into word lists by using the morphological analyzer MeCab-NEologd [12] [13]

We constructed the *artist dictionary*, which consists of lists of synonyms for each artist name. These synonyms (e.g., nicknames) were obtained mainly from the artist-name list in Uta-Map⁴. We also extracted some acronyms of the artist names by seeing the obtained corpus. This dictionary was used to normalize the artist names found in the corpus. We also implemented the preprocessor that remove noises like URLs and face marks.

We used word2vec[14] to obtain word embedding vectors where the parameters were set as follows:

- algorithm = skip-gram,
- dimension size = 100,
- window size = 15,
- word frequency threshold = 5.

²It was larger than 50,000 because we might extract multiple lines from one profile text.

³This is an imaginary example because of privacy issues.

⁴<https://www.utamap.com/>

4.3. Visualization by t-SNE

Obtained similarity between artists can be used to visualize music artist relations. We implemented a system where a user give two artist names as a query, and system returns the music artist map considered as *similar* to one or two given artists. Visualization was performed by using t-SNE [15], which embeds high-dimensional vectors into 2-dimentional points where two points become near if the distance between two original high-dimension vectors is small.

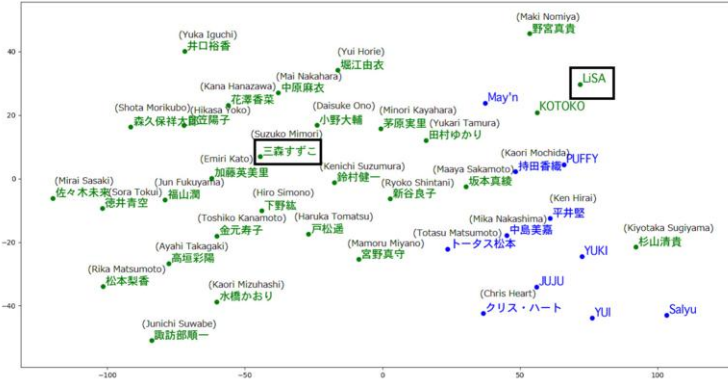


Figure 2. Example Result Using Wikipedia

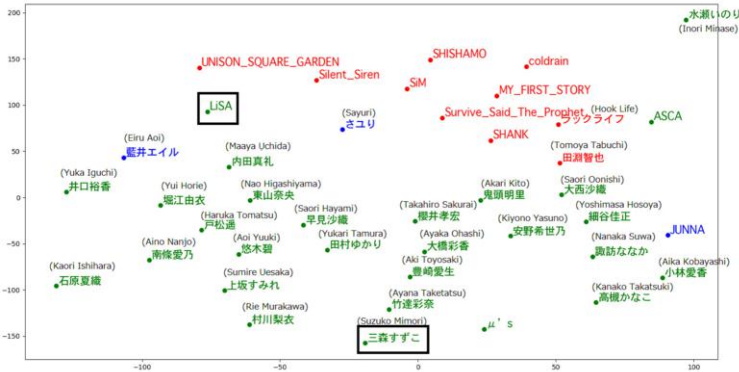


Figure 3. Example Result by Proposed Method

As described later, we tested two types of vectors: *Wikipedia vectors* learned by using Wikipedia texts and *profile vectors* learned by our proposed method. Results are shown in Figure 2 (using Wikipedia text) and 3 (using profile texts) for the query “LiSA” and “Suzuko Mimori”, both of which are Japanese Voice Actors, but the former is also a rock artist. In these figures, generally speaking, names with Kanji characters are of voice actors, and names with alphabets are for rock artists.

We observed that the results using profile texts (Figure 3) gave more comprehensive visualization where rock artists (upper half, colored red in Figure 3) were located near

“Lisa” and female voice actor names (lower half, colored green in Figure 3) were located near “Suzuko Mimori” than results using Wikipedia texts (Figure 2). In Figure 2, some voice actors and major music artists were listed (green names indicate the name of voice actors (including male and female ones) and blue names indicate the name of J-POP artists), but easy-to-understand structures were not observed. For example, voice actors listed in Figure 2 include both male and female ones, while the most of voice actors listed in Figure 3 (our method) were female voice actors which can be considered more similar to the query artists (both of them were female ones).

5. Experiments

We compared two types of embedding vectors: *Wikipedia vectors* provided by Shiro-Yagi Corp.⁵ which is pretrained on Japanese Wikipedia texts, and *profile vectors* obtained by using our method which uses Twitter profiles as a corpus. We call the former *Wikipedia vectors* and the latter *profile vectors*.

We selected 10 query artists (2 for each genre excluding “others” category) for evaluation. The Twitter profile corpus was divided into a training (80%) and test(20%) set, and we re-train our model using the training set. For each query artist q , we collected the test set profile texts that included q . The task is to predict the artist names other than q included in each collected profile text. Therefore, the experiment is to test if we can predict a user’s taste by using vectors obtained using other users’ tastes.

We used *average precision* [16] for the evaluation metric. We ranked all artist names using cosine similarity of vectors of each artist and the query artist q . Given the ranked list of artists $\langle c_1, c_2, \dots, c_n \rangle$, we calculate average precision for each profile text that includes artist names $S = \{q, s_1, s_2, \dots\}$ as follows:

$$\frac{1}{|S|} \sum_{1 \leq k \leq n} r_k \cdot \text{precision}(k),$$

where $\text{precision}(k)$ is the accuracy (i.e., ratio of correct answers to all answers) of the top k candidates, and r_k represents whether the k -th artist is relevant (1) or not (0). (In other words, $r_k = 1$ if $c_k \in S$, and $r_k = 0$ otherwise.)

Table 1. Average Precision by using profile and Wikipedia vectors

Genre	Wikipedia	Profile (proposed)
Rock	0.0287	0.109
J-POP	0.0786	0.107
Alternative Pops	0.0204	0.188
Idols	0.0749	0.310
Anime	0.0210	0.0689

Results are shown in Table 1 and Figure 4. We observed high average precision in the results by the proposed method, especially in the Idols genre, compared to the Wikipedia vectors. We think the reasons for good results in Idols genre is that this genre is relatively “exclusive” which means that the fans of an idol are likely to choose another

⁵<https://aial.shiroyagi.co.jp/2017/02/japanese-word2vec-model-builder/>

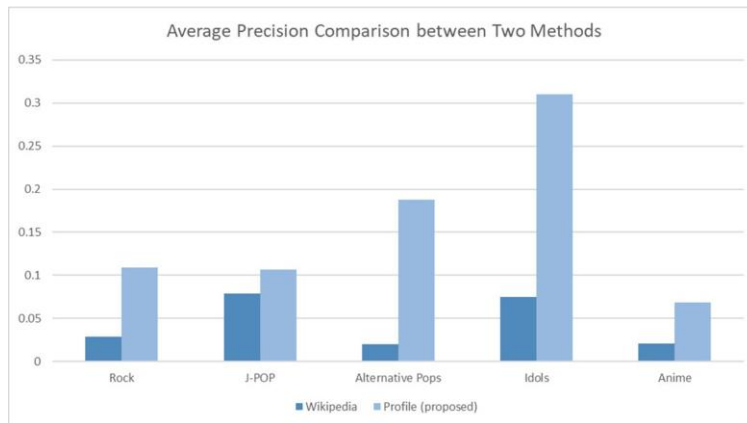


Figure 4. Comparison of Average Precision between Two Methods

idol as another artist to listen to. On the other hand, for J-POP the difference between two methods was small, suggesting that J-POP genres do not have such strong exclusiveness probably because the genre is more general (i.e., contain various kinds of artists) than other genres.

6. Conclusions and Future Work

In this paper, we proposed a new artist recommendation algorithm using *Twitter profile texts* to reflect people's tastes on music artists more directly. We also validated our results by visualizing the list of artists obtained by using two different queries using t-SNE. We observed that the proposed method provided more discriminative results than a method using Wikipedia texts in some genres.

Future work includes hybrid approaches of profile and Wikipedia texts, which may provide profile-based taste-oriented recommendation as well as Wikipedia-based exhaustive recommendations simultaneously. Developing systems with integrated ranking algorithms that consider not only artist similarities but also song similarities or genre similarities in one scoring function is also important future work.

Acknowledgement

This work was supported by JSPS KAKENHI Grant Numbers JP18K11549, JP20K12027.

References

- [1] Jannach D, Kamehkhosh I, Bonnin G. Music Recommendations: Algorithms, Practical Challenges and Applications. In: Berkovsky S, Cantador I, Tikk D, editors. Collaborative Recommendations: Algorithms, Practical Challenges and Applications. World Scientific; 2018. p.481-518.
- [2] Yoshii K, Goto M, Komatani K, Ogata T, Okuno HG. Hybrid collaborative and content-based music recommendation using probabilistic model with latent user preferences. In: Proceedings of the 7th International Conference on Music Information Retrieval (ISMIR); 2006. p. 296-301.

- [3] Moling O, Baltrunas L, Ricci F. Optimal radio channel recommendations with explicit and implicit feedback. In: Proceedings of the sixth ACM conference on Recommender systems (RecSys '12); 2012. p. 75-82.
- [4] Hartono P, Yoshitake R. Automatic Playlist Generation from Self-Organizing Music Map. *Journal of Signal Processing*. 2013; 17(1):11-19.
- [5] Hijikata Y, Iwahama K, Nishida S. Content - based Music Filtering System using Decision Tree and its Evaluation. *IPSJ SIG Technical Reports*. 2004; 2004-DBS-133:17-24. (In Japanese).
- [6] Mimura N, Ushijima T. Can we see the fans from SNS? - Extraction of fan characteristics of music artists using Twitter -. In: Proceedings of the DEIM Forum; 2017. D8-1. (In Japanese).
- [7] Sasai D. ArtistVector: Artist Feature Extraction with Web Document Embeddings. *IPSJ Technical Report*. 2018; 2018-NL-236(3):1-7. (In Japanese).
- [8] Hirota M, Okada R, Nakanishi T, Kitagawa T. Dynamic Context-Dependent Artist Network Generation for Japanese Music Artists. In: Proceedings of the DEIM Forum; 2016. E1-1. (In Japanese).
- [9] Hyung Z, Lee K, Lee K. Music recommendation using text analysis on song requests to radio stations. *Expert Systems with Applications*. 2014; 41(5):2608-2618.
- [10] Joshi A, Bhattacharyya P, Carman MJ. Political Issue Extraction Model: A Novel Hierarchical Topic Model That Uses Tweets By Political And Non-Political Authors. In: Proceedings of WASSA, NAACL-HLT; 2016. p. 82-90.
- [11] Yoshida M, Matsumoto K, Kita K. Modeling Relations Between Profiles and Texts. In: Proceedings of AIRS 2018; 2018. p. 103-109.
- [12] Kudo T. MeCab: Yet Another Part-of-Speech and Morphological Analyzer, "<http://taku910.github.io/mecab/>", 2013.
- [13] Kudo T, Yamamoto K, Matsumoto Y. Applying Conditional Random Fields to Japanese Morphological Analysis. In: Proceedings of the 2004 Conference on Empirical Methods in Natural Language Processing (EMNLP-2004); 2004. p. 230-237.
- [14] Mikolov T, Sutskever I, Chen K, Corrado GS, Dean J. Distributed representations of words and phrases and their compositionality. In: Proceedings of the Advances in neural information processing systems; 2013. p. 3111-3119.
- [15] Maaten LVD, Hinton G. Visualizing data using t-SNE. *Journal of Machine Learning Research*. 2008 Nov;9:2579-2605.
- [16] Chakrabarti S. Mining the Web : Discovering Knowledge from Hypertext Data. Morgan-Kaufmann Publishers; 2002. 368 p.

A New Approach for the Detection of Concrete Cracks Based on Adaptive Morphological Filtering

Huan Hou and Weiguo Lin¹

College of Information Science and Technology, Beijing University of Chemical Technology, Beijing 100029, China

Abstract. Cracks are an important sign of distress of concrete bridges and may reduce their service life and safety. For the case where there are stains, peeling, scratches, and uneven illumination on the surface of concrete bridges, and where it is difficult to accurately detect complete cracks, this paper proposes a new method to connect the breaks in cracks by adaptive morphological dilation based on crack direction. Most of the existing crack image detection methods attempt to achieve high detection accuracy by increasing the algorithm complexity but sacrifice real-time detection efficiency. A multiple filtering method based on a few adaptive feature thresholds is proposed to filter non-cracks and obtain a clear crack image by analyzing the morphological characteristic differences between real cracks and noise and pseudo-cracks. The experimental results show that the proposed method can effectively improve the integrity of cracks, remove different noise and pseudo-cracks, without modeling, and has a higher detection accuracy and speed, which is suitable for practical engineering applications.

Keywords. concrete crack detection, infrared image, morphology, multiple feature thresholds, adaptive filtering

1. Introduction

Bridges play an important role in transportation. Most modern bridges are constructed from reinforced concrete, which can be damaged by natural disasters, environmental temperature, aging of building materials, overload, and other factors. This reduces bridge lifespan, safety, and transport efficiency [1]. Cracks are a common defect in bridges, which belong to the first stage of bridge hazards. They not only affect the normal use of bridges, but also induce other damage [2]. Therefore, crack detection and evaluation of the surface of bridge structures play an important role in the maintenance of the structural health and reliability of concrete bridges [3]. Traditional manual crack detection methods are time-consuming, laborious, dangerous, and subjective, and cannot meet the requirements of high efficiency, automatic detection, and convenient accessibility [4].

¹ Corresponding Author: Weiguo Lin, College of Information Science and Technology, Beijing University of Chemical Technology, Beijing 100029, China; Email: linwg@mail.buct.edu.cn

The development of high-speed camera technology and large storage hardware makes it straightforward to collect road images in real time. Therefore, image-based technology provides an efficient and economical way to detect cracks. Combined with unmanned aerial vehicles (UAVs) and portable equipment, this area has attracted more and more attention from academic research and industry [5]. Image-based crack detection processing mainly includes image noise reduction, crack extraction, and crack recognition. Su and Yang [6] proposed a morphological segmentation algorithm based on edge detection to realize the automatic detection of cracks on concrete surfaces. In order to make use of the local structural features of cracks, Shi et al. [7] proposed the CrackForest method to detect road cracks automatically based on random structured forests, which can effectively suppress noise. However, this method requires manual threshold selection to segment the image. Zhao et al. [8] regarded each crack gray image as a parametric surface, and cluster the candidate points by geometric representation and anisotropy of cracks to detect inconspicuous cracks. Jahanshahi et al. [9] proposed a non-contact remote sensing crack detection and quantization method based on 3D scene reconstruction, image processing, and pattern recognition. This method uses depth perception to detect cracks and quantify their width, which has high reliability, but the 3D image requires more computation and cannot achieve real-time performance.

In order to improve crack detection performance, Lee et al. [10] combine morphology with a neural network to detect, measure, and analyze the width, length, direction, and pattern of cracks. Jang et al. [11] proposed a concrete crack detection approach based on deep learning (DL). This method uses hybrid images, which combine visual and infrared thermal imaging images, and improves the convolutional neural network (CNN) structure, which can automatically detect macro and micro cracks while minimizing the false alarm rate. Nhung et al. [12] applied a CNN to detect cracks in pavement images, achieving high accuracy without image preprocessing. Although the CNN-based method has high detection accuracy, it requires a large number of labeled images including actual crack and non-crack images to support the training process. It also requires a large amount of computation and high-performance hardware, taking a long time to run.

Due to the complex geographical and natural environment and concrete surface roughness, the collected concrete images have problems such as spalling, stains, scratches, and uneven illumination, which affect the detection accuracy. Most crack detection algorithms cannot address these problems simultaneously. Compared with ordinary images, infrared image detection greatly reduces the impact of these problems. Any object produces thermal radiation. The intensity of the infrared radiation of the object is not only related to the material type, morphological characteristics, and chemical and physical structure (such as surface oxidation, roughness, etc.), but is also related to the temperature. In the application of concrete crack detection, by analyzing infrared thermal imaging and comparing the difference of the infrared radiation distribution between the crack area and the surrounding concrete surface, the morphology and location of cracks are determined to achieve the detection of crack defects [13]. Tashan et al. [14] used an active infrared thermal imaging detection method to investigate carbon fiber reinforced polymer concrete samples containing various artificial and loading cracks on the concrete surface. It can detect the location and width of cracks well, but it is affected by the heating angle and position. Jang et al. [15] proposed a line laser thermography scanning system for multiple crack evaluation on a concrete structure, and infrared images are used to successfully visualize and

evaluate multiple cracks. However, the detection speed is slow, and the system is only designed for use with large laboratory equipment.

In this paper, infrared images are used to detect concrete cracks. Generally, crack detection methods based on image processing often have the problem of crack breaks after threshold segmentation, resulting in low detection accuracy and incomplete cracks detected. This paper proposes a new method of morphological dilation based on the direction of cracks to connect the breaks and improve the integrity of the crack. Most existing crack image detection methods try to achieve higher detection accuracy by increasing the algorithm complexity, but at the same time sacrifice the real-time detection efficiency. Taking into account the difference in the morphological characteristics of the connected domain between cracks and noise, a multi-filtering method based on adaptive feature thresholds is proposed to remove non-cracks and detect more complete cracks. The method does not need to establish a crack diagnosis model, and has a high detection accuracy rate, which not only improves the applicability of the method, but also ensures real-time performance.

2. Infrared image crack detection method

In the process of the automatic detection of cracks in concrete bridge images, the collected infrared images have large noise interference due to light, equipment noise, and other reasons. Therefore, it is necessary to preprocess the image first to improve the quality, and then perform image background removal and threshold segmentation. After this, the binary image is subjected to morphological dilation based on the crack direction to improve the integrity of the crack, and finally, adaptive morphological filtering is performed to obtain the detection result. The flow chart of the crack detection method proposed in this paper is shown in Figure 1.

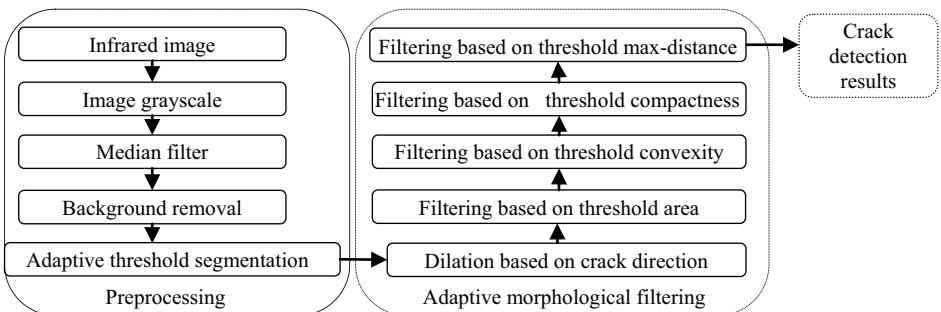


Figure 1. Flow chart of the crack detection processes.

2.1. Connected domain feature distribution for crack infrared images

After threshold segmentation, binary images can be obtained. The image domain composed of target pixels with the same pixel value and adjacent positions is called the connected domain. Pixels of the same crack target usually have connectivity. In this paper, by analyzing the differences in the morphological characteristics of the connected domains between cracks, noise, and pseudo-cracks, several connected domain features are proposed, and then the distribution characteristics of the features are analyzed. The features of the crack connected domain used in this paper mainly

include: (1) The area of the connected domain A; (2) Convexity feature CV; (3) Compactness feature COM; (4) The max distance L in the connected domain [16-19].

Figure 2 shows the binary images with and without cracks after background subtraction and adaptive threshold segmentation [19]. The distributions of the four kinds of features mentioned above are shown in Figure 3(a). It can be seen that the two curves for crack and non-crack images are significantly different because of the influence of the crack features, in which the positions of the crack features are marked with small circles. For the image with cracks, the kernel smoothing density estimation (ksdensity) curves for the four features were obtained and then their normal distribution $N(a * \mu_i, (b * \sigma_i)^2)$ curves are obtained, as shown in Figure 3(b). It can be seen that for the infrared image with cracks, most of the connected domains are still noise and pseudo-cracks, with only one or a few real cracks. Therefore, the above four features of noise and pseudo-cracks which account for the majority are basically within the range $(\mu - 2\sigma, \mu + 2\sigma)$ of the normal distribution $N(a * \mu_i, (b * \sigma_i)^2)$, while the features of real cracks (marked by dots) are distributed outside this range.

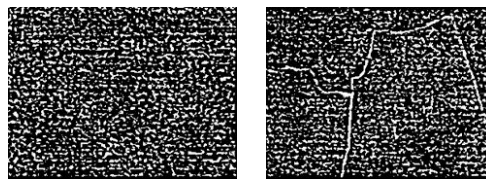
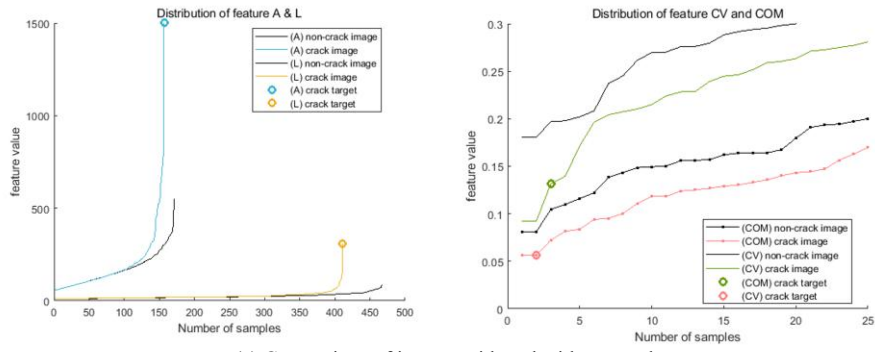
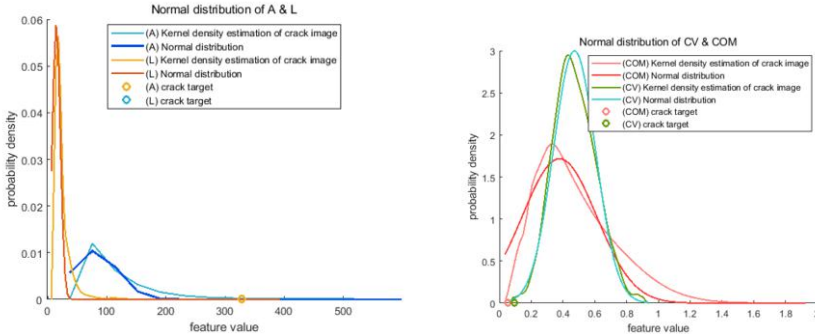


Figure 2. Images after background removal and segmentation.



(a) Comparison of images with and without cracks.



(b) Distribution of crack image features.

Figure 3. Distribution and comparison of connected domain features in infrared images.

Through the statistical analysis of the experimental results, the parameters a and b that fit the normal distribution can be obtained. Several infrared images with cracks are randomly selected as samples, and experimental statistical analysis is conducted for the four features to obtain the parameters a and b that minimize the mean squared error (MSE) of the fitting normal distribution $N(a * \mu_i, (b * \sigma_i)^2)$. According to the results, the normal distribution $N(\mu, \sigma^2)$ and the feature value distributions of the four connected domain features in the image are as follows:

- (1) $F(A) \sim N(0.6\mu_1, (\sigma_1/4)^2)$, $T_A > 0.6\mu_1 + \sigma_1/2$.
- (2) $F(CV) \sim N(\mu_2, \sigma_2^2)$, $T_{CV} < \mu_2 - 2\sigma_2$.
- (3) $F(COM) \sim N(0.6\mu_3, \sigma_3^2)$, $T_{COM} < 0.6\mu_3 - \sigma_3$.
- (4) $F(L) \sim N(0.6\mu_4, (\sigma_4/4)^2)$, $T_L > \mu_4 + \sigma_4/2$.

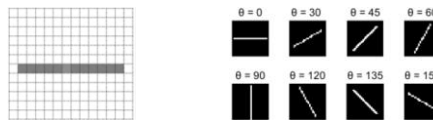
Here, T_A , T_{CV} , T_{COM} , and T_L can be used as the four adaptive crack feature thresholds which are the basis for selecting the target connected domains that conform to crack characteristics in the image. According to these adaptive thresholds, multi-stage filtering can be performed on noise and pseudo-cracks.

2.2. Adaptive dilation based on crack direction

After threshold segmentation, multiple breaks often appear in the image, resulting in incomplete cracks. In the basic operations of morphology, dilation will fill the edge breaks or holes, but usually the dilation operation will connect the target crack with surrounding noise, destroying the real shape of the crack. In this paper, an adaptive dilation method based on the crack direction is proposed, which can enhance the completeness of cracks and ensure that the shape of cracks is unchanged to a certain extent. The method first constructs structural elements that can adapt to the direction of the crack connected domain, which determines the direction of the subsequent dilation operation. Second, only the connected domains conforming to crack characteristics are processed by morphological dilation, while the noise domains are not, which protects the edge of the cracks and also reduces the amount of operations.

(1). For the image B_0 after threshold segmentation, the adjacent target connected domains A_n with larger areas and less compactness are selected, which are more consistent with crack characteristics. An initial horizontal structural element S_0 is constructed with a length of 12 pixels, as shown in Figure 4(a). (n represents the n -th target connected domain.)

(2). The angle of domain A_n is θ_n , which is the angle between the major axis of the same standard second order center distance ellipse and the positive x -axis. S_0 rotates at the angle of θ_n to construct the adaptive structural element S_n , so S_n is in the same direction as A_n . Figure 4(b) shows examples of a structural element rotated at different angles.



(a) Initial element. (b) Examples of adaptive structural element S_n .
Figure 4. Construction of adaptive structural elements with angles of θ_n .

(3). The structural element S_n is used for adaptive morphological dilation with the domain A_n ; the result is fused with the original image B_0 to obtain whole image B_n .

(4). Steps 2 and 3 are repeated until the adaptive dilation of all target domains is completed; the final image B_N is obtained, as shown in Eq. (1).

$$B_n = (A_n \oplus S_n) \cup B_{n-1} \quad (n = 1, 2, \dots, N) \quad (1)$$

This method extends each target domain towards both ends, and thus connects the two adjacent crack fragments. The red circle mark on Figure 5(a) is one of the crack breaks after threshold segmentation, and Figure 5(d) is the crack fragment in the circle.

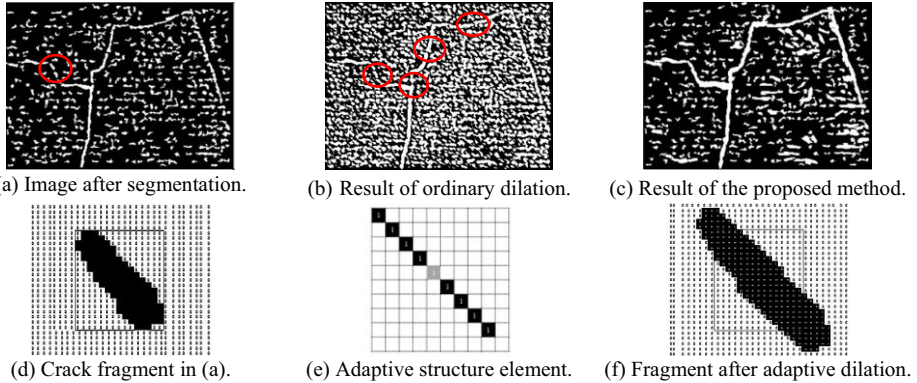


Figure 5. Result of adaptive dilation based on crack direction:(a)-(c), (d)-(f).

Figure 5(e) shows the structural element that is adaptively constructed according to the angle of the fragment θ . When Figure 5(d) is dilated with this structural element, the obtained image is dilated along the direction of θ and does not expand in other directions, as shown in Figure 5(f). Therefore, the dilated crack fragments can be connected to adjacent crack parts, making the crack more complete. Figure 5(b) is the result of common morphological dilation. It can be seen that the morphological operations are performed on each noise and crack fragment; however, there are still multiple crack breaks in the red circle mark. As shown in Figure 5(c), after the application of the method of adaptive dilation based on crack direction given in this paper, crack breaks are completely connected, and only the domains which conform to the crack characteristics have been dilated.

2.3. Multiple filtering based on adaptive feature thresholds

After dilation, the cracks are relatively complete, but it is necessary to further remove non-cracks by filtering. Filtering by using a feature threshold alone is not ideal. A multiple filtering method based on adaptive feature thresholds is proposed. According to the analysis of the results of the feature distributions in Section 2.1, four adaptive feature thresholds, namely T_A , T_{CV} , T_{COM} , and T_L , can be used for filtering, one after another. The process is as follows:

(1). Filtering based on the connected domain area. The image after adaptive dilation is denoted as $f_0(i, j)$, then the connected domain $C_k(x, y)$ can be extracted, the area of each domain is A_k , and the total number is N_A . $f_0(i, j)$ is filtered based on the area adaptive threshold T_A . $f_1(i, j)$ is obtained, as shown in Eq. (2).

$$f_1(i, j) = \begin{cases} 0, & f_0(i, j) \in C_k(x, y) \text{ and } A_k > T_A, k = 1, 2, \dots, N_A \\ f_0(i, j), & \text{otherwise} \end{cases} \quad (2)$$

(2). Filtering based on connected domain convexity. Extract all connected domains $D_k(x, y)$ from $f_1(i, j)$; the convexity of each domain is CV_k and the total number is N_{CV} . The adaptive threshold T_{CV} is used to filter $f_1(i, j)$. $f_2(i, j)$ is obtained, as in Eq. (3).

$$f_2(i, j) = \begin{cases} 0, & f_1(i, j) \in D_k(x, y) \text{ and } CV_k > T_{CV}, k = 1, 2 \dots N_{CV} \\ f_1(i, j), & \text{otherwise} \end{cases} \quad (3)$$

(3). Filtering based on connected domain compactness. Extract connected domains $E_k(x, y)$ from $f_2(i, j)$; the compactness of each domain is COM_k and the total is N_{COM} . Use the adaptive threshold T_{COM} to filter $f_2(i, j)$. $f_3(i, j)$ is obtained, as in Eq. (4).

$$f_3(i, j) = \begin{cases} 0, & f_2(i, j) \in E_k(x, y) \text{ and } COM_k > T_{COM}, k = 1, 2 \dots N_{COM} \\ f_2(i, j), & \text{otherwise} \end{cases} \quad (4)$$

(4). Filtering based on connected domain max-distance. Extract connected domains $F_k(x, y)$ from $f_3(i, j)$; the maximum distance of each domain is L_k and the total number is N_L . Use the adaptive threshold T_L to filter $f_3(i, j)$. $f_4(i, j)$ is obtained, as in Eq. (5).

$$f_4(i, j) = \begin{cases} 0, & f_3(i, j) \in F_k(x, y) \text{ and } L_k < T_L, k = 1, 2 \dots N_L \\ f_3(i, j), & \text{otherwise} \end{cases} \quad (5)$$

The result of the four-stage adaptive morphological filtering is the final crack detection result, as shown in Figure 6. It can be seen that without modeling, the multiple filtering method in this paper can effectively filter out almost all noise and pseudo-cracks, and the cracks in the obtained image are complete and clear. Figure 7 shows the filtering result for an image with cracks without adaptive dilation based on the crack direction. It can be seen that the crack breaks are serious. Therefore, comparing Figure 6 and Figure 7, we can see that the adaptive dilation method proposed in this paper can effectively fill crack breaks and improve the crack integrity, and to a certain extent provide a guarantee for the accuracy of the multi-level filtering based on adaptive thresholds.

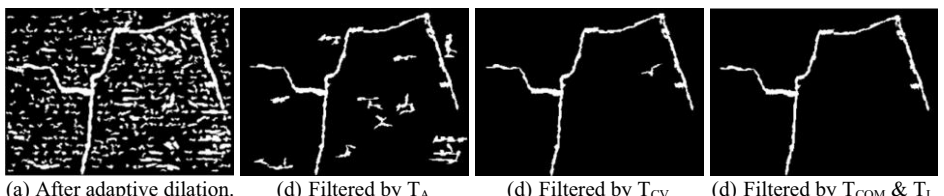
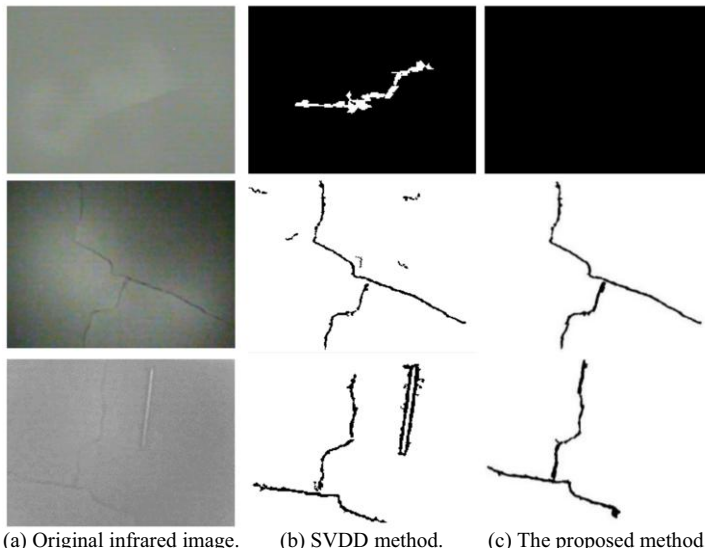


Figure 6. Result of multiple adaptive feature threshold filtering:(a)-(d).



Figure 7. Result of multiple filtering based on adaptive feature thresholds without adaptive dilation:(a)-(b).



(a) Original infrared image. (b) SVDD method. (c) The proposed method.

Figure 8. Original infrared image and detection result.

The test results of this method and Support Vector Data Description (SVDD) [19] are compared in Figure 8. The crack image detected by SVDD usually has breaks, and there are still some noise and pseudo-cracks in the image, which need to be identified one by one to distinguish them from a real crack. Based on the proposed method, when there is no crack in the original image, the method can accurately detect no crack in the image. In the case of uneven illumination, the method can still accurately detect clear and complete crack images. A disturbing object on the concrete surface will also be filtered out, leaving only the crack image.

3. Validity of the method

Some quantitative indicators are used to evaluate the performance of the detection methods and the results of this paper [20]. For the crack image detection results, TP (true positives) is the number of crack images detected correctly, TN (true negatives) is the number of non-crack images detected correctly, FP (false positives) is the number of non-crack images detected as crack images, and FN (false negatives) is the number of crack images detected as non-crack images.

The test sample images were taken from laboratory concrete samples and bridge surfaces using the TC388 uncooled focal plane infrared sensor module with maximum supported resolution of 640×480 pixels, including 123 crack images and 43 non-crack images, with a ratio of 3:1. For the image processing and filtering method proposed in this paper, as shown in Figure 1, the results are shown in Table 1. For further comparative verification, we selected 43 infrared images with cracks and 43 images without cracks, and compared the results with those of the algorithm CrackIT [21-22] and SVDD [19] in recent years, as shown in Table 2.

Table 1. Detection performance

TP	TN	FP	FN	Accuracy	Precision	Recall	FPR
121	40	3	2	96.99%	97.58%	98.37%	6.98%

Table 2. Detection accuracy of the three algorithms

Crack IT method	SVDD method	The proposed method
70.34%	92.49%	95.35%

Table 1 and Table 2 show that the proposed crack detection algorithm can not only filter out most of the interference and pseudo-cracks, but also has higher detection accuracy. In actual images, the detection accuracy of the CrackIT algorithm is not ideal due to uneven illumination, etc. In this paper, by using the difference of morphological characteristics between real cracks and noise and pseudo-cracks, the proposed adaptive morphological dilation and multiple filtering based on adaptive feature thresholds method can obtain and detect real cracks effectively, with a high detection accuracy of 95.35%. This method has a fast processing speed and a detection time of 0.35s, which meets the requirements of real-time detection of concrete bridge cracks and is suitable for practical engineering applications.

4. Conclusion

This paper proposed a real-time crack detection method for bridge concrete based on infrared images. Generally, crack detection methods based on image processing often have the problem of crack breaks after threshold segmentation, resulting in low detection accuracy or incomplete cracks detected. To address this problem, an adaptive morphological dilation method based on crack direction is proposed in this paper, which can not only enhance the completeness of crack images, but also protect the crack edges to a certain extent. Most of the existing crack image detection methods attempt to achieve high detection accuracy by increasing the algorithm complexity, which is not suitable for application scenarios that require real-time detection. This paper proposed a detection method using multiple filtering based on adaptive feature thresholds, which can filter out almost all noise and pseudo-cracks, and finally detect complete real cracks without modeling. It is simple and reliable, with a detection accuracy that can reach 95.35%. It has a fast processing speed and takes 0.35 seconds for detection, which meets the requirements of real-time processing and is suitable for practical engineering applications.

References

- [1]. Zhang J, Wang FY, Wang K, et al. Data-Driven Intelligent Transportation Systems: A Survey. *IEEE T. Intel. Transp.* 2011, 12(4):1624-1639.
- [2]. Miguel G, David B, Oscar M, Llorca DF, Sotelo MA. Adaptive road crack detection system by pavement classification. *Sensor. Basel.* 2011,11(10):9628-9657.
- [3]. Feizi-Derakhshi, Mohammad-Reza, Azarafza. Computer modeling of crack propagation in concrete retaining walls: A case stud. *Comput. Concrete.* 2017,19(5):509-514.
- [4]. Dai Y, Wang P, et al. Asphalt pavement pothole detection and segmentation based on wavelet energy field. *Math. Prob. Eng.* 2017(8), 1-13.
- [5]. Zou Q, Cao Y, Li Q. CrackTree: automatic crack detection from pavement images. *Pattern Recognition Letters.* 2012, 33(3):227-238.
- [6]. Su T, Yang M. Morphological segmentation based on edge detection-II for automatic concrete crack measurement. *Computers & Concrete.* 2018,21(6):727-73.
- [7]. Shi Y, Cui L, Qi Z, Fan M, Chen Z. Automatic road crack detection using random structured forests. *IEEE Transactions on Intelligent Transportation Systems.* 2016, 17(12): 3434-3445.
- [8]. Zhao G, Wang T, Ye J. Anisotropic clustering on surfaces for crack extraction. *Machine Vision & Applications.* 2015,26:675-688

- [9]. Jahanshahi MR, Masri SF, et al. An innovative methodology for detection and quantification of cracks through incorporation of depth perception. *Machine Vision and Applications*. 2013, 24(2):227-241.
- [10]. Lee B Y, Kim Y, Yi S T, et al. Automated image processing technique for detecting and analyzing concrete surface cracks. *Structure and Infrastructure Engineering*. 2013, 9(6): 567-577.
- [11]. Jang K, Kim N, An Y K. Deep learning-based autonomous concrete crack evaluation through hybrid image scanning. *Structural Health Monitoring*. 2019, 1475921718821719
- [12]. Nguyen N T H, Le T H, Perry S, et al. Pavement Crack Detection using Convolutional Neural Network. ACM Association for Computing Machinery, Da Nang, Viet Nam, December.2018.
- [13]. Ye H W, Duan X, Yang J C. Research on fatigue crack detection of steel bridge based on infrared thermal imaging. *National Bridge Academic Conference*. 2014,180-185.
- [14]. Tashan J, Al-Mahaidi R. Detection of cracks in concrete strengthened with CFRP systems using infrared thermography. *Composites Part B Engineering*. 2014, 64:116-125.
- [15]. Jang K, An Y K. Multiple crack evaluation on concrete using a line laser thermography scanning system. *SMART STRUCTURES AND SYSTEMS*. 2018, 22(2):201-207.
- [16]. Xu Z, Zhao X, Song H, et al. Asphalt pavement crack recognition algorithm based on histogram estimation and shape analysis. *CHINESE JOURNAL OF SCIENTIFIC*. 2010(10):102-108.
- [17]. Xu G, et al. A method for surface fracture extraction of structures based on the characteristics of multiple connected domains. *Huazhong Univ.of Sci.& Tech.(Natural Science Edition)*. 2019, 47(10):52-55+68.
- [18]. Fujita Y, Hamamoto Y. A robust automatic crack detection method from noisy concrete surfaces. *Machine Vision & Applications*. 2011, 22(2):245-254.
- [19]. Lin W G, Sun Y C, Yang Q N, Lin Y R. Real-time comprehensive image processing system for detecting concrete bridges crack. *Computers and Concrete*. 2019,23 (6): 445-457.
- [20]. Prasanna P, Dana K J, Gucunski N, et al. Automated crack detection on concrete bridges. *IEEE T. Autom Sci. Eng*. 2016, 13(2):591-599.
- [21]. Oliveira H, Correia P L. Automatic road crack detection and characterization. *IEEE T. Intell. Transp*.2013,14(1):155-168.
- [22]. Oliveira H, Correia P. CrackIT-an image processing toolbox for crack detection and characterization. *IEEE International Conference on Image Processing*, Paris, France, October. 2014.

Hardware Detection Method of Transmission Line Patrol Inspection Image Based on Improved YOLOV4 Model

Wang Ning¹, Zhao Hanghang, Zheng Wulue, Wang Chaoshuo

CSG EHV Power Transmission Company, China

Abstract. In order to solve the problem of intelligent hardware detection in aerial images, a hardware target detection method based on improved YOLOV4 model is proposed. In order to solve the problems of dense hardware and occlusion in aerial images, the improved network based on channel and spatial hybrid attention mechanism can further improve the detection effect of dense occlusion hardware and reduce image false detection and missed detection. In order to solve the problem that there is a great error in the position of the detection frame caused by the interference between the hardware and the hardware and between the hardware and the background, the prior frame is optimized by K-means++, and it is determined that the anchors generated by K=12 is the best, and the detection boxes are more suitable for the target. The experimental results show that the proposed method solves the problems of missing detection, misdetection and inaccurate detection frame to some extent, in which the mAP (mean Average Precision) value of the performance index is increased from 65.03% to 70.72%. The research can lay a good foundation for further state detection and fault diagnosis of typical hardware.

Keywords. Hardware; YOLOV4; target detection; anchor optimization; mixed attention mechanism

1. Introduction

Transmission line fault is one of the important causes of large-scale power outages, and line operation and maintenance is an important link to ensure the safety of power system. Hardware is a metal component widely used in transmission lines[1]. High-precision automatic detection of hardware targets in aerial inspection images of transmission lines is the basis of its state detection and fault diagnosis.

The aerial hardware data set has the characteristics of diverse shapes of similar objects, diverse target angles, complex background and widespread target density. Even if the corresponding model parameters are adjusted and improved for YOLOV4[2], there are still two problems: (1). Due to a large number of shielding between the hardware and the hardware or between the hardware and the background, as well as the blurring of the features between the hardware and the background, the

¹ Corresponding Author, Wang Ning, CSG EHV Power Transmission Company, Guangzhou, China; E-mail: wangning1@ehv.csg.cn.

regression of the detection frame is not accurate. (2). For the dense part of the hardware, there will be the problem of misdetection and omission of small fittings.

Some common methods of hardware inspection are introduced in section 2, and their shortcomings are analyzed. In order to effectively solve the above two problems in section 3, this paper makes two improvements based on the YOLOV4 model. Aiming at the problems of dense hardware and occlusion in aerial images, an improved network based on channel and spatial hybrid attention mechanism is used in section 3.1 to improve the detection effect of the model on dense occlusion hardware and reduce image misdetection and missed detection. In order to solve the problem that there is a great error in the position of the detection frame caused by the interference between the hardware and the hardware and between the hardware and the background, the prior frame is optimized by using K-means++ in section 3.2, and it is determined that the anchors generated by K=12 is the best, and the detection frame is more suitable for the target to improve the accuracy of model detection. The experimental environment and data set information are given in section 4, and our model is analyzed quantitatively and qualitatively. The effect of the model is compared with two evaluation indicators, and then the test results are qualitatively analyzed. In section 5, the improved YOLOV4 is summarized.

2. Research status

With the increasing maturity of target recognition algorithm, the intelligent image processing technology of power system patrol inspection has also made great progress. At present, the existing transmission line image hardware detection methods are mainly divided into two categories: one is transmission line hardware recognition and detection based on traditional image processing and machine learning algorithm, the other is transmission line hardware recognition and detection based on deep learning algorithm [3]. The transmission line image recognition algorithms based on traditional image processing and machine learning algorithms mainly include: traditional power component recognition algorithms which rely on manually designed feature descriptors such as SIFT (scale invariant feature transformation), edge detector and HOG (directional gradient histogram)[4]. A step-by-step identification method of insulators based on target suggestion algorithm and structure search is proposed in reference [5]. Reference[6]after preprocessing the aerial image, the Haar features of the shock hammer are extracted from the image to train the AdaBoost classifier, and a method based on multi-view matching is proposed to reduce the missed detection rate of the shock hammer. The identification and detection of transmission line fittings based on deep learning algorithm mainly includes: in reference [7], FasterR-CNN[8]model is used in the detection of voltage sharing ring and shock hammer. In reference [9], a target decomposition and aggregation algorithm based on YOLOV3[10]model is proposed for insulator target detection in aerial images. As the latest deep learning target detection model based on regression method, YOLOV4 has high recognition accuracy and recognition speed. In view of the dense target set of transmission line hardware data, this paper improves the YOLOV4 model and achieves excellent results in 13 kinds of hardware detection.

3. Research methods

YOLOV4 is an object detection model which has been used in a variety of detectors since the release of YOLOV3, which can improve the detection accuracy of tricks, and improve on the basis of YOLOV3. Compared with YOLOV3 and YOLOV4, it not only ensures the speed, but also greatly improves the detection accuracy of the model. YOLOV4 has mainly made the following changes. For the backbone of feature extraction, they use CSPDarknet-53, compared to YOLOV3's Darknet, which uses cross-stage partial connection. The spatial pyramid pool [11] is used as the neck of the CSPDarknet-53 because it increases the receptive field, distinguishes the most important features, and does not slow down. The path aggregation network [12] is used instead of the feature pyramid network [13]. For the header, they used the original YOLOV3 network.

We recommend adding the following to YOLOV4, and we use the following methods to improve hardware detection on the hardware dataset.

3.1. Mixed Attention (MA)

Because the aerial image hardware detection is different from the existing general target detection, the existing classical general target detection mainly deals with images with a size of 1000×600 or less, while the size of the aerial images captured by the actual UAV patrol line is about 5000×3000 , of which more than 96% of the targets account for less than 0.05% of the images. Too small target proportion leads to a large number of missed detection. The use of multi-scale target detection in YOLOV4 can improve this problem. In the existing model, whether down-sampling the image or feature image to a fixed size will greatly lose the important information of the small target in the aerial image. In order to solve this problem, this paper uses the MA, to add MA to the down-sampling, which can make the model focus on the target feature more easily, so as to improve the detection rate of hardware.

First of all, the original attention mechanism of YOLOV4 is improved. On the basis of the spatial attention mechanism improved by the author, the information in the effective region can be more highlighted by adding the channel attention mechanism. The structure of the improved channel and space mixed attention mechanism is shown in figure 1. By adding the channel attention mechanism, the input features are averaged and maximized along the channel dimension. The output of the two is combined to get the feature descriptor. Finally, the convolution operation is used to encode, and the spatial attention map is obtained. The characteristic graph dimension of the output of the whole channel and spatial attention mechanism is the same as the input dimension, there is no need to make great changes to the network structure, and the parameters of the full connection layer are compressed according to the dimension reduction ratio of rust 16, which can weigh the balance between performance and propagation speed [14]. Due to the introduction of a more complex structure, the speed is slightly slower than the original spatial attention mechanism module, and the introduced computing time is mainly focused on the full connection layer and the pooled part of the channel. The full connection layer is used in the channel attention module, and the full connection layer is used because it has a global receptive field. in the channel attention module, what we need to get is the weight of each channel. This actually needs to include global information. The above improvements can not only help the network to classify and

locate objects more accurately, but also improve the problem of missing detection of small hardware under dense targets.

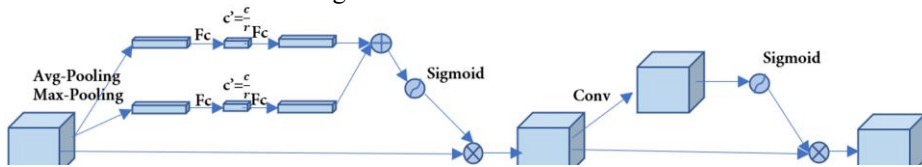


Figure 1. Based on channel and spatial attention mechanism.

3.2. Prior Anchor Optimization (PAO)

In the one-stage object detection algorithm, a prior anchor is widely used to set the initial dimension of the bounding box. YOLOV4 uses the K-means algorithm to generate nine prior anchor, from the coco dataset. In order to solve the defect caused by the random initialization of the clustering center in the original K-means algorithm, this paper introduces K-means++ to optimize the K clustering centers according to the following ideas: suppose n initial clustering centers have been selected ($0 < n < K$). When selecting the $n + 1$ cluster center, the farther away from the current n cluster center will have a higher probability of being selected as the $n + 1$ cluster center. The random method is also used when selecting the first clustering center ($n=1$). It can be said that this is also in line with our intuition: of course, the clustering centers are as far away from each other as possible. Although this improvement is intuitive and simple, it is very effective.

In order to determine the k value, we need to make a tradeoff between the ideal overlap value and the tolerable training time[15]. Increasing the k value will certainly increase the IoU(overlap)[16], but it will also greatly increase the computational overhead, because the number of convolution filters will increase linearly, thus increasing the training time. In the experiment, we draw the curve of the average IOU versus the K value, as shown in the figure, if the best K value is estimated according to the ElbowMethod method, if a certain K value makes the slope of the average IOU change obviously, then this K value is what we want. We find that the average IoU value of K=12 is 74.10% (while that of K=9 is 70.29%).

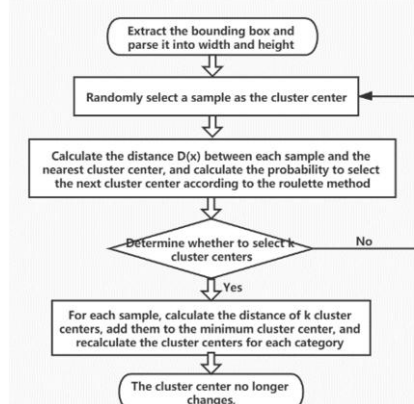


Figure 2. K-means++ Algorithm flowchart

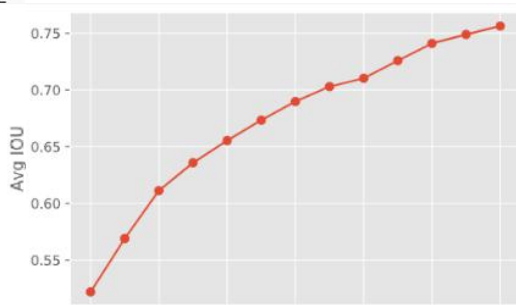


Figure 3. K-Avg IOU curve graph

4. Experimental results and analysis

The data set used in the first phase of this experiment includes 13 kinds of hardware targets, a total of 3774 images and 8738 tags, in which the ratio of training set to test set is 8:2. Most of the image sizes in the data set are 5000×4000 pixels, the input size of the GPU used is GTX1080, network is 416x416, the learning rate is set to 0.0013Maxbatchessbands 26000, the learning rate is adjusted in 20800 and 23400 iterations, and the weight is attenuated to 0.0005 using mosaic data enhancement.

In YOLOV4+MA, we use the improved channel and space hybrid attention mechanism, which can make the model better focus on the useful features in the image during training and detection, improve the problem of missed detection of dense targets, help to overcome the problem of image detection under different weather conditions, and improve the map@0.5 by 1 point.

In YOLOV4+PAO, we use IOU as a metric and Elbow Method to estimate the optimal K value of 12. Although the training time of the 12 prior anchor, is increased a little, the detection box generated by the optimized prior anchor, is more consistent with the real target, and the map@0.5 can be improved by 4 points.

With the comprehensive use of MA and PAO in YOLOV4, the experimental results are shown in Table 1, which can improve map@0.5 by 5.7 points.

Table 1. The original yolov4 and the method presented in this paper are used to detect the AP (Average Precision) values of each type of fittings and the mAP@0.5 values of 13 types of fittings in the transmission line aerial photograph data (YOLOV4 uses IoU > 0.5 by default).

Classes	YOLOV4	YOLOV4+MA+PAO
pre-twisted suspension clamp	45.36%	56.16%
bag-type suspension clamp	89.17%	91.81%
compression-type strain clamp	44.44%	45.24%
wedge-type strain clamp	48.46%	60.11%
hanging board	58.00%	61.17%
u-type hanging ring	70.48%	66.02%
yoke plate	55.49%	58.83%
parallel groove clamp	89.18%	92.14%
shockproof hammer	71.49%	77.19%
spacer	90.45%	89.75%
grading ring	23.21%	52.98%
shielded ring	92.99%	92.35%
adjusting board	66.71%	75.60%
map@0.5	65.03%	70.72%

In view of the fact that misdetection and omission have a great impact on the operation and maintenance of transmission lines, in order to meet the needs of hardware fault detection in actual power inspection, the practical effect of the combination of identification algorithm and company inspection work is realized. In addition to using the general evaluation index mAP in the field of target detection, this paper also uses the artificial intelligence algorithm evaluation method (val), which comprehensively measures the application effect of recall rate recall, accuracy precision and average accuracy AP, which is organized by the national network operation and inspection department. Its calculation formula is as follows:

$$\text{val} = 0.3 * \text{recall} + 0.2 * \text{precision} + 0.5\text{mAP} \quad (1)$$

It can be seen from Table 2 that the comprehensive use of PAO and MA, model has a higher recall rate, which can improve the problem of missing detection of hardware and improve the accuracy of detection, which is very important in the actual inspection task.

Table 2. Compare the original YOLOV4 and the method of this paper on the hardware data set for recall, precision, map and val of the test set.

Method	Recall	Precision	Map	Val
YOLOV4	0.69	0.76	0.65	0.693
YOLOV4+PAO+MA	0.74	0.8	0.707	0.736

In order to more intuitively show the high-precision detection performance and targeted improvement effect of this method, this paper increases the visualization experiment of the test data results. Figure 4 (a), (c) and (e) are the detection results of some images in the hardware image test set using only the adjusted original YOLOV4 model. Figure 4 (b), (d) and (f) are the detection results of the comprehensive application of PAO/MA method, including the target category, score and boundary box. As can be seen from figure 4 (a) and figure 4 (b), the light intensity of this sample is high due to the influence of weather. In this method, there is no missed detection, at the same time, the coincidence degree of the boundary box is higher, there is no serious deformation of the detection box, and too much redundant information is not classified into the detection frame. As can be seen from figure 4 (c) and figure 4 (d), for dense hardware detection, two small fittings in the original YOLOV4, u-type hanging ring and hanging board, have been missed, but all of them have been detected by this method. As can be seen in figure 4 (e) and figure 4(f), one of the lifting-type suspension clamps is disturbed by another heavy hammer fitting, which leads to false detection of fittings. The YOLOV4 model does not have a good generalization ability for this situation, but after using this method, the model can detect this interference more completely, indicating that it has better generalization performance.

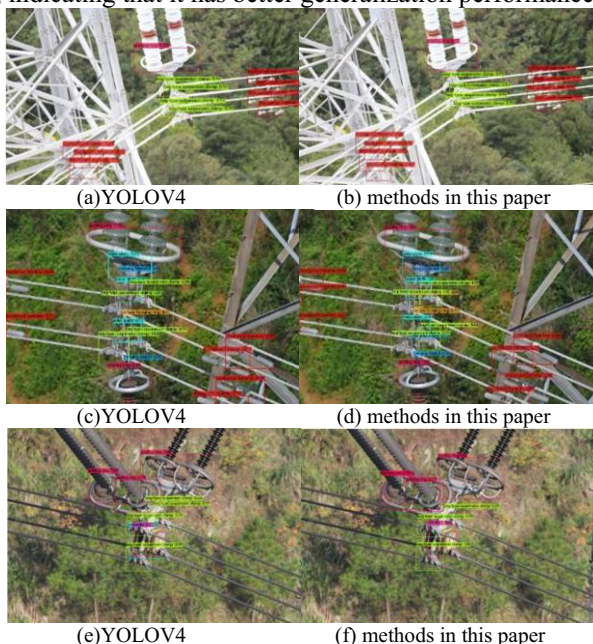


Figure 4. Visualization of YOLOV4 and methods in this paper

5. Conclusion

In this paper, a hardware detection method of transmission line aerial image based on improved YOLOV4 model is proposed. The improved mixed attention mechanism is used in YOLOV4 model, which can better detect small hardware with complex background and dense targets, optimize a priori anchor, and make the detection frame better match the real target frame. The improved detection method shows the excellent performance of small target and dense target detection under complex background, which improves the average accuracy of multi-targets to 5.69%, which lays a foundation for the subsequent defect state detection of hardware and its surface bolts. The method of this paper is quick to deploy and easy to operate, and can be extended to other application scenarios. In the future work, we will focus on solving the problem of model compression in order to deal with the embedded environment with limited space.

References

- [1] JIANG Xiuchen, LIU Yadong, FU Xiaofei, XU Peng, WANG Shaoqing, SHENG Gehao. Construction Ideas and Development Trends of Transmission and Distribution Equipment of the Ubiquitous Power Internet of Things[J]. High Voltage Engineering, 2019,45(5): 1345-1351.
- [2] Bochkovskiy, A., Wang C.,Mark Liao, H. (2020). "YOLOv4: Optimal Speed and Accuracy of Object Detection".arXiv:2004.10934v1 [cs.CV] 2020, 23 Apr.
- [3] WANG Wanguo, TIAN Bing, LIU Yue, LIU Liang and LI Jianxiang. Study on the electrical devices detection in UAV images based on region based convolutional neural networks[J]. Journal of Geo-information Science, 2017, 19(2):256-263.
- [4] Zhang Xiaochun, Ouyang Guangze, He Hongying, Ding Yujie. Zero-insulator detection based on infrared images matching[J]. Electrical Measurement & Instrumentation, 2019,56(6):100-105.
- [5] Zhai Yongjie, Wang Di, Zhao Zhenbing. Recognition Method of Insulator Based on Object Proposals and Structure Research[J]. Journal of North China Electric Power University, 2016, (4):66-71.
- [6] Wang Sen. Research on Algorithms of Vibration Damper Detection on Power Line Image[D]. Beijing:Beijing Jiaotong University Masters's Degree Thesis, 2017.
- [7] Tang Yong, Han Jun, Wei Wen Li, Ding Jian, Peng Xin Jun. Research on part recognition and defect detection of transmissionline in deep learning[J]. Electronic Measurement Technology, 2018, 41(6): 60-65.
- [8] Ren S, He K, Girshick R, et al. Faster R-CNN: Towards Real-Time Object Detection with Region Proposal Networks[J]. IEEE Transactions on Pattern Analysis & Machine Intelligence, 2017, 39(6): 1137-1149
- [9] Gao Qiang, Lian Qiwang. Research on target detection of insulator in aerial image[J]. Electrical Measurement & Instrumentation, 2019, 56(5): 119-123.
- [10] YOLOV3: An Incremental Improvement. Dataset available from <https://pjreddie.com/media/files/papers/YOLOv3.pdf>.
- [11] Kaiming He, Xiangyu Zhang, Shaoqing Ren, and Jian Sun.Spatial pyramid pooling in deep convolutional networks for visual recognition. IEEE Transactions on Pattern Analysis and Machine Intelligence (TPAMI), 2015, 2, 4, 7, 37(9):1904–1916.
- [12] Shu Liu, Lu Qi, Haifang Qin, Jianping Shi, and Jiaya Jia., Path aggregation network for instance segmentation. In Proceedings of the IEEE Conference on Computer Vision and Pattern Recognition (CVPR), 2018, pages 8759–8768.
- [13] Tsung-Yi Lin, Piotr Dollár, Ross Girshick, Kaiming He,Bharath Hariharan, and Serge Belongie. Feature pyramid networks for object detection. In Proceedings of the IEEE Conference on Computer Vision and Pattern Recognition (CVPR), 2017. 2, pages 2117–2125.
- [14] Woo, S., Park, J., Lee, J., & Kweon, I. CBAM: Convolutional Block Attention Module. (2018)ArXiv, abs/1807.06521.
- [15] Redmon, J., & Farhadi, A.. YOLO9000: better, faster, stronger. In Proceedings of the IEEE conference on computer vision and pattern recognition. 2017, pp. 7263-7271.
- [16] Zheng, Z.; Wang, P.; Liu, W.; Li, J.; Ye, R.; and Ren, D. (2020). Distance-IoU Loss: Faster and Better Learning for Bounding Box Regression. AAAI 2020

The Relation of Career Adaptability to Values Realization Degree and Organizational Citizenship Behavior

Qingsong Zhu¹, Ruiting Tan, Ping Wang

Sichuan University, Chengdu, Sichuan

Abstract. The sudden outbreak of the pandemic COVID-19 inevitably has a great impact on economic and social development. Therefore, the innovation-driven value becomes more and more prominent. Through literature review, it is not difficult to find that values have gradually become an important reference standard for organizations to select talents for their teams, as well as an important reference factor for studying organizational citizenship behavior. In order to explore the relationship between values realization degree and organizational citizenship behavior, this investigation based on the social interaction theory was conducting using a sample of enterprise staff (N=358). In this paper, LISRELV9.2 and SPSS21.0 were used to analyze the sample data, including descriptive statistical analysis, common variance deviation test, reliability and validity test, one-way ANOVA, correlation analysis, regression analysis, and validation of mediating effects. The results showed that values realization degree positively predicted organizational citizenship behavior, and job satisfaction played an intermediary role in the relationship between values realization degree and organizational citizenship behavior. Besides, there were some differences between the relation that work values realization degree and organizational citizenship behavior acted on organizational citizenship behavior.

Keywords. Work values realization degree, life values realization degree, job satisfaction, organizational citizenship behavior

1. Introduction

With the blurring of organizational boundaries in modern enterprises, the work contents become more challenging. Organizational citizenship behavior was the positive behavior of employees beyond their work roles and was not easily affected by work regulations or work formulations, and could promote organizational performance and innovative behavior [1]. Hence, how to promote organizational citizenship behavior had attracted more and more attention in organizational management.

According to previous literature, values, as the basis for understanding individual attitude cognition and intrinsic motivation, played a leading role in individual behavior. It was an important variable that studying organizational citizenship behavior. The predictive effect of values on organizational citizenship behavior had been widely recognized by researchers [2]. However, the majority of scholars mainly discussed the

¹ Corresponding Author: Ruiting Tan, Sichuan University, Chengdu, Sichuan, China; E-mail: 574409032@qq.com

influence of values and organizational citizenship behavior from the perspective of individual cognition and behavior, and ignored the role of the environment and emotional attitude. Values were only intrinsic values formed by employees, which could not effectively explain the interaction between employee values and the organizational environment. According to the social interaction theory, human socialization was inseparable from environment, and individual behavior was the product of the interaction between internal cognition and environment. In other words, employees participate in organizational activities and cannot be separated from the organizational environment, it is particularly important to explore the relationship between values and the interactive results of the environment and organizational citizenship behaviors. Besides, in an enterprise, the interaction between employee values and the organization will form value perception or evaluation of the organization. Based on this interactive result, employees tended to form emotional attitudes and made decisions about whether to conduct organizational citizenship behavior.

Therefore, based on the perspective of social interaction theory, this paper introduced the values realization degree as an effective predictor variable and measured the work values and life values realization degree in the organization. In the end, this paper made it easier for managers to track the data of values realization degree to accurately predict employee behavior and made reference to management decisions and enriched the theoretical study of values and behaviors.

2. Hypothesis and model construction

2.1 Values realization degree and organizational citizenship behavior

Values realization degree refers to the degree which is satisfied or realized in the organizational environment. It is the result of the interaction between individual motivation and organizational environment [3]. Organizational citizenship behavior is an extra role behavior which is not subject to formal regulations and is beneficial to the organization and team [4]. Organizational citizenship behavior has different cultural backgrounds. The spirit of western social psychology lies in individual orientation, while the essence of social psychology in China lies in relationship orientation, and the behavior of employees in China will be affected by the individual relationship background [5]. According to the social interaction theory, the socialization of individual cannot be separated from environment. In organizational context, employee behavior is influenced by the interaction between personal motivation and the organizational environment. If the values of the employees are satisfied well, this interactive result will strengthen the work motivation and attitude of the employees, and further stimulate the employees to make a series of extra-role behaviors. XingChun Xu, a domestic scholar, found that the higher the work values realization degree, the stronger the sense of organizational belonging felt by employees [6]. So they were more likely to take extra-role actions and to repay the satisfaction of the organization to its own work values.

2.2 The mediating role of job satisfaction

Job satisfaction is based on the psychological feeling of the working environment [7]. Smith & Kendall et al. believed that job satisfaction is an emotional response which is based on the gap between employees' expectations and reality [8]. Scholars agreed that the degree of employees' satisfaction with work depends on the degree of job adaptation. When values realization degree in the organization is high, the needs of employees at the individual level will be well satisfied. Employees were more likely to promote the positive emotional state of employees. Meanwhile, job satisfaction had a direct predictive effect on employee behavior [9]. The higher job satisfaction was, the easier it was for employees to generate positive emotions and implement behaviors beneficial to the organization, such as high performance and organizational citizenship behaviors [10]. Organ & Ryan also found that job satisfaction and organizational citizenship behavior were positively correlated. In addition, job satisfaction was closely related to their values orientation [10]. When the organization meets employees' material and spiritual expectations, employees tend to spontaneously reflect high levels of role and out of role behavior performance based on positive emotions [11].

Based on the above analysis, this article made the following hypothesis.

H1a. Life values realization degree positively affect organizational citizenship behavior.

H1b. Work values realization degree positively affect organizational citizenship behavior.

H2a. Life values realization degree positively affect job satisfaction.

H2b. Work values realization degree positively affect job satisfaction.

H3. Job satisfaction is significantly positively correlated with organizational citizenship behavior.

H4a. Job satisfaction mediates the relationship between work values realization degree and organizational citizenship behavior.

H4b. Job satisfaction mediates the relationship between life values realization degree and organizational citizenship behavior.

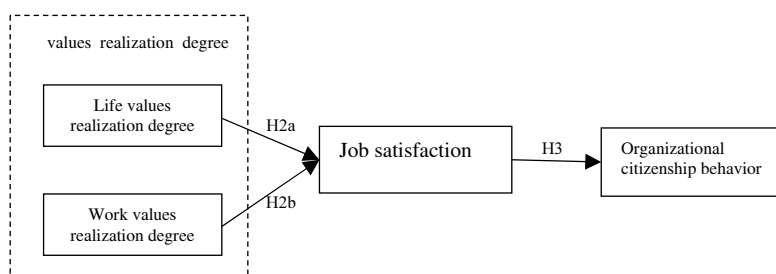


Figure 1. Research framework and model

3. Methods

The study selected 36 enterprises from Beijing, Shanghai, Zhejiang, Sichuan, Chongqing and Hubei to recover questionnaires, covering more than 20 industries, for example, Internet, electronics, finance, water and electricity. Meanwhile, in order to avoid homology error, the work values realization degree questionnaire and the job satisfaction questionnaire were filled out by the employees. But the organizational citizenship behavior was matched by the supervisor. A total of 461 sets of questionnaires were distributed and 385 questionnaires were recovered, with an effective recovery rate of 92.9%. All participants are voluntary and the questionnaires are made anonymous.

4. Results

4.1 Reliability and validity test

According to confirmatory factor analysis results (Table 1), Values realization degree scale (X^2/df) was close to 1, RMR was less than 0.05, GFI, AGFI, CFI, IFI and other indicators were all greater than 0.8. Therefore, the scale selected in this paper has a good validity. The job satisfaction and organizational citizenship behavior scale (X^2/df) is close to 1, RMR is less than 0.05, GFI, AGFI, CFI, IFI and other indicators are greater than 0.7. Therefore, the scale selected in this paper has a good validity, and its reliability and validity has also been verified to some extent in previous studies of scholars.

Table 1: Results of confirmatory factor analysis

Index	df	X^2/df	GFI	AGFI	CFI	IFI	RMR
VRD	2.45	0.81	0.79	0.89	0.87	0.89	0.04
JS	3.23	0.79	0.76	0.81	0.79	0.82	0.04
OCB	3.11	0.82	0.78	0.84	0.79	0.77	0.04

Note: VRD= Values realization degree; JS=Job satisfaction; OCB= organizational citizenship behavior.

4.2 Correlation analysis

The results of bivariate correlation analysis (Table 2) showed that there was a significant positive correlation between life values realization degree and work values realization degree ($r=0.537$, $p<0.01$), job satisfaction ($r=0.294$, $p<0.01$), and organizational citizenship behavior ($r=0.263$, $p<0.01$). so H1a was preliminarily verified. There was a significant positive correlation between work value realization and organizational citizenship behavior ($r=0.262$, $p<0.01$) and job satisfaction ($r=0.248$, $p<0.01$). so H1b was preliminarily verified. Besides, there was a significant positive correlation between employee satisfaction and organizational citizenship behavior ($r=0.158$, $p<0.01$), and a significant positive correlation between work value realization and organizational citizenship behavior ($r=0.312$, $p<0.01$). So H3 was preliminarily established.

Table 2. Correlation analysis

	Position	Time	Sex	Age	LVRD	WVRD	OCB	JS
Position	1	-.052	.162**	-.180**	-.069	-.063	.028	-.049
Time	-.052	1	-.020	.399**	-.038	-.123*	-.131*	-.083
Sex	.162**	-.020	1	-.017	.151**	.037	.114*	.046
Age	-.180**	.399**	-.017	1	-.080	-.067	-.122*	.103
LVRD	-.069	-.038	.151**	-.080	1	.537**	.263**	.294**
WVRD	-.063	-.123*	.037	-.067	.537**	1	.262**	.384**
OCB	.028	-.131*	.114*	-.122*	.263**	.262**	1	.158**
JS	-.049	-.083	.046	.103	.294**	.384**	.158**	1

Note: * $p<0.05$, ** $p<0.01$, *** $p<0.001$; LVRD=Life values realization degree;

WVRD= work values realization degree; OCB= organizational citizenship behaviour; JS=Job satisfaction;

4.3 Hypothesis test

According to the results of the regression analysis (Table 3), such as age, these variables had no significant influence on job satisfaction and organizational citizenship behavior. The VIF value of each variable was less than 1.500, which was far less than the critical value of 10. Therefore, there was no linear correlation in the equation, which does not affect the test results. In model 2, the regression equation of life value realization degree and job satisfaction is significant ($p<0.001$). In terms of regression coefficient ($r=0.297$, $p<0.001$), life values realization degree has a significant positive prediction effect on job satisfaction, so H2a is verified. In model 3, the regression variance between the life values realization degree and organizational citizenship behavior was significant ($r=0.246$, $p<0.001$). so H1a was established. In model 4, the regression equation of job satisfaction and organizational citizenship behavior was significant ($P<0.05$). From the regression coefficient ($r=0.179$, $P<0.001$), job satisfaction had a significant positive correlation with organizational citizenship behavior of employees. So H3 was established. In model 5, life values realization degree also had a positive prediction effect on the organizational citizenship behavior ($p<0.001$), but the mediating effect of job satisfaction was not significant ($p>0.05$). So H4a was not verified. According to the hypothesis test results (Table 3), the mediating effect of job satisfaction on life values realization degree and organizational citizenship behavior was not significant, and the interval (BootLLCI=-.0052, BootULCI=.0613) contains 0, that was, hypothesis H4a was not valid (Table 4).

Table 3. The regression analysis of life values realization degree, job satisfaction and organization citizenship behavior.

	Job satisfaction			organizational citizenship behavior			
	model1	model2	VIF	model3	model4	model5	VIF
Position	0.016	-0.01	1.079	0.054	0.028	0.054	1.091
Time	-0.100	-0.129	1.202	-0.071	-0.078	-0.064	1.213
Sex	0.074	0.001	1.055	0.076	0.062	0.069	1.032
Age	-0.066	0.17	1.25	-0.062	-0.088	-0.074	1.271
LVRD		0.297**	1.038	0.246**		0.208**	1.145
JS					0.179**	0.089	1.129
R2	0.027	0.114		0.085	0.058	0.091	
F	1.869	30.633		17.432	8.998	1.85	
ΔR2	0.012	0.085		0.058	0.031	0.006	

Note: *p<0.05, **p<0.01, ***p<0.001; LVRD=Life values realization degree; JS=Job satisfaction

Table 4. The intermediary test of job satisfaction in life values realization degree and organizational citizenship behavior.

OUTCOME VARIABLE							
organizational citizenship behavior							
Model Summary							
	R	R-SQ	MSE	F	DF1	DF2	P
Model	0.2625	0.0689	0.2575	10.3234	-0.071	-0.078	-0.064
	coeff	se	t	P	LLCL	ULCI	
Constant	-0.015	0.0302	-0.4973	0.6193	-0.0745	0.0445	
Vlues	0.1823	0.0518	3.52	0.0005	0.0804	0.1675	
DIRECT AND INDIRECT EFFECTS OF X ON Y							
Direct effect of X on Y							
	Effect	Se	t	p	LLCI	ULCI	
	0.1823	0.0518	3.52	0.0005	0.0804	0.2843	
Indirect effect (s) of X on Y							
Job satisfaction	Effect	BootSE	BootLLCI	BootULCI			
	0.0261	0.017	-0.0052	0.0613			

According to the test results, after controlling for the variables such as age and these variables, the VIF values of each variable were far less than the critical value of 10. So there was no linear correlation in this equation. In model 2, the regression equation of work values realization degree and job satisfaction was significant ($p<0.01$). From the regression coefficient ($r=0.297$, $p<0.01$), the work values realization degree had a significant positive prediction effect on employee satisfaction. so H2b was verified. In model 3, the regression equation of work values realization degree and organizational citizenship behavior was significantly positively correlated ($p<0.01$), and the prediction effect was significant ($r=0.227$, $p<0.01$). so H1b was established. In model 4, job satisfaction had a significant positive correlation with organizational citizenship behavior ($r=0.179$, $p<0.01$). Therefore H3 was verified.

In model 4, job satisfaction was significantly mediated ($p<0.05$) between the work values realization degree and organizational citizenship behavior. So H4b was verified.

Table 5. The intermediate inspection of work values realization degree and organizational citizenship behavior

	Job satisfaction			organizational citizenship behavior			
	model1	Model2	VIF	Model3	Model4	Model5	VIF
Position	-0.041	-0.01	1.079	0.056	0.028	0.057	1.091
Time	-0.134	-0.129	1.202	-0.096	-0.078	-0.081	1.213
sex	0.049	0.001	1.055	0.047	0.062	0.043	1.032
age	0.147	0.17	1.25	-0.05	-0.088	-0.067	1.271
GZJZG		0.297**	1.038	0.227**		0.190**	1.145
MYD					0.179**	0.123*	1.129
R2	0.029	0.114		0.093	0.058	0.089	
F	2.367	30.633		20.918	8.998	3.982	
ΔR2	0.129	0.085		0.060	0.031	0.013	

Note: * $p<0.05$, ** $p<0.01$, *** $p<0.001$; WVRD= work values realization degree; JS=Job satisfaction;

5. Discussion

5.1 Conclusion and revelation

The following conclusions are drawn. (1) Values realization degree positively predicts organizational citizenship behavior. (2) Values realization degree positively affects job satisfaction. Employees will form an emotional attitude based on their perception that values are satisfied. (3) Job satisfaction plays an intermediary role in the relationship between values realization degree and organizational citizenship behavior. (4) The life

values realization degree and the work values realization degree have different influence mechanisms on organizational citizenship behavior. The life values realization degree directly affects organizational citizenship behavior. But the work values realization degree influences organizational citizenship behavior through employee satisfaction.

5.2 Implications

First of all, pay attention to the application of employees' values realization degree in management practice. In the selection process, the enterprise presents the relevant information of the organization to the employees reasonably, such as corporate culture, team atmosphere, remuneration, job responsibilities and career development channels. In this way, employees' views and choices on various aspects of the organization are sought to predict the extent to which employees' values are realized in the organizational environment. Then a high reliability and validity assessment tool is established or introduced to achieve the realization of employees' values.

Besides, focus on the role of job satisfaction within the organization and management practices. Enrich the ways and means of obtaining job satisfaction, establish a positive and active two-way feedback mechanism, and break the situation of a single, top-down all-employee survey or satisfaction survey. Secondly, do a good job in analyzing employee satisfaction and reasonable use of job satisfaction of employee behavior.

Finally, exert the influence of organizational environment. By strengthening positive organizational citizenship behaviors, organizations can guide the change of employees' cognition and attitude. For example, talent and organizational development management or organizational values management department seek for employees with high frequency of organizational citizenship behavior to conduct one-to-one interview and communication. The relevant departments conduct personal case publicity in the form of offline lecture forum or online sharing and interaction, create pacesetters of organizational citizenship behavior, and inspire other organizational citizenship behavior.

5.3 Limitations and future research

Although the relationship between value realization degree and organizational citizenship behavior is clarified, some research results have been obtained, but the research still has some limitations. Firstly, the research method adopted in this paper is relatively single, which makes it difficult to fully and accurately express the values of the research. Later researcher can adopt more diversified research methods, such as the combination of interview, observation and questionnaire. Besides, the current research on employee values of intergenerational differences is relatively new. In the future, the researcher can consider the influence mechanism of the value realization degree of the post-90s, post-80s and post-70s generation on the behavior of organizational citizens, and explore the difference of the influence of the value realization degree of different age groups on organizational citizens.

References

- [1] Super DE. A Life-Space Approach to Career Development [J]. Journal of Occupational Psychology, 1980, 16 (3):282-298.
- [2] Kheckholm C K M. Value and value orientation in the theory of action: an exploratiou in definition and classification, Cambridge: Harvard University Press, 1951.
- [3] Qingsong Zhu. An empirical study on the value realization degree matching between employees and organizations and its role [D]. Sichuan University, 2007. Organ D W. Organizational citizenship behavior: The good sol-dier syndrome. Lexington, MA: Lexington Books. 1988.
- [4] Xiaolin Zhang, Zhenjiang Qi. Theory of organizational citizenship behavior and its application [J]. Psychology dynamics, 2001, 9 (4): 352-360.
- [5] Xingchun Xu. Research on the working values of university teachers and their influence effect [D]. Chongqing: southwest university, 2007.
- [6] Hoppock. Job Satisfaction [M].New York: Harper&Row.1935:236-245.
- [7] Smith,Kendall & Hulin. The measurement of Satisfaction in Work and Retirement: A Strategy for the Study of Attitudes [M]. Chicago: Rand McNally and Company. 1969: 166-188.
- [8] Qiwen Qin,Jingzhao Yao,li genqiang. Research on the relationship between work values of enterprise employees and organizational citizenship behavior [J]. Psychological science, 2007, 30 (4): 958-960.
- [9] Hofmans J, De Gieter S,Pepermans R. Individual differences in the relationship between satisfaction with job rewards and job satisfaction[J]. Journal of Vocational Behavior, 2013, 82(1):1-9.
- [10] Robbins, Stephen P. Organizational Behavior; Concepts, Controversies, and Applications [M]. Prentice Hall (Englewood Cliffs, N.J),1993.
- [11] Wiese, B. S.,Freund,A. M.,& Baltes,P. B. Subjective career success and emotional well-being: Longitudinal predictive power of selection, optimization, and compensation. Journal of Vocational Behavior. 2002, 60, 321–335.

Research on the Internal Relationship Characteristics and Their Influences of Knowledge Sharing Multilevel Network in Q&A Community

Chen Xiaohui^{a,1} and Hu Ping^a

^aSchool of Management, Xi'an Jiaotong University

Abstract. The virtual communities have become the main position for people to create and share content in today's society. It not only realizes the dissemination of knowledge and information, but also promotes the formation of the relationship between users. The traditional related studies treat all information in Internet as knowledge, which deviate from the real situation. Therefore, this paper uses text classification technology to classify the answer texts under the topic of "English learning" in the "Zhihu" Q&A community, and extract the real knowledge under the topic. On this basis, a multilevel network about answer-users' knowledge sharing is constructed, and three subgroups with different users' node degree are divided. The multilevel network exponential random graph models are used to explore the influence of local structural characteristics formed by the relationship between users on the whole multilevel network. The results show that: When the node degrees of answer-users are small and the network structure is stable, the initiative of sharing knowledge is small and the homogeneity of knowledge content is high; if there are structural holes in the network, answer-users will create an obvious clustering effect, and the heterogeneity of shared knowledge is high; for the subgroup with the largest answer-users' node degree, the relationship between users is tight and the network structure is stable, then the shared knowledge is more heterogeneous.

Key words. Knowledge sharing; multilevel network ERGMs; text classification

1. Introduction

The transmission of information and knowledge resources based on the Internet has become a mainstream trend. In online Q&A communities, users can ask questions freely and other users will participate in answering questions, which realizes the transfer of knowledge and information. Users' activities may affect the complex information flow within the platform, thus forming a huge social network with levels of nesting. Based on the theories of social capital, social exchange and social cognition, many studies analyze the influencing factors of knowledge sharing in virtual communities [1],[2] and the factors that may affect users' motivation and willingness of

¹ Chen Xiaohui, School of Management, Xi'an Jiaotong University, Xi'an 710049, China; E-mail: 842430599@qq.com.

knowledge sharing in virtual communities [3],[4],[5],[6]. Moreover, the researchers also explore the factors that promote the knowledge sharing behavior of community members [7],[8]. It can be seen that the studies mainly from the perspective of "users" and pay less attention to the impact of local structure generated by the relationship between users on the whole network.

In addition, most of them ignore the interaction between different networks and treat all information as knowledge. Thus, this paper uses the text classification method to classify the answer texts from "Zhihu" Q&A community and extract the real knowledge. In addition, it constructs a multilevel network of answer-users' knowledge sharing and uses the multilevel network exponential random graph models (ERGMs) to explore the possible relationship characteristics created by different network levels' interaction and the influences of the local network structures represented by these relationship characteristics on the overall network.

2. ERGMs and Multilevel network ERGMs

ERGMs can investigate the influence of some local substructures on the whole network through the statistical analysis of network structures. It can draw a conclusion by comparing the statistical results of real network data with the expected values of the variables in the model simulation results [9]. At present, people have gradually extended this kind of researches to more complex fields, such as ERGMs for affiliation network [10] and multilevel network [11].

Multilevel network ERGMs examine multiple networks and the interaction effects between these networks. Due to the complexities and difficulties in this method, the main study is about the model specification and variable selection [12]. Recently, there are few studies apply this method to the real networks [13],[14]. It could explore the possible local structure variables exist in the multilevel network and the interaction effects among different network levels. Different from the traditional empirical research methods, it is an exploratory empirical study method, which helps us to discover the internal features of real networks. Therefore, we use it to achieve the research objectives.

3. Research data and method

3.1 Data

In this study, we use Python to crawl the relevant users' information, questions and answers of "English Learning" topic in Zhihu from 9th November of 2017 to 13th January of 2018. Finally, 6296 answer texts and 6296 answer-users are collected.

At present, there is no standard classification thesaurus for Chinese text classification. Therefore, based on the classification system of Zhihu platform, combined with the classification modes of NetEase, Sina Weibo and other virtual communities, this study constructs the "English learning" answer texts classification vocabulary with 13 tags (Examination, Grammar, Word, Institution, Speaking, Pronunciation, Method, Translation, Materials, Software, Listening, Reading and

Writing). We use the sequence to sequence (Seq2seq) algorithm and combine with the Encoder-decoder module of LSRTM model to improve the algorithm, and finally get 3768 answer texts with tags.

3.2 Multilevel network construction

The multilevel network ERGMs include three levels, Network A and network B are two different levels of network, and the affiliation network generated by their relationship, namely network X, is the middle network [11]. The specific model equation is as follows,

$$P(A = a, B = b, X = x) = \frac{1}{\kappa(\theta)} \exp (\sum \theta_Q Z_Q(a) + \theta_Q Z_Q(x) + \theta_Q Z_Q(b) + \theta_Q Z_Q(a, x) + \theta_Q Z_Q(b, x) + \theta_Q Z_Q(a, b, x)) \quad (1)$$

Where, $Z_Q(a)$, $Z_Q(b)$ and $Z_Q(x)$ represent the network effects of networks A, B and X respectively. $Z_Q(a, x)$, $Z_Q(b, x)$ and $Z_Q(a, b, x)$ are the interaction effects between networks A and X, networks B and X, and three networks A, B, and X, respectively.

A multilevel network about answer-users' knowledge sharing is constructed as follows: **Answer-users network (A)**: If two answer-users answered a same question, their matrix position in the network is marked as 1, otherwise it is 0. **Knowledge network (B)**: According to the results of text classification, the answer texts of users can be divided into 13 knowledge tags. If two different tags appear in a same answer, the matrix position in the network is marked as 1, otherwise it is 0. **Affiliation network (X)**: If one answer user's text contains one Knowledge tag, they are defined as related, and the matrix position is marked as 1, otherwise it is 0.

Network subgroup extraction: Due to the low density of the answer-users network (0.0035), it is difficult to analyze the overall network after text classification. Therefore, we use the node degree method in Pajek to partition the answer-users network. Moreover, the FR algorithm is used to visualize the network [15]. Then, we can extract three subgroups with 54, 66 and 116 node degree, respectively.

4. Model Estimation

Since one of the difficulties of multilevel network ERGMs is model convergence, this paper analyzes the possible network effects in the model and finally obtains the corresponding convergence model of three subgroups. Table 1 shows the parameter estimation results of each model. If the absolute value of the parameter is greater than 2 times of the standard deviation, it is considered to be significant.

Table1: Estimation results of three multilevel networks

Network level	Effects	subgroup 1	subgroup 2	subgroup 3
Network A	Cycle4A	--	0.0001*	--
	EdgeB	-8.7794	-0.0832	1.6366
	Star2B	1.8891	--	-0.2822
Network B	Star3B	-0.4082	--	--
	TriangleB	--	-0.2468	--
	ATB	--	--	0.3114
Network X	XEdge	-2.6599*	--	--
	XACB	0.0938*	-0.035*	-0.0283*
Network B&X	Star2BX	0.4375	--	--
	StarAB1X	-0.2728	--	--
	L3XBX	0.0029	--	--
	EXTB	0.0031	--	--

Note: “*” represents that the parameter estimation result of the variable is significant.

(1) Answer-users network (Network A): The results in Table1 show that under the premise of model convergence, no network effect of network A is found in subgroup1 and 3. This is because the network (A) density of the two subgroups is 1, which means that all nodes are fully connected and the network structures are stable. The network density of subgroup 2 is 0.5, there are unconnected nodes and the parameter estimation result of variable Cycle4A is positive significantly. This parameter reflects the clustering effects in network A. It shows that when there are unrelated nodes in network A, there will be more clusters in the multilevel network. In these small clusters, the relationship between answer-users will be closer, and the knowledge contribution behavior of answering-users will be affected by other users associated with them. Knowledge is transferred to each other in these small clusters to form a closure. Compared with other network structures, this closed structure can make users in the clusters receive more kinds of knowledge, and the transmission performance of knowledge in such clusters would be better. The results of subgroup2 show that when there are obvious structure holes in network A, the aggregation characteristics among answer-users in the multilevel network are more obvious.

(2) Affiliation network (Network X): Network X reflects the knowledge sharing behavior of answer-users. Table1 shows that XEdge participates in the converging of subgroup1 model and is negative significantly. It means that in the subgroup with the smallest node degree of answer-users, people are less inclined to share knowledge. According to social capital theory, the interaction between users has a positive relationship with the amount of knowledge sharing [3]. The parameter XACB indicates the homogeneity tendency of knowledge content shared by different answer-users. When XACB is positive and significant, the more answer-users share the same kind of knowledge. A negative XACB indicates that users pay more attention to the heterogeneity of content when sharing knowledge. Sharing original knowledge can improve users' status and popularity in the platform, and the competition among similar users also makes the answer-users output different knowledge from others. According

to social network analysis theory, the characteristics of users in social network can be expressed as their status in the network, that is, the network reputation of users [16]. The higher the network reputation, the more popular the users are in the network, and the more other users have established relationships with them. For answer-users, sharing original knowledge can make them stand out in the platform and improve their popularity. The recognition of other users to these original knowledges will promote answer-users to get more attention, thus changing their relationship structures, enhancing their reputation in the network and gaining more authoritative network status. On the other hand, if answer-users want to improve their network reputation, they need to create original knowledge which is different from other competitors, improve the attraction of their output content, so as to obtain more recognition and attract more people to establish relations with them.

To sum up, in subgroup 1, the relationship between answer-users is less close than the other two subgroups, and users share less knowledge. At the same time, the knowledge sharing content of users in the corresponding multilevel network of this subgroup is relatively high. For subgroups 2 and 3, the users pay more attention to the heterogeneity of their knowledge output so as to get more attention in the platform. According to the results of network A, there are obvious aggregation characteristics among the answer-users in subgroup 2, and the knowledge heterogeneity shared by these users is higher, which once again confirms the relationship between the closeness of the answer-users and the heterogeneity of knowledge output.

If the absolute value of the goodness of fit t-value is less than 2, it means that the goodness of fit of the model is good, which can fully explain the sample network [11]. The results show that all variables of three models have passed the goodness of fit test, so the results of model estimation are reasonable and meaningful.

5. Conclusion

To sum up, the structural characteristics and relationship compositions of the answer-users network have a significant impact on the knowledge sharing multilevel network, which not only affects the enthusiasm of users to share knowledge, but also affects the heterogeneity of the shared knowledge content. Meanwhile, the shared knowledge content also could affect the relationship between answer-users. In the multilevel network, the structural characteristics and relationship compositions of answer-users network are closely related to the network composed of their shared knowledge. Firstly, relationship structures of answer-users network affect their enthusiasm to share knowledge. When there are fewer associated users in the network and the less edges between answer-users, the narrower the scope of knowledge transmission they share. Therefore, the less sense of achievement the answer-users can obtain from the network, and they are more inclined to output less knowledge. On the contrary, when there are more edges between users, they share knowledge more actively in order to obtain higher sense of achievement and higher network reputation. Secondly, when there are more clusters in answer-users network, these aggregated users respond more closely, and knowledge transferred better between them. However, the higher the homogeneity of shared knowledge content, the lower the probability of being noticed and recognized. In order to stand out from the competition, users tend to output heterogeneous content. In addition, the greater the degree of nodes in answer-users network, the wider the range of knowledge dissemination. Similarly, in

order to distinguish from other answer-users and gain higher reputation in the network, they are more likely to share knowledge with high heterogeneity. This paper extends the social network analysis about knowledge sharing in virtual communities to the multilevel network's extent. The relationship generated by answer-users and the content characteristics of knowledge are integrated to analyze the relationship between local substructures in different network levels and its impact on the whole multilevel network. The relationship characteristics and structural variables that affect the knowledge sharing of users are explored.

In view of the fact that this paper is an exploratory study, it still has some limitations. First, the research does not consider the users' attributes, and how different attributes affect the multilevel network. Second, it only selects the sample data under the topic of "English learning". Whether there are obvious differences in the network under different topics needs further analysis and research.

References

- [1] Li Y, Shan SQ, Li H, et al. An Empirical Study on Knowledge Sharing towards Emergency Events in Virtual Communities. *Management Review*. 2012, 24(11): 88-98+130.
- [2] Moghavvemi S, Sharabati M, Paramanathan T, et al. The impact of perceived enjoyment, perceived reciprocal benefits and knowledge power on students' knowledge sharing through Facebook. *International Journal of Management Education*. 2017, 15(1): 1-12.
- [3] Chiu CM., Hsu MH, Wang G. Understanding knowledge sharing in virtual communities: an integration of social capital and social cognitive theories. *Decision Support Systems*. 2006, 42(3): 1872-1888.
- [4] Chen IYL, Chen NS, Kinshuk. Examining the Factors Influencing Participants' Knowledge Sharing Behavior in Virtual Learning Communities. *Journal of Educational Technology & Society*. 2009, 12(1): 134-148.
- [5] Chang HH, Chuang SS. Social capital and individual motivations on knowledge sharing: participant involvement as a moderator. *Information & Management*. 2011, 48: 9-18.
- [6] Zhang X, Liu S, Deng Z, et al. Knowledge sharing motivations in online health communities: A comparative study of health professionals and normal users. *Computers in Human Behavior*. 2017, 75: 797-810.
- [7] Sun SY, Ju TL, Chung HF, et al. Influence on Willingness of Virtual Community's Knowledge Sharing: Based on Social Capital Theory and Habitual Domain. *International Journal of Human & Social Sciences*. 2010, (53): 142.
- [8] Jin JH, Li YJ, Zhong XJ, et al. Why users contribute knowledge to online communities. *Information & Management*. 2015, 52(7): 840-849.
- [9] Frank O, Strauss D. Markov graphs. *Journal of the American Statistical Association*. 1986, 81(395): 832-842.
- [10] Wang P, Sharpe K, Robins GL, Pattison PE. Exponential random graph (p^*) models for affiliation networks. *Social Networks*. 2009, 31: 12-25.
- [11] Wang P, Robins G, Pattison P, Lazega E. Exponential random graph models for multilevel networks. *Social Networks*. 2013, 35: 96-115.
- [12] Wang P, Robins G, Pattison P, Lazega E. Social selection models for multilevel networks. *Social Networks*. 2016, 44: 346-362.
- [13] Smith M, Gorgoni S, Cronin B. International production and trade in a high-tech industry: A multilevel network analysis. *Social Networks*. 2019, 59: 50-60.
- [14] Mcglashan J, Haye KDL, Wang P, et al. Collaboration in Complex Systems: Multilevel Network Analysis for Community-Based Obesity Prevention Interventions[J]. *Scientific Reports*. 2019, 9. doi:10.1038/s41598-019-47759-4.
- [15] Fruchterman TMJ, Reingold EM. Graph drawing by force—direct placement. *Software-Practice and Experience*. 1991, 21(11): 1129-1164.
- [16] Wasserman S. *Social Network Analysis: Methods and Applications*[M]. China Renmin University Press, 2004: 125-160.

Characterizing Eating Disorder Issues on Sina Weibo

Jingyun Tang, Guang Yu¹, Zheng Wang, Xiaoxu Yao

School of Management, Harbin Institute of Technology, Harbin, Heilongjiang, China

Abstract. Eating disorder (ED) was not learned well in China. To contribute to an understanding of the prevalence of EDs in China and to identify individuals with ED tendencies, we randomly selected one million Sina Weibo (social media platform similar to twitter) users and collected all their postings related to ED keywords. Using thematic analysis and sentiment analysis our study proposes an approach for identifying ED-prone people, the use of which reveals the current situation with regard to EDs in China. The identified ED-prone people were all willing to share information about diet, body shape and slimming while reporting their disease condition. Most of these users were young females, who were active on social media but in a negative frame of mind. With the method proposed in this study, it is possible to identify individuals with an ED and carry out timely intervention via social media at a very low cost.

Keywords. Eating disorder; anorexia; social media; Sina Weibo

1. Introduction

The mantra of “regard being slender as beauty” has come to influence the perception of beauty among Chinese in recent years, and extreme measures taken to lose weight have led to eating disorders (EDs) that have become a serious problem hindering the healthy development of Chinese adolescents[1, 2]. Presently about 0.5% to 2% of people worldwide, dominated by teenagers, are suffering from an eating disorder (ED)[3], which includes incomplete forms of anorexia nervosa and bulimia nervosa. With a fatality rate of 5% to 6 %, anorexia nervosa (AN) is the most fatal of all mental diseases[4].

Since individuals usually try to conceal ED symptoms[5]. It is particularly difficult to detect people with an ED in order to treat them in a timely manner. Given the often secretive nature of EDs, those with an ED may seek social support or resources online. Online social media offers anonymity and thus users have few scruples in expressing themselves, which makes social media the best tool for those with an ED to search for other users suffering from the same disease whom they can discuss their problems with, and seek support and advice from[6, 7]. The emergence of social media platforms provides an effective method to identify individuals with an ED and to help understand the development of EDs at a very low cost.

Sina Weibo, which is similar to Twitter, is the largest platform of user information sharing, circulation and acquisition in China. In the past two years, one of the hot

¹ Corresponding Author: Guang Yu, Harbin Institute of Technology, No.92, Xidazhi Street, Nangang District, Harbin City, Heilongjiang Province, China; Email:yug@hit.edu.cn

topics on Weibo has been the “skinny craze”. For example, the posts of “A4 waist” (the width of the waist is smaller than that of an A4 paper, namely, 210mm) has reached 270 million and the number of people participating in the discussion has reached 302,000. Another example is the throwing down of “skinny craze” challenges by posting photos. These kinds of activities are undoubtedly putting potential ED people at risk. In addition, because of the openness and anonymity of Weibo, users may post and discuss private matters without scruples. Therefore, it is worthwhile to probe into China's ED population using Weibo data sources.

2. Literature Review

In recent years, more and more researchers use social media data to study psychological diseases[8,9]. The research on ED based on social media mainly focuses on the following aspects:

First, the relationship between the social media and ED has been mainly explored. Some researchers have found that the frequent use of social media had a stronger correlation with body image concerns and ED[10-12]. A study showed positive linear relationship between the time of social media use and reported ED behaviors[13,14]. In addition, a study showed that there is a link between online ED content browsing and offline ED behavior[15].

Second, some studies focus on online Pro-ED community[16]. Some studies by the hashtag (for example, #proana, pro-ED) or keywords found those communities openly supporting ED on social media[17]. Through content analysis, it was found that the community content was consistent with the behavior of ED psychiatry, and the community members expressed support for these behaviors[18]. After the characteristics and posting information of users in these communities were tracked and analyzed, it was found that all such communities aggravate ED[19]. A study have established text classifiers to identify the risk pro-ED information by characterizing removed Pro-ED social media content[20].

Finally, studies from another perspective have also found that the Internet and social media can act as a platform to provide ED assessment and intervening measures, to decrease body image dissatisfaction and disordered eating patterns, and to reduce the morbidity of high-risk groups[21, 22]. The Internet and social media can also reduce the barriers for treatment, and provide an easy anonymous environment to encourage ED groups to conduct self-management[23, 24].

Therefore, social media does not only intensify ED hazards but is also the best methods for medical personnel to conduct assessments and take intervening measures. However, most of the existing research is based on Facebook and twitter, which are not available in China. As the prevalence of eating disorders in China is increasing year by year, it is necessary to investigate ED in social media.

In this study, an investigation is carried out into the population with EDs in China by extracting data from Weibo. Firstly, a general description of the current situation of EDs in China and an analysis of ED topics that users discuss via social media is provided; secondly, the personal features of ED users in China are revealed. Findings from this study are expected to provide a theoretical basis for the active intervention and treatment of ED users via social media.

3. Methods

3.1 Data collection

API (Application Programming Interface) was used to randomly collect approximately 394 million postings of one million users from Weibo. These users were randomly sampled and all their postings were collected. These original data included posting text, posting time, and user information such as age, gender, region, number of followings, and number of followers. These data were publicly available but the study hides all traceable user information for the protection of the users' privacy. Ethical review was not required because we only used publicly available data in this study.

Selection of postings

3.2 Selection of postings

From the data sets collected, we retrieved all posting texts related to ED by keyword search. This was achieved by reading a plethora of articles and postings on Chinese ED websites and post bars in order to find words that best embody the characteristics of ED. To avoid collecting noisy data, some commonly used words and terms such as dieting, slimming, and losing weight were not adopted. All postings that contained the keyword “eating disorder”, “anorexia”, “bulimia”, “emetic”, “self-induced vomiting”, were retrieved from the postings. The number of the selected ED-related postings was 33,230.

Not all posts containing the keyword are disclosed ED. In order to extract the content related to ED, two trained researchers with mental health experience then independently labeled the postings and a codebook was created for differentiating the 33,230 postings according to content; they coded all the postings by using the codebook independently[25]. Each of the postings was discussed and an agreement on the final assigned code was made. A third PhD researcher was introduced to code a sample of 1,000 postings randomly selected from all 33,230 postings to compute the inter-rater reliability. Cohen's kappa test is often used to check the inter-coder reliability[26,27]. The inter-rater reliability for each theme was as follows.

- A. Users suffering from ED ($\kappa > 0.4$)
- B. Users express wish to develop AN ($\kappa > 0.4$)
- C. Users disclosing the behaviors of disordered eating ($\kappa < 0.4$)
- D. Sharing medical information on ED, news, exaggeration ($\kappa > 0.4$)

Obviously, not all postings that contained keyword(s) reflect disclosure of ED(type D), and the quantity and kappa value for disclosing the behaviors of disordered eating were too small(type C). Finally, 1,145 postings (type A) and 96 postings (type B) were identified as disclosure of an ED and adopted for further analysis.

3.3 Themes

To identify ultimate themes of the postings that expressed disclosure of an ED, the two experienced members separately coded each of the 1,145 (type A) postings and 96 (type B) postings. The third member then was introduced to code the postings. Finally, Cohen's kappa test was conducted.

3.4 Demographics characteristics

It should be noted that 1,114 users posted the 1,145 postings that expressed symptoms of suffering from ED, while 94 users posted the 96 postings that expressed a wish to develop AN - these two types of users are referred to as eating disorder-prone (ED-prone) users. To verify the result, 910,000 users were randomly selected from Weibo as a comparison group, and Pearson chi-square was adopted to compare the characteristics of ED-prone users and typical users (from the comparison group) on the gender distribution. Wilcoxon Rank Sum and Signed Rank Test[28] were used to determine whether the medians of user's age, postings, followings and followers were statistically significant between the ED and typical users. $P < 0.05$ was considered statistically significant.

3.5 Sentiment analysis

To explore the emotional states of the postings posted by ED-prone users, all of their postings were retrieved from the database. The number of these postings was 775,066 and 61,930. For comparison, 120,000 postings from typical users were randomly selected.

It is impossible to classify a large number of postings manually, so we need to build a text classifier. A long short-term memory(LSTM) network is a type of recurrent neural network (RNN)[29], which is widely used in natural language processing tasks. Based on the LSTM algorithm, sentiment classifiers were built. Detection was considered as a binary classification problem (emotion states of each posting, namely, positive or negative). For the supervised classification problem, a training data set is necessary. Therefore, 30,000 postings were randomly selected from the postings of 1 million users. Three trained researchers independently labeled the postings, and majority rule was adopted when there was disagreement. Ten-folded cross-validation and accuracy were selected as measures to assess the performance of the classifiers. Experimental results suggested that the classifiers achieved the highest accuracy with 93%.

After the emotional state of each post was determined, the negative emotion score of each user was calculated; that is, the proportion of the number of postings with negative emotion stated to that of the total postings of a user. The higher the proportion is, the stronger the user's negative emotion.

3.6 Influencing factors of negative emotion and mental health

To identify the influencing factors of negative emotion of ED-prone users, the 1,000 posts randomly selected from all acquired postings with negative emotion states, were labeled. Users having a high negative emotion score were also examined to see whether they posted other psychological comorbidity messages.

4. Results

4.1 Themes

Postings containing the keywords were selected. The majority of postings were excluded because of sharing medical information and because kappa values were too small. Finally, 1,145 postings (type A) were identified as users suffering from an ED, in which AN accounted for 89.69% and bulimia 8.47%. In addition, 96 postings (type B) expressed their wish to develop AN. These postings were further coded to explore the themes of EDs in the postings. Themes identified in the postings are presented in Table 1.

Table 1 Themes of ED-related postings.

Thematic analysis	Kappa value	Quantity (proportion)	example
Type A			
1 disclosure of ED only	0.880	423, 36.94%	I am tormented by AN, and will die soon! This is God's punishment to me, and I will take the consequences!
2 description of symptoms and behaviors, including eating, body shape, and slimming	0.833	610, 53.28%	I still fail to do exercises but be tormented by Bulimia today./Now I am sitting in the classroom, and only thinking about which snack to eat./After calculation, I found the snack's calorific value is more than 1,000 kilocalories /If I eat the snack, at least two days of my exercises will lose effect.
3 seeking help	0.614	74, 6.46%	I have an eating disorder, who can help me?
4 taken measures	0.556	38, 3.31%	I must have a good meal to overcome ED.
Type B			
1 expressing wish to develop AN only	0.780	88, 91.67%	I hope to develop anorexia.
2 seeking a method for develop AN	0.780	8, 8.25%	I want to develop anorexia, and who can help me?

For type A, the most common theme of the postings (n=610, 53.28%) was describing their condition and behavior in eating, body shape, slimming and so on. Most users take pleasure in sharing and exchanging their own ED condition. The second most popular theme was disclosure of ED (423, 36.94%). Only 6.46% (n=74) of the postings attempted to seek help from others. About 3% (n=38) of the postings mentioned some measures taken to prevent or reduce ED. For type B, the most common theme of the postings (n=88, 91.67%) was expressing a wish to develop AN only.

4.2 Demographic characteristics

To better understand the difference between ED-prone users and typical users, it was decided to characterize the characteristics of the ED-prone Weibo users. Five variables of gender, age, number of postings, number of followings, and number of followers were used.

Table 2 Demographic characteristics of ED-prone users

	typical users	A Users suffering from ED	P _A	B Users express wish to develop AN	P _B
Gender					
Male	417180(43.79%)	196(17.59%)	P<0.001	9(9.57%)	P<0.001
Female	535577(56.21%)	918(78.19%)		85(90.43%)	
Age					
(10-60)		(15-38)		(17-33)	
25%	21	22		20	
Median	24	24	P=0.01443	23	P=0.01524
75%	28	26		26	
Number of postings					
25%	96	318		247	
Median	280	686	P<0.001	485	P<0.001
75%	728	1311		1133	
Number of followings					
25%	92	140		138	
Median	185	242	P<0.001	277	P<0.001
75%	341	421		454	
Number of followers					
25%	67	147		124	
Median	141	246	P<0.001	228	P<0.001
75%	280	386		472	

Table 2 shows the comparative result between demographic characteristics of groups with ED-prone and typical groups. The result of Pearson's chi-squared test shows that the gender distribution difference between the two groups has statistical significance. Analysis of gender distribution illustrates that females tend to have an ED more frequently than males, and a higher proportion of female users express a wish to develop AN. Results of Wilcoxon Rank Sum and Signed Rank Test show a statistical significance in the median difference in users' age, number of postings, followings, and followers. The age distribution was relatively young. Both the ED-prone users are more active and both their number of postings and followings are larger than those of typical Weibo users.

4.3 Sentiment analysis

Through sentiment classification of all postings of ED-prone users, it was found that compared with typical users, ED-prone users show stronger negative emotion.

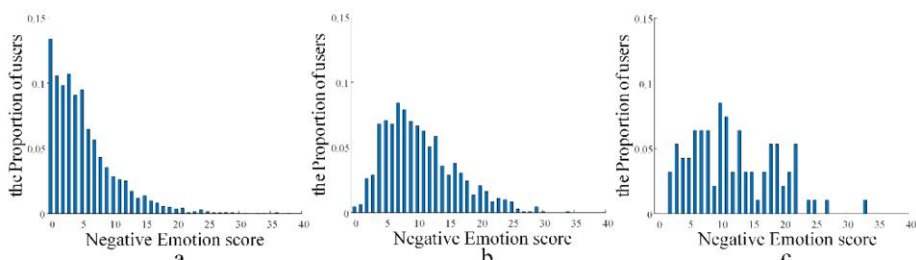


Figure 1 Distribution of negative emotion score of users; abscissa: negative emotion score, ordinate: the proportion of users

A distribution graph of negative emotion score of each user was produced (see Figure 1). It can be seen that most of the typical users had a low negative emotion score (Figure 1(a)). In most cases however, among users suffering from an ED more negative emotion exist (Figure 1(b)); among the users expressing a wish to develop AN, there was generally deeper negative emotion and a relatively average distribution of scores (Figure 1(c)), which might be related to the limited data size.

4.4 Influencing factors of negative emotion and mental health

The main reasons for negative emotion reflected by the sampled posts and the corresponding proportions are as follows:

- A. Physical complaint, such as illness, stomachache, hunger, insomnia, etc. (23%)
- B. Dissatisfied with self-image (4%)
- C. Life stress; work, study, and family affairs (33%)
- D. Weather and environment (7%)
- E. Not mentioned (33%)

Users with high negative emotion score also disclosed other mental problems: 53 users posted that they were suffering from depression, 14 users posted that they had anxiety disorder, and 13 users out of these showed a suicidal tendency more than once.

5. Discussion

This study examined the postings in Weibo related to those who are ED-prone, which reflects the status of EDs in China and identifies the problems of managing ED-prone users.

From the sample database, it was found that most of the 1,114 users posted that they were suffering from the ED appeared to have AN. These 1,114 users accounted for a relatively small proportion of the selected users. In the data labelling process, a large part of the data was deleted because of some users' misunderstanding of AN. Most of them considered a poor appetite for a period of time as a sign of AN, which indicates that there is a lack of general knowledge of EDs in China and that the majority are not aware of the AN disease.

The proportions of different themes of Weibo postings related to ED-prone users suggests that the users, in most cases, tend to talk about their own conditions because they might have no idea of how to seek help, or feel reluctant to ask for assistance with overcoming their ED. Those themes play an important role in establishing stronger links between these users and the exchange of information is expected to facilitate the identification of more online users with an ED. Therefore, it is necessary to proactively identify this group of users and render assistance by offering low-cost online intervention measures promptly to prevent the disease from getting worse.

In this study, 94 users expressed a wish to have AN. These users might be under great pressure imposed by the concept that regards being slender as beautiful, which has had a dramatic impact on the public through vigorous media promotions. Secondly, a group of pro-AN users (e.g., "Pro-Ana") is likely to emerge on the Internet and social media if there is no efficient control over relevant information and the users themselves. Studies have revealed that the users of "Pro-Ana" websites or online communities tend to share extreme weight loss measures with each other and learn skills via the Internet. In addition, these active and influential websites and online communities tend to be a risk factor for deterioration of EDs among users. To mitigate the risk, online guidance for correctly grasping healthcare concepts should be provided for the public and proper

measures for weight control and beneficial healthcare should be introduced to reduce the incidence of EDs.

The study also statistically analyzed the demographic characteristics of ED-prone users. First, gender distribution is consistent with previous studies by finding many more female users than male users[11, 30]. This significant gender difference implies that more attention should be paid to female users in future studies so as to customize health information provided during online management and control. Second, from the age statistics we found that users between the ages of 20 to 30 years old account for the largest proportion among users who are ED-prone. Previous studies usually restricted samples to teenagers under 18 years old or college students[2, 31]. However, such sample selection is unsuitable for studies on EDs in China. Therefore future studies should enlarge the age range of samples. Third, the number of postings, followings, and followers of both the two types of users are much larger than those of typical users. We think this may be related to the lack of identity in 'real life' and so they take pleasure in exchanging information and acquiring support through the anonymous environment of social media. However, since it is easy for them to receive wrong health information this way, it is very important to carry out online management and control for ED-prone users.

This study found that most of the ED-prone users showed negative emotions and tended to complain about their poor health, such as stomachache or hunger that might result from an ED. There are potential factors brought on by such negative emotions, such as discontentment with oneself, tremendous pressure, and anxiety, all of which are likely to cause or aggravate EDs. Moreover, identification of these factors may be essential for the treatment of the disease. These findings about physical and mental phenomena enable professionals to provide online assistance and guidance for users in terms of psychotherapy, nutrition counseling, and foundation of support groups. Apart from this, it was also noted that those with strong negative emotions had other psychological comorbidities, such as depression, anxiety disorder and even suicidal tendencies. The results suggest that the effects and treatment of these comorbidities should be taken into consideration when prescribing treatment and developing prevention plans for patients suffering from an ED.

Without further study or diagnosis by professional doctors, we cannot be sure whether the users in the study reporting their ED are really developing an ED. However, we think these users are potential ED patients, and this is an important step for helping ED patients. In addition, some users in their postings do not specifically mention the term ED but instead describe their extreme slimming behavior. Furthermore, most postings in Weibo only include one or two sentences, which restrict demarcation of EDs and as a result such content failed to pass the Cohen's kappa test and were not analyzed. Further studies are needed for identifying the relationship between particular symptoms and user activity on social media.

All in all, EDs are a serious and even fatal disease. This paper is the first to carry out an investigation of EDs based on social media. Most of the previous studies identified potential ED patients through traditional epidemiology or clinical methods that are resource and time intense. Nevertheless, this study provides medical researchers and health care service organizations with a smart method at a lower cost to identify and efficiently assist the population with EDs. It allows professionals to offer healthcare information and psychological guidance online, provide ED-prone users with assistance to combat the disease in the earlier stages, and strengthen online regulations on risk factors for EDs; more studies should be conducted to facilitate the

implementation of these plans. It is hoped that the findings of this study can enable mental health organizations in China to obtain a deeper understanding of the condition of the ED population and play a significant part in effectively preventing EDs and reducing incidence of the disease in China.

6. Conclusion

This is the first survey of ED on Chinese social media. We use keyword method to identify individuals with ED tendency. Through themes analysis, we find that ED-prone individuals are willing to share and exchange their own ED condition, and unwilling to seek help actively. Some users have made public their desire to get AN. These behaviors are very dangerous, which show there is still a lack of awareness of ED problem in China. According to the demographic characteristics, most of ED users are young women and more active than the general users. In addition, the sentiment analysis is conducted to estimate the negative emotion of ED-prone users of social media and the possibility of suffering from other mental comorbidities. It is possible that the findings of this study enable mental health organizations in China to obtain a deeper understanding of the condition of the ED population. This study also plays a significant role in effectively preventing EDs and reducing incidence of the disease in China.

References

- [1] Lian, Q. G.; Zuo, X. Y.; Mao, Y. Y.; Luo, S.; Zhang, S. C.; Tu, X. W.; Lou, C. H.; Zhou, W. J. Anorexia nervosa, depression and suicidal thoughts among Chinese adolescents: a national school-based cross-sectional study. *Environ Health Prev* 2017, 22–30. 10.1186/s12199-017-0639-2.
- [2] Chang, W.-w.; Nie, M.; Kang, Y.-w.; He, L.-p.; Jin, Y.-l.; Yao, Y.-s., Subclinical eating disorders in female medical students in Anhui, China: a cross-sectional study. *Nutr. Hosp.* 2015, 31,1771-1777. 10.3305/nh.2015.31.4.8456.
- [3] Campbell, K.; Peebles, R., Eating disorders in children and adolescents: state of the art review. *Pediatrics* 2014, 134, 582-592. 10.1542/peds.2014-0194.
- [4] Arcelus, J.; Mitchell, A. J.; Wales, J.; Nielsen, S., Mortality rates in patients with anorexia nervosa and other eating disorders: a meta-analysis of 36 studies. *Arch Gen Psychiat.* 2011, 68, 724-731. 10.1001/archgenpsychiatry.2011.74
- [5] Richardson, R.; Richards, D. A., Designing a search strategy for locating self-help books for people with depression. *Health Info Libr J* 2006, 23, 294-295. 10.1111/j.1471-1842.2006.00667.x
- [6] Brotsky, S. R.; Giles, D., Inside the “pro-ana” community: A covert online participant observation. *Eat. Disord.* 2007, 15, 93-109. 10.1080/10640260701190600
- [7] Fox, N.; Ward, K.; O'rourke, A., Pro - anorexia, weight - loss drugs and the internet: an ‘anti - recovery’explanatory model of anorexia. *Sociol. Health Ill.* 2005, 27, 944-971. 10.1111/j.1467-9566.2005.00465.x
- [8] Jingyun, T.; Guang, Y.; Xiaoxu, Y. A Comparative Study of Online Depression Communities in China. *International Journal of Environmental Research and Public Health.* 2020 17(14):5023 10.3390/ijerph17145023
- [9] Santarossa S , Woodruff S J . #SocialMedia: Exploring the Relationship of Social Networking Sites on Body Image, Self-Esteem, and Eating Disorders[J]. *Social Media + Society*,3,2(2017-5-01), 2017, 3(2):205630511770440.
- [10] Holland, G.; Tiggemann, M., A systematic review of the impact of the use of social networking sites on body image and disordered eating outcomes. *Body image* 2016, 17, 100-110. 10.1016/j.bodyim.2016.02.008
- [11] Saffran, K.; Fitzsimmons - Craft, E. E.; Kass, A. E.; Wilfley, D. E.; Taylor, C. B.; Trockel, M., Facebook usage among those who have received treatment for an eating disorder in a group setting. *Int. J. Eating Disord.* 2016, 49, 764-777. 10.1002/eat.22567
- [12] Tiggemann M , Slater A . NetTweens: The Internet and Body Image Concerns in Preteenage Girls[J]. *Journal of Early Adolescence*, 2013, 34(5):606-620.

- [13] Fardouly J , Vartanian L R . Negative comparisons about one's appearance mediate the relationship between Facebook usage and body image concerns[J]. *Body Image*, 2015, 12(jan.):82-88.
- [14] Sidani J E , Shensa A , Hoffman B , et al. The Association between Social Media Use and Eating Concerns among US Young Adults[J]. *Journal of the Academy of Nutrition & Dietetics*, 2016:1465-1472.
- [15] Branley D B , Covey J . Is exposure to online content depicting risky behavior related to viewers' own risky behavior offline?[J]. *Computers in Human Behavior*, 2017, 75:283-287.
- [16] Branley D B , Judith C . Pro-ana versus Pro-recovery: A Content Analytic Comparison of Social Media Users' Communication about Eating Disorders on Twitter and Tumblr[J]. *Frontiers in Psychology*, 2017, 8:1356..
- [17] Arseniev-Koehler, A.; Lee, H.; McCormick, T.; Moreno, M. A., # Proana: Pro-eating disorder socialization on twitter. *J. Adolesc. Health* 2016, 58, 659-664. 10.1016/j.jadohealth.2016.02.012
- [18] Sowles S J , Mcleary M , Optican A , et al. A content analysis of an online pro-eating disorder community on Reddit[J]. *Body Image*, 2018, 24:137-144.
- [19] Bert, F.; Gualano, M. R.; Camussi, E.; Siliquini, R., Risks and threats of social media websites: twitter and the proana movement. *Cyberpsychology Behav. Soc. Netw.* 2016, 19, 233-238. 10.1089/cyber.2015.0553
- [20] Chancellor S , Lin Z J , Choudhury M D . "This Post Will Just Get Taken Down": Characterizing Removed Pro-Eating Disorder Social Media Content[C]// the 2016 CHI Conference. ACM, 2016.
- [21] Taylor, C. B.; Bryson, S.; Luce, K. H.; Cunning, D.; Doyle, A. C.; Abascal, L. B.; Rockwell, R.; Dev, P.; Winzelberg, A. J.; Wilfley, D. E., Prevention of eating disorders in at-risk college-age women. *Arch Gen Psychiat.* 2006, 63, 881-888. 10.1001/archpsyc.63.8.881
- [22] Zabinski, M. F.; Pung, M. A.; Wilfley, D. E.; Eppstein, D. L.; Winzelberg, A. J.; Celio, A.; Taylor, C. B., Reducing risk factors for eating disorders: Targeting at - risk women with a computerized psychoeducational program. *Int. J. Eating Disord.* 2001, 29, 401-408. 10.1002/eat.1036
- [23] Forkner-Dunn, J., Internet-based patient self-care: the next generation of health care delivery. *J. Med. Internet Res.* 2003, 5. 10.2196/jmir.5.2.e8
- [24] Ybarra, M. L.; Eaton, W. W., Internet-based mental health interventions. *Mental health services research* 2005, 7, 75-87. 10.1007/s11020-005-3779-8
- [25] Gery W. Ryan, H. R. B., Techniques to identify themes. *Field Methods* 2003, 15, 85-109.
- [26] Xianyun T , Philip B , Shuang S , et al. Characterizing Depression Issues on Sina Weibo[J]. *International Journal of Environmental Research & Public Health*, 2018, 15(4):764.
- [27] Yao X , Yu G , Tian X , et al. Patterns and Longitudinal Changes in Negative Emotions of People with Depression on Sina Weibo[J]. *Telemedicine and e-Health*, 2019, 26(6):734-743
- [28] Siegel, S., Nonparametric statistics for the behavioral sciences. 1956.
- [29] Hochreiter, S.; Schmidhuber, J., Long short-term memory. *Neural Comput* 1997, 9, 1735-1780. 10.1162/neco.1997.9.8.1735
- [30] Tong, J.; Miao, S.; Wang, J.; Yang, F.; Lai, H.; Zhang, C.; Zhang, Y.; Hsu, G., A two-stage epidemiologic study on prevalence of eating disorders in female university students in Wuhan, China. *Soc. Psychiatry Psychiatr. Epidemiol.* 2014, 49, 499. 10.1007/s00127-013-0694-y
- [31] Lee, S.; Lee, A. M., Disordered eating in three communities of China: A comparative study of female high school students in Hong Kong, Shenzhen, and rural Hunan. *Int. J. Eating Disord.* 2000, 27, 317-327. 10.1002/(SICI)1098-108X(200004)27:3<317::AID-EAT9>3.3.CO;2-U

Optimization of Transit Scheduling Combined with Short-Turn Service Based on Real-Time Passenger Flow

Ailing HUANG^a, Yijing MIAO^a and Jiarui LI^{a,b,1}

^a*Key Laboratory of comprehensive transportation big data application technology,
Beijing Jiaotong University, Beijing 100044, P.R.China*

^b*STV Inc, Los Angeles, CA 90017, U.S.A.*

Abstract. In view of a series of problems, such as unable to meet the needs of passengers, high full load ratio or waste of carrying capacity on unbalanced passenger flow sections caused by the all-stop fleet scheduling in the urban public transit system, this paper proposed a bus combination scheduling strategy with considering short-turn service based on the imbalance coefficient of passenger flow and a method to determine the turning back point. A combined dispatching optimization model is established with the objective function of minimizing the total system cost which includes the waiting time cost of passengers, the congestion feeling cost and the operation cost of public transit enterprises. The headways of short-turn and all-stop scheme are optimized by the combined scheduling model, and the solution method is proposed. Taking Beijing No. A bus line as an empirical analysis object, the real-time passenger flow and vehicle data in a working day are collected and analyzed, and the optimized scheme of short-turn service combination scheduling is obtained. The results show that compared with the traditional all-stop fleet scheduling, the optimized short-turn service combination scheduling can reduce the fleet size by 4.9% and effectively improve the operation efficiency and system benefits.

Keywords. Public transit; combined scheduling; short-turn service; total system cost; operation

1. Introduction

The problems related to public transit operation are the focus and difficulty of public transit research. At present, the bus dispatching in major cities in China is still based on all-stop fleet scheduling, which often leads to a surge in passenger flow and traffic congestion during peak hours. Therefore, it is an important topic to explore the rationalization of urban public transit routes and vehicle scheduling optimization.

At present, the research on all-stop fleet scheduling has been very in-depth. Cancela summarized the international representative research work on bus dispatching and network design [1]. The traditional bus dispatching research focuses on dealing with the unbalanced spatial and temporal distribution of passenger flow, with the purpose of saving passenger travel cost [2-4]. The main research directions include bus timetable formulation [5-7], departure frequency optimization [8-10], routes scheduling

¹ Jiarui LI, 1055 W 7th St #3150, Los Angeles, CA 90017; E-mail: jiarui.li@stvinc.com

optimization [11-12]. In recent years, many achievements have been made in bus combination scheduling design. Among them, short-turn service is considered as a feasible way to reduce the cost, and due to the limited number of research, it is worth further study.

In order to adapt to the travel demand of the section with the highest passenger load and prevent overloading, Canca *et al.* [13] proposed a model to increase the departure frequency of certain stops on the line and balance the vehicle occupancy level. The setting of turning back point should shorten the passenger travel time on the premise of ensuring the service quality. Cheng [14] used the "cutting method" to determine the stops of short-turn bus lines, and established the optimization model of short-turn service combination scheduling with the optimization objectives of passenger waiting cost, congestion cost and bus operation cost under different scheduling modes. In this proposed model, the all-stop and short-turn service depart in a certain proportion, and different proportions represent different departure modes. Cortés *et al.* [15] established an optimal scheduling model for short-turn service on single line. It is proved that the total cost can be reduced by reducing the extra operating cost of empty vehicles. According to the theory of deficit function, in the process of combined dispatching of all-stop and short-turn service, Hu *et al.* [16] realized all departures of single line with the least number of vehicles by properly inserting idle vehicles, making full use of idle vehicles and reducing the operation cost of public transit group. Based on the passenger flow data, Cao [17] took the passenger waiting and riding satisfaction and the bus company satisfaction as the objective function, used the power weighted sum method to process the multi-objective function, established a single objective public transport scheduling model, and used the improved genetic algorithm to solve the problem. Chen *et al.* [18] constructed a combined scheduling model under the conditions of limited vehicle capacity and random passenger travel, and verified the model and solution method through an example. Wei *et al.* [19] put forward a kind of multi-objective single line combined dispatching method for stop-skipping service, and discussed the relationship among departure frequency, turning back point and cost with an example. Canca *et al.* [20] proposed a short-turn service scheduling strategy under the premise of ensuring certain service quality to reduce waiting time of passengers. Zhang *et al.* [21] established a mixed scheduling model of stop-skipped and short-turn service based on real-time data. Compared with the traditional scheduling mode, the hybrid scheduling strategies can effectively reduce the total cost of public transit system. On the basis of considering the number of passengers waiting to be transported due to the limitation of vehicle capacity and the dwelling time, Gao [22] set up the short-turn service combination scheduling model with the weighted sum of passenger travel cost and bus enterprise cost as the objective function, where the scheduling mode and departure interval as the decision variables. Ming *et al.* [23] discussed the combination of different departure modes and intervals, established a combination bus scheduling model with uncertain departure frequency, then compared and proved that multi-mode combined bus dispatching can effectively reduce the system time cost. On this basis, Liu [24] proposed a hybrid heuristic algorithm combining particle swarm optimization algorithm and pattern search algorithm to solve the problem of combination scheduling model with different departure frequencies. Luo [25] established an all-stop combined dispatching model with the objective function of minimizing the operating cost of passengers and bus companies by adopting appropriate departure strategy of vehicle groups to optimize the

original departure interval and adjust the driving plan to realize comparatively even distribution of passenger flow.

Taken together, the existing research, especially the practical application on the mode of combined bus dispatching is still in its infancy. Although more research of bus scheduling optimization has been conducted for many years, several questions remain open in the study of combined scheduling optimization with short-turn service. Since nowadays the real-time data like passenger flow is available via collecting smart card records, which has higher accuracy and reliability, the method of determining short-turn service point needs to be further explored. It is more reasonable to use the real-time passenger flow data and the actual traffic conditions as the data source of model input to judge the turning back point of short-turn service. It means that a systematic framework of designing transit combination scheduling scheme based on the real-time data needs to design. In addition, most of the studies only chooses one of the user cost and operation cost as the objective function, and accordingly, the optimized results cannot reflect the benefits and effectiveness more completely. Moreover, the cost in different scheduling schemes also need to be studied in detail. Therefore, the systematic objective needs to be optimized further with considering both the benefits of users and operators, and the benefit of optimized scheme is worth to be discussed more comprehensively. All of these factors should be thoroughly considered in the modeling framework. To address the research limitations that are discussed above, this paper designs a framework to judge the short-turn point based on the real-time passenger flow, and proposes a model and solution algorithm to optimize the bus combination scheduling scheme. In our model, different scheduling strategies combined with all-stop and short-turn services are designed and the minimum sum of the cost of both sides are regarded as the optimization goal from the perspectives of passengers and public transit enterprises. Particularly, besides the waiting cost, the congestion feeling cost of passengers is taken into account in our modeling framework to reflect more real external cost. Moreover, to evaluate the feasibility of the proposed model and algorithm, this paper conducts a case study of a bus line in Beijing by using the real data and makes an analysis on the optimized results. The results shows that our proposed method can greatly reduce the cost of passengers and operator, and improve the operational efficiency. The main purpose of this paper is to optimize the bus scheduling by formulating a feasible and effective combined dispatching strategy, reduce the passenger cost and the operation cost, and evacuate the passenger flow in peak period immediately and effectively. The proposed method can be applied to the operation and scheduling practice by public transit enterprises in the future.

The remainder of this paper is organized as follows. The second part gives the description of research object, and the judgement and planning framework of short-turn service combination dispatching mode. In the third part, based on the previous steps, the bus combination schedule model is proposed and the solving method is given. A case study is conducted in the fourth section to illustrate the specific application of the proposed methodology, where a satisfactory results comparison is discussed. The last section concludes this paper and suggests feasible directions for future study.

2. Framework of bus combination scheduling design with real-time passenger flow

2.1. Bus dispatching mode

Vehicle scheduling is a variety of methods adopted in the preparation of public transit operation plan. According to the passenger flow distribution, the combined bus dispatching is a bus dispatching mode supplemented by other dispatching forms on the basis of all-stop service.

- All-stop service

The all-stop service refers to the scheduling form in which the bus stops in sequence at the passing stop, does not skip stops in the middle, and finally stops at the terminal.

- Short-turn service

Short-turn service is a kind of scheduling mode that stops at specific stops or sections with large passenger flow. It stops at each stop in the operation section. According to the setting of initial and terminal stops, it can be divided into three forms: midway turning back, turning back from midway stop to another midway stop, and turning back from midway stop to terminal stop.

2.2. Judgment of combination dispatching mode with considering short-turn service

Based on the unbalanced coefficient, the judgment method of short-turn service combination dispatching mode is constructed. It can be expressed by the road section unbalanced coefficient K_{si} or section passenger flow difference ΔQ_i , as shown in Eq. (1) and (2)

$$K_{si} = \frac{\underline{Q}_{si}}{\overline{Q}_n} \quad (1)$$

$$\Delta Q_i = Q_{si} - \overline{Q}_n \quad (2)$$

In Eq. (1) and (2), \underline{Q}_{si} , \overline{Q}_n respectively refer to the passenger flow of road section i and the average section passenger flow within the statistical time.

When the passenger flow is high and the unbalanced coefficient of road section $K_{si} > 1.2$, it can be considered to carry out short-turn service combination scheduling in the section, so as to reduce the congestion of passenger flow in peak road section. The specific determination steps are as follow:

- Step 1: Make statistics on the passenger flow of to be investigated, and calculate the road section unbalance coefficients of the upward and downward directions respectively;
- Step 2: According to the criteria of short-turn service, determine the stop which will operate the short-turn service. Table 1 is the judgment standard of the short-turn service;

Table 1. Criteria for judging short-turn service

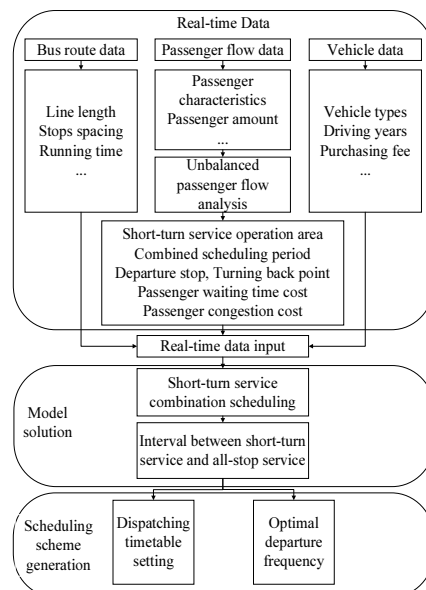
Judgment index	Condition	Remarks
Unbalanced coefficient of road section	$K_{si} > K_s^0$	Generally, $K_s^0 = 1.2 \sim 1.5$
Section passenger flow difference	$\Delta Q_i \geq \eta q_0$	Generally, $\eta = 2 \sim 4$, q_0 is the rated capacity of the vehicle

- Step 3: To evaluate and investigate the traffic condition of routes and sections where short-turn service will be set up to judge whether the selected stop is feasible;
- Step 4: Test the vehicles used in the section to determine the vehicle types and total fleet size of the bus line;
- Step 5: Formulate the departure interval and timetable for the all-stop and short-turn service.

In addition to using the unbalanced coefficient method to determine the short-turn service dispatching mode, it is also necessary to consider the actual road traffic conditions, the scale of public transit enterprises, the economic level of urban residents and other factors, so as to formulate a dispatching scheme which is beneficial to both passengers and public transit enterprises.

2.3. Design process of combination scheduling scheme based on real-time flow

When the short-turn service combination is determined, the combined scheduling model of all-stop and short-turn service is established. The real-time passenger flow data and vehicle data is input into the model. Through solution, the optimized departure interval is obtained, and the corresponding departure schedule and driving scheme are formulated. The specific process is shown in Figure 1.

**Figure 1.** Flow chart of combined scheduling

3. Bus combination schedule modeling and solution

3.1. Model establishment

3.1.1. Assumptions

- The principle of bus passengers is that the passengers who arrive at bus stop first have priority and obey the uniform distribution;
- The types of bus vehicles are consistent, and there are no multiple types;
- The fixed cost of public transit enterprises is related to the fleet size of bus line;
- The variable cost of public transit enterprises is related to vehicle fuel consumption;
- There is no transfer between all-stop service and short-turn service;
- In the combined dispatching, the difference of stopping time between the all-stop service and short-turn service is not considered.

3.1.2. Parameters

The model parameter definition of the short-turn service combination scheduling model is shown in Table 2.

Table 2. Model variable table

Parameter symbol	Meaning	Unit
i	Stop serial number	-
μ	Sequence of short-turn service departure stop	-
φ	Turning back point sequence of short-turn service	-
m	Parameters of combined dispatching mode, $m = 0, 1, 2$; where 0 is the all-stop scheduling, 1 is the combined scheduling of one all-stop service and short-turn combination, and 2 is two all-stop service and short-turn combination scheduling	-
ε	Parameters of congestion penalty cost coefficient	-
l_i	Stop spacing	km
L	Total length of bus line	km
L_s	Length of short-turn service line	km
τ	Study duration	min
h_0	Departure interval under whole vehicle scheduling	min
h_1	Time interval of the next short-turn service after an all-stop service	min
h_2	Time interval of the next all-stop service after a short-turn service	min

f	Total departures	second
r_{ik}	Arrival rate of passengers getting on at stop i and off at stop k	person/min
$P_i^{(m)}$	Under mode m , the number of boarding passengers at stop i	person
$Q_i^{(m)}$	Under mode m , the number of alighting passengers at stop i	person
$N_i^{(m)}$	Under mode m , the cumulative number of passengers between stop i and $i+1$	person
$W_i^{(m)}$	Under mode m , the waiting time cost of passengers at stop i	yuan
$Y_i^{(m)}$	Under mode m , when the full load ratio exceeds maximum load rate, the congestion feeling cost of passengers from stop i to $i+1$	yuan
$\rho_i^{(m)}$	Under mode m , and the congestion penalty cost coefficient between stop i and $i+1$	yuan/person·km
b	Rated capacity	person/vehicle
$A_i^{(m)}$	Full load ratio of vehicle at stop i	-
A_0	Critical load ratio	-
α	Passenger's waiting time cost	yuan/person·min
β	fuel consumption of one vehicle	yuan/km
T	Average one-way travel time of all-stop service in peak hours	min
T_s	Average one-way travel time of short-turn service in peak hours	min
ξ	Bus purchase cost	yuan/vehicle
c	Number of drivers per bus	people
d	Number of bus seats	individual
R_0	Driver's daily wage	yuan/person·day
S_0	Daily vehicle maintenance fee	yuan/vehicle·day
θ	Permitted driving years of vehicles	year
u_{\min}	Minimum fleet size	vehicle

3.1.3. Objective function

In order to ensure the interests of both passengers and public transit enterprises, the objective function of the short-turn service combination scheduling model constructed

in this paper includes two parts: passenger cost and operation cost of public transit enterprises.

(1) Passenger cost

The cost of passengers is the sum of waiting cost and congestion cost. The time cost in the bus is not considered because it is not related to bus departure mode. The following is the analysis of different departure conditions.

1) When $m = 0$, that is, the bus line only takes the all-stop, the cost of passengers is defined as:

$$C^{(0)} = \sum_{i=1}^{n-1} (W_i^{(0)} + Y_i^{(0)}) \quad (3)$$

In Eq. (3), the calculation of $W_i^{(0)}$, $Y_i^{(0)}$ is as follow:

$$\begin{cases} W_i^{(0)} = \frac{1}{2} \alpha \sum_{k=i+1}^n r_{ik} h_0^2 \\ Y_i^{(0)} = \rho_i^{(0)} (N_i^{(0)} - d) l_i, \quad i=1,2,3,\dots,n-1 \end{cases} \quad (4)$$

Where, $N_i^{(0)}$ is as shown in Eq. (5); $\rho_i^{(0)}$ is as shown in Eq. (6).

$$N_i^0 = N_{i-1}^0 + P_i^0 - Q_i^0 = N_{i-1}^{(0)} + \sum_{k=i+1}^n r_{ik} h_0 - \sum_{l=1}^{i-1} r_{li} h_0 \quad (5)$$

In Eq. (5), $Q_1^{(0)} = 0$, $N_1^{(0)} = P_1^{(0)}$.

$$\rho_i^{(0)} = \begin{cases} \varepsilon A_i^0, 0 \leq \varepsilon \leq 1, A_i^0 \geq A_0 \\ 0, A_i^0 < A_0 \end{cases} \quad (6)$$

In Eq. (6), the calculation of $A_i^{(0)}$ is as follow:

$$A_i^{(0)} = \frac{N_i^{(0)}}{b} \quad (7)$$

2) When $m = 1$, a combined dispatching of one all-stop service and the short-turn service is issued. The stop sequence of short-turn service is $\mu, \mu+1, \dots, \varphi$, then the passenger cost of short-turn service is defined as:

$$C^{(1)} = \sum_{i=\mu}^{\varphi-1} (W_i^{(1)} + Y_i^{(1)}) \quad (8)$$

In Eq. (8), the calculation of $W_i^{(1)}$, $Y_i^{(1)}$ is as follow:

$$\begin{cases} W_i^{(1)} = \frac{1}{2} \alpha \sum_{k=i+1}^{\varphi} r_{ik} h_1^2 \\ Y_i^{(1)} = \rho_i^{(1)} (N_i^{(1)} - d) l_i, \quad i = \mu, \mu+1, \dots, \varphi-1 \end{cases} \quad (9)$$

In Eq. (9), $N_i^{(1)}$ can be calculated by Eq. (10), and $\rho_i^{(1)}$ can be calculated by Eq. (11).

$$N_i^{(1)} = N_{i-1}^{(1)} + P_i^{(1)} - Q_i^{(1)} = N_{i-1}^{(1)} + \sum_{k=i+1}^{\varphi} r_{ik} h_1 - \sum_{l=\mu}^{i-1} r_{il} h_1 \quad (10)$$

In Eq. (10), there is $Q_\mu^{(1)} = 0$, $N_\mu^{(1)} = P_\mu^{(1)}$, $i = \mu, \mu+1, \dots, \varphi-1$.

$$\rho_i^{(1)} = \begin{cases} \varepsilon A_i^{(1)}, & 0 \leq \varepsilon \leq 1, A_i^{(1)} \geq A_0 \\ 0, & A_i^{(1)} < A_0 \end{cases} \quad (11)$$

In Eq. (11), the calculation of $A_i^{(1)}$ is as follow:

$$A_i^{(1)} = \frac{N_i^{(1)}}{b} \quad (12)$$

3) When $m = 2$, the passenger cost of the all-stop scheduling is defined as:

$$C^{(2)} = \sum_{i=1}^{n-1} (W_i^{(2)} + Y_i^{(2)}) = \sum_{i=1}^{\mu-1} W_i^{(2)} + \sum_{i=\mu}^{\varphi-1} W_i^{(2)} + \sum_{i=\varphi}^{n-1} W_i^{(2)} + \sum_{i=1}^{n-1} Y_i^{(2)} \quad (13)$$

In Eq. (13), the location relationship between stop i and the range of short-turn service section should be considered when calculating $W_i^{(2)}$, which is discussed in the following different cases.

a) When $1 \leq i \leq \mu-1$ or $\varphi \leq i \leq n-1$, stop i is not within the scope of short-turn service section, passengers need to wait for the next all-stop service:

During period $h_1 + h_2$, the sum of passengers boarding at stop i , which is denoted as $P_i^{(2)}$, can be expressed as

$$P_i^{(2)} = \sum_{k=i+1}^n r_{ik} (h_1 + h_2), \quad 1 \leq i \leq \mu-1 \text{ or } \varphi \leq i \leq n-1 \quad (14)$$

Then the average waiting time of passengers is $\frac{1}{2}(h_1 + h_2)$, and the calculation of passengers waiting time cost $W_i^{(2)}$ is obtained as follow:

$$W_i^{(2)} = \frac{1}{2} \alpha \sum_{k=i+1}^n r_{ik} (h_1 + h_2)^2 \quad (15)$$

b) When $\mu \leq i \leq \varphi-1$, that is, stop i is within the range of short-turn service section:

At this time, the number of passengers who do not take short-turn service bus because they cannot reach their destination directly is $\sum_{k=\varphi+1}^n r_{ik} h_1$, and the waiting time

cost of these passengers is $\frac{1}{2} \alpha \sum_{k=\varphi+1}^n r_{ik} (h_1 + h_2) h_1$. The waiting time cost of the new

arrival passengers arriving before the arrival of short-turn service is $\frac{1}{2} \alpha \sum_{k=i+1}^n r_{ik} h_2^2$,

thus the calculation of passengers waiting time cost $W_i^{(2)}$ is obtained as follow:

$$W_i^{(2)} = \frac{1}{2} \alpha \sum_{k=\varphi+1}^n r_{ik} (h_1 + h_2) h_1 + \frac{1}{2} \alpha \sum_{k=i+1}^n r_{ik} h_2^2, \quad \mu \leq i \leq \varphi - 1 \quad (16)$$

In Eq. (16), the calculation of $Y_i^{(2)}$ is as follow:

$$Y_i^{(2)} = \rho^{(2)} (N_i^{(2)} - d) l_i, \quad i = 1, 2, \dots, n-1 \quad (17)$$

In Eq. (17), $N_i^{(2)}$ is the cumulative passenger flow from stop i to $i+1$, which can be expressed as:

$$N_i^{(2)} = N_{i-1}^{(2)} + P_i^{(2)} - Q_i^{(2)} \quad (18)$$

To sum up, the passenger cost of all-stop scheduling can be expressed by Eq. (19) - (21)

$$C^{(2)} = \sum_{i=1}^{\mu-1} \left[\frac{1}{2} \alpha \sum_{k=i+1}^n r_{ik} (h_1 + h_2)^2 \right] + \sum_{i=\mu}^{\varphi-1} \left[\frac{1}{2} \alpha \sum_{k=\varphi+1}^n r_{ik} (h_1 + h_2) h_1 + \frac{1}{2} \alpha \sum_{k=i+1}^n r_{ik} h_2^2 \right] \quad (19)$$

$$\begin{aligned} & + \sum_{i=\varphi}^{n-1} \left[\frac{1}{2} \alpha \sum_{k=i+1}^n r_{ik} (h_1 + h_2)^2 \right] + \sum_{i=1}^{n-1} \rho_i^{(2)} (N_i^{(2)} - d) l_i \\ & \begin{cases} N_{i-1}^{(2)} + \sum_{k=i+1}^n r_{ik} (h_1 + h_2) - \sum_{l=1}^{i-1} r_{il} (h_1 + h_2), N_i^{(2)} = P_i^{(2)}, 1 \leq i \leq \mu - 1 \\ N_{\mu-1}^{(2)} + \sum_{k=\varphi+1}^n r_{uk} h_1 + \sum_{k=\mu+1}^n r_{uk} h_2 - \sum_{l=1}^{\mu-1} r_{il} (h_1 + h_2), i = \mu \end{cases} \end{aligned} \quad (20)$$

$$N_i^{(2)} = \begin{cases} N_{i-1}^{(2)} + \sum_{k=\varphi+1}^n r_{ik} h_1 + \sum_{k=i+1}^n r_{ik} h_2 - \sum_{l=1}^{\mu-1} r_{il} (h_1 + h_2) - \sum_{l=\mu}^{i-1} r_{il} h_2, \mu < i \leq \varphi - 1 \\ N_{\varphi-1}^{(2)} + \sum_{k=\varphi+1}^n r_{\varphi k} (h_1 + h_2) - \sum_{l=1}^{\varphi-1} r_{l\varphi} (h_1 + h_2) - \sum_{l=\varphi}^{i-1} r_{l\varphi} h_2, i = \varphi \\ N_{i-1}^{(2)} + \sum_{k=i+1}^n r_{ik} (h_1 + h_2) - \sum_{l=1}^{\mu-1} r_{il} (h_1 + h_2) - \sum_{l=\mu}^{\varphi-1} r_{il} h_2 - \sum_{l=\varphi}^{n-1} r_{il} (h_1 + h_2), \varphi < i \leq n - 1 \end{cases}$$

$$\rho_i^{(2)} = \begin{cases} \varepsilon A_i^{(2)}, 0 \leq \varepsilon \leq 1, A_i^{(2)} \geq A_0 \\ 0, A_i^{(2)} < A_0 \end{cases}, A_i^{(2)} = \frac{N_i^{(2)}}{b} \quad (21)$$

(2) Bus operation cost

In this paper, the total operating cost of public transit enterprises is divided into two parts, one is the fixed investment cost, the other is operating variable cost.

1) Fixed investment cost

The fixed investment cost of public transit enterprises is related to the minimum fleet size, as shown in Eq. (22)

$$U = (\phi + R + S_0) u_{\min} \quad (22)$$

In Eq. (22), ϕ is the daily depreciation cost of each vehicle, as shown in Eq. (22); R is the daily wage of drivers on each bus, as shown in Eq. (23);

$$\phi = \frac{\xi}{\theta \times 365 \times 24} \times T_r \quad (23)$$

$$R = cR_0 \quad (24)$$

2) Operating variable costs

In the variable cost side, this paper mainly considers the fuel consumption with increase of vehicle mileage. The total fuel consumption can be divided into the fuel consumption of all-stop service B_0 and that of the short-turn service B_1 . The calculation is shown in Eq. (25) and (26) respectively

$$B_0 = \beta L \quad (25)$$

$$B_1 = \beta L_s \quad (26)$$

Thus, the variable cost of bus operation B is expressed as follow:

$$B = B_0 f_0 + B_1 f_1 \quad (27)$$

In Eq. (27), f_0 , f_1 is the departure times of all-stop service and short-turn service in the study period respectively.

To sum up, the total system cost calculated by the objective function can be obtained from the sum of passenger costs and operating costs of public transit enterprises in different situations.

When $m = 1$, there is one all-stop service participating in the combined dispatching. The objective function of combined dispatching is shown in Eq. (28) - (30). Where, the departure times of all-stop service are equal to the departure times of short-turn service.

$$\min Z^{(1)} = \omega_1 [C^{(0)} f_0 + C^{(1)} f_1] + \omega_2 [B_0 f_0 + B_1 f_1 + U] \quad (28)$$

$$f_0 = f_1 = \frac{\tau}{h_1 + h_2} \quad (29)$$

$$B_0 = \beta L, B_1 = \beta L_s \quad (30)$$

Where, ω_1 and ω_2 are the weight coefficients of relative total cost of public transit enterprises and passengers, and $0 < \omega_1, \omega_2 < 1$, $\omega_1 + \omega_2 = 1$.

When $m = 2$, there are two all-stop service participating in the combined dispatching, and the departure times of all-stop service are twice of that of the short-turn service. The objective function of combined dispatching is shown in Eq. (31) - (33)

$$\min Z^{(2)} = \omega_1 \left[C^{(0)} f_0 + C^{(1)} f_1 + C^{(2)} \times \frac{1}{2} f_0 \right] + \omega_2 [B_0 f_0 + B_1 f_1 + U(u_{\min})] \quad (31)$$

$$f_0 = 2f_1 = \frac{2\tau}{h_0 + h_1 + h_2} \quad (32)$$

$$B_0 = \beta L, B_1 = \beta L_s \quad (33)$$

Thus, the objective function can be generalized to general situation. When m is any value, the objective value of combined scheduling is shown in Eq. (34) - (36):

$$\min Z^{(m)} = \omega_1 \left[C^{(0)} \times \frac{m-1}{m} f_0 + C^{(1)} f_1 + C^{(2)} \times \frac{1}{m} f_2 \right] + \omega_2 [B_0 f_0 + U(u_{\min})] \quad (34)$$

$$f_0 = mf_1 = \frac{m\tau}{(m-1)h_0 + h_1 + h_2}, m = 1, 2, 3, \dots \quad (35)$$

$$B_0 = \beta L, B_1 = \beta L_s \quad (36)$$

When the bus dispatching form is whole vehicle scheduling, the objective function is shown in Eq. (37) - (39):

$$\min Z^{(1)} = \omega_1 C^{(0)} f_0 + \omega_2 [B_0 f_0 + U(u_{\min})] \quad (37)$$

$$f_0 = \frac{\tau}{h_0} \quad (38)$$

$$B_0 = \beta L \quad (39)$$

3.1.4. Constraints

In order to meet the needs of passengers and limited by the fleet size, bus companies will set the departure interval according to actual bus line conditions. When the specified maximum and minimum departure intervals are h_{\max} and h_{\min} respectively, it is necessary to ensure that:

$$\begin{cases} h_{\min} \leq h_0 \leq h_{\max} \\ h_{\min} \leq h_1 \leq h_{\max} \\ h_{\min} \leq h_2 \leq h_{\max} \end{cases} \quad (40)$$

3.2. Model solution

Analysis of objective function $\min Z^{(m)}$: the value range of h_0, h_1, h_2 is $[h_{\min}, h_{\max}]$, and under the determined value of m , the model solution is to solve a nonlinear optimal problem. Matlab is used to search the total cost to get an optimal solution satisfying $\min Z^{(m)}$, and then the corresponding value of h_0, h_1, h_2 under the optimal target value is obtained.

The traditional mathematical method to calculate the optimal solution will lead to too much calculation, which is often unrealistic. Because of its own characteristics, genetic algorithm has a strong formula in solving such problems, so genetic algorithm is used to solve the model [21].

The improvement and function expansion of standard genetic algorithm can be divided into four steps: initialization, fitness calculation, genetic operation to produce offspring, and judgment of termination conditions.

3.2.1. Initialization and parameter selection

- Coding

First, the decision variable is encoded as a binary number, that is, a chromosome X. The relationship between the precision (p bit after the decimal point) and the encoding length (binary string dimension q) is as follows:

$$2^{q-1} < (h_{\max} - h_{\min})10^p \leq 2^q - 1 \quad (41)$$

- Initialization

When determining the initial population, the population size (N chromosomes) should be determined first. This process is equivalent to randomly selecting N points as the initial solution in the optimization solution space, which is, selecting a set of strings or individuals $X_i, i = 1, 2, \dots, N$.

- Parameter selection

The crossover probability P_c and the mutation probability P_m are determined.

3.2.2. Calculation of population fitness

Since the objective function of the model proposed in this paper is minimal, Eq. (42) is taken as the fitness function:

$$F(X) = \begin{cases} C_{\max} - f(X), & C_{\max} - f(X) > 0 \\ 0, & C_{\max} - f(X) \leq 0 \end{cases} \quad (42)$$

Where C_{\max} is the maximum estimate of $f(X)$.

3.2.3. Genetic manipulation

- Selection

In this paper, the Elitist Method and Tournament Selection Method are combined. Where Elitist Method: The individuals with the highest fitness in the population do not carry out pairing exchange, but directly replicate to the next generation; Tournament Selection Method: According to a certain number of individuals randomly selected in the population, the individuals with high fitness are saved to the next generation (in this paper, the tournament scale is selected as 2).

- Crossover

In this paper, the partial matched crossover (PMX) is adopted. PMX operation was proposed by Goldberg and Lingle in 1985. In PMX operation, two exchange points are randomly generated, and the region between the two points is defined as the matching area, and the matching area of two parents is exchanged.

- Mutation

In this algorithm, insertion mutation is used according to probability P_m . A gene is randomly selected from the chromosome and inserted into other sites at random.

3.2.4. Termination conditions

Before reaching the maximum algebra, judge whether the average fitness value of successive generations of individuals has not changed, or the change value is less than a certain minimum threshold. If so, the iterative process of the algorithm converges and the algorithm ends. Otherwise, replace the previous generation population with the new generation population obtained through selection, crossover and mutation, and return to the selection operation to continue the cycle execution.

4. Case study

4.1. Data acquisition and analysis

Taking Beijing No. A bus line as an example, there are 24 stops along the up-line. Along the way, there are several subway transfer stations, school surrounding stops and some other crowded areas.

The real-time passenger flow data is collected and analyzed through smart card database. The data collection period is selected as 6:00-22:00. By comparing the passenger flow changes on weekdays and holidays, it is found that there is an obvious imbalance of passenger flow on weekdays. Therefore, it is necessary to optimize the bus scheduling on weekdays. Figure 2 shows the passenger flow variation of bus No. A on weekdays and holidays.

Data statistics: the statistical interval is one hour. The passenger flow data in upward and downward directions of are counted. Taking 6:00-12:00 on weekdays as an example, the passenger flow data is shown in Figure 3.

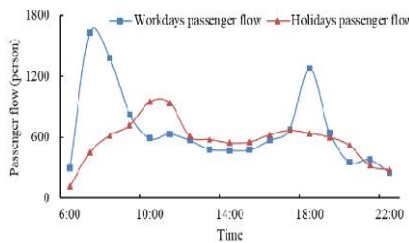


Figure 2. Passenger flow variation of working days and holidays

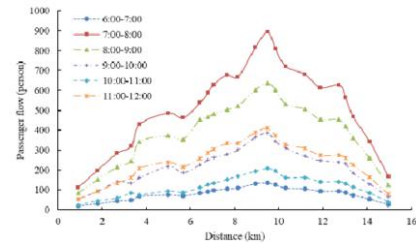


Figure 3. Passenger flow chart

In Figure 3, the ordinate represents passenger flow of the road section, and the abscissa represents the distance between the specific stop and departure stop. It can be seen that the passenger flow in middle section is relatively large, especially during 7:00-8:00 and 8:00-9:00, the passenger flow is relatively concentrated. Therefore, combined with the actual operation situation, it is necessary to optimize the original scheduling scheme by short-turn vehicle combination scheduling. Taking 7:00-8:00 as an example, the calculation results of unbalanced coefficient of road sections are shown in Table 3.

Table 3. Unbalanced coefficient of road section from 7:00 to 8:00

Section	Passenger flow	Unbalanced coefficient of road section	Section	Passenger flow	Unbalanced coefficient of road section
1-2	112	0.204007	13-14	836	1.522769
2-3	199	0.362477	14-15	894	1.628415

3-4	284	0.517304	15-16	810	1.47541
4-5	320	0.582878	16-17	711	1.295082
5-6	430	0.783242	17-18	681	1.240437
6-7	499	0.908925	18-19	604	1.100182
7-8	452	0.823315	19-20	601	1.094718
8-9	537	0.978142	20-21	544	0.990893
9-10	588	1.071038	21-22	468	0.852459
10-11	629	1.145719	22-23	344	0.626594
11-12	679	1.236794	23-24	168	0.306011
12-13	697	1.269581			

4.2. Judgment of combined scheduling mode

Through the statistical analysis of real-time passenger flow, it is found that in 7:00-8:00, 8:00-9:00 and 17:00-18:00, 18:00-19:00, the passenger flow are relatively large and concentrated. After calculating the unbalanced coefficient of road section and conducting on-the-spot investigation, it is found that short-turn service should be set up in these four periods, and the turning back points are stop 11 and 18. In other periods, although some sections meet the judgment conditions, the passenger flow difference is not obvious, the all-stop service dispatching mode is continued. Input parameter setting Through investigation on bus No. A operation group and consulting relevant data, the input parameter values of the model are obtained, as shown in Table 4.

Table 4. Parameter settings

Symbol	Meaning of parameters	Value
μ	Short-turn service departure stop	11
φ	Turning back point of short-turn service	17
τ	Duration of model study	60 min
L	Total length of line	14.96 km
L_s	Length of short-turn service line	4.12 km
n	Total number of bus stops	24
d	Number of bus seats	24 persons/vehicle
b	Rated capacity	90 passengers/vehicle
α_f	Unit time cost of passengers in off-peak hours	114 yuan/person· min
α_g	Unit time cost of passengers in peak hours	114 yuan/person· min
A_0	Critical load ratio	1.2
ε	Parameters of congestion penalty cost coefficient	0.4
β	Unit fuel consumption	1.42 yuan/km
T	Average one-way travel time of all-stop service in peak hours	61 min
T_s	Average one-way travel time of short-turn service in peak hours	22 min
ζ	Bus purchase cost	300,000 yuan
c	Number of drivers per bus	1
R_0	Driver's daily wage	100 yuan/person· day

S_0	Daily vehicle maintenance fee	66.7 yuan/vehicle· day
θ	Permitted driving years of vehicles	13 years
h_{\min}	Minimum headway	1.5 min
h_{\max}	Maximum headway	20 min
ω_1	Weight coefficient of passenger cost in total cost	0.45
ω_2	Weight coefficient of public transit cost in total cost	0.55

4.3. Result analysis

By solving the single scheduling model and combined scheduling model respectively, the calculation results of the optimal departure interval and frequency under the combined scheduling of all-stop and short-turn are obtained, as shown in Tables 5 and 6.

Table 5. Calculation results of departure frequency and interval under two dispatching modes

Time interval	All-stop fleet scheduling		Combined scheduling with short-turn service		
	h_0 (min)	f_0 (vehicle/h)	h_1 (min)	h_2 (min)	f_0 (vehicle/h)
7:00-8:00	3.5	17.1	3.6	3.1	8.95
8:00-9:00	4.3	14.0	3.9	3.7	7.89
17:00-18:00	4.2	14.3	4.4	3.5	7.59
18:00-19:00	3.7	16.2	3.7	3.2	8.69

Table 6. Calculation results of total departure frequency in different intervals

Time interval	Within short-turn service range		Out of short-turn service range	
	Single (vehicle/h)	Combination (vehicle/h)	Single (vehicle/h)	Combination (vehicle/h)
7:00-8:00	17.1	17.9	17.1	8.95
8:00-9:00	14.0	15.7	14.0	7.89
17:00-18:00	14.3	15.2	14.3	7.59
18:00-19:00	16.2	17.3	16.2	8.69

From Table 5 and 6, it can be found that within the scope of short-turn service section, the departure frequency of combined dispatching mode has been improved, which can better meet the passenger demand of the section with large passenger flow; outside the scope of short-turn service section, the departure frequency of combined dispatching mode is significantly lower than that of the single dispatching mode, which has a positive significance for passenger evacuation and cost saving in peak hours.

Table 7 shows the cost calculation results of single all-stop service dispatching and short-turn service combination dispatching. Meanwhile, Figure 4-6 visually shows the cost comparison before and after the optimization of dispatching mode, in which the total system cost is the sum of passenger cost and bus operation cost.

Table 7. Cost comparison of single all-stop and short-turn service combined scheduling (yuan / h)

Time interval	7:00-8:00			8:00-9:00		
	Single	Combination	Variation	Single	Combination	Variation
Passenger cost	502	759	+257	482	654	+172
Operation costs	1618	1246	-372	1484	1237	-247
Total system cost	2120	2005	-115	1966	1891	-75
Time interval	17:00-18:00			18:00-19:00		

	Single	Combination	Variation	Single	Combination	Variation
Passenger cost	461	669	+208	437	699	+262
Operation costs	1602	1328	-274	1454	1132	-322
Total system cost	2063	1997	-66	1891	1831	-60

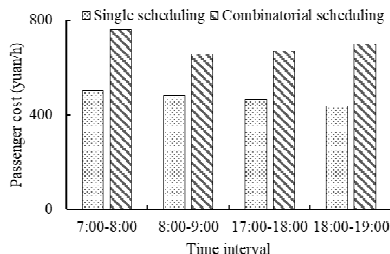


Figure 4. Comparison of passenger cost

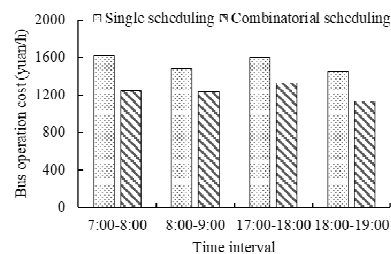


Figure 5. Comparison of bus operation cost

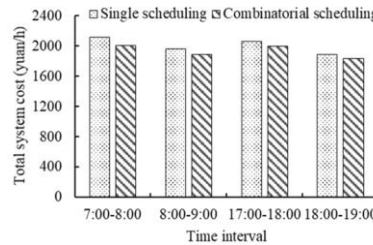


Figure 6. Comparison of total system cost

From Figure 4, Figure 5 and Figure 6, it can be seen that compared with all-stop fleet scheduling, the operation cost of bus companies under combined scheduling scheme is greatly reduced, which can effectively save the total system cost. According to the calculation results of optimal departure frequency and departure interval, the departure interval of other time periods is solved, and the optimal departure interval of each period in whole working day is obtained consequently, as shown in Table 8.

Table 8. Optimal departure interval of each period

Time interval	Scheduling	h_0 (min)	Departure interval	
			h_0 (min)	h_0 (min)
6:00-7:00	Single	11	-	-
	Single	3.5	-	-
7:00-8:00	Combination	-	3.6	3.1
	Single	4.3	-	-
8:00-9:00	Combination	-	3.9	3.7
	Single	4.3	-	-
9:00-10:00	Single	10	-	-
10:00-11:00	Single	8	-	-
11:00-12:00	Single	9	-	-
12:00-13:00	Single	7	-	-
13:00-14:00	Single	10	-	-
14:00-15:00	Single	11	-	-
15:00-16:00	Single	12	-	-
16:00-17:00	Single	9	-	-
17:00-18:00	Single	4.2	-	-
	Combination	-	4.4	3.5
18:00-19:00	Single	3.7	-	-
	Combination	-	3.7	3.2
19:00-20:00	Single	7	-	-
20:00-21:00	Single	9	-	-
21:00-22:00	Single	12	-	-

According to the calculation results of optimal departure interval in Table 9, the departure schedule of single dispatching and short-turn combined dispatching can be compiled. In this paper, the smooth transition uniform departure schedule is used to set the departure frequency at the transition of different periods of single scheduling, as shown in Table 9. Figure 7 shows the cumulative departure frequency of 6:00-12:00.

Table 9. Departure frequency of different periods

Time interval	Departure frequency (vehicle/h)	Time interval	Departure frequency (vehicle/h)
6:00-7:00	5.45	14:00-15:00	5.45
7:00-8:00	17.13	15:00-16:00	5.00
8:00-9:00	13.95	16:00-17:00	6.67
9:00-10:00	6	17:00-18:00	14.29
10:00-11:00	7.5	18:00-19:00	16.22
11:00-12:00	6.67	19:00-20:00	8.57
12:00-13:00	8.57	20:00-21:00	6.67
13:00-14:00	6.00	21:00-22:00	5.00

Taking the transition section between 6:00-7:00 and 7:00-8:00 as an example, the method for determining departure time is shown in Figure 8. It can be seen from the figure that the departure interval at the transition of two periods is 7:02.

Parameters of genetic algorithm: population size $N = 100$; crossover probability $P_c = 0.95$, mutation probability $P_m = 0.01$, maximum number of genetic iterations $i = 100$, and genetic convergence threshold $\delta = 1$.

Finally, the departure time of the bus line is calculated. Previous studies have shown that for the schedule optimization of public transit, the results that are obtained by genetic algorithm are more accurate and reliable[26,27].In order to verify the accuracy of genetic algorithm for solving the proposed model, two widely used heuristic algorithms, simulated annealing algorithm and ant colony algorithm, are compared with the calculation results of genetic algorithm, and it can be found that when the parameters of the three algorithms are within a certain range, the difference between the calculation results is within an acceptable range. In summary, the output of genetic algorithm optimization iteration is taken as the final calculation result. Take 6:00-8:00 as an example, as shown in Table 10. The all-stop scheduling is represented by "0" and the short-turn scheduling is represented by "1".

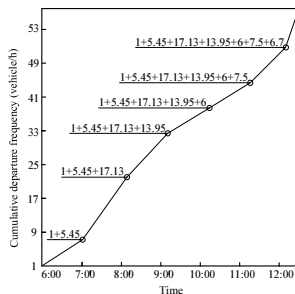


Figure 7. Cumulative departure frequency transition curve of single all-stop dispatching

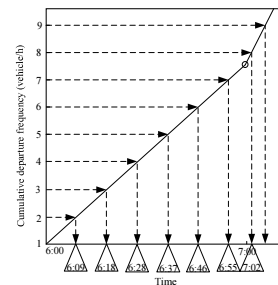


Figure 8. Determination of departure time of section between 6:00-7:00 and 7:00-8:00

Table 10. Departure schedule during 6:00-8:00 under two different bus dispatching modes

No.	Single		Combination		No.	Single		Combination	
	Departure time	Type	Departure time	Type		Departure time	Type	Departure time	Type
1	6:00 AM	0	6:00 AM	0	13	7:19 AM	0	7:20 AM	1
2	6:09 AM	0	6:09 AM	0	14	7:23 AM	0	7:23 AM	0
3	6:18 AM	0	6:18 AM	0	15	7:26 AM	0	7:26 AM	1
4	6:28 AM	0	6:28 AM	0	16	7:30 AM	0	7:29 AM	0
5	6:37 AM	0	6:37 AM	0	17	7:33 AM	0	7:33 AM	1
6	6:46 AM	0	6:46 AM	0	18	7:37 AM	0	7:36 AM	0
7	6:55 AM	0	6:55 AM	0	19	7:40 AM	0	7:40 AM	1
8	7:02 AM	0	7:02 AM	0	20	7:44 AM	0	7:43 AM	0
9	7:05 AM	0	7:06 AM	1	21	7:47 AM	0	7:47 AM	1
10	7:09 AM	0	7:09 AM	0	22	7:51 AM	0	7:50 AM	0
11	7:12 AM	0	7:13 AM	1	23	7:54 AM	0	7:54 AM	1
12	7:16 AM	0	7:16 AM	0	24	7:58 AM	0	7:57 AM	0

By analyzing the two different scheduling schemes, it can be calculated that the running time of short-turn scheduling is 122min and that of the all-stop scheduling is 210min. During the peak period 7:00~10:30, the combined dispatching mode has 45 total departure shift, in which 4 short-turn service are dispatched, and the minimum fleet size is 41. Compared with the all-stop fleet scheduling, the short-turn service combined dispatching reduces the fleet size by 4.9%.

From Eq. (28), the unit vehicle cost per day can be calculated:

$$\phi + R + S_0 = \frac{\xi}{\theta \times 365 \times 24} \times T_r + c \cdot R_0 + S_0 = \frac{480000 \times 16}{8 \times 365 \times 24} + 2 \times \frac{3500}{30} + \frac{2000}{30} \approx 409.5 \text{ (yuan/vehicle-day)}$$

According to the calculation results, the combined dispatching mode can save 819 yuan of operation cost every day and effectively improve its economic benefits.

5. Conclusion and further research

This paper presents a method to determine the short-turn service combination scheme based on the unbalanced coefficient of passenger flow and a method to determine the section stop. A combinatorial scheduling optimization model is established to minimize the total system cost. The empirical analysis shows that, compared with the single scheduling mode, the optimized short-turn service combination scheduling not only has a better adaptability to peak passenger flow, but also can reduce the departure frequency outside the range of shorting-turning bus section. Our contributions are summarized as follows: (1) On the basis of taking into account the cost of passengers and public transit enterprises, a combined scheduling model of short-turning service is established with considering different scheduling strategies, and the solution algorithm is designed. (2) A framework of designing bus combination scheduling scheme based on real-time data is proposed, and the processing method of obtaining passenger flow data based on bus smart card is studied, which can determine the short-turn point more accurately and present the practical instructions to transit operators. (3) A case study of the No. A bus line in Beijing for the service time of a whole day is carried out, the analysis results show that the short-turning service is necessary for the peak hours in working day. By compared with the actual operation, the departure scheme and total

cost are presented, which shows the feasibility and effectiveness of our proposed method.

Although the proposed combined dispatching model can effectively solve the problems existing in the public transit dispatching, the scope of public transport dispatching is relatively wide. In terms of model generalization, it is necessary to evaluate the model under different parameters by adjusting the value of variables according to actual situation in different regions. In addition, some limitations in this paper need further study: (1) Only the peak passenger flow of a single bus line is analyzed in this paper. However, the research scope can be expanded to further study the regional dispatching optimization. (2) This paper does not design other scheduling forms, such as the combined scheduling of all-stop service, short-turn service and stop-skipped bus. The impact of more complex scheduling forms on the cost of passengers and bus companies is worth further consideration. (3) Last but not least, only static combined scheduling scheme is obtained, and the intelligent dynamic combined scheduling model and the more efficiently solution algorithm should be studied in the future.

Acknowledgments

The authors would like to express their sincere gratitude for the funding support provided by the National Key R&D Program of China (Grant No.2018YFB1601200).

References

- [1] Cancela H, Mautton A, Urquhart ME. Mathematical programming formulations for transit network design. *Transportation Research Part B: Methodological*. 2015 Jul; 77:17-37.
- [2] Cancela H, Mautton A, Urquhart ME. Mathematical programming formulations for transit network design. *Transportation Research Part B: Methodological*. 2015 Jul; 77:17-37.
- [3] Liu T, Ceder A. Deficit function related to public transit: 50 year retrospective, new developments, and prospects. *Transportation Research Part B: Methodological*. 2017 Jun; 100:1-19.
- [4] Deng LB, Gao W, Zhou WL, et al. Optimal Design of Feeder-bus Network Related to Urban Rail Line based on Transfer System. 2013, 96:2383-2394.
- [5] Wenxin Li, Qiyuan Peng, Qinlin Li, et al. Joint Operating Revenue and Passenger Travel Cost Optimization in Urban Rail Transit. 2018, 2018:1-15
- [6] Tomáš R, Shadi SA, Yousef M et al. Train timetable design under elastic passenger demand. *Transportation Research Part B*. 2018, 111
- [7] Peña D, Tchernykh A, Nesmachnow S, Massobrio R, Feokitistov A, Bychkov I, et al. Operating cost and quality of service optimization for multi-vehicle-type timetabling for urban bus systems. *Journal of Parallel and Distributed Computing*. 2019 Nov; 133:272-85.
- [8] Liu T, Ceder A, Chowdhury S. Integrated public transport timetable synchronization with vehicle scheduling. *Transportmetrica A: Transport Science*. 2017 Jul; 13(10):932-54.
- [9] AlKheder S, AlRukabi F, Zaqqouq A. Optimal bus frequency for Kuwait public transit company: A cost view. 2018 Aug; 41:312-9.
- [10] Giesen R, Martínez H, Mauttne A, Urquhart ME, et al. A method for solving the multi-objective transit frequency optimization problem. *Journal of Advanced Transportation*. 2017 Apr; 50(8):2323-37.
- [11] Berrebi SJ, Watkins KE, Laval JA. A real-time bus dispatching policy to minimize passenger wait on a high frequency route. *Transportation Research Part B: Methodological*. 2015 Nov; 81(2):377-89.
- [12] Park C, Lee J, Sohn SY. Recommendation of feeder bus routes using neural network embedding-based optimization. *Transportation Research Part A: Policy and Practice*. 2019 Aug; 126:329-41.
- [13] John J, Bartholdi, et al. A self-coordinating bus route to resist bus bunching. *Transportation Research Part B Methodological*, 2012 Oct;46(4):481-91

- [14] Canca D, Barrena E, Laporte G, et al. A short-turning policy for the management of demand disruptions in rapid transit systems. *Annals of Operations Research*. 2016 Jul; 246(1-2):145-66.
- [15] Cheng SJ. Research on short-turn vehicle combinational scheduling method for bus route. Huazhong University of Science and Technology. 2013.
- [16] Cortés CE, Jara-Díaz S, Tirachini A. Integration short turning and deadheading in the optimization of transit services. *Transportation Research Part A: Policy and Practice*. 2011 Jun; 45(5): 419-34.
- [17] Hu BY, Wang XK, Chen WQ. Study on combinational scheduling between inter-zone vehicle and regular vehicle for urban public transit. *Journal of Wuhan University of Technology (Transportation Science & Engineering)*. 2012 Dec; 36(6):1192-95.
- [18] Cao YL. Study on the optimal model and solution for the problem of public transport dispatch. *Experiment Science and Technology* 2011 Aug;9(4):27-30,182
- [19] Chen JX, Liu ZY, Zhu SL, Wang W. Design of limited-stop bus service with capacity constraint and stochastic travel time. *Transportation Research Part E: Logistics and Transportation Review*. 2015 Nov; 83:1-15.
- [20] Wei M, Chen XW, Sun B. Multi-objective single line transit mixed scheduling model considering express bus service. *Journal of Transportation Systems Engineering and Information Technology*. 2015 Apr; 15(2):169-74,181.
- [21] Canca D, Barrena E, Laporte G, Ortega FA. A short-turning policy for the management of demand disruptions in rapid transit systems. *Annals of Operations Research*. 2014 Jul; 246(1-2): 145–66.
- [22] Zhang H, Zhao SZ, Cao Y, Liu HS, Liang SD. Real-time integrated limited-stop and short-turn service control with stochastic travel time. *Journal of advanced transportation*. 2017 Jul; 2017(746):1-9.
- [23] Gao L. Research and application of vehicle bus combined scheduling model for urban public interval bus. Dalian Maritime University. 2017.
- [24] Ming J, Zhang GJ, Liu YD. Combinatorial optimization model of multi-modal transit scheduling. *Computer Science*. 2015 Sept; 42(9):263-7.
- [25] Liu C. Research on single line bus scheduling problem based on hybrid heuristic algorithm. Beijing Jiaotong University. 2016.
- [26] Huang AL, Dou ZQ, Qi LZ, Wang LW. Flexible Route Optimization for Demand-Responsive Public Transit Service. *Journal of Transportation Engineering, Part A: Systems*, 2020.Sep;146(12): 04020132
- [27] Xiong, J, He Z, Guan W, Ran B. Optimal timetable development for community shuttle network with metro stations. *Transportation Research Part C: Emerging*. 2015 Nov; 60: 540–565.

Monitoring the Development Quality of College Students Based on Knowledge Graph

Aiyan Wu¹ and Yongmei Zhang

School of Information Science and Technology, North China University of Technology

Abstract. With the rapid development of higher education, how to innovate management means and ensure the quality of education is an urgent problem faced by higher education management. The paper focuses on a large number of data that include students' enrollment performance, family status, lessons performance, volunteer service, competition, rewards and punishments, social practice, etc. And it puts forward an education quality monitoring means that uses knowledge graph to reveal students' development and can guide the development of students according to the needs of local talents. The means includes three parts: the current situation of students' development, the early warning of development and the guidance of development. Finally, taking the postgraduate education in School of Information Science and Technology, North China University of Technology as an example, it demonstrates the feasibility and effectiveness of the means.

Keywords. Knowledge graph, higher education, quality monitoring

1. Introduction

With the development of China's higher education, the focus of its development has shifted from expanding its scale to improving its quality. Therefore, the management of education in universities is facing an urgent problem that is how to steadily improve the quality of education with the current large scale of undergraduate enrollment. And higher education informatization is an important means to solve this dilemma.[1-2] "Ten year development plan of education informatization (2011-2020)" issued by the Ministry of education of China clearly points out that[3] "education informatization is an effective way to promote education reform and improve quality of education."

In the process of education informatization in China, the education informatization platform has been mature and widely used in universities, which greatly facilitates the education management and has accumulated a lot of data information. However, how to transform all kinds of scattered and large-scale management data (in trillions of bytes) into information that can be understood by educational administrators and guide their work (in thousands of bytes), is a hot issue in the development of higher education informatization, and also the key to the innovative development and quality improvement of higher education[4]. At present, there are relatively excellent research results [5-7], such as practice monitoring, curriculum monitoring, and employment monitoring, etc. However, all aspects of students' development should interact and

¹ Corresponding Author: Aiyan Wu, E-mail: wuaiyan@ncut.edu.cn. The paper is supported by project of subject construction (NO.218051360020XN113).

promote each other. So, we can better improve the quality of education with the overall research. This is also the new task of education informatization.

The research of knowledge graph can provide a feasible research method for the new task of higher education informatization under the new stage. It consists of two parts. One is to acquire knowledge with big data technology; the other is to display the knowledge with graphs, which is one of the most advanced information technologies. And it can integrate all kinds of information and discover knowledge from the massive and complicated words, symbols and digital information [8]. Therefore, how to use knowledge graph to mine and show the laws in the process of education, and then guide the daily work of universities? The paper analyzes these problems in monitoring the development quality of college students, and proposes a means on monitoring the development quality of college students based on knowledge graph that includes knowledge graph of student development, big data monitoring and early warning of student development, and analysis of student development oriented by talent demand. It has realized the integration, analysis and display of scattered students' information with knowledge graph.

2. Problems in monitoring the development quality of college students

2.1. Dispersion and fragmentation of students' development information

Whether monitoring a professional development quality or a individual, it is to monitor the overall indicators, because the result will be one-sided by monitoring part indicators. However, in the process of training students from enrollment to graduation, the indexes information is complex and scattered, and even stored in different management departments. They include students' enrollment performance, family status, lessons performance, volunteer service, competition, rewards and punishments, social practice, etc. [9-10]. University administrators in different positions have access to only the part information about own work, so it is difficult to know the dynamic development of students and the gap between their current situation and training objectives. Access to comprehensive information requires the collaborative operation of multi-post staff, which can not be achieved under normal working conditions [11]. However, in order to achieve accurate monitoring of students' development quality, it is necessary to monitor the overall information of individuals. Therefore, how to systematically understand the overall information in the cultivation process is the primary problem in the monitoring process.

2.2. Lack of early warning mechanism

The management standards of colleges and universities are different. Each counselor is basically responsible for 200 students, and each educational administration personnel is responsible for a major specialty [12]. In fact, with the popularization of higher education, a counselor must manage far more than 200 students, and a management staff has to face the academic management of nearly a thousand students, or even more. This is all the more so for those universities located in first tier cities such as Beijing, Shanghai and Shenzhen. On the one hand, fine manual management is difficult to achieve, on the other hand, students who fail in many courses are regarded as academic difficulties. It's hard to change the academic dilemma, which is the key problem [13].

Often such students can not graduate smoothly, that is the failure in training. Any result is not achieved overnight. If we can timely find out abnormality in the long process of development, especially in the early stage of emergence, the academic guidance of our university staff can play a better role. So, to reduce the training failure cases, how can we discover the individuals with academic difficulties among thousands of students before the academic difficulties have developed? It is not easy to find abnormal individual performance from all kinds of complex training information, and it is impossible to achieve without advanced information technology.

2.3. The backward tracking technology of college students' employment quality

The quality of students' development is good or not, which depends on their employment evaluation. Therefore, the local talent demand should be the guidance of students' development in order to achieve a better match between students and employment companies. The existing quality tracking of students' employment is mainly based on questionnaire survey or company satisfaction survey [14]. On the one hand, the coverage of the survey is not complete. On the other hand, it is lack of sustainability. There is no dynamic development tracking of a whole major. At present, the tracking technology only can get a research report. Either it does not play a practical role in the development of specialty, or it does. However, due to the limitations of research, it can not play an effective role in guiding specialty construction. In addition, it is difficult to accurately reflect the professional market demand by the results of irregular and limited research [15]. The comprehensive and sustainable research should depend on advanced information technology.

These current sustainable researches of college students' employment quality have lagged behind the needs of education development. So, based on the needs of local talent, how to rely on advanced information technology to achieve the accurate guidance of students' development?

3. Monitoring means of college students' development based on knowledge graph

In view of the above problems, the main idea of this means is as follows. The scattered information is integrated with distributed database technology, and the student development database is constructed based on the campus LAN. On the one hand, the big data association mining technology is used to discover the crisis factors that affect learning, and they are stored in a crisis database. On the other hand, we use big data classification technology to find the correlation between the quality of students' employment and the data of students' development. So, we can classify students' development indicators according to different employment, and build a knowledge base of students' development oriented by employment demand. Finally, the knowledge graph is used for visualization display. One is to display the dynamic development of students during the school period, and the gap between the indicators and the professional training objectives; the other is to show the gap between the development of the students and the target of graduation. Once the crisis event is triggered and then academic warning will appear, we can clearly see the situation of students from individual knowledge graph, including the relationship between students, academic performance, extracurricular development, etc.

3.1. Knowledge graph of college Students' development

The knowledge graph can integrate the distributed information in the process of student development. And it dynamically can not only show the various indicators of students' individual development, but also show the gap between individual students and professional training. A knowledge graph of an individual student makes all individual development information clear and be shared, so that the administration personnel can check the personal development of students at any time and guide them accordingly. At the same time, it can also help students to understand their academic situation as a whole and correct their self-development timely.

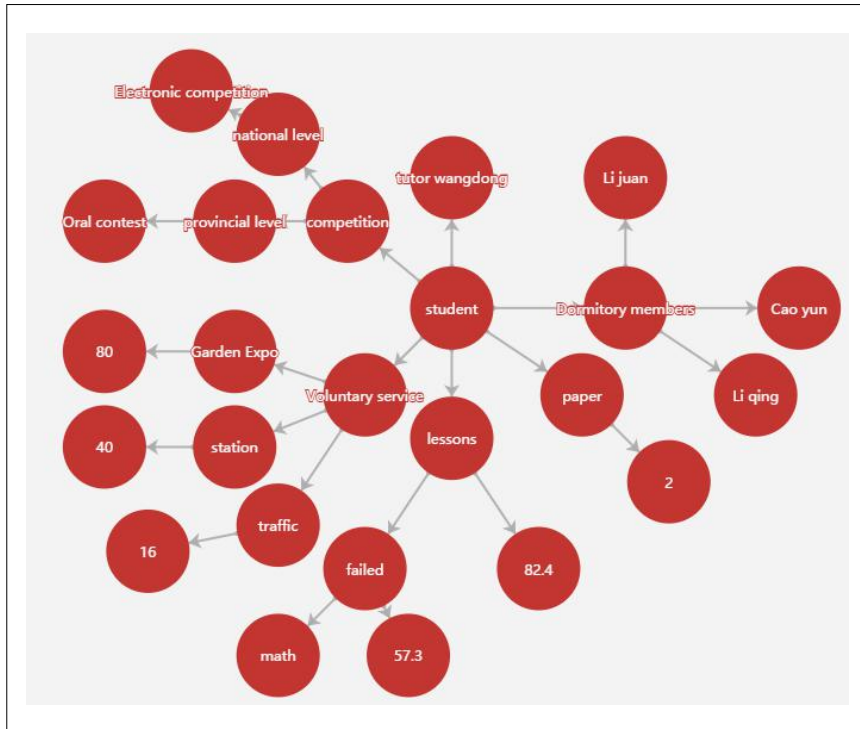


Figure1. The graph of a postgraduate in school

Firstly, the concept model of the knowledge graph should be constructed. Taking students as the noumenon, it defines the development indicators of students as attributes, and the relationship between development indicators as the correlation of attributes.

Secondly, its data model should be constructed. Its concept mode will be instantiated with attribute set and relation set.

Thirdly, the database of student development information is integrated. It is a distributed relational database, which integrates the information of various management platforms.

Fourthly, the knowledge graph is realized. Formal language can be used to describe the research information. And the knowledge graph of students' development can be realized with Protege program.

3.2. Early warning mechanism of college students' development crisis

There are some significant associations between the results of students' academic development and the training factors, and they can be discovered with the big data intelligent analysis technology. So, the database of student development rules is constructed. Once the impact event is triggered or the individual student deviates from the normal development path, it will quickly remind the university administrators and the students themselves. Before the emergence of academic difficulties, problem individuals can be found in time, such as failure in several courses. So we can guide the students to solve the difficulties earlier. In the case of more students and less management, reducing failed individuals is of great significance to improve the students' development quality in higher education stage.

Firstly, the information of students' development is discretized. There are many types of students' development information. In order to realize its' comprehensive analysis and operation, we should first discretize the information. The discrete range of the various development information is determined based on the big data intelligent computing model, so as to realize the discretization of all information.

Secondly, the mathematical model of dynamic warning is constructed. The rules are represented by mathematical models to realize the reasoning of early warning. The "and" mode is used to express the relationship among multiple conditions.

Thirdly, the warning of academic is established. The early warning system can automatically warn the students with learning difficulties in advance. According to the warning information, we can make academic supervision more detailed and accurate with the knowledge graph of students' development.

3.3. The optimization of college students' development oriented by talent demand

The big data technology can analyze the local vocational recruitment demand in recent years, and excavate the matching path of personal career goals with local talent demand. So we can get the association between different posts demand and key links of student development, and form association rules to guide students' development. Taking local talent demand as the guidance and individual career demand as the goal, we can guide students to develop with higher target to achieve students' career satisfaction and employers' satisfaction. This can make local universities better train applied talents for the local.

Firstly, we define the range of matching degree between employment target and actual employment.

Secondly, we mine the relationship between students' development links and post demand with the association analysis method based on big data. Because the data of individual students are independent, the parallel operation mechanism is used to extract the conditions of excellent students' development and the relationship between the conditions and the employment.

Thirdly, the association rules database is built. Based on the extracted association, the employment data is taken as the antecedent, and the student development information is taken as the consequent to build the association rule database.

Fourthly, the research results are used to guide the development of students. From students' career goals, including employment quality and employment type, we can know the conditions that students need to meet with intelligent reasoning. Combined with the knowledge graph of students' development, we can make clear the direction

that students need to work hard, and then help students get more targeted guidance.

4. Application cases

Taking the postgraduates in School of Information Science and Technology, North China University of Technology as an example is following. In recent years, the number of students enrolled has tripled. At present, there are more than 600 postgraduates on campus. One educational administration and one counselor are assigned to their daily management. The above-mentioned means is used to build a management platform, which realizes multi-department collaborative office.

Students with academic difficulties are found in time with early warning mechanism, and their problems are comprehensively understood and analyzed from their individual knowledge graph, and the key guidance is given to effectively help them out of their learning difficulties. Since 2014, there are 15 students with academic early warning in the college. Among them, 13 students have improved their academic status after guidance (seeing Table 1 for details over the years), and eight of them have successfully graduated and obtained satisfactory job positions, and five of them have come out of their academic difficulties at school, and one of them needs further guidance, and one of them has dropped out of school. The effect of academic warning function has achieved remarkable results with the knowledge graph of student individual.

Table 1. Academic warning situation

year	2014	2015	2016	2017	2018	2019	2020
number of students warned	3	1	2	4	2	3	0
number of students improved	2	1	2	3	2	3	0

In addition, students' development is guided by employment demand based on the knowledge graph of individual development, which promotes students to know their own learning objectives and development plans. This not only promotes students to graduate smoothly, but also improves their employment satisfaction. Since the student development has been differently guided according to the employment demand, the employment rate of the college has been 100% in the past five years, and the employment satisfaction is higher than local level. (see Figure 2).

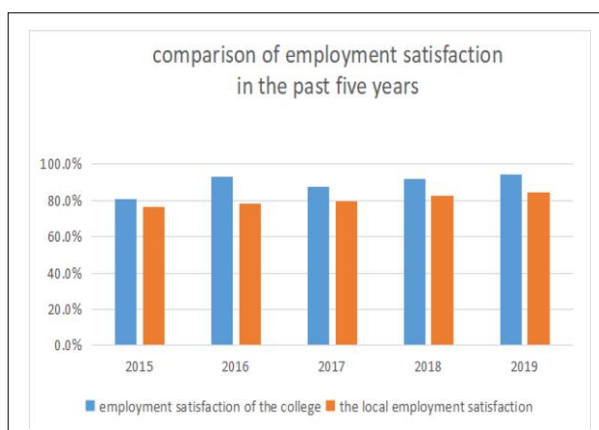


Figure 2. Comparison of employment satisfaction in the past five years

With the help of knowledge graph, satisfactory results have been achieved in improving students' academic performance and employ quality. The platform can display students' personal information comprehensively, which greatly facilitates the coordination of multi-department staffs and promotes the management effect.

5. Conclusion

The informatization process of higher education has achieved the stage of informatization of management platform. It is an important to discover rules and guide practical work. And the relevant research is of great significance to improve the quality of talents in higher education. The development of knowledge graph meets the actual needs of higher education informatization. The monitoring means of college students' development based on knowledge graph is effective and feasible. It can integrate the scattered information of students, display the dynamic development of students, and effectively promote the management of students' training.

References

- [1] YING Huiqiong, SU Rong. Promoting practical teaching in applied undergraduate colleges by quality monitoring data. Research and exploration in laboratory. 2020, 39(1):236-240.
- [2] WU Jin, ZHANG Yu, HUANG Lifei .Improving the quality of postgraduate training for professional degrees in applied universities. Education and vocation. 2020, (03): 34-41.
- [3] FENG Shilan, TAN Ya, JIN Wenwang, JIANG Cheng. The quality of higher education in China and the starting salary of college graduates: a quantitative study based on the survey of employment status of college graduates across the country. World economics collection, 2019, (03): 73-84.
- [4] WANG Xingyu. The value turn of the evaluation of the learning achievement of American college students. Development and evaluation of higher education. 2019, 35(05):27-37+114-115.
- [5] ZHU Hong. Research on the high-quality development path of international student education. Jiangsu higher education. 2020,(01):64-71.
- [6] YANG Dongxiao. Research on the strategies of improving the quality of postgraduate courses from the perspective of course subject incentives. Degree and postgraduate education. 2020, (01):43-47.
- [7] PAN Zisong, YAN Cen. A survey of college students' employment situation under the guidance of improving employment quality. Heilongjiang higher education research. 2019, 37(12):139-142.
- [8] YING Shuang. Constructing a graduate education quality system with interactive growth between subjects—based on the perspective of psychological contract and service essence. Degrees and graduate education. 2019, (12):7-12.
- [9] WANG Jing. Research on the ideological and political work system and team building strategies in colleges and universities. Research in higher engineering education. 2019,(S1):303-304+308.
- [10] TAN Chuansheng. Research on the innovation of practice education mechanism in colleges and universities.School party building and ideological education. 2019, (24): 61-63.
- [11] CAI Yun, SHI Banghong .Improvement of the model of the measurement factors of higher education quality. China higher education research. 2019, (04):74-79.
- [12] PENG Zhengxia, LU Genshu, LI Lijie. Analysis on the influencing factors and paths of university graduates' employment quality. China higher education research. 2020, (01): 57-64.
- [13] PENG Zhengxia, LU Genshu. Gender differences in employment quality of university graduates: an analysis based on multi-group structural equation model. Fudan education forum. 2020, 18(01):59-67.
- [14] XIE Weiqun, XU Shuo, YU Liying .Evaluation and improvement of the quality of innovative and entrepreneurial talent training. Science and Technology of Chinese Universities. 2019, (11):41-44.
- [15] YANG Yi, XIA Huixian. The conception and realization path of the diversified cultivation of doctoral students—based on the reflection of 20 years of research on the quality of doctoral education in my country. Graduate education research. 2020, (01): 15-21.

Hierarchy Spatial-Temporal Transformer for Action Recognition in Short Videos

Guoyong Cai, Yumeng Cai¹

*GuangXi Key Laboratory of Trusted Software, Guilin University of Electronic
Technology, Guilin, China*

Abstract. Short videos action recognition based on deep learning has made a series of important progress; most of the proposed methods are based on 3D Convolution neural networks (3D CNN) and Two Stream architecture. However, 3D CNN has a large number of parameters and Two Stream networks cannot learn features well enough. This work aims to build a network to learn better features and reduce the scale of parameters. A Hierarchy Spatial-Temporal Transformer model is proposed, which is based on Two Stream architecture and hierarchy inference. The model is divided into three modules: Hierarchy Residual Reformer, Spatial Attention Module, and Temporal-Spatial Attention Module. In the model, each frame's image is firstly transformed into a spatial visual feature map. Secondly, spatial feature learning is performed by spatial attention to generating attention spatial feature maps. Finally, the generated attention spatial feature map is incorporated with temporal feature vectors to generate a final representation for classification experiments. Experiment results in the hmdb51 and ucf101 data set showed that the proposed model achieved better accuracy than the state-of-art baseline models

Keywords. Spatial feature learning; hierarchy inference; spatial-temporal attention

1. Introduction

Video learning, which goal is to learn the content feature in each frame, consists of various tasks, such as object tracking, temporal action localization, action recognition, and et al. Action recognition in video learning has been researched for years but still a challenging task. Compared to single image recognition, temporal information between video frames must be considered for action recognition [1]; the computing efficiency must be considered due to the real-time property of video streams.

Recently, many researchers have developed novel methods for action recognition by using 3D Convolution Neural Network [2] or by Two Stream Convolution Neural Network(2S CNN) [3], which incorporate spatial and temporal CNN to extract spatial and temporal feature from each video frame.

¹ Corresponding Author: Yumeng Cai, GuangXi Key Laboratory of Trusted Software, Guilin University of Electronic Technology, Guilin, China. Email: cymqqqq@gmail.com

3D CNN can learn the features well in the video, but it has large scale parameters and is low efficient; 2S CNN can not learn the spatial and temporal feature in video accurately. Some works have explored methods of using spatial-temporal relation information, such as the C3D network [4], R3D network [5], but they still can not learn video features well.

To address the problem of reducing the parameter scale of 3D CNN, the paper used the mask network to avoid redundancy computation when learning spatial features in continuous frames.

To learn better features, the paper proposed to use the hierarchical inference principle designed in paper [6]. The hierarchy inference can calculate the posterior probability $p(y|x, z, w; \theta)$ under given initial prior knowledge $p_\theta(w)$ and conditional probability $p_\theta(z|w), p_\theta(y|x, z)$ in continuous states, where x, y, z, w is denoted be the feature map and θ represents the parameter of the network in this work. This will help us to design more useful learning models that can learn better features. The spatial feature of the image in the first frame can be taken as initial prior to infer the action context of the spatial features in the next frame.

This paper proposed a novel model, Hierarchy Spatial-Temporal Transformer, to learn the spatial-temporal related information based on Two Stream CNN and incorporates hierarchy inference. The main contributions of this paper are listed as follows.

- (1). A Hierarchy Residual Reformer is proposed to calculate the spatial feature similarity between every two frames.
- (2). A hierarchy residual network that incorporates the hierarchy inference method is proposed to calculate action feature similarity.
- (3). Spatial attention and a hybrid spatial-temporal transformer are designed to learn spatial-temporal related information.

2. Related Works

Action recognition methods can be divided into three types: 3D CNN, 2S CNN, and the combination of 3D CNN and 2S CNN.

Baccouche and Ji et al. [7] first proposed 3D convolution for action recognition; and then Ji et al.[8] further proposed two techniques to exploit prior information for the 3D CNN. One is that the original image, image gradient, and optical flow of adjacent frames were all used as input of their network, and the other is that they also used 3D convolution to learn the motion information between each frame. Based on 3D convolution, Tran et al. [9] proposed spatial and temporal feature 3D convolution (C3D) for action recognition, and their experiments showed that the convolution network in the temporal direction works best when the size of the convolution kernel is $1 \times 1 \times 3$. The reason is that C3D can handle multiple frames at a time. However, due to its scale of weight and parameters, C3D is difficult to train. To reduce the parameter scale and weight of C3D, Qiu et al. [10] decompose the 3D CNN into a 2D spatial

convolution and 1D temporal convolution. Then the two convolution networks are connected in series or parallel, and finally, a residual network is combined to construct a pseudo 3D (P3D) network. Based on the C3D network, Xu et al.[11] proposed Faster R-CNN to extract features from the input video clips, then extract candidate temporal information, and finally used Region of Interesting network(RoI)[12] to aggregate the features. Different from the C3D network, Faster R-CNN is mainly used for Object Detection. Shou et al.[13] proposed multi-stages CNN (MSCNN) for action recognition. Different from the above 3D networks, three different 3D convolution networks are proposed in MSCNN to perform different tasks.

Karpathy et al.[14] first proposed a 2S CNN for action recognition. One branch of the two-stream network inputs the spatial RGB image, and the other branch inputs the temporal-dimensional optical flow information of each frame. The final convolution features of the two branches are stitched together as the input into fully-connected layers to perform the action classification task. Based on a two-stream network, Zolfaghari et al. [15] proposed an efficient convolution network (ECO) for online video action recognition. Because the adjacent frames of the video have information redundancy, ECO samples several frames from the video. 2D convolution is used to extract spatial features of each frame, then the spatial features are stitched along the temporal dimension, and finally, the temporal relationship between each frame is captured by 3D convolution. The performance of ECO is better than 2S CNN. Based on 2S CNN, Tran et al. [16] proposed a residual two-stream network (ResNet (2+1)D) for action recognition. In their model, 3D convolution is decomposed integral into a 2D spatial convolution, and a 1D temporal convolution and spatial and temporal convolution are used to extract spatial features and temporal dimensional optical flow features respectively.

Shou et al.[17] proposed overlapping convolution networks (CDC) for action recognition, CDC incorporates 2S CNN and 3D CNN to obtain classification prediction score according to each frame. Then spatial convolution is used for down-sampling in the spatial dimension, and temporal-transposed convolution is used for up-sampling in the temporal dimension. Finally, spatial and temporal features are fused to classify actions.

Although C3D, P3D, and MSCNN networks have some improvements in performance, the computational efficiency is very low and the parameters scale is still large. The ECO, ResNet (2+1)D has some improvements in computational efficiency, but the ability to learn feature is still not enhanced.

3. Hierarchy Spatial-Temporal Transformer

In this section, the proposed model, the Hierarchy Spatial-Temporal Transformer, is presented and the overall architecture of the model is shown in figure 1. The hierarchy spatial-temporal transformer consists of three components: hierarchy residual reformer, spatial attention module, and spatial-temporal attention module. The Hierarchy residual reformer aims to transform short video into spatial visual feature maps and learn

temporal features. The spatial attention module incorporates an attention mechanism to perform spatial feature learning for producing spatial attention vector. The spatial-temporal attention module aims to fuse the spatial feature vector and temporal feature to produce final features. The details the components are given in the following section 3.1-3.3.

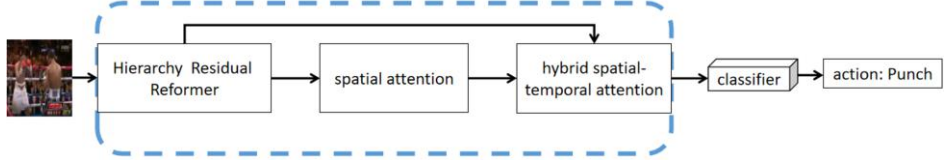


Figure 1 Overall Architecture of The Model

3.1 Hierarchy Residual Reformer

In figure 2, the hierarchy residual reformer consists of three parts: temporal convolution, spatial-visual slide window, and hierarchy residual network. Temporal convolution is used to extract the optical flow feature of each frame. The spatial visual slide window contains a merge operation that is used to aggregate features of two frames and spatial visual normalization (SVN) module that is used to calculate spatial feature similarity of images in two frames. The hierarchy inference method is applied by the hierarchy residual network to calculate the action similarity of the spatial visual feature map. In figure 2, each video that the time is within thirty seconds is clipped into 16 frames, denoted by x_1 to x_{16} .

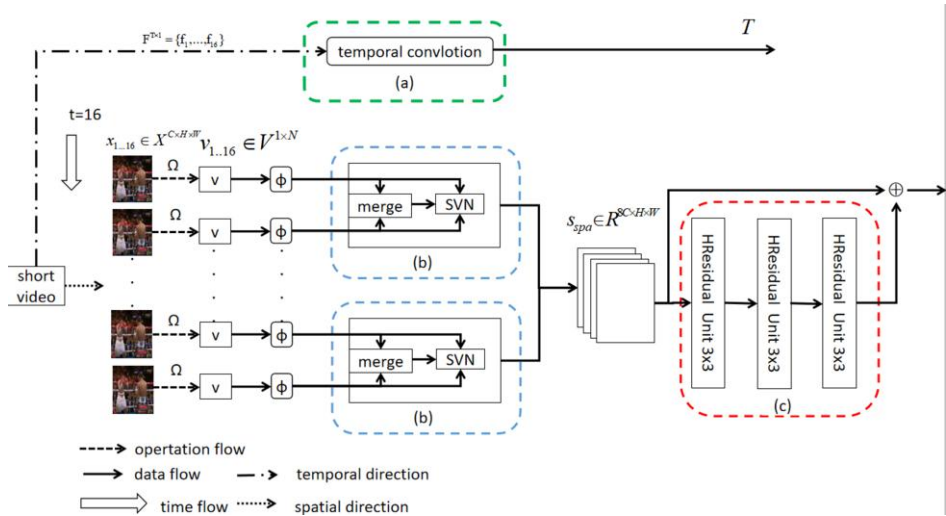


Figure 2 Hierarchy Residual Reformer

In this work, the short video is transformed by a map function along the spatial direction that is denoted by a 2D image of each frame $X^{C \times H \times W} = \{x_1, \dots, x_{16}\}$, where

C , H , W represents a channel, height, and width of the image, respectively. And the short video is learned by a temporal convolution along the temporal direction that is in the form of motion across the frames is denoted by continuous multi-frame optical flow $F^{1 \times N} = \{f_1, \dots, f_{16}\}$, where N represents the numbers of frames. Optical flow is the motion of objects between consecutive frames of the sequence; it is obtained by the function inside the OpenCV.

A green part of figure 2(a), temporal convolution $\text{temporal_CNN}(f)$ that is denoted by a 3D CNN layer with kernel size $1 \times 1 \times 3$ is used to extract optical flow motions along the temporal direction to produce the temporal feature T , the operation is denoted by equation(1).

$$T = \text{temporal_CNN}(f) \quad (1)$$

The images $x_{1 \dots 16}$ are firstly processed by channel shuffle[18] operation that is a tensor operation inside the Pytorch framework to help information flow across feature channels. Then a map function $\Omega : x \rightarrow v, x \in X^{C \times H \times W}, v \in V^{1 \times N}$, where $N = C \times H \times W$, is used to transform the processed images $x_{1 \dots 16}$ into feature vectors $v_{1 \dots 16}$, where Ω represents a fully-connected neural network. The feature vector is flattened into a 3D tensor by the reshape function that is inside the Pytorch framework. The tensor is then learned by a 3D CNN layer Φ with kernel size $1 \times 3 \times 3$.

In figure 2(b) that is marked by a blue square, the output of the 3D CNN layer is then sent to a spatial visual slide window, which consists of a merge operation that is denoted by equation(2) and a spatial visual normalization(SVN) module. The goal of the merge operation is to aggregate features of two frames to produce the spatial feature ξ .

$$\xi = \Phi(v_i) \oplus \Phi(v_{i+1}) \quad (2)$$

where \oplus represents matrix addition. Φ represents 3D CNN with kernel size $1 \times 3 \times 3$.

The goal of the SVN module is to calculate the similarity of spatial features while keeping the data distribution consistent. The procedure of SVN includes the following steps. First, the feature vector of two frames is used to calculate mean value u , denoted by equation (3).

$$u = \frac{1}{M} \sum_{i=1}^M \|\Phi(v_i) - \Phi(v_{i+1})\| \quad (3)$$

where M represents the number of frames.

In the second step, the mean value and the feature vector of the i^{th} frame are used as the input to calculate variance, the operation is shown by equation (4). Equation (5) is used to perform a normalization operation that keeps the data distribution consistent and reduces the complexity of the model and obtain feature map s , where ε represents noise from Gaussian distribution. ξ, μ, σ represents the output of equation(2), equation(3), and equation(4), respectively. The output of equation (5) is stacked together to produce the final spatial feature map $s_{spa} \in R^{8C \times H \times W}$, where the channel numbers C of each window is stacked together to 8C, and the operation is denoted by equation(6), where CONCAT represents connect operation.

$$\sigma = \frac{1}{M} \sum_{i=1}^M \|\Phi(v_i) - u\|^2 \quad (4)$$

$$s = \frac{\xi - u}{\sqrt{\sigma + \varepsilon}} \quad (5)$$

$$s_{spa} = \text{CONCAT}[s_1, \dots, s_8] \quad (6)$$

In figure 2(c) that is marked by a red square, the hierarchy residual network is performed to learn the feature of the action context of each spatial-visual feature map. The detail of the HResidual unit spatial_CNN() is given in figure 3. The HResidual unit consists of a 3D CNN layer, a down-sample module φ , a δ module, and a LeakyReLU activation function. The goal of this module is to produce a spatial feature $s \in R^{C \times H \times W}$, the overview operation of this module is denoted by equation(7):

$$s = \text{spatial_CNN}(s_{spa}^i; \theta) + s_{spa}^{i-1} \quad (7)$$

where s_{spa}^i represents the spatial-visual feature of the i^{th} channel.

A 3D CNN layer Φ with kernel size 1x3x3 is firstly performed to learn the spatial visual feature. The down-sample module is then used to extract the maximum value of the feature map, and function δ is used to calculate similarity that is a conditional probability under given spatial- visual feature map of the i^{th} channel, the operation is denoted by equation (8).

$$\text{spatial_CNN}(s_{spa}^i; \theta) = \varphi(W_{s_{spa}^{i-1}}^T * \Phi(s_{spa}^i)) + \text{LeakyReLU}(W_{s_{spa}^{i-1}}^T * \delta(s_{spa}^i, \Phi(s_{spa}^i))) \quad (8)$$

where φ, δ represents the down-sample module and action feature similarity computation module, respectively. LeakyReLU represents activation function. $W_{s_{spa}^i}^T$

represents the weight matrix of the action feature. θ represents the hyper-parameters of the neural network.

Finally, a mask is used to measure the weights of the action of two frames. If the similarity of action of the two frames is low, then the Hadamard product is performed, otherwise, the only operation that is performed of the part is convolution. The advantage of this operation is that only features with significant weight are calculated, which can greatly reduce the scale of the parameter. The operation is denoted by equation (9), where \otimes represents Hadmard product. $*$ represents a matrix product.

$$\delta(s_{spa}^i, \Phi(s_{spa}^i)) = (1 - \text{mask}(s_{spa}^i)) * \Phi(s_{spa}^i) + \text{mask}(s_{spa}^i) * \Phi(s_{spa}^i) \otimes W_{s_{spa}^i} \quad (9)$$

After all operations of this part are accomplished, the final feature is converged into one backbone to produce the final spatial-visual feature s , where \oplus represents matrix addition.

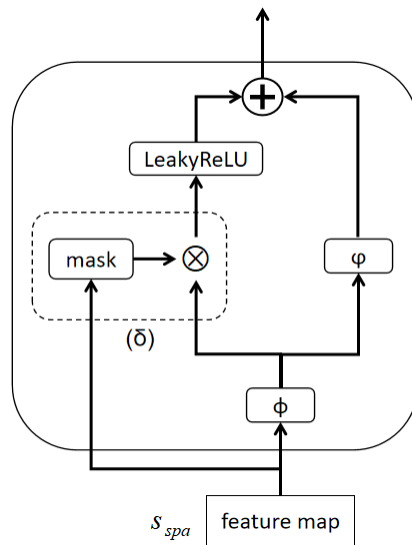


Figure 3 HResidual Unit

where mask represents a 3D convolution layer with kernel size 1x3x3 and output 1 channel.

3.2 Spatial feature attention

In figure 4, spatial feature attention consists of two Gaussian error linear units(GELU), a softmax function, and a single-layer feed-forward neural network f. The two spatial feature maps s^1, s^2 are used as the input to spatial attention module that is incorporated attention mechanism to further learn better spatial feature.

Two Gaussian error linear units(GELU) is used for spatial-visual feature learning, because which takes advantage of Dropout operation[19] and non-linear activation function to prevent model over-fitted and enhance the learning ability of the model. Then Hadmard product is performed to fuse two features, the operation is shown by equation(10).

$$\gamma = \text{GeLU}(s^1) \otimes \text{GeLU}(s^2) \quad (10)$$

where \otimes represents Hadmard product.

For attention, the fused feature is sent to the softmax function that is denoted by equation(11) is used to obtain the attention score β .

$$\beta = \text{softmax}(\gamma) \quad (11)$$

The fused feature γ and the output of softmax function are used as the input to the single-layer feed-forward neural network f that is denoted by equation(12) to generate an attention feature vector λ .

$$\lambda = f(\beta, \gamma) \quad (12)$$

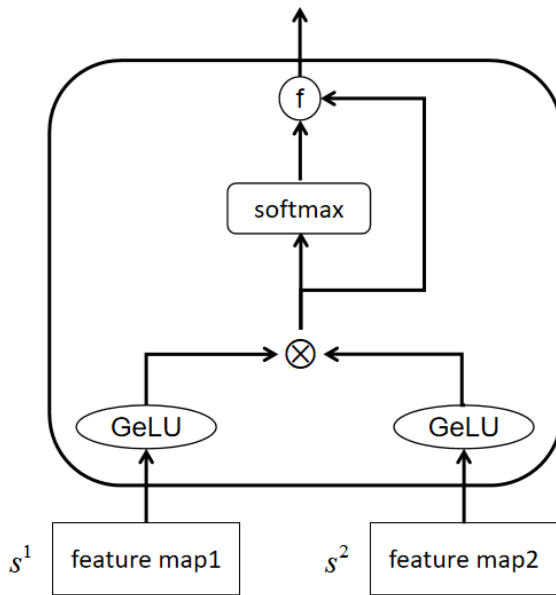


Figure 4 spatial feature attention module

3.3 Hybrid spatial-temporal attention

In figure 5, to incorporate spatial and temporal features to produce the final feature, the hybrid spatial-temporal attention module that is inspired by the Google transformer [20] is proposed. The hybrid spatial-temporal attention consists of a split function, a

pair of the max-pooling network, a fully-connected network, and a block-in attention module which is given by figure 7 in detail.

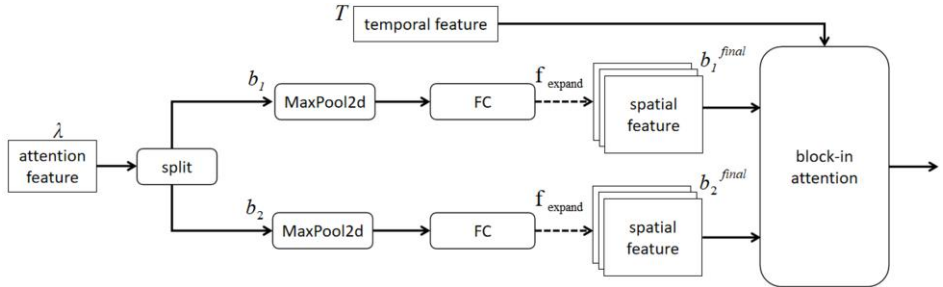


Figure 5 spatial-temporal attention module

The output of the spatial attention module is used as the input, and then the attention feature λ is divided into two branches $b_1, b_2 \in \mathbb{R}^{2C \times H/2 \times W/2}$, the operation is denoted by equation (13). In figure 6, the principle of split function is that numbers of channel C are divided into 2C through a tensor operation that can enhance the ability of information interaction between channels for image; the operation is denoted by equation (14).

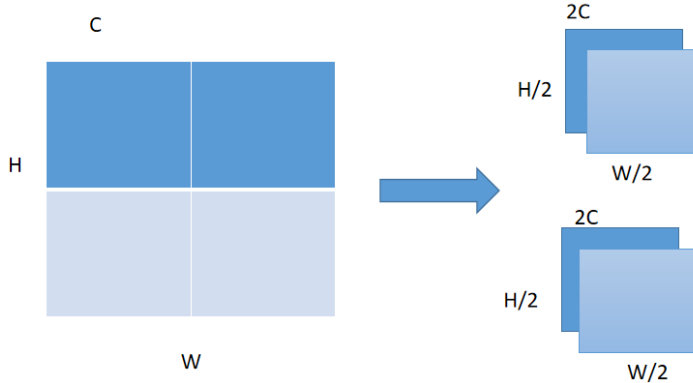


Figure 6 channels split

$$b_1 = b_2 = \text{split}_{2c}(\lambda) \quad (13)$$

$$\text{split}_{2c}[C, H, W] = [[C, H/2, W/2], [C, H/2, W/2]] \quad (14)$$

Then, the feature map of each branch is processed by max-pooling, fully-connected layer fc respectively, the operation is denoted by equation(15). Finally, the expand function f_{expand} that is denoted by equation(16) is used to expand the numbers of the channel to feature map $b_1^{\text{final}}, b_2^{\text{final}} \in \mathbb{R}^{C \times H \times W}$ to enhance the

information redundancy between channels, the operation of this part is denoted by equation(16).

$$\begin{aligned} b_1^{final} &= f_{scale}(fc(F_{max}(b_1))) \\ b_2^{final} &= f_{scale}(fc(F_{max}(b_2))) \end{aligned} \quad (15)$$

$$f_{expand}(2C, H/2, W/2) = [C, H, W] \quad (16)$$

In figure 7, the feature map b_1^{final} , b_2^{final} and the temporal feature T are used as input to the block-in attention module. The block-in module consists of matrix product operation, softmax function, and element-wise product operation.

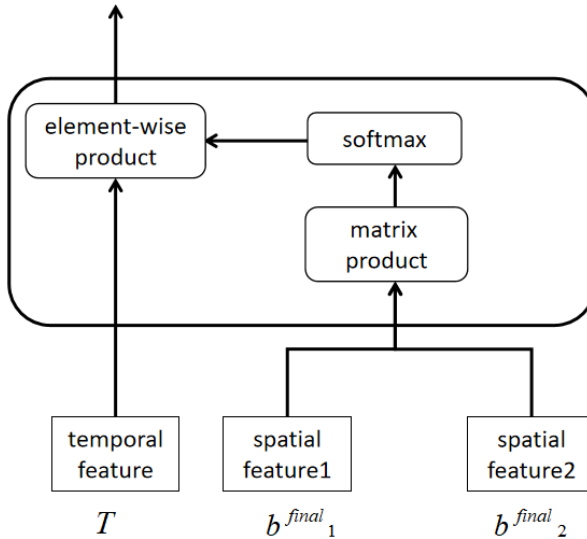


Figure 7 block-in attention module

Matrix product is firstly performed to fuse two feature maps to enrich the information of spatial features. Then the softmax operation is performed to obtain the hybrid attention score. Finally, the attention score and temporal feature T are used as the input to perform the element-wise product to obtain the final attention feature vector, then the feature vector is sent to the classifier to predict the final result, the operation of this part is denoted by equation (17).

$$\begin{aligned} &\text{transformer}(T, b_1^{final}, b_2^{final}) \\ &= \text{softmax}\left(\frac{\text{mat}(W_1^T b_1^{final}, W_2^T b_2^{final})}{\sqrt{\max(1, b)}} \bullet T\right) \\ &= \text{softmax}\left(\frac{W_1^T * b_1^{final} + W_2^T * b_2^{final}}{\sqrt{\max(1, b)}} \bullet T\right) \end{aligned} \quad (17)$$

where W_1^T, W_2^T represents the weight matrix of b^{final}_1, b^{final}_2 , respectively. * represents a matrix product. • represents an element-wise product.

4. Experiment

This section starts with the data set and training details, followed by network architectures, e.g. R3D, R2Plus1D[21], C3D, Hierarchy Spatial-Temporal transformer, and result.

Data Set HMDB51[22] is used in our model, which includes 51 action categories and 7000 short videos, and the UCF101 data set which includes 101 action categories and 30000 short videos. Both of them are open-source data set that contains various scenes in daily life, and a word is used to describe the characters in the scene are doing certain actions, such as running, brushing teeth, playing football, etc.

Training Details In this work, the model is trained in a completely supervised manner on the HMDB51 and UCF101 data set, meaning video sequences is the only needed information. As a video process, a variable t is denoted by the frame rate and set it to 16, to decode the short videos with a frame rate of 16fps, and resize all frames to 224x224x3. In this experiment, the kernel size of the first HResidual Unit is reshaped as 1x1 in every layer to reduce the parameter scale. ResNet-21 and VGG-13 are used as a backbone network. The model is trained end-to-end using a batch size of 64 for 100 iterations with an Adam optimizer. Four-way Tesla P100 GPU is used in this experiment for two days on average. The learning rate has different settings for four different networks: for C3D networks, the experiment found that when the learning rate is set to 0.1, the loss function will appear, NAN, so it is set to 0.0001. When the learning rates of R2Plus1D and R3D are set to 0.001, the network converges the fastest. The learning rate of the hierarchy spatial-temporal transformer proposed in this work is set to 0.01.

Network Architecture The overall network architecture is listed in Table1. The network from left to right in the table is sorted in order of the parameter scale. ResNet[23] with layer size 4,7,7,3 and VGG[24] with layer size 4, 3, 3, 3 is used as the backbone network. The three columns on the left are the baseline models, in which C3D and R2Plus1D network all use 3 x 3 kernel with stride 2. The model R3D uses 7 x 7 convolution with input channel 3 and stride 2, then passes through a maximum pooling layer with kernel size 3 x 3 and stride 2. Our model hierarchy spatial-temporal transformer, three sections in the table is interpreted as a three-stage calculation model, which are: hierarchy residual reformer, spatial attention module, and hybrid spatial-temporal attention. Finally, all modes are processed by global average pooling and fully-connected layers, and then classified by Softmax.

Table 1. The four columns refer to ResNet-21. In detail is the general shape of a residual block, including filter sizes and feature dimensions. The number of stacked blocks on each stage is presented on the right of the grid. Batch norm suggests Batch Normalization. The symbol FC indicates the output dimension of the two fully-connected layers.

Output	C3D	R2Plus1D	R3D	HST transformer
224x224	3 x 3,64,stride 2	3 x 3,64,stride 2	7 x 7,3,stride 2	1x1,3,stride 1
112x112	Relu activation	relu activation	3 x 3 max pool,stride 2	LeakyReLU activation
112x112	3 x 3 , 64 3 x 3 , 64 x4 3 x 3 , 128	7 x 7 , 3 x4 3 x 3 , 64	3 x 3 , 64 Batch Norm x4 3 x 3 ,128	1 x 1 , 64 three stages x4 3 x 3 ,128
56 x 56	3 x 3 , 128 3 x 3 , 128 x6 3 x 3 , 256	7 x 7 , 64 x6 3 x 3 ,128	3 x 3 ,128 Batch Norm x6 3 x 3 ,256	1 x 1 , 64 three stages x6 3 x 3 ,128
28 x 28	3 x 3 , 256 3 x 3 , 256 x6 3 x 3 , 512	7 x 7 , 128 x6 3 x 3 , 256	3 x 3 ,256 Batch Norm x6 3 x 3 ,512	1 x 1 , 64 three stages x6 3 x 3 ,128
14 x 14	3 x 3 , 512 3 x 3 , 512 x3 3 x 3 , 512	7 x 7 , 256 x3 3 x 3 , 512	3 x 3 , 512 Batch Norm x3 3 x 3 , 512	1 x 1 , 64 three stages x3 3 x 3 ,128
7 x 7	3 x 3 global average pool, 1024 FC, softmax	3 x 3 global average pool, 1024 FC, softmax	3 x 3 global average pool, 1024 FC, softmax	3 x 3 global average pool, 1024 FC, softmax

Table 2. List of the baseline model and our model, as well as the backbone network, parameter scale, and accuracy.

Model	Dataset	Backbone	Params(M)	Acc(%)
C3D	HMDB51	ResNet-21	78.20M	76.54%
R2Plus1D	HMDB51	ResNet-21	65.53M	80.64%
R3D	HMDB51	ResNet-21	57.68M	83.25%
Hierarchy Spatial-Temporal Transformer	HMDB51	ResNet-21	35.54M	85.53%

Table 3. The four columns refer to VGG-13. In detail is the general shape of a VGG block, including filter sizes and feature dimensions. The number of stacked blocks on each stage is presented on the right of the grid. Batch norm suggests Batch Normalization. The symbol FC indicates the output dimension of the two fully-connected layers.HST short for Hierarchy Spatial-Temporal Transformer

Output	C3D	R2Plus1D	R3D	HST transformer
224x224	3 x 3,64,stride 2	3 x 3,64,stride 2	7 x 7,3,stride 2	1x1,3,stride 1
112x112	Relu activation	Relu activation	3 x 3 max pool,stride 2	LeakyReLU activation
112x112	3 x 3 , 64 3 x 3 , 64 x4 3 x 3 , 128	7 x 7 , 3 x4 3 x 3 , 64	3 x 3 , 64 Batch Norm x4 3 x 3 ,128	1 x 1 , 64 three stages x4 3 x 3 ,128

56 x 56	3 x 3 , 128 3 x 3 , 128 x3 3 x 3 , 256	7 x 7 , 64 X3 3 x 3 ,128	3 x 3 ,128 Batch Norm x3 3 x 3 ,256	1 x 1 , 64 three stages x3 3 x 3 ,128
28 x 28	3 x 3 , 256 3 x 3 , 256 x3 3 x 3 , 512	7 x 7 , 128 X3 3 x 3 ,256	3 x 3 ,256 Batch Norm x3 3 x 3 ,512	1 x 1 , 64 three stages x3 3 x 3 ,128
14 x 14	3 x 3 , 512 3 x 3 , 512 x3 3 x 3 , 512	7 x 7 , 256 x3 3 x 3 ,512	3 x 3 ,512 Batch Norm x3 3 x 3 ,512	1 x 1 , 64 three stages x3 3 x 3 ,128
7 x 7	3 x 3 global average pool, 1024 FC, softmax	3 x 3 global average pool, 1024 FC, softmax	3 x 3 global average pool, 1024 FC, softmax	3 x 3 global average pool, 1024 FC, softmax

Table 4. List of the baseline model and our model, as well as the backbone network, parameter scale, and accuracy.

Model	Dataset	Backbone	Params(M)	Acc(%)
C3D	UCF101	VGG-13	42.5M	77.89%
R2Plus1D	UCF101	VGG-13	35.8M	79.3%
R3D	UCF101	VGG-13	26.78M	82.65%
Hierarchy Spatial-Temporal Transformer	UCF101	VGG-13	24.1M	86.3%

The following results of inference from the cases were selected from the HMDB51 and UCF101 data set. We took four frames from the test short videos and four different videos from UCF101 test videos. The actions of the two figures are ApplyLipStick and BaseBallPitch and the upper left corner of the figure suggests the current action and the probability of recognition, as shown in Figure 8 and Figure 9.



Figure 8 result of test short video from HMDB51

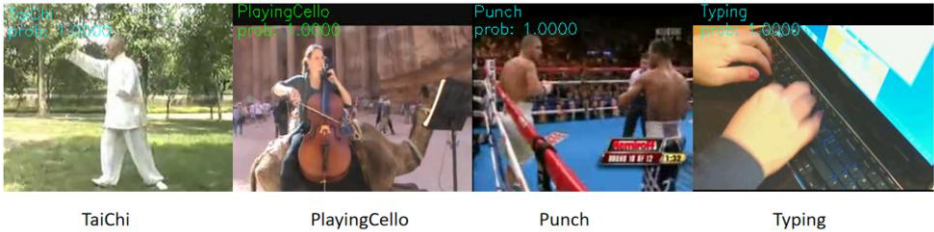


Figure 9 result of test short video from UCF101

5. Conclusion

This work proposed a hierarchy spatial-temporal transformer mainly addresses the problem that how to enhance the ability to learn the spatial feature of the network in action recognition of short videos and reduce parameter scale. The work introduces a hierarchy inference method that is incorporated attention mechanisms to further learn the spatial feature. The model consists of three components: hierarchy residual reformer that transforms video vector into a spatial visual feature map, spatial attention module that is used to further learn spatial feature, and spatial-temporal attention that incorporates spatial and temporal features to produce the final hybrid feature vector. The result suggests that accuracy of the model better than the baseline model. However, due to the limitation of hardware resources, the model in this work can only handle short videos within 30 seconds, and cannot handle large-scale videos. In the future, we will continue to study better local building modules to study the field of action recognition in short videos.

Reference

- [1] X. Wang, R. Girshick, A. Gupta, and K. He, "Non-local Neural Networks," arXiv 1711.07971.
- [2] K. Hara, H. Kataoka, and Y. Satoh, "Can Spatiotemporal 3D CNNs Retrace the History of 2D CNNs and ImageNet?", arXiv 1711.09577.
- [3] X. Li, W. Wang, X. Hu, and J. Yang, "Selective Kernel Networks," arXiv 1903.06586.
- [4] Z. Shou, D. Wang, and S.-F. Chang, "Temporal Action Localization in Untrimmed Videos via Multi-stage CNNs," arXiv 1601.02129.
- [5] L. Wang, W. Li, W. Li, and L. Van Gool, "Appearance-and-Relation Networks for Video Classification," arXiv 1711.09125.
- [6] Yoon, KiJung & Liao, Renjie & Xiong, Yuwen & Zhang, Lisa & Fetaya, Ethan & Urtasun, Raquel & Zemel, Richard & Pitkow, Xaq. (2019). Inference in Probabilistic Graphical Models by Graph Neural Networks. arXiv 1803.07710.
- [7] Baccouche M., Mamalet F., Wolf C., Garcia C., Baskurt A. (2011) Sequential Deep Learning for Human Action Recognition. In: Salah A.A., Lepri B. (eds) Human Behavior Understanding. HBU 2011. Lecture Notes in Computer Science, vol 7065. Springer, Berlin, Heidelberg.
- [8] D. Tran, L. Bourdev, R. Fergus, L. Torresani and M. Paluri, "Learning Spatiotemporal Features with 3D Convolutional Networks," 2015 IEEE International Conference on Computer Vision (ICCV), Santiago, 2015, pp. 4489-4497.
- [9] S. Ji, W. Xu, M. Yang and K. Yu, "3D Convolutional Neural Networks for Human Action Recognition," in IEEE Transactions on Pattern Analysis and Machine Intelligence, 2013, Jan., vol. 35, no. 1, pp. 221-231.
- [10] Z. Qiu, T. Yao, and T. Mei, "Learning Spatio-Temporal Representation with Pseudo-3D Residual Networks," arXiv 1711.10305.
- [11] H. Xu, A. Das, and K. Saenko, "R-C3D: Region Convolutional 3D Network for Temporal Activity Detection," arXiv 1703.07814.

- [12] W. Du, Y. Wang and Y. Qiao, "RPAN: An End-to-End Recurrent Pose-Attention Network for Action Recognition in Videos," 2017 IEEE International Conference on Computer Vision (ICCV), Venice, 2017, pp. 3745-3754.
- [13] J. Gao, Z. Yang, C. Sun, K. Chen, and R. Nevatia, "TURN TAP: Temporal Unit Regression Network for Temporal Action Proposals," arXiv 1703.06189.
- [14] A. Karpathy, G. Toderici, S. Shetty, T. Leung, R. Sukthankar and L. Fei-Fei, "Large-Scale Video Classification with Convolutional Neural Networks," 2014 IEEE Conference on Computer Vision and Pattern Recognition, Columbus, OH, 2014, pp. 1725-1732.
- [15] M. Zolfaghari, K. Singh, and T. Brox, "ECO: Efficient Convolutional Network for Online Video Understanding," arXiv 1804.09066.
- [16] D. Tran, H. Wang, L. Torresani, J. Ray, Y. LeCun and M. Paluri, "A Closer Look at Spatiotemporal Convolutions for Action Recognition," 2018 IEEE/CVF Conference on Computer Vision and Pattern Recognition, Salt Lake City, UT, 2018, pp. 6450-6459.
- [17] Z. Shou, J. Chan, A. Zareian, K. Miyazawa, and S.-F. Chang, "CDC: Convolutional-De-Convolutional Networks for Precise Temporal Action Localization in Untrimmed Videos," arXiv 1703.01515.
- [18] J. Carreira and A. Zisserman, "Quo Vadis, Action Recognition? A New Model and the Kinetics Dataset," arXiv 1705.07750.
- [19] X. Zhang, X. Zhou, M. Lin and J. Sun, "ShuffleNet: An Extremely Efficient Convolutional Neural Network for Mobile Devices," 2018 IEEE/CVF Conference on Computer Vision and Pattern Recognition, Salt Lake City, UT, 2018, pp. 6848-6856.
- [20] Vaswani, Ashish & Shazeer, Noam & Parmar, Niki & Uszkoreit, Jakob & Jones, Llion & Gomez, Aidan & Kaiser, Lukasz & Polosukhin, Illia. (2017). Attention Is All You Need. ArXiv, abs/1706.03762
- [21] C. Szegedy et al., "Going deeper with convolutions," 2015 IEEE Conference on Computer Vision and Pattern Recognition (CVPR), Boston, MA, 2015, pp. 1-9.
- [22] H. Kuehne, H. Jhuang, E. Garrote, T. Poggio and T. Serre, "HMDB: A large video database for human motion recognition," 2011 International Conference on Computer Vision, Barcelona, 2011, pp. 2556-2563
- [23] K. He, X. Zhang, S. Ren and J. Sun, "Deep Residual Learning for Image Recognition," 2016 IEEE Conference on Computer Vision and Pattern Recognition (CVPR), Las Vegas, NV, 2016, pp. 770-778.
- [24] Simonyan, Karen & Zisserman, Andrew. (2014). Very Deep Convolutional Networks for Large-Scale Image Recognition. arXiv 1409.1556.

A Brief Review of Relation Extraction Based on Pre-Trained Language Models

Tiange Xu and Fu Zhang¹

School of Computer Science & Engineering, Northeastern University, Shenyang, China

Abstract. Relation extraction is to extract the semantic relation between entity pairs in text, and it is a key point in building Knowledge Graphs and information extraction. The rapid development of deep learning in recent years has resulted in rich research results in relation extraction tasks. At present, the accuracy of relation extraction tasks based on pre-trained language models such as BERT exceeds the methods based on Convolutional or Recurrent Neural Networks. This review mainly summarizes the research progress of pre-trained language models such as BERT in supervised learning and distant supervision relation extraction. In addition, the directions for future research and some comparisons and analyses are discussed in our whole survey. The survey may help readers understand and catch some key techniques about the issue, and identify some future research directions.

Keywords. Relation Extraction, Pre-trained Language Models, Review

1. Introduction

Relation extraction plays an important role in the fields of Knowledge Graph, Machine Translation, Text Data Mining, and Information Extraction. Relation extraction has attracted widespread attention in international conferences on AI and NLP, and has achieved a series of research results. The traditional relation extraction methods are divided into rule-based learning, supervised learning, weakly supervised learning, and unsupervised learning [1], [2], [3], [4], [5], [6], [7]. In particular, the supervised learning requires manual labeling of a large amount of data, which needs to spend a lot of manpower and financial resources. Therefore, much work has proposed methods based on weak supervision and unsupervised learning to solve the problem of manual labeling.

Over the years, there are many traditional relation extraction methods [1], [8], [9]. Subsequently, some problems have also appeared, such as manually labeling a large amount of data, manually constructing Part-of-Speech Tagging or Dependency Analysis, and low accuracy. Fortunately, with the rapid development of deep learning technologies, researchers widely use deep learning methods to solve the relation extraction problems. Various methods by using Convolutional Neural Networks (CNN) models or Recurrent Neural Network (RNN) models have been proposed successively (see [10], [11], [12], [13], [14] in detail). Especially, the accuracy of relation extraction after the pre-trained language model BERT proposed by Devlin et al. [15] in 2018 has been further improved. Since the pre-trained language models can get more lexical,

¹ Corresponding Author Fu Zhang is with the School of Computer Science and Engineering, Northeastern University, Shenyang, China, PhD, Associate Professor, email: zhangfu@cse.neu.edu.cn

syntactic and semantic features, the relation extraction methods based on pre-trained language models have higher accuracy than the relation extraction methods based on CNN or RNN models. In particular, the mainstream pre-trained models based on Transformer (including BERT, GPT-2, Transformer-XL, XLNet, ROBERTa, ALBERT, etc.) almost occupy the relatively top positions in various of NLP tasks [16], [17], [18].

There are some surveys of relation extraction methods [19], [20], [21], [22], [23], [24]. Although up to now a huge number of relation extraction methods based on pre-trained language models (e.g., BERT [15]) have been proposed in the literature, to the best of our knowledge, detailed and in-depth reviews on these studies are scarce. In this paper, we provide a full up-to-date overview of the current state of the art in the existing relation extraction methods based on pre-trained language models. Regarding all the existing approaches, we make more detailed and in-depth comparisons and discussions, and we classify the existing approaches into supervised learning and distant supervision. In addition, the directions for future research and some comparisons and analyses are discussed in our whole survey. The survey may help readers understand and catch some key techniques about the issue, and identify some future research directions.

2. Development and Classification of Relation Extraction

In 1998, the last Message Understanding Conference (MUC) funded by the Defense Advanced Research Project Agency (DARPA) introduced the entity relation extraction task for the first time. Template Relation in MUC is the earliest description of entity relations [25], [26].

In 1999, the National Institute of Standards and Technology (NIST) organized an Automatic Content Extraction (ACE) evaluation, and one of the important evaluation tasks was entity relation extraction. The ACE entity relation corpus specifies 7 categories of entities, including people, organizations, facilities, premises, geopolitical entities, vehicles, and weapons, each of which is divided into multiple subcategories [23]. Since 2009, ACE has been included in Text Analysis Conference (TAC) and has become a major component of Knowledge Base Population (KBP) [27].

The entity relation extraction involved in MUC and ACE evaluation meetings is limited to a few types of entity relations between named entities (including person names, place names, organizational names, etc.), such as employment relations, geographical relations, person-society organizational relations, etc. SemEval (Semantic Evaluation) is another important evaluation conference in the field of information extraction after MUC and ACE [23]. This conference attracted a large number of institutions and research institutions to participate in the evaluation. SemEval-2007 evaluation task 4 [28] defines the entity relation between 7 common nouns or noun phrases, but the English corpus it provides is small. Subsequently, SemEval-2010 evaluation task 8 [29] enriched and perfected it, and expanded the entity relation types to 9 types, namely: Cause-Effect, Instrument-Agency, Product-Producer, Content-Container, Entity-Origin, Entity-Destination, Component-Whole, Member-Collection, Message-Topic. Considering the order of the entity pairs in the sentence instance, the “Other” class is introduced to describe instances that do not belong to the aforementioned relation types, and a total of 19 entity relations are generated [23].

Relation extraction methods are mainly divided into traditional methods based on machine learning and deep learning methods based on neural networks. The traditional

methods based on machine learning are mainly divided into rule matching, supervised learning, weak supervised learning and unsupervised learning. Deep learning methods based on neural networks are mainly divided into supervised learning and distant supervision. Among them, supervised learning mainly adopts pipeline method and joint learning method. Figure 1 describes the classifications and methods of relation extraction.

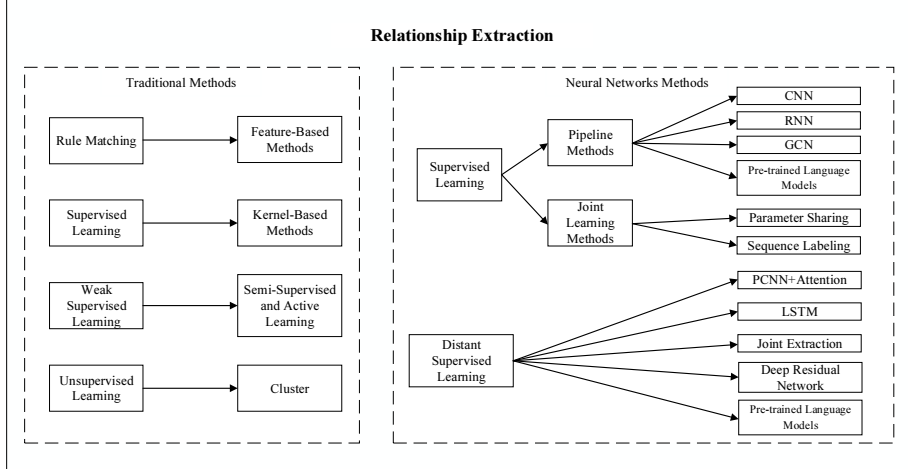


Figure 1. The classifications and methods of relation extraction.

3. Relation Extraction Datasets and Evaluation Criteria

In recent years, the standard datasets used for the evaluation of relation extraction are mainly (also see [24]): SemEval-2010 Task 8 [29], ACE2004 [30], ACE2005 [31], TACRED [32], CoNLL04 [33], FewRel [34], NYT [35], ADE Corpus [36], WebNLG [37], SciERC [38], and DocRED [39]. The relation extraction in the supervised learning mainly uses MUC [26], ACE2004 [30], ACE2005 [31], SemEval-2010 Task 8 [29], TACRED [32], and FewRel [34]. The relation extraction in the distant supervision mainly uses NYT [35] and DocRED [39].

In the supervised methods setting, relation extraction is expressed as a classification task and hence, metrics like Precision, Recall and F-Measure are used for performance evaluation [24]. In detail, Precision and Recall are evaluated based on TP (True Positive), TN (True Negative), FP (False Positive) and FN (False Negative). Suppose that TP is the number of correctly predicted relation instances, $TP + FP$ is the total number of predicted relation instances, and $TP + FN$ is the total number of relation instances, then these metrics are defined as follows:

$$\text{Precision } P = \frac{TP}{TP + FP} \quad (1)$$

$$\text{Recall } R = \frac{TP}{TP + FN} \quad (2)$$

$$\text{F - Measure } F1 = \frac{2 P R}{P + R} \quad (3)$$

4. Relation Extraction by Supervised Learning based on Pre-trained Language Models

Pre-trained language models such as BERT in supervised learning relation extraction methods have deeper depths and can capture longer distance information than previous CNN-based or RNN-based supervised learning relation extraction methods. Researchers have further improved the accuracy of relation extraction by changing BERT's coding method, input-output structure, combining other models, and using knowledge base or knowledge base information. Table 1 summarizes and compares several supervised learning relation extraction methods based on BERT or pre-trained language models.

Table 1. Comparison of different supervised learning relation extraction models.

Model	Technology	Use External Knowledge Base	Dataset	F1 Score
R-BERT [40]	BERT	No	SemEval-2010 Task 8	89.25
BERT _{EM} + MTB [41]	Matching the Blanks + BERT	Using Matching the Blanks	SemEval-2010 Task 8	89.5
			TACRED	71.5
			KBP37	69.3
EPGNN [42]	BERT+GCN	No	SemEval-2010 Task 8	90.2
			ACE2005	77.1
Know-Bert-W+W [43]	BERT+KAR	Wikipedia and WordNet	TACRED	71.5
			SemEval-2010 Task 8	89.1
Entity-Aware BERT [44]	BERT + Entity-Aware + Self-Attention	No	SemEval-2018 Task 7	83.9
			SemEval-2010 Task 8	89.0
TRE [45]	Pre-trained Transformer + Byte Pair Encoding	No	TACRED	67.4
			SemEval-2010 Task 8	87.1
ERNIE [46]	BERT+KG Embedding + TransE [47]	Knowledge Graph	TACRED	67.97
			FewRel	88.32
BERT-LSTM-base [48]	BERT + BiLSTM + WordPiece tokenizer [49]	No	TACRED	67.8
SpERT [50]	BERT + Span Classification+ Span filtering	No	ADE	78.84
		No	CoNLL04	71.47
		SciBERT [51] as a sentence encoder	SciERC	50.84
DYGIE++ [52]	BERT + Span Enumeration + Span Graph Propagation	No	ACE2005	63.4
			SciERC	48.4
			WLPC [53]	65.9

Wu et al. [40] proposed an R-BERT model for relation extraction tasks in 2019. In order to strengthen the BERT model to obtain the relation information between the entity e_1 and the entity e_2 , they add the head entities and tail entities with symbols "\$" and "#", respectively. There is a sentence s and two entities e_1 and e_2 , and they suppose H is BERT's output and the final hidden state. After BERT, they get the vectors H_i to H_j and H_k to H_m , which are the final hidden vectors for the two entities e_1 and e_2 . In order to obtain the vector representations for the entity e_1 and the entity e_2 , they use the average operation. They add an activation operation and a fully connected layer to H_i to H_j and H_k to H_m , and get the output H'_i and H'_j for e_1 and e_2 . They concatenate H'_o (an activation operation and a fully connected layer to the first token '[CLS]'), H'_i , H'_j and then add a fully connected layer and a Softmax layer.

Further, the model is evaluated based on the performance metrics $F1$. In the following we show the calculation process of $F1$ score through examples (e.g., the

relation Component-Whole(e_2, e_1) from the training file in the SemEval-2010 Task 8 dataset. In detail, given a snapshot of few rows of the dataset:

- sentence₁*: The system as described above has its greatest application in an arrayed < e_1 >configuration</ e_1 > of antenna < e_2 >elements</ e_2 >.
- sentence₂*: The girl showed a photo of apple < e_1 >tree</ e_1 > < e_2 >blossom</ e_2 > on a fruit tree in the Central Valley.
- sentence₃*: The < e_1 >provinces</ e_1 > are divided into < e_2 >counties</ e_2 > (Shahrestan), and subdivided into districts (Bakhsh) and sub-districts (Dehestan).

If the model predicts the relation in the first sentence $sentence_1$ is Component-Whole(e_2, e_1), the second sentence $sentence_2$ is Other and the third sentence $sentence_3$ is None (i.e., the model doesn't predict the relation in the third sentence $sentence_3$). In this case, we know the predicted relation in the first sentence $sentence_1$ is right, the second and third sentences are wrong. As we know, TP is a number, which means the relation in the sentence is Component-Whole(e_2, e_1) and the predicted relation in the sentence is also Component-Whole(e_2, e_1); FP is a number, which means the relation in the sentence isn't Component-Whole(e_2, e_1) but the predicted relation in the sentence is Component-Whole(e_2, e_1); FN is a number, which means the relation in the sentence is Component-Whole(e_2, e_1) but the predicted relation in the sentence isn't Component-Whole(e_2, e_1). Then we can get TP is 1 easily. Because all the relations in three sentences are Component-Whole(e_2, e_1), we can get FP is 0. Because the predicted relations in the sentence $sentence_2$ and $sentence_3$ are wrong, we can get FN is 2. Eventually, we can calculate $Precision = 1/1 = 100\%$, $Recall = 1/3 = 33.3\%$ and $F1$ score = 50%. Finally, the R-BERT model [40] achieved $F1$ score at 89.25 on SemEval-2010 Task 8. Figure 2 shows the architecture of the R-BERT model.

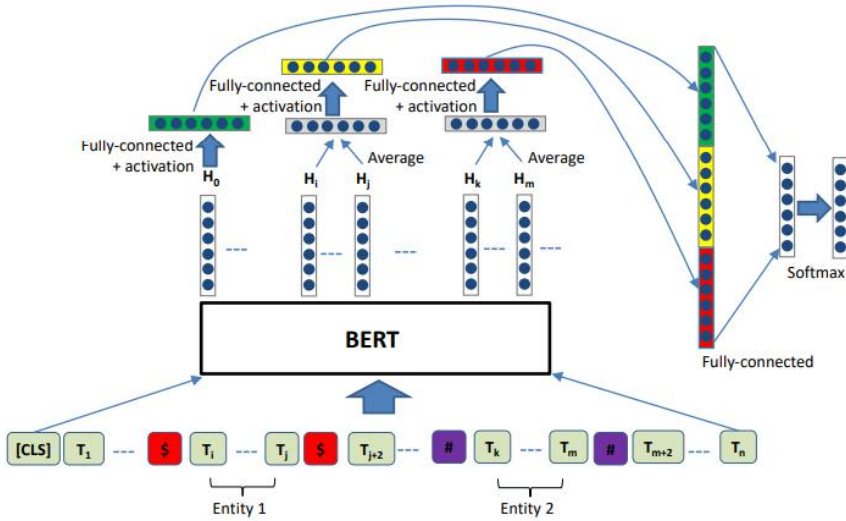


Figure 2. The architecture of the R-BERT model.

Soares et al. [41] proposed a $BERT_{EM} + MTB$ model for relation extraction tasks in 2019. They first proposed the task of MTB (Matching the Blanks), assuming that if two sentences contain the same entity pair, their relation representation should be as similar as possible, otherwise the similarity should be as low as possible. That is, r and r' representing similar relations, and their inner products $f_\theta(r) \cdot f_\theta(r')$ should be high. If

input two sentences into the model and get the relation representation, according to the above assumption, the model only needs the information of the entities in the sentence (comparing whether the entity pairs are the same) to minimize the error. Therefore, they replace the entities in the sentence with the special mark "[BLANK]" according to a certain probability ($\alpha = 0.7$), so that the BERT_{EM} + MTB model models the context information in the sentence except the entity. The loss of the pre-trained model is the loss in the Bert Masked Language Model and the loss of the similarity of the relation. The Matching the Blanks pre-trained dataset was built from Wikipedia. The model is initialized with the parameters of Bert-Large, pre-trained on Matching the Blanks, and fine-tuned on the specific relation extraction task. Matching the Blanks task can complete the relation extraction task without a training set, and it performs well on small datasets.

After presenting the MTB, the author discussed different input and output methods of BERT. The input method is how to specify the position of two entities in the input. There are three types, which are STANDARD: standard input, without specifying the position of the entity; POSITIONAL EMB: position embedding, set the segment type of *entity*₁ and *entity*₂ tokens to 1 and 2; ENTITY MARKER: Entity mark, use the special mark entity position on both sides of *entity*₁ and *entity*₂. The output method is how to get the relational representation from the output of the last layer of BERT. There are three types, which are [CLS]: [CLS] token is used as the relational representation; MENTION POOL: use max pooling on the token representations of the two entities, and then concatenate to obtain the relation representation; ENTITY START: use a special token at the start position of two entities, spliced together as a relation representation. The paper tested the performance of different structures on SemEval-2010 Task8, KBP37, TACRED, and FewRel. They found that the ENTITY MARKER input method and ENTITY START output method performed best on all datasets. They achieved F1 score at 89.5 on SemEval-2010 Task 8 and F1 score at 71.5 on TACRED and F1 score at 69.3 on KBP37.

Zhao et al. [42] proposed an EPGNN model for relation extraction tasks in 2019. They noticed that the relation between entity pairs in a sentence can be indicated by other sentences containing the same entity pair, so the dependency relation between entity pairs in relation extraction also needs to be modeled. Therefore, they proposed the concept of entity pairs graph and used Graph Convolutional Network (GCN) to combine the semantic features and graph topological features. The BERT model was used to encode the context information.

In the model construction, they used the method of Wu et al. [40]. In order to make the BERT model capture the relation information between the two entities, the head entity and the tail entity were added with the symbols "\$" and "#". Then, the sentence is encoded and input into the BERT model. The "[CLS]" at the beginning of the sentence and the hidden layer vector corresponding to the two entities are averaged and fully connected as the semantic feature of the sentence. After the average is connected, it is input to the multi-layer graph convolution network to obtain the graph topology. Finally, the semantic features of the sentences are connected to the graph topology features and input to the Softmax layer to obtain the relation extraction results. Figure 3 shows the architecture of EPGNN model. They achieved F1 score at 90.2 on SemEval-2010 Task 8 and F1 score at 77.1 on ACE2005.

Peters et al. [43] proposed the Know-Bert-W + W model for relation extraction tasks in 2019. For incorporate the structured information in the Knowledge Base into a large-scale pre-trained model, they proposed a Knowledge Attention and

Recontextualization (KAR) component. Know-Bert model integrates knowledge bases (KB) into BERT through KAR. The author proposes three KnowBert models: KnowBert-Wiki, KnowBert-WordNet, and KnowBert-W + W (including Wikipedia and WordNet). Among them, KnowBert-W + W adds the Wikipedia knowledge base to the 10 and 11 layers of BERT (Base), and WordNet to the 11 and 12 layers of BERT (Base). They achieved F1 score at 71.5 on TACRED and F1 score at 89.1 on SemEval-2010 Task 8.

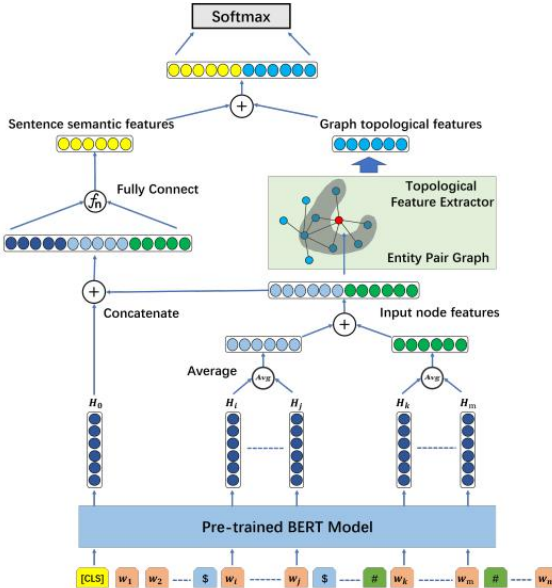


Figure 3. The architecture of EPGNN model.

Wang et al. [44] proposed the Entity-Aware BERT model for relation extraction tasks in 2019. They found that the existing Multiple Entity-Relations (MER) extraction uses a variant of Single Relation Extraction (SRE), which requires Multiple-Pass encoding when inputting the paragraph, resulting in costly calculations. It is expensive and difficult to handle long sentences. They proposed a One-Pass encoding method to solve this problem.

This method is based on BERT with a structured prediction layer to enable BERT to predict multiple relations using a single encoding, and has an entity-aware self-attention mechanism that can inject relation information with entities in hidden state. The key is to use the relative distance between words and entities to encode the location information of each entity. This information is propagated in different layers through attention computation. They achieved F1 score at 83.9 on SemEval-2018 Task 7 and F1 score at 89.0 on SemEval-2010 Task 8.

Alt et al. [45] proposed a TRE model for relation extraction tasks in 2019. Because the traditional method of relation extractions based on semantic and syntactic features requires a large amount of labeled data, which limits the generalization ability of the model, the author proposes a TRE (Transformer for Relation Extraction) model, which uses a pre-trained deep language model to capture the relation between entities. Through the unsupervised pre-training process, the model can learn implicit semantic features of sentences. They achieved F1 score at 67.4 on TACRED and F1 score at 87.1 on the SemEval-2010 Task 8.

Zhang et al. [46] proposed the ERNIE model for relation extraction tasks in 2019. They found that the previous researchers rarely thought of combining information in the Knowledge Graph (KG) when solving the relation extraction task. Therefore, they used large-scale corpora and knowledge maps to train Enhanced Language Representation with Informative Entities (ERNIE) models.

In order to solve the problem of structured knowledge coding and hybrid information fusion, they adopted two methods when constructing the ERNIE model. The first is to identify named entities in the text and match the corresponding named entities in the Knowledge Graph. They don't use the KG's graph-based information directly. They use algorithms like TransE [47] to encode the graph structure of KGs and make the informative entity embeddings as ERNIE's input. They use the MLM (Masked Language Model) and the Next Sentence Prediction as the pre-trained objectives like BERT. In addition, a method of randomly masking named entities in the input text and selecting appropriate named entities from the Knowledge Graph through ERNIE and using both context and Knowledge Graph information are also designed.

Shi et al. [48] proposed a BERT-LSTM-base model for relation extraction tasks in 2019. They found that most existing relation extraction methods rely on lexical and syntactic features, such as Part-of-Speech Tags, Syntactic Trees, Dependency Trees, and Global Decoding Constraints. Although these features improve the accuracy of relation extraction, these features are not suitable for every language, can't improve the robustness of the model, and even reduce the accuracy. Therefore, the author proposes a method that does not use external features and only uses a simple BERT model for relation extraction.

The input sentence is first converted into a "[CLS] sentence [SEP] subject [SEP] object [SEP]" form. To prevent overfitting, replace the subject and object with other symbols such as "[CLS] [S-PER] was born in [O-LOC] [SEP] Obama [SEP] Honolulu [SEP]". The input is then tokenized by the WordPiece tokenizer [49] and fed into the BERT encoder. The position vector is merged with the context vector to input a one-layer BiLSTM. The final hidden states in each direction of the BiLSTM are used for prediction with a one-hidden-layer Multilayer Perceptron (MLP). They achieved F1 score at 67.8 on the TACRED.

Eberts et al. [50] proposed a SpERT model for relation extraction tasks in 2019. They proposed a span-based joint learning model with BERT as the core, which can simultaneously extract entities and relations in sentences. Unlike traditional BIO or BILOU labels, the span-based model can identify overlapping entities. The author found that there are three aspects that help the model improve performance. The first is the negative samples in the same sentence, the second is the localized context representation, and the third is the fine-tuning of the pre-trained model. In addition, the model proposed by the author is also lightweight.

Wadden et al. [52] proposed the DYGIE ++ model for named entity recognition tasks, relation extraction tasks, event extraction tasks, and coreference resolution tasks. The model consists of 4 parts and the structure is shown in the Figure 4. The first part is Token Encoding. DYGIE++ uses BERT for token representations using a "sliding window" approach, feeding each sentence to BERT together with a size- L neighborhood of surrounding sentences. The second part is Span Enumeration. Spans of text are enumerated and constructed by concatenating the tokens representing their left and right endpoints, together with a learned span width embedding. The third part is Span Graph Propagation. A graph structure is generated dynamically based on the model's current best guess at the relations present among the spans in the document.

The fourth part is multi-task classification. The re-contextualized representations are input to scoring functions which make predictions for each of the end tasks. They use a two-layer feedforward neural net (FFNN) as the scoring function. Their F1 score on the relation extraction subtasks in ACE05, SciERC, and WLPC reached 63.4, 48.4, and 65.9, respectively.

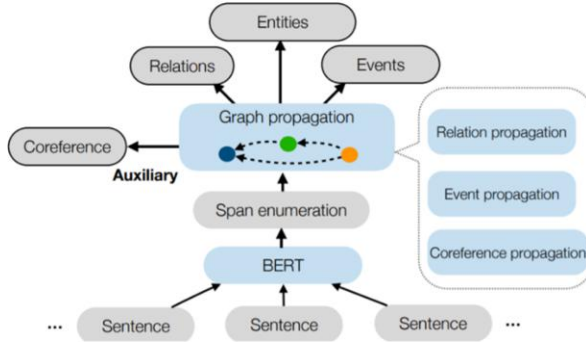


Figure 4. The architecture of DYGIE ++ model.

5. Relation extraction by distant supervision based on pre-trained language models

Distant supervision is a common method in relation extraction. This method was proposed by Mintz et al. [54] on ACL2009, and its main assumption is: if there is a relation between two entities, all sentences containing these two entities may show this relation. Riedel et al. [35] argue that this assumption is too strong, and propose at-least-once assumption: If there is a relation between two entities, at least one of all sentences containing the two entities expresses the relation. Based on this, Riedel et al. [35] modeled distant supervision as a multi-instance learning problem, and aggregated all sentences containing the same entity pair into a bag, and classified these bags. Hoffmann et al. [55] and Surdeanu et al. [56] observed that there may be more than one relation on an entity pair, so a multi-label learning method was added based on multi-instance learning. The method of distant supervision relation extraction requires aligning an unlabeled corpus to a known knowledge base. The most commonly used dataset is the NYT formed by Riedel et al. [57] aligning the New York Times with Freebase. Table 2 summarizes and compares several distant supervision relation extraction methods based on BERT or other pre-trained language models.

Table 2. Comparing different distant supervision relation extraction models.

Model	Technology	Dataset	F1 Score
HBT [58]	BERT + HBT	NYT	87.5
		WebNLG	88.8
BERT-Two-Step [59]	BERT + BiLinear	DocRED	53.92
REDN [60]	BERT + relation computing layer + Sigmoid classifier	SemEval-2010 Task 8	91.0
		NYT	89.8
		WebNLG	96.3

Wei et al. [58] proposed an HBT model for relation extraction tasks in 2019. They found that most of the previous work did not solve the overlapping triple problem. This

problem brings challenges to traditional sequence labeling methods, and it also brings difficulties to relation extraction methods, because previous works considered that an entity has at most one relation to each other. Zeng et al. [61] and Fu et al. [62] both noticed this problem and proposed some improvements. However, there are still shortcomings. They all treat all relations as independent labels and assign them to entity pairs, which makes the relation extraction task complicated. The author proposes a brand-new method for this problem, that is, to find the most likely object and relation based on the identified subject. They implemented this method in an End-to-End Hierarchical Binary Tagging (HBT) framework. The architecture of the model is shown in Figure 5.

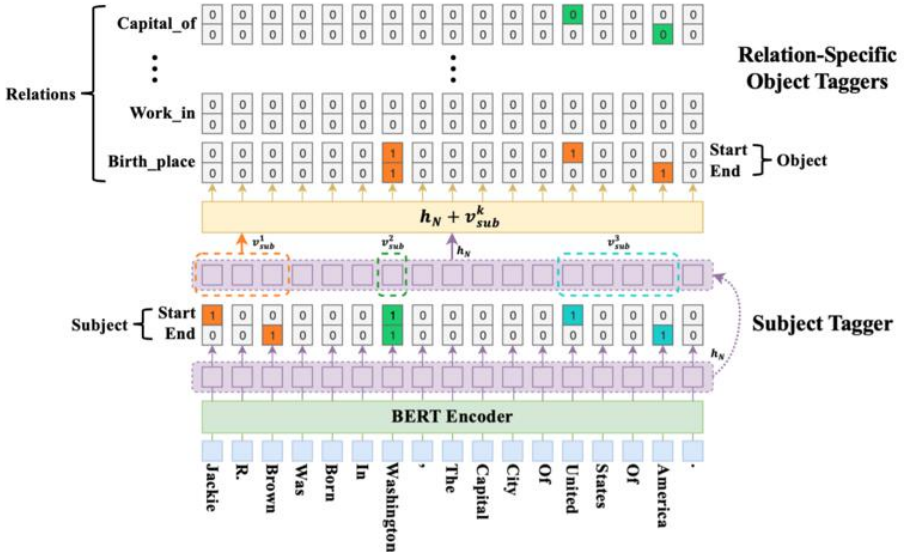


Figure 5. The architecture of HBT model.

Wang et al. [59] proposed a BERT-Two-Step model in 2019, and made progress in document-level relation extraction. They found that most of previous work focused on sentence-level data and did not focus on document-level data. A new document-level dataset DocRED based on distant supervision was released in 2019 [63], filling this gap. They found that using two steps can improve the accuracy of the model. The first step is to predict whether there is a relation between a pair of entities, and the second step is to predict the relation based on a given entity pair.

Li et al. [60] pointed out that the original standard tasks of pre-trained language model do not include the relation extraction and thus proposed a new downstream architecture of PLMs (Pre-trained Language Models) to deal with supervised relation extraction problems. Their works attempt to leverage the power of the pre-trained language models and promote the accuracy of relation extraction tasks. To achieve this goal, they implemented three improvements. First, they use BERT as encoder to extract head and tail entities embeddings from two layers. Second, in a sequence's each token, they calculate a parameterized asymmetric kernel inner-product matrix via all the head and tail embeddings. Third, they give up using Softmax classifier and choose Sigmoid classifier. Besides, for each entity pair they use the average probability of token pairs. It is regarded as the final probability for the entity pair which has a certain relation. Their method reached F1 score at 91.0 on SemEval-2010 Task 8 and F1 score at 89.8 on NYT and F1 score at 96.3 on WebNLG.

6. Results and Discussions

This section makes some results and discussions about the different models as mentioned in the previous Sections 4 and 5. Through comparison as shown in Table 3, it is concluded that each model uses different bright-spot techniques to obtain performance improvement, so that the reader can compare the advantages of each model.

Table 3. Comparisons of different relation extraction models.

Model	The main bright spots
R-BERT [40]	The model marks entities with \$ and # to enhance BERT's ability to capture entities.
BERT _{EM} +MTB [41]	Matching the Blanks improves the accuracy of relation extraction. Using ENEYITY MARKER input and ENTITY START output further improves the performance of BERT.
EPGNN [42]	The model marks entities with \$ and # to enhance BERT's ability to capture entities. The model uses GCN to extract the topological structure of the entity pair graph, which is combined with the semantic information of the sentence to further improve the accuracy of relation extraction.
Know-Bert-W+W [43]	The Know-Bert model integrates knowledge bases (KB) into BERT through KAR, so that the model can combine information from external knowledge bases, thereby improving the accuracy of relation extraction.
Entity-Aware BERT [44]	The model uses One-Pass encoding to solve the problem of Multiple Entity-Relations (MER) extraction. Entity-Aware and Self-Attention mechanisms can inject relation information for multiple entities in each hidden state, thereby improving the accuracy of MER extraction.
TRE [45]	The model uses multiple layers of Transformer to encode the input sequence. In terms of input expression, the input sentence is encoded using Byte Pair Encoding (BPE), which improves the model's ability to learn hidden semantic features.
ERNIE [46]	The model incorporates Knowledge Graph (KG) information during the training process of the multi-layer Transformer model, so that it can learn structured knowledge from KG, thereby improving the accuracy of relation extraction.
BERT-LSTM-base [48]	BERT combined with BiLSTM improves the robustness of the model.
SpERT [50]	Based on the Span-Based joint learning model with BERT as the core, overlapping entities can be extracted. After the sentences are encoded by the BERT layer, the overlapping entities are identified by the Span Classification layer and the Span Filtering layer, and the relation between the entities is obtained by the Relation Classification layer.
DYGIE ++ [52]	The model solves a variety of tasks by encoding sentences with BERT, spanning enumeration and span graph propagation.
HBT [58]	In order to solve the overlapping triple problem, the model uses a Hierarchical Binary Tagging (HBT) framework to extract the subjects and objects in the overlapping triples and the relation between them.
BERT-Two-Step [59]	To solve the problem of document-level data extraction, the model uses two steps to improve the accuracy of the model. The first step is to predict whether there is a relation between a pair of entities, and the second step is to predict relation based on a given entity pair.
REDN [60]	The method implemented three improvements to establish an effective downstream model that is competent for the relation extraction tasks. The first is using BERT as encoder. The second is using a parameterized asymmetric kernel inner product matrix. The third is using Sigmoid classifier instead of the Softmax classifier.

7. Conclusions and Future Research Directions

In this paper we provided a review of relation extraction based on pre-trained language models. The survey in this paper may help readers know and catch some key techniques about this issue and may identify some future research directions. After the

release of pre-trained language models such as BERT, they have shown great potential in relation extraction, which has greatly improved the accuracy in a short time. However, the researches on relation extraction are still in a developing stage. The following issues may be important in order for relation extraction technologies to be more widely adoptable in many application domains:

- Document-level relation extraction: Most of the current relation extraction tasks focus on extracting relations between entity pairs in a sentence, but rarely focus on document-level data. The combination of coreference resolution and relation extraction is a solution to this problem. Peng et al. [64] proposed a general relation extraction framework based on Graph LSTM in 2017, which can be easily extended to cross-sentence N-gram relation extraction. Hence the relation extraction based on graph structure is the solution to this problem.
- Mislabeled of distant supervision: Mislabeled of distant supervision is the most important factor affecting the accuracy of relation extraction [24]. At present, this problem is mainly solved by three methods: The first is an instance selection method. By using the Attention mechanism to assign different weights to sentences of different confidence levels or using multi-instance learning to label test bags, the weight of mislabeled instances noise is reduced. The second method used by Fan et al. [65] and Luo et al. [66] restore the true labels by modeling the process of noise generation. The third is that Qin et al. [67] introduced deep reinforcement learning into distant supervision, and put example sentences with no target relation into the negative set. The mislabeling of distant supervision is an important problem.
- Relation extraction uses knowledge base and Knowledge Graph information: It is one of the difficult points to effectively use the knowledge base and Knowledge Graph information to make a large amount of structured knowledge to help the relation extraction. Peters et al. [43] used the KAR layer to incorporate the knowledge base information, and Zhang et al. [46] used the TransE [47] algorithm to match the entities in the Knowledge Graph with the entities in the training corpus when the pre-trained model was trained. And their model obtained structured information by using the method above.
- Interpretability of BERT model: Jawahar et al. [68] and Bouaoui et al. [69] respectively explored BERT's deep-level representation learning and induction of relation knowledge from BERT in 2019. This is a very necessary thing. First, it can help us understand the limitations of BERT more clearly, so as to improve BERT or figure out its application scope. Second, it helps to explore the interpretability of BERT. Future research can start from this aspect and further explore the interpretability of deep neural networks.
- Identify the relation of overlapping entities: The relation of overlapping entities recognition has always been an obstacle to further improving the accuracy of relation extraction. Zheng et al. [70], Katiyar et al. [71], Zeng et al. [61], and Fu et al. [62] have all done some research on this problem, but none have achieved particularly good results. The method in [58] may well solve this problem, but there is still room for further research on cross-sentence and document-level relation extraction.

Acknowledgments

The authors thank the anonymous referees for their valuable comments and suggestions. The work is supported by the National Natural Science Foundation of China (61672139).

References

- [1] Bach N, Badaskar S. A review of relation extraction. *Literature review for Language and Statistics II*. 2007; 2: 1-15.
- [2] Kambhatla N. Combining lexical, syntactic, and semantic features with maximum entropy models for extracting relations. *ACL on Interactive poster and demonstration sessions*, 2004. p. 22-25.
- [3] Zhao S, Grishman R. Extracting relations with integrated information using kernel methods. *ACL*, 2005. p. 419-426.
- [4] Jiang J, Zhai C X. A systematic exploration of the feature space for relation extraction. *NAACL-HLT*, 2007. p. 113-120.
- [5] Zelenko D, Aone C, Richardella A. Kernel methods for relation extraction. *Journal of machine learning research*. 2003; 3(2): 1083-1106.
- [6] Culotta A, Sorensen J. Dependency tree kernels for relation extraction. *ACL*, 2004. p. 423-429.
- [7] Bunescu R C, Mooney R J. A shortest path dependency kernel for relation extraction. *HLT/EMNLP*, 2005. p. 724-731.
- [8] Alisa Smirnova and Philippe Cudré-Mauroux. Relation extraction using distant supervision: a survey. *ACM Computing Surveys*. 2019; 51(5): 1-35.
- [9] Konstantinova N. Review of relation extraction methods: what is new out there?. *International Conference on Analysis of Images, Social Networks and Texts*, 2014. p. 15-28.
- [10] Socher R, Huval B, Manning C D, et al. Semantic compositionality through recursive matrix-vector spaces. *EMNLP-CoNLL*, 2012. p. 1201-1211.
- [11] Zeng D, Liu K, Lai S, et al. Relation classification via convolutional deep neural network. *COLING*, 2014. p. 2335-2344.
- [12] Xu K, Feng Y, Huang S, et al. Semantic relation classification via convolutional neural networks with simple negative sampling. *EMNLP*, 2015. p. 536-540.
- [13] Vu N T, Adel H, Gupta P, et al. Combining recurrent and convolutional neural networks for relation classification. *NAACL-HLT*, 2016. p. 534-539.
- [14] Xu Y, Mou L, Li G, et al. Classifying relations via long short term memory networks along shortest dependency paths. *EMNLP*, 2015. p. 1785-1794.
- [15] Devlin J, Chang M W, Lee K, et al. Bert: Pre-training of deep bidirectional transformers for language understanding. *NAACL-HLT*, 2019. p. 4171-4186.
- [16] SuperGLUE. <https://super.gluebenchmark.com>.
- [17] NLP-progress. <https://nlpprogress.com>.
- [18] AI2. <https://leaderboard.allenai.org>.
- [19] Kumar S. A survey of deep learning methods for relation extraction. *arXiv preprint arXiv:1705.03645*, 2017.
- [20] Li A, Wang X, Wang W, et al. A survey of relation extraction of knowledge graphs. *Asia-Pacific Web (APWeb) and Web-Age Information Management (WAIM) Joint International Conference on Web and Big Data*, 2019. p. 52-66.
- [21] Goyal K, Bhattacharyya P. Literature survey on relation extraction and relational learning. *Indian Institute of Technology*. 2017; 1-19.
- [22] Zhang Q, Chen M, Liu L. A review on entity relation extraction. *Second International Conference on Mechanical, Control and Computer Engineering*, 2017. p. 178-183.
- [23] Liu S Y, Li Y C, Guo Z G, Wang B, Chen G. Review of entity relation extraction. *Journal of Information Engineering University*. 2016; 17(05): 541-547.
- [24] E HH, Zhang WJ, et al. Survey of entity relationship extraction based on deep learning. *Journal of Software*. 2019; 30(6): 1793-1818.
- [25] Chinchor N, Marsh E. Muc-7 information extraction task definition. *Proceeding of the seventh message understanding conference (MUC-7)*, 1998. p. 359-367.
- [26] Chinchor N A. Overview of muc-7/met-2. *Science Applications International Corp San Diego CA*, 1998.

- [27] McNamee P, Dang H T, Simpson H, et al. An evaluation of technologies for knowledge base population. LREC, 2010. p. 369-372.
- [28] Girju R, Nakov P, Nastase V, et al. Semeval-2007 task 04: Classification of semantic relations between nominals. Proceedings of the Fourth International Workshop on Semantic Evaluations (SemEval), 2007. p. 13-18.
- [29] Hendrickx I, Kim S N, Kozareva Z, et al. Semeval-2010 task 8: Multi-way Classification of Semantic Relations between Pairs of Nominals. Proceedings of the Workshop on Semantic Evaluations: Recent Achievements and Future Directions, 2009. p. 94-99.
- [30] ACE 2004. [EB/OL]. <https://catalog.ldc.upenn.edu/LDC2005T09>.
- [31] ACE 2005. <https://catalog.ldc.upenn.edu/LDC2006T06>.
- [32] TACRED. [EB/OL]. <https://nlp.stanford.edu/projects/tacred/>.
- [33] Roth D, Yih W. A linear programming formulation for global inference in natural language tasks. Illinois univ at urbana-champaign dept of computer science, 2004.
- [34] Han X, Zhu H, Yu P, et al. Fewrel: A large-scale supervised few-shot relation classification dataset with state-of-the-art evaluation. EMNLP, 2018. p. 4803-4809.
- [35] Riedel S, Yao L, McCallum A. Modeling relations and their mentions without labeled text. Joint European Conference on Machine Learning and Knowledge Discovery in Databases, 2010. p. 148-163.
- [36] Gurulingappa H, Rajput A M, Roberts A, et al. Development of a benchmark corpus to support the automatic extraction of drug-related adverse effects from medical case reports. Journal of biomedical informatics. 2012; 45(5): 885-892.
- [37] Gardent C, Shimorina A, Narayan S, et al. Creating training corpora for nlg micro-planning. ACL, 2017. p. 179-188.
- [38] Luan Y, He L, Ostendorf M, et al. Multi-task identification of entities, relations, and coreference for scientific knowledge graph construction. EMNLP, 2018. p. 3219-3232.
- [39] Yao Y, Ye D, Li P, et al. Docred: A large-scale document-level relation extraction dataset. ACL, 2019. p. 764-777.
- [40] Wu S, He Y. Enriching pre-trained language model with entity information for relation classification. CIKM, 2019. p. 2361-2364.
- [41] Soares L B, Fitzgerald N, Ling J, et al. Matching the blanks: distributional similarity for relation learning. ACL, 2019. p. 2895-2905.
- [42] Zhao Y, Wan H, Gao J, et al. Improving relation classification by entity pair graph. Asian Conference on Machine Learning, 2019. p. 1156-1171.
- [43] Peters M E, Neumann M, Logan I V, et al. Knowledge enhanced contextual word representations. EMNLP-IJCNLP, 2019. p. 43-54.
- [44] Wang H, Tan M, Yu M, et al. Extracting multiple-relations in one-pass with pre-trained transformers. ACL, 2019. p. 1371-1377.
- [45] Alt C, Hübner M, Hennig L. Improving relation extraction by pre-trained language representations. arXiv preprint arXiv:1906.03088, 2019.
- [46] Zhang Z, Han X, Liu Z, et al. ERNIE: enhanced language representation with informative entities. ACL, 2019. p. 1441-1451.
- [47] Bordes A, Usunier N, Garcia-Duran A, et al. Translating embeddings for modeling multi-relational data. Advances in neural information processing systems, 2013. p. 2787-2795.
- [48] Shi P, Lin J. Simple BERT models for relation extraction and semantic role labeling. arXiv preprint arXiv:1904.05255, 2019.
- [49] Sennrich R, Haddow B, Birch A. Neural machine translation of rare words with subword units. ACL, 2016. p. 1715-1725.
- [50] Eberts M, Ulges A. Span-based joint entity and relation extraction with transformer pre-training. arXiv preprint arXiv:1909.07755, 2019.
- [51] Beltagy I, Lo K, Cohan A. SciBERT: A pretrained language model for scientific text. EMNLP-IJCNLP, 2019. p. 3606-3611.
- [52] Wadden D, Wennberg U, Luan Y, et al. Entity, relation, and event extraction with contextualized span representations. EMNLP-IJCNLP, 2019. p. 5788-5793.
- [53] Kulkarni C, Xu W, et al. An annotated corpus for machine reading of instructions in wet lab protocols. NAACL, 2018. p. 97-106.
- [54] Mintz M, Bills S, Snow R, et al. Distant supervision for relation extraction without labeled data. ACL and AFNLP, 2009. p. 1003-1011.
- [55] Hoffmann R, Zhang C, Ling X, et al. Knowledge-based weak supervision for information extraction of overlapping relations. ACL, 2011. p. 541-550.
- [56] Surdeanu M, Tibshirani J, Nallapati R, et al. Multi-instance multi-label learning for relation extraction. EMNLP-CoNLL, 2012. p. 455-465.
- [57] Sandhaus E. The new york times annotated corpus. Linguistic Data Consortium, Philadelphia, 2008.

- [58] Wei, Zhepei, et al. A novel hierarchical binary tagging framework for joint extraction of entities and relations. arXiv preprint arXiv:1909.03227, 2019.
- [59] Wang H, Focke C, Sylvester R, et al. Fine-tune Bert for DocRED with two-step process. arXiv preprint arXiv:1909.11898, 2019.
- [60] Li C, Tian Y. Downstream model design of pre-trained language model for relation extraction task. arXiv preprint arXiv:2004.03786, 2020.
- [61] Zeng X, Zeng D, et al. Extracting relational facts by an end-to-end neural model with copy mechanism. ACL, 2018, p. 506-514.
- [62] Fu T J, Li P H, Ma W Y. Graphrel: Modeling text as relational graphs for joint entity and relation extraction. ACL, 2019, p. 1409-1418.
- [63] Yuan Yao, Deming Ye, Peng Li, et al. DocRED: A large-scale document-level relation extraction dataset. ACL, 2019, p. 764-777.
- [64] Peng N, Poon H, Quirk C, Toutanova K, Yih WT. Cross-sentence N-ary relation extraction with graph LSTMs. Transactions of the Association for Computational Linguistics. 2017; 5: 101-115.
- [65] Fan M, Zhao D, Zhou Q, et al. Distant supervision for relation extraction with matrix completion. ACL, 2014, p. 839-849.
- [66] Luo B, et al. Learning with noise: Enhance distantly supervised relation extraction with dynamic transition matrix. ACL, 2017, p. 430-439.
- [67] Qin P, Xu W, Wang WY. Robust distant supervision relation extraction via deep reinforcement learning. ACL, 2018, p. 2137-2147.
- [68] Jawahar G, Sagot B, Seddah D, et al. What does BERT learn about the structure of language?. ACL, 2019, p. 3651-3657.
- [69] Bouraoui Z, Camacho-Collados J, Schockaert S. Inducing Relational Knowledge from BERT. AAAI, 2019, p. 1-8.
- [70] Zheng S, Wang F, et al. Joint extraction of entities and relations based on a novel tagging scheme. ACL, 2017, p. 1227-1236.
- [71] Katiyar A, Cardie C. Going out on a limb: Joint extraction of entity mentions and relations without dependency trees. ACL, 2017, p. 917-928.

This page intentionally left blank

Subject Index

academic fraud	390	compounds	351
academic journals	522	concrete crack detection	690
acceleration approach	234	constructivist learning theory	201
accurate identification	168	convex optimization	589
adaptive filtering	690	convolutional neural	
advantages analysis	522	network	43, 93, 261
Alzheimer's disease	93	coupling co-location pattern	
analysis model of power theft	101	(CCP)	290
anchor optimization	700	Covid-19	201
anorexia	722	customer churn	78
artificial intelligence	247, 390, 413	cutting part	636
ASCII art	608	cyberbullying	223
attention mechanism	304	D numbers	146
attribute reduction	234	data augmentation	608
automatic marshalling model	627	data envelopment analysis	619
behavior prediction	304	data mining	210
belief functions	146	data partition	528
bibliometric method	522	data scarcity	656
bibliometry	390	data sharing	423
big data	436, 522	deep learning	93, 194, 405, 413, 481
big data application	423	delivery tracking	397
bilateration	546	descriptors	351
bisecting k-means	351	diagonal stabilization	589
blockchain	423, 436	differential privacy	671
boolean function	324	dimensionality reduction	160
BP-Firefly neural networks	636	distance matrices	457
broad learning system	474	distance metrics	146
cascaded cost volume filtering	405	distributed environment	378
cast iron components	656	distributed representation	492
chinese herbal medicine	351	DIVA model	52
chromatography data	113	eating disorder	722
citrus juice	474	ecosystem	580
classification	210	edge refinement	405
classifier	474	EdTech	201
Cloud ERP	553, 580	EEG signal	52
Cloud ERP ecosystem security		electricity anti-theft	125
evaluation system	580	electricity information acquisition	
cluster	304	system	101
code analysis	514	electricity substitution	168
code search	514	electricity theft prediction model	125
cognitive robotic system	601	electronic nose	474
collaborative filtering	261	employment relationship	619
combined scheduling	732	end-to-end	481

energy landscape paving	536	HMM	78
ensemble learning	93	human pose estimation	481
enterprise station railway	627	human-computer interaction	247
ERP	413	human-following	546
evaluation	25	hybrid network(s)	481, 492
evolutionary algorithm	324	hyperbola	546
face generation	273	hypergraphs	457
face tag	273	improved decision tree algorithm	101
facial expression analysis	43	indicator system	168
fatigue related properties		infrared image	690
prediction	656	innovation	25
fault diagnosis	636	integration	25
feature extraction	160	internet of things (IoT)	397
features of sub-deep convolutional		interval observers	589
layers	43	job satisfaction	707
federated learning	423, 436	k-means cluster analysis	180
fine tuning	608	k-nearest neighbour	370
fine-grained reading behavior	562	key phrase extraction	360
focused crawler	536	knowledge graph	753
following mobile robot	601	knowledge inference	492
FPCA	113	knowledge mapping	492
FTA-Petri net models	636	knowledge sharing	716
function identification	324	L ₁ performance	135
functional data analysis	113	language models	390
functional discrimination by local		large-scale data	528
likelihood	113	laws	223
fuzzy logic	255	LearningToRank	261
fuzzy logic system	656	life values realization degree	707
fuzzy mappings	7	linear matrix inequalities	589
game experience	247	link evaluation	536
GAN	1	local abnormal signal extraction	340
generation ability	528	local search	324
generative adversarial network	273	logit model	113
genetic algorithm	125, 324	Lorenz-96 model	449
gH-derivative	7	LSTM	304
gH-differentiability	7	machine learning	33, 210, 528
gH-directional differentiability	7	magnetic levitation motor	16
gH-partial derivative	7	Mahalanobis distance	370
global positioning system	397	management	378
Global Terrorism Database (GTD)	210	mapping property	546
GPS	397	MapReduce model	180
granular computing	643	marketing models	255
granular computing	234	mass spectroscopic data	113
grey model	125	maximal clique	290
hardware	700	measurement	66
hierarchies	643	measurement error	66
hierarchy inference	760	membranous nephropathy	
high efficiency video coding	315	diagnosis	160
higher education	753	metric geometry	457

metric spaces	457	public organizations	378
Metzlerian Takagi-Sugeno fuzzy systems	589	public transit	732
microscopic hyperspectral imaging	160	pythagorean fuzzy set	643
mitigation	223	python platform	101
mixed attention mechanism	700	quality monitoring	753
moment of inertia	16	rainstorm disasters	536
morphology	690	random subspace method	33
multi-classifier ensemble	33	random variable	66
multi-granularity	234	rate distortion optimization	315
multi-layer convolutional layer feature fusion	43	recommend system	261
multilevel network ERGMs	716	recommendations system	1
multiple feature thresholds	690	recurrent neural network	261
music recommendation	682	reinforcement learning	663
natural gas	194	relation extraction	775
natural language generation	390	review	775
natural language processing	360, 390	RFPG	663
nearest neighborhoods	457	risk	223
neighborhood rough set	234	robust filtering	449
network	25	robustness	449
neural network(s)	1, 125, 492	sales management	413
NIR spectroscopic data	113	sample adaptive offset	315
no reward value	663	scheduling methods and constraint sets	627
noise	52	scientific and educational complex	25
observation error covariance	449	security evaluation index	553
obstacle avoidance	601	sentiment analysis	194
operation	732	sequence quadratic programming method	16
optimization design	16	server log	304
ordered logit regression	180	sharing	436
ordinary least squares estimator	152	short-turn service	732
organizational citizenship behavior	707	Sina Weibo	722
outlier detection	370	small sample	340
persistent homology	457	social exchange	619
pipeline leak detection	340	social media	722
Pitman's closeness criterion	152	social networks	223
platform	436	socio-economic efficiency	25
polar coordinates	671	sparse decomposition	52
position type	671	spatial data mining	290
positive polynomial fuzzy system (PPFS)	135	spatial feature learning	760
pre-trained language models	775	spatial series data	370
prediction	78	spatial-temporal attention	760
prediction network	663	stability analysis	135
price trend prediction	194	staged	481
pricing tools	255	static code recommendation	514
privacy and security	378	static output feedback (SOF)	135
		stereo matching	405
		strong support	101
		sub-pixel consistency check	405

sum of squares (SOS)	135	uncertainty measures	643
support vector regression	528	user reading behavior preference	
symbolic regression	324	model	562
target detection	340, 700	user reading interest model	562
text analysis	580	variance	66
text classification	716	virtual reality	201
text mining	553	visual interaction	247
time series function	324	visual saliency	315
total system cost	732	VR games	247
trajectory data protection	671	waveform data	113
transfer learning	93, 608	weighted mixed estimator	152
trilateration	546	women's social status	180
TV program	360	work engagement	619
Twitter analysis	360	work values realization degree	707
Twitter profiles	682	XGBoost algorithm	168
unbalanced data	33	YOLOV4	700
uncertainty	66		

Author Index

A, Monika	210	Hu, P.	716
Ahn, H.	546, 601	Huang, A.	732
Alam, M.	210	Jia, P.	474
Bai, Y.	449	Jiao, L.	52
Bao, Y.-e.	7	Jin, P.	423
Bartoli, A.	390	Khusainov, M.	25
Cai, G.	760	Kirihara, T.	360
Cai, J.	671	Kita, K.	360, 608, 682
Cai, Y.	514, 760	Kohno, S.	682
Chen, F.	125	Krokavec, D.	589
Chen, Q.	413	Lai, P.	553
Chen, X.	101, 125, 168, 562, 716	Laksaci, A.	113
Cheng, Q.	273	Lam, H.-K.	135
Choi, Y.-H.	397	Lee, S.C.	546, 601
Cui, H.	474	Li, B.	514
D, Babitha	210	Li, F.	528
Dairo, A.	255	Li, H.	194
Dang, V.C.	546	Li, J.	732
Demongeot, J.	113	Li, L.	93
Ding, S.	66	Li, R.	33
Ding, Y.	492	Li, T.	7, 194
Dioszegi, A.	656	Li, W.	160
Dou, H.	234, 643	Lin, L.	457
Du, X.	273	Lin, W.	340, 690
Du, Y.	273	Lin, Y.	93
Duan, Z.	315	Liu, F.	135
Fang, Y.	553, 580	Liu, G.	194
Fei, L.	146	Liu, J.	413, 528, 536
Feng, Y.	146, 663	Liu, K.	423, 436
Filasová, A.	589	Liu, L.	663
Fourlakidis, V.	656	Liu, P.	619
Fu, S.	514	Liu, Q.	16
Fujisawa, A.	608	Liu, X.	180
Fung, K.-C.	397	Liu, Y.	93, 619
Gao, B.	168	Liu, Z.	514, 536
Gao, Y.	370, 553	Lu, G.	627
Gong, L.	436	Luo, C.	180
Guo, J.	514, 627	Luo, X.	234, 643
Guo, Y.	671	Lv, M.	160
Hamié, A.	113	Mafla Gallegos, L.E.	223, 378
Han, X.	194	Matayoshi, M.	324
Han, Z.	261, 273	Matsumoto, K.	360, 608, 682
Hou, H.	690	Medvet, E.	390

Meng, A.	135	Wang, K.	619
Meng, H.	43	Wang, L.	290, 351
Miao, Y.	732	Wang, N.	700
Naranjo Sánchez, B.A.	378	Wang, P.	707
Ng, T.-H.	397	Wang, X.	351
Nguyen, D.Q.N.	457	Wang, Y.	449, 474, 562
Ohta, K.	608	Wang, Z.	135, 580, 722
Ou, Y.	93	Wei, Z.	168
Ouassou, I.	113	Wen, J.	627
P, Rajesh	210	Wu, A.	753
Pei, Y.	194	Wu, B.	16
Peng, X.	474	Wu, F.	405
Poon, C.-T.	397	Wu, H.	522
Prosvetov, A.V.	1	Wu, J.	152
Qi, X.	101, 125	Wu, P.	290
Qiu, J.	93	Wu, Q.	522
Qiu, Y.	413, 671	Wu, Y.	351, 671
Rach, M.	201	Xi, W.	247
Rachdi, M.	113	Xie, F.	351
Rao, X.	234	Xie, Z.	627
Scott, R.	201	Xing, C.	66
Seo, H.C.	546, 601	Xing, H.	261, 273
Shan, N.	315	Xing, L.	457
Shang, Y.	304	Xu, K.	16
Shen, Y.	261	Xu, N.	627
Shi, H.	66	Xu, T.	643, 775
Slavikovsky, A.	25	Xu, Z.	101, 125
Song, D.	636	Yan, J.	370
Song, J.	234, 643	Yan, T.	43
Song, Y.	528	Yan, X.	234
Su, Q.	553, 580	Yang, B.	273
Sun, L.	671	Yang, J.	423, 436
Szűcs, K.	255	Yang, M.	180, 405
Tacuri López, I.L.	223	Yang, X.	643
Tahernehzadi, M.	210	Yang, Z.	536
Tallón-Ballesteros, A.J.	v	Yao, S.	16
Tan, H.	656	Yao, X.	722
Tan, R.	707	Ye, X.	66
Tang, J.	722	Yoshida, M.	360, 608, 682
Tao, R.	160	Yu, B.	78
Tarasov, V.	656	Yu, G.	722
Terán Terranova, Y.J.	378	Yu, Y.	370
Toapanta Toapanta, S.M.	223, 378	Yu, Z.	663
Van Dang, C.	601	Yuan, F.	43
Vladimirova, O.	25	Yuan, X.	481
Wang, A.	194	Yuen, M.-C.	397
Wang, C.	700	Zhang, D.	492
Wang, H.	481, 492	Zhang, F.	775
Wang, J.	481	Zhang, J.	528

Zhang, L.	7, 101, 125, 351	Zheng, W.	700
Zhang, Q.	423, 436	Zhou, N.	52
Zhang, S.	52, 351	Zhou, S.	290
Zhang, W.	536	Zhou, W.	315
Zhang, Y.	753	Zhou, W.-B.	33
Zhang, Z.	340, 671	Zhu, F.	101, 125
Zhao, G.	423	Zhu, H.	78
Zhao, H.	700	Zhu, L.	436
Zhao, Y.	168	Zhu, Q.	707

This page intentionally left blank